Studies in Systems, Decision and Control 152

Gerasimos Rigatos · Krishna Busawon

Robotic Manipulators and Vehicles

Control, Estimation and Filtering

Springer

Studies in Systems, Decision and Control

Volume 152

Series editor

Janusz Kacprzyk, Polish Academy of Sciences, Warsaw, Poland
e-mail: kacprzyk@ibspan.waw.pl

The series “Studies in Systems, Decision and Control” (SSDC) covers both new developments and advances, as well as the state of the art, in the various areas of broadly perceived systems, decision making and control- quickly, up to date and with a high quality. The intent is to cover the theory, applications, and perspectives on the state of the art and future developments relevant to systems, decision making, control, complex processes and related areas, as embedded in the fields of engineering, computer science, physics, economics, social and life sciences, as well as the paradigms and methodologies behind them. The series contains monographs, textbooks, lecture notes and edited volumes in systems, decision making and control spanning the areas of Cyber-Physical Systems, Autonomous Systems, Sensor Networks, Control Systems, Energy Systems, Automotive Systems, Biological Systems, Vehicular Networking and Connected Vehicles, Aerospace Systems, Automation, Manufacturing, Smart Grids, Nonlinear Systems, Power Systems, Robotics, Social Systems, Economic Systems and other. Of particular value to both the contributors and the readership are the short publication timeframe and the world-wide distribution and exposure which enable both a wide and rapid dissemination of research output.

More information about this series at http://www.springer.com/series/13304

Gerasimos Rigatos · Krishna Busawon

Robotic Manipulators and Vehicles

Control, Estimation and Filtering

Springer

Gerasimos Rigatos
Industrial Automation Unit
Industrial Systems Institute
Rion Patras
Greece

Krishna Busawon
Nonlinear Control Group
Northumbria University
Newcastle-upon-Tyne
UK

ISSN 2198-4182 ISSN 2198-4190 (electronic)
Studies in Systems, Decision and Control
ISBN 978-3-319-77850-1 ISBN 978-3-319-77851-8 (eBook)
https://doi.org/10.1007/978-3-319-77851-8

Library of Congress Control Number: 2018934938

Printed on acid-free paper

This Springer imprint is published by the registered company Springer International Publishing AG part of Springer Nature
The registered company address is: Gewerbestrasse 11, 6330 Cham, Switzerland

To the memory of my father George Rigatos (1933–2017)

Foreword

The aim of the monograph is to solve control, estimation and filtering problems in advanced models of robotic manipulators and vehicles. The methods to be developed are generic and applicable to a wide range of robotic systems. The methods are of assured stability and of proven robustness thus confirming the reliable function of robotic manipulators and vehicles under variable operating conditions, model uncertainty and external disturbances. The following types of robotic manipulators are examined: multi-DOF rigid-link robots, manipulators subject to input/output delays, underactuated robots and redundant manipulators, closed-chain robotic systems and flexible-link robots. Moreover, the following types of robotic vehicles are examined: automatic ground vehicles (AGVs), unmanned aerial vehicles (UAVs), unmanned surface vessels (USVs), autonomous underwater vessels (AUVs) and various types of cooperating autonomous vehicles.

Robotic manipulators and vehicles exhibit complicated dynamics and kinematics. As a consequence, the solution of the associated problems of nonlinear control, nonlinear estimation and nonlinear filtering is still an open research problem. Despite progress in developing advanced robotic mechanisms and elaborated robotic vehicles, control schemes for robots lack often a global stability proof and may rely on heuristically tuned PID controllers that allow functioning only around local operating points. Moreover, estimation and filtering schemes for robots may lack convergence proof (as for instance in the case of neural modelling approaches or in the case of state estimation with the Extended Kalman Filter). Due to the aforementioned reasons, the precision of robots in tasks execution is hindered while their safe and uninterrupted functioning may be also at risk. To overcome these shortfalls, the monograph presents nonlinear control methods for robotic manipulators and vehicles which are globally asymptotically stable, while they also exhibit sufficient robustness to external perturbations. Moreover, the monograph presents nonlinear estimation methods for robots which are of proven convergence thus allowing for real-time identification of the manipulators' and vehicles' unknown

dynamics. Finally, the monograph presents optimal and convergent filtering methods for robotic manipulators and vehicles which allow for their reliable functioning through the processing of measurements from a small number of sensors.

In the area of robotic manipulators (including industrial robots), one can distinguish between two main problems: (i) robots operating in a free working space, with indicative application examples in robotic welding, painting or laser and plasma cutting and (ii) robots performing compliance tasks, with indicative application examples in assembling, finishing of metal surfaces and polishing. When the robotic manipulators operate in a free environment, then kinematic and dynamic analysis provides the means for designing a control law that will move appropriately their end-effector and will enable the completion of the scheduled tasks. (ii) In the case of compliance (force control) tasks, the objective is not only to control the end effectors position but also to regulate the force developed due to contact with a surface. The monograph's results in this field aim at treating also the simultaneous position and force control problem of robotic manipulators.

In the area of mobile robots and autonomous vehicles, one has to handle nonholonomic constraints and to avoid potential singularities in the design of the control law. Again the kinematic and dynamic models of the mobile robots provide the basis for deriving a controller that will enable tracking of desirable trajectories. Several applications can be noted such as path tracking by autonomous mobile robots and automatic ground vehicles (AGVs), motion control of articulated and off-road land vehicles, trajectory tracking and dynamic positioning of surface and underwater vessels (USVs and AUVs) and flight control of unmanned aerial vehicles (UAVs). Apart from controller's design, path planning and motion planning are problems to solve. The monograph's results in this area aim particularly at handling problems of advanced difficulty for autonomous vehicles, e.g. when the unmanned vehicle operates in an unknown environment with moving obstacles and stochastic uncertainties in the measurements provided by its sensors.

The monograph is primarily addressed to the academic community. The contents of the monograph offer a useful insight to researchers in the areas of robotics and automation about key problems on nonlinear control estimation and filtering. On the other side, the monograph offers the knowhow about the handling of uncertainty in the dynamics or in the kinematic model of robotic manipulators and vehicles. It also analyses the implementation stages of new estimation and filtering techniques and demonstrates their use in the modelling of robotic manipulators and autonomous vehicles. The aforementioned topics cover a large research area including robotic arms and mobile robots or drones of various types. The contents of the monograph can be used for the development of late undergraduate and of postgraduate courses in robotics, in several engineering departments. Moreover, the monograph is addressed to engineers working on robotics applications and on industrial automation. The methods developed in it are applicable in industry and in

several manufacturing tasks as well as in intelligent transportation systems Therefore, the monograph's approach to the problems of control, estimation and filtering for robotic manipulators and autonomous vehicles can be of use by engineers treating practical robotic applications.

Rion Patras, Greece
Newcastle-upon-Tyne, UK
October 2017

Dr. Gerasimos Rigatos
Dr. Krishna Busawon

Preface

The monograph treats problems of (i) nonlinear control, estimation and filtering for robotic manipulators (multi-DOF rigid-link robots, robots subject to input–output delays, underactuated manipulators, redundant manipulators and closed-chain robotic mechanisms) and (ii) nonlinear control, estimation and filtering for robotic manipulators (automatic ground vehicles, unmanned aerial vehicles, unmanned surface vessels, autonomous underwater vessels and cooperating mobile robots). The monograph attempts a thorough coverage of the entire range of applications of robotic manipulators and autonomous vehicles. The nonlinear control and estimation methods it develops are of generic use and suitable for a wide range of robotic systems. Such methods can improve robustness, precision and fault tolerance in robotic manipulators and vehicles while they also enable the reliable functioning of these systems under variable conditions, model uncertainty and external perturbations. Through a balance between the theoretical and the applications part, the monograph's results and methods can be assimilated and used by both researchers or members of the academic community and by engineers. The monograph can be a useful contribution to robotics research and a reference guide for engineers working on practical robotic applications.

The content of the monograph's chapters is outlined in the following:

Chapter 1: Rigid-link manipulators and model-based control. The chapter analyses the model-based nonlinear control approaches for multi-DOF rigid-link robots, that is (i) control using global linearization methods, and (ii) control based on approximate linearization methods. As far as approach (i) is concerned, that is methods based on global linearization, these are techniques for the transformation of the nonlinear dynamics of the robotic system to equivalent linear state-space descriptions for which one can design state feedback controllers and can also solve the associated state estimation (filtering) problem. One can classify here methods mainly based on the theory of differentially flat systems. Differentially flat systems form the widest class of systems to which global linearization-based nonlinear control can be applied. Control of rigid-link robotic manipulators becomes of elevated difficulty when the robot is subject to input–output time delays. However, global linearization methods can offer efficient solution even in the latter case. As

far as approach (ii) is concerned, solutions are pursued to the problem of nonlinear control of robots with the use of local linear models (defined around local equilibria). For such local linear models, feedback controllers of proven stability can be developed. One can select the parameters of such local controllers in a manner that assures the robustness of the control loop to both external perturbations and to model's parametric uncertainty.

Chapter 2: Underactuated robotic manipulators. Control of underactuated robots has received significant attention and its application areas comprise several types of industrial and service robotic manipulators. The purpose of research in this area is to design robotic mechanisms that can be controlled despite having a number of actuators that are smaller than their degrees of freedom. This approach can reduce the cost and weight of robots or can provide robotic systems with tolerance to actuators' failures. Again the control problem for such robots is treated with (i) global linearization methods, (ii) approximate linearization approaches and (iii) Lyapunov methods. To achieve model-free control of underactuated manipulators, improved estimation approaches are developed, allowing the real-time identification of their unknown dynamics or kinematics. Moreover, to implement feedback control of underactuated robots through the measurement of a limited number of the robot's state variables, nonlinear filtering methods of proven convergence are developed.

Chapter 3: Rigid-Link manipulators and model-free control. The chapter analyses model-free nonlinear control approaches for multi-DOF rigid-link robots, based on Lyapunov methods. There, one comes against problems of minimization of Lyapunov functions so as to assure the asymptotic stability of the control loop. Model-free control takes often the form of indirect adaptive control. In such a case, the design of the controller is not based on prior knowledge of the robot's dynamics. With the use of adaptive algorithms and elaborated estimation methods, it is possible to identify in real-time the unknown dynamics of the robots and subsequently to use this information in the control loop, thus arriving at indirect adaptive control schemes. Finally, the development of nonlinear filtering methods for robotic manipulators allows the implementation of feedback control through measuring of only a small number of the robot's state variables. Global stability is proven for the control loop that comprises both the nonlinear controller of the robot's dynamics nonlinear filters that estimate the robot's state vector from indirect measurements.

Chapter 4: Closed-chain robotic systems and mechanisms. Control of closed-chain robots is a non-trivial problem because it is often associated with complicated dynamic and kinematics models exhibiting nonlinearities. Unlike robotic manipulators with a free end-effector, closed-chain robotic mechanisms include actuators which are usually placed on a fixed base. On the one side, this enables to develop mechatronic systems with low moving inertia and fast motion control. On the other side, this may incur underactuation problems. Comparing to open-chain robots, closed-chain robotic mechanisms have many advantages such as high stiffness, high accuracy, and high payload-to-weight ratio. To solve the nonlinear control problem of closed-chain robotic systems, the following approaches

are proposed (i) nonlinear control using global linearization methods, (ii) nonlinear control using approximate linearization methods and (iii) nonlinear control using Lyapunov methods. Besides applying model-free control for such a type of robotic manipulators, online estimation algorithms of the unknown dynamics of the robot can be considered once again. The global asymptotic stability of the control which relies on the real-time estimation of the robot's dynamics is proven. Moreover, as in the previously analysed closed-chain manipulator models, to implement feedback control through the measurement of a limited number of the closed-chain robot's state vector, nonlinear filtering methods of proven convergence are developed.

Chapter 5: Flexible-link robots. Control for flexible-link robots is a non-trivial problem that has increased difficulty comparing to the control of rigid-link manipulators. This is because the dynamic model of the flexible-link robot contains the non-linear rigid-link motion coupled with the distributed effects of the links' flexibility. This coupling depends on the inertia matrix of the flexible manipulator while the vibration characteristics are determined by structural properties of the links such as the damping and stiffness parameters. Moreover, in contrast to rigid-link robots, the dynamic model of flexible-link robots is an infinite dimensional one. The model exhibits a certain number of mechanical degrees of freedom associated to the rotational motion of the robot's joints and has also an infinite number of degrees of freedom associated to the vibration modes in which the deformation of the flexible link is decomposed The controller of a flexible manipulator must achieve the same motion objectives as in the case of a rigid manipulator, i.e. tracking of specific joints position and velocity setpoints. Additionally, it must also stabilize and asymptotically eliminate the vibrations of the flexible links that are naturally excited by the joints' rotational motion. A first approach for the control of flexible-link robots is to consider the vibration modes as additional state variables and to develop stabilizing feedback controller for the extended state-space model of the flexible manipulator. To this end, one can use again (i) control based on global linearization methods, (ii) control based on Lyapunov methods (energy-based control). Again, global asymptotic stability for this control approach can be demonstrated. On the other side, nonlinear filtering methods can be used for implementing state feedback control of the manipulator's state vector through the measurement of a limited number of elements from the flexible robot's state vector.

Chapter 6: Micro-manipulators. Microrobots can be used in the manipulation and precise positioning of micro-objects, as well as in several microelectronics applications. Microrobotics is primarily concerned with control problems of microelectromechanical systems (MEMS). Specific problems one encounters in the development of microrobotic systems and MEMS are the imprecision about the microrobot's dynamic model and the inability to measure specific state vector elements in it. This in turn signifies that the design of feedback controllers for such systems has to be sufficiently robust to compensate for unmodelled dynamics or for parametric uncertainty. To this end, one can consider either model-free control methods of proven stability (such as adaptive neurofuzzy control schemes), or

model-based control methods capable of eliminating the effects of modelling errors, parametric inconsistency and external perturbations (such as H-infinity control). Moreover, one has to implement state estimation-based feedback control methods, making use of robust state observers, that will allow for estimation of the entire state vector of the microrobot or MEMS through the processing of measurements from a small number of sensors.

Chapter 7: Unicycles and two-wheel autonomous ground vehicles. Models of unicycles and two-wheel autonomous vehicles can be used to describe the driving behaviour of autonomous ground vehicles in several cases. Robotization of such vehicles requires that several of their functionalities and driving tasks are automatically performed. To achieve this objective, the need of developing and using elaborated control and estimation methods for motorcycles has become apparent. To this end, several results have been developed aiming at solving the stabilization and path tracking problems for autonomous or semi-autonomous motorcycles. Due to underactuation in the motorcycle's model and the strong nonlinearities characterizing its state-space description, the solution of the associated motion problem is a difficult and challenging endeavour. To achieve a satisfactory solution of the problem of autonomous motorcycles driving, different nonlinear control methods can be considered such as global linearization-based control, as well as approximate linearization-based control approaches jointly with optimal control methods. To implement state estimation-based control for two-wheel autonomous vehicles, without the need to process measurements from a large number of on-board sensors, robust state estimation and filtering methods are proposed.

Chapter 8: Four-wheel autonomous ground vehicles. In the recent years, there has been significant effort in the design of intelligent four-wheel autonomous vehicles capable of operating in variable conditions. The precise modelling of the vehicles' dynamics improves the efficiency of vehicles controllers in adverse cases, for example in high velocity, when performing abrupt maneuvers, under mass and loads changes or when moving on rough terrain. Using model-based control approaches, it is possible to design a nonlinear controller that maintains the vehicle's motion characteristics according to given specifications. When the vehicle's dynamics is subject to modelling uncertainties or when there are unknown forces and torques exerted on the vehicle, it is important to be in position to estimate in real-time disturbances and unknown dynamics. In this direction, estimation for the unknown dynamics of the vehicle and state estimation-based control schemes have been developed. Feedback control of robotic ground vehicles can be primarily based on (i) global linearization approaches, (ii) approximate linearization approaches and (iii) Lyapunov methods. The control is applied to (a) four-wheel vehicles, and (b) articulated vehicles. Finally, to implement control of the ground vehicles through the measurement of a small number of its state variables, elaborated nonlinear filtering approaches are developed.

Chapter 9: Unmanned aerial vehicles. The multi-DOF dynamic model of unmanned aerial vehicles (UAVs) is a highly nonlinear one and its control can be performed again with (i) global linearization control methods, (ii) local linearization control methods and (iii) Lyapunov analysis-based methods. In approach (i), the

dynamic model of the UAV is transformed into an equivalent linear description through the application of a change of variables (diffeomorphisms). In (ii), the nonlinear model of the UAV is decomposed into local linear models for which linear feedback controllers are designed and next the aim is to select the feedback control gains so as to assure the global asymptotic stability of the control loop. In (iii), the objective is to define an energy function for the UAV (Lyapunov function) and to demonstrate that through suitable selection of the feedback control the first derivative of the energy function is always negative and thus the global stability of the control loop is assured. The latter approach is particularly suitable for model-free control of UAVs and takes the form of adaptive control methods. This chapter analyses the aforementioned control approaches for UAVs and proves global asymptotic stability for the aforementioned control approaches. The robustness of the developed control methods against model uncertainty and external perturbations is confirmed. Furthermore, elaborated nonlinear filtering approaches are developed that allow for accurate estimation of the state vector of the UAVs through the processing of measurements coming from a limited number of sensors.

Chapter 10: The problem of control and trajectory tracking for unmanned surface vessels (of the ship or hovercraft type) is non-trivial because the associated dynamic and kinematic models are complex nonlinear ones. A first problem that arises in controller design for unmanned surface vessels is that trajectory tracking has to be achieved despite modelling uncertainty and external perturbations and thus the control loop must exhibit sufficient robustness. Another problem that has to be dealt with is that the vessel's model is often underactuated (the propulsion system consists of less actuators than the vessel's degrees of freedom). The present chapter treats the problem of control of unmanned surface vessels. Solution to the associated control problem is provided through (i) global linearization methods, (ii) approximate linearization methods and (iii) Lyapunov methods. Moreover, for the accurate localization of the vessel and for precise computation of its motion characteristics, advanced (and precisely validated) nonlinear filtering and distributed filtering are applied. These enable to perform fusion of the measurements of heterogeneous sensors and of state estimates provided by individual distributed filters that track the vessel's motion.

Chapter 11: Autonomous underwater vessels. The control of multi-DOF autonomous underwater vessels (AUVs) exhibits particular difficulties which are due to the complicated nonlinear model of the submersible vessels, the coupling between the system's control inputs and outputs, and the uncertainty about the values of their dynamic and kinematic model's parameters. Moreover, the AUVs' dynamic model is subject to external perturbations which are caused by variable sea conditions and sea currents. Consequently, an efficient control scheme for AUVs should not only compensate for the nonlinearities of the associated dynamic model, but should also exhibit robustness to model parameter variations and to external disturbances. To this end, the present chapter provides results on robust control of AUVs, as well as on adaptive control of such submersible vessels. Thus the control problem for autonomous underwater vessels is treated with (i) global linearization

methods (ii) approximate linearization methods and (iii) Lyapunov methods. The solution of the control problem requires a more elaborated procedure when the AUVs' dynamic model is underactuated, which means that the number of actuators included in its propulsion system is less than the number of its degrees of freedom. The methods developed in this chapter also treat the case of underactuated AUVs. Moreover, advanced estimation methods are used to identify in real time the unknown dynamics of the underwater vessels or disturbance forces and torques that affect them. This allows for the implementation of indirect control schemes for the AUVs. Additionally, for the precise localization of the AUVs and their safe navigation, elaborated nonlinear filtering methods are developed. These permit to solve problems of multi-sensor fusion as well as problems of decentralized state estimation with the use of spatially distributed nonlinear filters that track the AUVs motion.

Chapter 12: Cooperating autonomous vehicles. Distributed and coordinated control of autonomous vehicles (automatic ground vehicles, unmanned aerial vehicles, unmanned surface and underwater vessels) has received significant attention during the last years. In this chapter, a solution is developed first for the problem of distributed control of cooperating unmanned surface vessels (USVs) which chase a target. The distributed control aims at achieving the synchronized convergence of the autonomous vessels towards the target and at maintaining the cohesion of the vessels' team, while also avoiding collisions between the individuals vessels and collisions between them and obstacles in their motion plane. To estimate the motion characteristics of the target, distributed filtering is performed. To treat the distributed control problem for the cooperating unmanned surface vessels, a Lyapunov theory-based method is introduced. To treat the distributed filtering and state estimation in the multi-vessel system, one can apply established methods for decentralized state estimation. The proposed distributed control and filtering method can be used for surveillance and security tasks executed by multi-robot systems and in particular by multi-USV systems. The method for coordinated control of USVs is a generic one and thus applicable to various types of autonomous robots, such as automatic ground vehicles. A second part of the chapter is concerned with distributed control and cooperation of automatic ground vehicles (such as agricultural robotic vehicles). A global linearization approach is used to transform the nonlinear kinematic model of the vehicle into an equivalent linear form. In this linear description, both the control and state estimation problems of the individual vehicles can be solved, while it is also ascertained that the control loop is globally stable. Moreover, distributed filtering is performed for accomplishing multi-sensor fusion and distributed state estimates fusion. It is shown that the method assures the vehicles' precisely synchronized motion.

The problems of nonlinear control, estimation and filtering for robotic manipulators and for autonomous vehicles are non-trivial ones and the present monograph offers efficient solutions about them. Thus, the monograph is anticipated to be meaningful for members of the academic and research community, as well as to engineers working on practical robotics problems. The benefits from the application of the monograph's results are as follows: (i) the stability of the control loop for

robotic manipulators and autonomous vehicles is assured, (ii) convergence of estimation and filtering methods for the aforementioned robotic systems is also ascertained, (iii) the robotic control loops exhibit robustness to modelling uncertainty and external perturbations (iv) the implementation of feedback control does not have as a prerequisite the precise knowledge of the robots' dynamic or kinematic model. Actually, by following the monograph's results one can develop adaptive control methods which are entirely model-free (v) the presented methods are not constrained by any assumption about the form and structure of the controlled robotic system (vi) the implementation of feedback control does not require measurement of the entire state vector of the robots and can be performed through the processing of the readings from a limited number of sensors. All these reasons indicate that the technical and scientific impact of the present monograph will be noteworthy.

The monograph can be a reference for researchers working on elaborated robotic systems. Moreover, the content of the monograph can be exploited for teaching undergraduate or postgraduate courses on advanced robotic systems. Therefore, it can be used by both academic tutors and students as a reference source for such a course. Almost all departments of electrical, industrial and mechanical engineering, include in their curriculum robotics courses and nonlinear control courses. This means that the academic audience that will bear interest for such a monograph is very wide. Moreover, since studies on robotics and control theory and applications thereof are gaining importance, one should expect that in the following years the number of engineers that will use the monograph's methods on robotics and nonlinear control will also grow.

Athens, Greece — Dr. Gerasimos Rigatos, Electrical and Computer Engineer, Ph.D.
Newcastle, UK — Dr. Krishna Busawon, Electrical and Computer Engineer, Ph.D.
October 2017

Acknowledgements

The authors of the monograph would like to thank the reviewers of this manuscript, coming from the research and academic community, who have contributed to the improvement of this research work through their constructive comments.

Athens, Greece — Gerasimos Rigatos
Newcastle, UK — Krishna Busawon

Contents

1 Rigid-Link Manipulators: Model-Based Control 1
1.1 Chapter Overview 1
1.2 Kinematics and Dynamics of Rigid-Link Multi-DOF Manipulators 3
1.2.1 Outline 3
1.2.2 Dynamic Analysis of Rigid Link Robots 3
1.2.3 Kinematic Analysis of Rigid Link Robots 8
1.3 Model-Based Control of Rigid-Link Manipulators Using Global Linearization Methods 11
1.3.1 Outline 11
1.3.2 Differential Flatness Theory 11
1.3.3 Differential Flatness for MIMO Nonlinear Dynamical Systems 13
1.3.4 Global Linearization of a 2-DOF Robotic Manipulator 16
1.3.5 Simulation Tests 19
1.4 Model-Based Control of Rigid-Link Manipulators Using Approximate Linearization Methods 26
1.4.1 Outline 26
1.4.2 Dynamic Model of the Multi-DOF Robotic System 28
1.4.3 Approximate Linearization of the Robot's Dynamics 31
1.4.4 Design of an H-Infinity Nonlinear Feedback Controller 35
1.4.5 Computation of the Feedback Control Gains for the Approximately Linearized Robot 37
1.4.6 Riccati Equation Coefficients in Controller's Robustness 38

1.4.7 Lyapunov Stability Analysis 39
1.4.8 Simulation Tests 42
1.5 Model-Based Control of Rigid-Link Manipulators Under Time-Delays 49
1.5.1 Outline 49
1.5.2 State-Space Description of the Robotic Manipulator 50
1.5.3 Control of the Robotic Manipulator Under Known Time Delays 53
1.5.4 Differential Flatness of the Robot's Model 54
1.5.5 Control of the Robot Under Unknown Time Delays 55
1.5.6 Simulation Tests 60

2 Underactuated Robotic Manipulators 65
2.1 Chapter Overview 65
2.2 Nonlinear Optimal Control for Multi-DOF Underactuated Overhead Cranes 67
2.2.1 Outline 67
2.2.2 Dynamic Model of the Crane 69
2.2.3 Approximate Linearization of the Crane's Model 71
2.2.4 Design of an H-Infinity Nonlinear Feedback Controller 74
2.2.5 Lyapunov Stability Analysis 76
2.2.6 Robust State Estimation with the Use of the H-Infinity Kalman Filter 79
2.2.7 Simulation Tests 80
2.3 A Nonlinear Optimal Control Approach for Precise Functioning of Ship-Mounted Cranes 85
2.3.1 Outline 85
2.3.2 Dynamic Model of the Payload's Positioning System 87
2.3.3 Approximate Linearization of the Payload's Positioning System 88
2.3.4 Design of an H-Infinity Nonlinear Feedback Controller 90
2.3.5 The Nonlinear H-Infinity Control 91
2.3.6 Lyapunov Stability Analysis 93
2.3.7 Robust State Estimation with the Use of the H_∞ Kalman Filter 96
2.3.8 Simulation Tests 97

2.4 Nonlinear H-Infinity Control for Underactuated Systems: The Furuta Pendulum Example 98
2.4.1 Outline 98
2.4.2 Dynamic Model of Furuta's Penulum 101
2.4.3 Design of an H-Infinity Nonlinear Feedback Controller 104
2.4.4 Lyapunov Stability Analysis 106
2.4.5 Robust State Estimation with the Use of the H-Infinity Kalman Filter 109
2.4.6 Simulation Tests 110
2.5 A Nonlinear Optimal Control Approach for the Cart and Double-Pendulum System 113
2.5.1 Outline 113
2.5.2 Dynamic Model of the Cart and Double-Pendulum System 116
2.5.3 Approximate Linearization of the Cart and Double-Pendulum System 117
2.5.4 Design of an H-Infinity Nonlinear Feedback Controller 122
2.5.5 Lyapunov Stability Analysis 125
2.5.6 Robust State Estimation with the Use of the H_∞ Kalman Filter 128
2.5.7 Simulation Tests 128
2.6 Nonlinear Optimal Control for 3-DOF Underactuated Robotic Manipulators 136
2.6.1 Introduction 136
2.6.2 Dynamic Model of the Underactuated Manipulator 140
2.6.3 Approximate Linearization of the Underactuated Robot 145
2.6.4 Design of an H-Infinity Nonlinear Feedback Controller 147
2.6.5 Lyapunov Stability Analysis 151
2.6.6 Robust State Estimation with the Use of the H-Infinity Kalman Filter 155
2.6.7 Simulation Tests 156

3 Rigid-Link Manipulators: Model-Free Control 161
3.1 Chapter Overview 161
3.2 Model-Free Adaptive Control of Rigid-Link Manipulators Using State Feedback 162
3.2.1 Outline 162
3.2.2 Adaptive Control Based on Transformation of the Robot's Dynamics to a Canonical Form 164

3.2.3 Control Law . . . 165
3.2.4 Application of Flatness-Based Adaptive Fuzzy Control to Robotic Manipulators . . . 167
3.2.5 Lyapunov Stability Analysis . . . 172
3.2.6 Simulation Tests . . . 177
3.3 Model-Free Adaptive Control of Rigid-Link Manipulators Using Output Feedback . . . 183
3.3.1 Outline . . . 183
3.3.2 Transformation of MIMO Robotic Systems into the Brunovsky Form . . . 183
3.3.3 Control Law . . . 186
3.3.4 Estimation of the State Vector . . . 188
3.3.5 Application of Observer-Based Adaptive Fuzzy Control to Robotic Systems . . . 189
3.3.6 Dynamics of the Observation Error . . . 192
3.3.7 Approximation of Unknown System's Dynamics . . . 193
3.3.8 Lyapunov Stability Analysis . . . 194
3.3.9 Riccati Equation Coefficients in Observer-Based Adaptive Fuzzy Control . . . 200
3.3.10 Simulation Tests . . . 201
3.4 Adaptive H-Infinity Neurofuzzy Control for the Rotary Pendulum . . . 207
3.4.1 Outline . . . 207
3.4.2 Dynamic Model of the Rotary Pendulum . . . 208
3.4.3 Control System Dynamics . . . 208
3.4.4 Estimation of the Unknown Dynamics of the System . . . 210
3.4.5 Lyapunov Stability Analysis . . . 212
3.4.6 Simulation Tests . . . 216

4 Closed-Chain Robotic Systems and Mechanisms . . . 221
4.1 Chapter Overview . . . 221
4.2 Flatness-Based Control of Closed-Chain Kinematic Mechanisms . . . 222
4.2.1 Outline . . . 222
4.2.2 Dynamic Model of the Closed-Chain 2-DOF Robotic System . . . 224
4.2.3 Proof of the Robot's Dynamic Model Using the Euler–Lagrange Method . . . 227
4.2.4 Linearization of the Closed-Chain 2-DOF Robotic System Using Lie Algebra Theory . . . 232
4.2.5 Differential Flatness of the Closed-Chain 2-DOF Robotic System . . . 235

4.2.6 Derivative-Free Nonlinear Kalman Filter for the Closed-Chain 2-DOF Robotic System 238
4.2.7 Simulation Tests 241
4.3 Flatness-Based Adaptive Fuzzy Control of Closed-Chain Kinematic Mechanisms 246
4.3.1 Outline 246
4.3.2 Flatness-Based Adaptive Fuzzy Control 247
4.3.3 Lyapunov Stability Analysis 250
4.3.4 Simulation Tests 253
4.4 Nonlinear Optimal Control for Closed-Chain Kinematic Mechanisms 256
4.4.1 Outline 256
4.4.2 Approximate Linearization of the Closed-Chain Closed-Chain Robotic Mechanism 257
4.4.3 Design of an H-Infinity Nonlinear Feedback Controller 260
4.4.4 Lyapunov Stability Analysis 262
4.4.5 Robust State Estimation with the Use of the H-Infinity Kalman Filter 266
4.4.6 Simulation Tests 266

5 Flexible-Link Robots 271
5.1 Chapter Overview 272
5.2 Inverse Dynamics Control of Flexible-Link Robots 272
5.2.1 Outline 272
5.2.2 Model-Based Control of Flexible Link Robots 274
5.2.3 Energy-Based Control of Flexible Link Robots 277
5.2.4 Force Control in Flexible-Link Robots 280
5.2.5 Simulation Results 285
5.3 Sliding-Mode Control of Flexible-Link Manipulators 286
5.3.1 Outline 286
5.3.2 Design of a Sliding-Mode Controller 292
5.3.3 Estimation of the Non-measurable State Variables 295
5.3.4 Simulation Tests 296

6 Micro-manipulators 301
6.1 Chapter Overview 301
6.2 Adaptive Neurofuzzy Control of Microactuators 302
6.2.1 Outline 302
6.2.2 Dynamic Model of the Electrostatic Actuator 304
6.2.3 Linearization of the MEMS Model Using Lie Algebra 306
6.2.4 Differential Flatness of the Electrostatic Actuator 307

6.2.5 Adaptive Fuzzy Control of the MEMS Model Using Output Feedback 309
6.2.6 Lyapunov Stability Analysis 315
6.2.7 Simulation Tests 321
6.3 Nonlinear Optimal Control of Underactuated MEMS 325
6.3.1 Outline 325
6.3.2 Dynamic Model of MEMS 326
6.3.3 Approximate Linearization of the MEMS Dynamics 327
6.3.4 Design of an H-Infinity Nonlinear Feedback Controller 328
6.3.5 The Nonlinear H-Infinity Control 329
6.3.6 Lyapunov Stability Analysis 331
6.3.7 Robust State Estimation with the Use of the H-infinity Kalman Filter 334
6.3.8 Simulation Tests 335

7 Unicycles and Two-Wheel Autonomous Ground Vehicles 341
7.1 Chapter Overview 341
7.2 Nonlinear Optimal Control of the Robotic Unicycle 343
7.2.1 Outline 343
7.2.2 Linearization of the Robotic Vehicle's Kinematic Model 344
7.2.3 Linearization of the Unicycle Robot Through Taylor Series Expansion 344
7.2.4 The Nonlinear H-Infinity Control 346
7.2.5 Lyapunov Stability Analysis 348
7.2.6 Simulation Tests 350
7.3 Flatness-Based Control of the Robotic Unicycle 353
7.3.1 Outline 353
7.3.2 Application of Derivative-Free Kalman Filtering to UGVs 354
7.3.3 Simulation Tests 359
7.4 Nonlinear Optimal Control of Autonomous Two-Wheel Vehicles 373
7.4.1 Outline 373
7.4.2 Dynamic and Kinematic Model of the Riderless Motorcycle 374
7.4.3 Approximate Linearization of the Model of the Riderless Motorcycle 376
7.4.4 The Nonlinear H-Infinity Control 377

7.4.5 Lyapunov Stability Analysis 380
7.4.6 Robust State Estimation with the Use of the H-Infinity Kalman Filter 384
7.4.7 Simulation Tests 384

8 Four-Wheel Autonomous Ground Vehicles 391
8.1 Chapter Overview 391
8.2 Nonlinear Optimal Control of Four-Wheel Autonomous Ground Vehicles 393
8.2.1 Outline 393
8.2.2 Dynamic and Kinematic Model of the Vehicle 394
8.2.3 Approximate Linearization of the Four-Wheel Vehicle Dynamics 399
8.2.4 The Nonlinear H-Infinity Control 401
8.2.5 Min-Max Control and Disturbance Rejection 402
8.2.6 Lyapunov Stability Analysis 404
8.2.7 Robust State Estimation with the Use of the H-Infinity Kalman Filter 407
8.2.8 Simulation Tests 408
8.3 A Nonlinear H-Infinity Control Approach for an Autonomous Truck and Trailer System 415
8.3.1 Outline 415
8.3.2 Kinematic Model of the Truck and Trailer 416
8.3.3 The Nonlinear H-Infinity Control 419
8.3.4 Lyapunov Stability Analysis 421
8.3.5 Robust State Estimation with the Use of the H-Infinity Kalman Filter 424
8.3.6 Simulation Tests 425
8.4 Nonlinear Optimal Feedback Control of Four-Wheel Steering Autonomous Vehicles 427
8.4.1 Outline 427
8.4.2 Modelling of the Kinematics and Dynamics of the 4WS Autonomous Vehicle 429
8.4.3 Approximate Linearization of the Model of the 4WS Vehicle 434
8.4.4 The Nonlinear H-Infinity Control 438
8.4.5 Lyapunov Stability Analysis 441
8.4.6 Robust State Estimation Using the H-Infinity Kalman Filter 444
8.4.7 Simulation Tests 445

8.5 Flatness-Based Control for AGVs and Kalman Filter-Based Compensation of Disturbance Forces and Torques 453
8.5.1 Outline 453
8.5.2 Dynamic Model of the Vehicle 455
8.5.3 Flatness-Based Controller for the 3-DOF Vehicle Model 456
8.5.4 Estimation of Vehicle Disturbance Forces with the Derivative-Free Nonlinear Kalman Filter 459
8.5.5 Simulation Tests 462

9 Unmanned Aerial Vehicles 469
9.1 Chapter Overview 469
9.2 Control of UAVs Based on Global Linearization 470
9.2.1 Outline 470
9.2.2 Kinematic Model of the Quadropter 472
9.2.3 Euler–Lagrange Equations for the Quadropter 473
9.2.4 Design of Flatness-Based Control for the Quadrotor's Model 474
9.2.5 Estimation of the Quadrotor's Disturbance Forces and Torques with Kalman Filtering 476
9.2.6 Simulation Tests 479
9.3 Control of UAVs Based on Approximate Linearization 480
9.3.1 Outline 480
9.3.2 Dynamic Model of the UAV 484
9.3.3 Linearization of the UAV's Dynamic Model 485
9.3.4 Design of an H-Infinity Nonlinear Feedback Controller 489
9.3.5 Lyapunov Stability Analysis 492
9.3.6 Robust State Estimation with the Use of the H-Infinity Kalman Filter 495
9.3.7 Simulation Tests 497

10 Unmanned Surface Vessels 501
10.1 Chapter Overview 502
10.2 Nonlinear Control and Filtering for a 3-DOF Surface Vessel 503
10.2.1 Outline 503
10.2.2 Kinematic and Dynamic Models of Vessels for the Problem of Dynamic Positioning 504
10.2.3 Ship Actuator Model 507
10.2.4 Feedback Linearization for Ship Dynamic Positioning 508

10.2.5 Joint Estimation of the Ship's State Vector and of Unknown Additive Disturbances 510
10.2.6 Sensor Fusion for the Surface Vessel Using Kalman Filtering 511
10.2.7 Particle Filter-Based Sensor Fusion for Estimating the Ship's Motion and Disturbances 513
10.2.8 Simulation Tests 515
10.3 Flatness-Based Control for the Autonomous Hovercraft 532
10.3.1 Outline 532
10.3.2 State-Space Description of the Underactuated Hovercraft 533
10.3.3 Differential Flatness Properties of the Hovercraft's Model 540
10.3.4 Flatness-Based Control of the Hovercraft's Model 543
10.3.5 Disturbances' Compensation with the Use of the Derivative-Free Nonlinear Kalman Filter 548
10.3.6 Simulation Tests 550
10.4 A Nonlinear H-Infinity Control Approach for Underactuated Surface Vessels 554
10.4.1 Outline 554
10.4.2 Approximate Linearization of the Underactuated Vessel 555
10.4.3 Design of an H-Infinity Nonlinear Feedback Controller 557
10.4.4 Lyapunov Stability Analysis 560
10.4.5 Robust State Estimation with the Use of the H-Infinity Kalman Filter 563
10.4.6 Simulation Tests 564
10.5 Validation of Distributed Kalman Filtering for Ship Tracking Applications 570
10.5.1 Outline 570
10.5.2 Dynamic Model of Surface Vessels 572
10.5.3 Fuzzy Kalman Filtering for Ship Motion Estimation 572
10.5.4 Consistency of the Kalman Filter 578
10.5.5 Change Detection with the Local Statistical Approach 581
10.5.6 Simulation Tests 588

11 Autonomous Underwater Vessels 593
11.1 Chapter Overview 594
11.2 Global Linearization-Based Control of Autonomous Underwater Vessels 595

11.2.1 Outline . . . 595
11.2.2 The 6-DOF Dynamic Model of the AUV . . . 596
11.2.3 Differential Flatness of the AUV's Model . . . 600
11.2.4 Flatness-Based Control of the AUV . . . 601
11.2.5 Disturbances Compensation with the Derivative-Free Nonlinear Kalman Filter . . . 603
11.2.6 Simulation Tests . . . 605
11.3 Adaptive Fuzzy Control of Autonomous Submarines . . . 607
11.3.1 Outline . . . 607
11.3.2 The Dynamic Model of the Autonomous Submarine . . . 611
11.3.3 Estimation of the Submarine's Unknown Dynamics . . . 614
11.3.4 Flatness-Based Adaptive Fuzzy Control of the Submarine Dynamics . . . 617
11.3.5 Lyapunov Stability Analysis . . . 620
11.3.6 Simulation Tests . . . 625
11.4 Nonlinear Optimal Control of Autonomous Submarines . . . 628
11.4.1 Outline . . . 628
11.4.2 Approximate Linearization of the AUV's Model . . . 629
11.4.3 Design of an H-Infinity Nonlinear Feedback Controller . . . 632
11.4.4 The Nonlinear H-Infinity Control for the Autonomous Submarine . . . 633
11.4.5 Lyapunov Stability Analysis . . . 636
11.4.6 Robust State Estimation with the Use of the H-Infinity Kalman Filter . . . 638
11.4.7 Simulation Tests . . . 640

12 Cooperating Autonomous Vehicles . . . 643
12.1 Chapter Overview . . . 643
12.2 Cooperating Unmanned Surface Vessels . . . 644
12.2.1 Outline . . . 644
12.2.2 Target Tracking by Multi-robot Systems . . . 645
12.2.3 Distributed Motion Planning for the Multi-USV System . . . 649
12.2.4 Distributed State Estimation Using the Extended Information Filter . . . 655
12.2.5 Distributed State Estimation Using the Unscented Information Filter . . . 661

12.2.6 Filtering Using Differential Flatness Theory and Canonical Forms 669
12.2.7 Simulation Tests 672
12.3 Cooperating Unmanned Ground Vehicles 684
12.3.1 Outline 684
12.3.2 Localization and Path Planning for Cooperating Agricultural Robots 687
12.3.3 Derivative-Free Kalman Filtering for Unmanned Ground Vehicles 690
12.3.4 Simulation Tests 693

References 697

Index 727

Abbreviations

4WD	4-Wheel Drive
4WS	4-Wheel Steering
AC motor	Alternate Current Motor
AGV	Automatic Ground Vehicle
ARE	Algebraic Riccati Equation
ARMAX	Auto-Regressive Moving Average system with Noise
AUV	Autonomous Underwater Vessel
CRLB	Cramer-Rao Lower Bound
CT	Computed Torque Method
DEIF	Derivative-free Extended Information Filter
DGPS	Differential Global Positioning System
DH	Denavit-Hartenberg
DKF	Derivative-free nonlinear Kalman Filter
DOF	Degrees of Freedom
EIF	Extended Information Filter
EKF	Extended Kalman Filter
FDI	Fault Detection and Isolation
FKF	Fuzzy Kalman Filter
GLR	Generalized Likelihood Ratio
GPS	Global Positioning System
H_∞ control	H-infinity Control
H_∞ KF	H-infinity Kalman Filter
IF	Information Filter
IMU	Inertial Measurement Unit
KF	Kalman Filter
LMI	Linear Matrix Inequalities
LQG	Linear Quadratic Gaussian
LQR	Linear Quadratic Regulator
MEMS	Microelectromechanical Systems
MIMO	Multi-Input Multi-Output

MPC	Model Predictive Control
MSE	Mean Square Error
NES	Normalized Error Square
NME	Normalized Mean Error
NMPC	Nonlinear Model Predictive Control
PD	Proportional Derivative Control
PF	Particle Filter
PID	Proportional Integral Derivative Control
RMSE	Root Mean Square Error
RTK-GPS	Real-Time Kinematic GPS
SISO	Single-Input Single-Output
SMC	Sliding Model Control
UAV	Unmanned Aerial Vehicle
UGV	Unmanned Ground Vehicle
UIF	Unscented Information Filter
UKF	Unscented Kalman Filter
USV	Unmanned Surface Vessel

Chapter 1
Rigid-Link Manipulators: Model-Based Control

Abstract The chapter analyzes the model-based nonlinear control approaches for multi-DOF rigid-link robots, that is (i) control based on global linearization methods, and (ii) control based on approximate linearization methods. As far as approach (i) is concerned, that is methods relying on global linearization, these are techniques for the transformation of the nonlinear dynamics of the robotic system to equivalent linear state-space descriptions for which one can design state feedback controllers and can also solve the associated state estimation (filtering) problem. One can classify here methods mainly elaborating on the theory of differentially flat systems. Differentially flat systems form the widest class of systems to which global linearization-based nonlinear control can be applied. As far as approach (ii) is concerned. solutions are sought to the problem of nonlinear control of robots with the use of local linear models (defined around local equilibria). For such local linear models, feedback controllers of proven global stability can be developed. One can select the parameters of such local controllers in a manner that ensures the robustness of the control loop to both external perturbations and to model's parametric uncertainty. In particular the chapter develops the following topics: (a) Kinematics and dynamics of multi-DOF robotic manipulators. (b) Model-based control of rigid-link manipulators using global linearization methods, (c) Model-based control of rigid-link manipulators using approximate linearization methods, (d) Model-based control using global linearization methods for rigid-link manipulators subject to time-delays.

1.1 Chapter Overview

The present chapter develops the following topics: (a) Kinematics and dynamics of multi-DOF robotic manipulators. (b) Model-based control of rigid-link manipulators using global linearization methods, (c) Model-based control of rigid-link manipulators using approximate linearization methods, (d) Model-based control in the context of global linearization methods for rigid-link robots subject to time-delays.

With reference to (a) the objective of kinematic analysis is to create models that connect the velocities of the robotic manipulator in a cartesian reference frame with

G. Rigatos and K. Busawon, *Robotic Manipulators and Vehicles*,
Studies in Systems, Decision and Control 152,
https://doi.org/10.1007/978-3-319-77851-8_1

the angular velocities of the robot's joints. On the other side the purpose of dynamic analysis is to create models that connect the angular or cartesian accelerations of the manipulator with the torques and forces that are exerted on the manipulator by its actuators or by contact with objects and surfaces. In the first case only the lengths of the robot's links are included in the kinematic model whereas in the latter case the masses and moments of inertia of the robot's link are included in the dynamic model.

With reference to (b) the objective of global linearization-based control methods is to transform the robotic manipulator's model into an equivalent linear form, in which both the solution of the feedback control and state-estimation problem becomes possible. Such a transformation is enabled through a change of state variables (diffeomorphisms) and is possible for all models of robotic manipulators that satisfy the differential flatness property. This class of robotic models comprises both fully actuated and underactuated manipulators.

With reference to (c) the dynamic model of the robotic manipulator undergoes an approximate linearization around a temporary operating point which is recomputed at each sampling instant. The linearization procedure makes use of first-order Taylor series expansion for the manipulator's model and relies on the computation of the associated Jacobian matrices. For the approximately linearized model of the robot an H-infinity (optimal) controller is developed after solving an algebraic Riccati equation at each time step of the control method. The latter control scheme achieves stabilization and tracking control for nonlinear robotic manipulators without the need to use the elaborated state-space transformations met in global linearization-based control methods.

With reference to (d) by applying Taylor series expansion to the terms of the robotic manipulator the time-derivatives of the control variables of the initial nonlinear model of the manipulator emerge as additional control inputs. Next, dynamic extension is performed which means that the state-space model of the robot is extended by including in it as additional control variables its initial control inputs. For the extended state-space description of the manipulator it is proven that differential flatness properties hold. This signifies that the extended state-space model is input-output linearizable and in this latter form the solution of the stabilization and control problem becomes possible. Moreover, it is shown that time-delays effects in the model of the robotic manipulator can be represented as additive disturbance terms affecting its input-output linearized description. With the use of a differential flatness theory-based filtering approach, which is the Derivative-free nonlinear Kalman Filter in the form of a disturbance observer, the real-time estimation of the aforementioned perturbation inputs is enabled. This, in turn allows for the computation of a control law that compensates for the time-delays effects.

1.2 Kinematics and Dynamics of Rigid-Link Multi-DOF Manipulators

1.2.1 Outline

Knowledge and understanding of the dynamic and kinematic model of robotic systems can help to increase productivity, cut-off production costs, and to improve working conditions and safety in industrial environments. This need has resulted in the development of modeling and control methods for robotic systems, and of optimization methods aiming at a more profitable functioning of robotic manipulators. Precise modelling of manipulators' dynamics and kinematics can help in handling more efficiently the associated control, estimation and filtering problems.

1.2.2 Dynamic Analysis of Rigid Link Robots

In the area of multl-DOF robotic manipulators one can distinguish between two main problems: (i) robots operating in a free working space, as in the case of robotic welding, painting, or laser and plasma cutting and (ii) robots performing compliance tasks, as in the case of assembling, finishing of stiff surfaces and polishing. When the robotic manipulator operates in a free environment then kinematic and dynamic analysis provide the means for designing a control law that will move appropriately the robot's end effector and will enable the completion of the scheduled tasks. The dynamic model of a multi-DOF rigid-link robotic manipulator, as the one depicted in Fig. 1.1, is obtained from the Euler-Lagrange principle, that is

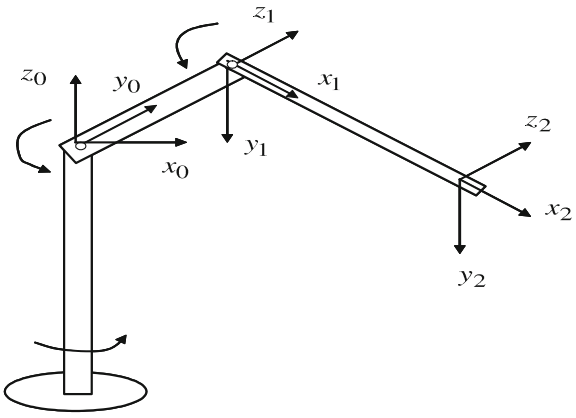

Fig. 1.1 A 3-DOF robotic manipulator with rigid links

$$\frac{\partial}{\partial t}\frac{\partial L}{\partial \dot{q}_i} - \frac{\partial L}{\partial q_i} = T_i \tag{1.1}$$

where L is the robot's Lagrangian, that is the difference between its kinematic and potential energy, q_i is the turn angle of the ith joint of the manipulator, $\dot{q}_i$ is the angular velocity of the jth joint and T_i is the actuator's torque that provides motion to the ith joint. A generic rigid-link dynamic model obtained from this procedure is:

$$D(\theta)\ddot{\theta} + h(\theta, \dot{\theta}) + G(\theta) = k(r_g\theta_m - \theta) \tag{1.2}$$

where $T(\theta) = k(r_g\theta_m - \theta)$ represents the control input vector (torque). In the latter relation, k is an elasticity coefficient and r_g denotes gears ratio, i.e. joints flexibility is introduced in the dynamic model of the manipulator [225, 226, 268]. The elements of the inertia matrix $D(\theta)$, the Coriolis and centrifugal forces matrix $h(\theta, \dot{\theta})$ and the gravity matrix $G(\theta)$ can be found in [155].

The physical characteristics of the manipulator and the range of values that the different variables of the system acquire in a real working environment can be defined for every type of industrial robot. The coordinates frames attached to each joint are defined using the Denavit-Hartenberg method and are depicted in Fig. 1.1. The Denavit-Hartenberg parameters for the general case of a 6-DOF robot are defined in [17] and their indicative values are given in Table 1.1:

The rigid link coordinates system and its parameters are depicted in Fig. 1.2. Considering the ith and the $(i-1)$th reference frames, the parameters of the Denavit-Hartenberg representation are defined as follows:

1. θ_i is the joint angle from the x_{i-1} axis to the x_i axis, about the z_{i-1} axis (using the right hand rule).
2. d_i is the distance from the origin of the $(i-1)$th coordinate frame to the intersection of the z_{i-1} axis, with the x_i axis along the z_{i-1} axis
3. α_i is the offset distance from the intersection of the z_{i-1} axis with the x_i axis to the origin of the ith frame along the x_i axis (or the shortest distance between the z_{i-1} and z_i axes).
4. a_i is the offset angle from the z_{i-1} axis to the z_i axis about the x_i axis (using the right hand rule)

The elements of the inertia matrix $D(\theta)$, the Coriolis and centrifugal forces matrix $h(\theta, \dot{\theta})$ and the gravity matrix $G(\theta)$ appearing in Eq. (1.2) are defined in [155] and

Table 1.1 Denavit-Hartenberg parameters

i	θ_i	a_i	α_i	d_i	Joint range ^{o}
1	90	−90	0	0	−160 to 160
2	0	0	431.8mm	149.08mm	−225 to 45
3	90	90	−20.32mm	0	−45 to 225
4	0	−90	0	433.07mm	−110 to 170
5	0	90	0	0	−100 to 100
6	0	0	0	56.25mm	−266 to 266

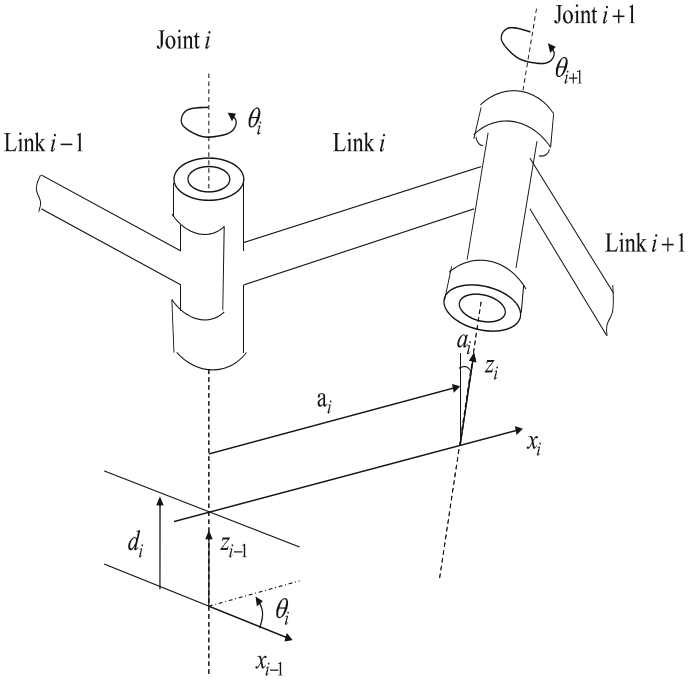

Fig. 1.2 Rigid link coordinates system and its parameters

for a 3-DOF robot are given by

$$D(\theta) = \begin{pmatrix} m_2 l_2^2 + m_3(l_2 S_2 + l_3 S_{23})^2 & 0 & 0 \\ 0 & m_2 l_2^2 + m_3(l_2^2 + 2 l_2 l_3 C_3 + l_3^2) & m_3 l_3 (l_2 C_3 + l_3) \\ 0 & m_3 l_3 (l_2 C_3 + l_3) & m_3 l_3^2 \end{pmatrix} \tag{1.3}$$

$$h(\theta, \dot{\theta}) = \begin{pmatrix} 2[m_2 l_2^2 S_2 C_2 + m_3(l_2 S_2 + l_3 S_{23})(l_2 S_2 + l_3 C_{23})]\dot{\theta}_1 \dot{\theta}_2 + 2 m_3 l_3 C_{23}(l_2 S_2 + l_3 S_{23})\dot{\theta}_1 \dot{\theta}_3 \\ -2 m_3 l_2 l_3 S_3 \dot{\theta}_2 \dot{\theta}_3 - m_3 l_2 l_3 S_3 \dot{\theta}_3^2 - [m_2 l_2 S_2 C_2 + m_2(l_2 S_2 + l_3 S_{23})(l_2 C_2 + l_3 C_{23})]\dot{\theta}_1^2 \\ -m_3(l_2 S_2 + l_3 S_{23}) l_3 C_{23} \dot{\theta}_1^2 + m_2 l_2 l_3 S_3 \dot{\theta}_2^2 + m_3 l_3 \dot{\theta}_2 \dot{\theta}_3 \end{pmatrix} \tag{1.4}$$

$$G(\theta) = \begin{pmatrix} 0 \\ -m_2 g l_2 S_2 - m_3 g(l_2 S_2 + l_3 S_{23}) \\ m_3 g l_3 S_{23} \end{pmatrix} \tag{1.5}$$

where S_i and C_i, denote $sin(\theta_i)$ and $cos(\theta_i)$ respectively, with $i = 1, 2, 3$, while S_{ij} denotes $sin(\theta_i + \theta_j)$ and C_{ij} denotes $cos(\theta_i + \theta_j)$.

For the dynamic model of the 3-DOF robot shown in Fig. 1.1 and with its dynamics described in Eq. (1.2), it holds that

$$\theta = [\theta_1, \theta_2, \theta_3]^T, \dot{\theta} = [\dot{\theta}_1, \dot{\theta}_2, \dot{\theta}_3]^T, \ddot{\theta} = [\ddot{\theta}_1, \ddot{\theta}_2, \ddot{\theta}_3]^T \tag{1.6}$$

where θ is the vector of the joints angles, $\dot{\theta}$ is the vector of the angular velocities and $\ddot{\theta}$ is the vector of angular accelerations. Consequently, the robot's state vector is defined as $x \in R^{6\times 1}$, and its derivative is given by $\dot{x} \in R^{6\times 1}$,

$$x = [\theta_1, \theta_2, \theta_3, \dot{\theta}_1, \dot{\theta}_2, \dot{\theta}_3]^T, \dot{x} = [\dot{\theta}_1, \dot{\theta}_2, \dot{\theta}_3, \ddot{\theta}_1, \ddot{\theta}_2, \ddot{\theta}_3]^T \tag{1.7}$$

Then, Eq. (1.2) is written as

$$\begin{aligned} \ddot{\theta} &= D(\theta)^{-1}[-h(\theta, \dot{\theta}) - G(\theta) + k(r_g\theta_m - \theta)] \Rightarrow \\ \ddot{\theta} &= D(\theta)^{-1}[-h(\theta, \dot{\theta}) - G(\theta) + T(\theta)] \end{aligned} \tag{1.8}$$

where $T(\theta) = k(r_g\theta_m - \theta)$. The control input $u \in R^{3\times 1}$ is defined as

$$u = D(\theta)^{-1}[-h(\theta, \dot{\theta}) - G(\theta) + T(\theta)] \tag{1.9}$$

Moreover, it holds that $\dot{x}_1 = x_4$, $\dot{x}_2 = x_5$ and $\dot{x}_3 = x_6$. Taking $0_{3\times 3}$ to be 3×3 matrix with zero elements, and $I_{3\times 3}$ to be the identity 3×3 matrix one obtains

$$\begin{pmatrix} \dot{x}_1 \\ \dot{x}_2 \\ \dot{x}_3 \end{pmatrix} = \begin{pmatrix} 0_{3\times 3} & I_{3\times 3} \end{pmatrix} x + \begin{pmatrix} 0_{3\times 3} \end{pmatrix} u \tag{1.10}$$

Furthermore, it holds that

$$\begin{pmatrix} \dot{x}_4 \\ \dot{x}_5 \\ \dot{x}_6 \end{pmatrix} = \begin{pmatrix} 0_{3\times 3} & 0_{3\times 3} \end{pmatrix} x + \begin{pmatrix} I_{3\times 3} \end{pmatrix} u \tag{1.11}$$

Thus, finally the robot's dynamic model can be written in a linear state-space form given by

$$\dot{x} = Ax + Bu \tag{1.12}$$

with

$$A = \begin{pmatrix} 0_{3\times 3} & I_{3\times 3} \\ 0_{3\times 3} & 0_{3\times 3} \end{pmatrix}, \quad B = \begin{pmatrix} 0_{3\times 3} \\ I_{3\times 3} \end{pmatrix} \tag{1.13}$$

The reference trajectories vector for the joints of the manipulator is defined as $x_d = [x_{d_1}, x_{d_2}, x_{d_3}]^T$. The control input given in Eq. (1.9) can be complemented with feedback terms of the outputs tracking vector of the manipulator that is $e = [e_1, e_2, e_3]^T = [x_1 - x_{d_1}, x_2 - x_{d_2}, x_3 - x_{d_3}]^T$. Thus by defining, the diagonal feedback gain matrices $K_p = \text{diag}[k_{p_1}, k_{p_2}, k_{p_3}]$ and $K_d = \text{diag}[k_{d_1}, k_{d_2}, k_{d_3}]$ and also by selecting the feedback control input to be

$$u = \ddot{x}_d - K_d\dot{e} - K_p e \tag{1.14}$$

one arrives at the linearized and decoupled form of the manipulator's dynamics

$$\ddot{e} + K_d\dot{e} + K_p e = 0_{3\times 1} \tag{1.15}$$

or equivalently

$$\ddot{e}_i + k_{d_i}\dot{e}_i + k_{p_i}e_i = 0 \;\; i = 1, 2, 3 \tag{1.16}$$

By selecting the feedback gains $K_{p_i} > 0$ and $K_{d_i} > 0$ so as the characteristic polynomial $p(s) = s^2 + k_{d_i}s + k_{p_i}$ is Hurwitz stable, that is to have roots exclusively at the left complex semi-plane one has that the tracking error for the ith joint of the robot is asymptotically eliminated. This is described by

$$\begin{gathered} \lim_{t\to\infty} e_i(t) = 0 \Rightarrow \\ \lim_{t\to\infty} x_i(t) = x_{d_i}(t), \;\; i = 1, 2, 3 \end{gathered} \tag{1.17}$$

The control input that is actually generated by the actuators of the manipulator is given by

$$\begin{gathered} u = \ddot{x}_d - K_d\dot{e} - \dot{K}_p e \Rightarrow D(\theta)^{-1}[-h(\theta, \dot{\theta}) - G(\theta) + T(\theta)] = \ddot{x}_d - K_d\dot{e} - K_p e \Rightarrow \\ T(\theta) = D(\theta)[\ddot{x}_d - K_d\dot{e} - K_p e] + h(\theta, \dot{\theta}) + G(\theta) \end{gathered} \tag{1.18}$$

This is the computed torque method. This stands for a special case of control of robots based on global linearization methods and on transformation of the manipulator's dynamics to a new linear and decoupled state-space description. The transition from the continuous time differential equations of Eq. (1.2) that describe the dynamics of the robotic manipulator, to the state-space description of Eq. (1.12) that is used in the simulation experiments can be carried out using established discretization methods and after choosing an appropriate sampling rate. Alternatively, the robot's dynamics can be simulated through numerical solution of the associated differential equations, given in Eq. (1.2).

1.2.3 Kinematic Analysis of Rigid Link Robots

Using the rigid-link reference system depicted in Fig. 1.2, a joint axis is established (for each joint i) at the connection of two links. This joint axis has two normals connected to it, one for each end of the links. The relative position of two such connected links (link $i-1$ and link i) is given by d_i which is the distance measured along the joint axis between the normals. The joint angle θ_i between the normals is measured in a plane that is taken to be normal to joint axis. Parameters d_i and θ_i are called the distance and angle between the adjacent links, respectively, and define the relative position of neighboring links.

A link i ($i = 1, \ldots, 6$) is connected to at most two other links, i.e link $i-1$ and link $i+1$ and two joint axes are established at the end of each connection. A fixed configuration between joints can be obtained by parameters a_i and α_i which are defined as follows: The parameter a_i is the shortest distance measured along the common normal between the joint axes, while α_i is the angle between the joint axes measured in a plane perpendicular to a_i. Equivalently, a_i and α_i are called the *length* and *twist angle* of link i.

An orthonormal cartesian coordinate system (x_i, y_i, z_i) can be established for each link at its joint axis, where $i = 1, 2, \ldots, n$ ($n =$ number of degrees of freedom) plus the base coordinate frame. Since a rotary joint has only one degree of freedom each (x_i, y_i, z_i) coordinate frame of a robot arm corresponds to joint $i+1$ and is fixed in link i. Moreover, since the ith coordinate system is fixed in link i it moves together with link i. Thus, the nth coordinate frame moves the end-effector (link n). The base coordinates are defined as the 0th coordinate frame (x_0, y_0, z_0) which is also the inertial coordinate frame of the robot arm. Thus for a six-axis robot arm, there are seven coordinate frames namely (x_0, y_0, z_0), (x_1, y_1, z_1), $\ldots$, (x_6, y_6, z_6). Every coordinate frame is determined and established on the basis of three rules:

1. The z_{i-1} axis lies along the axis of motion of the ith joint.
2. The x_i axis is normal to the z_{i-1} axis and point away from it.
3. The y_i axis completes the right-handed coordinate system as required.

By these rules one is free to choose the location of coordinate frame 0 anywhere in the supporting base, as long as the z_0 axis lies along the axis of motion of the first joint. The last (nth) coordinate frame, can be placed anywhere in the robot's hand, as long as the x_n axis is normal to the z_{n-1} axis.

Once the Denavit-Hartneberg (D-H) coordinate system has been established for each link (according to the analysis given in Sect. 1.2.2), a homogeneous transformation matrix can easily be developed relating the ith coordinate frame to the $(i-1)$th coordinate frame. Thus, a point r_i expressed in the ith coordinate system may be expressed in the $(i-1)$th coordinate system as r_{i-1} by performing the following successive transformations:

1. Rotate about the z_{i-1} axis of an angle θ_i to align the x_{i-1} axis with the x_i axis (x_{i-1} axis is parallel to x_i axis and pointing in the same direction).

2. Translate along the z_{i-1} axis a distance of d_i to bring the x_{i-1} and x_i axes into coincidence.
3. Translate along the x_i axis a distance of α_i to bring the two origins, as well as the x axis into coincidence.
4. Rotate about the x_i axis an angle of a_i to bring the two coordinate systems into coincidence.

Each of these four operations can be expressed by a basic homogeneous rotation-translation matrix and the product of these four basic homogeneous transformation matrices yields a composite homogeneous transformation matrix ${}^{i-1}A_i$, known as the D-H transformation matrix for adjacent coordinate frames i and $i-1$. Thus,

$$
\begin{aligned}
&{}^{i-1}A_i = T_{z,d}T_{z,\theta}T_{x,\alpha}T_{x,a} = \\
&= \begin{pmatrix} 1 & 0 & 0 & 0 \\ 0 & 1 & 0 & 0 \\ 0 & 0 & 1 & d_i \\ 0 & 0 & 0 & 1 \end{pmatrix} \cdot \begin{pmatrix} cos(\theta_i) & -sin(\theta_i) & 0 & 0 \\ sin(\theta_i) & cos(\theta_i) & 0 & 0 \\ 0 & 0 & 1 & 0 \\ 0 & 0 & 0 & 1 \end{pmatrix} \cdot \begin{pmatrix} 1 & 0 & 0 & \alpha_i \\ 0 & 1 & 0 & 0 \\ 0 & 0 & 1 & 0 \\ 0 & 0 & 0 & 1 \end{pmatrix} \cdot \begin{pmatrix} 1 & 0 & 0 & 0 \\ 0 & cos(a_i) & -sin(a_i) & 0 \\ 0 & sin(a_i) & cos(a_i) & 0 \\ 0 & 0 & 0 & 1 \end{pmatrix}, \\
&\text{i.e.}\, {}^{i-1}A_i = \begin{pmatrix} cos(\theta_i) & -cos(a_i)sin(\theta_i) & sin(a_i)sin(\theta_i) & \alpha_i cos(\theta_i) \\ sin(\theta_i) & cos(a_i)cos(\theta_i) & -sin(a_i)cos(\theta_i) & \alpha_i sin(\theta_i) \\ 0 & sin(a_i) & cos(a_i) & d_i \\ 0 & 0 & 0 & 1 \end{pmatrix}
\end{aligned} \tag{1.19}
$$

The inverse of this transformation enables transition from the reference system i to the reference system $i-1$.

$$
[{}^{i-1}A_i]^{-1} = {}^{i}A_{i-1} = \begin{pmatrix} cos(\theta_i) & sin(\theta_i) & 0 & -\alpha_i \\ -cos(a_i)sin(\theta_i) & cos(a_i)cos(\theta_i) & sin(a_i) & -d_i sin(a_i) \\ sin(a_i)sin(\theta_i) & -sin(a_i)cos(\theta_i) & cos(a_i) & -d_i cos(a_i) \\ 0 & 0 & 0 & 1 \end{pmatrix} \tag{1.20}
$$

where α_i, a_i, d_i are constants while θ_i is the joint variable for a revolute joint. For a prismatic joint, the joint variable is d_i, while a_i, α_i and θ_i are constants. In this case, ${}^{i-1}A_i$ becomes

$$
{}^{i-1}A_i = T_{z,\theta}T_{z,d}T_{x,\alpha} = \begin{pmatrix} cos(\theta_i) & -cos(a_i)sin(\theta_i) & sin(a_i)sin(\theta_i) & 0 \\ sin(\theta_i) & cos(a_i)cos(\theta_i) & -sin(a_i)cos(\theta_i) & 0 \\ 0 & sin(a_i) & cos(a_i) & d_i \\ 0 & 0 & 0 & 1 \end{pmatrix} \tag{1.21}
$$

and its inverse is

$$[^{i-1}A_i]^{-1} = {}^{i}A_{i-1} = \begin{pmatrix} cos(\theta_i) & sin(\theta_i) & 0 & 0 \\ -cos(a_i)sin(\theta_i) & cos(a_i)cos(\theta_i) & sin(a_i) & -d_i sin(a_i) \\ sin(a_i)sin(\theta_i) & -sin(a_i)cos(\theta_i) & cos(a_i) & -d_i cos(a_i) \\ 0 & 0 & 0 & 1 \end{pmatrix} \tag{1.22}$$

Using the $[^{i-1}A_i]^{-1}$ matrix, one can relate a point p_i at the examined link i, and expressed in homogeneous coordinates with respect to the coordinate system i, to the coordinate system $i-1$ established at link $i-1$ by

$$p_{i-1} = [^{i-1}A_i]^{-1} p_i \tag{1.23}$$

where $p_{i-1} = (x_{i-1}, y_{i-1}, z_{i-1}, 1)^T$ and $p_i = (x_i, y_i, z_i)^T$. For the six-DOF robotic manipulator the associate coordinates transformation matrices $^{i-1}A_i$ are given by

$$\begin{aligned} {}^0A_1 &= \begin{pmatrix} C_1 & 0 & -S_1 & 0 \\ S_1 & 0 & C_1 & 0 \\ 0 & -1 & 0 & 0 \\ 0 & 0 & 0 & 1 \end{pmatrix}, \quad {}^1A_2 = \begin{pmatrix} C_2 & -S_2 & 0 & \alpha_2 C_2 \\ S_2 & C_2 & 0 & \alpha_2 S_2 \\ 0 & 0 & 1 & d_2 \\ 0 & 0 & 0 & 1 \end{pmatrix} \\ {}^2A_3 &= \begin{pmatrix} C_3 & 0 & S_3 & \alpha_3 C_3 \\ S_3 & 0 & -C_3 & \alpha_3 S_3 \\ 0 & 1 & 0 & 0 \\ 0 & 0 & 0 & 1 \end{pmatrix}, \quad {}^3A_4 = \begin{pmatrix} C_4 & 0 & -S_4 & 0 \\ S_4 & 0 & C_4 & 0 \\ 0 & -1 & 0 & d_4 \\ 0 & 0 & 0 & 1 \end{pmatrix} \\ {}^4A_5 &= \begin{pmatrix} C_5 & 0 & S_5 & 0 \\ S_5 & 0 & -C_5 & 0 \\ 0 & 1 & 0 & 0 \\ 0 & 0 & 0 & 1 \end{pmatrix} \quad {}^5A_6 = \begin{pmatrix} C_6 & -S_6 & 0 & 0 \\ S_5 & C_6 & 0 & 0 \\ 0 & 0 & 1 & d_6 \\ 0 & 0 & 0 & 1 \end{pmatrix} \end{aligned} \tag{1.24}$$

$$\begin{aligned} T_1 &= {}^0A_1 {}^1A_2 {}^2A_3 = \begin{pmatrix} C_1C_{23} & -S_1 & C_1S_{23} & \alpha_2C_1C_2 + \alpha_3C_1C_{23} - d_2S_1 \\ S_1C_{23} & C_1 & S_1S_{23} & \alpha_2S_1C_2 + \alpha_3S_1C_{23} - d_2C_1 \\ -S_{23} & 0 & C_{23} & -\alpha_2S_2 - \alpha_3S_{23} \\ 0 & 0 & 0 & 1 \end{pmatrix} \\ T_2 &= {}^3A_4 {}^4A_5 {}^5A_6 = \begin{pmatrix} C_4C_5C_6 - S_4S_6 & -C_4C_5S_6 - S_4C_6 & C_4S_5 & d_6C_4S_5 \\ S_4C_5C_6 + C_4S_6 & -S_4C_5S_6 + C_4C_6 & S_4S_5 & d_6S_4S_5 \\ -S_5C_6 & S_5S_6 & C_5 & d_6C_5 + d_4 \\ 0 & 0 & 0 & 1 \end{pmatrix} \end{aligned} \tag{1.25}$$

where $C_i = cos(\theta_i)$, $S_i = sin(\theta_i)$, $C_{ij} = cos(\theta_i + \theta_j)$, $S_{ij} = sin(\theta_i + \theta_j)$. The homogeneous matrix ^0T_i which specifies the location of the ith coordinate frame with

respect to the base coordinate system is the chain product of successive coordinate transformation matrices of ${}^{i-1}A_i$ and is expressed as

$$\begin{aligned} {}^0T_i &= {}^0A_1\,{}^1A_2 \cdots {}^{i-1}A_i = \Pi_{j=1}^{i} A_j \text{ for } i = 1, 2, \ldots, n \\ &= \begin{pmatrix} x_i & y_i & z_i & p_i \\ 0 & 0 & 0 & 1 \end{pmatrix} = \begin{pmatrix} {}^0R_i & {}^0p_i \\ 0 & 1 \end{pmatrix} \end{aligned} \tag{1.26}$$

1.3 Model-Based Control of Rigid-Link Manipulators Using Global Linearization Methods

1.3.1 Outline

Manipulators control based on global linearization, comprises techniques for the transformation of the nonlinear dynamics of the robotic system to equivalent linear state-space descriptions for which one can design state feedback controllers and can also solve the associated state estimation (filtering) problem. The widest class of robot control methods comprises approaches based on the theory of differentially flat systems. Alternatively, one can consider control methods based on Lie algebra. Differential flatness theory is currently a main direction in the analysis of nonlinear dynamical systems [450, 476, 519]. To conclude if a dynamical system is differentially flat, the following should be examined: (i) the existence of the so-called flat output, i.e. a new variable which is expressed as a function of the system's state variables. It should hold that the flat output and its derivatives are not coupled in the form of an ordinary differential equation, (ii) the components of the system (i.e. state variables and control input) should be expressed as functions of the flat output and its derivatives [145, 254, 267, 322, 439, 572]. Differential flatness theory enables transformation to a linearized form (canonical Brunovsky form) for which the design of the controller becomes easier. Moreover, by showing that a system is differentially flat one can easily design a reference trajectory as a function of the so-called flat output and can find a control law that ensures tracking of this desirable trajectory [145, 572]. Robotic manipulators are differentially flat MIMO nonlinear dynamical systems which after applying the differential flatness theory can be written in the Brunovksy (canonical) form [322].

1.3.2 Differential Flatness Theory

1.3.2.1 Overview of Differential Flatness Theory

Differential flatness theory can be applied to the generic class of systems $\dot{x} = f(x, u)$. In this study, the interest is in dynamic models of the form of Eq. (1.27).

$$\dot{x} = f(x,t) + g(x,t)u \tag{1.27}$$

The principles of differential flatness theory have been extensively studied in the relevant bibliography [57, 145, 254, 267, 322, 450, 476, 519, 572]: A finite dimensional system is considered. This can be written in the form of an ordinary differential equation (ODE), i.e. $S_i(w, \dot{w}, \ddot{w}, \ldots, w^{(i)}) = 0, \quad i = 1, 2, \ldots, q$. The term w denotes the system variables (these variables are for instance the elements of the system's state vector and the control input) while $w^{(i)}$, $i = 1, 2, \ldots, q$ are the associated derivatives. Such a system is said to be differentially flat if there exists a set of m functions $y = (y_1, \ldots, y_m)$ of the system's variables and of their time-derivatives, i.e. $y_i = \phi(w, \dot{w}, \ddot{w}, \ldots, w^{(\alpha_i)})$, $i = 1, \ldots, m$ satisfying the following two conditions [145, 322]:

1. There does not exist any differential relation of the form $R(y, \dot{y}, \ldots, y^{(\beta)}) = 0$ which implies that the derivatives of the flat output are not coupled in the sense of an ODE, or equivalently it can be said that the flat output is differentially independent.
2. All system variables (i.e. the elements of the system's state vector w and the control input) can be expressed using only the flat output y and its time derivatives $w_i = \psi_i(y, \dot{y}, \ldots, y^{(\gamma_i)})$, $i = 1, \ldots, s$. An equivalent definition of differentially flat systems is as follows:

Definition: The system $\dot{x} = f(x,u)$, $x \in R^n$, $u \in R^m$ is differentially flat if there exist relations

$$\begin{aligned} h &: R^n \times (R^m)^{r+1} \to R^m, \\ \phi &: (R^m)^r \to R^n \text{ and} \\ \psi &: (R^m)^{r+1} \to R^m \end{aligned} \tag{1.28}$$

such that

$$\begin{aligned} y &= h(x, u, \dot{u}, \ldots, u^{(r)}), \\ x &= \phi(y, \dot{y}, \ldots, y^{(r-1)}), \text{ and} \\ u &= \psi(y, \dot{y}, \ldots, y^{(r-1)}, y^{(r)}). \end{aligned} \tag{1.29}$$

This means that all system dynamics can be expressed as a function of the flat output and its derivatives, therefore the state vector and the control input can be written as

$$\begin{aligned} x(t) &= \phi(y(t), \dot{y}(t), \ldots, y^{(r-1)}(t)), \text{ and} \\ u(t) &= \psi(y(t), \dot{y}(t), \ldots, y^{(r)}(t)) \end{aligned} \tag{1.30}$$

1.3.2.2 Classes of Differentially Flat Systems

For certain classes of dynamical systems it has been proven that they satisfy differential flatness properties. The following classes of nonlinear differentially flat systems are presented [57, 322]:

1. Affine in-the-input systems: The dynamics of such systems is given by:

$$\dot{x} = f(x) + \sum_{i=1}^{m} g_i(x)u_i \tag{1.31}$$

From Eq. (1.31) it can be concluded that the above state equation can also describe MIMO dynamical systems. Without loss of generality it is assumed that $G = [g_1, \ldots, g_m]$ is of rank m. In case that the flat outputs of the aforementioned system are only functions of states x, then this class of dynamical systems is called 0-flat. It has been proven that a dynamical affine system with n states and $n - 1$ inputs is 0-flat if it is controllable.

2. Driftless systems: These are systems of the form

$$\dot{x} = \sum_{i=1}^{m} f_i(x)u_i \tag{1.32}$$

For driftless systems with two inputs, i.e.

$$\dot{x} = f_1(x)u_1 + f_2(x)u_2 \tag{1.33}$$

the flatness property holds, if and only if the rank of matrix $E_{k+1} := \{E_k, [E_k, E_k]\}$, $k \geq 0$ with $E_0 := \{f_1, f_2\}$ is equal to $k + 2$ for $k = 0, \ldots, n - 2$. It has been proven that a driftless system that is differentially flat, is also 0-flat.

Moreover, for flat systems with n states and $n - 2$ control inputs, i.e.

$$\dot{x} = \sum_{i=1}^{n-2} u_i f_i(x) \; x \in R^n \tag{1.34}$$

the flatness property holds, if controllability also holds. Furthermore, the system is 0-flat if n is even.

1.3.3 Differential Flatness for MIMO Nonlinear Dynamical Systems

1.3.3.1 Conditions for Applying Differential Flatness Theory

The transformation of MIMO robotic systems into the canonical (Brunovsky) from, through the application of differential flatness theory, will be explained first. Next, a new control method for such systems will be developed, also in accordance to differential flatness theory. It will be shown that the proposed control and filtering

methods can be efficiently applied to the model of the nonlinear MIMO robotic manipulators.

The MIMO nonlinear robotic system can be written as a state-space model of the form $\dot{x} = f(x, u)$. Moreover, the previous state-space description can be transformed to the form of an affine in-the-input system by adding an integrator to each input [57, 267]. In the latter case one obtains

$$\dot{x} = f(x) + \sum_{i=1}^{m} g_i(x) u_i \tag{1.35}$$

The following definitions are now used [457]:

(i) Lie derivative: $L_f h(x)$ stands for the Lie derivative $L_f h(x) = (\nabla h) f$ and the repeated Lie derivatives are recursively defined as $L_f^0 h = h$ for $i = 0$, $L_f^i h = L_f L_f^{i-1} h = \nabla L_f^{i-1} h f$ for $i = 1, 2, \ldots$.
(ii) Lie Bracket: $ad_f^i g$ stands for a Lie Bracket which is defined recursively as $ad_f^i g = [f, ad_f^{i-1} g]$ with $ad_f^0 g = g$ and $ad_f g = [f, g] = \nabla g f - \nabla f g$.
If the system of Eq. (1.35) can be linearized by a diffeomorphism $z = \phi(x)$ and a static state feedback $u = \alpha(x) + \beta(x) v$ into the following form

$$\begin{gathered} \dot{z}_{i,j} = z_{i+1,j} \text{ for } 1 \leq j \leq m \text{ and } 1 \leq i \leq v_j - 1 \\ \dot{z}_{v_{i,j}} = v_j \end{gathered} \tag{1.36}$$

with $\sum_{j=1}^{m} v_j = n$, then $y_j = z_{1,j}$ for $1 \leq j \leq m$ are the 0-flat outputs which can be written as functions of only the elements of the state vector x. To provide conditions for transforming the system of Eq. (1.35) into the canonical form described in Eq. (1.36) the following theorem has been stated [57]:

Theorem: For nonlinear systems described by Eq. (1.35) the following variables are defined: (i) $G_0 = \text{span}[g_1, \ldots, g_m]$, (ii) $G_1 = \text{span}[g_1, \ldots, g_m, ad_f g_1, \ldots, ad_f g_m]$, $\cdots$ (k) $G_k = \text{span}\{ad_f^j g_i \text{ for } 0 \leq j \leq k, \ 1 \leq i \leq m\}$. Then, the linearization problem for the system of Eq. (1.35) can be solved if and only if: (1). The dimension of G_i, $i = 1, \ldots, k$ is constant for $x \in X \subseteq R^n$ and for $1 \leq i \leq n - 1$, (2). The dimension of G_{n-1} if of order n, (3). The distribution G_k is involutive for each $1 \leq k \leq n - 2$.

1.3.3.2 Transformation of the Nonlinear MIMO Dynamics into a Canonical State-Space Form

It is assumed now that after defining the flat outputs of the previous state-space description of the nonlinear MIMO dynamics and after expressing the robotic system's state variables and control inputs as functions of the flat output and of the associated derivatives, the robotic system can be transformed in the Brunovsky canonical form:

$$\begin{aligned}
&\dot{x}_1 = x_2 \\
&\dots \\
&\dot{x}_{r_1-1} = x_{r_1} \\
&\dot{x}_{r_1} = f_1(x) + \textstyle\sum_{j=1}^{p} g_{1_j}(x)u_j + d_1 \\
&\dot{x}_{r_1+1} = x_{r_1+2} \\
&\dots \\
&\dot{x}_{p-1} = x_p \\
&\dot{x}_p = f_p(x) + \textstyle\sum_{j=1}^{p} g_{p_j}(x)u_j + d_p
\end{aligned} \qquad \begin{aligned}
&y_1 = x_1 \\
&\dots \\
&y_p = x_{n-r_p+1}
\end{aligned} \tag{1.37}$$

where $x = [x_1, \dots, x_n]^T$ is the state vector of the transformed system (according to the differential flatness formulation), $u = [u_1, \dots, u_p]^T$ is the set of control inputs, $y = [y_1, \dots, y_p]^T$ is the output vector, f_i are the drift functions and $g_{i,j}$, $i, j = 1, 2, \dots, p$ are smooth functions corresponding to the control input gains, while d_j is a variable associated to external disturbances. It holds that $r_1 + r_2 + \dots + r_p = n$. After writing the initial nonlinear system into the canonical (Brunovsky) form it holds

$$y_i^{(r_i)} = f_i(x) + \textstyle\sum_{j=1}^{p} g_{ij}(x)u_j + d_j \tag{1.38}$$

Next the following vectors and matrices can be defined: $f(x) = [f_1(x), \dots, f_n(x)]^T$, $g(x) = [g_1(x), \dots, g_n(x)]^T$, with $g_i(x) = [g_{1i}(x), \dots, g_{pi}(x)]^T$, $A = diag[A_1, \dots, A_p]$, and $B = diag[B_1, \dots, B_p], C^T = diag[C_1, \dots, C_p]$, $d = [d_1, \dots, d_p]^T$, where matrix A has the MIMO canonical form, i.e. with block-diagonal elements

$$\begin{aligned}
A_i &= \begin{pmatrix} 0 & 1 & \cdots & 0 \\ 0 & 0 & \cdots & 0 \\ \vdots & \vdots & \dots & \vdots \\ 0 & 0 & \cdots & 1 \\ 0 & 0 & \cdots & 0 \end{pmatrix}_{r_i \times r_i} \\
B_i^T &= \begin{pmatrix} 0 & 0 & \cdots & 0 & 1 \end{pmatrix}_{1 \times r_i} \\
C_i &= \begin{pmatrix} 1 & 0 & \cdots & 0 & 0 \end{pmatrix}_{1 \times r_i}
\end{aligned} \tag{1.39}$$

Thus, Eq. (1.38) can be written in state-space form

$$\begin{aligned}
\dot{x} &= Ax + Bv + B\tilde{d} \\
y &= Cx
\end{aligned} \tag{1.40}$$

where the control input is written as $v = f(x) + g(x)u$. The system of Eqs. (1.39) and (1.40) is in controller and observer canonical form.

1.3.4 Global Linearization of a 2-DOF Robotic Manipulator

Following the previous analysis and without loss of generality, a 2-DOF rigid link robotic manipulator is considered. The dynamic model of the robot is given by

$$\begin{pmatrix} M_{11} & M_{12} \\ M_{21} & M_{22} \end{pmatrix} \begin{pmatrix} \ddot{\theta}_1 \\ \ddot{\theta}_2 \end{pmatrix} + \begin{pmatrix} F_1(\theta, \dot{\theta}) \\ F_2(\theta, \dot{\theta}) \end{pmatrix} + \begin{pmatrix} G_1(\theta) \\ G_2(\theta) \end{pmatrix} = \begin{pmatrix} T_1 \\ T_2 \end{pmatrix} \tag{1.41}$$

or equivalently

$$\begin{aligned} \begin{pmatrix} \ddot{\theta}_1 \\ \ddot{\theta}_2 \end{pmatrix} = & - \begin{pmatrix} M_{11} & M_{12} \\ M_{21} & M_{22} \end{pmatrix}^{-1} \begin{pmatrix} F_1(\theta, \dot{\theta}) \\ F_2(\theta, \dot{\theta}) \end{pmatrix} - \\ & - \begin{pmatrix} M_{11} & M_{12} \\ M_{21} & M_{22} \end{pmatrix}^{-1} \begin{pmatrix} G_1(\theta) \\ G_2(\theta) \end{pmatrix} + \begin{pmatrix} M_{11} & M_{12} \\ M_{21} & M_{22} \end{pmatrix}^{-1} \begin{pmatrix} T_1 \\ T_2 \end{pmatrix} \end{aligned} \tag{1.42}$$

Denoting the inverse of the inertia matrix as

$$\begin{pmatrix} M_{11} & M_{12} \\ M_{21} & M_{22} \end{pmatrix} = \begin{pmatrix} N_{11} & N_{12} \\ N_{21} & N_{22} \end{pmatrix} \tag{1.43}$$

then one obtains

$$\begin{pmatrix} \ddot{\theta}_1 \\ \ddot{\theta}_2 \end{pmatrix} = - \begin{pmatrix} N_{11} & N_{12} \\ N_{21} & N_{22} \end{pmatrix} \begin{pmatrix} F_1(\theta, \dot{\theta}) \\ F_2(\theta, \dot{\theta}) \end{pmatrix} - \begin{pmatrix} N_{11} & N_{12} \\ N_{21} & N_{22} \end{pmatrix} \begin{pmatrix} G_1(\theta) \\ G_2(\theta) \end{pmatrix} + \begin{pmatrix} N_{11} & N_{12} \\ N_{21} & N_{22} \end{pmatrix} \begin{pmatrix} T_1 \\ T_2 \end{pmatrix} \tag{1.44}$$

or equivalently

$$\begin{pmatrix} \ddot{\theta}_1 \\ \ddot{\theta}_2 \end{pmatrix} = \begin{pmatrix} -N_{11} F_1(\theta, \dot{\theta}) - N_{12} F_2(\theta, \dot{\theta}) - N_{11} G_1(\theta) - N_{12} G_2(\theta) + N_{11} T_1 + N_{12} T_2 \\ -N_{21} F_2(\theta, \dot{\theta}) - N_{22} F_2(\theta, \dot{\theta}) - N_{21} G_1(\theta) - N_{22} G_2(\theta) + N_{21} T_1 + N_{22} T_2 \end{pmatrix} \tag{1.45}$$

which can be also written as

$$\ddot{\theta}_1 = -N_{11} F_1(\theta, \dot{\theta}) - N_{12} F_2(\theta, \dot{\theta}) - N_{11} G_1(\theta) - N_{12} G_2(\theta) + \begin{pmatrix} N_{11} & N_{12} \end{pmatrix} \begin{pmatrix} T_1 \\ T_2 \end{pmatrix} \tag{1.46}$$

$$\ddot{\theta}_2 = -N_{21} F_1(\theta, \dot{\theta}) - N_{22} F_2(\theta, \dot{\theta}) - N_{21} G_1(\theta) - N_{22} G_2(\theta) + \begin{pmatrix} N_{21} & N_{22} \end{pmatrix} \begin{pmatrix} T_1 \\ T_2 \end{pmatrix} \tag{1.47}$$

The following state variables are defined

$$x_1 = \theta_1 \; x_2 = \dot{\theta}_1 \; x_3 = \theta_2 \; x_4 = \dot{\theta}_2 \tag{1.48}$$

It holds that

$$\begin{aligned} \ddot{x}_1 &= f_1(x) + g_1(x)u \\ \ddot{x}_3 &= f_2(x) + g_2(x)u \end{aligned} \tag{1.49}$$

where

$$\begin{aligned} f_1(x) = -N_{11}F_1(\theta, \dot{\theta}) - N_{12}F_2(\theta, \dot{\theta}) - N_{11}G_1(\theta) - N_{12}G_2(\theta) \; \in \; R^{1\times 1} \\ g_1(x) = [N_{11} \; N_{12}] \; \in R^{1\times 2} \\ f_2(x) = -N_{21}F_1(\theta, \dot{\theta}) - N_{22}F_2(\theta, \dot{\theta}) - N_{21}G_1(\theta) - N_{22}G_2(\theta) \; \in \; R^{1\times 1} \\ g_2(x) = [N_{21} \; N_{22}] \; \in R^{2\times 2} \end{aligned} \tag{1.50}$$

The flat output is defined as

$$y = [\theta_1, \theta_2] = [x_1, x_3] \tag{1.51}$$

It holds that

$$\begin{aligned} \dot{x}_1 &= x_2 \\ \dot{x}_2 &= f_1(x) + g_1(x)u \\ \dot{x}_3 &= x_4 \\ \dot{x}_4 &= f_2(x) + g_2(x)u \end{aligned} \tag{1.52}$$

therefore all system state variables can be written as functions of the flat output y and its derivatives. The same holds for the control input u

$$\begin{aligned} x_1 = [1\;0]y^T \; x_2 = [1\;0]\dot{y}^T \\ x_3 = [0\;1]y^T \; x_2 = [0\;1]\dot{y}^T \end{aligned} \tag{1.53}$$

Moreover, from Eq. (1.52) it holds

$$\begin{pmatrix} \ddot{x}_1 \\ \ddot{x}_3 \end{pmatrix} = \begin{pmatrix} f_1(x) \\ f_2(x) \end{pmatrix} + \begin{pmatrix} g_1(x) \\ g_2(x) \end{pmatrix} u \;\text{ i.e. }\; u = \begin{pmatrix} g_1(x) \\ g_2(x) \end{pmatrix}^{-1} \left\{ \begin{pmatrix} \ddot{x}_1 \\ \ddot{x}_3 \end{pmatrix} - \begin{pmatrix} f_1(x) \\ f_2(x) \end{pmatrix} \right\} \tag{1.54}$$

Knowing that $x = h(y, \dot{y})$ one finally obtains

$$u = \begin{pmatrix} g_1(h(y,\dot{y})) \\ g_2(h(y,\dot{y})) \end{pmatrix}^{-1} \left\{ \begin{pmatrix} [1\;0]\ddot{y}^T \\ [0\;1]\ddot{y}^T \end{pmatrix} - \begin{pmatrix} f_1(h(y,\dot{y})) \\ f_2(h(y,\dot{y})) \end{pmatrix} \right\} \tag{1.55}$$

Therefore, the considered robotic system is a differentially flat one. Next, considering also the effects of additive disturbances to the joints of the robotic manipulator the dynamic model becomes

$$\begin{aligned} \ddot{x}_1 &= f_1(x,t) + g_1(x,t)u + \tilde{d}_1 \\ \ddot{x}_3 &= f_2(x,t) + g_2(x,t)u + \tilde{d}_2 \end{aligned} \tag{1.56}$$

$$\begin{pmatrix} \ddot{x}_1 \\ \ddot{x}_3 \end{pmatrix} = \begin{pmatrix} f_1(x,t) \\ f_2(x,t) \end{pmatrix} + \begin{pmatrix} g_1(x,t) \\ g_2(x,t) \end{pmatrix} u + \begin{pmatrix} \tilde{d}_1 \\ \tilde{d}_2 \end{pmatrix} \tag{1.57}$$

Moreover, the following control input is defined

$$u = \begin{pmatrix} g_1(x,t) \\ g_2(x,t) \end{pmatrix}^{-1} \left\{ \begin{pmatrix} \ddot{x}_1^d \\ \ddot{x}_3^d \end{pmatrix} - \begin{pmatrix} f_1(x,t) \\ f_2(x,t) \end{pmatrix} - \begin{pmatrix} K_1^T \\ K_2^T \end{pmatrix} e + \begin{pmatrix} u_{c_1} \\ u_{c_2} \end{pmatrix} \right\} \tag{1.58}$$

where $[u_{c_1}\ u_{c_2}]^T$ is a supervisory control term that is used for the compensation of the model's uncertainties as well as of the external disturbances and $K_i^T = [k_1^i, k_2^i, \ldots, k_{n-1}^i, k_n^i]$ are the rows of the error feedback gain matrix [447, 457].

Additionally, the differentially flat robotic model is written in the Brunovsky (canonical) form. Considering the state vector $x \in R^{4\times 1}$, with the state variables defined in Eq. (1.48), the following matrices are defined

$$A = \begin{pmatrix} 0\ 1\ 0\ 0 \\ 0\ 0\ 0\ 0 \\ 0\ 0\ 0\ 1 \\ 0\ 0\ 0\ 0 \end{pmatrix}, \quad B = \begin{pmatrix} 0\ 0 \\ 1\ 0 \\ 0\ 0 \\ 0\ 1 \end{pmatrix}, \quad C = \begin{pmatrix} 1\ 0\ 0\ 0 \\ 0\ 0\ 1\ 0 \end{pmatrix} \tag{1.59}$$

Using the matrices of Eq. (1.59) one obtains the Brunovsky form of the MIMO robot model dynamics

$$\begin{aligned} \dot{x} &= Ax + Bv \\ y &= Cx \end{aligned} \tag{1.60}$$

where the new input v is given by

$$v = \begin{pmatrix} f_1(x,t) \\ f_2(x,t) \end{pmatrix} + \begin{pmatrix} g_1(x,t) \\ g_2(x,t) \end{pmatrix} u + \begin{pmatrix} \tilde{d}_1 \\ \tilde{d}_2 \end{pmatrix} \tag{1.61}$$

Moreover, considering that the model's structure and parameters are known and that the additive input disturbance $\tilde{d}_i, \quad i = 1, 2, \ldots$ are also known, but the system's state vector is obtained by an estimation procedure, then the following feedback linearizing control input is defined

$$u = \begin{pmatrix} g_1(x,t) \\ g_2(x,t) \end{pmatrix}^{-1} \left\{ \begin{pmatrix} \ddot{x}_1^d \\ \ddot{x}_3^d \end{pmatrix} - \begin{pmatrix} f_1(x,t) \\ f_2(x,t) \end{pmatrix} - \begin{pmatrix} K_1^T \\ K_2^T \end{pmatrix} e + \begin{pmatrix} u_{c_1} \\ u_{c_2} \end{pmatrix} \right\} \tag{1.62}$$

where $[u_{c_1} \; u_{c_2}]^T$ is a supervisory control term that is used for the compensation of the model's uncertainties as well as of the external disturbances and $K_i^T = [k_1^i, k_2^i, \ldots, k_{n-1}^i, k_n^i]$ are the rows of the feedback gain matrix, while $\hat{x}$ is the estimated value of the system's state vector [447, 457]. It is also noted that to perform simultaneous state and disturbances estimation one can consider results on disturbance observers within a Kalman Filter framework [450].

Finally, the differentially flat robotic model is written in the Brunovsky (canonical) form. Considering the state vector $x \in R^{4\times 1}$, with the state variables defined in Eq. (3.29), the following matrices are defined

$$A = \begin{pmatrix} 0 & 1 & 0 & 0 \\ 0 & 0 & 0 & 0 \\ 0 & 0 & 0 & 1 \\ 0 & 0 & 0 & 0 \end{pmatrix}, \quad B = \begin{pmatrix} 0 & 0 \\ 1 & 0 \\ 0 & 0 \\ 0 & 1 \end{pmatrix}, \quad C = \begin{pmatrix} 1 & 0 & 0 & 0 \\ 0 & 0 & 1 & 0 \end{pmatrix} \tag{1.63}$$

Using the matrices of Eq. (1.63) one obtains the Brunovsky form of the MIMO robot model dynamics

$$\begin{aligned} \dot{x} &= Ax + Bv \\ y &= Cx \end{aligned} \tag{1.64}$$

where the new input v is given by

$$v = \begin{pmatrix} f_1(x,t) \\ f_2(x,t) \end{pmatrix} + \begin{pmatrix} g_1(x,t) \\ g_2(x,t) \end{pmatrix} u + \begin{pmatrix} \tilde{d}_1 \\ \tilde{d}_2 \end{pmatrix} \tag{1.65}$$

For the model of Eq. (1.64) is is possible to apply feedback control after measuring only the outputs of the model, that is the joint angles. The non-measurable elements of the state vector are estimated with the use of Kalman Filtering. In such a case, matrices A, B and C of Eq. (1.63) are turned into discrete-time ones using common discretization methods. These discrete-time matrices are denoted as A_d, B_d and C_d respectively. For the robotic model of Eqs. (1.64) and (1.65) state estimation can be performed using the Kalman Filter recursion, as described in [457].

1.3.5 Simulation Tests

The performance of the proposed global linearization-based control was tested in the model of a 2-DOF rigid-link robotic manipulator (Fig. 1.3). The differentially flat model of the robot and its transformation to the Brunovksy form has been analyzed

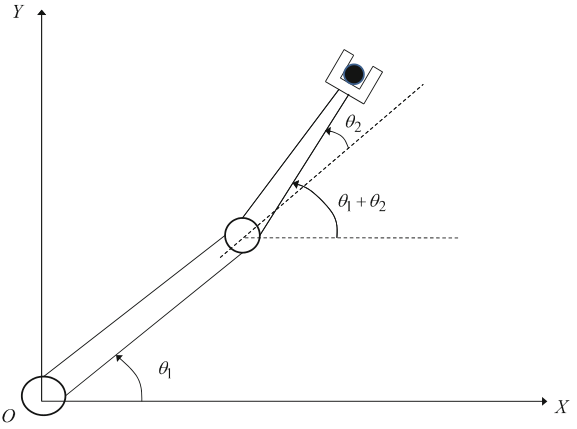

Fig. 1.3 A 2-DOF rigid-link robotic manipulator

in the previous section. The flat outputs were taken to be the robot's joint angles $y_1 = x_1$ and $y_2 = x_3$. It has been proven that all state variables of the robotic model and the associated control inputs, i.e. the torques applied by the motors to the links' joints can be written as functions of the flat output $[y_1, y_2]$ and of the associated derivatives.

Two different set-points were studied: (i) a sinusoidal signal of amplitude 1.0 and period $T = 10$ s, (ii) a see-saw set-point of amplitude 0.30 and period $T = 10$ s. At the beginning of the second half of the simulation time an additive sinusoidal disturbance of amplitude $A = 0.5$ and period $T = 10$ s was applied to the system. The approximations $\hat{f}$ and $\hat{g}$ were used in the derivation of the control law. To implement state estimation-based control after measuring only x_1 and x_3 the Kalman Filter has been applied on the linearized equivalent model of the robot.

The position and velocity variations for the sinusoidal set-point for the first joint of the robotic manipulator are depicted in Fig. 1.4. For the second joint of the 2-DOF robot the tracking of the position and velocity setpoints is depicted in Fig. 1.5. The control inputs (motor torques) applied to the first and second joint of the robotic manipulator are shown in Fig. 1.6.

The performance of the state estimation-based control has been also tested in the tracking of a see-saw set-point. The position and velocity variation of the first joint are demonstrated in Fig. 1.7. Similarly, the tracking of the position and velocity reference setpoints for the second joint are depicted in Fig. 1.8. The control signal in the case of tracking of a tracking a see-saw setpoint by the two joints of the robotic manipulator is shown in Fig. 1.9. The estimated state variables were denoted as green line whereas the real state variables were denoted as blue lines.

Moreover, state estimation with Kalman Filtering on the linearized equivalent model of the robot (Derivative-free nonlinear Kalman Filter (DKF) [457]) was tested against the Extended Kalman Filter which is among the most commonly used estimation methods for nonlinear dynamical systems. In the latter case, the position and velocity variations for the sinusoidal set-point for the first joint of the robotic

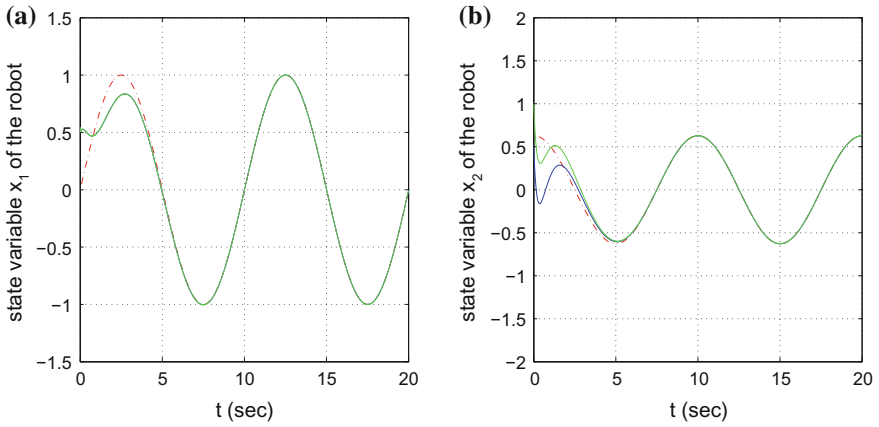

Fig. 1.4 Control with global linearization and Kalman Filtering: **a** Tracking of a sinusoidal position set-point (dashed line) by the angle of the first joint of the robot (continuous line) **b** Tracking of a sinusoidal velocity set-point (dashed line) by the angular velocity of the first joint of the robot (continuous line)

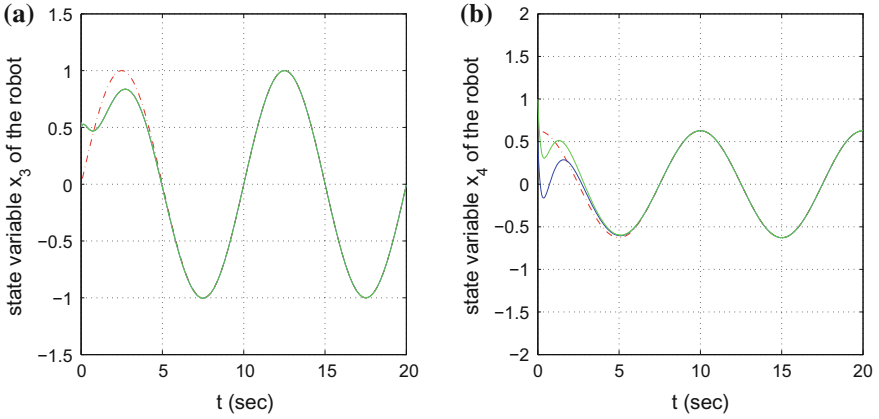

Fig. 1.5 Control with global linearization and Kalman Filtering: **a** Tracking of a sinusoidal position set-point (dashed line) by the angle of the second joint of the robot (continuous line) **b** Tracking of a sinusoidal velocity set-point (dashed line) by the angular velocity of the second joint of the robot (continuous line)

manipulator are depicted in Fig. 1.10. For the second joint of the 2-DOF robot the tracking of the position and velocity setpoints is depicted in Fig. 1.11. The control inputs (motor torques) applied to the first and second joint of the robotic manipulator are shown in Fig. 1.12.

The performance of the state estimation-based control is also tested in the tracking of a see-saw set-point. The position and velocity variation of the first joint are demonstrated in Fig. 1.13. Similarly, the tracking of the position and velocity refer-

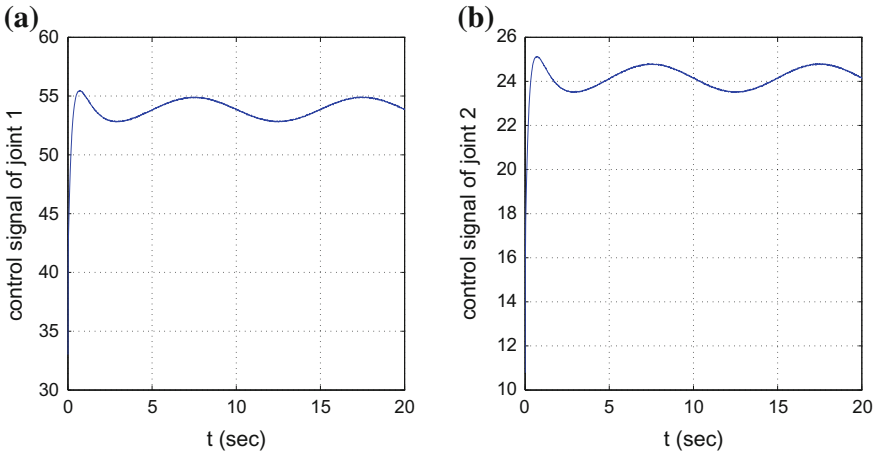

Fig. 1.6 Tracking of a sinusoidal setpoint by the 2-DOF robotic manipulator with the use of the derivative-free Kalman Filter: **a** Control input (motor torque) applied to the first joint **b** Control input (motor torque) applied to the second joint

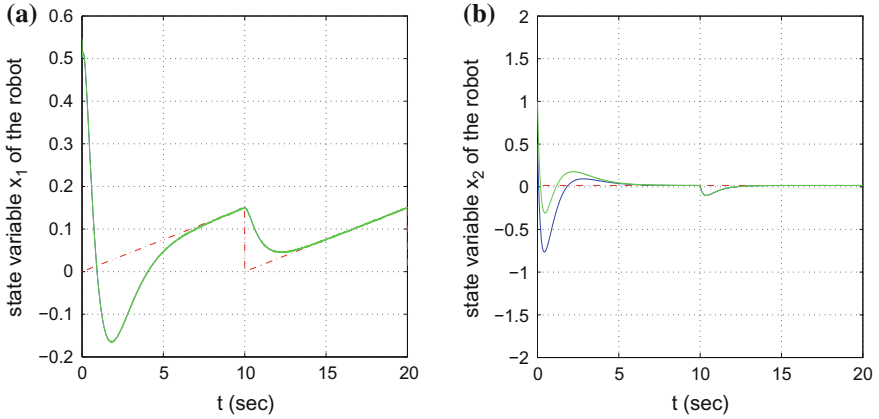

Fig. 1.7 Control with global linearization and Kalman Filtering: **a** Tracking of a seesaw position set-point (dashed line) by the angle of the first joint of the robot (continuous line) **b** Tracking of a seesaw velocity set-point (dashed line) by the angular velocity of the first joint of the robot (continuous line)

ence setpoints for the second joint are depicted in Fig. 1.14. The control signal in the case of tracking a see-saw setpoint by the two joints of the robotic manipulator is shown in Fig. 1.15.

Comparing the estimation performed by the derivative-free MIMO nonlinear Kalman Filter with the one performed by the Extended Kalman Filter it can be noticed that the derivative-free filtering approach results in more accurate state estimates. Moreover, comparing the associated state estimation-based control loop that

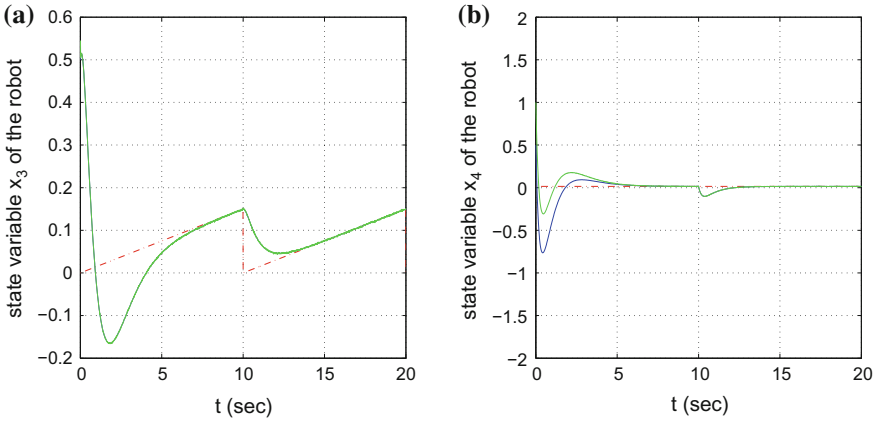

Fig. 1.8 Control with global linearization and Kalman Filtering: **a** Tracking of a seesaw position set-point (dashed line) by the angle of the second joint of the robot (continuous line) Control with global linearization and Kalman Filtering Tracking of a seesaw velocity set-point (dashed line) by the angular velocity of the second joint of the robot (continuous line)

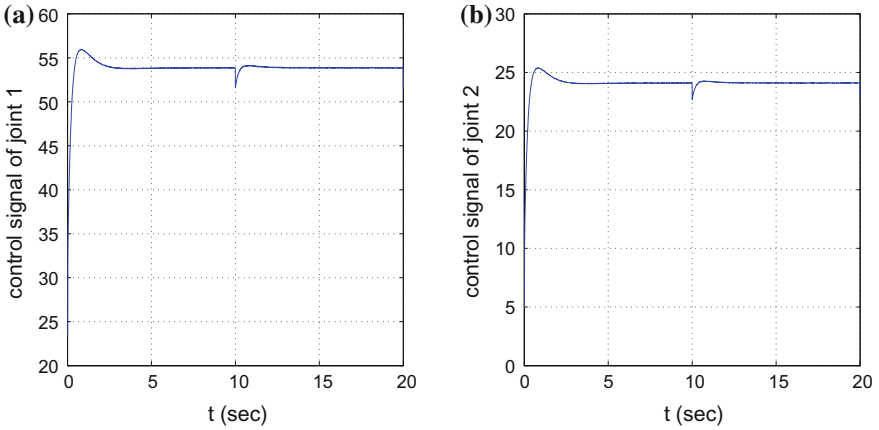

Fig. 1.9 Control with global linearization and Kalman Filtering: Tracking of a seesaw setpoint by the 2-DOF robotic manipulator with the use of the derivative-free Kalman Filter: **a** Control input (motor torque) applied to the first joint **b** Control input (motor torque) applied to the second joint

was based on the derivative-free MIMO nonlinear Kalman Filter to the control that was based on the Extended Kalman Filter it was observed that the first control scheme was significantly more robust and capable of tracking with better accuracy the desirable trajectories. These findings show the suitability of the considered derivative-free MIMO nonlinear Kalman Filter for tracking, control and fault diagnosis tasks.

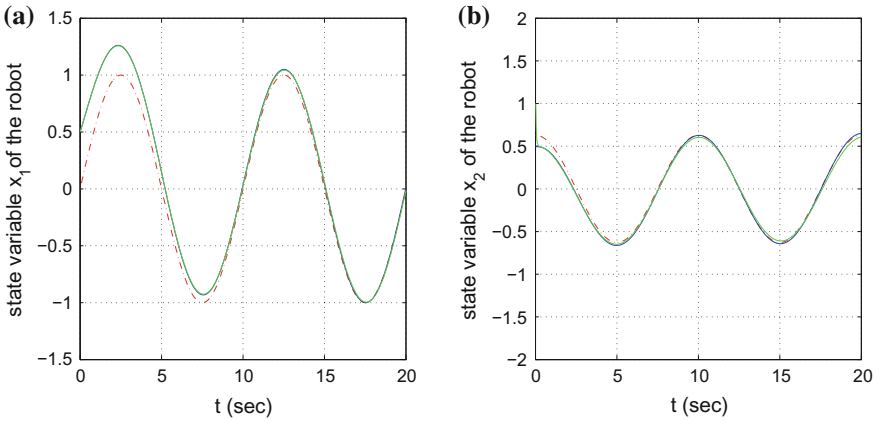

Fig. 1.10 Control with computed torque method and Extended Kalman Filtering: **a** Tracking of a sinusoidal position set-point (dashed line) by the angle of the first joint of the robot (continuous line) **b** Tracking of a sinusoidal velocity set-point (dashed line) by the angular velocity of the first joint of the robot (continuous line)

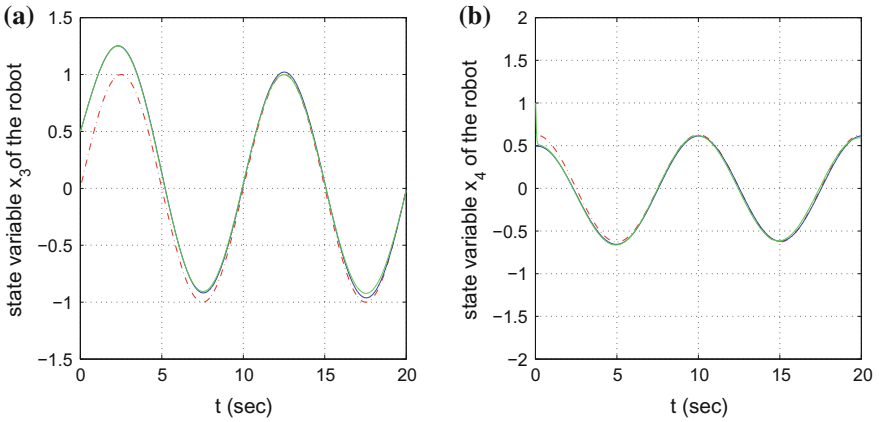

Fig. 1.11 Control with computed torque method and Extended Kalman Filtering: **a** Tracking of a sinusoidal position set-point (dashed line) by the angle of the second joint of the robot (continuous line) **b** Tracking of a sinusoidal velocity set-point (dashed line) by the angular velocity of the second joint of the robot (continuous line)

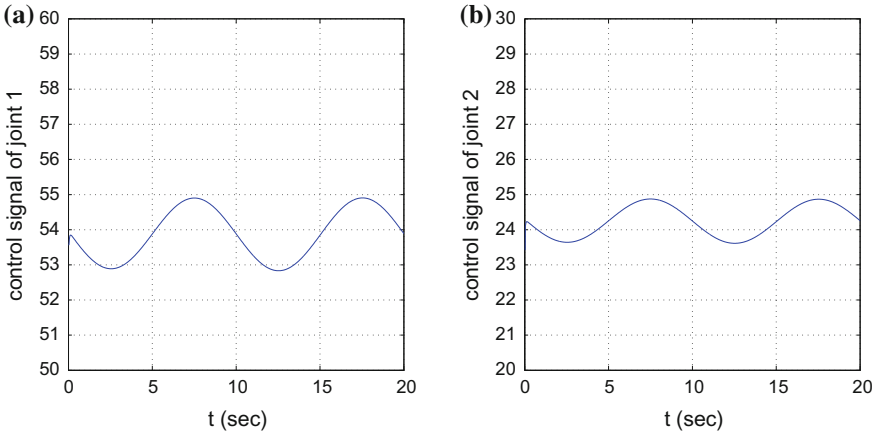

Fig. 1.12 Tracking of a sinusoidal setpoint by the 2-DOF robotic manipulator with the use of the Extended Kalman Filter: **a** Control input (motor torque) applied to the first joint **b** Control input (motor torque) applied to the second joint

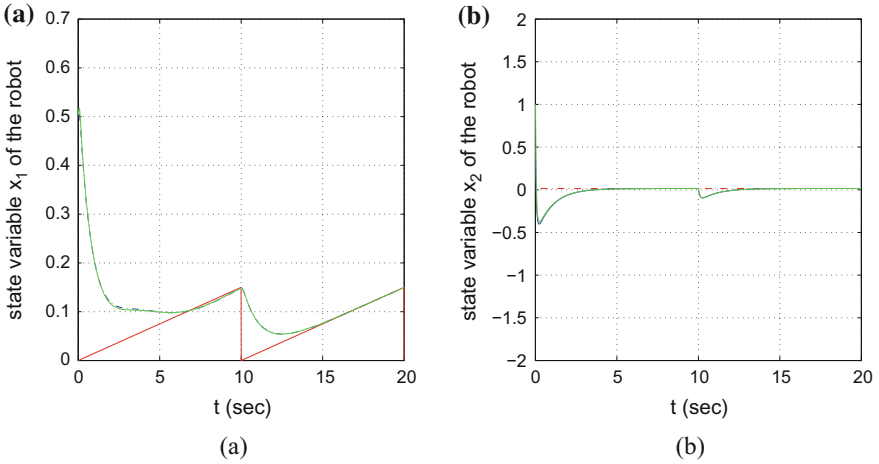

Fig. 1.13 Control with computed torque method and Extended Kalman Filtering: **a** Tracking of a seesaw position set-point (dashed line) by the angle of the first joint of the robot (continuous line) **b** Tracking of a seesaw velocity set-point (dashed line) by the angular velocity of the first joint of the robot (continuous line)

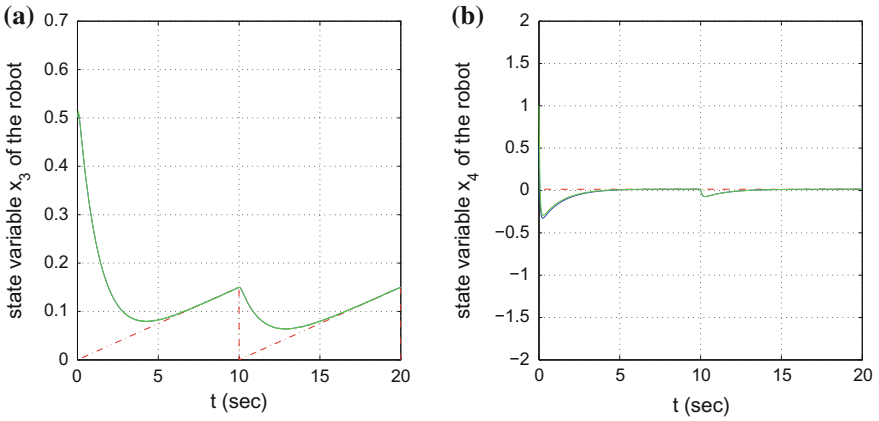

Fig. 1.14 Control with computed torque method and Extended Kalman Filtering: **a** Tracking of a seesaw position set-point (dashed line) by the angle of the second joint of the robot (continuous line) **b** Tracking of a seesaw velocity set-point (dashed line) by the angular velocity of the second joint of the robot (continuous line)

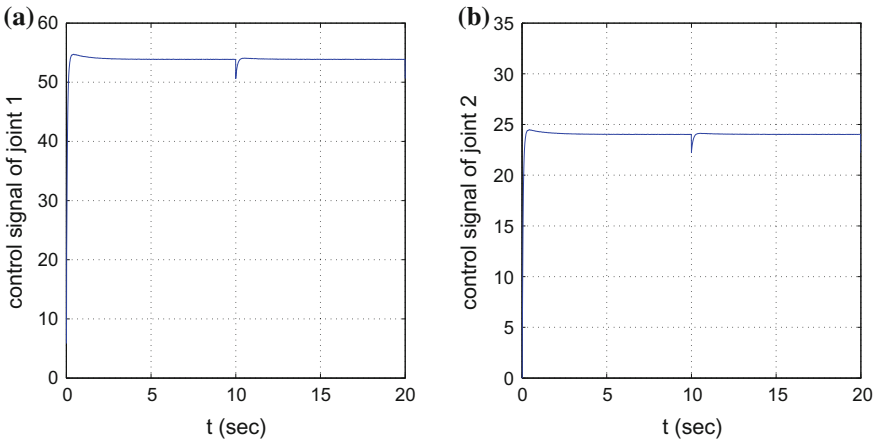

Fig. 1.15 Tracking of a seesaw setpoint by the 2-DOF robotic manipulator with the Extended Kalman Filter: **a** Control input (motor torque) applied to the first joint **b** Control input (motor torque) applied to the second joint

1.4 Model-Based Control of Rigid-Link Manipulators Using Approximate Linearization Methods

1.4.1 Outline

As previously analyzed, the problem of nonlinear control for multi-DOF robotic manipulators is a nontrivial one [86, 233, 372, 377, 403, 484]. In this section a new

method for H-infinity nonlinear control of robotic manipulators is developed and the associated stability proof is provided. In the preceding section it has been shown that existing methods for control of robotic manipulators can be based on global linearization transformations and static state feedback and among these methods the computed torque approach is the most popular one. As already explained, such control methods are based on the transformation of the nonlinear manipulator into an equivalent form of new state variables in which the robot's dynamics is given by a linear and decoupled model. For the latter description of the robot the design of a state feedback controller becomes possible [230, 450, 452, 457, 519].

In this section a different approach for the control of multi-DOF robotic manipulators is proposed, making use of local linearization of the robot's dynamics and applying H-infinity control theory [10, 132, 243, 305, 528]. The nonlinear dynamical model of the robot is subject to local linearization through a Taylor series expansion and the computation of the associated Jacobian matrices [33, 431, 463]. The selection of the linearization point (equilibrium) is performed using the present value of the state vector and the control input of the robotic model. The resulting linearized model of the robot contains also an uncertainty term which is due to the linearization error and this is compensated with the application of an H-infinity feedback control scheme [417, 466].

Actually, the solution of the H-infinity control problem for the linearized dynamics of the robot stands for a min-max differential game in which the control input tries to minimize a cost functional expressing the tracking error for the robot's state variables while the disturbance and model uncertainty input tries to maximize it [133, 402, 404, 564, 605]. The computation of the controller's feedback gain is performed by solving an algebraic Riccati equation at each iteration of the algorithm. The stability of the control method is demonstrated through Lyapunov analysis. It is proven that despite the existence of model uncertainties and external perturbations in the robot's dynamic model, the H-infinity tracking performance condition can be attained. This addresses robustness issues which are a prerequisite in the design of robot control systems [156, 499]. Under moderate conditions, this can also confirm the system's asymptotic stability.

The main features of nonlinear H-infinity control for multi-DOF robotic manipulators are outlined as follows: (i) the new control approach does not make use of linearizing transformations (diffeomorphisms) of the robot's description but acts directly on the robot's nonlinear model, (ii) the H-infinity control approach follows optimal control theory for the computation of the control signal (iii) the new control approach makes use of local linearization and requires the computation of Jacobian matrices in the robot's dynamic model, (iv) the computation of the controller's feedback gains relies on the solution of an algebraic Riccati equation and this is performed at each stage of the control algorithm, (v) yet simple the control method provides good tracking accuracy and exhibits robustness to modelling errors and external perturbations.

1.4.2 Dynamic Model of the Multi-DOF Robotic System

The dynamic model of the 2-DOF rigid-link robot which is depicted again in Fig. 1.3, and under the assumption that the masses of the links are concentrated at the links' end is given by

$$D(\theta)\ddot{\theta} + h(\theta, \dot{\theta}) + g(\theta) = \tau \tag{1.66}$$

where $D(\theta)$ is the inertia matrix

$$D(\theta) = \begin{pmatrix} (m_1 + m_2)l_1^2 + m_1 l_2^2 + 2m_2 l_1 l_2 cos(\theta_2) & m_2 l_2^2 + m_2 l_1 l_2 cos(\theta_2) \\ m_2 l_2^2 + m_2 l_1 l_2 cos(\theta_2) & m_2 l_2 (l_1 + l_2) cos(\theta_2) \end{pmatrix} \tag{1.67}$$

$h(\theta, \dot{\theta})$ is the Coriolis and centrifugal forces vector

$$h(\theta, \dot{\theta}) = \begin{pmatrix} -m_2 l_1^2 sin(\theta_2)\dot{\theta}_2^2 - 2m_2 l_1^2 sin(\theta_2)\dot{\theta}_1\dot{\theta}_2 \\ m_2 l_1^2 sin(\theta_2)\dot{\theta}_1^2 \end{pmatrix} \tag{1.68}$$

$g(\theta)$ is the gravitational forces vector

$$g(\theta) = \begin{pmatrix} (m_1 + m_2) g l_1 cos(\theta_1) + m_2 g l_2 cos(\theta_1 + \theta_2) \\ m_2 g l_2 cos(\theta_1 + \theta_2) \end{pmatrix} \tag{1.69}$$

and $\tau(t)$ is the control inputs vector consisting of the torques that are generated by the motors mounted on the robot's joints.

It holds that

$$D^{-1}(\theta) = \frac{1}{detD} \begin{pmatrix} m_2 l_2 (l_1 + l_2) cos(\theta_2) & -m_2 l_2^2 + m_2 l_1 l_2 cos(\theta_2) \\ -m_2 l_2^2 + m_2 l_1 l_2 cos(\theta_2) & (m_1 + m_2) l_1^2 + m_2 l_2^2 + 2m_2 l_1 l_2 cos(\theta_2) \end{pmatrix} \tag{1.70}$$

where the determinant of D is

$$\begin{gathered} detD = [(m_1 + m_2)l_1^2 + m_2 l_2^2 + 2m_2 l_1 l_2 cos(\theta_2)][m_2 l_2 (l_1 + l_2) cos(\theta_2)] - \\ -[m_2 l_2^2 + m_2 l_1 l_2 cos(\theta_2)]^2 \Rightarrow \\ detD = (m_1 + m_2) m_2 l_1^2 l_2 (l_1 + l_2) cos(\theta_2) + m_2^2 l_2^3 (l_1 + l_2) cos(\theta_2) + 2m_2^2 l_1 l_2^2 (l_1 + \\ + l_2) cos^2(\theta_2) - m_2^2 l_2^4 - m_2^2 l_1^2 l_2^2 cos^2(\theta_2) - 2m_2^2 l_1 l_2^3 cos(\theta_2) \end{gathered} \tag{1.71}$$

Without loss of generality, the following parameters' values are assumed: $m_1 = 1$ kg, $m_2 = 1$ kg, $l_1 = 1$ m, $l_2 = 1$ m and $g = 10$ m/s^2. Thus the inverse of the inertia matrix $D(\theta)$ becomes

$$D^{-1}(\theta) = \frac{1}{detD}\begin{pmatrix} 2cos(\theta_2) & -1+cos(\theta_2) \\ -1+cos(\theta_2) & 2+2cos(\theta_2) \end{pmatrix} \tag{1.72}$$

with

$$detD = 4cos(\theta_2) + 3cos^2(\theta_2) - 1 \tag{1.73}$$

For the previously given values of the parameters in the robot's model one has

$$h(\theta, \dot{\theta}) = \begin{pmatrix} -sin(\theta_2)\dot{\theta}_2^2 - 2sin(\theta_2)\dot{\theta}_1\dot{\theta}_2 \\ sin(\theta_2)\dot{\theta}_1^2 \end{pmatrix} \tag{1.74}$$

$$g(\theta) = \begin{pmatrix} 10cos(\theta_1) + 10cos(\theta_1+\theta_2) \\ 10cos(\theta_1+\theta_2) \end{pmatrix} \tag{1.75}$$

Using the above one gets

$$-D^{-1}(\theta)h(\theta,\dot{\theta}) = \frac{-1}{detD}\cdot \begin{pmatrix} 2cos(\theta_2) & -1+cos(\theta_2) \\ -1+cos(\theta_2) & 2+2cos(\theta_2) \end{pmatrix} \begin{pmatrix} -sin(\theta_2)\dot{\theta}_2^2 - 2sin(\theta_2)\dot{\theta}_1\dot{\theta}_2 \\ sin(\theta)_2\dot{\theta}_1^2 \end{pmatrix} \tag{1.76}$$

or equivalently

$$-D^{-1}(\theta)h(\theta,\dot{\theta}) = \frac{-1}{detD}\cdot \begin{pmatrix} 2cos(\theta_2)[-sin(\theta_2)\dot{\theta}_2^2 - 2sin(\theta_2)\dot{\theta}_1\dot{\theta}_2] + [-1+cos(\theta_2)]sin(\theta)_2\dot{\theta}_1^2 \\ [-1+cos(\theta_2)][-sin(\theta_2)\dot{\theta}_2^2 - 2sin(\theta_2)\dot{\theta}_1\dot{\theta}_2] + [2+2cos(\theta_2)]sin(\theta)_2\dot{\theta}_1^2 \end{pmatrix} \tag{1.77}$$

Alternatively,

$$-D^{-1}(\theta)g(\theta) = -\frac{1}{detD}\cdot \begin{pmatrix} 2cos(\theta_2) & -1+cos(\theta_2) \\ -1+cos(\theta_2) & 2+2cos(\theta_2) \end{pmatrix} \begin{pmatrix} 10cos(\theta_1) + 10cos(\theta_1+\theta_2) \\ 10cos(\theta_1+\theta_2) \end{pmatrix} \tag{1.78}$$

or equivalently

$$-D^{-1}(\theta)g(\theta) = \frac{-1}{detD}\cdot \begin{pmatrix} 2cos(\theta_2)[10cos(\theta_1) + 10cos(\theta_1+\theta_2)] + [-1+cos(\theta_2)]10cos(\theta_1+\theta_2) \\ [-1+cos(\theta_2)][10cos(\theta_1) + 10cos(\theta_1+\theta_2)] + [2+2cos(\theta_2)]10cos(\theta_1+\theta_2) \end{pmatrix} \tag{1.79}$$

Next, by defining the state variables $x_1 = \theta_1$, $x_2 = \dot{\theta}_1$, $x_3 = \theta_2$ and $x_4 = \dot{\theta}_2$ one gets

$$D^{-1}(\theta) = \begin{pmatrix} \dfrac{2cos(x_3)}{4cos(x_3) + 3cos^2(x_3) - 1} & \dfrac{-1 + cos(x_3)}{4cos(x_3) + 3cos^2(x_3) - 1} \\ \dfrac{-1 + cos(x_3)}{4cos(x_3) + 3cos^2(x_3) - 1} & \dfrac{2 + 2cos(x_3)}{4cos(x_3) + 3cos^2(x_3) - 1} \end{pmatrix} \tag{1.80}$$

and also

$$-D^{-1}(\theta)h(\theta, \dot{\theta}) = -\begin{pmatrix} \dfrac{2cos(x_3)[-sin(x_3)x_4^2 - 2sin(x_3)x_2x_4] + [-1 + cos(x_3)]sin(x_3)x_2^2}{4cos(x_3) + 3cos^2(x_3) - 1} \\ \dfrac{[1 + cos(x_3)][-sin(x_3)x_4^2 - 2sin(x_3)x_2x_4] + [2 + 2cos(x_3)]sin(x_3)x_2^2}{4cos(x_3) + 3cos^2(x_3) - 1} \end{pmatrix} \tag{1.81}$$

and similarly

$$-D^{-1}(\theta)g(\theta) = -\begin{pmatrix} \dfrac{2cos(x_3)[10cos(x_1) + 10cos(x_1 + x_3)] + [-1 + cos(x_3)][10cos(x_1 + x_3)]}{4cos(x_3) + 3cos^2(x_3) - 1} \\ \dfrac{[-1 + cos(x_3)][10cos(x_1) + 10cos(x_1 + x_3)] + [2 + 2cos(x_3)]10cos(x_1 + x_3)}{4cos(x_3) + 3cos^2(x_3) - 1} \end{pmatrix} \tag{1.82}$$

The state-space equations of the robotic model are

$$\begin{pmatrix} \ddot{x}_1 \\ \ddot{x}_3 \end{pmatrix} = -D^{-1}(\theta)h(\theta, \dot{\theta}) - D^{-1}(\theta)g(\theta) - D^{-1}(\theta)\tau \tag{1.83}$$

and using that the state vector is $x = [x_1, x_2, x_3, x_4]^T = [\theta_1, \dot{\theta}_1, \theta_2, \dot{\theta}_2]^T$ and the control inputs vector is $\tau = [\tau_1, \tau_2]^T = [u_1, u_2]^T$ the above system can be written as,

$$\dot{x} = f(x) + g_a(x)u_1 + g_b(x)u_2 \tag{1.84}$$

or equivalently

$$\begin{pmatrix} \dot{x}_1 \\ \dot{x}_2 \\ \dot{x}_3 \\ \dot{x}_4 \end{pmatrix} = \begin{pmatrix} f_1 \\ f_2 \\ f_3 \\ f_4 \end{pmatrix} + \begin{pmatrix} g_{a_1} \\ g_{a_2} \\ g_{a_3} \\ g_{a_4} \end{pmatrix} u_1 + \begin{pmatrix} g_{b_1} \\ g_{b_2} \\ g_{b_3} \\ g_{b_4} \end{pmatrix} u_2 \tag{1.85}$$

with

$$f_1 = x_2 \tag{1.86}$$

$$f_2 = -\frac{2cos(x_3)[-sin(x_3)x_4^2 - 2sin(x_3)x_2x_4] + [-1 + cos(x_3)]sin(x_3)x_2^2}{4cos(x_3) + 3cos^2(x_3) - 1} - \\ -\frac{2cos(x_3)[10cos(x_1) + 10cos(x_1 + x_3)] + [-1 + cos(x_3)][10cos(x_1 + x_3)]}{4cos(x_3) + 3cos^2(x_3) - 1} \tag{1.87}$$

$$f_3 = x_4 \tag{1.88}$$

$$f_4 = -\frac{[1 + cos(x_3)][-sin(x_3)x_4^2 - 2sin(x_3)x_2x_4] + [2 + 2cos(x_3)]sin(x_3)x_2^2}{4cos(x_3) + 3cos^2(x_3) - 1} \\ -\frac{[-1 + cos(x_3)][10cos(x_1) + 10cos(x_1 + x_3)] + [2 + 2cos(x_3)]10cos(x_1 + x_3)}{4cos(x_3) + 3cos^2(x_3) - 1} \tag{1.89}$$

Moreover, one has

$$\begin{array}{cc} g_{a_1} = 0 & g_{b_1} = 0 \\ g_{a_2} = \dfrac{2cos(x_3)}{4cos(x_3) + 3cos^2(x_3) - 1} & g_{b_2} = \dfrac{-1cos(x_3)}{4cos(x_3) + 3cos^2(x_3) - 1} \\ g_{a_3} = 0 & g_{b_3} = 0 \\ g_{a_4} = \dfrac{-1 + cos(x_3)}{4cos(x_3) + 3cos^2(x_3) - 1} & g_{b_4} = \dfrac{2 + 2cos(x_3)}{4cos(x_3) + 3cos^2(x_3) - 1} \end{array} \tag{1.90}$$

1.4.3 Approximate Linearization of the Robot's Dynamics

The linearization procedure for the robotic model, which is shown in Fig. 1.3, takes place around the operating point (x^*, u^*), which is the present value of the robot's state vector x^* and the value of the control input vector u^* applied at the last iteration of the control algorithm. The linearization procedure gives

$$\dot{x} = [\nabla_x f \mid_{(x^*,u^*)} + \nabla_x g_a u_1 \mid_{(x^*,u^*)} + \nabla_x g_b u_2 \mid_{(x^*,u^*)}]x + g_a u_1 + g_b u_2 + d_1 \tag{1.91}$$

and thus, by defining the linearization error as d_1 and matrices A, B as

$$A = \nabla_x f \mid_{(x^*,u^*)} + \nabla_x g_a u_1 \mid_{(x^*,u^*)} + \nabla_x g_b u_2 \mid_{(x^*,u^*)} \tag{1.92}$$

$$B = [g_a \; g_b] \tag{1.93}$$

one obtains the linearized description of the robot

$$\dot{x} = Ax + Bu + d_1 \tag{1.94}$$

Using the linearized description of the robotic system $\dot{x} = Ax + Bu + d_1$, the design of the feedback controller can be performed after applying the H-infinity control theory.

Computation of Jacobian matrices of the robot's dynamics: The Jacobian matrices of the model of the 2-DOF robotic manipulator are defined as

$$\nabla_x f\ |_{(x^*,u^*)} = \begin{pmatrix} \frac{\partial f_1}{\partial x_1} & \frac{\partial f_1}{\partial x_2} & \frac{\partial f_1}{\partial x_3} & \frac{\partial f_1}{\partial x_4} \\ \frac{\partial f_2}{\partial x_1} & \frac{\partial f_2}{\partial x_2} & \frac{\partial f_2}{\partial x_3} & \frac{\partial f_2}{\partial x_4} \\ \frac{\partial f_3}{\partial x_1} & \frac{\partial f_3}{\partial x_2} & \frac{\partial f_3}{\partial x_3} & \frac{\partial f_3}{\partial x_4} \\ \frac{\partial f_4}{\partial x_1} & \frac{\partial f_4}{\partial x_2} & \frac{\partial f_4}{\partial x_3} & \frac{\partial f_4}{\partial x_4} \end{pmatrix}_{(x^*,u^*)} \tag{1.95}$$

$$\nabla_x g_a\ |_{(x^*,u^*)} = \begin{pmatrix} \frac{\partial g_{a1}}{\partial x_1} & \frac{\partial g_{a1}}{\partial x_2} & \frac{\partial g_{a1}}{\partial x_3} & \frac{\partial g_{a1}}{\partial x_4} \\ \frac{\partial g_{a2}}{\partial x_1} & \frac{\partial g_{a2}}{\partial x_2} & \frac{\partial g_{a2}}{\partial x_3} & \frac{\partial g_{a2}}{\partial x_4} \\ \frac{\partial g_{a3}}{\partial x_1} & \frac{\partial g_{a3}}{\partial x_2} & \frac{\partial g_{a3}}{\partial x_3} & \frac{\partial g_{a3}}{\partial x_4} \\ \frac{\partial g_{a4}}{\partial x_1} & \frac{\partial g_{a4}}{\partial x_2} & \frac{\partial g_{a4}}{\partial x_3} & \frac{\partial g_{a4}}{\partial x_4} \end{pmatrix}_{(x^*,u^*)} \tag{1.96}$$

$$\nabla_x g_b\ |_{(x^*,u^*)} = \begin{pmatrix} \frac{\partial g_{b1}}{\partial x_1} & \frac{\partial g_{b1}}{\partial x_2} & \frac{\partial g_{b1}}{\partial x_3} & \frac{\partial g_{b1}}{\partial x_4} \\ \frac{\partial g_{b2}}{\partial x_1} & \frac{\partial g_{b2}}{\partial x_2} & \frac{\partial g_{b2}}{\partial x_3} & \frac{\partial g_{b2}}{\partial x_4} \\ \frac{\partial g_{b3}}{\partial x_1} & \frac{\partial g_{b3}}{\partial x_2} & \frac{\partial g_{b3}}{\partial x_3} & \frac{\partial g_{b3}}{\partial x_4} \\ \frac{\partial g_{b4}}{\partial x_1} & \frac{\partial g_{b4}}{\partial x_2} & \frac{\partial g_{b4}}{\partial x_3} & \frac{\partial g_{b4}}{\partial x_4} \end{pmatrix}_{(x^*,u^*)} \tag{1.97}$$

where

$$\frac{\partial f_1}{\partial x_1} = 0 \; \frac{\partial f_1}{\partial x_2} = 1 \; \frac{\partial f_1}{\partial x_3} = 0 \; \frac{\partial f_1}{\partial x_4} = 0 \tag{1.98}$$

$$\frac{\partial f_2}{\partial x_1} = -\frac{2cos(x_3)[10cos(x_1) + 10cos(x_1 + x_3)] + [-1 + cos(x_3)][10cos(x_1 + x_3)]}{4cos(x_3) + 3cos^2(x_3) - 1} \tag{1.99}$$

$$\begin{aligned}\frac{\partial f_2}{\partial x_2} = &-\frac{-2cos(x_3)2sin(x_3)x_4 + [-1 + cos(x_3)]sin(x_3)2x_2}{4cos(x_3) + 3cos^2(x_3) - 1} \\ &-\frac{2cos(x_3)10sin(x_1 + x_3)}{4cos(x_3) + 3cos^2(x_3) - 1}\end{aligned} \tag{1.100}$$

$$\begin{aligned}\frac{\partial f_2}{\partial x_3} = &-\left\{\frac{-2sin(x_3)[-sin(x_3)x_4^2 - 2sin(x_3)x_2x_4] + 2cos(x_3)[cos(x_3)x_4^2 - 2cos(x_3)x_2x_4]}{[4cos(x_3) + 3cos^2(x_3) - 1]^2}\right. \\ &\left.+\frac{[-sin(x_3)]sin(x_3)x_2^2 + [-1 + cos(x_3)]cos(x_3)x_2^2}{[4cos(x_3) + 3cos^2(x_3) - 1]^2}\right\}[4cos(x_3) + 3cos^2(x_3) - 1] \\ &-\left\{\frac{2sin(x_3)[10cos(x_1) + 10cos(x_1 + x_3)] - 2cos(x_3)10sin(x_1 + x_3)}{[4cos(x_3) + 3cos^2(x_3) - 1]^2}\right. \\ &\left.+\frac{[-sin(x_3)][10cos(x_1 + x_3)] - [-1 + cos(x_3)]sin(x_1 + x_3)}{[4cos(x_3) + 3cos^2(x_3) - 1]^2}\right\}[4cos(x_3) + 3cos^2(x_3) - 1] \\ &\left\{+\frac{2cos(x_3)[-sin(x_3)x_4^2 - 2sin(x_3)x_2x_4] + [-1 + cos(x_3)]sin(x_3)x_2^2}{[4cos(x_3) + 3cos^2(x_3) - 1]^2}\right. \\ &\left.+\frac{2cos(x_3)[10cos(x_1) + 10cos(x_1 + x_3)] + [-1 + cos(x_3)][10cos(x_1 + x_3)]}{[4cos(x_3) + 3cos^2(x_3) - 1]^2}\right\}[-4sin(x_3) - 6cos(x_3)sin(x_3)]\end{aligned} \tag{1.101}$$

$$\frac{\partial f_2}{\partial x_4} = \frac{2cos(x_3)[-sin(x_3)2x_4 - 2sin(x_3)x_2]}{4cos(x_3) + 3cos^2(x_3) - 1} \tag{1.102}$$

$$\frac{\partial f_3}{\partial x_1} = 0 \; \frac{\partial f_3}{\partial x_2} = 0 \; \frac{\partial f_3}{\partial x_3} = 0 \; \frac{\partial f_3}{\partial x_4} = 1 \tag{1.103}$$

$$\frac{\partial f_4}{\partial x_1} = -\frac{[-1 + cos(x_3)][-10sin(x_1) - 10sin(x_1 + x_3)] - [2 + 2cos(x_3)]10sin(x_1 + x_3)}{4cos(x_3) + 3cos^2(x_3) - 1} \tag{1.104}$$

$$\frac{\partial f_4}{\partial x_2} = -\frac{[1 + cos(x_3)][-2sin(x_3)x_4] + [2 + 2cos(x_3)]sin(x_3)2x_2}{4cos(x_3) + 3cos^2(x_3) - 1} \tag{1.105}$$

$$\frac{\partial f_4}{\partial x_3} = -\left\{\frac{-sin(x_3)[-sin(x_3)x_4^2 - 2sin(x_3)x_2x_4] + [1+cos(x_3)][cos(x_3)x_4^2 - 2cos(x_3)x_2x_4]}{[4cos(x_3)+3cos^2(x_3)-1]^2} + \frac{-2sin(x_3)sin(x_3)x_2^2 + [2+2cos(x_3)]cos(x_3)x_2^2}{[4cos(x_3)+3cos^2(x_3)-1]^2}\right\}[4cos(x_3)+3cos^2(x_3)-1]$$
$$-\left\{\frac{-sin(x_3)[10cos(x_1)+10cos(x_1+x_3)] + [-1+cos(x_3)][-10sin(x_3)-10sin(x_1+x_3)]}{[4cos(x_3)+3cos^2(x_3)-1]^2} + \frac{-2sin(x_3)10cos(x_1+x_3) - [2+2cos(x_3)]10sin(x_1+x_3)}{[4cos(x_3)+3cos^2(x_3)-1]^2}\right\}[4cos(x_3)+3cos^2(x_3)-1]$$
$$\left\{\frac{[1+cos(x_3)][-sin(x_3)x_4^2 - 2sin(x_3)x_2x_4] + [2+2cos(x_3)]sin(x_3)x_2^2}{[4cos(x_3)+3cos^2(x_3)-1]^2} + \frac{[-1+cos(x_3)][10cos(x_1)+10cos(x_1+x_3)] + [2+2cos(x_3)]10cos(x_1+x_3)}{[4cos(x_3)+3cos^2(x_3)-1]^2}\right\}[-4sin(x_3) - 6cos(x_3)sin(x_3)] \tag{1.106}$$

$$\frac{\partial f_4}{\partial x_4} = \frac{[1+cos(x_3)][-sin(x_3)2x_4 - 2sin(x_3)x_2]}{4cos(x_3)+3cos^2(x_3)-1} \tag{1.107}$$

In a similar manner one computes

$$\frac{\partial g_{a1}}{\partial x_1} = 0 \;\; \frac{\partial g_{a1}}{\partial x_2} = 0 \;\; \frac{\partial g_{a1}}{\partial x_3} = 0 \;\; \frac{\partial g_{a1}}{\partial x_4} = 0 \tag{1.108}$$

$$\frac{\partial g_{a2}}{\partial x_1} = 0 \;\; \frac{\partial g_{a2}}{\partial x_2} = 0 \;\; \frac{\partial g_{a2}}{\partial x_4} = 0 \tag{1.109}$$

$$\frac{\partial g_{a2}}{\partial x_3} = \frac{-2sin(x_3)[4cos(x_3)+4cos^2(x_3)-1] + 2cos(x_3)[-4sin(x_3) - 6sin(x_3)cos(x_3)]}{[4cos(x_3)+3cos^2(x_3)-1]^2} \tag{1.110}$$

$$\frac{\partial g_{a3}}{\partial x_1} = 0 \;\; \frac{\partial g_{a3}}{\partial x_2} = 0 \;\; \frac{\partial g_{a3}}{\partial x_3} = 0 \;\; \frac{\partial g_{a3}}{\partial x_4} = 0 \tag{1.111}$$

$$\frac{\partial g_{a2}}{\partial x_1} = 0 \;\; \frac{\partial g_{a2}}{\partial x_2} = 0 \;\; \frac{\partial g_{a2}}{\partial x_4} = 0 \tag{1.112}$$

$$\frac{\partial g_{a2}}{\partial x_3} = \frac{-sin(x_3)[4cos(x_3)+4cos^2(x_3)-1] + [-1+cos(x_3)][4sin(x_3)+6sin(x_3)cos(x_3)]}{[4cos(x_3)+3cos^2(x_3)-1]^2} \tag{1.113}$$

while one also obtains

$$\frac{\partial g_{b1}}{\partial x_1} = 0 \;\; \frac{\partial g_{b1}}{\partial x_2} = 0 \;\; \frac{\partial g_{b1}}{\partial x_3} = 0 \;\; \frac{\partial g_{b1}}{\partial x_4} = 0 \tag{1.114}$$

$$\frac{\partial g_{b2}}{\partial x_1} = 0 \quad \frac{\partial g_{b2}}{\partial x_2} = 0 \quad \frac{\partial g_{b2}}{\partial x_3} = 0 \tag{1.115}$$

$$\frac{\partial g_{b2}}{\partial x_3} = \frac{-sin(x_3)[4cos(x_3) + 4cos^2(x_3) - 1] + [-1 + cos(x_3)][4sin(x_3) + 6sin(x_3)cos(x_3)]}{[4cos(x_3) + 3cos^2(x_3) - 1]^2} \tag{1.116}$$

$$\frac{\partial g_{b3}}{\partial x_1} = 0 \quad \frac{\partial g_{b3}}{\partial x_2} = 0 \quad \frac{\partial g_{b3}}{\partial x_3} = 0 \quad \frac{\partial g_{b3}}{\partial x_4} = 0 \tag{1.117}$$

$$\frac{\partial g_{b4}}{\partial x_1} = 0 \quad \frac{\partial g_{b4}}{\partial x_2} = 0 \quad \frac{\partial g_{b4}}{\partial x_3} = 0 \tag{1.118}$$

$$\frac{\partial g_{b4}}{\partial x_3} = \frac{-2sin(x_3)[4cos(x_3) + 4cos^2(x_3) - 1] + [2 + 2cos(x_3)][4sin(x_3) + 6sin(x_3)cos(x_3)]}{[4cos(x_3) + 3cos^2(x_3) - 1]^2} \tag{1.119}$$

1.4.4 Design of an H-Infinity Nonlinear Feedback Controller

1.4.4.1 Equivalent Linearized Dynamics of the Robot

After linearization round its current operating point, the robot's dynamic model is written as

$$\dot{x} = Ax + Bu + d_1 \tag{1.120}$$

Parameter d_1 stands for the linearization error in the robot's dynamic model appearing in Eq. (1.120). The reference setpoints for the robot's state vector are denoted by $\mathbf{x_d} = [x_1^d, \ldots, x_4^d]$. Tracking of this trajectory is achieved after applying the control input u^*. At every time instant the control input u^* is assumed to differ from the control input u appearing in Eq. (1.120) by an amount equal to Δu, that is $u^* = u + \Delta u$

$$\dot{x}_d = Ax_d + Bu^* + d_2 \tag{1.121}$$

The dynamics of the controlled system described in Eq. (1.120) can be also written as

$$\dot{x} = Ax + Bu + Bu^* - Bu^* + d_1 \tag{1.122}$$

and by denoting $d_3 = -Bu^* + d_1$ as an aggregate disturbance term one obtains

$$\dot{x} = Ax + Bu + Bu^* + d_3 \tag{1.123}$$

By subtracting Eq. (1.121) from Eq. (1.123) one has

$$\dot{x} - \dot{x}_d = A(x - x_d) + Bu + d_3 - d_2 \tag{1.124}$$

By defining the tracking error as $e = x - x_d$ and the aggregate disturbance term as $\tilde{d} = d_3 - d_2$, the tracking error dynamics becomes

$$\dot{e} = Ae + Bu + \tilde{d} \tag{1.125}$$

The above linearized form of the robot's model can be efficiently controlled after applying an H-infinity feedback control scheme.

1.4.4.2 The Nonlinear H-Infinity Control

The initial nonlinear model of the robotic manipulator is in the form

$$\dot{x} = f(x, u) \;\; x \in R^n, \; u \in R^m \tag{1.126}$$

Linearization of the system (multi-DOF robot) is performed at each iteration of the control algorithm around its present operating point $(x^*, u^*) = (x(t), u(t - T_s))$. The linearized equivalent of the system is described by

$$\dot{x} = Ax + Bu + L\tilde{d} \;\; x \in R^n, \; u \in R^m, \; \tilde{d} \in R^q \tag{1.127}$$

where matrices A and B are obtained from the computation of the Jacobians

$$A = \begin{pmatrix} \frac{\partial f_1}{\partial x_1} & \frac{\partial f_1}{\partial x_2} & \cdots & \frac{\partial f_1}{\partial x_n} \\ \frac{\partial f_2}{\partial x_1} & \frac{\partial f_2}{\partial x_2} & \cdots & \frac{\partial f_2}{\partial x_n} \\ \cdots & \cdots & \cdots & \cdots \\ \frac{\partial f_n}{\partial x_1} & \frac{\partial f_n}{\partial x_2} & \cdots & \frac{\partial f_n}{\partial x_n} \end{pmatrix} |_{(x^*,u^*)} \; B = \begin{pmatrix} \frac{\partial f_1}{\partial u_1} & \frac{\partial f_1}{\partial u_2} & \cdots & \frac{\partial f_1}{\partial u_m} \\ \frac{\partial f_2}{\partial u_1} & \frac{\partial f_2}{\partial u_2} & \cdots & \frac{\partial f_2}{\partial u_m} \\ \cdots & \cdots & \cdots & \cdots \\ \frac{\partial f_n}{\partial u_1} & \frac{\partial f_n}{\partial u_2} & \cdots & \frac{\partial f_n}{\partial u_m} \end{pmatrix} |_{(x^*,u^*)} \tag{1.128}$$

and vector $\tilde{d}$ denotes disturbance terms due to linearization errors. The problem of disturbance rejection for the linearized model that is described by

$$\begin{aligned} \dot{x} &= Ax + Bu + L\tilde{d} \\ y &= Cx \end{aligned} \tag{1.129}$$

where $x \in R^n$, $u \in R^m$, $\tilde{d} \in R^q$ and $y \in R^p$, cannot be handled efficiently if the classical LQR control scheme is applied. This is because of the existence of

the perturbation term $\tilde{d}$. The disturbance term $\tilde{d}$ apart from modeling (parametric) uncertainty and external perturbation terms can also represent noise terms of any distribution.

In the H_∞ control approach, a feedback control scheme is designed for trajectory tracking by the system's state vector and simultaneous disturbance rejection, considering that the disturbance affects the system in the worst possible manner. The disturbances' effects are incorporated in the following quadratic cost function:

$$\begin{aligned} J(t) &= \tfrac{1}{2}\int_0^T [y^T(t)y(t)+ \\ &+ru^T(t)u(t) - \rho^2\tilde{d}^T(t)\tilde{d}(t)]dt, \quad r, \rho > 0 \end{aligned} \tag{1.130}$$

The significance of the negative sign in the cost function's term that is associated with the perturbation variable $\tilde{d}(t)$ is that the disturbance tries to maximize the cost function $J(t)$ while the control signal $u(t)$ tries to minimize it. The physical meaning of the relation given above is that the control signal and the disturbances compete to each other within a min-max differential game. This problem of mini-max optimization can be written as

$$min_u max_{\tilde{d}} J(u, \tilde{d}) \tag{1.131}$$

The objective of the optimization procedure is to compute a control signal $u(t)$ which can compensate for the worst possible disturbance, that is externally imposed to the robotic system. However, the solution to the min-max optimization problem is directly related to the value of the parameter ρ. This means that there is an upper bound in the disturbances magnitude that can be annihilated by the control signal.

1.4.5 Computation of the Feedback Control Gains for the Approximately Linearized Robot

For the linearized system given by Eq. (1.129) the cost function of Eq. (1.130) is defined, where the coefficient r determines the penalization of the control input and the weight coefficient ρ determines the reward of the disturbances' effects.

It is assumed that (i) The energy that is transferred from the disturbances signal $\tilde{d}(t)$ is bounded, that is $\int_0^\infty \tilde{d}^T(t)\tilde{d}(t)dt < \infty$, (ii) the matrices $[A, B]$ and $[A, L]$ are stabilizable, (iii) the matrix $[A, C]$ is detectable. Then, the optimal feedback control law is given by

$$u(t) = -Kx(t) \tag{1.132}$$

with

$$K = \tfrac{1}{r}B^T P \tag{1.133}$$

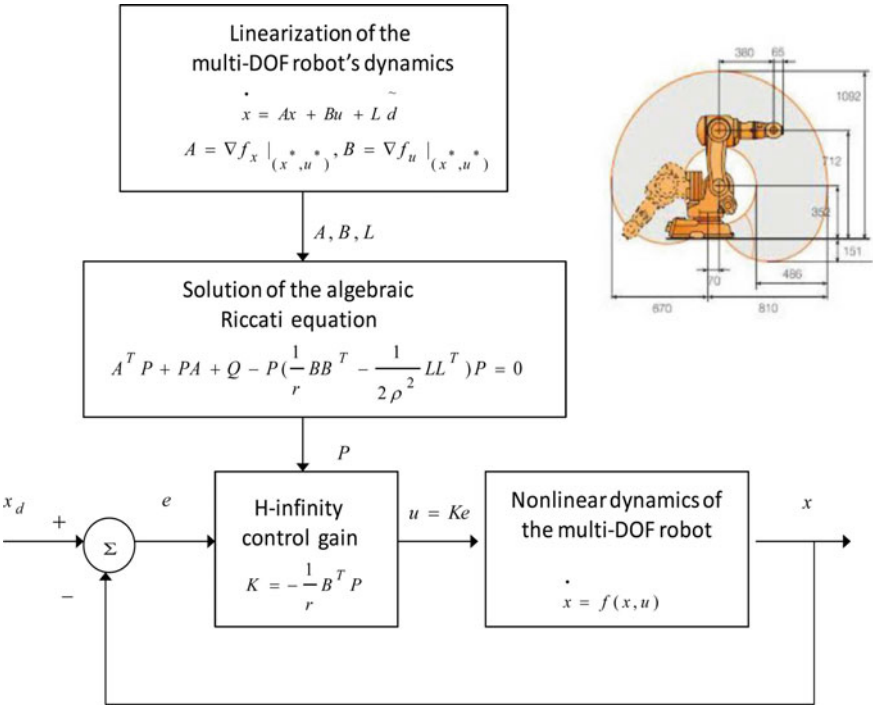

Fig. 1.16 Diagram of the control scheme for the multi-DOF robotic manipulator

where P is a positive semi-definite symmetric matrix which is obtained from the solution of the Riccati equation

$$A^T P + PA + Q - P\left(\tfrac{1}{r}BB^T - \tfrac{1}{2\rho^2}LL^T\right)P = 0 \tag{1.134}$$

where Q is also a positive definite symmetric matrix. The worst case disturbance is given by

$$\tilde{d}(t) = \tfrac{1}{\rho^2}L^T P x(t) \tag{1.135}$$

The diagram of the considered control loop is depicted in Fig. 1.16.

1.4.6 Riccati Equation Coefficients in Controller's Robustness

The parameter ρ in Eq. (1.130), is an indication of the closed-loop system robustness. If the values of $\rho > 0$ are excessively decreased with respect to r, then the solution

of the Riccati equation is no longer a positive definite matrix. Consequently there is a lower bound ρ_{min} of ρ for which the H_∞ control problem has a solution. The acceptable values of ρ lie in the interval $[\rho_{min}, \infty)$. If ρ_{min} is found and used in the design of the H_∞ controller, then the closed-loop system will have increased robustness. Otherwise, if a value $\rho > \rho_{min}$ is used, then an admissible stabilizing H_∞ controller will be derived but it will be a suboptimal one. The Hamiltonian matrix

$$H = \begin{pmatrix} A & -(\frac{1}{r}BB^T - \frac{1}{\rho^2}LL^T) \\ -Q & -A^T \end{pmatrix} \tag{1.136}$$

provides a criterion for the existence of a solution of the Riccati equation Eq. (1.134). A necessary condition for the solution of the algebraic Riccati equation to be a positive semi-definite symmetric matrix is that H has no imaginary eigenvalues [450].

1.4.7 Lyapunov Stability Analysis

Through Lyapunov stability analysis it will be shown that the proposed nonlinear control scheme guarantees H_∞ tracking performance for the robotic manipulator, and that in case of bounded disturbance terms asymptotic convergence to the reference setpoints is achieved. The tracking error dynamics for the multi-DOF robot is written in the form

$$\dot{e} = Ae + Bu + L\tilde{d} \tag{1.137}$$

where in the robot's case $L = I \in R^4$ with I being the identity matrix. Variable $\tilde{d}$ denotes model uncertainties and external disturbances of the robot's model. The following Lyapunov function is considered

$$V = \tfrac{1}{2}e^T Pe \tag{1.138}$$

where $e = x - x_d$ is the tracking error. By differentiating with respect to time one obtains

$$\begin{gathered} \dot{V} = \tfrac{1}{2}\dot{e}^T Pe + \tfrac{1}{2}eP\dot{e} \Rightarrow \\ \dot{V} = \tfrac{1}{2}[Ae + Bu + L\tilde{d}]^T Pe + \tfrac{1}{2}e^T P[Ae + Bu + L\tilde{d}] \Rightarrow \end{gathered} \tag{1.139}$$

$$\begin{gathered} \dot{V} = \tfrac{1}{2}[e^T A^T + u^T B^T + \tilde{d}^T L^T]Pe + \\ + \tfrac{1}{2}e^T P[Ae + Bu + L\tilde{d}] \Rightarrow \end{gathered} \tag{1.140}$$

$$\begin{gathered} \dot{V} = \tfrac{1}{2}e^T A^T Pe + \tfrac{1}{2}u^T B^T Pe + \tfrac{1}{2}\tilde{d}^T L^T Pe + \\ \tfrac{1}{2}e^T PAe + \tfrac{1}{2}e^T PBu + \tfrac{1}{2}e^T PL\tilde{d} \end{gathered} \tag{1.141}$$

The previous equation is rewritten as

$$\begin{aligned}\dot{V} = \tfrac{1}{2}e^T(A^T P + PA)e + (\tfrac{1}{2}u^T B^T Pe + \tfrac{1}{2}e^T PBu) + \\ +(\tfrac{1}{2}\tilde{d}^T L^T Pe + \tfrac{1}{2}e^T PL\tilde{d})\end{aligned} \tag{1.142}$$

Assumption: For given positive definite matrix Q and coefficients r and ρ there exists a positive definite matrix P, which is the solution of the following matrix equation

$$A^T P + PA = -Q + P\left(\tfrac{2}{r}BB^T - \tfrac{1}{\rho^2}LL^T\right)P \tag{1.143}$$

Moreover, the following feedback control law is applied to the system

$$u = -\tfrac{1}{r}B^T Pe \tag{1.144}$$

By substituting Eqs. (1.143) and (1.144) one obtains

$$\begin{aligned}\dot{V} = \tfrac{1}{2}e^T\left[-Q + P\left(\tfrac{2}{r}BB^T - \tfrac{1}{\rho^2}LL^T\right)P\right]e + \\ +e^T PB\left(-\tfrac{1}{r}B^T Pe\right) + e^T PL\tilde{d} \Rightarrow\end{aligned} \tag{1.145}$$

$$\begin{aligned}\dot{V} = -\tfrac{1}{2}e^T Qe + \tfrac{1}{r}e^T PBB^T Pe - \tfrac{1}{2\rho^2}e^T PLL^T Pe \\ -\tfrac{1}{r}e^T PBB^T Pe + e^T PL\tilde{d}\end{aligned} \tag{1.146}$$

which after intermediate operations gives

$$\dot{V} = -\tfrac{1}{2}e^T Qe - \tfrac{1}{2\rho^2}e^T PLL^T Pe + e^T PL\tilde{d} \tag{1.147}$$

or, equivalently

$$\begin{aligned}\dot{V} = -\tfrac{1}{2}e^T Qe - \tfrac{1}{2\rho^2}e^T PLL^T Pe + \\ +\tfrac{1}{2}e^T PL\tilde{d} + \tfrac{1}{2}\tilde{d}^T L^T Pe\end{aligned} \tag{1.148}$$

Lemma: The following inequality holds

$$\tfrac{1}{2}e^T L\tilde{d} + \tfrac{1}{2}\tilde{d}L^T Pe - \tfrac{1}{2\rho^2}e^T PLL^T Pe \leq \tfrac{1}{2}\rho^2\tilde{d}^T\tilde{d} \tag{1.149}$$

Proof The binomial $(\rho\alpha - \frac{1}{\rho}b)^2$ is considered. Expanding the left part of the above inequality one gets

$$\begin{aligned}\rho^2a^2 + \tfrac{1}{\rho^2}b^2 - 2ab \geq 0 \Rightarrow \tfrac{1}{2}\rho^2a^2 + \tfrac{1}{2\rho^2}b^2 - ab \geq 0 \Rightarrow \\ ab - \tfrac{1}{2\rho^2}b^2 \leq \tfrac{1}{2}\rho^2a^2 \Rightarrow \tfrac{1}{2}ab + \tfrac{1}{2}ab - \tfrac{1}{2\rho^2}b^2 \leq \tfrac{1}{2}\rho^2a^2\end{aligned} \tag{1.150}$$

The following substitutions are carried out: $a = \tilde{d}$ and $b = e^T PL$ and the previous relation becomes

$$\tfrac{1}{2}\tilde{d}^T L^T Pe + \tfrac{1}{2}e^T PL\tilde{d} - \tfrac{1}{2\rho^2}e^T PLL^T Pe \leq \tfrac{1}{2}\rho^2\tilde{d}^T\tilde{d} \tag{1.151}$$

Equation (1.151) is substituted in Eq. (1.148) and the inequality is enforced, thus giving

$$\dot{V} \leq -\tfrac{1}{2}e^T Qe + \tfrac{1}{2}\rho^2\tilde{d}^T\tilde{d} \tag{1.152}$$

Equation (1.152) shows that the H_∞ tracking performance criterion is satisfied. The integration of $\dot{V}$ from 0 to T gives

$$\begin{gathered}\int_0^T \dot{V}(t)dt \leq -\tfrac{1}{2}\int_0^T ||e||_Q^2 dt + \tfrac{1}{2}\rho^2\int_0^T ||\tilde{d}||^2 dt \Rightarrow \\ 2V(T) + \int_0^T ||e||_Q^2 dt \leq 2V(0) + \rho^2\int_0^T ||\tilde{d}||^2 dt\end{gathered} \tag{1.153}$$

Moreover, if there exists a positive constant $M_d > 0$ such that

$$\int_0^\infty ||\tilde{d}||^2 dt \leq M_d \tag{1.154}$$

then one gets

$$\int_0^\infty ||e||_Q^2 dt \leq 2V(0) + \rho^2 M_d \tag{1.155}$$

Thus, the integral $\int_0^\infty ||e||_Q^2 dt$ is bounded. Moreover, $V(T)$ is bounded and from the definition of the Lyapunov function V in Eq. (1.138) it becomes clear that $e(t)$ will be also bounded since $e(t) \in \Omega_e = \{e | e^T Pe \leq 2V(0) + \rho^2 M_d\}$. According to the above and with the use of Barbalat's Lemma one obtains $\lim_{t\to\infty} e(t) = 0$.

The outline of the global stability proof is that at each iteration of the control algorithm the state vector of the robotic system converges towards the temporary equilibrium and the temporary equilibrium in turn converges towards the reference trajectory. Thus, the control scheme exhibits global asymptotic stability properties and not local stability. Assume the ith iteration of the control algorithm and the ith time interval about which a positive definite symmetric matrix P is obtained from the solution of the Riccati Equation appearing in Eq. (1.143). By following the stages of the stability proof one arrives at Eq. (1.152) which shows that the H-infinity tracking performance criterion holds. By selecting the attenuation coefficient ρ to be sufficiently small and in particular to satisfy $\rho^2 < ||e||_Q^2 / ||\tilde{d}||^2$ one has that the first derivative of the Lyapunov function is upper bounded by 0. Therefore for the ith time interval it is proven that the Lyapunov function defined in Eq. (1.138) is a decreasing one. This signifies that between the beginning and the end of the ith time interval there will be a drop of the value of the Lyapunov function and since matrix P is a positive definite one, the only way for this to happen is the Euclidean norm of the state vector error e to be decreasing. This means that comparing to the

beginning of each time interval, the distance of the state vector error from 0 at the end of the time interval has been diminished. Consequently as the iterations of the control algorithm advance the tracking error will approach zero, and this is a global asymptotic stability condition.

1.4.8 Simulation Tests

The tracking performance of the proposed nonlinear H-infinity control algorithm was confirmed in the case of tracking of different reference setpoints by two different types of multi-DOF robotic manipulators: (i) a planar 2-DOF robot, (ii) a 2-DOF manipulator with a dynamic model subjected to the effects of gravitational forces. In both cases it was confirmed that the applied control method achieved precise tracking of the joints' reference setpoints. The convergence of the joints' angles to the desirable values was fast, while the variation of the control input was smooth and remained within moderate ranges.

First, the results about the motion of the joints of the planar 2-DOF robot are given. It was considered that the motion of the robot was taking place in the horizontal plane at zero height. Consequently Eq. (1.159) did not contain the vector of gravitational forces $g(\theta)$. In Figs. 1.17, 1.18 and 1.19 one can note how under the proposed control scheme the angles of the joints of the multi-DOF planar robotic manipulator converge to a constant reference setpoint. Equivalently in Figs. 1.20, 1.21 and 1.22 one can note how under the proposed control scheme the angles of the joints of the multi-DOF planar robotic manipulator track a sinusoidal reference setpoint.

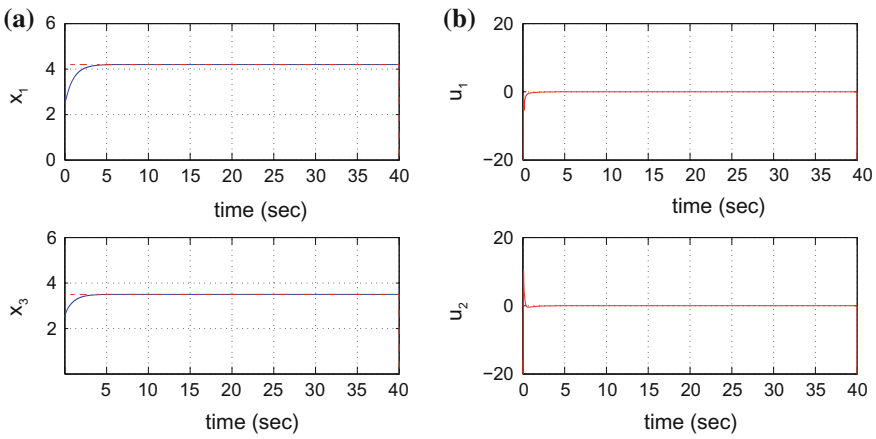

Fig. 1.17 **a** Tracking of a constant reference setpoint by the joints $x_1 = \theta_1$ and $x_3 = \theta_2$ of a 2-DOF planar robot manipulator, **b** the associated control inputs u_1 and u_2

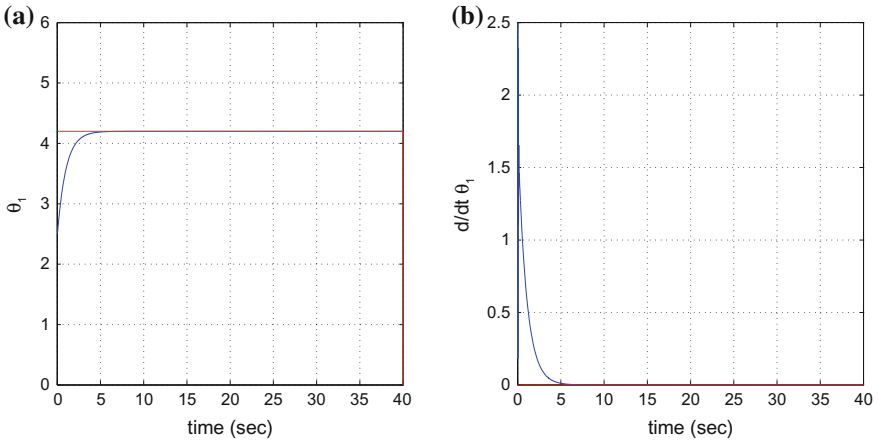

Fig. 1.18 **a** Tracking of a constant reference setpoint by the joints θ_1 of a 2-DOF planar robot manipulator, **b** angular velocity $\dot{\theta}_1$

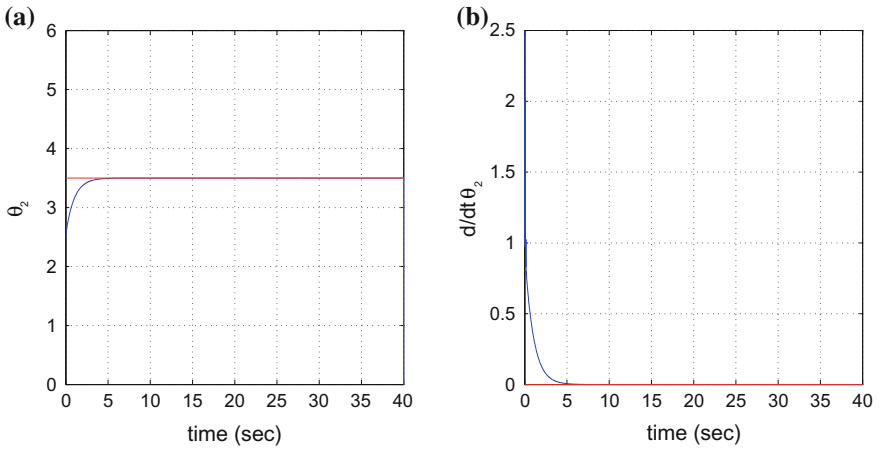

Fig. 1.19 **a** Tracking of a constant reference setpoint by the joints θ_2 of a 2-DOF planar robot manipulator, **b** angular velocity $\dot{\theta}_2$

Next, results about the convergence to reference setpoints of the joints of the 2-DOF robotic model subjected to gravitational forces are presented. The dynamic model of the robot was that of Eq. (1.159). It was considered that the motion of the robot takes place in the cartesian space and consequently the vector of gravitational forces $g(\theta)$ had non-zero values. In Figs. 1.23, 1.24 and 1.25 one can observe how under the proposed control scheme the angles of the joints of the multi-DOF robotic manipulator convergence to a constant reference setpoint. Equivalently in Figs. 1.26, 1.27 and 1.28 one can note how under the proposed control scheme the angles of the joints of the multi-DOF robotic manipulator track a sinusoidal reference setpoint.

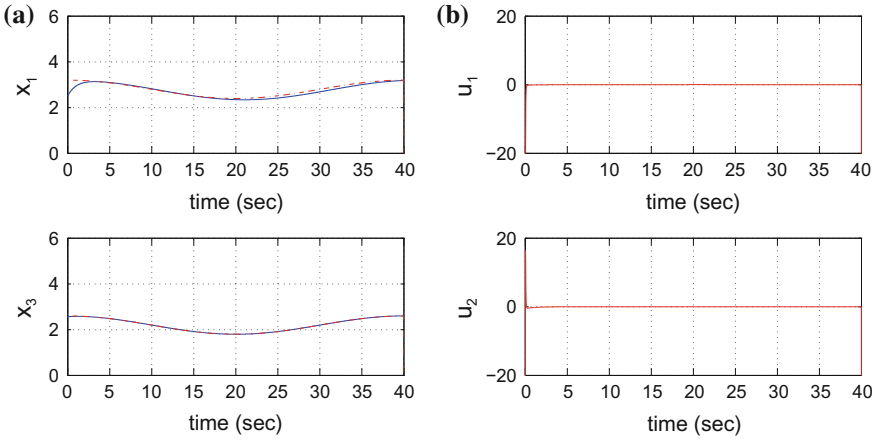

Fig. 1.20 **a** Tracking of a sinusoidal reference setpoint by the joints $x_1 = \theta_1$ and $x_3 = \theta_2$ of a 2-DOF planar robot manipulator, **b** the associated control inputs u_1 and u_2

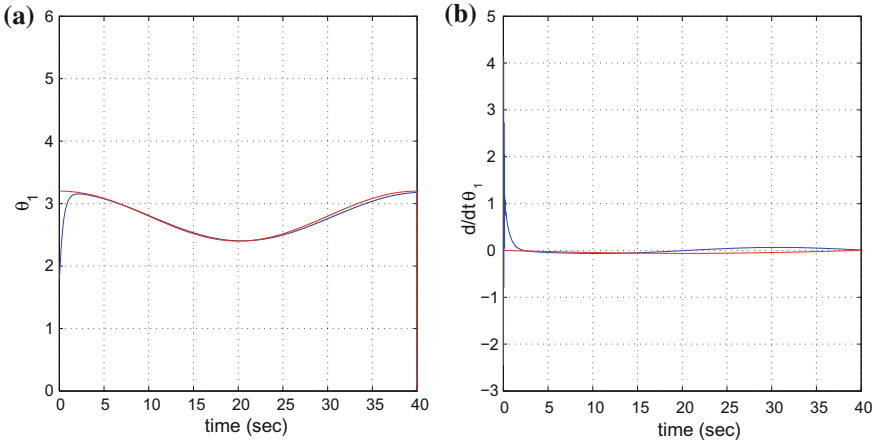

Fig. 1.21 **a** Tracking of a sinusoidal reference setpoint by the joints θ_1 of a 2-DOF planar robot manipulator, **b** angular velocity $\dot{\theta}_1$

The tracking accuracy of the presented control method (H_∞) was compared against the one of the computed torque method (CT) in the case of several reference setpoints (path 1: a constant angle setpoint, path 2: a linearly increasing angle setpoint, path 3; a sinusoidal angle setpoint). The obtained results are given in Tables 1.2 and 1.3. The proposed nonlinear H-infinity control method was based on approximate linearization of the dynamic model of the robot, whereas the computed torque method made use of global linearization. Despite this the performance of the nonlinear H-infinity control was equally good to the performance of control based on the computed torque method.

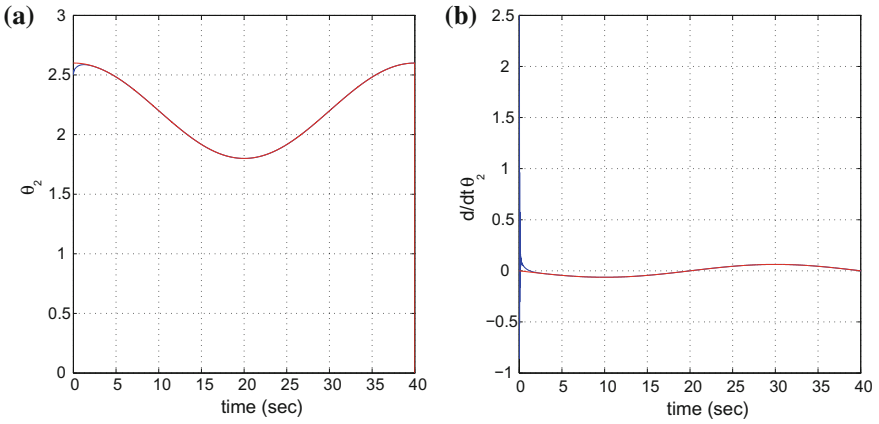

Fig. 1.22 **a** Tracking of a sinusoidal reference setpoint by the joints θ_2 of a 2-DOF planar robot manipulator, **b** angular velocity $\dot{\theta}_2$

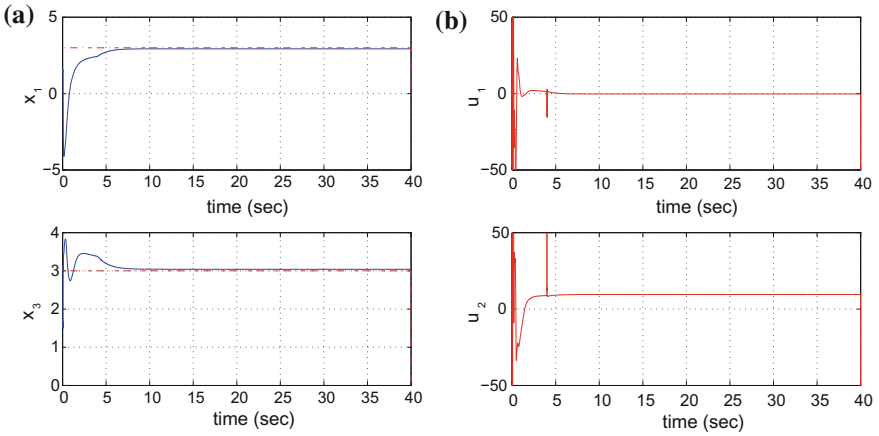

Fig. 1.23 **a** Tracking of a constant reference setpoint by the joints $x_1 = \theta_1$ and $x_3 = \theta_2$ of a 2-DOF robot manipulator that was subjected to gravitational forces, **b** the associated control inputs u_1 and u_2

The tracking performance of the nonlinear H-infinity control method for the model of the 2-DOF manipulator and under additive disturbances affecting element $g_{a,2}(x)$ of the input gain functions $g_a(x)$ of Eq. (1.84) is outlined in Table 1.4. It can be noticed that despite model perturbations the tracking accuracy of the control method remained satisfactory.

Comparison of the proposed control method to PD or PID controllers can confirm the improved performance and reliability of nonlinear H-infinity control. Actually, when PD or PID controllers are applied to nonlinear dynamical systems, such as robotic manipulators, global asymptotic stability of the control loop usually cannot

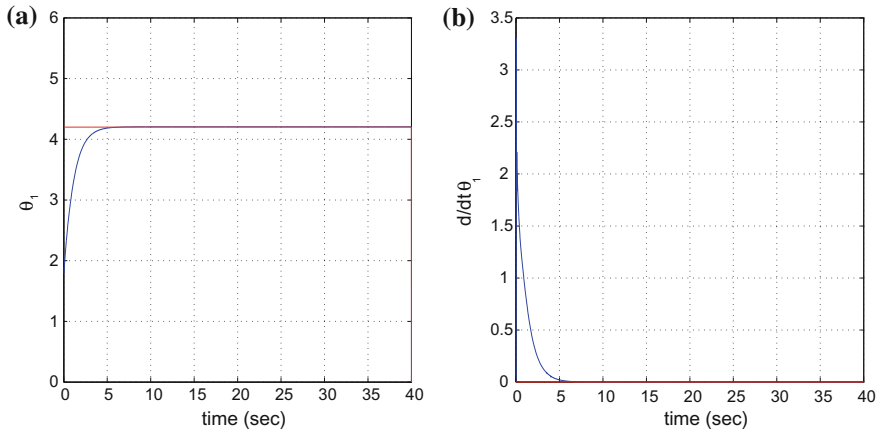

Fig. 1.24 **a** Tracking of a constant reference setpoint by the joint θ_1 of a 2-DOF robot manipulator that was subjected to gravitational forces, **b** angular velocity $\dot{\theta}_1$

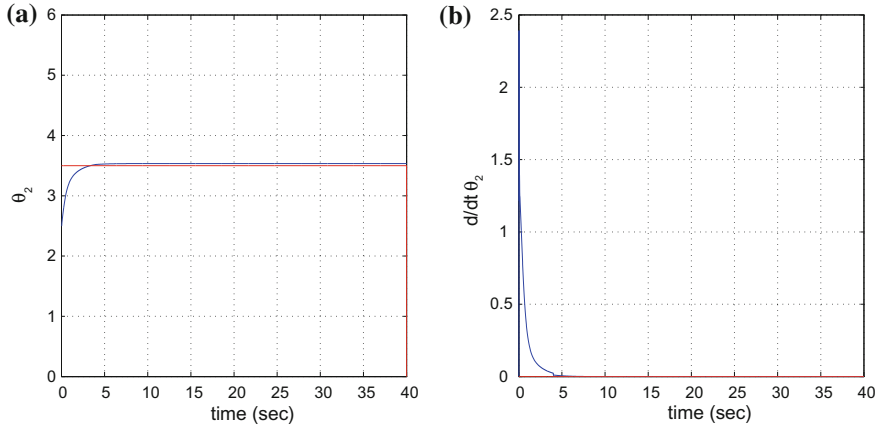

Fig. 1.25 **a** Tracking of a constant reference setpoint by the joint θ_2 of a 2-DOF robot manipulator that was subjected to gravitational forces, **b** angular velocity $\dot{\theta}_2$

be proven. The functioning of PID controllers remains valid only at local operating points (equilibria) where the nonlinear system can be approximated by an equivalent robotic model. When the operating conditions change or when the robotic system is subject to modelling uncertainty or to external perturbations, the stability of the control loop is likely to be lost. On the other hand, the nonlinear H-infinity control of the robotic manipulator is proven to have global asymptotic stability properties and to be robust as described by the H-infinity tracking performance criterion of Eq. (1.152).

The improved performance of nonlinear H-infinity control comparing to LQR/LQG control can be also confirmed. The LQR control method is the solution to the

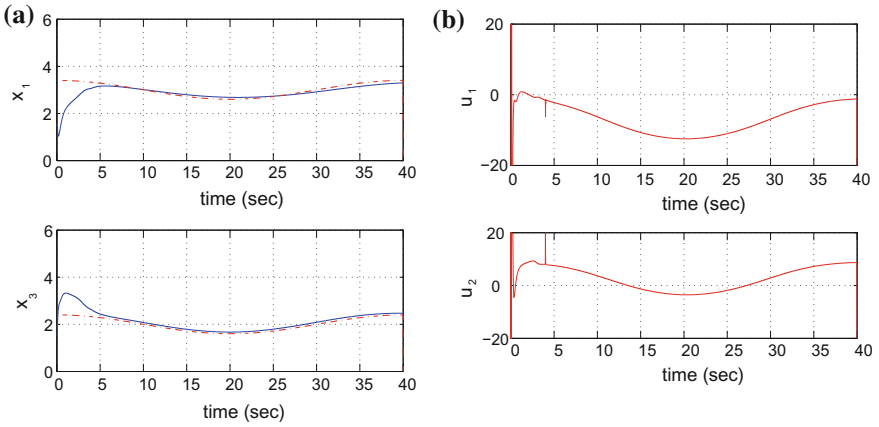

Fig. 1.26 **a** Tracking of a sinusoidal reference setpoint by the joints $x_1 = \theta_1$ and $x_3 = \theta_2$ of a 2-DOF planar robot manipulator that was subjected to gravitational forces, **b** the associated control inputs u_1 and u_2

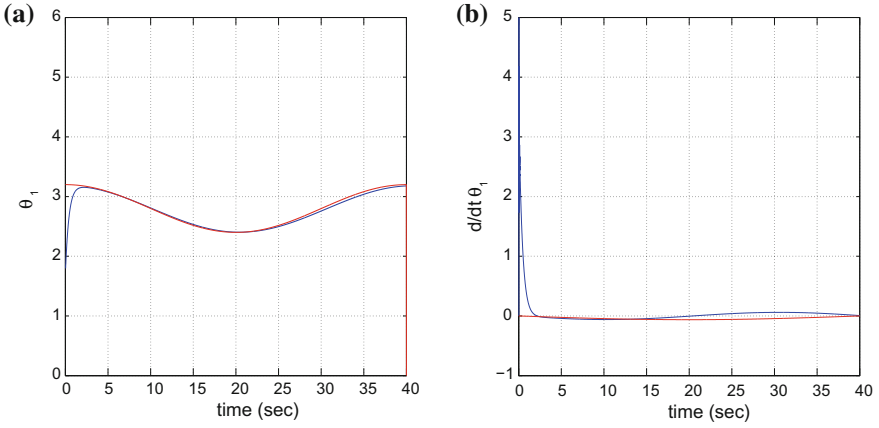

Fig. 1.27 **a** Tracking of a sinusoidal reference setpoint by the joint θ_1 of a 2-DOF robot manipulator that was subjected to gravitational forces, **b** angular velocity $\dot{\theta}_1$

optimal control method according to Bellman's optimality principle and following minimization of the associated Hamiltonian of the system (the latter consisting of a first term representing a quadratic cost function and of a second term representing the state-space equation of the system). The LQG control approach is the solution of the joint optimal control and optimal state estimation problem (Kalman Filtering) for linear dynamical systems. The solution of the optimal control problem through LQR is possible provided that the system's state-space equation is a linear one and provided also that no external disturbances or model uncertainty terms exist in the system's dynamics. On the other side the solution of the optimal control problem

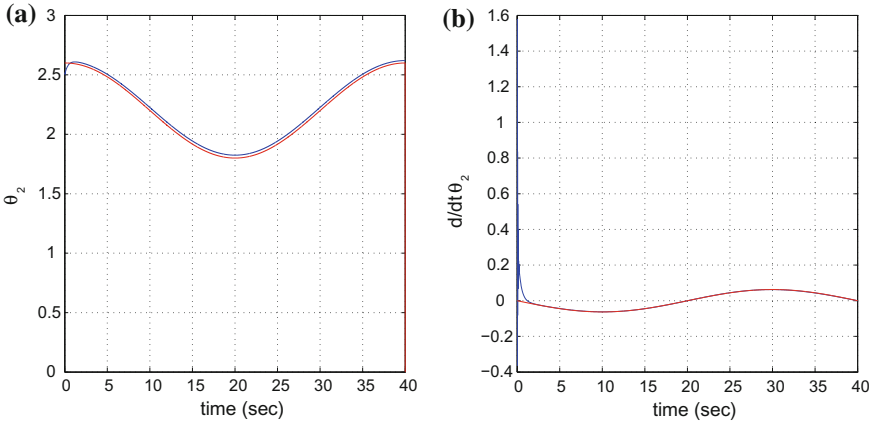

Fig. 1.28 **a** Tracking of a sinusoidal reference setpoint by the joint θ_2 of a 2-DOF robot manipulator that was subjected to gravitational forces, **b** angular velocity $\dot{\theta}_2$

Table 1.2 RMSE of the robot's state variables (planar robot)

No	RMSEx_1	RMSEx_2	RMSEx_3	RMSEx_4
path 1 CT	$8.4{\cdot}10^{-3}$	$0.1{\cdot}10^{-3}$	$7.0{\cdot}10^{-3}$	$0.1{\cdot}10^{-3}$
path 1 H_∞	$8.4{\cdot}10^{-3}$	$0.1{\cdot}10^{-3}$	$7.0{\cdot}10^{-3}$	$0.1{\cdot}10^{-3}$
path 2 CT	$9.2{\cdot}10^{-3}$	$0.1{\cdot}10^{-3}$	$7.8{\cdot}10^{-3}$	$0.1{\cdot}10^{-3}$
path 2 H_∞	$9.2{\cdot}10^{-3}$	$0.1{\cdot}10^{-3}$	$7.8{\cdot}10^{-3}$	$0.1{\cdot}10^{-3}$
path 3 CT	$4.8{\cdot}10^{-3}$	$1.1{\cdot}10^{-3}$	$3.6{\cdot}10^{-3}$	$0.1{\cdot}10^{-3}$
path 3 H_∞	$4.8{\cdot}10^{-3}$	$1.0{\cdot}10^{-3}$	$3.6{\cdot}10^{-3}$	$0.1{\cdot}10^{-3}$

in case that the robotic system is characterized by nonlinear dynamics is a non-trivial problem and the iterative optimization solutions which have been proposed for it are not always of assured convergence to a minimum. The nonlinear optimal control problem becomes much more complicated when the system is subject to model uncertainty and external perturbations. The present section has proposed a solution to the nonlinear optimal control problem under model uncertainties and external perturbations. The method is of proven stability and robustness. This control approach is based on approximate linearization of the nonlinear system's dynamics around a temporary equilibrium that is recomputed at each iteration of the control algorithm. It has been proven that the state vector of the system is made to converge to the temporary equilibrium while progressively the equilibrium also converges to the reference trajectories. This comes to explain the stability and convergence to optimum properties of the proposed control method.

Table 1.3 RMSE of the robot's state variables (cartesian space)

No	RMSEx_1	RMSEx_2	RMSEx_3	RMSEx_4
path 1 CT	$8.4{\cdot}10^{-3}$	$0.1{\cdot}10^{-3}$	$7.0{\cdot}10^{-3}$	$0.1{\cdot}10^{-3}$
path 1 H_∞	$8.4{\cdot}10^{-3}$	$0.1{\cdot}10^{-3}$	$7.2{\cdot}10^{-3}$	$0.1{\cdot}10^{-3}$
path 2 CT	$9.2{\cdot}10^{-3}$	$0.1{\cdot}10^{-3}$	$7.8{\cdot}10^{-3}$	$0.1{\cdot}10^{-3}$
path 2 H_∞	$9.6{\cdot}10^{-3}$	$0.1{\cdot}10^{-3}$	$7.9{\cdot}10^{-3}$	$0.1{\cdot}10^{-3}$
path 3 CT	$5.8{\cdot}10^{-3}$	$0.5{\cdot}10^{-3}$	$3.6{\cdot}10^{-3}$	$0.1{\cdot}10^{-3}$
path 3 H_∞	$5.3{\cdot}10^{-3}$	$0.9{\cdot}10^{-3}$	$4.0{\cdot}10^{-3}$	$0.1{\cdot}10^{-3}$

Table 1.4 RMSE of state variables under model disturbance

No	% change	RMSEx_1	RMSEx_2	RMSEx_3	RMSEx_4
1	0	$8.4{\cdot}10^{-3}$	$0.1{\cdot}10^{-3}$	$7.2{\cdot}10^{-3}$	$0.1{\cdot}10^{-4}$
2	50	$8.4{\cdot}10^{-3}$	$0.1{\cdot}10^{-3}$	$7.3{\cdot}10^{-3}$	$0.1{\cdot}10^{-4}$
3	100	$8.4{\cdot}10^{-3}$	$0.1{\cdot}10^{-3}$	$7.8{\cdot}10^{-3}$	$0.1{\cdot}10^{-4}$
4	150	$8.4{\cdot}10^{-3}$	$0.1{\cdot}10^{-3}$	$8.7{\cdot}10^{-3}$	$0.1{\cdot}10^{-4}$
5	200	$8.4{\cdot}10^{-3}$	$0.1{\cdot}10^{-3}$	$9.4{\cdot}10^{-3}$	$0.1{\cdot}10^{-4}$

1.5 Model-Based Control of Rigid-Link Manipulators Under Time-Delays

1.5.1 Outline

The previous sections have analyzed the problem of embedded control of the robotic manipulator, meaning that the controller and the actuators were both on the robot's side. Unlike this, networked control schemes arise when the robot is teleoperated and the controller is separately placed from the robot's actuators, at a distant location. Networked control of robotic manipulators is a non-trivial problem and up to now several approaches for its solution have been attempted. One can distinguish: (i) global linearization-based control methods which try to develop linearizing transformations of the system's state-space description capable of incorporating the effects of time-delays either to the control input's and to the system's outputs or to the system's state variables [61, 64, 65, 147, 321, 468] (ii) approximate linearization-based control methods which take into account the presence of time delays in the linearization they perform around local operating points on the system's state-space description [178, 200] (iii) Lyapunov-based control methods which dynamically adapt the controller's gains aiming at compensating for model uncertainty and time-delays effects [300, 397] (iv) the use of filters as smoothers that incorporate delayed measurements in the estimation procedure about the system's state vector (v) the use of filters as predictors that give a several steps-ahead estimate of the system's state variables which is turn is used for the computation of the control input. In particular the use of

diffeomorphisms (state variable transformations) for treating the problems of time-delays in the design of controllers and state estimators has been analyzed in [63, 161, 185, 537, 644]. Several findings about the design of state-observers for dynamical systems subject to time delays can be also found in [160, 165, 585, 642, 643, 645]

In the present section a control method is developed, for the compensation of time-delays effects in the control loop of robotic manipulators, after making use of differential flatness theory and of the associated global linearization of the robot's dynamics [145, 267, 465, 467, 519, 572]. By performing Taylor-series expansion to the control terms of the robotic manipulator which are subject to time-delays, the time-derivative of its control variables emerge as new control inputs. Next, dynamic extension is implemented which means that the state vector of the manipulator is extended by introducing as additional state-vector elements the initial control inputs of the system. The extended state-space description of the robotic manipulator is shown to be differentially flat and this signifies that it can be transformed into an input-output linearized form. In its latter linearized description the design of a stabilizing state feedback controller becomes possible [450, 457, 459].

Moreover, it is shown that unknown time-delays in the control inputs and the measured outputs of the manipulator can be represented as additive disturbance terms affecting the robot. For the compensation of such perturbations, which are induced by time-delays, the Derivative-free nonlinear Kalman Filter is used as a disturbance observer. This filter consists of the implementation of the Kalman Filter on the linearized equivalent model of the robot [33, 431, 463]. It also comprises an inverse transformation based on differential flatness diffeomorphisms that provides estimates of the state variables in the initial nonlinear dynamics of the robot. Under the form of a disturbance observer, the Derivative-free nonlinear Kalman Filter provides real-time estimates of the unknown perturbations that affect the manipulator's control inputs and which are due time-delays in the robot's dynamic model. By obtaining accurate estimates of these cumulative disturbance terms their compensation becomes also possible. The global stability properties of the control scheme are proven.

1.5.2 State-Space Description of the Robotic Manipulator

The dynamic model of the robotic manipulator is given by

$$D(\theta)\ddot{\theta} + h(\theta, \dot{\theta}) + g(\theta) = T(t - \tau) \tag{1.156}$$

where, $\theta \in R^{n\times 1}$, is the vector of the joints angles, $\dot{\theta} \in R^{n\times 1}$, is the vector of the joints angular velocities, $D(\theta) \in R^{n\times n}$ is the inertia matrix, $h(\theta, \dot{\theta}) \in R^{n\times 1}$ is the Coriolis and centrifugal terms matrix and $g(\theta) \in R^{n\times 1}$ is the gravitational terms matrix, whereas $T(t - \tau) \in R^{n\times 1}$ is the joint torques vector subjected to a time-delay equal to τ. Equivalently, one has

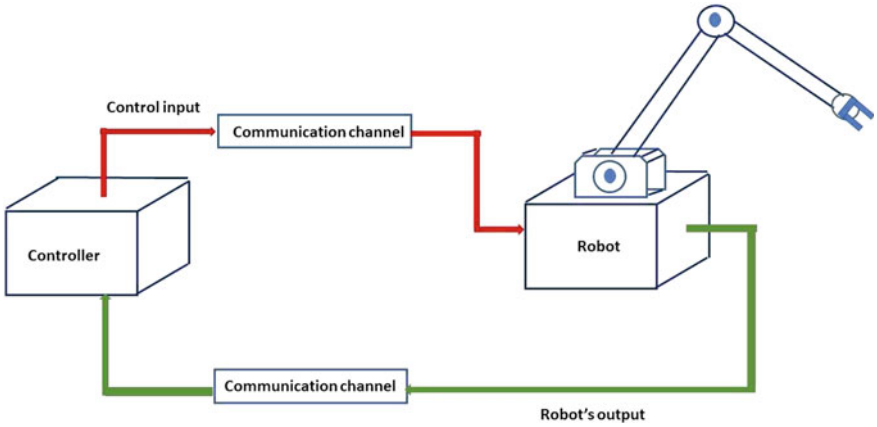

Fig. 1.29 Networked control of the robotic manipulator under input/output delays

$$\ddot{\theta} = -D^{-1}(\theta)h(\theta, \dot{\theta}) - D^{-1}(\theta)g(\theta) + D^{-1}(\theta)T(t-\tau) \tag{1.157}$$

The torques vector $T(t-\tau)$ which constitutes the control input of the system is expanded with the first-order Taylor series method around the present time instant t, thus giving

$$\begin{aligned} T(t-\tau) &= T(t) + \dot{T}(t)(\tfrac{-\tau}{1!}) \Rightarrow \\ T(t-\tau) &= T(t) - \tau\dot{T}(t) \end{aligned} \tag{1.158}$$

To solve the control problem of the robotic manipulator under time-delays the concept of dynamic extension is applied. This means that the robot's state vector $x = [\theta_1, \dot{\theta}_1, \theta_2, \dot{\theta}_2, \ldots, \theta_n, \dot{\theta}_n]$ is extended by including as additional state variables in it, the elements of the control input. Thus, the extended state vector becomes $x_e = [\theta_1, \dot{\theta}_1, \theta_2, \dot{\theta}_2, \ldots, \theta_n, \dot{\theta}_n, T_1, T_2, \ldots, T_n]$.

The dynamic model of the 2-DOF rigid-link robot which is depicted again in Fig. 1.29. As noted above, and under the assumption that the masses of the links are concentrated at the links' end the dynamic model of the manipulator is given by

$$D(\theta)\ddot{\theta} + h(\theta, \dot{\theta}) + g(\theta) = T(t-\tau) \tag{1.159}$$

where $D(\theta)$ is the inertia matrix

$$D(\theta) = \begin{pmatrix} (m_1+m_2)l_1^2 + m_1 l_2^2 + 2m_2 l_1 l_2 cos(\theta_2) & m_2 l_2^2 + m_2 l_1 l_2 cos(\theta_2) \\ m_2 l_2^2 + m_2 l_1 l_2 cos(\theta_2) & m_2 l_2 (l_1 + l_2) cos(\theta_2) \end{pmatrix} \tag{1.160}$$

$h(\theta, \dot{\theta})$ is the Coriolis and centrifugal forces vector

$$h(\theta, \dot{\theta}) = \begin{pmatrix} -m_2 l_1^2 sin(\theta_2)\dot{\theta}_2^2 - 2m_2 l_1^2 sin(\theta_2)\dot{\theta}_1\dot{\theta}_2 \\ m_2 l_1^2 sin(\theta_2)\dot{\theta}_1^2 \end{pmatrix} \tag{1.161}$$

$g(\theta)$ is the gravitational forces vector

$$g(\theta) = \begin{pmatrix} (m_1 + m_2) g l_1 cos(\theta_1) + m_2 g l_2 cos(\theta_1 + \theta_2) \\ m_2 g l_2 cos(\theta_1 + \theta_2) \end{pmatrix} \tag{1.162}$$

and $\tau(t)$ is the control inputs vector consisting of the torques that are generated by the motors mounted on the robot's joints.

Following the stages previously presented about the inversion of the inertia matrix $D^{-1}(\theta)$ and about the computation of the products $D^{-1}(\theta)h(\theta, \dot{\theta})$ and $D^{-1}(\theta)g(\theta)$, the state-space equations of the robotic model are

$$\begin{pmatrix} \ddot{x}_1 \\ \ddot{x}_3 \end{pmatrix} = -D^{-1}(\theta)h(\theta, \dot{\theta}) - D^{-1}(\theta)g(\theta) - D^{-1}(\theta)T(t - \tau) \tag{1.163}$$

and using that the state vector is $x = [x_1, x_2, x_3, x_4]^T = [\theta_1, \dot{\theta}_1, \theta_2, \dot{\theta}_2]^T$ and the control inputs vector is $T(t - \tau) = [T_1(t - \tau), T_2(t - \tau)]^T = [u_1, u_2]^T$ this is also written in the form

$$\dot{x} = f(x) + g_a(x)u_1 + g_b(x)u_2 \tag{1.164}$$

or equivalently

$$\begin{pmatrix} \dot{x}_1 \\ \dot{x}_2 \\ \dot{x}_3 \\ \dot{x}_4 \end{pmatrix} = \begin{pmatrix} f_1 \\ f_2 \\ f_3 \\ f_4 \end{pmatrix} + \begin{pmatrix} g_{a_1} \\ g_{a_2} \\ g_{a_3} \\ g_{a_4} \end{pmatrix} u_1 + \begin{pmatrix} g_{b_1} \\ g_{b_2} \\ g_{b_3} \\ g_{b_4} \end{pmatrix} u_2 \tag{1.165}$$

with

$$f_1 = x_2 \tag{1.166}$$

$$f_2 = -\frac{2cos(x_3)[-sin(x_3)x_4^2 - 2sin(x_3)x_2x_4] + [-1 + cos(x_3)]sin(x_3)x_2^2}{4cos(x_3) + 3cos^2(x_3) - 1} - \\ - \frac{2cos(x_3)[10cos(x_1) + 10cos(x_1 + x_3)] + [-1 + cos(x_3)][10cos(x_1 + x_3)]}{4cos(x_3) + 3cos^2(x_3) - 1} \tag{1.167}$$

$$f_3 = x_4 \tag{1.168}$$

$$f_4 = -\frac{[1+cos(x_3)][-sin(x_3)x_4^2 - 2sin(x_3)x_2x_4] + [2+2cos(x_3)]sin(x_3)x_2^2}{4cos(x_3)+3cos^2(x_3)-1} \\ -\frac{[-1+cos(x_3)][10cos(x_1)+10cos(x_1+x_3)] + [2+2cos(x_3)]10cos(x_1+x_3)}{4cos(x_3)+3cos^2(x_3)-1} \tag{1.169}$$

Moreover, one has

$$\begin{array}{cc} g_{a_1} = 0 & g_{b_1} = 0 \\ g_{a_2} = \dfrac{2cos(x_3)}{4cos(x_3)+3cos^2(x_3)-1} & g_{b_2} = \dfrac{-1cos(x_3)}{4cos(x_3)+3cos^2(x_3)-1} \\ g_{a_3} = 0 & g_{b_3} = 0 \\ g_{a_4} = \dfrac{-1+cos(x_3)}{4cos(x_3)+3cos^2(x_3)-1} & g_{b_4} = \dfrac{2+2cos(x_3)}{4cos(x_3)+3cos^2(x_3)-1} \end{array} \tag{1.170}$$

1.5.3 Control of the Robotic Manipulator Under Known Time Delays

1.5.3.1 State-Space Description of the Robot Under Time Delays

About the time-delayed control inputs of the manipulator $u_1 = T_1(t-\tau_1)$ and $u_2 = T_2(t-\tau_2)$, and by denoting as additional state variables $x_5 = T_1(t), x_6 = T_2(t)$, it holds that

$$\begin{array}{c} u_1 = T_1(t) - \tau_1\dot{T}_1(t) \Rightarrow u_1 = x_5 - \tau_1\tilde{u_1} \\ \dot{x}_5 = \tilde{u}_1 \end{array} \tag{1.171}$$

$$\begin{array}{c} u_2 = T_2(t) - \tau_2\dot{T}_2(t) \Rightarrow u_2 = x_6 - \tau_2\tilde{u_2} \\ \dot{x}_6 = \tilde{u}_2 \end{array} \tag{1.172}$$

Thus, the extended state-space model of the 2-DOF robot becomes:

$$\begin{array}{c} \dot{x}_1 = x_2 \\ \dot{x}_2 = f_2(x) + g_{a_2}(x)[x_5 - \tau_1\tilde{u}_1] + g_{b_2}(x)[x_6 - \tau_2\tilde{u}_2] \\ \dot{x}_3 = x_4 \\ \dot{x}_4 = f_4(x) + g_{a_4}(x)[x_5 - \tau_1\tilde{u}_1] + g_{b_4}(x)[x_6 - \tau_2\tilde{u}_2] \\ \dot{x}_5 = \tilde{u}_1 \\ \dot{x}_6 = \tilde{u}_2 \end{array} \tag{1.173}$$

1.5.4 Differential Flatness of the Robot's Model

The flat outputs of the robotic system under time delays are taken to be $y = [y_1, y_2] = [x_1, x_3]$. From the first row of the state-space model of Eq. (1.173) one has

$$x_2 = \dot{x_1} \Rightarrow x_2 = h_a(y, \dot{y}) \tag{1.174}$$

From the third row of the state-space model of Eq. (1.173) one has

$$x_4 = \dot{x_3} \Rightarrow x_2 = h_b(y, \dot{y}) \tag{1.175}$$

From the second and fourth row of the state-space model of Eq. (1.173) one has

$$\begin{pmatrix} \dot{x}_2 \\ \dot{x}_4 \end{pmatrix} = \begin{pmatrix} f_2(x) + g_{a_2}(x)x_5 + g_{b_2}(x)x_6 \\ f_4(x) + g_{a_4}(x)x_5 + g_{b_4}(x)x_6 \end{pmatrix} + \begin{pmatrix} g_{a_2}(x)(-\tau_1) & g_{b_2}(x)(-\tau_2) \\ g_{a_4}(x)(-\tau_1) & g_{b_4}(x)(-\tau_2) \end{pmatrix} \begin{pmatrix} \tilde{u}_1 \\ \tilde{u}_2 \end{pmatrix} \tag{1.176}$$

By considering x_5 and x_6 as time-varying parameters for the model of the first four state space equations (zero dynamics) one can solve Eq. (1.176) with respect to $\tilde{u}_1$ and $\tilde{u}_2$, thus obtaining

$$\begin{pmatrix} \tilde{u}_1 \\ \tilde{u}_2 \end{pmatrix} = \begin{pmatrix} g_{a_2}(x)(-\tau_1) & g_{b_2}(x)(-\tau_2) \\ g_{a_4}(x)(-\tau_1) & g_{b_4}(x)(-\tau_2) \end{pmatrix}^{-1} \{ \begin{pmatrix} \dot{x}_2 \\ \dot{x}_4 \end{pmatrix} - \begin{pmatrix} f_2(x) + g_{a_2}(x)x_5 + g_{b_2}(x)x_6 \\ f_4(x) + g_{a_4}(x)x_5 + g_{b_4}(x)x_6 \end{pmatrix} \} \tag{1.177}$$

The previous equation signifies that

$$\tilde{u}_1 = h_c(y, \dot{y}) \;\; \tilde{u}_2 = h_d(y, \dot{y}) \tag{1.178}$$

Consequently, all state variables and the control inputs of the robotic manipulator's model are written as differential functions of the flat output, and the robotic model is a differentially flat one.

1.5.4.1 Transformation of the Robot's Model into an Input-Output Linearized Form

By proving that the model of the robotic manipulator is a differentially flat one its transformation into an input-output linearized form is possible (Lie-Backlund equivalence). The second and the fourth row of the previous state-space model of the 2-DOF robotic manipulator are rewritten as

$$\begin{aligned}\ddot{x}_1 &= [f_2(x) + g_{a_2}(x)x_5 + g_{b_2}(x)x_6] - \tau_1 g_{a_2}(x)\tilde{u}_1 - \tau_2 g_{b_2}(x)\tilde{u}_2 \\ \ddot{x}_3 &= [f_4(x) + g_{a_4}(x)x_5 + g_{b_4}(x)x_6] - \tau_1 g_{a_4}(x)\tilde{u}_1 - \tau_2 g_{b_4}(x)\tilde{u}_2\end{aligned} \tag{1.179}$$

and by defining $F_1 = [f_2(x) + g_{a_2}(x)x_5 + g_{b_2}(x)x_6]$, $G_{11}(x) = -\tau_1 g_{a_2}(x)$, $G_{12} = -\tau_2 g_{b_2}(x)$ as well as $F_2(x) = [f_4(x) + g_{a_4}(x)x_5 + g_{b_4}(x)x_6]$, $G_{21} = -\tau_2 g_{a_4}(x)$, $G_{22} = -\tau_2 g_{b_4}(x)$, the previous dynamic model is rewritten as

$$\begin{aligned}\ddot{x}_1 &= F_1(x) + G_{11}(x)\tilde{u}_1 + G_{12}(x)\tilde{u}_2 \\ \ddot{x}_3 &= F_2(x) + G_{21}(x)\tilde{u}_1 + G_{22}(x)\tilde{u}_2\end{aligned} \tag{1.180}$$

or in matrix form

$$\begin{pmatrix}\ddot{x}_1 \\ \ddot{x}_3\end{pmatrix} = \begin{pmatrix}F_1(x) \\ F_2(x)\end{pmatrix} + \begin{pmatrix}G_{11}(x) & G_{12}(x) \\ G_{21}(x) & G_{22}(x)\end{pmatrix}\begin{pmatrix}\tilde{u}_1 \\ \tilde{u}_2\end{pmatrix} \tag{1.181}$$

The following notation is used $v_1 = F_1 + G_{11}\tilde{u}_1 + G_{12}\tilde{u}_2$ and $v_2 = F_2 + G_{21}\tilde{u}_1 + G_{22}\tilde{u}_2$. The stabilizing feedback control that is exerted on the robot is

$$\begin{aligned}v_1 &= \ddot{x}_1^d - K_{d_1}(\dot{x}_1 - \dot{x}_1^d) - K_{p_1}(x_1 - x_1^d) \\ v_2 &= \ddot{x}_3^d - K_{d_2}(\dot{x}_3 - \dot{x}_3^d) - K_{p_2}(x_3 - x_3^d)\end{aligned} \tag{1.182}$$

where the feedback control gains $K_{p_i} > 0, \quad i = 1, 2$ and $K_{d_i} > 0, \quad i = 1, 2$ are chosen such that the associated characteristic polynomials become Hurwitz stable, that is $\ddot{e}_1 + K_{d_1}\dot{e}_1 + K_{p_1}e_1 = 0$ and $\ddot{e}_3 + K_{d_2}\dot{e}_3 + K_{p_2}e_3 = 0$.

The control input variables $\tilde{u}_1$ and $\tilde{u}_2$ are computed next from the following relation

$$\begin{pmatrix}\tilde{u}_1 \\ \tilde{u}_2\end{pmatrix} = \begin{pmatrix}G_{11} & G_{12} \\ G_{21} & G_{22}\end{pmatrix}^{-1}\begin{pmatrix}v_1 - F_1 \\ v_2 - F_2\end{pmatrix} \tag{1.183}$$

Finally, the control inputs that are exerted on the robotic system comprise the integrals of $\tilde{u}_1$ and $\tilde{u}_2$, that is $u_1 = \int_0^t \tilde{u}_1(t)dt$ and $u_2 = \int_0^t \tilde{u}_2(t)dt$.

1.5.5 Control of the Robot Under Unknown Time Delays

Next, the case in which time-delays τ_1, τ_2 are unknown or subject to uncertainty, is considered. The model of the robotic manipulator given in Eq. (1.180) is re-examined and uncertainty about the time delays τ_1 and τ_2 is assumed. This in-turn incurs perturbation terms at the control input gains of the dynamic model of the robot. Thus, it holds that

$$\begin{aligned}\ddot{x}_1 &= [f_2(x) + g_{a_2}(x)x_5 + g_{b_2}(x)x_6] - [\tau_1 + \Delta\tau_1]g_{a_2}(x)\tilde{u}_1 - [\tau_2 + \Delta\tau_2]g_{b_2}(x)\tilde{u}_2 \\ \ddot{x}_3 &= [f_4(x) + g_{a_4}(x)x_5 + g_{b_4}(x)x_6] - [\tau_1 + \Delta\tau_1]g_{a_4}(x)\tilde{u}_1 - [\tau_2 + \Delta\tau_2]g_{b_4}(x)\tilde{u}_2\end{aligned} \tag{1.184}$$

The previous state-space representation is also written as

$$\begin{aligned}\ddot{x}_1 &= [f_2(x) + g_{a_2}(x)x_5 + g_{b_2}(x)x_6] - \tau_1 g_{a_2}(x)\tilde{u}_1 - \\ &\quad -\tau_2 g_{b_2}(x)\tilde{u}_2 - \Delta\tau_1 g_{a_2}(x)\tilde{u}_1 - \Delta\tau_2 g_{b_2}(x)\tilde{u}_2 \\ \ddot{x}_3 &= [f_4(x) + g_{a_4}(x)x_5 + g_{b_4}(x)x_6] - \tau_1 g_{a_4}(x)\tilde{u}_1 - \\ &\quad -\tau_2 g_{b_4}(x)\tilde{u}_2 - \Delta\tau_1 g_{a_4}(x)\tilde{u}_1 - \Delta\tau_2 g_{b_4}(x)\tilde{u}_2\end{aligned} \tag{1.185}$$

or equivalently it can be written in the form

$$\begin{aligned}\ddot{x}_1 &= F_1 + G_{11}\tilde{u}_1 + G_{12}\tilde{u}_2 - \Delta G_{11}\tilde{u}_1 - \Delta G_{12}\tilde{u}_2 \\ \ddot{x}_3 &= F_2 + G_{21}\tilde{u}_1 + G_{22}\tilde{u}_2 - \Delta G_{21}\tilde{u}_1 - \Delta G_{22}\tilde{u}_2\end{aligned} \tag{1.186}$$

First, the following disturbance terms due to time delays of the control inputs are defined: $\tilde{d_{b_1}} = -\Delta G_{11}\tilde{u}_1 - \Delta G_{12}\tilde{u}_2$ and $\tilde{d_{b_2}} = -\Delta G_{21}\tilde{u}_1 - \Delta G_{22}\tilde{u}_2$.

Moreover, by considering time delays in the feedback of the robot's output to the controller one can define: $v_1 + \tilde{d_{a_1}} = F_1 + G_{11}\tilde{u}_1 + G_{12}\tilde{u}_2$, and $v_2 + \tilde{d_{a_2}} = F_2 + G_{21}\tilde{u}_1 + G_{22}\tilde{u}_2$.

Consequently, one obtains the following compact form of the robotic manipulator's dynamics under variable time delays:

$$\begin{aligned}\ddot{x}_1 &= v_1 + \tilde{d_{a_1}} + \tilde{d_{b_1}} \Rightarrow \ddot{x}_1 = v_1 + \tilde{d}_1 \\ \ddot{x}_3 &= v_2 + \tilde{d_{a_2}} + \tilde{d_{b_2}} \Rightarrow \ddot{x}_3 = v_2 + \tilde{d}_2\end{aligned} \tag{1.187}$$

In such a case the stabilizing control input requires a precise estimation of the aggregate disturbance terms $\tilde{d}_1$ and $\tilde{d}_2$ and takes the form:

$$\begin{aligned}v_1 &= \ddot{x}_1^d - K_{d_1}(\dot{x}_1 - \dot{x}_1^d) - K_{p_1}(x_1 - x_1^d) - \hat{\tilde{d}}_1 \\ v_2 &= \ddot{x}_2^d - K_{d_2}(\dot{x}_2 - \dot{x}_2^d) - K_{p_2}(x_2 - x_2^d) - \hat{\tilde{d}}_2\end{aligned} \tag{1.188}$$

These estimates can be obtained with the use of a Kalman Filter-based disturbance observer. This approach is known as Derivative-free nonlinear Kalman Filter because it consists of the Kalman Filter recursion applied to the input-output linearized model of the robotic manipulator that was obtained through the previously analyzed procedure [457].

To compensate for the effects of the unknown time delays, the precise estimation of $\tilde{d}_1$ and $\tilde{d}_2$ is needed. This will be obtained with the use of the above-mentioned Kalman Filter, redesigned as a disturbance observer. It is assumed that $\tilde{d}_1$ and $\tilde{d}_2$ are described by their nth order derivative (for instance $n = 2$) and the associated initial conditions, that is

$$\ddot{\tilde{d}}_1 = f_{d_1} \; \ddot{\tilde{d}}_2 = f_{d_2} \tag{1.189}$$

However, since estimation of $\tilde{d}_1$ and $\tilde{d}_2$ is going to be performed with the use of stochastic filtering, knowledge about initial conditions becomes obsolete. Next, the previously analyzed input-output linearized form of the robotic manipulator, given in Eq. (1.187), is considered. An extended state-space form of the system is obtained by defining the disturbance terms and their time derivatives as additional state variables. Actually, the extended state vector of the system comprises the following state variables: $z_1 = x_1, z_2 = \dot{x}_1, z_3 = x_3, z_4 = \dot{x}_3, z_5 = \tilde{d}_1, z_6 = \dot{\tilde{d}}_1, z_7 = \tilde{d}_2, z_8 = \dot{\tilde{d}}_2$. Next, using Eq. (1.187) and the new definition of state variables the extended state-space description of the system is obtained:

$$\begin{aligned} \dot{z}_1 &= z_2 \quad \dot{z_5} = z_6 \\ \dot{z}_2 &= v_1 + z_5 \; \dot{z_6} = f_{d_1} \\ \dot{z}_3 &= z_4 \quad \dot{z}_7 = z_8 \\ \dot{z}_4 &= v_2 + z_7 \; \dot{z}_8 = f_{d_2} \end{aligned} \tag{1.190}$$

The extended state-space description of the robot can be also written in matrix form

$$\begin{pmatrix} \dot{z}_1 \\ \dot{z}_2 \\ \dot{z}_3 \\ \dot{z}_4 \\ \dot{z}_5 \\ \dot{z}_6 \\ \dot{z}_7 \\ \dot{z}_8 \end{pmatrix} = \begin{pmatrix} 0\,1\,0\,0\,0\,0\,0\,0 \\ 0\,0\,0\,0\,1\,0\,0\,0 \\ 0\,0\,0\,1\,0\,0\,0\,0 \\ 0\,0\,0\,0\,0\,0\,1\,0 \\ 0\,0\,0\,0\,0\,1\,0\,0 \\ 0\,0\,0\,0\,0\,0\,0\,0 \\ 0\,0\,0\,0\,0\,0\,0\,1 \\ 0\,0\,0\,0\,0\,0\,0\,0 \end{pmatrix} \begin{pmatrix} z_1 \\ z_2 \\ z_3 \\ z_4 \\ z_5 \\ z_6 \\ z_7 \\ z_8 \end{pmatrix} + \begin{pmatrix} 0\,0\,0\,0 \\ 1\,0\,0\,0 \\ 0\,0\,0\,0 \\ 0\,1\,0\,0 \\ 0\,0\,0\,0 \\ 0\,0\,1\,0 \\ 0\,0\,0\,0 \\ 0\,0\,0\,1 \end{pmatrix} \begin{pmatrix} v_1 \\ v_2 \\ f_{d_1} \\ f_{d_2} \end{pmatrix} \tag{1.191}$$

while by denoting the state vector of the system as $Z_e = [z_1, z_2, z_3, z_4, z_5, z_6, z_7, z_8]^T$, the measurement equation is obtained from the following relation

$$\begin{pmatrix} z_1^m \\ z_3^m \end{pmatrix} = \begin{pmatrix} 1\,0\,0\,0\,0\,0\,0\,0 \\ 0\,0\,1\,0\,0\,0\,0\,0 \end{pmatrix} Z_e \tag{1.192}$$

Thus, one has a state-space description for the dynamics of the robotic manipulator under time-delays of the inputs and outputs,in the following matrix form:

$$\begin{aligned} \dot{z}_e &= A_e z_e + B_e v_e \\ z_e^m &= C_e z_e \end{aligned} \tag{1.193}$$

For the state-space model of Eq. (1.193) one can perform simultaneous estimation of the non-measurable state vector elements z_2, z_4 as well as estimation of the unknown disturbance terms due to time delays $z_5 = \tilde{d}_1$ and $z_7 = \tilde{d}_2$, with the use of a disturbance observer

$$\begin{aligned} \dot{\hat{z}}_e &= A_o \hat{z}_e + B_o v_o + K_f (z_e^m - \hat{z}_e^m) \\ \hat{z}_e^m &= C_o \hat{z}_e \end{aligned} \tag{1.194}$$

where $A_o = A_e$, $C_o = C_e$ and

$$B_o^T = \begin{pmatrix} 0 & 1 & 0 & 0 & 0 & 0 & 0 & 0 \\ 0 & 0 & 0 & 1 & 0 & 0 & 0 & 0 \end{pmatrix} \tag{1.195}$$

and K_f is the estimator's gain which is obtained by applying the Kalman Filter recursion to the input-output linearized model of the system (Derivative-free nonlinear Kalman Filter). Before implementing Kalman Filtering the state-space model of Eq. (1.194) undergoes discretization with common discretization techniques and its discrete-time equivalent is obtained. The discrete-time equivalents of matrices A_o, B_o and C_o are denoted as A_d, B_d and C_d, respectively. The discrete-time disturbance observer is given by

$$\begin{aligned} \hat{z}_e(k+1) &= A_d \hat{z}_e(k) + B_d v_o(k) + K_f(k)(z_e^m(k) - \hat{z}_e^m(k)) \\ \hat{z}_e^m &= C_d \hat{z}_e(k) \end{aligned} \tag{1.196}$$

The Kalman Filter-based disturbance observer for the state and disturbance estimation problem comprises a *measurement update* and a *time update* stage.

measurement update:

$$\begin{aligned} K_f(k) &= P^-(k) C_d^T [C_d P^-(k) C_d^T + R(k)]^{-1} \\ \hat{x}(k) &= \hat{x}^-(k) + K_f(k)[z_e^m(k) - \hat{z}_e^m(k)] \\ P(k) &= P^-(k) - K_f(k) C_d P^-(k) \end{aligned} \tag{1.197}$$

time update:

$$\begin{aligned} P^-(k+1) &= A_d P(k) A_d^T + Q(k) \\ \hat{x}^-(k+1) &= A_d \hat{x}(k) + B_d v_o(k) \end{aligned} \tag{1.198}$$

where $Q(k)$ is the process noise covariance matrix and $R(k)$ is the measurement noise covariance matrix. By ensuring through the above estimation procedure that $\lim_{t\to\infty} \hat{\tilde{d}}_1 = \tilde{d}_1$ and $\lim_{t\to\infty} \hat{\tilde{d}}_2 = \tilde{d}_2$ one has also the following conditions about elimination of the state variables tracking error

$$\begin{aligned} &\lim_{t\to\infty} x_1(t) = x_1^d(t) \ \lim_{t\to\infty} x_2(t) = x_2^d(t) \\ &\lim_{t\to\infty} x_3(t) = x_3^d(t) \ \lim_{t\to\infty} x_4(t) = x_3^d(t) \end{aligned} \tag{1.199}$$

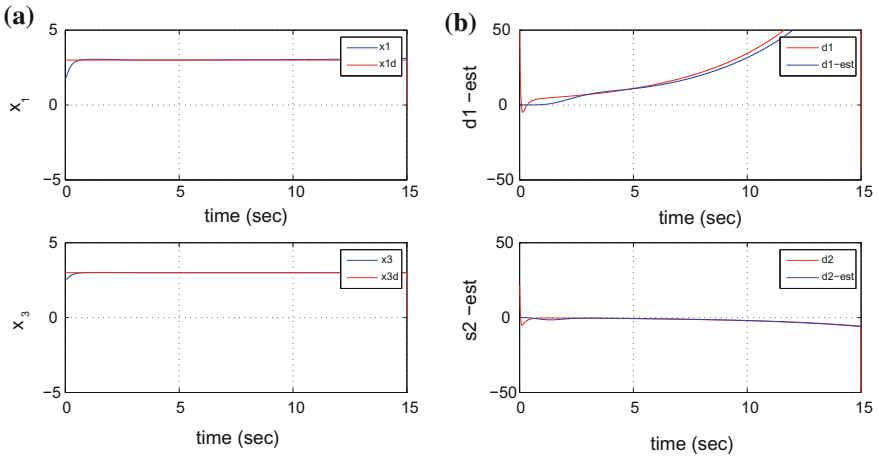

Fig. 1.30 Setpoint 1 - $\tau_1 = 0.29$ s, $\Delta\tau_1 = 0.18$ s, $\tau_2 = 0.27$ s, $\Delta\tau_2 = 0.18$ s: **a** Convergence of the joint angles of the robot x_1, x_3 to the reference setpoints **b** Estimation of disturbance terms d_1, d_2 which are due to the uncertainty about time delays $\Delta\tau_1$, $\Delta\tau_2$

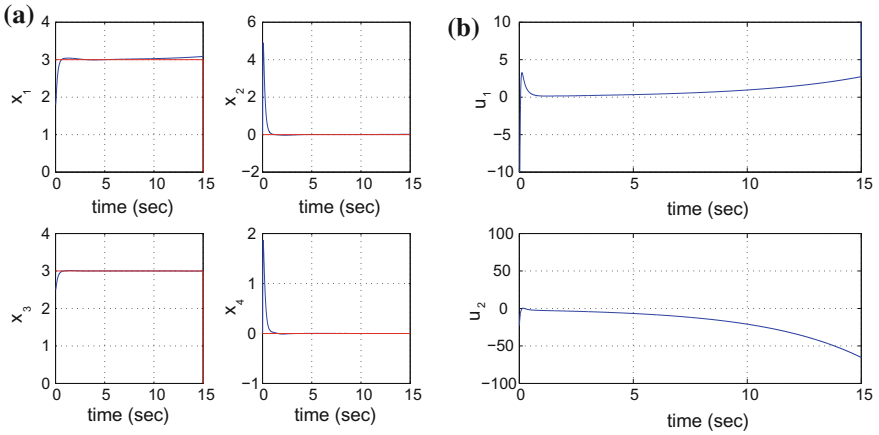

Fig. 1.31 Setpoint 1 - $\tau_1 = 0.29$ s, $\Delta\tau_1 = 0.18$ s, $\tau_2 = 0.27$ s, $\Delta\tau_2 = 0.18$ s: **a** Convergence of state variables x_1 to x_4 of the robotic manipulator to the reference setpoints **b** Control inputs $\tilde{u}_1, \tilde{u}_2$ of the extended state-space model of the robot

which means that both the position and angular velocity tracking errors for the robot's joints are eliminated, despite the existence of time-delays.

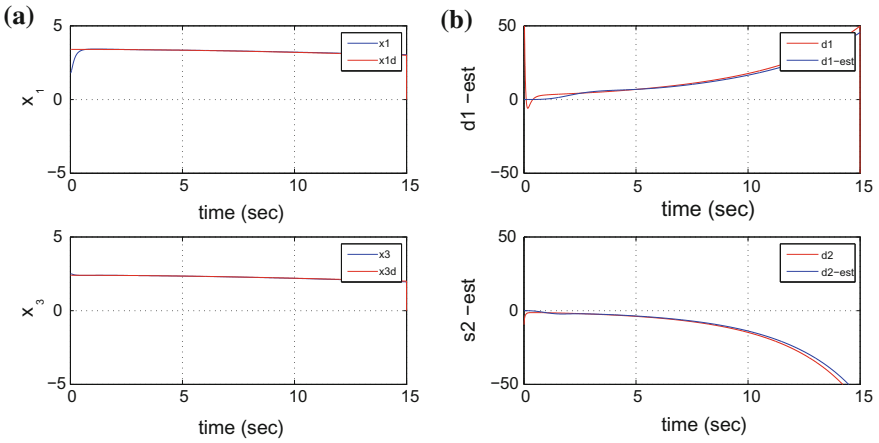

Fig. 1.32 (Setpoint 2 - $\tau_1 = 0.29$ s, $\Delta\tau_1 = 0.19$ s, $\tau_2 = 0.27$ s, $\Delta\tau_2 = 0.17$ s: **a** Convergence of the joint angles of the robot x_1, x_3 to the reference setpoints **b** Estimation of disturbance terms d_1, d_2 which are due to the uncertainty about time delays $\Delta\tau_1$, $\Delta\tau_2$

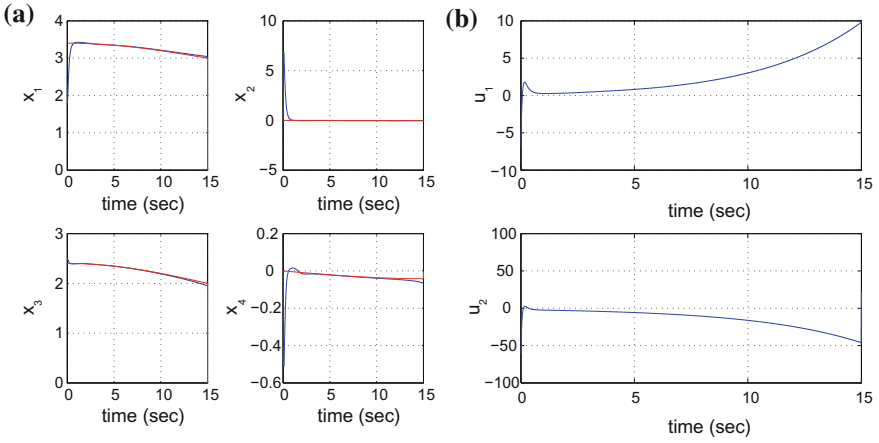

Fig. 1.33 Setpoint 2 - $\tau_1 = 0.29$ s, $\Delta\tau_1 = 0.19$ s, $\tau_2 = 0.27$ s, $\Delta\tau_2 = 0.17$ s: **a** Convergence of state variables x_1 to x_4 of the robotic manipulator to the reference setpoints **b** Control inputs $\tilde{u}_1, \tilde{u}_2$ of the extended state-space model of the robot

1.5.6 Simulation Tests

The performance of the proposed flatness-based control scheme for the compensation of time-delays in the control loop of robotic manipulators has been further confirmed through simulation experiments. The robot's control loop was sampled at $f_s = 2$ kHz. The obtained results demonstrate that the state variables of the robotic manipulator converge to the reference setpoints despite the existence of time-delays of variable

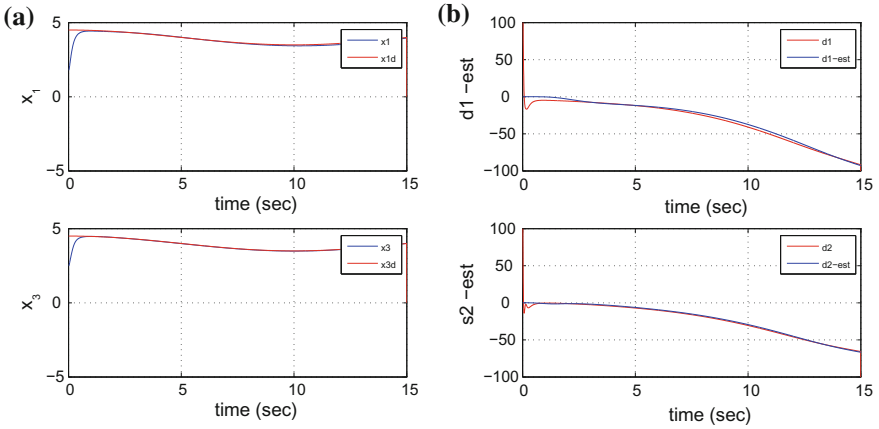

Fig. 1.34 Setpoint 3 - $\tau_1 = 0.25$ s, $\Delta\tau_1 = 0.19$ s, $\tau_2 = 0.24$ s, $\Delta\tau_2 = 0.20$ s: **a** Convergence of the joint angles of the robot x_1, x_3 to the reference setpoints **b** Estimation of disturbance terms d_1, d_2 which are due to the uncertainty about time delays $\Delta\tau_1$, $\Delta\tau_2$

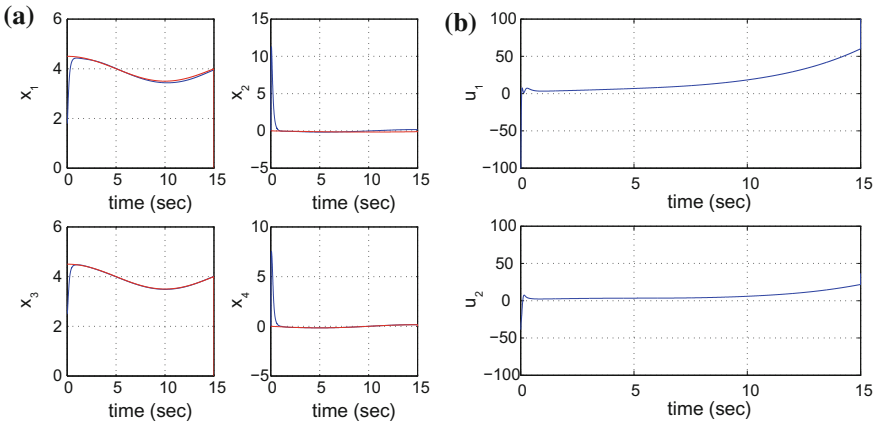

Fig. 1.35 Setpoint 3 - $\tau_1 = 0.25$ s, $\Delta\tau_1 = 0.19$ s, $\tau_2 = 0.24$ s, $\Delta\tau_2 = 0.20$ s: **a** Convergence of state variables x_1 to x_4 of the robotic manipulator to the reference setpoints **b** Control inputs $\tilde{u}_1, \tilde{u}_2$ of the extended state-space model of the robot

duration. The obtained results are given in Figs. 1.30, 1.31, 1.32, 1.33, 1.34, 1.35, 1.36, 1.37, 1.38 and 1.39.

The controller's design makes use of the input-output linearized extended state-space description of the robotic manipulator. According, to Eq. (1.185) the control input that finally is exerted on the robotic manipulator comprises the terms $\tilde{u}_1$ and $\tilde{u}_2$ which in adherence to Eq. (1.181) are functions of the joint angles' tracking errors and of their derivatives. Moreover, this control input comprises the integral terms $\int_0^t \tilde{u}_1 dt$ and $\int_0^t \tilde{u}_2 dt$. Thus, it can be stated that the control input that is applied to

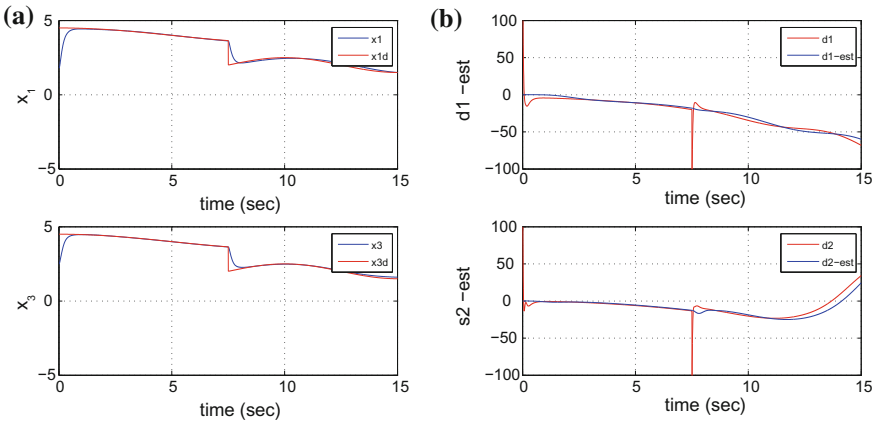

Fig. 1.36 Setpoint 4 - $\tau_1 = 0.27$ s, $\Delta\tau_1 = 0.19$ s, $\tau_2 = 0.25$ s, $\Delta\tau_2 = 0.16$ s: **a** Convergence of the joint angles of the robot x_1, x_3 to the reference setpoints **b** Estimation of disturbance terms d_1, d_2 which are due to the uncertainty about time delays $\Delta\tau_1$, $\Delta\tau_2$

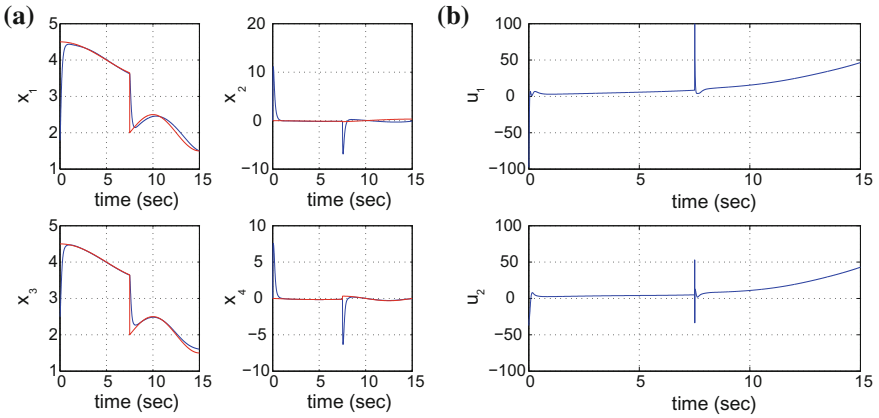

Fig. 1.37 Setpoint 4 - $\tau_1 = 0.27$ s, $\Delta\tau_1 = 0.19$ s, $\tau_2 = 0.25$ s, $\Delta\tau_2 = 0.16$ s: **a** Convergence of state variables x_1 to x_4 of the robotic manipulator to the reference setpoints **b** Control inputs $\tilde{u}_1$, $\tilde{u}_2$ of the extended state-space model of the robot

the nonlinear and multivariable model of the robotic manipulator is finally of the proportional-integral type.

The Derivative-free nonlinear Kalman Filter is used as a disturbance observer, that is capable of estimating in real-time the cumulative perturbation terms that are exerted on the control inputs of the extended state-space model of the manipulator and which are due to time-delays in its dynamic model. The associated results are shown in Figs. 1.30b, 1.31, 1.32, 1.33, 1.34, 1.35, 1.36, 1.37, 1.38 and 1.39b. It can be noticed that the estimated variables $\hat{\tilde{d}}_1$ and $\hat{\tilde{d}}_2$ converge rapidly to the real variables of

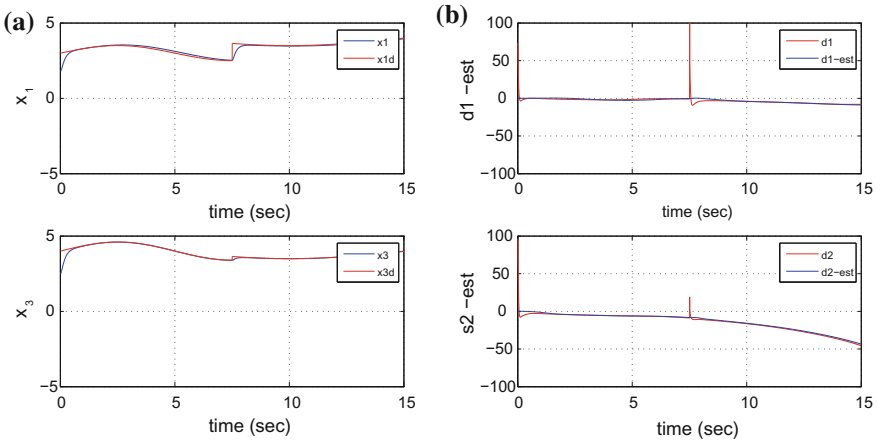

Fig. 1.38 Setpoint 5 - $\tau_1 = 0.30$ s, $\Delta\tau_1 = 0.19$ s, $\tau_2 = 0.28$ s, $\Delta\tau_2 = 0.19$ s: **a** Convergence of the joint angles of the robot x_1, x_3 to the reference setpoints **b** Estimation of disturbance terms d_1, d_2 which are due to the uncertainty about time delays $\Delta\tau_1$, $\Delta\tau_2$

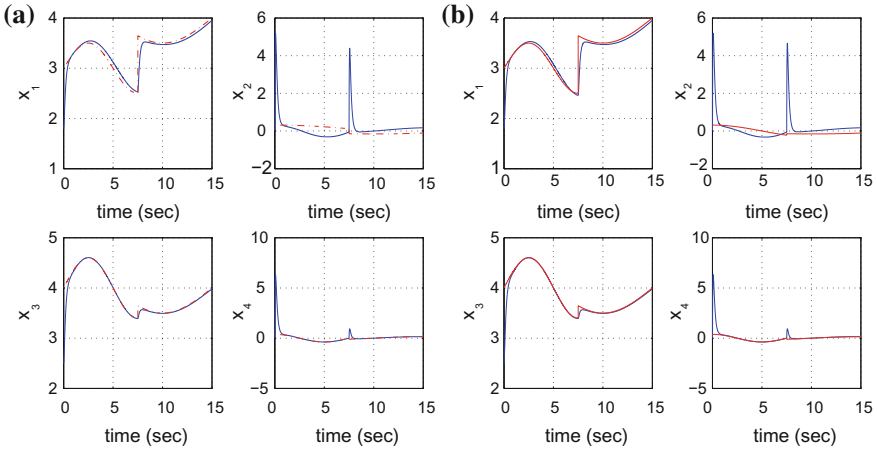

Fig. 1.39 Setpoint 5 - $\tau_1 = 0.30$ s, $\Delta\tau_1 = 0.19$ s, $\tau_2 = 0.28$ s, $\Delta\tau_2 = 0.19$ s: **a** Convergence of state variables x_1 to x_4 of the robotic manipulator to the reference setpoints **b** Control inputs $\tilde{u}_1$, $\tilde{u}_2$ of the extended state-space model of the robot

the cumulative disturbance terms $\tilde{d}_1$ and $\tilde{d}_2$ and that the associated estimation error was practically eliminated.

Chapter 2
Underactuated Robotic Manipulators

Abstract Control of underactuated robots has received significant attention and its application areas comprise several types of industrial and service robotic manipulators. The purpose of research in this area is to design robotic mechanisms that can be controlled despite having a number of actuators that is smaller than their degrees of freedom. This approach can reduce the cost and weight of robots or can provide robotic systems with tolerance to actuators failures. Again the control problem for such robots can be treated with (i) global linearization methods, (ii) approximate linearization approaches and (iii) Lyapunov methods. To achieve model-free control of underactuated manipulators, improved estimation approaches are developed, allowing the real-time identification of their unknown dynamics or kinematics. Moreover, to implement feedback control of underactuated robots through the measurement of a limited number of the robot's state variables, nonlinear filtering methods of proven convergence are developed. In particular the chapter develops the following topics: (a) Nonlinear optimal control for multi-DOF underactuated overhead cranes, (b) Nonlinear optimal control for ship-mounted cranes (c) Nonlinear optimal control for the rotary (Furuta's) pendulum, (d) Nonlinear optimal control for the cart and double-pendulum system, and (e) Nonlinear optimal control for a 3-DOF underactuated robotic arm

2.1 Chapter Overview

The present chapter develops the following topics: (a) Nonlinear optimal control for multi-DOF underactuated overhead cranes, (b) Nonlinear optimal control for ship-mounted cranes (c) Nonlinear optimal control for the rotary (Furuta's) pendulum, (d) Nonlinear optimal control for the cart and double-pendulum system, and (e) Nonlinear optimal control for a 3-DOF underactuated robotic arm.

With reference to (a) the dynamic model of the overhead crane undergoes approximate linearization around local operating points which are redefined at each iteration of the control algorithm. The crane's system is underactuated because it receives only two external inputs, namely a force that allows the motion of its bridge component

G. Rigatos and K. Busawon, *Robotic Manipulators and Vehicles*,
Studies in Systems, Decision and Control 152,
https://doi.org/10.1007/978-3-319-77851-8_2

along the x axis and a force that allows the motion of its trolley component along the y axis. A solution to the control problem of this underactuated system is obtained by applying nonlinear H-infinity control. For the approximate linearization of the system's dynamics, Taylor series expansion is performed through the computation of the associated Jacobian matrices. Next, for the linearized equivalent model of the crane an H-infinity feedback controller is designed.

With reference to (b) a nonlinear optimal control approach is developed for the precise functioning of ship-mounted cranes. The problem is of elevated difficulty because of the nonlinearities of the associated dynamic model, the time-delays appearing in some of its state variables and the underactuation with reference to the model's control input. The considered crane model comprises a winch that is rotated by an AC motor which in turn controls the submergence of a payload in the water. The objective is to control precisely the payload's vertical position, despite the effect of hydrodynamic forces and of the vessel's heave motion. The dynamic model of the ship-mounted crane system undergoes approximate linearization around a temporary operating point that is re-computed at each iteration of the control algorithm. For the approximately linearized system an optimal (H-infinity) controller is designed. The global stability properties of the control method is proven through Lyapunov analysis.

With reference to (c) The rotary pendulum's dynamic model is first transformed to an equivalent form after applying partial feedback linearization. The later description of the pendulum's dynamics undergoes approximate linearization which takes place round a temporary operating point (equilibrium) recomputed at each iteration of the control algorithm. For the approximately linearized model of the pendulum the optimal (H-infinity) control problem is solved.

With reference to (d) a nonlinear H-infinity (optimal) control approach is proposed for the nonlinear model of the cart and double-pendulum system. The control of the cart and double-pendulum system is known to exhibit a high degree of difficulty due to nonlinearities and underactuation. Actually, there are three degrees of freedom (the longitudinal motion of the cart and the two rotational motions of the poles that constitute the double pendulum) which have to be controlled with only one input (the force exerted on the cart). To solve this non-trivial control problem, the dynamic model of the cart and double-pendulum system undergoes first approximate linearization around a temporary operating point (equilibrium) which is recomputed at each iteration of the control algorithm. For the approximately linearized model of the cart and double-pendulum a stabilizing H-infinity (optimal) controller is developed.

With reference to (e) a nonlinear H-infinity (optimal) control approach is developed for the problem of end-effector trajectory tracking in 3-DOF planar underactuated robotic manipulators. First, the state-space model of the underactuated manipulator is subject to a transformation which results into a new description of its dynamics. Next, the new dynamic model of the underactuated manipulator undergoes approximate linearization, round a local operating point. Furthermore, an H-infinity feedback controller is designed. The feedback gain is computed after solving an algebraic Riccati equation at each iteration of the control algorithm. Through Lyapunov stability analysis it is proven that the control loop satisfies an H-infinity tracking performance

criterion, which signifies elevated robustness to model uncertainty and external perturbations. Moreover, under moderate conditions the global asymptotic stability of the control loop is proven. In all aforementioned cases (a)–(e) the global asymptotic stability properties for the models of the underactuated robotic systems are proven through Lyapunov analysis.

2.2 Nonlinear Optimal Control for Multi-DOF Underactuated Overhead Cranes

2.2.1 Outline

Overhead cranes are nonlinear underactuated electromechanical systems and their control is a nontrivial problem [141, 168, 289, 532, 539]. Cranes have been extensively used in factories and industrial sites, in workshops and building constructions, in loading and unloading of ships at ports and in several other applications requiring the pick and placement of heavy payloads [534, 595, 597, 629, 646]. However, due to the fast motion of their trolley part excessive swing of the payload may be caused (Fig. 2.1). On the one side the trolley is required to move fast so as to accomplish the payload placement tasks in short time. On the other side this fast motion causes undesirable oscillations of the payload which have to be rapidly and efficiently suppressed by the crane's control system [112, 139, 188, 196, 535]. The difficulty in achieving simultaneously fast motion of the trolley and rapid attenuation of the payload's oscillations comes from the fact that the crane's control system is underactuated [97, 325, 360, 568, 596]. In this section a 4-DOF underactuated overhead crane is considered (Fig. 2.1). The crane exhibits four degrees of freedom associated with the motion of its bridge component along the x-axis, with the motion of its trolley component along the bridge (the latter defining also the y axis), while there are also two angles θ_x and θ_y defining the displacement of the payload from the vertical position and with respect to the x and y axes respectively. Due to strong nonlinearities and the limited actuation that the system receives, the crane's control problem is complex [91, 168, 538, 594]. As explained, the system is underactuated because it receives only two external inputs, namely a force that allows the motion of the bridge along the x axis and a force that allows the motion of the trolley along the y axis [597].

To solve the control and stabilization problem for the 4-DOF crane, in this section an H-infinity nonlinear control approach is proposed. The nonlinear model of the crane undergoes approximate linearization, around a temporary equilibrium which is recomputed at each iteration of the control algorithm. This equilibrium consists of the present value of the crane's state vector and the last value of the control inputs vector that was exerted on it [461, 466]. The linearization follows the concept of Taylor series expansion and requires the computation of Jacobian matrices [33, 431, 463, 564]. The modelling error which is due to the truncation of higher

order terms in the Taylor series expansion is considered to be a perturbation that is compensated by the robustness of the control algorithm.

For the linearized model of the overhead crane an H-infinity feedback controller is designed. This controller represents the solution to a min-max differential game in which the controller tries to minimize a quadratic cost functional associated with the tracking error of the crane's state vector while the model uncertainty and disturbance terms try to minimize it. The feedback gain of the H-infinity controller is obtained from the solution of an algebraic Riccati equation [450, 452, 457, 459, 460]. This procedure is repeated at each iteration of the control method. The stability of the control scheme is confirmed through Lyapunov analysis. First, it is shown that the control system satisfies the H-infinity tracking performance criterion and this signifies elevated robustness against parametric uncertainty and external disturbances. Moreover, under moderate conditions it is proven that the control scheme is globally asymptotically stable.

Additionally, to implement state estimation-based feedback control of the overhead crane through measuring only a subset of its state vector elements, the H-infinity Kalman Filter is used [169, 511]. The H-infinity Kalman Filter is an optimal state estimator under imprecision of the dynamic model of the crane. This allows for reconstructing the entire state vector of the crane after obtaining measurements from sensors that record specific state variables of it. The H-infinity Kalman Filter comprises two-stages, an update in measurement and an update in time. The estimation method uses in its recursion the update of a modified state vector error covariance matrix, and finally provides optimal estimation of the state vector under model uncertainty or exogenous perturbations.

The solution achieved by the proposed nonlinear H-infinity control method exhibits several advantages which are outlined in the following: (i) it is applied directly on the nonlinear dynamical model of the overhead crane and not on an equivalent linearized description of it, (ii) It avoids the elaborated linearizing transformations (diffeomorphisms) which can be met in global linearization-based control methods for robotic manipulators, (iii) the controller is designed according to optimal control principles which implies the best trade-off between precise tracking of the reference setpoints on the one side and moderate variations of the control inputs on the other side (iv) the control method exhibits significant robustness to parametric uncertainty, modelling errors as well as to external perturbations (v) the computational implementation of the control method is simple since it requires only the solution of an algebraic Riccati equation. It is noted that other control methods such as Model Predictive Control (MPC) would be unsuitable for application to the crane's model because of the model's nonlinearity. Moreover, Nonlinear Model Predictive Control (NMPC) would not be of assured stability and convergence. On the other side, the proposed nonlinear H-infinity control approach is of proven global asymptotic stability. Finally, it is noted that comparing to energy-based control methods the proposed nonlinear optimal control method appears again to have better performance because it is computationally simpler, it avoids singularities, and avoids intuition in the selection of the energy function to be minimized as well as in the selection of the feedback terms and parameters of the stabilizing controller.

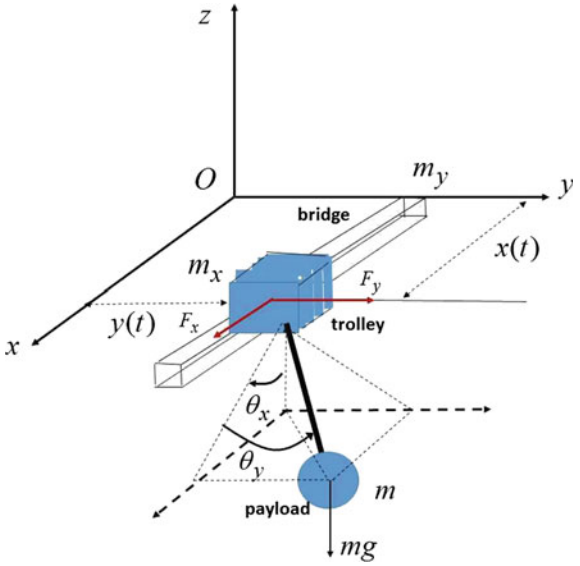

Fig. 2.1 Reference axes for the model of the underactuated crane

2.2.2 Dynamic Model of the Crane

Using Euler–Lagrange analysis, the dynamic model of the underactuated crane (Fig. 2.1) is shown to be described by the following set of differential equations [535, 597]:

$$\begin{gathered}(m+m_x)\ddot{x}+mlcos(\theta_x)cos(\theta_y)\ddot{\theta}_x-mlsin(\theta_x)sin(\theta_y)\ddot{\theta}_y- \\ -mlsin(\theta_x)cos(\theta_y)\dot{\theta}_y^2-2mlcos(\theta_x)sin(\theta_y)\dot{\theta}_x\dot{\theta}_y- \\ mlsin(\theta_x)cos(\theta_y)\dot{\theta}_y^2=F_x\end{gathered} \tag{2.1}$$

$$(m+m_y)\ddot{y}+mlcos(\theta_y)\ddot{\theta}_y-mlsin(\theta_y)\dot{\theta}_y^2=F_y \tag{2.2}$$

$$\begin{gathered}mlcos(\theta_x)cos(\theta_y)\ddot{x}+ml^2cos^2(\theta_y)\ddot{\theta}_x- \\ -2ml^2sin(\theta_y)cos(\theta_y)\dot{\theta}_x\dot{\theta}_y+mglsin(\theta_x)cos(\theta_y)=0\end{gathered} \tag{2.3}$$

$$\begin{gathered}mlsin(\theta_x)sin(\theta_y)\ddot{x}-mlcos(\theta_x)\ddot{y}-ml^2\ddot{\theta}_y- \\ -ml^2sin(\theta_y)cos(\theta_y)\dot{\theta}_x^2-mglcos(\theta_x)sin(\theta_y)=0\end{gathered} \tag{2.4}$$

In the previous equations m is the payload mass, m_x is the trolley mass, m_y is the bridge mass, l is the length of the cable and g is the gravitational acceleration. Moreover, $x(t)$ is the displacement of the trolley along the x-axis, $y(t)$ is the displacement of the trolley along the y axis, θ_x is the swing angle related to the displacement of the payload from its vertical position and along the x axis, θ_y is the swing angle related to the displacement of the payload from its vertical position and along the y axis,

F_x is the control force along the x-axis which is exerted on the bridge and F_y is the control force along the y-axis which is exerted on the trolley.

Next, using Eqs. (2.1) and (2.2) to define the new control inputs

$$\begin{aligned} u_x = &-\frac{mlcos(\theta_x)cos(\theta_y)\ddot{\theta}_x}{(m+m_x)} + \frac{mlsin(\theta_x)sin(\theta_y)\ddot{\theta}_y}{(m+m_x)} + \\ &+ \frac{mlsin(\theta_x)cos(\theta_y)\dot{\theta}_y^2}{(m+m_x)} + \frac{2mlcos(\theta_x)sin(\theta_y)\dot{\theta}_x\dot{\theta}_y}{(m+m_x)} + \\ &+ \frac{mlsin(\theta_x)cos(\theta_y)\dot{\theta}_y^2}{(m+m_x)} + \frac{1}{(m+m_x)}F_x \end{aligned} \tag{2.5}$$

$$u_y = -\frac{mlcos(\theta_y)\ddot{\theta}_y}{(m+m_y)} + \frac{mlsin(\theta_y)\dot{\theta}_y^2}{(m+m_y)} + \frac{1}{(m+m_y)}F_y \tag{2.6}$$

the following state-space model is obtained for the underactuated crane [597]

$$\ddot{x} = u_x \tag{2.7}$$

$$\ddot{y} = u_y \tag{2.8}$$

$$\ddot{\theta}_x = \frac{1}{lcos(\theta_y)}[2lsin(\theta_y)\dot{\theta}_x\dot{\theta}_y - gsin(\theta_x - u_xcos(\theta)_x] \tag{2.9}$$

$$\ddot{\theta}_y = \frac{1}{l}[u_xsin(\theta_x)sin(\theta_y) - u_ycos(\theta_y) - lsin(\theta_y)cos(\theta_y)\dot{\theta}_x^2 - gcos(\theta_x)sin(\theta_y)] \tag{2.10}$$

Thus by defining the state vector $q = [x, y, \theta_x, \theta_y, \dot{x}, \dot{y}, \dot{\theta}_x, \dot{\theta}_y]^T$, the model of the underactuated crane is written in the state-space form [597]

$$\dot{q} = f(q) + g(q)u \tag{2.11}$$

where $u = [u_1, u_2]^T$ and

$$f(q) = \begin{pmatrix} \dot{x} \\ \dot{y} \\ \dot{\theta}_x \\ \dot{\theta}_y \\ 0 \\ 0 \\ \frac{1}{lcos(\theta_y)}[2lsin(\theta_y)\dot{\theta}_x\dot{\theta}_y - gsin(\theta_x)] \\ \frac{1}{l}[-lsin(\theta_y)cos(\theta_y)\dot{\theta}_x^2 - gcos(\theta_x)sin(\theta_y)] \end{pmatrix} \quad g(q) = \begin{pmatrix} 0 & 0 \\ 0 & 0 \\ 0 & 0 \\ 0 & 0 \\ 1 & 0 \\ 0 & 1 \\ -\frac{cos(\theta_x)}{lcos(\theta_x)} & 0 \\ \frac{sin(\theta_x)sin(\theta_y)}{l} & -\frac{cos(\theta_y)}{l} \end{pmatrix} \tag{2.12}$$

Next, using the state variables notation $x_1 = x$, $x_2 = y$, $x_3 = \theta_x$, $x_4 = \theta_y$, $x_5 = \dot{x}$, $x_6 = \dot{y}$, $x_7 = \dot{\theta}_x$ and $x_8 = \dot{\theta}_y$ one obtains the following state-space description

$$\dot{x} = f(x) + g(x)u \tag{2.13}$$

where $u = [u_1, u_2]^T$ and

$$f(x) = \begin{pmatrix} x_5 \\ x_6 \\ x_7 \\ x_8 \\ 0 \\ 0 \\ \frac{1}{lcos(x_4)}[2lsin(x_4)x_7x_8 - gsin(x_3)] \\ \frac{1}{l}[-lsin(x_4)cos(x_4)x_3^2 - gcos(x_3)sin(x_4)] \end{pmatrix} \quad g(x) = \begin{pmatrix} 0 & 0 \\ 0 & 0 \\ 0 & 0 \\ 0 & 0 \\ 1 & 0 \\ 0 & 1 \\ -\frac{cos(x_3)}{lcos(x_4)} & 0 \\ \frac{sin(x_3)sin(x_4)}{l} & -\frac{cos(x_4)}{l} \end{pmatrix} \tag{2.14}$$

2.2.3 Approximate Linearization of the Crane's Model

The model of the overhead crane is linearized around the temporary equilibrium (x^*, y^*) by performing Taylor series expansion and by computing the associated Jacobian matrices [461, 466]

$$\dot{x} = Ax + Bu + \tilde{d} \tag{2.15}$$

where matrices A and B are the system's Jacobians

$$A = [\nabla_x f(x) + \nabla_x g(x)u] \mid_{(x^*,u^*)} \tag{2.16}$$

$$B = g(x) \mid_{(x^*,u^*)} \tag{2.17}$$

Ihe Jacobian matrices of the system are computed after considering the vector fields appearing in the state-space description of the system, that is $f = [f_1, \cdot, f_8]^T$, and $g = [g_1, g_2]$ with $g_1 = [g_{11} \ldots, g_{18}]^T$, $g_2 = [g_{21} \ldots, g_{28}]^T$. Thus the Jacobian matrices are given by

$$\nabla_x f = \quad \nabla_x g_1 = \quad \nabla_x g_2 =$$

$$\begin{pmatrix} \frac{\partial f_1}{\partial x_1} & \frac{\partial f_1}{\partial x_2} & \cdots & \frac{\partial f_1}{\partial x_8} \\ \frac{\partial f_2}{\partial x_1} & \frac{\partial f_2}{\partial x_2} & \cdots & \frac{\partial f_2}{\partial x_8} \\ \cdots & \cdots & \cdots & \cdots \\ \frac{\partial f_8}{\partial x_1} & \frac{\partial f_8}{\partial x_2} & \cdots & \frac{\partial f_8}{\partial x_8} \end{pmatrix} \begin{pmatrix} \frac{\partial g_{11}}{\partial x_1} & \frac{\partial g_{11}}{\partial x_2} & \cdots & \frac{\partial g_{11}}{\partial x_8} \\ \frac{\partial g_{12}}{\partial x_1} & \frac{\partial g_{12}}{\partial x_2} & \cdots & \frac{\partial g_{12}}{\partial x_8} \\ \cdots & \cdots & \cdots & \cdots \\ \frac{\partial g_{18}}{\partial x_1} & \frac{\partial g_{18}}{\partial x_2} & \cdots & \frac{\partial g_{18}}{\partial x_8} \end{pmatrix} \begin{pmatrix} \frac{\partial g_{21}}{\partial x_1} & \frac{\partial g_{21}}{\partial x_2} & \cdots & \frac{\partial g_{21}}{\partial x_8} \\ \frac{\partial g_{22}}{\partial x_1} & \frac{\partial g_{22}}{\partial x_2} & \cdots & \frac{\partial g_{22}}{\partial x_8} \\ \cdots & \cdots & \cdots & \cdots \\ \frac{\partial g_{28}}{\partial x_1} & \frac{\partial g_{28}}{\partial x_2} & \cdots & \frac{\partial g_{28}}{\partial x_8} \end{pmatrix} \tag{2.18}$$

The elements of the Jacobian matrix $\nabla_x f$ are as follows:

1st row of $\nabla_x f$: $\frac{\partial f_1}{\partial x_1} = 0$, $\frac{\partial f_1}{\partial x_2} = 0$, $\frac{\partial f_1}{\partial x_3} = 0$, $\frac{\partial f_1}{\partial x_4} = 0$, $\frac{\partial f_1}{\partial x_5} = 1$, $\frac{\partial f_1}{\partial x_6} = 0$, $\frac{\partial f_1}{\partial x_7} = 0$ and $\frac{\partial f_1}{\partial x_8} = 0$.

2nd row of $\nabla_x f$: $\frac{\partial f_2}{\partial x_1} = 0$, $\frac{\partial f_2}{\partial x_2} = 0$, $\frac{\partial f_2}{\partial x_3} = 0$, $\frac{\partial f_2}{\partial x_4} = 0$, $\frac{\partial f_2}{\partial x_5} = 0$, $\frac{\partial f_2}{\partial x_6} = 1$, $\frac{\partial f_2}{\partial x_7} = 0$ and $\frac{\partial f_2}{\partial x_8} = 0$.

3rd row of $\nabla_x f$: $\frac{\partial f_3}{\partial x_1} = 0$, $\frac{\partial f_3}{\partial x_2} = 0$, $\frac{\partial f_3}{\partial x_3} = 0$, $\frac{\partial f_3}{\partial x_4} = 0$, $\frac{\partial f_3}{\partial x_5} = 0$, $\frac{\partial f_3}{\partial x_6} = 0$, $\frac{\partial f_3}{\partial x_7} = 1$ and $\frac{\partial f_3}{\partial x_8} = 0$.

4th row of $\nabla_x f$: $\frac{\partial f_4}{\partial x_1} = 0$, $\frac{\partial f_4}{\partial x_2} = 0$, $\frac{\partial f_4}{\partial x_3} = 0$, $\frac{\partial f_4}{\partial x_4} = 0$, $\frac{\partial f_4}{\partial x_5} = 0$, $\frac{\partial f_4}{\partial x_6} = 0$, $\frac{\partial f_4}{\partial x_7} = 0$ and $\frac{\partial f_4}{\partial x_8} = 1$.

5th row of $\nabla_x f$: $\frac{\partial f_5}{\partial x_1} = 0$, $\frac{\partial f_5}{\partial x_2} = 0$, $\frac{\partial f_5}{\partial x_3} = 0$, $\frac{\partial f_5}{\partial x_4} = 0$, $\frac{\partial f_5}{\partial x_5} = 0$, $\frac{\partial f_5}{\partial x_6} = 0$, $\frac{\partial f_5}{\partial x_7} = 0$ and $\frac{\partial f_5}{\partial x_8} = 0$.

6th row of $\nabla_x f$: $\frac{\partial f_6}{\partial x_1} = 0$, $\frac{\partial f_6}{\partial x_2} = 0$, $\frac{\partial f_6}{\partial x_3} = 0$, $\frac{\partial f_6}{\partial x_4} = 0$, $\frac{\partial f_6}{\partial x_5} = 0$, $\frac{\partial f_6}{\partial x_6} = 0$, $\frac{\partial f_6}{\partial x_7} = 0$ and $\frac{\partial f_6}{\partial x_8} = 0$.

7th row of $\nabla_x f$: $\frac{\partial f_7}{\partial x_1} = 0$, $\frac{\partial f_7}{\partial x_2} = 0$, $\frac{\partial f_7}{\partial x_3} = \frac{-gcos(x_3)}{lcos(x_4)}$, $\frac{\partial f_7}{\partial x_4} = 2x_7x_8 + \frac{[2lsin(x_4)x_7x_8 - gcos(x_3)][lsin(x_4)]}{[lcos(x_4)]^2}$, $\frac{\partial f_7}{\partial x_5} = 0$, $\frac{\partial f_7}{\partial x_6} = 0$, $\frac{\partial f_7}{\partial x_7} = \frac{2sin(x_4)x_8}{cos(x_4)}$, $\frac{\partial f_7}{\partial x_8} = \frac{2sin(x_4)x_7}{cos(x_4)}$.

8th row of $\nabla_x f$: $\frac{\partial f_8}{\partial x_1} = 0$, $\frac{\partial f_8}{\partial x_2} = 0$, $\frac{\partial f_8}{\partial x_3} = \frac{lsin(x_4)sin(x_3)x_5^2 + gsin(x_3)cos(x_4)}{l}$, $\frac{\partial f_8}{\partial x_4} = \frac{-lcos(x_4)cos(x_3)x_5^2 + gcos(x_3)sin(x_4)}{l}$, $\frac{\partial f_8}{\partial x_5} = -2sin(x_4)cos(x_3)x_5$, $\frac{\partial f_8}{\partial x_6} = 0$, $\frac{\partial f_8}{\partial x_7} = 0$, $\frac{\partial f_8}{\partial x_8} = 0$.

The elements of the Jacobian matrix $\nabla_x g_1$ are as follows:

1st row of $\nabla_x g_1$: $\frac{\partial g_{11}}{\partial x_1} = 0$, $\frac{\partial g_{11}}{\partial x_2} = 0$, $\frac{\partial g_{11}}{\partial x_3} = 0$, $\frac{\partial g_{11}}{\partial x_4} = 0$, $\frac{\partial g_{11}}{\partial x_5} = 0$, $\frac{\partial g_{11}}{\partial x_6} = 0$, $\frac{\partial g_{11}}{\partial x_7} = 0$, $\frac{\partial g_{11}}{\partial x_8} = 0$.

2nd row of $\nabla_x g_1$: $\frac{\partial g_{12}}{\partial x_1} = 0$, $\frac{\partial g_{12}}{\partial x_2} = 0$, $\frac{\partial g_{12}}{\partial x_3} = 0$, $\frac{\partial g_{12}}{\partial x_4} = 0$, $\frac{\partial g_{12}}{\partial x_5} = 0$, $\frac{\partial g_{12}}{\partial x_6} = 0$, $\frac{\partial g_{12}}{\partial x_7} = 0$, $\frac{\partial g_{12}}{\partial x_8} = 0$.

3rd row of $\nabla_x g_1$: $\frac{\partial g_{13}}{\partial x_1} = 0$, $\frac{\partial g_{13}}{\partial x_2} = 0$, $\frac{\partial g_{13}}{\partial x_3} = 0$, $\frac{\partial g_{13}}{\partial x_4} = 0$, $\frac{\partial g_{13}}{\partial x_5} = 0$, $\frac{\partial g_{13}}{\partial x_6} = 0$, $\frac{\partial g_{13}}{\partial x_7} = 0$, $\frac{\partial g_{13}}{\partial x_8} = 0$.

4th row of $\nabla_x g_1$: $\frac{\partial g_{14}}{\partial x_1} = 0$, $\frac{\partial g_{14}}{\partial x_2} = 0$, $\frac{\partial g_{14}}{\partial x_3} = 0$, $\frac{\partial g_{14}}{\partial x_4} = 0$, $\frac{\partial g_{14}}{\partial x_5} = 0$, $\frac{\partial g_{14}}{\partial x_6} = 0$, $\frac{\partial g_{14}}{\partial x_7} = 0$, $\frac{\partial g_{14}}{\partial x_8} = 0$.

5th row of $\nabla_x g_1$: $\frac{\partial g_{15}}{\partial x_1} = 0$, $\frac{\partial g_{15}}{\partial x_2} = 0$, $\frac{\partial g_{15}}{\partial x_3} = 0$, $\frac{\partial g_{15}}{\partial x_4} = 0$, $\frac{\partial g_{15}}{\partial x_5} = 0$, $\frac{\partial g_{15}}{\partial x_6} = 0$, $\frac{\partial g_{15}}{\partial x_7} = 0$, $\frac{\partial g_{15}}{\partial x_8} = 0$.

6th row of $\nabla_x g_1$: $\frac{\partial g_{16}}{\partial x_1} = 0$, $\frac{\partial g_{16}}{\partial x_2} = 0$, $\frac{\partial g_{16}}{\partial x_3} = 0$, $\frac{\partial g_{16}}{\partial x_4} = 0$, $\frac{\partial g_{16}}{\partial x_5} = 0$, $\frac{\partial g_{16}}{\partial x_6} = 0$, $\frac{\partial g_{16}}{\partial x_7} = 0$, $\frac{\partial g_{16}}{\partial x_8} = 0$.

7th row of $\nabla_x g_1$: $\frac{\partial g_{17}}{\partial x_1}=0$, $\frac{\partial g_{17}}{\partial x_2}=0$, $\frac{\partial g_{17}}{\partial x_3}=\frac{sin(x_3)}{lcos(x_3)}$, $\frac{\partial g_{16}}{\partial x_4}=-\frac{sin(x_3)sin(x_4)}{lcos^2(x_4)}$, $\frac{\partial g_{17}}{\partial x_5}=0$, $\frac{\partial g_{17}}{\partial x_6}=0$, $\frac{\partial g_{17}}{\partial x_7}=0$, $\frac{\partial g_{17}}{\partial x_8}=0$.

8th row of $\nabla_x g_1$: $\frac{\partial g_{18}}{\partial x_1}=0$, $\frac{\partial g_{18}}{\partial x_2}=0$, $\frac{\partial g_{18}}{\partial x_3}=\frac{cos(x_3)sin(x_4)}{l}$, $\frac{\partial g_{18}}{\partial x_4}=\frac{sin(x_3)cos(x_4)}{l}$, $\frac{\partial g_{18}}{\partial x_5}=0$, $\frac{\partial g_{18}}{\partial x_6}=0$, $\frac{\partial g_{18}}{\partial x_7}=0$, $\frac{\partial g_{18}}{\partial x_8}=0$.

The elements of the Jacobian matrix $\nabla_x g_2$ are as follows:

1st row of $\nabla_x g_2$: $\frac{\partial g_{21}}{\partial x_1}=0$, $\frac{\partial g_{21}}{\partial x_2}=0$, $\frac{\partial g_{21}}{\partial x_3}=0$, $\frac{\partial g_{21}}{\partial x_4}=0$, $\frac{\partial g_{21}}{\partial x_5}=0$, $\frac{\partial g_{21}}{\partial x_6}=0$, $\frac{\partial g_{21}}{\partial x_7}=0$, $\frac{\partial g_{21}}{\partial x_8}=0$.

2nd row of $\nabla_x g_2$: $\frac{\partial g_{22}}{\partial x_1}=0$, $\frac{\partial g_{22}}{\partial x_2}=0$, $\frac{\partial g_{22}}{\partial x_3}=0$, $\frac{\partial g_{22}}{\partial x_4}=0$, $\frac{\partial g_{22}}{\partial x_5}=0$, $\frac{\partial g_{22}}{\partial x_6}=0$, $\frac{\partial g_{22}}{\partial x_7}=0$, $\frac{\partial g_{22}}{\partial x_8}=0$.

3rd row of $\nabla_x g_2$: $\frac{\partial g_{23}}{\partial x_1}=0$, $\frac{\partial g_{23}}{\partial x_2}=0$, $\frac{\partial g_{23}}{\partial x_3}=0$, $\frac{\partial g_{23}}{\partial x_4}=0$, $\frac{\partial g_{23}}{\partial x_5}=0$, $\frac{\partial g_{23}}{\partial x_6}=0$, $\frac{\partial g_{23}}{\partial x_7}=0$, $\frac{\partial g_{23}}{\partial x_8}=0$.

4th row of $\nabla_x g_2$: $\frac{\partial g_{24}}{\partial x_1}=0$, $\frac{\partial g_{24}}{\partial x_2}=0$, $\frac{\partial g_{24}}{\partial x_3}=0$, $\frac{\partial g_{24}}{\partial x_4}=0$, $\frac{\partial g_{24}}{\partial x_5}=0$, $\frac{\partial g_{24}}{\partial x_6}=0$, $\frac{\partial g_{24}}{\partial x_7}=0$, $\frac{\partial g_{24}}{\partial x_8}=0$.

5th row of $\nabla_x g_2$: $\frac{\partial g_{25}}{\partial x_1}=0$, $\frac{\partial g_{25}}{\partial x_2}=0$, $\frac{\partial g_{25}}{\partial x_3}=0$, $\frac{\partial g_{25}}{\partial x_4}=0$, $\frac{\partial g_{25}}{\partial x_5}=0$, $\frac{\partial g_{25}}{\partial x_6}=0$, $\frac{\partial g_{25}}{\partial x_7}=0$, $\frac{\partial g_{25}}{\partial x_8}=0$.

6th row of $\nabla_x g_2$: $\frac{\partial g_{26}}{\partial x_1}=0$, $\frac{\partial g_{26}}{\partial x_2}=0$, $\frac{\partial g_{26}}{\partial x_3}=0$, $\frac{\partial g_{26}}{\partial x_4}=0$, $\frac{\partial g_{26}}{\partial x_5}=0$, $\frac{\partial g_{26}}{\partial x_6}=0$, $\frac{\partial g_{26}}{\partial x_7}=0$, $\frac{\partial g_{26}}{\partial x_8}=0$.

7th row of $\nabla_x g_2$: $\frac{\partial g_{27}}{\partial x_1}=0$, $\frac{\partial g_{27}}{\partial x_2}=0$, $\frac{\partial g_{27}}{\partial x_3}=0$, $\frac{\partial g_{27}}{\partial x_4}=0$, $\frac{\partial g_{27}}{\partial x_5}=0$, $\frac{\partial g_{27}}{\partial x_6}=0$, $\frac{\partial g_{27}}{\partial x_7}=0$, $\frac{\partial g_{27}}{\partial x_8}=0$.

8th row of $\nabla_x g_2$: $\frac{\partial g_{28}}{\partial x_1}=0$, $\frac{\partial g_{28}}{\partial x_2}=0$, $\frac{\partial g_{28}}{\partial x_3}=0$, $\frac{\partial g_{28}}{\partial x_4}=0$, $\frac{\partial g_{28}}{\partial x_5}=0$, $\frac{\partial g_{28}}{\partial x_6}=0$, $\frac{\partial g_{28}}{\partial x_7}=0$, $\frac{\partial g_{28}}{\partial x_8}=0$.

As previously noted, about the linearized state-space description of the system it holds that

$$\begin{aligned} A &= \nabla_x[f(x)+g(x)u]\mid_{(x^*,u^*)} = \nabla_x[f(x)+g_1(x)u_1+g_2(x)u_2]\mid_{(x^*,u^*)} \\ B &= \nabla_u[f(x)+g(x)u]\mid_{(x^*,u^*)} = \nabla_u[f(x)+g_1(x)u_1+g_2(x)u_2]\mid_{(x^*,u^*)} = g(x) \end{aligned} \tag{2.19}$$

2.2.4 Design of an H-Infinity Nonlinear Feedback Controller

2.2.4.1 Equivalent Linearized Dynamics of the Crane

After linearization around its current operating point, the crane's dynamic model is written as

$$\dot{x} = Ax + Bu + d_1 \tag{2.20}$$

Parameter d_1 stands for the linearization error in the crane's dynamic model appearing in Eq. (2.20). The reference setpoints for the crane's state vector are denoted by $\mathbf{x_d} = [x_1^d, \ldots, x_8^d]$. Tracking of this trajectory is achieved after applying the control input u^*. At every time instant the control input u^* is assumed to differ from the control input u appearing in Eq. (2.20) by an amount equal to Δu, that is $u^* = u + \Delta u$

$$\dot{x}_d = Ax_d + Bu^* + d_2 \tag{2.21}$$

The dynamics of the controlled system described in Eq. (2.20) can be also written as

$$\dot{x} = Ax + Bu + Bu^* - Bu^* + d_1 \tag{2.22}$$

and by denoting $d_3 = -Bu^* + d_1$ as an aggregate disturbance term one obtains

$$\dot{x} = Ax + Bu + Bu^* + d_3 \tag{2.23}$$

By subtracting Eq. (2.21) from (2.23) one has

$$\dot{x} - \dot{x}_d = A(x - x_d) + Bu + d_3 - d_2 \tag{2.24}$$

By denoting the tracking error as $e = x - x_d$ and the aggregate disturbance term as $\tilde{d} = d_3 - d_2$, the tracking error dynamics becomes

$$\dot{e} = Ae + Bu + \tilde{d} \tag{2.25}$$

The above linearized form of the crane's model can be efficiently controlled after applying an H-infinity feedback control scheme.

2.2.4.2 The Nonlinear H-Infinity Control

The initial nonlinear model of the underactuated crane is in the form

$$\dot{x} = \tilde{f}(x, u) \;\; x \in R^n, \;\; u \in R^m \tag{2.26}$$

Linearization of the system (multi-DOF crane) is performed at each iteration of the control algorithm round its present operating point $(x^*, u^*) = (x(t), u(t - T_s))$, where T_s is the sampling period. The linearized equivalent model of the system is described by

$$\dot{x} = Ax + Bu + L\tilde{d} \quad x \in R^n, \; u \in R^m, \; \tilde{d} \in R^q \tag{2.27}$$

where matrices A and B are obtained from the computation of the Jacobians of the crane's state-space description and vector $\tilde{d}$ denotes disturbance terms due to linearization errors. The problem of disturbance rejection for the linearized model that is described by

$$\begin{aligned} \dot{x} &= Ax + Bu + L\tilde{d} \\ y &= Cx \end{aligned} \tag{2.28}$$

where $x \in R^n$, $u \in R^m$, $\tilde{d} \in R^q$ and $y \in R^p$, cannot be handled efficiently if the classical LQR control scheme is applied. This is because of the existence of the perturbation term $\tilde{d}$ in the linearized model of the crane. The disturbance term $\tilde{d}$ apart from modeling (parametric) uncertainty and external perturbation terms can also represent noise terms of any distribution.

In the H_∞ control approach, a feedback control scheme is designed for trajectory tracking by the system's state vector and simultaneous disturbance rejection, considering that the disturbance affects the system in the worst possible manner. As already explained in Chap. 1, disturbances' effect are incorporated in the following quadratic cost function:

$$J(t) = \frac{1}{2}\int_0^T [y^T(t)y(t) + ru^T(t)u(t) - \rho^2 \tilde{d}^T(t)\tilde{d}(t)]dt, \quad r, \rho > 0 \tag{2.29}$$

The significance of the negative sign in the cost function's term that is associated with the perturbation variable $\tilde{d}(t)$ is that the disturbance tries to maximize the cost function $J(t)$ while the control signal $u(t)$ tries to minimize it. The physical meaning of the relation given above is that the control signal and the disturbances compete to each other within a min-max differential game. This problem of min-max optimization can be written as

$$min_u max_{\tilde{d}} J(u, \tilde{d}) \tag{2.30}$$

The objective of the optimization procedure is to compute a control signal $u(t)$ which can compensate for the worst possible disturbance, that is externally imposed to the overhead crane system. However, the solution to the min-max optimization problem is directly related to the value of the parameter ρ. This means that there is an upper bound in the disturbances magnitude that can be annihilated by the crane's control signal.

2.2.4.3 Computation of the Feedback Control Gains

For the linearized system given by Eq. (2.75) the cost function of Eq. (2.76) is defined, where the coefficient r determines the penalization of the control input and the weight coefficient ρ determines the reward of the disturbances' effects.

It is assumed that (i) The energy that is transferred from the disturbances signal $\tilde{d}(t)$ is bounded, that is $\int_0^\infty \tilde{d}^T(t)\tilde{d}(t)dt < \infty$, (ii) the matrices $[A, B]$ and $[A, L]$ of the linearized model of the crane are stabilizable, (iii) the matrix $[A, C]$ is detectable. Then, the optimal feedback control law is given by

$$u(t) = -Kx(t) \tag{2.31}$$

with

$$K = \frac{1}{r}B^T P \tag{2.32}$$

where P is a positive semi-definite symmetric matrix which is obtained from the solution of the Riccati equation

$$A^T P + PA + Q - P\left(\frac{1}{r}BB^T - \frac{1}{2\rho^2}LL^T\right)P = 0 \tag{2.33}$$

where Q is also a positive definite symmetric matrix. The worst case disturbance is given by

$$\tilde{d}(t) = \frac{1}{\rho^2}L^T Px(t) \tag{2.34}$$

The diagram of the considered control loop is depicted in Fig. 2.2.

2.2.5 *Lyapunov Stability Analysis*

Through Lyapunov stability analysis it will be shown that the proposed nonlinear control scheme ensures H_∞ tracking performance for the crane, and that in case of bounded disturbance terms asymptotic convergence to the reference setpoints is achieved. The tracking error dynamics for the underactuated crane is written in the form

$$\dot{e} = Ae + Bu + L\tilde{d} \tag{2.35}$$

where in the crane's case $L = I \in R^8$ with I being the identity matrix. Variable $\tilde{d}$ denotes model uncertainties and external disturbances of the crane's model. The following Lyapunov function is considered

$$V = \frac{1}{2}e^T Pe \tag{2.36}$$

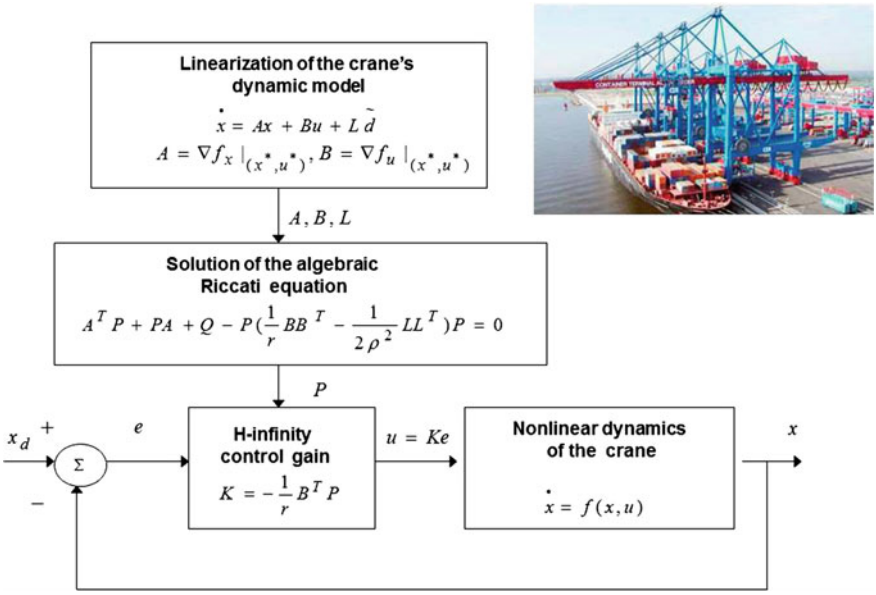

Fig. 2.2 Diagram of the control scheme for the underactuated crane

where $e = x - x_d$ is the tracking error. By differentiating with respect to time one obtains

$$\begin{gathered}\dot{V} = \tfrac{1}{2}\dot{e}^T Pe + \tfrac{1}{2}eP\dot{e} \Rightarrow \\ \dot{V} = \tfrac{1}{2}[Ae + Bu + L\tilde{d}]^T Pe + \tfrac{1}{2}e^T P[Ae + Bu + L\tilde{d}] \Rightarrow\end{gathered} \tag{2.37}$$

$$\begin{gathered}\dot{V} = \tfrac{1}{2}[e^T A^T + u^T B^T + \tilde{d}^T L^T]Pe + \\ + \tfrac{1}{2}e^T P[Ae + Bu + L\tilde{d}] \Rightarrow\end{gathered} \tag{2.38}$$

$$\begin{gathered}\dot{V} = \tfrac{1}{2}e^T A^T Pe + \tfrac{1}{2}u^T B^T Pe + \tfrac{1}{2}\tilde{d}^T L^T Pe + \\ \tfrac{1}{2}e^T PAe + \tfrac{1}{2}e^T PBu + \tfrac{1}{2}e^T PL\tilde{d}\end{gathered} \tag{2.39}$$

The previous equation is rewritten as

$$\begin{gathered}\dot{V} = \tfrac{1}{2}e^T(A^T P + PA)e + \left(\tfrac{1}{2}u^T B^T Pe + \tfrac{1}{2}e^T PBu\right) + \\ + \left(\tfrac{1}{2}\tilde{d}^T L^T Pe + \tfrac{1}{2}e^T PL\tilde{d}\right)\end{gathered} \tag{2.40}$$

Assumption: For given positive definite matrix Q and coefficients r and ρ there exists a positive definite matrix P, which is the solution of the following matrix equation

$$A^T P + PA = -Q + P\left(\tfrac{2}{r}BB^T - \tfrac{1}{\rho^2}LL^T\right)P \tag{2.41}$$

Moreover, the following feedback control law is applied to the system

$$u = -\tfrac{1}{r} B^T P e \tag{2.42}$$

By substituting Eqs. (2.41) and (2.42) one obtains

$$\begin{gathered} \dot{V} = \tfrac{1}{2} e^T \left[-Q + P \left(\tfrac{2}{r} B B^T - \tfrac{1}{\rho^2} L L^T \right) P \right] e + \\ + e^T P B \left(-\tfrac{1}{r} B^T P e \right) + e^T P L \tilde{d} \Rightarrow \end{gathered} \tag{2.43}$$

$$\begin{gathered} \dot{V} = -\tfrac{1}{2} e^T Q e + \tfrac{1}{r} e^T P B B^T P e - \tfrac{1}{2\rho^2} e^T P L L^T P e \\ - \tfrac{1}{r} e^T P B B^T P e + e^T P L \tilde{d} \end{gathered} \tag{2.44}$$

which after intermediate operations gives

$$\dot{V} = -\tfrac{1}{2} e^T Q e - \tfrac{1}{2\rho^2} e^T P L L^T P e + e^T P L \tilde{d} \tag{2.45}$$

or, equivalently

$$\begin{gathered} \dot{V} = -\tfrac{1}{2} e^T Q e - \tfrac{1}{2\rho^2} e^T P L L^T P e + \\ + \tfrac{1}{2} e^T P L \tilde{d} + \tfrac{1}{2} \tilde{d}^T L^T P e \end{gathered} \tag{2.46}$$

Lemma: The following inequality holds

$$\tfrac{1}{2} e^T P L \tilde{d} + \tfrac{1}{2} \tilde{d} L^T P e - \tfrac{1}{2\rho^2} e^T P L L^T P e \leq \tfrac{1}{2} \rho^2 \tilde{d}^T \tilde{d} \tag{2.47}$$

Proof: The binomial $(\rho\alpha - \frac{1}{\rho} b)^2$ is considered. Expanding the left part of the above inequality one gets

$$\begin{gathered} \rho^2 a^2 + \tfrac{1}{\rho^2} b^2 - 2ab \geq 0 \Rightarrow \tfrac{1}{2} \rho^2 a^2 + \tfrac{1}{2\rho^2} b^2 - ab \geq 0 \Rightarrow \\ ab - \tfrac{1}{2\rho^2} b^2 \leq \tfrac{1}{2} \rho^2 a^2 \Rightarrow \tfrac{1}{2} ab + \tfrac{1}{2} ab - \tfrac{1}{2\rho^2} b^2 \leq \tfrac{1}{2} \rho^2 a^2 \end{gathered} \tag{2.48}$$

The following substitutions are carried out: $a = \tilde{d}$ and $b = e^T P L$ and the previous relation becomes

$$\tfrac{1}{2} \tilde{d}^T L^T P e + \tfrac{1}{2} e^T P L \tilde{d} - \tfrac{1}{2\rho^2} e^T P L L^T P e \leq \tfrac{1}{2} \rho^2 \tilde{d}^T \tilde{d} \tag{2.49}$$

Equation (2.49) is substituted in Eq. (2.46) and the inequality is enforced, thus giving

$$\dot{V} \leq -\tfrac{1}{2} e^T Q e + \tfrac{1}{2} \rho^2 \tilde{d}^T \tilde{d} \tag{2.50}$$

Equation (2.50) shows that the H_∞ tracking performance criterion is satisfied. The integration of $\dot{V}$ from 0 to T gives

$$\begin{aligned} &\int_0^T \dot{V}(t)dt \leq -\tfrac{1}{2}\int_0^T ||e||_Q^2 dt + \tfrac{1}{2}\rho^2 \int_0^T ||\tilde{d}||^2 dt \Rightarrow \\ &2V(T) + \int_0^T ||e||_Q^2 dt \leq 2V(0) + \rho^2 \int_0^T ||\tilde{d}||^2 dt \end{aligned} \tag{2.51}$$

Moreover, if there exists a positive constant $M_d > 0$ such that

$$\int_0^\infty ||\tilde{d}||^2 dt \leq M_d \tag{2.52}$$

then one gets

$$\int_0^\infty ||e||_Q^2 dt \leq 2V(0) + \rho^2 M_d \tag{2.53}$$

Thus, the integral $\int_0^\infty ||e||_Q^2 dt$ is bounded. Moreover, $V(T)$ is bounded and from the definition of the Lyapunov function V in Eq. (2.36) it becomes clear that $e(t)$ will be also bounded since $e(t) \in \Omega_e = \{e | e^T P e \leq 2V(0) + \rho^2 M_d\}$. According to the above and with the use of Barbalat's Lemma one obtains $lim_{t\to\infty} e(t) = 0$.

Elaborating on the above, it can be noted that the proof of global asymptotic stability for the control loop of the underactuated crane is based on Eq. (2.50) and on the application of Barbalat's Lemma. It uses the condition of Eq. (2.52) about the boundedness of the square of the aggregate disturbance and modelling error term $\tilde{d}$ that affects the model. However, as explained above the proof of global asymptotic stability is not restricted by this condition. By selecting the attenuation coefficient ρ to be sufficiently small and in particular to satisfy $\rho^2 < ||e||_Q^2 / ||\tilde{d}||^2$ one has that the first derivative of the Lyapunov function is upper bounded by 0. Therefore for the ith time interval it is proven that the Lyapunov function defined in Eq. (2.36) is a decreasing one. This also ensures the Lyapunov function of the system defined in Eq. (29) will always have a negative first-order derivative.

2.2.6 *Robust State Estimation with the Use of the H-Infinity Kalman Filter*

The control loop has to be implemented with the use of information provided by a small number of sensors and by processing only a small number of state variables. To reconstruct the missing information about the state vector of the overhead crane it is proposed to use a filtering scheme and based on it to apply state estimation-based control [169, 457, 511]. The recursion of the H_∞ Kalman Filter, for the model of the crane, can be formulated in terms of a *measurement update* and a *time update* part

Measurement update:

$$\begin{aligned} D(k) &= [I - \theta W(k) P^-(k) + C^T(k) R(k)^{-1} C(k) P^-(k)]^{-1} \\ K(k) &= P^-(k) D(k) C^T(k) R(k)^{-1} \\ \hat{x}(k) &= \hat{x}^-(k) + K(k)[y(k) - C\hat{x}^-(k)] \end{aligned} \tag{2.54}$$

Time update:

$$\begin{aligned} \hat{x}^{-}(k+1) &= A(k)x(k) + B(k)u(k) \\ P^{-}(k+1) &= A(k)P^{-}(k)D(k)A^{T}(k) + Q(k) \end{aligned} \tag{2.55}$$

where it is assumed that parameter θ is sufficiently small to assure that the covariance matrix $P^{-}(k)^{-1} - \theta W(k) + C^{T}(k)R(k)^{-1}C(k)$ will be positive definite. When $\theta = 0$ the H_{∞} Kalman Filter becomes equivalent to the standard Kalman Filter. One can measure only a part of the state vector of the crane, and estimate through filtering the rest of the state vector elements. Moreover, the proposed Kalman filtering method can be used for sensor fusion purposes.

2.2.7 Simulation Tests

The performed simulation tests have demonstrated the excellent tracking performance of the H-infinity nonlinear control scheme in the case of the stabilization and control problem of the underactuated crane. The computation of the feedback control gain was based on the solution of the algebraic Riccati equation given in Eq. (2.41), through a procedure that was repeated at each iteration of the control method. The obtained results are depicted in Figs. 2.3, 2.4, 2.5, 2.6, 2.7 and 2.8. The simulation tests' diagrams evaluate the performance of the proposed nonlinear H-infinity control method for the problem of control of the 4-DOF overhead crane with respect to the following indexes: (i) accuracy of tracking of the reference trajectories measured in RMSE (Root Mean Square Error) (ii) avoidance of abrupt variations of the control inputs and avoidance of actuators saturation, (iii) robustness to model uncertainty and external perturbations. It can be confirmed that fast and accurate convergence of the state variables of the crane to the reference setpoints was achieved. Moreover, it can be seen that the variation of the control inputs remained smooth and within moderate ranges. Despite underactuation, the control method's performance was satisfactory and precise tracking of the reference setpoints was achieved.

In the presented simulation experiments state estimation-based control has been implemented. Out of the 8 state variables of the underactuated crane only 4 where considered to be measurable. These were the cartesian coordinates of the crane x and y and the displacement angles of the payload θ_x and θ_y. The rest of the state variables, describing the time derivatives of the cartesian coordinates of the crane and the time derivatives of the payload's displacement angles were indirectly estimated with the use of the H-infinity Kalman Filter. The real value of each state variable has been plotted in blue, the estimated value has been plotted in green, while the associated reference setpoint has been plotted in red. It can be noticed that despite model uncertainty the H-infinity Kalman Filter achieved accurate estimation of the real values of the state vector elements. In this manner the robustness of the state estimation-based H-infinity control scheme was also improved.

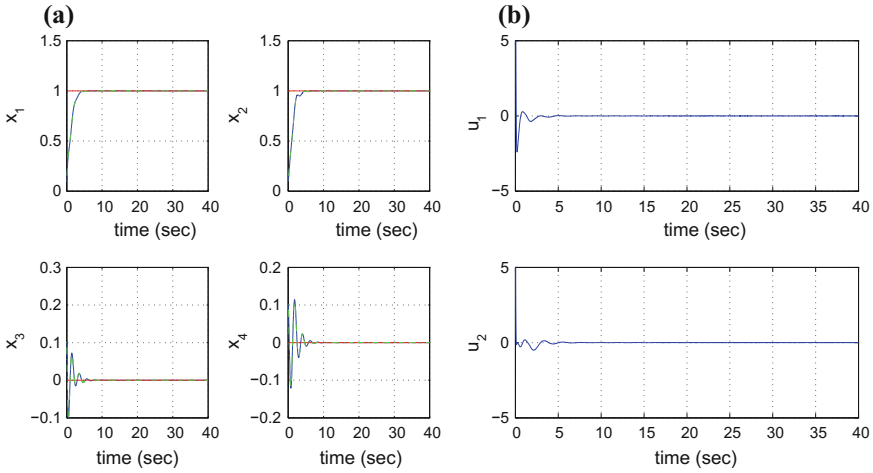

Fig. 2.3 Reference path 1: **a** Convergence of the state variables of the crane $x_1 = x$, $x_2 = y$, $x_3 = \theta_x$ and $x_4 = \theta_y$ (blue line: real value, green line: estimated value by the H-infinity filter) to the associated reference values (red line). **b** Control inputs u_1 and u_2 applied to the control system

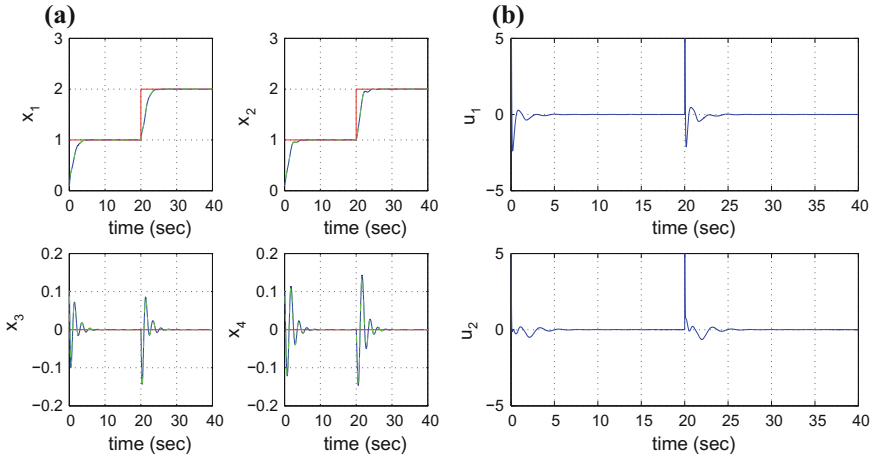

Fig. 2.4 Reference path 2: **a** Convergence of the state variables of the crane $x_1 = x$, $x_2 = y$, $x_3 = \theta_x$ and $x_4 = \theta_y$ (blue line: real value, green line: estimated value by the H-infinity filter) to the associated reference values (red line). **b** Control inputs u_1 and u_2 applied to the control system

Yet computationally simple, the proposed H_∞ control scheme has an excellent performance. Comparing to the control of underactuated cranes that can be based on global linearization methods [457, 629] the presented nonlinear H_∞ control scheme is equally efficient in setpoint tracking while also retaining optimal control features.

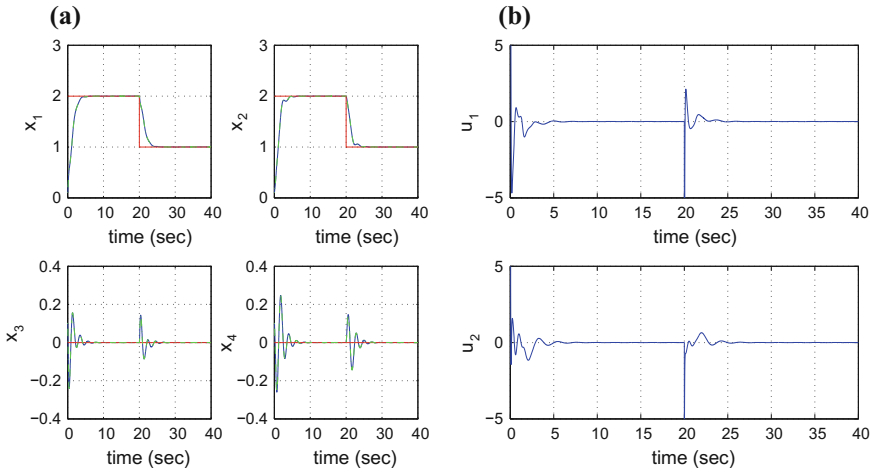

Fig. 2.5 Reference path 3: **a** Convergence of the state variables of the crane $x_1 = x$, $x_2 = y$, $x_3 = \theta_x$ and $x_4 = \theta_y$ (blue line: real value, green line: estimated value by the H-infinity filter) to the associated reference values (red line). **b** Control inputs u_1 and u_2 applied to the control system

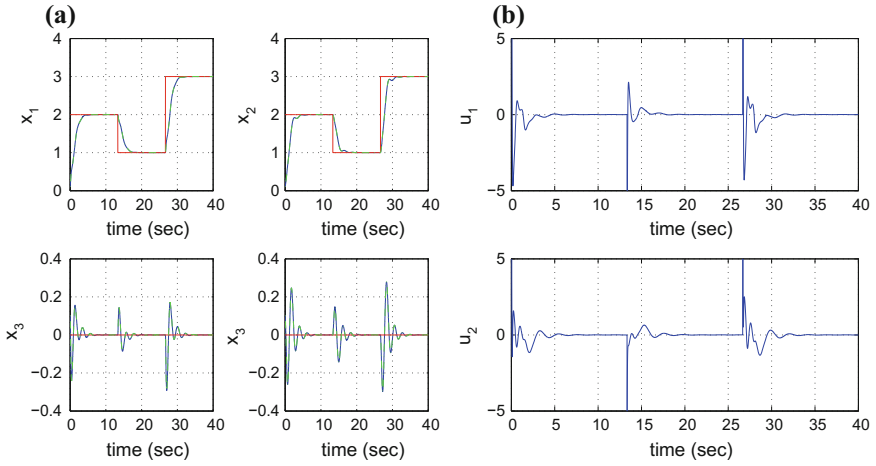

Fig. 2.6 Reference path 4: **a** Convergence of the state variables of the crane $x_1 = x$, $x_2 = y$, $x_3 = \theta_x$ and $x_4 = \theta_y$ (blue line: real value, green line: estimated value by the H-infinity filter) to the associated reference values (red line). **b** Control inputs u_1 and u_2 applied to the control system

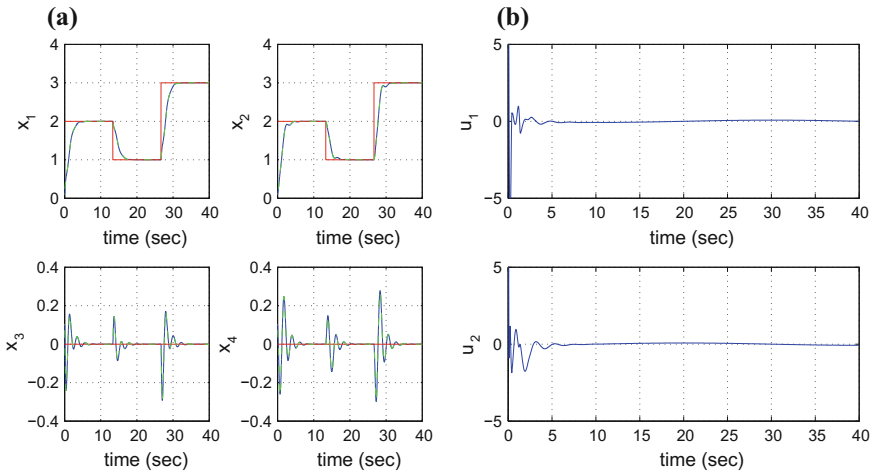

Fig. 2.7 Reference path 5: **a** Convergence of the state variables of the crane $x_1 = x$, $x_2 = y$, $x_3 = \theta_x$ and $x_4 = \theta_y$ (blue line: real value, green line: estimated value by the H-infinity filter) to the associated reference values (red line). **b** Control inputs u_1 and u_2 applied to the control system

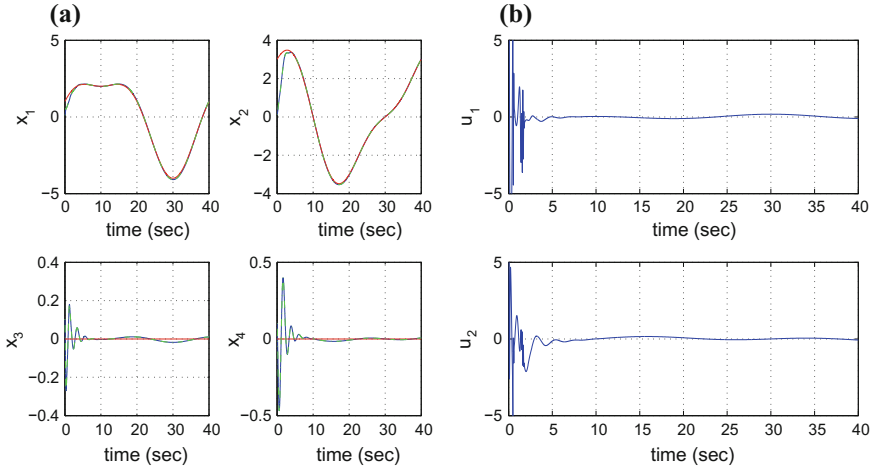

Fig. 2.8 Reference path 6: **a** Convergence of the state variables of the crane $x_1 = x$, $x_2 = y$, $x_3 = \theta_x$ and $x_4 = \theta_y$ (blue line: real value, green line: estimated value by the H-infinity filter) to the associated reference values (red line). **b** Control inputs u_1 and u_2 applied to the control system

Table 2.1 RMSE of the crane's state variables

Path	RMSEx_1	RMSEx_2	RMSEx_3	RMSEx_4	RMSEx_5	RMSEx_6	RMSEx_7	RMSEx_8
1	$1.26{\cdot}10^{-6}$	$2.36{\cdot}10^{-6}$	$0.02{\cdot}10^{-6}$	$0.03{\cdot}10^{-6}$	$0.12{\cdot}10^{-6}$	$0.26{\cdot}10^{-6}$	$0.05{\cdot}10^{-6}$	$0.10{\cdot}10^{-6}$
2	$0.85{\cdot}10^{-6}$	$0.36{\cdot}10^{-6}$	$0.11{\cdot}10^{-6}$	$0.19{\cdot}10^{-6}$	$0.21{\cdot}10^{-6}$	$0.53{\cdot}10^{-6}$	$0.30{\cdot}10^{-6}$	$0.70{\cdot}10^{-6}$
3	$0.65{\cdot}10^{-6}$	$0.17{\cdot}10^{-6}$	$0.11{\cdot}10^{-6}$	$0.20{\cdot}10^{-6}$	$0.24{\cdot}10^{-6}$	$0.32{\cdot}10^{-6}$	$0.29{\cdot}10^{-6}$	$0.72{\cdot}10^{-6}$
4	$0.04{\cdot}10^{-4}$	$0.06{\cdot}10^{-4}$	$0.07{\cdot}10^{-4}$	$0.17{\cdot}10^{-4}$	$0.10{\cdot}10^{-4}$	$0.25{\cdot}10^{-4}$	$0.24{\cdot}10^{-4}$	$0.41{\cdot}10^{-4}$
5	$9.00{\cdot}10^{-4}$	$5.00{\cdot}10^{-4}$	$10.0{\cdot}10^{-4}$	$4.00{\cdot}10^{-4}$	$3.00{\cdot}10^{-4}$	$1.00{\cdot}10^{-4}$	$1.00{\cdot}10^{-4}$	$2.00{\cdot}10^{-4}$
6	$9.47{\cdot}10^{-4}$	$4.00{\cdot}10^{-4}$	$4.00{\cdot}10^{-4}$	$2.00{\cdot}10^{-4}$	$2.00{\cdot}10^{-4}$	$9.00{\cdot}10^{-4}$	$4.00{\cdot}10^{-6}$	$2.00{\cdot}10^{-4}$

Table 2.2 RMSE of state variables under model disturbance

Δa (%)	RMSEx_1	RMSEx_2	RMSEx_3	RMSEx_4	RMSEx_5	RMSEx_6	RMSEx_7	RMSEx_8
0	$0.04{\cdot}10^{-4}$	$0.06{\cdot}10^{-4}$	$0.07{\cdot}10^{-4}$	$0.17{\cdot}10^{-4}$	$0.10{\cdot}10^{-4}$	$0.23{\cdot}10^{-4}$	$0.24{\cdot}10^{-4}$	$0.41{\cdot}10^{-4}$
25	$0.25{\cdot}10^{-4}$	$25.0{\cdot}10^{-4}$	$0.07{\cdot}10^{-4}$	$0.17{\cdot}10^{-4}$	$0.10{\cdot}10^{-4}$	$2.09{\cdot}10^{-4}$	$0.24{\cdot}10^{-4}$	$0.40{\cdot}10^{-4}$
50	$0.48{\cdot}10^{-4}$	$49.0{\cdot}10^{-4}$	$0.06{\cdot}10^{-4}$	$0.16{\cdot}10^{-4}$	$0.11{\cdot}10^{-4}$	$4.08{\cdot}10^{-4}$	$0.24{\cdot}10^{-4}$	$0.40{\cdot}10^{-4}$
75	$0.74{\cdot}10^{-4}$	$72.0{\cdot}10^{-4}$	$0.06{\cdot}10^{-4}$	$0.16{\cdot}10^{-4}$	$0.12{\cdot}10^{-4}$	$6.04{\cdot}10^{-4}$	$0.24{\cdot}10^{-4}$	$0.40{\cdot}10^{-4}$
100	$0.96{\cdot}10^{-4}$	$96.0{\cdot}10^{-4}$	$0.06{\cdot}10^{-4}$	$0.16{\cdot}10^{-4}$	$0.13{\cdot}10^{-4}$	$7.36{\cdot}10^{-4}$	$0.24{\cdot}10^{-4}$	$0.39{\cdot}10^{-4}$

Table 2.3 RMSE of state variables under model disturbance

Δa (%)	RMSEx_1	RMSEx_2	RMSEx_3	RMSEx_4	RMSEx_5	RMSEx_6	RMSEx_7	RMSEx_8
0	$0.04{\cdot}10^{-4}$	$0.06{\cdot}10^{-4}$	$0.07{\cdot}10^{-4}$	$0.17{\cdot}10^{-4}$	$0.10{\cdot}10^{-4}$	$0.23{\cdot}10^{-4}$	$0.24{\cdot}10^{-4}$	$0.41{\cdot}10^{-4}$
25	$1.00{\cdot}10^{-4}$	$15.0{\cdot}10^{-4}$	$0.06{\cdot}10^{-4}$	$0.16{\cdot}10^{-4}$	$0.11{\cdot}10^{-4}$	$1.29{\cdot}10^{-4}$	$0.24{\cdot}10^{-4}$	$0.39{\cdot}10^{-4}$
50	$1.83{\cdot}10^{-4}$	$29.0{\cdot}10^{-4}$	$0.06{\cdot}10^{-4}$	$0.13{\cdot}10^{-4}$	$0.19{\cdot}10^{-4}$	$2.46{\cdot}10^{-4}$	$0.23{\cdot}10^{-4}$	$0.38{\cdot}10^{-4}$
75	$3.66{\cdot}10^{-4}$	$43.0{\cdot}10^{-4}$	$0.06{\cdot}10^{-4}$	$0.15{\cdot}10^{-4}$	$0.33{\cdot}10^{-4}$	$3.58{\cdot}10^{-4}$	$0.23{\cdot}10^{-4}$	$0.37{\cdot}10^{-4}$
100	$6.05{\cdot}10^{-4}$	$52.0{\cdot}10^{-4}$	$0.06{\cdot}10^{-4}$	$0.14{\cdot}10^{-4}$	$0.52{\cdot}10^{-4}$	$4.66{\cdot}10^{-4}$	$0.26{\cdot}10^{-4}$	$0.36{\cdot}10^{-4}$

The tracking accuracy of the presented H_∞ control method has been monitored in the case of several reference setpoints. The obtained results are given in Table 2.1.

The tracking performance of the nonlinear H-infinity control method for the model of the multi-DOF robotic system and under disturbances, imposing a change equal to $\Delta a\%$ to the first element of the 7th row of the drift function $f(x)$ of Eq. (2.12), is outlined in Table 2.2. It can be noticed that despite model perturbations the tracking accuracy of the control method remained satisfactory.

Moreover, the tracking performance of the nonlinear H-infinity control method for the model of the 2-DOF manipulator and under disturbances, imposing a change equal to $\Delta a\%$ to the first element of the 8th row of the drift function $f(x)$ of Eq. (2.12), is outlined in Table 2.3. It can be noticed that despite model perturbations the tracking accuracy of the control method remained satisfactory.

H-infinity control in its classical implementation is addressed to linear dynamical systems. The 4-DOF overhead crane model considered in this section is a highly

nonlinear one. Therefore, the application of the classical H-infinity control to it would be inadequate. To enable the solution of control and stabilization of the overhead crane under model uncertainty, the H-infinity control is applied to the crane's linearized model which is obtained after performing first order Taylor series expansion for the crane's state-space description. Jointly, the crane's linearization procedure and the application of the H-infinity control method to the approximately linearized model form the nonlinear H-infinity control approach. It is noted that other control methods such as the Model Predictive Control (MPC) would be unsuitable for application to the crane's model because of the model's nonlinearity. Moreover, Nonlinear Model Predictive Control (NMPC) may not be of assured stability and convergence. On the other side, the proposed nonlinear H-infinity control approach is of proven global asymptotic stability.

For the control problem of the overhead crane one can also consider energy-based methods, where the control input is chosen from minimization of a function that comprises the kinematic and the dynamic model of the crane [535]. Such a type of control has been also applied in [450]. Energy-based control methods have been successfully used in many robotic systems, however some of the shortfalls they may exhibit are outlined as follows (i) they rely on an intuitive procedure about the selection of the energy function of the robotic system (ii) they need an intuitive parametrization and tuning of the feedback controller, (iii) they are computationally more demanding because they need more intermediate calculations to arrive at the form that the stabilizing feedback controller should have, (iv) they do not assure the avoidance of singularities, (v) their performance appears to be debatable in terms of transients for both the state variables and control inputs. On the other side, the proposed nonlinear H-infinity control method has clear and easy to implement stages. It requires only (i) the approximate linearization of the robotic system's dynamic model using Taylor expansion and the computation of Jacobian matrices, (ii) the solution of an algebraic Riccati equation that allows for computing the controller's feedback gain. Besides this control method retains the advantages of optimal control, that is best trade-off between accuracy of tracking of the reference trajectories and minimal variations of the control input.

2.3 A Nonlinear Optimal Control Approach for Precise Functioning of Ship-Mounted Cranes

2.3.1 Outline

The need for precise functioning of ship-mounted cranes is apparent in tasks carried out in vessels and offshore platforms aiming at accurately submerging various payloads. To annihilate the effect of hydrodynamic forces and of the vessel's heave motion, methods for cranes nonlinear control and in particular for active heave motion control have been developed [124, 125, 533, 593]. Indicative approaches to the modeling of the electromechanical parts of ship-mounted cranes and heave compensation

systems can be found in [27, 177, 385, 400, 588]. Attempts for the robust functioning of ship-mounted cranes and of the associated payload positioning systems have been presented in [95, 186, 331, 488, 619]. In this section, the ship-mounted crane and payload positioning system is activated by a winch which in turn is driven by an AC motor. The winch controls the submergence of a payload in the water as well as the payload's vertical position (depth). The payload's positioning is affected by hydrodynamic forces and the lift force that is exerted by the crane. Moreover. due to the heave motion of the of the vessel, the payload's motion is also affected by a disturbance term that the control scheme has to compensate for. The problem of control of the payload's position is a nontrivial one because of the nonlinearities of the associated state-space description, and because of time-delays that appear in specific state variables of it. Furthermore, this system is underactuated because of receiving only one control input while having two degrees of freedom [239–242, 285, 304, 357].

There have been attempts to solve this control problem with the use of global linearization methods [240]. The approach of the present section follows an approximate linearization method. The dynamic model of the active heave compensation system undergoes approximate linearization, around a temporary operating point (equilibrium) which is recomputed at each iteration of the control method [423, 461, 466]. This equilibrium comprises the present value of the payload's positioning system state vector and the last value of the control input that was applied to it. The linearization makes use of Taylor series expansion and of the computation of the system's Jacobian's matrices [33, 463, 564]. The modelling error which is due to truncation of higher order terms in the Taylor series expansion is considered to be a perturbation that is compensated by the robustness of the control algorithm. For the approximately linearized model of the payload's positioning system an H-infinity (optimal controller) is designed that is finally capable of compensating the heave motion's effects.

The H-infinity controller stands for the solution to the optimal control problem of the payload's positioning system under model uncertainty and external perturbations. It actually implements the solution to a min-max differential game in which the control input tries to minimize a cost function comprising a quadratic term of the tracking error of the system's state vector, whereas the model uncertainty and external disturbance terms try to maximize this cost functional. To select the controller's feedback gain, an algebraic Riccati equation is solved at each time step of the control method [305, 450, 457, 459]. The stability of the payload's positioning system is proven through Lyapunov analysis. First, it is proven that the control loop satisfies the H-infinity tracking performance criterion. This signifies elevated robustness against model uncertainties and external disturbances. Moreover, under moderate conditions it is proven that the control method is globally asymptotically stable. Finally, to implement state estimation-based feedback control after measuring only a small number of the system's state variables, the H-infinity Kalman Filter has been used as a robust state estimator [169, 511].

2.3.2 Dynamic Model of the Payload's Positioning System

The ship-mounted crane and the associated payload positioning system is shown in Figs. 2.9 and 2.10. The state-space description of the payload's positioning system is given by the state vector $x = [\phi_w, \dot{\phi}_w, z_P, \dot{z}_P]^T$, where ϕ is the turn angle of the winch and z_p is the position of the submerged payload on the z-axis. A detailed analysis of this model follows the stages presented in [240]. The state-space equations of the model are:

$$\begin{pmatrix} \dot{x}_1 \\ \dot{x}_2 \\ \dot{x}_3 \\ \dot{z}_4 \end{pmatrix} = \begin{pmatrix} x_2 \\ -\frac{1}{T_w} x_2 + \frac{K_w}{T_w} u \\ x_4 \\ \frac{1}{m_s}[\beta - \alpha x_4 |x_4| - c_r(x_3 - \gamma r_w x_1(t - T_d))] \end{pmatrix} \tag{2.56}$$

while the measurable output is the depth of the payload z_p. In particular the state variables of the model are defined as: $x_1 = \phi_{r,t}$ is the turn angle of the crane, $x_2 = \dot{\phi}_{r,t}$ is the rotational speed of the crane, $x_3 = z_p$ is the position of the payload along the z-axis and $\dot{z}_p$ is the velocity of the payload along the z-axis, as shown in Figs. 2.9 and 2.10. Moreover, the term $x_1(t - T_d)$ denotes that time-delay equal to T_d affects state variable x_1.

About parameter β one has $\beta = F_g - \rho_w g(V(z_r)) + \frac{1}{2} l_w A_r$, where with reference to Fig. 2.10, $V(z_r)$ is the submerged volume of the load, l_w is the nominal length of the rope, A_r is the cross-sectional area of the submerged rope . About parameter m_s one has $m_s = m_{eq} + A_{33} + \rho_w V(z_r)$, where A_{33} is the added mass of the rope, and is given by $A_{33} = \rho_w C_a V(z_r)$ where C_a is the added mass coefficient which depends on the shape of the object, and ρ_w is the density of the water. Additionally, m_{eq} is the mass of the load plus the mass of the rope, F_g is the gravitational force, $\rho_w g(V(z_r))$ is a lift force, while $\gamma = l_p + z_c(0)$, where l_p is the length (height) of the payload and z_c is the position of the end tip of the crane on the z-axis.

Due to the heave motion of the vessel, an unknown acceleration term equal to $\ddot{z}_c$ affects the motion of the payload, while a term dependent on $\dot{z}_p$ affects the tension of the rope (see [240]). These are perturbations which can be included in the state-space model of Eq. (2.56) by adding a cumulative disturbance term d_h to its fourth row. This unknown disturbance term is anticipated to be compensated by the robustness of the H-infinity control method.

$$\begin{pmatrix} \dot{x}_1 \\ \dot{x}_2 \\ \dot{x}_3 \\ \dot{z}_4 \end{pmatrix} = \begin{pmatrix} x_2 \\ -\frac{1}{T_w} x_2 + \frac{K_w}{T_w} u \\ x_4 \\ \frac{1}{m_s}[\beta - \alpha x_4 |x_4| - c_r(x_3 - \gamma r_w x_1(t - T_d))] + d_h \end{pmatrix} \tag{2.57}$$

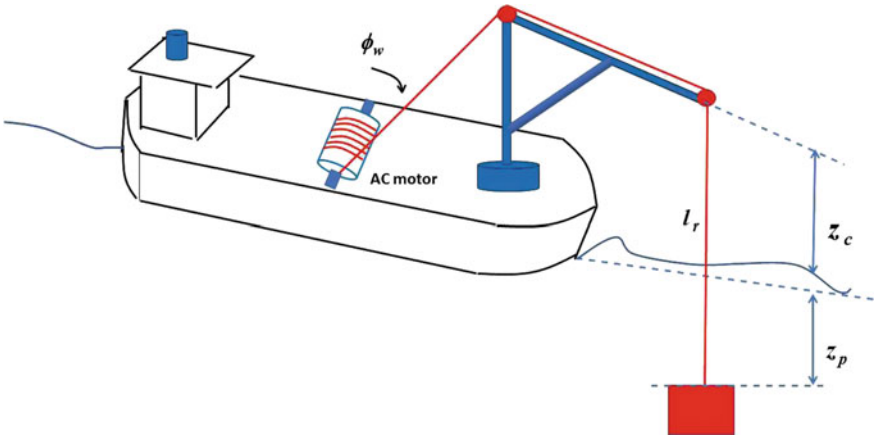

Fig. 2.9 Ship-mounted crane and payload positioning system

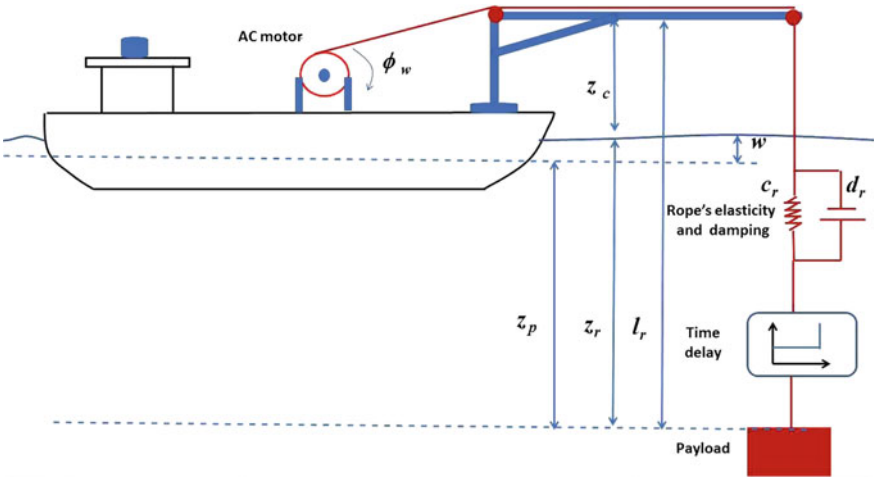

Fig. 2.10 Coordinates for the ship-mounted crane and its payload positioning system

2.3.3 *Approximate Linearization of the Payload's Positioning System*

The state variable $x_1(t - T_d)$ which exhibits time-delay in the state-space model of Eq. (2.56) is approximated with the use of first-order Taylor series expansion

$$\begin{aligned} x_1(t - T_d) &= x_1(t) - T_d \dot{x}_1(t) \Rightarrow \\ x_1(t - T_d) &= x_1(t) - T_d x_2 \end{aligned} \tag{2.58}$$

Consequently, the state-space model of the system under time-delays becomes

$$\begin{pmatrix} \dot{x}_1 \\ \dot{x}_2 \\ \dot{x}_3 \\ \dot{z}_4 \end{pmatrix} = \begin{pmatrix} x_2 \\ -\frac{1}{T_w}x_2 + \frac{K_w}{T_w}u \\ x_4 \\ \frac{1}{m_s}[\beta - \alpha x_4|x_4| - c_r(x_3 - \gamma r_w(x_1 - T_d x_2))] \end{pmatrix} \tag{2.59}$$

The previous state-space model can be also written in vector form:

$$\begin{pmatrix} \dot{x}_1 \\ \dot{x}_2 \\ \dot{x}_3 \\ \dot{z}_4 \end{pmatrix} = \begin{pmatrix} x_2 \\ -\frac{1}{T_w}x_2 \\ x_4 \\ \frac{1}{m_s}[\beta - \alpha x_4|x_4| - c_r(x_3 - \gamma r_w(x_1 - T_d x_2))] \end{pmatrix} + \begin{pmatrix} 0 \\ \frac{k_w}{T_w} \\ 0 \\ 0 \end{pmatrix} u \tag{2.60}$$

By defining the time-varying variable $\tilde{a} = a$ if $x_4 > 0$ and $\tilde{a} = -a$ if $x_4 < 0$ one has the following state-space description

$$\dot{x} = f(x) + g(x)u \tag{2.61}$$

where

$$f(x) = \begin{pmatrix} x_2 \\ -\frac{1}{T_w}x_2 \\ x_4 \\ \frac{1}{m_s}[\beta - \tilde{a}x_4^2 - c_r(x_3 - \gamma r_w(x_1 - T_d x_2))] \end{pmatrix} \quad g(x) = \begin{pmatrix} 0 \\ \frac{k_w}{T_w} \\ 0 \\ 0 \end{pmatrix} \tag{2.62}$$

The state-space model of the payload's positioning system undergoes approximate linearization around the temporary operating point (x^*, u^*), where x^* is the present value of the system's state vector and u^* is the last value of the control input that was exerted on it. To carry out linearization the computation of the associated Jacobian matrices is needed.

$$\nabla_x f(x) = \begin{pmatrix} \frac{\partial f_1}{\partial x_1} & \frac{\partial f_1}{\partial x_2} & \frac{\partial f_1}{\partial x_3} & \frac{\partial f_1}{\partial x_4} \\ \frac{\partial f_2}{\partial x_1} & \frac{\partial f_2}{\partial x_2} & \frac{\partial f_2}{\partial x_3} & \frac{\partial f_2}{\partial x_4} \\ \frac{\partial f_3}{\partial x_1} & \frac{\partial f_3}{\partial x_2} & \frac{\partial f_3}{\partial x_3} & \frac{\partial f_3}{\partial x_4} \\ \frac{\partial f_4}{\partial x_1} & \frac{\partial f_4}{\partial x_2} & \frac{\partial f_4}{\partial x_3} & \frac{\partial f_4}{\partial x_4} \end{pmatrix} \tag{2.63}$$

About the first row of $\nabla_x f(x)$ one has: $\frac{\partial f_1}{\partial x_1} = 0$, $\frac{\partial f_1}{\partial x_2} = 1$, $\frac{\partial f_1}{\partial x_3} = 0$, $\frac{\partial f_1}{\partial x_4} = 0$.

About the second row of $\nabla_x f(x)$ one has: $\frac{\partial f_2}{\partial x_1} = 0$, $\frac{\partial f_2}{\partial x_2} = -\frac{1}{T_w}$, $\frac{\partial f_2}{\partial x_3} = 0$, $\frac{\partial f_2}{\partial x_4} = 0$.

About the third row of $\nabla_x f(x)$ one has: $\frac{\partial f_3}{\partial x_1} = 0$, $\frac{\partial f_3}{\partial x_2} = 0$, $\frac{\partial f_3}{\partial x_3} = 0$, $\frac{\partial f_3}{\partial x_4} = 1$.

About the fourth row of $\nabla_x f(x)$ one has: $\frac{\partial f_4}{\partial x_1} = -\frac{\gamma r_w}{m_s}$, $\frac{\partial f_4}{\partial x_2} = \frac{\gamma r_w T_d}{m_s}$, $\frac{\partial f_4}{\partial x_3} = -\frac{c_r}{m_s}$, $\frac{\partial f_4}{\partial x_4} = -\frac{2\tilde{a}x_4}{m_s}$.

About the Jacobian matrix $\nabla_u(g(x)u) = g(x)$ one has $\nabla_u(g(x)u) = [0\ \frac{k_w}{T_w}\ 0\ 0]^T$. Thus the approximately linearized system is

$$\dot{x} = Ax + Bu + \tilde{d} \tag{2.64}$$

where $\tilde{d}$ is a disturbance which is due to the truncation of higher-order terms in the Taylor series expansion and matrices A, B are defined as:

$$A = \nabla_x[f(x) + g(x)u] \mid_{(x^*,u^*)} \Rightarrow A = \nabla_x f(x) \mid_{(x^*,u^*)} \tag{2.65}$$

$$B = \nabla_u[f(x) + g(x)u] \mid_{(x^*,u^*)} \Rightarrow B = g(x) \mid_{(x^*,u^*)} \tag{2.66}$$

2.3.4 Design of an H-Infinity Nonlinear Feedback Controller

2.3.4.1 Equivalent Linearized Dynamics of the Payload's Positioning System

After linearization around its current operating point, the dynamic model of the payload's positioning system is written as

$$\dot{x} = Ax + Bu + d_1 \tag{2.67}$$

Parameter d_1 stands for the linearization error in the dynamic model of the payload's positioning system appearing in Eq. (2.67). The reference setpoints for the payload's positioning system state vector are denoted by $\mathbf{x_d} = [x_1^d, \ldots, x_6^d]$. Tracking of this trajectory is achieved after applying the control input u^*. At every time instant the control input u^* is assumed to differ from the control input u appearing in Eq. (2.67) by an amount equal to Δu, that is $u^* = u + \Delta u$

$$\dot{x}_d = Ax_d + Bu^* + d_2 \tag{2.68}$$

The dynamics of the controlled system described in Eq. (2.67) can be also written as

$$\dot{x} = Ax + Bu + Bu^* - Bu^* + d_1 \tag{2.69}$$

and by denoting $d_3 = -Bu^* + d_1$ as an aggregate disturbance term one obtains

$$\dot{x} = Ax + Bu + Bu^* + d_3 \tag{2.70}$$

By subtracting Eq. (2.68) from (2.70) one has

$$\dot{x} - \dot{x}_d = A(x - x_d) + Bu + d_3 - d_2 \tag{2.71}$$

By denoting the tracking error as $e = x - x_d$ and the aggregate disturbance term as $\tilde{d} = d_3 - d_2$, the tracking error dynamics becomes

$$\dot{e} = Ae + Bu + \tilde{d} \tag{2.72}$$

The above linearized form of the payload's positioning system can be efficiently controlled after applying an H-infinity feedback control scheme.

2.3.5 The Nonlinear H-Infinity Control

2.3.5.1 The H-infinity control approach

The initial nonlinear model of the payload's positioning system is in the form

$$\dot{x} = \tilde{f}(x, u) \;\; x \in R^n, \; u \in R^m \tag{2.73}$$

Linearization of the system, that is of the ship-mounted crane and payload's positioning system, is performed at each iteration of the control algorithm round its present operating point $(x^*, u^*) = (x(t), u(t - T_s))$, where T_s is the sampling period. The linearized equivalent model of the system is described by

$$\dot{x} = Ax + Bu + L\tilde{d} \;\; x \in R^n, \; u \in R^m, \; \tilde{d} \in R^q \tag{2.74}$$

where matrices A and B are obtained from the computation of the system's Jacobians and vector $\tilde{d}$ denotes disturbance terms due to linearization errors. The problem of disturbance rejection for the linearized model that is described by

$$\begin{aligned} \dot{x} &= Ax + Bu + L\tilde{d} \\ y &= Cx \end{aligned} \tag{2.75}$$

where $x \in R^n$, $u \in R^m$, $\tilde{d} \in R^q$ and $y \in R^p$, cannot be handled efficiently if the classical LQR control scheme is applied. This is because of the existence of the perturbation term $\tilde{d}$. The disturbance term $\tilde{d}$ apart from modeling (parametric) uncertainty and external perturbation terms can also represent noise terms of any distribution.

In the H_∞ control approach, a feedback control scheme is designed for trajectory tracking by the system's state vector and simultaneous disturbance rejection, considering that the disturbance affects the system in the worst possible manner. The disturbances' effects are incorporated in the following quadratic cost function:

$$J(t) = \tfrac{1}{2}\int_0^T [y^T(t)y(t) + ru^T(t)u(t) - \rho^2 \tilde{d}^T(t)\tilde{d}(t)]dt, \;\; r, \rho > 0 \tag{2.76}$$

As already explained, the significance of the negative sign in the cost function's term that is associated with the perturbation variable $\tilde{d}(t)$ is that the disturbance tries to maximize the cost function $J(t)$ while the control signal $u(t)$ tries to minimize

it. The physical meaning of the relation given above is that the control signal and the disturbances compete to each other within a min-max differential game. This problem of min-max optimization can be written as

$$min_u max_{\tilde{d}} J(u, \tilde{d}) \tag{2.77}$$

The objective of the optimization procedure is to compute a control signal $u(t)$ which can compensate for the worst possible disturbance, that is externally imposed to the system. However, the solution to the min-max optimization problem is directly related to the value of the parameter ρ. This means that there is an upper bound in the disturbances magnitude that can be annihilated by the control signal.

2.3.5.2 Computation of the Feedback Control Gains

For the linearized system given by Eq. (2.75) the cost function of Eq. (2.76) is defined, where the coefficient r determines the penalization of the control input and the weight coefficient ρ determines the reward of the disturbances' effects.

It is assumed that (i) The energy that is transferred from the disturbances signal $\tilde{d}(t)$ is bounded, that is $\int_0^\infty \tilde{d}^T(t)\tilde{d}(t)dt < \infty$, (ii) the matrices $[A, B]$ and $[A, L]$ are stabilizable, (iii) the matrix $[A, C]$ is detectable. Then, the optimal feedback control law is given by

$$u(t) = -Kx(t) \tag{2.78}$$

with

$$K = \frac{1}{r} B^T P \tag{2.79}$$

where P is a positive semi-definite symmetric matrix which is obtained from the solution of the Riccati equation

$$A^T P + PA + Q - P\left(\frac{1}{r} BB^T - \frac{1}{2\rho^2} LL^T\right) P = 0 \tag{2.80}$$

where Q is also a positive definite symmetric matrix. The worst case disturbance is given by

$$\tilde{d}(t) = \frac{1}{\rho^2} L^T P x(t) \tag{2.81}$$

The diagram of the considered control loop is depicted in Fig. 2.11.

2.3.5.3 Riccati Equation Coefficients in H-Infinity Control Robustness

As already analyzed, parameter ρ in Eq. (2.76), is an indication of the closed-loop system robustness. If the values of $\rho > 0$ are excessively decreased with respect to r, then the solution of the Riccati equation is no longer a positive definite matrix.

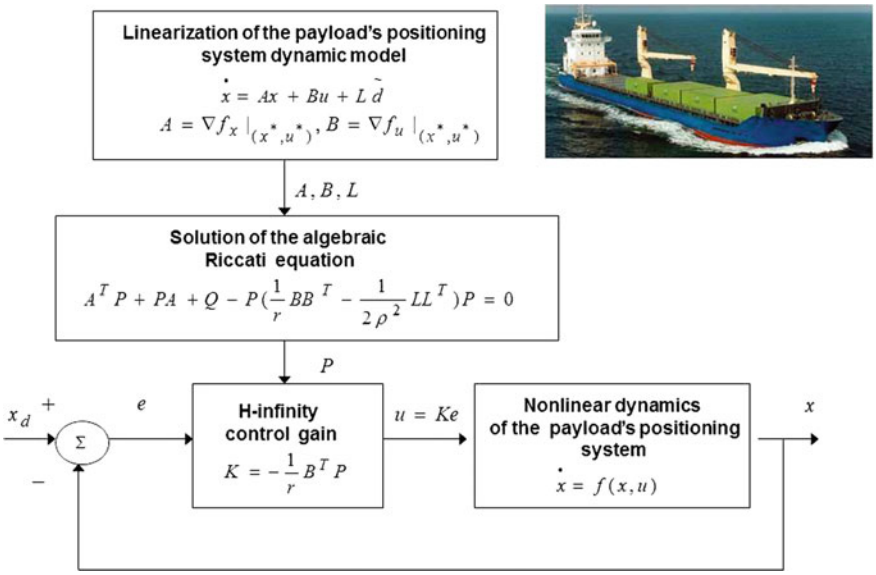

Fig. 2.11 Diagram of the control scheme for the ship-mounted crane and payload positioning system

Consequently there is a lower bound ρ_{min} of ρ for which the H_∞ control problem has a solution. The acceptable values of ρ lie in the interval $[\rho_{min}, \infty)$. If ρ_{min} is found and used in the design of the H_∞ controller, then the closed-loop system will have increased robustness. Unlike this, if a value $\rho > \rho_{min}$ is used, then an admissible stabilizing H_∞ controller will be derived but it will be a suboptimal one. The Hamiltonian matrix

$$H = \begin{pmatrix} A & -(\frac{1}{r}BB^T - \frac{1}{\rho^2}LL^T) \\ -Q & -A^T \end{pmatrix} \tag{2.82}$$

provides a criterion for the existence of a solution of the Riccati equation (2.80). A necessary condition for the solution of the algebraic Riccati equation to be a positive semi-definite symmetric matrix is that H has no imaginary eigenvalues [450].

2.3.6 *Lyapunov Stability Analysis*

Through Lyapunov stability analysis it will be shown again that the proposed nonlinear control scheme assures H_∞ tracking performance for the ship-mounted crane and the payload's positioning system, and that in case of bounded disturbance terms asymptotic convergence to the reference setpoints is achieved. The tracking error dynamics for the payload's positioning system is written in the form

$$\dot{e} = Ae + Bu + L\tilde{d} \tag{2.83}$$

where in the case of the payload's positioning system $L = I \in R^4$ with I being the identity matrix. Variable $\tilde{d}$ denotes model uncertainties and external disturbances of the payload's positioning system. The following Lyapunov equation is considered

$$V = \tfrac{1}{2} e^T P e \tag{2.84}$$

where $e = x - x_d$ is the tracking error. By differentiating with respect to time one obtains

$$\begin{gathered} \dot{V} = \tfrac{1}{2}\dot{e}^T P e + \tfrac{1}{2} e P \dot{e} \Rightarrow \\ \dot{V} = \tfrac{1}{2}[Ae + Bu + L\tilde{d}]^T P e + \tfrac{1}{2} e^T P [Ae + Bu + L\tilde{d}] \Rightarrow \end{gathered} \tag{2.85}$$

$$\begin{gathered} \dot{V} = \tfrac{1}{2}[e^T A^T + u^T B^T + \tilde{d}^T L^T] P e + \\ + \tfrac{1}{2} e^T P [Ae + Bu + L\tilde{d}] \Rightarrow \end{gathered} \tag{2.86}$$

$$\begin{gathered} \dot{V} = \tfrac{1}{2} e^T A^T P e + \tfrac{1}{2} u^T B^T P e + \tfrac{1}{2} \tilde{d}^T L^T P e + \\ \tfrac{1}{2} e^T P A e + \tfrac{1}{2} e^T P B u + \tfrac{1}{2} e^T P L \tilde{d} \end{gathered} \tag{2.87}$$

The previous equation is rewritten as

$$\begin{gathered} \dot{V} = \tfrac{1}{2} e^T (A^T P + P A) e + \left(\tfrac{1}{2} u^T B^T P e + \tfrac{1}{2} e^T P B u \right) + \\ + \left(\tfrac{1}{2} \tilde{d}^T L^T P e + \tfrac{1}{2} e^T P L \tilde{d} \right) \end{gathered} \tag{2.88}$$

Assumption: For given positive definite matrix Q and coefficients r and ρ there exists a positive definite matrix P, which is the solution of the following matrix equation

$$A^T P + P A = -Q + P \left(\tfrac{2}{r} B B^T - \tfrac{1}{\rho^2} L L^T \right) P \tag{2.89}$$

Moreover, the following feedback control law is applied to the system

$$u = -\tfrac{1}{r} B^T P e \tag{2.90}$$

By substituting Eqs. (2.89) and (2.90) one obtains

$$\begin{gathered} \dot{V} = \tfrac{1}{2} e^T \left[-Q + P \left(\tfrac{2}{r} B B^T - \tfrac{1}{\rho^2} L L^T \right) P \right] e + \\ + e^T P B \left(-\tfrac{1}{r} B^T P e \right) + e^T P L \tilde{d} \Rightarrow \end{gathered} \tag{2.91}$$

$$\begin{gathered} \dot{V} = -\tfrac{1}{2} e^T Q e + \tfrac{1}{r} e^T P B B^T P e - \tfrac{1}{2\rho^2} e^T P L L^T P e \\ - \tfrac{1}{r} e^T P B B^T P e + e^T P L \tilde{d} \end{gathered} \tag{2.92}$$

which after intermediate operations gives

$$\dot{V} = -\frac{1}{2}e^T Qe - \frac{1}{2\rho^2}e^T PLL^T Pe + e^T PL\tilde{d} \tag{2.93}$$

or, equivalently

$$\begin{aligned}\dot{V} = -\frac{1}{2}e^T Qe - \frac{1}{2\rho^2}e^T PLL^T Pe + \\ + \frac{1}{2}e^T PL\tilde{d} + \frac{1}{2}\tilde{d}^T L^T Pe\end{aligned} \tag{2.94}$$

Lemma: The following inequality holds

$$\frac{1}{2}e^T PL\tilde{d} + \frac{1}{2}\tilde{d}L^T Pe - \frac{1}{2\rho^2}e^T PLL^T Pe \leq \frac{1}{2}\rho^2\tilde{d}^T\tilde{d} \tag{2.95}$$

Proof: The binomial $(\rho\alpha - \frac{1}{\rho}b)^2$ is considered. Expanding the left part of the above inequality one gets

$$\begin{aligned}\rho^2a^2 + \frac{1}{\rho^2}b^2 - 2ab \geq 0 \Rightarrow \frac{1}{2}\rho^2a^2 + \frac{1}{2\rho^2}b^2 - ab \geq 0 \Rightarrow \\ ab - \frac{1}{2\rho^2}b^2 \leq \frac{1}{2}\rho^2a^2 \Rightarrow \frac{1}{2}ab + \frac{1}{2}ab - \frac{1}{2\rho^2}b^2 \leq \frac{1}{2}\rho^2a^2\end{aligned} \tag{2.96}$$

The following substitutions are carried out: $a = \tilde{d}$ and $b = e^T PL$ and the previous relation becomes

$$\frac{1}{2}\tilde{d}^T L^T Pe + \frac{1}{2}e^T PL\tilde{d} - \frac{1}{2\rho^2}e^T PLL^T Pe \leq \frac{1}{2}\rho^2\tilde{d}^T\tilde{d} \tag{2.97}$$

Equation (2.97) is substituted in Eq. (2.94) and the inequality is enforced, thus giving

$$\dot{V} \leq -\frac{1}{2}e^T Qe + \frac{1}{2}\rho^2\tilde{d}^T\tilde{d} \tag{2.98}$$

Equation (2.98) shows that the H_∞ tracking performance criterion is satisfied. The integration of $\dot{V}$ from 0 to T gives

$$\begin{aligned}\int_0^T \dot{V}(t)dt \leq -\frac{1}{2}\int_0^T ||e||_Q^2 dt + \frac{1}{2}\rho^2\int_0^T ||\tilde{d}||^2 dt \Rightarrow \\ 2V(T) + \int_0^T ||e||_Q^2 dt \leq 2V(0) + \rho^2\int_0^T ||\tilde{d}||^2 dt\end{aligned} \tag{2.99}$$

Moreover, if there exists a positive constant $M_d > 0$ such that

$$\int_0^\infty ||\tilde{d}||^2 dt \leq M_d \tag{2.100}$$

then one gets

$$\int_0^\infty ||e||_Q^2 dt \leq 2V(0) + \rho^2 M_d \tag{2.101}$$

Thus, the integral $\int_0^\infty ||e||_Q^2 dt$ is bounded. Moreover, $V(T)$ is bounded and from the definition of the Lyapunov function V in Eq. (2.84) it becomes clear that $e(t)$ will

be also bounded since $e(t) \in \Omega_e = \{e | e^T P e \leq 2V(0) + \rho^2 M_d\}$. According to the above and with the use of Barbalat's Lemma one obtains $lim_{t\to\infty} e(t) = 0$.

Elaborating on the above, it can be noted that the proof of global asymptotic stability for the control loop of the ship-mounted crane and the payload's positioning system is based on Eq. (2.98) and on the application of Barbalat's Lemma. It uses the condition of Eq. (2.100) about the boundedness of the square of the aggregate disturbance and modelling error term $\tilde{d}$ that affects the model. However, the proof of global asymptotic stability is not restricted by this condition. By selecting the attenuation coefficient ρ to be sufficiently small and in particular to satisfy $\rho^2 < ||e||_Q^2 / ||\tilde{d}||^2$ one has that the first derivative of the Lyapunov function is upper bounded by 0. Therefore for the ith time interval it is proven that the Lyapunov function defined in Eq. (2.84) is a decreasing one. This also assures the Lyapunov function of the ship-mounted crane system will always have a negative first-order derivative.

2.3.7 *Robust State Estimation with the Use of the H_∞ Kalman Filter*

The control loop has to be implemented with the use of information provided by a small number of sensors and by processing only a small number of state variables. To reconstruct the missing information about the state vector of the payload's positioning system it is proposed to use a filtering scheme and based on it to apply state estimation-based control [169, 457, 511]. The recursion of the H_∞ Kalman Filter, for the model of the payload's positioning system, can be formulated in terms of a *measurement update* and a *time update* part

Measurement update:

$$\begin{aligned} D(k) &= [I - \theta W(k) P^-(k) + C^T(k) R(k)^{-1} C(k) P^-(k)]^{-1} \\ K(k) &= P^-(k) D(k) C^T(k) R(k)^{-1} \\ \hat{x}(k) &= \hat{x}^-(k) + K(k)[y(k) - C\hat{x}^-(k)] \end{aligned} \tag{2.102}$$

Time update:

$$\begin{aligned} \hat{x}^-(k+1) &= A(k)x(k) + B(k)u(k) \\ P^-(k+1) &= A(k)P^-(k)D(k)A^T(k) + Q(k) \end{aligned} \tag{2.103}$$

where it is assumed that parameter θ is sufficiently small to assure that the covariance matrix $P^-(k)^{-1} - \theta W(k) + C^T(k) R(k)^{-1} C(k)$ will be positive definite. When $\theta = 0$ the H_∞ Kalman Filter becomes equivalent to the standard Kalman Filter. One can measure only the depth $x_3 = z_p$ of the payload, and can estimate through filtering the rest of the state vector elements. Moreover, the proposed Kalman filtering method can be used for sensor fusion purposes.

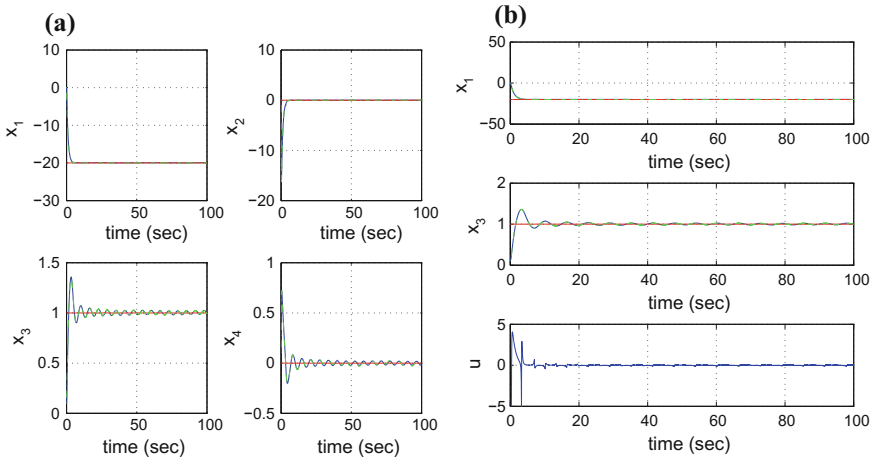

Fig. 2.12 Tracking of setpoint 1: **a** Convergence of the state variables of the payload's positioning system x_i $i = 1, \ldots, 4$ (blue lines) to the reference setpoints (red lines) and associated state estimates (green lines). **b** Diagrams about convergence of state variables $x_1 = \phi_w$, and $x_3 = z_p$ to their reference setpoint, and diagram depicting the variations of the control input

2.3.8 *Simulation Tests*

The performance of the considered control scheme for the ship-mounted crane and the payload's positioning system was tested through simulation experiments. The effect of the heave's motion, as shown in the fourth row of Eq. (2.57), was described by a sinusoidal disturbance term $d_h(t)$. The obtained results are depicted in Figs. 2.12, 2.13, 2.14, 2.15 and 2.16. It can be observed that convergence of the state variables to the reference setpoints was achieved and this in turn signifies that precise positioning of the payload is accomplished. The only measurable state variable was the depth of the payload $z_3 = z_p$. In the provided simulation results the real value of the state variables of the payload's positioning system is printed in blue, the estimated value provided by the H-infinity Kalman Filter is printed in green, whereas the associated reference setpoints are depicted in red.

The transient performance of the control algorithm is determined by the selection of parameters r, ρ and Q which appear in the algebraic Riccati equation of Eq. (2.89). The robustness of the control method is affected by the selection of the H-infinity attenuation coefficient ρ. By selecting the value of ρ to be sufficiently small, so as the H-infinity tracking performance condition of Eq. (11.123) to hold, one assures also the global asymptotic stability of the control loop and the elimination of the state vector's tracking error. The smallest value of ρ for which the Riccati equation of Eq. (2.89) can be solved is the one that provides the control loop with maximum robustness.

Yet computational simple the section's approach provides an efficient solution to the problem of precise functioning of ship-mounted cranes and of the associated

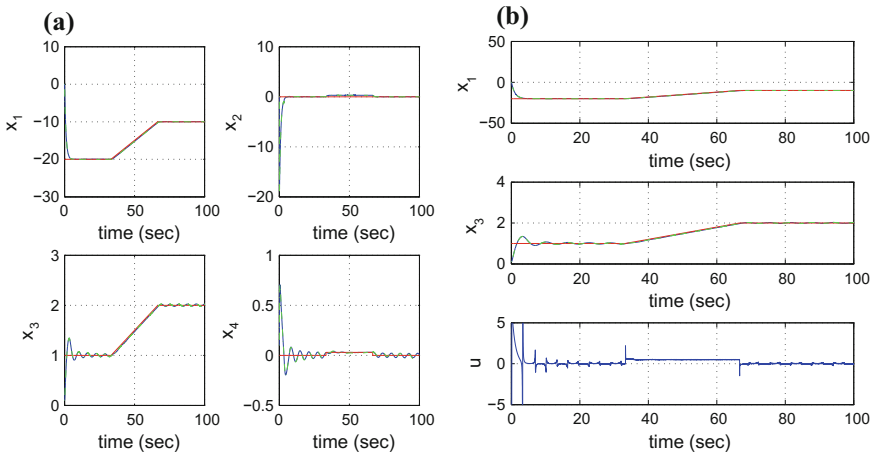

Fig. 2.13 Tracking of setpoint 2: **a** Convergence of the state variables of the payload's positioning system x_i $i = 1, \ldots, 4$ (blue lines) to the reference setpoints (red lines) and associated state estimates (green lines). **b** Diagrams about convergence of state variables $x_1 = \phi_w$, and $x_3 = z_p$ to their reference setpoint, and diagram depicting the variations of the control input

payload's positioning systems. Comparing to other methods for the same problem, the advantages of the sections's approach are outlined as follows: (i) the nonlinear optimal control scheme is directly applied on the nonlinear model of the payload's positioning system and unlike global linearization-based control does not require its transformation into a linear form through elaborated changes of state variables (diffeomorphisms), (ii) the method retains the typical advantages of optimal control, that is precise tracking of the reference setpoints at moderate variation of the control inputs, (iii) unlike nonlinear model predictive control the proposed nonlinear optimal control method is of proven stability and convergence to an optimum, (iv) the proposed control method does not require the state-space model of the payload's positioning system to be in a specific form (e.g. triangular, canonical etc.)

2.4 Nonlinear H-Infinity Control for Underactuated Systems: The Furuta Pendulum Example

2.4.1 Outline

As noted in the previous section, control of underactuated systems is a topic of primary importance in the area of nonlinear dynamical systems [153, 347, 378, 506, 520]. A typical underactuated system is Furuta's pendulum, also known as rotary pendulum. The system has two degrees of freedom while it receives only one

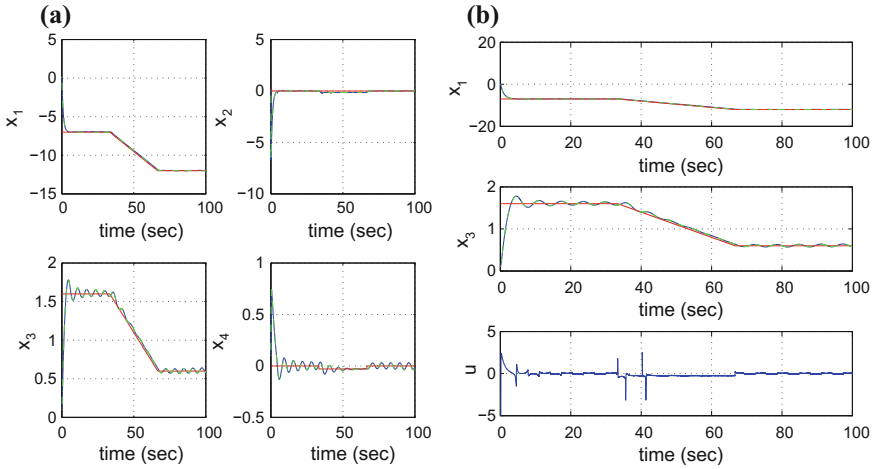

Fig. 2.14 Tracking of setpoint 3: **a** Convergence of the state variables of the payload's positioning system x_i $i = 1, \ldots, 4$ (blue lines) to the reference setpoints (red lines) and associated state estimates (green lines). **b** Diagrams about convergence of state variables $x_1 = \phi_w$, and $x_3 = z_p$ to their reference setpoint, and diagram depicting the variations of the control input

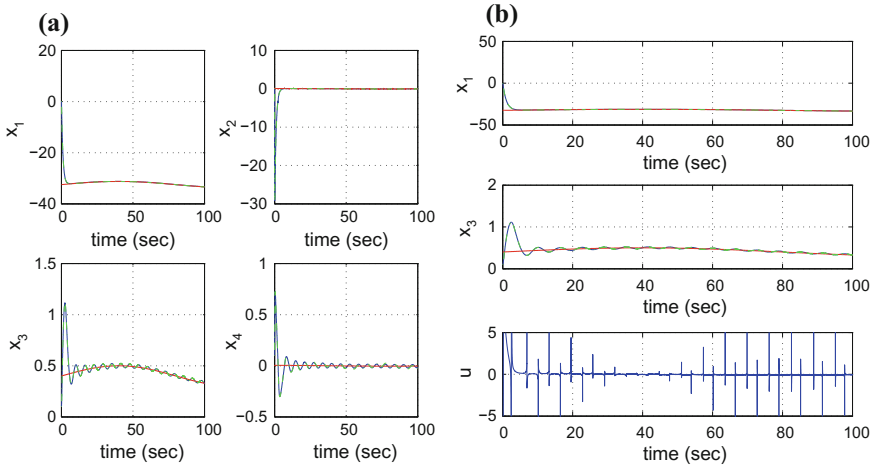

Fig. 2.15 Tracking of setpoint 4: **a** Convergence of the state variables of the payload's positioning system x_i $i = 1, \ldots, 4$ (blue lines) to the reference setpoints (red lines) and associated state estimates (green lines). **b** Diagrams about convergence of state variables $x_1 = \phi_w$, and $x_3 = z_p$ to their reference setpoint, and diagram depicting the variations of the control input

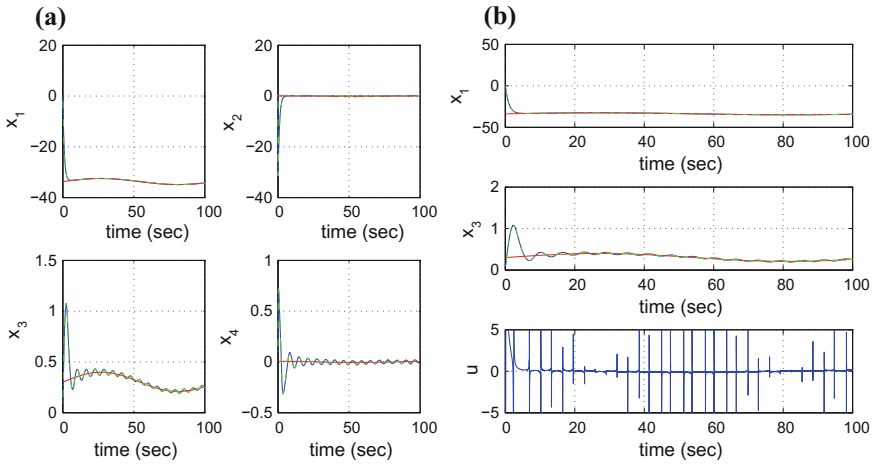

Fig. 2.16 Tracking of setpoint 5: **a** Convergence of the state variables of the payload's positioning system x_i $i = 1, \ldots, 4$ (blue lines) to the reference setpoints (red lines) and associated state estimates (green lines). **b** Diagrams about convergence of state variables $x_1 = \phi_w$, and $x_3 = z_p$ to their reference setpoint, and diagram depicting the variations of the control input

control input [299, 326, 527, 544, 630]. Besides, the system exhibits strong nonlinear characteristics due to the appearance of nonlinear gravitational and Coriolis terms in it [18, 78, 137, 244, 640]. Furthermore, the system is not linearizable through state feedback and in its nonlinear form it is not differentially flat. As a result its transformation into a linear equivalent state-space form through a change of state variables (diffeomorphisms) is not a straightforward and easy to implement procedure [3–5, 405, 406]. For these reasons the control of Furuta's pendulum is a non-trivial problem.

In this section, a nonlinear optimal (H-infinity) control approach to the problem of Furuta's pendulum is developed. The pendulum's model first undergoes a partial state feedback linearization which allows to express half of its state-space description into a linear form. For the aggregate model, which remains nonlinear, approximate linearization is performed around a temporary operating point (equilibrium) which is updated at each iteration of the control algorithm. The equilibrium is defined by the present value of the pendulum's state vector and the last value of the control input that was exerted on it [461, 466]. The linearization makes use of Taylor series expansion [33, 431, 463]. To obtain the linearized state-space model of the pendulum it is required to compute the associated Jacobian matrices. The modelling error which is due to the truncation of higher-order terms in the Taylor series expansion is considered as a perturbation that is compensated by the robustness of the control algorithm.

For the approximately linearized model of the rotary pendulum an H-infinity stabilizing feedback controller is defined. It represents the solution to a min-max differential game in which the controller tries to minimize a cost functional comprising a quadratic term of the state vector error of the pendulum, while the disturbance inputs

try to maximize it. The controller's feedback gain is computed from the solution of an algebraic Riccati equation that is also performed at each iteration of the control method [450, 452, 457, 459, 460]. The stability properties of the control scheme are confirmed through Lyapunov analysis. First it is proven that the H-infinity tracking performance criterion is satisfied. This indicates elevated robustness against modelling uncertainties and external perturbations. Moreover, under moderate conditions it is proven that the pendulum's control loop exhibits global asymptotic stability properties. Finally, to implement state estimation-based feedback control of the rotary pendulum the H-infinity Kalman Filter is used to compute the system's state vector through the processing of its outputs' measurements [169, 511].

Comparing to the proposed nonlinear optimal control method, other nonlinear control schemes for the rotary pendulum are assessed as follows: Global linearization-based control schemes, such as Lie-algebra based control require the intuitive definition of linearizing outputs as well as the application of elaborated state variables transformations (diffeomorphisms). Due to applying the control input to the linearized equivalent model of the dynamical system and not to the initial nonlinear model such methods may come against singularity problems. Additionally, in the case of underactuation the application of global linearization-based control schemes may require dynamic extension, that is the inclusion of the control inputs and their derivatives in the extended state vector of the system and in the form of additional state variables. Moreover, the application of Model Predictive Control schemes is not possible because this method requires that the dynamics of the control system is a linear one, whereas the Furuta pendulum is a strongly nonlinear one. Additionally, Nonlinear Model Predictive Control trying to extend MPC to the nonlinear case, is not of assured convergence to an optimum and the performance of its iterative search for an optimum is dependent on its parametrization and on initial conditions. Furthermore, the application of sliding-mode control to underactuated systems (such as the model of the Furuta pendulum) is hindered by the fact that such systems are usually not found into a canonical form, so the definition of the sliding surface is not a task that can be directly accomplished. Finally, the application of backstepping control in the case of underactuated robotic systems is not recommended because such systems are not found a-priori into a triangular form [194, 313, 379, 483, 542].

2.4.2 Dynamic Model of Furuta's Penulum

2.4.2.1 State-Space Description of the Pendulum

The dynamic model of Furuta's pendulum, as obtained from the application of the Euler–Lagrange method, is given by [506]:

$$\begin{gathered}(\alpha+\beta+sin^2(\theta))\ddot{\phi}+\gamma cos(\theta)\ddot{\theta}+2\beta\dot{\theta}\dot{\phi}sin(\theta)cos(\theta)-\gamma\dot{\theta}^2sin(\theta)=T\\ \gamma cos(\theta)\ddot{\phi}+\beta\ddot{\theta}-\beta\dot{\phi}^2sin(\theta)cos(\theta)-\delta sin(\theta)=0\end{gathered} \tag{2.104}$$

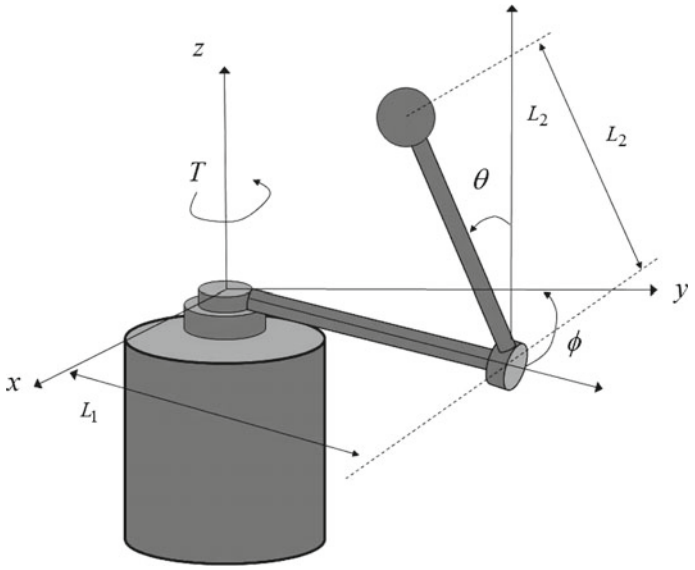

Fig. 2.17 Diagram of Furuta's pendulum

In this model ϕ is the angle of the arm with $\dot{\phi}$ and $\ddot{\phi}$ to stand for the associated angular velocity and the angular acceleration, θ is the angle of the pendulum with $\dot{\theta}$ and $\ddot{\theta}$ to stand for the associated angular velocity and angular acceleration, while α, β, γ and δ are parameters comprising the masses and lengths of the two links of the pendulum. The control input (torque) that is applied to the arm and which is generated by a DC motor is denoted as T. The diagram of Furuta's pendulum is depicted in Fig. 2.17. The system is underactuated because it has only one control input while having two degrees of freedom.

After applying a partial feedback linearization transformation through the relation

$$T = (\alpha + \beta sin^2(\theta))u + \gamma cos(\theta)\ddot{\theta} + 2\beta\dot{\theta}\dot{\phi}sin(\theta)cos(\theta) - \gamma\dot{\theta}^2 sin(\theta) \quad (2.105)$$

the dynamic model of Furuta's pendulum is written as

$$\begin{aligned} \ddot{\phi} &= u \\ \ddot{\theta} &= \frac{\dot{\phi}^2\beta\sin(\theta)cos(\theta)+\delta sin(\theta)-\gamma cos(\theta)u}{\beta} \end{aligned} \quad (2.106)$$

where the control input in the transformed nonlinear model of Eq. (2.106) is denoted as u. Next, by defining the state variables $x_1 = \phi$, $x_2 = \dot{\phi}$, $x_3 = \theta$ and $x_4 = \dot{\theta}$ one arrives at the following state-space description of the pendulum

$$\dot{x} = f(x) + g(x)u \quad (2.107)$$

where $x \in R^{4\times 1}$, $u \in R^{1\times 1}$, $f(x) \in R^{4\times 1}$ and $g(x) \in R^{4\times 1}$ and vector fields $f(x)$ and $g(x)$ are given by

$$f(x) = \begin{pmatrix} x_2 \\ 0 \\ x_4 \\ \frac{x_2^2 \beta sin(\theta) cos(\theta) + \delta sin(\theta)}{\beta} \end{pmatrix} g(x) = \begin{pmatrix} 0 \\ 1 \\ 0 \\ \frac{-\gamma cos(\theta)}{\beta} \end{pmatrix} \tag{2.108}$$

2.4.2.2 Approximate Linearization of the Pendulum's Dynamics

Approximate linearization for the pendulum's state-space model takes place around a time-varying equilibrium which is re-computed at each time instant and which consists of the present value of system's state vector x^* and of the last value of the control inputs vector u^* that was applied on it. This results into a linearized state-space description of the form

$$\dot{x} = Ax + Bu + \tilde{d} \tag{2.109}$$

where $\tilde{d}$ is the modelling error due to approximate linearization and truncation of higher-order terms in the Taylor series expansion, while matrices A and B are given by

$$\begin{gathered} A = \nabla_x [f(x) + g(x)u] \mid_{(x^*,u^*)} \Rightarrow A = \nabla_x [f(x) \mid_{(x^*,u^*)} + \nabla_x [g(x)u \mid_{(x^*,u^*)}] \\ B = \nabla_u [f(x) + g(x)u] \mid_{(x^*,u^*)} \Rightarrow B = g(x) \mid_{(x^*,u^*)} \end{gathered} \tag{2.110}$$

Next, the elements of the model's Jacobian matrix $\nabla_x f(x)$ are computed:

First row of $\nabla_x f(x)$: $\frac{\partial f_1}{\partial x_1} = 0$, $\frac{\partial f_1}{\partial x_2} = 1$, $\frac{\partial f_1}{\partial x_3} = 0$, and $\frac{\partial f_1}{\partial x_4} = 0$.

Second row of $\nabla_x f(x)$: $\frac{\partial f_2}{\partial x_1} = 0$, $\frac{\partial f_2}{\partial x_2} = 0$, $\frac{\partial f_2}{\partial x_3} = 0$, and $\frac{\partial f_2}{\partial x_4} = 0$.

Third row of $\nabla_x f(x)$: $\frac{\partial f_3}{\partial x_1} = 0$, $\frac{\partial f_3}{\partial x_2} = 0$, $\frac{\partial f_3}{\partial x_3} = 0$, and $\frac{\partial f_3}{\partial x_4} =$ '1.

Fourth row of $\nabla_x f(x)$: $\nabla_x f(x)$: $\frac{\partial f_4}{\partial x_1} = 0$, $\frac{\partial f_4}{\partial x_2} = 2x_2 sin(x_3) cos(x_3)$, $\frac{\partial f_4}{\partial x_3} = \frac{x_2^2 \beta [cos^2(x_3) - sin^2(x_3)] + \delta cos(x_3)}{\beta}$, and $\frac{\partial f_4}{\partial x_4} = 0$.

In a similar manner, the elements of the model's Jacobian matrix $\nabla_x g(x)$ are computed:

First row of $\nabla_x g(x)$: $\frac{\partial g_1}{\partial x_1} = 0$, $\frac{\partial g_1}{\partial x_2} = 0$, $\frac{\partial g_1}{\partial x_3} = 0$, and $\frac{\partial g_1}{\partial x_4} = 0$.

Second row of $\nabla_x g(x)$: $\frac{\partial g_2}{\partial x_1} = 0$, $\frac{\partial g_2}{\partial x_2} = 0$, $\frac{\partial g_2}{\partial x_3} = 0$, and $\frac{\partial g_2}{\partial x_4} = 0$.

Third row of $\nabla_x g(x)$: $\frac{\partial g_3}{\partial x_1} = 0$, $\frac{\partial g_3}{\partial x_2} = 0$, $\frac{\partial g_3}{\partial x_3} = 0$, and $\frac{\partial g_3}{\partial x_4} = 0$.

Fourth row of $\nabla_x g(x)$: $\frac{\partial g_4}{\partial x_1} = 0$, $\frac{\partial g_4}{\partial x_2} = 0$, $\frac{\partial g_4}{\partial x_3} = \frac{\gamma sin(x_3)}{\beta}$, and $\frac{\partial g_4}{\partial x_4} = 0$.

For the previous approximately linearized model of Fututa's pendulum H-infinity feedback control is applied [450, 457, 459] (Fig. 2.17).

2.4.3 Design of an H-Infinity Nonlinear Feedback Controller

2.4.3.1 Equivalent Linearized Dynamics of the Pendulum

After linearization around its current operating point, the pendulum's dynamic model is written as

$$\dot{x} = Ax + Bu + d_1 \tag{2.111}$$

As noted in the previous section, parameter d_1 stands for the linearization error in the pendulum's dynamic model appearing in Eq. (2.111). The reference setpoints for the pendulum's state vector are denoted by $\mathbf{x_d} = [x_1^d, \ldots, x_6^d]$. Tracking of this trajectory is achieved after applying the control input u^*. At every time instant the control input u^* is assumed to differ from the control input u appearing in Eq. (2.111) by an amount equal to Δu, that is $u^* = u + \Delta u$

$$\dot{x}_d = Ax_d + Bu^* + d_2 \tag{2.112}$$

The dynamics of the controlled system described in Eq. (2.67) can be also written as

$$\dot{x} = Ax + Bu + Bu^* - Bu^* + d_1 \tag{2.113}$$

and by denoting $d_3 = -Bu^* + d_1$ as an aggregate disturbance term one obtains

$$\dot{x} = Ax + Bu + Bu^* + d_3 \tag{2.114}$$

By subtracting Eq. (2.112) from (2.114) one has

$$\dot{x} - \dot{x}_d = A(x - x_d) + Bu + d_3 - d_2 \tag{2.115}$$

By denoting the tracking error as $e = x - x_d$ and the aggregate disturbance term as $\tilde{d} = d_3 - d_2$, the tracking error dynamics becomes

$$\dot{e} = Ae + Bu + \tilde{d} \tag{2.116}$$

The above linearized form of the pendulum's model can be efficiently controlled after applying an H-infinity feedback control scheme.

2.4.3.2 The Nonlinear H-Infinity Control

The initial nonlinear model of the underactuated rotary pendulum is in the form

$$\dot{x} = \tilde{f}(x, u) \;\; x \in R^n, \; u \in R^m \tag{2.117}$$

Linearization of the system (underactuated pendulum) is performed at each iteration of the control algorithm round its present operating point $(x^*, u^*) = (x(t), u(t - T_s))$, where T_s is the sampling period. The linearized equivalent model of the system is described by

$$\dot{x} = Ax + Bu + L\tilde{d} \;\; x \in R^n, \; u \in R^m, \; \tilde{d} \in R^q \tag{2.118}$$

where matrices A and B are obtained from the computation of the Jacobian matrices of the pendulum's state-space description and vector $\tilde{d}$ denotes disturbance terms due to linearization errors. The problem of disturbance rejection for the linearized model that is described by

$$\begin{aligned} \dot{x} &= Ax + Bu + L\tilde{d} \\ y &= Cx \end{aligned} \tag{2.119}$$

where $x \in R^n$, $u \in R^m$, $\tilde{d} \in R^q$ and $y \in R^p$, cannot be handled efficiently if the classical LQR control scheme is applied. This is because of the existence of the perturbation term $\tilde{d}$. The disturbance term $\tilde{d}$ apart from modeling (parametric) uncertainty and external perturbation terms can also represent noise terms of any distribution.

In the H_∞ control approach, a feedback control scheme is designed for trajectory tracking by the rotary pendulum's state vector and simultaneous disturbance rejection, considering that the disturbance affects the system in the worst possible manner. The disturbances' effects are incorporated in the following quadratic cost function:

$$J(t) = \tfrac{1}{2}\int_0^T [y^T(t)y(t) + ru^T(t)u(t) - \rho^2\tilde{d}^T(t)\tilde{d}(t)]dt, \;\; r, \rho > 0 \tag{2.120}$$

As also noted in the previous section, the significance of the negative sign in the cost function's term that is associated with the perturbation variable $\tilde{d}(t)$ is that the disturbance tries to maximize the cost function $J(t)$ while the control signal $u(t)$ tries to minimize it. In adherence to the previous section, the physical meaning of the relation given above is that the control signal of the pendulum and the disturbances compete to each other within a min-max differential game. This problem of min-max optimization can be written as

$$min_u max_{\tilde{d}} J(u, \tilde{d}) \tag{2.121}$$

Once again, the objective of the optimization procedure is to compute a control signal $u(t)$ which can compensate for the worst possible disturbance, that is externally imposed to the system. As explained, the solution to such a type of min-max opti-

mization problem is directly related to the value of the parameter ρ. This means that there is an upper bound in the disturbances magnitude that can be annihilated by the control signal.

2.4.3.3 Computation of the Feedback Control Gains

For the linearized system given by Eq. (2.119) the cost function of Eq. (2.120) is defined, where the coefficient r determines the penalization of the control input and the weight coefficient ρ determines the reward of the disturbances' effects.

It is assumed again that (i) The energy that is transferred from the disturbances signal $\tilde{d}(t)$ is bounded, that is $\int_0^\infty \tilde{d}^T(t)\tilde{d}(t)dt < \infty$, (ii) the matrices $[A, B]$ and $[A, L]$ are stabilizable, (iii) the matrix $[A, C]$ is detectable. Then, the optimal feedback control law is given by

$$u(t) = -Kx(t) \tag{2.122}$$

with

$$K = \frac{1}{r}B^T P \tag{2.123}$$

where P is a positive semi-definite symmetric matrix which is obtained from the solution of the Riccati equation

$$A^T P + PA + Q - P\left(\frac{1}{r}BB^T - \frac{1}{2\rho^2}LL^T\right)P = 0 \tag{2.124}$$

where Q is also a positive definite symmetric matrix. The worst case disturbance is given by

$$\tilde{d}(t) = \frac{1}{\rho^2}L^T Px(t) \tag{2.125}$$

The diagram of the considered control loop is depicted in Fig. 2.18.

2.4.4 Lyapunov Stability Analysis

Through Lyapunov stability analysis it will be shown that the proposed nonlinear control scheme assures H_∞ tracking performance for the pendulum, and that in case of bounded disturbance terms asymptotic convergence to the reference setpoints is achieved. The tracking error dynamics for the underactuated pendulum is written in the form

$$\dot{e} = Ae + Bu + L\tilde{d} \tag{2.126}$$

where in the pendulum's case $L = I \in R^4$ with I being the identity matrix. Variable $\tilde{d}$ denotes model uncertainties and external disturbances of the pendulum's model. The following Lyapunov function is considered

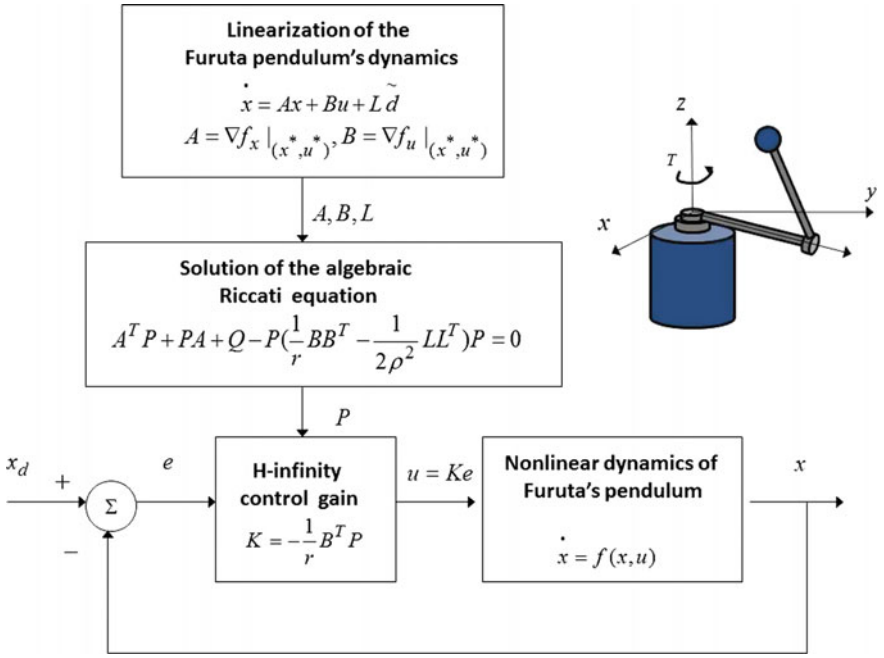

Fig. 2.18 Nonlinear H-infinity control loop for Furuta's pendulum: An H-infinity controller is applied to the approximately linearized model of the pendulum, which is obtained after Taylor series expansion of its state-space description

$$V = \tfrac{1}{2} e^T P e \tag{2.127}$$

where $e = x - x_d$ is the tracking error. By differentiating with respect to time and by using the previous technique one obtains

$$\begin{gathered} \dot{V} = \tfrac{1}{2}\dot{e}^T P e + \tfrac{1}{2} e P \dot{e} \Rightarrow \\ \dot{V} = \tfrac{1}{2}[Ae + Bu + L\tilde{d}]^T P e + \tfrac{1}{2} e^T P [Ae + Bu + L\tilde{d}] \Rightarrow \end{gathered} \tag{2.128}$$

$$\begin{gathered} \dot{V} = \tfrac{1}{2}[e^T A^T + u^T B^T + \tilde{d}^T L^T] P e + \\ + \tfrac{1}{2} e^T P [Ae + Bu + L\tilde{d}] \Rightarrow \end{gathered} \tag{2.129}$$

$$\begin{gathered} \dot{V} = \tfrac{1}{2} e^T A^T P e + \tfrac{1}{2} u^T B^T P e + \tfrac{1}{2}\tilde{d}^T L^T P e + \\ \tfrac{1}{2} e^T P A e + \tfrac{1}{2} e^T P B u + \tfrac{1}{2} e^T P L \tilde{d} \end{gathered} \tag{2.130}$$

The previous equation is rewritten as

$$\dot{V} = \tfrac{1}{2}e^T(A^T P + PA)e + \left(\tfrac{1}{2}u^T B^T Pe + \tfrac{1}{2}e^T PBu\right) + \\ + \left(\tfrac{1}{2}\tilde{d}^T L^T Pe + \tfrac{1}{2}e^T PL\tilde{d}\right) \tag{2.131}$$

Assumption: For given positive definite matrix Q and coefficients r and ρ there exists a positive definite matrix P, which is the solution of the following matrix equation

$$A^T P + PA = -Q + P\left(\tfrac{2}{r}BB^T - \tfrac{1}{\rho^2}LL^T\right)P \tag{2.132}$$

Moreover, the following feedback control law is applied to the system

$$u = -\tfrac{1}{r}B^T Pe \tag{2.133}$$

By substituting Eqs. (2.132) and (2.133) one obtains

$$\dot{V} = \tfrac{1}{2}e^T\left[-Q + P\left(\tfrac{2}{r}BB^T - \tfrac{1}{\rho^2}LL^T\right)P\right]e + \\ + e^T PB\left(-\tfrac{1}{r}B^T Pe\right) + e^T PL\tilde{d} \Rightarrow \tag{2.134}$$

$$\dot{V} = -\tfrac{1}{2}e^T Qe + \tfrac{1}{r}e^T PBB^T Pe - \tfrac{1}{2\rho^2}e^T PLL^T Pe \\ - \tfrac{1}{r}e^T PBB^T Pe + e^T PL\tilde{d} \tag{2.135}$$

which after intermediate operations gives

$$\dot{V} = -\tfrac{1}{2}e^T Qe - \tfrac{1}{2\rho^2}e^T PLL^T Pe + e^T PL\tilde{d} \tag{2.136}$$

or, equivalently

$$\dot{V} = -\tfrac{1}{2}e^T Qe - \tfrac{1}{2\rho^2}e^T PLL^T Pe + \\ + \tfrac{1}{2}e^T PL\tilde{d} + \tfrac{1}{2}\tilde{d}^T L^T Pe \tag{2.137}$$

Lemma: The following inequality holds

$$\tfrac{1}{2}e^T PL\tilde{d} + \tfrac{1}{2}\tilde{d}L^T Pe - \tfrac{1}{2\rho^2}e^T PLL^T Pe \leq \tfrac{1}{2}\rho^2\tilde{d}^T\tilde{d} \tag{2.138}$$

Proof: The binomial $(\rho\alpha - \frac{1}{\rho}b)^2$ is considered. Expanding the left part of the above inequality one gets

$$\rho^2 a^2 + \tfrac{1}{\rho^2}b^2 - 2ab \geq 0 \Rightarrow \tfrac{1}{2}\rho^2 a^2 + \tfrac{1}{2\rho^2}b^2 - ab \geq 0 \Rightarrow \\ ab - \tfrac{1}{2\rho^2}b^2 \leq \tfrac{1}{2}\rho^2 a^2 \Rightarrow \tfrac{1}{2}ab + \tfrac{1}{2}ab - \tfrac{1}{2\rho^2}b^2 \leq \tfrac{1}{2}\rho^2 a^2 \tag{2.139}$$

The following substitutions are carried out: $a = \tilde{d}$ and $b = e^T PL$ and the previous relation becomes

$$\frac{1}{2}\tilde{d}^T L^T P e + \frac{1}{2} e^T P L \tilde{d} - \frac{1}{2\rho^2} e^T P L L^T P e \leq \frac{1}{2}\rho^2 \tilde{d}^T \tilde{d} \tag{2.140}$$

Equation (2.140) is substituted in Eq. (2.137) and the inequality is enforced, thus giving

$$\dot{V} \leq -\frac{1}{2} e^T Q e + \frac{1}{2}\rho^2 \tilde{d}^T \tilde{d} \tag{2.141}$$

Equation (2.141) shows that the H_∞ tracking performance criterion is satisfied. The integration of $\dot{V}$ from 0 to T gives

$$\begin{aligned} &\int_0^T \dot{V}(t)dt \leq -\frac{1}{2}\int_0^T ||e||_Q^2 dt + \frac{1}{2}\rho^2 \int_0^T ||\tilde{d}||^2 dt \Rightarrow \\ &2V(T) + \int_0^T ||e||_Q^2 dt \leq 2V(0) + \rho^2 \int_0^T ||\tilde{d}||^2 dt \end{aligned} \tag{2.142}$$

Moreover, if there exists a positive constant $M_d > 0$ such that

$$\int_0^\infty ||\tilde{d}||^2 dt \leq M_d \tag{2.143}$$

then one gets

$$\int_0^\infty ||e||_Q^2 dt \leq 2V(0) + \rho^2 M_d \tag{2.144}$$

Thus, the integral $\int_0^\infty ||e||_Q^2 dt$ is bounded. Moreover, $V(T)$ is bounded and from the definition of the Lyapunov function V in Eq. (2.127) it becomes clear that $e(t)$ will be also bounded since $e(t) \in \Omega_e = \{e | e^T P e \leq 2V(0) + \rho^2 M_d\}$. According to the above and with the use of Barbalat's Lemma one obtains $lim_{t\to\infty} e(t) = 0$.

Elaboratiing on the above, it can be noted that the proof of global asymptotic stability for the control loop of the underactuated pendulum relies on Eq. (2.141) and on the application of Barbalat's Lemma. It uses the condition of Eq. (2.143) about the boundedness of the square of the aggregate disturbance and modelling error term $\tilde{d}$ that affects the model of the rotary pendulum. However, as explained above the proof of global asymptotic stability is not restricted by this condition. By selecting the attenuation coefficient ρ to be sufficiently small and in particular to satisfy $\rho^2 < ||e||_Q^2 / ||\tilde{d}||^2$ one has that the first derivative of the Lyapunov function is upper bounded by 0. Therefore for the ith time interval it is proven that the Lyapunov function defined in Eq. (2.127) is a decreasing one. This also assures the Lyapunov function of the rotary pendulum defined in Eq. (2.127) will always have a negative first-order derivative.

2.4.5 *Robust State Estimation with the Use of the H-Infinity Kalman Filter*

The control loop of the rotary pendulum can be implemented with the use of information provided by a small number of sensors and by processing only a small number

of state variables. To reconstruct the missing information about the state vector of Furuta's (rotary) pendulum it is proposed to use a filtering scheme and based on it to apply state estimation-based control [169, 511]. The recursion of the H_∞ Kalman Filter, for the model of the pendulum, can be formulated in terms of a *measurement update* and a *time update* part.
Measurement update:

$$\begin{aligned} D(k) &= [I - \theta W(k)P^-(k) + C^T(k)R(k)^{-1}C(k)P^-(k)]^{-1} \\ K(k) &= P^-(k)D(k)C^T(k)R(k)^{-1} \\ \hat{x}(k) &= \hat{x}^-(k) + K(k)[y(k) - C\hat{x}^-(k)] \end{aligned} \tag{2.145}$$

Time update:

$$\begin{aligned} \hat{x}^-(k+1) &= A(k)x(k) + B(k)u(k) \\ P^-(k+1) &= A(k)P^-(k)D(k)A^T(k) + Q(k) \end{aligned} \tag{2.146}$$

where it is assumed that parameter θ is sufficiently small to assure that the covariance matrix $P^-(k)^{-1} - \theta W(k) + C^T(k)R(k)^{-1}C(k)$ will be positive definite. When $\theta = 0$ the H_∞ Kalman Filter becomes equivalent to the standard Kalman Filter. One can measure only a part of the state vector of the pendulum, and can estimate through filtering the rest of its state vector elements.

2.4.6 Simulation Tests

After applying nonlinear H-infinity control to the dynamic model of Furuta's pendulum given in Eq. (2.106) convergence of all state variables of the pendulum to the reference setpoints was achieved. For the computation of the feedback gain of the H-infinity controller the algebraic Riccati equation appearing in Eq. (2.132) had to be repetitively solved at each iteration of the control method. The obtained results ate given in Fig. 2.19, 2.20, 2.21, 2.22, 2.23, 2.24 and 2.25. The variation of the control signal remained smooth.

In the presented simulation experiments state estimation-based control has been implemented. Out of the 4 state variables of the underactuated pendulum only 2 where considered to be measurable. These were the rotational angle of the arm ϕ and the rotation angle of the pendulum θ. The rest of the state variables, describing the time derivatives of the turn angles, that is the angular velocities, for the arm and the pendulum were indirectly estimated with the use of the H-infinity Kalman Filter. The real value of each state variable has been plotted in blue, the estimated value has been plotted in green, while the associated reference setpoint has been plotted in red. It can be noticed that despite model uncertainty the H-infinity Kalman Filter achieved accurate estimation of the real values of the state vector elements. In this manner the robustness of the state estimation-based H-infinity control scheme was also improved. Moreover, the tracking accuracy of the control method and the

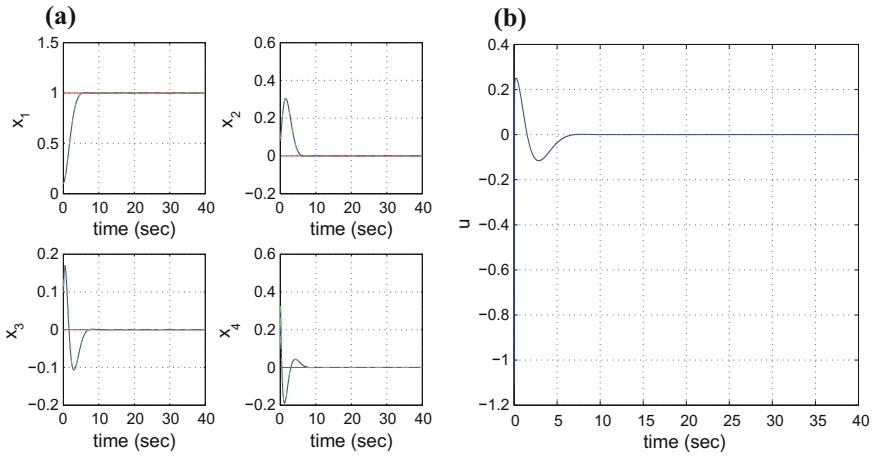

Fig. 2.19 Test case 1: **a** Tracking of reference setpoints (red-lines) by the state variables x_1-x_4 of Furuta's pendulum (blue lines) and state variables' estimates (green lines). **b** Control input

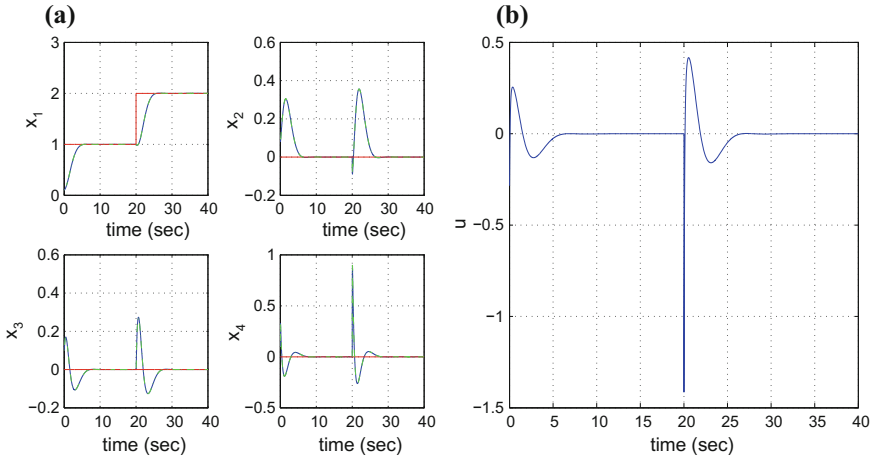

Fig. 2.20 Test case 2: **a** Tracking of reference setpoints (red-lines) by the state variables x_1-x_4 of Furuta's pendulum (blue lines) and state variables' estimates (green lines). **b** Control input

precision under which the state variables of the rotary (Furuta's) pendulum could converge to the reference setpoints is given in Table 2.4. Additionally, the robustness of the control method to parametric variations is given in Table 2.5. It it is shown that despite changes in the value of parameter β of the pendulum 's model given in Eq. (2.107) the tracking accuracy remained satisfactory.

Comparing to control methods for underactuated systems which make use of global linearization techniques, the main properties of the nonlinear H-infinity control scheme for the rotary pendulum are outlined as follows: (i) it is applied directly on the nonlinear dynamical model of the underactuated pendulum and does not

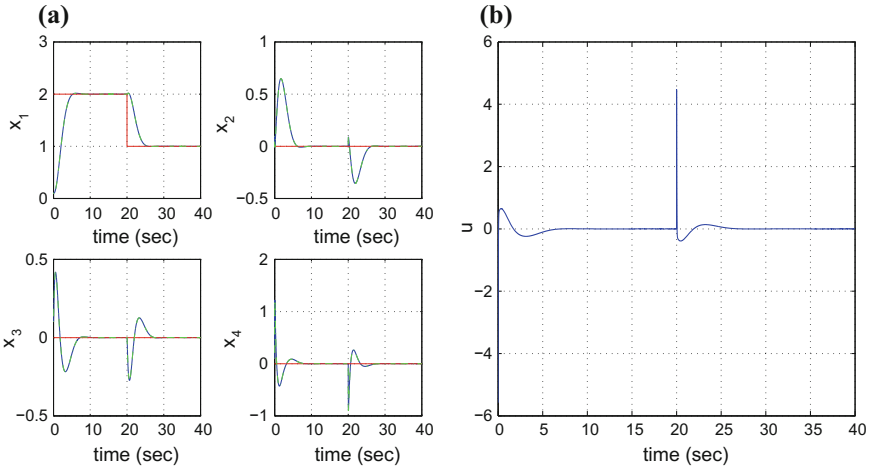

Fig. 2.21 Test case 3: **a** Tracking of reference setpoints (red-lines) by the state variables x_1-x_4 of Furuta's pendulum (blue lines) and state variables' estimates (green lines). **b** Control input

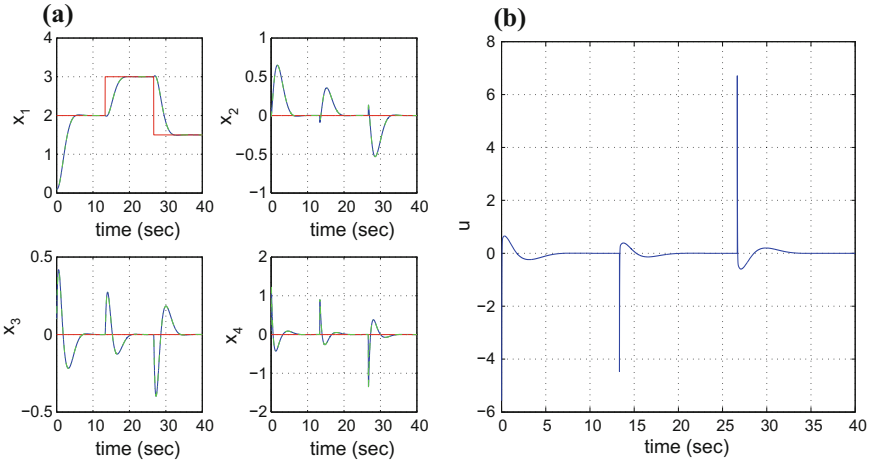

Fig. 2.22 Test case 4: **a** Tracking of reference setpoints (red-lines) by the state variables x_1-x_4 of Furuta's pendulum (blue lines) and state variables' estimates (green lines). **b** Control input

require the computation of diffeomorphisms (change of variables) that can bring the system into an equivalent linearized form, (ii) the computation of the feedback control signal follows an optimal control concept and requires the solution of an algebraic Riccati equation at each iteration of the control algorithm, (iii) the method retains the advantages of optimal control, that is minimization of the tracking error for the state variables of the rotary pendulum, while also keeping the moderate the variations of the control input.

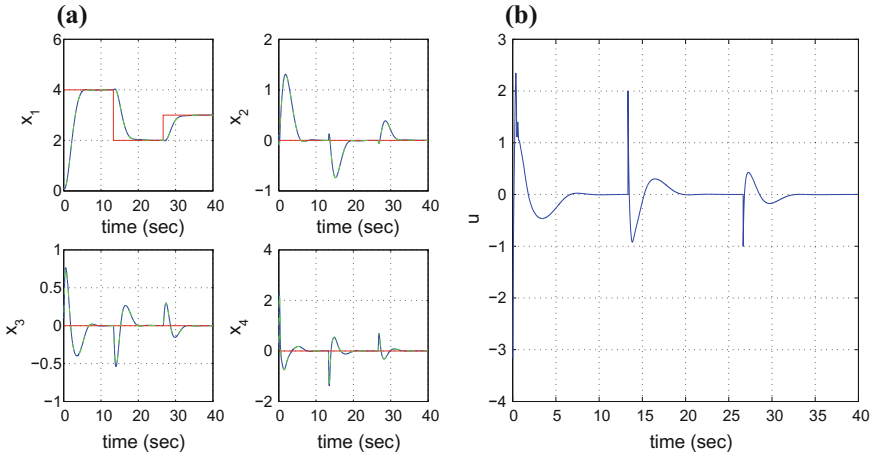

Fig. 2.23 Test case 5: **a** Tracking of reference setpoints (red-lines) by the state variables x_1-x_4 of Furuta's pendulum (blue lines) and state variables' estimates (green lines). **b** Control input

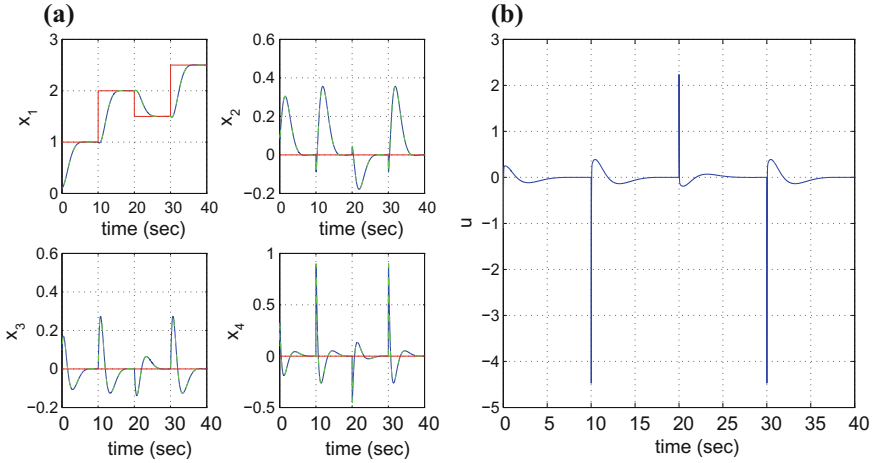

Fig. 2.24 Test case 6: **a** Tracking of reference setpoints (red-lines) by the state variables x_1-x_4 of Furuta's pendulum (blue lines) and state variables' estimates (green lines). **b** Control input

2.5 A Nonlinear Optimal Control Approach for the Cart and Double-Pendulum System

2.5.1 Outline

As it has been already analyzed, control of pendulum systems is an important research area because it is the basis for solving stabilization and trajectory tracking problems

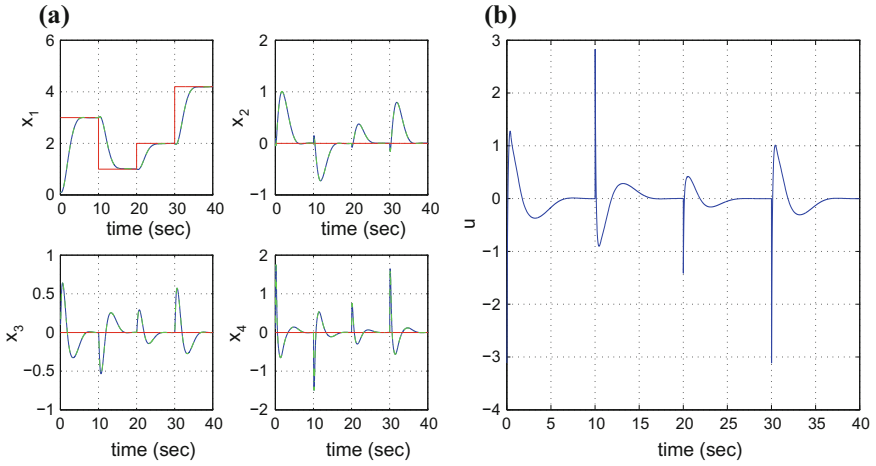

Fig. 2.25 Test case 7: **a** Tracking of reference setpoints (red-lines) by the state variables x_1-x_4 of Furuta's pendulum (blue lines) and state variables' estimates (green lines). **b** Control input

Table 2.4 RMSE of the pendulum state variables

Setpoint	RMSE x_1	RMSE x_2	RMSE x_3	RMSE x_4
1	$0.24{\cdot}10^{-5}$	$0.27{\cdot}10^{-5}$	$0.04{\cdot}10^{-5}$	$0.19{\cdot}10^{-5}$
2	$0.31{\cdot}10^{-5}$	$0.32{\cdot}10^{-5}$	$0.05{\cdot}10^{-5}$	$0.18{\cdot}10^{-5}$
3	$0.11{\cdot}10^{-5}$	$0.20{\cdot}10^{-5}$	$0.04{\cdot}10^{-5}$	$0.18{\cdot}10^{-5}$
4	$1.41{\cdot}10^{-5}$	$1.10{\cdot}10^{-5}$	$0.09{\cdot}10^{-5}$	$0.26{\cdot}10^{-5}$
5	$2.56{\cdot}10^{-5}$	$1.88{\cdot}10^{-5}$	$0.15{\cdot}10^{-5}$	$0.29{\cdot}10^{-5}$
6	$3.74{\cdot}10^{-5}$	$1.88{\cdot}10^{-5}$	$0.34{\cdot}10^{-5}$	$0.63{\cdot}10^{-5}$

Table 2.5 RMSE of pendulum under disturbances

Δa (%)	RMSE x_1	RMSE x_2	RMSE x_3	RMSE x_4
0	$0.31{\cdot}10^{-5}$	$0.32{\cdot}10^{-5}$	$0.05{\cdot}10^{-5}$	$0.18{\cdot}10^{-5}$
10	$0.22{\cdot}10^{-5}$	$0.36{\cdot}10^{-5}$	$0.06{\cdot}10^{-5}$	$0.21{\cdot}10^{-5}$
20	$0.17{\cdot}10^{-5}$	$0.35{\cdot}10^{-5}$	$0.05{\cdot}10^{-5}$	$0.20{\cdot}10^{-5}$
30	$0.24{\cdot}10^{-5}$	$0.20{\cdot}10^{-5}$	$0.05{\cdot}10^{-5}$	$0.25{\cdot}10^{-5}$
40	$0.14{\cdot}10^{-5}$	$0.19{\cdot}10^{-5}$	$0.05{\cdot}10^{-5}$	$0.35{\cdot}10^{-5}$
50	$0.23{\cdot}10^{-5}$	$0.36{\cdot}10^{-5}$	$0.06{\cdot}10^{-5}$	$0.39{\cdot}10^{-5}$
60	$0.12{\cdot}10^{-5}$	$0.32{\cdot}10^{-5}$	$0.07{\cdot}10^{-5}$	$0.46{\cdot}10^{-5}$

for robotic systems and electromechanical systems characterized by complex nonlinear dynamics and underactuation [8, 130, 236, 342, 354, 647]. The problem of trajectory tracking and stabilization for multi-pendulum systems has been studied in [121, 302, 558, 614]. Moroever, several results on nonlinear control of pendulum systems exhibiting underactuation have been presented [80, 237, 380, 591, 638]. In particular the control of the cart and double-pendulum system, either in the form of an overhead crane or in the form of an inverted pendulum has been analyzed in several studies [175, 539, 548, 600, 613]. The present section proposes a nonlinear optimal (H-infinity) control approach for the cart and double-pendulum system [450, 457, 459]. The control problem of the cart and double-pendulum system is acknowledged to be of high difficulty because of the strong nonlinearities characterizing its dynamics and because of the model's underactuation. Actually, there are three degrees of freedom (the longitudinal motion of the cart and the rotational motions of the poles that the constitute the double pendulum) which have to be controlled by only one control input (which is the force exerted on the cart).

To solve the control problem for the cart and double-pendulum system the associated dynamic model is first subject to approximate linearization around a temporary operating point (equilibrium) [417, 461, 466]. This operating point is defined by the present value of the system's state vector and the last value of the control inputs vector that was applied on it. The linearization makes use of first order Taylor series expansion and of the computation of the model's Jacobian matrices [33, 431, 463]. The modelling error which is due to the truncation of higher-order terms in the Taylor series expansion is considered to be a disturbance that is compensated by the robustness of the control method. For the approximately linearized model of the cart and double-pendulum system an H-infinity (optimal) controller is designed.

H-infinity control for the cart and double-pendulum model provides solution to the system's optimal control problem under model uncertainty and external perturbations [305, 564]. H-infinity control is the solution to a min-max differential game in which the control inputs try to minimize a quadratic cost function defined the square of the state vector's tracking error, whereas the disturbance and model uncertainty terms try to maximize this cost function. As analyzed in previous sections, the selection of the feedback gain of the H-infinity controller requires the solution of an algebraic Riccati equation at each step of the control method. The stability of the control scheme is proven through Lyapunov analysis. First, it is shown that the control method achieves the H-infinity tracking performance criterion which signifies elevated robustness to model uncertainty and external perturbations. Next, it is shown that the control loop satisfies also conditions for global asymptotic stability. Furthermore, to implement the nonlinear optimal control scheme though partial measurement of the cart and double pendulum's state vector, the H-infinity Kalman filter is proposed as a robust state estimator [169, 511].

2.5.2 Dynamic Model of the Cart and Double-Pendulum System

The diagram of the cart and double-pendulum system is depicted in Fig. 2.26. The following parameters of the model are defined: l_1 is the length of pole 1, l_2 is the length of pole 2, F is the force that is exerted on the cart, g is the acceleration of gravity, m_c is the mass of the cart, m_1 is the mass of pole 1 and m_2 is the mass of pole 2.

The dynamic model of the cart and double-pendulum system is obtained with the application of Euler–Lagrange analysis and is given by [539, 548]:

$$\begin{aligned}(m_1+m_2+m_c)\ddot{x}+(m_1+m_2)l_1(\ddot{\theta}_1)cos(\theta_1)-\dot{\theta}_1^2 sin(\theta_1)+\\ +m_2 l_2\ddot{\theta}_2 cos(\theta_2)-m_2 l_2\dot{\theta}_2^2 sin(\theta_2)=F\end{aligned} \tag{2.147}$$

$$\begin{aligned}(m_1+m_2)l_1 cos(\theta_1)\ddot{x}+(m_1+m_2)l_1^2\ddot{\theta}_1+m_2 l_1 l_2 cos(\theta_1-\theta_2)\ddot{\theta}_2+\\ +m_2 l_1 l_2 sin(\theta_1-\theta_2)\dot{\theta}_1^2+(m_1+m_2)g l_1 sin(\theta)_1=0\end{aligned} \tag{2.148}$$

$$\begin{aligned}m_2 l_2\ddot{x}cos(\theta_1)+m_2 l_1 l_2 cos(\theta_1-\theta_2)\ddot{\theta}_1+m_2 l_2^2\ddot{\theta}_2-\\ -m_2 l_1 l_2\dot{\theta}_1^2 sin(\theta_1-\theta_2)+m_2 g l_2 sin(\theta_2)=0\end{aligned} \tag{2.149}$$

By reformulating the state-space equations an equivalent description of the cart and double-pendulum system is obtained, where the following state variables x_i, $i=1,\ldots,6$ are defined: $x_1=\theta_1$ that is the rotation angle of the first pole, $x_2=\dot{\theta}_1$,

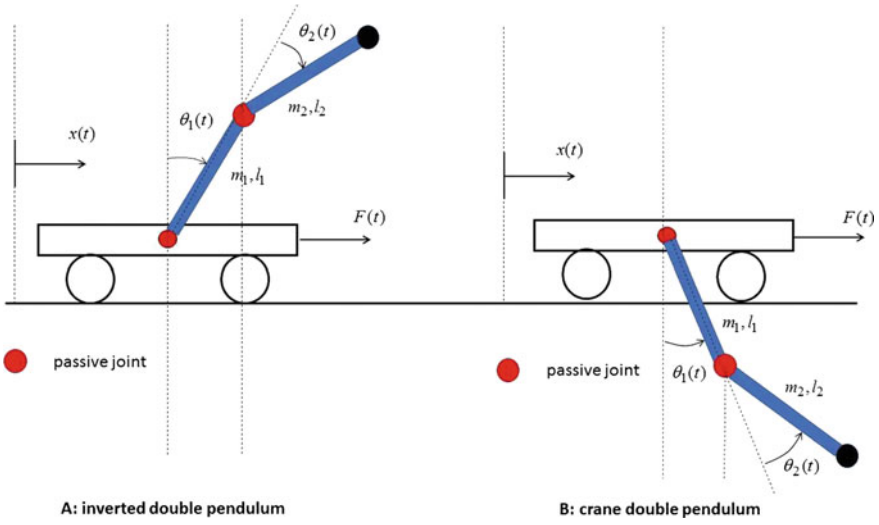

Fig. 2.26 The cart and double-pendulum system: **a** as inverted pendulum, **b** as crane

$x_3 = \theta_2$ that is the rotation angle of the second pole, $x_4 = \dot{\theta}_2$, $x_5 = x$ that is the linear displacement of the cart and $x_6 = \dot{x}$. The control input of the states-space model is denoted as $u = F$ that is the force exerted on the cart [539, 548]:

$$\begin{aligned} \dot{x}_1 &= f_1 = x_2 \\ \dot{x}_2 &= f_2 = g_1 + b_{p_1} F \\ \dot{x}_3 &= f_3 = x_4 \\ \dot{x}_4 &= f_4 = g_2 + b_{p_2} F \\ \dot{x}_5 &= f_5 = x_6 \\ \dot{x}_6 &= f_6 = g_3 + b_{c_3} F \end{aligned} \tag{2.150}$$

where one complements the previous model with the incusion of additive input disturbance variables. The terms of tne model given in Eq. (2.150) are defined as follows [539, 548]:

$$g_1 = \frac{A_{21}}{l_1 m_1} sin(x_3 - x_1) + \frac{1}{l_1} g sin(x_1) - \frac{A_{11}}{l_1 m_2} cos(x_1) sin(x_1) \tag{2.151}$$

$$g_2 = \frac{A_{11}}{l_1 m_1} sin(x_3 - x_1) \tag{2.152}$$

$$g_3 = \frac{A_{11}}{m_c} sin(x_1) \tag{2.153}$$

while one has $b_{p_1} = \frac{A_{22}}{l_1 m_1} sin(x_3 - x_1) - \frac{cos(x_1)}{l_1 m_c} - \frac{A_{12}}{l_1 m_1} cos(x_1) sin(x_1)$, $b_{p_2} = \frac{A_{12}}{l_2 m_1}$ $sin(x_3 - x_1)$, $b_{c_3} = \frac{1}{m_1} + \frac{A_{12}}{m_c} sin(x)$, $a_{11} = \frac{1}{m_1} + \frac{sin^2(x_1)}{m_c}$, $a_{22} = \frac{1}{m_1} + \frac{1}{m_c}$, $\Delta = a_{11} a_{12} - a_{12}{}^2$, $A_{12} = -\frac{a_{22} sin(x_1)}{\Delta m_c}$, $A_{21} = \frac{a_{22}(l_1)\dot{x}_1^2 - g cos(x_1) - a_{12} l_2 \dot{x}_3^2}{\Delta}$, $A_{22} = \frac{a_{12} sin(x_1)}{\Delta m_c}$.

2.5.3 *Approximate Linearization of the Cart and Double-Pendulum System*

In vector-fields form the state-space model of the cart and double-pendulum system is written as

$$\begin{pmatrix} \dot{x}_1 \\ \dot{x}_2 \\ \dot{x}_3 \\ \dot{x}_4 \\ \dot{x}_5 \\ \dot{x}_6 \end{pmatrix} = \begin{pmatrix} f_1(x) \\ f_2(x) \\ f_3(x) \\ f_4(x) \\ f_5(x) \\ f_6(x) \end{pmatrix} + \begin{pmatrix} g_1(x) \\ g_2(x) \\ g_3(x) \\ g_4(x) \\ g_5(x) \\ g_6(x) \end{pmatrix} F \tag{2.154}$$

and by substituting the elements of vector fields $f(x) \in R^{6\times 1}$ and $g(x) \in R^{6\times 1}$ one has:

$$\begin{pmatrix}\dot{x}_1\\ \dot{x}_2\\ \dot{x}_3\\ \dot{x}_4\\ \dot{x}_5\\ \dot{x}_6\end{pmatrix}=\begin{pmatrix} x_2\\ \frac{A_{21}}{l_1m_2}sin(x_3-x_1)+\frac{1}{l_1}gsin(x_1)-\frac{A_{11}}{l_1m_c}cos(x_1)sin(x_1)\\ x_4\\ \frac{A_{11}}{l_2m_1}sin(x_3-x_1)\\ x_6\\ \frac{A_{11}}{m_c}sin(x_1)\end{pmatrix}+ \\ +\begin{pmatrix}0\\ \frac{A_{22}}{l_1m_1}sin(x_3-x_1)-\frac{cos(x_1)}{l_1m_1}\\ 0\\ \frac{A_{12}}{l_2m_1}sin(x_3-x_1)\\ 0\\ \frac{1}{m_c}+\frac{A_{12}}{m_c}sin(x_1)\end{pmatrix}F \tag{2.155}$$

As noted above, the system is in the state-space form:

$$\dot{x}=f(x)+g(x)u \tag{2.156}$$

The state-space model of the cart and double-pendulum undergoes approximate linearization around a temporary operating point (equilibrium) (x^*, u^*) which is recomputed at each step of the control algorithm and which is defined by the present value of the system's state vector x^* and the last value of the control input u^* that was exerted on it. The linearized system has the following description

$$\dot{x}=Ax+Bu+\tilde{d} \tag{2.157}$$

where $\tilde{d}$ is the disturbance's vector, representing the model inaccuracy due to the approximate linearization as well as the effects of external perturbations, while matrices A and B are computed from the system's Jacobian matrices

$$A=[\nabla_x f(x)+\nabla_x g(x)u]\mid_{(x^*,u^*)} \tag{2.158}$$

$$\begin{gathered}B=[\nabla_u f(x)+\nabla_u g(x)u]\mid_{(x^*,u^*)}\\ \Rightarrow B=g(x)\mid_{x^*}\end{gathered} \tag{2.159}$$

The Jacobian matrices of the system are written as follows

$$\nabla_x f(x)=\begin{pmatrix}\frac{\partial f_1}{\partial x_1} & \frac{\partial f_1}{\partial x_2} & \dots & \frac{\partial f_1}{\partial x_6}\\ \frac{\partial f_2}{\partial x_1} & \frac{\partial f_2}{\partial x_2} & \dots & \frac{\partial f_2}{\partial x_6}\\ \dots & \dots & \dots & \dots\\ \frac{\partial f_6}{\partial x_1} & \frac{\partial f_6}{\partial x_2} & \dots & \frac{\partial f_6}{\partial x_6}\end{pmatrix}\nabla_x g(x)=\begin{pmatrix}\frac{\partial g_1}{\partial x_1} & \frac{\partial g_1}{\partial x_2} & \dots & \frac{\partial g_1}{\partial x_6}\\ \frac{\partial g_2}{\partial x_1} & \frac{\partial g_2}{\partial x_2} & \dots & \frac{\partial g_2}{\partial x_6}\\ \dots & \dots & \dots & \dots\\ \frac{\partial g_6}{\partial x_1} & \frac{\partial g_6}{\partial x_2} & \dots & \frac{\partial g_6}{\partial x_6}\end{pmatrix} \tag{2.160}$$

in particular, the elements of the Jacobian matrix $\nabla_x f(x)$ are computed as follows:

1st row of the Jacobian matrix:

$\frac{\partial f_1}{\partial x_1} = 0$, $\frac{\partial f_1}{\partial x_2} = 1$, $\frac{\partial f_1}{\partial x_3} = 0$, $\frac{\partial f_1}{\partial x_4} = 0$, $\frac{\partial f_1}{\partial x_5} = 0$, $\frac{\partial f_1}{\partial x_6} = 0$.

2nd row of the Jacobian matrix: $\frac{\partial f_2}{\partial x_1} = \frac{\frac{\partial A_{21}}{\partial x_1}}{l_1 m_1} sin(x_3 - x_1) - \frac{A_{21}}{l_1 m_1} cos(x_3 - x_1) + \frac{g}{l_1} cos(x_1) + \frac{\frac{\partial A_{11}}{\partial x_1}}{l_1 m_c} cos(x_1) sin(x_1) + \frac{A_{11}}{l_1 m_c}[sin^2(x_1) - cos^2(x_1)]$, $\frac{\partial f_2}{\partial x_2} = \frac{\frac{\partial A_{21}}{\partial x_2}}{l_1 m_1} sin(x_3 - x_1) + \frac{\frac{\partial A_{11}}{\partial x_2}}{l_1 m_c} cos(x_1) sin(x_1)$, $\frac{\partial f_2}{\partial x_3} = \frac{\frac{\partial A_{21}}{\partial x_3}}{l_1 m_1} sin(x_3 - x_1) + \frac{A_{21}}{l_1 m_1} cos(x_3 - x_1) + \frac{\frac{\partial A_{11}}{\partial x_3}}{l_1 m_c} cos(x_1) sin(x_1)$, $\frac{\partial f_2}{\partial x_4} = \frac{\frac{\partial A_{21}}{\partial x_4}}{l_1 m_1} sin(x_3 - x_1)$, $\frac{\partial f_2}{\partial x_5} = 0$, $\frac{\partial f_2}{\partial x_6} = 0$

3rd row of the Jacobian matrix: $\frac{\partial f_3}{\partial x_1} = 0$, $\frac{\partial f_3}{\partial x_2} = 0$, $\frac{\partial f_3}{\partial x_3} = 0$, $\frac{\partial f_3}{\partial x_4} = 1$, $\frac{\partial f_3}{\partial x_5} = 0$, $\frac{\partial f_3}{\partial x_6} = 0$.

4th row of the Jacobian matrix: $\frac{\partial f_4}{\partial x_1} = \frac{\frac{\partial A_{11}}{\partial x_1}}{l_1 m_1} sin(x_3 - x_1) - \frac{A_{11}}{l_2 m_1} cos(x_3 - x_1)$, $\frac{\partial f_4}{\partial x_2} = \frac{\frac{\partial A_{11}}{\partial x_2}}{l_1 m_1} sin(x_3 - x_1)$, $\frac{\partial f_4}{\partial x_3} = \frac{\frac{\partial A_{11}}{\partial x_3}}{l_1 m_1} sin(x_3 - x_1) + \frac{A_{11}}{l_2 m_1} cos(x_3 - x_1)$, $\frac{\partial f_4}{\partial x_4} = 0$, $\frac{\partial f_4}{\partial x_5} = 0$, $\frac{\partial f_4}{\partial x_6} = 0$

5th row of the Jacobian matrix:: $\frac{\partial f_5}{\partial x_1} = 0$, $\frac{\partial f_5}{\partial x_2} = 0$, $\frac{\partial f_5}{\partial x_3} = 0$, $\frac{\partial f_5}{\partial x_4} = 0$, $\frac{\partial f_5}{\partial x_5} = 0$, $\frac{\partial f_5}{\partial x_6} = 1$.

6th row of the Jacobian matrix: $\frac{\partial f_6}{\partial x_1} = \frac{\frac{\partial A_{11}}{\partial x_1}}{m_c} sin(x_1) - \frac{A_{11}}{m_c} cos(x_1)$, $\frac{\partial f_6}{\partial x_2} = \frac{\frac{\partial A_{11}}{\partial x_2}}{m_c} sin(x_1)$, $\frac{\partial f_6}{\partial x_3} = \frac{\frac{\partial A_{11}}{\partial x_3}}{m_c} sin(x_1)$. $\frac{\partial f_6}{\partial x_4} = 0$, $\frac{\partial f_6}{\partial x_5} = 0$, $\frac{\partial f_6}{\partial x_6} = 0$.

The elements of the Jacobian matrix $\nabla_x g(x)$ are computed as follows:

1st row of the Jacobian matrix: $\frac{\partial g_1}{\partial x_1} = 0$, $\frac{\partial g_1}{\partial x_2} = 0$, $\frac{\partial g_1}{\partial x_3} = 0$, $\frac{\partial g_1}{\partial x_4} = 0$, $\frac{\partial g_1}{\partial x_5} = 0$, $\frac{\partial g_1}{\partial x_6} = 0$.

2nd row of the Jacobian matrix: $\frac{\partial g_2}{\partial x_1} = \frac{\frac{\partial A_{22}}{\partial x_1}}{l_1 m_1} sin(x_3 - x_1) - \frac{A_{22}}{l_1 m_1} cos(x_3 - x_1) + \frac{sin(x_1)}{l_1 m_c} - \frac{\frac{\partial A_{12}}{\partial x_1}}{l_1 m_c} cos(x_1) sin(x_1) + \frac{A_{12}}{l_1 m_c}[sin^2(x_1) - cos^2(x_1)]$, $\frac{\partial g_2}{\partial x_2} = \frac{\frac{\partial A_{22}}{\partial x_2}}{l_1 m_1} sin(x_3 - x_1) - \frac{\frac{\partial A_{12}}{\partial x_2}}{l_1 m_c} cos(x_1) sin(x_1)$ $\frac{\partial g_2}{\partial x_3} = \frac{\frac{\partial A_{22}}{\partial x_3}}{l_1 m_1} sin(x_3 - x_1) + \frac{A_{22}}{l_1 m_1} cos(x_3 - x_1)$, $\frac{\partial g_2}{\partial x_4} = 0$, $\frac{\partial g_2}{\partial x_5} = 0$. $\frac{\partial g_2}{\partial x_6} = 0$.

3rd row of the Jacobian matrix: $\frac{\partial g_3}{\partial x_1} = 0$, $\frac{\partial g_3}{\partial x_2} = 0$, $\frac{\partial g_3}{\partial x_3} = 0$, $\frac{\partial g_3}{\partial x_4} = 0$, $\frac{\partial g_3}{\partial x_5} = 0$, $\frac{\partial g_3}{\partial x_6} = 0$.

4th row of the Jacobian matrix: $\frac{\partial g_4}{\partial x_1} = \frac{\frac{\partial A_{12}}{\partial x_1}}{l_2 m_1} sin(x_3 - x_1) - \frac{A_{12}}{l_2 m_1} cos(x_3 - x_1)$, $\frac{\partial g_4}{\partial x_2} = \frac{\frac{\partial A_{12}}{\partial x_2}}{l_2 m_1} sin(x_3 - x_1)$, $\frac{\partial g_4}{\partial x_3} = \frac{\frac{\partial A_{12}}{\partial x_3}}{l_2 m_1} sin(x_3 - x_1)$, $\frac{\partial g_4}{\partial x_4} = 0$, $\frac{\partial g_4}{\partial x_5} = 0$, $\frac{\partial g_4}{\partial x_6} = 0$

5th row of the Jacobian matrix: $\frac{\partial g_5}{\partial x_1} = 0$, $\frac{\partial g_5}{\partial x_2} = 0$, $\frac{\partial g_5}{\partial x_3} = 0$, $\frac{\partial g_5}{\partial x_4} = 0$, $\frac{\partial g_5}{\partial x_5} = 0$, $\frac{\partial g_5}{\partial x_6} = 0$.

6th row of the Jacobian matrix: $\frac{\partial g_6}{\partial x_1} = \frac{\frac{\partial A_{12}}{\partial x_1}}{m_c} sin(x_1) + \frac{A_{12}}{m_c} cos(x_1)$ $\frac{\partial g_6}{\partial x_2} = \frac{\frac{\partial A_{12}}{\partial x_2}}{m_c} sin(x_1)$, $\frac{\partial g_6}{\partial x_3} = \frac{\frac{\partial A_{12}}{\partial x_3}}{m_c} sin(x_1)$, $\frac{\partial g_6}{\partial x_4} = 0$, $\frac{\partial g_6}{\partial x_5} = 0$, $\frac{\partial g_6}{\partial x_6} = 0$

Next the computation of the partial derivatives of the variables A_{11}, A_{12}, A_{21} and A_{22} with respect to the state variables of the system x_i $i = 1, 2, \ldots, 6$ is given. It holds that

$$A_{11} = \frac{-a_{12}(l_1 x_1^2 - gcos(x_1)) + a_{11} l_2 x_2^2}{\Delta} \tag{2.161}$$

The derivatives of A_{11} with respect to the state vector elements x_i $i = 1, \ldots, 6$ are computed as follows:

$$\frac{\partial A_{11}}{\partial x_1} = \frac{[-\frac{\partial a_{12}}{\partial x_1}(l_1 x_2^2 - gcos(x_1)) - a_{12} gsin(x_1) + \frac{\partial a_{11}}{\partial x_1} l_2 x_4^2]\Delta}{\Delta^2} - \frac{[-a_{12}(l_1 x_2^2 - gcos(x_1)) + a_{11} l_2 x_4^2]\frac{\partial \Delta}{\partial x_1}}{\Delta^2}$$

$$\frac{\partial A_{11}}{\partial x_2} = \frac{[-\frac{\partial a_{12}}{\partial x_2}(l_1 x_2^2 - gcos(x_1)) - a_{12}(2 l_1 x_2) + \frac{\partial a_{11}}{\partial x_2} l_2 x_4^2]\Delta}{\Delta^2} - \frac{[-a_{12}(l_1 x_2^2 - gcos(x_1)) + a_{11} l_2 x_4^2]\frac{\partial \Delta}{\partial x_2}}{\Delta^2}$$

$$\frac{\partial A_{11}}{\partial x_3} = \frac{[-\frac{\partial a_{12}}{\partial x_3}(l_1 x_2^2 - gcos(x_1)) + \frac{\partial a_{11}}{\partial x_3} l_2 x_4^2]\Delta}{\Delta^2} - \frac{[-a_{12}(l_1 x_2^2 - gcos(x_1)) + a_{11} l_2 x_4^2]\frac{\partial \Delta}{\partial x_3}}{\Delta^2}$$

$$\frac{\partial A_{11}}{\partial x_4} = \frac{[-\frac{\partial a_{12}}{\partial x_4}(l_1 x_2^2 - gcos(x_1)) + \frac{\partial a_{11}}{\partial x_4} l_2 x_4^2 + 2 a_{11} l_2 x_4]\Delta}{\Delta^2} - \frac{[-a_{12}(l_1 x_2^2 - gcos(x_1)) + a_{11} l_2 x_4^2]\frac{\partial \Delta}{\partial x_4}}{\Delta^2}$$

$$\frac{\partial A_{11}}{\partial x_5} = \frac{[-\frac{\partial a_{12}}{\partial x_5}(l_1 x_2^2 - gcos(x_1)) + \frac{\partial a_{11}}{\partial x_5} l_2 x_4^2]\Delta}{\Delta^2} - \frac{[-a_{12}(l_1 x_2^2 - gcos(x_1)) + a_{11} l_2 x_4^2]\frac{\partial \Delta}{\partial x_5}}{\Delta^2}$$

$$\frac{\partial A_{11}}{\partial x_6} = \frac{[-\frac{\partial a_{12}}{\partial x_6}(l_1 x_2^2 - gcos(x_1)) + \frac{\partial a_{11}}{\partial x_6} l_2 x_4^2]\Delta}{\Delta^2} - \frac{[-a_{12}(l_1 x_2^2 - gcos(x_1)) + a_{11} l_2 x_4^2]\frac{\partial \Delta}{\partial x_6}}{\Delta^2}$$

It holds that

$$A_{12} = -\frac{a_{22} sin(x_1)}{\Delta} \tag{2.162}$$

The derivatives of A_{12} with respect to the state vector elements x_i $i = 1, \ldots, 6$ are computed as follows:

$$\frac{\partial A_{12}}{\partial x_1} = -\frac{[\frac{\partial a_{22}}{\partial x_1} sin(x_1) + a_{22} cos(x_1)]\Delta}{m_c \Delta^2} + \frac{a_{22} sin(x_1)\frac{\partial \Delta}{\partial x_1}}{m_c \Delta^2}$$

$$\frac{\partial A_{12}}{\partial x_2} = -\frac{[\frac{\partial a_{22}}{\partial x_2} sin(x_1)]\Delta}{m_c \Delta^2} + \frac{a_{22} sin(x_1)\frac{\partial \Delta}{\partial x_2}}{m_c \Delta^2}$$

$$\frac{\partial A_{12}}{\partial x_3} = -\frac{[\frac{\partial a_{22}}{\partial x_3} sin(x_1)]\Delta}{m_c \Delta^2} + \frac{a_{22} sin(x_1) \frac{\partial \Delta}{\partial x_3}}{m_c \Delta^2}$$

$$\frac{\partial A_{12}}{\partial x_4} = -\frac{[\frac{\partial a_{22}}{\partial x_4} sin(x_1)]\Delta}{m_c \Delta^2} + \frac{a_{22} sin(x_1) \frac{\partial \Delta}{\partial x_4}}{m_c \Delta^2}$$

$$\frac{\partial A_{12}}{\partial x_5} = -\frac{[\frac{\partial a_{22}}{\partial x_5} sin(x_1)]\Delta}{m_c \Delta^2} + \frac{a_{22} sin(x_1) \frac{\partial \Delta}{\partial x_5}}{m_c \Delta^2}$$

$$\frac{\partial A_{12}}{\partial x_6} = -\frac{[\frac{\partial a_{22}}{\partial x_6} sin(x_1)]\Delta}{m_c \Delta^2} + \frac{a_{22} sin(x_1) \frac{\partial \Delta}{\partial x_6}}{m_c \Delta^2}$$

It holds that

$$A_{21} = \frac{a_{22}(l_1 x_1^2 - g cos(x_1)) - a_{12} l_2 x_4^2}{\Delta} \tag{2.163}$$

The derivatives of A_{21} with respect to the state vector elements x_i $i = 1, \ldots, 4$ are computed as follows:

$$\frac{\partial A_{21}}{\partial x_1} = \frac{[-\frac{\partial a_{22}}{\partial x_1}(l_1 x_2^2 - g cos(x_1)) - a_{22} g sin(x_1) + \frac{\partial a_{12}}{\partial x_1} l_2 x_4^2]\Delta}{\Delta^2} - \frac{[-a_{22}(l_1 x_2^2 - g cos(x_1)) + a_{12} l_2 x_4^2]\frac{\partial \Delta}{\partial x_1}}{\Delta^2}$$

$$\frac{\partial A_{21}}{\partial x_2} = \frac{[-\frac{\partial a_{22}}{\partial x_2}(l_1 x_2^2 - g cos(x_1)) - a_{22}(2 l_1 x_2) + \frac{\partial a_{12}}{\partial x_2} l_2 x_4^2]\Delta}{\Delta^2} - \frac{[-a_{22}(l_1 x_2^2 - g cos(x_1)) + a_{12} l_2 x_4^2]\frac{\partial \Delta}{\partial x_2}}{\Delta^2}$$

$$\frac{\partial A_{21}}{\partial x_3} = \frac{[-\frac{\partial a_{22}}{\partial x_3}(l_1 x_2^2 - g cos(x_1)) + \frac{\partial a_{12}}{\partial x_3} l_2 x_4^2]\Delta}{\Delta^2} - \frac{[-a_{22}(l_1 x_2^2 - g cos(x_1)) + a_{12} l_2 x_4^2]\frac{\partial \Delta}{\partial x_3}}{\Delta^2}$$

$$\frac{\partial A_{21}}{\partial x_4} = \frac{[-\frac{\partial a_{22}}{\partial x_4}(l_1 x_2^2 - g cos(x_1)) + \frac{\partial a_{12}}{\partial x_4} l_2 x_4^2 + 2 a_{12} l_2 x_4]\Delta}{\Delta^2} - \frac{[-a_{22}(l_1 x_2^2 - g cos(x_1)) + a_{12} l_2 x_4^2]\frac{\partial \Delta}{\partial x_4}}{\Delta^2}$$

$$\frac{\partial A_{21}}{\partial x_5} = \frac{[-\frac{\partial a_{22}}{\partial x_5}(l_1 x_2^2 - g cos(x_1)) + \frac{\partial a_{12}}{\partial x_5} l_2 x_4^2]\Delta}{\Delta^2} - \frac{[-a_{22}(l_1 x_2^2 - g cos(x_1)) + a_{12} l_2 x_4^2]\frac{\partial \Delta}{\partial x_5}}{\Delta^2}$$

$$\frac{\partial A_{21}}{\partial x_6} = \frac{[-\frac{\partial a_{22}}{\partial x_6}(l_1 x_2^2 - g cos(x_1)) + \frac{\partial a_{12}}{\partial x_6} l_2 x_4^2]\Delta}{\Delta^2} - \frac{[-a_{22}(l_1 x_2^2 - g cos(x_1)) + a_{12} l_2 x_4^2]\frac{\partial \Delta}{\partial x_6}}{\Delta^2}$$

It holds that

$$A_{22} = \frac{a_{12} sin(x_1)}{m_c \Delta} \tag{2.164}$$

The derivatives of A_{22} with respect to the state vector elements x_i $i = 1, \ldots, 4$ are computed as follows:

$$\frac{\partial A_{22}}{\partial x_1} = \frac{[\frac{\partial a_{12}}{\partial x_1} sin(x_1) + a_{12} cos(x_1)]\Delta}{m_c \Delta^2} + \frac{a_{12} sin(x_1) \frac{\partial \Delta}{\partial x_1}}{m_c \Delta^2}$$

$$\frac{\partial A_{22}}{\partial x_2} = \frac{[\frac{\partial a_{12}}{\partial x_2} sin(x_1)]\Delta}{m_c \Delta^2} + \frac{a_{12} sin(x_1) \frac{\partial \Delta}{\partial x_2}}{m_c \Delta^2}$$

$$\frac{\partial A_{22}}{\partial x_3} = \frac{[\frac{\partial a_{12}}{\partial x_3} sin(x_1)]\Delta}{m_c \Delta^2} + \frac{a_{12} sin(x_1) \frac{\partial \Delta}{\partial x_3}}{m_c \Delta^2}$$

$$\frac{\partial A_{22}}{\partial x_4} = \frac{[\frac{\partial a_{12}}{\partial x_4} sin(x_1)]\Delta}{m_c \Delta^2} + \frac{a_{12} sin(x_1) \frac{\partial \Delta}{\partial x_4}}{m_c \Delta^2}$$

$$\frac{\partial A_{22}}{\partial x_5} = \frac{[\frac{\partial a_{12}}{\partial x_5} sin(x_1)]\Delta}{m_c \Delta^2} + \frac{a_{12} sin(x_1) \frac{\partial \Delta}{\partial x_5}}{m_c \Delta^2}$$

$$\frac{\partial A_{22}}{\partial x_6} = \frac{[\frac{\partial a_{12}}{\partial x_6} sin(x_1)]\Delta}{m_c \Delta^2} + \frac{a_{12} sin(x_1) \frac{\partial \Delta}{\partial x_6}}{m_c \Delta^2}$$

Finally, about the partial derivatives of the parameters a_{11}, a_{12} and a_{21}, with respect to the state variables of the x_i $i = 1, \ldots, 6$ one has

$$\frac{\partial a_{11}}{\partial x_1} = \frac{2}{m_c} sin(x_1) cos(x_1),\ \frac{\partial a_{11}}{\partial x_2} = 0,\ \frac{\partial a_{11}}{\partial x_3} = 0,\ \frac{\partial a_{11}}{\partial x_4} = 0,\ \frac{\partial a_{11}}{\partial x_5} = 0,\ \frac{\partial a_{11}}{\partial x_6} = 0.$$

$$\frac{\partial a_{12}}{\partial x_1} = \frac{-sin(x_3 - x_1)}{m_c},\ \frac{\partial a_{12}}{\partial x_2} = 0,\ \frac{\partial a_{12}}{\partial x_3} = \frac{sin(x_3 - x_1)}{m_c},\ \frac{\partial a_{12}}{\partial x_4} = 0,\ \frac{\partial a_{12}}{\partial x_5} = 0,\ \frac{\partial a_{12}}{\partial x_6} = 0.$$

$$\frac{\partial a_{22}}{\partial x_1} = 0,\ \frac{\partial a_{22}}{\partial x_2} = 0,\ \frac{\partial a_{22}}{\partial x_3} = 0,\ \frac{\partial a_{22}}{\partial x_4} = 0,\ \frac{\partial a_{22}}{\partial x_5} = 0,\ \frac{\partial a_{22}}{\partial x_6} = 0.$$

Moreover, considering that $\frac{\partial a_{22}}{\partial x_i} = 0, i = 1, \ldots, 6$, the derivatives of $\Delta = a_{11} a_{22} - a_{12}^2$ with respect to the state vector elements x_i, $i = 1, \ldots, 6$ are computed as follows:

$$\frac{\partial \Delta}{\partial x_1} = \frac{\partial a_{11}}{\partial x_1} a_{22} - 2 a_{12} \frac{\partial a_{12}}{\partial x_1}$$

$$\frac{\partial \Delta}{\partial x_2} = \frac{\partial a_{11}}{\partial x_2} a_{22} - 2 a_{12} \frac{\partial a_{12}}{\partial x_2}$$

$$\frac{\partial \Delta}{\partial x_3} = \frac{\partial a_{11}}{\partial x_3} a_{22} - 2 a_{12} \frac{\partial a_{12}}{\partial x_3}$$

$$\frac{\partial \Delta}{\partial x_4} = \frac{\partial a_{11}}{\partial x_4} a_{22} - 2 a_{12} \frac{\partial a_{12}}{\partial x_4}$$

$$\frac{\partial \Delta}{\partial x_5} = \frac{\partial a_{11}}{\partial x_5} a_{22} - 2 a_{12} \frac{\partial a_{12}}{\partial x_5}$$

$$\frac{\partial \Delta}{\partial x_6} = \frac{\partial a_{11}}{\partial x_6} a_{22} - 2 a_{12} \frac{\partial a_{12}}{\partial x_6}$$

2.5.4 *Design of an H-Infinity Nonlinear Feedback Controller*

2.5.4.1 Equivalent Linearized Dynamics of the Cart and Double-Pendulum System

After linearization around its current operating point, the dynamic model of the cart and double-pendulum system is written as

$$\dot{x} = Ax + Bu + d_1 \tag{2.165}$$

As in previous applications of the linearization procedure, parameter d_1 stands for the linearization error in the dynamic model of the cart and double pendulum appearing in Eq. (2.165). The reference setpoints for the cart and double pendulum's state vector are denoted by $\mathbf{x_d} = [x_1^d, \ldots, x_6^d]$. Tracking of this trajectory is achieved after

applying the control input u^*. At every time instant the control input u^* is assumed to differ from the control input u appearing in Eq. (2.165) by an amount equal to Δu, that is $u^* = u + \Delta u$

$$\dot{x}_d = Ax_d + Bu^* + d_2 \tag{2.166}$$

The dynamics of the controlled system described in Eq. (2.165) can be also written as

$$\dot{x} = Ax + Bu + Bu^* - Bu^* + d_1 \tag{2.167}$$

and by denoting $d_3 = -Bu^* + d_1$ as an aggregate disturbance term one obtains

$$\dot{x} = Ax + Bu + Bu^* + d_3 \tag{2.168}$$

By subtracting Eq. (2.166) from (2.168) one has

$$\dot{x} - \dot{x}_d = A(x - x_d) + Bu + d_3 - d_2 \tag{2.169}$$

By denoting the tracking error as $e = x - x_d$ and the aggregate disturbance term as $\tilde{d} = d_3 - d_2$, the tracking error dynamics becomes

$$\dot{e} = Ae + Bu + \tilde{d} \tag{2.170}$$

The above linearized form of the model of the cart and double-pendulum can be efficiently controlled after applying an H-infinity feedback control scheme.

2.5.4.2 The Nonlinear H-Infinity Control

The initial nonlinear model of the underactuated model of the cart and double-pendulum is in the form

$$\dot{x} = \tilde{f}(x, u) \;\; x \in R^n, \;\; u \in R^m \tag{2.171}$$

Linearization of the multi-DOF model of the cart and double-pendulum is performed at each iteration of the control algorithm around its present operating point $(x^*, u^*) = (x(t), u(t - T_s))$, where T_s is the sampling period. The linearized equivalent model of the system is described by

$$\dot{x} = Ax + Bu + L\tilde{d} \;\; x \in R^n, \;\; u \in R^m, \;\; \tilde{d} \in R^q \tag{2.172}$$

where matrices A and B are obtained from the computation of the Jacobians given in Eq. (2.160), and vector $\tilde{d}$ denotes disturbance terms due to linearization errors. As explained, the problem of disturbance rejection for the linearized model that is described by

$$\begin{aligned} \dot{x} &= Ax + Bu + L\tilde{d} \\ y &= Cx \end{aligned} \tag{2.173}$$

where $x \in R^n$, $u \in R^m$, $\tilde{d} \in R^q$ and $y \in R^p$, cannot be handled efficiently if the classical LQR control scheme is applied. This is because of the existence of the perturbation term $\tilde{d}$. The disturbance term $\tilde{d}$ apart from modeling (parametric) uncertainty and external perturbation terms can also represent noise terms of any distribution.

As already explained in the previous application of the H_∞ control, a feedback control scheme is designed for trajectory tracking by the system's state vector and simultaneous disturbance rejection, considering that the disturbance affects the system in the worst possible manner. The disturbances' effects are incorporated in the following quadratic cost function:

$$J(t) = \frac{1}{2}\int_0^T [y^T(t)y(t) + ru^T(t)u(t) - \rho^2 \tilde{d}^T(t)\tilde{d}(t)]dt, \quad r, \rho > 0 \tag{2.174}$$

The significance of the negative sign in the cost function's term that is associated with the perturbation variable $\tilde{d}(t)$ is that the disturbance tries to maximize the cost function $J(t)$ while the control signal $u(t)$ tries to minimize it. The physical meaning of the relation given above is that the control signal and the disturbances compete to each other within a min-max differential game. This problem of min-max optimization can be written as $min_u max_{\tilde{d}} J(u, \tilde{d})$.

As previously noted, the objective of the optimization procedure is to compute a control signal $u(t)$ which can compensate for the worst possible disturbance, that is externally imposed to the cart and double-pendulum system. However, the solution to the min-max optimization problem is directly related to the value of the parameter ρ. This means that there is an upper bound in the disturbances magnitude that can be annihilated by the control signal.

2.5.4.3 Computation of the Feedback Control Gains

For the linearized system given by Eq. (2.173) the cost function of Eq. (2.174) is defined, where the coefficient r determines the penalization of the control input and the weight coefficient ρ determines the reward of the disturbances' effects.

It is assumed that (i) The energy that is transferred from the disturbances signal $\tilde{d}(t)$ is bounded, that is $\int_0^\infty \tilde{d}^T(t)\tilde{d}(t)dt < \infty$, (ii) the matrices $[A, B]$ and $[A, L]$ are stabilizable, (iii) the matrix $[A, C]$ is detectable. Then, the optimal feedback control law is given by

$$u(t) = -Kx(t) \tag{2.175}$$

with $K = \frac{1}{r}B^T P$, where P is a positive semi-definite symmetric matrix which is obtained from the solution of the Riccati equation

$$A^T P + PA + Q - P(\frac{1}{r}BB^T - \frac{1}{2\rho^2}LL^T)P = 0 \tag{2.176}$$

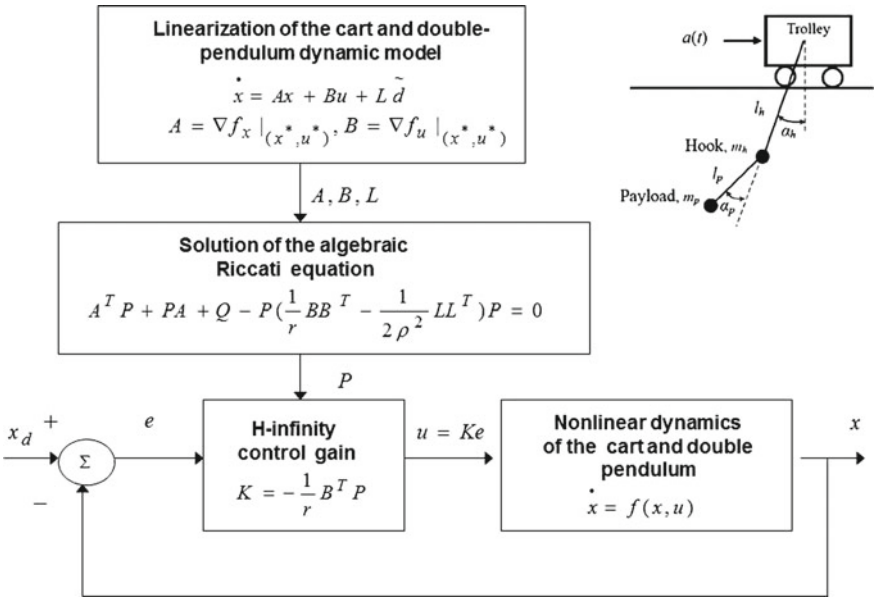

Fig. 2.27 Diagram of the control scheme for the cart and double-pendulum system

where Q is also a positive definite symmetric matrix. The worst case disturbance is given by $\tilde{d}(t) = \frac{1}{\rho^2}L^T Px(t)$. The above Riccati equation has to be solved at each time-step of the control method. The diagram of the considered control loop is depicted in Fig. 2.27.

2.5.5 *Lyapunov Stability Analysis*

Through Lyapunov stability analysis it will be shown that the proposed nonlinear control scheme assures H_∞ tracking performance for the cart and double-pendulum system, and that in case of bounded disturbance terms asymptotic convergence to the reference setpoints is achieved. The tracking error dynamics for the underactuated model of the cart and double-pendulum is written in the form

$$\dot{e} = Ae + Bu + L\tilde{d} \tag{2.177}$$

where in the cart and double-pendulum's case $L = I \in R^6$ with I being the identity matrix. Variable $\tilde{d}$ denotes model uncertainties and external disturbances of the cart and double pendulum's model. The following Lyapunov function is considered

$$V = \frac{1}{2}e^T Pe \tag{2.178}$$

where $e = x - x_d$ is the tracking error. By differentiating with respect to time and by following the previous technique, one obtains

$$\begin{gathered} \dot{V} = \tfrac{1}{2}\dot{e}^T P e + \tfrac{1}{2} e^T P \dot{e} \Rightarrow \\ \dot{V} = \tfrac{1}{2}[Ae + Bu + L\tilde{d}]^T P e + \tfrac{1}{2} e^T P [Ae + Bu + L\tilde{d}] \Rightarrow \end{gathered} \tag{2.179}$$

$$\begin{gathered} \dot{V} = \tfrac{1}{2}[e^T A^T + u^T B^T + \tilde{d}^T L^T] P e + \\ + \tfrac{1}{2} e^T P [Ae + Bu + L\tilde{d}] \Rightarrow \end{gathered} \tag{2.180}$$

$$\begin{gathered} \dot{V} = \tfrac{1}{2} e^T A^T P e + \tfrac{1}{2} u^T B^T P e + \tfrac{1}{2} \tilde{d}^T L^T P e + \\ \tfrac{1}{2} e^T P A e + \tfrac{1}{2} e^T P B u + \tfrac{1}{2} e^T P L \tilde{d} \end{gathered} \tag{2.181}$$

The previous equation is rewritten as

$$\begin{gathered} \dot{V} = \tfrac{1}{2} e^T (A^T P + P A) e + \left(\tfrac{1}{2} u^T B^T P e + \tfrac{1}{2} e^T P B u\right) + \\ + \left(\tfrac{1}{2} \tilde{d}^T L^T P e + \tfrac{1}{2} e^T P L \tilde{d}\right) \end{gathered} \tag{2.182}$$

Assumption: For given positive definite matrix Q and coefficients r and ρ there exists a positive definite matrix P, which is the solution of the following matrix equation

$$A^T P + P A = -Q + P \left(\tfrac{2}{r} B B^T - \tfrac{1}{\rho^2} L L^T\right) P \tag{2.183}$$

Moreover, the following feedback control law is applied to the system

$$u = -\tfrac{1}{r} B^T P e \tag{2.184}$$

By substituting Eqs. (2.183) and (2.184) one obtains

$$\begin{gathered} \dot{V} = \tfrac{1}{2} e^T \left[-Q + P \left(\tfrac{2}{r} B B^T - \tfrac{1}{\rho^2} L L^T\right) P\right] e + \\ + e^T P B \left(-\tfrac{1}{r} B^T P e\right) + e^T P L \tilde{d} \Rightarrow \end{gathered} \tag{2.185}$$

$$\begin{gathered} \dot{V} = -\tfrac{1}{2} e^T Q e + \tfrac{1}{r} e^T P B B^T P e - \tfrac{1}{2\rho^2} e^T P L L^T P e \\ - \tfrac{1}{r} e^T P B B^T P e + e^T P L \tilde{d} \end{gathered} \tag{2.186}$$

which after intermediate operations gives

$$\dot{V} = -\tfrac{1}{2} e^T Q e - \tfrac{1}{2\rho^2} e^T P L L^T P e + e^T P L \tilde{d} \tag{2.187}$$

or, equivalently

$$\begin{aligned}\dot{V} = -\tfrac{1}{2}e^T Qe - \tfrac{1}{2\rho^2}e^T PLL^T Pe + \\ + \tfrac{1}{2}e^T PL\tilde{d} + \tfrac{1}{2}\tilde{d}^T L^T Pe\end{aligned} \tag{2.188}$$

Lemma: The following inequality holds

$$\tfrac{1}{2}e^T PL\tilde{d} + \tfrac{1}{2}\tilde{d}L^T Pe - \tfrac{1}{2\rho^2}e^T PLL^T Pe \leq \tfrac{1}{2}\rho^2\tilde{d}^T\tilde{d} \tag{2.189}$$

Proof: The binomial $(\rho\alpha - \frac{1}{\rho}b)^2$ is considered. Expanding the left part of the above inequality one gets

$$\begin{aligned}\rho^2a^2 + \tfrac{1}{\rho^2}b^2 - 2ab \geq 0 \Rightarrow \tfrac{1}{2}\rho^2a^2 + \tfrac{1}{2\rho^2}b^2 - ab \geq 0 \Rightarrow \\ ab - \tfrac{1}{2\rho^2}b^2 \leq \tfrac{1}{2}\rho^2a^2 \Rightarrow \tfrac{1}{2}ab + \tfrac{1}{2}ab - \tfrac{1}{2\rho^2}b^2 \leq \tfrac{1}{2}\rho^2a^2\end{aligned} \tag{2.190}$$

The following substitutions are carried out: $a = \tilde{d}$ and $b = e^T PL$ and the previous relation becomes

$$\tfrac{1}{2}\tilde{d}^T L^T Pe + \tfrac{1}{2}e^T PL\tilde{d} - \tfrac{1}{2\rho^2}e^T PLL^T Pe \leq \tfrac{1}{2}\rho^2\tilde{d}^T\tilde{d} \tag{2.191}$$

Equation (2.191) is substituted in Eq. (2.188) and the inequality is enforced, thus giving

$$\dot{V} \leq -\tfrac{1}{2}e^T Qe + \tfrac{1}{2}\rho^2\tilde{d}^T\tilde{d} \tag{2.192}$$

Equation (2.192) shows that the H_∞ tracking performance criterion is satisfied. The integration of $\dot{V}$ from 0 to T gives

$$\begin{aligned}\int_0^T \dot{V}(t)dt \leq -\tfrac{1}{2}\int_0^T ||e||_Q^2 dt + \tfrac{1}{2}\rho^2\int_0^T ||\tilde{d}||^2 dt \Rightarrow \\ 2V(T) + \int_0^T ||e||_Q^2 dt \leq 2V(0) + \rho^2\int_0^T ||\tilde{d}||^2 dt\end{aligned} \tag{2.193}$$

Moreover, if there exists a positive constant $M_d > 0$ such that

$$\int_0^\infty ||\tilde{d}||^2 dt \leq M_d \tag{2.194}$$

then one gets

$$\int_0^\infty ||e||_Q^2 dt \leq 2V(0) + \rho^2 M_d \tag{2.195}$$

Thus, the integral $\int_0^\infty ||e||_Q^2 dt$ is bounded. Moreover, $V(T)$ is bounded and from the definition of the Lyapunov function V in Eq. (2.178) it becomes clear that $e(t)$ will be also bounded since $e(t) \in \Omega_e = \{e | e^T Pe \leq 2V(0) + \rho^2 M_d\}$. According to the above and with the use of Barbalat's Lemma one obtains $lim_{t\to\infty} e(t) = 0$.

Elaborating on the above, it can be noted that the proof of global asymptotic stability for the control loop of the underactuated cart and double-pendulum relies on Eq. (2.192) and on the application of Barbalat's Lemma. It uses the condition of Eq. (2.194) about the boundedness of the square of the aggregate disturbance and

modelling error term $\tilde{d}$ that affects the model. However, as explained above the proof of global asymptotic stability is not restricted by this condition. By selecting the attenuation coefficient ρ to be sufficiently small and in particular to satisfy $\rho^2 < ||e||_Q^2 / ||\tilde{d}||^2$ one has that the first derivative of the Lyapunov function is upper bounded by 0. Therefore for the ith time interval it is proven that the Lyapunov function defined in Eq. (2.178) is a decreasing one. This also assures that the Lyapunov function of the rotary pendulum defined in Eq. (2.171) will always have a negative first-order derivative.

2.5.6 Robust State Estimation with the Use of the H_∞ Kalman Filter

The control loop for the cart and double-pendulum system can be implemented with the use of information provided by a small number of sensors and by processing only a small number of state variables. To reconstruct the missing information about the state vector of the cart and double pendulum it is proposed to use a filtering scheme and based on it to apply state estimation-based control [169, 457, 459, 511]. The recursion of the H_∞ Kalman Filter, for the model of the cart and double-pendulum system, can be formulated in terms of a *measurement update* and a *time update* part

Measurement update:

$$\begin{aligned} D(k) &= [I - \theta W(k) P^-(k) + C^T(k) R(k)^{-1} C(k) P^-(k)]^{-1} \\ K(k) &= P^-(k) D(k) C^T(k) R(k)^{-1} \\ \hat{x}(k) &= \hat{x}^-(k) + K(k)[y(k) - C\hat{x}^-(k)] \end{aligned} \tag{2.196}$$

Time update:

$$\begin{aligned} \hat{x}^-(k+1) &= A(k)x(k) + B(k)u(k) \\ P^-(k+1) &= A(k)P^-(k)D(k)A^T(k) + Q(k) \end{aligned} \tag{2.197}$$

where it is assumed that parameter θ is sufficiently small to assure that the covariance matrix $P^-(k)^{-1} - \theta W(k) + C^T(k) R(k)^{-1} C(k)$ will be positive definite. When $\theta = 0$ the H_∞ Kalman Filter becomes equivalent to the standard Kalman Filter. One can measure only a part of the state vector of the cart and double-pendulum system, for instance $x_1 = \theta_1$, $x_3 = \theta_2$, and $x_5 = x$, and can estimate through filtering the rest of the state vector elements.

2.5.7 Simulation Tests

The performance and the tracking accuracy of the nonlinear optimal (H-infinity) control scheme for the cart and double-pendulum system has been demonstrated

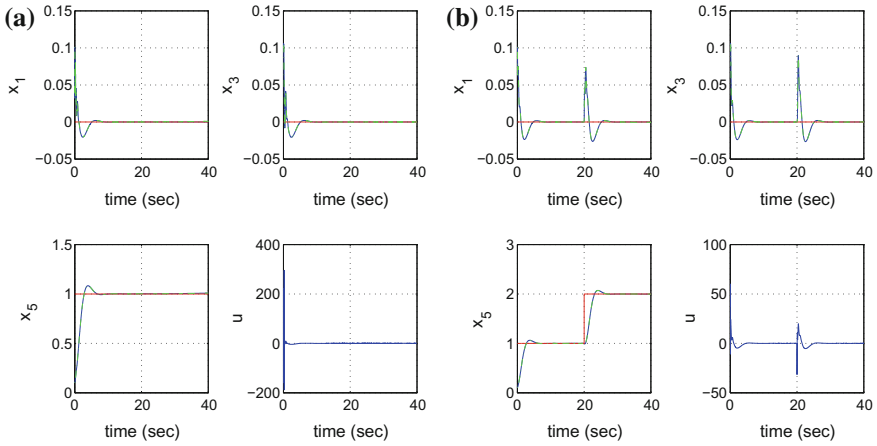

Fig. 2.28 Tracking of reference setpoints by the state variables $x_1 = \theta_1, x_3 = \theta_2$ and $x_5 = x$ of the cart and double pendulum system (blue lines: real values, green lines: estimated values, red lines: setpoints), and variation of the control input u. **a** Test case 1. **b** Test case 2

through simulation experiments. It has been shown that the under the proposed control approach fast and accurate tracking of all reference setpoints was achieved by the state vector elements of the cart and double-pendulum system. The obtained results are depicted in Figs. 2.28, 2.29, 2.30 and 2.31. In these diagrams, the reference setpoints are given with a red-line, the real value of the state variables is plotted with a blue line whereas, its estimated value is plotted with a green line.

For the design of the H-infinity feedback controller it was necessary to solve repetitively and at each iteration of the control algorithm the algebraic Riccati equation given in Eq. (2.183). The implementation of the proposed nonlinear H-infinity control scheme depends on the existence of a solution for the aforementioned Riccati equation. Actually, the smallest value of the attenuation coefficient ρ for which such a solution exists is the one that supplies the control method with maximum robustness. By selecting parameter ρ to be sufficiently small it can be assured that the inequality given in Eq. (2.192) holds and moreover that the first derivative of the system's Lyapunov function will be upper bounded by 0. This ascertains the global asymptotic stability of the control loop.

For the implementation of state estimation-based control, the H-infinity Kalman Filter has been used as a robust state estimator. It has been shown that it is possible to control and stabilize the cart and double-pendulum system by measuring only a small number of its state vector elements (such as $x_1 = \theta_1, x_3 = \theta_2$ and $x_5 = x$) and by estimating the rest of these elements with the use of the Kalman Filter. Despite the approximate linearization of the system's dynamics and despite the use of the estimated state vector in the control loop, the nonlinear H-infinity control scheme for the cart and double-pendulum system had a very satisfactory performance.

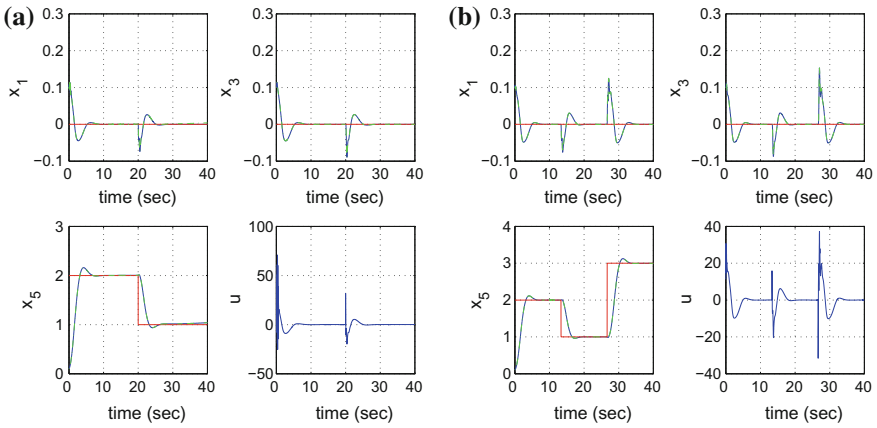

Fig. 2.29 Tracking of reference setpoints by the state variables $x_1 = \theta_1, x_3 = \theta_2$ and $x_5 = x$ of the cart and double pendulum system (blue lines: real values, green lines: estimated values, red lines: setpoints), and variation of the control input u. **a** Test case 3. **b** Test case 4

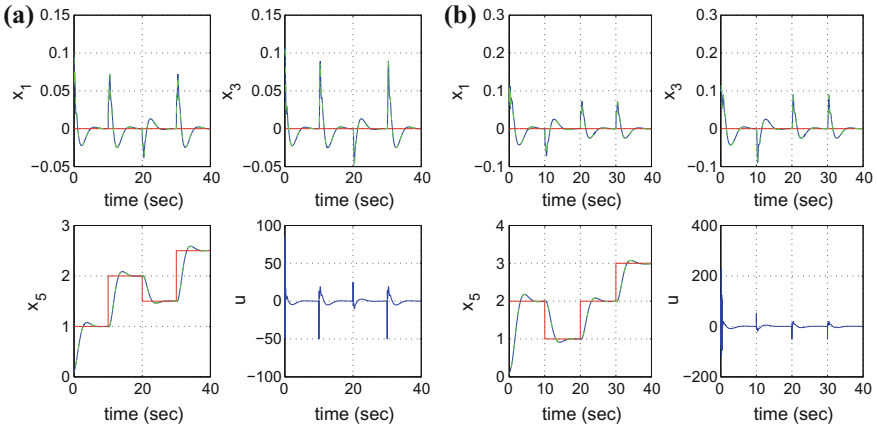

Fig. 2.30 Tracking of reference setpoints by the state variables $x_1 = \theta_1, x_3 = \theta_2$ and $x_5 = x$ of the cart and double pendulum system (blue lines: real values, green lines: estimated values, red lines: setpoints), and variation of the control input u. **a** Test case 3. **b** Test case 4

The tracking performance of the nonlinear optimal control algorithm, and particularly the RMSE for state variables $x_1 = \theta_1$, $x_3 = \theta_2$ and $x_5 = x$ is outlined in Table 2.6. The robustness of the control method against perturbations affecting the parameters of the cart and double-pendulum system is given in Table 2.7, which also appears next. The specific results are related with a change in the mass of the cart, up to 60% from the associated nominal value. Detailed diagrams about the variation of the state variables $x_i, i = 1, \ldots, 6$ of the cart and double-pendulum system and

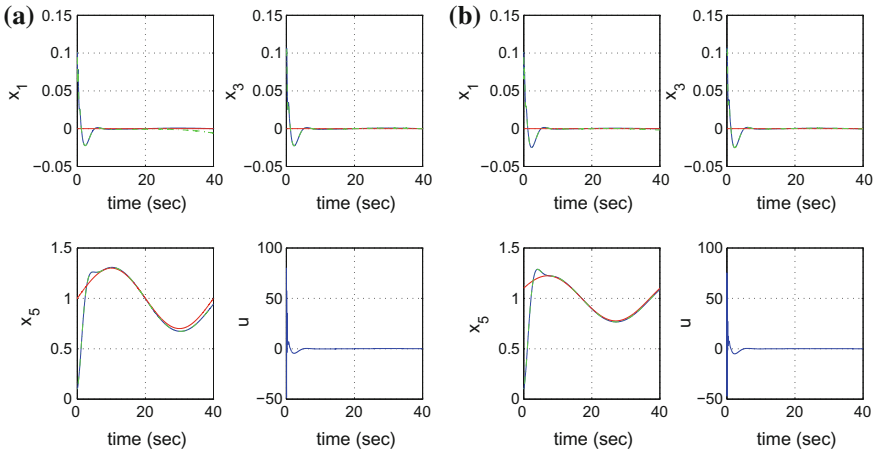

Fig. 2.31 Tracking of reference setpoints by the state variables $x_1 = \theta_1, x_3 = \theta_2$ and $x_5 = x$ of the cart and double pendulum system (blue lines: real values, green lines: estimated values, red lines: setpoints), and variation of the control input u. **a** Test case 7. **b** Test case 8

Table 2.6 RMSE of $x_1 = \theta_1, x_3 = \theta_2$ and $x_5 = x$

No test	RMSE x_1	RMSE x_3	RMSE x_5
1	$9.45{\cdot}10^{-7}$	$9.67{\cdot}10^{-7}$	$8.28{\cdot}10^{-4}$
2	$7.33{\cdot}10^{-7}$	$7.62{\cdot}10^{-7}$	$7.05{\cdot}10^{-4}$
3	$8.82{\cdot}10^{-7}$	$9.12{\cdot}10^{-7}$	$5.43{\cdot}10^{-4}$
4	$3.16{\cdot}10^{-6}$	$3.19{\cdot}10^{-6}$	$5.15{\cdot}10^{-4}$
5	$6.37{\cdot}10^{-5}$	$6.42{\cdot}10^{-5}$	$7.35{\cdot}10^{-5}$
6	$6.34{\cdot}10^{-5}$	$6.38{\cdot}10^{-5}$	$8.57{\cdot}10^{-4}$
7	$1.38{\cdot}10^{-5}$	$1.38{\cdot}10^{-5}$	$1.32{\cdot}10^{-4}$
8	$5.23{\cdot}10^{-6}$	$5.21{\cdot}10^{-6}$	$6.67{\cdot}10^{-5}$

Table 2.7 RMSE of x_1, x_3 and x_5 under disturbance

Δa (%)	RMSE x_1	RMSE x_3	RMSE x_5
0	$9.45{\cdot}10^{-7}$	$9.67{\cdot}10^{-7}$	$8.28{\cdot}10^{-4}$
20	$1.65{\cdot}10^{-6}$	$1.66{\cdot}10^{-6}$	$7.55{\cdot}10^{-4}$
30	$1.77{\cdot}10^{-6}$	$1.77{\cdot}10^{-6}$	$1.70{\cdot}10^{-3}$
40	$1.26{\cdot}10^{-6}$	$1.26{\cdot}10^{-6}$	$4.46{\cdot}10^{-4}$
50	$4.02{\cdot}10^{-6}$	$4.03{\cdot}10^{-6}$	$3.90{\cdot}10^{-3}$
60	$1.02{\cdot}10^{-5}$	$1.02{\cdot}10^{-5}$	$4.20{\cdot}10^{-3}$

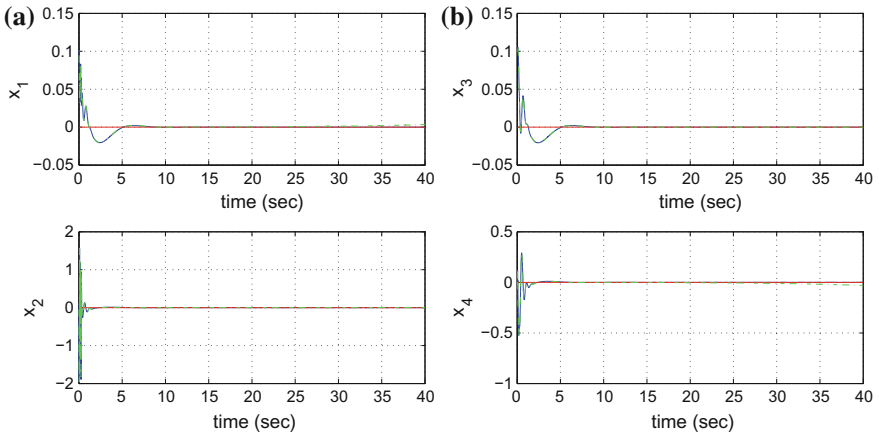

Fig. 2.32 Tracking of reference setpoint 1: **a** State variables $x_1 = \theta_1$ and $x_2 = \dot{\theta}_1$ of the cart and double pendulum system (blue lines: real values, green lines: estimated values, red lines: setpoints), **b** State variables $x_3 = \theta_2$ and $x_4 = \dot{\theta}_2$ of the cart and double-pendulum system (blue lines: real values, green lines: estimated values, red lines: setpoints)

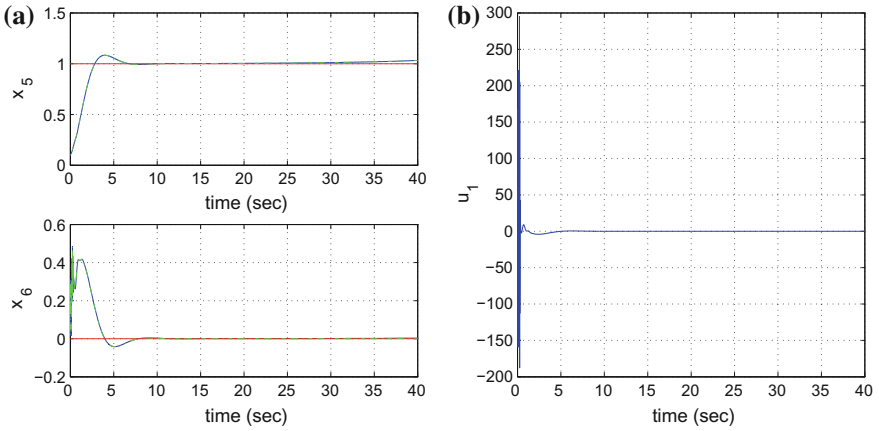

Fig. 2.33 Tracking of reference setpoint 1: **a** State variables $x_5 = x$ and $x_6 = \dot{x}$ of the cart and double pendulum system (blue lines: real values, green lines: estimated values, red lines: setpoints), **b** Control input u of the cart and double-pendulum system (blue line)

their convergence to the associated reference setpoints has been given in Appendix II at the end of manuscript. These diagrams appear in Figs. 2.32, 2.33, 2.34, 2.35, 2.36, 2.37, 2.38, 2.39, 2.40, 2.41, 2.42, 2.43, 2.44, 2.45, 2.46 and 2.47. Moreover, diagrams showing also in detail the variation of the control input u have been also provided.

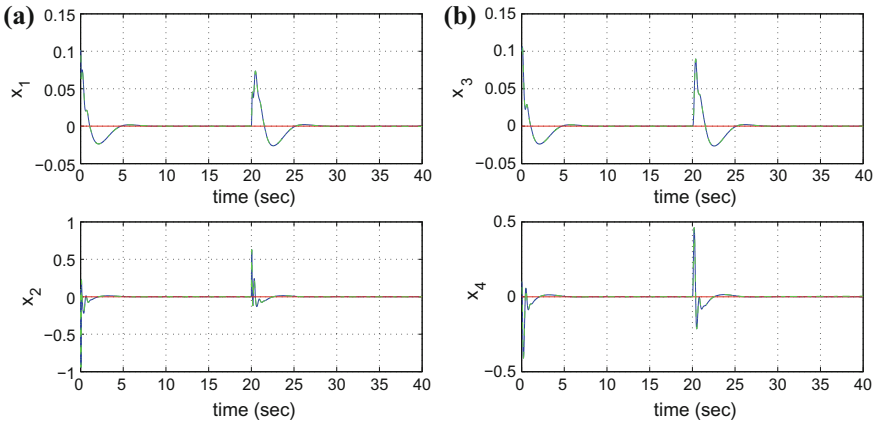

Fig. 2.34 Tracking of reference setpoint 2: **a** State variables $x_1 = \theta_1$ and $x_2 = \dot{\theta}_1$ of the cart and double-pendulum system (blue lines: real values, green lines: estimated values, red lines: setpoints), **b** State variables $x_3 = \theta_2$ and $x_4 = \dot{\theta}_2$ of the cart and double-pendulum system (blue lines: real values, green lines: estimated values, red lines: setpoints)

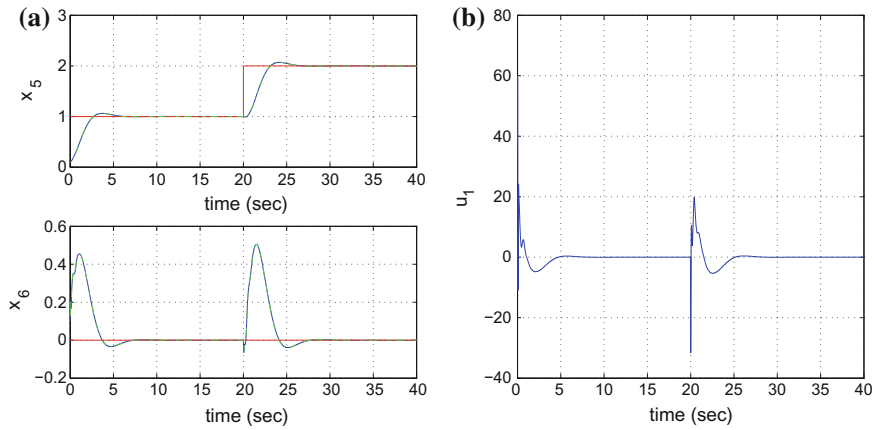

Fig. 2.35 Tracking of reference setpoint 2: **a** State variables $x_5 = x$ and $x_6 = \dot{x}$ of the cart and double-pendulum system (blue lines: real values, green lines: estimated values, red lines: setpoints), **b** Control input u of the cart and double-pendulum system (blue line)

Tracking performance of the nonlinear optimal control method for the cart and double-pendulum system:
The variation in time of the state variables $x_i,\ i = 1, \ldots, 6$, where $x_1 = \theta_1, x_2 = \dot{\theta}_1$, $x_3 = \theta_2$, $x_4 = \dot{\theta}_2$, $x_5 = x$ and $x_6 = \dot{x}$, as well as of the control input $u = F$ of the cart and double-pendulum system is shown in the following diagrams:

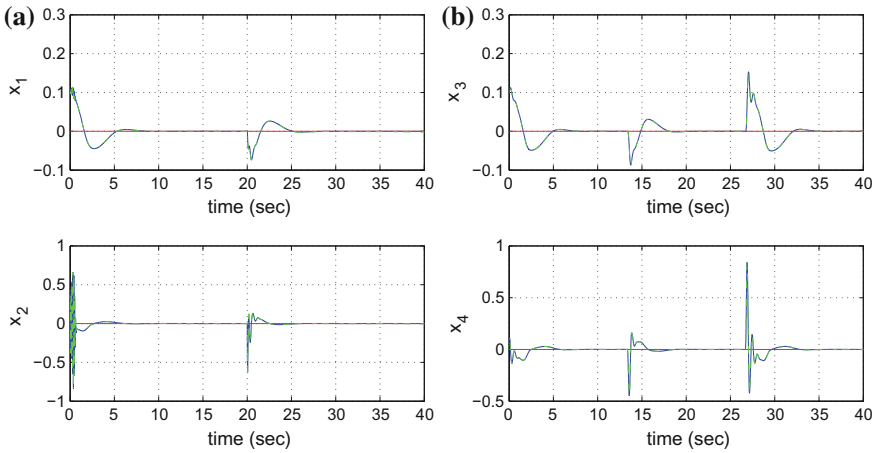

Fig. 2.36 Tracking of reference setpoint 3: **a** State variables $x_1 = \theta_1$ and $x_2 = \dot{\theta}_1$ of the cart and double-pendulum system (blue lines: real values, green lines: estimated values, red lines: setpoints), **b** State variables $x_3 = \theta_2$ and $x_4 = \dot{\theta}_2$ of the cart and double-pendulum system (blue lines: real values, green lines: estimated values, red lines: setpoints)

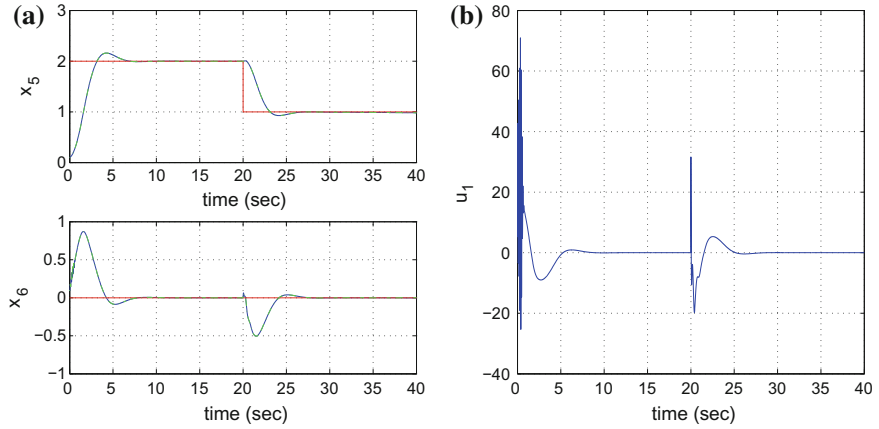

Fig. 2.37 Tracking of reference setpoint 3: **a** State variables $x_5 = x$ and $x_6 = \dot{x}$ of the cart and double-pendulum system (blue lines: real values, green lines: estimated values, red lines: setpoints), **b** Control input u of the cart and double-pendulum system (blue line)

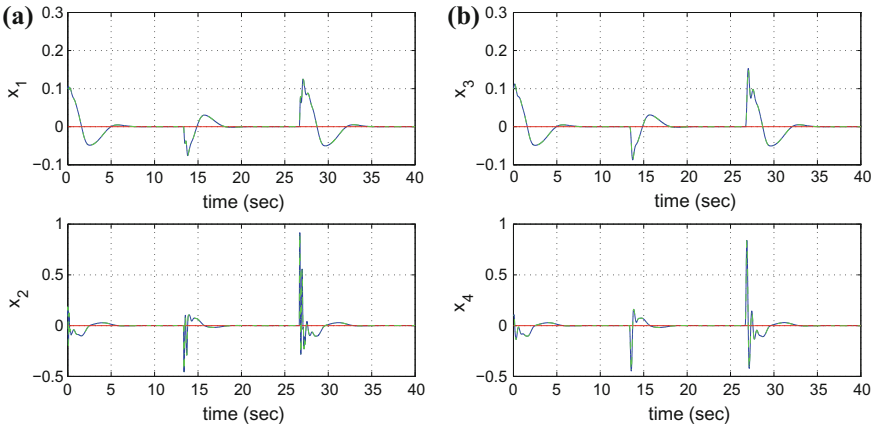

Fig. 2.38 Tracking of reference setpoint 4: **a** State variables $x_1 = \theta_1$ and $x_2 = \dot{\theta}_1$ of the cart and double-pendulum system (blue lines: real values, green lines: estimated values, red lines: setpoints), **b** State variables $x_3 = \theta_2$ and $x_4 = \dot{\theta}_2$ of the cart and double-pendulum system (blue lines: real values, green lines: estimated values, red lines: setpoints)

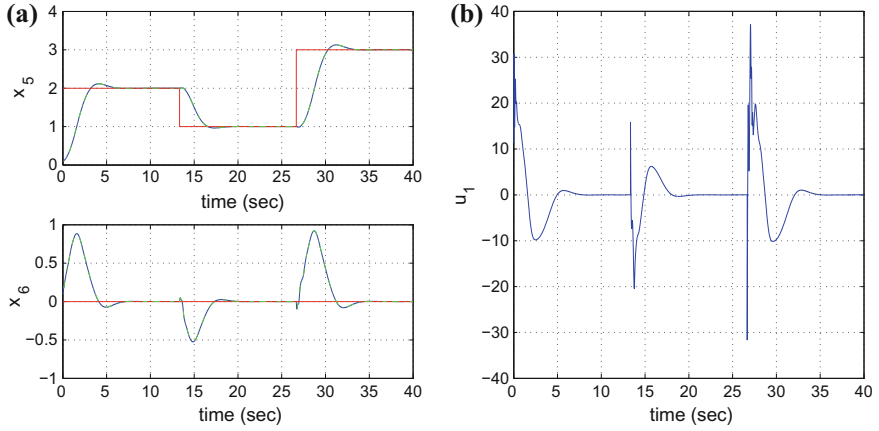

Fig. 2.39 Tracking of reference setpoint 4: **a** State variables $x_5 = x$ and $x_6 = \dot{x}$ of the cart and double-pendulum system (blue lines: real values, green lines: estimated values, red lines: setpoints), **b** Control input u of the cart and double-pendulum system (blue line)

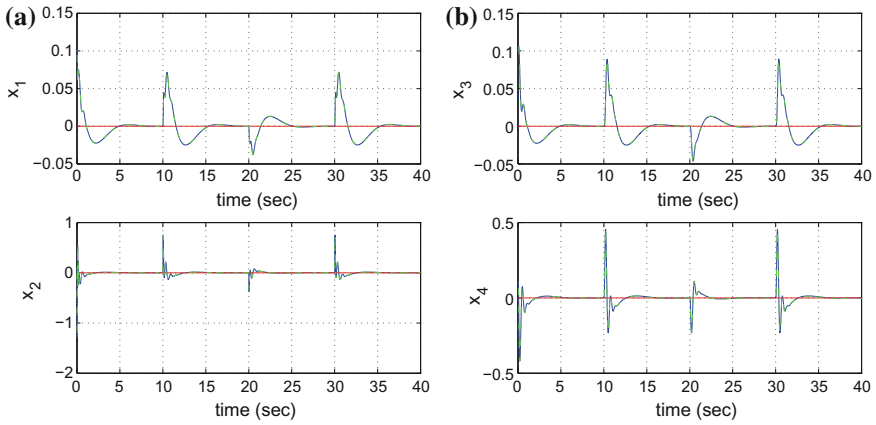

Fig. 2.40 Tracking of reference setpoint 5: **a** State variables $x_1 = \theta_1$ and $x_2 = \dot{\theta}_1$ of the cart and double-pendulum system (blue lines: real values, green lines: estimated values, red lines: setpoints), **b** State variables $x_3 = \theta_2$ and $x_4 = \dot{\theta}_2$ of the cart and double-pendulum system (blue lines: real values, green lines: estimated values, red lines: setpoints)

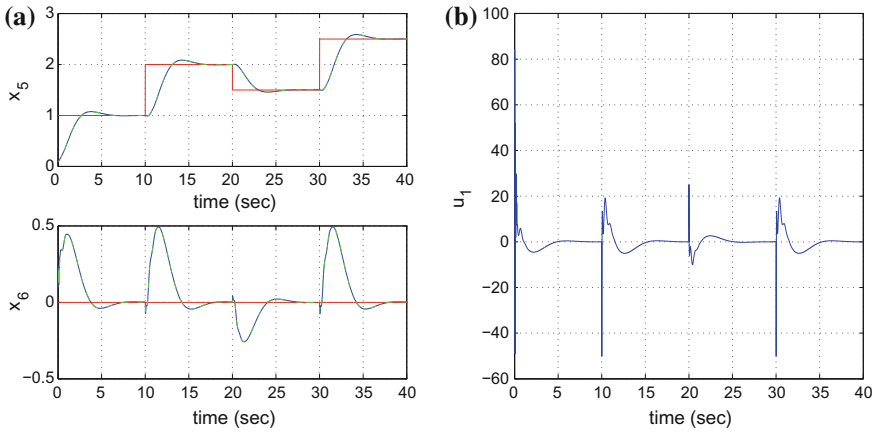

Fig. 2.41 Tracking of reference setpoint 5: **a** State variables $x_5 = x$ and $x_6 = \dot{x}$ of the cart and double-pendulum system (blue lines: real values, green lines: estimated values, red lines: setpoints), **b** Control input u of the cart and double-pendulum system (blue line)

2.6 Nonlinear Optimal Control for 3-DOF Underactuated Robotic Manipulators

2.6.1 Introduction

Control of underactuated robotic manipulators, that is robotic arms including both active and passive joints is a non-trivial problem due to the need of controlling the

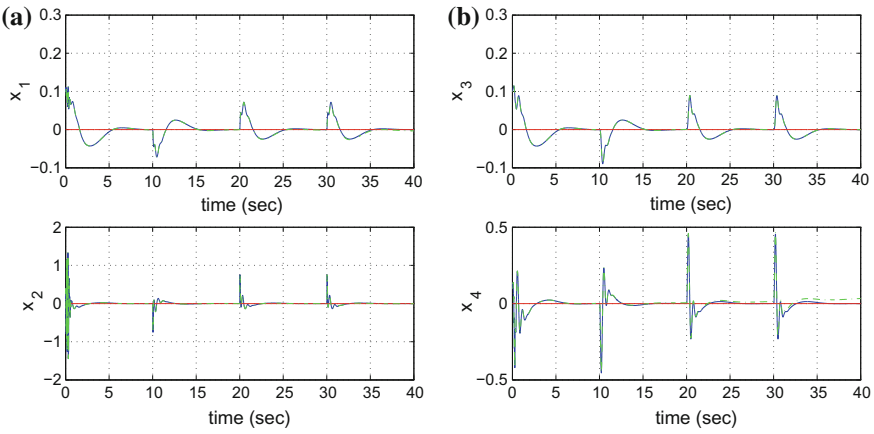

Fig. 2.42 Tracking of reference setpoint 6: **a** State variables $x_1 = \theta_1$ and $x_2 = \dot{\theta}_1$ of the cart and double-pendulum system (blue lines: real values, green lines: estimated values, red lines: setpoints), **b** State variables $x_3 = \theta_2$ and $x_4 = \dot{\theta}_2$ of the cart and double-pendulum system (blue lines: real values, green lines: estimated values, red lines: setpoints)

nonlinear robot dynamics with the use of a small number of actuators [19, 28, 352, 393, 485]. There are cases in which robotic manipularoes exhibit underactuation because of their design characteristics. Additionally there are cases in which the number of actuators is chosen to be smaller than the robot's degrees of freedom aiming at reducing the manipulator's weight and its power consumption. Moreover, solving the problem of control of a robot in underactuation signifies a fault tolerant functioning of the manipulator and that the robot's performance will remain reliable even if specific actuators undergo a failure [209, 307, 308, 473, 502]. A main approach in the control of underactuated manipulators is based on global linearization methods and the transformation of the robot's dynamic model into an equivalent linear form through a change of state variables (diffeomorphisms) [116–118, 208, 489]. Another major approach in the solution of the underactuated manipulators control problem is energy-based control in which the control inputs are computed through the minimization of a suitably chosen Lyapunov function of the robotic system [9, 210, 245, 247, 603, 628].

In this section a new method for the control of underactuated robotic manipulators has been developed, with the use of a nonlinear optimal (H-infinity) control approach [450, 457, 459]. The case of a 3-DOF robotic manipulator that comprises two active and one passive joint has been considered. The associated dynamic model consists of two equations describing the translational motion of the last (unactuated) link of the robot and one equation describing the rotational motion of this link. After initial transformations on the robot's dynamic model, an equivalent state-space description of the manipulator was obtained. For the latter description of the robot's dynamics a nonlinear optimal feedback controller has been designed, that was capable of making the state variables of the robot track any desirable trajectory.

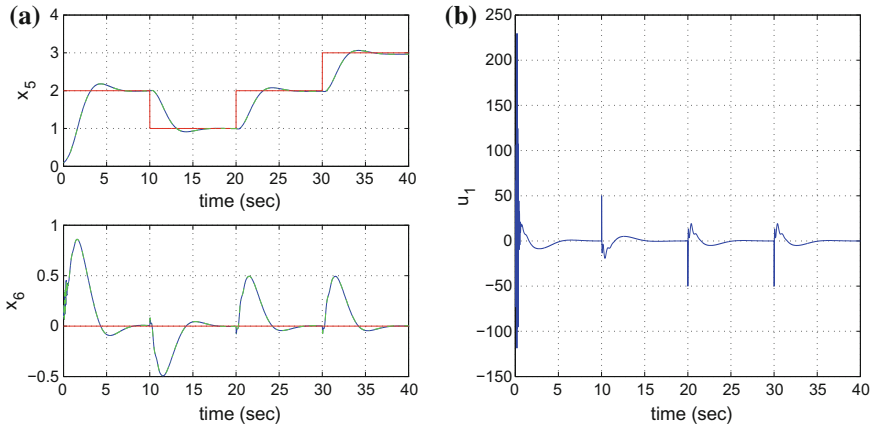

Fig. 2.43 Tracking of reference setpoint 6: **a** State variables $x_5 = x$ and $x_6 = \dot{x}$ of the cart and double-pendulum system (blue lines: real values, green lines: estimated values, red lines: setpoints), **b** Control input u of the cart and double-pendulum system (blue line)

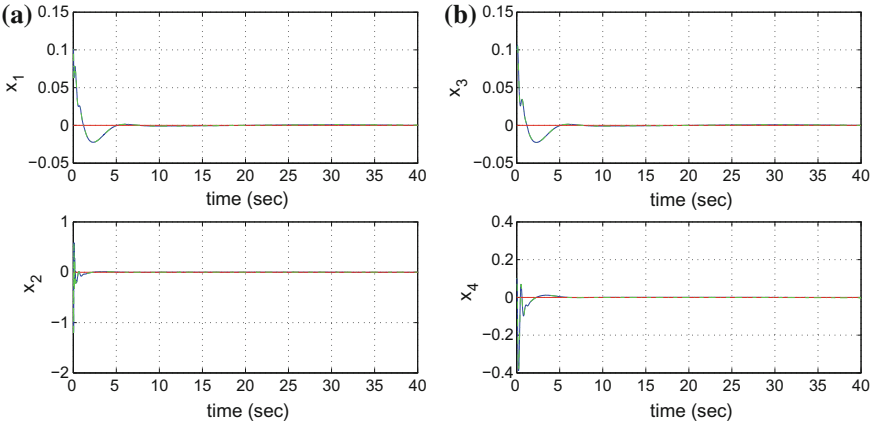

Fig. 2.44 Tracking of reference setpoint 7: **a** State variables $x_1 = \theta_1$ and $x_2 = \dot{\theta}_1$ of the cart and double-pendulum system (blue lines: real values, green lines: estimated values, red lines: setpoints), **b** State variables $x_3 = \theta_2$ and $x_4 = \dot{\theta}_2$ of the cart and double-pendulum system (blue lines: real values, green lines: estimated values, red lines: setpoints)

To achieve the design of the stabilizing feedback controller, the equivalent model of the underactuated manipulator was subject first to approximate linearization. The linearization is performed around a time-varying operating point (equilibrium) which is re-computed at each iteration of the control algorithm. This equilibrium is defined by the present value of the robotic system's state vector and of the last value of the control inputs vector that was exerted on it. The approximate linearization is based on first-order Taylor series expansion of the robotic model and on computation of the

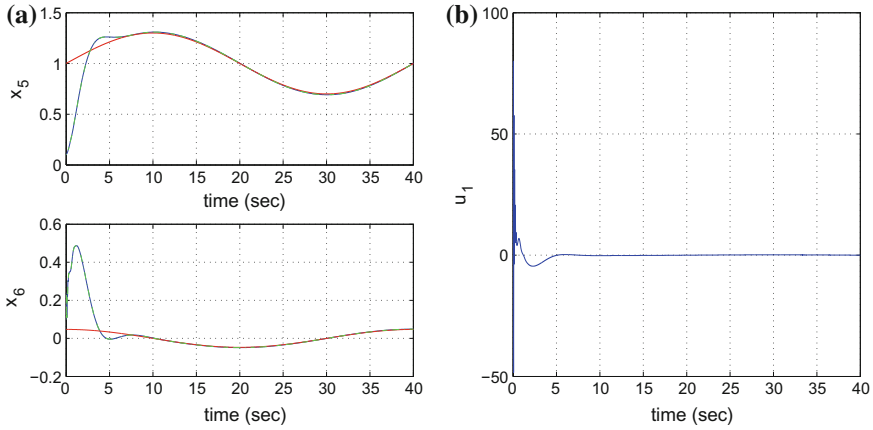

Fig. 2.45 Tracking of reference setpoint 7: **a** State variables $x_5 = x$ and $x_6 = \dot{x}$ of the cart and double-pendulum system (blue lines: real values, green lines: estimated values, red lines: setpoints), **b** Control input u of the cart and double-pendulum system (blue line)

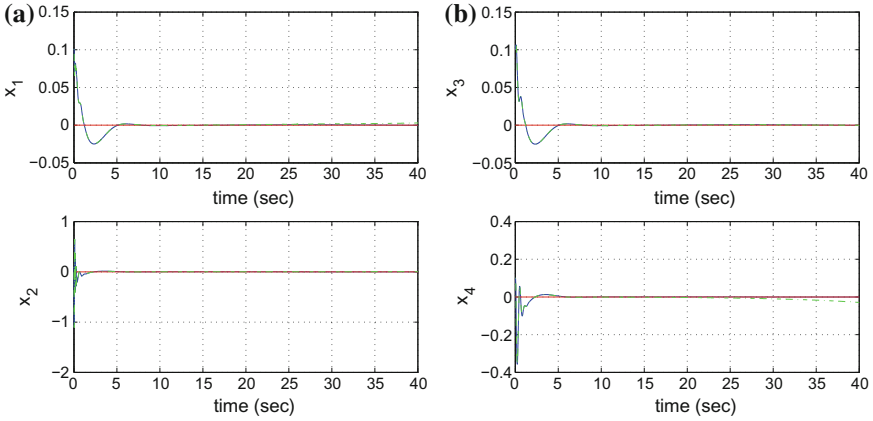

Fig. 2.46 Tracking of reference setpoint 8: **a** State variables $x_1 = \theta_1$ and $x_2 = \dot{\theta}_1$ of the cart and double-pendulum system (blue lines: real values, green lines: estimated values, red lines: setpoints), **b** State variables $x_3 = \theta_2$ and $x_4 = \dot{\theta}_2$ of the cart and double-pendulum system (blue lines: real values, green lines: estimated values, red lines: setpoints)

associated Jacobian matrices [33, 431, 461, 463]. The modelling error which is due to the truncation of higher-order terms in the Taylor series expansion is considered to be a perturbation which is compensated by the robustness of the control algorithm.

For the approximately linearized model of the underactuated manipulator an optimal (H-infinity) feedback controller is designed. This controller represents a solution to a min-max differential game, taking place between the controller (which tries to minimize a cost function incorporating a a quadratic term of the state vector's error) and the model uncertainty and disturbance terms (which try to maximize this cost

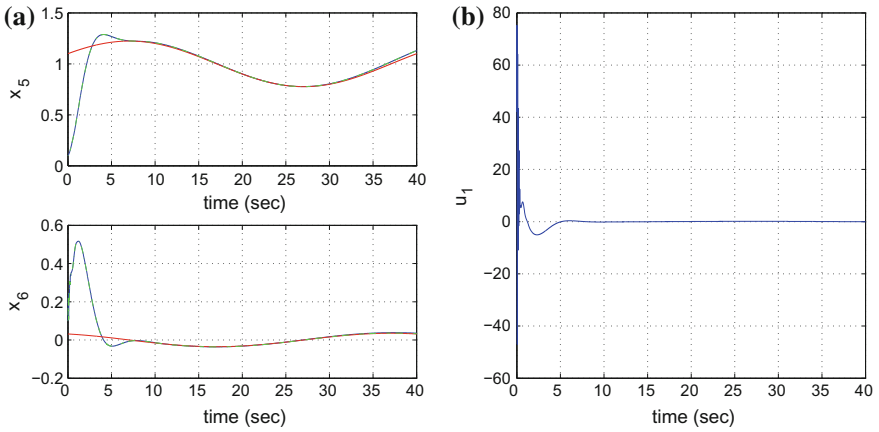

Fig. 2.47 Tracking of reference setpoint 8: **a** State variables $x_5 = x$ and $x_6 = \dot{x}$ of the cart and double-pendulum system (blue lines: real values, green lines: estimated values, red lines: setpoints), **b** Control input u of the cart and double-pendulum system (blue line)

function). The computation of the feedback control gain requires the repetitive solution of an algebraic Riccati equation which also takes place at each step of the control method [132, 305, 564].

The stability of the nonlinear optimal control method is proven through Lyapunov analysis. First, it is demonstrated that the control method satisfies the H-infinity tracking performance criterion. This signifies elevated robustness against model uncertainty and external perturbations. Moreover, under moderate conditions it is proven that the control scheme has global asymptotic stability features. Finally, to implement state estimation -based control for the underactuated robotic manipulator without the need to measure its entire state vector, the H-infinity Kalman Filter is used as a robust state estimator [169, 511].

2.6.2 *Dynamic Model of the Underactuated Manipulator*

The considered 3-DOF robotic manipulator comprises 2 active joints rotated by DC motors and 1 passive joint that receives no actuation. After some preliminary transformations, the dynamic model of the 3-DOF underactuated manipulator (Fig. 2.48) is written in cartesian coordinates as follows [19, 117]:

$$\begin{aligned} \ddot{x}_p &= u_1 cos(\theta) \\ \ddot{y_p} &= u_1 sin(\theta) \\ \ddot{\theta} &= \tfrac{1}{\lambda} u_2 \end{aligned} \tag{2.198}$$

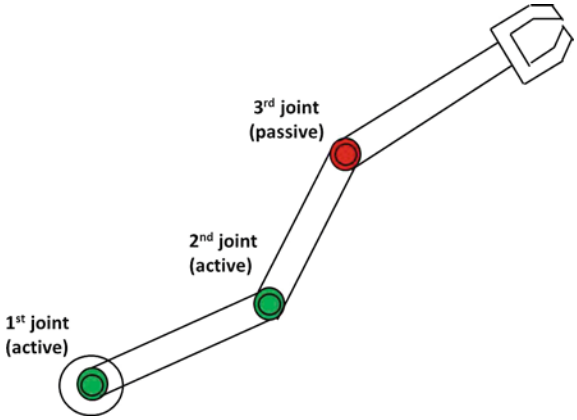

Fig. 2.48 Diagram of the 3-DOF underactuated manipulator, comprising 2 active and 1 passive joint

where $\lambda = (ml^2 + I)/ml$ with I to stand for the moment of inertia of the third link (for rotation round its center of symmetry), m to be the mass of this link, and l to be the distance of the center of gravity of the third link from its basis. Moreover x_p, y_p are the cartesian coordinates of the center of gravity third link, θ is the orientation angle of the third link with respect to a reference frame mounted on its basis and u_1, u_2 are transformed control inputs to be defined next.

Next, the stages of computation of the dynamic model describing the translational and rotational motion performed by the third link of the robot are analyzed. The cartesian coordinates (x_p, y_p) of the center of gravity of the third link are connected to the cartesian coordinates of the joint at the basis of the link (x, y), through the following relation:

$$\begin{aligned} x_p &= x + lcos(\theta) \\ y_p &= y + lsin(\theta) \end{aligned} \tag{2.199}$$

The forces affecting the translational motion of the third link are F_x and F_y, expressed in the reference frame of the joint of this robot, as shown in Fig. 2.49. It holds that

$$\begin{aligned} F_x &= m\ddot{x}_p \\ F_y &= m\ddot{y}_p \end{aligned} \tag{2.200}$$

About the acceleration of the center of gravity of the third link it holds

$$\begin{aligned} \dot{x}_p &= \dot{x} - lsin(\theta)\dot{\theta} \Rightarrow \\ \ddot{x}_p &= \ddot{x} - lcos(\theta)\dot{\theta}^2 - lsin(\theta)\ddot{\theta} \end{aligned} \tag{2.201}$$

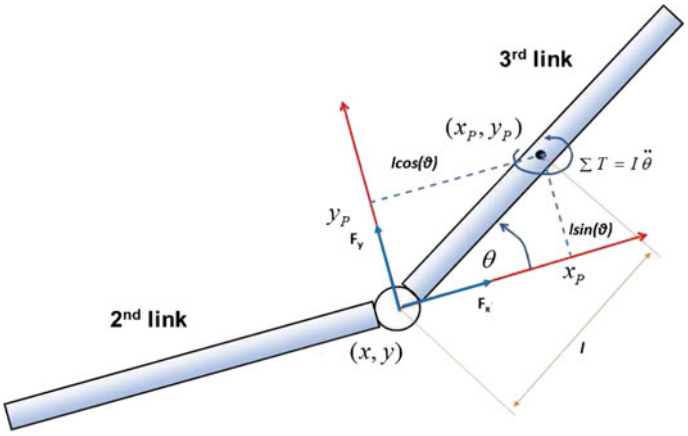

Fig. 2.49 Positioning reference frame for the 3rd rink of the underactuated manipulator

$$\begin{aligned} \dot{y}_p &= \dot{y} + lcos(\theta)\dot{\theta} \Rightarrow \\ \ddot{y}_p &= \ddot{y} - lsin(\theta)\ddot{\theta} + lcos(\theta)\ddot{\theta} \end{aligned} \tag{2.202}$$

Consequently, the equations of the translational motion of the third link become [19, 117]

$$\begin{aligned} F_x &= m(\ddot{x} - lcos(\theta)\dot{\theta}^2 - lsin(\theta)\ddot{\theta} \Rightarrow \\ F_x &= m\ddot{x} - mlcos(\theta)\dot{\theta}^2 - mlsin(\theta)\ddot{\theta} \end{aligned} \tag{2.203}$$

$$\begin{aligned} F_y &= m(\ddot{y} - lsin(\theta)\dot{\theta}^2 + lcos(\theta)\ddot{\theta}) \Rightarrow \\ F_y &= m\ddot{y} - mlcos(\theta)\dot{\theta}^2 + mlcos(\theta)\ddot{(\theta)} \end{aligned} \tag{2.204}$$

The third link performs also a rotational motion which is due to torques generated by forces F_x and F_y. Since there is no actuator at the passive joint and consequently the associated mechanical torque is $T_\theta = 0$, it holds that

$$F_x(-lsin(\theta)) + F_y(lcos(\theta)) + T_\theta = I\ddot{\theta} \tag{2.205}$$

By substituting Eqs. (2.203) and (2.204) in (2.205) one obtains

$$\begin{aligned} &(m\ddot{x} - mlcos(\theta)\dot{\theta}^2 - mlsin(\theta)\ddot{\theta})(-lsin(\theta)) + \\ &+ (m\ddot{y} - mlcos(\theta)\dot{\theta}^2 + mlcos(\theta)\ddot{(\theta)})(lcos(\theta)) = -I\ddot{\theta} \end{aligned} \tag{2.206}$$

and after intermediate operations one arrives at

$$-ml\ddot{x}sin(\theta) + ml\ddot{y}cos(\theta) + (ml^2 + I)\ddot{\theta} = 0 \tag{2.207}$$

Moreover, after setting $\lambda = \frac{ml^2+I}{ml}$ one arrives at the following equation about the rotational equation of the third link [19, 117]

$$m\ddot{x} = F_x + mlcos(\theta)\dot{\theta}^2 + mlsin(\theta)\ddot{\theta} \tag{2.208}$$

$$m\ddot{y} = F_y + mlsin(\theta)\dot{\theta}^2 - mlcos(\theta)\ddot{\theta} \tag{2.209}$$

$$\lambda\ddot{\theta} = \ddot{x}sin(\theta) - \ddot{y}cos(\theta) \tag{2.210}$$

Equivalently, the equations of motion of the third link can be written as

$$\ddot{x} = \ddot{x}_p + lcos(\theta)\dot{\theta}^2 + lsin(\theta)\ddot{\theta} \tag{2.211}$$

$$\ddot{y} = \ddot{y}_p + lsin(\theta)\dot{\theta}^2 - lcos(\theta)\ddot{\theta} \tag{2.212}$$

$$\ddot{\theta} = \tfrac{1}{\lambda}\ddot{x}sin(\theta) - \tfrac{1}{\lambda}\ddot{y}cos(\theta) \tag{2.213}$$

By substituting Eqs. (2.211) and (2.212) into (2.213) one gets

$$\begin{aligned}\ddot{\theta} = \tfrac{1}{\lambda}[\ddot{x}_p + lcos(\theta)\dot{\theta}^2 + lsin(\theta)\ddot{(\theta)}]sin(\theta) - \\ - \tfrac{1}{\lambda}[\ddot{y}_p + mlsin(\theta)\dot{\theta}^2 - mlcos(\theta)\ddot{(\theta)}]cos(\theta)\end{aligned} \tag{2.214}$$

Considering a case in which $l = \lambda$ (that is all mass of the third link is taken to be concentrated at its center of gravity), Eq. (2.214) of the rotational motion of the third link of the underactuated 3-DOF robotic manipulator becomes

$$0 = \ddot{x}_p sin(\theta) - \ddot{y}_p cos(\theta) \tag{2.215}$$

Moreover, about the angular acceleration of the center of gravity of the third link of the underactuated manipulator, this is expressed in a reference frame with its horizontal axis being aligned with the link and is decomposed into two orthogonal components a_x and a_y. Thus it holds

$$\begin{aligned}\ddot{x}_p = acos(\theta) = a_x \\ \ddot{y}_p = asin(\theta) = a_y\end{aligned} \tag{2.216}$$

The acceleration of the joint of the third link $(\ddot{x}, \ddot{y})$, expressed in the reference frame of the joint of this link, is related to $(\ddot{x}_p, \ddot{y}_p)$ through a rotation's transformation. This gives

$$\begin{aligned}\ddot{x} = a_x cos(\theta) + a_y sin(\theta) \\ \ddot{y} = a_x sin(\theta) - a_y cos(\theta)\end{aligned} \tag{2.217}$$

By substituting Eqs. (2.211) and (2.212) into (2.213) one gets

$$\begin{aligned}\ddot{\theta} = \tfrac{1}{\lambda}[a_x cos(\theta) + a_y sin(\theta)]sin(\theta) - \\ - \tfrac{1}{\lambda}[a_x sin(\theta) - a_y cos(\theta)]cos(\theta)\end{aligned} \tag{2.218}$$

which after intermediate operations gives

$$\ddot{\theta} = \tfrac{1}{\lambda} a_y \tag{2.219}$$

By substituting the first row of Eqs. (2.217) and (2.215) into (2.211) one gets

$$a_x cos(\theta) + a_y sin(\theta) = \ddot{x}_p + lcos(\theta)\dot{\theta}^2 + lsin(\theta)\tfrac{1}{\lambda} a_y \tag{2.220}$$

which after intermediate operations gives

$$\ddot{x}_p = (a_x - l\dot{\theta}^2)cos(\theta) \tag{2.221}$$

By substituting the second row of Eqs. (2.217) and (2.215) into (2.212) one gets

$$a_x sin(\theta) - a_y cos(\theta) = \ddot{y}_p + lsin(\theta)\dot{\theta}^2 - lcos(\theta)\tfrac{1}{\lambda} a_y \tag{2.222}$$

which after intermediate operations gives

$$\ddot{y}_p = (a_x - l\dot{\theta}^2)sin(\theta) \tag{2.223}$$

Consequently, the equations of motion of the third link of the 3-DOF underactuated robotic manipulator are written as

$$\begin{aligned}\ddot{x}_p &= (a_x - l\dot{\theta}^2)cos(\theta) \\ \ddot{y}_p &= (a_x - l\dot{\theta}^2)sin(\theta) \\ \ddot{\theta} &= \tfrac{1}{\lambda} a_y\end{aligned} \tag{2.224}$$

The new control inputs of the robotic system are defined

$$\begin{aligned}u_1 &= a_x - l\dot{\theta}^2 \\ u_2 &= a_y\end{aligned} \tag{2.225}$$

After substituting Eq. (2.225) into (2.226) one obtains the following form of the dynamics of the third-link in the 3-DOF underactuated robotic manipularor

$$\begin{aligned}\ddot{x}_p &= u_1 cos(\theta) \\ \ddot{y}_p &= u_1 sin(\theta) \\ \ddot{\theta} &= \tfrac{1}{\lambda} u_2\end{aligned} \tag{2.226}$$

The problem of control of the motion of the third-link of the robot will be solved using the dynamic model of Eq. (2.226), which is also the previously defined model of Eq. (2.198).

2.6.3 Approximate Linearization of the Underactuated Robot

Next, the dynamic model of the robot's unactuated link, given in Eq. (2.226) is considered. By defining the state vector $x = [x_1, x_2, x_3, x_4, x_5, x_6]^T = [x_p, y_p, \theta, \dot{x}_p, \dot{y}_p, \dot{\theta}^T]$, the dynamic model of the underactuated 3-DOF robotic manipulator is

$$\begin{pmatrix} \dot{x}_1 \\ \dot{x}_2 \\ \dot{x}_3 \\ \dot{x}_4 \\ \dot{x}_5 \\ \dot{x}_6 \end{pmatrix} = \begin{pmatrix} x_4 \\ x_5 \\ x_6 \\ 0 \\ 0 \\ 0 \end{pmatrix} + \begin{pmatrix} 0 & 0 \\ 0 & 0 \\ 0 & 0 \\ cos(x_3) & 0 \\ sin(x_3) & 0 \\ 0 & \frac{1}{\lambda} \end{pmatrix} \begin{pmatrix} u_1 \\ u_2 \end{pmatrix} \tag{2.227}$$

where (x_1, x_2) are the cartesian coordinates of the center of gravity of the third-link of the manipulator, x_3 is the turn angle of the third link with respect to the reference frame of the joint found at its basis, and u_1, u_2 are the previously defined transformed control inputs which are applied on this link.

Linearization of the robot's dynamic model will be performed round a local equilibrium (x^*, u^*). To this end, the dynamics model of Eq. (2.227) is written in the form:

$$\dot{x} = f(x) + g(x)u \tag{2.228}$$

where the state vector $x \in R^6$ was defined before and

$$f(x) = \begin{pmatrix} x_4 \\ x_5 \\ x_6 \\ 0 \\ 0 \\ 0 \end{pmatrix} \quad g(x) = \begin{pmatrix} 0 & 0 \\ 0 & 0 \\ 0 & 0 \\ cos(x_3) & 0 \\ sin(x_3) & 0 \\ 0 & \frac{1}{\lambda} \end{pmatrix} \tag{2.229}$$

The linearization of the underactuated robot's model round the temporary equilibrium gives

$$\dot{x} = Ax + Bu \tag{2.230}$$

where

$$A = \nabla_x [f(x) + g(x)u] \mid_{(x^*, u^*)} \tag{2.231}$$

$$B = \nabla_u [f(x) + g(x)u] \mid_{(x^*, u^*)} \Rightarrow B = g(x) \mid_{(x^*, u^*)} \tag{2.232}$$

By denoting the columns of matrix $g(x) = [g_1(x), g_2(x)]$, for the Jacobian matrix $A = \nabla_x [f(x) + g(x)u] \mid_{(x^*,u^*)}$, it holds that

$$A = \nabla_x f(x) + \nabla_x g_1(x)u] \mid_{(x^*,u^*)} \tag{2.233}$$

where the Jacobian matrix $\nabla_x f(x)$ is given by

$$\nabla_x f(x) = \begin{pmatrix} \frac{\partial f_1}{\partial x_1} & \frac{\partial f_1}{\partial x_2} & \frac{\partial f_1}{\partial x_3} & \cdots & \frac{\partial f_1}{\partial x_6} \\ \frac{\partial f_2}{\partial x_1} & \frac{\partial f_2}{\partial x_2} & \frac{\partial f_2}{\partial x_3} & \cdots & \frac{\partial f_2}{\partial x_6} \\ \cdots & \cdots & \cdots & \cdots & \\ \frac{\partial f_6}{\partial x_1} & \frac{\partial f_6}{\partial x_2} & \frac{\partial f_6}{\partial x_3} & \cdots & \frac{\partial f_6}{\partial x_6} \end{pmatrix} \tag{2.234}$$

For the first row of the aforementioned Jacobian matrix one has:

$$\frac{\partial f_1}{\partial x_1} = 0,\ \frac{\partial f_1}{\partial x_2} = 0,\ \frac{\partial f_1}{\partial x_3} = 0,\ \frac{\partial f_1}{\partial x_4} = 1,\ \frac{\partial f_1}{\partial x_5} = 0,\ \frac{\partial f_1}{\partial x_6} = 0.$$

For the second row of the aforementioned Jacobian matrix one has:

$$\frac{\partial f_2}{\partial x_1} = 0,\ \frac{\partial f_2}{\partial x_2} = 0,\ \frac{\partial f_2}{\partial x_3} = 0,\ \frac{\partial f_2}{\partial x_4} = 0,\ \frac{\partial f_2}{\partial x_5} = 1,\ \frac{\partial f_2}{\partial x_6} = 0.$$

For the third row of the aforementioned Jacobian matrix one has:

$$\frac{\partial f_3}{\partial x_1} = 0,\ \frac{\partial f_3}{\partial x_2} = 0,\ \frac{\partial f_3}{\partial x_3} = 0,\ \frac{\partial f_3}{\partial x_4} = 0,\ \frac{\partial f_3}{\partial x_5} = 0,\ \frac{\partial f_3}{\partial x_6} = 1.$$

For the fourth row of the aforementioned Jacobian matrix one has:

$$\frac{\partial f_4}{\partial x_1} = 0,\ \frac{\partial f_4}{\partial x_2} = 0,\ \frac{\partial f_4}{\partial x_3} = 0,\ \frac{\partial f_4}{\partial x_4} = 0,\ \frac{\partial f_4}{\partial x_5} = 0,\ \frac{\partial f_4}{\partial x_6} 0.$$

For the fifth row of the aforementioned Jacobian matrix one has:

$$\frac{\partial f_5}{\partial x_1} = 0,\ \frac{\partial f_5}{\partial x_2} = 0,\ \frac{\partial f_5}{\partial x_3} = 0,\ \frac{\partial f_5}{\partial x_4} = 0,\ \frac{\partial f_5}{\partial x_5} = 0,\ \frac{\partial f_5}{\partial x_6} = 0.$$

For the sixth row of the aforementioned Jacobian matrix one has:

$$\frac{\partial f_6}{\partial x_1} = 0,\ \frac{\partial f_6}{\partial x_2} = 0,\ \frac{\partial f_6}{\partial x_3} = 0,\ \frac{\partial f_6}{\partial x_4} = 0,\ \frac{\partial f_6}{\partial x_5} = 0,\ \frac{\partial f_6}{\partial x_6} = 0.$$

Similarly, the Jacobian matrix $\nabla_x g_1(x)$ is given by

$$\nabla_x g_1(x) = \begin{pmatrix} \frac{\partial g_{11}}{\partial x_1} & \frac{\partial g_{11}}{\partial x_2} & \frac{\partial g_{11}}{\partial x_3} & \cdots & \frac{\partial g_{11}}{\partial x_6} \\ \frac{\partial g_{21}}{\partial x_1} & \frac{\partial g_{21}}{\partial x_2} & \frac{\partial g_{21}}{\partial x_3} & \cdots & \frac{\partial g_{21}}{\partial x_6} \\ \cdots & \cdots & \cdots & \cdots & \\ \frac{\partial g_{61}}{\partial x_1} & \frac{\partial g_{61}}{\partial x_2} & \frac{\partial g_{61}}{\partial x_3} & \cdots & \frac{\partial g_{61}}{\partial x_6} \end{pmatrix} \tag{2.235}$$

For the first row of the aforementioned Jacobian matrix one has:

$$\frac{\partial g_{11}}{\partial x_1} = 0, \frac{\partial g_{11}}{\partial x_2} = 0, \frac{\partial g_{11}}{\partial x_3} = 0, \frac{\partial g_{11}}{\partial x_4} = 0, \frac{\partial g_{11}}{\partial x_5} = 0, \frac{\partial g_{11}}{\partial x_6} = 0.$$

For the second row of the aforementioned Jacobian matrix one has:

$$\frac{\partial g_{21}}{\partial x_1} = 0, \frac{\partial g_{21}}{\partial x_2} = 0, \frac{\partial g_{21}}{\partial x_3} = 0, \frac{\partial g_{21}}{\partial x_4} = 0, \frac{\partial g_{21}}{\partial x_5} = 0, \frac{\partial g_{21}}{\partial x_6} = 0.$$

For the third row of the aforementioned Jacobian matrix one has:

$$\frac{\partial g_{31}}{\partial x_1} = 0, \frac{\partial g_{31}}{\partial x_2} = 0, \frac{\partial g_{31}}{\partial x_3} = 0, \frac{\partial g_{31}}{\partial x_4} = 0, \frac{\partial g_{31}}{\partial x_5} = 0, \frac{\partial g_{31}}{\partial x_6} = 0.$$

For the fourth row of the aforementioned Jacobian matrix one has:

$$\frac{\partial g_{41}}{\partial x_1} = 0, \frac{\partial g_{41}}{\partial x_2} = 0, \frac{\partial g_{41}}{\partial x_3} = -sin(x_3), \frac{\partial g_{41}}{\partial x_4} = 0, \frac{\partial g_{41}}{\partial x_5} = 0, \frac{\partial g_{41}}{\partial x_6} 0.$$

For the fifth row of the aforementioned Jacobian matrix one has:

$$\frac{\partial g_{51}}{\partial x_1} = 0, \frac{\partial g_{51}}{\partial x_2} = 0, \frac{\partial g_{51}}{\partial x_3} = cos(x_3), \frac{\partial g_{51}}{\partial x_4} = 0, \frac{\partial g_{51}}{\partial x_5} = 0, \frac{\partial g_{51}}{\partial x_6} = 0.$$

For the sixth row of the aforementioned Jacobian matrix one has:

$$\frac{\partial g_{61}}{\partial x_1} = 0, \frac{\partial g_{61}}{\partial x_2} = 0, \frac{\partial g_{61}}{\partial x_3} = 0, \frac{\partial g_{61}}{\partial x_4} = 0, \frac{\partial g_{61}}{\partial x_5} = 0, \frac{\partial g_{61}}{\partial x_6} = 0.$$

2.6.4 Design of an H-Infinity Nonlinear Feedback Controller

2.6.4.1 Equivalent Linearized Dynamics of the Robot

After linearization round its current operating point, the dynamic model for the third link of the underactuated robotic manipulator is written as

$$\dot{x} = Ax + Bu + d_1 \tag{2.236}$$

Parameter d_1 stands for the linearization error in the link's dynamic model appearing in Eq. (2.236). The reference setpoints for the state vector of the aforementioned dynamic model are denoted by $\mathbf{x_d} = [x_1^d, \ldots, x_4^d]$. Tracking of this trajectory is achieved after applying the control input u^*. At every time instant the control input u^* is assumed to differ from the control input u appearing in Eq. (2.236) by an amount equal to Δu, that is $u^* = u + \Delta u$

$$\dot{x}_d = Ax_d + Bu^* + d_2 \tag{2.237}$$

The dynamics of the controlled system described in Eq. (2.236) can be also written as

$$\dot{x} = Ax + Bu + Bu^* - Bu^* + d_1 \tag{2.238}$$

and by denoting $d_3 = -Bu^* + d_1$ as an aggregate disturbance term one obtains

$$\dot{x} = Ax + Bu + Bu^* + d_3 \tag{2.239}$$

By subtracting Eq. (2.237) from (2.239) one has

$$\dot{x} - \dot{x}_d = A(x - x_d) + Bu + d_3 - d_2 \tag{2.240}$$

By denoting the tracking error as $e = x - x_d$ and the aggregate disturbance term as $\tilde{d} = d_3 - d_2$, the tracking error dynamics becomes

$$\dot{e} = Ae + Bu + \tilde{d} \tag{2.241}$$

The above linearized form of the robot's model can be efficiently controlled after applying an H-infinity feedback control scheme.

2.6.4.2 The Nonlinear H-Infinity Control

The initial nonlinear model of the third link of the underactuated robot is in the form

$$\dot{x} = f(x, u) \;\; x \in R^n, \;\; u \in R^m \tag{2.242}$$

Linearization of the system (unactuated link of the 3-DOF robot) is performed at each iteration of the control algorithm round its present operating point $(x^*, u^*) = (x(t), u(t - T_s))$. The linearized equivalent of the system is described by

$$\dot{x} = Ax + Bu + L\tilde{d} \;\; x \in R^n, \;\; u \in R^m, \;\; \tilde{d} \in R^q \tag{2.243}$$

where matrices A and B are obtained from the computation of the Jacobians of the 3-DOF underactuated manipulator, and vector $\tilde{d}$ denotes disturbance terms due to linearization errors. The problem of disturbance rejection for the linearized model that is described by

$$\begin{aligned} \dot{x} &= Ax + Bu + L\tilde{d} \\ y &= Cx \end{aligned} \tag{2.244}$$

where $x \in R^n$, $u \in R^m$, $\tilde{d} \in R^q$ and $y \in R^p$, cannot be handled efficiently if the classical LQR control scheme is applied. This is because of the existence of the perturbation term $\tilde{d}$. The disturbance term $\tilde{d}$ apart from modeling (parametric) uncertainty and external perturbation terms can also represent noise terms of any distribution.

In the H_∞ control approach, a feedback control scheme is designed for trajectory tracking by the system's state vector and simultaneous disturbance rejection, considering that the disturbance affects the system in the worst possible manner. The disturbances' effects are incorporated in the following quadratic cost function:

$$\begin{array}{c} J(t) = \frac{1}{2}\int_0^T [y^T(t)y(t) + \\ + ru^T(t)u(t) - \rho^2 \tilde{d}^T(t)\tilde{d}(t)]dt, \quad r, \rho > 0 \end{array} \tag{2.245}$$

The significance of the negative sign in the cost function's term that is associated with the perturbation variable $\tilde{d}(t)$ is that the disturbance tries to maximize the cost function $J(t)$ while the control signal $u(t)$ tries to minimize it. The physical meaning of the relation given above is that the control signal and the disturbances compete to each other within a min-max differential game. This problem of min-max optimization can be written as

$$min_u max_{\tilde{d}} J(u, \tilde{d}) \tag{2.246}$$

As previously noted, the objective of the optimization procedure is to compute a control signal $u(t)$ which can compensate for the worst possible disturbance, that is externally imposed to the system. However, the solution to the min-max optimization problem is directly related to the value of the parameter ρ. This means that there is an upper bound in the disturbances magnitude that can be annihilated by the control signal.

2.6.4.3 Computation of the Feedback Control Gains

For the linearized system given by Eq. (2.244) the cost function of Eq. (2.245) is defined, where the coefficient r determines the penalization of the control input and the weight coefficient ρ determines the reward of the disturbances' effects.

It is assumed that (i) The energy that is transferred from the disturbances signal $\tilde{d}(t)$ is bounded, that is $\int_0^\infty \tilde{d}^T(t)\tilde{d}(t)dt < \infty$, (ii) the matrices $[A, B]$ and $[A, L]$ are stabilizable, (iii) the matrix $[A, C]$ is detectable. Then, the optimal feedback control law is given by

$$u(t) = -Kx(t) \tag{2.247}$$

with

$$K = \frac{1}{r}B^T P \tag{2.248}$$

where P is a positive semi-definite symmetric matrix which is obtained from the solution of the Riccati equation

$$A^T P + PA + Q - P\left(\frac{1}{r}BB^T - \frac{1}{2\rho^2}LL^T\right)P = 0 \tag{2.249}$$

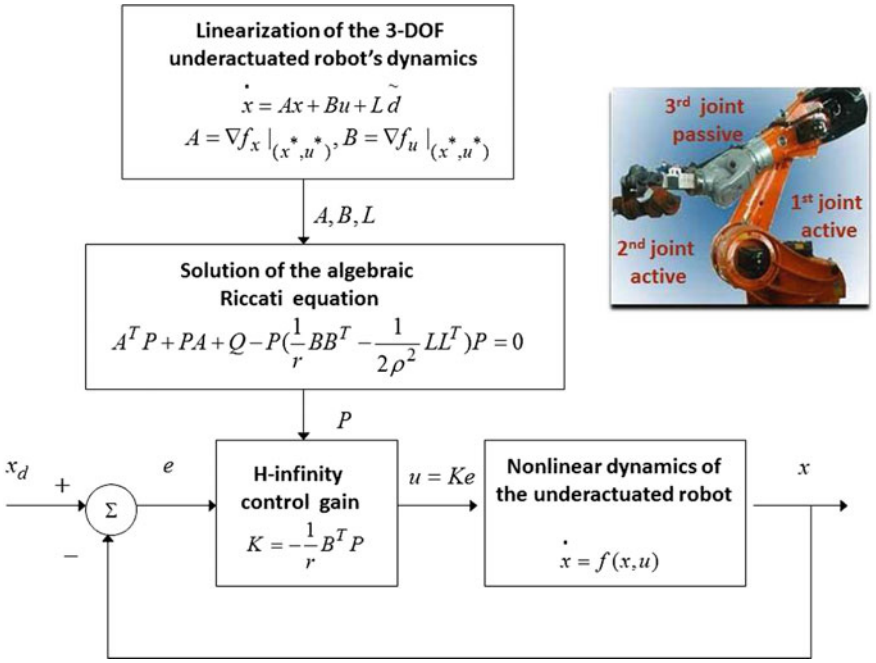

Fig. 2.50 Diagram of the control scheme for the underactuated 3-DOF robotic manipulator

where Q is also a positive definite symmetric matrix. The worst case disturbance is given by

$$\tilde{d}(t) = \frac{1}{\rho^2} L^T P x(t) \tag{2.250}$$

The diagram of the considered control loop is depicted in Fig. 2.50.

2.6.4.4 Riccati Equation Coefficients in H-Infinity Control Robustness

The parameter ρ in Eq. (2.245), is an indication of the closed-loop system robustness. If the values of $\rho > 0$ are excessively decreased with respect to r, then the solution of the Riccati equation is no longer a positive definite matrix. Consequently there is a lower bound ρ_{min} of ρ for which the H_∞ control problem has a solution. The acceptable values of ρ lie in the interval $[\rho_{min}, \infty)$. If ρ_{min} is found and used in the design of the H_∞ controller, then the closed-loop system will have increased robustness. Unlike this, if a value $\rho > \rho_{min}$ is used, then an admissible stabilizing H_∞ controller will be derived but it will be a suboptimal one. The Hamiltonian matrix

$$H = \begin{pmatrix} A & -(\frac{1}{r}BB^T - \frac{1}{\rho^2}LL^T) \\ -Q & -A^T \end{pmatrix} \tag{2.251}$$

provides a criterion for the existence of a solution of the Riccati equation (2.249). A necessary condition for the solution of the algebraic Riccati equation to be a positive semi-definite symmetric matrix is that H has no imaginary eigenvalues [450].

2.6.5 Lyapunov Stability Analysis

Through Lyapunov stability analysis it will be shown that the proposed nonlinear control scheme assures H_∞ tracking performance for the underactuated 3-DOF robotic manipulator, and that in case of bounded disturbance terms asymptotic convergence to the reference setpoints is achieved. The tracking error dynamics for the unactuated link of the 3-DOF robot is written in the form

$$\dot{e} = Ae + Bu + L\tilde{d} \tag{2.252}$$

where in the robot's case $L = I \in R^6$ with I being the identity matrix. Variable $\tilde{d}$ denotes model uncertainties and external disturbances of the robot's model. The following Lyapunov function is considered

$$V = \tfrac{1}{2} e^T P e \tag{2.253}$$

where $e = x - x_d$ is the tracking error. By differentiating with respect to time and by following the previous method one obtains

$$\begin{gathered} \dot{V} = \tfrac{1}{2}\dot{e}^T P e + \tfrac{1}{2} e P \dot{e} \Rightarrow \\ \dot{V} = \tfrac{1}{2}[Ae + Bu + L\tilde{d}]^T P e + \tfrac{1}{2} e^T P [Ae + Bu + L\tilde{d}] \Rightarrow \end{gathered} \tag{2.254}$$

$$\begin{gathered} \dot{V} = \tfrac{1}{2}[e^T A^T + u^T B^T + \tilde{d}^T L^T] P e + \\ + \tfrac{1}{2} e^T P [Ae + Bu + L\tilde{d}] \Rightarrow \end{gathered} \tag{2.255}$$

$$\begin{gathered} \dot{V} = \tfrac{1}{2} e^T A^T P e + \tfrac{1}{2} u^T B^T P e + \tfrac{1}{2}\tilde{d}^T L^T P e + \\ \tfrac{1}{2} e^T P A e + \tfrac{1}{2} e^T P B u + \tfrac{1}{2} e^T P L \tilde{d} \end{gathered} \tag{2.256}$$

The previous equation is rewritten as

$$\begin{gathered} \dot{V} = \tfrac{1}{2} e^T (A^T P + P A) e + \left(\tfrac{1}{2} u^T B^T P e + \tfrac{1}{2} e^T P B u\right) + \\ + \left(\tfrac{1}{2}\tilde{d}^T L^T P e + \tfrac{1}{2} e^T P L \tilde{d}\right) \end{gathered} \tag{2.257}$$

Assumption: For given positive definite matrix Q and coefficients r and ρ there exists a positive definite matrix P, which is the solution of the following matrix equation

$$A^T P + PA = -Q + P\left(\frac{2}{r}BB^T - \frac{1}{\rho^2}LL^T\right)P \tag{2.258}$$

Moreover, the following feedback control law is applied to the system

$$u = -\frac{1}{r}B^T Pe \tag{2.259}$$

By substituting Eqs. (2.258) and (2.259) one obtains

$$\begin{gathered}\dot{V} = \frac{1}{2}e^T[-Q + P(\frac{2}{r}BB^T - \frac{1}{\rho^2}LL^T)P]e + \\ + e^T PB(-\frac{1}{r}B^T Pe) + e^T PL\tilde{d} \Rightarrow\end{gathered} \tag{2.260}$$

$$\begin{gathered}\dot{V} = -\frac{1}{2}e^T Qe + \frac{1}{r}e^T PBB^T Pe - \frac{1}{2\rho^2}e^T PLL^T Pe \\ - \frac{1}{r}e^T PBB^T Pe + e^T PL\tilde{d}\end{gathered} \tag{2.261}$$

which after intermediate operations gives

$$\dot{V} = -\frac{1}{2}e^T Qe - \frac{1}{2\rho^2}e^T PLL^T Pe + e^T PL\tilde{d} \tag{2.262}$$

or, equivalently

$$\begin{gathered}\dot{V} = -\frac{1}{2}e^T Qe - \frac{1}{2\rho^2}e^T PLL^T Pe + \\ + \frac{1}{2}e^T PL\tilde{d} + \frac{1}{2}\tilde{d}^T L^T Pe\end{gathered} \tag{2.263}$$

Lemma: The following inequality holds

$$\frac{1}{2}e^T L\tilde{d} + \frac{1}{2}\tilde{d}L^T Pe - \frac{1}{2\rho^2}e^T PLL^T Pe \leq \frac{1}{2}\rho^2\tilde{d}^T\tilde{d} \tag{2.264}$$

Proof: The binomial $(\rho\alpha - \frac{1}{\rho}b)^2$ is considered. Expanding the left part of the above inequality one gets

$$\begin{gathered}\rho^2a^2 + \frac{1}{\rho^2}b^2 - 2ab \geq 0 \Rightarrow \frac{1}{2}\rho^2a^2 + \frac{1}{2\rho^2}b^2 - ab \geq 0 \Rightarrow \\ ab - \frac{1}{2\rho^2}b^2 \leq \frac{1}{2}\rho^2a^2 \Rightarrow \frac{1}{2}ab + \frac{1}{2}ab - \frac{1}{2\rho^2}b^2 \leq \frac{1}{2}\rho^2a^2\end{gathered} \tag{2.265}$$

The following substitutions are carried out: $a = \tilde{d}$ and $b = e^T PL$ and the previous relation becomes

$$\frac{1}{2}\tilde{d}^T L^T Pe + \frac{1}{2}e^T PL\tilde{d} - \frac{1}{2\rho^2}e^T PLL^T Pe \leq \frac{1}{2}\rho^2\tilde{d}^T\tilde{d} \tag{2.266}$$

Equation (2.266) is substituted in Eq. (2.263) and the inequality is enforced, thus giving

$$\dot{V} \leq -\frac{1}{2}e^T Qe + \frac{1}{2}\rho^2\tilde{d}^T\tilde{d} \tag{2.267}$$

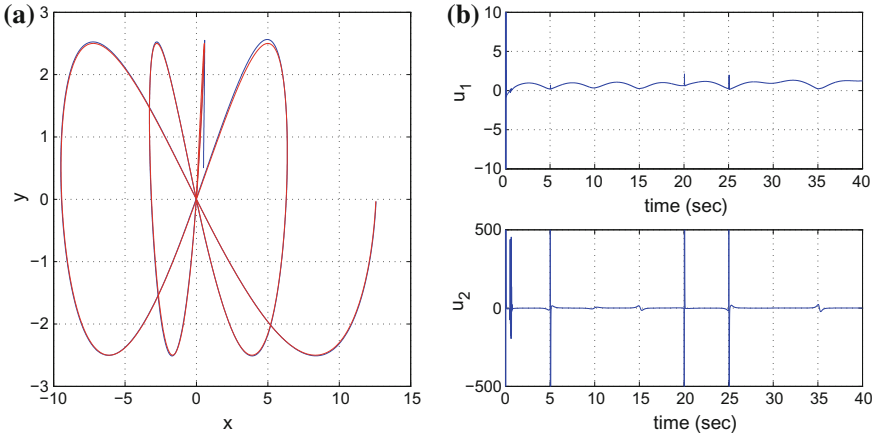

Fig. 2.51 Control of the underactuated 3-DOF robotic manipultor - Case 1 : **a** path followed by the robot's third-link in the xy cartesian coordinates frame (blue line) and reference path (red line), **b** control inputs u_i $i = 1, 2$ applied to the robot

Equation (2.267) shows that the H_∞ tracking performance criterion is satisfied. The integration of $\dot{V}$ from 0 to T gives

$$\begin{aligned} &\int_0^T \dot{V}(t)dt \leq -\tfrac{1}{2}\int_0^T ||e||_Q^2 dt + \tfrac{1}{2}\rho^2 \int_0^T ||\tilde{d}||^2 dt \Rightarrow \\ &2V(T) + \int_0^T ||e||_Q^2 dt \leq 2V(0) + \rho^2 \int_0^T ||\tilde{d}||^2 dt \end{aligned} \tag{2.268}$$

Moreover, if there exists a positive constant $M_d > 0$ such that

$$\int_0^\infty ||\tilde{d}||^2 dt \leq M_d \tag{2.269}$$

then one gets

$$\int_0^\infty ||e||_Q^2 dt \leq 2V(0) + \rho^2 M_d \tag{2.270}$$

Thus, the integral $\int_0^\infty ||e||_Q^2 dt$ is bounded. Moreover, $V(T)$ is bounded and from the definition of the Lyapunov function V in Eq. (2.253) it becomes clear that $e(t)$ will be also bounded since $e(t) \in \Omega_e = \{e | e^T P e \leq 2V(0) + \rho^2 M_d\}$. According to the above and with the use of Barbalat's Lemma one obtains $\lim_{t\to\infty} e(t) = 0$.

The outline of the global stability proof is that at each iteration of the control algorithm the state vector of the underactuated robotic manipulator converges towards the temporary equilibrium and the temporary equilibrium in turn converges towards the reference trajectory. Thus, the control scheme exhibits global asymptotic stability properties and not local stability. Assume the ith iteration of the control algorithm and the ith time interval about which a positive definite symmetric matrix P is obtained

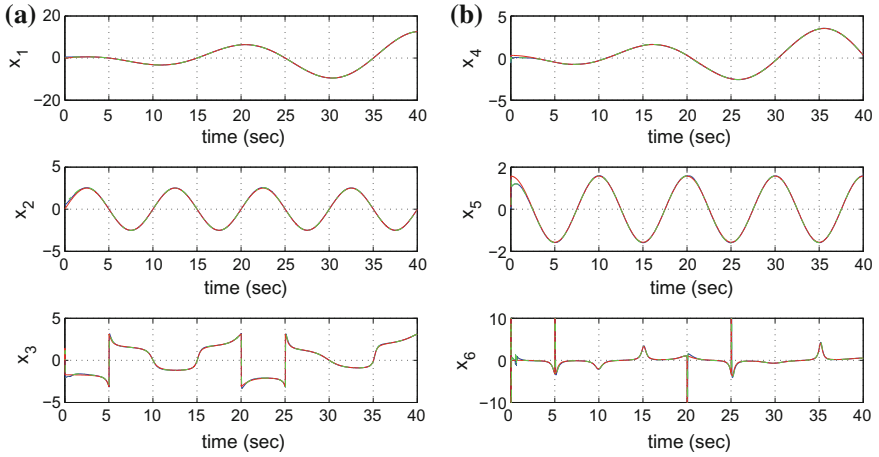

Fig. 2.52 Control of the underactuated 3-DOF robotic manipultor - Case 1 : **a** convergence of state variables x_i, $i = 1, 2, 3$ (blue line) and of their estimated values (green lines) to the reference setpoints (red line), **b** convergence of state variables x_i, $i = 4, 5, 6$ (blue line) and of their estimated values (green lines) to the reference setpoints (red line)

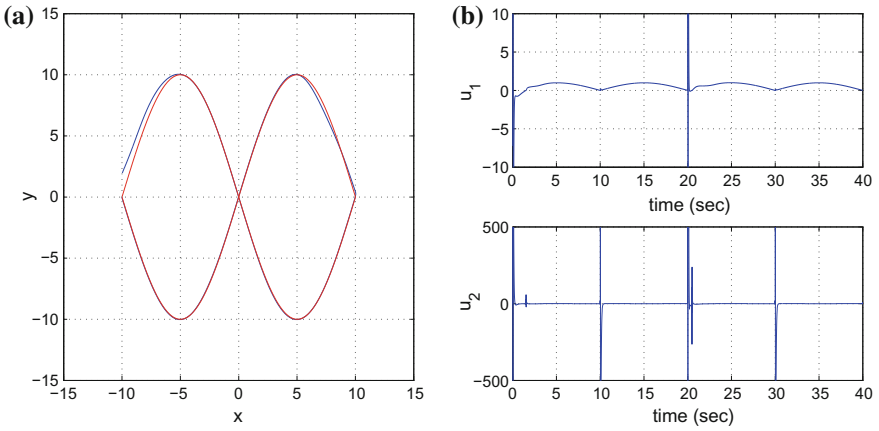

Fig. 2.53 Control of the underactuated 3-DOF robotic manipultor - Case 2 : **a** path followed by the robot's third-link in the xy cartesian coordinates frame (blue line) and reference path (red line), **b** control inputs u_i $i = 1, 2$ applied to the robot

from the solution of the Riccati Equation appearing in Eq. (2.258). By following the stages of the stability proof one arrives at Eq. (2.267) which shows that the H-infinity tracking performance criterion holds. By selecting the attenuation coefficient ρ to be sufficiently small and in particular to satisfy $\rho^2 < ||e||_Q^2 / ||\tilde{d}||^2$ one has that the first derivative of the Lyapunov function is upper bounded by 0. Therefore for the ith time interval it is proven that the Lyapunov function defined in Eq. (2.253) is a

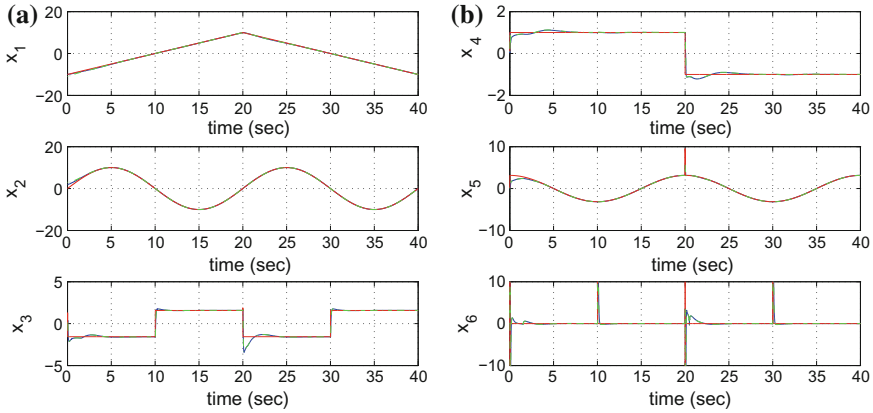

Fig. 2.54 Control of the underactuated 3-DOF robotic manipultor - Case 2 : **a** convergence of state variables x_i, $i = 1, 2, 3$ (blue line) and of their estimated values (green lines) to the reference setpoints (red line), **b** convergence of state variables x_i, $i = 4, 5, 6$ (blue line) and of their estimated values (green lines) to the reference setpoints (red line)

decreasing one. This signifies that between the beginning and the end of the ith time interval there will be a drop of the value of the Lyapunov function and since matrix P is a positive definite one, the only way for this to happen is the Euclidean norm of the state vector error e to be decreasing. This means that comparing to the beginning of each time interval, the distance of the state vector error from 0 at the end of the time interval has diminished. Consequently as the iterations of the control algorithm advance the tracking error will approach zero, and this is a global asymptotic stability condition.

2.6.6 Robust State Estimation with the Use of the H-Infinity Kalman Filter

The control loop has to be implemented with the use of information provided by a small number of sensors and by processing only a small number of state variables. To reconstruct the missing information about the state vector of the unactuated link of the 3-DOF robotic manipulator it is proposed to use a filtering scheme and based on it to apply state estimation-based control [457]. The recursion of the H_∞ Kalman Filter, for the model of the underactuated manipulator, can be formulated in terms of a *measurement update* and a *time update* part.

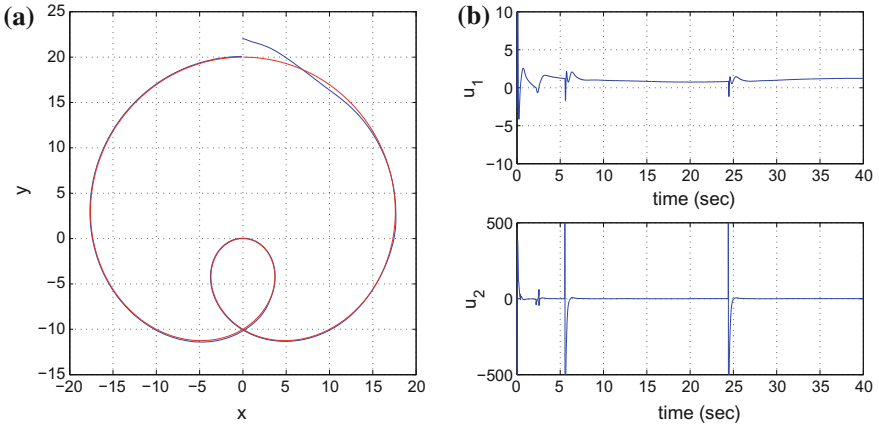

Fig. 2.55 Control of the underactuated 3-DOF robotic manipultor - Case 3 : **a** path followed by the robot's third-link in the xy cartesian coordinates frame (blue line) and reference path (red line), **b** control inputs u_i $i = 1, 2$ applied to the robot

Measurement update:

$$\begin{aligned} D(k) &= [I - \theta W(k)P^{-}(k) + C^{T}(k)R(k)^{-1}C(k)P^{-}(k)]^{-1} \\ K(k) &= P^{-}(k)D(k)C^{T}(k)R(k)^{-1} \\ \hat{x}(k) &= \hat{x}^{-}(k) + K(k)[y(k) - C\hat{x}^{-}(k)] \end{aligned} \tag{2.271}$$

Time update:

$$\begin{aligned} \hat{x}^{-}(k+1) &= A(k)x(k) + B(k)u(k) \\ P^{-}(k+1) &= A(k)P^{-}(k)D(k)A^{T}(k) + Q(k) \end{aligned} \tag{2.272}$$

where it is assumed that parameter θ is sufficiently small to assure that the covariance matrix $P^{-}(k)^{-1} - \theta W(k) + C^{T}(k)R(k)^{-1}C(k)$ will be positive definite. When $\theta = 0$ the H_{∞} Kalman Filter becomes equivalent to the standard Kalman Filter. One can measure only a part of the state vector of the robotic system, and estimate through filtering the rest of the state vector elements. Moreover, the proposed Kalman filtering method can be used for sensor fusion purposes.

2.6.7 Simulation Tests

The efficiency of the previously analyzed control scheme, developed at the unactuated joint of the manipulator, has been tested through simulation experiments. The obtained results are given in Figs. 2.51, 2.52, 2.53, 2.54, 2.55, 2.56, 2.57, 2.58, 2.59 and 2.60. The real value of the state variable of the underactuated robot is denoted

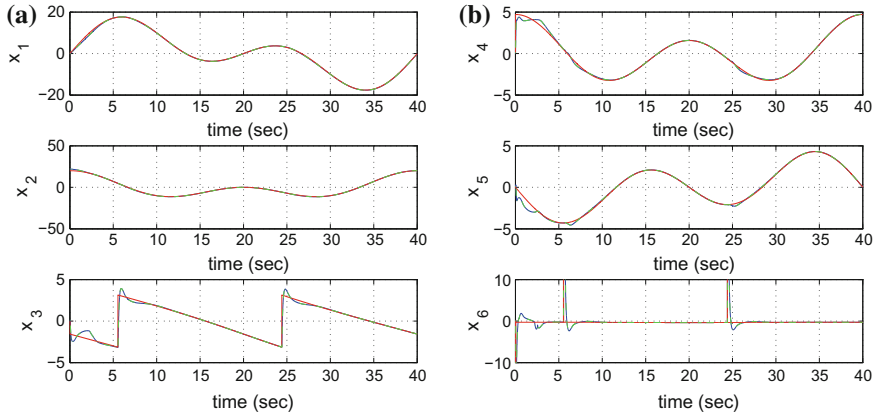

Fig. 2.56 Control of the underactuated 3-DOF robotic manipulator - Case 3 : **a** convergence of state variables x_i, $i = 1, 2, 3$ (blue line) and of their estimated values (green lines) to the reference setpoints (red line), **b** convergence of state variables x_i, $i = 4, 5, 6$ (blue line) and of their estimated values (green lines) to the reference setpoints (red line)

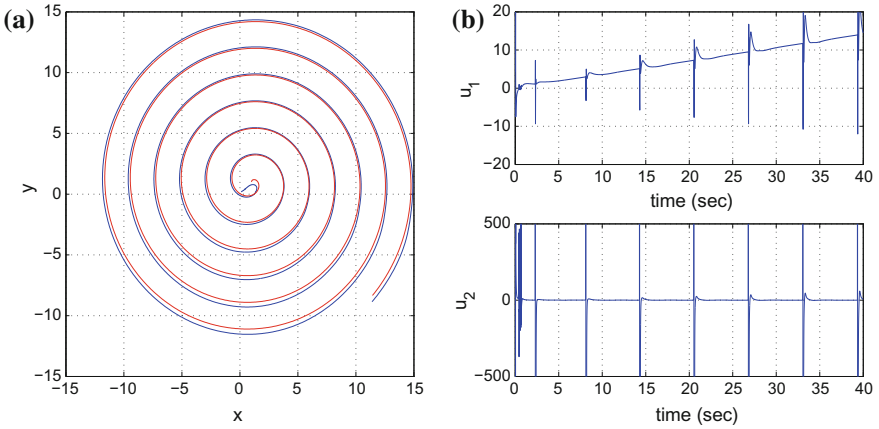

Fig. 2.57 Control of the underactuated 3-DOF robotic manipulator - Case 4 : **a** path followed by the robot's third-link in the xy cartesian coordinates frame (blue line) and reference path (red line), **b** control inputs u_i $i = 1, 2$ applied to the robot

with blue colour, the estimated value is denoted with green colour while the reference setpoints are denoted with red colour. It can be noticed that the proposed nonlinear optimal control scheme achieved fast and accurate tracking of all reference setpoints while the variations of the control input remained smooth. For the computation of the feedback gain of the H-infinity controller the algebraic Riccati equation given in Eq. (2.258) had to be solved at each step of the control method. In the presented simulation experiments sensorless control for the model of the underactuated robotic manipulator has been implemented, where the only state variables being measured

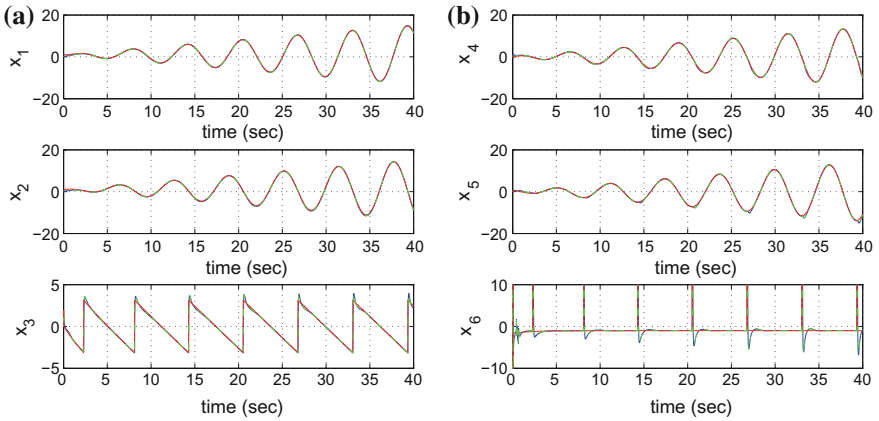

Fig. 2.58 Control of the underactuated 3-DOF robotic manipulator - Case 4 : **a** convergence of state variables $x_i,\ i = 1, 2, 3$ (blue line) and of their estimated values (green lines) to the reference setpoints (red line), **b** convergence of state variables $x_i,\ i = 4, 5, 6$ (blue line) and of their estimated values (green lines) to the reference setpoints (red line)

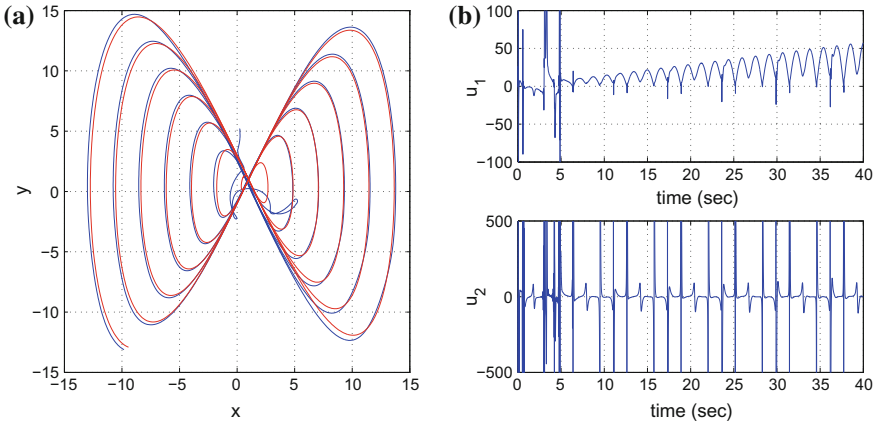

Fig. 2.59 Control of the underactuated 3-DOF robotic manipulator - Case 5 : **a** path followed by the robot's third-link in the xy cartesian coordinates frame (blue line) and reference path (red line), **b** control inputs $u_i\ i = 1, 2$ applied to the robot

were the unactuated link's cartesian coordinates $x_1 = x_p$ and $x_2 = y_p$. The real values of the robot's state variables are plotted in blue colour, the values of the state variables which were estimated by the H-infinity Kalman Filter are plotted in green colour, while the associated reference setpoints are printed in red colour.

It is of worth to note that despite its computational simplicity the proposed nonlinear H-infinity control method for 3-DOF underactuated robotic manipulators is very efficient and exhibits specific advantages: (i) it is applied directly on the nonlinear dynamical model of the underactuated robot and not on an equivalent linearized

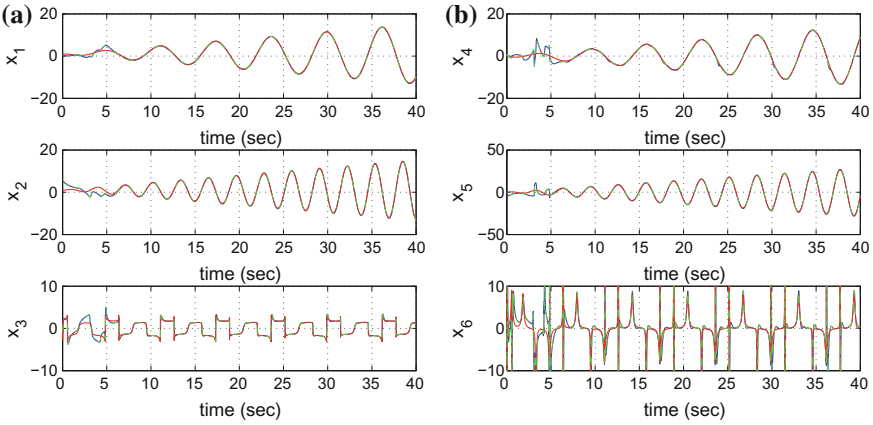

Fig. 2.60 Control of the underactuated 3-DOF robotic manipulator - Case 5 : **a** convergence of state variables x_i, $i = 1, 2, 3$ (blue line) and of their estimated values (green lines) to the reference setpoints (red line), **b** convergence of state variables x_i, $i = 4, 5, 6$ (blue line) and of their estimated values (green lines) to the reference setpoints (red line)

description of it, (ii) It avoids the elaborated linearizing transformations (diffeomorphisms) which can be met in global linearization-based control methods for robotic systems, (iii) the controller is designed according to optimal control principles which implies the best trade-off between precise tracking of the reference setpoints on the one side and moderate variations of the control inputs on the other side (iv) the control method exhibits significant robustness to parametric uncertainty, modelling errors as well as to external perturbations (v) the computational implementation of the control method is simple since it requires only the solution of an algebraic Riccati equation.

Chapter 3
Rigid-Link Manipulators: Model-Free Control

Abstract The chapter analyzes model-free nonlinear control approaches for multi-DOF rigid-link robots, based on Lyapunov methods. There, one comes against problems of minimization of Lyapunov functions so as to ensure the asymptotic stability of the control loop. Model-free control takes often the form of indirect adaptive control. In such a case the design of the controller is not based on prior knowledge of the robot's dynamics. With the use of adaptive algorithms and elaborated estimation methods it is possible to identify in real-time the unknown dynamics of the robots and subsequently to use this information in the control loop, thus arriving at indirect adaptive control schemes. Finally, the development of nonlinear state-estimation methods for robotic manipulators allows the implementation of feedback control through measuring of only a small number of the robot's state variables. Global stability is proven for the control loop that comprises both the nonlinear controller of the robot's dynamics and nonlinear observers that estimate the robot's state vector from indirect measurements. In particular, the chapter develops the following topics: (a) Model-free adaptive control of rigid-link manipulators using full-state feedback, (ii) Model-free adaptive control of rigid-link manipulators using output feedback, (iii) Model-free adaptive control of the underactuated rotary (Furuta's) pendulum.

3.1 Chapter Overview

The present chapter develops the following topics: (a) Model-free adaptive control of rigid-link manipulators using full-state feedback, (ii) Model-free adaptive control of rigid-link manipulators using output feedback, (c) Model-free control of the underactuated rotary (Furuta's) pendulum.

With reference to (a) the solution of the adaptive control problem for the robotic manipulator exploits the differential flatness properties of the manipulator and its transformation into an equivalent input-output linearized form. In this latter description the control input that is applied to the robot comprises the unknown functions of the manipulator's nonlinear dynamics. These unknown functions are online identified with the use of neurofuzzy approximators and the obtained function estimators

G. Rigatos and K. Busawon, *Robotic Manipulators and Vehicles*,
Studies in Systems, Decision and Control 152,
https://doi.org/10.1007/978-3-319-77851-8_3

are used in a feedback control scheme that finally stabilizes the robot and makes it track accurately all reference trajectories. The global asymptotic stability properties of the control method are proven through Lyapunov analysis.

With reference to (b) the adaptive control problem for robotic manipulators becomes more complicated since apart from the unknown dynamic model of the robot, its state vector is also considered to be only partially measurable. To solve the estimation problem for the non-measurable state vector elements of the manipulator a state observer is included in the adaptive control loop. Again the global asymptotic stability properties of the control method are proven through Lyapunov analysis.

With reference to (c) an adaptive controller is developed for the case that the dynamic model of the rotary (Furuta's) pendulum is unknown. In such a case neurofuzzy networks are used to estimate the elements of the matrices which constitute the approximately linearized model of the pendulum. Actually, neurofuzzy networks are employed for learning the constituent functions of the rotary pendulum's dynamic model. Based on these function estimates the rotary pendulum's Jacobian matrices are also obtained and this allows the implementation of an adaptive H-infinity neurofuzzy control scheme. To ensure the stability of the control loop, the learning rate of the neurofuzzy approximators is chosen from the requirement the first derivative of the system's Lyapunov function to be always a negative one.

3.2 Model-Free Adaptive Control of Rigid-Link Manipulators Using State Feedback

3.2.1 Outline

There has been significant research effort among the members of the robotic systems community in the design of nonlinear control systems, particularly for robotic systems with partially known or unknown dynamics. The application of global linearization techniques has enabled advancements in this research direction [415, 435, 561, 581, 582]. These techniques can be applied to nonlinear systems, with not exactly known dynamics. Based on the universal approximation theorem, many stable adaptive fuzzy control schemes have been developed for unknown single-input single-output (SISO) and unknown multi-input multi-output (MIMO) dynamical systems [83, 89, 277, 524, 562]. The capability of neurofuzzy controllers to compensate for model parametric uncertainties, external disturbances, as well as for incomplete measurement of the system's state vector has been analyzed in several studies [14, 108, 274, 504, 559]. Moreover results on neural and fuzzy control have been presented for both the case that the complete state vector of the dynamical system is measurable, as well as for the case that the state vector of the system is not measurable and has to be reconstructed with the use of a state observer [92, 158, 294, 395, 560]. To improve the robustness of these control schemes a supervisory control term is added to the control signal which can take the form of sliding mode

control or H_∞ control [85, 88, 280]. In this section an approach to the design of robust controllers for MIMO nonlinear robotic systems of unknown dynamics will be developed according to flatness-based control theory. This approach extends the class of nonlinear robotic systems to which adaptive fuzzy control can be applied.

Flatness-based control is currently a main direction of research in the design of nonlinear control systems [450, 476, 519]. The section proposes flatness-based adaptive fuzzy control for MIMO nonlinear robotic systems with unknown parameters. As already noted in the previous chapter, to find out if a dynamical system is differentially flat, the following should be examined: (i) the existence of the so-called flat output, i.e. a new variable which is expressed as a function of the system's state variables. It should hold that the flat output and its derivatives should not be coupled in the form of an ordinary differential equation, (ii) the components of the system (i.e. state variables and control input) should be expressed as differential functions of the flat output [145, 182, 183, 254, 267, 445, 572]. Differential flatness is a property characterising classes of systems. Expressing all system variables as functions of the flat output and its derivatives enables transformation to a linearized form for which the design of the controller becomes easier. Moreover, by showing that a system is differentially flat one can easily design a reference trajectory as a function of the so-called flat output and can find a control law that ensures tracking of this trajectory [145, 572].

Flatness-based control can be also applied to robotic systems characterized by model uncertainties and exogenous disturbances [182, 183]. In [415] it was shown that flatness-based adaptive fuzzy control can be developed for single-input nonlinear dynamical systems with uncertain model. In this section, the results of [415] are generalized and applied to multi-input multi-output (MIMO) robotic systems. The section is concerned with differentially flat multi-input multi-output (MIMO) robotic systems which can be written in the Brunovksy (canonical) form. Transformation into the Brunovksy form can be achieved for systems that admit static feedback linearization (i.e. a change of coordinates for both the system state variables and the system's control input). Single-input differentially flat robotic systems admit static feedback linearization and therefore can be finally written in the Brunovsky form [322]. Moreover, multi-input robotic systems which satisfy the differential flatness properties can be also transformed to an equivalent canonical linear form (input-output linearized form), after a change of their state variables (diffeomorphisms).

After transforming a MIMO system into the canonical form, the resulting control inputs are shown to contain nonlinear elements which depend on the system's parameters. If the parameters of the system are unknown, then the nonlinear terms which appear in the control inputs can be approximated with the use of nonlinear regressors (e.g. neuro-fuzzy networks). In this section it is shown that a suitable learning law can be defined for the aforementioned neuro-fuzzy approximators so as to preserve the closed-loop system stability. Lyapunov stability analysis proves also that the proposed flatness-based adaptive fuzzy control scheme results in H_∞ tracking performance, in accordance to the results of [436, 447, 457].

3.2.2 *Adaptive Control Based on Transformation of the Robot's Dynamics to a Canonical Form*

In Chap. 1 it was shown that, by applying differential flatness theory, the model of the multi-DOF robotic manipulator (see for instance Fig. 1.3), can be written in state-space form of Eq. (1.40), that is

$$\begin{aligned} \dot{x} &= Ax + B[f(x) + g(x)u + \tilde{d}] \\ y &= Cx \end{aligned} \tag{3.1}$$

which can be also written in the equivalent form:

$$\begin{aligned} \dot{x} &= Ax + Bv + B\tilde{d} \\ y &= Cx \end{aligned} \tag{3.2}$$

where $v = f(x) + g(x)u$.

The reference setpoints for the robot's outputs $y_1, \ldots, y_p$, that is for the joints' angles, are denoted as $y_{1m}, \ldots, y_{pm}$, thus for the associated tracking errors it holds

$$\begin{aligned} e_1 &= y_1 - y_{1m} \\ e_2 &= y_2 - y_{2m} \\ &\cdots \\ e_p &= y_p - y_{pm} \end{aligned} \tag{3.3}$$

The error vector of the outputs the transformed MIMO robotic system is denoted as

$$\begin{aligned} E_1 &= [e_1, \ldots, e_p]^T \\ y_m &= [y_{1m}, \ldots, y_{pm}]^T \\ &\cdots \\ y_m^{(r)} &= [y_{1m}^{(r)}, \ldots, y_{pm}^{(r)}]^T \end{aligned} \tag{3.4}$$

where $y_{im}^{(r)}$ denotes the rth order derivative of the ith reference output of the MIMO robotic model. Thus, one can also define the following vectors: (i) a vector containing the state variables of the system and the associated derivatives, (ii) a vector containing the reference outputs of the system and the associated derivatives

$$x = [x_1, \ldots, x_1^{r_1-1}, \ldots, x_p, \ldots, x_p^{r_p-1}]^T \tag{3.5}$$

$$Y_m = [y_{1m}, \ldots, y_{1m}^{r_1-1}, \ldots, y_{pm}, \ldots, y_{pm}^{r_p-1}]^T \tag{3.6}$$

while in a similar manner one can define a vector containing the tracking error of the robotic system's outputs and the associated derivatives

$$e = Y_m - x = [e_1, \ldots, e_1^{r_1-1}, \ldots, e_p, \ldots, e_p^{r_p-1}]^T \tag{3.7}$$

It is assumed that matrix $g(x)$ is a nonsingular one, i.e. $g^{-1}(x)$ exists and is bounded for all $x \in U_x$, where $U_x \subset R^n$ is a compact set. In any case, the problem of singularities in matrix $g(x)$ can be avoided by appropriately modifying the state feedback-based control input.

The objective of the adaptive fuzzy controller, denoted as $u = u(x, e|\theta)$ is: (i) all the signals involved in the controller's design are bounded and it holds that $lim_{t\to\infty} e = 0$, (ii) the H_∞ tracking performance criterion is achieved for a prescribed attenuation level.

In the presence of non-gaussian disturbances w_d, successful tracking of the reference signal is denoted by the H_∞ criterion [436, 561]:

$$\int_0^T e^T Q e dt \leq \rho^2 \int_0^T w_d{}^T w_d dt \tag{3.8}$$

where ρ is the attenuation level and corresponds to the maximum singular value of the transfer function $G(s)$ of the linearized model associated to Eq. (3.2).

From the H_∞ control theory, the H_∞ norm of a linear system with transfer function $G(s)$, is denoted by $||G||_\infty$ and is defined as $||G||_\infty = sup_\omega \sigma_{max}[G(j\omega)]$ [436, 447, 457]. In this definition *sup* denotes the supremum or least upper bound of the function $\sigma_{max}[G(j(\omega)]$, and thus the H_∞ norm of $G(s)$ is the maximum value of $\sigma_{max}[G(j(\omega)]$ over all frequencies ω. H_∞ norm has a physically meaningful interpretation when considering the system $y(s) = G(s)u(s)$. When this system is driven with a unit sinusoidal input at a specific frequency, $\sigma_{max}|G(j\omega)|$ is the largest possible output for the corresponding sinusoidal intput. Thus, the H_∞ norm is the largest possible amplification over all frequencies of a sinusoidal input.

3.2.3 Control Law

The control signal of the MIMO nonlinear system which has been transformed into the Brunovsky form as described by Eq. (3.2) contains the unknown nonlinear functions $f(x)$ and $g(x)$, through the transformed control input $v = f(x) + g(x)u$. These can be approximated by

$$\begin{aligned} \hat{f}(x|\theta_f) &= \Phi_f(x)\theta_f \\ \hat{g}(x|\theta_g) &= \Phi_g(x)\theta_g \end{aligned} \tag{3.9}$$

where

$$\Phi_f(x) = (\xi_f^1(x), \xi_f^2(x), \ldots \xi_f^n(x))^T \tag{3.10}$$

with $\xi_f^i(x), \imath = 1, \ldots, n$ being the vector of kernel functions (e.g. normalized fuzzy Gaussian membership functions), where

$$\xi_f^i(x) = (\phi_f^{i,1}(x), \phi_f^{i,2}(x), \ldots, \phi_f^{i,N}(x)) \tag{3.11}$$

thus giving

$$\Phi_f(x) = \begin{pmatrix} \phi_f^{1,1}(x) & \phi_f^{1,2}(x) & \cdots & \phi_f^{1,N}(x) \\ \phi_f^{2,1}(x) & \phi_f^{2,2}(x) & \cdots & \phi_f^{2,N}(x) \\ \cdots & \cdots & \cdots & \cdots \\ \phi_f^{n,1}(x) & \phi_f^{n,2}(x) & \cdots & \phi_f^{n,N}(x) \end{pmatrix} \tag{3.12}$$

while the weights vector is defined as

$$\theta_f{}^T = \left(\theta_f^1, \theta_f^2, \ldots \theta_f^N\right) \tag{3.13}$$

$j = 1, \ldots, N$ is the number of basis functions that is used to approximate the components of function f which are denoted as $i = 1, \ldots, n$. Thus, one obtains the relation of Eq. (3.9), i.e. $\hat{f}(x|\theta_f) = \Phi_f(x)\theta_f$.

In a similar manner, for the approximation of function g one has

$$\Phi_g(x) = \left(\xi_g^1(x), \xi_g^2(x), \ldots \xi_g^N(x)\right)^T \tag{3.14}$$

with $\xi_g^i(x), \imath = 1, \ldots, N$ being the vector of kernel functions (e.g. normalized fuzzy Gaussian membership functions), where

$$\xi_g^i(x) = \left(\phi_g^{i,1}(x), \phi_g^{i,2}(x), \ldots, \phi_g^{i,N}(x)\right) \tag{3.15}$$

thus giving

$$\Phi_g(x) = \begin{pmatrix} \phi_g^{1,1}(x) & \phi_g^{1,2}(x) & \cdots & \phi_g^{1,N}(x) \\ \phi_g^{2,1}(x) & \phi_g^{2,2}(x) & \cdots & \phi_g^{2,N}(x) \\ \cdots & \cdots & \cdots & \cdots \\ \phi_g^{n,1}(x) & \phi_g^{n,2}(x) & \cdots & \phi_g^{n,N}(x) \end{pmatrix} \tag{3.16}$$

while the weights vector is defined as

$$\theta_g = \left(\theta_g^1, \theta_g^2, \ldots, \theta_g^p\right)^T \tag{3.17}$$

where the components of matrix θ_g are defined as

$$\theta_g^j = \left(\theta_{g_1}^j, \theta_{g_2}^j, \ldots \theta_{g_N}^j\right) \tag{3.18}$$

$j = 1, \ldots, N$ is the number of basis functions that is used to approximate the components of function g which are denoted as $i = 1, \ldots, n$. Thus one obtains about matrix $\theta_g \in R^{N \times p}$

$$\theta_g = \begin{pmatrix} \theta_{g_1}^1 & \theta_{g_1}^2 & \cdots & \theta_{g_1}^p \\ \theta_{g_2}^1 & \theta_{g_2}^2 & \cdots & \theta_{g_2}^p \\ \cdots & \cdots & \cdots & \cdots \\ \theta_{g_N}^1 & \theta_{g_N}^2 & \cdots & \theta_{g_N}^p \end{pmatrix} \tag{3.19}$$

It holds that

$$g = \begin{pmatrix} g_1 \\ g_2 \\ \cdots \\ g_n \end{pmatrix} = \begin{pmatrix} g_1^1 & g_1^2 & \cdots & g_1^p \\ g_2^1 & g_2^2 & \cdots & g_2^p \\ \cdots & \cdots & \cdots & \cdots \\ g_n^1 & g_n^2 & \cdots & g_n^p \end{pmatrix} \tag{3.20}$$

Using the above, one finally has the relation of Eq. (3.9), i.e. $\hat{g}(x|\theta_g) = \Phi_g(x)\theta_g$.

If the state variables of the system are available for measurement then a state-feedback control law can be formulated as

$$u = \hat{g}^{-1}(x|\theta_g)[-\hat{f}(x|\theta_f) + y_m^{(r)} + K^T e + u_c] \tag{3.21}$$

where $\hat{f}(x|\theta_f)$ and $\hat{g}(x|\theta_g)$ are neurofuzzy models to approximate $f(x)$ and $g(x)$, respectively. u_c is a supervisory control term, e.g. an H_∞ control term that is used to compensate for the effects of modelling inaccuracies and external disturbances. Using the system's state-space description of Eq. (3.1) the control term u_c is defined as

$$u_c = -\tfrac{1}{r} B^T P e \tag{3.22}$$

Moreover, K^T is the feedback gain matrix that assures that the characteristic polynomial of matrix $A - BK^T$ will be a Hurwitz one.

3.2.4 *Application of Flatness-Based Adaptive Fuzzy Control to Robotic Manipulators*

The previous examined 2-DOF rigid link robotic manipulator, shown in Fig. 3.1 is considered again. The dynamic model of the robot is given by

$$\begin{pmatrix} M_{11} & M_{12} \\ M_{21} & M_{22} \end{pmatrix} \begin{pmatrix} \ddot{\theta}_1 \\ \ddot{\theta}_2 \end{pmatrix} + \begin{pmatrix} F_1(\theta, \dot{\theta}) \\ F_2(\theta, \dot{\theta}) \end{pmatrix} + \begin{pmatrix} G_1(\theta) \\ G_2(\theta) \end{pmatrix} = \begin{pmatrix} T_1 \\ T_2 \end{pmatrix} \tag{3.23}$$

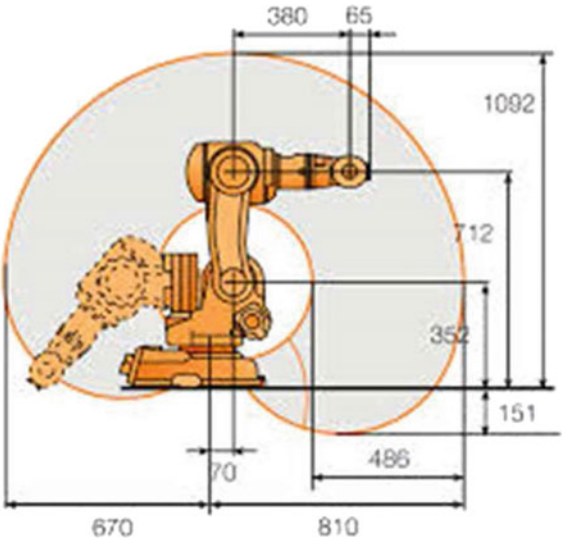

Fig. 3.1 A 2-DOF rigid-link robotic manipulator

or equivalently

$$\begin{pmatrix}\ddot{\theta}_1\\ \ddot{\theta}_2\end{pmatrix} = -\begin{pmatrix}M_{11}\ M_{12}\\ M_{21}\ M_{22}\end{pmatrix}^{-1}\begin{pmatrix}F_1(\theta,\dot{\theta})\\ F_2(\theta,\dot{\theta})\end{pmatrix} - \\ -\begin{pmatrix}M_{11}\ M_{12}\\ M_{21}\ M_{22}\end{pmatrix}^{-1}\begin{pmatrix}G_1(\theta)\\ G_2(\theta)\end{pmatrix} + \begin{pmatrix}M_{11}\ M_{12}\\ M_{21}\ M_{22}\end{pmatrix}^{-1}\begin{pmatrix}T_1\\ T_2\end{pmatrix} \tag{3.24}$$

As explained in Chap. 1, by denoting the inverse of the inertia matrix as

$$\begin{pmatrix}M_{11}\ M_{12}\\ M_{21}\ M_{22}\end{pmatrix} = \begin{pmatrix}N_{11}\ N_{12}\\ N_{21}\ N_{22}\end{pmatrix} \tag{3.25}$$

then one obtains

$$\begin{pmatrix}\ddot{\theta}_1\\ \ddot{\theta}_2\end{pmatrix} = -\begin{pmatrix}N_{11}\ N_{12}\\ N_{21}\ N_{22}\end{pmatrix}\begin{pmatrix}F_1(\theta,\dot{\theta})\\ F_2(\theta,\dot{\theta})\end{pmatrix} - \\ -\begin{pmatrix}N_{11}\ N_{12}\\ N_{21}\ N_{22}\end{pmatrix}\begin{pmatrix}G_1(\theta)\\ G_2(\theta)\end{pmatrix} + \begin{pmatrix}N_{11}\ N_{12}\\ N_{21}\ N_{22}\end{pmatrix}\begin{pmatrix}T_1\\ T_2\end{pmatrix} \tag{3.26}$$

which can be also written as

$$\ddot{\theta}_1 = -N_{11}F_1(\theta,\dot{\theta}) - N_{12}F_2(\theta,\dot{\theta}) - \\ -N_{11}G_1(\theta) - N_{12}G_2(\theta) + N_{11}T_1 + N_{12}T_2 \tag{3.27}$$

$$\ddot{\theta}_2 = -N_{21}F_1(\theta,\dot{\theta}) - N_{22}F_2(\theta,\dot{\theta}) - \\ = N_{21}G_1(\theta) - N_{22}G_2(\theta) + N_{21}T_1 + N_{22}T_2 \tag{3.28}$$

The following state variables are defined

$$x_1 = \theta_1 \; x_2 = \dot{\theta}_1 \; x_3 = \theta_2 \; x_4 = \dot{\theta}_2 \tag{3.29}$$

It holds that

$$\begin{aligned} \ddot{x}_1 &= f_1(x) + g_1(x)u \\ \ddot{x}_3 &= f_2(x) + g_2(x)u \end{aligned} \tag{3.30}$$

where

$$\begin{aligned} f_1(x) = -N_{11}F_1(\theta, \dot{\theta}) - N_{12}F_2(\theta, \dot{\theta}) - \\ -N_{11}G_1(\theta) - N_{12}G_2(\theta) \; \in \; R^{1\times 1} \\ g_1(x) = [N_{11} \; N_{12}] \; \in R^{1\times 2} \\ f_2(x) = -N_{21}F_2(\theta, \dot{\theta}) - N_{22}F_2(\theta, \dot{\theta}) - \\ -N_{21}G_1(\theta) - N_{22}G_2(\theta) \; \in \; R^{1\times 1} \\ g_2(x) = [N_{21} \; N_{22}] \; \in R^{2\times 2} \end{aligned} \tag{3.31}$$

The flat output is defined as

$$y = [\theta_1, \theta_2] = [x_1, x_3] \tag{3.32}$$

It holds that

$$\begin{aligned} \dot{x}_1 &= x_2 \\ \dot{x}_2 &= f_1(x) + g_1(x)u \\ \dot{x}_3 &= x_4 \\ \dot{x}_4 &= f_2(x) + g_2(x)u \end{aligned} \tag{3.33}$$

therefore all system state variables can be written as functions of the flat output y and its derivatives. The same holds for the control input u

$$\begin{aligned} x_1 = [1\;0]y^T \; x_2 = [1\;0]\dot{y}^T \\ x_3 = [0\;1]y^T \; x_4 = [0\;1]\dot{y}^T \end{aligned} \tag{3.34}$$

Moreover, from Eq. (3.33) it holds

$$\begin{aligned} \begin{pmatrix} \ddot{x}_1 \\ \ddot{x}_3 \end{pmatrix} = \begin{pmatrix} f_1(x) \\ f_2(x) \end{pmatrix} + \begin{pmatrix} g_1(x) \\ g_2(x) \end{pmatrix} u \; i.e. \\ u = \begin{pmatrix} g_1(x) \\ g_2(x) \end{pmatrix}^{-1} \left\{ \begin{pmatrix} \ddot{x}_1 \\ \ddot{x}_3 \end{pmatrix} - \begin{pmatrix} f_1(x) \\ f_2(x) \end{pmatrix} \right\} \end{aligned} \tag{3.35}$$

Knowing that $x = h(y, \dot{y})$ one finally obtains

$$u = \begin{pmatrix} g_1(h(y,\dot{y})) \\ g_2(h(y,\dot{y})) \end{pmatrix}^{-1} \left\{ \begin{pmatrix} [1\;0]\ddot{y}^T \\ [0\;1]\ddot{y}^T \end{pmatrix} - \begin{pmatrix} f_1(h(y,\dot{y})) \\ f_2(h(y,\dot{y})) \end{pmatrix} \right\} \tag{3.36}$$

Therefore, as it has already been proven, the considered robotic system is a differentially flat one. Next, taking into account also the effects of additive disturbances to the joints of the robotic manipulator the dynamic model becomes

$$\begin{aligned} \ddot{x}_1 &= f_1(x,t) + g_1(x,t)u + \tilde{d}_1 \\ \ddot{x}_3 &= f_2(x,t) + g_2(x,t)u + \tilde{d}_2 \end{aligned} \tag{3.37}$$

$$\begin{pmatrix} \ddot{x}_1 \\ \ddot{x}_3 \end{pmatrix} = \begin{pmatrix} f_1(x,t) \\ f_2(x,t) \end{pmatrix} + \begin{pmatrix} g_1(x,t) \\ g_2(x,t) \end{pmatrix} u + \begin{pmatrix} \tilde{d}_1 \\ \tilde{d}_2 \end{pmatrix} \tag{3.38}$$

The following control input is defined

$$u = \begin{pmatrix} \hat{g}_1(x,t) \\ \hat{g}_2(x,t) \end{pmatrix}^{-1} \cdot \left\{ \begin{pmatrix} \ddot{x}_1^d \\ \ddot{x}_3^d \end{pmatrix} - \begin{pmatrix} \hat{f}_1(x,t) \\ \hat{f}_2(x,t) \end{pmatrix} - \begin{pmatrix} K_1^T \\ K_2^T \end{pmatrix} e + \begin{pmatrix} u_{c_1} \\ u_{c_2} \end{pmatrix} \right\} \tag{3.39}$$

where $[u_{c_1} \; u_{c_2}]^T$ is a robust control term that is used for the compensation of the model's uncertainties as well as of the external disturbances. The feedback control gain is defined as $K_i^T = [k_1^i, k_2^i, \ldots, k_{n-1}^i, k_n^i]$.

Substituting Eq. (3.39) into (3.38) the closed-loop tracking error dynamics is obtained

$$\begin{aligned} \begin{pmatrix} \ddot{x}_1 \\ \ddot{x}_3 \end{pmatrix} &= \begin{pmatrix} f_1(x,t) \\ f_2(x,t) \end{pmatrix} + \begin{pmatrix} g_1(x,t) \\ g_2(x,t) \end{pmatrix} \begin{pmatrix} \hat{g}_1(x,t) \\ \hat{g}_2(x,t) \end{pmatrix}^{-1} \\ &\left\{ \begin{pmatrix} \ddot{x}_1^d \\ \ddot{x}_3^d \end{pmatrix} - \begin{pmatrix} \hat{f}_1(x,t) \\ \hat{f}_2(x,t) \end{pmatrix} - \begin{pmatrix} K_1^T \\ K_2^T \end{pmatrix} e + \begin{pmatrix} u_{c_1} \\ u_{c_2} \end{pmatrix} \right\} + \begin{pmatrix} \tilde{d}_1 \\ \tilde{d}_2 \end{pmatrix} \end{aligned} \tag{3.40}$$

Equation (3.40) can now be written as

$$\begin{aligned} \begin{pmatrix} \ddot{x}_1 \\ \ddot{x}_3 \end{pmatrix} &= \begin{pmatrix} f_1(x,t) \\ f_2(x,t) \end{pmatrix} + \\ &+ \left\{ \begin{pmatrix} g_1(x,t) - \hat{g}_1(x,t) \\ g_2(x,t) - \hat{g}_2(x,t) \end{pmatrix} + \begin{pmatrix} \hat{g}_1(x,t) \\ \hat{g}_2(x,t) \end{pmatrix} \right\} \begin{pmatrix} \hat{g}_1(x,t) \\ \hat{g}_2(x,t) \end{pmatrix}^{-1} \cdot \\ &\cdot \left\{ \begin{pmatrix} \ddot{x}_1^d \\ \ddot{x}_3^d \end{pmatrix} - \begin{pmatrix} \hat{f}_1(x,t) \\ \hat{f}_2(x,t) \end{pmatrix} - \begin{pmatrix} K_1^T \\ K_2^T \end{pmatrix} e + \begin{pmatrix} u_{c_1} \\ u_{c_2} \end{pmatrix} \right\} + \begin{pmatrix} \tilde{d}_1 \\ \tilde{d}_2 \end{pmatrix} \end{aligned} \tag{3.41}$$

and using Eq. (3.39) this results into

$$\begin{aligned} \begin{pmatrix} \ddot{e}_1 \\ \ddot{e}_3 \end{pmatrix} &= \begin{pmatrix} f_1(x,t) - \hat{f}_1(x,t) \\ f_2(x,t) - \hat{f}_2(x,t) \end{pmatrix} + \\ &+ \begin{pmatrix} g_1(x,t) - \hat{g}_1(x,t) \\ g_2(x,t) - \hat{g}_2(x,t) \end{pmatrix} u - \begin{pmatrix} K_1^T \\ K_2^T \end{pmatrix} e + \begin{pmatrix} u_{c_1} \\ u_{c_2} \end{pmatrix} + \begin{pmatrix} \tilde{d}_1 \\ \tilde{d}_2 \end{pmatrix} \end{aligned} \tag{3.42}$$

The following description for the approximation error is defined

$$w = \begin{pmatrix} f_1(x,t) - \hat{f}_1(x,t) \\ f_2(x,t) - \hat{f}_2(x,t) \end{pmatrix} + \begin{pmatrix} g_1(x,t) - \hat{g}_1(x,t) \\ g_2(x,t) - \hat{g}_2(x,t) \end{pmatrix} u \tag{3.43}$$

Moreover, the following matrices are defined

$$\begin{gathered} A = \begin{pmatrix} 0\ 1\ 0\ 0 \\ 0\ 0\ 0\ 0 \\ 0\ 0\ 0\ 1 \\ 0\ 0\ 0\ 0 \end{pmatrix}, \quad B = \begin{pmatrix} 0\ 0 \\ 1\ 0 \\ 0\ 0 \\ 0\ 1 \end{pmatrix} \\ K^T = \begin{pmatrix} K_1^1\ K_2^1\ K_3^1\ K_4^1 \\ K_1^2\ K_2^2\ K_3^2\ K_4^2 \end{pmatrix} \end{gathered} \tag{3.44}$$

Using matrices A, B, K^T, Eq. (3.42) is written in the following form

$$\begin{gathered} \dot{e} = (A - BK^T)e + Bu_c + \\ + B\{\begin{pmatrix} f_1(x,t) - \hat{f}_1(x,t) \\ f_2(x,t) - \hat{f}_2(x,t) \end{pmatrix} + \\ + \begin{pmatrix} g_1(x,t) - \hat{g}_1(x,t) \\ g_2(x,t) - \hat{g}_2(x,t) \end{pmatrix} u + \tilde{d}\} \end{gathered} \tag{3.45}$$

Next, the following approximators of the unknown system dynamics are defined

$$\hat{f}(x) = \begin{pmatrix} \hat{f}_1(x|\theta_f)\ x \in R^{4\times 1}\ \hat{f}_1(x|\theta_f)\ \in\ R^{1\times 1} \\ \hat{f}_2(x|\theta_f)\ x \in R^{4\times 1}\ \hat{f}_2(x|\theta_f)\ \in\ R^{1\times 1} \end{pmatrix} \tag{3.46}$$

with kernel functions

$$\phi_f^{i,j}(x) = \frac{\prod_{j=1}^{n} \mu_{A_j^i}(x_j)}{\sum_{i=1}^{N} \prod_{j=1}^{n} \mu_{A_j^i}(x_j)} \tag{3.47}$$

where $l = 1, 2$ and $\mu_{A_j^i}(x)$ is the ith membership function of the antecedent (IF) part of the lth fuzzy rule.

Similarly, the following approximators of the unknown system dynamics are defined

$$\hat{g}(x) = \begin{pmatrix} \hat{g}_1(x|\theta_g)\ x \in R^{4\times 1}\ \hat{g}_1(x|\theta_g)\ \in\ R^{1\times 2} \\ \hat{g}_2(x|\theta_g)\ x \in R^{4\times 1}\ \hat{g}_2(x|\theta_g)\ \in\ R^{1\times 2} \end{pmatrix} \tag{3.48}$$

The values of the weights that result in optimal approximation are

$$\begin{gathered} \theta_f^* = arg\ min_{\theta_f \in M_{\theta_f}} [sup_{x\in U_x} (f(x) - \hat{f}(x|\theta_f))] \\ \theta_g^* = arg\ min_{\theta_g \in M_{\theta_g}} [sup_{x\in U_x} (g(x) - \hat{g}(x|\theta_g))] \end{gathered} \tag{3.49}$$

where the variation ranges for the weights are defined as

$$\begin{array}{l} M_{\theta_f} = \{\theta_f \in R^h : \ ||\theta_f|| \leq m_{\theta_f}\} \\ M_{\theta_g} = \{\theta_g \in R^h : \ ||\theta_g|| \leq m_{\theta_g}\} \end{array} \tag{3.50}$$

Taking the value of the approximation error defined in Eq. (3.43) that corresponds to the optimal values of the weights vectors θ_f^* and θ_g^* one has

$$w = \left(f(x,t) - \hat{f}(x|\theta_f^*)\right) + \left(g(x,t) - \hat{g}(x|\theta_g^*)\right) u \tag{3.51}$$

which is next written as

$$\begin{array}{c} w = \left(f(x,t) - \hat{f}(x|\theta_f) + \hat{f}(x|\theta_f) - \hat{f}(x|\theta_f^*)\right) + \\ + \left(g(x,t) - \hat{g}(x|\theta_g) + \hat{g}(x|\theta_g) - \hat{g}(x|\theta_g^*)\right) u \end{array} \tag{3.52}$$

which can be also written in the following form

$$w = \left(w_a + w_b\right) \tag{3.53}$$

where

$$w_a = \{[f(x,t) - \hat{f}(x|\theta_f)] + [g(x,t) - \hat{g}(x|\theta_g)]\} u \tag{3.54}$$

$$w_b = \{[f(x,t) - \hat{f}(x|\theta_f^*)] + [g(x,t) - \hat{g}(x|\theta_g^*)]\} u \tag{3.55}$$

Moreover, the following weights error vectors are defined

$$\begin{array}{l} \tilde{\theta}_f = \theta_f - \theta_f^* \\ \tilde{\theta}_g = \theta_g - \theta_g^*. \end{array} \tag{3.56}$$

3.2.5 Lyapunov Stability Analysis

3.2.5.1 Stability Proof for the Control Loop

The following quadratic Lyapunov function is defined

$$V = \frac{1}{2} e^T P e + \frac{1}{2\gamma_1} \tilde{\theta}_f^T \tilde{\theta}_f + \frac{1}{2\gamma_2} tr[\tilde{\theta}_g^T \tilde{\theta}_g] \tag{3.57}$$

Parameter γ_1 is the learning rate used in the adaptation of the weights of the neurofuzzy approximator for $f(x)$, while parameter γ_2 is the learning rate used in the adaptation of the weights of the neurofuzzy approximation for $g(x)$. It holds that

$$\dot{V} = \tfrac{1}{2} \dot{e}^T P e + \tfrac{1}{2} e^T P \dot{e} + \tfrac{1}{\gamma_1} \dot{\tilde{\theta}}_f^T \tilde{\theta}_f + \tfrac{1}{\gamma_2} tr[\dot{\tilde{\theta}}_g^T \tilde{\theta}_g] \tag{3.58}$$

The tracking error dynamics is described by

$$\begin{aligned}\dot{e} = (A - BK^T)e + Bu_c + B\left\{\begin{pmatrix} f_1(x,t) - \hat{f}_1(x,t) \\ f_2(x,t) - \hat{f}_2(x,t)\end{pmatrix} + \right. \\ \left. + \begin{pmatrix} g_1(x,t) - \hat{g}_1(x,t) \\ g_2(x,t) - \hat{g}_2(x,t)\end{pmatrix} \begin{pmatrix} \hat{g}_1(x,t) \\ \hat{g}_2(x,t)\end{pmatrix}^{-1} u + \tilde{d}\right\}\end{aligned} \tag{3.59}$$

and defining the approximation error

$$w = \begin{pmatrix} f_1(x,t) - \hat{f}_1(x,t) \\ f_2(x,t) - \hat{f}_2(x,t)\end{pmatrix} + \begin{pmatrix} g_1(x,t) - \hat{g}_1(x,t) \\ g_2(x,t) - \hat{g}_2(x,t)\end{pmatrix} \begin{pmatrix} \hat{g}_1(x,t) \\ \hat{g}_2(x,t)\end{pmatrix}^{-1} u \tag{3.60}$$

the previous relation can be also written as

$$\dot{e} = (A - BK^T)e + Bu_c + B(w + \tilde{d}) \tag{3.61}$$

From Eq. (3.58) one obtains

$$\begin{aligned}\dot{V} = \tfrac{1}{2}\{e^T(A - BK^T)^T + u_c^T B^T + \\ +(w + \tilde{d})^T B^T\}Pe + \tfrac{1}{2}e^T P\{(A - BK^T)e + \\ +Bu_c + B(w + \tilde{d})\} + \tfrac{1}{\gamma_1}\dot{\tilde{\theta}}_f^T\tilde{\theta}_f + \tfrac{1}{\gamma_2}tr[\dot{\tilde{\theta}}_g^T\tilde{\theta}_g]\end{aligned} \tag{3.62}$$

which in turn yields

$$\begin{aligned}\dot{V} = \tfrac{1}{2}e^T\{(A - BK^T)^T P + P(A - BK^T)\}e + \\ \tfrac{1}{2}2e^T PBu_c + \tfrac{1}{2}2B^T Pe(w + \tilde{d}) + \\ +\tfrac{1}{\gamma_1}\dot{\tilde{\theta}}_f^T\tilde{\theta}_f + \tfrac{1}{\gamma_2}tr[\dot{\tilde{\theta}}_g^T\tilde{\theta}_g]\end{aligned} \tag{3.63}$$

Assumption 1: For given positive definite matrix Q there exists a positive definite matrix P, which is the solution of the following matrix equation

$$(A - BK^T)^T P + P(A - BK^T) - PB(\tfrac{2}{r} - \tfrac{1}{\rho^2})B^T P + Q = 0 \tag{3.64}$$

Substituting Eqs. (3.64) and (3.22) into $\dot{V}$ yields after some operations

$$\begin{aligned}\dot{V} = \tfrac{1}{2}e^T\{-Q + PB(\tfrac{2}{r} - \tfrac{1}{\rho^2})B^T P\}e + \\ e^T PB\{-\tfrac{1}{r}B^T Pe\} + B^T P(w + \tilde{d}) + \\ +\tfrac{1}{\gamma_1}\dot{\tilde{\theta}}_f^T\tilde{\theta}_f + \tfrac{1}{\gamma_2}tr[\dot{\tilde{\theta}}_g^T\tilde{\theta}_g]\end{aligned} \tag{3.65}$$

Therefore it holds

$$\begin{array}{c}\dot{V} = -\frac{1}{2}e^T Qe - \frac{1}{2\rho^2}e^T PBB^T Pe + e^T PB(w + \tilde{d}) + \\ \frac{1}{\gamma_1}\dot{\tilde{\theta}}_f^T \tilde{\theta}_f + \frac{1}{\gamma_2} tr[\dot{\tilde{\theta}}_g^T \tilde{\theta}_g]\end{array} \tag{3.66}$$

It also holds that

$$\begin{array}{c}\dot{\tilde{\theta}}_f = \dot{\theta}_f - \dot{\theta}_f^* = \dot{\theta}_f \\ \dot{\tilde{\theta}}_g = \dot{\theta}_g - \dot{\theta}_g^* = \dot{\theta}_g\end{array} \tag{3.67}$$

The following weights adaptation law is used

$$\begin{array}{c}\dot{\theta}_f = -\gamma_1 \Phi(x)^T B^T Pe \\ \dot{\theta}_g = -\gamma_2 \Phi(x)^T B^T Peu^T\end{array} \tag{3.68}$$

where assuming N fuzzy rules and associated kernel functions the matrices dimensions are $\theta_f \in R^{N\times 1}$, $\theta_g \in R^{N\times 2}$, $\Phi(x) \in R^{2\times N}$, $B \in R^{4\times 2}$, $P \in R^{4\times 4}$ and $e \in R^{4\times 1}$. Therefore it holds

$$\begin{array}{c}\dot{V} = -\frac{1}{2}e^T Qe - \frac{1}{2\rho^2}e^T PBB^T Pe + e^T PB(w + \tilde{d}) + \\ + \frac{1}{\gamma_1}(-\gamma_1)e^T PB\Phi(x)(\theta_f - \theta_f^*) + \\ + \frac{1}{\gamma_2}(-\gamma_2) tr[ue^T PB\Phi(x)(\theta_g - \theta_g^*)]\end{array} \tag{3.69}$$

or

$$\begin{array}{c}\dot{V} = -\frac{1}{2}e^T Qe - \frac{1}{2\rho^2}e^T PBB^T Pe + e^T PB(w + \tilde{d}) + \\ + \frac{1}{\gamma_1}(-\gamma_1)e^T PB\Phi(x)(\theta_f - \theta_f^*) + \\ + \frac{1}{\gamma_2}(-\gamma_2) tr[ue^T PB(\hat{g}(x|\theta_g) - \hat{g}(x|\theta_g^*)]\end{array} \tag{3.70}$$

Taking into account that $u \in R^{2\times 1}$ and $e^T PB(\hat{g}(x|\theta_g) - \hat{g}(x|\theta_g^*)) \in R^{1\times 2}$ it holds

$$\begin{array}{c}\dot{V} = -\frac{1}{2}e^T Qe - \frac{1}{2\rho^2}e^T PBB^T Pe + e^T PB(w + \tilde{d}) + \\ + \frac{1}{\gamma_1}(-\gamma_1)e^T PB\Phi(x)(\theta_f - \theta_f^*) + \\ + \frac{1}{\gamma_2}(-\gamma_2) tr[e^T PB(\hat{g}(x|\theta_g) - \hat{g}(x|\theta_g^*))u]\end{array} \tag{3.71}$$

Since $e^T PB(\hat{g}(x|\theta_g) - \hat{g}(x|\theta_g^*))u \in R^{1\times 1}$ it holds

$$\begin{array}{c}tr(e^T PB(\hat{g}(x|\theta_g) - \hat{g}(x|\theta_g^*)u) = \\ = e^T PB(\hat{g}(x|\theta_g) - \hat{g}(x|\theta_g^*))u\end{array} \tag{3.72}$$

Therefore, one finally obtains

$$\begin{array}{c}\dot{V} = -\frac{1}{2}e^T Qe - \frac{1}{2\rho^2}e^T PBB^T Pe + e^T PB(w + \tilde{d}) + \\ + \frac{1}{\gamma_1}(-\gamma_1)e^T PB\Phi(x)(\theta_f - \theta_f^*) + \\ + \frac{1}{\gamma_2}(-\gamma_2)e^T PB(\hat{g}(x|\theta_g) - \hat{g}(x|\theta_g^*))u\end{array} \tag{3.73}$$

Next the following approximation error is defined

$$w_\alpha = [\hat{f}(x|\theta_f^*) - \hat{f}(x|\theta_f)] + [\hat{g}(x|\theta_g^*) - \hat{g}(x|\theta_g)]u \tag{3.74}$$

Thus, one obtains

$$\begin{array}{c} \dot{V} = -\frac{1}{2}e^T Qe - \frac{1}{2\rho^2}e^T PBB^T Pe + \\ +e^T PB(w + \tilde{d}) + e^T PBw_\alpha \end{array} \tag{3.75}$$

Denoting the aggregate approximation error and disturbances vector as

$$w_1 = w + \tilde{d} + w_\alpha \tag{3.76}$$

the derivative of the Lyapunov function becomes

$$\dot{V} = -\frac{1}{2}e^T Qe - \frac{1}{2\rho^2}e^T PBB^T Pe + e^T PBw_1 \tag{3.77}$$

which in turn is written as

$$\begin{array}{c} \dot{V} = -\frac{1}{2}e^T Qe - \frac{1}{2\rho^2}e^T PBB^T Pe + \\ +\frac{1}{2}e^T PBw_1 + \frac{1}{2}w_1^T B^T Pe \end{array} \tag{3.78}$$

The following Lemma is now used:
Lemma: The following inequality holds:

$$\frac{1}{2}e^T PBw_1 + \frac{1}{2}w_1^T B^T Pe - \frac{1}{2\rho^2}e^T PBB^T Pe \leq \frac{1}{2}\rho^2 w_1^T w_1 \tag{3.79}$$

Proof: The binomial $(\rho a - \frac{1}{\rho}b)^2 \geq 0$ is considered. Expanding the left part of the above inequality one gets

$$\begin{array}{c} \rho^2 a^2 + \frac{1}{\rho^2}b^2 - 2ab \geq 0 \Rightarrow \frac{1}{2}\rho^2 a^2 + \frac{1}{2\rho^2}b^2 - ab \geq 0 \Rightarrow \\ ab - \frac{1}{2\rho^2}b^2 \leq \frac{1}{2}\rho^2 a^2 \Rightarrow \frac{1}{2}ab + \frac{1}{2}ab - \frac{1}{2\rho^2}b^2 \leq \frac{1}{2}\rho^2 a^2 \end{array} \tag{3.80}$$

The following substitutions are carried out: $a = w_1$ and $b = e^T PB$ and the previous relation becomes

$$\begin{array}{c} \frac{1}{2}w_1^T B^T Pe + \frac{1}{2}e^T PBw_1 - \\ -\frac{1}{2\rho^2}e^T PBB^T Pe \leq \frac{1}{2}\rho^2 w_1^T w_1 \end{array} \tag{3.81}$$

The previous inequality is used in $\dot{V}$, and the right part of the associated inequality is enforced

$$\dot{V} \leq -\frac{1}{2}e^T Qe + \frac{1}{2}\rho^2 w_1^T w_1 \tag{3.82}$$

Equation (3.82) can be used to show that the H_∞ performance criterion is satisfied. The integration of $\dot{V}$ from 0 to T gives

$$\begin{array}{c} \int_0^T \dot{V}(t)dt \leq -\frac{1}{2}\int_0^T ||e||^2 dt + \frac{1}{2}\rho^2 \int_0^T ||w_1||^2 dt \Rightarrow \\ 2V(T) + \int_0^T ||e||_Q^2 dt \leq 2V(0) + \rho^2 \int_0^T ||w_1||^2 dt \end{array} \tag{3.83}$$

Moreover, if there exists a positive constant $M_w > 0$ such that

$$\int_0^\infty ||w_1||^2 dt \leq M_w \tag{3.84}$$

then one gets

$$\int_0^\infty ||e||_Q^2 dt \leq 2V(0) + \rho^2 M_w \tag{3.85}$$

Thus, the integral $\int_0^\infty ||e||_Q^2 dt$ is bounded and according to Barbalat's Lemma one obtains $lim_{t\to\infty} e(t) = 0$.

3.2.5.2 Riccati Equation Coefficients in H_∞ Control Robustness

The linearized tracking error dynamics of the robotic manipulator in Eq. (3.61) is considered again, i.e.

$$\dot{e} = (A - BK^T)e + Bu_c + B(w + \tilde{d})$$

The aim of H_∞ control is to eliminate the impact of the modelling errors $w = [f(x,t) - \hat{f}(x,t)] + [g(x,t) - \hat{g}(x,t)]u$ and the external disturbances $\tilde{d}$ which are not white noise signals. This implies the minimization of the quadratic cost function [243, 305]:

$$\begin{array}{c} J(t) = \frac{1}{2}\int_0^T e^T(t)e(t) + ru_c^T(t)u_c(t) - \\ -\rho^2(w + \tilde{d})^T(w + \tilde{d})dt, \quad r, \rho > 0 \end{array} \tag{3.86}$$

The weight r determines how much the control signal should be penalized and the weight ρ determines how much the disturbances influence should be rewarded in the sense of a min-max differential game. The H_∞ control law is $u(t) = -\frac{1}{r}B^T P e(t)$ where P is the positive definite symmetric matrix derived from the algebraic Riccati equation Eq. (3.64).

The parameter ρ in Eq. (3.86), is an indication of the closed-loop system robustness. If the values of $\rho > 0$ are excessively decreased with respect to r, then the solution of the Riccati equation is no longer a positive definite matrix. Consequently there is a lower bound ρ_{min} of ρ for which the H_∞ control problem has a solution. The acceptable values of ρ lie in the interval $[\rho_{min}, \infty)$. If ρ_{min} is found and used in the design of the H_∞ controller, then the closed-loop system will have elevated

robustness. Otherwise, if a value $\rho > \rho_{min}$ is used, then an admissible stabilizing H_∞ controller will be derived but it will be a suboptimal one. The Hamiltonian matrix

$$H = \begin{pmatrix} A & -(\frac{2}{r} - \frac{1}{\rho^2})BB^T \\ -Q & -A^T \end{pmatrix} \tag{3.87}$$

provides a criterion for the existence of a solution of the Riccati equation Eq. (3.64). A necessary condition for the solution of the algebraic Riccati equation to be a positive semi-definite symmetric matrix is that H has no imaginary eigenvalues [132, 459].

3.2.6 Simulation Tests

The performance of the proposed flatness-based adaptive fuzzy MIMO controller was tested in the previously analyzed model of the 2-DOF rigid-link robotic manipulator (Fig. 3.1). The control loop is depicted in Fig. 3.2. The differentially flat model of the robot and its transformation to the Brunovksy form has been analyzed in Sect. 3.3.5. The flat outputs were taken to be the robot's joint angles $y_1 = x_1$ and $y_2 = x_3$. It has been proven that all state variables of the robotic model and the associated control inputs, i.e. the torques applied by the motors to the links' joints can be written as functions of the flat output $[y_1, y_2]$ and of the associated derivatives.

The state feedback gain was $K \in R^{2\times 4}$. The basis functions used in the estimation of $f_i(x,t),\ i = 1, 2$ and $g_{ij}(x,t),\ i = 1, 2,\ j = 1, 2$ were $\mu_{A_j}(\hat{x}) = e^{(\frac{\hat{x}-c_j}{\sigma})^2}, j = 1, \ldots, 3$. Since there are four inputs x_1, $\dot{x}_1$ and x_2, $\dot{x}_2$ and their range of variation comprises 3 fuzzy sets, for the approximation of functions $f_i(x,t)\ i = 1, 2$, there will be 81 fuzzy rules of the form:

$$\begin{aligned} &R^l : IF\ \ x_1\ \ is\ \ A_1^l\ \ AND\ \ \dot{x}_1\ \ is\ \ A_2^l \\ &AND\ \ x_3\ \ is\ \ A_3^l\ \ AND\ \ \dot{x}_3\ \ is\ \ A_4^l\ \ THEN\ \ \hat{f}_i^l\ \ is\ \ b^l \end{aligned} \tag{3.88}$$

and $\hat{f}_i(x,t) = \frac{\sum_{l=1}^{81} \hat{f}_i^l \prod_{i=1}^{4} \mu_{A_i}^l(x_i)}{\sum_{l=1}^{81} \prod_{i=1}^{4} \mu_{A_i}^l(x_i)}$. The centers $c_i^{(l)},\ i = 1, \ldots, 4$ and the variances $v^{(l)}$ of each rule are as follows (Table 3.1)

In the considered fuzzy rule-base there are four input parameters in the antecedent parts of the fuzzy rules, i.e. $x_1 = \theta_1, x_2 = \dot{\theta}_1, x_3 = \theta_2$ and $x_4 = \dot{\theta}_4$. Each parameter is partitioned into 3 fuzzy sets. Therefore by taking all possible combinations between the fuzzy sets one has $3^4 = 81$ fuzzy rules. The finer the partition of the input variables into fuzzy sets is, the more accurate the approximation of the nonlinear system dynamics by the neuro-fuzzy model is expected to be (although some of the rules of the fuzzy rule base may not be sufficiently activated due to little coverage of the associated region of the patterns space by input data). However, considering a large number of fuzzy sets for each input variable induces the curse of dimensionality which means that there is an excessive and rather unnecessary increase in the number of the adaptable parameters that constitute the neuro-fuzzy model.

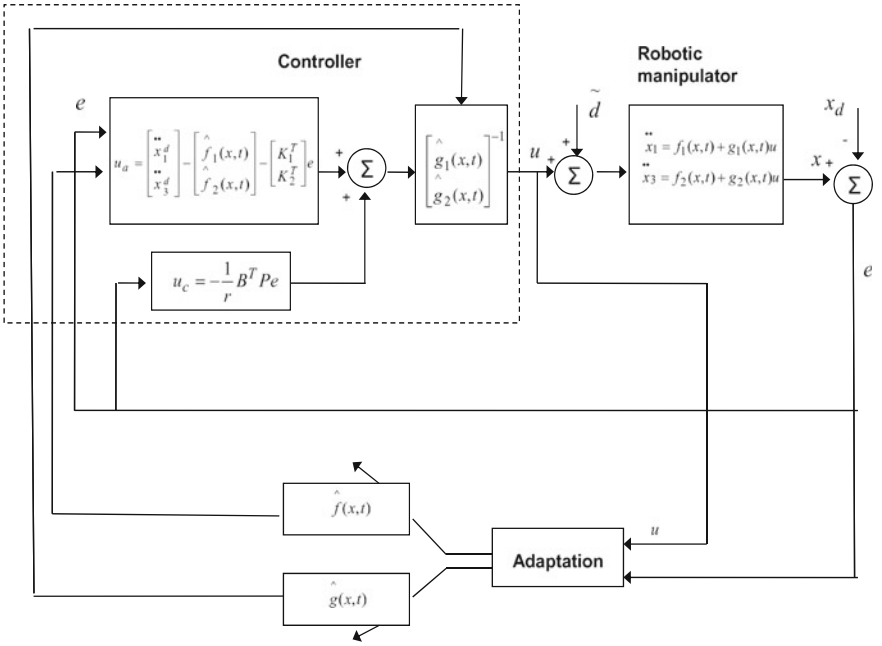

Fig. 3.2 Flatness-based adaptive-fuzzy control loop for the robotic manipulator

Table 3.1 Parameters of the fuzzy rule base

Rule	$c_1^{(l)}$	$c_2^{(l)}$	$c_3^{(l)}$	$c_4^{(l)}$	$v^{(l)}$
$R^{(1)}$	−1.0	−1.0	−1.0	−0.5	3
$R^{(2)}$	−1.0	−1.0	−1.0	0.0	3
$R^{(3)}$	−1.0	−1.0	−1.0	−1.0	3
$R^{(4)}$	−1.0	−1.0	0.0	−0.5	3
$R^{(5)}$	−1.0	−1.0	0.0	0.0	3
$R^{(6)}$	−1.0	−1.0	0.0	0.5	3
...	...	...	...	...	...
...	...	...	...	...	...
$R^{(81)}$	1.0	1.0	1.0	0.5	3

The estimation of the control input gain functions $\hat{g}_{ij}(x, t)$ $i = 1, 2$ was derived in a similar way. The overall simulation time was $t_s = 40$ s. The time step was taken to be 0.01 s. In the beginning of the training of the neuro-fuzzy approximators their weights were initialized to zero. Moreover, the elements of the robot's state vector were also initialized to zero. The positive definite matrix $P \in R^{4\times4}$ stems from the solution of the algebraic Riccati equation (3.64), for Q also positive definite.

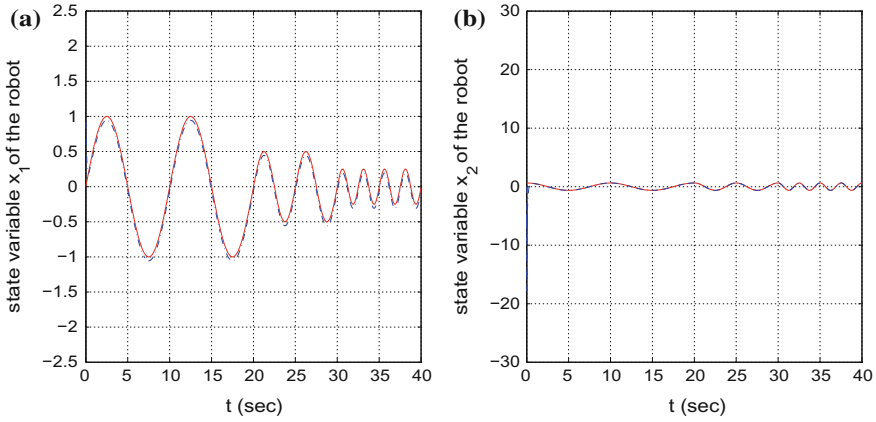

Fig. 3.3 **a** Tracking of a sinusoidal position set-point by joint 1 of the robot, **b** Tracking of sinusoidal velocity setpoint by joint 1 of the robot

Tracking of two different setpoints is demonstrated: (i) a sinusoidal signal of variable amplitude and frequency, (ii) a see-saw set-point of amplitude 0.30 and period $T = 20$ s. The approximations $\hat{f}$ and $\hat{g}$ were used in the derivation of the control law, given by Eq. (3.21). To show the disturbance rejection capability of the proposed adaptive fuzzy controller, at the beginning of the second half of the simulation time additive sinusoidal disturbances of amplitude $A = 0.5$ and period $T = 10$ s were applied to the robot's joints. The external disturbances which appear as additive torques to the robot's joints can be due to a force F exerted on the manipulator's end-effector (e.g. due to contact with a surface) and which through the relation $T = J^T F$ (J stands for the Jacobian matrix of the robot's kinematic model) generates torques on the joints.

In the simulation results that follow the position and velocity setpoints are noted as continuous lines while the position and velocity signals of the robot's joints are denoted as dashed lines. The position and velocity variation for the first joint of the robotic manipulator when tracking a sinusoidal set-point is depicted in Fig. 3.3. For the second joint of the 2-DOF robot the tracking of the position and velocity setpoint is depicted in Fig. 3.4. The control inputs (motor torques) applied to the first and second joint of the robotic manipulator are shown in Fig. 3.5.

The performance of the proposed flatness-based adaptive fuzzy control is also tested in the tracking of a see-saw set-point. This is a reference signal characterized by discontinuities. It serves as a good example for testing the accuracy of tracking of the proposed adaptive fuzzy control scheme and its stabilization features in case of set-points that exhibit abrupt variations. It is shown that after suitable tuning of the feedback gain matrix K defined in Eq. (3.44) precise tracking of the see-saw setpoint can be achieved, with fast elimination of the tracking error. The controller is also suitable for compensating the effects of the additive torques disturbance that is applied to the robot's joints.

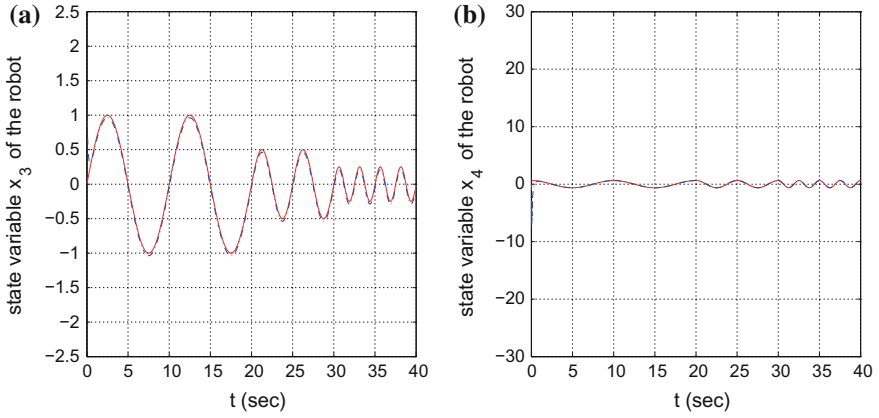

Fig. 3.4 **a** Tracking of a sinusoidal position set-point by joint 2 of the robot, **b** Tracking of sinusoidal velocity setpoint by joint 2 of the robot

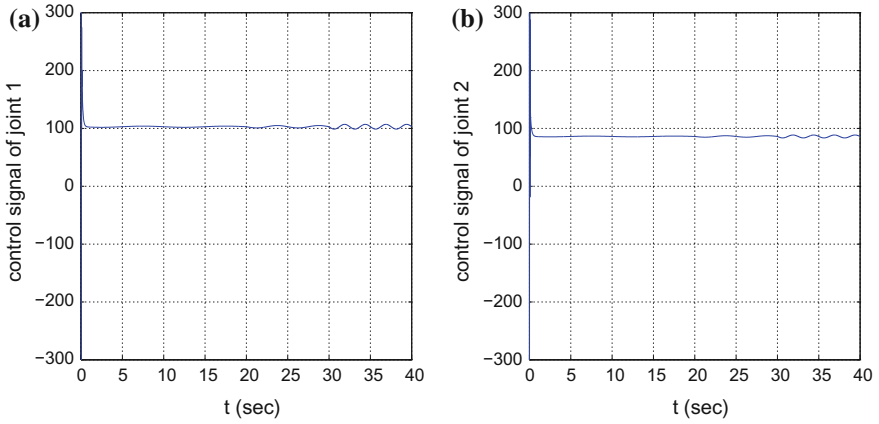

Fig. 3.5 **a** Tracking of a sinusoidal setpoint: Control input to joint 1, **b** Tracking of a sinusoidal setpoint: Control input to joint 2

The position and velocity variation of the first joint is demonstrated in Fig. 3.6. Similarly, the tracking of the position and velocity reference setpoint for the second joint is depicted in Fig. 3.7. The control signal in the case of tracking a see-saw setpoint by the two joints of the robotic manipulator is shown in Fig. 3.8.

Finally, the approximation of function $g_2^2(x, t)$ in the case of tracking of a sinusoidal and a seesaw setpoint is shown in Fig. 3.9 (and is marked as a dashed line).

The RMSE (root mean square error) of the examined control loop is also calculated (assuming the same parameters of the controller) in the case of tracking of previous setpoints (a) sinusoidal setpoint of variable amplitude/frequency and (b) seesaw setpoint. The results are summarized in Table 3.2. It can be observed that the examined

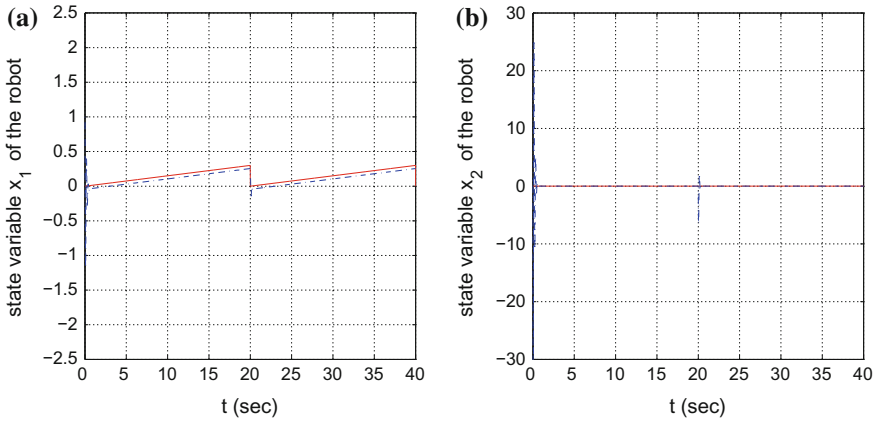

Fig. 3.6 **a** Tracking of a seesaw position set-point by joint 1 of the robot, **b** Tracking of seesaw velocity setpoint by joint 1 of the robot

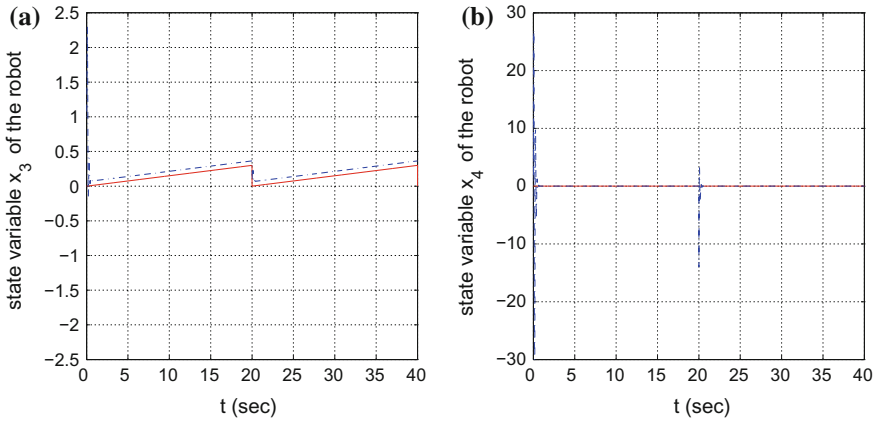

Fig. 3.7 **a** Tracking of a seesaw position set-point by joint 2 of the robot, **b** Tracking of seesaw velocity setpoint by joint 2 of the robot

controller, apart from elimination of the tracking error for the parameters of the robot's state vector achieves also good transient performance. Taking into account that no prior knowledge about the robot's dynamics has been used by the controller, and at the first iterations of the control loop the controller undergoes self-tuning (learning of values for specific gains) the transient characteristics of the control scheme can be also deemed as quite satisfactory.

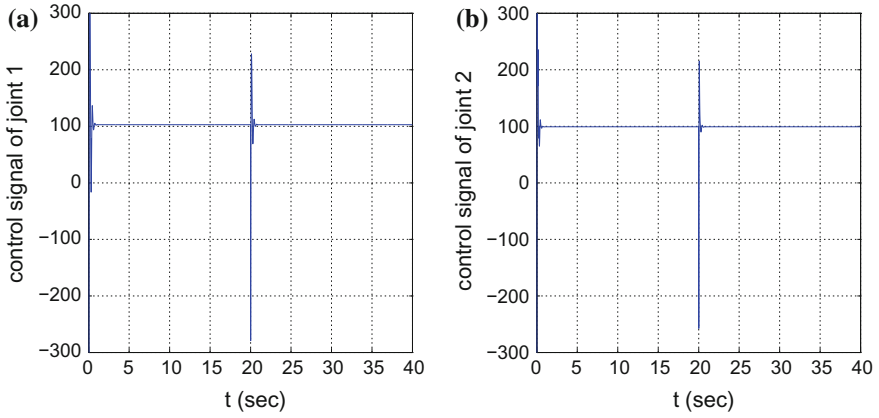

Fig. 3.8 **a** Tracking of a seesaw setpoint: Control input to joint 1, **b** Tracking of a seesaw setpoint: Control input to joint 2

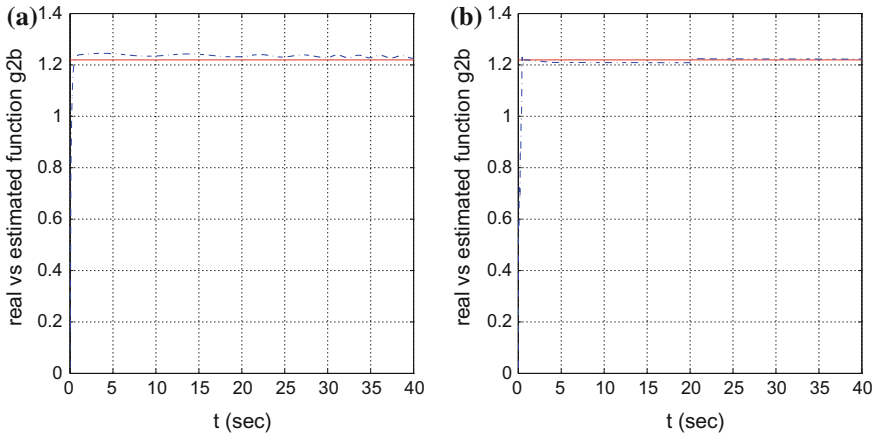

Fig. 3.9 **a** Approximation of function $g_2^2(x, t)$ when tracking a sinusoidal setpoint, **b** Approximation of function $g_2^2(x, t)$ when tracking a seesaw setpoint

Table 3.2 RMSE of joints' angles

parameter	θ_1	θ_2
$RMSE_a$	0.0085	0.0028
$RMSE_b$	0.0175	0.0145

3.3 Model-Free Adaptive Control of Rigid-Link Manipulators Using Output Feedback

3.3.1 Outline

The present section proposes a solution to the problem of observer-based adaptive fuzzy control for nonlinear robotic manipulators). The objective of this section is to design an adaptive fuzzy controller for multi-DOF robotic arms, under the constraint that only the system's output is measured, which is the joints' angles of the robot. The control algorithm aims at satisfying the H_∞ tracking performance criterion, which means that the influence of the modeling errors and the external disturbances on the tracking error is attenuated to an arbitrary desirable level. After transforming the MIMO robotic system into the canonical form, the resulting control inputs are shown to contain nonlinear elements which depend on the system's parameters. Since the parameters of the robot's dynamic model are unknown, then the nonlinear terms which appear in the control inputs have to be approximated with the use of neuro-fuzzy networks. Moreover, since only the system's output is measurable the complete state vector has to be reconstructed with the use of a state observer. In this section it is shown that a suitable learning law can be defined for the aforementioned neuro-fuzzy approximators so as to preserve the closed-loop system stability. Lyapunov stability analysis proves also that the proposed observer-based adaptive fuzzy control scheme results in H_∞ tracking performance, in accordance to the results of [436, 447, 457].

For the design of the observer-based adaptive fuzzy controller one has to solve two Riccati equations, where the first one is associated with the controller and the second one is associated with the observer. Parameters that affect the closed-loop robustness are: (i) the feedback gain vector K, (ii) the observer's gain vector K_o, (iii) the positive definite matrices P_1 and P_2 which stem from the solution of the two algebraic Riccati equations and which weigh the above mentioned observer and controller terms. The proposed control architecture guarantees that, the output of the closed-loop system will asymptotically track the desired trajectory and that H_∞ performance will be achieved.

3.3.2 Transformation of MIMO Robotic Systems into the Brunovsky Form

It is assumed once again that after defining the flat outputs of the initial MIMO nonlinear robotic system that was initially described in Sect. 1.3.4, and after expressing the system state variables and control inputs as functions of the flat output and of the associated derivatives, the system can be transformed in the Brunovsky canonical form:

$$\begin{aligned}
&\dot{x}_1 = x_2 \\
&\dot{x}_2 = x_3 \\
&\cdots \\
&\dot{x}_{r_1-1} = x_{r_1} \\
&\dot{x}_{r_1} = f_1(x) + \textstyle\sum_{j=1}^{p} g_{1_j}(x)u_j + d_1 \\
&\dot{x}_{r_1+1} = x_{r_1+2} \\
&\dot{x}_{r_1+2} = x_{r_1+3} \\
&\cdots \\
&\dot{x}_{p-1} = x_p \\
&\dot{x}_p = f_p(x) + \textstyle\sum_{j=1}^{p} g_{p_j}(x)u_j + d_p
\end{aligned} \qquad \begin{aligned}
&y_1 = x_1 \\
&\cdots \\
&y_i = x_{r_i} \\
&\cdots \\
&y_p = x_{n-r_p+1}
\end{aligned} \tag{3.89}$$

where $x = [x_1, \ldots, x_n]^T$ is the state vector of the transformed system (according to the differential flatness formulation), $u = [u_1, \ldots, u_p]^T$ is the set of control inputs, $y = [y_1, \ldots, y_p]^T$ is the output vector, f_i are the drift functions and $g_{i,j},\ i, j = 1, 2, \ldots, p$ are smooth functions corresponding to the control input gains, while d_j is a variable associated to external disturbances. In holds that $r_1 + r_2 + \cdots + r_p = n$. Having written the initial nonlinear robotic system into the canonical (Brunovsky) form it holds

$$y_i^{(r_i)} = f_i(x) + \textstyle\sum_{j=1}^{p} g_{ij}(x)u_j + d_j \tag{3.90}$$

Equivalently, in vector form, one has the following description for the system dynamics

$$y^{(r)} = f(x) + g(x)u + d \tag{3.91}$$

where the following vectors and matrices are be defined

$$\begin{aligned}
&y^{(r)} = [y_1^{(r_1)}, \ldots, y_p^{(r_p)}] \\
&f(x) = [f_1(x), \ldots, f_p(x)]^T \\
&g(x) = [g_1(x), \ldots, g_p(x)] \\
&with\ g_i(x) = [g_{1i}(x), \ldots, g_{pi}(x)]^T \\
&A = diag[A_1, \ldots, A_p],\quad B = diag[B_1, \ldots, B_p] \\
&C^T = diag[C_1, \ldots, C_p],\quad d = [d_1, \ldots, d_p]^T
\end{aligned} \tag{3.92}$$

while matrix A has the MIMO canonical form, i.e. with elements

$$A_i = \begin{pmatrix} 0 & 1 & \cdots & 0 \\ 0 & 0 & \cdots & 0 \\ \vdots & \vdots & \ldots & \vdots \\ 0 & 0 & \cdots & 1 \\ 0 & 0 & \cdots & 0 \end{pmatrix}_{r_i \times r_i} \qquad \begin{aligned} B_i^T &= \begin{pmatrix} 0 & 0 & \cdots & 0 & 1 \end{pmatrix}_{1 \times r_i} \\ C_i &= \begin{pmatrix} 1 & 0 & \cdots & 0 & 0 \end{pmatrix}_{1 \times r_i} \end{aligned} \tag{3.93}$$

Thus, as previously shown, Eq. (3.90) can be written in state-space form

$$\begin{array}{c} \dot{x} = Ax + B[f(x) + g(x)u + \tilde{d}] \\ y = C^T x \end{array} \tag{3.94}$$

which can be also written in the equivalent form:

$$\begin{array}{c} \dot{x} = Ax + Bv + B\tilde{d} \\ y = C^T x \end{array} \tag{3.95}$$

where $v = f(x) + g(x)u$. The reference setpoints for the system's outputs $y_1, \ldots, y_p$ are denoted as $y_{1m}, \ldots, y_{pm}$, thus for the associated tracking errors it holds

$$\begin{array}{c} e_1 = y_1 - y_{1m} \\ e_2 = y_2 - y_{2m} \\ \cdots \\ e_p = y_p - y_{pm} \end{array} \tag{3.96}$$

The error vector of the outputs of the transformed MIMO system is denoted as

$$\begin{array}{c} E_1 = [e_1, \ldots, e_p]^T \\ y_m = [y_{1m}, \ldots, y_{pm}]^T \\ \cdots \\ y_m^{(r)} = [y_{1m}^{(r)}, \ldots, y_{pm}^{(r)}]^T \end{array} \tag{3.97}$$

where $y_{im}^{(r)}$ denotes the rth order derivative of the ith reference output of the MIMO dynamical system, as analyzed in Sect. 3.2. Thus, one can also define the following vectors: (i) a vector containing the state variables of the system and the associated derivatives, (ii) a vector containing the reference outputs of the system and the associated derivatives

$$x = [x_1, \ldots, x_1^{r_1 - 1}, \ldots, x_p, \ldots, x_p^{r_p - 1}]^T \tag{3.98}$$

$$Y_m = [y_{1m}, \ldots, y_{1m}^{r_1 - 1}, \ldots, y_{pm}, \ldots, y_{pm}^{r_p - 1}]^T \tag{3.99}$$

while in a similar manner one can define a vector containing the tracking error of the system's outputs and the associated derivatives

$$e = Y_m - x = [e_1, \ldots, e_1^{r_1 - 1}, \ldots, e_p, \ldots, e_p^{r_p - 1}]^T \tag{3.100}$$

It is assumed that matrix $g(x)$ is a nonsingular one, i.e. $g^{-1}(x)$ exists and is bounded for all $x \in U_x$, where $U_x \subset R^n$ is a compact set. In any case, the problem of singularities in matrix $g(x)$ can be handled by appropriately modifying the state feedback-based control input.

The objective of the adaptive fuzzy controller, denoted as $u = u(x, e|\theta)$ is: all the signals involved in the controller's design are bounded and it holds that $lim_{t\to\infty} e = 0$, (ii) the H_∞ tracking performance criterion is achieved for a prescribed attenuation level.

In the presence of non-gaussian disturbances w_d, successful tracking of the reference signal is denoted by the H_∞ criterion [436, 561]:

$$\int_0^T e^T Q e dt \leq \rho^2 \int_0^T {w_d}^T w_d dt \tag{3.101}$$

where ρ is the attenuation level and corresponds to the maximum singular value of the transfer function $G(s)$ of the linearized model associated to Eqs. (3.94) and (3.95).

3.3.3 Control Law

The control signal of the MIMO nonlinear robotic system which has been transformed into the Brunovsky form as described by Eq. (3.95) contains the unknown nonlinear functions $f(x)$ and $g(x)$. As explained in Sect. 2.2, in case that the complete state vector x is measurable these unknown functions can be approximated by

$$\begin{aligned} \hat{f}(x|\theta_f) &= \Phi_f(x)\theta_f \\ \hat{g}(x|\theta_g) &= \Phi_g(x)\theta_g \end{aligned} \tag{3.102}$$

where

$$\Phi_f(x) = (\xi_f^1(x), \xi_f^2(x), \ldots \xi_f^n(x))^T \tag{3.103}$$

with $\xi_f^i(x), \imath = 1, \ldots, n$ being the vector of kernel functions (e.g. normalized fuzzy Gaussian membership functions), where

$$\xi_f^i(x) = (\phi_f^{i,1}(x), \phi_f^{i,2}(x), \cdots, \phi_f^{i,N}(x)) \tag{3.104}$$

thus giving

$$\Phi_f(x) = \begin{pmatrix} \phi_f^{1,1}(x) & \phi_f^{1,2}(x) & \cdots & \phi_f^{1,N}(x) \\ \phi_f^{2,1}(x) & \phi_f^{2,2}(x) & \cdots & \phi_f^{2,N}(x) \\ \cdots & \cdots & \cdots & \cdots \\ \phi_f^{n,1}(x) & \phi_f^{n,2}(x) & \cdots & \phi_f^{n,N}(x) \end{pmatrix} \tag{3.105}$$

while the weights vector is defined as

$$\theta_f{}^T = \left(\theta_f^1, \theta_f^2, \ldots \theta_f^N\right) \tag{3.106}$$

$j = 1, \ldots, N$ is the number of basis functions that is used to approximate the components of function f which are denoted as $i = 1, \ldots, n$. Thus, one obtains the relation of Eq. (3.102), i.e. $\hat{f}(x|\theta_f) = \Phi_f(x)\theta_f$.

In a similar manner, for the approximation of function g one has

$$\Phi_g(x) = \left(\xi_g^1(x), \xi_g^2(x), \ldots \xi_g^N(x)\right)^T \tag{3.107}$$

with $\xi_g^i(x), \imath = 1, \ldots, N$ being the vector of kernel functions (e.g. normalized fuzzy Gaussian membership functions), where

$$\xi_g^i(x) = \left(\phi_g^{i,1}(x), \phi_g^{i,2}(x), \ldots, \phi_g^{i,N}(x)\right) \tag{3.108}$$

thus giving

$$\Phi_g(x) = \begin{pmatrix} \phi_g^{1,1}(x) & \phi_g^{1,2}(x) & \cdots & \phi_g^{1,N}(x) \\ \phi_g^{2,1}(x) & \phi_g^{2,2}(x) & \cdots & \phi_g^{2,N}(x) \\ \cdots & \cdots & \cdots & \cdots \\ \phi_g^{n,1}(x) & \phi_g^{n,2}(x) & \cdots & \phi_g^{n,N}(x) \end{pmatrix} \tag{3.109}$$

while the weights vector is defined as

$$\theta_g = \left(\theta_g^1, \theta_g^2, \ldots, \theta_g^p\right) \tag{3.110}$$

where the components of matrix θ_g are defined as

$$\theta_g^j = \left(\theta_{g_1}^j, \theta_{g_2}^j, \ldots \theta_{g_N}^j\right)^T \tag{3.111}$$

$j = 1, \ldots, p$ is the number of basis functions that is used to approximate the components of function g which are denoted as $i = 1, \ldots, n$. Thus one obtains about matrix $\theta_g \in R^{N \times p}$

$$\theta_g = \begin{pmatrix} \theta_{g_1}^1 & \theta_{g_1}^2 & \cdots & \theta_{g_1}^p \\ \theta_{g_2}^1 & \theta_{g_2}^2 & \cdots & \theta_{g_2}^p \\ \cdots & \cdots & \cdots & \cdots \\ \theta_{g_N}^1 & \theta_{g_N}^2 & \cdots & \theta_{g_N}^p \end{pmatrix} \tag{3.112}$$

It holds that

$$g = \begin{pmatrix} g_1 \\ g_2 \\ \cdots \\ g_n \end{pmatrix} = \begin{pmatrix} g_1^1 & g_1^2 & \cdots & g_1^p \\ g_2^1 & g_2^2 & \cdots & g_2^p \\ \cdots & \cdots & \cdots & \cdots \\ g_n^1 & g_n^2 & \cdots & g_n^p \end{pmatrix} \tag{3.113}$$

Using the above, one finally has the relation of Eq. (3.102), i.e. $\hat{g}(x|\theta_g) = \Phi_g(x)\theta_g$. If the state variables of the system are available for measurement then a state-feedback control law can be formulated as

$$u = \hat{g}^{-1}(x|\theta_g)[-\hat{f}(x|\theta_f) + y_m^{(r)} - K^T e + u_c] \tag{3.114}$$

where $\hat{f}(x|\theta_f)$ and $\hat{g}(x|\theta_g)$ are fuzzy models to approximate $f(x)$ and $g(x)$, respectively. u_c is a supervisory control term, e.g. H_∞ control term that is used to compensate for the effects of modelling inaccuracies and external disturbances. Moreover, K^T is the feedback gain matrix that assures that the characteristic polynomial of matrix $A - BK^T$ will be a Hurwitz one.

3.3.4 *Estimation of the State Vector*

The control of the system described by Eq. (3.91) becomes more complicated when the state vector x of the robotic manipulator is not directly measurable and has to be reconstructed through a state observer. The following definitions are used

- error of the state vector $e = x - x_m$
- error of the estimated state vector $\hat{e} = \hat{x} - x_m$
- observation error $\tilde{e} = e - \hat{e} = (x - x_m) - (\hat{x} - x_m)$

When an observer is used to reconstruct the state vector, the control law of Eq. (3.114) is written as

$$u = \hat{g}^{-1}(\hat{x}|\theta_g)[-\hat{f}(\hat{x}|\theta_f) + y_m^{(r)} - K^T \hat{e} + u_c] \tag{3.115}$$

Applying Eq. (3.115) to the nonlinear system described by Eq. (3.91), results into

$$\begin{gathered} y^{(r)} = f(x) + g(x)\hat{g}^{-1}(\hat{x})[-\hat{f}(\hat{x}) + y_m^{(r)} - K^T\hat{e} + u_c] + d \Rightarrow \\ y^{(r)} = f(x) + [g(x) - \hat{g}(\hat{x}) + \hat{g}(\hat{x})]\hat{g}^{-1}(\hat{x})[-\hat{f}(\hat{x}) + y_m^{(r)} - K^T\hat{e} + u_c] + d \Rightarrow \\ y^{(r)} = [f(x) - \hat{f}(\hat{x})] + [g(x) - \hat{g}(\hat{x})]u + y_m^{(r)} - K^T\hat{e} + u_c + d \end{gathered} \tag{3.116}$$

It holds $e = x - x_m \Rightarrow y^{(r)} = e^{(r)} + y_m^{(r)}$. Substituting $y^{(r)}$ in the above equation gives

$$e^{(r)} + y_m^{(r)} = y_m^{(r)} - K^T\hat{e} + u_c + [f(x) - \hat{f}(\hat{x})] + \\ + [g(x) - \hat{g}(\hat{x})]u + d \tag{3.117}$$

and equivalently

$$\dot{e} = Ae - BK^T\hat{e} + Bu_c + B\{[f(x) - \hat{f}(\hat{x})] + \\ + [g(x) - \hat{g}(\hat{x})]u + \tilde{d}\} \tag{3.118}$$

$$e_1 = C^T e \tag{3.119}$$

where $e = [e^1, e^2, \ldots, e^p]^T$ with $e^i = [e_i, \dot{e}_i, \ddot{e}_i, \ldots, e_i^{r_i-1}]^T$, $i = 1, 2, \ldots, p$ and equivalently $\hat{e} = [\hat{e}^1, \hat{e}^2, \ldots, \hat{e}^p]^T$ with $\hat{e}^i = [\hat{e}_i, \hat{\dot{e}}_i, \hat{\ddot{e}}_i, \ldots, \hat{e}_i^{r_i-1}]^T$, $i = 1, 2, \ldots, p$. Matrices A, B and C have been defined in Eq. (3.93).

A state observer is designed according to Eqs. (3.118) and (3.119) and is given by [561]:

$$\dot{\hat{e}} = A\hat{e} - BK^T\hat{e} + K_o[e_1 - C^T\hat{e}] \tag{3.120}$$

$$\hat{e}_1 = C^T\hat{e} \tag{3.121}$$

The feedback gain matrix is denoted as $K \in R^{n\times p}$. The observation gain matrix is denoted as $K_o \in R^{n\times p}$ and its elements are selected so as to assure the asymptotic elimination of the observation error.

3.3.5 *Application of Observer-Based Adaptive Fuzzy Control to Robotic Systems*

As shown in the previous section, for the 2-DOF rigid-link robotic manipulator, it holds that

$$\begin{aligned} \ddot{x}_1 &= f_1(x) + g_1(x)u \\ \ddot{x}_3 &= f_2(x) + g_2(x)u \end{aligned} \tag{3.122}$$

where

$$\begin{aligned} f_1(x) &= -N_{11}F_1(\theta, \dot{\theta}) - N_{12}F_2(\theta, \dot{\theta}) - \\ &\quad -N_{11}G_1(\theta) - N_{12}G_2(\theta) \in R^{1\times 1} \\ g_1(x) &= [N_{11}\ N_{12}] \in R^{1\times 2} \\ f_2(x) &= -N_{21}F_2(\theta, \dot{\theta}) - N_{22}F_2(\theta, \dot{\theta}) - \\ &\quad -N_{21}G_1(\theta) - N_{22}G_2(\theta) \in R^{1\times 1} \\ g_2(x) &= [N_{21}\ N_{22}] \in R^{2\times 2} \end{aligned} \tag{3.123}$$

The flat output is defined as

$$y = [\theta_1, \theta_2] = [x_1, x_3] \tag{3.124}$$

It holds that

$$\begin{aligned} \dot{x}_1 &= x_2 \\ \dot{x}_2 &= f_1(x) + g_1(x)u \\ \dot{x}_3 &= x_4 \\ \dot{x}_4 &= f_2(x) + g_2(x)u \end{aligned} \tag{3.125}$$

therefore all system state variables can be written as functions of the flat output y and its derivatives. The same holds for the control input u

$$\begin{aligned} x_1 &= [1\ 0]y^T \ x_2 = [1\ 0]\dot{y}^T \\ x_3 &= [0\ 1]y^T \ x_4 = [0\ 1]\dot{y}^T \end{aligned} \tag{3.126}$$

Moreover, from Eq. (3.125) it holds

$$\begin{aligned} \begin{pmatrix} \ddot{x}_1 \\ \ddot{x}_3 \end{pmatrix} &= \begin{pmatrix} f_1(x) \\ f_2(x) \end{pmatrix} + \begin{pmatrix} g_1(x) \\ g_2(x) \end{pmatrix} u \ i.e. \\ u &= \begin{pmatrix} g_1(x) \\ g_2(x) \end{pmatrix}^{-1} \left\{ \begin{pmatrix} \ddot{x}_1 \\ \ddot{x}_3 \end{pmatrix} - \begin{pmatrix} f_1(x) \\ f_2(x) \end{pmatrix} \right\} \end{aligned} \tag{3.127}$$

Knowing that $x = h(y, \dot{y})$ one finally obtains

$$u = \begin{pmatrix} g_1(h(y,\dot{y})) \\ g_2(h(y,\dot{y})) \end{pmatrix}^{-1} \left\{ \begin{pmatrix} [1\ 0]\ddot{y}^T \\ [0\ 1]\ddot{y}^T \end{pmatrix} - \begin{pmatrix} f_1(h(y,\dot{y})) \\ f_2(h(y,\dot{y})) \end{pmatrix} \right\} \tag{3.128}$$

Therefore, as already proven in the previous section, the considered robotic system is a differentially flat one. Next, taking into account also the effects of additive disturbances to the joints of the robotic manipulator the dynamic model becomes

$$\begin{aligned} \ddot{x}_1 &= f_1(x,t) + g_1(x,t)u + d_1 \\ \ddot{x}_3 &= f_2(x,t) + g_2(x,t)u + d_2 \end{aligned} \tag{3.129}$$

$$\begin{pmatrix} \ddot{x}_1 \\ \ddot{x}_3 \end{pmatrix} = \begin{pmatrix} f_1(x,t) \\ f_2(x,t) \end{pmatrix} + \begin{pmatrix} g_1(x,t) \\ g_2(x,t) \end{pmatrix} u + \begin{pmatrix} d_1 \\ d_2 \end{pmatrix} \tag{3.130}$$

The stabilizing control input for the robot dynamics will be now generated using the estimated value for the nonlinear functions $\hat{f}$ and $\hat{g}$. The following control input is defined

$$u = \begin{pmatrix} \hat{g}_1(x,t) \\ \hat{g}_2(x,t) \end{pmatrix}^{-1} \{ \begin{pmatrix} \ddot{x}_1^d \\ \ddot{x}_3^d \end{pmatrix} - \begin{pmatrix} \hat{f}_1(x,t) \\ \hat{f}_2(x,t) \end{pmatrix} - \begin{pmatrix} K_1^T \\ K_2^T \end{pmatrix} e + \begin{pmatrix} u_{c_1} \\ u_{c_2} \end{pmatrix} \} \tag{3.131}$$

where $[u_{c_1}\ u_{c_2}]^T$ is a robust control term that is used for the compensation of the model's uncertainties as well as of the external disturbances, and the rows of the feedback gain matrix K are $K_i^T = [k_1^i, k_2^i, \ldots, k_{n-1}^i, k_n^i]$. Substituting Eq. (3.131) into (3.130) the closed-loop tracking error dynamics is obtained

$$\begin{pmatrix} \ddot{x}_1 \\ \ddot{x}_3 \end{pmatrix} = \begin{pmatrix} f_1(x,t) \\ f_2(x,t) \end{pmatrix} + \begin{pmatrix} g_1(x,t) \\ g_2(x,t) \end{pmatrix} \begin{pmatrix} \hat{g}_1(x,t) \\ \hat{g}_2(x,t) \end{pmatrix}^{-1} \cdot \cdot \left\{ \begin{pmatrix} \ddot{x}_1^d \\ \ddot{x}_3^d \end{pmatrix} - \begin{pmatrix} \hat{f}_1(x,t) \\ \hat{f}_2(x,t) \end{pmatrix} - \begin{pmatrix} K_1^T \\ K_2^T \end{pmatrix} e + \begin{pmatrix} u_{c_1} \\ u_{c_2} \end{pmatrix} \right\} + \begin{pmatrix} d_1 \\ d_2 \end{pmatrix} \tag{3.132}$$

Equation (3.132) can now be written as

$$\begin{pmatrix} \ddot{x}_1 \\ \ddot{x}_3 \end{pmatrix} = \begin{pmatrix} f_1(x,t) \\ f_2(x,t) \end{pmatrix} + \{ \begin{pmatrix} g_1(x,t) - \hat{g}_1(x,t) \\ g_2(x,t) - \hat{g}_2(x,t) \end{pmatrix} + + \begin{pmatrix} \hat{g}_1(x,t) \\ \hat{g}_2(x,t) \end{pmatrix} \} \begin{pmatrix} \hat{g}_1(x,t) \\ \hat{g}_2(x,t) \end{pmatrix}^{-1} \cdot \left\{ \begin{pmatrix} \ddot{x}_1^d \\ \ddot{x}_3^d \end{pmatrix} - \begin{pmatrix} \hat{f}_1(x,t) \\ \hat{f}_2(x,t) \end{pmatrix} - \begin{pmatrix} K_1^T \\ K_2^T \end{pmatrix} e + \begin{pmatrix} u_{c_1} \\ u_{c_2} \end{pmatrix} \right\} + \begin{pmatrix} d_1 \\ d_2 \end{pmatrix} \tag{3.133}$$

and using Eq. (3.131) this results into

$$\begin{pmatrix} \ddot{e}_1 \\ \ddot{e}_3 \end{pmatrix} = \begin{pmatrix} f_1(x,t) - \hat{f}_1(x,t) \\ f_2(x,t) - \hat{f}_2(x,t) \end{pmatrix} + \begin{pmatrix} g_1(x,t) - \hat{g}_1(x,t) \\ g_2(x,t) - \hat{g}_2(x,t) \end{pmatrix} u - - \begin{pmatrix} K_1^T \\ K_2^T \end{pmatrix} e + \begin{pmatrix} u_{c_1} \\ u_{c_2} \end{pmatrix} + \begin{pmatrix} d_1 \\ d_2 \end{pmatrix} \tag{3.134}$$

The following description for the approximation error is defined

$$w = \begin{pmatrix} f_1(x,t) - \hat{f}_1(x,t) \\ f_2(x,t) - \hat{f}_2(x,t) \end{pmatrix} + \begin{pmatrix} g_1(x,t) - \hat{g}_1(x,t) \\ g_2(x,t) - \hat{g}_2(x,t) \end{pmatrix} u \tag{3.135}$$

Moreover, the following matrices are defined

$$A = \begin{pmatrix} 0\ 1\ 0\ 0 \\ 0\ 0\ 0\ 0 \\ 0\ 0\ 0\ 1 \\ 0\ 0\ 0\ 0 \end{pmatrix}, \quad B = \begin{pmatrix} 0\ 0 \\ 1\ 0 \\ 0\ 0 \\ 0\ 1 \end{pmatrix}$$
$$K^T = \begin{pmatrix} K_1^1 & K_2^1 & K_3^1 & K_4^1 \\ K_1^2 & K_2^2 & K_3^2 & K_4^2 \end{pmatrix} \tag{3.136}$$

Using matrices A, B, K^T, Eq. (3.134) is written in the following form

$$\begin{aligned}\dot{e} = (A - BK^T)e + Bu_c + B\{&\begin{pmatrix} f_1(x,t) - \hat{f}_1(x,t) \\ f_2(x,t) - \hat{f}_2(x,t) \end{pmatrix} + \\ &+ \begin{pmatrix} g_1(x,t) - \hat{g}_1(x,t) \\ g_2(x,t) - \hat{g}_2(x,t) \end{pmatrix} u + \tilde{d}\}\end{aligned} \tag{3.137}$$

When the estimated state vector $\hat{x}$ is used in the feedback control loop, equivalently to Eq. (3.118) one has

$$\begin{aligned}\dot{e} = Ae - BK^T\hat{e} + Bu_c + B\Bigg\{&\begin{pmatrix} f_1(x,t) - \hat{f}_1(\hat{x},t) \\ f_2(x,t) - \hat{f}_2(\hat{x},t) \end{pmatrix} + \\ &+ \begin{pmatrix} g_1(x,t) - \hat{g}_1(\hat{x},t) \\ g_2(x,t) - \hat{g}_2(\hat{x},t) \end{pmatrix} u + \tilde{d}\Bigg\}\end{aligned} \tag{3.138}$$

and considering that the approximation error w is now denoted as

$$w = \begin{pmatrix} f_1(x,t) - \hat{f}_1(\hat{x},t) \\ f_2(x,t) - \hat{f}_2(\hat{x},t) \end{pmatrix} + \begin{pmatrix} g_1(x,t) - \hat{g}_1(\hat{x},t) \\ g_2(x,t) - \hat{g}_2(\hat{x},t) \end{pmatrix} u \tag{3.139}$$

Equation (3.138) can be also written as

$$\dot{e} = Ae - BK^T\hat{e} + Bu_c + Bw + B\tilde{d} \tag{3.140}$$

The associated state observer will be described again by Eqs. (3.120) and (3.121).

3.3.6 *Dynamics of the Observation Error*

The observation error is defined as $\tilde{e} = e - \hat{e} = x - \hat{x}$. Substructing Eq. (3.120) from (3.118) as well as Eq. (3.121) from (3.119) one gets

$$\begin{gathered}\dot{e} - \dot{\hat{e}} = A(e - \hat{e}) + Bu_c + B\{[f(x,t) - \hat{f}(\hat{x},t)] + \\ + [g(x,t) - \hat{g}(\hat{x},t)]u + \tilde{d}\} - K_o C^T(e - \hat{e}) \\ e_1 - \hat{e}_1 = C^T(e - \hat{e})\end{gathered}$$

or equivalently

$$\begin{gathered}\dot{\tilde{e}} = A\tilde{e} + Bu_c + B\{[f(x,t) - \hat{f}(\hat{x},t)] + [g(x,t) - \hat{g}(\hat{x},t)]u + \tilde{d}\} - K_o C^T\tilde{e} \\ \tilde{e}_1 = C^T\tilde{e}\end{gathered}$$

which can be written as

$$\dot{\tilde{e}} = (A - K_o C^T)\tilde{e} + Bu_c + B\{[f(x,t) - \hat{f}(\hat{x},t)] + [g(x,t) - \hat{g}(\hat{x},t)]u + \tilde{d}\} \tag{3.141}$$

$$\tilde{e}_1 = C^T \tilde{e} \tag{3.142}$$

or equivalently, it can be written as

$$\dot{\tilde{e}} = (A - K_o C^T)\tilde{e} + Bu_c + Bw + \tilde{d} \tag{3.143}$$

$$\tilde{e}_1 = C^T \tilde{e}. \tag{3.144}$$

3.3.7 Approximation of Unknown System's Dynamics

Next, the following approximators of the unknown system dynamics are defined

$$\hat{f}(\hat{x}) = \begin{pmatrix} \hat{f}_1(\hat{x}|\theta_f)\ \hat{x} \in R^{4\times 1}\ \hat{f}_1(\hat{x}|\theta_f)\ \in\ R^{1\times 1} \\ \hat{f}_2(\hat{x}|\theta_f)\ \hat{x} \in R^{4\times 1}\ \hat{f}_2(\hat{x}|\theta_f)\ \in\ R^{1\times 1} \end{pmatrix} \tag{3.145}$$

with kernel functions

$$\phi_f^{i,j}(\hat{x}) = \frac{\prod_{j=1}^{n} \mu_{A_j^i}(\hat{x}_j)}{\sum_{i=1}^{N} \prod_{j=1}^{n} \mu_{A_j^i}(\hat{x}_j)} \tag{3.146}$$

where $l = 1, 2, \hat{x}$ is the estimate of the state vector and $\mu_{A_j^i}(\hat{x})$ is the ith membership function of the antecedent (IF) part of the lth fuzzy rule. Similarly, the following approximators of the unknown dynamics of the robotic manipulator are defined

$$\hat{g}(\hat{x}) = \begin{pmatrix} \hat{g}_1(\hat{x}|\theta_g)\ \hat{x} \in R^{4\times 1}\ \hat{g}_1(\hat{x}|\theta_g)\ \in\ R^{1\times 2} \\ \hat{g}_2(\hat{x}|\theta_g)\ \hat{x} \in R^{4\times 1}\ \hat{g}_2(\hat{x}|\theta_g)\ \in\ R^{1\times 2} \end{pmatrix} \tag{3.147}$$

The values of the weights that result in optimal approximation are

$$\begin{aligned} \theta_f^* &= arg\ min_{\theta_f \in M_{\theta_f}} [sup_{\hat{x}\in U_{\hat{x}}} (f(x) - \hat{f}(\hat{x}|\theta_f))] \\ \theta_g^* &= arg\ min_{\theta_g \in M_{\theta_g}} [sup_{\hat{x}\in U_{\hat{x}}} (g(x) - \hat{g}(\hat{x}|\theta_g))] \end{aligned} \tag{3.148}$$

where the variation ranges for the weights are defined as

$$\begin{aligned} M_{\theta_f} &= \{\theta_f \in R^h :\ ||\theta_f|| \leq m_{\theta_f}\} \\ M_{\theta_g} &= \{\theta_g \in R^h :\ ||\theta_g|| \leq m_{\theta_g}\} \end{aligned} \tag{3.149}$$

The value of the approximation error defined in Eq. (3.135) that corresponds to the optimal values of the weights vectors θ_f^* and θ_g^* is given by

$$w = \left(f(x,t) - \hat{f}(\hat{x}|\theta_f^*)\right) + \left(g(x,t) - \hat{g}(\hat{x}|\theta_g^*)\right)u \tag{3.150}$$

which is next written as

$$\begin{aligned} w = &\left(f(x,t) - \hat{f}(\hat{x}|\theta_f) + \hat{f}(\hat{x}|\theta_f) - \hat{f}(\hat{x}|\theta_f^*)\right) + \\ &+ \left(g(x,t) - \hat{g}(\hat{x}|\theta_g) + \hat{g}(\hat{x}|\theta_g) - \hat{g}(\hat{x}|\theta_g^*)\right)u \end{aligned} \tag{3.151}$$

which can be also written in the following form

$$w = \left(w_a + w_b\right) \tag{3.152}$$

where

$$w_a = \{[f(x,t) - \hat{f}(\hat{x}|\theta_f)] + [g(x,t) - \hat{g}(\hat{x}|\theta_g)]\}u \tag{3.153}$$

$$w_b = \{[\hat{f}(\hat{x}|\theta_f) - \hat{f}(\hat{x}|\theta_f^*)] + [\hat{g}(\hat{x},\theta_g) - \hat{g}(\hat{x}|\theta_g^*)]\}u \tag{3.154}$$

Moreover, the following weights error vectors are defined

$$\begin{aligned} \tilde{\theta}_f &= \theta_f - \theta_f^* \\ \tilde{\theta}_g &= \theta_g - \theta_g^*. \end{aligned} \tag{3.155}$$

3.3.8 Lyapunov Stability Analysis

3.3.8.1 Design of the Lyapunov Function

In the case of observer-based adaptive fuzzy control with the use of differential flatness theory, the adaptation law of the neurofuzzy approximators weights θ_f and θ_g as well as the supervisory control term u_c are derived from the requirement for a negative first-order derivative of a suitably chosen Lyapunov function. Extending the results presented in Sect. 3.2.5, the Lyapunov function is now defined as

$$V = \tfrac{1}{2}\hat{e}^T P_1 \hat{e} + \tfrac{1}{2}\tilde{e}^T P_2 \tilde{e} + \tfrac{1}{2\gamma_1}\tilde{\theta}_f^T \tilde{\theta}_f + \tfrac{1}{2\gamma_2} tr[\tilde{\theta}_g^T \tilde{\theta}_g] \tag{3.156}$$

The selection of the Lyapunov function relies on the following principle of indirect adaptive control $\hat{e} : \lim_{t\to\infty} \hat{x}(t) = x_d(t)$ and $\tilde{e} : \lim_{t\to\infty} \hat{x}(t) = x(t)$. This yields $\lim_{t\to\infty} x(t) = x_d(t)$. Substituting Eqs. (3.120), (3.121), (3.141), (3.142) into (3.156) and differentiating results into

$$\begin{gathered}\dot{V}=\tfrac{1}{2}\dot{\hat{e}}^{T}P_{1}\hat{e}+\tfrac{1}{2}\hat{e}^{T}P_{1}\dot{\hat{e}}+\tfrac{1}{2}\dot{\tilde{e}}^{T}P_{2}\tilde{e}+\tfrac{1}{2}\tilde{e}^{T}P_{2}\dot{\tilde{e}}+\\+\tfrac{1}{\gamma_{1}}\dot{\tilde{\theta}}_{f}^{T}\tilde{\theta}_{f}+\tfrac{1}{\gamma_{2}}tr[\dot{\tilde{\theta}}_{g}^{T}\tilde{\theta}_{g}]\Rightarrow\end{gathered}\tag{3.157}$$

$$\begin{gathered}\dot{V}=\tfrac{1}{2}\{(A-BK^{T})\hat{e}+K_{o}C^{T}\tilde{e}\}^{T}P_{1}\hat{e}+\tfrac{1}{2}\hat{e}^{T}P_{1}\{(A-BK^{T})\hat{e}+K_{o}C^{T}\tilde{e}\}+\\+\tfrac{1}{2}\{(A-K_{o}C^{T})\tilde{e}+Bu_{c}+B\tilde{d}+Bw\}^{T}P_{2}\tilde{e}+\\+\tfrac{1}{2}\tilde{e}^{T}P_{2}\{(A-K_{o}C^{T})\tilde{e}+Bu_{c}+B\tilde{d}+Bw\}+\\+\tfrac{1}{\gamma_{1}}\dot{\tilde{\theta}}_{f}^{T}\tilde{\theta}_{f}+\tfrac{1}{\gamma_{2}}tr[\dot{\tilde{\theta}}_{g}^{T}\tilde{\theta}_{g}]\Rightarrow\end{gathered}\tag{3.158}$$

$$\begin{gathered}\dot{V}=\tfrac{1}{2}\{\hat{e}^{T}(A-BK^{T})^{T}+\tilde{e}^{T}CK_{o}^{T}\}P_{1}\hat{e}+\tfrac{1}{2}\hat{e}^{T}P_{1}\{(A-BK^{T})\hat{e}+K_{o}C^{T}\tilde{e}\}+\\+\tfrac{1}{2}\{\tilde{e}^{T}(A-K_{o}C^{T})^{T}+u_{c}^{T}B^{T}+w^{T}B^{T}+\tilde{d}^{T}B^{T}\}P_{2}\tilde{e}+\\\tfrac{1}{2}\tilde{e}^{T}P_{2}\{(A-K_{o}C^{T})\tilde{e}+Bu_{c}+Bw+B\tilde{d}\}+\tfrac{1}{\gamma_{1}}\dot{\tilde{\theta}}_{f}^{T}\tilde{\theta}_{f}+\tfrac{1}{\gamma_{2}}tr[\dot{\tilde{\theta}}_{g}^{T}\tilde{\theta}_{g}]\Rightarrow\end{gathered}\tag{3.159}$$

$$\begin{gathered}\dot{V}=\tfrac{1}{2}\hat{e}^{T}(A-BK^{T})^{T}P_{1}\hat{e}+\tfrac{1}{2}\tilde{e}^{T}CK_{o}^{T}P_{1}\hat{e}+\\+\tfrac{1}{2}\hat{e}^{T}P_{1}(A-BK^{T})\hat{e}+\tfrac{1}{2}\hat{e}^{T}P_{1}K_{o}C^{T}\tilde{e}+\\+\tfrac{1}{2}\tilde{e}^{T}(A-K_{o}C^{T})^{T}P_{2}\tilde{e}+\tfrac{1}{2}(u_{c}^{T}+w^{T}+\tilde{d}^{T})B^{T}P_{2}\tilde{e}+\\+\tfrac{1}{2}\tilde{e}^{T}P_{2}(A-K_{o}C^{T})\tilde{e}+\tfrac{1}{2}\tilde{e}^{T}P_{2}B(u_{c}+w+\tilde{d})+\\+\tfrac{1}{\gamma_{1}}\dot{\tilde{\theta}}_{f}^{T}\tilde{\theta}_{f}+\tfrac{1}{\gamma_{2}}tr[\dot{\tilde{\theta}}_{g}^{T}\tilde{\theta}_{g}]\end{gathered}\tag{3.160}$$

Assumption 1: For given positive definite matrices Q_1 and Q_2 there exist positive definite matrices P_1 and P_2, which are the solution of the following Riccati equations [561]

$$(A-BK^{T})^{T}P_{1}+P_{1}(A-BK^{T})+Q_{1}=0\tag{3.161}$$

$$\begin{gathered}(A-K_{o}C^{T})^{T}P_{2}+P_{2}(A-K_{o}C^{T})-\\-P_{2}B\left(\tfrac{2}{r}-\tfrac{1}{\rho^{2}}\right)B^{T}P_{2}+Q_{2}=0\end{gathered}\tag{3.162}$$

The conditions given in Eqs. (3.161)–(3.162) are related to the requirement that the systems described by Eqs. (3.120), (3.121), (3.141), (3.142) have stable eigenvalues. Substituting Eqs. (3.161)–(3.162) into $\dot{V}$ yields

$$\begin{gathered}\dot{V}=\tfrac{1}{2}\hat{e}^{T}\{(A-BK^{T})^{T}P_{1}+P_{1}(A-BK^{T})\}\hat{e}+\tilde{e}^{T}CK_{o}^{T}P_{1}\hat{e}+\\+\tfrac{1}{2}\tilde{e}^{T}\{(A-K_{o}C^{T})^{T}P_{2}+P_{2}(A-K_{o}C^{T})\}\tilde{e}+\\+\tilde{e}^{T}P_{2}B(u_{c}+w+\tilde{d})+\tfrac{1}{\gamma_{1}}\dot{\tilde{\theta}}_{f}^{T}\tilde{\theta}_{f}+\tfrac{1}{\gamma_{2}}tr[\dot{\tilde{\theta}}_{g}^{T}\tilde{\theta}_{g}]\end{gathered}\tag{3.163}$$

that is

$$\dot{V} = -\tfrac{1}{2}\hat{e}^T Q_1 \hat{e} + \tilde{e}^T C K_o^T P_1 \hat{e} - \tfrac{1}{2}\tilde{e}^T \left\{ Q_2 - P_2 B \left(\tfrac{2}{r} - \tfrac{1}{\rho^2} \right) B^T P_2 \right\} \tilde{e} + \\ + \tilde{e}^T P_2 B (u_c + w + \tilde{d}) + \tfrac{1}{\gamma_1} \dot{\tilde{\theta}}_f^T \tilde{\theta}_f + \tfrac{1}{\gamma_2} tr[\dot{\tilde{\theta}}_g^T \tilde{\theta}_g] \tag{3.164}$$

The supervisory control u_c is decomposed in two terms, u_a and u_b.

- The control term u_a is given by

$$u_a = -\frac{1}{r} \tilde{e}^T P_2 B + \Delta u_a \tag{3.165}$$

where assuming that the measurable elements of vector $\tilde{e}$ are $\{\tilde{e}_1, \tilde{e_3}, \ldots, \tilde{e_k}\}$, the term Δu_a is such that

$$-\tfrac{1}{r}\tilde{e}^T P_2 B + \Delta u_a = -\tfrac{1}{r} \begin{pmatrix} p_{11}\tilde{e}_1 + p_{13}\tilde{e}_3 + \cdots + p_{1k}\tilde{e}_k \\ p_{13}\tilde{e}_1 + p_{33}\tilde{e}_3 + \cdots + p_{3k}\tilde{e}_k \\ \cdots \quad \cdots \\ p_{1k}\tilde{e}_1 + p_{3k}\tilde{e}_3 + \cdots + p_{kk}\tilde{e}_k \end{pmatrix} \tag{3.166}$$

- The control term u_b is given by

$$u_b = -[(P_2 B)^T (P_2 B)]^{-1} (P_2 B)^T C K_o^T P_1 \hat{e} \tag{3.167}$$

- u_a is an H_∞ control used for the compensation of the approximation error w and the additive disturbance $\tilde{d}$. Its first component $-\frac{1}{r}\tilde{e}^T P_2 B$ has been chosen so as to compensate for the term $\frac{1}{r}\tilde{e}^T P_2 B B^T P_2 \tilde{e}$, which appears in Eq. (3.164). By including also the second component Δu_a, one has that u_a is computed based only on the feedback of the measurable variables $\{\tilde{e}_1, \tilde{e_3}, \ldots, \tilde{e_k}\}$, out of the complete vector $\tilde{e} = [\tilde{e}_1, \tilde{e}_2, \ldots, \tilde{e}_n]$. According to Eq. (3.165) u_a is written as $u_a = -\frac{1}{r}\tilde{e}^T P_2 B + \Delta u_a$.
- u_b is a control used for the compensation of the observation error (the control term u_b has been chosen so as to satisfy the condition $\tilde{e}^T P_2 B u_b = -\tilde{e}^T C K_o^T P_1 \hat{e}$.

The control scheme is depicted in Fig. 3.10

Substituting Eqs. (3.165) and (3.167) in $\dot{V}$ and assuming that Eqs. (3.161) and (3.162) hold, one gets

$$\dot{V} = -\tfrac{1}{2}\hat{e}^T Q_1 \hat{e} + \tilde{e}^T C K_o^T P_1 \hat{e} - \tfrac{1}{2}\tilde{e}^T Q_2 \tilde{e} + \tfrac{1}{r}\tilde{e}^T P_2 B B^T P_2 \tilde{e} - \tfrac{1}{2\rho^2}\tilde{e}^T P_2 B B^T P_2 \tilde{e} + \\ + \tilde{e}^T P_2 B u_a + \tilde{e}^T P_2 B u_b + \tilde{e}^T P_2 B (w + \tilde{d}) + \tfrac{1}{\gamma_1} \dot{\tilde{\theta}}_f^T \tilde{\theta}_f + \tfrac{1}{\gamma_2} tr[\dot{\tilde{\theta}}_g^T \tilde{\theta}_g] \tag{3.168}$$

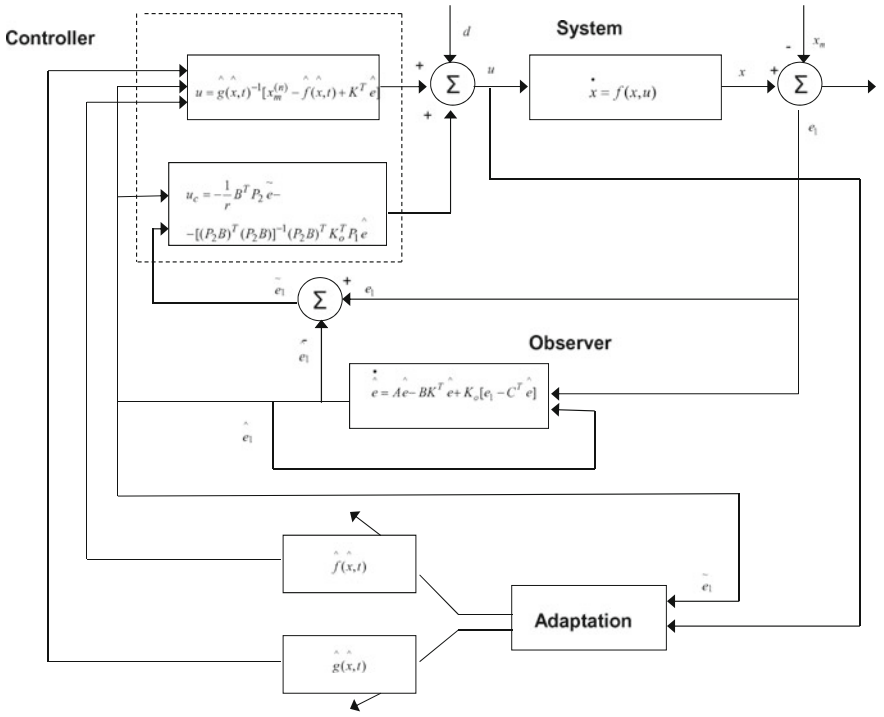

Fig. 3.10 The proposed observer-based control scheme for the multi-DOF robotic manipulator

or equivalently,

$$\begin{aligned}\dot{V} = &-\tfrac{1}{2}\hat{e}^T Q_1 \hat{e} - \tfrac{1}{2}\tilde{e}^T Q_2 \tilde{e} - \tfrac{1}{2\rho^2}\tilde{e}^T P_2 B B^T P_2 \tilde{e} + \\ &+\tilde{e}^T P_2 B(w + \tilde{d} + \Delta u_a) + \tfrac{1}{\gamma_1}\dot{\tilde{\theta}}_f^T \tilde{\theta}_f + \tfrac{1}{\gamma_2} tr[\dot{\tilde{\theta}}_g^T \tilde{\theta}_g]\end{aligned} \tag{3.169}$$

It holds that $\dot{\tilde{\theta}}_f = \dot{\theta}_f - \dot{\theta}_f^* = \dot{\theta}_f$ and $\dot{\tilde{\theta}}_g = \dot{\theta}_g - \dot{\theta}_g^* = \dot{\theta}_g$. The following weight adaptation laws are considered:

$$\begin{aligned}\dot{\theta}_f &= -\gamma_1 \Phi(\hat{x})^T B^T P_2 \tilde{e} \\ \dot{\theta}_g &= -\gamma_2 \Phi(\hat{x})^T B^T P_2 \tilde{e} u^T\end{aligned} \tag{3.170}$$

where assuming N fuzzy rules and associated kernel functions the matrices dimensions are $\theta_f \in R^{N\times 1}$, $\theta_g \in R^{N\times 2}$, $\Phi(x) \in R^{2\times N}$, $B \in R^{4\times 2}$, $P \in R^{4\times 4}$ and $\tilde{e} \in R^{4\times 1}$.

The update of θ_f is a gradient type algorithm. The update of θ_g is also a gradient type algorithm, where u_c implicitly tunes the adaptation gain γ_2 [33, 457, 463]. Substituting Eq. (3.170) in $\dot{V}$ gives

$$\begin{array}{c}\dot{V} = -\frac{1}{2}\hat{e}^T Q_1 \hat{e} - \frac{1}{2}\tilde{e}^T Q_2 \tilde{e} - \frac{1}{2\rho^2}\tilde{e}^T P_2 B B^T P_2 \tilde{e} + B^T P_2 \tilde{e}(w + d + \Delta u_a) + \\ + \frac{1}{\gamma_1}(-\gamma_1)\tilde{e}^T P_2 B \Phi(\hat{x})(\theta_f - \theta_f^*) + \\ + \frac{1}{\gamma_2}(-\gamma_2) tr[u\tilde{e}^T P_2 B \Phi(\hat{x})(\theta_g - \theta_g^*)]\end{array} \tag{3.171}$$

or

$$\begin{array}{c}\dot{V} = -\frac{1}{2}\hat{e}^T Q_1 \hat{e} - \frac{1}{2}\tilde{e}^T Q_2 \tilde{e} - \frac{1}{2\rho^2}\tilde{e}^T P_2 B B^T P_2 \tilde{e} + B^T P_2 \tilde{e}(w + \tilde{d} + \Delta u_a) + \\ + \frac{1}{\gamma_1}(-\gamma_1)\tilde{e}^T P_2 B \Phi(\hat{x})(\theta_f - \theta_f^*) + \\ + \frac{1}{\gamma_2}(-\gamma_2) tr[u\tilde{e}^T P_2 B(\hat{g}(\hat{x}|\theta_g) - \hat{g}(\hat{x}|\theta_g^*))]\end{array} \tag{3.172}$$

Taking into account that $u \in R^{2\times 1}$ and $\tilde{e}^T PB(\hat{g}(x|\theta_g) - \hat{g}(x|\theta_g^*)) \in R^{1\times 2}$ it holds

$$\begin{array}{c}\dot{V} = -\frac{1}{2}\hat{e}^T Q_1 \hat{e} - \frac{1}{2}\tilde{e}^T Q_2 \tilde{e} - \frac{1}{2\rho^2}\tilde{e}^T P_2 B B^T P_2 \tilde{e} + B^T P_2 \tilde{e}(w + \tilde{d} + \Delta u_a) + \\ + \frac{1}{\gamma_1}(-\gamma_1)\tilde{e}^T P_2 B \Phi(\hat{x})(\theta_f - \theta_f^*) + \\ + \frac{1}{\gamma_2}(-\gamma_2) tr[\tilde{e}^T P_2 B(\hat{g}(\hat{x}|\theta_g) - \hat{g}(\hat{x}|\theta_g^*))u]\end{array} \tag{3.173}$$

Since $\tilde{e}^T P_2 B(\hat{g}(\hat{x}|\theta_g) - \hat{g}(\hat{x}|\theta_g^*))u \in R^{1\times 1}$ it holds

$$\begin{array}{c} tr(\tilde{e}^T P_2 B(\hat{g}(x|\theta_g) - \hat{g}(x|\theta_g^*)u) = \\ = \tilde{e}^T P_2 B(\hat{g}(x|\theta_g) - \hat{g}(x|\theta_g^*))u\end{array} \tag{3.174}$$

Therefore, one finally obtains

$$\begin{array}{c}\dot{V} = -\frac{1}{2}\hat{e}^T Q_1 \hat{e} - \frac{1}{2}\tilde{e}^T Q_2 \tilde{e} - \frac{1}{2\rho^2}\tilde{e}^T P_2 B B^T P_2 \tilde{e} + B^T P_2 \tilde{e}(w + \tilde{d} + \Delta u_a) + \\ + \frac{1}{\gamma_1}(-\gamma_1)\tilde{e}^T P_2 B \Phi(\hat{x})(\theta_f - \theta_f^*) + \\ + \frac{1}{\gamma_2}(-\gamma_2)\tilde{e}^T P_2 B(\hat{g}(\hat{x}|\theta_g) - \hat{g}(\hat{x}|\theta_g^*))u\end{array} \tag{3.175}$$

Next, the following approximation error is defined

$$w_\alpha = [\hat{f}(\hat{x}|\theta_f^*) - \hat{f}(\hat{x}|\theta_f)] + [\hat{g}(\hat{x}|\theta_g^*) - \hat{g}(\hat{x}|\theta_g)]u \tag{3.176}$$

Thus, one obtains

$$\begin{array}{c}\dot{V} = -\frac{1}{2}\hat{e}^T Q_1 \hat{e} - \frac{1}{2}\tilde{e}^T Q_2 \tilde{e} - \frac{1}{2\rho^2}\tilde{e}^T P_2 B B^T P_2 \tilde{e} + \\ + B^T P_2 \tilde{e}(w + \tilde{d}) + \tilde{e}^T P_2 B w_\alpha\end{array} \tag{3.177}$$

Denoting the aggregate approximation error and disturbances vector as

$$w_1 = w + \tilde{d} + w_\alpha + \Delta u_a \tag{3.178}$$

the derivative of the Lyapunov function becomes

$$\dot{V} = -\frac{1}{2}\hat{e}^T Q_1 \hat{e} - \frac{1}{2}\tilde{e}^T Q_2 \tilde{e} - \frac{1}{2\rho^2}\tilde{e}^T P_2 B B^T P_2 \tilde{e} + \tilde{e}^T P_2 B w_1 \tag{3.179}$$

which in turn is written as

$$\begin{gathered}\dot{V} = -\frac{1}{2}\hat{e}^T Q_1 \hat{e} - \frac{1}{2}\tilde{e}^T Q_2 \tilde{e} - \frac{1}{2\rho^2}\tilde{e}^T P_2 B B^T P_2 \tilde{e} + \\ + \frac{1}{2}\tilde{e}^T P B w_1 + \frac{1}{2} w_1^T B^T P_2 \tilde{e}\end{gathered} \tag{3.180}$$

Lemma: The following inequality holds

$$\begin{gathered}\frac{1}{2}\tilde{e}^T P_2 B w_1 + \frac{1}{2} w_1^T B^T P_2 \tilde{e} - \frac{1}{2\rho^2}\tilde{e}^T P_2 B B^T P_2 \tilde{e} \\ \leq \frac{1}{2}\rho^2 w_1^T w_1\end{gathered} \tag{3.181}$$

Proof: The binomial $(\rho a - \frac{1}{\rho} b)^2 \geq 0$ is considered. Expanding the left part of the above inequality one gets

$$\begin{gathered}\rho^2 a^2 + \frac{1}{\rho^2} b^2 - 2ab \geq 0 \Rightarrow \\ \frac{1}{2}\rho^2 a^2 + \frac{1}{2\rho^2} b^2 - ab \geq 0 \Rightarrow \\ ab - \frac{1}{2\rho^2} b^2 \leq \frac{1}{2}\rho^2 a^2 \Rightarrow \\ \frac{1}{2} ab + \frac{1}{2} ab - \frac{1}{2\rho^2} b^2 \leq \frac{1}{2}\rho^2 a^2\end{gathered} \tag{3.182}$$

The following substitutions are carried out: $a = w_1$ and $b = \tilde{e}^T P_2 B$ and the previous relation becomes

$$\begin{gathered}\frac{1}{2} w_1^T B^T P_2 \tilde{e} + \frac{1}{2}\tilde{e}^T P_2 B w_1 - \frac{1}{2\rho^2}\tilde{e}^T P_2 B B^T P_2 \tilde{e} \\ \leq \frac{1}{2}\rho^2 w_1^T w_1\end{gathered} \tag{3.183}$$

The above relation is used in $\dot{V}$, and the right part of the associated inequality is enforced

$$\dot{V} \leq -\frac{1}{2}\hat{e}^T Q_1 \hat{e} - \frac{1}{2}\tilde{e}^T Q_2 \tilde{e} + \frac{1}{2}\rho^2 w_1^T w_1 \tag{3.184}$$

Thus, Eq. (3.184) can be written as

$$\dot{V} \leq -\frac{1}{2} E^T Q E + \frac{1}{2}\rho^2 w_1^T w_1 \tag{3.185}$$

where

$$E = \begin{pmatrix} \hat{e} \\ \tilde{e} \end{pmatrix}, \quad Q = \begin{pmatrix} Q_1 & 0 \\ 0 & Q_2 \end{pmatrix} = diag[Q_1, Q_2] \tag{3.186}$$

As explained in Sect. 3.4, a sufficiently small value for the attenuation coefficient ρ assures that the right part of Eq. (3.185) will be upper bounded by 0.

Hence, the H_∞ performance criterion is derived. For ρ sufficiently small Eq. (3.184) will be true and the H_∞ tracking criterion will be satisfied. In that case, the integration of $\dot{V}$ from 0 to T gives

$$\begin{array}{c} \int_0^T \dot{V}(t)dt \leq -\frac{1}{2}\int_0^T ||E||^2 dt + \frac{1}{2}\rho^2 \int_0^T ||w_1||^2 dt \Rightarrow \\ 2V(T) - 2V(0) \leq -\int_0^T ||E||_Q^2 dt + \rho^2 \int_0^T ||w_1||^2 dt \Rightarrow \\ 2V(T) + \int_0^T ||E||_Q^2 dt \leq 2V(0) + \rho^2 \int_0^T ||w_1||^2 dt \end{array} \tag{3.187}$$

It is assumed that there exists a positive constant $M_w > 0$ such that $\int_0^\infty ||w_1||^2 dt \leq M_w$. Therefore for the integral $\int_0^T ||E||_Q^2 dt$ one gets

$$\int_0^\infty ||E||_Q^2 dt \leq 2V(0) + \rho^2 M_w \tag{3.188}$$

Thus, the integral $\int_0^\infty ||E||_Q^2 dt$ is bounded and according to Barbalat's Lemma

$$\begin{array}{c} \lim_{t\to\infty} E(t) = 0 \Rightarrow \\ \lim_{t\to\infty} \hat{e}(t) = 0 \\ \lim_{t\to\infty} \tilde{e}(t) = 0 \end{array} \tag{3.189}$$

Therefore $\lim_{t\to\infty} e(t) = 0$.

3.3.9 *Riccati Equation Coefficients in Observer-Based Adaptive Fuzzy Control*

The linear system of Eqs. (3.141) and (3.142) is considered again

$$\begin{array}{c} \dot{\tilde{e}} = (A - K_o C^T)\tilde{e} + Bu_c + B\{[f(x,t) - \hat{f}(\hat{x},t)] + [g(x,t) - \hat{g}(\hat{x},t)]u + \tilde{d}\} \\ e_1 = C^T \tilde{e} \end{array}$$

The aim of H_∞ control is to eliminate the impact of the modelling errors $w = [f(x,t) - \hat{f}(\hat{x},t)] + [g(x,t) - \hat{g}(\hat{x},t)]u$ and the external disturbances $\tilde{d}$ which are not white noise signals. This implies the minimization of the quadratic cost function [132, 243, 305]:

$$\begin{array}{c} J(t) = \frac{1}{2}\int_0^T \tilde{e}^T(t)\tilde{e}(t) + ru_c^T(t)u_c(t) - \\ -\rho^2(w + \tilde{d})^T(w + \tilde{d})dt, \quad r, \rho > 0 \end{array} \tag{3.190}$$

As previously pointed out, the weight r determines how much the control signal should be penalized and the weight ρ determines how much the disturbances influence should be rewarded in the sense of a min-max differential game. The control input u_c has been defined as the sum of the terms described in Eqs. (3.165) and (3.167).

Parameter ρ in Eq. (3.190), is an indication of the closed-loop system robustness. If the values of $\rho > 0$ are excessively decreased with respect to r, then the solution of the Riccati equation is no longer a positive definite matrix. Consequently there is a lower bound ρ_{min} of ρ for which the H_∞ control problem has a solution. The acceptable values of ρ lie in the interval $[\rho_{min}, \infty)$. If ρ_{min} is found and used in the design of the H_∞ controller, then the closed-loop system will have have elevated robustness. Unlike this, if a value $\rho > \rho_{min}$ is used, then an admissible stabilizing H_∞ controller will be derived but it will be a suboptimal one. The Hamiltonian matrix

$$H = \begin{pmatrix} A - K_o C^T & -(\frac{2}{r} - \frac{1}{\rho^2})BB^T \\ -Q & -(A - K_o C^T)^T \end{pmatrix} \tag{3.191}$$

provides a criterion for the existence of a solution of the Riccati equation Eq. (3.162). A necessary condition for the solution of the algebraic Riccati equation to be a positive semi-definite symmetric matrix is that H has no imaginary eigenvalues [132, 457].

It is noted that several methods on adaptive neural/fuzzy control of nonlinear dynamical systems assume that the system is already described in the canonical Brunovsky form. However, for the majority of electro-mechanical systems this does not hold. For example, robotic manipulators, unmanned aerial vehicles, land vehicles, surface and underwater vehicle models, are some examples of robotic systems which are not inherently found in the canonical form [450]. Adaptive fuzzy control methods usually try to invert the system's dynamics, and thus to succeed convergence of its output to the desirable setpoints, starting from a description of the system in the canonical form. This means that the system is taken to be a-priori in the description given in Eq. (3.95), however in the majority of electromechanical systems the dynamics is in the form of Eq. (3.37). Differential flatness theory enables to transform the system's description $\dot{x} = f(x, u)$ into that of Eq. (3.95) and from that point on to develop adaptive control schemes. Consequently, differential flatness theory extends the class of nonlinear robotic systems to which adaptive neural/fuzzy control can be applied and this is a significant benefit for adaptive control theory. Additional results about adaptive fuzzy controllers which make use of transformations into canonical forms can be found in [399, 609, 617].

3.3.10 Simulation Tests

The performance of the proposed observer-based adaptive fuzzy MIMO controller was tested in the benchmark problem of the 2-DOF rigid-link robotic manipulator (Fig. 3.11). The differentially flat model of the robot and its transformation to the Brunovksy form has been analyzed in Sect. 3.3.5.

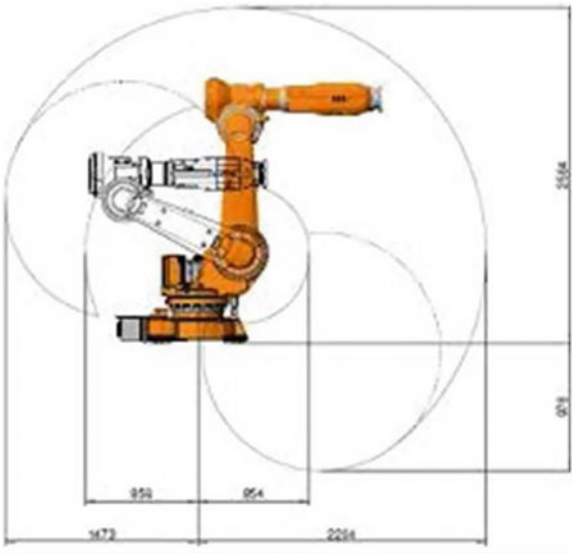

Fig. 3.11 A multi-DOF robotic manipulator controlled by an observer-based adaptive fuzzy control scheme

The state feedback gain was $K \in R^{2\times 4}$. The basis functions used in the estimation of $f_i(\hat{x}, t),\ i = 1, 2$ and $g_{ij}(\hat{x}, t),\ i = 1, 2,\ j = 1, 2$ were $\mu_{A_j}(\hat{x}) = e^{(\frac{\hat{x}-c_j}{\sigma})^2}, j = 1, \ldots, 3$. Since there are four inputs $\hat{x}_1, \dot{\hat{x}}_1$ and $\hat{x}_3, \dot{\hat{x}}_3$ and each one of them consists of 3 fuzzy sets, for the approximation of functions $f_i(\hat{x}, t)\ i = 1, \ldots, 3$, there will be 81 fuzzy rules of the form:

$$\begin{aligned} &R^l : IF\ \ \hat{x}_1\ \ is\ \ A_1^l\ \ AND\ \ \dot{\hat{x}}_1\ \ is\ \ A_2^l \\ &AND\ \ \hat{x}_3\ \ is\ \ A_3^l\ \ AND\ \ \dot{\hat{x}}_3\ \ is\ \ A_4^l\ \ THEN\ \ \hat{f}_i^l\ \ is\ \ b^l \end{aligned} \tag{3.192}$$

The aggregate output of the neuro-fuzzy approximator (rule-base) is $\hat{f}_i(\hat{x}, t) = \frac{\sum_{l=1}^{81} \hat{f}_i^l \prod_{i=1}^{4} \mu_{A_i}^l(\hat{x}_i)}{\sum_{l=1}^{81} \prod_{i=1}^{4} \mu_{A_i}^l(\hat{x}_i)}$. The centers $c_i^{(l)},\ i = 1, \ldots, 4$ and the variances $v^{(l)}$ of each rule are summarized in Table 3.3.

The estimation of the control input gain functions $\hat{g}_{ij}(\hat{x}, t)\ i = 1, 2$ was derived in a similar way. The overall simulation time was $t_s = 40$ s. The sampling period was taken to be 0.01 s. In the beginning of the training of the neuro-fuzzy approximators their weights were initialized to zero. Moreover, the elements of the robot's state vector were also initialized to zero. The positive definite matrices $P_1 \in R^{4\times 4}$ and $P_2 \in R^{4\times 4}$ stem from the solution of the algebraic Riccati equations given in Eqs. (3.161) and (3.162), for Q_1 and Q_2 also positive definite.

The approximations $\hat{f}$ and $\hat{g}$ were used in the derivation of the control law, given by Eq. (3.115). To show the disturbance rejection capability of the proposed adaptive fuzzy controller, at the beginning of the second half of the simulation time additive sinusoidal disturbances of amplitude $A = 0.5$ and period $T = 10$ s were applied to the robot's joints.

Table 3.3 Parameters of the fuzzy rule base

Rule	$c_1^{(l)}$	$c_2^{(l)}$	$c_3^{(l)}$	$c_4^{(l)}$	$v^{(l)}$
$R^{(1)}$	−1.0	−1.0	−1.0	−1.0	3
$R^{(2)}$	−1.0	−1.0	−1.0	0.0	3
$R^{(3)}$	−1.0	−1.0	−1.0	1.0	3
$R^{(4)}$	−1.0	−1.0	0.0	−1.0	3
$R^{(5)}$	−1.0	−1.0	0.0	0.0	3
$R^{(6)}$	−1.0	−1.0	0.0	1.0	3
...	...	...	...	...	...
...	...	...	...	...	...
$R^{(81)}$	1.0	1.0	1.0	1.0	3

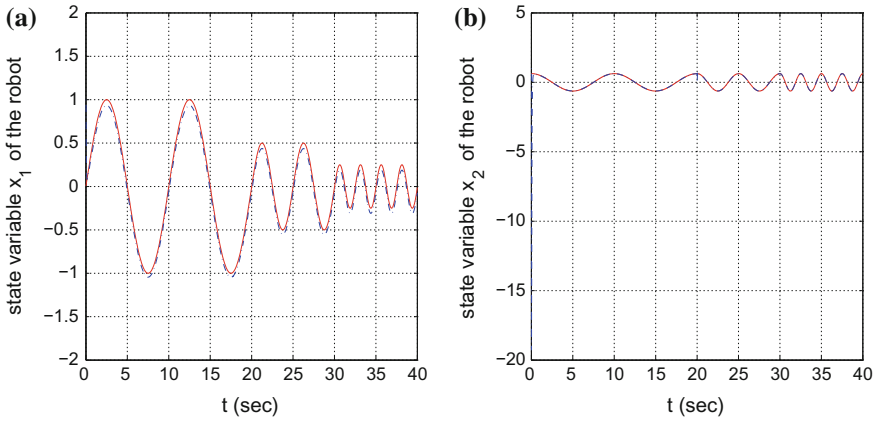

Fig. 3.12 **a** Tracking of a sinusoidal position set-point by joint 1 of the robot. **b** Tracking of sinusoidal velocity setpoint by joint 1 of the robot

In the simulation results that follow, the position and velocity setpoints are noted as continuous red lines while the position and velocity signals of the robot's joints are denoted as dashed blue lines. The position variation for the first joint of the robotic manipulator when tracking a sinusoidal set-point is depicted in Fig. 3.12a, while the velocity variation is shown in Fig. 3.12b. For the second joint of the 2-DOF robot the tracking of the position setpoint is depicted in Fig. 3.13a while the tracking of the velocity setpoint is shown in Fig. 3.13b. The control inputs (motor torques) applied to the first and second joint of the robotic manipulator are shown in Fig. 3.14a and in Fig. 3.14b, respectively.

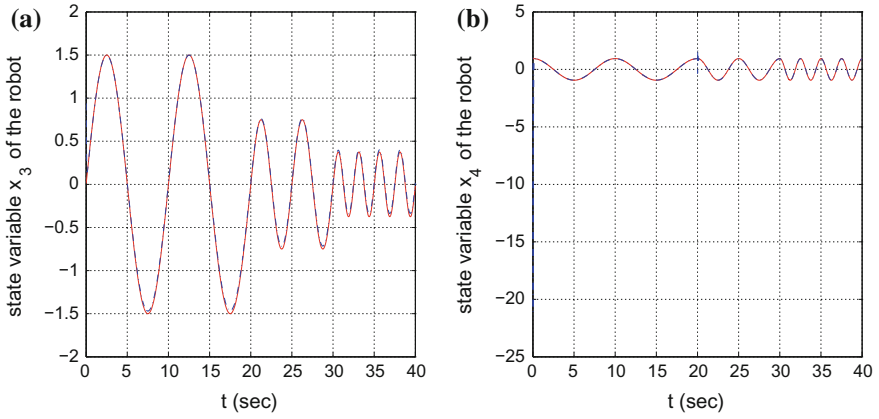

Fig. 3.13 **a** Tracking of a sinusoidal position set-point by joint 2 of the robot. **b** Tracking of sinusoidal velocity setpoint by joint 2 of the robot

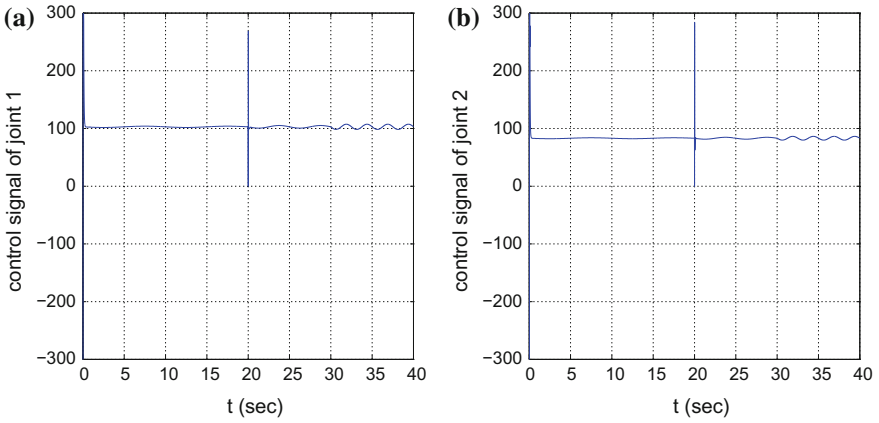

Fig. 3.14 Tracking of a sinusoidal setpoint: **a** Control input to joint 1 of the robot **b** Control input to joint 2 of the robot

The performance of the proposed observer-based adaptive fuzzy control scheme was also tested in the case of various other setpoints. The associated results, about the accuracy of tracking of the state vector elements, are shown in Figs. 3.15 and 3.16. The control loop enabled fast convergence of the state variables to the desirable setpoints although there was no previous knowledge about the dynamic model of the robotic manipulator and despite the effects of external disturbances.

The RMSE (root mean square error) of the examined control loop is also calculated (assuming the same parameters of the controller) in the case of tracking of the previous setpoints: (a) the piecewise constant setpoint of Fig. 3.15a, (b) the sinusoidal setpoint of Fig. 3.15b, (c) the seesaw setpoint of Fig. 3.16a, (d) the setpoint

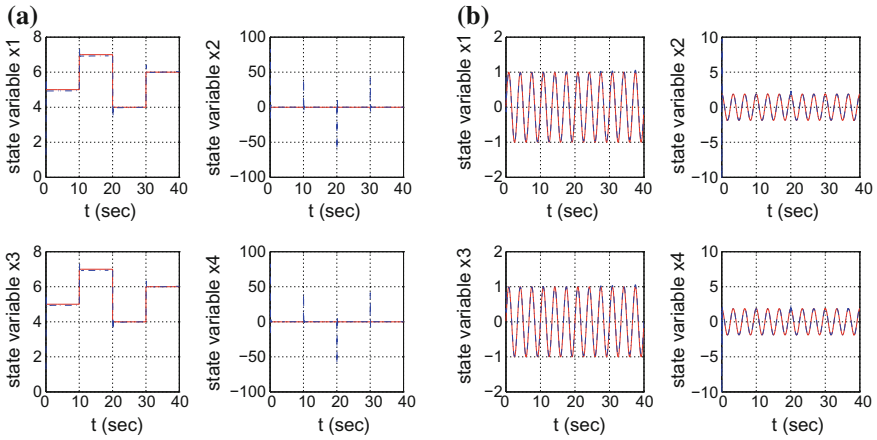

Fig. 3.15 Convergence of state vector elements of the robot to the desirable setpoints: **a** when tracking a piecewise constant setpoint **b** when tracking a sinusoidal setpoint

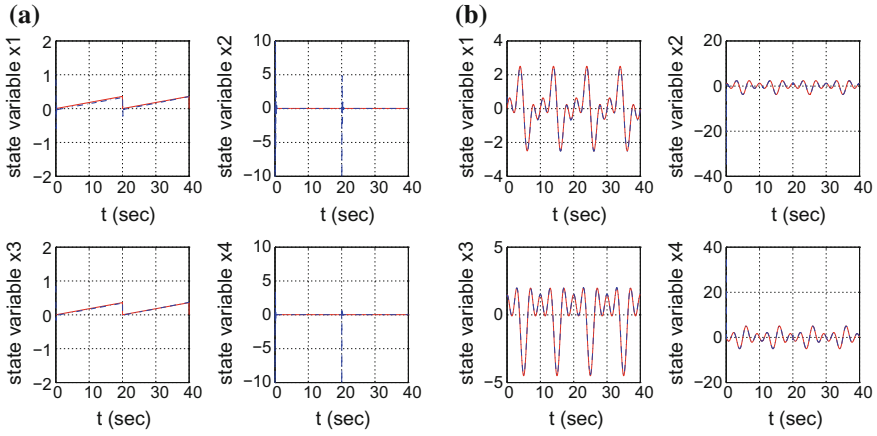

Fig. 3.16 Convergence of state vector elements of the robot to the desirable setpoints: **a** when tracking a seesaw setpoint **b** when tracking a setpoint obtained from the sum of different sinusoidal signals

obtained from the sum of different sinusoidal signals as shown in Fig. 3.16b. The results are summarized in Table 3.4. It can be seen that the transient characteristics of the control scheme are also quite satisfactory.

Through the presented simulation experiments it has been shown that the adaptive control method achieves excellent accuracy in the tracking of the reference setpoints. This is a confirmation of the stability analysis that resulted in an H-infinity tracking performance criterion and in an asymptotic stability condition. Moreover, it has been shown that the control input exhibits smooth variations. This is an advantage

Table 3.4 RMSE of joints' angles

parameter	θ_1	θ_2
$RMSE_a$	0.0471	0.0449
$RMSE_b$	0.0418	0.0427
$RMSE_c$	0.0495	0.0288
$RMSE_d$	0.0449	0.0472

comparing, for instance, to adaptive fuzzy sliding mode control since in the latter case there are abrupt control input variations. What is also important to compare is the extent of the class of robotic systems to which the various control methods can be applied and the constraining assumptions made about the structure of the controlled systems. From this point of view, the proposed "Differential flatness theory approach to observer-based adaptive fuzzy control of MIMO nonlinear dynamical systems outperforms all other adaptive neural/fuzzy control methods. The method can be applied to any type of MIMO differentially flat systems that admit a transformation to the canonical Brunovsky form and does not require the system's dynamic model to have a particular structure (e.g. affine-in-the-input, triangular or other). Besides, the control method relies exclusively on feedback of the outputs of the system and does not require measurements of all elements of the state vector. Performing estimation of the state vector instead or precise measurements of the state variables has significant advantages. It is less costly because it requires less sensors to be used in the control loop. It reduces the faulty conditions for the control loop because it is free of sensors that frequently undergo failures when used in harsh operating conditions of robotic systems (such as robotic manipulators, autonomous ground vehicles, aerial vehicles, unmanned surface and underwater vessels or other).

The definition of the parameters of the fuzzy rule base (81 rules) has been given in Table 3.5. For the two-DOF robotic model considered as application example, the number of the rules is computed as follows: there are four input variables in the antecedent part of the each rule, namely position and angular velocity for each one of the robot's joints. Each input variable is partitioned into three fuzzy sets, therefore taking into account all possible combinations of the fuzzy sets to which the input variables can be assigned one has $3^4 = 81$ fuzzy rules. The placement of the centers of the fuzzy sets at specific points of the four-dimensional state-space is performed following the so-called grid partitioning. This means that the centers of the fuzzy sets are chosen to occupy equally distant positions along the axes of the input variables. This results in a uniform coverage of the state space.

3.4 Adaptive H-Infinity Neurofuzzy Control for the Rotary Pendulum

3.4.1 Outline

Next, the problem of adaptive (model-free) control of the rotary pendulum is treated. Adaptive control of underactuated robotic systems is a significant problem because (i) in several cases the number of available control inputs (actuators) is less than the number of degrees of freedom of the robot, (ii) the dynamic model of such robotic systems is often unknown [153, 347, 378, 506, 520]. A typical underactuated system is Furuta's pendulum, also known as rotational pendulum. As analyzed in the previous sections, this system has two degrees of freedom while it receives only one control input [299, 326, 527, 544, 630]. Besides, the system exhibits strong nonlinear characteristics due to the appearance of nonlinear gravitational and Coriolis terms in it [18, 78, 137, 244, 640]. Furthermore, the system is not linearizable through state feedback and in its nonlinear form it is not differentially flat. As a result its transformation into a linear equivalent state-space form through a change of state variables (diffeomorphisms) can be a burdening procedure [3–5, 405, 406]. Additionally, the pendulum's dynamic model may be subject to parametric uncertainty and variation or to external perturbations thus making model-based approaches for the solution of the associated control problem be unreliable. For these reasons adaptive control of the rotary (Furuta's) pendulum is a non-trivial problem [577, 606].

In this section, an adaptive H-infinity neurofuzzy control method is applied to the dynamic model of the rotary (Furuta's) pendulum. As noted above, this control problem is of elevated difficulty because the pendulum exhibits strong nonlinearities while it is also an underactuated system (there are two degrees of freedom and only one control input). Besides, in the model-free case, as for instance when the values of the model parameters are unknown (lengths and weights of the pendulum's links) the control problem's complexity is further raised. To solve this control problem, the pendulum's model was first subject to approximate linearization round a temporary equilibrium that was recomputed at each iteration of the control method. The equilibrium is defined by the present value of the pendulum's state vector and the last value of the control input that was exerted on it [461, 466]. The linearization procedure is relies on Taylor series expansion and on the computation of the pendulum's Jacobian matrices [431, 463].

For the approximately linearized model of the pendulum and for the case of a known dynamical model it would be possible to achieve stabilization by using an H-infinity feedback controller. Such a controller would provide a solution to the nonlinear H-infinity (optimal) control problem of the pendulum [450, 452, 457, 459, 460]. Its feedback gain would be computed from the repetitive solution of an algebraic Riccati equation, taking place at each iteration of the control method. However, the dynamic model of the pendulum is actually unknown and to solve the H-infinity control problem, an indirect adaptive control scheme based on neurofuzzy estimators is developed. Neurofuzzy networks are employed to approximate in real

time the functions that constitute the unknown dynamics of the rotary pendulum. Next these functions' estimates are used to approximate the system's Jacobians. Finally, by using the approximated Jacobian in the algebraic Riccati equation the feedback gain of the H-infinity controller is obtained.

The stability properties of this adaptive neurofuzzy control scheme are analyzed with the use of the Lyapunov method [450, 457, 460]. First, it is shown that the H-infinity tracking performance criterion holds for the control loop that comprises: (i) the rotary pendulum of unknown dynamics, (ii) the neurofuzzy approximators that estimate the system's unknown dynamics and (iii) the H-infinity feedback controller. At a second stage, it is shown that the control loop exhibits global asymptotic stability properties. The learning rate of the neurofuzzy approximators is chosen in a manner that assures that the first derivative of the system's Lyapunov function will always be a negative one. Through simulation experiments, the excellent tracking performance of the control method is further confirmed.

3.4.2 Dynamic Model of the Rotary Pendulum

3.4.3 Control System Dynamics

As demonstrated before, the rotary pendulum's model belongs to the wider class of affine-in-the-input systems which can be described in the form

$$\dot{x} = f(x) + g(x)u \tag{3.193}$$

where $x \in R^n$ and $u \in R$. The system undergoes approximate linearization through Taylor series expansion at a temporary equilibrium (x^*, u^*) which is defined by the present value of the state vector u^* and the last value of the control input that was applied on the system. In accordance to the previously given analysis, the linearization procedure is based on the computation of Jacobian matrices:

$$\begin{array}{cc} A = \nabla_x [f(x) + g(x)u]_{(x^*,u^*)} \Rightarrow & B = \nabla_u [f(x) + g(x)u]_{(x^*,u^*)} \Rightarrow \\ A = \nabla_x \tilde{f} \mid_{(x^*,u^*)} & B = \nabla_u \tilde{f} \mid_{(x^*,u^*)} \end{array} \tag{3.194}$$

which, after denoting $\tilde{f}(x, u) = [f(x) + g(x)u]$ yields

$$A = \begin{pmatrix} \frac{\partial \tilde{f}_1}{\partial x_1} & \frac{\partial \tilde{f}_1}{\partial x_2} & \cdots & \frac{\partial \tilde{f}_1}{\partial x_n} \\ \frac{\partial \tilde{f}_2}{\partial x_1} & \frac{\partial \tilde{f}_2}{\partial x_2} & \cdots & \frac{\partial \tilde{f}_2}{\partial x_n} \\ \cdots & \cdots & \cdots & \cdots \\ \cdots & \cdots & \cdots & \cdots \\ \frac{\partial \tilde{f}_n}{\partial x_1} & \frac{\partial \tilde{f}_n}{\partial x_2} & \cdots & \frac{\partial \tilde{f}_n}{\partial x_n} \end{pmatrix} \quad B = \begin{pmatrix} g_1 \\ g_2 \\ \cdots \\ \cdots \\ g_n \end{pmatrix} \tag{3.195}$$

Using that the effects of linearization error due to truncation of higher order terms in the Taylor series expansion are denoted with the vector d_1, the dynamics of the approximately linearized system is given by

$$\dot{x} = Ax + Bu + d_1 \tag{3.196}$$

Moreover, considering that u^* is the control signal which achieves perfect tracking of the reference trajectories x_d one has

$$\dot{x}_d = Ax_d + Bu^* + d_2 \tag{3.197}$$

where $u^* = u + \Delta u$. From Eq. (3.196) one obtains

$$\dot{x} = Ax + Bu + Bu^* - Bu^* + d_1 \tag{3.198}$$

and by denoting $d_3 = -Bu^* + d_1$ one gets

$$\dot{x} = Ax + Bu + Bu^* + d_3 \tag{3.199}$$

By subtracting Eq. (3.197) from (3.199) one has

$$\begin{gathered} \dot{x} - \dot{x}^* = A(x - x^*) + Bu + d_3 - d_1 \Rightarrow \\ \dot{e} = Ae + Bu + L\tilde{d} \end{gathered} \tag{3.200}$$

where $A \in R^{n \times n}$, $B \in R^{n \times 1}$ and $L = I_n$ that is the identity matrix of dimension n. Equation (3.200) denotes the tracking error dynamics for the model that is obtained from approximate linearization, when the stabilizing feedback control u (e.g. H-infinity control) is applied on it.

In case that functions $f(x)$ and $g(x)$ in Eq. (3.193) are unknown, one has to compute the Jacobian matrices $A = \nabla_x [f(x) + g(x)u]|_{(x^*, u^*)}$ and $B = \nabla_u [f(x) + g(x)u]|_{(x^*, u^*)}$ using the estimated values of functions $f(x)$ and $g(x)$. The estimates $\hat{f}(x)$ and $\hat{g}(x)$ can be obtained from neurofuzzy networks. In such a case the estimated values of the Jacobian matrices are computed as follows:

$$\begin{gathered} \hat{A} = \nabla_x [\hat{f}(x) + \hat{g}(x)u]_{(x^*, u^*)} \Rightarrow \quad \hat{B} = \nabla_u [\hat{f}(x) + \hat{g}(x)u]_{(x^*, u^*)} \Rightarrow \\ \hat{A} = \nabla_x \hat{\tilde{f}}_{(x^*, u^*)} \qquad\qquad \hat{B} = \hat{g}(x) \end{gathered} \tag{3.201}$$

which, after denoting $\hat{\tilde{f}}(x, u) = [\hat{f}(x) + \hat{g}(x)u]$ gives

$$\hat{A} = \begin{pmatrix} \frac{\partial \hat{f}_1}{\partial x_1} & \frac{\partial \hat{f}_1}{\partial x_2} & \cdots & \frac{\partial \hat{f}_1}{\partial x_n} \\ \frac{\partial \hat{f}_2}{\partial x_1} & \frac{\partial \hat{f}_2}{\partial x_2} & \cdots & \frac{\partial \hat{f}_2}{\partial x_n} \\ \cdots & \cdots & \cdots & \cdots \\ \cdots & \cdots & \cdots & \cdots \\ \frac{\partial \hat{f}_n}{\partial x_1} & \frac{\partial \hat{f}_n}{\partial x_2} & \cdots & \frac{\partial \hat{f}_n}{\partial x_n} \end{pmatrix} \hat{B} = \begin{pmatrix} \hat{g}_1 \\ \hat{g}_2 \\ \cdots \\ \cdots \\ \hat{g}_n \end{pmatrix} \tag{3.202}$$

When using a model of the system that is based on the approximated Jacobians $\hat{A}$ and $\hat{B}$ the tracking error dynamics is given by

$$\dot{\hat{e}} = \hat{A}\hat{e} + \hat{B}u + \hat{L}\tilde{d} \tag{3.203}$$

where the feedback control input can be obtained from an H-infinity control law as $u = -\frac{1}{r}\hat{B}^T P\hat{e}$ and matrix P will be obtained from the solution of the algebraic Riccati equation of the generic form

$$\hat{A}^T P + P\hat{A} + Q - P\left(\frac{1}{r}\hat{B}\hat{B}^T - \frac{1}{\rho^2}\hat{L}\hat{L}^T\right)P = 0. \tag{3.204}$$

3.4.4 Estimation of the Unknown Dynamics of the System

For the estimation of the unknown dynamics of the rotary pendulum one proceeds as follows: It is considered that the unknown functions $f(x)$ and $g(x)$ that constitute the dynamic model of the system can be approximated by a neurofuzzy network (Fig. 3.17)

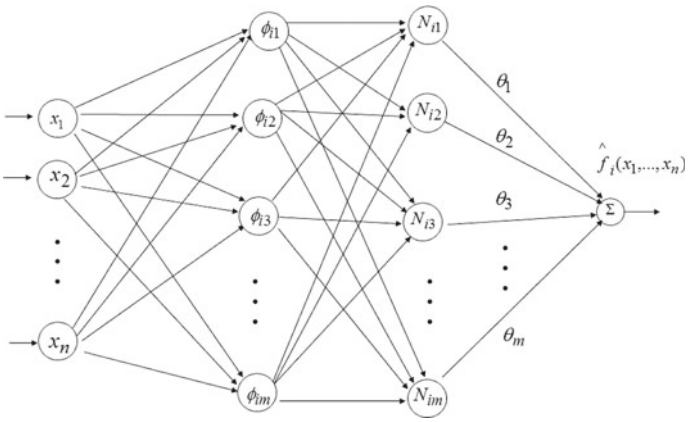

Fig. 3.17 Neurofuzzy approximator for estimating the unknown dynamics of the system: Φ_{ij} are kernel functions, N_{ij} are normalized kernel functions, and θ_j are weights

$$\hat{f}(x) = \begin{pmatrix} \hat{f}_1(x) \\ \hat{f}_2(x) \\ \cdots \\ \cdots \\ \hat{f}_n(x) \end{pmatrix} = \begin{pmatrix} \phi_{11}(x) & \phi_{12}(x) & \cdots & \phi_{1m}(x) \\ \phi_{21}(x) & \phi_{22}(x) & \cdots & \phi_{2m}(x) \\ \cdots & \cdots & \cdots & \cdots \\ \cdots & \cdots & \cdots & \cdots \\ \phi_{n1}(x) & \phi_{n2}(x) & \cdots & \phi_{nm}(x) \end{pmatrix} \begin{pmatrix} \theta_1^f \\ \theta_2^f \\ \cdots \\ \cdots \\ \theta_m^f \end{pmatrix} \tag{3.205}$$

$$\hat{g}(x) = \begin{pmatrix} \hat{g}_1(x) \\ \hat{g}_2(x) \\ \cdots \\ \cdots \\ \hat{g}_n(x) \end{pmatrix} = \begin{pmatrix} \phi_{11}(x) & \phi_{12}(x) & \cdots & \phi_{1m}(x) \\ \phi_{21}(x) & \phi_{22}(x) & \cdots & \phi_{2m}(x) \\ \cdots & \cdots & \cdots & \cdots \\ \cdots & \cdots & \cdots & \cdots \\ \phi_{n1}(x) & \phi_{n2}(x) & \cdots & \phi_{nm}(x) \end{pmatrix} \begin{pmatrix} \theta_1^g \\ \theta_2^g \\ \cdots \\ \cdots \\ \theta_m^g \end{pmatrix} \tag{3.206}$$

where $\phi_{ij}(x)$, $i = 1, 2, \ldots, n$, $j = 1, 2, \ldots, n$ are kernel functions, while θ_i^f, θ_i^g, $i = 1, 2, \ldots, n$ are the weights of the neural approximators for functions f and g respectively. Equivalently, it holds that

$$\hat{f}(x) = \Phi(x)\theta_f \quad \hat{g}(x) = \Phi(x)\theta_g \tag{3.207}$$

where $\hat{f}(x) \in R^{n\times 1}, \Phi(x) \in R^{n\times m}, \theta_f(x) \in R^{m\times 1}, \hat{g}(x) \in R^{n\times 1}$ and $\theta_g(x) \in R^{m\times 1}$. The elements of matrix $\Phi(x) \in R^{n\times m}$ are the kernel functions $\phi_{ij}(x)$, $i = 1, \ldots, n$, $j = 1, \ldots, m$ which are defined as

$$\phi_{ij}(x) = \frac{\prod_{i=1}^{n} \mu_{A^{i,j}}(x_i)}{\sum_{k=1}^{n} \prod_{i=1}^{m} \mu_{A^{i,k}}(x_i)} \tag{3.208}$$

The value of the weight vector θ_f that achieves optimal approximation of function f is denoted as θ_f^*. Equivalently, the value of the weight vector θ_g that achieves optimal approximation of function g is denoted as θ_g^*.

The weight vector errors for the approximation of functions $f(x)$ and $g(x)$ are defined as

$$\tilde{\theta}_f = \theta_f - \theta_f^* \; \tilde{\theta}_g = \theta_g - \theta_g^* \tag{3.209}$$

Using Eq. (3.205) one has about the approximations of functions $\hat{f}(x)$ and $\hat{g}(x)$:

$$\hat{f} = \begin{pmatrix} \hat{f}_1 \\ \hat{f}_2 \\ \cdots \\ \cdots \\ \hat{f}_n \end{pmatrix} = \begin{pmatrix} \sum_{i=1}^{m} \theta_i^f \phi_{i1}(x) \\ \sum_{i=1}^{m} \theta_i^f \phi_{i2}(x) \\ \cdots \\ \cdots \\ \sum_{i=1}^{m} \theta_i^f \phi_{in}(x) \end{pmatrix} \; \hat{g} = \begin{pmatrix} \hat{g}_1 \\ \hat{g}_2 \\ \cdots \\ \cdots \\ \hat{g}_n \end{pmatrix} = \begin{pmatrix} \sum_{i=1}^{m} \theta_i^g \phi_{i1}(x) \\ \sum_{i=1}^{m} \theta_i^g \phi_{i2}(x) \\ \cdots \\ \cdots \\ \sum_{i=1}^{m} \theta_i^g \phi_{in}(x) \end{pmatrix} \tag{3.210}$$

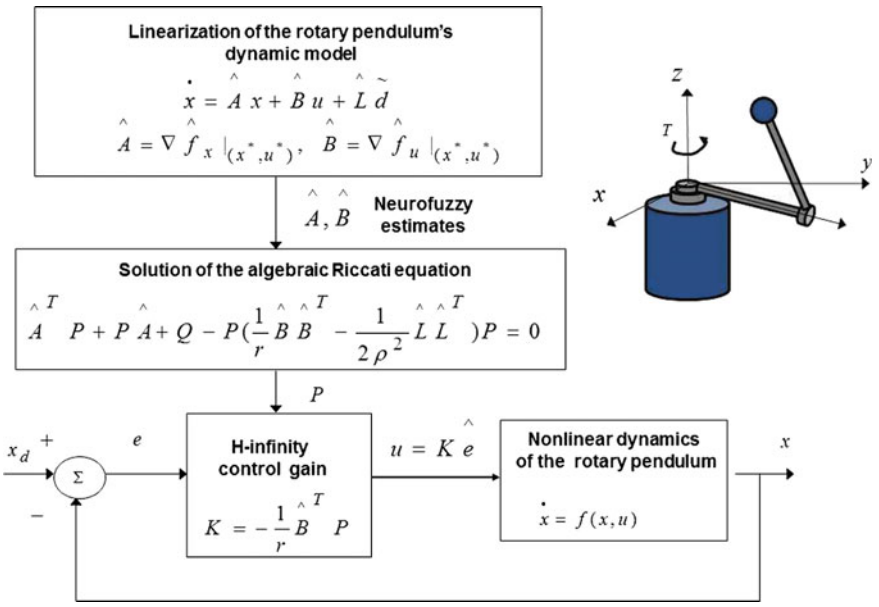

Fig. 3.18 Adaptive neurofuzzy H-infinity control loop of the rotary pendulum

Thus, the approximation of the Jacobians of vector fields $\hat{f}(x)$ and $\hat{g}(x)$ becomes

$$\nabla_x \hat{f}(x) = \begin{pmatrix} \frac{\partial \hat{f}_1(x)}{\partial x_1} & \frac{\partial \hat{f}_1(x)}{\partial x_2} & \cdots & \frac{\partial \hat{f}_1(x)}{\partial x_n} \\ \frac{\partial \hat{f}_2(x)}{\partial x_1} & \frac{\partial \hat{f}_2(x)}{\partial x_2} & \cdots & \frac{\partial \hat{f}_2(x)}{\partial x_n} \\ \cdots & \cdots & \cdots & \cdots \\ \frac{\partial \hat{f}_n(x)}{\partial x_1} & \frac{\partial \hat{f}_n(x)}{\partial x_2} & \cdots & \frac{\partial \hat{f}_n(x)}{\partial x_n} \end{pmatrix} \nabla_x \hat{g}(x) = \begin{pmatrix} \frac{\partial \hat{g}_1(x)}{\partial x_1} & \frac{\partial \hat{g}_1(x)}{\partial x_2} & \cdots & \frac{\partial \hat{g}_1(x)}{\partial x_n} \\ \frac{\partial \hat{g}_2(x)}{\partial x_1} & \frac{\partial \hat{g}_2(x)}{\partial x_2} & \cdots & \frac{\partial \hat{g}_2(x)}{\partial x_n} \\ \cdots & \cdots & \cdots & \cdots \\ \frac{\partial \hat{g}_n(x)}{\partial x_1} & \frac{\partial \hat{g}_n(x)}{\partial x_2} & \cdots & \frac{\partial \hat{g}_n(x)}{\partial x_n} \end{pmatrix} \quad (3.211)$$

The above relations can be used in the approximately linearized model of the system, after setting $\hat{A} = [\nabla_x \hat{f}(x) + \nabla_x \hat{g}(x)u]\,|_{(x^*,u^*)}$ and $\hat{B} = \hat{g}(x)\,|_{(x^*,u^*)}$.

The diagram of the proposed adaptive neurofuzzy H-infinity control loop for the rotary pendulum, is depicted in Fig. 3.18.

3.4.5 Lyapunov Stability Analysis

For the dynamic model of the rotary pendulum, the following Lyapunov function is defined

$$V = \tfrac{1}{2}\hat{e}^T P\hat{e} + \tfrac{1}{2\gamma_1}\tilde{\theta}_f^T\tilde{\theta}_f + \tfrac{1}{2\gamma_2}\tilde{\theta}_g^T\tilde{\theta}_g \quad (3.212)$$

By differentiating Eq. (3.212) with respect to time one obtains

$$\dot{V} = \tfrac{1}{2}\dot{\hat{e}}^T P\hat{e} + \tfrac{1}{2}\hat{e^T} P\dot{\hat{e}} + \tfrac{1}{\gamma_1}\dot{\hat{\theta}}_f^T\tilde{\theta}_f + \tfrac{1}{\gamma_2}\dot{\tilde{\theta}}_g^T\tilde{\theta}_g \tag{3.213}$$

and using that the tracking error dynamics for the model comprising $\hat{A}$ and $\hat{B}$ is given by

$$\dot{\hat{e}} = \hat{A}\hat{e} + \hat{B}u + \hat{L}\tilde{d} \tag{3.214}$$

then one obtains

$$\begin{gathered}\dot{V} = \tfrac{1}{2}(\hat{e}^T\hat{A}^T + u^T\hat{B} + \tilde{d}^T\hat{L}^T)P\hat{e} + \tfrac{1}{2}\hat{e}^T P(\hat{A}\hat{e} + \hat{B}u + \hat{L}\tilde{d}) + \\ + \tfrac{1}{\gamma_1}\dot{\tilde{\theta}}_f^T\tilde{\theta}_f + \tfrac{1}{\gamma_2}\dot{\tilde{\theta}}_g^T\tilde{\theta}_g +\end{gathered} \tag{3.215}$$

The feedback control signal is

$$u = -\tfrac{1}{r}\hat{B}^T Pe \tag{3.216}$$

where P comes from the solution of a Riccati equation. By advancing with computations one gets

$$\begin{gathered}\dot{V} = \tfrac{1}{2}\hat{e}^T\hat{A}^T P\hat{e} + \tfrac{1}{2}u^T\hat{B}^T P\hat{e} + \tfrac{1}{2}\tilde{d}^T\hat{L}^T P\hat{e} \\ + \tfrac{1}{2}\hat{e}^T P\hat{A}\hat{e} + \tfrac{1}{2}\hat{e}^T P\hat{B}u + \tfrac{1}{2}\hat{e}^T P\hat{L}\tilde{d} \\ + \tfrac{1}{\gamma_1}\dot{\tilde{\theta}}_f^T\tilde{\theta}_f + \tfrac{1}{\gamma_2}\dot{\tilde{\theta}}_g^T\tilde{\theta}_g\end{gathered} \tag{3.217}$$

By grouping terms in the above equation one obtains

$$\begin{gathered}\dot{V} = \tfrac{1}{2}\hat{e}^T\left(\hat{A}P + P\hat{A} - \tfrac{1}{r}P\hat{B}\hat{B}^T P\right)\hat{e} + \tilde{d}^T\hat{L}^T P\hat{e} + \\ + \tfrac{1}{\gamma_1}\dot{\tilde{\theta}}_f^T\tilde{\theta}_f + \tfrac{1}{\gamma_2}\dot{\tilde{\theta}}_g^T\tilde{\theta}_g\end{gathered} \tag{3.218}$$

Assumption: The following algebraic Riccati equation is considered to admit as solution a positive definite symmetric matrix P

$$\hat{A}P + P\hat{A} + Q - \tfrac{1}{r}P\hat{B}\hat{B}^T P + \tfrac{1}{2\rho^2}P\hat{L}\hat{L}^T P = 0 \tag{3.219}$$

The above algebraic Riccati equation is equivalently written as

$$\hat{A}P + P\hat{A} - \tfrac{1}{r}P\hat{B}\hat{B}^T P = -Q - \tfrac{1}{2\rho^2}P\hat{L}\hat{L}^T P = 0 \tag{3.220}$$

By substituting Eq. (3.220) into (3.218) one has

$$\begin{gathered}\dot{V} = -\tfrac{1}{2}\hat{e}^T Q\hat{e} - \tfrac{1}{2\rho^2}\hat{e}^T P\hat{L}\hat{L}^T P\hat{e} + \hat{e}^T P\hat{L}\tilde{d} + \\ + \tfrac{1}{\gamma_1}\dot{\tilde{\theta}}_f^T\tilde{\theta}_f + \tfrac{1}{\gamma_2}\dot{\tilde{\theta}}_g^T\tilde{\theta}_g\end{gathered} \tag{3.221}$$

Next, the following weights adaptation laws are considered

$$\begin{array}{c}\dot{\theta}_f = -\gamma_1 \phi^T \hat{L}^T P \hat{e} \;\text{ or }\; \dot{\theta}_f^T = -\gamma_1 \hat{e}^T P \hat{L} \Phi \\ \dot{\theta}_g = -\gamma_2 \phi^T \hat{L}^T P \hat{e} u \text{ or } \dot{\theta}_g^T = -\gamma_2 u \hat{e}^T P \hat{L} \Phi\end{array} \tag{3.222}$$

By substituting the weights' adaptation laws of Eq. (3.222) into (3.221) one has

$$\begin{array}{c}\dot{V} = -\frac{1}{2}\hat{e}^T Q \hat{e} - \frac{1}{2\rho^2}\hat{e}^T P \hat{L}\hat{L}^T P \hat{e} + \hat{e}^T P \hat{L}\tilde{d} + \\ + \frac{1}{\gamma_1}(-\gamma_1)\hat{e}^T p \hat{L} \Phi (\theta_f - \theta_f^*) + \frac{1}{\gamma_2}(-\gamma_2)\hat{e}^T p \hat{L} \Phi (\theta_g - \theta_g^*) u\end{array} \tag{3.223}$$

By elaborating on computations in the previous relation one gets

$$\begin{array}{c}\dot{V} = -\frac{1}{2}\hat{e}^T Q \hat{e} - \frac{1}{2\rho^2}\hat{e}^T P \hat{L}\hat{L}^T P \hat{e} + \hat{e}^T P \hat{L}\tilde{d} + \\ -\hat{e}^T P \hat{L}\{[\hat{f}(x|\theta_f) - \hat{f}(x|\theta_f^*)] + [\hat{g}(x|\theta_g) - \hat{g}(x|\theta_g^*)]u\}\end{array} \tag{3.224}$$

Actually the modelling error term w_a is

$$\begin{array}{c}w_a = [\hat{f}(x|\theta_f) - \hat{f}(x|\theta_f^*)] + [\hat{g}(x|\theta_g) - \hat{g}(x|\theta_g^*)]u \;\text{ or} \\ w_a = [\hat{f}(x|\theta_f) + \hat{g}(x|\theta_g)u] - [\hat{f}(x|\theta_f^*) + \hat{g}(x|\theta_g^*)u]\end{array} \tag{3.225}$$

denotes the difference in the approximation of the nonlinear dynamics of the rotary pendulum $\dot{x} = f(x) + g(x)u$ when described with neural networks of weights θ_f, θ_g and when described with neural networks having the optimal estimation weights θ_f^*, θ_g^*. By substituting w_a in Eq. (3.224) one obtains

$$\dot{V} = -\frac{1}{2}\hat{e}^T Q \hat{e} - \frac{1}{2\rho^2}\hat{e}^T P \hat{L}\hat{L}^T P \hat{e} + \hat{e}^T P \hat{L}\tilde{d} - \hat{e}^T P \hat{L} w_a \tag{3.226}$$

By defining $w_1 = \tilde{d} - w_a$ one has

$$\dot{V} = -\frac{1}{2}\hat{e}^T Q \hat{e} - \frac{1}{2\rho^2}\hat{e}^T P \hat{L}\hat{L}^T P \hat{e} + \hat{e}^T P \hat{L} w_1 \tag{3.227}$$

Equation (3.228) is written in the equivalent form

$$\begin{array}{c}\dot{V} = -\frac{1}{2}\hat{e}^T Q \hat{e} - \frac{1}{2\rho^2}\hat{e}^T P \hat{L}\hat{L}^T P \hat{e} + \\ + \frac{1}{2}\hat{e}^T P \hat{L} w_1 + \frac{1}{2} w_1^T \hat{L}^T \hat{e}\end{array} \tag{3.228}$$

Lemma: The following inequality holds

$$\frac{1}{2}\hat{e}^T P \hat{L} w_1 + \frac{1}{2} w_1 \hat{L}^T P \hat{e} - \frac{1}{2\rho^2}\hat{e}^T P \hat{L}\hat{L}^T P \hat{e} \leq \frac{1}{2}\rho^2 w_1^T w_1 \tag{3.229}$$

Proof: The binomial $(\rho\alpha - \frac{1}{\rho}b)^2$ is considered. Expanding the left part of the above inequality one gets

$$\begin{array}{c}\rho^2a^2+\frac{1}{\rho^2}b^2-2ab\geq 0\Rightarrow \frac{1}{2}\rho^2a^2+\frac{1}{2\rho^2}b^2-ab\geq 0\Rightarrow\\ ab-\frac{1}{2\rho^2}b^2\leq \frac{1}{2}\rho^2a^2\Rightarrow \frac{1}{2}ab+\frac{1}{2}ab-\frac{1}{2\rho^2}b^2\leq \frac{1}{2}\rho^2a^2\end{array} \tag{3.230}$$

The following substitutions are carried out: $a = w_1$ and $b = \hat{e}^T P\hat{L}$ and the previous relation becomes

$$\frac{1}{2}w_1^T\hat{L}^T P\hat{e}+\frac{1}{2}\hat{e}^T P\hat{L}w_1-\frac{1}{2\rho^2}\hat{e}^T P\hat{L}\hat{L}^T P\hat{e}\leq\frac{1}{2}\rho^2w_1^Tw_1 \tag{3.231}$$

Equation (3.231) signifies the completion of the Lemma's proof. Equation (3.231) is substituted in Eq. (3.228) and the inequality is enforced, thus giving

$$\dot{V}\leq-\frac{1}{2}\hat{e}^TQ\hat{e}+\frac{1}{2}\rho^2w_1^Tw_1 \tag{3.232}$$

Equation (3.232) shows that the H_∞ tracking performance criterion is satisfied. This implies that the effect that the modelling error and external perturbations may have on the control system is finally taken into account by the condition defining the sign of the first derivative of the system's Lyapunov function. If the disturbance term w_1 vanishes then one has a clear asymptotic stability condition. By selecting the attenuation coefficient ρ to be sufficiently small and in particular to satisfy $\rho^2 < ||\hat{e}||_Q^2/||w_1||^2$ one has that the first derivative of the Lyapunov function is upper bounded by 0. Therefore for each time interval it is proven that the Lyapunov function defined in Eq. (3.212) is a decreasing one, and that at every time instant its value keeps on diminishing. This also assures that the first-order derivative of the Lyapunov function of the system defined in Eq. (3.212) will be always negative.

Equivalently to the above, the integration of $\dot{V}$ from 0 to T gives

$$\begin{array}{c}\int_0^T\dot{V}(t)dt\leq-\frac{1}{2}\int_0^T||\hat{e}||_Q^2dt+\frac{1}{2}\rho^2\int_0^T||w_1||^2dt\Rightarrow\\ 2V(T)+\int_0^T||\hat{e}||_Q^2dt\leq 2V(0)+\rho^2\int_0^T||w_1||^2dt\end{array} \tag{3.233}$$

Moreover, if there exists a positive constant $M_d > 0$ such that

$$\int_0^\infty||w_1||^2dt\leq M_d \tag{3.234}$$

then one gets

$$\int_0^\infty||\hat{e}||_Q^2dt\leq 2V(0)+\rho^2M_d \tag{3.235}$$

Thus, the integral $\int_0^\infty||\hat{e}||_Q^2dt$ is bounded. Moreover, $V(T)$ is bounded and from the definition of the Lyapunov function V in Eq. (3.212) it becomes clear that $\hat{e}(t)$ will be also bounded since $\hat{e}(t) \in \Omega_{\hat{e}} = \{\hat{e}|\hat{e}^TP\hat{e}\leq 2V(0)+\rho^2M_d\}$. According to the above and with the use of Barbalat's Lemma one obtains $lim_{t\to\infty}\hat{e}(t) = 0$.

3.4.6 Simulation Tests

In the implementation of simulation tests about the adaptive neurofuzzy H-infinity control method of Furuta's pendulum it has been assumed that the parameters of the pendulum's model were unknown, For the computation of the feedback control law, the Riccati equation appearing in Eq. (3.220) had to be solved at each iteration of the control method. This in turn made use of the Jacobian matrices $\hat{A} = \nabla_x[\hat{f}(x) + \hat{g}(x)u]$ and $\hat{B} = \nabla_u[\hat{f}(x) + \hat{g}(x)u]$ which were approximated with the use of neurofuzzy estimators. The obtained results are depicted in Figs. 3.19, 3.20, 3.21, 3.22, 3.23, 3.24 and 3.25.

The approximation of the unknown functions $\hat{f}(x)$ and $\hat{g}(x)$ was performed with the use of neurofuzzy estimators. There are four input fuzzy variables x_i associated with the state variables of the pendulum, that is $x_1 = \phi$, $x_2 = \dot{\phi}$, $x_3 = \theta$ and $x_4 = \dot{\theta}$. Considering that each one of them is analyzed into three fuzzy sets A_i, then there should be in aggregate $3^4 = 81$ fuzzy rules. The aggregate fuzzy rule base takes the form given in Table 3.5. Each neurofuzzy estimator comprises rules of the form

$$\begin{aligned} &R^l : IF\ \ x_1\ \ is\ \ A_1^l\ \ AND\ \ x_2\ \ is\ \ A_2^l \\ &AND\ \ x_3\ \ is\ \ A_3^l\ \ AND\ \ x_4\ \ is\ \ A_4^l\ \ THEN\ \ \hat{f}_i^l\ \ is\ \ b^l \end{aligned} \tag{3.236}$$

where $l = 1, \ldots, 81$ and $\hat{f}(x,t) = \frac{\sum_{l=1}^{81} \hat{f}_i^l \prod_{i=1}^{4} \mu_{A_i^l}(x_i)}{\sum_{l=1}^{81} \prod_{i=1}^{4} \mu_{A_i^l}(x_i)}$. Indicative (dimensionless) values for the placement on a spatial grid of the centers $c_i^{(l)}$, $i = 1, \ldots, 4$ and about the variances $v^{(l)}$ of each rule are as follows (Table 3.5):

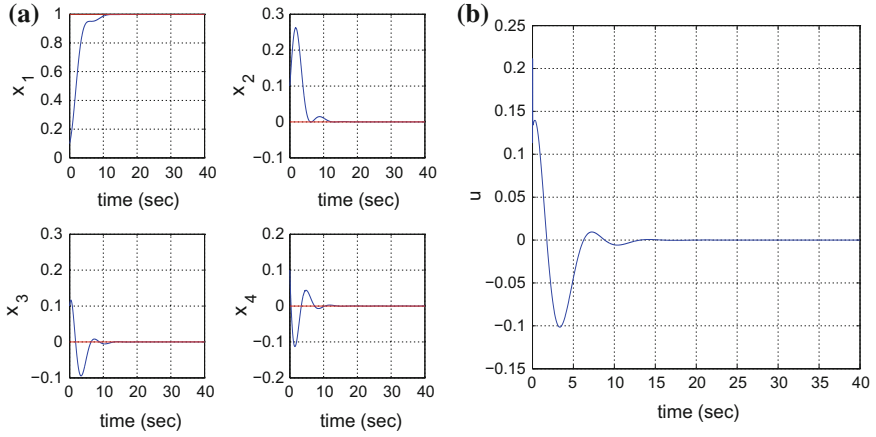

Fig. 3.19 H-infinity neural adaptive control of the underactuated rotary pendulum: **a** Tracking of setpoint 1 by the state variables x_i, $i = 1, \ldots, 4$ of the pendulum **b** control input u

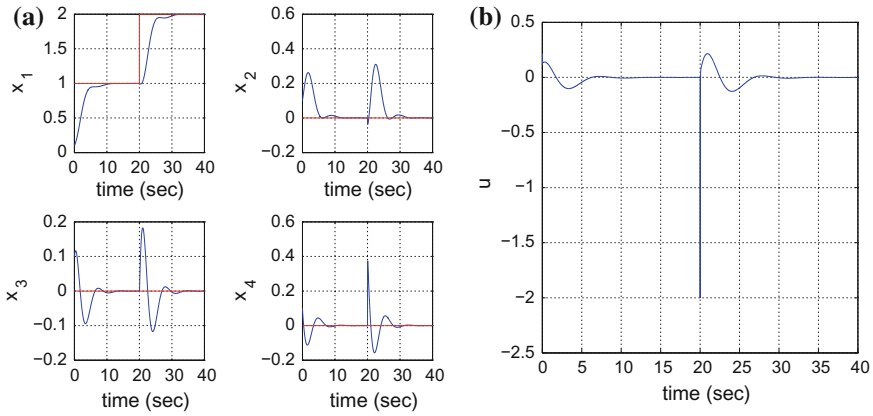

Fig. 3.20 H-infinity neural adaptive control of the underactuated rotary pendulum: **a** Tracking of setpoint 2 by the state variables $x_i,\ i = 1, \ldots, 4$ of the pendulum **b** control input u

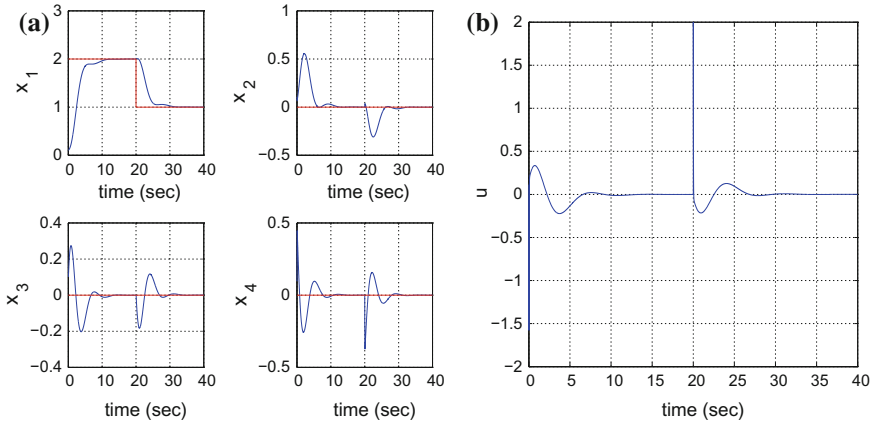

Fig. 3.21 H-infinity neural adaptive control of the underactuated rotary pendulum: **a** Tracking of setpoint 3 by the state variables $x_i,\ i = 1, \ldots, 4$ of the pendulum **b** control input u

The finer the partition of the input variables into fuzzy sets is, the more accurate the approximation of the nonlinear system dynamics by the neuro-fuzzy model is expected to be (although some of the rules of the fuzzy rule base may not be sufficiently activated due to little coverage of the associated region of the patterns space by input data). However, considering a large number of fuzzy sets for each input

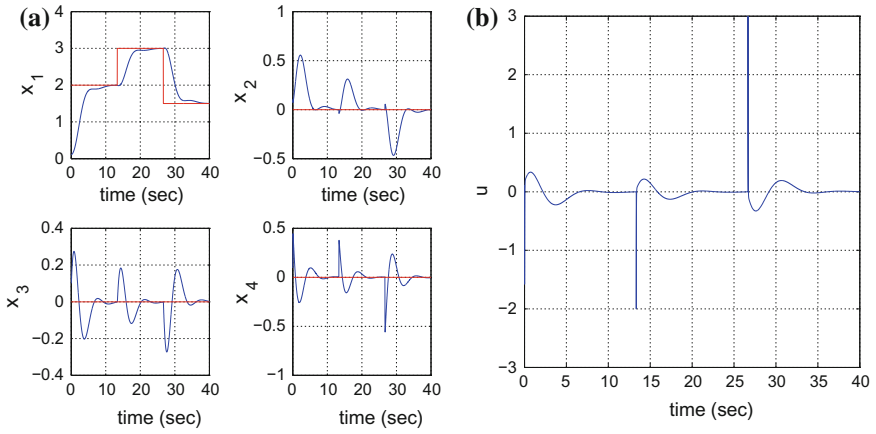

Fig. 3.22 H-infinity neural adaptive control of the underactuated rotary pendulum: **a** Tracking of setpoint 4 by the state variables $x_i,\ i = 1, \ldots, 4$ of the pendulum **b** control input u

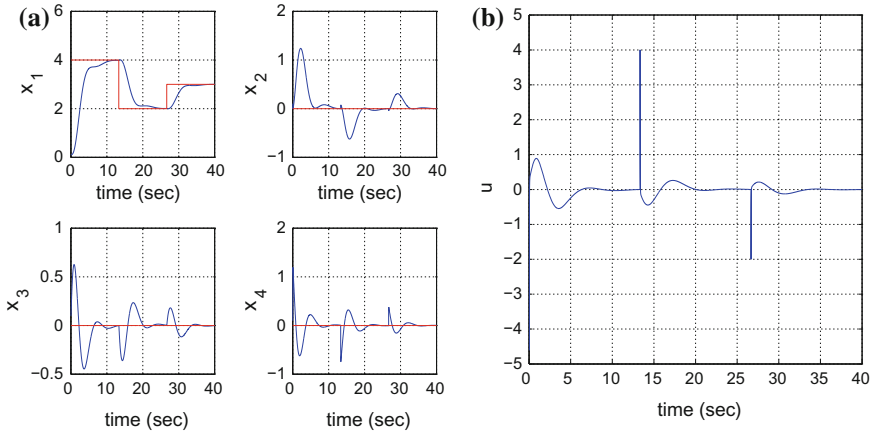

Fig. 3.23 H-infinity neural adaptive control of the underactuated rotary pendulum: **a** Tracking of setpoint 5 by the state variables $x_i,\ i = 1, \ldots, 4$ of the pendulum **b** control input u

variable induces the curse of dimensionality which means that there is an excessive and rather unnecessary increase in the number of the adaptable parameters that constitute the neuro-fuzzy model.

From Figs. 3.19, 3.20, 3.21, 3.22, 3.23, 3.24 and 3.25, it can be noticed that the proposed control method achieves fast and accurate tracking of the reference setpoints for the state variables of the rotary pendulum. The associated variations of the control

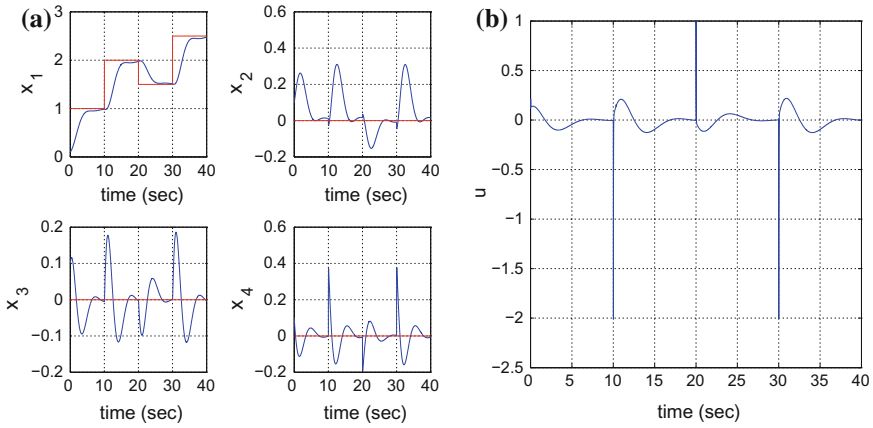

Fig. 3.24 H-infinity neural adaptive control of the underactuated rotary pendulum: **a** Tracking of setpoint 6 by the state variables $x_i,\ i = 1, \ldots, 4$ of the pendulum **b** control input u

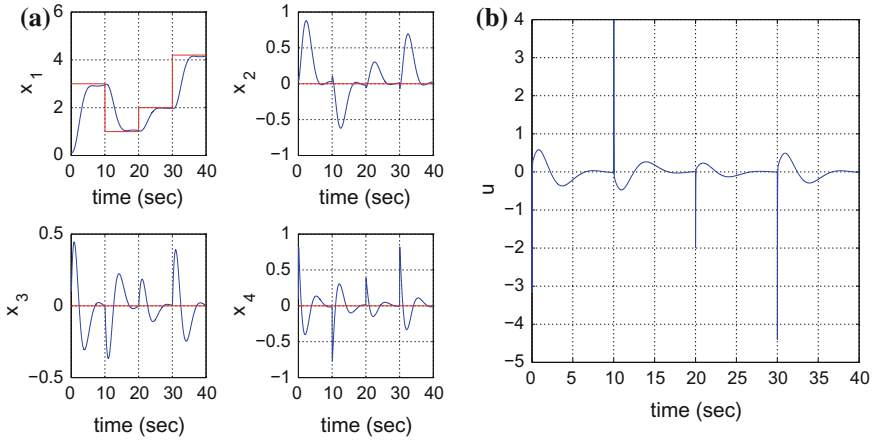

Fig. 3.25 H-infinity neural adaptive control of the underactuated rotary pendulum: **a** Tracking of setpoint 7 by the state variables $x_i,\ i = 1, \ldots, 4$ of the pendulum **b** control input u

input remained moderate. This comes to confirm the previously given theoretical analysis about the stability and convergence of the proposed control scheme and to show its application to underactuated robotic systems.

Table 3.5 Parameters of the fuzzy rule base

Rule	$c_1^{(l)}$	$c_2^{(l)}$	$c_3^{(l)}$	$c_4^{(l)}$	$v^{(l)}$
$R^{(1)}$	-1.0	-1.0	-1.0	-1.0	3
$R^{(2)}$	-1.0	-1.0	-1.0	0.0	3
$R^{(3)}$	-1.0	-1.0	-1.0	1.0	3
$R^{(4)}$	-1.0	-1.0	0.0	-1.0	3
$R^{(5)}$	-1.0	-1.0	0.0	0.0	3
$R^{(6)}$	-1.0	-1.0	0.0	1.0	3
...	...	...	...	...	
$R^{(25)}$	-1.0	1.0	1.0	-1.0	3
$R^{(26)}$	-1.0	1.0	1.0	0.0	3
$R^{(27)}$	-1.0	1.0	1.0	1.0	3
...	...	...	...	...	
$R^{(81)}$	1.0	1.0	1.0	1.0	3

Chapter 4
Closed-Chain Robotic Systems and Mechanisms

Abstract Control of closed-chain robots is a non-trivial problem because it is often associated with complicated dynamic and kinematics models exhibiting nonlinearities. Unlike robotic manipulators with a free end-effector, closed-chain robotic mechanisms include actuators which are usually placed on a fixed base. On the one side this enables to develop robotic and mechatronic systems with low moving inertia and fast motion control. On the other side this may incur underactuation problems. Comparing to open-chain robots, closed-chain robotic mechanisms have many advantages such as high stiffness, high accuracy, and high payload-to-weight ratio To solve the nonlinear control problem of closed-chain robotic systems the following approaches are proposed (i) nonlinear control based on global linearization methods, (ii) nonlinear control based on approximate linearization methods and (iii) nonlinear control based on Lyapunov methods. Besides to apply model-free control for such a type of robotic manipulators, online estimation algorithms of the unknown dynamics of the robot can be considered once again. The global asymptotic stability of the control based on the real-time estimation of the robot's dynamics is proven. Moreover, as in the previously analysed multi-DOF manipulator models, to implement feedback control through the measurement of a limited number of the closed-chain robot's state vector elements, nonlinear filtering methods of proven convergence are developed. In particular the chapter analyzes the following topics: (a) Model-based control of closed-chain kinematic mechanisms with the use of differential flatness theory, (b) Flatness-based adaptive fuzzy control of closed-chain kinematic mechanisms (c) Nonlinear optimal control for closed-chain kinematic mechanisms.

4.1 Chapter Overview

The present chapter develops the following topics: (a) Model-based control of closed-chain kinematic mechanisms with the use of differential flatness theory, (b) Flatness-based adaptive fuzzy control of closed-chain kinematic mechanisms (c) Nonlinear optimal control for closed-chain kinematic mechanisms.

With reference to (a) global linearization-based control for underactuated closed-chain robotic systems is considered. Using differential flatness theory it is shown

G. Rigatos and K. Busawon, *Robotic Manipulators and Vehicles*,
Studies in Systems, Decision and Control 152,
https://doi.org/10.1007/978-3-319-77851-8_4

that the model of a closed-chain 2-DOF robotic manipulator can be transformed to linear canonical form. For the linearized equivalent of the robotic system it is demonstrated that a state feedback controller can be designed. Since certain elements of the state vector of the linearized system can not be measured directly, it is proposed to estimate them with the use of a differential flatness theory-based implementation of the Kalman Filter, the so-called Derivative-free nonlinear Kalman Filter (DKF). Moreover, by redesigning the Kalman Filter as a disturbance observer, it is shown that one can estimate simultaneously external disturbances terms that affect the robotic model or disturbance terms which are associated with parametric uncertainty.

With reference to (b) an adaptive fuzzy controller is designed for the previously noted closed-chain 2-DOF robotic manipulator, under the constraint that the system's model is unknown. After transforming the robotic system into the canonical form, the resulting control inputs are shown to contain nonlinear elements which depend on the system's parameters. The nonlinear terms which appear in the control inputs are approximated with the use of neuro-fuzzy networks. It is shown that a suitable learning law can be defined for the aforementioned neuro-fuzzy approximators so as to preserve the closed-loop system stability.

With reference to (c) the previously noted dynamic model of the closed-chain robotic mechanism undergoes approximate linearization, round a local operating point. This local equilibrium is re-calculated at each iteration of the control program. The linearization relies on Taylor series expansion and the computation of the associated Jacobian matrices. Next, an H-infinity feedback controller is designed. The feedback gain is computed after solving an algebraic Riccati equation at each iteration of the control algorithm. In all cases (a) to (c) the global asymptotic stability of the considered control schemes for the manipulators of closed-chain kinematics was proven through Lyapunov analysis.

4.2 Flatness-Based Control of Closed-Chain Kinematic Mechanisms

4.2.1 Outline

Control of underactuated closed-chain robots has received significant attention. The design of robotic mechanisms that can be controlled with a smaller number of actuators than their degrees of freedom enables to reduce cost and weight of robots and to achieve robustness in the case of actuators' failures [150, 197, 245, 246, 308, 356, 599, 636]. The control problem of underactuated robotic manipulators has been studied in several research articles during the last years. In [150] the property of differential flatness for a class of planar under-actuated open-chain robots having a specific inertia distribution, but driven by only one or two actuators has been analyzed. In [636] it was shown that closed chain underactuated robots satisfy differential flatness properties and this enables their transformation into a linearized form for

which the design of a feedback controller becomes easier. In [599] energy-based control for underactuated robotic manipulators has been proposed. In [245, 246] a Lyapunov-based approach to the design of efficient control for underactuated robots is proposed. In [356] passive velocity control and decoupling vector field control have been applied to the control of underactuated mechanical systems. In [308] the problem of point-to-point control for underactuated robotic manipulators has been presented. In [197] an open-loop vibrational control for an underactuated mechanical system has been studied.

Unlike robotic manipulators with a free end-effector, machines with closed chains include actuators which are usually placed on a fixed base. This enables to develop mechatronic systems with low moving inertia and fast motion control. The particular problem studied in this section is the controller design for a closed-chain mechatronic system, characterized by model uncertainty and subjected to external perturbations. Moreover, the control system is an underactuated one, which means that the number of actuators is less than the number of degrees of freedom in the associated dynamic model. Underactuation can be met in: (1) mobile manipulators carrying out cooperative tasks, (2) fixed-base robots that manipulate elastically deformable objects [159, 413, 474, 475, 563, 637]. Underactuated closed-chain robotic systems, containing fewer actuators than the degrees of freedom have little been studied. This is mainly due to strong nonlinearities of the associated dynamic model and the complexity in the controller's design.

In this section an approach to solve the problem of closed-chain underactuated robots is developed with the use of a flatness-based controller and a Kalman Filter-based disturbances estimator. Dynamic analysis for the closed-chain underactuated robot is first provided. Closed-chain robotic models can be underactuated and the efficient suppression of disturbance inputs is important for attaining the performance objectives of the control loop. The elements of the state vector are variables denoting the linear displacement and the rotation of the robot's joints. The control input to the model is the torque applied by an actuator to a joint that is mounted on a fixed base. Disturbance inputs can be due to model uncertainties or external perturbation forces and torques.

First, Lie algebra is used to perform input-output linearization to the robot's model. This enables to introduce a state-space transformation (diffeomorphism) which brings the system to the linear canonical Brunovsky form. Next, it is shown how a controller for the aforementioned robot model can be obtained through the application of differential flatness theory. The flat output for the robot's model is a nonlinear function of the linear and rotational displacement of the robot's joints [1, 151]. By expressing all state variables and the control input of the robotic model as functions of the flat output and its derivatives the system's dynamic model is transformed into the linear Brunovksy (canonical) form [57, 145, 254, 267, 322, 450, 476, 519, 572]. For the latter model it is possible to design a state feedback controller that enables accurate tracking of position and velocity set-points by the robot's joints. However, since measurements are available only for certain elements of the transformed state vector, to implement a state feedback control loop, the rest of the elements of the robot's transformed state vector have to be estimated with the use of an observer or filter. To this end the concept of *Derivative-free*

nonlinear Kalman Filtering is employed. By avoiding linearization approximations, the proposed filtering method improves the accuracy of estimation of the system's state variables [424, 438, 457].

A particular difficulty, in the case of state estimation for the robotic model is the existence of the unmodeled disturbance forces. It is shown that it is possible to redesign the Kalman Filter in the form of a disturbance observer and using the estimation of the disturbance to develop an auxiliary control input that compensates for the disturbances effects [87, 105, 106, 180, 341, 367]. In this way the robot's control system can become robust with respect to uncertainties in the model's parameters or uncertainties about external forces and torques. It is also noted that in terms of computation speed the proposed Kalman Filter-based disturbance estimator is faster than disturbance estimators that may rely on other nonlinear filtering approaches (e.g. Extended Kalman Filter, Unscented Kalman Filter or Particle Filter) thus becoming advantageous for the real-time estimation of the unknown dynamics of the robot. The efficiency of the proposed control and Kalman Filter-based disturbances estimation scheme is evaluated through numerical simulation tests. It has been shown that the accurate estimation of the disturbance forces which are exerted on the robot enables their efficient compensation. This is achieved by introducing an additional element in the controller that produces a counter-disturbance input based on the estimated value for the disturbance variable. This control scheme finally results in minimizing the effects of the disturbances that affect the robot.

4.2.2 Dynamic Model of the Closed-Chain 2-DOF Robotic System

The considered closed-chain 2-DOF robotic system depicted in Fig. 4.1 consists of four bodies: (i) bodies 1 and 2 are two sliders with masses m_1 and m_2 respectively [150, 636]. Body 3 is connected with a revolute joint to body 1 and has mass m_3, length l_3 while its moment of inertia is I_3. Similarly body 4 is connected to body 2 with a revolute joint, has mass m_4, length l_4 while the associated moment of inertia is I_4. The motion of the system takes place in the 2D xy plane depicted in Fig. 4.1 while its dynamics is subjected to gravity.

The state variables for the robotic system are as follows $q = [q_1, q_3, q_2, q_4]^T$: q_1 is the displacement of mass m_1 along the x-axis, q_3 is the turn angle of body 3 round the revolute joint A. q_2 is the displacement of m_2 along the x-axis and q_4 is the turn angle of body 4 round the revolute joint B. The following geometric constraints hold:

$$\begin{aligned} l_3 sin(q_3) &= l_4 sin(q_4) \\ q_1 + l_3 cos(q_3) &= q_2 + l_4 cos(q_4) \end{aligned} \tag{4.1}$$

The control inputs exerted on the robotic model are the horizontal force F_1 that causes the displacement of mass m_1 along the x-axis, the torque T_3 that causes the rotation of the link with length l_3 round the revolute joint A, the horizontal force

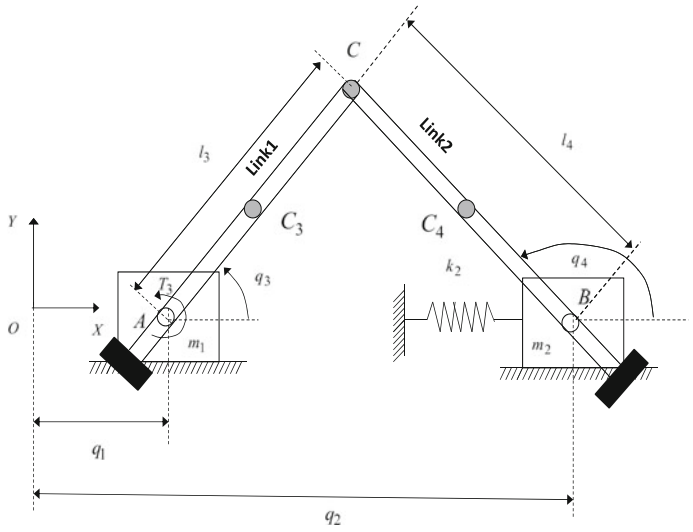

Fig. 4.1 A two-part underactuated robotic system constituting a closed-chain mechanism

F_2 that causes the displacement of mass m_2 along the x-axis and the torque T_4 that causes the rotation of the link with length l_4 round the revolute joint B. Thus, in the most generic case the input vector can be $u = [f_1, T_3, f_2, T_4]^T$. According to the Euler–Lagrange analysis the dynamic model of the robotic manipulator is obtained (the complete proof is given in the following subsection 4.2.3)

$$A(q)\ddot{q} + h(q, \dot{q}) = u \tag{4.2}$$

where

$$A(q) = \begin{pmatrix} a_{11} & a_{12} & 0 & 0 \\ a_{21} & a_{22} & 0 & 0 \\ 0 & 0 & a_{33} & a_{34} \\ 0 & 0 & a_{43} & a_{44} \end{pmatrix} \tag{4.3}$$

with $a_{11} = m_1 + m_3$, $a_{12} = a_{21} = -m_3 l_{c_3} sin(q_3)$, $a_{22} = m_3 l_{c_3}^2 + I_3$, $a_{33} = m_2 + m_4$, $a_{34} = a_{43} = -m_4 l_{c_4} sin(q_4)$, $a_{44} = m_4 l_{c_4}^2 + I_4$, and

$$h(q, \dot{q}) = \begin{pmatrix} -m_3 l_{c_3} cos(q_3)\dot{q}_3^2 \\ m_3 g l_{c_3} cos(q_3) \\ -m_4 l_{c_4} cos(q_4)\dot{q}_4^2 \\ m_4 g l_{c_4} cos(q_4) \end{pmatrix} \tag{4.4}$$

Next, the case in which $l_3 = l_4$ is examined. Moreover, it is considered that the mass m_2 is connected to a spring with elasticity k_2, while at the revolute joint of the second link l_4 there is also a torsional spring with elasticity coefficient k_4. Finally, it is

assumed that the only inputs applied to the robotic model are $u_1 = f_1$ and $u_2 = T_3$. The dynamic model of the robot becomes [636]

$$A(q_l)\ddot{q}_l + h(q_l, \dot{q}_l) = [u_1, u_2]^T \tag{4.5}$$

where $q_l = [q_1, q_3]^T$ and $q = [q_1, q_2, q_3, q_4]^T$. The inertia and Coriolis matrices are defined as [636]

$$A(q_l) = \begin{pmatrix} M_1 + M_2 & -2M_2 l_3 sin(q_3) \\ -2M_2 l_3 sin(q_3) & I_3 + I_4 + 4M_2 l_3^2 sin^2(q_3) \end{pmatrix} \tag{4.6}$$

$$h(q_l, \dot{q}_l) = \begin{pmatrix} -2M_2 l_3 \dot{q}_3^2 cos(q_3) + k_2 l_d \\ k_4(q_3 - \pi) + 2l_3 sin(q_3)(2M_2 l_3 \dot{q}_3^2 cos(q_3) - k_2 l_d) \end{pmatrix} \tag{4.7}$$

where $M_1 = m_1 + m_3$, $M_2 = m_2 + m_4$, $l_d = q_1 + 2l_3 cos(q_3) - L$. Denoting $x = [q_1, q_3, \dot{q}_1, \dot{q}_3]^T$ the robot's dynamic model can be written in the following state-space form:

$$\dot{x} = f(x) + g_1(x)u_1 + g_2(x)u_2 \tag{4.8}$$

where

$$f(x) = \begin{pmatrix} \dot{q}_1 \\ \dot{q}_3 \\ \dfrac{-k_2 l_d (I_3 + I_4) + 2l_3 M_2 (k_2(\pi - q_3) sin(q_3) + (I_3 + I_4)\dot{q}_3^2 cos(q_3)}{M_2(I_3 + I_4) + M_1(I_3 + I_4 + 4M_2 l_3^2 sin^2(q_3)))} \\ \dfrac{k_4(M_1 + M_2)(\pi - q_3) + 2I_3 M_1 sin(q_3)(k_2 l_d - 2l_3 M_2 \dot{q}_3^2 cos(q_3))}{M_2(I_3 + I_4) + M_1(I_3 + I_4 + 4M_2 l_3^2 sin^2(q_3))} \end{pmatrix} \tag{4.9}$$

$$g_1(x) = \begin{pmatrix} 0 \\ 0 \\ \dfrac{I_3 + I_4 + 4M_2 l_3^2 sin^2(q_3)}{(I_3 + I_4)M_2 + M_1(I_3 + I_4 + 4M_2 l_3^2 sin^2(q_3))} \\ \dfrac{2M_2 l_3 sin(q_3)}{(I_3 + I_4)M_2 + M_1(I_3 + I_4 + 4M_2 l_3^2 sin^2(q_3))} \end{pmatrix} \tag{4.10}$$

$$g_2(x) = \begin{pmatrix} 0 \\ 0 \\ \dfrac{2M_2 l_3 sin(q_3)}{(I_3 + I_4)M_2 + M_1(I_3 + I_4 + 4M_2 l_3^2 sin^2(q_3))} \\ \dfrac{M_1 + M_2}{(I_3 + I_4)M_2 + M_1(I_3 + I_4 + 4M_2 l_3^2 sin^2(q_3))} \end{pmatrix} \tag{4.11}$$

The robotic system is underactuated when only one of the control inputs is enabled. It can be proven that when the only input is $u_1 = F_1$ then the robotic system is not static feedback linearizable.

Next, the case in which the only control input is $u_2 = T_3$ is examined. When $k_2 \neq 0$ and $k_4 = 0$ then the robotic model is static feedback linearizable. Equivalently this means that (i) the distribution $D_3 =< g(x), ad_{f(x)}g(x), ad^2_{f(x)}g(x), ad^3_{f(x)}g(x) >$ has full rank and (ii) the vector fields $D_0 =< g(x) >$, $D_1 =< g(x), ad_{f(x)}g(x) >$ and $D_2 =< g(x), ad_{f(x)}g(x), ad^2_{f(x)}g(x) >$ are involutive. The previous conditions (i) and (ii) are necessary and sufficient conditions for Lie algebra-based input-to-state linearization for nonlinear dynamical systems. A detailed analysis on input-to-state and input-output linearization of nonlinear dynamical systems is given in [457].

4.2.3 *Proof of the Robot's Dynamic Model Using the Euler–Lagrange Method*

The closed chain robotic system of Fig. 4.2, presented initially in Sect. 4.2.2 is considered again. This comprises four masses, out of which mass m_1 and mass m_2 slide along the x-axis, while masses m_3 and m_4 associated with links l_3 and l_4 perform both translational and rotational motion in the xy-plane.

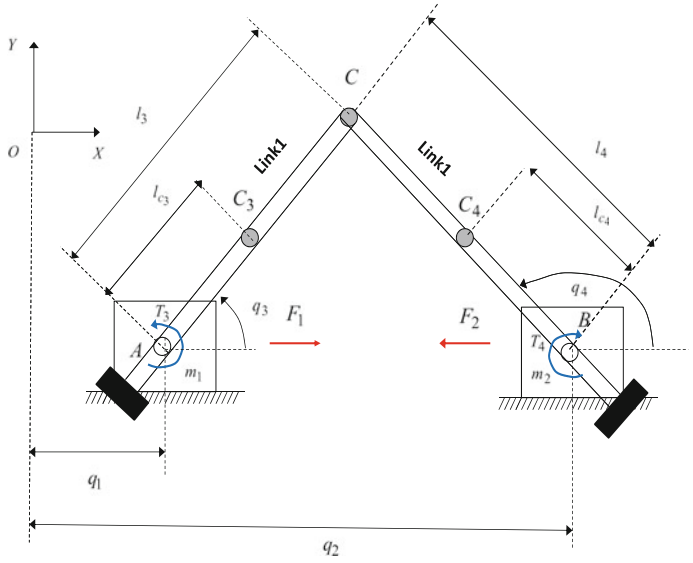

Fig. 4.2 The closed chain robotic system, comprising two sliding masses m_1 and m_2 and two rotating links with masses m_3 and m_4

For mass m_1 one has that the potential energy is $P_1 = 0$ while the kinetic energy is $K_1 = \frac{1}{2} m_1 \dot{q}_1^2$. For mass m_2 one has again that the potential energy is $P_2 = 0$ while the kinetic energy is $K_2 = \frac{1}{2} m_2 \dot{q}_2^2$.

For mass m_3 the potential energy is given by

$$P_3 = m_3 g l_{c_3} sin(q_3) \tag{4.12}$$

The kinetic energy of mass m_3 (link l_3) is due to both translational motion and rotational motion. Denoting by I_3 the moment of inertia for the rotation of the link l_3 one has the kinetic energy that is associated with the rotational motion is $K_{3,1} = \frac{1}{2} I_3 \dot{q}_3^2$. The kinetic energy of link l_3 that is associated with the translational motion is denoted as $K_{3,2}$ and is given by

$$K_{3,2} = \frac{1}{2} m_3 \dot{C}_3 \dot{C}_3^T \tag{4.13}$$

$\dot{C}_3$ is the velocity of the center of gravity of mass (link) 3 in cartesian coordinates. Using that the position of the center of gravity of link 3 is the vector

$$C_3 = [q_1 + l_{c_3} cos(q_3), \quad l_{c_3} sin(q_3)] \tag{4.14}$$

its velocity is computed as follows

$$\dot{C}_3 = [\dot{q}_1 - l_{c_3} sin(q_3) \dot{q}_3, \quad l_{c_3} cos(q_3) \dot{q}_3] \tag{4.15}$$

Thus, using Eq. (4.15) the kinetic energy of link 3 that is due to its translational motion is given by

$$\begin{gathered} K_{3,2} = \frac{1}{2} m_3 \dot{C}_3 \dot{C}_3^T \Rightarrow \\ K_{3,2} = \frac{1}{2} m_3 [(\dot{q}_1 - l_{c_3} sin(q_3) \dot{q}_3)^2 + (l_{c_3} cos(q_3) \dot{q}_3)^2] \Rightarrow \\ K_{3,2} = \frac{1}{2} m_3 [\dot{q}_1^2 + l_{c_3}^2 \dot{q}_3^2 - 2 l_{c_3} sin(q_3) \dot{q}_1 \dot{q}_3] \end{gathered} \tag{4.16}$$

Using $K_{3,1}$ and $K_{3,2}$ one has that the aggregate kinetic energy of mass (link) m_3 is

$$K_3 = \frac{1}{2} I_3 \dot{q}_3^2 + \frac{1}{2} m_3 [\dot{q}_1^2 + l_{c_3}^2 \dot{q}_3^2 - 2 l_{c_3} sin(q_3) \dot{q}_1 \dot{q}_3] \tag{4.17}$$

For mass m_4 the potential energy is given by

$$P_4 = m_4 g l_{c_4} sin(q_4) \tag{4.18}$$

The kinetic energy of mass m_4 (link l_4) is due to both translational motion and rotational motion. Denoting by I_4 the moment of inertia for the rotation of the link l_4 one has the kinetic energy that is associated with the rotational motion is $K_{4,1} = \frac{1}{2} I_4 \dot{q}_4^2$. The kinetic energy of link l_4 that is associated with the translational motion is denoted as $K_{4,2}$ and is given by

$$K_{4,2} = \frac{1}{2} m_4 \dot{C}_4 \dot{C}_4^T \tag{4.19}$$

$\dot{C}_4$ is the velocity of the center of gravity of mass (link) 4 in cartesian coordinates. Using that the position of the center of gravity of link 4 is the vector

$$C_4 = [q_2 + l_{c_4} cos(q_4), \quad l_{c_4} sin(q_4)] \tag{4.20}$$

its velocity is computed as follows

$$\dot{C}_4 = [\dot{q}_2 - l_{c_4} sin(q_4)\dot{q}_4, \quad l_{c_4} cos(q_4)\dot{q}_4] \tag{4.21}$$

Thus, using Eq. (4.21) the kinetic energy of link 4 that is due to its translational motion is given by

$$\begin{gathered} K_{4,2} = \tfrac{1}{2} m_4 \dot{C}_4 \dot{C}_4^T \Rightarrow \\ K_{4,2} = \tfrac{1}{2} m_4 [(\dot{q}_2 - l_{c_4} sin(q_4)\dot{q}_4)^2 + (l_{c_4} cos(q_4)\dot{q}_4)^2] \Rightarrow \\ K_{4,2} = \tfrac{1}{2} m_4 [\dot{q}_4^2 + l_{c_4}^2 \dot{q}_4^2 - 2 l_{c_4} sin(q_4)\dot{q}_2 \dot{q}_4] \end{gathered} \tag{4.22}$$

Using $K_{4,1}$ and $K_{4,2}$ one has that the aggregate kinetic energy of mass (link) m_4 is

$$K_4 = \tfrac{1}{2} I_4 \dot{q}_4^2 + \tfrac{1}{2} m_4 [\dot{q}_2^2 + l_{c_4}^2 \dot{q}_4^2 - 2 l_{c_4} sin(q_4)\dot{q}_2 \dot{q}_4] \tag{4.23}$$

The Lagrangian of the considered robotic system (closed kinematic mechanism) is given by

$$L = \textstyle\sum_{i=1}^{4} K_i - \sum_{i=1}^{4} P_i \Rightarrow$$

$$\begin{gathered} L = \tfrac{1}{2} m_1 \dot{q}_1^2 + \tfrac{1}{2} m_2 \dot{q}_2^2 + \\ + \tfrac{1}{2} I_3 \dot{q}_3^2 + \tfrac{1}{2} m_3 [\dot{q}_1^2 + l_{c_3}^2 \dot{q}_3^2 - 2 l_{c_3} sin(q_3)\dot{q}_1 \dot{q}_3] + \\ + \tfrac{1}{2} I_4 \dot{q}_4^2 + \tfrac{1}{2} m_4 [\dot{q}_2^2 + l_{c_4}^2 \dot{q}_4^2 - 2 l_{c_4} sin(q_4)\dot{q}_2 \dot{q}_4] + \\ - m_3 g l_{c_3} sin(q_3) - m_4 g l_{c_4} sin(q_4) \end{gathered} \tag{4.24}$$

Next, it can be computed that

$$\tfrac{\partial L}{\partial \dot{q}_1} = m_1 \dot{q}_1 + m_3 \dot{q}_1 + m_3 l_{c_3} sin(q_3)\dot{q}_3 \tag{4.25}$$

and by differentiating Eq. (4.25) with respect to time gives

$$\tfrac{\partial}{\partial t} \tfrac{\partial L}{\partial \dot{q}_1} = (m_1 + m_3)\ddot{q}_1 - m_3 l_{c_3} cos(q_3)\dot{q}_3^2 - m_3 l_{c_3} sin(q_3)\ddot{q}_3 \tag{4.26}$$

while one also obtains

$$\tfrac{\partial L}{\partial q_1} = 0 \tag{4.27}$$

In a similar manner one computes

$$\tfrac{\partial L}{\partial \dot{q}_2} = m_2 \dot{q}_2 + m_4 \dot{q}_2 - m_4 l_{c_4} sin(q_4)\dot{q}_4 \tag{4.28}$$

and by differentiating Eq. (4.28) with respect to time gives

$$\frac{\partial}{\partial t}\frac{\partial L}{\partial \dot{q}_2} = (m_2 + m_4)\ddot{q}_2 - m_4 l_{c_4} cos(q_4)\dot{q}_4^2 - m_4 l_{c_4} sin(q_4)\ddot{q}_4 \tag{4.29}$$

while one also obtains

$$\frac{\partial L}{\partial q_2} = 0 \tag{4.30}$$

In an equivalent way one finds

$$\frac{\partial L}{\partial \dot{q}_3} = I_3\dot{q}_3 + m_3 l_{c_3}^2\dot{q}_3 - m_3 l_{c_3} sin(q_3)\dot{q}_1 \tag{4.31}$$

and by differentiating Eq. (4.31) with respect to time gives

$$\frac{\partial}{\partial t}\frac{\partial L}{\partial \dot{q}_3} = I_3\ddot{q}_3 + m_3 l_{c_3}^2\ddot{q}_3 - m_3 l_{c_3} cos(q_3)\dot{q}_1\dot{q}_3 - m_3 l_{c_3} sin(q_3)\ddot{q}_1 \tag{4.32}$$

while one also obtains

$$\frac{\partial L}{\partial q_3} = -m_3 l_{c_3} cos(q_3)\dot{q}_1\dot{q}_3 - m_3 g l_{c_3} cos(q_3) \tag{4.33}$$

Following the same procedure one gets

$$\frac{\partial L}{\partial \dot{q}_4} = I_4\dot{q}_4 + m_4 l_{c_4}^2\dot{q}_4 - m_4 l_{c_4} sin(q_4)\dot{q}_2 \tag{4.34}$$

and by differentiating Eq. (4.34) with respect to time gives

$$\frac{\partial}{\partial t}\frac{\partial L}{\partial \dot{q}_4} = I_4\ddot{q}_4 + m_4 l_{c_4}^2\ddot{q}_4 - m_4 l_{c_4} cos(q_4)\dot{q}_2\dot{q}_4 - m_4 l_{c_4} sin(q_4)\ddot{q}_2 \tag{4.35}$$

while one also obtains

$$\frac{\partial L}{\partial q_4} = -m_4 l_{c_4} cos(q_4)\dot{q}_2\dot{q}_4 - m_4 g l_{c_4} cos(q_4) \tag{4.36}$$

Next, by using the previous equations and by applying the Euler–Lagrange principle one gets

$$\begin{aligned} &\frac{\partial}{\partial t}\frac{\partial L}{\partial \dot{q}_1} - \frac{\partial L}{\partial q_1} = F_1 \Rightarrow \\ &(m_1 + m_3)\ddot{q}_1 - m_3 l_{c_3} sin(q3)\ddot{q}_3 - m_3 l_{c_3} cos(q_3)\dot{q}_3^2 = F_1 \end{aligned} \tag{4.37}$$

$$\begin{aligned} &\frac{\partial}{\partial t}\frac{\partial L}{\partial \dot{q}_2} - \frac{\partial L}{\partial q_2} = F_2 \Rightarrow \\ &(m_2 + m_4)\ddot{q}_2 - m_4 l_{c_4} sin(q4)\ddot{q}_4 - m_4 l_{c_4} cos(q_4)\dot{q}_4^2 = F_2 \end{aligned} \tag{4.38}$$

$$\begin{array}{l}\frac{\partial}{\partial t}\frac{\partial L}{\partial \dot{q}_3}-\frac{\partial L}{\partial q_3}=T_1\Rightarrow\\ -m_3 l_{c_3} sin(q_3)\ddot{q}_1+(I_3+m_3 l_{c_3}^2)\ddot{q}_3-m_3 l_{c_3} cos(q_3)\dot{q}_1\dot{q}_3+\\ +m_3 l_{c_3} cos(q_3)\dot{q}_1\dot{q}_3+m_3 g l_{c_3} cos(q_3)=T_1\Rightarrow\end{array} \tag{4.39}$$

$$-m_3 l_{c_3} sin(q_3)\ddot{q}_1+(I_3+m_3 l_{c_3}^2)\ddot{q}_3+m_3 g l_{c_3} cos(q_3)=T_1$$

$$\begin{array}{l}\frac{\partial}{\partial t}\frac{\partial L}{\partial \dot{q}_4}-\frac{\partial L}{\partial q_4}=T_2\Rightarrow\\ -m_4 l_{c_4} sin(q_4)\ddot{q}_2+(I_4+m_4 l_{c_4}^2)\ddot{q}_4-m_4 l_{c_4} cos(q_4)\dot{q}_2\dot{q}_4+\\ +m_4 l_{c_4} cos(q_4)\dot{q}_2\dot{q}_4+m_4 g l_{c_4} cos(q_4)=T_2\Rightarrow\end{array} \tag{4.40}$$

$$-m_4 l_{c_4} sin(q_4)\ddot{q}_2+(I_4+m_4 l_{c_4}^2)\ddot{q}_4+m_4 g l_{c_4} cos(q_4)=T_2$$

By considering the state vector $\tilde{q}=[q_1,q_3,q_2,q_4]^T$ and by grouping together Eqs. (4.37), (4.39) and (4.38), (4.40) one has

$$\begin{array}{l}(m_1+m_3)\ddot{q}_1-m_3 l_{c_3} sin(q3)\ddot{q}_3-m_3 l_{c_3} cos(q_3)\dot{q}_3^2=F_1\\ -m_3 l_{c_3} sin(q_3)\ddot{q}_1+(I_3+m_3 l_{c_3}^2)\ddot{q}_3+m_3 g l_{c_3} cos(q_3)=T_1\end{array} \tag{4.41}$$

$$\begin{array}{l}(m_2+m_4)\ddot{q}_2-m_4 l_{c_4} sin(q4)\ddot{q}_4-m_4 l_{c_4} cos(q_4)\dot{q}_4^2=F_2\\ -m_4 l_{c_4} sin(q_4)\ddot{q}_2+(I_4+m_4 l_{c_4}^2)\ddot{q}_4+m_4 g l_{c_4} cos(q_4)=T_2\end{array} \tag{4.42}$$

Equations (4.41) and (4.42) can now be written in matrix form

$$\begin{pmatrix}(m_1+m_3) & -m_3 l_{c_3} sin(q_3) & 0 & 0\\ -m_3 l_{c_3} sin(q_3) & (I_3+m_3 l_{c_3}^2) & 0 & 0\\ 0 & 0 & (m_2+m_4) & -m_4 l_{c_4} sin(q_4)\\ 0 & 0 & -m_4 l_{c_4} sin(q_4) & (I_4+m_4 l_{c_4}^2)\end{pmatrix}\begin{pmatrix}\ddot{q}_1\\ \ddot{q}_2\\ \ddot{q}_3\\ \ddot{q}_4\end{pmatrix}+$$
$$+\begin{pmatrix}-m_3 l_{c_3} cos(q_3)\dot{q}_3^2\\ m_3 g l_{c_3} cos(q_3)\\ -m_4 l_{c_4} cos(q_4)\dot{q}_4^2\\ m_4 g l_{c_4} cos(q_4)\end{pmatrix}=\begin{pmatrix}F_1\\ T_1\\ F_2\\ T_2\end{pmatrix} \tag{4.43}$$

Equation (4.43) can also take the compact matrix form

$$A(\tilde{q})\ddot{\tilde{q}}+h(\tilde{q},\dot{\tilde{q}})=\tilde{u} \tag{4.44}$$

This is the description of the robotic mechanism which has been given in Eqs. (4.2)–(4.4).

4.2.4 Linearization of the Closed-Chain 2-DOF Robotic System Using Lie Algebra Theory

The following variable (linearizing output) is defined first

$$z_1 = y = h_1(q) = (M_1 + M_2)q_1 + 2M_2 l_3 cos(q_3) \tag{4.45}$$

Applying Lie-algebra theory, it holds that [230]

$$\begin{gathered} z_2 = L_f h_1 = \begin{pmatrix} \frac{\partial h_1}{\partial q_1} & \frac{\partial h_1}{\partial q_3} & \frac{\partial h_1}{\partial \dot{q}_1} & \frac{\partial h_1}{\partial \dot{q}_3} \end{pmatrix} \begin{pmatrix} f_1 \\ f_2 \\ f_3 \\ f_4 \end{pmatrix} \Rightarrow \\ z_2 = L_f h_1 = \begin{pmatrix} (M_1 + M_2 & -2M_2 l_3 sin(q_3) & 0 & 0) \end{pmatrix} \begin{pmatrix} f_1 \\ f_2 \\ f_3 \\ f_4 \end{pmatrix} \Rightarrow \\ z_2 = L_f h_1 = (M_1 + M_2) f_1 - 2M_2 l_3 sin(q_3) f_2 \Rightarrow \\ z_2 = L_f h_1 = (M_1 + M_2)\dot{q}_1 - 2M_2 l_3 sin(q_3)\dot{q}_3 \end{gathered} \tag{4.46}$$

Similarly, it holds

$$\begin{gathered} z_3 = L_f^2 h_1 = \begin{pmatrix} \frac{\partial z_2}{\partial q_1} & \frac{\partial z_2}{\partial q_3} & \frac{\partial z_2}{\partial \dot{q}_1} & \frac{\partial z_2}{\partial \dot{q}_3} \end{pmatrix} \begin{pmatrix} f_1 \\ f_2 \\ f_3 \\ f_4 \end{pmatrix} \Rightarrow \\ z_3 = L_f^2 h_1 = \begin{pmatrix} 0 & -2M_2 l_3 cos(q_3)\dot{q}_3 & (M_1 + M_2) & -2M_2 l_3 sin(q_3) \end{pmatrix} \begin{pmatrix} f_1 \\ f_2 \\ f_3 \\ f_4 \end{pmatrix} \Rightarrow \\ z_3 = L_f^2 h_1 = (M_1 + M_2) f_3 - 2M_2 l_3 sin(q_3) f_4 - 2M_2 l_3 cos(q_3)\dot{q}_3 f_2 \end{gathered} \tag{4.47}$$

It holds that

$$\begin{aligned} \ddot{q}_1 &= f_3 + g_{a_3} u_1 + g_{b_3} u_2 \Rightarrow \ddot{q}_1 = f_3 + g_{b_3} u_2 \Rightarrow f_3 = \ddot{q}_1 - g_{b_3} u_2 \\ \ddot{q}_3 &= f_4 + g_{a_4} u_1 + g_{b_4} u_2 \Rightarrow \ddot{q}_4 = f_4 + g_{b_4} u_2 \Rightarrow f_4 = \ddot{q}_3 - g_{b_4} u_2 \end{aligned} \tag{4.48}$$

Therefore, it holds

$$\begin{gathered} z_3 = (M_1 + M_2)f_3 - 2M_2 l_3 sin(q_3)f_4 - 2M_2 l_3 cos(\dot{q}_3)f_2 \Rightarrow \\ z_3 = (M_1 + M_2)\ddot{q}_1 - (M_1 + M_2)g_{b_2}u_2 - 2M_2 l_3 sin(q_3)\ddot{q}_3 + 2M_2 l_3 sin(q_3)g_{b_4}u_2 - \\ -2M_2 l_3 cos(q_3)\dot{q}_3^2 \Rightarrow \end{gathered} \tag{4.49}$$

or equivalently

$$\begin{gathered} z_3 = (M_1 + M_2)\ddot{q}_1 - 2M_2 l_3 sin(q_3)\ddot{q}_3 \\ -\frac{(M_1 + M_2)2M_2 l_3 sin(q_3)}{(I_3 + I_4)M_2 + M_1(I_3 + I_4 + 4M_2 l_3^2 sin^2(q_3))}u_2 \\ +\frac{(M_1 + M_2)2M_2 l_3 sin(q_3)}{(I_3 + I_4)M_2 + M_1(I_3 + I_4 + 4M_2 l_3^2 sin^2(q_3))}u_2 \\ -2M_2 l_3 cos(q_3)\dot{q}_3^2 \end{gathered} \tag{4.50}$$

Consequently, it holds that

$$z_3 = (M_1 + M_2)\ddot{q}_1 - 2M_2 l_3 sin(q_3)\ddot{q}_3 - 2M_2 l_3 \dot{q}_3^2 cos(q_3) \tag{4.51}$$

Using Eqs. (4.5)–(4.7) one obtains that

$$(M_1 + M_2)\ddot{q}_1 - 2M_2 l_3 sin(q_3)\ddot{q}_3 = 2M_2 l_3 \dot{q}_3^2 cos(q_3) - k_2 l_d + u_1 \tag{4.52}$$

with $u_1 = 0$ due to underactuation. Therefore, it holds

$$\begin{gathered} z_3 = 2M_2 l_3 \dot{q}_3^2 cos(q_3) - k_2 l_d - 2M_2 l_3 \dot{q}_3^2 cos(q_3) \Rightarrow \\ z_3 = -k_2 l_d \Rightarrow z_3 = -k_2(q_1 + 2l_3 cos(q_3) - L) \end{gathered} \tag{4.53}$$

Similarly, one has

$$\begin{gathered} z_4 = L_f^3 h_1(q) = \begin{pmatrix} \frac{\partial z_3}{\partial q_1} & \frac{\partial z_3}{\partial q_3} & \frac{\partial z_3}{\partial \dot{q}_1} & \frac{\partial z_3}{\partial \dot{q}_3} \end{pmatrix} \begin{pmatrix} f_1 \\ f_2 \\ f_3 \\ f_4 \end{pmatrix} \Rightarrow \\ z_4 = \begin{pmatrix} -k_2 & 2k_2 l_3 sin(q_3) & 0 & 0 \end{pmatrix} \begin{pmatrix} f_1 \\ f_2 \\ f_3 \\ f_4 \end{pmatrix} \Rightarrow \\ z_4 = -k_2 f_1 + 2k_2 l_3 sin(q_3)f_2 \Rightarrow z_4 = -k_2 \dot{q}_1 + 2k_2 l_3 sin(q_3)\dot{q}_3 \end{gathered} \tag{4.54}$$

Moreover, it holds that

$$\dot{z}_4 = L_f^4 h_1 + L_{g_a} L_f^3 h_1 u_1 + L_{g_b} L_f^3 h_1 u_2 \tag{4.55}$$

Additionally,

$$\begin{gathered} L_f^4 h_1 = \begin{pmatrix} \frac{\partial z_4}{\partial q_1} & \frac{\partial z_4}{\partial q_3} & \frac{\partial z_4}{\partial \dot{q}_1} & \frac{\partial z_4}{\partial \dot{q}_3} \end{pmatrix} \begin{pmatrix} f_1 \\ f_2 \\ f_3 \\ f_4 \end{pmatrix} \Rightarrow \\ L_f^4 h_1 = \begin{pmatrix} 0 & 2k_2 l_3 cos(q_3)\dot{q}_3 & -k_2 & 2k_2 l_3 sin(q_3) \end{pmatrix} \begin{pmatrix} f_1 \\ f_2 \\ f_3 \\ f_4 \end{pmatrix} \Rightarrow \\ L_f^4 h_1 = 2k_2 l_3 cos(q_3)\dot{q}_3 f_2 - k_2 f_3 + 2k_2 l_3 sin(q_3) f_4 \Rightarrow \\ L_f^4 h_1 = 2k_2 l_3 cos(q_3)\dot{q}_3^2 - k_2 f_3 + 2k_2 l_3 sin(q_3) f_4 \end{gathered} \tag{4.56}$$

It holds that $u_1 = 0$ and

$$\begin{gathered} L_{g_b} L_f^3 h_1 = \begin{pmatrix} \frac{\partial z_4}{\partial q_1} & \frac{\partial z_4}{\partial q_3} & \frac{\partial z_4}{\partial \dot{q}_1} & \frac{\partial z_4}{\partial \dot{q}_3} \end{pmatrix} \begin{pmatrix} g_{b_1} \\ g_{b_2} \\ g_{b_3} \\ g_{b_4} \end{pmatrix} \Rightarrow \\ L_{g_b} L_f^3 h_1 = \begin{pmatrix} 0 & 2k_3 l_3 cos(q_3)\dot{q}_3 & -k_2 & 2k_2 l_3 sin(q_3) \end{pmatrix} \begin{pmatrix} g_{b_1} \\ g_{b_2} \\ g_{b_3} \\ g_{b_4} \end{pmatrix} \end{gathered} \tag{4.57}$$

which can be also written as

$$\begin{gathered} L_{g_b} L_f^3 h_1 = -k_2 \frac{2M_2 l_3 sin(q_3)}{(I_3 + I_4)M_2 + M_1(I_3 + I_4 + 4M_2 l_3^2 sin^2(q_3))} + \\ +2k_2 l_3 sin(q_3) \frac{M_1 + M_2}{(I_3 + I_4)M_2 + M_1(I_3 + I_4 + 4M_2 l_3^2 sin^2(q_3))} \Rightarrow \\ L_{g_b} L_f^3 h_1 = \frac{2k_2 l_3 sin(q_3) M_1}{(I_3 + I_4)M_2 + M_1(I_3 + I_4 + 4M_2 l_3^2 sin^2(q_3))} \end{gathered} \tag{4.58}$$

Using next the relation

$$\dot{z}_4 = L_f^{(4)} h_1 + L_{g_a} L_f^3 h_1 u_1 + L_{g_b} L_f^3 h_1 u_2 = v \tag{4.59}$$

and that $\dot{z}_1 = z_2, \dot{z}_2 = z_3, \dot{z}_3 = z_4$ one has that the robotic model can be finally written in the linear canonical (Brunovsky) form

$$\begin{pmatrix} \dot{z}_1 \\ \dot{z}_2 \\ \dot{z}_3 \\ \dot{z}_4 \end{pmatrix} = \begin{pmatrix} 0 & 1 & 0 & 0 \\ 0 & 0 & 1 & 0 \\ 0 & 0 & 0 & 1 \\ 0 & 0 & 0 & 0 \end{pmatrix} \begin{pmatrix} z_1 \\ z_2 \\ z_3 \\ z_4 \end{pmatrix} + \begin{pmatrix} 0 \\ 0 \\ 0 \\ 1 \end{pmatrix} v \tag{4.60}$$

For the linearized system, a suitable feedback control law is

$$v = \dot{z}_4^d - k_1(z_4 - z_4^d) - k_2(z_3 - z_3^d) - k_3(z_2 - z_2^d) - k_4(z_1 - z_1^d) \tag{4.61}$$

After computing the control input v, one can also find the control input that should be really applied to the robotic system. Using that $u_1 = 0$, it holds that

$$\begin{gathered} v = L_f^{(4)} h_1 + L_{g_a} L_f^{(3)} h_1 u_1 + L_{g_b} L_f^{(3)} h_1 u_2 \Rightarrow \\ u_2 = \frac{1}{L_{g_b} L_f^{(3)} h_1} (v - L_f^{(4)} h_1). \end{gathered} \tag{4.62}$$

4.2.5 *Differential Flatness of the Closed-Chain 2-DOF Robotic System*

4.2.5.1 Differential Flatness Proof for the Closed-Chain 2-DOF Robotic System

The following flat output is chosen:

$$y = (M_1 + M_2) q_1 + 2 M_2 l_3 cos(q_3) \tag{4.63}$$

Then, one has

$$\begin{gathered} \dot{y} = (M_1 + M_2) \dot{q}_1 - 2 M_2 l_3 sin(q_3) \dot{q}_3 \Rightarrow \\ \ddot{y} = (M_1 + M_2) \ddot{q}_1 - 2 M_2 l_3 sin(q_3) \ddot{q}_3 - 2 M_2 l_3 cos(q_3) \dot{q}_3^2 \end{gathered} \tag{4.64}$$

Using Eqs. (4.2)–(4.4) it holds that

$$(M_1 + M_2) \ddot{q}_1 - 2 M_2 l_3 sin(q_3) \ddot{q}_3 = 2 M_2 l_3 \dot{q}_3^2 cos(q_3) - k_2 l_d + u_1 \tag{4.65}$$

where due to underactuation one has $u_1 = F_1 = 0$. Therefore, it holds

$$\ddot{y} = -k_2 l_d \Rightarrow \ddot{y} = -k_2 (q_1 + 2 l_3 cos(q_3) - L) \tag{4.66}$$

Consequently

$$y^{(3)} = -k_2 [\dot{q}_1 - 2 l_3 sin(q_3) \dot{q}_3] \tag{4.67}$$

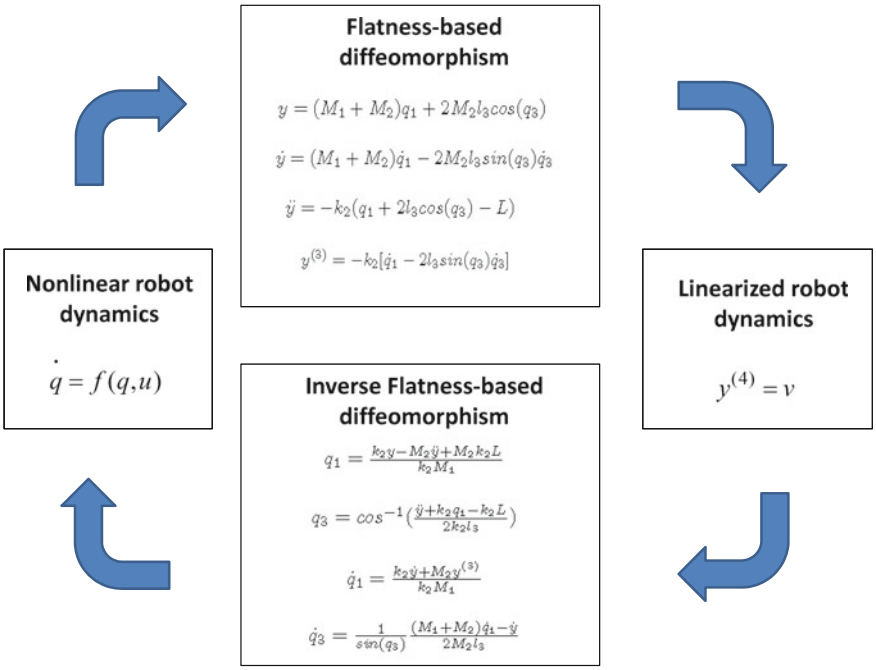

Fig. 4.3 Flatness-based diffeomorphism and its inverse, enabling the implementation of nonlinear control for the underactuated robotic mechanism

and respectively

$$y^{(4)} = -k_2\ddot{q}_1 + 2k_2 l_3 cos(q_3)\dot{q}_3^2 + 2k_2 l_3 sin(q_3)\ddot{q}_3 \tag{4.68}$$

From Eq. (4.63) describing the flat output and from the equations of its higher order derivatives one has a set of equations which can be solved with respect to the state variables q_1, q_3, $\dot{q}_1$ and $\dot{q}_3$ (Fig. 4.3). It holds that

$$q_1 = \frac{k_2 y - M_2 \ddot{y} + M_2 k_2 L}{k_2 M_1} \tag{4.69}$$

$$q_3 = cos^{-1}\left(\frac{\ddot{y} + k_2 q_1 - k_2 L}{2k_2 l_3}\right) \tag{4.70}$$

$$\dot{q}_1 = \frac{k_2 \dot{y} + M_2 y^{(3)}}{k_2 M_1} \tag{4.71}$$

$$\dot{q}_3 = \frac{1}{sin(q_3)} \frac{(M_1 + M_2)\dot{q}_1 - \dot{y}}{2M_2 l_3} \tag{4.72}$$

Having expressed the elements of the state vector q as functions of the flat output and its derivatives and knowing that $\ddot{q}_1 = f_3 + g_{a_3}u_1 + g_{b_3}u_2$ and $\ddot{q}_3 = f_4 + g_{a_4}u_1 + g_{b_4}u_2$ one concludes that the control inputs u_1 and u_2 can be also written as functions of the flat output and its derivatives. Therefore, the robotic system stands for a differentially flat model.

4.2.5.2 Design of a Flatness-Based Controller for the Closed-Chain 2-DOF Robotic System

From the relation $\dot{q} = f(q) + g_a(q)u_1 + g_b(q)u_2$ and the associated relations about $f(q)$, $g_a q$ and $g_b(q)$ it holds

$$\ddot{q}_1 = f_3 + g_{a_3}u_1 + g_{b_3}u_2 \Rightarrow \ddot{q}_1 = f_3 + g_{b_3}u_2 \Rightarrow$$

$$\ddot{q}_1 = \frac{-k_2 l_d (I_3 + I_4) + 2l_3 M_2 [K_4(\pi - q_3)sin(q_3) + (I_3 + I_4)\dot{q}_3^2 cos(q_3)}{M_2(I_3 + I_4) + M_1(I_3 + I_4 + 4M_2 l_3^2 sin^2(q_3))} + \\ + \frac{2M_2 l_3 sin(q_3)}{(I_3 + I_4)M_2 + M_1(I_3 + I_4 + 4M_2 l_3^2 sin^2(q_3))} u2 \tag{4.73}$$

Equivalently, one has

$$\ddot{q}_3 = f_4 + g_{a_4}u_1 + g_{b_4}u_2 \Rightarrow \ddot{q}_3 = f_3 + g_{b_4}u_2 \Rightarrow$$

$$\ddot{q}_3 = \frac{k_4(M_1 + M_2)(\pi - q_3) + 2l_3 M_1 sin(q_3)[K_2 l_d - 2l_3 M_2 \dot{q}_3^2 cos(q_3)]}{M_2(I_3 + I_4) + M_1(I_3 + I_4 + 4M_2 l_3^2 sin^2(q_3))} + \\ + \frac{M_1 + M_2}{(I_3 + I_4)M_2 + M_1(I_3 + I_4 + 4M_2 l_3^2 sin^2(q_3))} u2 \tag{4.74}$$

The flat output of the closed-chain robot has been chosen to be $y = (M_1 + M_2)q_1 + 2M_2 l_3 cos(q_3)$. Consequently, after successive differentiations, one has

$$\begin{gathered} y^{(4)} = -k_2 \ddot{q}_1 + 2k_2 l_3 cos(q_3)\dot{q}_3^2 + 2k_2 l_3 sin(q_3)\ddot{q}_3 \Rightarrow \\ y^{(4)} = -k_2(f_3 + g_{b_3})u_2 + 2k_2 l_3 cos(q_3)\dot{q}_3^2 + 2k_2 l_3 sin(q_3)(f_4 + g_{b_4}u_2) \Rightarrow \\ y^{(4)} = 2k_2 l_3 cos(q_3)\dot{q}_3^2 - k_2 f_3 + 2k_2 l_3 sin(q_3) f_4 + [-k_2 g_{b_3} + 2k_2 l_3 sin(q_3) g_{b_4}]u_2 \Rightarrow \\ y^{(4)} = f_v + g_v u \Rightarrow y^{(4)} = v \end{gathered} \tag{4.75}$$

where $v = f_v + g_v u_2$ with

$$\begin{gathered} f_v = 2k_2 l_3 cos(q_3)\dot{q}_3^2 - k_2 f_3 + 2k_2 l_3 sin(q_3) f_4 \\ g_v = -k_2 g_{b_3} + 2k_2 l_3 sin(q_3) g_{b_4} \end{gathered} \tag{4.76}$$

The following new state variables are defined $z_1 = y, z_2 = \dot{y}, z_3 = \ddot{y}$ and $z_4 = y^{(3)}$. For the new state variables a description of the system in the linear canonical (Brunovsky) form is obtained

$$\begin{pmatrix} \dot{z}_1 \\ \dot{z}_2 \\ \dot{z}_3 \\ \dot{z}_4 \end{pmatrix} = \begin{pmatrix} 0\,1\,0\,0 \\ 0\,0\,1\,0 \\ 0\,0\,0\,1 \\ 0\,0\,0\,0 \end{pmatrix} \begin{pmatrix} z_1 \\ z_2 \\ z_3 \\ z_4 \end{pmatrix} + \begin{pmatrix} 0 \\ 0 \\ 0 \\ 1 \end{pmatrix} v \tag{4.77}$$

Considering that the linear displacement of the left part of the kinematic chain q_1 is measurable, and that the same holds for the turn angle q_3 of joint A, one has that the flat output $y = (M_1 + M_2)q_1 + 2M_2 l_3 cos(q_3)$ is also a measurable variable.

Using the description of system in the linear canonical form, the appropriate control law is

$$v = \dot{z}_4^d - k_1(z_4 - z_4^d)) - k_2(z_3 - z_3^d) - k_3(z_2 - z_2^d) - k_4(z_1 - z_1^d) \tag{4.78}$$

After computing the control input v, one can also find the control input that should be really applied to the robotic system. The following relation is used:

$$v = f_v + g_v u_2 \Rightarrow u_2 = g_v^{-1}(v - f_v). \tag{4.79}$$

4.2.6 Derivative-Free Nonlinear Kalman Filter for the Closed-Chain 2-DOF Robotic System

4.2.6.1 State Estimation with the Derivative-Free Nonlinear Kalman Filter

The concept of global linearizing transformations has been extensively analyzed and previous results about state estimation through transformation to linear canonical forms can be found in [424, 438, 457]. It was shown that the dynamical model of the underactuated closed-chain robot can be written in the MIMO canonical form of Eq. (4.77). Thus one has a MIMO linear model of the form

$$\begin{aligned} \dot{y}_f &= A_f y_f + B_f v \\ z_f &= C_f y_f \end{aligned} \tag{4.80}$$

where $z_f = [z_1, z_2, z_3, z_4]^T$ and matrices A_f,B_f,C_f are in the form

$$A_f = \begin{pmatrix} 0\,1\,0\,0 \\ 0\,0\,1\,0 \\ 0\,0\,0\,1 \\ 0\,0\,0\,0 \end{pmatrix} \; B_f = \begin{pmatrix} 0 \\ 0 \\ 0 \\ 1 \end{pmatrix} \; C_f^T = \begin{pmatrix} 1 \\ 0 \\ 0 \\ 0 \end{pmatrix} \tag{4.81}$$

where the measurable variables $y = z_1$ is associated with the linear displacement and the rotational motion of joint A (Fig. 4.1) in the robotic model. For the aforementioned model, and after carrying out discretization of matrices A_f, B_f and C_f with common

discretization methods one can apply linear Kalman filtering. This is *Derivative-free nonlinear Kalman Filtering* for the model of the robot which is performed without the need to compute Jacobian matrices and does not introduce numerical errors due to approximative linearization with Taylor series expansion.

4.2.6.2 Kalman Filter-Based Estimation of Robot Disturbance Forces

Disturbances affecting the robot's model can be due to: (i) uncertainty and changes in model parameters, (ii) unknown external torques exerted on the robot's joints, (iii) unknown forces exerted on the masses of the robotic mechanism (e.g. friction). Considering the effects of disturbances on the robotic model and after applying a transform on the system's state variables according to the differential flatness theory it has been shown that the robot model is described by

$$z_1^{(4)} = v + \phi(\tau) \tag{4.82}$$

The robot's state space model of Eq. (4.77) will be extended to take into account also the dynamics and the effects of the disturbance input $\phi(t)$. The extended state vector of the robot model is defined as $z \in R^{8\times 1}$ with $z_1 = y, z_2 = \dot{y}, z_3 = \ddot{y}, z_4 = y^{(3)}$, $z_5 = \phi, z_6 = \dot{\phi}, z_7 = \ddot{\phi}, z_8 = \phi^{(3)}$. The dynamics of the disturbance is assumed to be defined by its fourth order derivative, i.e. $\phi^{(4)} = f_d(y, \dot{y}, \ddot{y}, y^{(3)})$. Thus one has the extended state-space model

$$\begin{gathered} \dot{z} = \tilde{A}\cdot z + \tilde{B}\cdot\tilde{v} \\ q = \tilde{C}z \end{gathered} \tag{4.83}$$

with

$$\tilde{A} = \begin{pmatrix} 0&1&0&0&0&0&0&0 \\ 0&0&1&0&0&0&0&0 \\ 0&0&0&1&0&0&0&0 \\ 0&0&0&0&1&0&0&0 \\ 0&0&0&0&0&1&0&0 \\ 0&0&0&0&0&0&1&0 \\ 0&0&0&0&0&0&0&1 \\ 0&0&0&0&0&0&0&0 \end{pmatrix}, \tilde{B} = \begin{pmatrix} 0&0 \\ 0&0 \\ 0&0 \\ 1&0 \\ 0&0 \\ 0&0 \\ 0&0 \\ 0&1 \end{pmatrix}, \tilde{C}^T = \begin{pmatrix} 1 \\ 0 \\ 0 \\ 0 \\ 0 \\ 0 \\ 0 \\ 0 \end{pmatrix} \tag{4.84}$$

where the measurable variable is z_1 and the control input is

$$\tilde{v} = \left(u,\ \phi^{(4)}\right)^T \tag{4.85}$$

The disturbance estimator has the following structure

$$\begin{gathered} \dot{\hat{z}} = \tilde{A}_o\cdot\hat{z} + \tilde{B}_o\cdot\tilde{v} + K(z_1 - \hat{z}_1) \\ \hat{z}_1 = \tilde{C}_o\hat{y} \end{gathered} \tag{4.86}$$

where the estimator's gain $K \in R^{8\times 1}$ and matrices $\tilde{A}_o$, $\tilde{B}_o$ and $\tilde{C}_o$ are defined as

$$\tilde{A}_o = \begin{pmatrix} 0&1&0&0&0&0&0&0\\ 0&0&1&0&0&0&0&0\\ 0&0&0&1&0&0&0&0\\ 0&0&0&0&1&0&0&0\\ 0&0&0&0&0&1&0&0\\ 0&0&0&0&0&0&1&0\\ 0&0&0&0&0&0&0&1\\ 0&0&0&0&0&0&0&0 \end{pmatrix}, \tilde{B}_o = \begin{pmatrix} 0&0\\ 0&0\\ 0&0\\ 1&0\\ 0&0\\ 0&0\\ 0&0\\ 0&0 \end{pmatrix}, \tilde{C}_o^T = \begin{pmatrix} 1\\ 0\\ 0\\ 0\\ 0\\ 0\\ 0\\ 0 \end{pmatrix} \tag{4.87}$$

The disturbance estimator's gain $K \in R^{8\times 1}$ will be computed through the Kalman Filter recursion.

Defining as $\tilde{A}_d$, $\tilde{B}_d$, and $\tilde{C}_d$, the discrete-time equivalents of matrices $\tilde{A}_o$, $\tilde{B}_o$ and $\tilde{C}_o$ respectively, a Derivative-free nonlinear Kalman Filter can be designed for the aforementioned representation of the system dynamics [33, 190, 222, 432]. The associated Kalman Filter-based disturbance estimator is given by

measurement update:

$$\begin{aligned} K(k) &= P^-(k)\tilde{C}_d^T[\tilde{C}_d \cdot P^-(k)\tilde{C}_d^T + R]^{-1}\\ \hat{z}(k) &= \hat{z}^-(k) + K(k)[z(k) - \tilde{C}_d\hat{z}^-(k)]\\ P(k) &= P^-(k) - K(k)\tilde{C}_d P^-(k) \end{aligned} \tag{4.88}$$

time update:

$$\begin{aligned} P^-(k+1) &= \tilde{A}_d(k)P(k)\tilde{A}_d^T(k) + Q(k)\\ \hat{z}^-(k+1) &= \tilde{A}_d(k)\hat{z}(k) + \tilde{B}_d(k)\tilde{v}(k) \end{aligned} \tag{4.89}$$

To compensate for the effects of the disturbance forces it suffices to use in the control loop the modified control input vector $v_1 = u - \hat{\phi}(t)$.

By transforming the nonlinear dynamic model of the robot into the canonical form of Eq. (4.82), one obtains an equivalent linear description having multiple poles at the origin. Such a system, can be easily stabilized, using pole placement methods. Thus, by applying state feedback, it is shown in this section that a closed loop system can be obtained having poles exclusively in the left complex semi-plane. Next, considering that Kalman Filter-based estimation of the state vector is used for the implementation of the state feedback control scheme, it becomes clear that the stability and robustness properties of the control loop are finally those of LQG control.

It is known that a function $\phi(t)$ can been represented either through explicit knowledge of its mathematical formulation or through knowledge of its n-th order derivative and of the associated initial conditions. The latter case is assumed in this section for the description of the dynamics of the disturbance term $\phi(t)$. Thus, it is considered that $\phi(t)$ is equivalently described by knowledge of the time derivatives of order n, that is $\phi^{(n)}(t)$ and of the associated initial conditions $\phi(0), \ldots, \phi^{(n-1)}(0)$,

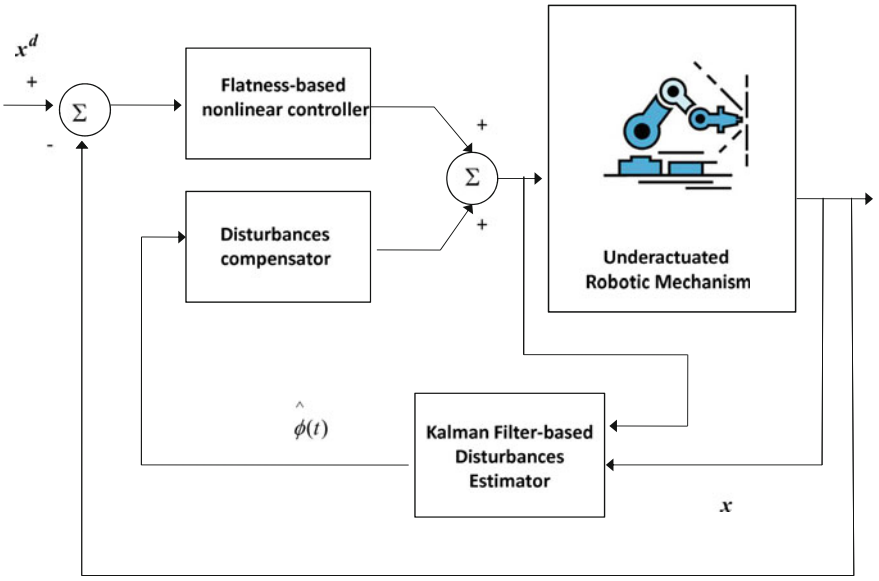

Fig. 4.4 Control scheme for the closed-chain underactuated robot consisting of a flatness-based control term and a Kalman Filter-based disturbances estimator

while without loss of generality it is considered that the order of derivation is $n = 4$. Moreover, since the reconstruction of $\phi(t)$ is performed with the use of Kalman Filtering, and the convergence of this estimation algorithm is not dependent on initial conditions, the use of the initial conditions becomes finally unnecessary in the estimation procedure for $\phi(t)$.

4.2.7 Simulation Tests

The efficiency of the proposed Kalman Filter-based control scheme for the underactuated robotic manipulator (Fig. 4.4) was evaluated in the tracking of various setpoints for state variable q_1 i.e. the linear displacement of mass M_1 of the mechanism and state variable q_3, i.e. the rotation angle of joint A. The mass displacement has been measured in m while the joint's turn angle has been measured in rad.

As it can be observed in Figs. 4.5a, 4.6, 4.7 and 4.8a the proposed control scheme enabled accurate tracking of the reference setpoints by the robot's state variables. Moreover, as it can be confirmed in Figs. 4.5b, 4.6, 4.7 and 4.8b the tracking error for the state variables of the robot, converged rapidly to zero.

Additionally, as it can be seen in Figs. 4.9 and 4.10, the Kalman Filter-based disturbance estimator was capable of identifying in real-time the external disturbances that affected the robotic system. By including an additional term in the control loop

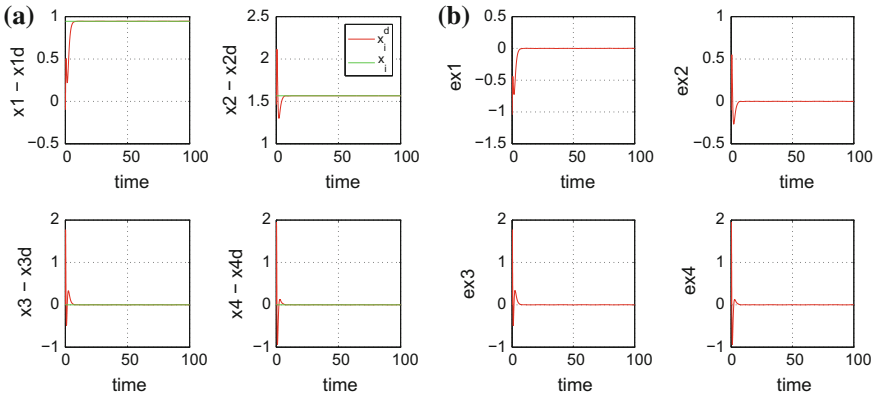

Fig. 4.5 Tracking of setpoint 1 **a** Convergence of the robot's state variables to reference setpoints **b** Variation of the tracking error

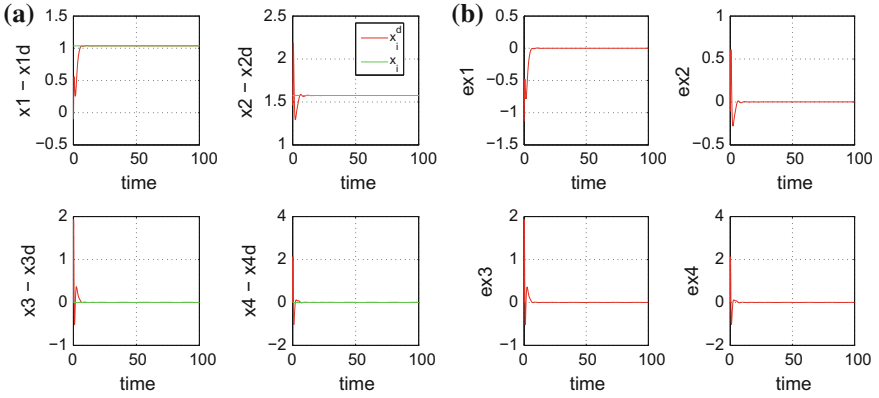

Fig. 4.6 Tracking of setpoint 2 **a** Convergence of the robot's state variables to reference setpoints **b** Variation of the tracking error

that was based on the disturbances estimation it became possible to compensate for the disturbances effects.

Finally, Table 4.1 presents the tracking RMSE (root mean square error) and the % tracking error for the state variables x_i, $i = 1, \ldots, 4$ of the underactuated robot modeled by Eq. (4.8), in the case of the three reference setpoints depicted in Figs. 4.6, 4.7 and 4.8. The joints angles x_1, x_3 have been measured in rad, while the joints' angular velocities have been measured in rad/sec. It can be noticed that the proposed control and state estimation scheme assures good tracking performance.

Finally, to elaborate on the performance indexes for the proposed control scheme, Table 4.2 is given next. This provides the percentage of improvement of the tracking accuracy due to the use of the Kalman Filter-based disturbance observer in the control

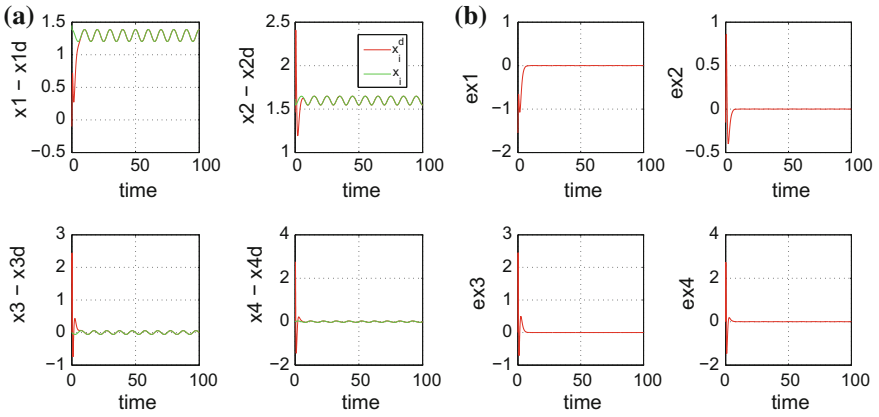

Fig. 4.7 Tracking of setpoint 3 **a** Convergence of the robot's state variables to reference setpoints **b** Variation of the tracking error

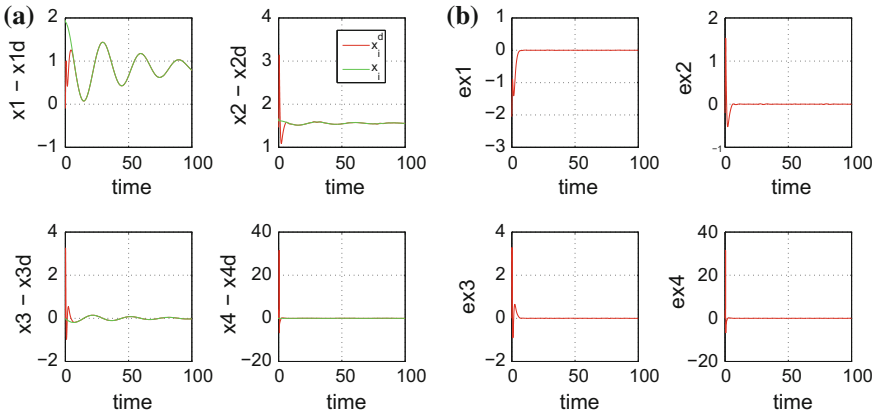

Fig. 4.8 Tracking of setpoint 4 **a** Convergence of the robot's state variables to reference setpoints **b** Variation of the tracking error

Table 4.1 RMSE and % tracking error for the robot's state variables

	$RMSE_1$	% $error_1$	$RMSE_2$	% $error_2$	$RMSE_3$	% $error_3$	$RMSE_4$	% $error_4$
x_1	0.0062	0.0313	0.0003	0.0142	0.0024	0.0125	0.0025	0.0128
x_2	0.0004	0.0039	0.0002	0.0335	0.0028	0.0281	0.0035	0.0352
x_3	0.0020	0.0102	0.0002	0.0115	0.0012	0.0064	0.0028	0.0141
x_4	0.0004	0.0048	0.0003	0.0266	0.0025	0.0255	0.0026	0.0264

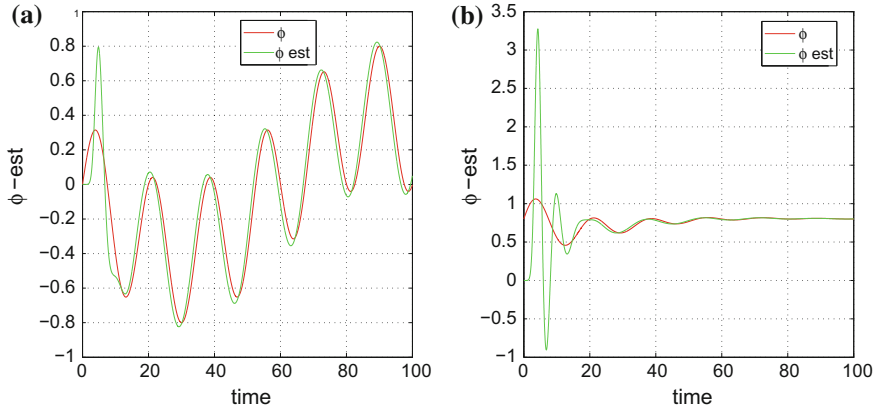

Fig. 4.9 **a** Tracking of setpoint 1: estimation of disturbance input, **b** Tracking of setpoint 2: estimation of disturbance input

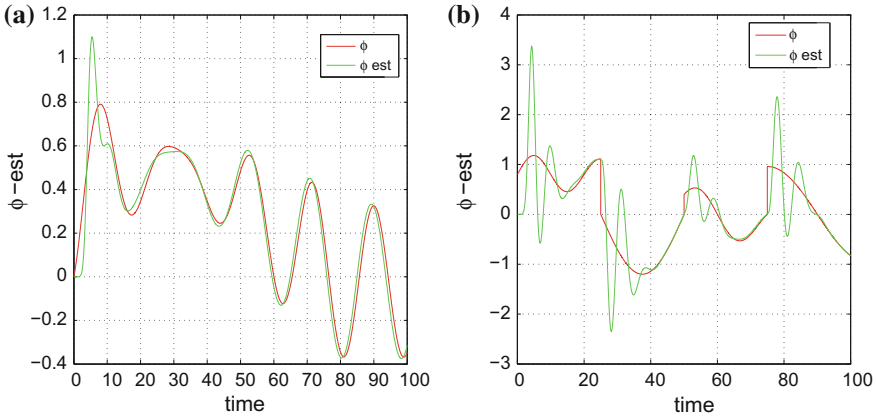

Fig. 4.10 **a** Tracking of setpoint 3: estimation of disturbance input, **b** Tracking of setpoint 4: estimation of disturbance input

loop. It can be noticed that the Derivative-free nonlinear Kalman Filter enables to reduce tracking error for all state variables of the robot $x_i,\ i = 1, \ldots, 4$.

The proposed control scheme is a stochastic one since the estimated state vector variables of the underactuated robotic manipulator are used in the computation of the nonlinear feedback control law. Thus the nonlinear feedback controller and the nonlinear Kalman Filter for the underactuated robot work in parallel and the one uses the computation produced by the other within the same sampling interval. It is remarkable, that despite lack of measurements from the complete state vector of the robot and despite the effects of external perturbations the proposed state

Table 4.2 Percentage % of improvement of robot's tracking accuracy

	Setpoint_1	Setpoint_2	Setpoint_3	Setpoint_4
x_1	97.93	100.00	93.10	100.00
x_2	100.00	100.00	100.00	100.00
x_3	98.92	93.33	100.00	40.00
x_4	100.00	100.00	100.00	100.00

estimation-based control scheme remains stable and provides accurate tracking of the reference setpoints for all robot joints.

Proportional integral derivative (PID) control is insufficient in treating nonlinear control problems for systems of complex dynamics, such as underactuated robotic manipulators, because the tuning of the PID controller parameters is based on heuristics and remains valid only round local operating points. Usually PID control is not followed by stability analysis and thus the functioning of the associated control loop is based on heuristics. For this reason it has been considered that comparison of the control method analyzed in the previous sections against PID control would be little informative since PID control is known to have poor performance in such a type of control problems [450].

It is noted that, control of underactuated robots is a nontrivial problem since the control algorithm does not have to cope exclusively with nonlinearities and coupling effects in the manipulator dynamics but has also to perform efficiently in underactuation which means that the number of control inputs is less than the number of degrees of freedom of the manipulator. The proposed control method succeeds global linearization after a change of coordinates (diffeomorphism) that is applied to the robot's model. The linearization of the underactuated manipulator is global because it is effective in the complete state-space of the robot and unlike approximate linearization methods does not introduce numerical errors. The linearized model of the robot has multiple poles at the origin and this implies an infinite gain margin and a sufficiently large phase margin. By applying feedback control on the linearized equivalent model of the robot its poles are transferred to the left complex semiplane thus assuring asymptotic stability. Moreover, the use of the Derivative-free nonlinear Kalman Filter in the control loop enables to estimate dynamically and compensate for the disturbances' effects. About feedback control under the effect of disturbance terms it is pointed out that the stability properties of the robot's feedback control loop are those of LQG control.

Moreover it is outlined that, solving the problem of state estimation for the underactuated robot is important because not all state variables are directly measurable and because the estimation of disturbance terms enables their compensation thus also making the feedback control loop be more robust. It is noted that the proposed filtering method is more accurate than other nonlinear estimation methods because it uses an exact linearization of the robot's dynamics and thus it remains free of the cumulative numerical errors which are caused in other filtering methods by

approximate linearization. Moreover, it has been proven that the Derivative-free nonlinear Kalman Filter is computationally faster than other nonlinear filtering methods due to working without the need to calculate repetitively an additional number of covariance matrices. Finally, unlike to what happens in other nonlinear filtering approaches, the proposed filtering method for the problem of state estimation of the nonlinear robotic manipulator preserves the improved accuracy of the linear Kalman Filtering.

As shown in the Euler–Lagrange analysis about the dynamic model of the considered robotic mechanism, both the modeling approach and the nonlinear control method are generic and can be applied to robotic systems of more degrees of freedom. Actually, in the Euler–Lagrange analysis it is shown that the computation of the kinematic and dynamic energy of the robot's links and of the Lagrangian of the robotic system enables to obtain the dynamic model of the robot in the general N-degrees of freedom case. Moreover, through the proposed control method it is shown that even in the case of underactuated robotic manipulators of more links and despite underactuation it is possible to obtain an equivalent linearized model for which the design of a state feedback controller becomes possible. By proving differential flatness properties for the robotic system, either referring to its initial model or to its extended model that is obtained after considering as additional state variables some of its control inputs (dynamic extension), it can be assured that an equivalent description for the robotic manipulator can be obtained in the linear canonical (Brunovsky) form. For the linearized equivalent model of the robot it is straightforward to apply linear state-feedback control design methods.

4.3 Flatness-Based Adaptive Fuzzy Control of Closed-Chain Kinematic Mechanisms

4.3.1 Outline

In the previous sections it has been shown that after transformation to the linear canonical form, the resulting control input for the underactuated robotic mechanism contains nonlinear elements which depend on the system's parameters. If the parameters of the system are unknown, then the nonlinear terms which appear in the control signal can be approximated with the use of neuro-fuzzy networks. In the present section it is shown that a suitable learning law can be defined for the aforementioned neuro-fuzzy approximators so as to preserve the closed-loop system stability. Lyapunov stability analysis proves also that the proposed flatness-based adaptive fuzzy control scheme results in H_∞ tracking performance, in accordance to the results of [436, 438, 447, 457].

Adaptive fuzzy control has been proven to be an efficient nonlinear control method [94, 203, 620]. The adaptive fuzzy control system based on differential flatness theory extends the class of systems to which indirect adaptive fuzzy control can

be applied. This is particularly important for the design of controllers, capable of efficiently compensating for modeling uncertainties and external disturbances in nonlinear dynamical systems. Unlike other adaptive fuzzy control schemes which are make use of several assumptions about the structure of the nonlinear system as well as about the uncertainty characterizing the system's model, the proposed adaptive fuzzy control scheme based on differential flatness theory offers an exact solution to the design of fuzzy controllers for unknown dynamical systems. The only assumption needed for the design of the controller and for succeeding H_∞ tracking performance for the control loop is that there exists a solution for a Riccati equation associated to the linearized error dynamics of the differentially flat model. This assumption is quite reasonable for several nonlinear systems, thus providing a systematic approach to the design of reliable controllers for such systems [414, 438].

4.3.2 Flatness-Based Adaptive Fuzzy Control

4.3.2.1 Nonlinear System Transformation into the Brunovsky Form

A single-input differentially flat dynamical system is considered again:

$$\dot{x} = f_s(x,t) + g_s(x,t)(u + \tilde{d}),\ x \in R^n,\ u \in R,\ \tilde{d} \in R \tag{4.90}$$

where $f_s(x,t)$, $g_s(x,t)$ are nonlinear vector fields defining the system's dynamics, u denotes the control input and $\tilde{d}$ denotes additive input disturbances. Knowing that the system of Eq. (4.90) is differentially flat, the next step is to try to write it into a Brunovsky form. For all differentially flat systems a transformation to an input-output linearized form is possible. This also holds for differentially flat single-input systems, such as the model of the underactuated closed-chain robot [322, 414].

The selected flat output is again denoted by y. Then, as analyzed in Section 1.3.2, for the state variables x_i of the system of Eq. (4.90) it holds

$$x_i = \phi_i(y, \dot{y}, \ldots, y^{(r-1)}), i = 1, \ldots, n \tag{4.91}$$

while for the control input it holds

$$u = \psi(y, \dot{y}, \ldots, y^{(r-1)}, y^{(r)}) \tag{4.92}$$

Introducing the new state variables $y_1 = y$ and $y_i = y^{(i-1)},\ i = 2, \ldots, n$, the initial system of Eq. (4.90) can be written in the Brunovsky form [182, 183]:

$$\begin{pmatrix} \dot{y}_1 \\ \dot{y}_2 \\ \cdots \\ \cdots \\ \dot{y}_{n-1} \\ \dot{y}_n \end{pmatrix} = \begin{pmatrix} 0 & 1 & 0 & \cdots & 0 \\ 0 & 0 & 1 & \cdots & 0 \\ \cdots & \cdots & \cdots & \cdots & \cdots \\ \cdots & \cdots & \cdots & \cdots & \cdots \\ 0 & 0 & 0 & \cdots & 1 \\ 0 & 0 & 0 & \cdots & 0 \end{pmatrix} \begin{pmatrix} y_1 \\ y_2 \\ \cdots \\ \cdots \\ y_{n-1} \\ y_n \end{pmatrix} + \begin{pmatrix} 0 \\ 0 \\ \cdots \\ \cdots \\ 0 \\ 1 \end{pmatrix} v \tag{4.93}$$

where $v = f(x,t) + g(x,t)(u + \tilde{d})$ is the control input for the linearized model, and $\tilde{d}$ denotes additive input disturbances. Thus one can use that

$$y^{(n)} = f(x,t) + g(x,t)(u + \tilde{d}) \tag{4.94}$$

where $f(x,t)$, $g(x,t)$ are unknown nonlinear functions, while as mentioned above $\tilde{d}$ is an unknown additive disturbance. It is possible to make the system's state vector x follow a given bounded reference trajectory x_d. In the presence of model uncertainties and external disturbances, denoted by w_d, successful tracking of the reference trajectory is provided by the H_∞ criterion [436, 561]:

$$\int_0^T e^T Q e dt \leq \rho^2 \int_0^T {w_d}^T w_d dt \tag{4.95}$$

where ρ is the attenuation level and corresponds to the maximum singular value of the transfer function $G(s)$ of the linearized model associated to Eqs. (4.93) and (4.94).

4.3.2.2 Control Law

For the measurable state vector x of the system of Eqs. (4.93) and (4.94), and for uncertain functions $f(x,t)$ and $g(x,t)$ an appropriate control law is

$$u = \frac{1}{\hat{g}(x,t)}[y_d^{(n)} - \hat{f}(x,t) - K^T e + u_c] \tag{4.96}$$

with $e = [e, \dot{e}, \ddot{e}, \cdots, e^{(n-1)}]^T$ and $e = y - y_d$, while the feedback gain matrix $K^T = [k_n, k_{n-1}, \ldots, k_1]$, is chosen such that the polynomial $e^{(n)} + k_1 e^{(n-1)} + k_2 e^{(n-2)} + \cdots + k_n e$ is Hurwitz. The control law of Eq. (4.96) results into

$$e^{(n)} = -K^T e + u_c + [f(x,t) - \hat{f}(x,t)] + [g(x,t) - \hat{g}(x,t)]u + g(x,t)\tilde{d} \tag{4.97}$$

where the supervisory control term u_c aims at the compensation of the approximation error

$$w = [f(x,t) - \hat{f}(x,t)] + [g(x,t) - \hat{g}(x,t)]u \tag{4.98}$$

as well as of the additive disturbance term $d_1 = g(x,t)\tilde{d}$. The above relation can be written in a state-equation form. The state vector is taken to be $e^T = [e, \dot{e}, \ldots, e^{(n-1)}]$, which after some operations yields

$$\dot{e} = (A - BK^T)e + Bu_c + B\{[f(x,t) - \hat{f}(x,t)] + [g(x,t) - \hat{g}(x,t)]u + d_1\} \tag{4.99}$$

where

$$A = \begin{pmatrix} 0 & 1 & 0 & \cdots\cdots & 0 \\ 0 & 0 & 1 & \cdots\cdots & 0 \\ \cdots & \cdots & \cdots & \cdots & \cdots \\ \cdots & \cdots & \cdots & \cdots & \cdots \\ 0 & 0 & 0 & \cdots\cdots & 1 \\ 0 & 0 & 0 & \cdots\cdots & 0 \end{pmatrix}, \quad B = \begin{pmatrix} 0 \\ 0 \\ \cdots \\ \cdots \\ 0 \\ 1 \end{pmatrix} \tag{4.100}$$

and $K = [k_n, k_{n-1}, \ldots, k_2, k_1]^T$. As explained above, the control signal u_c is an auxiliary control term, used for the compensation of $\tilde{d}$ and w, which can be selected according to H_∞ control theory:

$$u_c = -\tfrac{1}{r}B^T P e. \tag{4.101}$$

4.3.2.3 Approximators of Unknown System Dynamics

The approximation of functions $f(x,t)$ and $g(x,t)$ of Eq. (4.94) can be carried out with neuro-fuzzy networks (Fig. 4.11). The estimation of $f(x,t)$ and $g(x,t)$ can be written as [581, 582]:

$$\hat{f}(x|\theta_f) = \theta_f^T \phi(x), \quad \hat{g}(x|\theta_g) = \theta_g^T \phi(x), \tag{4.102}$$

where $\phi(x)$ are kernel functions with elements

$$\phi^l(x) = \frac{\prod_{i=1}^n \mu_{A_i^l}(x_i)}{\sum_{l=1}^N \prod_{i=1}^n \mu_{A_i^l}(x_i)} \quad l = 1, 2, \ldots, N \tag{4.103}$$

It is assumed that the weights θ_f and θ_g vary in the bounded areas M_{θ_f} and M_{θ_g} which are defined as

$$\begin{aligned} M_{\theta_f} &= \{\theta_f \in R^h : ||\theta_f|| \leq m_{\theta_f}\}, \\ M_{\theta_g} &= \{\theta_g \in R^h : ||\theta_g|| \leq m_{\theta_g}\} \end{aligned} \tag{4.104}$$

with m_{θ_f} and m_{θ_g} to be positive constants.

The values of θ_f and θ_g that give optimal approximation are:

$$\begin{aligned} \theta_f^* &= \arg\min_{\theta_f \in M_{\theta_f}} [sup_{x \in U_x} |f(x) - \hat{f}(x|\theta_f)|] \\ \theta_g^* &= \arg\min_{\theta_g \in M_{\theta_g}} [sup_{x \in U_x} |g(x) - \hat{g}(x|\theta_g)|] \end{aligned} \tag{4.105}$$

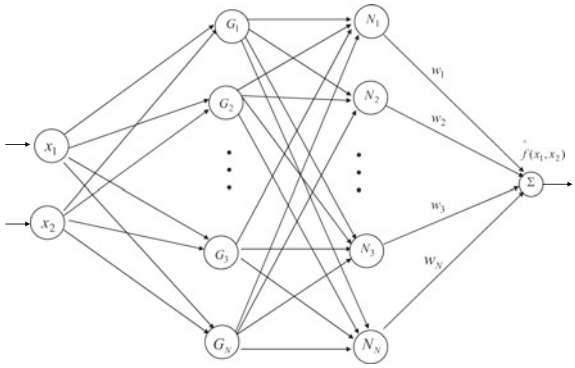

Fig. 4.11 Neuro-fuzzy approximator of the dynamics of the closed-chain robotic manipulator: G_i Gaussian basis function, N_i: normalization unit

The approximation error of $f(x, t)$ and $g(x, t)$ is given by

$$\begin{gathered} w = [\hat{f}(x, |\theta_f^*) - f(x, t)] + [\hat{g}(x|\theta_f^*) - g(x, t)]u \Rightarrow \\ w = \{[\hat{f}(x|\theta_f^*) - \hat{f}(x|\theta_f)] + [\hat{f}(x|\theta_f) - f(x, t)]\} + \\ + \{[\hat{g}(x|\theta_g^*) - \hat{g}(x|\theta_g)] + [\hat{g}(x|\theta_g) - g(x, t)]u\} \end{gathered} \tag{4.106}$$

where: i) $\hat{f}(x|\theta_f^*)$ is the approximation of f for the best estimation θ_f^* of the weights' vector θ_f, ii) $\hat{g}(x|\theta_g^*)$ is the approximation of g for the best estimation θ_g^* of the weights' vector θ_g.

The approximation error w can be decomposed into w_a and w_b, where

$$\begin{aligned} w_a &= [\hat{f}(x|\theta_f) - \hat{f}(x|\theta_f^*)] + [\hat{g}(x|\theta_g) - \hat{g}(x|\theta_g^*)]u \\ w_b &= [\hat{f}(x|\theta_f^*) - f(x, t)] + [\hat{g}(x|\theta_g^*) - g(x, t)]u \end{aligned} \tag{4.107}$$

Finally, the following two parameters are defined:

$$\begin{aligned} \tilde{\theta}_f &= \theta_f - \theta_f^* \\ \tilde{\theta}_g &= \theta_g - \theta_g^*. \end{aligned} \tag{4.108}$$

4.3.3 Lyapunov Stability Analysis

The adaptation law of the weights θ_f and θ_g as well as of the supervisory control term u_c is derived by the requirement for negative first-order derivative of the quadratic Lyapunov function

$$V = \frac{1}{2}e^T Pe + \frac{1}{2\gamma_1}\tilde{\theta}_f^T\tilde{\theta}_f + \frac{1}{2\gamma_2}\tilde{\theta}_g^T\tilde{\theta}_g \tag{4.109}$$

Substituting Eqs. (4.99) into (4.109) and differentiating gives

$$\begin{aligned} \dot{V} &= \tfrac{1}{2}\dot{e}^T Pe + \tfrac{1}{2}e^T P\dot{e} + \tfrac{1}{\gamma_1}\tilde{\theta}_f^T\dot{\tilde{\theta}}_f + \tfrac{1}{\gamma_2}\tilde{\theta}_g^T\dot{\tilde{\theta}}_g \Rightarrow \\ \dot{V} &= \tfrac{1}{2}e^T\{(A-BK^T)^T P + P(A-BK^T)\}e + \\ &+ B^T Pe(u_c + w + d_1) + \tfrac{1}{\gamma_1}\tilde{\theta}_f^T\dot{\tilde{\theta}}_f + \tfrac{1}{\gamma_2}\tilde{\theta}_g^T\dot{\tilde{\theta}}_g. \end{aligned} \tag{4.110}$$

Assumption 1: For given positive definite matrix Q and coefficients r and ρ there exists a positive definite matrix P, which is the solution of the following matrix equation

$$(A-BK^T)^T P + P(A-BK^T) - PB(\frac{2}{r} - \frac{1}{\rho^2})B^T P + Q = 0 \tag{4.111}$$

Substituting Eq. (4.111) into $\dot{V}$ yields after some operations

$$\begin{aligned} \dot{V} = -\tfrac{1}{2}e^T Qe + \tfrac{1}{2}e^T PB(\tfrac{2}{r} - \tfrac{1}{\rho^2})B^T Pe + B^T Pe(-\tfrac{1}{r}e^T PB) + \\ + B^T Pe(w + d_1) + \tfrac{1}{\gamma_1}\tilde{\theta}_f^T\dot{\tilde{\theta}}_f + \tfrac{1}{\gamma_2}\tilde{\theta}_g^T\dot{\tilde{\theta}}_g \end{aligned} \tag{4.112}$$

It holds that

$$\begin{aligned} \dot{\tilde{\theta}}_f &= \dot{\theta}_f - \dot{\theta}_f^* = \dot{\theta}_f \\ \dot{\tilde{\theta}}_g &= \dot{\theta}_g - \dot{\theta}_g^* = \dot{\theta}_g \end{aligned} \tag{4.113}$$

The following weight adaptation laws are considered [581]

$$\dot{\theta}_f = \begin{cases} -\gamma_1 e^T PB\phi(x) & \text{if } ||\theta_f|| < m_{\theta_f} \\ 0 & \text{if } ||\theta_f|| \geq m_{\theta_f} \end{cases} \tag{4.114}$$

$$\dot{\theta}_g = \begin{cases} -\gamma_2 e^T PB\phi(x)u_c & \text{if } ||\theta_g|| < m_{\theta_g} \\ 0 & \text{if } ||\theta_g|| \geq m_{\theta_g} \end{cases} \tag{4.115}$$

$\dot{\theta}_f$ and $\dot{\theta}_g$ are set to 0, when

$$||\theta_f|| \geq m_{\theta_f}, \quad ||\theta_g|| \geq m_{\theta_g}. \tag{4.116}$$

The update of θ_f stems from a gradient algorithm on the cost function $\frac{1}{2}(f - \hat{f})^2$. The update of θ_g is also of the gradient type, while u_c implicitly tunes the adaptation gain γ_2. Substituting Eqs. (4.114) and (4.115) in $\dot{V}$ finally gives

$$\begin{gathered}\dot{V} = -\frac{1}{2}e^T Qe - \frac{1}{2\rho^2}e^T PBB^T Pe + e^T PB(w + d_1) - \\ -e^T PB(\theta_f - \theta_f^*)^T \phi(x) - e^T PB(\theta_g - \theta_g^*)^T \phi(x) u_c \Rightarrow \\ \dot{V} = -\frac{1}{2}e^T Qe - \frac{1}{2\rho^2}e^T PBB^T Pe + e^T PB(w + d_1) + e^T PBw_\alpha .\end{gathered} \tag{4.117}$$

Denoting $w_1 = w + d_1 + w_\alpha$ one gets

$$\begin{gathered}\dot{V} = -\frac{1}{2}e^T Qe - \frac{1}{2\rho^2}e^T PBB^T Pe + e^T PBw_1 \text{ or equivalently,} \\ \dot{V} = -\frac{1}{2}e^T Qe - \frac{1}{2\rho^2}e^T PBB^T Pe + \frac{1}{2}e^T PBw_1 + \frac{1}{2}w_1^T B^T Pe\end{gathered} \tag{4.118}$$

Lemma: The following inequality holds:

$$\frac{1}{2}e^T PBw_1 + \frac{1}{2}w_1^T B^T Pe - \frac{1}{2\rho^2}e^T PBB^T Pe \le \frac{1}{2}\rho^2 w_1^T w_1 \tag{4.119}$$

Proof: The binomial $(\rho a - \frac{1}{\rho}b)^2 \ge 0$ is considered. Expanding the left part of the above inequality one gets

$$\begin{gathered}\rho^2 a^2 + \frac{1}{\rho^2}b^2 - 2ab \ge 0 \Rightarrow \frac{1}{2}\rho^2 a^2 + \frac{1}{2\rho^2}b^2 - ab \ge 0 \Rightarrow \\ ab - \frac{1}{2\rho^2}b^2 \le \frac{1}{2}\rho^2 a^2 \Rightarrow \frac{1}{2}ab + \frac{1}{2}ab - \frac{1}{2\rho^2}b^2 \le \frac{1}{2}\rho^2 a^2\end{gathered} \tag{4.120}$$

The following substitutions are carried out: $a = w_1$ and $b = e^T PB$ and the previous relation becomes

$$\frac{1}{2}w_1^T B^T Pe + \frac{1}{2}e^T PBw_1 - \frac{1}{2\rho^2}e^T PBB^T Pe \le \frac{1}{2}\rho^2 w_1^T w_1 \tag{4.121}$$

The previous inequality is used in $\dot{V}$, and the right part of the associated inequality is enforced

$$\dot{V} \le -\frac{1}{2}e^T Qe + \frac{1}{2}\rho^2 w_1^T w_1 \tag{4.122}$$

Equation (4.122) can be used to show that the H_∞ performance criterion is satisfied. For ρ sufficiently small the right part of the previous inequality will remain upper bounded by zero, and in this manner the asymptotic stability of the control loop is demonstrated. Additionally, the integration of $\dot{V}$ from 0 to T gives

$$\begin{gathered}\int_0^T \dot{V}(t)dt \le -\frac{1}{2}\int_0^T ||e||^2 dt + \frac{1}{2}\rho^2 \int_0^T ||w_1||^2 dt \Rightarrow \\ 2V(T) + \int_0^T ||e||_Q^2 dt \le 2V(0) + \rho^2 \int_0^T ||w_1||^2 dt\end{gathered} \tag{4.123}$$

Moreover, if there exists a positive constant $M_w > 0$ such that

$$\int_0^\infty ||w_1||^2 dt \le M_w \tag{4.124}$$

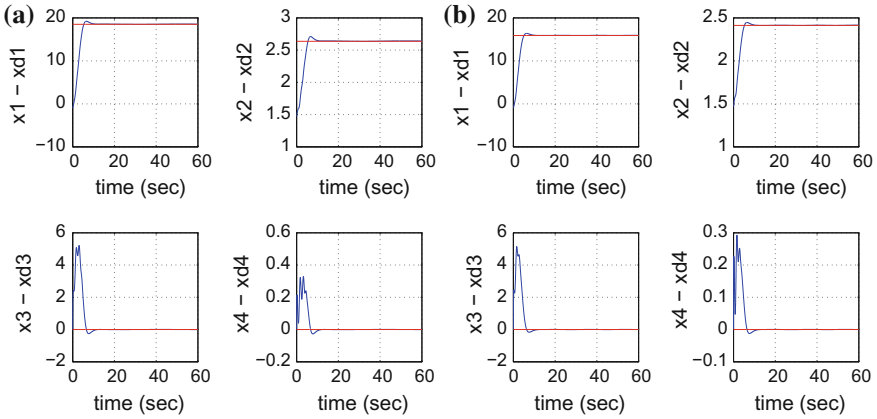

Fig. 4.12 Convergence of the robot's state variables (blue line): **a** setpoint 1 **b** setpoint 2 (red line)

then one gets

$$\int_0^{\infty} ||e||_Q^2 dt \leq 2V(0) + \rho^2 M_w \tag{4.125}$$

Thus, the integral $\int_0^{\infty} ||e||_Q^2 dt$ is bounded. Moreover, $V(T)$ is bounded and from the definition of the Lyapunov function V in Eq. (4.109) it becomes clear that $e(t)$ will be also bounded since $e(t) \in \Omega_e = \{e | e^T Pe \leq 2V(0) + \rho^2 M_w\}$. According to the above and with the use of Barbalat's Lemmaone obtains $lim_{t\to\infty} e(t) = 0$.

4.3.4 Simulation Tests

The efficiency of the proposed adaptive fuzzy control scheme for the underactuated robotic manipulator was evaluated in the tracking of various setpoints for state variable q_1 i.e. the linear displacement of mass M_1 of the mechanism and state variable q_3, i.e. the rotation angle of joint A. As it can be observed in Figs. 4.12, 4.13 and 4.14, the proposed control scheme enabled accurate tracking of the reference setpoints by the robot's state variables. Indicative results about the estimation of unknown functions $f_v(x, t)$ and $g_v(x, t)$ in the robot's dynamics by the neurofuzzy approximators is shown in Fig. 4.15. By including an additional term in the control loop that was based on the disturbances estimation it became possible to compensate for the disturbances effects.

Flatness-based adaptive fuzzy control approach is a completely model-free control method. It needs no prior knowledge about the system's dynamics (apart from the order of the system, and also needs no prior knowledge about the values of the parameters of the system's model). The proposed flatness-based adaptive fuzzy control approach can be applied to both robotic systems that admit static feedback linearization as well as to robotic models that admit dynamic feedback linearization.

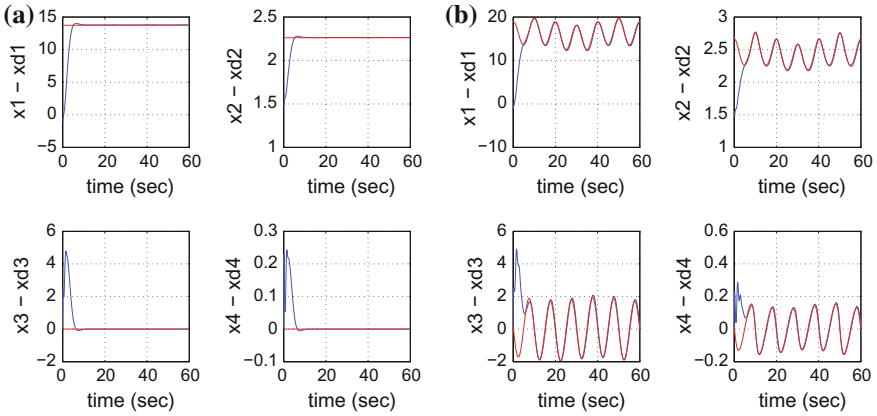

Fig. 4.13 Convergence of the robot's state variables (blue line): **a** to setpoint 3 **b** to setpoint 4 (red line)

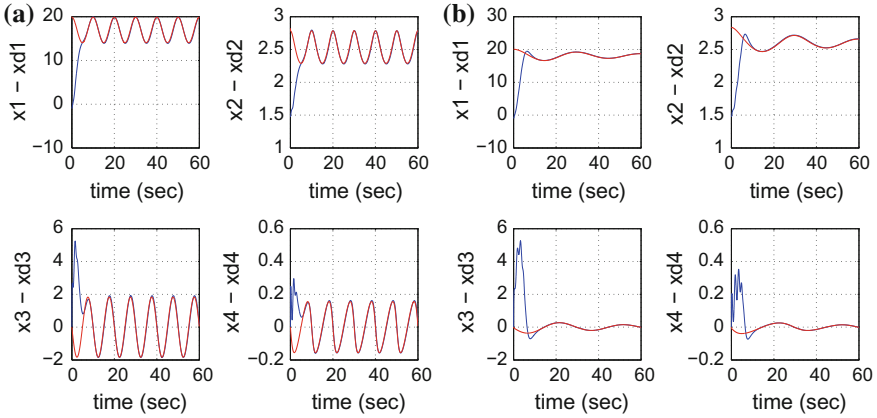

Fig. 4.14 Convergence of the robot's state variables (blue line): **a** to setpoint 5 **b** to setpoint 6 (red line)

The necessary and sufficient condition for the application of the proposed adaptive fuzzy control method is the robot system to be differentially flat. This enables the use of adaptive fuzzy control to a wide class of dynamical systems.

Flatness-based control can be applied to a wider class of dynamical systems than Lie algebra-based control. This is because the necessary and sufficient condition for the application of flatness-based adaptive fuzzy control is the system to differentially flat. This covers the widest class of nonlinear dynamical systems. On the other side, the necessary and sufficient condition for the application of Lie algebra-based control is the system to be input-to-state linearizable. This constrains the application of the method to a more narrow class of dynamical system. Besides, by using differential flatness theory one can solve simultaneously the control and state estimation

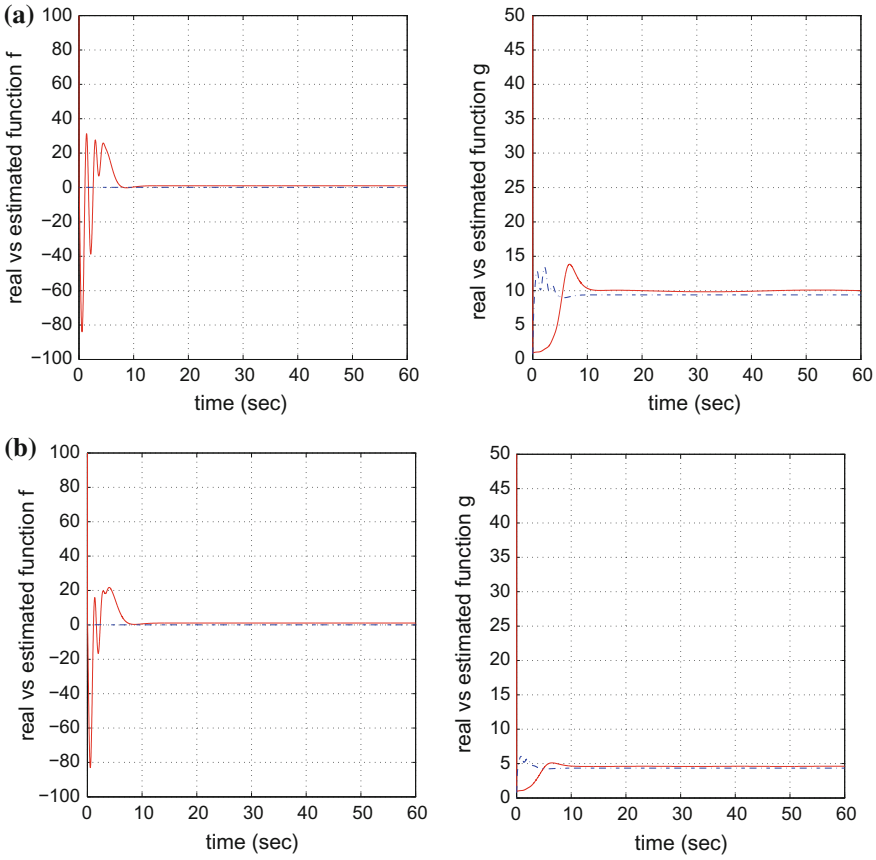

Fig. 4.15 Estimation of functions $f_v(x, t)$ and $g_v(x, t)$ of the robot dynamics by neurofuzzy networks when tracking: **a** setpoint 1 **b** setpoint 2

problem for the case of nonlinear underactuated robotic manipulators, without the need appearing in the Lie algebra-based approach for computing Jacobian matrices of the system's transformed state vector.

Comparison of flatness-based adaptive control to other nonlinear control methods (i) An alternative global linearization-based control method is Lie algebra-based control. However, as mentioned above this is applicable to a more constrained class of robotic systems. Moreover, to solve the associated state estimation and filtering problems the method requires the computation of Jacobian matrices, (ii) Another option is local linearization-based control methods. These make use of approximately linearized dynamical models of the robot which are obtained round local operating points (equilibria). This linearization procedure requires Taylor series expansion of the robotic model and the computation of Jacobian matrices. Besides, the use of an approximately linearized method introduces to the control loop inherent modelling

errors and perturbations which should be continuously suppressed by the robustness of the feedback controller.

4.4 Nonlinear Optimal Control for Closed-Chain Kinematic Mechanisms

4.4.1 Outline

In this section a nonlinear H-infinity control method is proposed for solving the problem of stabilization and trajectory tracking by the joints of an underactuated closed-chain multi-DOF robotic mechanism. The robot has the form of a closed kinematic chain and the control inputs are the torques that are generated by actuators mounted on its joints [286, 513–515]. The dynamic model of the robot undergoes approximate linearization around a temporary equilibrium which is redefined at each iteration of the control algorithm and which consists of the present value of the robot's state vector and of the last value of the control inputs vector that was exerted on the system. The approximate linearization is based on Taylor series expansion and on the computation of the associated Jacobian matrices [33, 431, 461, 463]. The modelling error which is due to truncation of higher-order terms in the Taylor series expansion is considered to be a disturbance that is compensated by the robustness of the control algorithm [450, 452, 457, 460].

For the linearized equivalent model of the robotic mechanism an H-infinity feedback controller is designed, actually giving solution to the nonlinear optimal control problem of the robot under model uncertainty and perturbations [132, 305, 564]. This controller implements the solution to a mini-max differential game, in which the disturbance inputs to the robotic model try to maximize a quadratic cost function while the control input tries to minimize it. The computation of the feedback control gain requires the solution of an algebraic Riccati equation at each iteration of the control program. Through Lyapunov stability analysis it is shown that the feedback control scheme satisfies an H-infinity tracking performance criterion, which signifies elevated robustness to modelling uncertainty and external perturbations. Moreover, under moderate conditions the global asymptotic stability of the control-loop is proven. To solve the state estimation problem for the closed-chain robotic mechanism and to implement state estimation-based control the H-infinity Kalman Filter is proposed [169, 511].

Despite its computational and conceptual simplicity the proposed control method has an excellent performance. Comparing to the control of closed-chain robotic systems that is based on global linearization methods, the following features can be attributed to the presented nonlinear H-infinity control scheme (i) it is applied directly on the nonlinear dynamical model of the closed-chain robotic mechanism and does not require the computation of diffeomorphisms (change of variables) that

will bring the system into an equivalent linearized form, (ii) the computation of the feedback control signal follows an optimal control concept and requires the solution of an algebraic Riccati equation at each iteration of the control algorithm, (iii) the control input is applied directly on the nonlinear model of the robot and not on a linearized equivalent description of it. In such a manner, inverse transformations that may come against singularity problems are not used in the computation of the real control input.

4.4.2 *Approximate Linearization of the Closed-Chain Closed-Chain Robotic Mechanism*

The closed-chain robotic mechanism has been depicted in Fig. 4.2. The dynamic model of the robotic mechanism has been shown to be

$$\dot{x} = f(x) + g_1(x)u_1 + g_2(x)u_2 \tag{4.126}$$

where the state vector is $x = [x_1, x_2, x_3, x_4]^T = [q_1, q_3, \dot{q}_1, \dot{q}_3]^T$, and vector fields $f(x)$, $g_1(x)$ and $g_2(x)$ are given by Eqs. (4.9), (4.10) and (4.11) respectively.

The robotic mechanism undergoes approximate linearization round its present operating point (x^*, u^*), where x^* denotes the present value of the state vector and u^* denotes the last value of the control input that was exerted on the system. This linearization procedure requires the computation of Jacobian matrices and gives

$$\dot{x} = Ax + Bu + \tilde{d} \tag{4.127}$$

where $\tilde{d}$ is the modelling error due to approximate linearization and cut-off of higher order terms in the Taylor series expansion, while matrices A and B are obtained from the computation of the Jacobian matrices

$$A = \nabla_x [f(x) + g_1(x)u_1 + g_2(x)u_2] \tag{4.128}$$

or by denoting $h(x, u) = [f(x) + g_1(x)u_1 + g_2(x)u_2]$ one has the following description for the Jacobian matrix of A

$$A = \begin{pmatrix} \frac{\partial h_1}{\partial x_1} & \frac{\partial h_1}{\partial x_2} & \frac{\partial h_1}{\partial x_3} & \frac{\partial h_1}{\partial x_4} \\ \frac{\partial h_2}{\partial x_1} & \frac{\partial h_2}{\partial x_2} & \frac{\partial h_2}{\partial x_3} & \frac{\partial h_2}{\partial x_4} \\ \frac{\partial h_3}{\partial x_1} & \frac{\partial h_3}{\partial x_2} & \frac{\partial h_3}{\partial x_3} & \frac{\partial h_3}{\partial x_4} \\ \frac{\partial h_4}{\partial x_1} & \frac{\partial h_4}{\partial x_2} & \frac{\partial h_4}{\partial x_3} & \frac{\partial h_4}{\partial x_4} \end{pmatrix} \tag{4.129}$$

For the first row of the Jacobian matrix $\nabla_x(f(x))$ it holds that $\frac{\partial f_1}{\partial x_1} = 0$, $\frac{\partial f_1}{\partial x_2} = 0$, $\frac{\partial f_1}{\partial x_3} = 1$, $\frac{\partial f_1}{\partial x_4} = 0$.

For the second row of the Jacobian matrix $\nabla_x(f(x))$ it holds that $\frac{\partial f_2}{\partial x_1} = 0$, $\frac{\partial f_2}{\partial x_2} = 0$, $\frac{\partial f_2}{\partial x_3} = 0$, $\frac{\partial f_2}{\partial x_4} = 1$.

For the third row of the Jacobian matrix $\nabla_x(f(x))$ it holds that $\frac{\partial f_3}{\partial x_1} = 0$, $\frac{\partial f_3}{\partial x_3} = 0$ and also

$$\frac{\partial f_3}{\partial x_2} = \frac{2l_3M_2(-k_2sin(x_2)+k_2(\pi-x_2)cos(x_2)-(I_3+I_4)x_4^2sin(x_2))\cdot[M_2(I_3+I_4)+M_1(I_3+I_4+4M_2l_3^2sin^2(x_2))]}{[M_2(I_3+I_4)+M_1(I_3+I_4+4M_2l_3^2sin^2(x_2))]^2} -$$

$$\frac{-[-k_2l_dI_3+I_4+2l_3M_2(k_2(\pi-x_2)sin(x_2)+(I_3+I_4)x_4^2cos(x_2))]\cdot[M_14M_2l_3^22sin(x_2)cos(x_2)]]}{[M_2(I_3+I_4)+M_1(I_3+I_4+4M_2l_3^2sin^2(x_2))]^2}$$

$$\frac{\partial f_3}{\partial x_4} = \frac{2l_3M_2(I_3+I_4)2x_4cos(x_2)}{[M_2(I_3+I_4)+M_1(I_3+I_4+4M_2l_3^2sin^2(x_2))]}$$

For the fourth row of the Jacobian matrix $\nabla_x(f(x))$ it holds that $\frac{\partial f_4}{\partial x_1} = 0$, $\frac{\partial f_4}{\partial x_3} = 0$ and also

$$\frac{\partial f_4}{\partial x_2} =$$

$$\frac{[-k_4(M_1+M_2)+2l_3M_2cos(x_2)(k_2l_d-2I_3M_2x_4^2cos(x_2))][M_2(I_3+I_4)+M_1(I_3+I_4+4M_2l_3^2sin^2(x_2))]}{[M_2(I_3+I_4)+M_1(I_3+I_4+4M_2l_3^2sin^2(x_2))]^2} +$$

$$+\frac{[2l_3M_2sin(x_2)(2I_3M_2x_4^2sin(x_2))][M_2(I_3+I_4)+M_1(I_3+I_4+4M_2l_3^2sin^2(x_2))]}{[M_2(I_3+I_4)+M_1(I_3+I_4+4M_2l_3^2sin^2(x_2))]^2}$$

$$-\frac{[k_4(M_1+M_2)(\pi-x_2)+2l_3M_1sin(x_2)(k_2l_d-2I_3M_2x_4^2cos(x_2))][M_1(4M_2l_3^2)2sin(x_2)cos(x_2)]}{[M_2(I_3+I_4)+M_1(I_3+I_4+4M_2l_3^2sin^2(x_2))]^2}$$

$$\frac{\partial f_4}{\partial x_4} = \frac{2l_3M_2sin(x_2)(-2I_3M_22x_4cos(x_2))}{[M_2(I_3+I_4)+M_1(I_3+I_4+4M_2l_3^2sin^2(x_2))]}$$

In a similar manner for the first row of the Jacobian matrix $\nabla_x(g_1(x))$ one computes: $\frac{\partial g_{11}(x)}{\partial x_1} = 0$, $\frac{\partial g_{11}(x)}{\partial x_2} = 0$, $\frac{\partial g_{11}(x)}{\partial x_3} = 0$, $\frac{\partial g_{11}(x)}{\partial x_4} = 0$.

For the second row of the Jacobian matrix $\nabla_x(g_1(x))$ one computes: $\frac{\partial g_{12}(x)}{\partial x_1} = 0$, $\frac{\partial g_{12}(x)}{\partial x_2} = 0$, $\frac{\partial g_{12}(x)}{\partial x_3} = 0$, $\frac{\partial g_{12}(x)}{\partial x_4} = 0$.

For the third row of the Jacobian matrix $\nabla_x(g_1(x))$ one computes: $\frac{\partial g_{13}(x)}{\partial x_1} = 0$, $\frac{\partial g_{13}(x)}{\partial x_3} = 0$, $\frac{\partial g_{13}(x)}{\partial x_4} = 0$ and also

$$\frac{\partial g_{13}(x)}{\partial x_2} = \frac{[4M_2I_3^22sin(x_2)cos(x_2)][(I_3+I_4)M_2+M_1(I_3+I_4+4M_2l_3^2sin^2(x_2))]}{[(I_3+I_4)M_2+M_1(I_3+I_4+4M_2l_3^2sin^2(x_2))]^2} -$$

$$-\frac{[I_3+I_4+4M_2l_3^2sin^2(x_2)][M_1(4M_2l_3^22sin(x_2)cos(x_2))]}{[(I_3+I_4)M_2+M_1(I_3+I_4+4M_2l_3^2sin^2(x_2))]^2}$$

For the fourth row of the Jacobian matrix $\nabla_x(g_1(x))$ one computes: $\frac{\partial g_{14}(x)}{\partial x_1} = 0$, $\frac{\partial g_{14}(x)}{\partial x_3} = 0$, $\frac{\partial g_{14}(x)}{\partial x_4} = 0$ and also

$$\frac{\partial g_{14}(x)}{\partial x_2} = \frac{[2M_2 l_3 cos(x_2)][(I_3+I_4)M_2+M_1(I_3+I_4+4M_2 l_3^2 sin^2(x_2))]}{[(I_3+I_4)M_2+M_1(I_3+I_4+4M_2 l_3^2 sin^2(x_2))]^2} -$$

$$- \frac{[2M_2 l_3 sin(x_2)][M_1 4M_2 l_3^2 2sin(x_2)cos(x_2)]}{[(I_3+I_4)M_2+M_1(I_3+I_4+4M_2 l_3^2 sin^2(x_2))]^2}$$

In a similar manner for the first row of the Jacobian matrix $\nabla_x(g_2(x))$ one computes: $\frac{\partial g_{21}(x)}{\partial x_1} = 0$, $\frac{\partial g_{21}(x)}{\partial x_2} = 0$, $\frac{\partial g_{21}(x)}{\partial x_3} = 0$, $\frac{\partial g_{21}(x)}{\partial x_4} = 0$.

For the second row of the Jacobian matrix $\nabla_x(g_2(x))$ one computes: $\frac{\partial g_{22}(x)}{\partial x_1} = 0$, $\frac{\partial g_{22}(x)}{\partial x_2} = 0$, $\frac{\partial g_{22}(x)}{\partial x_3} = 0$, $\frac{\partial g_{22}(x)}{\partial x_4} = 0$.

For the third row of the Jacobian matrix $\nabla_x(g_2(x))$ one computes: $\frac{\partial g_{23}(x)}{\partial x_1} = 0$, $\frac{\partial g_{23}(x)}{\partial x_3} = 0$, $\frac{\partial g_{23}(x)}{\partial x_4} = 0$ and also

$$\frac{\partial g_{23}(x)}{\partial x_2} = \frac{[2M_2 l_3 cos(x_2)][(I_3+I_4)M_2+M_1(I_3+I_4+M_2 l_3^2 sin^2(x_2))]}{[(I_3+I_4)M_2+M_1(I_3+I_4+4M_2 l_3^2 sin^2(x_2))]^2} -$$

$$- \frac{[2M_2 l_3 sin(x_2)][M_2 4M_2 l_3^2 2sin(x_2)cos(x_2)]}{[(I_3+I_4)M_2+M_1(I_3+I_4+4M_2 l_3^2 sin^2(x_2))]^2}$$

For the fourth row of the Jacobian matrix $\nabla_x(g_2(x))$ one computes: $\frac{\partial g_{24}(x)}{\partial x_1} = 0$, $\frac{\partial g_{24}(x)}{\partial x_3} = 0$, $\frac{\partial g_{24}(x)}{\partial x_4} = 0$ and also

$$\frac{\partial g_{24}(x)}{\partial x_2} = - \frac{[(M_1+M_2)M_2(4M_2 l_3^2 2sin(x_2)cos(x_2))]}{[(I_3+I_4)M_2+M_1(I_3+I_4+4M_2 l_3^2 sin^2(x_2))]^2}$$

For the elements of the Jacobian matrix $A = \nabla_x[f(x) + g_1(x)u_1 + g_2(x)u_2] \mid_{(x^*,u^*)}$ t holds that for $i = 1, \ldots, 4$ and $j = 1, \ldots, 4$

$$\frac{\partial h_i}{\partial x_j} = [\frac{\partial f_i}{\partial x_j} + \frac{\partial g_{1i}}{\partial x_j} u_1 + \frac{\partial g_{2i}}{\partial x_j} u_2] \mid_{(x^*,u^*)} \tag{4.130}$$

while in the case of underactuation of the robotic mechanism one has $u_1 = 0$, thus the elements of this Jacobian matrix become

$$\frac{\partial h_i}{\partial x_j} = [\frac{\partial f_i}{\partial x_j} + \frac{\partial g_{2i}}{\partial x_j} u_2] \mid_{(x^*,u^*)} \tag{4.131}$$

Moreover, it holds that

$$B = \nabla_u = [f(x) + g_1(x)u_1 + g_2(x)u_2] \mid_{(x^*,u^*)} \Rightarrow B = [g_1(x)\ g_2(x)] \tag{4.132}$$

It is also noted that, for the case of underactuation, that is when $u_1 = 0$, $u_2 \neq 0$ one has

$$B = g_2. \tag{4.133}$$

4.4.3 Design of an H-Infinity Nonlinear Feedback Controller

4.4.3.1 Equivalent Linearized Dynamics of the Closed-Chain Robotic Mechanism

After linearization round its current operating point, the dynamic model of the closed-chain robotic mechanism's dynamic model is written as

$$\dot{x} = Ax + Bu + d_1 \tag{4.134}$$

Parameter d_1 stands for the linearization error in the closed-chain robotic mechanism's dynamic model appearing in Eq. (4.134). The reference setpoints for the closed-chain robotic mechanism's state vector are denoted by $\mathbf{x_d} = [x_1^d, \ldots, x_4^d]$. Tracking of this trajectory is achieved after applying the control input u^*. At every time instant the control input u^* is assumed to differ from the control input u appearing in Eq. (4.134) by an amount equal to Δu, that is $u^* = u + \Delta u$

$$\dot{x}_d = Ax_d + Bu^* + d_2 \tag{4.135}$$

The dynamics of the controlled system described in Eq. (4.134) can be also written as

$$\dot{x} = Ax + Bu + Bu^* - Bu^* + d_1 \tag{4.136}$$

and by denoting $d_3 = -Bu^* + d_1$ as an aggregate disturbance term one obtains

$$\dot{x} = Ax + Bu + Bu^* + d_3 \tag{4.137}$$

By subtracting Eq. (4.135) from (4.137) one has

$$\dot{x} - \dot{x}_d = A(x - x_d) + Bu + d_3 - d_2 \tag{4.138}$$

By denoting the tracking error as $e = x - x_d$ and the aggregate disturbance term as $\tilde{d} = d_3 - d_2$, the tracking error dynamics becomes

$$\dot{e} = Ae + Bu + \tilde{d} \tag{4.139}$$

The above linearized form of the closed-chain robotic mechanism's model can be efficiently controlled after applying an H-infinity feedback control scheme.

4.4.3.2 The Nonlinear H-Infinity Control

The initial nonlinear model of the closed-chain robotic mechanism is in the form

$$\dot{x} = f(x, u) \;\; x \in R^n, \;\; u \in R^m \tag{4.140}$$

Linearization of the system (multi-DOF closed-chain robotic mechanism) is performed at each iteration of the control algorithm round its present operating point $(x^*, u^*) = (x(t), u(t - T_s))$. The linearized equivalent of the system is described by

$$\dot{x} = Ax + Bu + L\tilde{d} \;\; x \in R^n, \;\; u \in R^m, \;\; \tilde{d} \in R^q \tag{4.141}$$

where matrices A and B are obtained from the computation of the Jacobians of the closed-chain robotic system and vector $\tilde{d}$ denotes disturbance terms due to linearization errors. The problem of disturbance rejection for the linearized model that is described by

$$\begin{gathered} \dot{x} = Ax + Bu + L\tilde{d} \\ y = Cx \end{gathered} \tag{4.142}$$

where $x \in R^n$, $u \in R^m$, $\tilde{d} \in R^q$ and $y \in R^p$, cannot be handled efficiently if the classical LQR control scheme is applied. This is because of the existence of the perturbation term $\tilde{d}$. The disturbance term $\tilde{d}$ apart from modeling (parametric) uncertainty and external perturbation terms can also represent noise terms of any distribution.

In the H_∞ control approach, a feedback control scheme is designed for trajectory tracking by the closed–chain robotic system's state vector and simultaneous disturbance rejection, considering that the disturbance affects the system in the worst possible manner. The disturbances' effects are incorporated in the following quadratic cost function:

$$J(t) = \tfrac{1}{2}\int_0^T [y^T(t)y(t) + ru^T(t)u(t) - \rho^2 \tilde{d}^T(t)\tilde{d}(t)]dt, \;\; r, \rho > 0 \tag{4.143}$$

As explained in previous applications of the H-infinity control to robotic models, the significance of the negative sign in the cost function's term that is associated with the perturbation variable $\tilde{d}(t)$ is that the disturbance tries to maximize the cost function $J(t)$ while the control signal $u(t)$ tries to minimize it. The physical meaning of the relation given above is that the control signal and the disturbances compete to each other within a min-max differential game. This problem of min-max optimization can be written as

$$min_u max_{\tilde{d}} J(u, \tilde{d}) \tag{4.144}$$

The objective of the optimization procedure is to compute a control signal $u(t)$ which can compensate for the worst possible disturbance, that is externally imposed to the closed-chain robotic system. However, the solution to the min-max optimization

problem is directly related to the value of parameter ρ. This means that there is an upper bound in the disturbances magnitude that can be annihilated by the control signal.

4.4.3.3 Computation of the Feedback Control Gains

For the linearized system given by Eq. (4.142) the cost function of Eq. (4.143) is defined, where the coefficient r determines the penalization of the control input and the weight coefficient ρ determines the reward of the disturbances' effects.

It is assumed that (i) The energy that is transferred from the disturbances signal $\tilde{d}(t)$ is bounded, that is $\int_0^\infty \tilde{d}^T(t)\tilde{d}(t)dt < \infty$, (ii) the matrices $[A, B]$ and $[A, L]$ are stabilizable, (iii) the matrix $[A, C]$ is detectable. As shown in previous cases of application of H-infinity control, the optimal feedback control law is given by

$$u(t) = -Kx(t) \tag{4.145}$$

with

$$K = \frac{1}{r}B^T P \tag{4.146}$$

where P is a positive semi-definite symmetric matrix which is obtained from the solution of the Riccati equation

$$A^T P + PA + Q - P\left(\frac{1}{r}BB^T - \frac{1}{2\rho^2}LL^T\right)P = 0 \tag{4.147}$$

where Q is also a positive definite symmetric matrix. The worst case disturbance is given by

$$\tilde{d}(t) = \frac{1}{\rho^2}L^T P x(t) \tag{4.148}$$

The diagram of the considered control loop is depicted in Fig. 4.16.

4.4.4 Lyapunov Stability Analysis

Through Lyapunov stability analysis it will be shown that the proposed nonlinear control scheme assures H_∞ tracking performance for the closed-chain robotic mechanism, and that in case of bounded disturbance terms asymptotic convergence to the reference setpoints is achieved.

The tracking error dynamics for the closed-chain robotic mechanism is written in the form

$$\dot{e} = Ae + Bu + L\tilde{d} \tag{4.149}$$

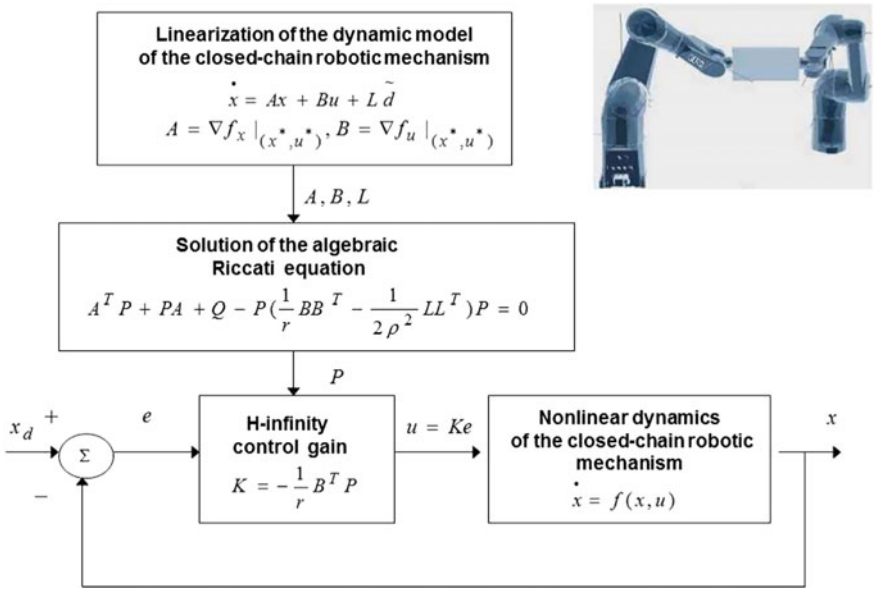

Fig. 4.16 Diagram of the control scheme for the closed-chain robotic mechanism

where in the closed-chain robotic mechanism's case $L = I \in R^4$ with I being the identity matrix. Variable $\tilde{d}$ denotes model uncertainties and external disturbances of the closed-chain robotic mechanism's model. The following Lyapunov function is considered

$$V = \tfrac{1}{2}e^T Pe \tag{4.150}$$

where $e = x - x_d$ is the tracking error. By differentiating with respect to time one obtains

$$\begin{gathered}\dot{V} = \tfrac{1}{2}\dot{e}^T Pe + \tfrac{1}{2}eP\dot{e} \Rightarrow \\ \dot{V} = \tfrac{1}{2}[Ae + Bu + L\tilde{d}]^T Pe + \tfrac{1}{2}e^T P[Ae + Bu + L\tilde{d}] \Rightarrow\end{gathered} \tag{4.151}$$

$$\begin{gathered}\dot{V} = \tfrac{1}{2}[e^T A^T + u^T B^T + \tilde{d}^T L^T]Pe + \\ + \tfrac{1}{2}e^T P[Ae + Bu + L\tilde{d}] \Rightarrow\end{gathered} \tag{4.152}$$

$$\begin{gathered}\dot{V} = \tfrac{1}{2}e^T A^T Pe + \tfrac{1}{2}u^T B^T Pe + \tfrac{1}{2}\tilde{d}^T L^T Pe + \\ \tfrac{1}{2}e^T PAe + \tfrac{1}{2}e^T PBu + \tfrac{1}{2}e^T PL\tilde{d}\end{gathered} \tag{4.153}$$

The previous equation is rewritten as

$$\begin{gathered}\dot{V} = \tfrac{1}{2}e^T(A^T P + PA)e + (\tfrac{1}{2}u^T B^T Pe + \tfrac{1}{2}e^T PBu) + \\ + (\tfrac{1}{2}\tilde{d}^T L^T Pe + \tfrac{1}{2}e^T PL\tilde{d})\end{gathered} \tag{4.154}$$

Assumption: For given positive definite matrix Q and coefficients r and ρ there exists a positive definite matrix P, which is the solution of the following matrix equation

$$A^T P + PA = -Q + P(\tfrac{2}{r}BB^T - \tfrac{1}{\rho^2}LL^T)P \tag{4.155}$$

Moreover, the following feedback control law is applied to the system

$$u = -\tfrac{1}{r}B^T Pe \tag{4.156}$$

By substituting Eqs. (4.155) and (4.156) one obtains

$$\begin{gathered}\dot{V} = \tfrac{1}{2}e^T[-Q + P(\tfrac{2}{r}BB^T - \tfrac{1}{\rho^2}LL^T)P]e + \\ + e^T PB(-\tfrac{1}{r}B^T Pe) + e^T PL\tilde{d} \Rightarrow\end{gathered} \tag{4.157}$$

$$\begin{gathered}\dot{V} = -\tfrac{1}{2}e^T Qe + \tfrac{1}{r}e^T PBB^T Pe - \tfrac{1}{2\rho^2}e^T PLL^T Pe \\ -\tfrac{1}{r}e^T PBB^T Pe + e^T PL\tilde{d}\end{gathered} \tag{4.158}$$

which after intermediate operations gives

$$\dot{V} = -\tfrac{1}{2}e^T Qe - \tfrac{1}{2\rho^2}e^T PLL^T Pe + e^T PL\tilde{d} \tag{4.159}$$

or, equivalently

$$\begin{gathered}\dot{V} = -\tfrac{1}{2}e^T Qe - \tfrac{1}{2\rho^2}e^T PLL^T Pe + \\ + \tfrac{1}{2}e^T PL\tilde{d} + \tfrac{1}{2}\tilde{d}^T L^T Pe\end{gathered} \tag{4.160}$$

Lemma: The following inequality holds

$$\tfrac{1}{2}e^T PL\tilde{d} + \tfrac{1}{2}\tilde{d}L^T Pe - \tfrac{1}{2\rho^2}e^T PLL^T Pe \leq \tfrac{1}{2}\rho^2\tilde{d}^T\tilde{d} \tag{4.161}$$

Proof: The binomial $(\rho\alpha - \frac{1}{\rho}b)^2$ is considered. Expanding the left part of the above inequality one gets

$$\begin{gathered}\rho^2 a^2 + \tfrac{1}{\rho^2}b^2 - 2ab \geq 0 \Rightarrow \tfrac{1}{2}\rho^2 a^2 + \tfrac{1}{2\rho^2}b^2 - ab \geq 0 \Rightarrow \\ ab - \tfrac{1}{2\rho^2}b^2 \leq \tfrac{1}{2}\rho^2 a^2 \Rightarrow \tfrac{1}{2}ab + \tfrac{1}{2}ab - \tfrac{1}{2\rho^2}b^2 \leq \tfrac{1}{2}\rho^2 a^2\end{gathered} \tag{4.162}$$

The following substitutions are carried out: $a = \tilde{d}$ and $b = e^T PL$ and the previous relation becomes

$$\tfrac{1}{2}\tilde{d}^T L^T Pe + \tfrac{1}{2}e^T PL\tilde{d} - \tfrac{1}{2\rho^2}e^T PLL^T Pe \leq \tfrac{1}{2}\rho^2\tilde{d}^T\tilde{d} \tag{4.163}$$

Equation (4.163) is substituted in Eq. (4.160) and the inequality is enforced, thus giving

$$\dot{V} \leq -\frac{1}{2}e^T Qe + \frac{1}{2}\rho^2 \tilde{d}^T \tilde{d} \tag{4.164}$$

Equation (4.164) shows that the H_∞ tracking performance criterion is satisfied. The integration of $\dot{V}$ from 0 to T gives

$$\begin{array}{c} \int_0^T \dot{V}(t)dt \leq -\frac{1}{2}\int_0^T ||e||_Q^2 dt + \frac{1}{2}\rho^2 \int_0^T ||\tilde{d}||^2 dt \Rightarrow \\ 2V(T) + \int_0^T ||e||_Q^2 dt \leq 2V(0) + \rho^2 \int_0^T ||\tilde{d}||^2 dt \end{array} \tag{4.165}$$

Moreover, if there exists a positive constant $M_d > 0$ such that

$$\int_0^\infty ||\tilde{d}||^2 dt \leq M_d \tag{4.166}$$

then one gets

$$\int_0^\infty ||e||_Q^2 dt \leq 2V(0) + \rho^2 M_d \tag{4.167}$$

Thus, the integral $\int_0^\infty ||e||_Q^2 dt$ is bounded. Moreover, $V(T)$ is bounded and from the definition of the Lyapunov function V in Eq. (4.150) it becomes clear that $e(t)$ will be also bounded since $e(t) \in \Omega_e = \{e | e^T Pe \leq 2V(0) + \rho^2 M_d\}$. According to the above and with the use of Barbalat's Lemma one obtains $lim_{t\to\infty} e(t) = 0$.

The outline of the global stability proof is that at each iteration of the control algorithm the state vector of the system converges towards the temporary equilibrium and the temporary equilibrium in turn converges towards the reference trajectory. Thus, the control scheme exhibits global asymptotic stability properties and not local stability. Assume the ith iteration of the control algorithm and the ith time interval about which a positive definite symmetric matrix P is obtained from the solution of the Riccati equation appearing in Eq. (4.155). By following the stages of the stability proof one arrives at Eq. (4.164) which shows that the H-infinity tracking performance criterion holds. By selecting the attenuation coefficient to be sufficiently small and in particular to satisfy $\rho^2 < ||e||_Q^2 / |\tilde{d}|^2$ one has that the first derivative of the Lyapunov function is upper bounded by 0. Therefore for the ith time interval it is proven that the Lyapunov function defined in Eq. (4.150) is a decreasing one. This signifies that between the beginning and the end of the ith time interval there will be a drop of the value of the Lyapunov function and since matrix P is a positive definite one, the only way for this to happen is the Euclidean norm of the state vector error e to be decreasing. This means that comparing to the beginning of each time interval, the distance of the state vector error from 0 at the end of the time interval has diminished. Consequently as the iterations of the control algorithm advance the tracking error will approach zero, and this is a global asymptotic stability condition.

4.4.5 Robust State Estimation with the Use of the H-Infinity Kalman Filter

The control loop can be implemented with the use of information provided by a small number of sensors and by processing only a small number of state variables. To reconstruct the missing information about the state vector of the closed-chain robotic mechanism it is proposed to use a filtering scheme and based on it to apply state estimation-based control [457]. The recursion of the H_∞ Kalman Filter, for the model of the robotic mechanism, can be formulated in terms of a *measurement update* and a *time update* part

Measurement update:

$$\begin{aligned} D(k) &= [I - \theta W(k)P^{-}(k) + C^{T}(k)R(k)^{-1}C(k)P^{-}(k)]^{-1} \\ K(k) &= P^{-}(k)D(k)C^{T}(k)R(k)^{-1} \\ \hat{x}(k) &= \hat{x}^{-}(k) + K(k)[y(k) - C\hat{x}^{-}(k)] \end{aligned} \tag{4.168}$$

Time update:

$$\begin{aligned} \hat{x}^{-}(k+1) &= A(k)x(k) + B(k)u(k) \\ P^{-}(k+1) &= A(k)P^{-}(k)D(k)A^{T}(k) + Q(k) \end{aligned} \tag{4.169}$$

where it is assumed that parameter θ is sufficiently small to assure that the covariance matrix $P^{-}(k)^{-1} - \theta W(k) + C^{T}(k)R(k)^{-1}C(k)$ will be positive definite. When $\theta = 0$ the H_∞ Kalman Filter becomes equivalent to the standard Kalman Filter. One can measure only a part of the state vector of the closed-chain robotic mechanism, and estimate through filtering the rest of the state vector elements. Moreover, the proposed Kalman filtering method can be used for sensor fusion purposes.

4.4.6 Simulation Tests

The performance of the proposed nonlinear optimal (H-infinity) control scheme in the problem of stabilization and trajectory tracking of closed-chain robotic mechanisms has been tested through simulation experiments. The implementation of the H-infinity feedback control required to solve at each iteration of the control algorithm the algebraic Riccati equation given in Eq. (4.147). The outcome of this equation was the positive definite symmetric matrix P and its value was dependent on the values of the weight matrix Q, as well of the gains r and ρ. These parameters determined the transient performance of the control scheme. The obtained results are depicted in Figs. 4.17a, 4.18, 4.19, 4.20, 4.21 and 4.22a. It can be observed that the H-infinity control method resulted in fast and accurate tracking of the reference setpoints. Moreover, from Figs. 4.17b, 4.18, 4.19, 4.20, 4.21 and 4.22b it can be confirmed that the associated control inputs varied smoothly.

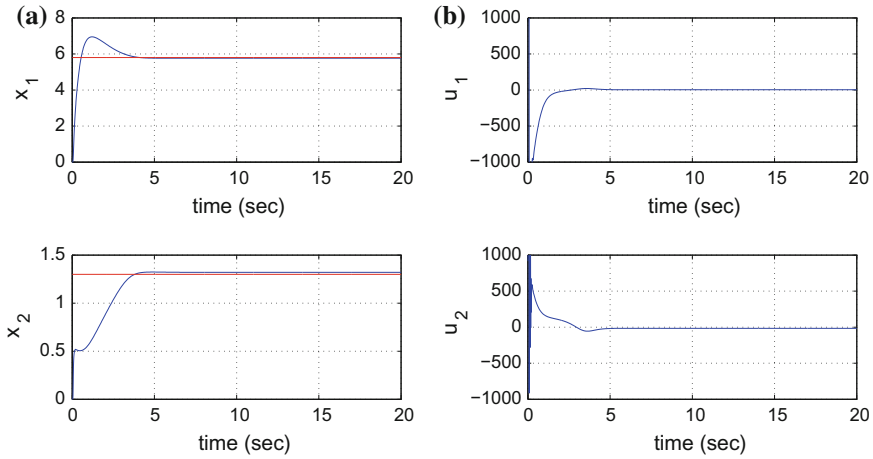

Fig. 4.17 Reference path 1: **a** Convergence of the state variables of the closed-chain robotic mechanism $x_1, = q_1$ and $x_2 = q_3$ (blue line) to the associated reference values (red line) **b** Control input $u_1 = F$ and $u_2 = T_3$ exerted on the robot

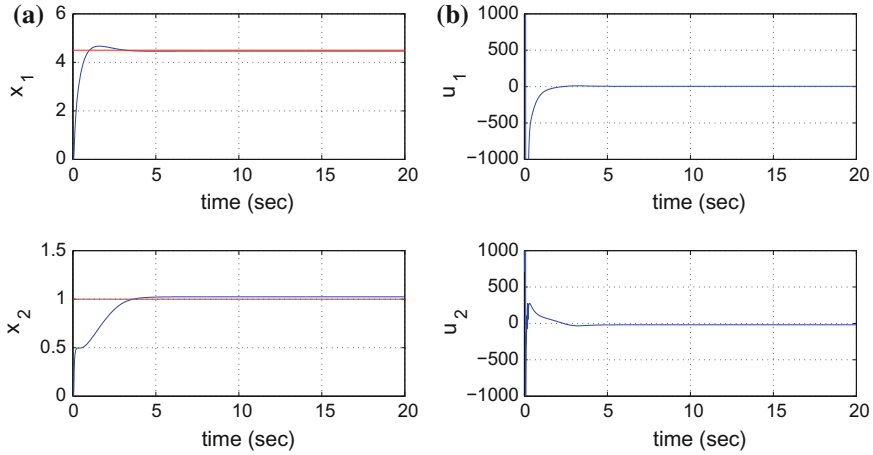

Fig. 4.18 Reference path 2: **a** Convergence of the state variables of the closed-chain robotic mechanism $x_1, = q_1$ and $x_2 = q_3$ (blue line) to the associated reference values (red line) **b** Control input $u_1 = F$ and $u_2 = T_3$ exerted on the robot

The tracking performance of the nonlinear H-infinity control method for the model of the closed-chain robotic mechanism and under parametric disturbances affecting the input gain functions $g_1(x)$ and $g_2(x)$ of Eq. (4.8) is outlined in Table 4.3. Moreover, the tracking performance of the H-infinity control algorithm under parametric disturbances (case No 5 of Table 4.3) is depicted in Fig. 4.23. It can be noticed

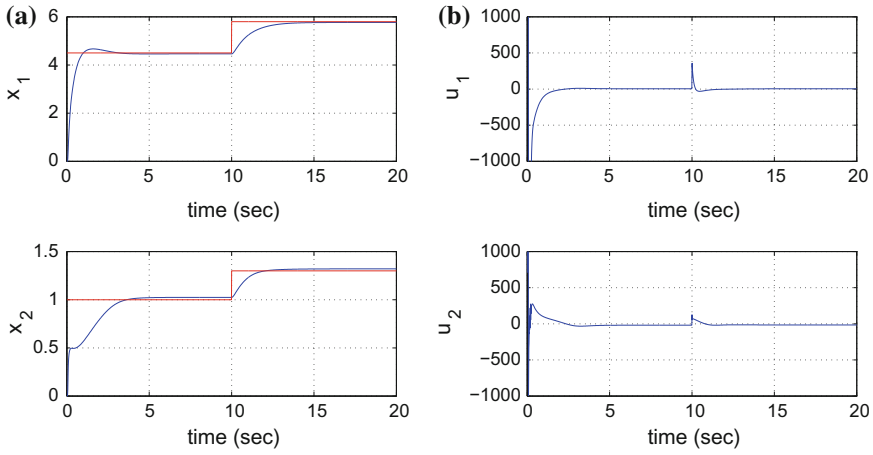

Fig. 4.19 Reference path 3: **a** Convergence of the state variables of the closed-chain robotic mechanism $x_1, = q_1$ and $x_2 = q_3$ (blue line) to the associated reference values (red line) **b** Control input $u_1 = F$ and $u_2 = T_3$ exerted on the robot

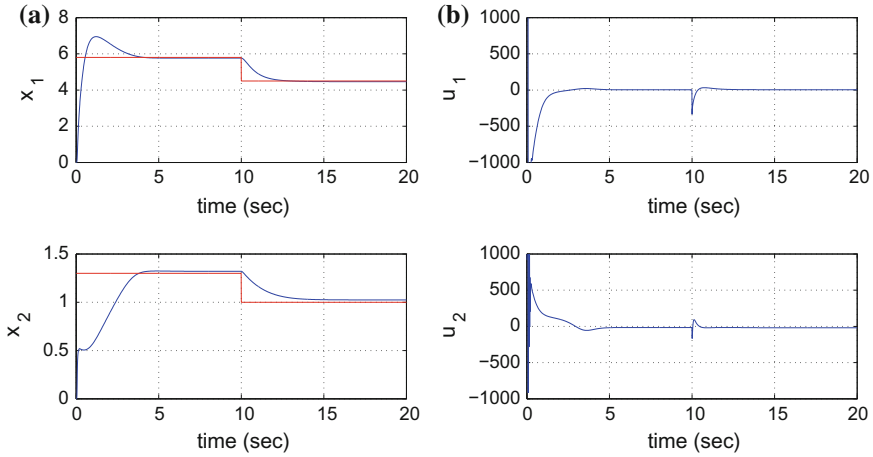

Fig. 4.20 Reference path 4: **a** Convergence of the state variables of the closed-chain robotic mechanism $x_1, = q_1$ and $x_2 = q_3$ (blue line) to the associated reference values (red line) **b** Control input $u_1 = F$ and $u_2 = T_3$ exerted on the robot

that despite parametric perturbations the tracking accuracy of the control method remained satisfactory.

It is worth mentioning that the H-infinity optimal control scheme has not been previously applied to closed-chain kinematic mechanisms [418, 420, 425]. The presented control method stands for a new result in the area of nonlinear control of robotic mechanisms. Moreover, it is noteworthy that there is no need to consider linearization at multiple operating points (equilibria). It suffices to consider one single

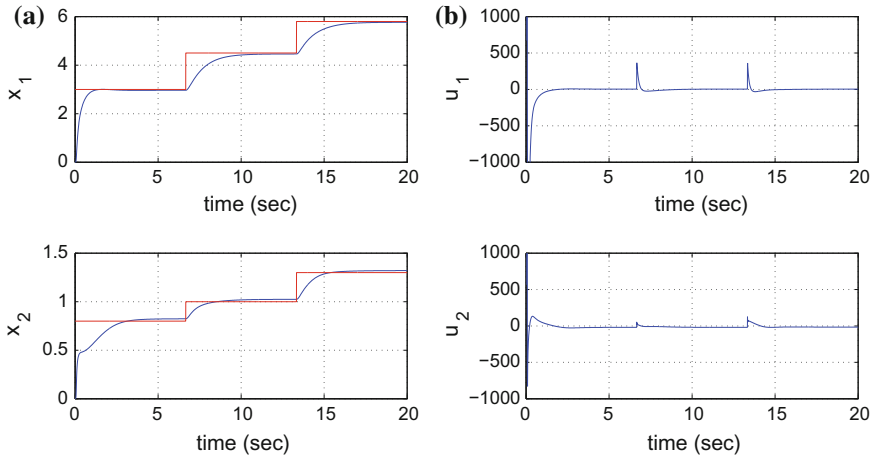

Fig. 4.21 Reference path 5: **a** Convergence of the state variables of the closed-chain robotic mechanism $x_1, = q_1$ and $x_2 = q_3$ (blue line) to the associated reference values (red line) **b** Control input $u_1 = F$ and $u_2 = T_3$ exerted on the robot

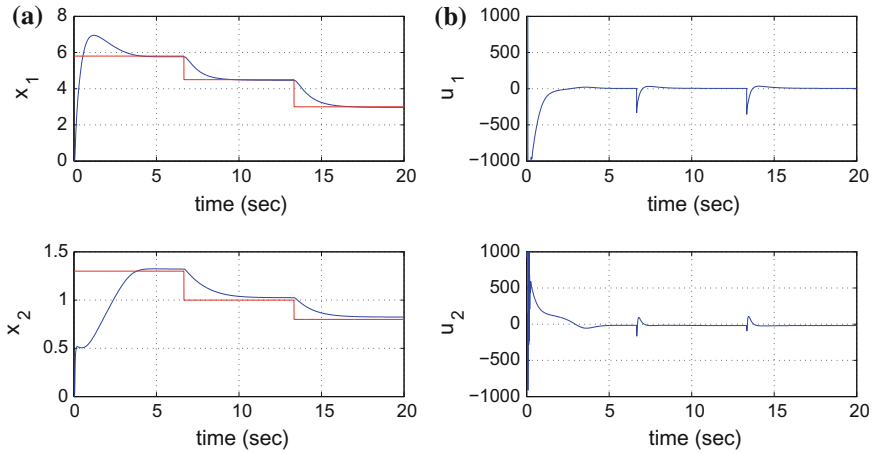

Fig. 4.22 Reference path 6: **a** Convergence of the state variables of the closed-chain robotic mechanism $x_1, = q_1$ and $x_2 = q_3$ (blue line) to the associated reference values (red line) **b** Control input $u_1 = F$ and $u_2 = T_3$ exerted on the robot

equilibrium at each iteration of the control method consisting of the present value of the system's state vector and the last value of the control inputs vector exerted on it. Unlike design of stabilizing feedback controllers based on the linearization of the state-space model round multiple operating points and making use of multiple linear local models, the proposed control method considers only one time-varying equilibrium which at each iteration of the control algorithm is made to converge towards the reference trajectory. Moreover, there is no need to design multiple local feedback

Table 4.3 RMSE of the robot's state variables

No	% change	RMSEx_1	RMSEx_2	RMSEx_3	RMSEx_4
1	0	$2.0{\cdot}10^{-4}$	$0.7{\cdot}10^{-4}$	$0.1{\cdot}10^{-4}$	$0.1{\cdot}10^{-4}$
2	50	$7.0{\cdot}10^{-4}$	$1.0{\cdot}10^{-4}$	$2.0{\cdot}10^{-4}$	$2.0{\cdot}10^{-4}$
3	100	$11.0{\cdot}10^{-4}$	$3.0{\cdot}10^{-4}$	$5.0{\cdot}10^{-4}$	$5.0{\cdot}10^{-4}$
4	150	$13.0{\cdot}10^{-4}$	$4.0{\cdot}10^{-4}$	$6.0{\cdot}10^{-4}$	$6.0{\cdot}10^{-4}$
5	200	$15.0{\cdot}10^{-4}$	$5.0{\cdot}10^{-4}$	$7.0{\cdot}10^{-4}$	$7.0{\cdot}10^{-4}$
6	250	$16.0{\cdot}10^{-4}$	$6.0{\cdot}10^{-4}$	$8.0{\cdot}10^{-4}$	$8.0{\cdot}10^{-4}$
7	300	$16.0{\cdot}10^{-4}$	$6.0{\cdot}10^{-4}$	$8.0{\cdot}10^{-4}$	$8.0{\cdot}10^{-4}$
8	350	$17.0{\cdot}10^{-4}$	$7.0{\cdot}10^{-4}$	$9.0{\cdot}10^{-4}$	$9.0{\cdot}10^{-4}$

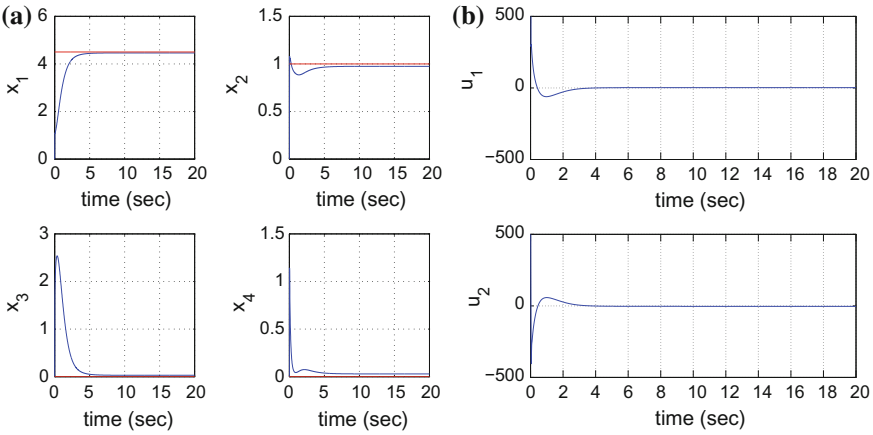

Fig. 4.23 Reference path 2 under parametric disturbances: **a** Convergence of the state variables of the closed-chain robotic mechanism $x_1, = q_1$ and $x_2 = q_3$ (blue line) to the associated reference values (red line) **b** Control input $u_1 = F$ and $u_2 = T_3$ exerted on the robot

controllers through the solution of multiple algebraic Riccati equations, each one related to a local linear model. Besides there is no need to find a common symmetric positive definite matrix P standing for the common solution of the multiple algebraic Riccati equations (approach followed in [457], Chap. 10). In the proposed H-infinity nonlinear control method, at each iteration of the control algorithm there is solution of one single algebraic Riccati equation and the positive definite symmetric matrix P which is obtained out of it is used for the design of the stabilizing feedback controller. The provided stability analysis relying on Eq. (4.164) proves finally global asymptotic stability properties for the control loop.

Chapter 5
Flexible-Link Robots

Abstract Control for flexible-link robots is a non-trivial problem that has elevated difficulty comparing to the control of rigid-link manipulators. This is because the dynamic model of the flexible-link robot contains the nonlinear rigid link motion coupled with the distributed effects of the links' flexibility. This coupling depends on the inertia matrix of the flexible manipulator while the vibration characteristics are determined by structural properties of the links such as the damping and stiffness parameters. Moreover, in contrast to the dynamic model of rigid-link robots the dynamic model of flexible-link robots is an infinite dimensional one. As in the case of the rigid-link manipulators there is a certain number of mechanical degrees of freedom associated to the rotational motion of the robot's joints and there is also an infinite number of degrees of freedom associated to the vibration modes in which the deformation of the flexible link is decomposed The controller of a flexible manipulator must achieve the same motion objectives as in the case of a rigid manipulator, i.e. tracking of specific joints position and velocity setpoints. Additionally, it must also stabilize and asymptotically eliminate the vibrations of the flexible-links that are naturally excited by the joints' rotational motion. A first approach for the control of flexible-link robots is to consider the vibration modes as additional state variables and to develop stabilizing feedback controller for the extended state-space model of the flexible manipulator. To this end, one can use again (i) control based on global linearization methods, (ii) control based on approximate linearization methods, (iii) control based on Lyapunov methods. Another approach to the solution of the control problem of flexible manipulators is to treat the robot as a distributed parameter system and to apply control directly to the partial differential equations models that describe the motion of the flexible links. Again global asymptotic stability for this control approach can be demonstrated. On the other side, nonlinear filtering methods can be used for implementing state estimation-based feedback control through the measurement of a limited number of elements from the flexible robot's state vector. In particular, the topics which are developed by the present chapter are as follows: (a) Inverse dynamics control of flexible-link robotic manipulators (b) sliding-mode control of flexible-link robotic manipulators.

G. Rigatos and K. Busawon, *Robotic Manipulators and Vehicles*,
Studies in Systems, Decision and Control 152,
https://doi.org/10.1007/978-3-319-77851-8_5

5.1 Chapter Overview

The topics which are developed by the present chapter are as follows: (a) Inverse dynamics control of flexible-link robotic manipulators (b) sliding-mode control of flexible-link robotic manipulators.

With reference to (a) a comparative study on representative methods for model-based and model-free control of flexible-link robots is given. Model-based techniques for the control of flexible-link robots such as inverse dynamics control can come up against limitations when an accurate model is unavailable, due to parameters uncertainty or truncation of high order vibration modes. On the other hand, model-free control methods, such as energy-based control can result in stabilization and satisfactory trajectory tracking performance of flexible-link robots.

With reference to (b) a robust control approach for a 2-link flexible robotic manipulator is developed that comprises sliding-mode control theory and Kalman Filtering. It is aimed to achieve: (i) simultaneous position control and suppression of the flexible structure vibrations. Assuming a known model of the robot dynamics, this can be achieved with the use of robust model-based control schemes, such as sliding-mode control, (ii) estimation of the complete state vector of the vibrating structure, so as to implement state-feedback control. To solve the latter problem, in this chapter, state estimation for the flexible-link robot is implemented with the use of Kalman Filtering. The fast recursion of the Kalman Filter provides real-time estimates of the robot's state vector through the processing of measurements coming from a limited number of sensors.

5.2 Inverse Dynamics Control of Flexible-Link Robots

5.2.1 Outline

Flexible-link robots comprise an important class of systems that include lightweight arms for assembly, civil infrastructure, bridge/vehicle systems, military applications and large-scale space structures. Modelling and vibration control of flexible systems have received a great deal of attention in recent years [224, 231, 442]. This section presents a comparative study on representative methods for model-based and model-free control of flexible-link robots. Conventional approaches to design a control system for a flexible-link robot often involve the development of a mathematical model describing the robot dynamics, and the application of analytical techniques to this model to derive an appropriate control law [22, 75, 119]. Usually, such a mathematical model consists of nonlinear partial differential equations, most of which are obtained using some approximation or simplification [224, 442]. The inverse dynamics model-based control for flexible link robots relies on modal analysis, i.e. on the assumption that the deformation of the flexible link can be written as a finite series expansion containing the elementary vibration modes [583]. However, this

inverse-dynamics model-based control may result into unsatisfactory performance when an accurate model is unavailable, due to parameters uncertainty or truncation of high order vibration modes [268].

Another model-based approach for the control of flexible-link robots is flatness-based control. Flatness-based control is a powerful tool for the control of distributed parameter systems which does not follow modal analysis but the description of the flexible robot using the concept of *differential flatness* [16, 39, 146]. It has been shown that flexible-link robots and flexible beams are flat systems and thus flatness-based control can be efficiently used for trajectory tracking of flexible-link manipulators [145, 337, 349, 476]. The decomposition of the desirable trajectory into a series of a reference flat output (Gevrey function) and its derivatives enables to generate open-loop control that assures tracking of the desirable trajectory. To achieve additional robustness a PID control loop can be designed to operate in parallel to the flatness-based controller of the flexible-link manipulator. Different model-based approaches for the control of flexible link manipulators have been also developed. In [365] wave-based control of flexible-link robots has been proposed. First a new wave-based model of uniform mass-spring systems was introduced and next this model was used to derive a control method for flexible-link robotic systems. In [41], a survey of model-based approaches for the control of flexible-link manipulators has been given.

To overcome the inefficiencies of the aforementioned inverse-dynamics control, model-free control methods have been studied [351, 529, 612]. A number of research papers employ model-free approaches for the control of flexible-link robots based on fuzzy logic and neural networks. In [557] control of a flexible manipulator with the use of a neuro-fuzzy method is described, where the weighting factor of the fuzzy logic controller is adjusted by the dynamic recurrent identification network. The controller works without any prior knowledge about the manipulator's dynamics. Control of the end-effector's position of a flexible-link manipulator with the use of a neural and a fuzzy controller has been presented in [531, 543, 575]. In [575] an intelligent optimal control for a nonlinear flexible robot arm driven by a permanent-magnet synchronous servo motor has been designed using a fuzzy neural network control approach. This consists of an optimal controller which minimizes a quadratic performance index and a fuzzy neural-network controller that learns the uncertain dynamics of the flexible manipulator. In [543] a fuzzy controller has been developed for a three-link robot with two rigid links and one flexible fore-arm. This controller's design is based on fuzzy Lyapunov synthesis where a Lyapunov candidate function has been chosen to derive the fuzzy rules. In [530] a neuro-fuzzy scheme has been proposed for position control of the end effector of a single-link flexible robot manipulator. The scale factors of the neuro-fuzzy controller are adapted on-line using a neural network which is trained with an improved back-propagation algorithm. In [73] two different neuro-fuzzy feed-forward controllers have been proposed to compensate for the nonlinearities of a flexible manipulator. In [412] the dynamics of a flexible link has been modeled using modal analysis and then an inverse dynamics fuzzy controller has been employed to obtain tracking and deflection control. In [503] a fuzzy logic controller has been applied to a flexible-link manipulator. In this distributed fuzzy logic controller the two velocity variables which have higher

importance have been grouped together as the inputs to a velocity fuzzy controller while the two displacement variables which have lower importance degrees have been used as inputs to a displacement fuzzy logic controller. In [204] adaptive control for a flexible-link manipulator has been achieved using a neuro-fuzzy time-delay controller. In [362] a genetic algorithm has been used to improve the performance of a fuzzy controller designed to compensate for the links' flexibility and the joints' flexibility of a robotic manipulator.

In this section the energy-based model-free control method of flexible-link robots is examined and shown to be equally effective to the model-based control methods. In the energy-based control method, instead of using the dynamical model of the links, the main stability results are derived with the use of the total energy and the energy-work relationship of the whole system [164, 491].

5.2.2 *Model-Based Control of Flexible Link Robots*

5.2.2.1 The Inverse Dynamics Control Method

A common approach in modelling of flexible-link robots is depends on the Euler-Bernoulli model [583]. This model consists of nonlinear partial differential equations, which are obtained using some approximation or simplification. In case of a single-link flexible manipulator the basic variables of this model are $w(x,t)$ which is the deformation of the flexible link, and $\theta(t)$ which is the joint's angle.

$$E \cdot I \cdot w''''(x,t) + \rho \ddot{w}(x,t) + \rho x \ddot{\theta}(t) = 0 \tag{5.1}$$

$$I_t \ddot{\theta}(t) + \rho \int_0^L x \ddot{w}(x,t) dx = T(t) \tag{5.2}$$

In Eqs. (5.1) and (5.2), $w''''(x,t) = \frac{\partial^4 w(x,t)}{\partial x^4}$,$\ddot{w}(x,t) = \frac{\partial^2 w(x,t)}{\partial t^2}$, while I_t is the moment of inertia of a rigid link of length L, ρ denotes the uniform mass density and EI is the uniform flexural rigidity with units $N \cdot m^2$. To calculate $w(x,t)$, instead of solving analytically the above partial differential equations, modal analysis can be used which assumes that $w(x,t)$ can be approximated by a weighted sum of orthogonal basis functions

$$w(x,t) = \sum_{i=1}^{n_e} \phi_i(x) v_i(t) \tag{5.3}$$

where index $i = [1, 2, \ldots, n_e]$ denotes the normal modes of vibration of the flexible link. Using modal analysis a dynamical model of finite-dimensions is derived for the flexible link robot. Without loss of generality assume a 2-link flexible robot (Fig. 5.1) and that only the first two vibration modes of each link are significant ($n_e = 2$). Σ_1 is a point on the first link with reference to which the deformation vector is measured.

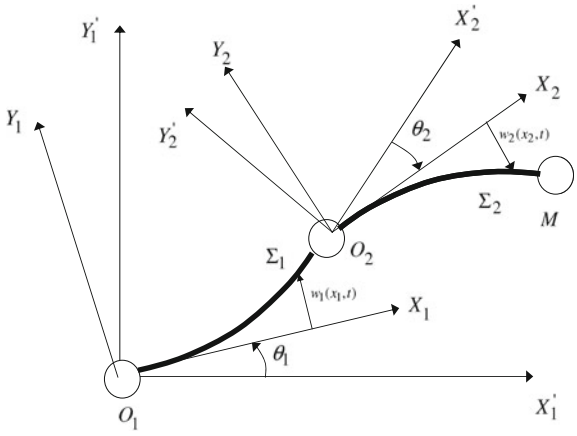

Fig. 5.1 A 2-DOF flexible-link robot

Similarly, Σ_2 is a point on the second link with reference to which the associated deformation vector is measured. In that case the dynamic model of the robot becomes [268, 583]:

$$\begin{pmatrix} M_{11}(z) & M_{12}(z) \\ M_{21}(z) & M_{22}(z) \end{pmatrix} \cdot \begin{pmatrix} \ddot{\theta} \\ \ddot{v} \end{pmatrix} + \begin{pmatrix} F_1(z,\dot{z}) \\ F_2(z,\dot{z}) \end{pmatrix} + \begin{pmatrix} 0_{2\times 2} & 0_{2\times 4} \\ 0_{4\times 2} & D(z) \end{pmatrix} \cdot \begin{pmatrix} \dot{\theta} \\ \dot{v} \end{pmatrix} + \\ + \begin{pmatrix} 0_{2\times 2} & 0_{2\times 4} \\ 0_{4\times 2} & K(z) \end{pmatrix} \cdot \begin{pmatrix} \theta \\ v \end{pmatrix} = \begin{pmatrix} T(t) \\ 0_{4\times 1} \end{pmatrix} \tag{5.4}$$

where $z = [\theta, v]^T$, with $\theta = [\theta_1, \theta_2]^T$, $v = [v_{11}, v_{12}, v_{21}, v_{22}]^T$ (vector of the vibration modes for links 1 and 2), and $[F_1(z,\dot{z}), F_2(z,\dot{z})]^T = [0,0]^T$ (centrifugal and Coriolis forces). The elements of the inertia matrix are: $M_{11} \in R^{2\times 2}$, $M_{12} \in R^{2\times 4}$, $M_{21} \in R^{4\times 2}$, $M_{22} \in R^{4\times 4}$. The damping and elasticity matrices of the aforementioned model are $D \in R^{4\times 4}$ and $K \in R^{4\times 4}$. Moreover the vector of the control torques is $T(t) = [T_1(t), T_2(t)]^T$.

The principle of inverse dynamics control is to transform the nonlinear system of Eq. (5.4) into a linear one, so that linear control techniques can be applied. From Eq. (5.4) it holds that:

$$M_{11}\ddot{\theta} + M_{12}\ddot{v} + F_1(z,\dot{z}) = T(t) \tag{5.5}$$

$$M_{21}\ddot{\theta} + M_{22}\ddot{v} + F_2(z,\dot{z}) + D\dot{v} + Kv = 0 \tag{5.6}$$

Equation (5.6) is solved with respect to $\ddot{v}$

$$\ddot{v} = -M_{22}^{-1}M_{21}\ddot{\theta} - M_{22}^{-1}F_2(z,\dot{z}) - M_{22}^{-1}D\dot{v} - M_{22}^{-1}Kv \tag{5.7}$$

Equation (5.7) is substituted in Eq. (5.5) which results into:

$$(M_{11} - M_{12}M_{22}^{-1}M_{21})\ddot{\theta} - M_{12}M_{22}^{-1}F_2(z,\dot{z}) - M_{12}M_{22}^{-1}D\dot{v} - M_{12}M_{22}^{-1}Kv + F_1(z,\dot{z}) = T(t) \tag{5.8}$$

The following control law is now introduced [583]:

$$T(t) = -M_{12}M_{22}^{-1}F_2(z,\dot{z}) - M_{12}M_{22}^{-1}D\dot{v} - \\ -M_{12}M_{22}^{-1}Kv + F_1(z,\dot{z}) + (M_{11} - M_{12}M_{22}^{-1}M_{21})u_0 \tag{5.9}$$

$$u_0 = \ddot{\theta}_d - K_d(\dot{\theta} - \dot{\theta}_d) - K_p(\theta - \theta_d) \tag{5.10}$$

By replacing Eqs. (5.9) in (5.8) one gets

$$(M_{11} - M_{12}M_{22}^{-1}M_{21})\ddot{\theta} - M_{12}M_{22}^{-1}F_2(z,\dot{z}) - M_{12}M_{22}^{-1}D\dot{v} - M_{12}M_{22}^{-1}Kv + F_1(z,\dot{z}) = \\ = -M_{12}M_{22}^{-1}F_2(z,\dot{z}) - M_{12}M_{22}^{-1}D\dot{v} - M_{12}M_{22}^{-1}Kv + F_1(z,\dot{z}) + (M_{11} - M_{12}M_{22}^{-1}M_{21})u_0$$

which finally results into

$$\ddot{\theta} = u_0 \tag{5.11}$$

Equation (5.11) implies that linearisation and decoupling of the robotic model has been achieved. Substituting Eqs. (5.10) into (5.11) gives:

$$\ddot{\theta} - \ddot{\theta}_d + K_d(\dot{\theta} - \dot{\theta}_d) + K_p(\theta - \theta_d) = 0 \Rightarrow \\ \ddot{e}(t) + K_d\dot{e}(t) + K_p e(t) = 0 \tag{5.12}$$

Gain matrices K_p and K_d are selected, so as to assure that the poles of Eq. (5.12) are in the left semiplane. This results into

$$lim_{t\to\infty}e(t) = 0 \Rightarrow lim_{t\to\infty}\theta(t) = \theta_d(t) \tag{5.13}$$

Consequently, for $\theta_d(t)$ =constant it holds $lim_{t\to\infty}\ddot{\theta}(t) = 0$. Then Eq. (5.7) gives

$$\ddot{v} = -M_{22}^{-1}F_2 - M_{22}^{-1}D\dot{v} - M_{22}^{-1}Kv \tag{5.14}$$

and for $F_2(z,\dot{z}) = 0$ results into

$$\ddot{v} + M_{22}^{-1}D\dot{v} + M_{22}^{-1}Kv = 0 \tag{5.15}$$

which is the differential equation of the free damped oscillator. Suitable selection of the damping matrix D and the elasticity matrix K assures that

$$lim_{t\to\infty}v(t) = 0 \tag{5.16}$$

5.2.2.2 Shortfalls of Inverse Dynamics Control for Flexible-Link Robots

The objective of the inverse-dynamics model-based control for flexible-link robots, that was presented in Sect. 5.2.2.1, is to force the rigid-mode variable $\theta(t)$ to follow

a desired trajectory or to converge to a certain set-point and at the same time to suppress the flexible modes of the links $v(t)$. However, this control approach appears several weaknesses [268]:
1. In general there are n_r flexible links, thus $\theta(t) \in R^{n_r}$. The control input available is $T(t) \in R^{n_r}$, since there is one actuator per link. Considering n_f flexible modes for each link means that $n_r \times n_f$ additional degrees of freedom are introduced. Thus appropriate control is required to suppress the vibrations. However, the number of control inputs is n_r which is less than the number of the degrees of freedom. Consequently, there is reduced control effectiveness.
2. The situation becomes more complicated, because by selecting the control input $T(t)$ to achieve practical tracking performance of the rigid variable $\theta(t)$, one actually destabilizes the flexible modes $v(t)$. This is due to the non-minimum phase nature of the zeros dynamics of the flexible-link arms.
3. Another drawback of model-based control is that the model of Eq. (5.4), is derived assuming a finite number of vibration modes. This simplification is not always applicable since higher-order modes may be excited. The proposed model-based control does not provide robustness to external disturbances.

5.2.3 Energy-Based Control of Flexible Link Robots

5.2.3.1 Energy-Based Control

To overcome the weaknesses of the inverse-dynamics model-based control for flexible link robots, model-free control methods have been proposed. Of interest is the energy-based control which requires only knowledge of the potential and kinetic energy of the flexible manipulator. Energy-based control of flexible-link robots assures closed-loop system stability in the case of constant set-points (point-to-point control).

The kinetic energy E_{kin} of a n-link flexible robot is given by [164, 583]

$$E_{kin} = \sum_{i=1}^{n} \frac{1}{2} \rho \int_0^{L_i} [\dot{p}_{x_i}^2 + \dot{p}_{y_i}^2] dx \tag{5.17}$$

In Eq. (5.17), p_{x_i} is the position of elementary segment of the ith link along x-axis, while p_{y_i} is the position of elementary segment of the ith link along y-axis. On the other hand the potential energy E_p of a planar n-link flexible robot is due to the links deformation and is given by

$$E_p = \sum_{i=1}^{n} \frac{1}{2} E I \int_0^{L_i} [\frac{\partial^2}{\partial x^2} w_i(x,t)]^2 dx \tag{5.18}$$

Thus to estimate the robot's potential energy, measurement of the flexible links strain $\frac{\partial^2 w_i(x,t)}{\partial x^2}$ is needed. The potential energy includes only the energy due to strain,

while the gravitational effect as well as longitudinal and torsional deformations are neglected.

Moreover, the energy provided to the flexible-link robot by the ith motor is given by

$$W_i = \int_0^t T_i(\tau)\dot{\theta}(\tau)d\tau \tag{5.19}$$

Consequently, the power of the ith motor is

$$P_i(t) = T_i(t)\dot{\theta}_i(t) \tag{5.20}$$

where $T_i(t)$ is the torque of the ith motor and $\dot{\theta}_i(t)$ is the motor's angular velocity. Thus, the aggregate motors energy is given by

$$W = \sum_{i=1}^{n}\int_0^t T_i(\tau)\dot{\theta}_i(\tau)d\tau \tag{5.21}$$

The energy that is provided to the flexible-link robot by its motors takes the form of: (i) potential energy (due to the deformation of the flexible links) and (ii) kinetic energy. This energy flow is described by

$$[E_{kin}(t) + E_p(t)] - [E_{kin}(0) + E_p(0)] = W \tag{5.22}$$

Energy-based control of flexible-link robots considers that the torque of the ith motor (control output) is based on a PD-type controller and is given by [164, 583]:

$$\begin{gathered} T_i(t) = -K_{p_i}[\theta_i(t) - \theta_{d_i}(t)] - K_{d_i}\dot{\theta}_i(t) - \\ -K_i w_i''(x,t)\int_0^t \dot{\theta}_i(s)w_i''(x,s)ds,\ i = 1,2,\ldots,n \end{gathered} \tag{5.23}$$

where K_{p_i} is the ith P control gain, K_{d_i} is the ith D control gain, θ_{d_i}, is the desirable angle of the ith link, K_i is also a positive (constant) gain, and $w_i(x,t)$ is the deformation of the ith link.

5.2.3.2 Stability Proof

The proposed control law of Eq. (5.23) assures the asymptotic stability of the closed-loop system in case of constant set-points (point to point control). The following Lyapunov (energy) function is considered [164, 583]:

$$V = E_{kin} + E_p + \frac{1}{2}\sum_{i=1}^{N} K_{p_i}[\theta_i(t) - \theta_{d_i}(t)]^2 + \frac{1}{2}\sum_{i=1}^{n} K_i[\int_0^t \dot{\theta}_i(s)w_i''(s,t)ds]^2 \tag{5.24}$$

where E_{kin} is given by Eq. (5.17) and denotes the kinetic energy of the robot's links, while E_p is given by Eq. (5.18) and denotes the potential energy of the robot's links due to deformation.

It holds that $V(t) > 0$ since $E_{kin} > 0$, $E_p > 0$, $\frac{1}{2}\sum_{i=1}^{n} K_{p_i}[\theta_i(t) - \theta_{d_i}(t)]^2 > 0$ and $\frac{1}{2}\sum_{i=1}^{n} K_i[\int_0^t \dot{\theta}_i(t) w_i(s,t)]^2 > 0$. Moreover, it holds that

$$\begin{array}{c}\dot{V}(t) = \dot{E}_{kin} + \dot{E}_p + \sum_{i=1}^{n} K_{p_i}[\theta_i(t) - \theta_{d_i}(t)]\dot{\theta}_i(t) + \\ \frac{1}{2}\sum_{i=1}^{n} 2K_i[\int_0^t \dot{\theta}_i(s,t) w_i''(s,t) ds][\dot{\theta}_i(t) w_i''(x,t)]\end{array} \tag{5.25}$$

while using Eqs. (5.20) and (5.22) the derivative of the robot's energy is found to be

$$\dot{E}_{kin}(t) + \dot{E}_p(t) = \sum_{i=1}^{n} T_i(t)\dot{\theta}_i(t) \tag{5.26}$$

where the torque generated by the ith motor is given by Eq. (5.23). By substituting Eqs. (5.26) and (5.23) in (5.25) one gets

$$\begin{array}{c}\dot{V}(t) = -\sum_{i=1}^{n} K_{p_i}[\theta_i(t) - \theta_{d_i}(t)]\dot{\theta}_i(t) - \\ -\sum_{i=1}^{n} K_{d_i}\dot{\theta}_i^2(t) - \sum_{i=1}^{n}[K_i w_i''(x,t)\int_0^t \dot{\theta}_i(s) w_i''(s,t) ds]\dot{\theta}_i(t) \\ +\sum_{i=1}^{n} K_{p_i}[\theta_i(t) - \theta_{d_i}(t)]\dot{\theta}_i(t) + \sum_{i=1}^{n}[K_i w_i''(x,t)\int_0^t \dot{\theta}_i(s) w_i''(s,t) ds]\dot{\theta}_i(t)\end{array} \tag{5.27}$$

which finally results into,

$$\dot{V}(t) = -\sum_{i=1}^{n} K_{d_i}\dot{\theta}_i^2 \tag{5.28}$$

Obviously, from Eq. (5.28) it holds that $\dot{V}(t) \leq 0$, which implies stability of the closed-loop system, but not asymptotic stability. Asymptotic stability can be proven as follows [583]: If the ith link did not converge to the desirable angle, i.e. $lim_{t\to\infty}\theta_i(t) = a_i \neq \theta_{d_i}(t)$ then the torque of the ith motor would become equal to a small positive constant. This is easy to prove from Eq. (5.23) where the terms $K_{d_i}\dot{\theta}_i(t) = 0$, $K_i w_i(x,t)\int_0^t \dot{\theta}_i(s) w_i''(s,t) ds = 0$, while the term $K_{p_i}[\theta_i(t) - \theta_{d_i}(t)] = K_{p_i} a_i$ becomes equal to a positive constant.

However, if $T_i(t) = \text{constant} \neq 0$ then the ith link should continue to rotate. This means that $\theta_i(t) \neq a_i$, which contradicts the initial assumption $lim_{t\to\infty}\theta_i(t) = a_i$. Therefore, it must hold $lim_{t\to\infty} T_i(t) = 0$ and $lim_{t\to\infty}\theta_i(t) = \theta_{d_i}(t)$. Consequently, $lim_{t\to\infty} V(t) = 0$.

The proposed energy-based controller is a decentralized controller since the control signals $T_i(t)$ of the ith motor are calculated using only the angle $\theta_i(t)$ and the deformation $w_i(x,t)$ of the ith link.

5.2.4 Force Control in Flexible-Link Robots

Up to now the study of control methods for flexible-link robots followed the assumption that the robot operated in the free space. However, when in contact with a surface, forces are exerted to robot's end-effector and a significant issue that has to be taken into account in the design of the robotic controller is force control. To solve the force control problem, a kinematic model of a flexible-link robot is first introduced.

5.2.4.1 Overview of the Kinematic Model of Flexible-Link Robots

Assume the ith link of the flexible-link robot and the associated rotating frame $O_i X_i Y_i$ (Fig. 5.1). Then the vector of coordinates of the end-effector M is given by

$$p_M^i = [x_i, w_i(x_i)]^T \tag{5.29}$$

The coordinates of the end-effector in the inertial frame $O_1 X_1^{'} Y_1^{'}$ is given by

$$p_M = r_i + W_i p_M^i \tag{5.30}$$

with

$$\begin{gathered} W_i = W_{i-1} E_{i-1} R_i = \hat{W}_{i-1} R_i \\ \hat{W}_0 = I \end{gathered} \tag{5.31}$$

where R_i is the rigid rotation matrix that aligns the rotating frame of the ith link to the inertial frame of the same link, and E_{i-1} is the flexible rotation matrix that aligns the inertial frame of link i to the rotational frame of link $i-1$:

$$R_i = \begin{pmatrix} cos(\theta_i) & -sin(\theta_i) \\ sin(\theta_i) & cos(\theta_i) \end{pmatrix}, \quad E_i = \begin{pmatrix} 1 & -w_{ie}^{'} \\ w_{ie}^{'} & 1 \end{pmatrix} = \begin{pmatrix} 1 & -\frac{\partial w_i}{\partial x_i} \\ \frac{\partial w_i}{\partial x_i} & 1 \end{pmatrix} \tag{5.32}$$

$$r_i = r_{i-1} + W_i r_i^{i-1} \tag{5.33}$$

where r_i^{i-1} is the distance vector between the origin of the and ith and the $i-1$th frame, r_i is the distance vector between the origin of the ith rotational frame and the inertial frame, and W_i is the rotation matrix calculated with the use of Eq. (5.31).

Using Eqs. (5.33) and (5.43) in the 2-DOF flexible-link robot depicted in Fig. 5.1, one obtains

$$r_2 = r_1 + W_1 r_2^1 = \begin{pmatrix} L_1 cos(\theta_1) - w_1(L_1, t) sin(\theta_1) \\ L_1 sin(\theta_1) + w_1(L_1, t) cos(\theta_1) \end{pmatrix} \tag{5.34}$$

$$p_M = r_2 + W_2 p_M^2 \tag{5.35}$$

where

$$p_M^2 = \begin{pmatrix} L_2 \\ w_2(L_2, t) \end{pmatrix}, W_2 = R_1 E_1 R_2 = \\ \begin{pmatrix} cos(\theta_1) & -sin(\theta_1) \\ sin(\theta_1) & cos(\theta_1) \end{pmatrix} \cdot \begin{pmatrix} 1 & -w'_{1e} \\ w'_{1e} & 1 \end{pmatrix} \cdot \begin{pmatrix} cos(\theta_2) & -sin(\theta_2) \\ sin(\theta_2) & cos(\theta_2) \end{pmatrix} \tag{5.36}$$

The differential kinematic model of the flexible-link robot can now be calculated. The coordinates of the end-effector in the inertial frame are given by Eq. (5.30). According to modal analysis the deformation $w_i(x_i, t)$ in normal modes of vibration is given by Eq. (5.3). Using the previous 2 equations the kinematic model can be written as a function of the joint angles θ and of the normal modes of vibration v.

$$p = k(\theta, v) \tag{5.37}$$

The velocity of the end-effector is calculated through the differentiation of Eq. (5.43).

$$\dot{p}_M = \dot{r}_i + \dot{W}_i p_M^i + W_i \dot{p}_M^i \tag{5.38}$$

Moreover, it holds that $\dot{r}_{i+1}^i = \dot{p}_M^i(L_i) = [0, \dot{w}_i(x_i = L_i)]^T$ since there is no longitudinal deformation ($\dot{x}_i = 0$). It also holds that

$$\dot{W}_i = \dot{\hat{W}}_{i-1} R_i + \hat{W}_{i-1} \dot{R}_i \\ \dot{\hat{W}}_i = \dot{W}_i E_i + W_i \dot{E}_i \tag{5.39}$$

It also holds that

$$\dot{R}_i = S R_i \dot{\theta}_i \\ \dot{E}_i = S \dot{w}'_{ie} \tag{5.40}$$

with $S = \begin{pmatrix} 0 & -1 \\ 1 & 0 \end{pmatrix}$. Substituting Eqs. (5.39) and (5.40) in (5.38) the differential kinematic model of the flexible-link robot is obtained:

$$\dot{p} = J_\theta(\theta, v)\dot{\theta} + J_v(\theta, v)\dot{v} \tag{5.41}$$

where

$J_\theta = \frac{\partial k}{\partial \theta}$: is the Jacobian with respect to θ
$J_v = \frac{\partial k}{\partial v}$: is the Jacobian with respect to v.
If the end-effector is in contact with the surface $\Omega(\theta)$ and is subject to contact-forces $F = [F_x, F_y]$ then the torques which are developed to the joints are:
$J_\theta^T F$: torques that produce the work associated with the rotation angle θ.
$J_v^T F$: torques that produce work associated with the deformation modes v.

The dynamic model of the flexible-link robot given in Eq. (5.4) is corrected into:

$$\begin{pmatrix} M_{11}(z) & M_{12}(z) \\ M_{21}(z) & M_{22}(z) \end{pmatrix} \begin{pmatrix} \ddot{\theta} \\ \ddot{v} \end{pmatrix} + \begin{pmatrix} F_1(z,\dot{z}) \\ F_2(z,\dot{z}) \end{pmatrix} + \\ + \begin{pmatrix} 0_{2\times 2} & 0_{2\times 4} \\ 0_{4\times 2} & D(z) \end{pmatrix} \begin{pmatrix} \dot{\theta} \\ \dot{v} \end{pmatrix} + \begin{pmatrix} 0_{2\times 2} & 0_{2\times 4} \\ 0_{4\times 2} & K(z) \end{pmatrix} \begin{pmatrix} \theta \\ v \end{pmatrix} = \begin{pmatrix} T(t) - J_\theta^T(\theta, v)F \\ -J_v^T(\theta, v)F \end{pmatrix} \tag{5.42}$$

For a two-link flexible robot of Fig. 5.1 one gets

$$p_M = \begin{pmatrix} L_1 cos(\theta_1) - w_1(L_1, t) sin(\theta_1) \\ L_1 sin(\theta_1) + w_1(L_1, t) cos(\theta_1) \end{pmatrix} + \\ + \begin{pmatrix} cos(\theta_1+\theta_2) - w_{1e}^{'} sin(\theta_1+\theta_2) & -sin(\theta_1+\theta_2) - w_{1e}^{'} cos(\theta_1+\theta_2) \\ sin(\theta_1+\theta_2) + w_{1e}^{'} cos(\theta_1+\theta_2) & cos(\theta_1+\theta_2) - w_{1e}^{'} sin(\theta_1+\theta_2) \end{pmatrix} \begin{pmatrix} L_2 \\ w_2 \end{pmatrix} \tag{5.43}$$

with

$$\begin{aligned} w_1(L_1, t) &= \phi_{11}(L_1) v_{11}(t) + \phi_{12}(L_1) v_{12}(t) \\ w_2(L_2, t) &= \phi_{21}(L_2) v_{21}(t) + \phi_{22}(L_2) v_{22}(t) \\ w_{1e}^{'} &= \frac{\partial w_1(x,t)}{\partial x}|_{x=L_1} = \phi_{11}^{'}(L_1) v_{11}(t) + \phi_{12}^{'}(L_1) v_{12}(t) \end{aligned} \tag{5.44}$$

The Jacobian J_θ is

$$J_\theta = \begin{pmatrix} \frac{\partial p_M^{(1)}}{\partial \theta_1} & \frac{\partial p_M^{(1)}}{\partial \theta_2} \\ \frac{\partial p_M^{(2)}}{\partial \theta_1} & \frac{\partial p_M^{(2)}}{\partial \theta_2} \end{pmatrix} \tag{5.45}$$

$$\frac{\partial p_M^{(1)}}{\partial \theta_1} = -L_1 sin(\theta_1) - w_1(L_1, t) cos(\theta_1) - L_2 sin(\theta_1+\theta_2) - \\ -L_2 w_{1e}^{'} cos(\theta_1+\theta_2) - w_2(L_2, t) cos(\theta_1+\theta_2) + w_2(L_2, t) w_{1e}^{'} sin(\theta_1+\theta_2)$$

$$\frac{\partial p_M^{(2)}}{\partial \theta_1} = L_1 cos(\theta_1) - w_1(L_1, t) sin(\theta_1) + L_2 cos(\theta_1+\theta_2) - L_2 w_{1e}^{'} sin(\theta_1+\theta_2) - \\ -w_2(L_2, t) sin(\theta_1+\theta_2) + w_2(L_2, t) w_{1e}^{'} cos(\theta_1+\theta_2)$$

$$\frac{\partial p_M^{(1)}}{\partial \theta_2} = -L_2 sin(\theta_1+\theta_2) - L_2 w_{1e}^{'} cos(\theta_1+\theta_2) - w_2(L_2, t) cos(\theta_1+\theta_2) + \\ +w_2(L_2, t) w_{1e}^{'} sin(\theta_1+\theta_2)$$

$$\frac{\partial p_M^{(2)}}{\partial \theta_2} = L_2 cos(\theta_1+\theta_2) - L_2 w_{1e}^{'} sin(\theta_1+\theta_2) - w_2(L_2, t) sin(\theta_1+\theta_2) - \\ -w_2(L_2, t) w_{1e}^{'} cos(\theta_1+\theta_2)$$

Similarly, the Jacobian J_v is calculated:

$$J_v = \begin{pmatrix} \frac{\partial p_M^{(1)}}{\partial v_{11}} & \frac{\partial p_M^{(1)}}{\partial v_{12}} & \frac{\partial p_M^{(1)}}{\partial v_{21}} & \frac{\partial p_M^{(1)}}{\partial v_{22}} \\ \frac{\partial p_M^{(2)}}{\partial v_{11}} & \frac{\partial p_M^{(2)}}{\partial v_{12}} & \frac{\partial p_M^{(2)}}{\partial v_{21}} & \frac{\partial p_M^{(2)}}{\partial v_{22}} \end{pmatrix} \tag{5.46}$$

$$\frac{\partial p_M^{(1)}}{\partial v_{11}} = -\phi_{11}(L_1) sin(\theta_1) - L_2 \phi_{11}^{'}(L_1) sin(\theta_1+\theta_2) - w_2(L_2, t) \phi_{11}^{'}(L_1) cos(\theta_1+\theta_2)$$

$$\frac{\partial p_M^{(1)}}{\partial v_{12}} = -\phi_{12}(L_1)sin(\theta_1) - L_2\phi_{12}^{'}(L_1)sin(\theta_1+\theta_2) - w_2(L_2,t)\phi_{12}^{'}(L_1)cos(\theta_1+\theta_2)$$

$$\frac{\partial p_M^{(1)}}{\partial v_{21}} = -\phi_{21}(L_2)sin(\theta_1+\theta_2) - \phi_{21}(L_2)w_{1e}^{'}cos(\theta_1+\theta_2)$$

$$\frac{\partial p_M^{(1)}}{\partial v_{22}} = -\phi_{22}(L_2)sin(\theta_1+\theta_2) - \phi_{22}(L_2)w_{1e}^{'}cos(\theta_1+\theta_2)$$

$$\frac{\partial p_M^{(2)}}{\partial v_{11}} = \phi_{11}(L_1)cos(\theta_1) + L_2\phi_{11}^{'}(L_1)cos(\theta_1+\theta_2) - w_2(L_2,t)\phi_{11}^{'}(L_1)sin(\theta_1+\theta_2)$$

$$\frac{\partial p_M^{(2)}}{\partial v_{12}} = \phi_{12}(L_1)cos(\theta_1) + L_2\phi_{12}^{'}(L_1)cos(\theta_1+\theta_2) - w_2(L_2,t)\phi_{12}^{'}(L_1)sin(\theta_1+\theta_2)$$

$$\frac{\partial p_M^{(2)}}{\partial v_{21}} = \phi_{21}(L_2)cos(\theta_1+\theta_2) - \phi_{21}(L_2)w_{1e}^{'}sin(\theta_1+\theta_2)$$

$$\frac{\partial p_M^{(2)}}{\partial v_{22}} = \phi_{22}(L_2)cos(\theta_1+\theta_2) - \phi_{22}(L_2)w_{1e}^{'}sin(\theta_1+\theta_2)$$

5.2.4.2 Interaction with the Compliant Surface

A simple model of elastic force due to contact of the end-effector with a surface is given by:

$$F = K_e\eta\eta^T(p - p_e) \tag{5.47}$$

where $p = k(\theta, v)$ are the coordinates of the end-effector which are calculated from the kinematic model, and η is a vector normal to the surface p_e. From the second line of the dynamic model of Eq. (5.42) one obtains:

$$M_{21}\ddot{\theta} + M_{22}\ddot{v} + D\dot{v} + Kv = -J_v^T(\theta, v)F \tag{5.48}$$

In the steady-state one obtains

$$\begin{gathered} v = -K^{-1}J_v^T(\theta,v)F - K^{-1}J_v^T(\theta,v)\eta K_e(p_n - p_{en}) \Rightarrow \\ v = -K^{-1}J_{vn}K_e(p_n - p_{en}) \end{gathered} \tag{5.49}$$

where $p_n = \eta^T p$, $p_{e_n} = \eta^T p_e$, and $J_{v_n} = J_v^T\eta$. The derivative of Eq. (5.49) with respect to t is calculated.

$$\begin{gathered} \dot{v} = \frac{\partial v}{\partial\theta}\frac{\partial\theta}{\partial t} = \frac{\partial}{\partial\theta}\{-K^{-1}J_{v_n}K_e(p_n - p_{en})\}\dot{\theta} \Rightarrow \\ \dot{v} = -K^{-1}\frac{\partial J_{v_n}}{\partial\theta}K_e(p_n - p_{en}) + K^{-1}J_{v_n}K_e\frac{\partial p_{e_n}}{\partial\theta}\dot{\theta} \end{gathered} \tag{5.50}$$

which finally results into

$$\dot{v} = -K^{-1}K_eJ_f(\theta)\dot{\theta} \tag{5.51}$$

with $J_f(\theta) = \frac{\partial J_{v_n}}{\partial\theta}K_e(p_n - p_{en}) + K^{-1}J_{v_n}K_e\frac{\partial p_{e_n}}{\partial\theta}$. Substituting Eq. (5.51) into (5.41) gives:

$$\begin{gathered}\dot{p} = J_\theta(\theta, v)\dot{\theta} + J_v(\theta, v)\{-K^{-1}K_e J_f(\theta)\} \Rightarrow \\ \dot{p} = \{J_\theta(\theta, v) - K^{-1}K_e J_v(\theta, v) J_f(\theta)\}\end{gathered} \tag{5.52}$$

The overall Jacobian matrix J_p is defined as:

$$J_p = J_\theta(\theta, v) - K^{-1}K_e J_v(\theta, v) J_f(\theta) \tag{5.53}$$

which relates the velocity of the end-effector with the angular velocity of the joints

$$\dot{p} = J_p(\theta, v)\dot{\theta} \tag{5.54}$$

5.2.4.3 Force Control

The desirable contact force along the normal vector of surface p_e is denoted as F_d and corresponds to the desirable position p_d. The relation between F_d and p_d is given by

$$p_{d_n} = \eta^T p_d = K_e^{-1} F_d + p_{e_n} \tag{5.55}$$

or equivalently $p_{d_n} - p_{e_n} = K_e^{-1} F_d \Rightarrow \eta^T p_d - \eta^T p_e = K_e^{-1} F_d$. Thus to succeed contact force equal to F_d the end-effector should reach the depth $\eta^T p_d - \eta^T p_e$. The design of the force controller comprises the following steps [509]:
1. For a certain force set-point F_d the corresponding position of the end-effector is calculated using Eq. (5.55).
2. Knowing p_d an inverse kinematics algorithm is used to calculate the associated joint angles θ_d and the vibration modes v_d.
3. The values of θ_d and v_d are used as set-points of a simple proportional-derivative joint controller, as the ones described in the previous sections.
The inverse kinematics problem can be solved with the use of an inverse kinematics algorithm which enables the calculation of θ_d and v_d through the following relation:

$$\dot{\theta} = J_P^T(\theta, v) K_p (p_d - p) \tag{5.56}$$

where J_p is the Jacobian of Eq. (5.53), p is the current position of the end-effector, p_d is the desirable position of the end-effector, and K_p is the diagonal feedback matrix of Eq. (5.56). The convergence conditions of the inverse kinenatics algorithm have been studied [509]. The calculated values θ_d and v_d which are associated with the desirable position p_d are introduced as set-points in the PD controller of each link. This is given in:

$$T(t) = K_1(\theta_d - \theta) + K_2\dot{\theta} + J_\theta^T(\theta_d, v_d) F_d n \tag{5.57}$$

where $F_d n = K_e[\eta^T p_d - \eta^T p_e]\eta$ and J_θ is the Jacobian of Eq. (5.45). The term $J_\theta^T F_d n$ is added to the control signal to compensate for the torques which are induced to the joints due to the contact forces.

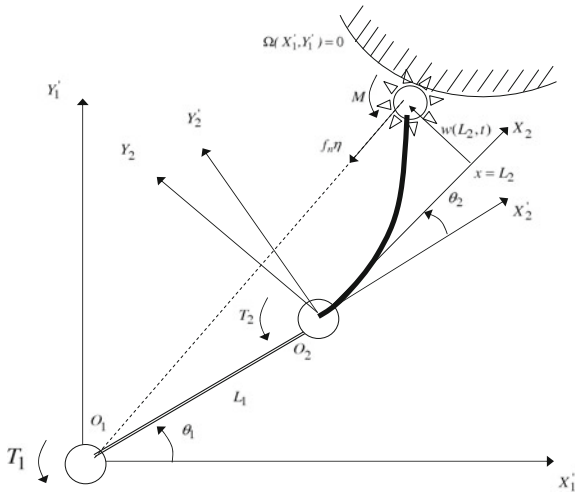

Fig. 5.2 A flexible-link robot which operates in the presence of compliance forces

The discrete-time solution of the inverse kinematics gives

$$\theta_d(k+1) = \theta_d(k) + T_s J_P^T(\theta_d(k), v_d(k)) K_p[p_d(k) - p(k)] \tag{5.58}$$

where the Jacobian J_p is given by Eq. (5.53), and T_s is the sampling period. From Eq. (5.51), one obtains iteratively the setpoints for the normal vibration modes,

$$v_d(k+1) = -K^{-1} K_e J_{v_n}(\theta_d(k))[p_n(k) - p_{e_n}(k)] \tag{5.59}$$

with $p_n = \eta^T p$, $p_{e_n} = \eta^T p_e$ and $J_{v_n} = J_v^T \eta$ (Fig. 5.2).

5.2.5 *Simulation Results*

The performance of the previously analyzed model-free control method (energy-based control) is compared to the performance of model-based techniques (inverse-dynamics control), in a simulation case study for planar 2-DOF manipulators (Fig. 5.2).

5.2.5.1 Model-Based Control of Flexible-Link Robots

The 2-DOF flexible link robot of Fig. 5.1 is considered. The robot is planar and consists of two flexible links of length $L_1 = 0.45\,\text{m}$ and $L_2 = 0.45\,\text{m}$, respectively. The dynamic model of the robot is given by Eq. (5.4). The elements of the inertia matrix M are:

$$M_{11} = \begin{pmatrix} 1 & 2 \\ 2 & 1 \end{pmatrix},\ M_{12} = M_{21}^T = \begin{pmatrix} 1 & 1 & 0.2 & 0.3 \\ 0.5 & 0.1 & 2 & 0.7 \end{pmatrix},\ M_{22} = \begin{pmatrix} 1 & 0 \\ 0 & 1 \end{pmatrix}$$

The damping matrix was taken to be $D = diag\{0.04, 0.08, 0.03, 0.06\}$ while the stiffness matrices was selected as $K = diag\{0.02, 0.04, 0.03, 0.06\}$. The inverse dynamics control law given in Eqs. (5.9) and (5.10) is employed. The selection of the gain matrices K_p and K_d determines the transient response of the closed loop system. The following controller gains have been considered: $K_p = diag\{0.2, 0.2\}$ and $K_d = diag\{0.1, 0.1\}$. The desirable joints positions are $\theta_{d_1} = 1$ rad and $\theta_{d_2} = 1.4$ rad. The performance of the model-based controller is given in Fig. 5.3.

Moreover, it is considered that an additive disturbance torque appears on each joint. The disturbance is given by $d_i(t) = 0.3cos(t)$. The performance of the model-based controller of the flexible-link robot in the presence of disturbance is depicted in Fig. 5.4. It can be seen that vibrations around the desirable joint positions cannot be eliminated.

5.2.5.2 Energy-Based Control

The same robotic model as in Sect. 5.3.4.1 is used to simulate the variation of the manipulator's joints with respect to time. Energy-based control of flexible-link robots is based on Eq. (5.23). The following controller gains have been used: $K_p = diag\{1.9, 5.6\}$, $K_d = diag\{7.2, 23.3\}$ and $K_i = diag\{0.1, 0.1\}$. The desirable joint positions are again $\theta_{d_1} = 1.0$ rad and $\theta_{d_2} = 1.4$ rad. To derive the control signal of Eq. (5.23) the strains at the base of each link were used, i.e. $w_i''(0, t)$. The performance of the energy-based controller in the case of the 2-DOF flexible link robot is shown in Fig. 5.5.

Moreover, the performance of the energy-based controller in presence of the external disturbances of Sect. 5.3.4.1 is given in Fig. 5.6. Suppression of the vibrations can be achieved if the elements of the gain matrix K_d are given higher values.

5.3 Sliding-Mode Control of Flexible-Link Manipulators

5.3.1 Outline

In the previous sections it has been pointed out that the control for flexible-link robots is a non-trivial problem that has elevated difficulty comparing to the control of rigid-link manipulators [450, 583]. This is because the dynamic model of the flexible-link robot contains the nonlinear rigid link motion coupled with the distributed effects of the links' flexibility. This coupling depends on the inertia matrix of the flexible manipulator while the vibration characteristics are determined by structural properties of the links such as the damping and stiffness parameters. Moreover, in contrast

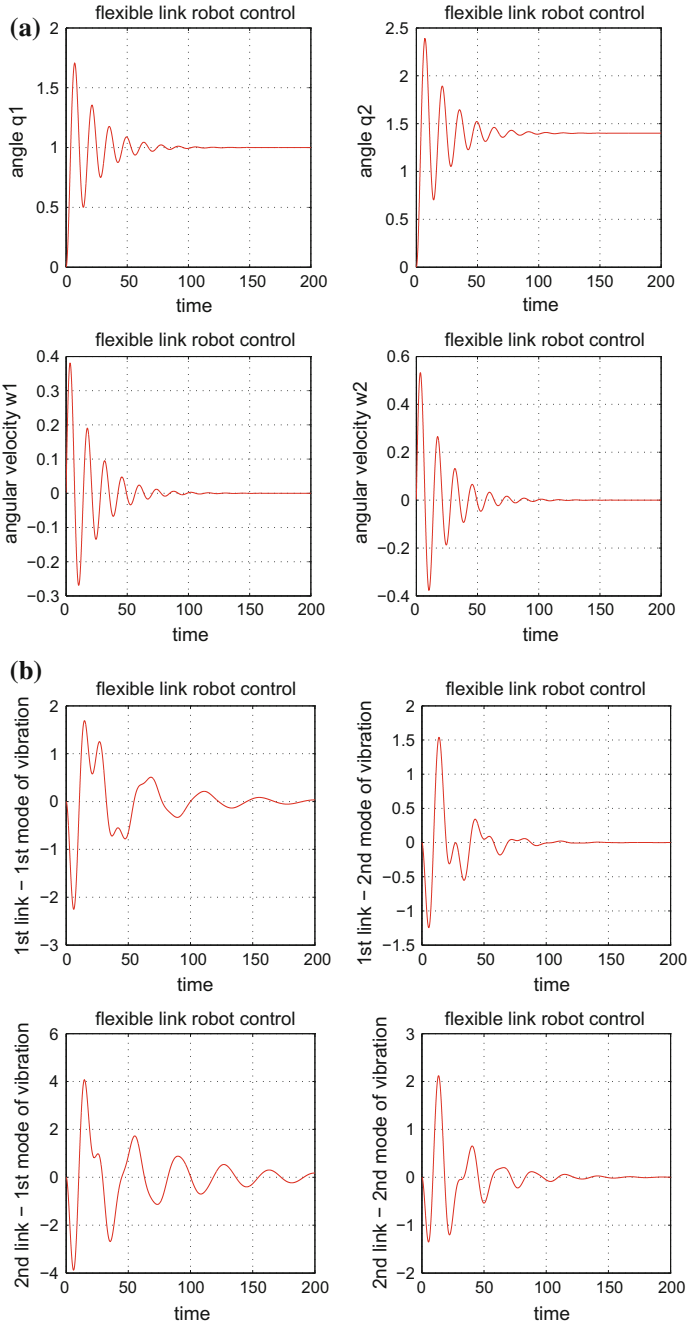

Fig. 5.3 Model-based control of a 2-link flexible robot **a** joints' angles and joints' angular velocity, **b** the first two vibration modes for each link

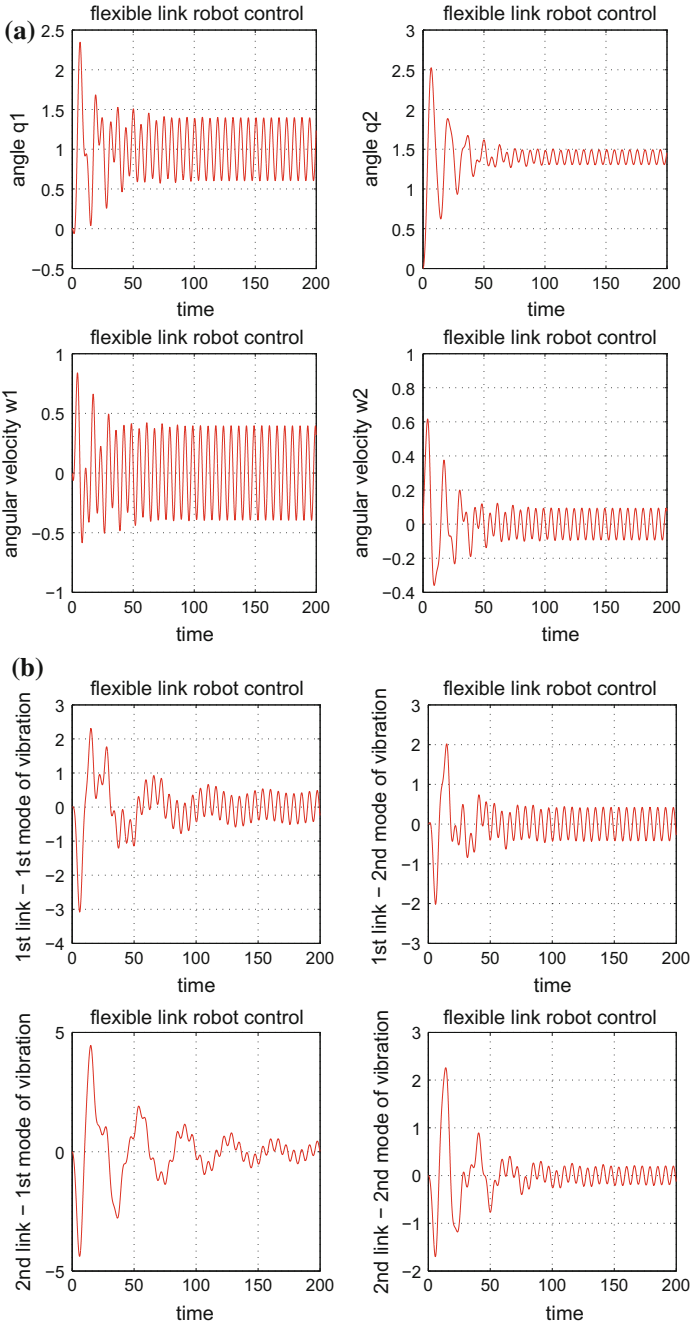

Fig. 5.4 Model-based control of a 2-link flexible robot in the presence of additive motor-torques disturbances **a** joints' angles and joints' angular velocity, **b** the first two vibration modes for each link

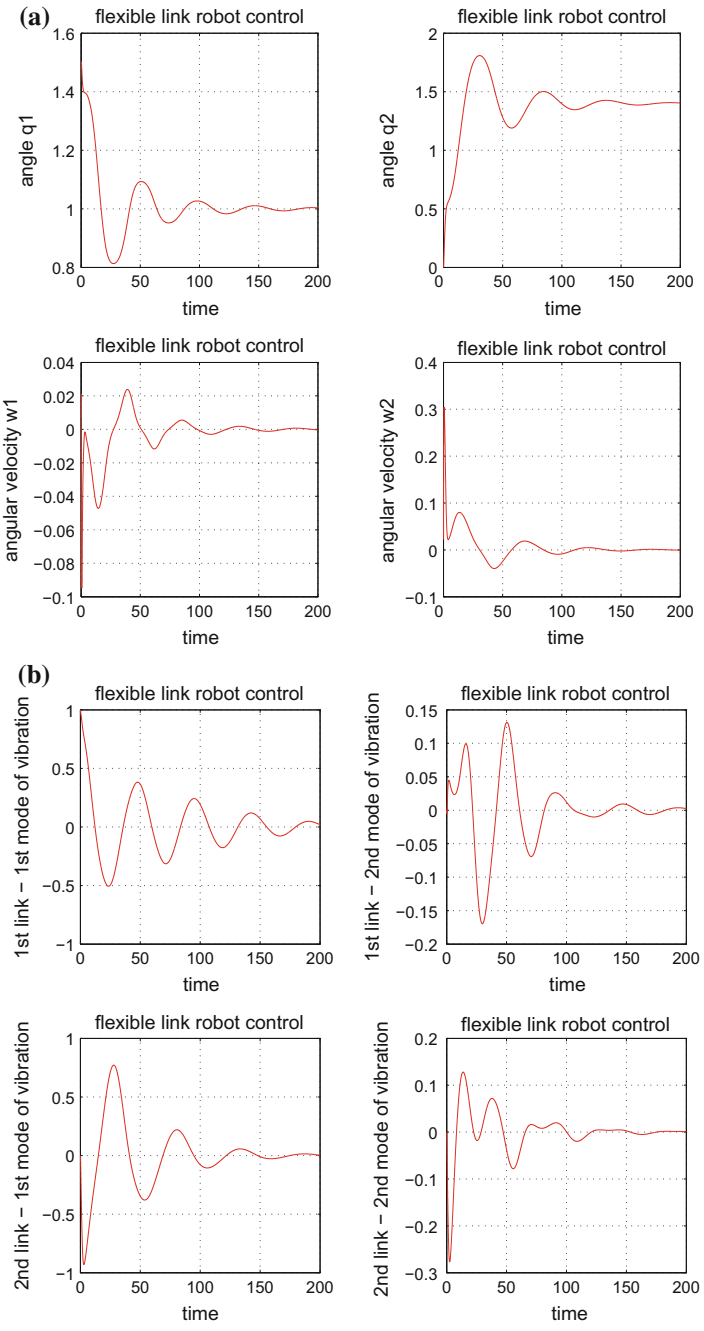

Fig. 5.5 Energy-based control of a 2-link flexible robot **a** joints' angles and joints' angular velocity, **b** the first two vibration modes for each link

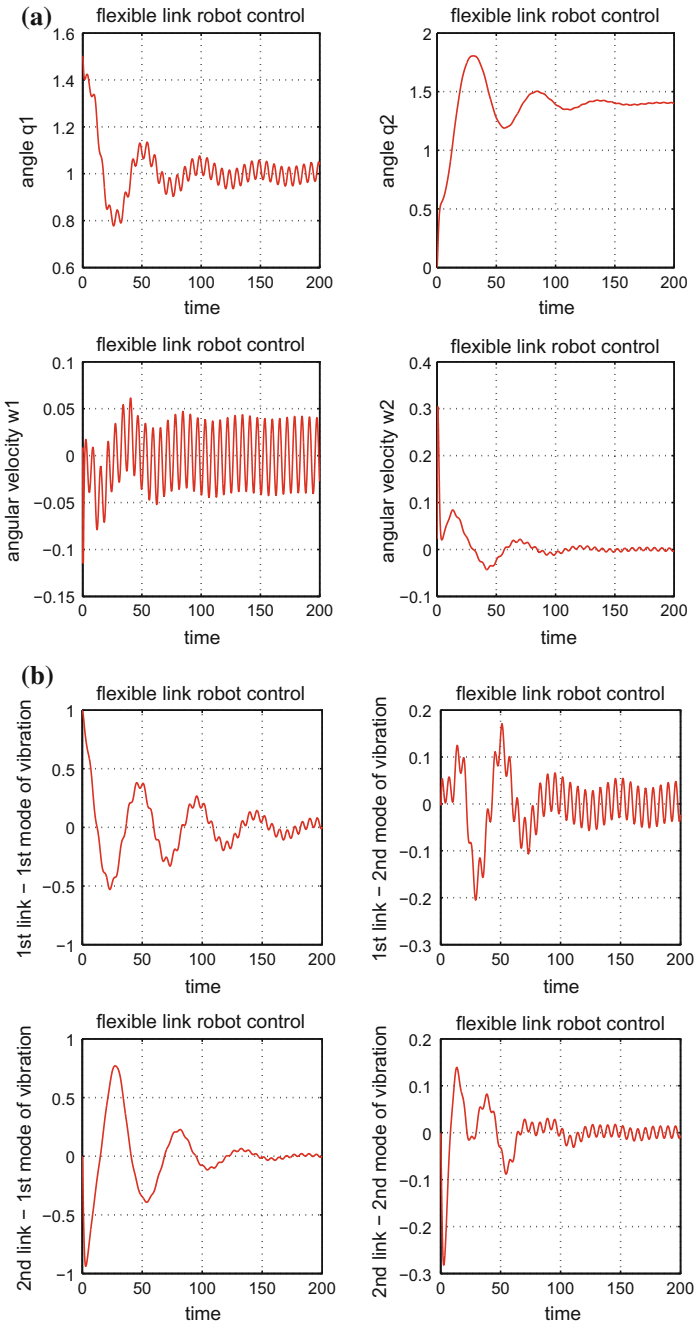

Fig. 5.6 Energy-based control of a 2-link flexible robot in the presence of additive motor-torques disturbances **a** joints' angles and joints' angular velocity, **b** the first two vibration modes for each link

to the dynamic model of rigid-link robots the dynamic model of flexible-link robots is an infinite dimensional one. As in the case of the rigid-link robot there is a certain number of mechanical degrees of freedom associated to the rotational motion of the robot's joints and there is also an infinite number of degrees of freedom associated to the vibration modes in which the deformation of the flexible link is decomposed [441]. The controller of a flexible manipulator must achieve the same motion objectives as in the case of a rigid manipulator, i.e. tracking of specific joints position and velocity setpoints. Additionally, it must also stabilize and asymptotically eliminate the vibrations of the flexible-links that are naturally excited by the joints rotational motion.

It has already been shown that the inverse dynamics model-based control for flexible-link robots relies on modal analysis, i.e. on the assumption that the deformation of the flexible link can be written as a finite series expansion containing the elementary vibration modes. However, this inverse-dynamics model-based control may result into unsatisfactory performance when an accurate model is unavailable, due to parameters uncertainty or truncation of high order vibration modes in the model [441]. Moreover, based on the state space formulation, the sliding mode control, which belongs to the wider class of the variable structure control schemes, is a nonlinear robust controller suitable for flexible-link manipulators. Sliding-mode control (SMC) can achieve simultaneous convergence of the flexible robot's joints angles and angular velocities to the desirable setpoints and efficient suppression of the flexible links vibrations. The inclusion of a switching control term in a sliding mode controller can provide robustness against parametric uncertainties and input disturbances [136, 229, 330].

As mentioned, sliding-mode control is a state-feedback based controller and its implementation requires knowledge of the complete state vector of the controlled system [204, 490]. However, there are certain elements in the state vector of the flexible-link robot which are difficult to measure, e.g. the vibration modes. Therefore, to apply sliding-mode control to the flexible manipulator it is necessary to use some kind of state estimator which can reconstruct the robot's state vector through the processing of measurements from a limited number of sensors, e.g. angles of the joints and the associated angular velocities [31, 361]. The Kalman Filter can provide real-time estimates of the state vector of the flexible link robot while assuring the optimality of estimation in the presence of measurement noises [222, 431].

Indicative results about filtering-based control for flexible-link robots can be noted. In [174] state feedback control for a flexible-link robot is implemented with the use of a state vector that is estimated through Kalman Filtering. Using fuzzy rules, an online adaptation of the covariance matrix of the Kalman Filter is performed which aims at improving the vibration suppression capabilities of the filtering-based control. In [290] a controller that follows the principles of singular perturbations theory is developed and the flexible-link robot model is decomposed into a fast and a slow dynamics subsystem. Then a two-time scale Kalman filter is designed for estimating the components of the robot's state vector associated both with the rigid (slow) and the flexible (fast) dynamics of the robot. The estimated state vector is used in the control loop. In [353] an observer-based control scheme for flexible-link

robots is developed where a fixed-gain state estimator processes measurements of the flexible-links' deformation. Lyapunov-like stability analysis is used to demonstrate the efficiency of the feedback control scheme. In [391] a method is proposed for improving the performance of flexible manipulators through the employment of robust state estimation techniques. The method is based on discrete-time Kalman filtering and sliding mode principles and is applied to the model of a 1-DOF flexible-link manipulator. Finally, in [25] the Extended Kalman Filter is redesigned in the form of a disturbance observer to estimate the disturbance forces that are exerted on the end-effector of a single-link flexible robotic manipulator. The forces' estimates provided by the filter are used in the robot's feedback control loop.

In this section it will be shown how a suitable formulation of the dynamic model of the flexible manipulator enables the application of the Kalman Filter recursion and provides accurate estimates of the robot's state vector which in turn can be used by a sliding-mode control loop. The present section extends and elaborates on the results of [437]. The performance of the proposed Kalman Filter-based sliding mode controller is also compared against the previously analyzed inverse dynamics control for flexible-link robots. As already discussed, in the latter method, by assuming a finite number of vibration modes, acontrol input is developed which inverts the dynamics of robotic system and eliminates the tracking error of its state variables [450, 583]. The evaluation of Kalman filter-based sliding-mode control against inverse dynamics control derives useful results on the efficiency of this control approach.

5.3.2 *Design of a Sliding-Mode Controller*

Sliding-mode control for flexible-link robots has been studied in several papers [136, 490]. In the sequel and for simplifying the presentation of the control scheme a 2-link flexible manipulator will be assumed, i.e. $n = 2$. The flexible-link robot model of Eq. (5.4) can be written as

$$\begin{pmatrix} \ddot{\theta} \\ \ddot{v} \end{pmatrix} = -\begin{pmatrix} M_{11} & M_{12} \\ M_{21} & M_{22} \end{pmatrix}^{-1} \{ \begin{pmatrix} 0 & 0 \\ 0 & D \end{pmatrix} \begin{pmatrix} \dot{\theta} \\ \dot{v} \end{pmatrix} + \begin{pmatrix} 0 & 0 \\ 0 & K \end{pmatrix} \begin{pmatrix} \theta \\ v \end{pmatrix} + + \begin{pmatrix} F_1 \\ F_2 \end{pmatrix} + \begin{pmatrix} G_1 \\ G_2 \end{pmatrix} - \begin{pmatrix} T \\ 0 \end{pmatrix} \} \tag{5.60}$$

The model of the flexible-link robot dynamics is written in state-space form after defining the following state vector:

$$x = [\theta_1, \theta_2, v_{11}, v_{12}, v_{21}, v_{22}, \dot{\theta}_1, \dot{\theta}_2, \dot{v}_{11}, \dot{v}_{12}, \dot{v}_{21}, \dot{v}_{22}]^T \tag{5.61}$$

The following notation is used for the inverse of the inertia matrix of the flexible-link robot

$$\begin{pmatrix} M_{11} & M_{12} \\ M_{21} & M_{22} \end{pmatrix}^{-1} = \begin{pmatrix} N_{11} & N_{12} \\ N_{21} & N_{22} \end{pmatrix} \tag{5.62}$$

where $N_{11} \in R^{2\times 2}$, $N_{12} \in R^{2\times 4}$, $N_{21} \in R^{4\times 2}$ and $N_{22} \in R^{4\times 4}$. It holds that

$$\ddot{\theta} = -N_{12}Kv - N_{12}D\dot{v} - N_{11}F_1 - N_{11}G_1 + N_{11}T \tag{5.63}$$

The elements of the damping matrix $D \in R^{4\times 4}$ are denoted as $D(i, j)$, where $D(i, j) \neq 0$ for $i = j$, while the elements of the stiffness matrix $K \in R^{4\times 4}$ are denoted as $K(i, j)$, where $K(i, j) \neq 0$ for $i = j$. Additionally the terms of the Coriolis and the gravitational vectors are $F = \left(F_1 \in R^{2\times 1},\ F_2 \in R^{4\times 1}\right)^T$ and $G = \left(G_1 \in R^{2\times 1},\ G_2 \in R^{4\times 1}\right)^T$. To obtain a more compact mathematical description in the design of the controller, and without loss of generality, in the rest of this section it will be considered that $F_2 = 0_{4\times 1}$ and $G_2 = 0_{4\times 1}$.

Therefore, one can write the dynamics of the joints of the flexible-link robot in a matrix form:

$$\begin{aligned} \ddot{x}_1 &= f_1(x) + g_1(x)u \\ \ddot{x}_2 &= f_2(x) + g_2(x)u \end{aligned} \tag{5.64}$$

where $u = \left(T_1\ T_2\right)^T$, $g_1(x) = \left(N_{11}(1, 1)\ N_{11}(1, 2)\right)$, $g_2(x) = \left(N_{11}(2, 1)\ N_{11}(2, 2)\right)$, while functions $f_1(x)$ and $f_2(x)$ are defined as

$$\begin{aligned} f_1(x) = \ & -N_{12}(1, 1)K(1, 1)x_3 - N_{12}(1, 2)K(2, 2)x_4 \\ & -N_{12}(1, 3)K(3, 3)x_5 - N_{12}(1, 4)K(4, 4)x_6 \\ & -N_{12}(1, 1)D(1, 1)x_9 - N_{12}(1, 2)D(2, 2)x_{10} \\ & -N_{12}(1, 3)D(3, 3)x_{11} - N_{12}(1, 4)D(4, 4)x_{12} \\ & -N_{11}(1, 1)F_1(1, 1) - N_{11}(1, 2)F_1(2, 1) \\ & -N_{11}(1, 1)G_1(1, 1) - N_{11}(1, 2)G_1(2, 1) \end{aligned} \tag{5.65}$$

$$\begin{aligned} f_2(x) = \ & -N_{12}(2, 1)K(1, 1)x_3 - N_{12}(2, 2)K(2, 2)x_4 \\ & -N_{12}(2, 3)K(3, 3)x_5 - N_{12}(2, 4)K(4, 4)x_6 \\ & -N_{12}(2, 1)D(1, 1)x_9 - N_{12}(2, 2)D(2, 2)x_{10} \\ & -N_{12}(2, 3)D(3, 3)x_{11} - N_{12}(2, 4)D(4, 4)x_{12} \\ & -N_{11}(2, 1)F_1(1, 1) - N_{11}(2, 2)F_1(2, 1) \\ & -N_{11}(2, 1)G_1(1, 1) - N_{11}(2, 2)G_1(2, 1) \end{aligned} \tag{5.66}$$

In the equations describing the joint dynamics the terms $g_1(x)$ and $g_2(x)$ depend on the elements of the inertia matrix of the flexible-link robot and are considered to be known. On the other hand, the terms $f_1(x)$ and $f_2(x)$ are considered to vary in uncertainty ranges, given by

$$|f_1 - \hat{f}_1| \leq \Delta F_1,\ |f_2 - \hat{f}_2| \leq \Delta F_2 \tag{5.67}$$

The following tracking error for the joints angles is defined:

$$e_1 = x_1 - x_1^d,\ e_2 = x_2 - x_2^d \tag{5.68}$$

The flexible-link robot's description given in Eq. (5.64) is in the input-output linear form and signifies also that the robotic system can be written in a canonical state-space form. Moreover, the sliding surface vector $s = [s_1, s_2]^T$ is defined with elements

$$s_1 = \dot{e}_1 + \lambda_1 e_1,\ s_2 = \dot{e}_2 + \lambda_2 e_2 \tag{5.69}$$

To achieve convergence of the tracking error to zero for the ith element of the state vector the following conditions should hold:

$$\frac{1}{2}\frac{d}{dt}s_i^2 \leq -\eta_i |s_i|,\quad \eta_i > 0,\quad i = 1, 2 \tag{5.70}$$

The sliding-mode control law is finally given by

$$u = \begin{pmatrix} g_1(x) \\ g_2(x) \end{pmatrix}^{-1} \cdot\cdot \begin{pmatrix} \ddot{x}_1^d - \hat{f}_1(x) - \lambda_1(\dot{x}_1 - \dot{x}_1^d) - k_1 sgn(s_1) \\ \ddot{x}_2^d - \hat{f}_2(x) - \lambda_2(\dot{x}_2 - \dot{x}_2^d) - k_2 sgn(s_2) \end{pmatrix} \tag{5.71}$$

To define the permissible values for the switching gains k_i $i = 1, 2$ the following conditions are used

$$\begin{gathered} \tfrac{1}{2}\tfrac{d}{dt}s_i^2 \leq -\eta_i |s_i| \Rightarrow s_i \dot{s}_i \leq -\eta_i |s_i| \Rightarrow \\ \left[f_i(x) + g_i(x)u - \ddot{x}_i^d + \lambda_i(\dot{x}_i - \dot{x}_i^d) \right] s_i \leq -\eta_i |s_i| \end{gathered} \tag{5.72}$$

The conditions given in Eq. (5.72) can be written as follows

$$\begin{gathered} \begin{pmatrix} s_1 & 0 \\ 0 & s_2 \end{pmatrix} \{ \begin{pmatrix} f_1(x) \\ f_2(x) \end{pmatrix} + \begin{pmatrix} g_1(x) \\ g_2(x) \end{pmatrix} u - \begin{pmatrix} \ddot{x}_1^d \\ \ddot{x}_2^d \end{pmatrix} + \\ + \begin{pmatrix} \lambda_1(\dot{x}_1 - \dot{x}_1^d) \\ \lambda_2(\dot{x}_2 - \dot{x}_2^d) \end{pmatrix} \} \leq \begin{pmatrix} -\eta_1 |s_1| \\ -\eta_2 |s_2| \end{pmatrix} \end{gathered} \tag{5.73}$$

Substituting in Eq. (5.73) the control law u that was calculated in Eq. (5.71), one obtains

$$\begin{pmatrix} s_1 & 0 \\ 0 & s_2 \end{pmatrix} \begin{pmatrix} f_1(x) - \hat{f}_1(x) - k_1 sgn(s_1) \\ f_2(x) - \hat{f}_2(x) - k_2 sgn(s_2) \end{pmatrix} \leq \begin{pmatrix} -\eta_1 |s_1| \\ -\eta_2 |s_2| \end{pmatrix} \tag{5.74}$$

or equivalently

$$\begin{gathered} (f_1(x) - \hat{f}_1(x) - k_1 sgn(s_1)) s_1 \leq -\eta_1 |s_1| \\ (f_2(x) - \hat{f}_2(x) - k_2 sgn(s_2)) s_2 \leq -\eta_2 |s_2| \end{gathered} \tag{5.75}$$

and using Eq. (5.67) one has

$$\begin{gathered} \Delta F_1 s_1 - k_1 sgn(s_1) s_1 \leq -\eta_1 |s_1| \\ \Delta F_2 s_2 - k_2 sgn(s_2) s_2 \leq -\eta_2 |s_2| \end{gathered} \tag{5.76}$$

or equivalently

$$\begin{array}{l} \Delta F_1 s_1 - k_1 |s_1| \leq -\eta_1 |s_1| \\ \Delta F_2 s_2 - k_2 |s_2| \leq -\eta_2 |s_2| \end{array} \tag{5.77}$$

The switching control gains are chosen to satisfy

$$k_1 = \Delta F_1 + \eta_1,\ k_2 = \Delta F_2 + \eta_2 \tag{5.78}$$

Substituting Eqs. (5.78) into (5.77) gives

$$\begin{array}{l} \Delta F_1 s_1 - \Delta F_1 |s_1| - \eta_1 |s_1| \leq -\eta_1 |s_1| \\ \Delta F_2 s_2 - \Delta F_2 |s_2| - \eta_2 |s_2| \leq -\eta_2 |s_2| \end{array} \tag{5.79}$$

or equivalently

$$\begin{array}{l} \Delta F_1 s_1 \leq \Delta F_1 |s_1| \\ \Delta F_2 s_2 \leq \Delta F_2 |s_2| \end{array} \tag{5.80}$$

This assures that $lim_{t \to \infty} s_i = 0,\ i = 1, 2$ and consequently the asymptotic elimination of the tracking error for the joints' angle and rotation speed.

5.3.3 *Estimation of the Non-measurable State Variables*

Knowing that certain elements of the state vector of the flexible-link robot are not directly measurable, e.g. vibration modes, it becomes necessary to estimate these variables with the use of a state observer or filter. Indicative research results on state estimation-based control for flexible-link robots have been given in [31, 204, 361]. To obtain a state estimation-based control scheme for the flexible manipulator, in this section the state-space description of the flexible-link robot dynamics in the form of Eq. (5.81) is used:

$$\begin{array}{c} \dot{x} = Ax + Bu_a \\ y = Cx \end{array} \tag{5.81}$$

where $x \in R^{12 \times 1}$ is the previously defined state vector, $u_a = [T_1 - F_1 - G_1, T_2 - F_1 - G_1]^T$, while matrices A and B are defined as

$$A = \begin{pmatrix} 0_{6\times 6} & I_{6\times 6} \\ [0_{2\times 2}, -N_{12}K] & [0_{2\times 2}, -N_{12}D] \\ [0_{4\times 2}, -N_{22}K] & [0_{4\times 2}, -N_{22}D] \end{pmatrix} \quad B = \begin{pmatrix} 0_{6\times 2} \\ N_{12} \\ N_{22} \end{pmatrix} \tag{5.82}$$

$$C = \begin{pmatrix} 1 & 0 & 0_{1\times 10} \\ 0 & 1 & 0_{1\times 10} \\ 0_{1\times 6} & 1 & 0_{1\times 5} \\ 0_{1\times 7} & 1 & 0_{1\times 4} \end{pmatrix} \tag{5.83}$$

Thus, it is considered that the measurable elements of the robot's state vector are the joints' angles and the joints' angular velocities. After applying common discretization methods the linear continuous-time model of the flexible-link robot of Eq. (5.81) is turned into a discrete-time linear model, which makes use of the discrete-time equivalents of matrices A, B and C defined in Eqs. (5.82) and (5.83).

For the latter discrete-time model the application of the recursion of the discrete-time Kalman Filter is possible. The discrete-time Kalman filter can be decomposed into two parts: (i) time update (prediction stage), and (ii) measurement update (correction stage) [222, 450, 457]. The first part employs an estimate of the state vector $x(k)$ made before the output measurement $y(k)$ is available (a priori estimate). The second part estimates $x(k)$ after $y(k)$ has become available (a posteriori estimate). The covariance matrices associated with $\hat{x}^-(k)$ and $\hat{x}(k)$ are defined as: $P^-(k) = Cov[e^-(k)] = E[e^-(k)e^-(k)^T]$ and $P(k) = Cov[e(k)] = E[e(k)e^T(k)]$.

Matrices A, B and C of the linear state-space model are defined in Eq. (5.82) and Eq. (5.83). Next, by applying common discretization methods (e.g. Tustin transform) the continuous-time linear model of the robot's dynamics is transformed into a linear discrete-time model where matrices A, B, and C are substituted by their discrete-time equivalents A_d, B_d and C_d. For this latter model, the application of the standard discrete-time Kalman Filter recursion is possible.

The recursion of the discrete-time Kalman Filter is formulated as:

measurement update:

$$\begin{aligned} K(k) &= P^-(k)C_d(k)^T[C_d(k)\cdot P^-(k)C_d(k)^T + R]^{-1} \\ \hat{x}(k) &= \hat{x}^-(k) + K(k)[y(k) - C_d(k)\hat{x}^-(k)] \\ P(k) &= P^-(k) - K(k)C_d(k)P^-(k) \end{aligned} \tag{5.84}$$

time update:

$$\begin{aligned} P^-(k+1) &= A_d(k)P(k)A_d^T(k) + Q(k) \\ \hat{x}^-(k+1) &= A_d(k)\hat{x}(k) + B(_dk)u(k) \end{aligned} \tag{5.85}$$

5.3.4 Simulation Tests

5.3.4.1 Inverse Dynamics Control for a 2-Link FLR

The 2-link flexible robot of Fig. 5.1 is considered. The robot consists of two flexible links of length $L_1 = 0.45\,\text{m}$ and $L_2 = 0.45\,\text{m}$, respectively. The dynamic model of the robot is given by Eq. (5.4). The elements of the inertia matrix M are:

$$\begin{aligned} M_{11} &= \begin{pmatrix} 1 & 2 \\ 2 & 1 \end{pmatrix}, \quad M_{22} = \begin{pmatrix} 1 & 0 \\ 0 & 1 \end{pmatrix} \\ M_{12} &= M_{21}^T = \begin{pmatrix} 1 & 1 & 0.2 & 0.3 \\ 0.5 & 0.1 & 2 & 0.7 \end{pmatrix} \end{aligned} \tag{5.86}$$

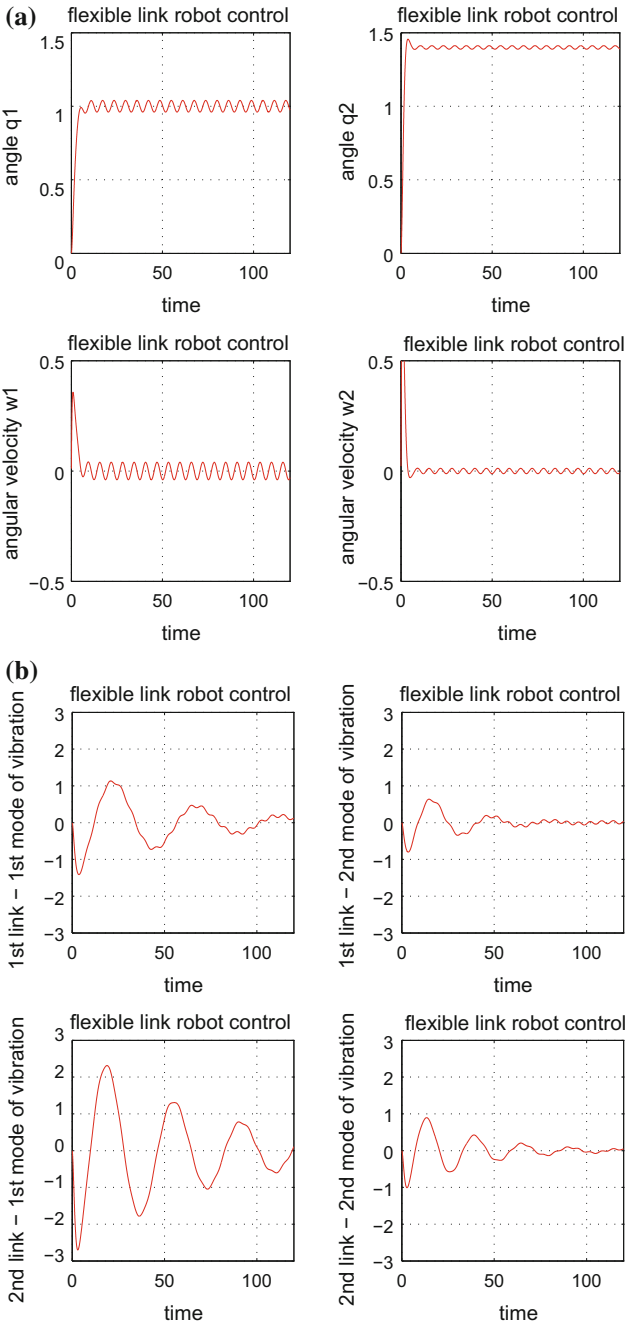

Fig. 5.7 **a** Inverse dynamics control of a 2-link flexible robot under additive motor-torques disturbances: joints' angles (rad) and joints' angular velocity (rad/sec) **b** Inverse dynamics control of a 2-link flexible robot under additive motor-torques disturbances: the first two vibration modes for each link

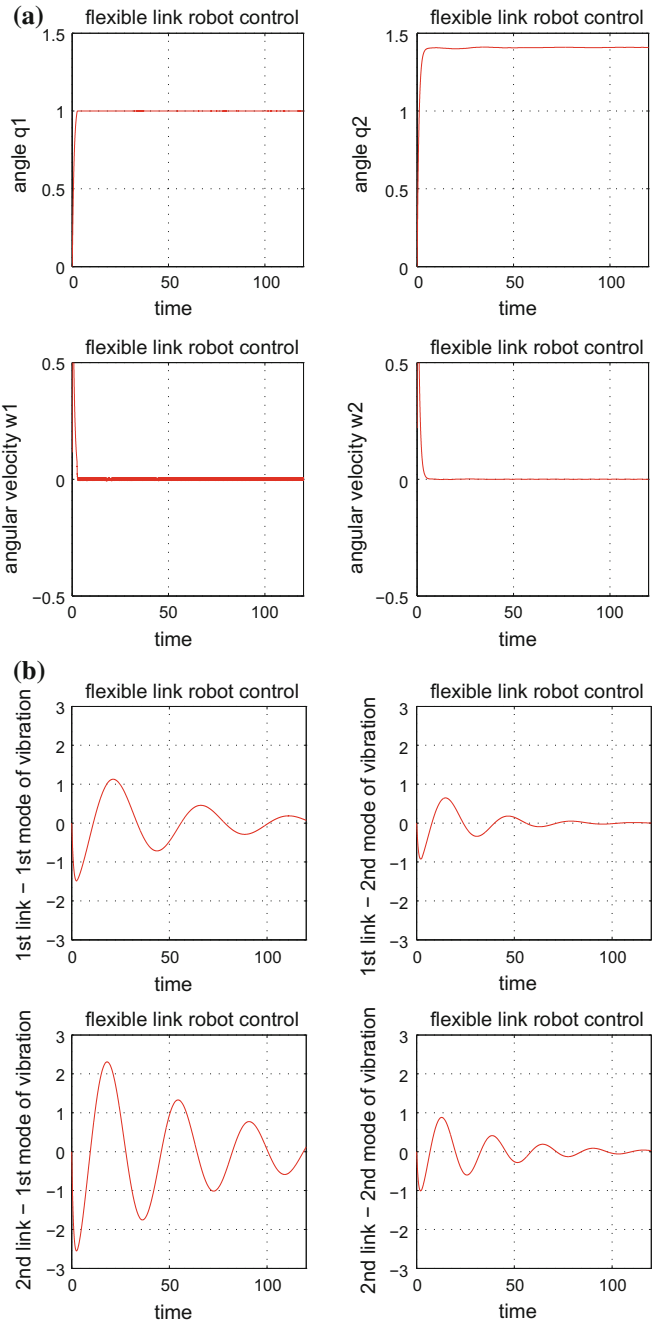

Fig. 5.8 **a** Sliding-mode control of a 2-link flexible robot under additive motor-torques disturbances: joints' angles (rad) and joints' angular velocity (rad/sec) for each link, **b** Sliding-mode control of a 2-link flexible robot under additive motor-torques disturbances: the first two vibration modes for each link

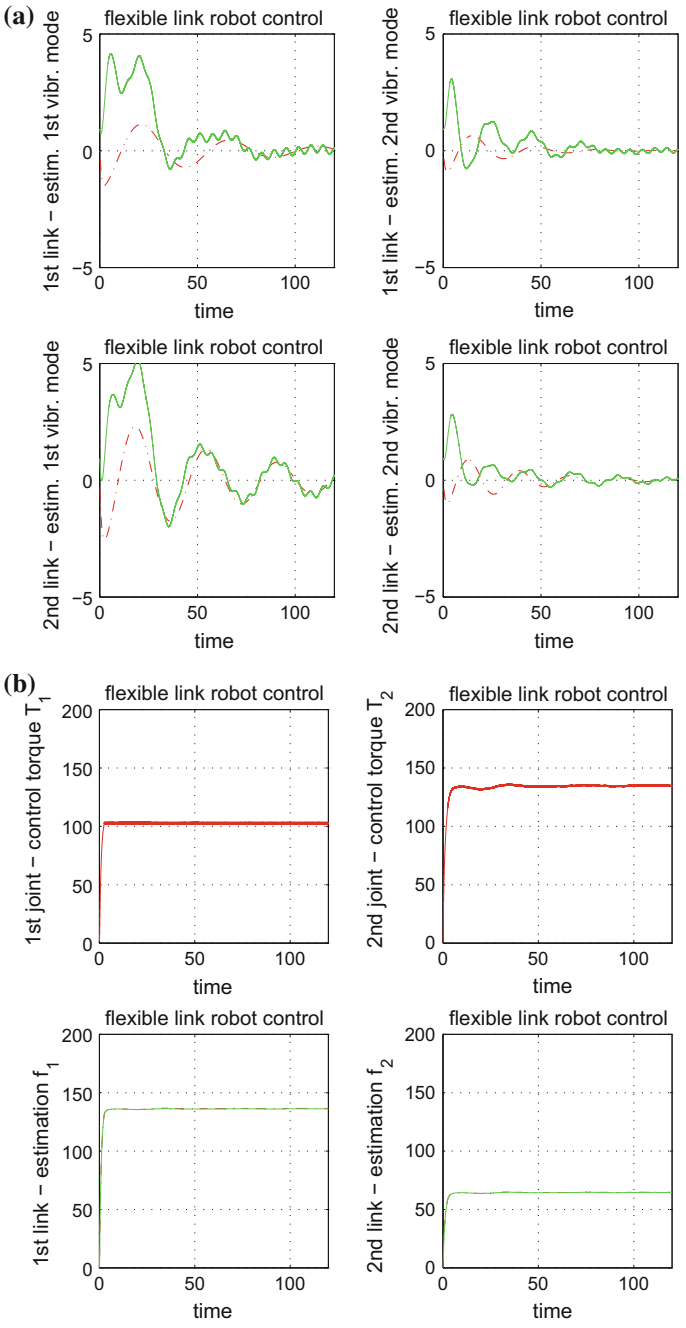

Fig. 5.9 **a** Estimates (continuous lines) of the non-measurable state vector elements of the flexible-link robot (vibration modes), provided by the Kalman Filter. **b** Top row: Control inputs (torques) $T_i,\ i = 1, 2$ applied to the joints of the flexible-link robot, Bottom row: estimation of function $f_i,\ i = 1, 2$ of the flexible-link dynamics

The damping matrix is $D = diag\{0.04, 0.08, 0.03, 0.06\}$ while the stiffness matrix is $K = diag\{0.02, 0.04, 0.03, 0.06\}$. The inverse dynamics control law given in Sect. 5.2.2 was employed. The selection of the gain matrices K_p and K_d determines the transient response of the closed loop system. The following controller gains have been considered: $K_p = diag\{10.5, 15.5\}$ and $K_d = diag\{10.9, 15.0\}$. The desirable joints' positions were $\theta_{d_1} = 1$ rad and $\theta_{d_2} = 1.4$ rad. It was considered that an additive disturbance torque $d_i(t) = 0.3cos(t)$ affected each joint.

In the simulation diagrams about angular position and velocity setpoint tracking, the horizontal axis represents time in sec, and since the robot's control takes place in the configuration space the vertical axis represents angle in rad and angular velocity in rad/sec. Moreover, as shown in Eq. (5.3), the vibration modes variables $v_i(t)$ are functions of time and are associated with the deformation of the flexible links $w(x, t)$. The performance of the model-based controller of the flexible-link robot in the presence of disturbance is depicted in Fig. 5.7. It can be seen that vibrations around the desirable joint positions cannot be eliminated.

5.3.4.2 Sliding-Mode Control for a 2-Link Flexible-Link Robot

The sliding-mode control scheme proposed in Sect. 5.3.2 was tested on the 2-link flexible robotic manipulator model. It was assumed that the complete state vector of the robot was not directly measurable. Thus, it was considered that only the joints' angles $\theta_i,\ i = 1, 2$ and the associated angular velocities $\dot{\theta}_i,\ i = 1, 2$ could be obtained through sensor measurements, whereas the vibration modes of the links $v_{11}, v_{12}, v_{21}, v_{22}$ were not measurable and had to be reconstructed with the use of the Kalman Filter.

The obtained results are depicted in Fig. 5.8a where convergence of the joints' angles and velocities to the desirable setpoints is shown. In Fig. 5.8b the evolution in time of the vibration modes of the flexible links is presented. Figure 5.9a presents the estimation of the flexible-links' vibration modes, provided by the Kalman Filter. It can be noticed that the Kalman Filter state estimates track with satisfactory accuracy the real values of the non-measurable state vector elements. Finally, Fig. 5.9b depicts the control inputs (torques) applied to the joints of the flexible-link robot.

From the simulation experiments it can be noticed that as the Kalman Filter-based sliding-mode controller, the energy-based controller is also efficient in controlling the position and in suppressing vibrations of the flexible links. However, an advantage of the Kalman Filter-based sliding mode control is that it achieves accurate tracking for any type of joint angle and velocity set-point whereas the convergence of the energy-based control is assured only in the case of constant set-points.

Chapter 6
Micro-manipulators

Abstract Microrobots can be used in the manipulation and precise positioning of micro-objects, as well as in several microelectronics applications. Microrobotics is primarily concerned with control problems of micro electromechanical systems (MEMS). Specific problems that one encounters when developing microrobotic systems and MEMS is the imprecision about the micro-robot's dynamic model and the inability to measure specific state vector elements in it. This in turn signifies that the design of feedback controllers for such systems has to be sufficiently robust to compensate for unmodelled dynamics or for parametric uncertainty. To this end one can consider either model-free control methods of proven stability (such as adaptive neurofuzzy control schemes), or model-based control methods capable of eliminating the effects of modelling errors, parametric inconsistency and external perturbations (such as H-infinity control). Moreover, one has to implement state estimation-based feedback control methods, making use of robust state observers, that will allow for estimation of the entire state vector of the microrobot or MEMS through the processing of measurements from a small number of sensors. In particular, the chapter treats the following topics: (a) Adaptive neurofuzzy control of micro-actuators, (b) Nonlinear optimal control of underactuated MEMS.

6.1 Chapter Overview

This chapter treats the following topics: (a) Adaptive neurofuzzy control of micro-actuators, (b) Nonlinear optimal control of underactuated MEMS.

With reference to (a) the chapter presents an adaptive fuzzy approach to the problem of control of electrostatically actuated MEMS, which is based on differential flatness theory and which uses exclusively output feedback. It is shown that the model of the electrostatically actuated MEMS is a differentially flat one and this permits to transform it to the so-called linear canonical form. For the new description of the system's dynamics the transformed control inputs contain unknown terms which depend on the system's parameters. To identify these terms adaptive fuzzy approximators are used in the control loop. Thus an adaptive fuzzy control scheme is

G. Rigatos and K. Busawon, *Robotic Manipulators and Vehicles*,
Studies in Systems, Decision and Control 152,
https://doi.org/10.1007/978-3-319-77851-8_6

implemented in which the unknown or unmodeled system dynamics is approximated by neurofuzzy networks and next this information is used by a feedback controller that makes the electrostatically activated MEMS converge to the desirable motion setpoints. This adaptive control scheme is exclusively implemented with the use of output feedback, while the state vector elements which are not directly measured are estimated with the use of a state observer that operates in the control loop. The learning rate of the adaptive fuzzy system is suitably computed from Lyapunov analysis, so as to ensure that both the learning procedure for the unknown system's parameters, the dynamics of the observer and the dynamics of the control loop will remain stable. The Lyapunov stability analysis depends on two Riccati equations, one associated with the feedback controller and one associated with the state observer.

With reference to (b) the chapter proposes a nonlinear optimal control method for solving the problem of control of coupled underactuated micro-electromechanical systems (MEMS). The MEMS model consists of a Van-der-Pol oscillator being elastically coupled with a forced Duffing oscillator. The dynamic model of the MEMS is approximately linearized around a temporary operating point with the use of first-order Taylor series expansion and after computing the Jacobian matrices of its state-space model. For the approximately linearized model of the MEMS a nonlinear optimal (H-infinity) feedback controller is designed. This controller stands for the solution of the MEMS optimal control problem under model uncertainty and external perturbations. The computation of the feedback control gain relies on the solution of an algebraic Riccati equation taking place at each time step of the control method. Finally, to achieve state estimation-based control through the measurement of a small number of the MEMS state vector elements, the H-infinity Kalman Filter is used as a robust state estimator. In both cases (a) and (b) the global asymptotic stability properties of the control scheme are proven through Lyapunov analysis.

6.2 Adaptive Neurofuzzy Control of Microactuators

6.2.1 Outline

As micro and nanotechnology develop fast, the use of MEMS and particularly of microactuators is rapidly deploying. One can note several systems where the use of microactuators has become indispensable and the solution of the associated control problems has become a prerequisite. In [501, 507, 649, 651] electrostatic microactuators are used in adaptive optics and optical communications. In [56, 327] microactuators are used for micromanipulation and precise positioning of microobjects. Several approaches to the control of microactuators have been proposed. In [263, 276, 550] adaptive control methods have been used. In [142, 607] solution of microactuation control problems through robust control approaches has been attempted. In [482] backstepping control has been used, while in [550] an output feedback control scheme has been implemented. Additional results for the stabilization and control

of microactuators have been presented in [192, 389]. In such control systems, convergence of the state vector elements to the associated reference setpoints has to be performed with accuracy, despite modeling uncertainties, parametric variations or external perturbations. Moreover, the reliable functioning of the control loop has to be assured despite difficulties in measuring the complete state vector of the MEMS. The present section develops a new method for the control of micro-electromechanical systems (MEMS) which is based on differential flatness theory. The considered control problem is a nontrivial one because of the of the unknown nonlinear dynamical model of the actuator and because of the constraint to implement the control using exclusively output feedback (it is little reliable and technically difficult to use sensor measurements for the monitoring of all state variables of the micro-actuator). The differential flatness theory control approach is based on an exact linearization of the MEMS dynamics which avoids the numerical errors of the approximate linearization that is performed by other nonlinear control methods [93, 235, 335, 454, 457].

First, the section shows that the dynamic model of the studied microactuator is a differentially flat one. This means that all its state variables and the control input can be written as functions of one single algebraic variable, which is the flat output, and also as functions of the flat output's derivatives [267, 450, 452, 476, 519]. This change of variables (differential flatness theory-based diffeomorphism) enables to transform the nonlinear model of the actuator into the linear canonical (Brunovsky) form [145, 334, 546, 572]. In the latter description of the MEMS, the transformed control input contains elements which are associated with the unknown nonlinear dynamics of the system. These are identified on-line with the use of neurofuzzy approximators and the estimated system dynamics is finally used for the computation of the control signal that will make the MEMS state vector track the desirable setpoints. Thus an adaptive fuzzy control scheme is implemented [457, 462]. The learning rate of the neurofuzzy approximators is determined by the requirement to assure that the Lyapunov function of the control loop will always have a negative first-order derivative.

Next, another problem that has to be dealt with was that only output feedback can be used for the implementation of the MEMS control scheme. The nonmeasurable state variables of the microactuator have to be reconstructed with the use of a state estimator (observer), which functions again inside the control loop. Thus, finally, the Lyapunov function for the proposed control scheme comprises three quadratic terms: (i) a term that describes the tracking error of the MEMS state variables from the reference setpoints, (ii) a term that describes the error in the estimation of the nonmeasurable state vector elements of the microactuator with respect to the reference setpoints, and (iii) a sum of quadratic terms associated with the distance of the weights of the neurofuzzy approximators from the values that give the best approximation of the unknown MEMS dynamics. It is proven that an adaptive (learning) control law can be found assuring that the Lyapunov function will continuously have a negative first order derivative, thus also confirming that the stability of the control loop will be preserved and that accurate tracking of the setpoints by the system's state variables will be achieved (H-infinity tracking performance).

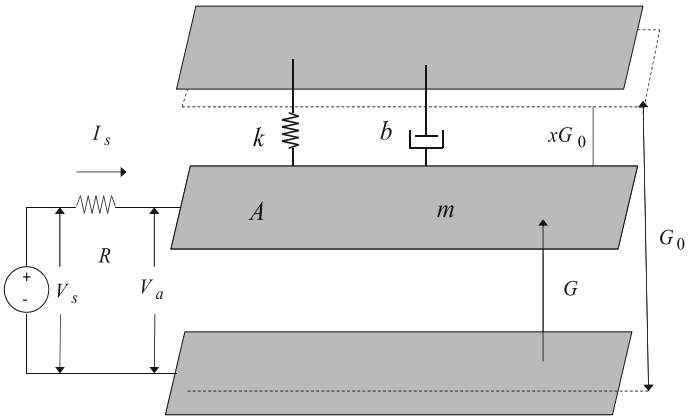

Fig. 6.1 Diagram of the 1-DOF parallel-plate electrostatic actuator

6.2.2 *Dynamic Model of the Electrostatic Actuator*

The considered MEMS (electrostatic microactuator) is depicted in Fig. 6.1. The dynamic model of the MEMS has been analyzed in [172, 199, 648, 650], where model-based control approaches have been mostly developed. It is assumed that $Q(t)$ is the charge of the device, while ε is the permitivity in the gap. Then the capacitance of the device is

$$C(t) = \frac{\varepsilon A}{G(t)} \tag{6.1}$$

while the attractive electrostatic force on the moving plate is

$$F(t) = \frac{V_a^2}{2}\frac{\partial C}{\partial G} = -\frac{\varepsilon A V_a^2}{2G^2(t)} = -\frac{Q^2(t)}{2\varepsilon A} \tag{6.2}$$

Thus, the equation of motion of the actuator is given by

$$m\ddot{G}(t) + b\dot{G}(t) + k(G(t) - G_0) = -\frac{Q^2(t)}{2\varepsilon A} \tag{6.3}$$

From Eqs. (6.2) and (6.3) it can be concluded that the electrostatic force F increases with the inverse square of the gap, while the restoring mechanical force which is associated with the term $k(G(t) - G_0)$ increases linearly with the plate deflection. A critical value for the voltage across the device is called pull-in voltage and is given by [651]

$$V_{pi} = \sqrt{\frac{8kG_0^2}{27C_0}} \tag{6.4}$$

It is assumed that the MEMS starts operating from an initially uncharged state at $t = 0$. Then the charge of the electrodes at time instant t is given by $Q(t) = \int_0^t I_s(\tau)d\tau$, or equivalently $\dot{Q}(t) = I_s(t)$. By applying Kirchhoff's voltage law one has for the current that goes through the resistor

$$\dot{Q}(t) = \frac{1}{R}\left(V_s(t) - \frac{Q(t)G(t)}{\varepsilon A}\right) \tag{6.5}$$

Next, the equations of the system's dynamics given in Eqs. (6.3)–(6.5) undergo a transformation which consists of a change of the time scale $\tau = \omega t$ and of the following normalization

$$\begin{aligned} x &= 1 - \tfrac{G}{G_0} \quad q = \tfrac{Q}{Q_{pi}} \\ u &= \tfrac{V_s}{V_{pi}} \quad i = \tfrac{I_s}{V_{pi}\omega_0 C_0}\ r = \omega_0 C_0 R \end{aligned} \tag{6.6}$$

where $C_0 = \frac{\varepsilon A}{G_0}$, $Q_{pi} = \frac{3}{2}C_0 V_{pi}$ is the pull-in charge corresponding to the pull-in voltage, $\omega_0 = \sqrt{k/m}$ is the undamped natural frequency, and $\zeta = \frac{b}{2m\omega_0}$ is the damping ratio. The normalized voltage across the actuator can be expressed in terms of normalized deflection x of the moveable electrode, that is $u_o = \frac{3}{2}q(1-x)$, while the dynamics of the normalized charge is $\dot{q} = \frac{2}{3}i$.

After the aforementioned normalization and transformation, the dynamic model of the microactuator is written as [651]

$$\begin{aligned} \dot{x} &= v \\ \dot{v} &= -2\zeta v - x + \frac{1}{3}q^2 \\ \dot{q} &= \frac{1}{r}q(1-x) + \frac{2}{3r}u \end{aligned} \tag{6.7}$$

In the previous state-space model: $\dot{x} = v$: is a variable denoting the speed of deflection of the moving electrode, q is a variable denoting the ratio between the actual change of the plates Q and the pull-in charge Q_{pi}. It holds that $q = \frac{Q}{Q_{p_i}}$, where $Q_{p_i} = \frac{3}{2}C_o V_{p_i}$ and V_{p_i} is the pull-in voltage.

Remark 1 The previously analyzed MEMS dynamics is a highly nonlinear one and nonlinear control methods have to be used for it. One can distinguish three main approaches in the control of nonlinear dynamical systems: (i) control based on global linearization methods, (ii) control based on approximate linearization methods, (iii) Lyapunov methods.

The results of the present section are mostly based on approach (iii) that is Lyapunov theory-based design of feedback controllers for dynamical systems of unknown model and of non completely measurable state vector. Comparing to methods (i) and (ii), approach (iii) is a completely model-free one. Therefore, the major

benefit from it is that there is no dependence on prior knowledge of the microactuator's dynamics. The main difficulty in the application of approach (iii) is that it may require operations between matrices of high dimension. Thus it becomes computationally more demanding than approaches (i) and (ii).

6.2.3 *Linearization of the MEMS Model Using Lie Algebra*

The MEMS nonlinear dynamics given in Eq. (6.7), with state vector defined as $x = [x, v, q]$, is also written in the form

$$\dot{x} = f(x) + g(x)u \tag{6.8}$$

where the vector fields $f(x)$ and $g(x)$ are defined as

$$f(x) = \begin{pmatrix} v \\ -2\zeta v - x + \frac{1}{2}q^2 \\ -\frac{1}{r}q(1-x) \end{pmatrix} g(x) = \begin{pmatrix} 0 \\ 0 \\ \frac{2}{3r} \end{pmatrix} \tag{6.9}$$

Using the above formulation, one can arrive at a linearized description of the MEMS dynamics using a differential geometric approach and the computation of Lie derivatives. The following state variables are defined: $z_1 = h_1(x) = x$, $z_2 = L_f h_1(x)$ and $z_3 = L_f^2 h_1(x)$. It holds that

$$\begin{gathered} z_2 = L_f h_1(x) \Rightarrow z_2 = \frac{\partial h_1}{\partial x_1} f_1 + \frac{\partial h_1}{\partial x_2} f_2 + \frac{\partial h_1}{\partial x_3} f_3 \Rightarrow \\ z_2 = 1 f_1 + 0 f_2 + 0 f_3 \Rightarrow z_2 = f_1 \Rightarrow z_2 = v \Rightarrow z_2 = \dot{x} \end{gathered} \tag{6.10}$$

In a similar manner one computes

$$\begin{gathered} z_3 = L_f^2 h_1(x) \Rightarrow z_3 = \frac{\partial z_2}{\partial x_1} f_1 + \frac{\partial z_2}{\partial x_2} f_2 + \frac{\partial z_2}{\partial x_3} f_3 \Rightarrow \\ z_3 = 0 f_1 + 1 f_2 + 0 f_3 \Rightarrow z_3 = \dot{v} \Rightarrow z_3 = \ddot{x} \end{gathered} \tag{6.11}$$

Moreover, one has that

$$\dot{z}_3 = x^{(3)} = L_f^3 h_1(x) + L_g L_f^2 h_1 x \cdot u \tag{6.12}$$

where

$$L_f^3 h_1(x) = L_f z_2 \Rightarrow L_f^3 h_1(x) = \frac{\partial z_3}{\partial x_1} f_1 + \frac{\partial z_3}{\partial x_2} f_2 + \frac{\partial z_3}{\partial x_3} f_3 \Rightarrow$$

$$L_f^3 h_1(x) = 1 f_1 - 2\zeta f_2 + \frac{2}{3} q f_3 \Rightarrow L_f^3 h_1(x) = v - 2\zeta \dot{v} + \frac{2}{3} q \left(-\frac{1}{r} q(1-x) \right) \Rightarrow$$

$$L_f^3 h_1(x) = \dot{y} - 2\zeta\ddot{y} + \frac{2}{3}q\left[-\frac{1}{r}q(1-x)\right] \Rightarrow L_f^3 h_1(x) = -2\zeta\ddot{y} - \dot{y} - \frac{1}{r}(1-y)\frac{2}{3}q^2 \Rightarrow$$

$$L_f^3 h_1(x) = -2\zeta\ddot{y} - \dot{y} - \frac{2}{r}(1-y)[\ddot{y} + 2\zeta\dot{y} + y] \tag{6.13}$$

Following a similar procedure one finds

$$\begin{gathered} L_g L_f^2 h_1(x) = L_g z_3 \Rightarrow L_g L_f^2 h_1(x) = \tfrac{\partial z_3}{\partial x_1} g_1 + \tfrac{\partial z_3}{\partial x_2} g_2 + \tfrac{\partial z_3}{\partial x_3} g_3 \Rightarrow \\ L_g L_f^2 h_1(x) = 1 g_1 - 2\zeta g_2 + \tfrac{2}{3} q g_3 \Rightarrow L_g L_f^2 h_1(x) = \tfrac{4}{9r} q \Rightarrow \\ L_g L_f^2 h_1(x) = \tfrac{4}{9r}\sqrt{3[\ddot{y} + 2\zeta\dot{y} + y]} \end{gathered} \tag{6.14}$$

For the linearized description of the MEMS dynamics given in Eq. (6.12), and using that $v = L_f^3 h_1(x) + L_g L_f^2 h_1(x) u$ one obtains the state-space description

$$\begin{pmatrix} \dot{z}_1 \\ \dot{z}_2 \\ \dot{z}_3 \end{pmatrix} = \begin{pmatrix} 0 & 1 & 0 \\ 0 & 0 & 1 \\ 0 & 0 & 0 \end{pmatrix} \begin{pmatrix} z_1 \\ z_2 \\ z_3 \end{pmatrix} + \begin{pmatrix} 0 \\ 0 \\ 1 \end{pmatrix} v \tag{6.15}$$

$$z^{meas} = \begin{pmatrix} 1 & 0 & 0 \end{pmatrix} \begin{pmatrix} z_1 \\ z_2 \\ z_3 \end{pmatrix} \tag{6.16}$$

For the linearized description of the system given in Eq. (6.25) the design of a state feedback controller is carried out as follows:

$$v = y_d^{(3)} - k_1(\ddot{y} - \ddot{y}_d) - k_2(\dot{y} - \dot{y}_d) - k_3(y - y_d) \tag{6.17}$$

which results in tracking error dynamics of the form

$$e^{(3)}(t) + k_1\ddot{e}(t) + k_2\dot{e}(t) + k_3 e(t) = 0 \tag{6.18}$$

By selecting the feedback gains k_i, $i = 1, 2, 3$ such that the characteristic polynomial of Eq. (6.31) to be a Hurwitz one, it is assured that $lim_{t\to\infty} e(t) = 0$.

6.2.4 Differential Flatness of the Electrostatic Actuator

6.2.4.1 Differential Flatness Properties of the Electrostatic Microactuator

The dynamic model of the electrostatic microactuator given in Eq. (6.7) is considered. The flat output of the model is taken to be be $y = x$. Therefore, it also holds $v = \dot{y}$. From the second row of the state space equations, given in Eq. (6.7) one has

$$\begin{gathered}\ddot{y} = -2\zeta\dot{y} - y + \tfrac{1}{3}q^2 \Rightarrow q^2 = 3[\ddot{y} + 2\zeta\dot{y} + y] \\ \Rightarrow q = \sqrt{3[\ddot{y} + 2\zeta\dot{y} + y]} \Rightarrow q = f_q(y, \dot{y}, \ddot{y})\end{gathered} \tag{6.19}$$

From the third row of the state space equations, given in Eq. (6.7) one has

$$u = \frac{3r}{2}\left[\dot{q} + \frac{1}{r}q(1-x)\right] \Rightarrow u = f_u(y, \dot{y}, \ddot{y}, y^{(3)}) \tag{6.20}$$

Since all state variables and the control input of the system are expressed as functions of the flat output and its derivatives, it is concluded that the model of the electrostatic actuator is a differentially flat one.

6.2.4.2 Linearization of the MEMS Model Using Differential Flatness Theory

From the second row of the state-space model given in Eq. (6.7) it holds that

$$\ddot{y} = -2\zeta\dot{y} - y + \frac{1}{3}q^2 \tag{6.21}$$

By deriving once more with respect to time one gets

$$y^{(3)} = -2\zeta\ddot{y} - \dot{y} + \frac{2}{3}q\dot{q} \tag{6.22}$$

By substituting the third row of the state-space model given in Eq. (6.7) one obtains

$$\begin{gathered}y^{(3)} = -2\zeta\ddot{y} - \dot{y} + \tfrac{2}{3}q\left[-\tfrac{1}{r}q(1-x) + \tfrac{2}{3r}u\right] \Rightarrow \\ y^{(3)} = -2\zeta\ddot{y} - \dot{y} - \tfrac{2}{3r}(1-x)q^2 + \tfrac{4}{9r}qu\end{gathered} \tag{6.23}$$

Next, using from Eq. (6.19) that $q^2 = \ddot{y} + 2\zeta\dot{y} + y$ or equivalently that $q = \sqrt{\ddot{y} + 2\zeta\dot{y} + y}$ the following relation is obtained

$$y^{(3)} = -2\zeta\ddot{y} - \dot{y} - \frac{2}{e}(1-y)[\ddot{y} + 2\zeta\dot{y} + y] + \frac{4}{9r}\sqrt{3[\ddot{y} + 2\zeta\dot{y} + y]}u \tag{6.24}$$

or equivalently

$$y^{(3)} = f(y, \dot{y}, \ddot{y}) + g(y, \dot{y}, \ddot{y})u \tag{6.25}$$

where

$$f(y, \dot{y}, \ddot{y}) = -2\zeta\ddot{y} - \dot{y} - \frac{2}{r}(1-y)[\ddot{y} + 2\zeta\dot{y} + y] \tag{6.26}$$

$$g(y, \dot{y}, \ddot{y}) = \frac{4}{9r}[\sqrt{3[\ddot{y} + 2\zeta\dot{y} + y]}] \tag{6.27}$$

For the linearized description of the MEMS dynamics given in Eq. (6.25), and using the notation $z_1 = y, z_2 = \dot{y}$ and $z_3 = \ddot{y}$, and $v = f(y, \dot{y}, \ddot{y}) + g(y, \dot{y}, \ddot{y})u$ one arrives also at the state-space description

$$\begin{pmatrix} \dot{z}_1 \\ \dot{z}_2 \\ \dot{z}_3 \end{pmatrix} = \begin{pmatrix} 0 & 1 & 0 \\ 0 & 0 & 1 \\ 0 & 0 & 0 \end{pmatrix} \begin{pmatrix} z_1 \\ z_2 \\ z_3 \end{pmatrix} + \begin{pmatrix} 0 \\ 0 \\ 1 \end{pmatrix} v \tag{6.28}$$

$$z^{meas} = \begin{pmatrix} 1 & 0 & 0 \end{pmatrix} \begin{pmatrix} z_1 \\ z_2 \\ z_3 \end{pmatrix} \tag{6.29}$$

For the linearized description of the system given in Eq. (6.25) the design of a state feedback controller is carried out as follows:

$$v = y_d^{(3)} - k_1(\ddot{y} - \ddot{y}_d) - k_2(\dot{y} - \dot{y}_d) - k_3(y - y_d) \tag{6.30}$$

which results in tracking error dynamics of the form

$$e^{(3)}(t) + k_1\ddot{e}(t) + k_2\dot{e}(t) + k_3e(t) = 0 \tag{6.31}$$

By selecting the feedback gains $k_i,\ i = 1, 2, 3$ such that the characteristic polynomial of Eq. (6.31) to be a Hurwitz one, it assured that $lim_{t\to\infty}e(t) = 0$.

6.2.5 *Adaptive Fuzzy Control of the MEMS Model Using Output Feedback*

6.2.5.1 Problem Statement

Adaptive fuzzy control aims at solving the microactuator's control problem in case that its dynamics is unknown and the state vector is not completely measurable. It has been shown that after applying the differential flatness theory-based transformation, the following non-linear SISO system is obtained:

$$x^{(n)} = f(x, t) + g(x, t)u + \tilde{d} \tag{6.32}$$

where $f(x, t)$, $g(x, t)$ are unknown nonlinear functions and $\tilde{d}$ is an unknown additive disturbance. The objective is to force the system's output $y = x$ to follow a

given bounded reference signal x_d. In the presence of non-Gaussian disturbances w, successful tracking of the reference signal is denoted by the H_∞ criterion [450, 457].

$$\int_0^T e^T Qedt \leq \rho^2 \int_0^T w^T wdt \tag{6.33}$$

where ρ is the attenuation level and corresponds to the maximum singular value of the transfer function $G(s)$ of the linearized equivalent of Eq. (6.32).

6.2.5.2 Transformation of Tracking into a Regulation Problem

The flatness-based adaptive fuzzy control approach for nonlinear systems control consists of the following steps : (i) linearization is applied; (ii) the unknown system dynamics are approximated by neural or fuzzy estimators, (iii) an H_∞ control term, is employed to compensate for estimation errors and external disturbances. If the state vector is not measurable, this can be reconstructed with the use of an observer.

For measurable state vector x, desirable state vector x_m and uncertain functions $f(x,t)$ and $g(x,t)$ an appropriate control law for (6.32) would be

$$u = \frac{1}{\hat{g}(x,t)}[x_m^{(n)} - \hat{f}(x,t) + K^T e + u_c] \tag{6.34}$$

where, $\hat{f}$ and $\hat{g}$ are the approximations of the unknown parts of the system dynamics f and g respectively, and which can be given by the outputs of suitably trained neuro-fuzzy networks. The term u_c denotes a supervisory controller which compensates for the approximation error $w = [f(x,t) - \hat{f}(x,t)] + [g(x,t) - \hat{g}(x,t)]u$, as well as for the additive disturbance $\tilde{d}$. Moreover the feedback control gains $K^T = [k_n, k_{n-1}, \ldots, k_1]$, and the vector of the state vector element's tracking error $e^T = [e, \dot{e}, \ddot{e}, \ldots, e^{(n-1)}]^T$ are chosen such that the polynomial $e^{(n)} + k_1 e^{(n-1)} + k_2 e^{(n-2)} + \cdots + k_n e$ is Hurwitz. The substitution of control law of Eq. (6.34) in (6.32) results into

$$\begin{gathered}
x^{(n)} = f(x,t) + g(x,t)\frac{1}{\hat{g}(x,t)}[x_m^{(n)} - \hat{f}(x,t) - K^T e + u_c] + \tilde{d} \Rightarrow \\
x^{(n)} = f(x,t) + \{\hat{g}(x,t) + [g(x,t) - \hat{g}(x,t)]\}\frac{1}{\hat{g}(x,t)}[x_m^{(n)} - \hat{f}(x,t) - K^T e + u_c] + \tilde{d} \Rightarrow \\
x^{(n)} = f(x,t) + \left\{\frac{\hat{g}(x,t)}{\hat{g}(x,t)}[x_m^{(n)} - \hat{f}(x,t) - K^T e + u_c] + [g(x,t) - \hat{g}(x,t)]u\right\} + \tilde{d} \Rightarrow \\
x^{(n)} = f(x,t) + x_m^{(n)} - \hat{f}(x,t) - K^T e + u_c + [g(x,t) - \hat{g}(x,t)]u + u_c + \tilde{d} \Rightarrow \\
x^{(n)} - x_m^{(n)} = -K^T e + [f(x,t) - \hat{f}(x,t)] + [g(x,t) - \hat{g}(x,t)]u + u_c + \tilde{d} \Rightarrow \\
x^{(n)} = -K^T e + u_c + [f(x,t) - \hat{f}(x,t)] + [g(x,t) - \hat{g}(x,t)]u + \tilde{d}
\end{gathered} \tag{6.35}$$

The above relation can be written in a state-equations form. The state vector is taken to be $e^T = [e, \dot{e}, \ldots, e^{(n-1)}]$, which yields

$$\dot{e} = Ae - BK^T e + Bu_c + B\{[f(x,t) - \hat{f}(x,t)] + [g(x,t) - \hat{g}(x,t)]u + \tilde{d}\} \tag{6.36}$$

or equivalently

$$\begin{gathered}\dot{e} = (A - BK^T)e + Bu_c + B\{[f(x,t) - \hat{f}(x,t)] + [g(x,t) - \hat{g}(x,t)]u + \tilde{d}\} \\ e_1 = C^T e\end{gathered} \tag{6.37}$$

where

$$\begin{aligned} A &= \begin{pmatrix} 0 & 1 & 0 & \cdots\cdots & 0 \\ 0 & 0 & 1 & \cdots\cdots & 0 \\ \cdots & \cdots & \cdots & \cdots & \cdots \\ \cdots & \cdots & \cdots & \cdots & \cdots \\ 0 & 0 & 0 & \cdots\cdots & 1 \\ 0 & 0 & 0 & \cdots\cdots & 0 \end{pmatrix} \\ B^T &= \left(0, 0, \cdots, 0, 1\right), \; C^T = \left(1, 0, \cdots, 0, 0\right) \\ K^T &= \left(k_0, k_1, \cdots, k_{n-2}, k_{n-1}\right) \end{aligned} \tag{6.38}$$

where e_1 denotes the output error $e_1 = x - x_m$. Eq. (6.37) describes a regulation problem.

6.2.5.3 Estimation of the State Vector

The control of the microactuator described by Eq. (6.32) becomes more complicated when the state vector x is not directly measurable and has to be reconstructed through a state observer. The following definitions are used

- error of the state vector $e = x - x_m$
- error of the estimated state vector $\hat{e} = \hat{x} - x_m$
- observation error $\tilde{e} = e - \hat{e} = (x - x_m) - (\hat{x} - x_m)$

When an observer is used to reconstruct the state vector, the control law of Eq. (6.34) is written as

$$u = \frac{1}{\hat{g}(\hat{x}, t)}[x_m^{(n)} - \hat{f}(\hat{x}, t) + K^T e + u_c] \tag{6.39}$$

Applying Eq. (6.39) to the nonlinear system described by Eq. (6.32), after some operations results into

$$x^{(n)} = x_m^{(n)} - K^T\hat{e} + u_c + [f(x,t) - \hat{f}(\hat{x},t)] + [g(x,t) - \hat{g}(\hat{x},t)]u + \tilde{d}$$

It holds $e = x - x_m \Rightarrow x^{(n)} = e^{(n)} + x_m^{(n)}$. Substituting $x^{(n)}$ in the above equation gives

$$\begin{aligned} e^{(n)} + x_m^{(n)} = x_m^{(n)} - K^T\hat{e} + u_c + [f(x,t) - \hat{f}(\hat{x},t)] + \\ + [g(x,t) - \hat{g}(\hat{x},t)]u + \tilde{d} \Rightarrow \end{aligned} \tag{6.40}$$

$$\begin{aligned} \dot{e} = Ae - BK^T\hat{e} + Bu_c + B\{[f(x,t) - \hat{f}(\hat{x},t)] + \\ + [g(x,t) - \hat{g}(\hat{x},t)]u + \tilde{d}\} \end{aligned} \tag{6.41}$$

$$e_1 = C^T e \tag{6.42}$$

where $e = [e, \dot{e}, \ddot{e}, \ldots, e^{(n-1)}]^T$, and $\hat{e} = [\hat{e}, \dot{\hat{e}}, \ddot{\hat{e}}, \ldots, \hat{e}^{(n-1)}]^T$.

The state observer is designed according to Eqs. (6.41) and (6.42) and is given by [457]:

$$\dot{\hat{e}} = A\hat{e} - BK^T\hat{e} + K_o[e_1 - C^T\hat{e}] \tag{6.43}$$

$$\hat{e}_1 = C^T\hat{e} \tag{6.44}$$

The observation gain $K_o = [k_{o_0}, k_{o_1}, \ldots, k_{o_{n-2}}, k_{o_{n-1}}]^T$ is selected so as to ensure the convergence of the observer.

6.2.5.4 The Additional Control Term u_c

The additional term u_c which appeared in Eq. (6.34) is also introduced in the observer-based control to compensate for:

- The external disturbances $\tilde{d}$
- The state vector estimation error $\tilde{e} = e - \hat{e} = x - \hat{x}$
- The approximation error of the nonlinear functions $f(x,t)$ and $g(x,t)$, denoted as $w = [f(x,t) - \hat{f}(\hat{x},t)] + [g(x,t) - \hat{g}(\hat{x},t)]u$

The control signal u_c consists of 2 terms, namely:

- the H_∞ control term, $u_a = -\frac{1}{r}B^T P\tilde{e}$ for the compensation of d and w
- the control term u_b for the compensation of the observation error $\tilde{e}$

6.2.5.5 Dynamics of the Observation Error

The observation error is defined as $\tilde{e} = e - \hat{e} = x - \hat{x}$. Subtracting Eq. (6.43) from (6.41) as well as Eq. (6.44) from (6.42) one gets

$$\dot{e} - \dot{\hat{e}} = A(e - \hat{e}) + Bu_c + B\{[f(x,t) - \hat{f}(\hat{x},t)] + \\ + [g(x,t) - \hat{g}(\hat{x},t)]u + \tilde{d}\} - K_o C^T (e - \hat{e})$$
$$e_1 - \hat{e}_1 = C^T (e - \hat{e})$$

that is

$$\dot{\tilde{e}} = A\tilde{e} + Bu_c + B\{[f(x,t) - \hat{f}(\hat{x},t)] + \\ + [g(x,t) - \hat{g}(\hat{x},t)]u + \tilde{d}\} - K_o C^T \tilde{e}$$
$$\tilde{e}_1 = C^T \tilde{e}$$

which can be written as

$$\dot{\tilde{e}} = (A - K_o C^T)\tilde{e} + Bu_c + B\{[f(x,t) - \hat{f}(\hat{x},t)] + [g(x,t) - \hat{g}(\hat{x},t)]u + \tilde{d}\} \tag{6.45}$$
$$\tilde{e}_1 = C\tilde{e} \tag{6.46}$$

6.2.5.6 Approximation of the Unknown MEMS Dynamics

Neurofuzzy networks can been trained on-line to approximate parts of the unknown dynamics of the microactuator,or to compensate for external disturbances. The approximation of functions $f(x,t)$ and $g(x,t)$ of Eq.(6.32) can be carried out with Takagi-Sugeno neuro-fuzzy networks of zero or first order (Fig. 6.2). These consist of rules of the form:

R^l : IF $\hat{x}$ is A_1^l AND $\dot{\hat{x}}$ is A_2^l AND $\cdots$ AND $\hat{x}^{(n-1)}$ is A_n^l THEN $\bar{y}^l = \sum_{i=1}^n w_i^l \hat{x}_i + b^l$, $l = 1, 2, \ldots, L$

The output of the neuro-fuzzy model is calculated by taking the average of the consequent part of the rules

$$\hat{y} = \frac{\sum_{l=1}^L \bar{y}^l \prod_{i=1}^n \mu_{A_i^l}(\hat{x}_i)}{\sum_{l=1}^L \prod_{i=1}^n \mu_{A_i^l}(\hat{x}_i)} \tag{6.47}$$

where $\mu_{A_i^l}$ is the membership function of x_i in the fuzzy set A_i^l. The training of the neuro-fuzzy networks is carried out with 1^{st} order gradient algorithms, in pattern mode, i.e. by processing only one data pair (x_i, y_i) at every time step i. The estimation of $f(x,t)$ and $g(x,t)$ can be written as

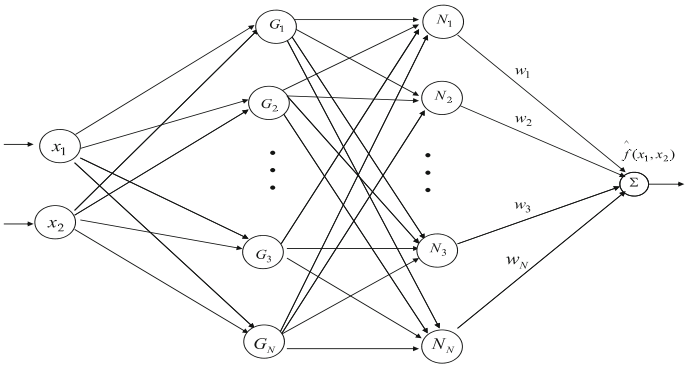

Fig. 6.2 Neuro-fuzzy approximator for the unknown dynamics of the mioroactuator: G_i Gaussian basis function, N_i: normalization unit

$$\begin{aligned} \hat{f}(\hat{x}|\theta_f) &= \theta_f^T \phi(\hat{x}) \\ \hat{g}(\hat{x}|\theta_g) &= \theta_g^T \phi(\hat{x}) \end{aligned} \tag{6.48}$$

where $\phi(\hat{x})$ are kernel functions with elements $\phi^l(\hat{x}) = \frac{\prod_{i=1}^{n} \mu_{A_i^l}(\hat{x}_i)}{\sum_{l=1}^{L} \prod_{i=1}^{n} \mu_{A_i^l}(\hat{x}_i)} \quad l = 1, 2, \cdots, L$. It is assumed that that the weights θ_f and θ_g vary in the bounded areas M_{θ_f} and M_{θ_g} which are defined as

$$\begin{aligned} M_{\theta_f} &= \{\theta_f \in R^h : ||\theta_f|| \leq m_{\theta_f}\} \\ M_{\theta_g} &= \{\theta_g \in R^h : ||\theta_g|| \leq m_{\theta_g}\} \end{aligned} \tag{6.49}$$

with m_{θ_f} and m_{θ_g} positive constants. The values of θ_f and θ_g for which optimal approximation is achieved are:

$$\begin{aligned} \theta_f^* &= arg\ min_{\theta_f \in M_{\theta_f}} [sup_{x \in U_x, \hat{x} \in U_{\hat{x}}} |f(x) - \hat{f}(\hat{x}|\theta_f)|] \\ \theta_g^* &= arg\ min_{\theta_g \in M_{\theta_g}} [sup_{x \in U_x, \hat{x} \in U_{\hat{x}}} |g(x) - \hat{g}(\hat{x}|\theta_g)|] \end{aligned}$$

The variation ranges of x and $\hat{x}$ are the compact sets

$$\begin{aligned} U_x &= \{x \in R^n : ||x|| \leq m_x < \infty\}, \\ U_{\hat{x}} &= \{\hat{x} \in R^n : ||\hat{x}|| \leq m_{\hat{x}} < \infty\} \end{aligned} \tag{6.50}$$

The approximation error of $f(x, t)$ and $g(x, t)$ is given by

$$\begin{aligned} w = [\hat{f}(\hat{x}|\theta_f^*) - f(x, t)] + [\hat{g}(\hat{x}|\theta_g^*) - g(x, t)]u \Rightarrow \\ w = \{[\hat{f}(\hat{x}|\theta_f^*) - f(x|\theta_f^*)] + [f(x|\theta_f^*) - f(x, t)]\} + \\ \{[\hat{g}(\hat{x}|\theta_g^*) - g(\hat{x}|\theta_g^*)] + [g(\hat{x}|\theta_g^*)g(x, t)]\}u \end{aligned} \tag{6.51}$$

where

- $\hat{f}(\hat{x}|\theta_f^*)$ is the approximation of f for the best estimation θ_f^* of the weights' vector θ_f.
- $\hat{g}(\hat{x}|\theta_g^*)$ is the approximation of g for the best estimation θ_g^* of the weights' vector θ_g.

The approximation error w can be decomposed into w_a and w_b, where

$$w_a = [\hat{f}(\hat{x}|\theta_f) - \hat{f}(\hat{x}|\theta_f^*)] + [\hat{g}(\hat{x}|\theta_g) - \hat{g}(\hat{x}|\theta_g^*)]u$$

$$w_b = [\hat{f}(\hat{x}|\theta_f^*) - f(x,t)] + [\hat{g}(\hat{x}|\theta_g^*) - g(x,t)]u$$

Finally, the following two parameters are defined:

$$\tilde{\theta}_f = \theta_f - \theta_f^*, \quad \tilde{\theta}_g = \theta_g - \theta_g^* \tag{6.52}$$

6.2.6 Lyapunov Stability Analysis

6.2.6.1 Design of the Lyapunov Function

The adaptation law of the neurofuzzy approximators' weights θ_f and θ_g as well as of the supervisory control term u_c for the microactuator's loop are derived from the requirement for negative definiteness of the Lyapunov function

$$V = \frac{1}{2}\hat{e}^T P_1 \hat{e} + \frac{1}{2}\tilde{e}^T P_2 \tilde{e} + \frac{1}{2\gamma_1}\tilde{\theta}_f^T \tilde{\theta}_f + \frac{1}{2\gamma_2}\tilde{\theta}_g^T \tilde{\theta}_g \tag{6.53}$$

The selection of the Lyapunov function relies on the following principle of indirect adaptive control $\hat{e} : \lim_{t\to\infty} \hat{x}(t) = x_d(t)$ and $\tilde{e} : \lim_{t\to\infty} \hat{x}(t) = x(t)$. This yields $\lim_{t\to\infty} x(t) = x_d(t)$. Substituting Eqs. (6.41), (6.42) and Eqs. (6.45), (6.46) into Eq. (6.53) and differentiating results into

$$\dot{V} = \frac{1}{2}\dot{\hat{e}}^T P_1 \hat{e} + \frac{1}{2}\hat{e}^T P_1 \dot{\hat{e}} + \frac{1}{2}\dot{\tilde{e}}^T P_2 \tilde{e} + \frac{1}{2}\tilde{e}^T P_2 \dot{\tilde{e}} + \frac{1}{\gamma_1}\tilde{\theta}_f^T \dot{\tilde{\theta}}_f + \frac{1}{\gamma_2}\tilde{\theta}_g^T \dot{\tilde{\theta}}_g \tag{6.54}$$

which in turn gives

$$\begin{gathered}\dot{V} = \tfrac{1}{2}\{(A - BK^T)\hat{e} + K_o C^T \tilde{e}\}^T P_1 \hat{e} + \tfrac{1}{2}\hat{e}^T P_1 \{(A - BK^T)\hat{e} + K_o C^T \tilde{e}\} + \\ + \tfrac{1}{2}\{(A - K_o C^T)\tilde{e} + Bu_c + Bd + Bw\}^T P_2 \tilde{e} + \tfrac{1}{2}\tilde{e}^T P_2 \{(A - K_o C^T)\tilde{e} + Bu_c + Bd + Bw\} + \\ + \tfrac{1}{\gamma_1}\tilde{\theta}_f^T \dot{\tilde{\theta}}_f + \tfrac{1}{\gamma_2}\tilde{\theta}_g^T \dot{\tilde{\theta}}_g\end{gathered} \tag{6.55}$$

or, equivalently

$$\begin{gathered}\dot{V}=\tfrac{1}{2}\{\hat{e}^T(A-BK^T)^T+\tilde{e}^TCK_o^T\}P_1\hat{e}+\tfrac{1}{2}\hat{e}^TP_1\{(A-BK^T)\hat{e}+K_oC^T\tilde{e}\}+\\+\tfrac{1}{2}\{\tilde{e}^T(A-K_oC^T)^T+B^Tu_c+B^Tw+B^Td\}P_2\tilde{e}+\tfrac{1}{2}\tilde{e}^TP_2\{(A-K_oC^T)\tilde{e}+Bu_c+Bw+Bd\}+\\+\tfrac{1}{\gamma_1}\tilde{\theta}_f^T\dot{\tilde{\theta}}_f+\tfrac{1}{\gamma_2}\tilde{\theta}_g^T\dot{\tilde{\theta}}_g\end{gathered}\tag{6.56}$$

$$\begin{gathered}\dot{V}=\tfrac{1}{2}\hat{e}^T(A-BK^T)^TP_1\hat{e}+\tfrac{1}{2}\tilde{e}^TCK_o^TP_1\hat{e}++\tfrac{1}{2}\hat{e}^TP_1(A-BK^T)\hat{e}+\tfrac{1}{2}\hat{e}^TP_1K_oC^T\tilde{e}+\\+\tfrac{1}{2}\tilde{e}^T(A-K_oC^T)^TP_2\tilde{e}+\tfrac{1}{2}B^TP_2\tilde{e}(u_c+w+d)+\tfrac{1}{2}\tilde{e}^TP_2(A-K_oC^T)\tilde{e}+\\+\tfrac{1}{2}\tilde{e}^TP_2B(u_c+w+d)+\tfrac{1}{\gamma_1}\tilde{\theta}_f^T\dot{\tilde{\theta}}_f+\tfrac{1}{\gamma_2}\tilde{\theta}_g^T\dot{\tilde{\theta}}_g\end{gathered}\tag{6.57}$$

Assumption 1: For given positive definite matrices Q_1 and Q_2 there exist positive definite matrices P_1 and P_2, which are the solution of the following Riccati equations [457]

$$(A-BK^T)^TP_1+P_1(A-BK^T)+Q_1=0\tag{6.58}$$

$$\begin{gathered}(A-K_oC^T)^TP_2+P_2(A-K_oC^T)-\\-P_2B(\tfrac{2}{r}-\tfrac{1}{\rho^2})B^TP_2+Q_2=0\end{gathered}\tag{6.59}$$

The conditions given in Eqs. (6.58)–(6.59) are related to the requirement that the systems described by Eqs. (6.43), (6.44) and Eqs. (6.45), (6.46) become asymptotically stable. Substituting Eqs. (6.58)–(6.59) into $\dot{V}$ yields

$$\begin{gathered}\dot{V}=\tfrac{1}{2}\hat{e}^T\{(A-BK^T)^TP_1+P_1(A-BK^T)\}\hat{e}+\tilde{e}^TCK_o^TP_1\hat{e}+\\+\tfrac{1}{2}\tilde{e}^T\{(A-K_oC^T)^TP_2+P_2(A-K_oC^T)\}\tilde{e}+B^TP_2\tilde{e}(u_c+w+d)+\\+\tfrac{1}{\gamma_1}\tilde{\theta}_f^T\dot{\tilde{\theta}}_f+\tfrac{1}{\gamma_2}\tilde{\theta}_g^T\dot{\tilde{\theta}}_g\end{gathered}\tag{6.60}$$

which is also written as

$$\begin{gathered}\dot{V}=-\tfrac{1}{2}\hat{e}^TQ_1\hat{e}+\tilde{e}^TCK_o^TP_1\hat{e}-\\-\tfrac{1}{2}\tilde{e}^T\{Q_2-P_2B(\tfrac{2}{r}-\tfrac{1}{\rho^2})B^TP_2\}\tilde{e}+B^TP_2\tilde{e}(u_c+w+d)+\\+\tfrac{1}{\gamma_1}\tilde{\theta}_f^T\dot{\tilde{\theta}}_f+\tfrac{1}{\gamma_2}\tilde{\theta}_g^T\dot{\tilde{\theta}}_g\end{gathered}\tag{6.61}$$

Following the concept analyzed in Chapter 3, the supervisory control u_c is decomposed in two terms, u_a and u_b

$$u_a=-\frac{1}{r}p_{1n}\tilde{e}_1=-\frac{1}{r}\tilde{e}^TP_2B+\frac{1}{r}(p_{2n}\tilde{e}_2+\cdots+p_{nn}\tilde{e}_n)=-\frac{1}{r}\tilde{e}^TP_2B+\Delta u_a\tag{6.62}$$

where p_{1n} stands for the last (n-th) element of the first row of matrix P_2, and

$$u_b = -[(P_2B)^T(P_2B)]^{-1}(P_2B)^T C K_o^T P_1 \hat{e} \tag{6.63}$$

- u_a is an H_∞ control used for the compensation of the approximation error w and the additive disturbance $\tilde{d}$. Its first component $-\frac{1}{r}\tilde{e}^T P_2 B$ has been chosen so as to compensate for the term $\frac{1}{r}\tilde{e}^T P_2 B B^T P_2 \tilde{e}$, which appears in Eq. (6.61). By subtracting the second component $-\frac{1}{r}(p_{2n}\tilde{e}_2 + \cdots + p_{nn}\tilde{e}_n)$ one has that $u_a = -\frac{1}{r} p_{1n}\tilde{e}_1$, which means that u_a is computed based on the feedback of the measurable variable $\tilde{e}_1$. Eq. (6.62) is finally rewritten as $u_a = -\frac{1}{r}\tilde{e}^T P_2 B + \Delta u_a$.
- u_b is a control used for the compensation of the observation error (the control term u_b has been chosen so as to satisfy the condition $\tilde{e}^T P_2 B u_b = -\tilde{e}^T C K_o^T P_1 \hat{e}$.

The control scheme is depicted in Fig. 6.3. Substituting Eqs. (6.62) and (6.63) in $\dot{V}$, one gets

$$\begin{gathered}\dot{V} = -\frac{1}{2}\hat{e}^T Q_1 \hat{e} + \tilde{e}^T C K_o^T P_1 \hat{e} - \frac{1}{2}\tilde{e}^T Q_2 \tilde{e} + \frac{1}{r}\tilde{e}^T P_2 B B^T P_2 \tilde{e} - \\ -\frac{1}{2\rho^2}\tilde{e}^T P_2 B B^T P_2 \tilde{e} + \tilde{e}^T P_2 B u_b - \frac{1}{r}\tilde{e}^T P_2 B B^T P_2 \tilde{e} + B^T P_2 \tilde{e}(w + d + \Delta u_a) + \\ + \frac{1}{\gamma_1}\tilde{\theta}_f^T \dot{\tilde{\theta}}_f + \frac{1}{\gamma_2}\tilde{\theta}_g^T \dot{\tilde{\theta}}_g\end{gathered} \tag{6.64}$$

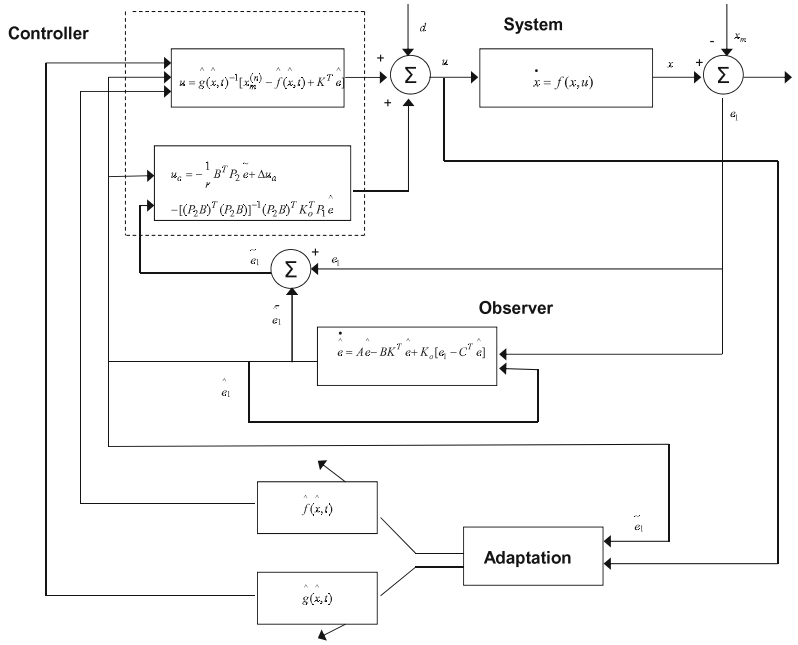

Fig. 6.3 The proposed adaptive-fuzzy control scheme

or equivalently,

$$\dot{V} = -\frac{1}{2}\hat{e}^T Q_1 \hat{e} - \frac{1}{2}\tilde{e}^T Q_2 \tilde{e} - \frac{1}{2\rho^2}\tilde{e}^T P_2 B B^T P_2 \tilde{e} + B^T P_2 \tilde{e}(w + d + \Delta u_a) + \\ + \frac{1}{\gamma_1}\tilde{\theta}_f^T \dot{\tilde{\theta}}_f + \frac{1}{\gamma_2}\tilde{\theta}_g^T \dot{\tilde{\theta}}_g \tag{6.65}$$

It holds that $\dot{\tilde{\theta}}_f = \dot{\theta}_f - \dot{\theta}_f^* = \dot{\theta}_f$ and $\dot{\tilde{\theta}}_g = \dot{\theta}_g - \dot{\theta}_g^* = \dot{\theta}_g$. The following weight adaptation laws are considered:

$$\dot{\theta}_f = \begin{cases} -\gamma_1 \tilde{e}^T P_2 B \phi(\hat{x}) \;\; if \;\; ||\theta_f|| < m_{\theta_f} \\ 0 \;\; ||\theta_f|| \geq m_{\theta_f} \end{cases} \tag{6.66}$$

$$\dot{\theta}_g = \begin{cases} -\gamma_2 \tilde{e}^T P_2 B \phi(\hat{x}) u_c \;\; if \;\; ||\theta_g|| < m_{\theta_g} \\ 0 \;\; ||\theta_g|| \geq m_{\theta_g} \end{cases} \tag{6.67}$$

To set $\dot{\theta}_f$ and $\dot{\theta}_g$ equal to 0, when $||\theta_f \geq m_{\theta_f}||$, and $||\theta_g \geq m_{\theta_g}||$ the projection operator is employed [450]:

$$P\{\gamma_1 \tilde{e}^T P_2 B \phi(\hat{x})\} = -\gamma_1 \tilde{e}^T P_2 B \phi(\hat{x}) + \\ + \gamma_1 \tilde{e}^T P_2 B \frac{\theta_f \theta_f^T}{||\theta_f||^2} \phi(\hat{x})$$

$$P\{\gamma_1 \tilde{e}^T P_2 B \phi(\hat{x}) u_c\} = -\gamma_1 \tilde{e}^T P_2 B \phi(\hat{x}) u_c + \\ + \gamma_1 \tilde{e}^T P_2 B \frac{\theta_f \theta_f^T}{||\theta_f||^2} \phi(\hat{x}) u_c$$

The update of θ_f stems from a gradient algorithm on the cost function $\frac{1}{2}(f - \hat{f})^2$ [33, 432]. The update of θ_g is also of the gradient type, while u_c implicitly tunes the adaptation gain γ_2. Substituting Eqs. (6.66) and (6.67) in $\dot{V}$ gives

$$\dot{V} = -\frac{1}{2}\hat{e}^T Q_1 \hat{e} - \frac{1}{2}\tilde{e}^T Q_2 \tilde{e} - \frac{1}{2\rho^2}\tilde{e}^T P_2 B B^T P_2 \tilde{e} + B^T P_2 \tilde{e}(w + d + \Delta u_a) + \\ + \frac{1}{\gamma_1}\tilde{\theta}_f^T(-\gamma_1 \tilde{e}^T P_2 B \phi(\hat{x})) + \frac{1}{\gamma_2}\tilde{\theta}_g^T(-\gamma_2 \tilde{e}^T P_2 B \phi(\hat{x}) u) \tag{6.68}$$

which is also written as

$$\dot{V} = -\frac{1}{2}\hat{e}^T Q_1 \hat{e} - \frac{1}{2}\tilde{e}^T Q_2 \tilde{e} - \frac{1}{2\rho^2}\tilde{e}^T P_2 B B^T P_2 \tilde{e} + \tilde{e}^T P_2 B(w + d + \Delta u_a) - \\ - \tilde{e}^T P_2 B \tilde{\theta}_f^T \phi(\hat{x}) - \tilde{e}^T P_2 B \tilde{\theta}_g^T \phi(\hat{x}) u \tag{6.69}$$

and using Eqs. (6.48) and (6.52) results into

$$\dot{V} = -\frac{1}{2}\hat{e}^T Q_1 \hat{e} - \frac{1}{2}\tilde{e}^T Q_2 \tilde{e} - \frac{1}{2\rho^2}\tilde{e}^T P_2 B B^T P_2 \tilde{e} + \tilde{e}^T P_2 B(w + d + \Delta u_a) - \\ - \tilde{e}^T P_2 B\{[\hat{f}(\hat{x}|\theta_f) + \hat{g}(\hat{x}|\theta_f) u] - [\hat{f}(\hat{x}|\theta_f^*) + \hat{g}(\hat{x}|\theta_g^*) u]\} \tag{6.70}$$

where $[\hat{f}(\hat{x}|\theta_f) + \hat{g}(\hat{x}|\theta_f)u] - [\hat{f}(\hat{x}|\theta_f^*) + \hat{g}(\hat{x}|\theta_g^*)u] = w_a$. Thus setting $w_1 = w + w_a + d + \Delta u_a$ one gets

$$\begin{aligned} \dot{V} &= -\tfrac{1}{2}\hat{e}^T Q_1 \hat{e} \tfrac{1}{2}\tilde{e}^T Q_2 \tilde{e} - \tfrac{1}{2\rho^2}\tilde{e}^T P_2 B B^T P_2 \tilde{e} + B^T P_2 \tilde{e} w_1 \Rightarrow \\ \dot{V} &= -\tfrac{1}{2}\hat{e}^T Q_1 \hat{e} \tfrac{1}{2}\tilde{e}^T Q_2 \tilde{e} - \tfrac{1}{2\rho^2}\tilde{e}^T P_2 B B^T P_2 \tilde{e} + \tfrac{1}{2} w_1^T B^T P_2 \tilde{e} + \tfrac{1}{2}\tilde{e}^T P_2 B w_1 \end{aligned} \tag{6.71}$$

Lemma: The following inequality holds

$$\tfrac{1}{2}\tilde{e}^T P_2 B w_1 + \tfrac{1}{2} w_1^T B^T P_2 \tilde{e} - \tfrac{1}{2\rho^2}\tilde{e}^T P_2 B B^T P_2 \tilde{e} \le \tfrac{1}{2}\rho^2 w_1^T w_1 \tag{6.72}$$

Proof: The binomial $(\rho a - \frac{1}{\rho} b)^2 \ge 0$ is considered. Expanding the left part of the above inequality one gets

$$\begin{aligned} &\rho^2 a^2 + \tfrac{1}{\rho^2} b^2 - 2ab \ge 0 \Rightarrow \tfrac{1}{2}\rho^2 a^2 + \tfrac{1}{2\rho^2} b^2 - ab \ge 0 \\ &\Rightarrow ab - \tfrac{1}{2\rho^2} b^2 \le \tfrac{1}{2}\rho^2 a^2 \Rightarrow \tfrac{1}{2}ab + \tfrac{1}{2}ab - \tfrac{1}{2\rho^2} b^2 \le \tfrac{1}{2}\rho^2 a^2 \end{aligned} \tag{6.73}$$

The following substitutions are carried out: $a = w_1$ and $b = \tilde{e}^T P_2 B$ and the previous relation becomes

$$\begin{aligned} &\tfrac{1}{2} w_1^T B^T P_2 \tilde{e} + \tfrac{1}{2}\tilde{e}^T P_2 B w_1 - \tfrac{1}{2\rho^2}\tilde{e}^T P_2 B B^T P_2 \tilde{e} \\ &\le \tfrac{1}{2}\rho^2 w_1^T w_1 \end{aligned} \tag{6.74}$$

The above inequality is used in $\dot{V}$, and the right part of the associated inequality is enforced

$$\dot{V} \le -\frac{1}{2}\hat{e}^T Q_1 \hat{e} - \frac{1}{2}\tilde{e}^T Q_2 \tilde{e} + \frac{1}{2}\rho^2 w_1^T w_1 \tag{6.75}$$

Thus, Eq. (6.75) can be written as

$$\dot{V} \le -\frac{1}{2} E^T Q E + \frac{1}{2}\rho^2 w_1^T w_1 \tag{6.76}$$

where

$$E = \begin{pmatrix} \hat{e} \\ \tilde{e} \end{pmatrix}, \quad Q = \begin{pmatrix} Q_1 & 0 \\ 0 & Q_2 \end{pmatrix} = diag[Q_1, Q_2] \tag{6.77}$$

Hence, the H_∞ performance criterion is derived. For ρ sufficiently small Eq. (6.75) will be true and the H_∞ tracking criterion will be satisfied. In that case, the integration of $\dot{V}$ from 0 to T gives

$$\int_0^T \dot{V}(t)dt \leq -\frac{1}{2}\int_0^T ||E||^2 dt + \frac{1}{2}\rho^2 \int_0^T ||w_1||^2 dt \Rightarrow$$
$$2V(T) - 2V(0) \leq -\int_0^T ||E||_Q^2 dt + \rho^2 \int_0^T ||w_1||^2 dt \Rightarrow$$
$$2V(T) + \int_0^T ||E||_Q^2 dt \leq 2V(0) + \rho^2 \int_0^T ||w_1||^2 dt$$

It is assumed that there exists a positive constant $M_w > 0$ such that $\int_0^\infty ||w_1||^2 dt \leq M_w$. Therefore for the integral $\int_0^T ||E||_Q^2 dt$ one gets

$$\int_0^\infty ||E||_Q^2 dt \leq 2V(0) + \rho^2 M_w \tag{6.78}$$

Thus, the integral $\int_0^\infty ||E||_Q^2 dt$ is bounded and according to Barbalat's Lemma

$$\lim_{t\to\infty} E(t) = 0 \Rightarrow \begin{matrix} \lim_{t\to\infty} \hat{e}(t) = 0 \\ \lim_{t\to\infty} \tilde{e}(t) = 0 \end{matrix}$$

Therefore $\lim_{t\to\infty} e(t) = 0$.

6.2.6.2 Riccati Equation Coefficients in H_∞ Control Robustness

Following the concept of the flatness-based adaptive fuzzy control which has been developed in previous sections, the linear system of Eqs. (6.45) and (6.46) is considered again

$$\dot{\tilde{e}} = (A - K_o C^T)\tilde{e} + Bu_c + B\{[f(x,t) - \hat{f}(\hat{x},t)] + [g(x,t) - \hat{g}(\hat{x},t)]u + \tilde{d}\}$$
$$e_1 = C^T \tilde{e}$$

Once again the aim of H_∞ control is to eliminate the impact of the modelling errors $w = [f(x,t) - \hat{f}(\hat{x},t)] + [g(x,t) - \hat{g}(\hat{x},t)]u$ and the external disturbances $\tilde{d}$ which are not white noise signals. This implies the minimization of the following quadratic cost function for the microactuator's state vector tracking problem [132, 243, 305]:

$$J(t) = \frac{1}{2}\int_0^T [\tilde{e}^T(t)\tilde{e}(t) + ru_c^T(t)u_c(t) - \rho^2(w + \tilde{d})^T(w + \tilde{d})]dt, \quad r, \rho > 0 \tag{6.79}$$

The weight r determines how much the control signal should be penalized and the weight ρ determines how much the disturbances influence should be rewarded in the sense of a min-max differential game. The control input u_c has been defined as the sum of the terms described in Eqs. (6.62) and (6.63).

The parameter ρ in Eq. (6.79), is an indication of the closed-loop system robustness. If the values of $\rho > 0$ are excessively decreased with respect to r, then the

solution of the Riccati equation is no longer a positive definite matrix. Consequently there is a lower bound ρ_{min} of ρ for which the H_∞ control problem has a solution. The acceptable values of ρ lie in the interval $[\rho_{min}, \infty)$. If ρ_{min} is found and used in the design of the H_∞ controller, then the closed-loop system will have increased robustness. Unlike this, if a value $\rho > \rho_{min}$ is used, then an admissible stabilizing H_∞ controller will be derived but it will be a suboptimal one. The Hamiltonian matrix

$$H = \begin{pmatrix} A - K_o C^T & -(\frac{2}{r} - \frac{1}{\rho^2}) B B^T \\ -Q & -(A - K_o C^T)^T \end{pmatrix} \tag{6.80}$$

provides a criterion for the existence of a solution of the Riccati equation Eq. (6.59). A necessary condition for the solution of the algebraic Riccati equation to be a positive semi-definite symmetric matrix is that H has no imaginary eigenvalues [132, 457].

6.2.7 Simulation Tests

The performance of the proposed output feedback-based adaptive fuzzy control approach for MEMS (microactuator) was tested in the case of tracking of several reference setpoints. The only measurable variable, used in the control loop was the microactuator's deflection variable x. Indicative variation ranges for the MEMS parameters are $\zeta \in [0.1, 3]$ and $r \in [0.1, 3]$ without excluding that these parameters may take values in wider intervals. In the simulation tests, the dynamic model of the MEMS, as well as the numerical values of its parameters were considered to be completely unknown.

The estimation of the unknown dynamics of the system with the use of neuro-fuzzy approximators has been explained in Sect. 6.2.5.6. Knowing that there are $i = 3$ state variables for the MEMS model and that each such variable comprises $n = 3$ fuzzy sets, the total number of rules in the fuzzy rule base should be $n^m = 3^3 = 27$. The aggregate output of the neuro-fuzzy approximator (rule-base) for function $f(x)$ is given by Eq. (6.47). The centers $c_i^{(l)}$, $i = 1, \ldots, 3$ and the variances $v^{(l)}$ of each rule are summarized in Table 6.1. Similar is the structure of the neuro-fuzzy approximator for function $g(x)$.

The control loop was based on simultaneous estimation of the unknown MEMS dynamics (this was performed with the use of neuro-fuzzy approximators) and of the nonmeasurable elements of the microactuator's state vector, that is of the deflections change rate $\dot{x}$ and of the charge of the plates q (this was performed with the use of the state observer). The obtained results are presented in Figs. 6.4, 6.5, 6.6, 6.7 and 6.8. The real values of the monitored parameters (state vector variables) are denoted with blue line, the estimated variables are denoted with green line and the reference setpoints are plotted as red lines. It can be noticed that differential flatness theory-based adaptive fuzzy control of the MEMS, achieved fast and accurate tracking of the reference setpoints.

Table 6.1 Table I: Parameters of the fuzzy rule base

Rule	$c_1^{(l)}$	$c_2^{(l)}$	$c_3^{(l)}$	$v^{(l)}$
$R^{(1)}$	-1.0	-1.0	-1.0	3
$R^{(2)}$	-1.0	-1.0	0.0	3
$R^{(3)}$	-1.0	-1.0	1.0	3
$R^{(4)}$	-1.0	0.0	-1.0	3
$R^{(5)}$	-1.0	0.0	0.0	3
$R^{(6)}$	-1.0	0.0	1.0	3
...	...	...	...	...
...	...	...	...	...
$R^{(27)}$	1.0	1.0	1.0	3

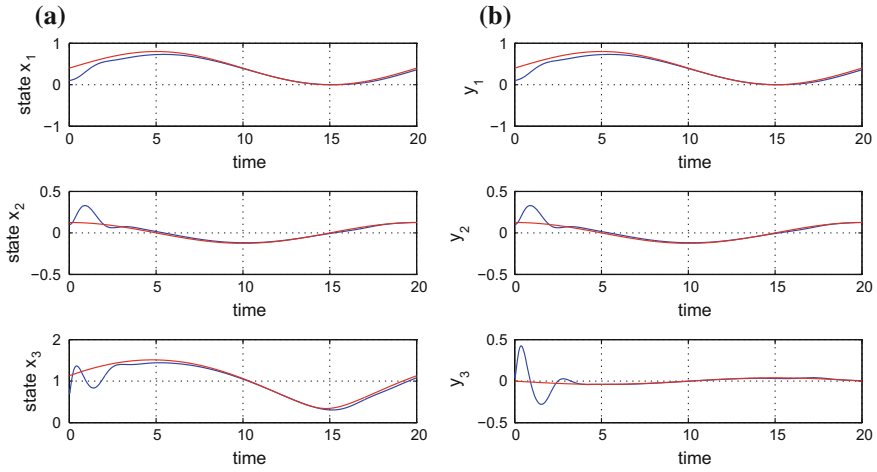

Fig. 6.4 Output feedback based adaptive fuzzy control of MEMS (microactuator) - Test 1: **a** state variables x_i, $i = 1, \ldots, 3$ of the initial nonlinear system, **b** transformed state variables y_i, $i = 1, \ldots, 3$ (blue line: real value, red line: setpoint)

The implementation of the proposed control scheme requires that the two algebraic Riccati equations which have been defined in Eqs. (6.58) and (6.59) are solved in each iteration of the control algorithm. These provide the positive definite matrices P_1 and P_2 which are used for the computation of the control signals u_a and u_b that have been defined in Eqs. (6.62) and (6.63). The transients of the state vector elements x_i, $i = 1, \ldots, 3$, are determined by the values given to the positive definite matrices Q_i, $i = 1, \ldots, 3$, as well as by the value of the parameter r and of the H-infinity coefficient (attenuation level) ρ. It has been confirmed that the variations of both x_i, $i = 1, \ldots, 3$ and of the control input u were smooth.

One can compare the proposed adaptive fuzzy control method for the electromechanically actuated MEMS against model-based control methods based on the approximate linearization of MEMS. The latter method consists of local

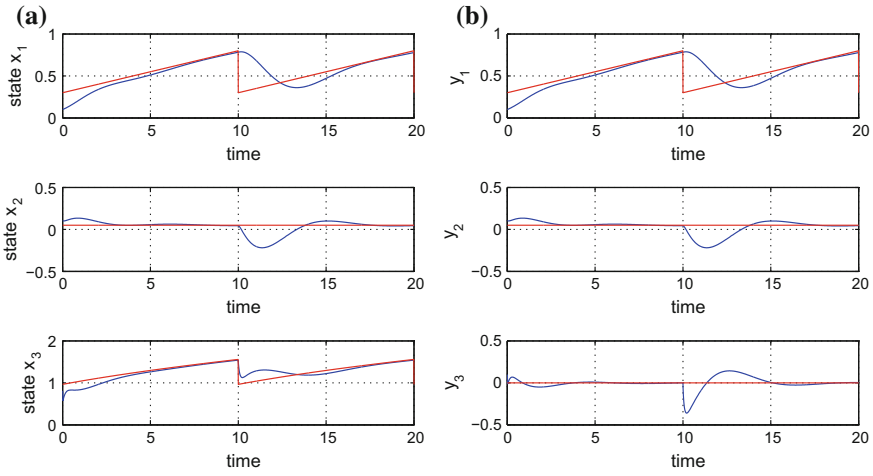

Fig. 6.5 Output feedback based adaptive fuzzy control of MEMS (microactuator) - Test 2: **a** state variables x_i, $i = 1, \ldots, 3$ of the initial nonlinear system, **b** transformed state variables y_i, $i = 1, \ldots, 3$ (blue line: real value, red line: setpoint)

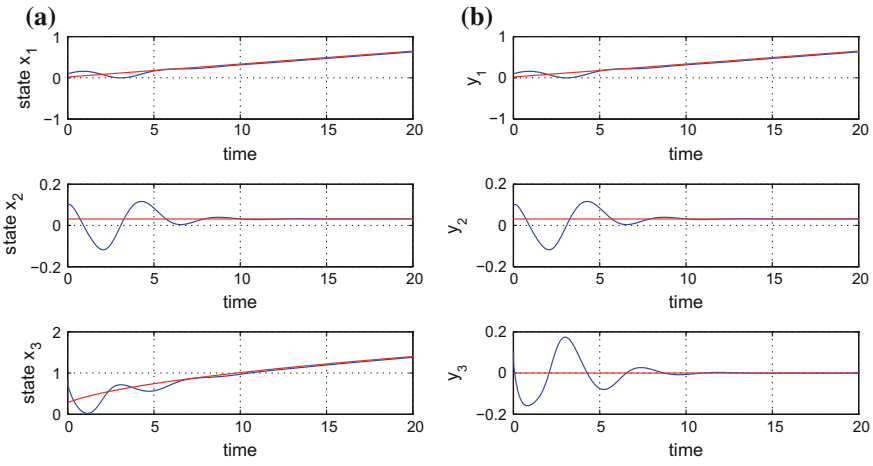

Fig. 6.6 Output feedback based adaptive fuzzy control of MEMS (microactuator) - Test 3: **a** state variables x_i, $i = 1, \ldots, 3$ of the initial nonlinear system, **b** transformed state variables y_i, $i = 1, \ldots, 3$ (blue line: real value, red line: setpoint)

linearization of the MEMS model round operating points and on the solution of LMIs and remains dependent on knowledge of the MEMS dynamics. In [456], it has been shown that although the proposed adaptive control scheme uses no prior knowledge about the system's dynamics it performs equally well to the aforemen-

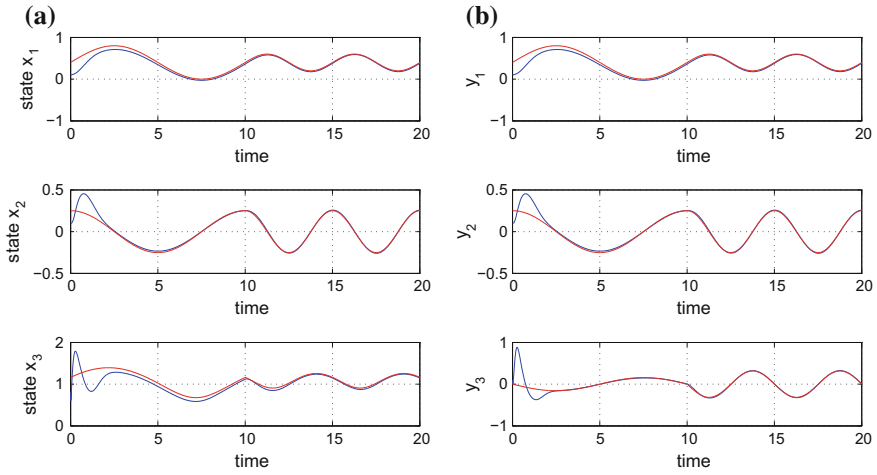

Fig. 6.7 Output feedback based adaptive fuzzy control of MEMS (microactuator) - Test 4: **a** state variables x_i, $i = 1, \ldots, 3$ of the initial nonlinear system, **b** transformed state variables y_i, $i = 1, \ldots, 3$ (blue line: real value, red line: setpoint)

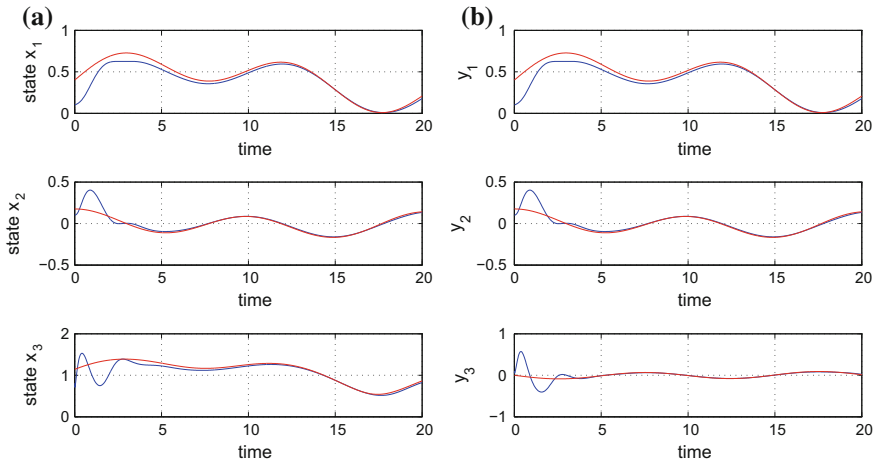

Fig. 6.8 Output feedback based adaptive fuzzy control of MEMS (microactuator) - Test 5: **a** state variables x_i, $i = 1, \ldots, 3$ of the initial nonlinear system, **b** transformed state variables y_i, $i = 1, \ldots, 3$ (blue line: real value, red line: setpoint)

tioned model-based control approach. The associated simulation results about the comparison of the two methods can be found in [456].

6.3 Nonlinear Optimal Control of Underactuated MEMS

6.3.1 Outline

Extending the analysis on the dynamics of microactuators that was given in the previous section, one can consider next micro-electromechanical systems (MEMS) which exhibit often the dynamics of nonlinear oscillators such as the Van-der-Pol oscillator and the Duffing oscillator [214, 215, 407, 409]. In certain cases these oscillator models are coupled and are described for instance by a Van-der-Pol oscillator driven by a forced Duffing oscillator [138, 266, 376, 579]. Such micro-electromechanical systems can exhibit complex and chaotic dynamics [29, 265, 339, 383]. In an aim to improve the precision and reliability of MEMS, nonlinear control of MEMS has been the subject of wide research during the last years [184, 336, 368, 384, 496]. However, taking into account the nonlinearities of their dynamic model and possible underactuation, the problem of control of these micro-electromechanical systems is considered as a non-trivial one [96, 120, 296, 338].

In this section a nonlinear optimal (H-infinity) control method is developed for the model of a MEMS described in the form of a Van-der-Pol oscillator elastically coupled with a forced Duffing oscillator. This MEMS receives control input only at the side of the Duffing oscillator. The MEMS dynamic model undergoes first approximate linearization around a temporary operating point (equilibrium) which is redefined at each iteration of the control method. This temporary equilibrium comprises the present value of the system's state vector and the last value of the control inputs vector that was applied on it. The linearization makes use of first-order Taylor series expansion and requires the computation of the system's Jacobian matrices [33, 431, 463] . The modelling error which is due to the truncation of higher order terms in the Taylor series expansion is considered to be a disturbance term which is finally compensated by the robustness of the control algorithm.

For the approximately linearized model of the MEMS an optimal (H-infinity) feedback controller is designed [461, 466]. As explained in the previous sections, the H-infinity controller represents the solution to the optimal control problem under model uncertainty and external perturbations. Actually, the H-infinity controller stands for the solution to a min-max differential game in which the control inputs try to minimize a cost function comprising a quadratic term of the state vector's tracking error, whereas the model uncertainty and the disturbance inputs try to maximize it [450, 457, 459]. For the computation of the feedback gain of the H-infinity controller an algebraic Riccati equation is solved repetitively at each time-step of the control method
[305, 564].

The stability of the proposed nonlinear optimal control method is proven through Lyapunov analysis. First, it is demonstrated that the control loop satisfies the H-infinity tracking performance criterion, which signifies elevated robustness against model uncertainty and external perturbations. Moreover, under moderate conditions it is shown that the control scheme has also global asymptotic stability properties. Finally, to implement state estimation-based control of the MEMS through the mea-

surement of a small number of its state vector elements, the H-infinity Kalman Filter is proposed as a robust state estimator [169, 511].

6.3.2 Dynamic Model of MEMS

The dynamic model of the coupled MEMS comprises a Van der Pol oscillator driven by a forced Duffing oscillator (Fig. 6.9). The variation in time of the Van der Pol oscillator is given by state variable z_1 while the variation in time of the Duffing oscillator is given by state variable z_2. Moreover, the control input to the MEMS is the sinusoidal voltage $V = ucos(\frac{\omega_d}{\omega_1}\tau)$, and thus one has the following dynamics [266, 376]

$$\begin{aligned} \ddot{z}_1 + \gamma_2(z_1^2 - 1)\dot{z}_1 + \left(\frac{\omega_2}{\omega_1}\right)^2 z_1 &= k(z_2 - z_1) \\ \ddot{z}_2 + \gamma_2\dot{z}_2 + \delta z_2^3 &= (z_1 - z_2) + ucos\left(\frac{\omega_d}{\omega_1}\tau\right) \end{aligned} \tag{6.81}$$

The following state variables are defined $x_1 = z_1$, $x_2 = \dot{z}_1$, $x_2 = z_2$ and $x_4 = \dot{z}_2$. Then, the state-space description of the system is given by

$$\begin{aligned} \dot{x}_1 &= x_2 \\ \dot{x}_2 &= -\gamma_1(x_1^2 - 1)x_2 - \left(\frac{\omega_2}{\omega_1}\right)^2 x_1 + k(x_2 - x_1) \\ \dot{x}_3 &= x_4 \\ \dot{x}_4 &= -\gamma_2 x_4 - \delta x_3^2 + k(x_1 - x_3) + ucos\left(\frac{\omega_d}{\omega_1}\tau\right) \end{aligned} \tag{6.82}$$

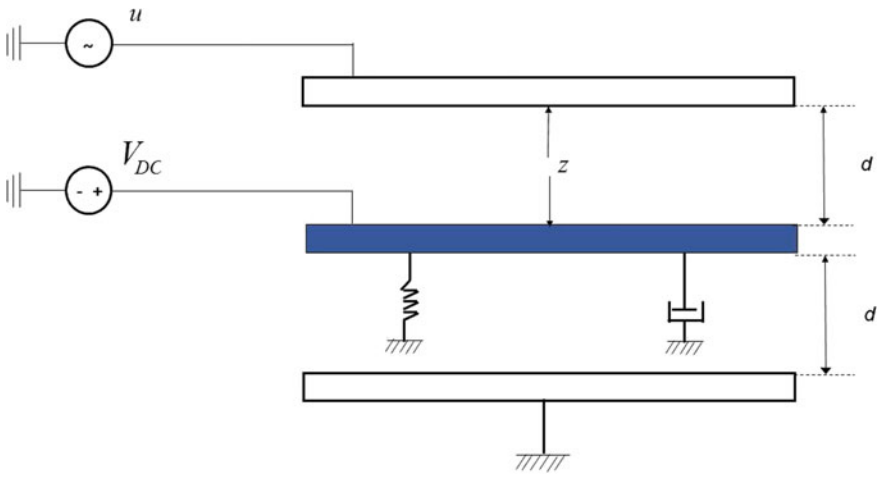

Fig. 6.9 Diagram of an electrostatically actuated MEMS, exhibiting the dynamics of a Duffing oscillator

Next, the system of the coupled Van der Pol and Duffing oscillators can be written in the following matrix form

$$\begin{pmatrix} \dot{x}_1 \\ \dot{x}_2 \\ \dot{x}_3 \\ \dot{x}_4 \end{pmatrix} = \begin{pmatrix} x_2 \\ -\gamma_1(x_1^2-1)x_2 - (\frac{\omega_2}{\omega_1})^2 x_1 + k(x_2 - x_1) \\ x_4 \\ \dot{x}_4 = -\gamma_2 x_4 - \delta x_3^2 + k(x_1 - x_3) \end{pmatrix} + \begin{pmatrix} 0 \\ 0 \\ 0 \\ cos(\frac{\omega_d}{\omega_1}\tau) \end{pmatrix} u \quad (6.83)$$

Thus by defining the vector fields $f(x)\ x \in R^{4\times 1}$ and $g(x)\ x \in R^{4\times 1}$ where

$$f(x) = \begin{pmatrix} x_2 \\ -\gamma_1(x_1^2-1)x_2 - (\frac{\omega_2}{\omega_1})^2 x_1 + k(x_2 - x_1) \\ x_4 \\ \dot{x}_4 = -\gamma_2 x_4 - \delta x_3^2 + k(x_1 - x_3) \end{pmatrix} g(x) = \begin{pmatrix} 0 \\ 0 \\ 0 \\ cos(\frac{\omega_d}{\omega_1}\tau) \end{pmatrix} u \quad (6.84)$$

one arrives at the states-space description

$$\dot{x} = f(x) + g(x)u \quad (6.85)$$

6.3.3 Approximate Linearization of the MEMS Dynamics

Approximate linearization of the MEMS dynamics given in Eq. (6.85) is performed around the temporary operating point (equilibrium) (x^*, u^*) which is re-defined at each iteration of the control algorithm by the present value of the system's state vector x^* and the last value of the control inputs vector u^* that was exerted on it. This results in the following linear state-space form of the system:

$$\dot{x} = Ax + Bu + \tilde{d} \quad (6.86)$$

where matrices A and B are defined as follows:

$$A = \nabla_x [f(x) + g(x)u] \mid_{(x^*,u^*)} \Rightarrow A = \nabla_x f(x) \mid_{(x^*)} \quad (6.87)$$

$$B = \nabla_u [f(x) + g(x)u] \mid_{(x^*,u^*)} \Rightarrow B = g(x) \quad (6.88)$$

About the Jacobian matrix $\nabla_x f(x) \mid_{(x^*)}$ one has

$$\nabla_x f(x) = \begin{pmatrix} \frac{\partial f_1}{\partial x_1} & \frac{\partial f_1}{\partial x_2} & \frac{\partial f_1}{\partial x_3} & \frac{\partial f_1}{\partial x_4} \\ \frac{\partial f_2}{\partial x_1} & \frac{\partial f_2}{\partial x_2} & \frac{\partial f_2}{\partial x_3} & \frac{\partial f_2}{\partial x_4} \\ \frac{\partial f_3}{\partial x_1} & \frac{\partial f_3}{\partial x_2} & \frac{\partial f_3}{\partial x_3} & \frac{\partial f_3}{\partial x_4} \\ \frac{\partial f_4}{\partial x_1} & \frac{\partial f_4}{\partial x_2} & \frac{\partial f_4}{\partial x_3} & \frac{\partial f_4}{\partial x_4} \end{pmatrix} \tag{6.89}$$

where the elements of the first row of $\nabla_x f(x)$ are: $\frac{\partial f_1}{\partial x_1} = 0$, $\frac{\partial f_1}{\partial x_2} = 1$, $\frac{\partial f_1}{\partial x_3} = 0$, and $\frac{\partial f_1}{\partial x_4} = 0$.

the elements of the second row of $\nabla_x f(x)$ are: $\frac{\partial f_2}{\partial x_1} = -\gamma_1 2x_1x_2 - (\frac{\omega_2}{\omega_1})^2 - k$, $\frac{\partial f_2}{\partial x_2} = -\gamma_1(x_1^2 - 1)$, $\frac{\partial f_2}{\partial x_3} = 1$, and $\frac{\partial f_2}{\partial x_4} = 0$.

the elements of the third row of $\nabla_x f(x)$ are: $\frac{\partial f_3}{\partial x_1} = 0$, $\frac{\partial f_3}{\partial x_2} = 0$, $\frac{\partial f_3}{\partial x_3} = 0$, and $\frac{\partial f_3}{\partial x_4} = 1$.

and the elements of the fourth row of $\nabla_x f(x)$ are: $\frac{\partial f_4}{\partial x_1} = k$, $\frac{\partial f_4}{\partial x_2} = 0$, $\frac{\partial f_4}{\partial x_3} = -2\delta x_3 - k$, and $\frac{\partial f_3}{\partial x_4} = -\gamma_1$.

6.3.4 Design of an H-Infinity Nonlinear Feedback Controller

6.3.4.1 Equivalent Linearized Dynamics of the MEMS

After linearization round its current operating point, the dynamic model of the MEMS is written as

$$\dot{x} = Ax + Bu + d_1 \tag{6.90}$$

Parameter d_1 stands for the linearization error in the dynamic model of the MEMS appearing in Eq. (6.90). The reference setpoints for the MEMS model state vector are denoted by $\mathbf{x_d} = [x_1^d, \ldots, x_6^d]$. Tracking of this trajectory is achieved after applying the control input u^*. At every time instant the control input u^* is assumed to differ from the control input u appearing in Eq. (6.90) by an amount equal to Δu, that is $u^* = u + \Delta u$

$$\dot{x}_d = Ax_d + Bu^* + d_2 \tag{6.91}$$

The dynamics of the controlled system described in Eq. (6.90) can be also written as

$$\dot{x} = Ax + Bu + Bu^* - Bu^* + d_1 \tag{6.92}$$

and by denoting $d_3 = -Bu^* + d_1$ as an aggregate disturbance term one obtains

$$\dot{x} = Ax + Bu + Bu^* + d_3 \tag{6.93}$$

By subtracting Eq. (6.91) from (6.93) one has

$$\dot{x} - \dot{x}_d = A(x - x_d) + Bu + d_3 - d_2 \tag{6.94}$$

By denoting the tracking error as $e = x - x_d$ and the aggregate disturbance term as $\tilde{d} = d_3 - d_2$, the tracking error dynamics becomes

$$\dot{e} = Ae + Bu + \tilde{d} \tag{6.95}$$

The above linearized form of the MEMS model can be efficiently controlled after applying an H-infinity feedback control scheme.

6.3.5 *The Nonlinear H-Infinity Control*

The initial nonlinear model of MEMS is in the form

$$\dot{x} = \tilde{f}(x, u) \;\; x \in R^n, \;\; u \in R^m \tag{6.96}$$

Linearization of the MEMS model that comprises coupled electromechanical oscillators is performed at each iteration of the control algorithm round its present operating point $(x^*, u^*) = (x(t), u(t - T_s))$, where T_s is the sampling period. The linearized equivalent model of the system is described by

$$\dot{x} = Ax + Bu + L\tilde{d} \;\; x \in R^n, \;\; u \in R^m, \;\; \tilde{d} \in R^q \tag{6.97}$$

where matrices A and B are obtained from the computation of the Jacobians of the MEMS model, and vector $\tilde{d}$ denotes disturbance terms due to linearization errors. The problem of disturbance rejection for the MEMS linearized model that is described by

$$\begin{aligned} \dot{x} &= Ax + Bu + L\tilde{d} \\ y &= Cx \end{aligned} \tag{6.98}$$

where $x \in R^n$, $u \in R^m$, $\tilde{d} \in R^q$ and $y \in R^p$, cannot be handled efficiently if the classical LQR control scheme is applied. This is because of the existence of the perturbation term $\tilde{d}$. The disturbance term $\tilde{d}$ apart from modeling (parametric) uncertainty and external perturbation terms can also represent noise terms of any distribution.

As explained in the application of the control method in previous sections, in the H_∞ control approach, a feedback control scheme is designed for trajectory tracking by the MEMS state vector and simultaneous disturbance rejection, considering that the disturbance affects the system in the worst possible manner. The disturbances' effects are incorporated in the following quadratic cost function:

$$J(t) = \frac{1}{2}\int_0^T [y^T(t)y(t) + ru^T(t)u(t) - \rho^2 \tilde{d}^T(t)\tilde{d}(t)]dt, \quad r, \rho > 0 \tag{6.99}$$

As mentioned in previous chapters, the significance of the negative sign in the cost function for the MEMS control loop is that this is associated with the perturbation variable $\tilde{d}(t)$ is that the disturbance tries to maximize the cost function $J(t)$ while the control signal $u(t)$ tries to minimize it. The physical meaning of the relation given above is that the control signal and the disturbances compete to each other within a min-max differential game. This problem of min-max optimization can be written as

$$min_u max_{\tilde{d}} J(u, \tilde{d}) \tag{6.100}$$

The objective of the optimization procedure is to compute a control signal $u(t)$ which can compensate for the worst possible disturbance, that is externally imposed to the MEMS. As explained in previous sections, the solution to the mini-max optimization problem is directly related to the value of the parameter ρ. This means that there is an upper bound in the disturbances magnitude that can be annihilated by the control signal.

6.3.5.1 Computation of the Feedback Control Gains

For the linearized model of the MEMS given by Eq. (6.98) the cost function of Eq. (6.99) is defined, where the coefficient r determines the penalization of the control input and the weight coefficient ρ determines the reward of the disturbances' effects.

In adherence to the analysis of the control method given in previous sections, it is assumed again that (i) The energy that is transferred from the disturbances signal $\tilde{d}(t)$ is bounded, that is $\int_0^\infty \tilde{d}^T(t)\tilde{d}(t)dt < \infty$, (ii) matrices $[A, B]$ and $[A, L]$ are stabilizable, (iii) matrix $[A, C]$ is detectable. Then, the optimal feedback control law is given by

$$u(t) = -Kx(t) \tag{6.101}$$

with

$$K = \frac{1}{r}B^T P \tag{6.102}$$

where P is a positive semi-definite symmetric matrix which is obtained from the solution of the Riccati equation

$$A^T P + PA + Q - P\left(\frac{1}{r}BB^T - \frac{1}{2\rho^2}LL^T\right)P = 0 \tag{6.103}$$

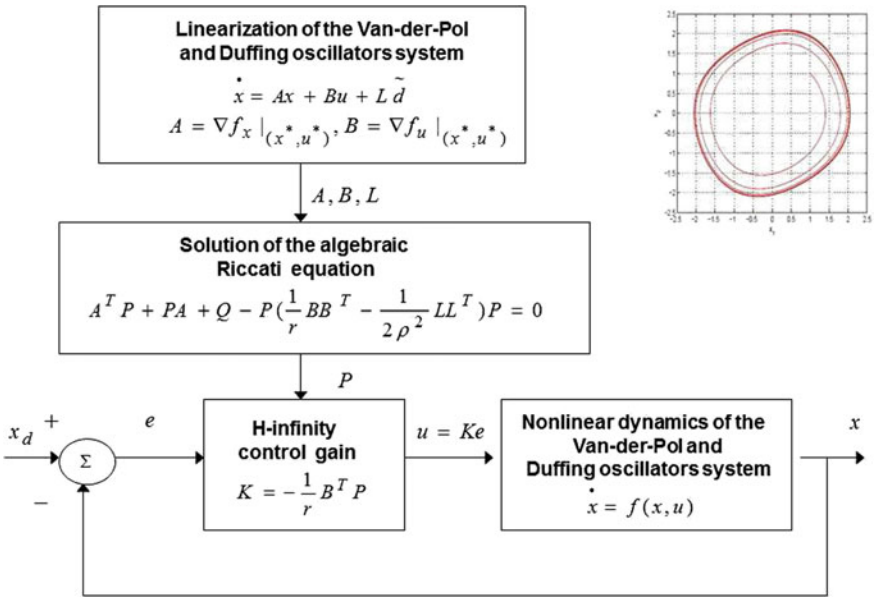

Fig. 6.10 Diagram of the control scheme for MEMS comprising a Van-der-Pol oscillator coupled with a forced Duffing oscillator

where Q is also a positive definite symmetric matrix. The worst case disturbance is given by

$$\tilde{d}(t) = \frac{1}{\rho^2} L^T P x(t) \tag{6.104}$$

The diagram of the MEMS control loop is depicted in Fig. 6.10.

6.3.6 *Lyapunov Stability Analysis*

Through Lyapunov stability analysis it will be shown that the proposed nonlinear control scheme assures H_∞ tracking performance for the MEMS model, and that in case of bounded disturbance terms asymptotic convergence to the reference setpoints is achieved. The tracking error dynamics for the MEMS model is written in the form

$$\dot{e} = Ae + Bu + L\tilde{d} \tag{6.105}$$

where in the MEMS case $L = I \in R^4$ with I being the identity matrix. Variable $\tilde{d}$ denotes model uncertainties and external disturbances of the micro-electromechanical system's model. The following Lyapunov equation is considered

$$V = \frac{1}{2} e^T P e \tag{6.106}$$

where $e = x - x_d$ is the tracking error. By differentiating with respect to time one obtains

$$\begin{gathered} \dot{V} = \tfrac{1}{2}\dot{e}^T P e + \tfrac{1}{2} e^T P \dot{e} \Rightarrow \\ \dot{V} = \tfrac{1}{2}[Ae + Bu + L\tilde{d}]^T P e + \tfrac{1}{2} e^T P [Ae + Bu + L\tilde{d}] \Rightarrow \end{gathered} \tag{6.107}$$

$$\begin{gathered} \dot{V} = \tfrac{1}{2}[e^T A^T + u^T B^T + \tilde{d}^T L^T] P e + \\ + \tfrac{1}{2} e^T P [Ae + Bu + L\tilde{d}] \Rightarrow \end{gathered} \tag{6.108}$$

$$\begin{gathered} \dot{V} = \tfrac{1}{2} e^T A^T P e + \tfrac{1}{2} u^T B^T P e + \tfrac{1}{2} \tilde{d}^T L^T P e + \\ \tfrac{1}{2} e^T P A e + \tfrac{1}{2} e^T P B u + \tfrac{1}{2} e^T P L \tilde{d} \end{gathered} \tag{6.109}$$

The previous equation is rewritten as

$$\begin{gathered} \dot{V} = \tfrac{1}{2} e^T (A^T P + P A) e + \left(\tfrac{1}{2} u^T B^T P e + \tfrac{1}{2} e^T P B u\right) + \\ + \left(\tfrac{1}{2} \tilde{d}^T L^T P e + \tfrac{1}{2} e^T P L \tilde{d}\right) \end{gathered} \tag{6.110}$$

Assumption: For given positive definite matrix Q and coefficients r and ρ there exists a positive definite matrix P, which is the solution of the following matrix equation

$$A^T P + P A = -Q + P \left(\frac{2}{r} B B^T - \frac{1}{\rho^2} L L^T\right) P \tag{6.111}$$

Moreover, the following feedback control law is applied to the system

$$u = -\frac{1}{r} B^T P e \tag{6.112}$$

By substituting Eqs. (6.111) and (6.112) one obtains

$$\begin{gathered} \dot{V} = \tfrac{1}{2} e^T \left[-Q + P \left(\tfrac{2}{r} B B^T - \tfrac{1}{\rho^2} L L^T\right) P\right] e + \\ + e^T P B \left(-\tfrac{1}{r} B^T P e\right) + e^T P L \tilde{d} \Rightarrow \end{gathered} \tag{6.113}$$

$$\begin{gathered} \dot{V} = -\tfrac{1}{2} e^T Q e + \tfrac{1}{r} e^T P B B^T P e - \tfrac{1}{2\rho^2} e^T P L L^T P e \\ -\tfrac{1}{r} e^T P B B^T P e + e^T P L \tilde{d} \end{gathered} \tag{6.114}$$

which after intermediate operations gives

$$\dot{V} = -\frac{1}{2} e^T Q e - \frac{1}{2\rho^2} e^T P L L^T P e + e^T P L \tilde{d} \tag{6.115}$$

or, equivalently

$$\begin{aligned}\dot{V} = -\tfrac{1}{2}e^T Qe - \tfrac{1}{2\rho^2}e^T PLL^T Pe + \\ +\tfrac{1}{2}e^T PL\tilde{d} + \tfrac{1}{2}\tilde{d}^T L^T Pe\end{aligned} \tag{6.116}$$

Lemma: The following inequality holds

$$\frac{1}{2}e^T PL\tilde{d} + \frac{1}{2}\tilde{d}L^T Pe - \frac{1}{2\rho^2}e^T PLL^T Pe \leq \frac{1}{2}\rho^2\tilde{d}^T\tilde{d} \tag{6.117}$$

Proof: The binomial $(\rho\alpha - \frac{1}{\rho}b)^2$ is considered. Expanding the left part of the above inequality one gets

$$\begin{aligned}\rho^2a^2 + \tfrac{1}{\rho^2}b^2 - 2ab \geq 0 \Rightarrow \tfrac{1}{2}\rho^2a^2 + \tfrac{1}{2\rho^2}b^2 - ab \geq 0 \Rightarrow \\ ab - \tfrac{1}{2\rho^2}b^2 \leq \tfrac{1}{2}\rho^2a^2 \Rightarrow \tfrac{1}{2}ab + \tfrac{1}{2}ab - \tfrac{1}{2\rho^2}b^2 \leq \tfrac{1}{2}\rho^2a^2\end{aligned} \tag{6.118}$$

The following substitutions are carried out: $a = \tilde{d}$ and $b = e^T PL$ and the previous relation becomes

$$\frac{1}{2}\tilde{d}^T L^T Pe + \frac{1}{2}e^T PL\tilde{d} - \frac{1}{2\rho^2}e^T PLL^T Pe \leq \frac{1}{2}\rho^2\tilde{d}^T\tilde{d} \tag{6.119}$$

Equations (6.119) is substituted in (6.116) and the inequality is enforced, thus giving

$$\dot{V} \leq -\frac{1}{2}e^T Qe + \frac{1}{2}\rho^2\tilde{d}^T\tilde{d} \tag{6.120}$$

Equation (6.120) shows that the H_∞ tracking performance criterion is satisfied. The integration of $\dot{V}$ from 0 to T gives

$$\begin{aligned}\int_0^T \dot{V}(t)dt \leq -\tfrac{1}{2}\int_0^T ||e||_Q^2 dt + \tfrac{1}{2}\rho^2\int_0^T ||\tilde{d}||^2 dt \Rightarrow \\ 2V(T) + \int_0^T ||e||_Q^2 dt \leq 2V(0) + \rho^2\int_0^T ||\tilde{d}||^2 dt\end{aligned} \tag{6.121}$$

Moreover, if there exists a positive constant $M_d > 0$ such that

$$\int_0^\infty ||\tilde{d}||^2 dt \leq M_d \tag{6.122}$$

then one gets

$$\int_0^\infty ||e||_Q^2 dt \leq 2V(0) + \rho^2 M_d \tag{6.123}$$

Thus, the integral $\int_0^\infty ||e||_Q^2 dt$ is bounded. Moreover, $V(T)$ is bounded and from the definition of the Lyapunov function V in Eq. (6.106) it becomes clear that $e(t)$ will

be also bounded since $e(t) \in \Omega_e = \{e | e^T P e \leq 2V(0) + \rho^2 M_d\}$. According to the above and with the use of Barbalat's Lemma one obtains $lim_{t\to\infty} e(t) = 0$.

Elaborating on the above, it can be noted that the proof of global asymptotic stability for the control loop of the MEMS model is based on Eq. (6.120) and on the application of Barbalat's Lemma. It uses the condition of Eq. (6.122) about the boundedness of the square of the aggregate disturbance and modelling error term $\tilde{d}$ that affects the model. However, as explained above the proof of global asymptotic stability is not restricted by this condition. By selecting the attenuation coefficient ρ to be sufficiently small and in particular to satisfy $\rho^2 < ||e||_Q^2 / ||\tilde{d}||^2$ one has that the first derivative of the Lyapunov function is upper bounded by 0. Therefore for the i-th time interval it is proven that the Lyapunov function defined in Eq (6.106) is a decreasing one. This also assures that the first derivative of the Lyapunov function of the system defined in Eq. (6.106) will always be negative.

6.3.7 *Robust State Estimation with the Use of the H-infinity Kalman Filter*

The MEMS control loop can be implemented with the use of information provided by a small number of sensors and by processing only a small number of state variables. To reconstruct the missing information about the state vector of the MEMS model it is proposed to use a filtering scheme and based on it to apply state estimation-based control [169, 457, 511]. The recursion of the H_∞ Kalman Filter, for the MEMS model, can be formulated in terms of a *measurement update* and a *time update* part

Measurement update:

$$\begin{aligned} D(k) &= [I - \theta W(k) P^-(k) + C^T(k) R(k)^{-1} C(k) P^-(k)]^{-1} \\ K(k) &= P^-(k) D(k) C^T(k) R(k)^{-1} \\ \hat{x}(k) &= \hat{x}^-(k) + K(k)[y(k) - C\hat{x}^-(k)] \end{aligned} \tag{6.124}$$

Time update:

$$\begin{aligned} \hat{x}^-(k+1) &= A(k)x(k) + B(k)u(k) \\ P^-(k+1) &= A(k)P^-(k)D(k)A^T(k) + Q(k) \end{aligned} \tag{6.125}$$

where it is assumed that parameter θ is sufficiently small to assure that the covariance matrix $P^-(k)^{-1} - \theta W(k) + C^T(k) R(k)^{-1} C(k)$ will be positive definite. When $\theta = 0$ the H_∞ Kalman Filter becomes equivalent to the standard Kalman Filter. One can measure only a part of the state vector of the MEMS (e.g. state variables x_1 and x_3), and can estimate through filtering the rest of the state vector elements.

6.3.8 Simulation Tests

6.3.8.1 Computation of Setpoints for the Model of the Coupled MEMS

The setpoints for the model of the coupled MEMS, that is if the Van der Pol Oscillator driven by the forced Duffing oscillator are computed by exploiting the model's differential flatness properties. The system is in triangular form and thus it is differentially flat, with flat output equal to $y = x_1$. From the first row of the state-space model of Eq. (6.83) it holds that $x_2 = \dot{x}_1$. Moreover, from the second row of the state-space model of Eq. (6.83) one obtains

$$x_3 = \frac{1}{k}\left[\dot{x}_2 + \gamma_1(x_1^2 - 1)x_2 + \left(\frac{\omega_2}{\omega_1}\right)^2 x_1 + kx_1\right] \tag{6.126}$$

From the third row of the state-space model it holds $x_4 = \dot{x}_3$. Additionally, from the fourth raw of the state-space model one has

$$u = \frac{1}{cos\left(\frac{\omega_d}{\omega_1}\tau\right)}[\dot{x}_4 + \gamma_2 x_4 + \delta x_3^2 - k(x_1 - x_3)] \tag{6.127}$$

Therefore, all state variables and the control inputs of the model can be expressed as differential functions of the flat output, and as a consequence the MEMS system consisting of the Van der Pol oscillator, driven by the Duffing oscillator, is a differentially flat one.

6.3.8.2 Simulation Diagrams

Simulation tests have been carried out to test the tracking accuracy of the proposed nonlinear optimal (H-infinity) control method for the MEMS that comprised the Van-del-Pol oscillator model, elastically coupled to the forced Duffing oscillator model. The obtained simulation result have confirmed that despite the nonlinearities and the underactuation in the MEMS state-space description the proposed control scheme achieves fast and accurate tracking of all reference setpoints, while also keeping moderate the variations of the control input. The simulation results are depicted in Figs. 6.11, 6.12, 6.13, 6.14, 6.15, 6.16, 6.17, 6.18 and 6.19, where the real values of the MEMS state variables are depicted in blue, the reference setpoints of the experiments are plotted in red while the estimated values of the state vector elements (provided by the H-infinity Kalman Filter) are printed in green.

The computation of the feedback gain of the H-infinity controller was based on the solution of the algebraic Riccati equation of Eq. (6.111), taking place at each time step of the control method. The selection of the attenuation coefficient ρ determines the robustness of the control algorithm as well as the existence of a solution in the

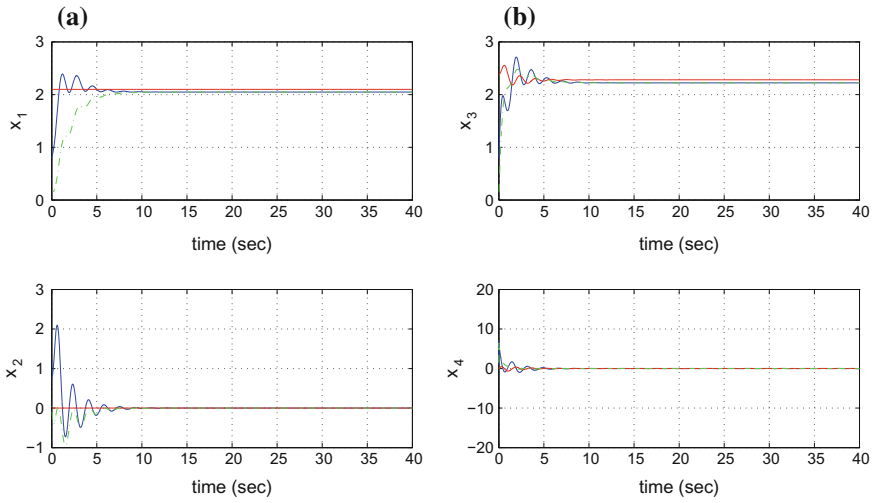

Fig. 6.11 Setpoint 1: **a** Convergence of state variables x_1 and x_2 of the MEMS (blue lines) to the reference setpoints (red lines) and estimates of them provided by the Kalman Filter (green lines), **b** Convergence of state variables x_3 and x_4 of the MEMS (blue lines) to the reference setpoints (red lines) and estimates of them provided by the Kalman Filter (green lines)

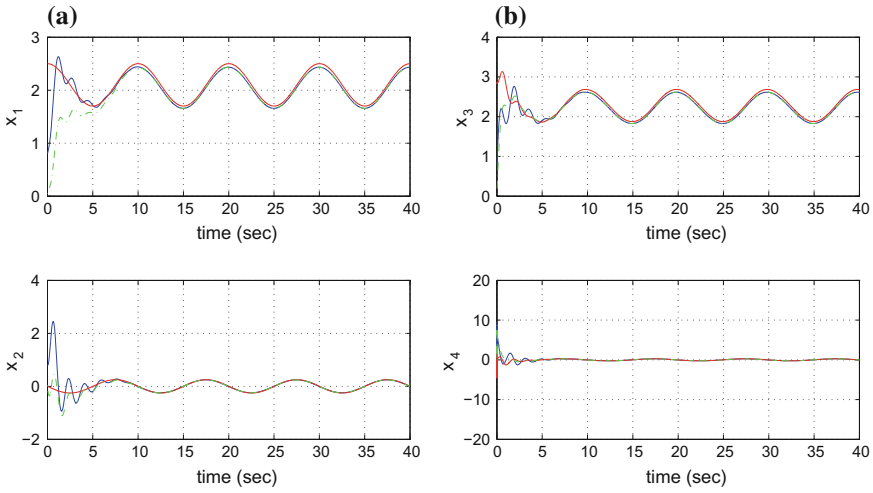

Fig. 6.12 Setpoint 2: **a** Convergence of state variables x_1 and x_2 of the MEMS (blue lines) to the reference setpoints (red lines) and estimates of them provided by the Kalman Filter (green lines), **b** Convergence of state variables x_3 and x_4 of the MEMS (blue lines) to the reference setpoints (red lines) and estimates of them provided by the Kalman Filter (green lines)

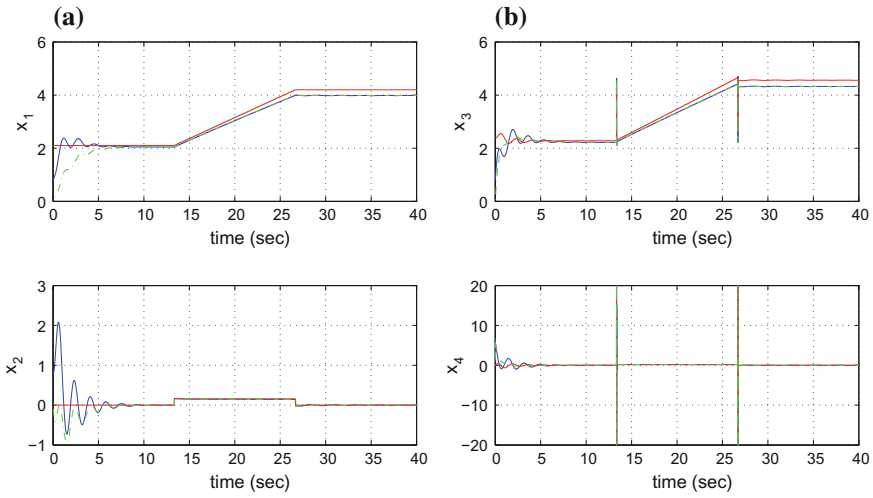

Fig. 6.13 Setpoint 3: **a** Convergence of state variables x_1 and x_2 of the MEMS (blue lines) to the reference setpoints (red lines) and estimates of them provided by the Kalman Filter (green lines), **b** Convergence of state variables x_3 and x_4 of the MEMS (blue lines) to the reference setpoints (red lines) and estimates of them provided by the Kalman Filter (green lines)

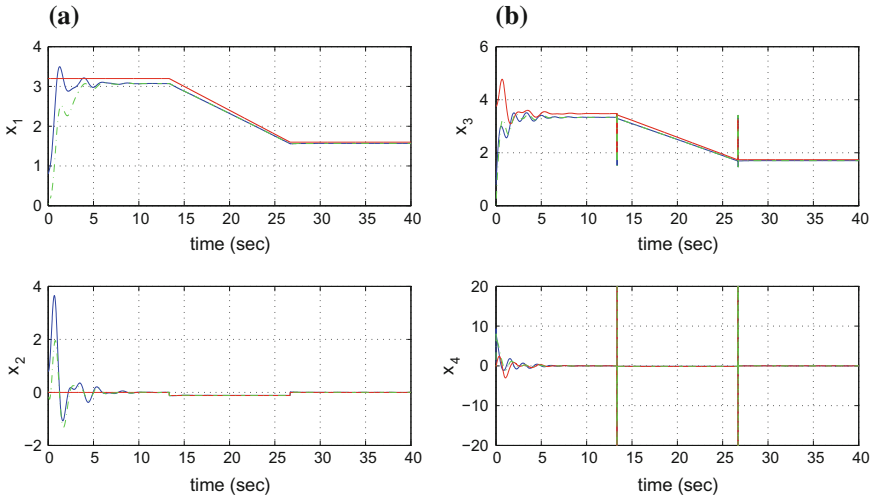

Fig. 6.14 Setpoint 4: **a** Convergence of state variables x_1 and x_2 of the MEMS (blue lines) to the reference setpoints (red lines) and estimates of them provided by the Kalman Filter (green lines), **b** Convergence of state variables x_3 and x_4 of the MEMS (blue lines) to the reference setpoints (red lines) and estimates of them provided by the Kalman Filter (green lines)

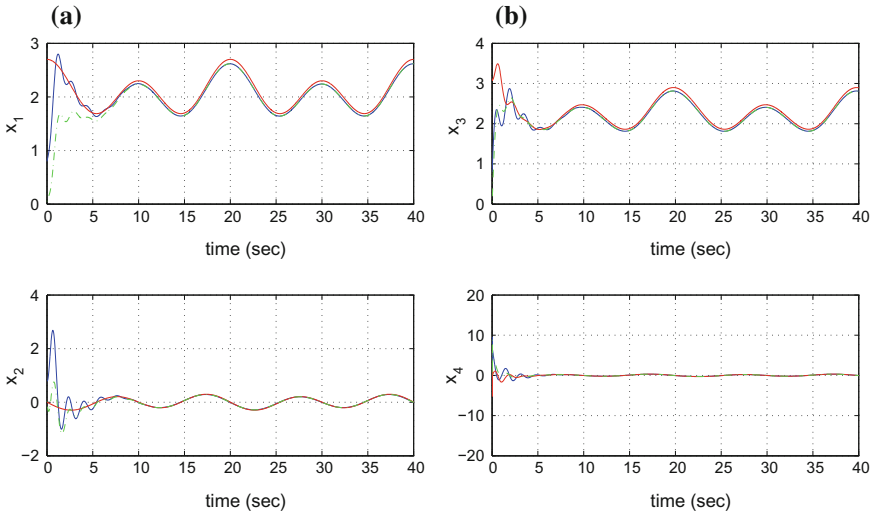

Fig. 6.15 Setpoint 5: **a** Convergence of state variables x_1 and x_2 of the MEMS (blue lines) to the reference setpoints (red lines) and estimates of them provided by the Kalman Filter (green lines), **b** Convergence of state variables x_3 and x_4 of the MEMS (blue lines) to the reference setpoints (red lines) and estimates of them provided by the Kalman Filter (green lines)

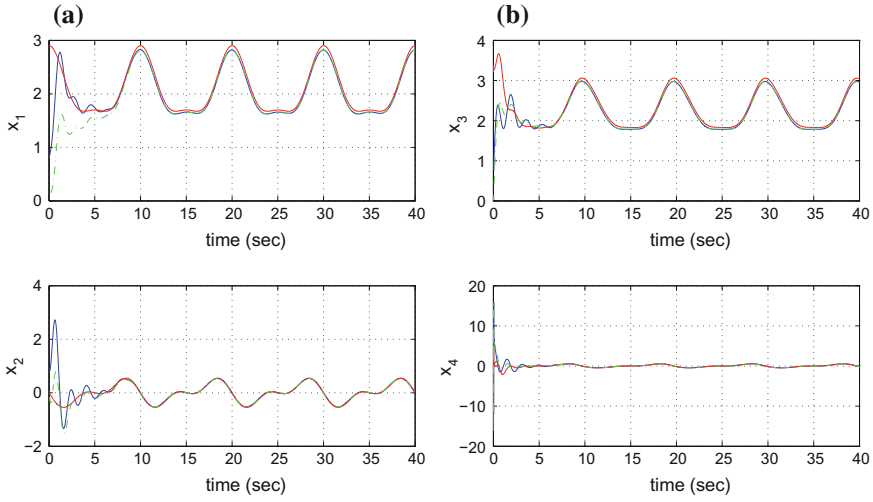

Fig. 6.16 Setpoint 6: **a** Convergence of state variables x_1 and x_2 of the MEMS (blue lines) to the reference setpoints (red lines) and estimates of them provided by the Kalman Filter (green lines), **b** Convergence of state variables x_3 and x_4 of the MEMS (blue lines) to the reference setpoints (red lines) and estimates of them provided by the Kalman Filter (green lines)

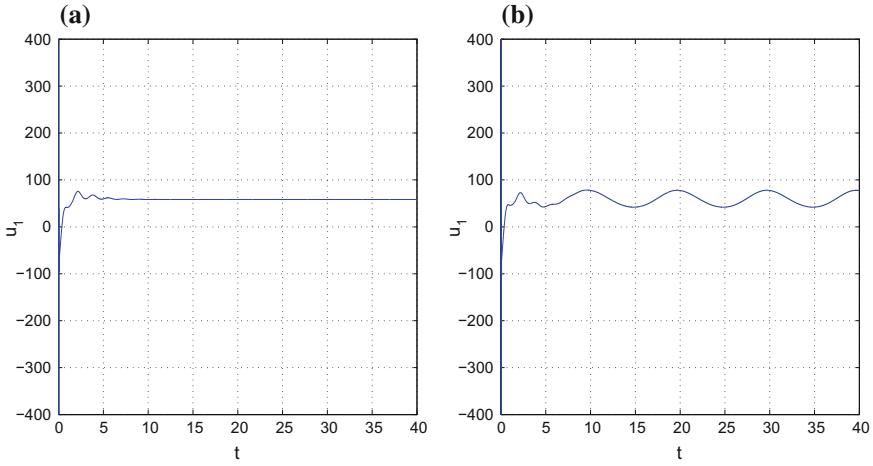

Fig. 6.17 Variation of the control input u applied to the MEMS **a** when tracking Setpoint 1, **b** when tracking Setpoint 2

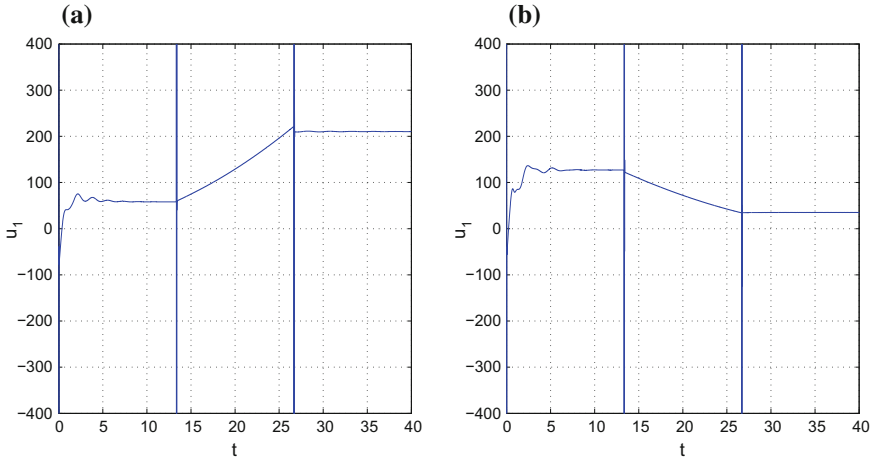

Fig. 6.18 Variation of the control input u applied to the MEMS **a** when tracking Setpoint 3, **b** when tracking Setpoint 4

aforementioned Riccati equation. As explained in the preceding sections, by selecting ρ to be sufficiently small the global asymptotic stability of the control method is assured. Moreover, the values of parameters ρ,r and of matrix Q appearing in Eq. (6.111) determine the transients of the control method.

By using the H-infinity Kalman Filter as a robust state estimator it has become possible to implement state estimation-based control through the measurement of selected state vector elements (for instance the position variables of the Van-der-Pol

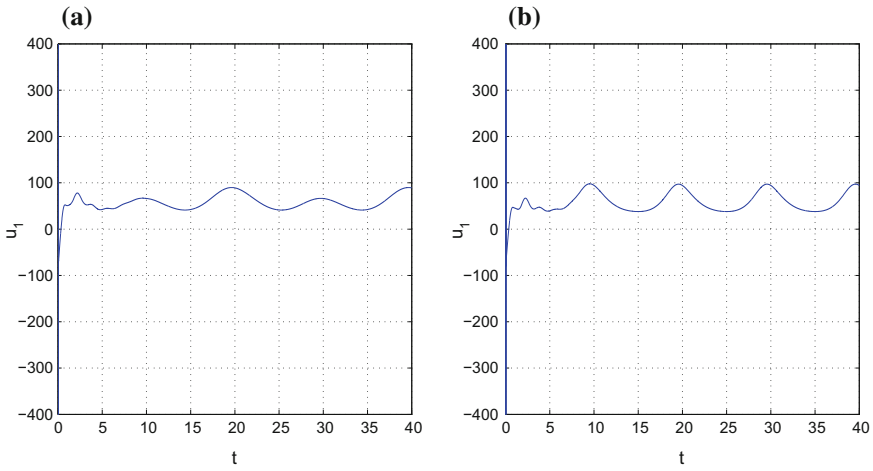

Fig. 6.19 Variation of the control input u applied to the MEMS **a** when tracking Setpoint 5, **b** when tracking Setpoint 6

and the Duffing oscillators). The rest of the state vector elements were estimated through the Kalman Filter's recursion. The use of a state estimator, in place of measurements of the entire state vector of the MEMS is important considering the difficulty of obtaining sensor measurements at the MEMS scale.

Chapter 7
Unicycles and Two-Wheel Autonomous Ground Vehicles

Abstract In complement to robotic manipulators, autonomous vehicles form the second large class of robotic systems. In this context, the autonomous or semi-autonomous navigation of unicycle-type and two-wheel vehicles, such as motorcycles, can be significantly improved through electronic control of the their stability properties. This will also allow for precise path following and for dexterous maneuvering. In this chapter, a nonlinear optimal control method is developed for solving the stabilization and path following problem of autonomous two-wheel vehicles. In the presented application examples either the kinematic or the joint kinematic-dynamic of the two-wheel vehicle undergoes approximate linearization around a temporary operating point which is recomputed at each iteration of the control algorithm. The linearization takes place using Taylor series expansion and the computation of the Jacobian matrices of the system's states-space model. For the approximately linearized model of the two-wheel vehicle an H-infinity feedback controller is designed. The computation of the feedback gain of the controller requires the repetitive solution of an algebraic Riccati equation, taking again place at each time-step of the control method. The concept of the control method is that at each time instant the system's state vector is made to converge to the temporary equilibrium, while this equilibrium is shifted towards the reference trajectory. Thus, asymptotically the state vector of the two-wheel vehicle converges to the reference setpoints. Through Lyapunov stability analysis the global asymptotic stability properties of the control method are proven In particular, the chapter treats the following topics: (a) Nonlinear optimal control of robotic unicycles, (b) Flatness-based control of robotic unicycles, and (c) Nonlinear optimal control of autonomous two-wheeled vehicles such as motorcycles.

7.1 Chapter Overview

The present chapter treats the following topics: (a) Nonlinear optimal control of robotic unicycles, (b) Flatness-based control of robotic unicycles, and (c) Nonlinear optimal control of autonomous two-wheeled vehicles such as motorcycles.

G. Rigatos and K. Busawon, *Robotic Manipulators and Vehicles*,
Studies in Systems, Decision and Control 152,
https://doi.org/10.1007/978-3-319-77851-8_7

With reference to (a) the chapter introduces a new control method for feedback control of autonomous robotic vehicles of the unicycle type. The control method consists of a repetitive solution of an H-infinity control problem for the mobile robot, that makes use of a locally linearized model of the robot and takes place at each iteration of the control algorithm. The vehicle's model is locally linearized round its current position through the computation of the associated Jacobian matrices. Using the linearized model of the vehicle an H-infinity feedback control law is computed. The known robustness features of H-infinity control enable to compensate for the errors of the approximate linearization, as well as to eliminate the effects of external perturbations.

With reference to (b) the chapter proposes a differential flatness theory-based implementation of the Kalman Filter (known as Derivative-free nonlinear Kalman Filter) and state estimation-based control for MIMO nonlinear dynamical systems, such as autonomous vehicles. The considered nonlinear filtering scheme which is based on differential flatness theory can be applied to the autonomous vehicle model without the need for calculation of Jacobian matrices, and in general extends the class of MIMO nonlinear systems for which derivative-free Kalman Filtering can be performed. Nonlinear systems such as unicycle-type autonomous vehicles, satisfying the differential flatness property, can be written in the Brunovsky (canonical) form via a transformation of their state variables and control inputs. After transforming the unicycle-type vehicle to the canonical form it is straightforward to apply the standard Kalman Filter recursion.

With reference to (c) the chapter demonstrates that the autonomous or semi-autonomous navigation of two-wheel vehicles, such as motorcycles, can be significantly improved through electronic control of the their stability properties. This will also allow for precise path following and for dexterous maneuvering. Actually, a nonlinear optimal control method is developed once again, for solving the stabilization and path following problem of autonomous motorcycles. The joint kinematic and dynamic model of the motorcycle undergoes approximate linearization around a temporary operating point which is recomputed at each iteration of the control algorithm. The linearization takes place using Taylor series expansion and the computation of the Jacobian matrices of the system's states-space model. For the approximately linearized model of the motorcycle an H-infinity feedback controller is designed. The computation of the feedback gain of the controller requires the repetitive solution of an algebraic Riccati equation, taking again place at each time-step of the control method. The concept of the control method is that at each time instant the autonomous motorcycle's state vector is made to converge to the temporary equilibrium, while this equilibrium is shifted towards the reference trajectory. Thus, asymptotically the state vector of the motorcycle converges to the reference setpoints. In all cases (a)–(c) the global asymptotic stability properties of the control method are proven through Lyapunov analysis.

7.2 Nonlinear Optimal Control of the Robotic Unicycle

7.2.1 Outline

Nonlinear and embedded control and autonomous navigation of robotic vehicles is of primary importance for the automotive industry. By succeeding motion control of the vehicle, safety in driving can be improved while other several practical problems, such as lane keeping and maneuvering or parallel parking can be solved [206, 207, 223, 278, 281, 425, 569, 574]. Up to now several research results have been developed to enable the steering control and autonomous navigation of vehicles. The developed methods are based on nonlinear control, such as differential geometry and differential flatness theory approaches as well as on Lyapunov stability theory [38, 90, 100, 262, 343, 486, 604]. In this section a new solution to the problem of autonomous vehicle navigation is given, using a linearization scheme together with H_∞ robust control theory [450].

The kinematic model of a unicycle robotic vehicle is considered as a case study, however the proposed approach can be also applied to other types of vehicles (such as four wheel vehicles, heavy duty vehicles, articulated vehicles etc.). Actually the present section proposes the application of an approximate linearization scheme for the kinematic model of the unicycle robotic vehicle. The linearization makes use of Taylor series expansion around the vehicle's current position. To perform this linearization the computation of Jacobian matrices is needed while the induced linearization error is treated as a disturbance. For the linearized equivalent of the vehicle's model an H_∞ feedback control scheme is developed. The formulation of the H_∞ control problem is based on the minimization of a quadratic cost function that comprises both the disturbance and the control input effects. The disturbance tries to maximize the cost function while the control signal tries to minimize it, within a min-max differential game.

Comparing to nonlinear feedback control approaches which rely on exact linearization (as the ones based on differential flatness theory and analyzed in [450, 452, 457]) the proposed H_∞ control scheme is assessed as follows: (i) it uses an approximate linearization approach of the vehicle's dynamic or kinematic model which does not follow the elaborated transformations (diffeomorphisms) of the exact linearization methods, (ii) it introduces additional disturbance error which is due to the approximate linearization of the system dynamics coming from the application of Taylor series expansion, (iii) it requires the computation of Jacobian matrices, (iv) unlike exact feedback linearization, the H_∞ control term has to compensate not only for modelling uncertainties and external disturbances but needs also to annihilate the effects of the cumulative linearization error, (v) the H_∞ control approach follows optimal control methods for the computation of the control signal, thus achieving accurate tracking of reference setpoints under moderate variations of the control input.

7.2.2 *Linearization of the Robotic Vehicle's Kinematic Model*

7.2.2.1 Approaches in Control of Nonlinear Robotic Vehicles

Motion control of unmanned vehicles is a nonlinear control problem. One can distinguish three main approaches in the design of nonlinear control systems: (i) control and filtering based on global linearization methods, (ii) control and filtering based on asymptotic linearization methods, (iii) Lyapunov methods.

As far as approach (i) is concerned, that is methods of global linearization, one can classify there methods for the transformation of nonlinear vehicles dynamics into equivalent linear state space form. For the linear equivalent forms of the vehicles dynamics one can design feedback controllers and can solve the problem of state estimation (filtering). In this area one can consider methods based on differential flatness theory and methods based on Lie algebra. These approaches avoid approximation errors in modelling and arrive at controllers of elevated precision and robustness, In this area, one can also distinguish a new nonlinear filtering method (Derivative-free nonlinear Kalman Filter) which is more precise and computationally faster than other nonlinear estimation approaches [450].

As far as approach (ii) is concerned, that is methods of asymptotic linearization, the focus is on robust and adaptive control with the use of a decomposition of the vehicles dynamics into a set of linear local models. One can pursue solutions to the problem of nonlinear control, relying on local linear models (around linearization points). For such systems one can select the parameters of the local controllers by following linear feedback controller design methods. These controllers achieve asymptotically, that is in the course of time, the compensation of the nonlinear system dynamics and the stabilization of the feedback control loops. In this research direction several results have been obtained about a new nonlinear H-infinity control method, which is based on the local and approximate linearization of the vehicles dynamics and which makes use of the computation of Jacobian matrices.

As far as approach (iii) is concerned, that is Lyapunov theory-based nonlinear control methods one comes against problems of minimization of the Lyapunov functions so as to compute control signals for nonlinear vehicle dynamics. For the development of Lyapunov-type controllers one can either exploit a model of the vehicle's dynamics, or can avoid completely the use of such a model as in the case of adaptive control. In the latter case, the vehicles dynamics is completely unknown and can be approximated by adaptive algorithms which are suitably designed so as to assure the stability and robustness of the control loop.

7.2.3 *Linearization of the Unicycle Robot Through Taylor Series Expansion*

A unicycle autonomous robotic vehicle is considered, as shown in Fig. 7.1. Its kinematic model is given by

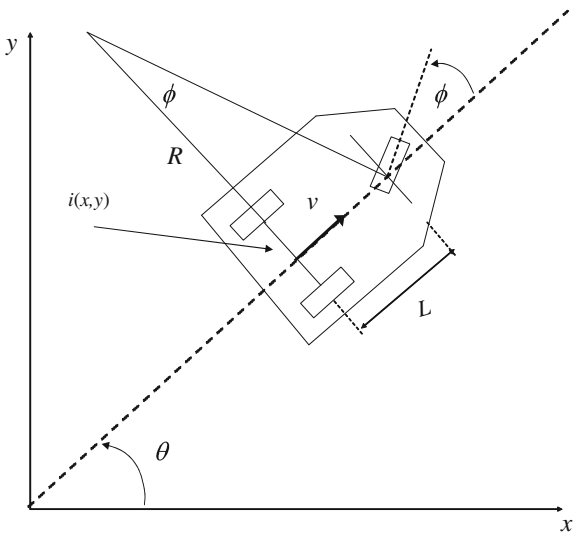

Fig. 7.1 The model of the autonomous robotic vehicle (cart-like vehicle)

$$\begin{pmatrix} \dot{x} \\ \dot{y} \\ \dot{\theta} \end{pmatrix} = \begin{pmatrix} cos(\theta) & 0 \\ sin(\theta) & 0 \\ 0 & 1 \end{pmatrix} \cdot \begin{pmatrix} v \\ \omega \end{pmatrix} \tag{7.1}$$

where x, y are the cartesian coordinates of the robot's center of gravity and θ is its orientation angle. Input v is the vehicle's linear velocity and ω is the vehicle's angular velocity for rotations round its transversal axis.

Considering linearization of the model round the current position of the robot and round the velocity value $v(t - T_s)$, where T_S is the sampling period, the Jacobian matrices of the robotic model are:

$$A = \begin{pmatrix} 0 & 0 & -v(t - T_s) \cdot sin(\theta) \\ 0 & 0 & v(t - T_s) \cdot cos(\theta) \\ 0 & 0 & 0 \end{pmatrix} \tag{7.2}$$

$$B = \begin{pmatrix} cos(\theta) & 0 \\ sin(\theta) & 0 \\ 0 & 1 \end{pmatrix} \tag{7.3}$$

The state vector of the robotic vehicle is denoted as $\mathbf{x} = [\mathbf{x}, \mathbf{y}, \boldsymbol{\theta}]^{\mathbf{T}}$ while the input vector is denoted as $u = [v, w]^T$. After linearization around its current position, the robot's kinematic model is written as

$$\dot{x} = Ax + Bu + d_1 \tag{7.4}$$

Parameter d_1 stands for the linearization error in the robot's kinematic model appearing in Eq. (7.4). The desirable trajectory of the robot is denoted by $\mathbf{x_d} = [\mathbf{x_d}, \mathbf{y_d}, \boldsymbol{\theta}_\mathbf{d}]$. Tracking of this trajectory is achieved after applying the control input u^*. At every time instant the control input u^* is assumed to differ from the control input u appearing in Eq. (7.4) by an amount equal to Δu, that is $u^* = u + \Delta u$

$$\dot{x}_d = Ax_d + Bu^* + d_2 \tag{7.5}$$

The dynamics of the controlled system described in Eq. (7.4) can be also written as

$$\dot{x} = Ax + Bu + Bu^* - Bu^* + d_1 \tag{7.6}$$

and by denoting $d_3 = -Bu^* + d_1$ as an aggregate disturbance term one obtains

$$\dot{x} = Ax + Bu + Bu^* + d_3 \tag{7.7}$$

By subtracting Eq. (7.5) from Eq. (7.7) one has

$$\dot{x} - \dot{x}_d = A(x - x_d) + Bu + d_3 - d_2 \tag{7.8}$$

By denoting the tracking error as $e = x - x_d$ and the aggregate disturbance term as $\tilde{d} = d_3 - d_2$, the tracking error dynamics becomes

$$\dot{e} = Ae + Bu + \tilde{d} \tag{7.9}$$

The above linearized form of the robotic model can be efficiently controlled after applying an H-infinity feedback control scheme.

7.2.4 The Nonlinear H-Infinity Control

7.2.4.1 Mini-Max Control and Disturbance Rejection

The initial nonlinear system is assumed to be in the form

$$\dot{x} = f(x, u) \;\; x \in R^n, \;\; u \in R^m \tag{7.10}$$

Linearization of the system (autonomous vehicle) is performed at each iteration of the control algorithm round its present operating point $(x^*, u^*) = (x(t), u(t - T_s))$. The linearized equivalent of the system is described by

$$\dot{x} = Ax + Bu + L\tilde{d} \;\; x \in R^n, \;\; u \in R^m, \;\; \tilde{d} \in R^q \tag{7.11}$$

where matrices A and B are obtained from the computation of the Jacobians

$$A = \begin{pmatrix} \frac{\partial f_1}{\partial x_1} & \frac{\partial f_1}{\partial x_2} & \cdots & \frac{\partial f_1}{\partial x_n} \\ \frac{\partial f_2}{\partial x_1} & \frac{\partial f_2}{\partial x_2} & \cdots & \frac{\partial f_2}{\partial x_n} \\ \cdots & \cdots & \cdots & \cdots \\ \frac{\partial f_n}{\partial x_1} & \frac{\partial f_n}{\partial x_2} & \cdots & \frac{\partial f_n}{\partial x_n} \end{pmatrix} |_{(x^*,u^*)} \tag{7.12}$$

$$B = \begin{pmatrix} \frac{\partial f_1}{\partial u_1} & \frac{\partial f_1}{\partial u_2} & \cdots & \frac{\partial f_1}{\partial u_m} \\ \frac{\partial f_2}{\partial u_1} & \frac{\partial f_2}{\partial u_2} & \cdots & \frac{\partial f_2}{\partial u_m} \\ \cdots & \cdots & \cdots & \cdots \\ \frac{\partial f_n}{\partial u_1} & \frac{\partial f_n}{\partial u_2} & \cdots & \frac{\partial f_n}{\partial u_m} \end{pmatrix} |_{(x^*,u^*)} \tag{7.13}$$

and vector $\tilde{d}$ denotes disturbance terms due to linearization errors. The problem of disturbance rejection for the linearized model that is described by

$$\begin{gathered} \dot{x} = Ax + Bu + Ld \\ y = Cx \end{gathered} \tag{7.14}$$

where $x \in R^n$, $u \in R^m$, $\tilde{d} \in R^q$ and $y \in R^p$, cannot be handled efficiently if the classical LQR control scheme is applied. This is because of the existence of the perturbation term d. The disturbance term d apart from modeling (parametric) uncertainty and external perturbation terms can also represent noise terms of any distribution.

As analyzed in previous applications of the H_∞ control approach, a feedback control scheme is designed for trajectory tracking by the system's state vector and simultaneous disturbance rejection, considering that the disturbance affects the system in the worst possible manner. The disturbances' effects are incorporated in the following quadratic cost function:

$$\begin{gathered} J(t) = \frac{1}{2}\int_0^T [y^T(t)y(t) + \\ + ru^T(t)u(t) - \rho^2 \tilde{d}^T(t)\tilde{d}(t)]dt, \quad r, \rho > 0 \end{gathered} \tag{7.15}$$

As pointed out in previous sections, the significance of the negative sign in the cost function's term that is associated with the perturbation variable $\tilde{d}(t)$ is that the disturbance tries to maximize the cost function $J(t)$ while the control signal $u(t)$ tries to minimize it. The physical meaning of the relation given above is that the control signal and the disturbances compete to each other within a min-max differential game. This problem of min-max optimization can be written as

$$min_u max_{\tilde{d}} J(u, \tilde{d}) \tag{7.16}$$

The objective of the optimization procedure is to compute a control signal $u(t)$ which can compensate for the worst possible disturbance, that is externally imposed to the unicycle vehicle. However, the solution to the min-max optimization problem is directly related to the value of the parameter ρ. This means that there is an upper bound in the disturbances magnitude that can be annihilated by the control signal.

7.2.4.2 H-Infinity Feedback Control

For the linearized system given by Eq. (7.14) the cost function of Eq. (7.15) is defined, where the coefficient r determines the penalization of the control input and the weight coefficient ρ determines the reward of the disturbances' effects. It is assumed that:

As in previous applications of the H-infinity control method, it is assumed that (i) The energy that is transferred from the disturbances signal $d(t)$ is bounded, that is $\int_0^\infty \tilde{d}^T(t)\tilde{d}(t)dt < \infty$, (ii) matrices $[AB]$ and $[AL]$ are stabilizable, (iii) matrix $[AC]$ is detectable. Then, the optimal feedback control law is given by

$$u(t) = -Kx(t) \tag{7.17}$$

with

$$K = \frac{1}{r}B^T P \tag{7.18}$$

where P is a positive semi-definite symmetric matrix which is obtained from the solution of the Riccati equation

$$A^T P + PA + Q - P(\frac{1}{r}BB^T - \frac{1}{2\rho^2}LL^T)P = 0 \tag{7.19}$$

where Q is also a positive definite symmetric matrix. The worst case disturbance is given by $\tilde{d}(t) = \frac{1}{\rho^2}L^T Px(t)$.

7.2.5 Lyapunov Stability Analysis

Through Lyapunov stability analysis it will be shown that the proposed nonlinear control scheme for the unicycle vehicle assures H_∞ tracking performance, and that in case of bounded disturbance terms asymptotic convergence to the reference setpoints is achieved. The tracking error dynamics for the robotic vehicle is written in the form

$$\dot{e} = Ae + Bu + L\tilde{d} \tag{7.20}$$

where in the unicycle robot's application example $L = I \in R^3$ with I being the identity matrix. The following Lyapunov function is considered

$$V = \frac{1}{2}e^T Pe \tag{7.21}$$

where $e = x - x_d$ is the tracking error. By differentiating with respect to time one obtains

$$\begin{gathered}\dot{V} = \tfrac{1}{2}\dot{e}^T Pe + \tfrac{1}{2}eP\dot{e} \Rightarrow \\ \dot{V} = \tfrac{1}{2}[Ae + Bu + L\tilde{d}]^T P + \tfrac{1}{2}e^T P[Ae + Bu + L\tilde{d}] \Rightarrow\end{gathered} \tag{7.22}$$

$$\begin{gathered}\dot{V} = \tfrac{1}{2}[e^T A^T + u^T B^T + \tilde{d}^T L^T]Pe + \\ + \tfrac{1}{2}e^T P[Ae + Bu + L\tilde{d}] \Rightarrow\end{gathered} \tag{7.23}$$

$$\begin{gathered}\dot{V} = \tfrac{1}{2}e^T A^T Pe + \tfrac{1}{2}u^T B^T Pe + \tfrac{1}{2}\tilde{d}^T L^T Pe + \\ \tfrac{1}{2}e^T PAe + \tfrac{1}{2}e^T PBu + \tfrac{1}{2}e^T PL\tilde{d}\end{gathered} \tag{7.24}$$

The previous equation is rewritten as

$$\begin{gathered}\dot{V} = \tfrac{1}{2}e^T(A^T P + PA)e + \left(\tfrac{1}{2}u^T B^T Pe + \tfrac{1}{2}e^T PBu\right) + \\ + \left(\tfrac{1}{2}\tilde{d}^T L^T Pe + \tfrac{1}{2}e^T PL\tilde{d}\right)\end{gathered} \tag{7.25}$$

Assumption: For given positive definite matrix Q and coefficients r and ρ there exists a positive definite matrix P, which is the solution of the following matrix equation

$$A^T P + PA = -Q + P\left(\tfrac{1}{r}BB^T - \tfrac{1}{2\rho^2}LL^T\right)P \tag{7.26}$$

Moreover, the following feedback control law is applied to the system

$$u = -\tfrac{1}{r}B^T Pe \tag{7.27}$$

By substituting Eq. (7.26) and Eq. (7.27) one obtains

$$\begin{gathered}\dot{V} = \tfrac{1}{2}e^T\left[-Q + P\left(\tfrac{1}{r}BB^T - \tfrac{1}{2\rho^2}LL^T\right)P\right]e + \\ + e^T PB\left(-\tfrac{1}{r}B^T Pe\right) + e^T PL\tilde{d} \Rightarrow\end{gathered} \tag{7.28}$$

$$\begin{gathered}\dot{V} = -\tfrac{1}{2}e^T Qe + \left(\tfrac{1}{r}PBB^T Pe - \tfrac{1}{2\rho^2}e^T PLL^T\right)Pe \\ -\tfrac{1}{r}e^T PBB^T Pe + e^T PL\tilde{d}\end{gathered} \tag{7.29}$$

which after intermediate operations gives

$$\dot{V} = -\tfrac{1}{2}e^T Qe - \tfrac{1}{2\rho^2}e^T PLL^T Pe + e^T PL\tilde{d} \tag{7.30}$$

or, equivalently

$$\begin{gathered}\dot{V} = -\tfrac{1}{2}e^T Qe - \tfrac{1}{2\rho^2}e^T PLL^T Pe + \\ + \tfrac{1}{2}e^T PL\tilde{d} + \tfrac{1}{2}\tilde{d}^T L^T Pe\end{gathered} \tag{7.31}$$

Lemma: The following inequality holds

$$\frac{1}{2}e^T L\tilde{d} + \frac{1}{2}\tilde{d}L^T Pe - \frac{1}{2\rho^2}e^T PLL^T Pe \leq \frac{1}{2}\rho^2\tilde{d}^T\tilde{d} \tag{7.32}$$

Proof: The binomial $(\rho\alpha - \frac{1}{\rho}b)^2$ is considered. Expanding the left part of the above inequality one gets

$$\begin{gathered}\rho^2a^2 + \frac{1}{\rho^2}b^2 - 2ab \geq 0 \Rightarrow \frac{1}{2}\rho^2a^2 + \frac{1}{2\rho^2}b^2 - ab \geq 0 \Rightarrow \\ ab - \frac{1}{2\rho^2}b^2 \leq \frac{1}{2}\rho^2a^2 \Rightarrow \frac{1}{2}ab + \frac{1}{2}ab - \frac{1}{2\rho^2}b^2 \leq \frac{1}{2}\rho^2a^2\end{gathered} \tag{7.33}$$

The following substitutions are carried out: $a = \tilde{d}$ and $b = e^T PL$ and the previous relation becomes

$$\frac{1}{2}\tilde{d}^T L^T Pe + \frac{1}{2}e^T PL\tilde{d} - \frac{1}{2\rho^2}e^T PLL^T Pe \leq \frac{1}{2}\rho^2\tilde{d}^T\tilde{d} \tag{7.34}$$

Equation (7.34) is substituted in Eq. (7.31) and the inequality is enforced, thus giving

$$\dot{V} \leq -\frac{1}{2}e^T Qe + \frac{1}{2}\rho^2\tilde{d}^T\tilde{d} \tag{7.35}$$

Equation (7.35) shows that the H_∞ tracking performance criterion is satisfied. The integration of $\dot{V}$ from 0 to T gives

$$\begin{gathered}\int_0^T \dot{V}(t)dt \leq -\frac{1}{2}\int_0^T ||e||_Q^2 dt + \frac{1}{2}\rho^2\int_0^T ||\tilde{d}||^2 dt \Rightarrow \\ 2V(T) + \int_0^T ||e||_Q^2 dt \leq 2V(0) + \rho^2\int_0^T ||\tilde{d}||^2 dt\end{gathered} \tag{7.36}$$

Moreover, if there exists a positive constant $M_d > 0$ such that

$$\int_0^\infty ||\tilde{d}||^2 dt \leq M_d \tag{7.37}$$

then one gets

$$\int_0^\infty ||e||_Q^2 dt \leq 2V(0) + \rho^2 M_d \tag{7.38}$$

Thus, the integral $\int_0^\infty ||e||_Q^2 dt$ is bounded. Moreover, $V(T)$ is bounded and from the definition of the Lyapunov function V in Eq. (7.21) it becomes clear that $e(t)$ will be also bounded since $e(t) \in \Omega_e = \{e | e^T Pe \leq 2V(0) + \rho^2 M_d\}$. According to the above and with the use of Barbalat's Lemma one obtains $lim_{t\to\infty} e(t) = 0$.

7.2.6 Simulation Tests

The performance of the proposed nonlinear H_∞ control scheme is tested is two examples: (i) when the mobile robot tracks a reference trajectory, (ii) when the unicycle robot performs the automated parallel parking task. In both cases the performance of the proposed controller was satisfactory, with minimum tracking error and fast

convergence to the reference setpoints. In the computation of the reference path, the coordinates of the reference trajectory in the 2D-plane (x_d, y_d) have been used, while the desirable steering angle has been computed by $\theta_d = tan^{-1}(\dot{y}_d/\dot{x}_d)$. The obtained results are depicted in Figs. 7.2, 7.3 and 7.4.

The tracking performance of the control method is shown in Table 7.1. It can be observed that the tracking error for all state variables of the unicycle robot was extremely small. Besides, in the simulation diagrams one can note the excellent transient performance of the control algorithm, which means that convergence to the

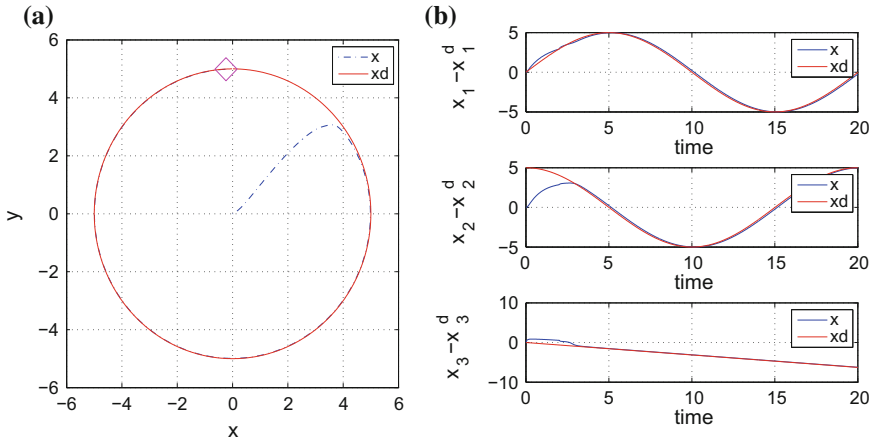

Fig. 7.2 **a** Plot of the circular $x - y$ trajectory followed by the mobile robot, **b** convergence of the robot's state variables $x_1 = x$, $x_2 = y$ and $x_3 = \theta$ to the associated reference setpoints

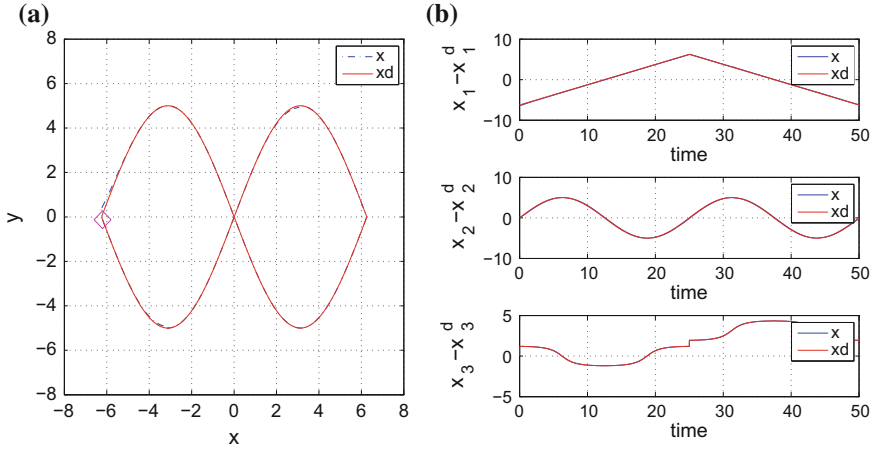

Fig. 7.3 **a** Plot of the eight-shaped $x - y$ trajectory followed by the mobile robot, **b** convergence of the robot's state variables $x_1 = x$, $x_2 = y$ and $x_3 = \theta$ to the associated reference setpoints

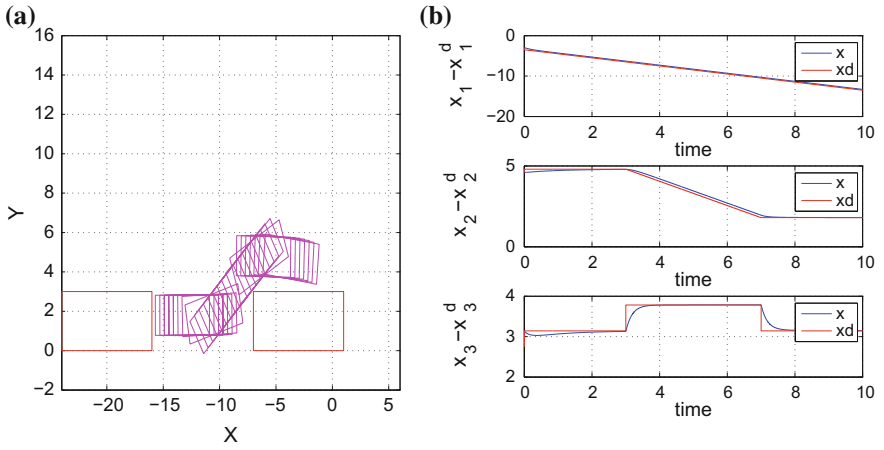

Fig. 7.4 **a** Plot of the $x - y$ trajectory followed by the mobile robot in case of the parallel parking maneuver, **b** convergence of the robot's state variables $x_1 = x, x_2 = y$ and $x_3 = \theta$ to the associated reference setpoints

Table 7.1 Tracking RMSE in the disturbance-free case

	$RMSE_x$	$RMSE_y$	$RMSE_\theta$
Path_1	$36.00 \cdot 10^{-4}$	$39.00 \cdot 10^{-4}$	$10.00 \cdot 10^{-4}$
Path_2	$7.90 \cdot 10^{-4}$	$12.00 \cdot 10^{-4}$	$2.40 \cdot 10^{-4}$

reference path was succeeded in a smooth manner, while also avoiding overshoot and oscillations.

It is pointed out that the errors and disturbances that affect the proposed control method are as follows: (i) linearization errors due to the truncation of higher order terms in the Taylor series expansion of the vehicle's nonlinear model, (ii) external perturbations that may affect the vehicle's motion. H-infinity control aims at providing maximum robustness to this kind of modeling errors and disturbances, and this is achieved through the appropriate selection of the attenuation coefficient ρ which appears in the associated Riccati equation. Actually, the minimum value of ρ for which there exists a solution for the algebraic Riccati equation (in the form of a positive definite symmetric matrix P) is the one that provides the control loop with maximum robustness. The above have been explained in Sect. 3.3 of manuscript.

Moreover, it is pointed out that the control method that is presented in this section and which is based on nonlinear H-infinity control theory can be compared against global linearization methods, e.g. those based on differential flatness theory and against Lyapunov-based methods (used by adaptive control schemes) [450, 452, 457]. As a general remark it can be stated that the nonlinear H-infinity control, yet conceptually more simple than the other two control approaches, is a reliable and efficient solution for the problem of autonomous vehicles' control. Besides,by avoiding

the intuitive definition of linearizing outputs and the elaborated computations associated with state variables' transformations met in global linearization-based control schemes, the nonlinear optimal control approach appears to be advantageous.

7.3 Flatness-Based Control of the Robotic Unicycle

7.3.1 Outline

In this section, using differential flatness theory, the nonlinear dynamics of the vehicle (e.g. the UGV of Fig. 7.5) is first subject to a linearization transformation. This makes possible (i) to design an efficient control law for trajectories tracking, and (ii) to apply to the nonlinear system a filtering method that it is based on the standard Kalman Filter recursion. Unlike the Extended Kalman Filter (EKF), the proposed filtering method provides estimates of the state vector of the UGV without the need for derivatives and Jacobians calculation. By avoiding linearization approximations, the proposed derivative-free nonlinear Kalman filtering method improves the accuracy of estimation of the system state variables, and results in smooth control signal variations and in minimization of the tracking error of the associated control loop.

Filtering-based state estimation for unmanned ground vehicles (UGVs) is a significant topic because it enables their accurate localization and autonomous navigation [45]. For nonlinear systems such as UGVs, and under the assumption of Gaussian noise, the Extended Kalman Filter (EKF) is frequently applied for estimating the non-measurable state variables through the processing of input and output sequences or

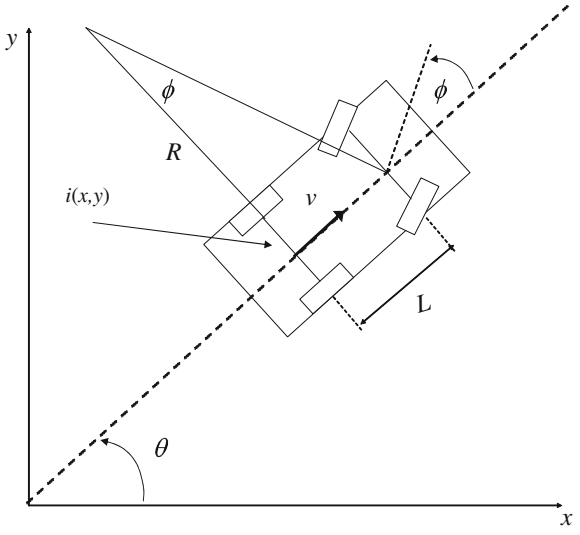

Fig. 7.5 The model of the 4-wheel autonomous vehicle (car-like vehicle) is approximated by that of the unicycle at moderate speeds

for obtaining estimates of the state vector through the fusion of measurements coming from various sensors [33, 190, 222, 359]. The Extended Kalman Filter is based on linearization of the system dynamics using a first order Taylor expansion [431, 432, 439, 445, 449, 601]. Although EKF is efficient in several estimation and fusion problems, it is characterized by cumulative errors due to the local linearization assumption and this may affect the accuracy of the UGV's motion estimation or even risk the stability of the UGV state estimation-based control loop.

The present section extends the results of [415, 433] towards nonlinear dynamical systems, such as UGVs, which are described by multi-input multi-output (MIMO) models. Actually, the section's results are applicable to differentially flat MIMO nonlinear dynamical systems which after employing the differential flatness theory can be written in the Brunovksy (canonical) form [254, 322]. Simulation experiments on the problem of autonomous navigation of a unicycle robotic vehicle are provided to test the performance of the proposed derivative-free Kalman Filter.

7.3.2 Application of Derivative-Free Kalman Filtering to UGVs

7.3.2.1 Kinematic Models for Autonomous Vehicles

The proposed method of derivative-free nonlinear Kalman Filtering (DKF) for MIMO nonlinear systems will be analyzed through an application example. Once again the kinematic model of a UGV (unicycle robotic vehicle) is considered. This is given by

$$\begin{aligned} \dot{x} &= vcos(\theta) \\ \dot{y} &= vsin(\theta) \\ \dot{\theta} = \omega &= \tfrac{v}{L} tan(\phi) \end{aligned} \tag{7.39}$$

where $v(t)$ is the velocity of the vehicle, L is the distance between the front and the rear wheel axis of the vehicle, θ is the angle between the transversal axis of the vehicle and axis OX, and ϕ is the angle of the steering wheel with respect to the transversal axis of the vehicle. As shown in previous sections, the position of such a vehicle is described by the coordinates (x, y) of the center of its rear axis and its orientation is given by the angle θ between the x-axis and the axis of the direction of the vehicle. The steering angle ϕ and the speed v are considered to be the inputs of the system.

The problem of control of autonomous ground vehicles (AGVs) of the unicycle-type is considered once more. The position of such a vehicle is described by the coordinates (x, y) of the center of its rear axis and its orientation is given by the angle θ between the x-axis and the axis of the direction of the vehicle. The steering angle ϕ and the speed u are considered to be the inputs of the system. The kinematic model of autonomous vehicles can be expressed in the general form [415]

$$\begin{pmatrix} \dot{x} \\ \dot{y} \\ \dot{\theta} \end{pmatrix} = \begin{pmatrix} cos(\theta) & 0 \\ sin(\theta) & 0 \\ 0 & 1 \end{pmatrix} \cdot \begin{pmatrix} v(t) \\ v(t)\rho(t) \end{pmatrix} \tag{7.40}$$

where (x, y) are the coordinates of the center of the vehicle's rear wheels axis, $v(t)$ is the velocity of the vehicle, and θ is the angle between the transversal axis of the vehicle and axis OX, while $\rho(t) = 1/r(t)$ is the curvature of the robot's path. The autonomous vehicle is a nonholonomic system. Nonholonomic systems are characterized by nonintegrable differential expressions, such as

$$\sum_{i=i}^{n} f_{ij}(q_1, q_2, \cdots, q_n, t)\dot{q}_i = 0, \;\; j = 1, 2, \cdots, m \tag{7.41}$$

where $\dot{q}_i$ represents the nth generalized coordinate (state variable), m is the number of equations defining the nonholonomic constraints, $\dot{q}_i$ represents the generalized speed and f_{ij} are nonlinear functions of q_i at time t. For the kinematic model of Eq. (7.40) the following nonholonomic constraint exists:

$$\dot{x}sin(\theta) - \dot{y}cos(\theta) = 0 \tag{7.42}$$

The curvature radius for any path can be written as

$$R(t) = \frac{1}{\rho(t)} = \frac{L}{tan(\phi)} \tag{7.43}$$

where L is the distance between the front and the back wheels, and ϕ (namely the steering angle) is the angle defined by the main axis of the vehicle and the velocity vector of the front wheel (for cart like vehicles as shown in Fig. 7.1, and for car-like vehicles as shown in Fig. 7.5). The value of $R(t)$ is usually bounded by R_{min}, the minimum curvature radius.

7.3.2.2 Controller Design for UGVs

Flatness-based control can be used for steering the vehicle along a desirable trajectory. In the case of the autonomous vehicle of Eq. (7.39) the flat output is the cartesian position of the center of the wheel axis, denoted as $\eta = (x, y)$, while the other model parameters can be written as:

$$v = \pm||\dot{\eta}|| \begin{pmatrix} cos(\theta) \\ sin(\theta) \end{pmatrix} = \frac{\dot{\eta}}{v} \; tan(\phi) = ldet(\dot{\eta}\ddot{\eta})/v^3 \tag{7.44}$$

where det stands for a matrix determinant. These formulas show simply that θ is the tangent angle of the curve and $tan(\phi)$ is the associated curvature. With

reference to a generic driftless nonlinear system $\dot{q},\ q \in R^n, w \in R^m$, dynamic feedback linearization consists in finding a feedback compensator of the form

$$\begin{aligned} \dot{\xi} &= \alpha(q,\xi) + b(q,\xi)u \\ w &= c(q,\xi) + d(q,\xi)u \end{aligned} \tag{7.45}$$

with state $\xi \in R^v$ and input $u \in R^m$, such that the closed-loop system of Eq. (7.39) and Eq. (7.45) is equivalent under a state transformation $z = T(q,\xi)$ to a linear system. The starting point is the selection of a m-dimensional output $\eta = h(q)$ to which a desired behavior can be assigned (this is the previously defined *flat output*). One then proceeds by successively differentiating the output until the input appears in a non-singular way. If the sum of the output differentiation orders equals the dimension $n + v$ of the extended state space, full input-state-output linearization is obtained. The closed-loop system is then equivalent to a set of decoupled input-output chains of integrators from u_i to η_i. The exact linearization procedure is illustrated for the vehicle's model of Eq. (7.39). As flat output $\eta = (x, y)$ the coordinates of the center of the wheel axis is considered. Differentiation with respect to time then yields [371, 439]

$$\dot{\eta} = \begin{pmatrix} \dot{x} \\ \dot{y} \end{pmatrix} = \begin{pmatrix} cos(\theta) & 0 \\ sin(\theta) & 0 \end{pmatrix} \cdot \begin{pmatrix} v \\ \omega \end{pmatrix} \tag{7.46}$$

showing that only v affects $\dot{\eta}$, while the angular velocity ω cannot be recovered from this first-order differential information. To proceed, one needs to add an integrator (whose state is denoted by ξ) on the linear velocity input

$$v = \xi,\ \dot{\xi} = \alpha \Rightarrow \dot{\eta} = \xi \begin{pmatrix} cos(\theta) \\ sin(\theta) \end{pmatrix} \tag{7.47}$$

where α denotes the linear acceleration of the vehicle. Differentiating further one obtains

$$\begin{aligned} \ddot{\eta} &= \dot{\xi} \begin{pmatrix} cos(\theta) \\ sin(\theta) \end{pmatrix} + \xi\dot{\theta} \begin{pmatrix} sin(\theta) \\ cos(\theta) \end{pmatrix} = \\ &= \begin{pmatrix} cos(\theta) & -\xi sin(\theta) \\ sin(\theta) & \xi cos(\theta) \end{pmatrix} \begin{pmatrix} \alpha \\ \omega \end{pmatrix} \end{aligned} \tag{7.48}$$

and the matrix multiplying the modified input (α, ω) is nonsingular if $\xi \neq 0$. Under this assumption one defines

$$\begin{pmatrix} \alpha \\ \omega \end{pmatrix} = \begin{pmatrix} cos(\theta) & -\xi sin(\theta) \\ sin(\theta) & \xi cos(\theta) \end{pmatrix} \cdot \begin{pmatrix} u_1 \\ u_2 \end{pmatrix} \tag{7.49}$$

and $\ddot{\eta}$ is denoted as

$$\ddot{\eta} = \begin{pmatrix} \ddot{\eta}_1 \\ \ddot{\eta}_2 \end{pmatrix} = \begin{pmatrix} u_1 \\ u_2 \end{pmatrix} = u \tag{7.50}$$

which means that the desirable linear acceleration and the desirable angular velocity can be expressed using the transformed control inputs u_1 and u_2. Then, the resulting dynamic compensator is (return to the initial control inputs v and ω)

$$\begin{aligned} \dot{\xi} &= u_1 cos(\theta) + u_2 sin(\theta) \\ v &= \xi \\ \omega &= \frac{u_2 cos(\theta) - u_1 sin(\theta)}{\xi} \end{aligned} \tag{7.51}$$

Being $\xi \in R$, it is $n + v = 3 + 1 = 4$, equal to the output differentiation order in Eq. (7.50). In the new coordinates

$$\begin{aligned} z_1 &= x \\ z_2 &= y \\ z_3 &= \dot{x} = \xi cos(\theta) \\ z_4 &= \dot{y} = \xi sin(\theta) \end{aligned} \tag{7.52}$$

The extended system is thus fully linearized and described by the chains of integrators, in Eq. (7.50), and can be rewritten as

$$\ddot{z}_1 = u_1, \quad \ddot{z}_2 = u_2 \tag{7.53}$$

The dynamic compensator of Eq. (7.51) has a potential singularity at $\xi = v = 0$, i.e. when the vehicle is not moving, which is a case not met while executing the trajectory tracking. It is noted however, that the occurrence of such a singularity is structural for non-holonomic systems. In general, this difficulty must be obviously taken into account when designing control laws on the equivalent linear model. A nonlinear controller for output trajectory tracking, based on dynamic feedback linearization, is easily derived. Assume that the autonomous vehicle must follow a smooth trajectory $(x_d(t), y_d(t))$ which is persistent, i.e. for which the nominal velocity $v_d = (\dot{x}_d^2 + \dot{y}_d^2)^{\frac{1}{2}}$ along the trajectory never goes to zeros (and thus singularities are avoided). On the equivalent and decoupled system of Eq. (7.53), one can easily design an exponentially stabilizing feedback for the desired trajectory, which has the form

$$\begin{aligned} u_1 &= \ddot{x}_d + k_{p_1}(x_d - x) + k_{d_1}(\dot{x}_d - \dot{x}) \\ u_2 &= \ddot{y}_d + k_{p_1}(y_d - y) + k_{d_1}(\dot{y}_d - \dot{y}) \end{aligned} \tag{7.54}$$

and which results in the following error dynamics for the closed-loop system

$$\begin{aligned} \ddot{e}_x + k_{d_1}\dot{e}_x + k_{p_1}e_x &= 0 \\ \ddot{e}_y + k_{d_2}\dot{e}_y + k_{p_2}e_y &= 0, \end{aligned} \tag{7.55}$$

where $e_x = x - x_d$ and $e_y = y - y_d$. The proportional-derivative gains are chosen as $k_{p_1} > 0$ and $k_{d_1} > 0$ for $i = 1, 2$. Knowing the control inputs u_1, u_2, for the linearized

system one can calculate the control inputs v and ω applied to the vehicle, using Eq. (7.45). The above result is valid, provided that the dynamic feedback compensator does not meet the singularity. In the general case of design of flatness-based controllers, the following theorem assures the avoidance of singularities in the proposed control law [371]:

Theorem: Let $\lambda_{11}, \lambda_{12}$ and $\lambda_{21}, \lambda_{22}$, be respectively the eigenvalues of two equations of the error dynamics, given in Eq. (7.45). Assume that, for $i = 1, 2$ it is $\lambda_{11} < \lambda_{12} < 0$ (negative real eigenvalues), and that λ_{i2} is sufficiently small. If

$$\min_{t \geq 0} || \begin{pmatrix} \dot{x}_d(t) \\ \dot{y}_d(t) \end{pmatrix} || \geq \begin{pmatrix} \dot{\epsilon}_x^0 \\ \dot{\epsilon}_y^0 \end{pmatrix} \tag{7.56}$$

with $\dot{\epsilon}_x^0 = \dot{\epsilon}_x(0) \neq 0$ and $\dot{\epsilon}_y^0 = \dot{\epsilon}_y(0) \neq 0$, then the singularity $\xi = 0$ is never met.

7.3.2.3 Derivative-Free Kalman Filtering for UGVs

It is assumed now that the vehicle's velocity has to be estimated through the processing of the sequence of position measurements by a filtering algorithm. To this end the derivative-free nonlinear Kalman Filter for MIMO nonlinear dynamical systems can been used. From the previous application of the differential flatness theory, it is possible to transform the initial nonlinear vehicle's model into a linearized equivalent model that is finally written in the Brunovsky form. Thus one arrives at Eq. (7.50) which means $\ddot{x} = u_1$ and $\ddot{y} = u_2$. Next, the state variables $x_1 = x$, $x_2 = \dot{x}$, $x_3 = y$ and $x_4 = \dot{y}$ are defined. Considering the state vector $x \in R^{4\times 1}$, the following matrices are also defined

$$A = \begin{pmatrix} 0 & 1 & 0 & 0 \\ 0 & 0 & 0 & 0 \\ 0 & 0 & 0 & 1 \\ 0 & 0 & 0 & 0 \end{pmatrix}, \quad B = \begin{pmatrix} 0 & 0 \\ 1 & 0 \\ 0 & 0 \\ 0 & 1 \end{pmatrix}, \quad C = \begin{pmatrix} 1 & 0 & 0 & 0 \\ 0 & 0 & 1 & 0 \end{pmatrix} \tag{7.57}$$

Using the matrices of Eq. (7.57) one obtains the Brunovsky form of the MIMO robot model

$$\begin{aligned} \dot{x} &= Ax + Bv \\ y &= Cx \end{aligned} \tag{7.58}$$

where the new input v is given by $v = [u_1(x, t), u_2(x, t)]^T$. For the unicycle robotic model of Eq. (7.58) state estimation can be performed using the standard Kalman Filter recursion, as described in Eqs. (4.88) and (4.89).

7.3.3 Simulation Tests

7.3.3.1 Extended Kalman Filter Based Navigation of the Autonomous Vehicle

The vehicle's kinematic model of Eq. (7.39) is considered. A GPS sensor or encoders placed at the vehicle's wheels can be used to provide measurements of the cartesian coordinates of the vehicle $x(t)$ and $y(t)$ (displacement of the vehicle), over a sampling period T. The values of the vehicle's velocity components along the x and y axes are not directly available and are estimated through the processing of the sequence of position measurements with the use of a filtering algorithm. Computing the vehicle's speed through the differentiation of the position measurements would introduce cumulative errors in the value of the vehicle's velocity, which in turn can affect the performance of the control loop. To avoid such errors an estimation of the vehicle's velocity is obtained through the processing of the sequence of position measurements with the use of a filtering algorithm.

Assuming a constant sampling period $\Delta t_k = T$ the measurement equation is $z(k+1) = \gamma(x(k)) + v(k)$, where $z(k)$ is the vector containing the sequence of measurements of the cartesian coordinates of the vehicle and $v(k)$ is the measurement noise vector.

$$z(k) = [x(k) + v_1(k), y(k) + v_2(k)], \ k = 1, 2, 3 \cdots \tag{7.59}$$

To obtain the Extended Kalman Filter (EKF), the kinematic model of the vehicle is linearized about the estimates $\hat{x}(k)$ and $\hat{x}^-(k)$, and the control input $U(k)$ is applied. Using that the continuous-time state-space description of the system is

$$\dot{x} = \phi(x, u) + wz = \gamma(x) + v \tag{7.60}$$

and by defining matrices $A = I + T_s J_x \phi(x, u)(x)$, $B = T_s J_u \phi(x, u)$ and $C = J_x \gamma(x)$ the linearized description of the system is obtained:

$$\begin{aligned} x(k+1) &= Ax + Bu(k) + w(k) \\ z(k) &= Cx(k) + v(k) \end{aligned} \tag{7.61}$$

The EKF recursion consists of the measurement update part and of the time update part as described in Eqs. (4.88) and (4.89), respectively.

One has to use the input gain matrix $B(k)$

$$B(k) = \begin{pmatrix} T_s cos(\theta(k)) & 0 \\ T_s sin(\theta(k)) & 0 \\ 0 & T \end{pmatrix} \tag{7.62}$$

and to compute the drift matrix $A(k)$ as follows

$$A(k) = \begin{pmatrix} 1 & 0 & -v(k)sin(\theta)T_s \\ 0 & 1 & v(k)cos(\theta)T_s \\ 0 & 0 & 1 \end{pmatrix} \tag{7.63}$$

while for the elements of the process noise covariance matrix which is given by $Q(k) = diag[\sigma^2(k), \sigma^2(k), \sigma^2(k)]$ indicative values would be $\sigma^2(k) = 10^{-3}$.

Using the estimated state vector, function $\phi(x)$ appearing in the state equations part and $\gamma(x)$ appearing in the measurements equations part of the vehicle's kinematic model become $\phi(\hat{x}(k)) = [\hat{x}(k), \hat{y}(k)]^T$, and $\gamma(\hat{x}(k)) = [\hat{x}(k), \hat{y}(k)]$, respectively. The associated Jacobian matrix $J_\gamma^T(\hat{x}^-(k))$ is given by

$$J_\gamma(\hat{x}^-(k)) = \begin{pmatrix} 1 & 0 & 0 \\ 0 & 1 & 0 \end{pmatrix} \tag{7.64}$$

The vehicle is steered by the flatness-based controller analyzed in Sect. 7.3.2

$$\begin{aligned} u_1 &= \ddot{x}_d + K_{p_1}(x_d - x) + K_{d_1}(\dot{x}_d - \dot{x}) \\ u_2 &= \ddot{y}_d + K_{p_2}(y_d - y) + K_{d_2}(\dot{y}_d - \dot{y}) \\ \dot{\xi} &= u_1 cos(\theta) + u_2 sin(\theta) \\ v = \xi, \;\; \omega &= \frac{u_2 cos(\theta) - u_1 sin(\theta)}{\xi} \end{aligned} \tag{7.65}$$

The use of EKF for estimating the vehicle's velocity along the x-axis (denoted as $\dot{x}$) and the vehicle's velocity along the y-axis (denoted as $\dot{y}$) enables the successful application of nonlinear steering control of Eq. (7.65).

Indicative results about tracking of the circular reference trajectory with use of the Extended Kalman Filter are shown in Figs. 7.6, 7.7, 7.8 and 7.9. In Fig. 7.6 one can notice the accuracy of tracking of the reference trajectory, achieved by the proposed state estimation-based control scheme. In Fig. 7.7 the accuracy of tracking of the x and y axis position setpoints is depicted. In Fig. 7.8, the associated x and y axis tracking errors are shown. Finally, in Fig. 7.9 the x and y axis velocity estimation errors are given.

Indicative results about tracking of the eight-shaped reference trajectory with use of the Extended Kalman Filter are shown in Figs. 7.10, 7.11 and 7.12 and 7.13. In Fig. 7.10 one can notice the accuracy of tracking of the reference trajectory, achieve by the proposed state estimation-based control scheme. In Fig. 7.11 the accuracy of tracking of the x and y axis position setpoints is depicted. In Fig. 7.12, the associated x and y axis tracking errors are shown. Finally, in Fig. 7.13 the x and y axis velocity estimation errors are given.

Indicative results about tracking of the complex-curved reference trajectory with use of the Extended Kalman Filter are shown in Figs. 7.14, 7.15, 7.16 and 7.17. In Fig. 7.14 one can notice the accuracy of tracking of the reference trajectory, achieve by the proposed state estimation-based control scheme. In Fig. 7.15 the accuracy of

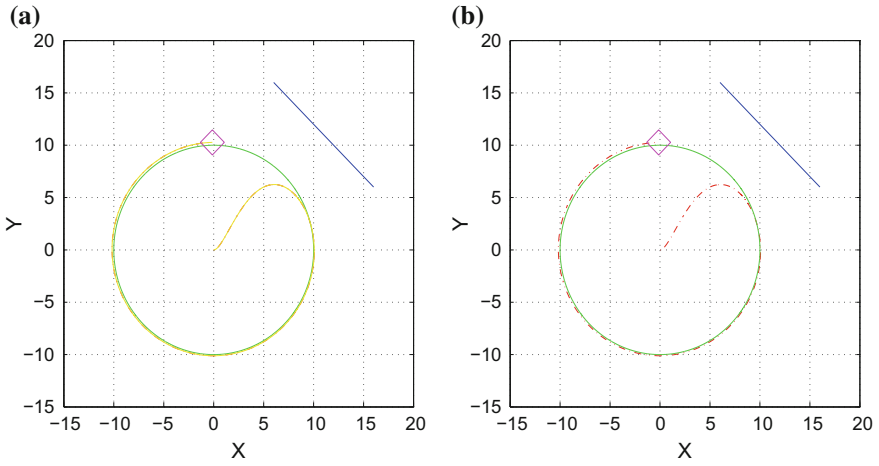

Fig. 7.6 **a** Tracking of a circular reference trajectory (green line) by the autonomous vehicle and associated estimation of the vehicle's position provided by the Extended Kalman Filter (continuous yellow line) **b** Tracking of a circular reference trajectory (green line) by the autonomous vehicle and real position of the vehicle (dashed red line)

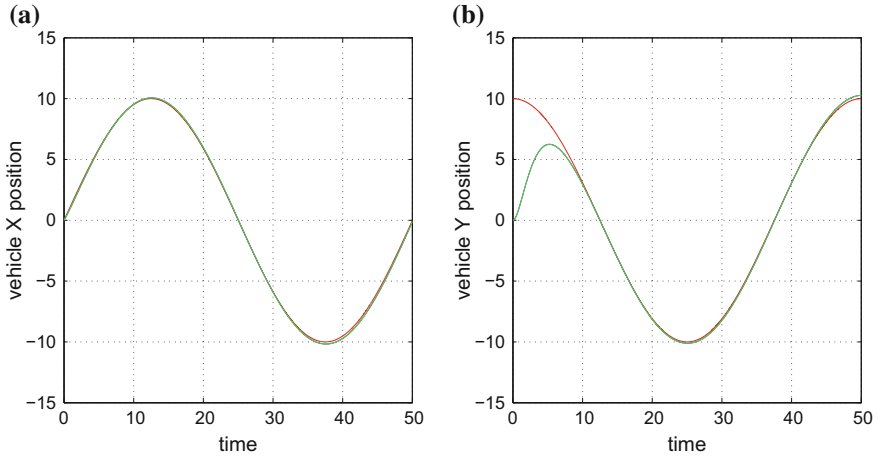

Fig. 7.7 Tracking of a circular reference trajectory with use of the EKF: **a** tracking of the x-axis reference set-point **b** tracking of the y-axis reference set-point

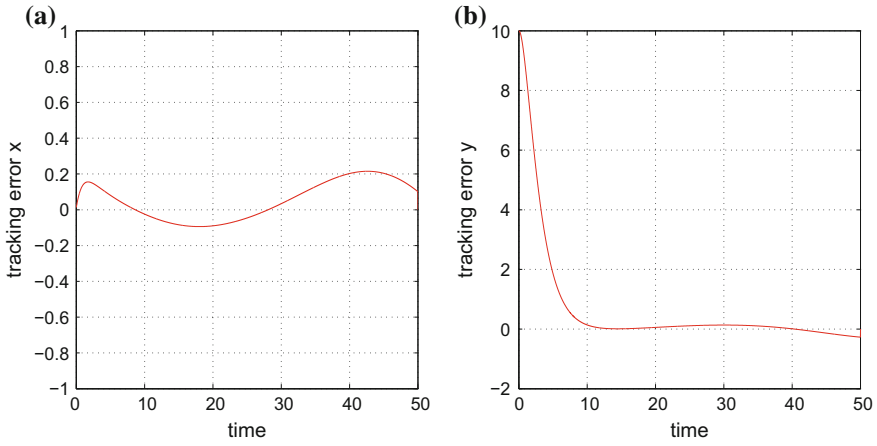

Fig. 7.8 Tracking of a circular reference trajectory with use of the EKF: **a** tracking error along the x-axis **b** tracking error along the y-axis

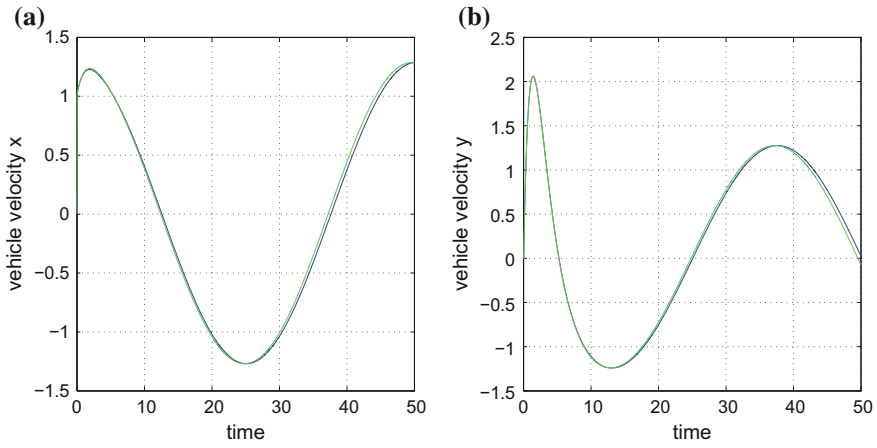

Fig. 7.9 Tracking of a circular reference trajectory by the autonomous vehicle with use of the EKF: **a** convergence of the estimated x-axis velocity (green line) to the associated real velocity (blue line) **b** convergence of the estimated y-axis velocity (green line) to the associated real velocity (green line)

tracking of the x and y axis position setpoints is depicted. In Fig. 7.16, the associated x and y axis tracking errors are shown. Finally, in Fig. 7.17 the x and y axis velocity estimation errors are given.

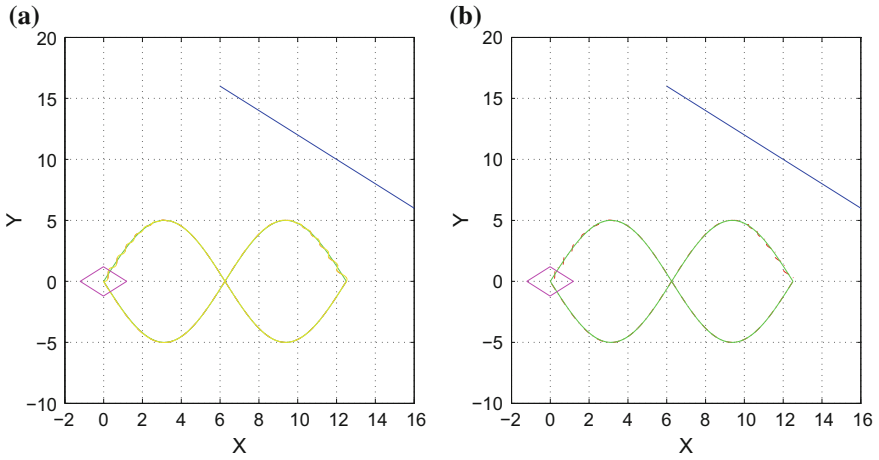

Fig. 7.10 **a** Tracking of an eight-shaped reference trajectory (green line) by the autonomous vehicle and associated estimation of the vehicle's position provided by the Extended Kalman Filter (yellow line) **b** Tracking of a circular reference trajectory (green line) by the autonomous vehicle and real position of the vehicle (dashed red line)

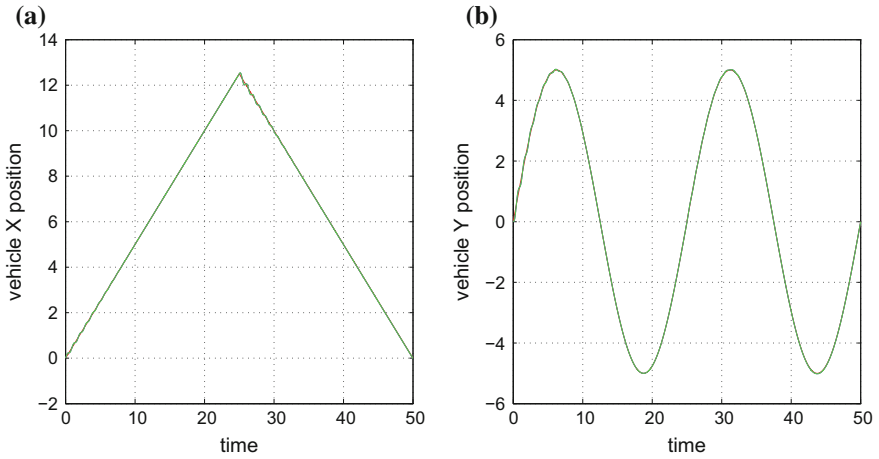

Fig. 7.11 Tracking of an eight-shaped reference trajectory with use of the EKF: **a** tracking of the x-axis reference set-point **b** tracking of the y-axis reference set-point

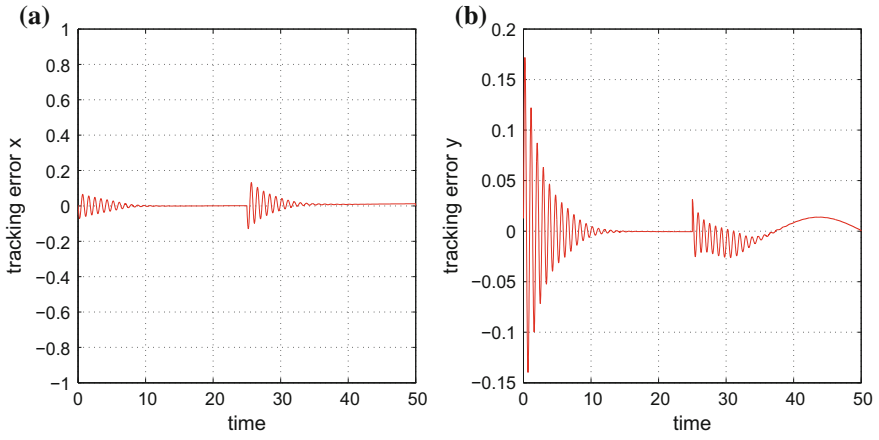

Fig. 7.12 Tracking of an eight-shaped reference trajectory with use of the EKF: **a** tracking error along the x-axis **b** tracking error along the y-axis

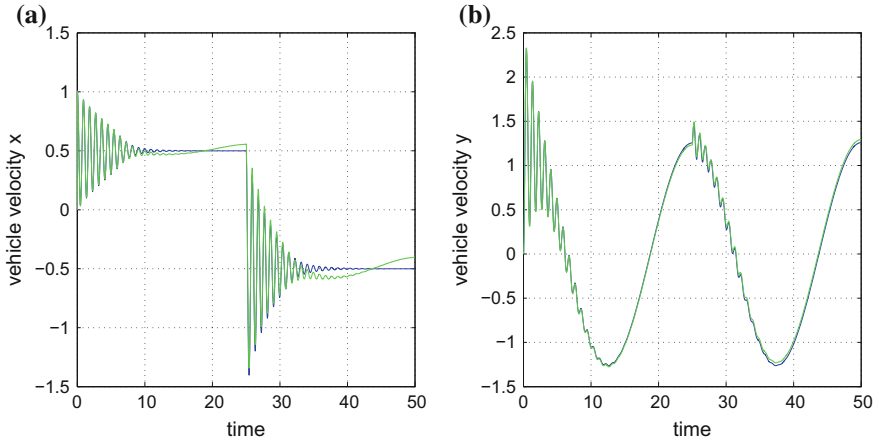

Fig. 7.13 Tracking of an eight-shaped reference trajectory by the autonomous vehicle with use of the EKF: **a** convergence of the estimated x-axis velocity (green line) to the associated real velocity (blue line) **b** convergence of the estimated y-axis velocity (green line) to the associated real velocity (green line)

7.3.3.2 Derivative-Free Kalman Filter Based Navigation of the Autonomous Vehicle

A second set of tests focused on the performance of the proposed Derivative-free nonlinear Kalman Filter (DKF) in the problem of state estimation-based control of an autonomous vehicle (cart-like robot) (Fig. 7.1). The differentially flat model of the autonomous vehicle and its transformation to the Brunovksy form has been

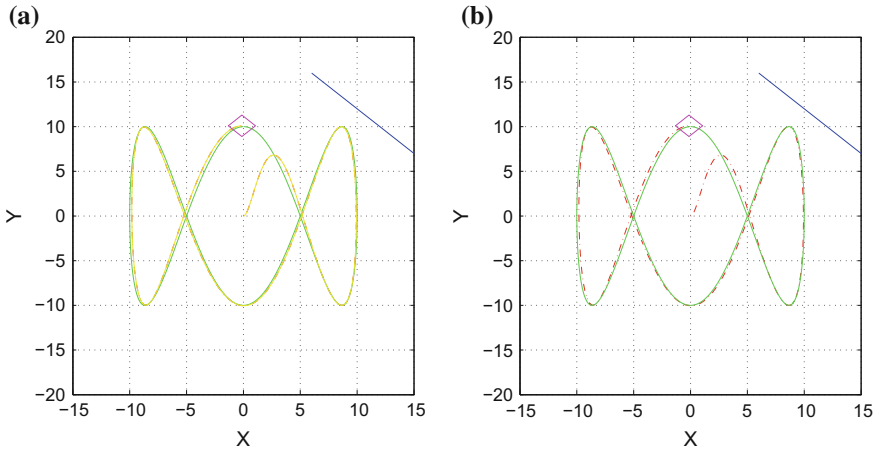

Fig. 7.14 **a** Tracking of a complex-curved reference trajectory (green line) by the autonomous vehicle and associated estimation of the vehicle's position provided by the Extended Kalman Filter (yellow line) **b** Tracking of a circular reference trajectory (green line) by the autonomous vehicle (red dashed line) and real position of the vehicle (dashed red line)

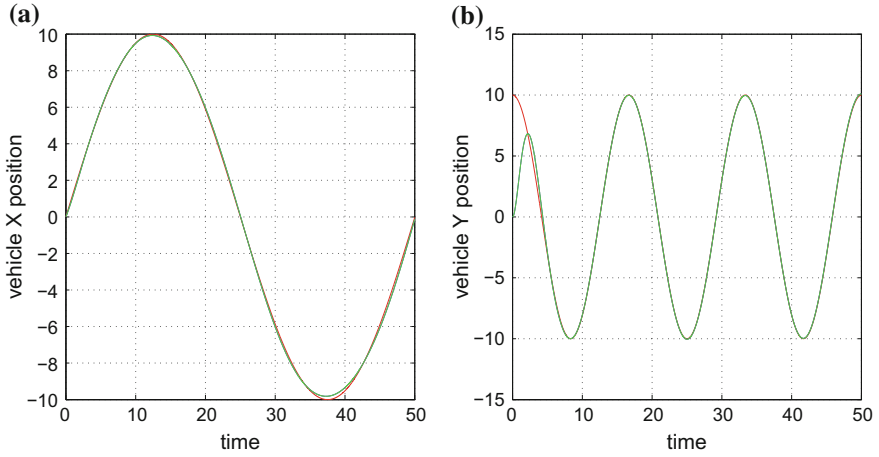

Fig. 7.15 Tracking of a complex-curved reference trajectory with use of the EKF: **a** tracking of the x-axis reference set-point **b** tracking of the y-axis reference set-point

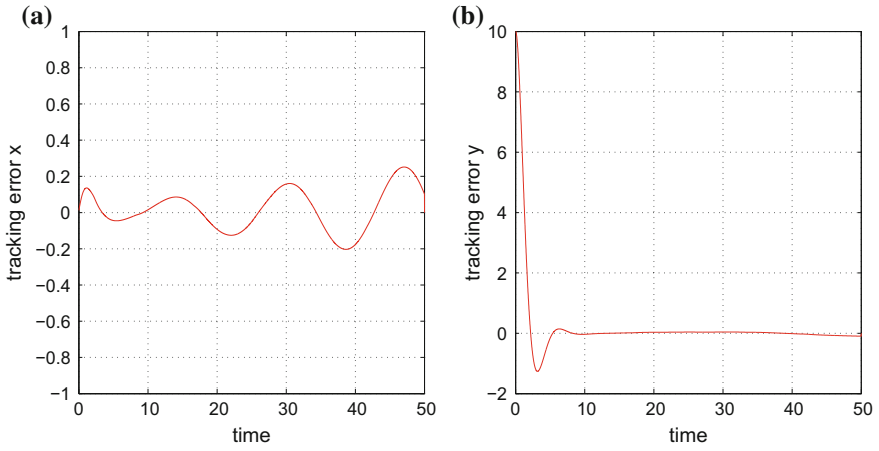

Fig. 7.16 Tracking of a complex-curved reference trajectory with use of the EKF: **a** tracking error along the x-axis **b** tracking error along the y-axis

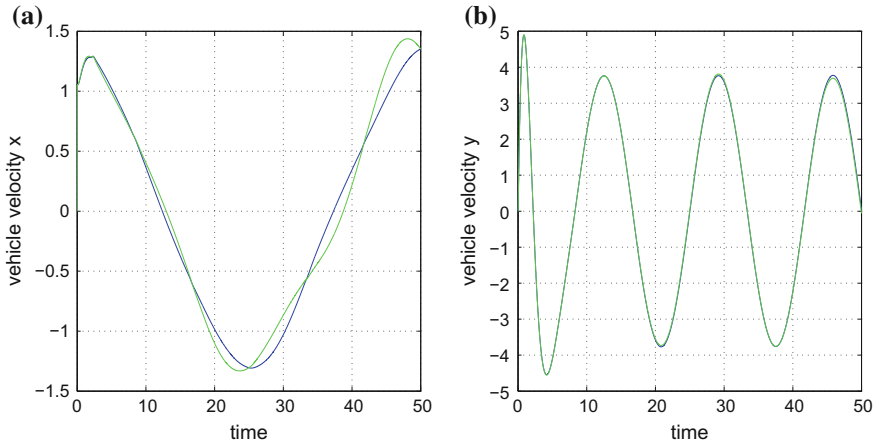

Fig. 7.17 Tracking of a complex-curved reference trajectory by the autonomous vehicle with use of the EKF: **a** convergence of the estimated x-axis velocity (green line) to the associated real velocity (blue line) **b** convergence of the estimated y-axis velocity (green line) to the associated real velocity (green line)

analyzed in Eqs. (7.39) and (7.46). The state estimation algorithm of the Derivative-free nonlinear Kalman Filter consisted of Eqs. (4.88) and (4.89). It was assumed that only measurements of the cartesian coordinates of the vehicle (displacement on the xy-plane) could be obtained through a GPS unit (localization of moderate accuracy), RTK-GPS (localization of higher accuracy) or through laser, visual and sonar sensors with reference to specific landmarks (the latter measuring approaches require transformation from a local to a global coordinates system).

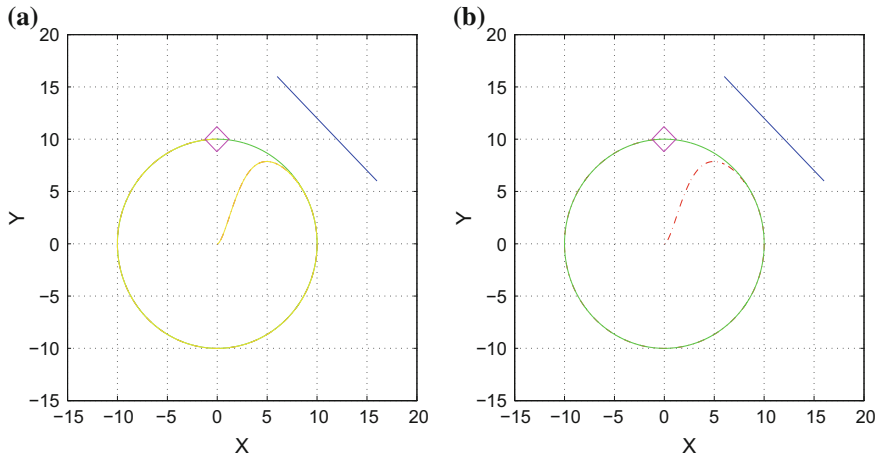

Fig. 7.18 **a** Tracking of a circular reference trajectory (green line) by the autonomous vehicle and associated estimation of the vehicle's position provided by the derivative-free Kalman Filter (yellow line) **b** Tracking of a circular reference trajectory (green line) by the autonomous vehicle and real position of the vehicle (dashed red line)

Indicative results about tracking of the circular reference trajectory with use of the Derivative-free nonlinear Kalman Filter are shown in Figs. 7.18, 7.19 and 7.20. Comparing the estimation performed by the derivative-free MIMO nonlinear Kalman Filter with the one performed by the Extended Kalman Filter it can be noticed that the derivative-free filtering approach results in more accurate state estimates.

Indicative results about tracking of the circular reference trajectory with use of the Derivative-free nonlinear Kalman Filter are shown in Figs. 7.18, 7.19 and 7.20. In Fig. 7.18 one can notice the accuracy of tracking of the reference trajectory, achieved by the proposed state estimation-based control scheme. In Fig. 7.19, the associated x and y axis tracking errors are shown. Finally, in Fig. 7.20 the x and y axis velocity estimation errors are given.

Indicative results about tracking of the eight-shaped reference trajectory with use of the Extended Kalman Filter are shown in Figs. 7.21, 7.22, 7.23 and 7.24. In Fig. 7.21 one can notice the accuracy of tracking of the reference trajectory, achieved by the proposed state estimation-based control scheme. In Fig. 7.22 the accuracy of tracking of the x and y axis position setpoints is depicted. In Fig. 7.23, the associated x and y axis tracking errors are shown. Finally, in Fig. 7.24 the x and y axis velocity estimation errors are given.

Indicative results about tracking of the complex-curved reference trajectory with use of the Extended Kalman Filter are shown in Figs. 7.25, 7.26, 7.27 and 7.28. In Fig. 7.25 one can notice the accuracy of tracking of the reference trajectory, achieved by the proposed state estimation-based control scheme. In Fig. 7.26 the accuracy of tracking of the x and y axis position setpoints is depicted. In Fig. 7.27, the associated

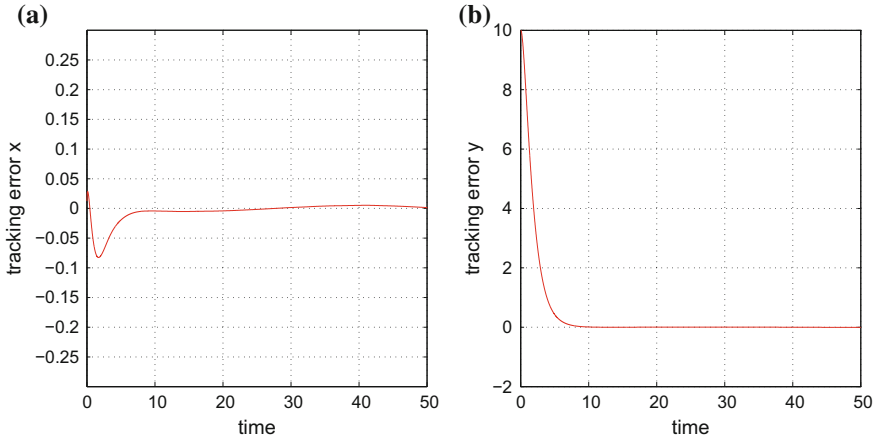

Fig. 7.19 Tracking of a circular reference trajectory with use if the DKF: **a** tracking error along the x-axis **b** tracking error along the y-axis

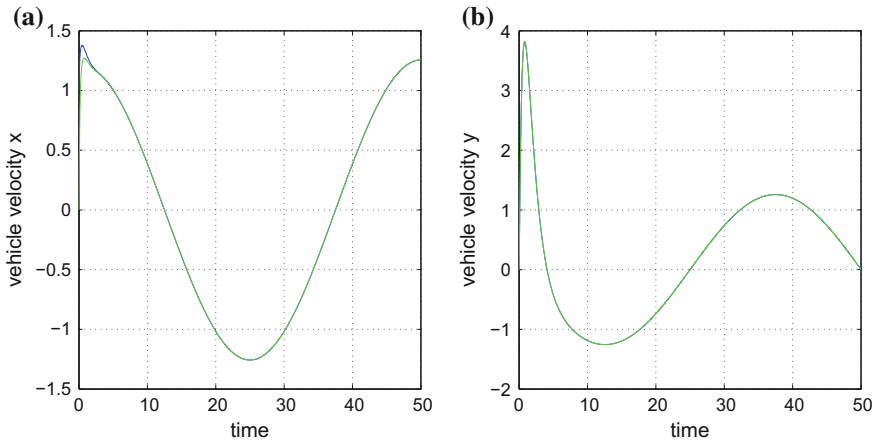

Fig. 7.20 Tracking of a circular reference trajectory by the autonomous vehicle with use of the DKF: **a** convergence of the estimated x-axis velocity (green line) to the associated real velocity (blue line) **b** convergence of the estimated y-axis velocity (green line) to the associated real velocity (green line)

x and y axis tracking errors are shown. Finally, in Fig. 7.28 the x and y axis velocity estimation errors are given.

Comparing the estimation performed by the Derivative-free nonlinear Kalman Filter with the one performed by the Extended Kalman Filter it can be noticed that the derivative-free filtering approach results in more accurate state estimates. Moreover, comparing the associated state estimation-based control loop of the autonomous vehicle that was based on the derivative-free MIMO nonlinear Kalman Filter to the

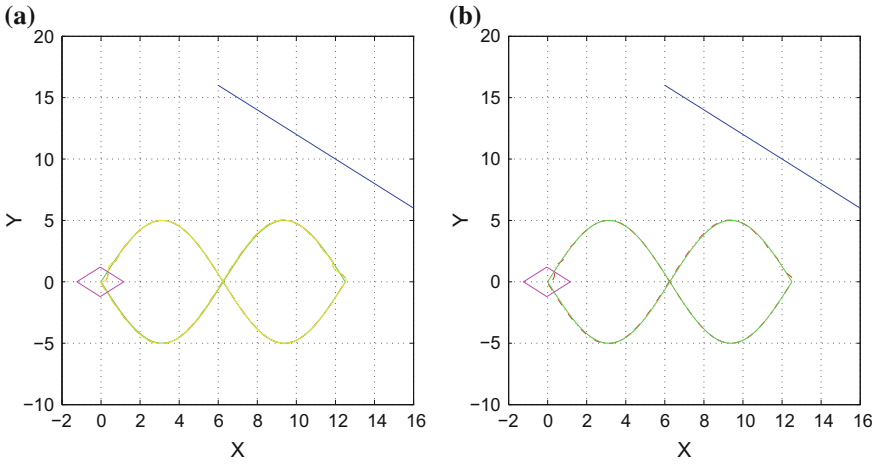

Fig. 7.21 **a** Tracking of an eight-shaped reference trajectory (green line) by the autonomous vehicle and associated estimation of the vehicle's position provided by the derivative-free Kalman Filter (yellow line) **b** Tracking of a circular reference trajectory (green line) by the autonomous vehicle and real position of the vehicle (dashed red line)

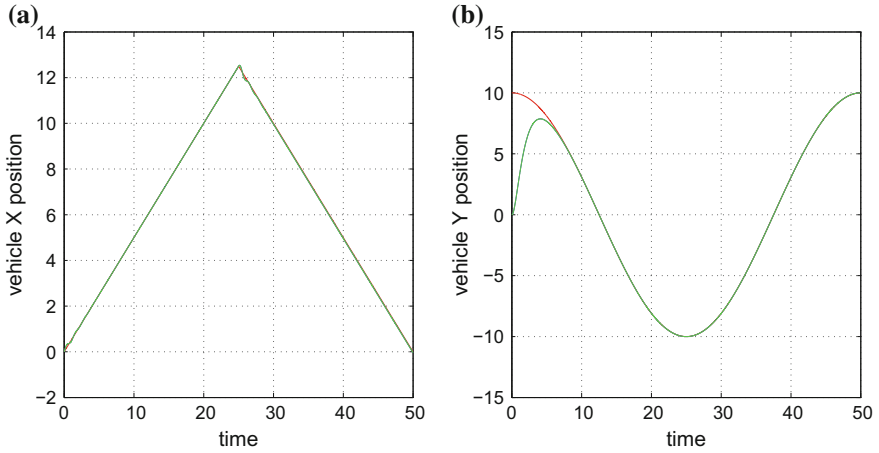

Fig. 7.22 Tracking of an eight-shaped reference trajectory with use of the DKF: **a** tracking of the x-axis reference set-point **b** tracking of the y-axis reference set-point

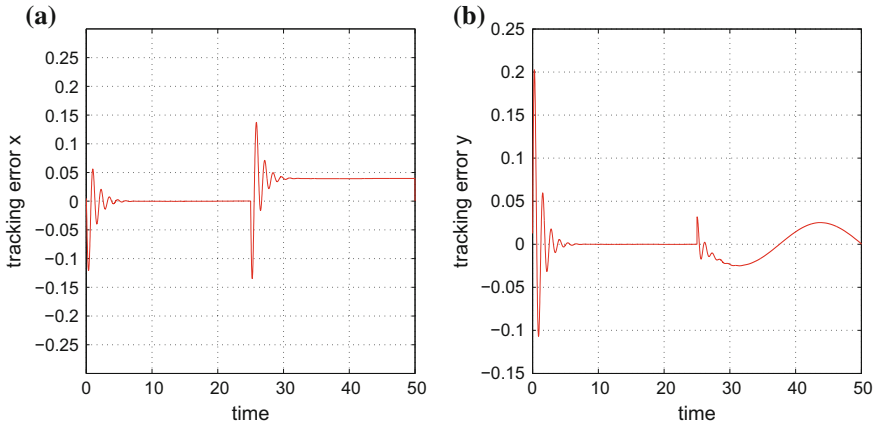

Fig. 7.23 Tracking of an eight-shaped reference trajectory with use of the DKF: **a** tracking error along the x-axis **b** tracking error along the y-axis

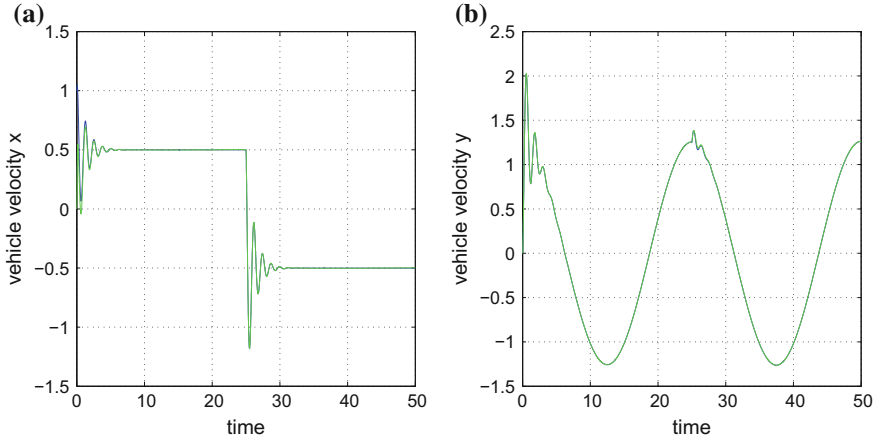

Fig. 7.24 Tracking of an eight-shaped reference trajectory by the autonomous vehicle with use of the DKF: **a** convergence of the estimated x-axis velocity (green line) to the associated real velocity (blue line) **b** convergence of the estimated y-axis velocity (green line) to the associated real velocity (green line)

control that relied on the Extended Kalman Filter it was observed that the first control scheme was significantly more robust and capable of tracking with better accuracy the desirable trajectories. These findings show the suitability of the considered Derivative-free nonlinear Kalman Filter for localization, control and autonomous navigation of autonomous vehicles. Finally, it is noted that the section's approach can be applied also to various types of 4-wheel robotic vehicles.

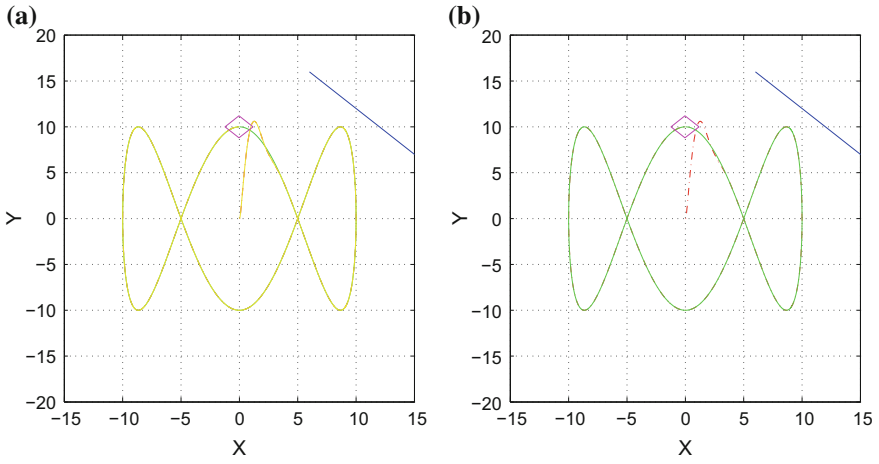

Fig. 7.25 **a** Tracking of a complex-curved reference trajectory (green line) by the autonomous vehicle and associated estimation of the vehicle's position provided by the derivative-free Kalman Filter (yellow line) **b** Tracking of a circular reference trajectory (green line) by the autonomous vehicle and real position of the vehicle (dashed red line)

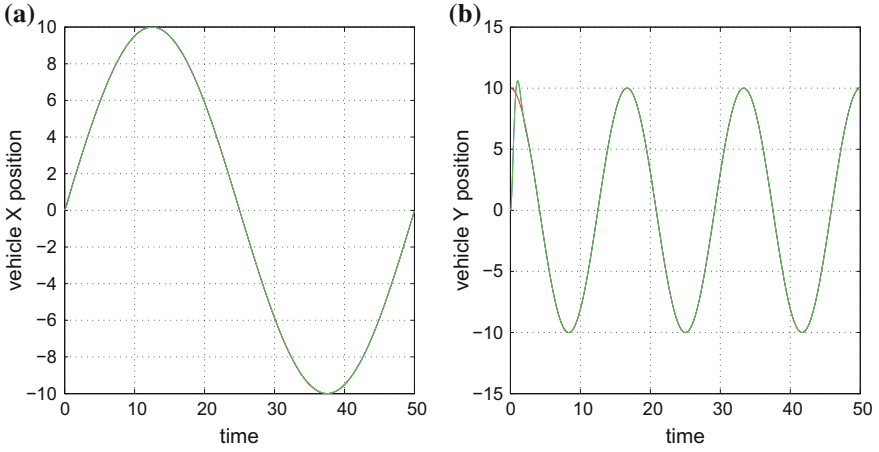

Fig. 7.26 Tracking of a complex-curved reference trajectory with use of the DKF: **a** tracking of the x-axis reference set-point **b** tracking of the y-axis reference set-point

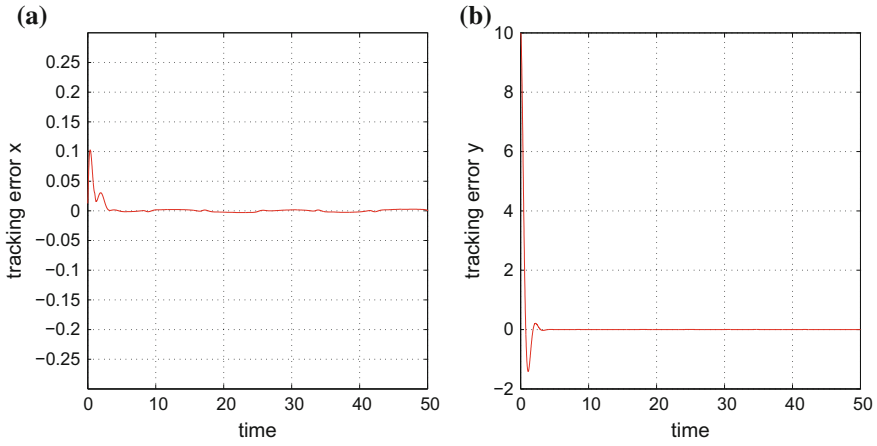

Fig. 7.27 Tracking of a complex-curved reference trajectory with use of the DKF: **a** tracking error along the x-axis **b** tracking error along the y-axis

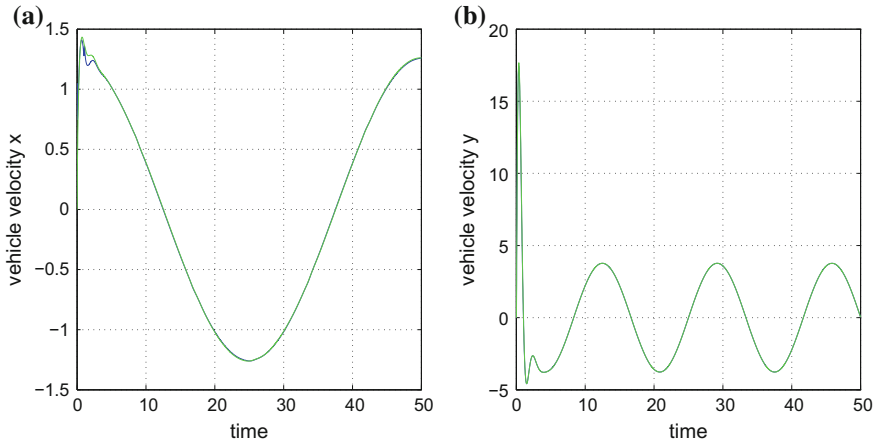

Fig. 7.28 Tracking of a complex-curved reference trajectory by the autonomous vehicle with use of the DKF: **a** convergence of the estimated x-axis velocity (green line) to the associated real velocity (blue line) **b** convergence of the estimated y-axis velocity (green line) to the associated real velocity (green line)

7.4 Nonlinear Optimal Control of Autonomous Two-Wheel Vehicles

7.4.1 Outline

Autonomous or semi-autonomous navigation of two-wheel vehicles such as motorcycles, requires that several of their functionalities and driving tasks, are automatically performed [74, 81, 154, 615, 626]. To achieve this objective, the need of developing and using elaborated control and estimation methods for motorcycles has become apparent [15, 324, 479, 481, 610]. To this end, several results have been developed aiming at solving the stabilization and path tracking problems for autonomous or semi-autonomous motorcycles [71, 104, 114, 173, 293, 410, 565]. Due to underactuation in the motorcycle's model and the strong nonlinearities characterizing its state-space description, the solution of the associated motion problem is a difficult and challenging endeavour [102, 103, 113, 115]. To achieve a satisfactory solution of the problem of autonomous motorcycles driving, in this section a nonlinear optimal (H-infinity) controller is developed [419, 461].

First, the joint kinematic and dynamic model of the motorcycle undergoes approximate linearization around a temporary operating point (equilibrium) which is recomputed at each iteration of the control method. This equilibrium is defined by the present value of the system's state vector and the last value of the control inputs vector that was exerted on it. The linearization procedure requires first order Taylor series expansion of the state-space description of the motorcycle and computation of the associated Jacobian matrices [33, 431, 463]. The modelling error which is due to the truncation of higher-order terms in the Taylor series expansion is considered to be a disturbance which is eliminated by the robustness of the control loop. Next, for the approximately linearized model of the motorcycle an optimal (H-infinity) feedback controller is designed.

The H-infinity controller represents the solution of the optimal control problem for the model of the autonomous motorcycle, under model uncertainty and external perturbations. It actually stands for the solution of a min-max differential game, in which the controller tries to minimize a cost function comprising a quadratic term of the state vector's tracking error, whereas the model uncertainty and external perturbation terms try to maximize this cost function. For the computation of the controller's feedback gain it is necessary to solve an algebraic Riccati equation at each time-step of the control method [450, 457, 459]. The stability properties of the control method are proven through Lyapunov analysis. First, it is demonstrated that the control loop of the motorcycle satisfies the H-infinity tracking performance criterion. This signifies elevated robustness against model uncertainty and external perturbations affecting the motorcycle's motion [305, 564]. Next, it is proven that the control loop is also globally asymptotically stable, which ascertains precise tracking of reference paths. Moreover, to implement a state estimation-based control scheme for the autonomous motorcycle, through the processing of measurements from a small number of on-board sensors, the H-infinity Kalman Filter is proposed as a robust state estimator [169, 511].

7.4.2 Dynamic and Kinematic Model of the Riderless Motorcycle

As noted above the control and stabilization problem of the autonomous motorcycle is a nontrivial one. The use of nonlinear optimal (H-infinity) control for this problem is in several aspects advantageous. Comparing for instance against global linearization-based control schemes, the proposed nonlinear optimal control does not require complicated transformations (diffeomorphisms) for bringing the state-space model of the system into an equivalent linear form. Besides, it does not come against singularity problems because for computing the control inputs that will be finally exerted on the vehicle's model there is no need to implement inverse transformations which in-turn imply matrices inversions. Comparing against other optimal control methods it can be noted that Model Predictive Control is unsuitable for the model of the autonomous motorcycle because such a control method is addressed to linear dynamical systems and cannot compensate for strong nonlinearities. It can be also noted that Nonlinear Model Predictive Control, being a popular optimal control approach for nonlinear dynamical systems is not of assured convergence while its iterative search for an optimum is dependent on initial parametrization. On the other side, backstepping control cannot be directly applied to the model of the of the autonomous motorcycle because this is not inherently found in the triangular form. Furthermore, the application of sliding-mode control is hindered by the fact that the model of the autonomous motorcycle is not found inherently into a canonical form. Finally, PID control which is widely used by practitioners in the area of robotics is an unreliable methodology because the tuning of such a controller is performed in a heuristic manner around local operating points where the unrealistic assumption is made that the dynamics of the autonomous motorcycle remains linear. Such a control method lacks a global stability proof.

The main parameters of the autonomous motorcycle are described in Fig. 7.29. By defining as $\sigma = \frac{tan(\delta)}{p}$ the joint kinematic and dynamic model of the riderless motorcycle is given by [154]

$$\dot{x} = vcos(\psi) \tag{7.66}$$

$$\dot{y} = vsin(\psi) \tag{7.67}$$

$$\dot{\psi} = v\frac{tan(\delta)}{p} \tag{7.68}$$

$$\ddot{\phi} = \frac{1}{h}\{gsin(\phi) + cos(\psi)[(1 + h\sigma sin(\phi))\sigma v^2 + h\ddot{\psi}]\} \tag{7.69}$$

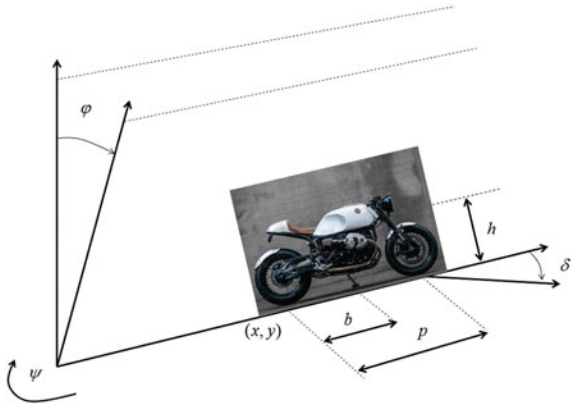

Fig. 7.29 Diagram of the two-wheel autonomous vehicle (riderless motorcycle)

By differentiating Eq. (7.68) one obtains [154]:

$$\ddot{\psi} = v\frac{\dot{\delta}}{pcos^2(\delta)} + \dot{v}\frac{\tan(\delta)}{p} \tag{7.70}$$

The following state variables are defined: $x_1 = x$, $x_2 = y$, $x_3 = \psi$, $x_4 = \phi$, $x_5 = \dot{\phi}$, $x_6 = v$, $x_7 = \delta$. Moreover, the following control inputs are defined $u_1 = \dot{v}$, $u_2 = \dot{\delta}$, that is the control inputs of the autonomous motorcycle are its acceleration and the rate of turn of the angle of its steering wheel. The state-space description of the system becomes:

$$\begin{gathered}
\dot{x}_1 = x_6 cos(x_3) \\
\dot{x}_2 = x_6 sin(x_3) \\
\dot{x}_3 = x_6\frac{tan(x_7)}{p} \\
\dot{x}_4 = x_5 \\
\dot{x}_5 = \frac{1}{h}\left\{gsin(x_4) + cos(x_4)\left[(1 + h\sigma sin(x_4))\sigma x_6^2 + bcos(x_4)\left(u_2\frac{x_6}{pcos^2(x_7)} + u_1\frac{tan(x_7)}{p}\right)\right]\right\} \\
\dot{x}_6 = u_1 \\
\dot{x}_7 = u_2
\end{gathered} \tag{7.71}$$

In vector form, one obtains the state-space description

$$\dot{x} = f(x) + G(x)u \tag{7.72}$$

where $G(x) = [g_1(x)\ g_2(x)]$ is the control inputs gain, or analytically

$$\begin{pmatrix}\dot{x}_1\\ \dot{x}_2\\ \dot{x}_3\\ \dot{x}_4\\ \dot{x}_5\\ \dot{x}_6\\ \dot{x}_7\end{pmatrix} = \begin{pmatrix} x_6 cos(x_3)\\ x_6 sin(x_3)\\ x_6 \frac{tan(x_7)}{p}\\ x_5\\ \frac{1}{h}\{g sin(x_4 + cos(x_4)[(1 + h\sigma sin(x_4))\sigma x_6^2])\}\\ 0\\ 0\end{pmatrix} + \\ + \begin{pmatrix} 0 & 0\\ 0 & 0\\ 0 & 0\\ 0 & 0\\ \frac{bcos(x_4)tan(x_7)}{p} & \frac{bcos(x_4)x_6}{pcos^2(x_7)}\\ 1 & 0\\ 0 & 1\end{pmatrix}\begin{pmatrix}u_1\\ u_2\end{pmatrix} \tag{7.73}$$

7.4.3 Approximate Linearization of the Model of the Riderless Motorcycle

Linearization is performed around the temporary operating point (x^*, u^*), where x^* is the present value of the state-vector of the two-wheel unmanned vehicle and u^* is the last value of the control input vector that was exerted on it. One has the linearized model $\dot{x} = Ax + Bu + \tilde{d}$ with:

$$A = \nabla_x[f(x) + G(x)u] \mid_{(x^*,u^*)} \Rightarrow \\ A = [\nabla_x f(x) + \nabla_x g_1(x)u_1 + \nabla_x g_2(x)u_2] \mid_{(x^*,u^*)} \tag{7.74}$$

$$B = \nabla_u[f(x) + G(x)u] \mid_{(x^*,u^*)} \Rightarrow \\ B = G(x) \mid_{(x^*,u^*)} \tag{7.75}$$

About the Jacobian matrix $\nabla_x f(x)|_{(x^*,u^*)}$ one has

$$\nabla_x f(x) \mid_{(x^*,u^*)} = \begin{pmatrix} \frac{\partial f_1}{\partial x_1} & \frac{\partial f_1}{\partial x_2} & \dots & \frac{\partial f_1}{\partial x_7}\\ \frac{\partial f_2}{\partial x_1} & \frac{\partial f_2}{\partial x_2} & \dots & \frac{\partial f_2}{\partial x_7}\\ \dots & \dots & \dots & \dots\\ \frac{\partial f_7}{\partial x_1} & \frac{\partial f_7}{\partial x_2} & \dots & \frac{\partial f_7}{\partial x_7}\end{pmatrix} \mid_{(x^*,u^*)} \tag{7.76}$$

For the first row of the Jacobian matrix $\nabla_x f(x)|_{(x^*,u^*)}$ it holds: $\frac{\partial f_1}{\partial x_1} = 0$, $\frac{\partial f_1}{\partial x_2} = 0$, $\frac{\partial f_1}{\partial x_3} = -x_6 sin(x_3)$, $\frac{\partial f_1}{\partial x_4} = 0$, $\frac{\partial f_1}{\partial x_5} = 0$, $\frac{\partial f_1}{\partial x_6} = cos(x_3)$, $\frac{\partial f_1}{\partial x_7} = 0$.

For the second row of the Jacobian matrix $\nabla_x f(x)|_{(x^*,u^*)}$ it holds: $\frac{\partial f_2}{\partial x_1} = 0$, $\frac{\partial f_2}{\partial x_2} = 0$, $\frac{\partial f_2}{\partial x_3} = x_6 cos(x_3)$, $\frac{\partial f_2}{\partial x_4} = 0$, $\frac{\partial f_2}{\partial x_5} = 0$, $\frac{\partial f_2}{\partial x_6} = 0 sin(x_3)$, $\frac{\partial f_1}{\partial x_7} = 0$.

For the third row of the Jacobian matrix $\nabla_x f(x)|_{(x^*,u^*)}$ it holds: $\frac{\partial f_3}{\partial x_1} = 0$, $\frac{\partial f_3}{\partial x_2} = 0$, $\frac{\partial f_3}{\partial x_3} = 0$, $\frac{\partial f_3}{\partial x_4} = 0$, $\frac{\partial f_3}{\partial x_5} = 0$, $\frac{\partial f_3}{\partial x_6} = \frac{tan(x_7)}{p}$, $\frac{\partial f_3}{\partial x_7} = x_6 \frac{1}{pcos^2(x_7)}$.

For the fourth row of the Jacobian matrix $\nabla_x f(x)|_{(x^*,u^*)}$ it holds: $\frac{\partial f_4}{\partial x_1} = 0$, $\frac{\partial f_4}{\partial x_2} = 0$, $\frac{\partial f_4}{\partial x_3} = 0$, $\frac{\partial f_4}{\partial x_4} = 0$, $\frac{\partial f_4}{\partial x_5} = 1$, $\frac{\partial f_4}{\partial x_6} = 0$, $\frac{\partial f_4}{\partial x_7} = 0$.

For the Jacobian's $\nabla_x f(x)|_{(x^*,u^*)}$ fifth row it holds: $\frac{\partial f_5}{\partial x_1} = 0$, $\frac{\partial f_5}{\partial x_2} = 0$, $\frac{\partial f_5}{\partial x_3} = 0$, $\frac{\partial f_5}{\partial x_4} = \frac{1}{h}\{gcos(x_4) - sin(x_4)[(1 + h\frac{tan(x_7)}{p}sin(x_4))\frac{tan(x_7)}{p}x_6^2] + cos(x_4)[h\frac{tan(x_7)}{p}cos(x_4)\frac{tan(x_7)}{p}x_6^2]\}$, $\frac{\partial f_5}{\partial x_5} = 0$, $\frac{\partial f_5}{\partial x_6} = \frac{1}{h}cos(x_4)[1 + h\frac{tan(x_7)}{p}sin(x_4))\frac{tan(x_7)}{p}2x_6]$, and continuing in a similar manner $\frac{\partial f_5}{\partial x_7} = \frac{1}{h}cos(x_4)\{[(h\frac{1}{pcos^2(x_7)}sin(x_4))\frac{tan(x_7)}{p}x_6^2] + [(1 + h\frac{tan(x_7)}{p}sin(x_4))\frac{1}{pcos^2(x_7)}x_6^2]\}$.

For the sixth row of the Jacobian matrix $\nabla_x f(x)|_{(x^*,u^*)}$ it holds: $\frac{\partial f_6}{\partial x_1} = 0$, $\frac{\partial f_6}{\partial x_2} = 0$, $\frac{\partial f_6}{\partial x_3} = 0$, $\frac{\partial f_6}{\partial x_4} = 0$, $\frac{\partial f_6}{\partial x_5} = 0$, $\frac{\partial f_6}{\partial x_6} = 0$, $\frac{\partial f_6}{\partial x_7} = 0$.

For the seventh row of the Jacobian matrix $\nabla_x f(x)|_{(x^*,u^*)}$ it holds: $\frac{\partial f_7}{\partial x_1} = 0$, $\frac{\partial f_7}{\partial x_2} = 0$, $\frac{\partial f_7}{\partial x_3} = 0$, $\frac{\partial f_7}{\partial x_4} = 0$, $\frac{\partial f_7}{\partial x_5} = 0$, $\frac{\partial f_7}{\partial x_6} = 0$, $\frac{\partial f_7}{\partial x_7} = 0$.

About the Jacobian matrix $\nabla_x g_1(x)|_{(x^*,u^*)}$ one has

$$\nabla_x g_1(x)\,|_{(x^*,u^*)} = \begin{pmatrix} 0\,0\,0 & 0 & 0\,0 & 0 \\ 0\,0\,0 & 0 & 0\,0 & 0 \\ 0\,0\,0 & 0 & 0\,0 & 0 \\ 0\,0\,0 & 0 & 0\,0 & 0 \\ 0\,0\,0 & bsin(x_4)\frac{tan(x_7)}{p} & 0\,0 & bcos(x_4)\frac{1}{pcos^2(x_7)} \\ 0\,0\,0 & 0 & 0\,0 & 0 \\ 0\,0\,0 & 0 & 0\,0 & 0 \end{pmatrix} |_{(x^*,u^*)} \tag{7.77}$$

About the Jacobian matrix $\nabla_x g_2(x)|_{(x^*,u^*)}$ one has

$$\nabla_x g_2(x)\,|_{(x^*,u^*)} = \begin{pmatrix} 0\,0\,0 & 0 & 0 & 0 & 0 \\ 0\,0\,0 & 0 & 0 & 0 & 0 \\ 0\,0\,0 & 0 & 0 & 0 & 0 \\ 0\,0\,0 & 0 & 0 & 0 & 0 \\ 0\,0\,0 & -\frac{bsin(x_4)x_6}{pcos^2(x_7)} & 0 & \frac{bcos(x_4)}{pcos^2(x_7)} & \frac{bcos(x_4)x_6sin(x_7)}{pcos^3(x_7)} \\ 0\,0\,0 & 0 & 0 & 0 & 0 \\ 0\,0\,0 & 0 & 0 & 0 & 0 \end{pmatrix} |_{(x^*,u^*)} \tag{7.78}$$

7.4.4 The Nonlinear H-Infinity Control

7.4.4.1 Tracking Error Dynamics for the Autonomous Motorcycle

The initial nonlinear model of the autonomous motorcycle is in the form

$$\dot{x} = f(x, u) \;\; x \in R^n, \;\; u \in R^m \tag{7.79}$$

Linearization of the model of the riderless motorcycle is performed at each iteration of the control algorithm round its present operating point $(x^*, u^*) = (x(t), u(t - T_s))$. The linearized equivalent of the autonomous motorcycle is described by

$$\dot{x} = Ax + Bu + L\tilde{d} \;\; x \in R^n, \;\; u \in R^m, \;\; \tilde{d} \in R^q \tag{7.80}$$

Thus, after linearization round its current operating point, the motorcycle's dynamic model is written as

$$\dot{x} = Ax + Bu + d_1 \tag{7.81}$$

Parameter d_1 stands for the linearization error in the two-wheel vehicle's dynamic model appearing in Eq. (7.81). The reference setpoints for the autonomous motorcycle are denoted by $\mathbf{x_d} = [x_1^d, \ldots, , x_6^d]$. Tracking of this trajectory is achieved after applying the control input u^*. At every time instant the control input u^* is assumed to differ from the control input u appearing in Eq. (7.81) by an amount equal to Δu, that is $u^* = u + \Delta u$

$$\dot{x}_d = Ax_d + Bu^* + d_2 \tag{7.82}$$

The joint kinematics and dynamics of the riderless motorcycle is described in Eq. (7.81) can be also written as

$$\dot{x} = Ax + Bu + Bu^* - Bu^* + d_1 \tag{7.83}$$

and by denoting $d_3 = -Bu^* + d_1$ as an aggregate disturbance term one obtains

$$\dot{x} = Ax + Bu + Bu^* + d_3 \tag{7.84}$$

By subtracting Eq. (7.82) from Eq. (7.84) one has

$$\dot{x} - \dot{x}_d = A(x - x_d) + Bu + d_3 - d_2 \tag{7.85}$$

By denoting the tracking error as $e = x - x_d$ and the aggregate disturbance term as $\tilde{d} = d_3 - d_2$, the tracking error dynamics becomes

$$\dot{e} = Ae + Bu + \tilde{d} \tag{7.86}$$

The above linearized form of the motorcycle's model can be efficiently controlled after applying an H-infinity feedback control scheme.

7.4.4.2 Min-Max Control and Disturbance Rejection

The initial nonlinear model of the riderless motorcycle is in the form

$$\dot{x} = f(x,u) \;\; x \in R^n, \;\; u \in R^m \tag{7.87}$$

Linearization of the joint kinematic and dynamic model of the autonomous two-wheel vehicle is performed at each iteration of the control algorithm round its present operating point $(x^*, u^*) = (x(t), u(t - T_s))$. The linearized equivalent model of the system is described by

$$\dot{x} = Ax + Bu + L\tilde{d} \;\; x \in R^n, \;\; u \in R^m, \;\; \tilde{d} \in R^q \tag{7.88}$$

where matrices A and B are obtained from the computation of the motorcycle's Jacobians, according to Eqs. (7.76), (7.77) and (7.78) and vector $\tilde{d}$ denotes disturbance terms due to linearization errors. The problem of disturbance rejection for the linearized model that is described by

$$\begin{gathered} \dot{x} = Ax + Bu + L\tilde{d} \\ y = Cx \end{gathered} \tag{7.89}$$

where $x \in R^n$, $u \in R^m$, $\tilde{d} \in R^q$ and $y \in R^p$, cannot be handled efficiently if the classical LQR control scheme is applied. This is because of the existence of the perturbation term $\tilde{d}$. The disturbance term $\tilde{d}$ apart from modeling (parametric) uncertainty and external perturbation terms can also represent noise terms of any distribution.

In the H_∞ control approach, a feedback control scheme is designed for trajectory tracking by the autonomous motorcycle's state vector and simultaneous disturbance rejection, considering that the disturbance affects the system in the worst possible manner. The disturbances' effect are incorporated in the following quadratic cost function:

$$J(t) = \tfrac{1}{2}\int_0^T [y^T(t)y(t) + ru^T(t)u(t) - \rho^2 \tilde{d}^T(t)\tilde{d}(t)]dt, \;\; r, \rho > 0 \tag{7.90}$$

As explained in the application of the H-infinity control presented in the previous sections, the significance of the negative sign in the cost function's term that is associated with the perturbation variable $\tilde{d}(t)$ is that the disturbance tries to maximize the cost function $J(t)$ while the control signal $u(t)$ tries to minimize it. The physical meaning of the relation given above is that the control signal and the disturbances compete to each other within a min-max differential game. This problem of min-max optimization can be written as

$$min_u max_{\tilde{d}} J(u, \tilde{d}) \tag{7.91}$$

The objective of the optimization procedure is to compute a control signal $u(t)$ which can compensate for the worst possible disturbance, that is externally imposed to the system of the two-wheel autonomous vehicle. However, the solution to the min-max optimization problem is directly related to the value of the parameter ρ. This means that there is an upper bound in the disturbances magnitude that can be annihilated by the control signal.

7.4.4.3 H-Infinity Feedback Control

For the linearized system given by Eq. (7.89) the cost function of Eq. (7.90) is defined, where the coefficient r determines the penalization of the control input and the weight coefficient ρ determines the reward of the disturbances' effects. It is assumed that (i) The energy that is transferred from the disturbances signal $\tilde{d}(t)$ is bounded, that is $\int_0^\infty \tilde{d}^T(t)\tilde{d}(t)dt < \infty$, (ii) matrices $[A, B]$ and $[A, L]$ are stabilizable, (iii) matrix $[A, C]$ is detectable. Then, the optimal feedback control law is given by

$$u(t) = -Kx(t) \tag{7.92}$$

with

$$K = \frac{1}{r}B^T P \tag{7.93}$$

where P is a positive semi-definite symmetric matrix which is obtained from the solution of the Riccati equation

$$A^T P + PA + Q - P\left(\frac{1}{r}BB^T - \frac{1}{2\rho^2}LL^T\right)P = 0 \tag{7.94}$$

where Q is also a positive definite symmetric matrix. The worst case disturbance is given by

$$\tilde{d}(t) = \frac{1}{\rho^2}L^T Px(t) \tag{7.95}$$

The diagram of the considered control loop is depicted in Fig. 7.30.

7.4.5 Lyapunov Stability Analysis

Through Lyapunov stability analysis it will be shown that the proposed nonlinear control scheme assures H_∞ tracking performance for the control loop of the riderless motorcycle. Moreover, under moderate conditions asymptotic stability is proven and convergence to the reference setpoints is achieved. The tracking error dynamics for the autonomous motorcycle is written in the form

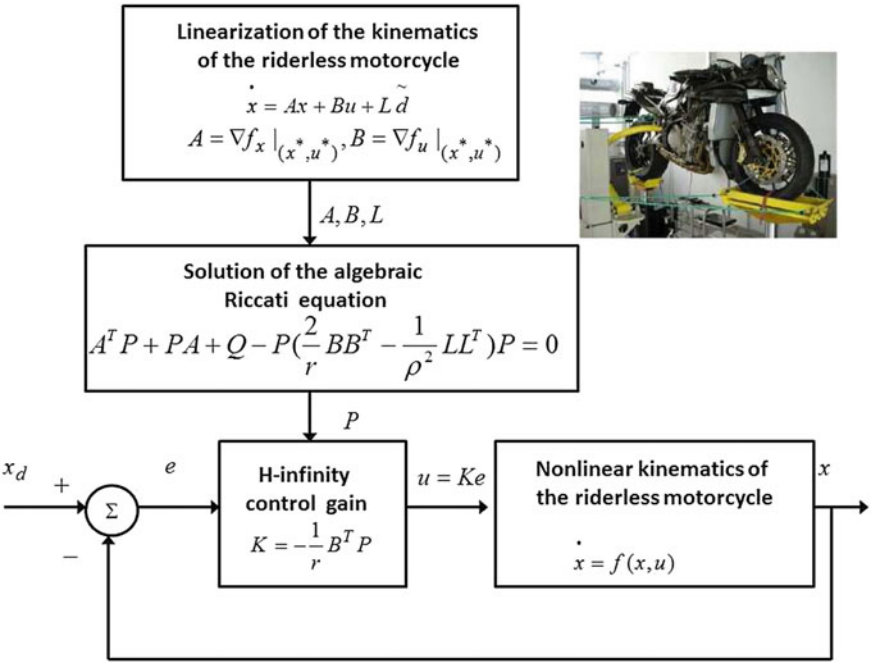

Fig. 7.30 Diagram of the nonlinear optimal control scheme for the 2-wheel autonomous vehicle (riderless motorcycle)

$$\dot{e} = Ae + Bu + L\tilde{d} \tag{7.96}$$

where in the motorcycle's case $L = I \in R^{7\times 7}$ with I being the identity matrix. Variable $\tilde{d}$ denotes model uncertainties and external disturbances of the vehicle's model. The following Lyapunov function is considered

$$V = \tfrac{1}{2}e^T Pe \tag{7.97}$$

where $e = x - x_d$ is the tracking error. By differentiating with respect to time one obtains

$$\begin{gathered} \dot{V} = \tfrac{1}{2}\dot{e}^T Pe + \tfrac{1}{2}eP\dot{e} \Rightarrow \\ \dot{V} = \tfrac{1}{2}[Ae + Bu + L\tilde{d}]^T P + \tfrac{1}{2}e^T P[Ae + Bu + L\tilde{d}] \Rightarrow \end{gathered} \tag{7.98}$$

$$\begin{gathered} \dot{V} = \tfrac{1}{2}[e^T A^T + u^T B^T + \tilde{d}^T L^T]Pe + \\ + \tfrac{1}{2}e^T P[Ae + Bu + L\tilde{d}] \Rightarrow \end{gathered} \tag{7.99}$$

$$\begin{gathered}\dot{V} = \tfrac{1}{2}e^T A^T Pe + \tfrac{1}{2}u^T B^T Pe + \tfrac{1}{2}\tilde{d}^T L^T Pe + \\ \tfrac{1}{2}e^T PAe + \tfrac{1}{2}e^T PBu + \tfrac{1}{2}e^T PL\tilde{d}\end{gathered} \tag{7.100}$$

The previous equation is rewritten as

$$\begin{gathered}\dot{V} = \tfrac{1}{2}e^T(A^T P + PA)e + \left(\tfrac{1}{2}u^T B^T Pe + \tfrac{1}{2}e^T PBu\right) + \\ + \left(\tfrac{1}{2}\tilde{d}^T L^T Pe + \tfrac{1}{2}e^T PL\tilde{d}\right)\end{gathered} \tag{7.101}$$

Assumption: For given positive definite matrix Q and coefficients r and ρ there exists a positive definite matrix P, which is the solution of the following matrix equation

$$A^T P + PA = -Q + P\left(\tfrac{2}{r}BB^T - \tfrac{1}{\rho^2}LL^T\right)P \tag{7.102}$$

Moreover, the following feedback control law is applied to the system

$$u = -\tfrac{1}{r}B^T Pe \tag{7.103}$$

By substituting Eqs. (7.102) and (7.103) one obtains

$$\begin{gathered}\dot{V} = \tfrac{1}{2}e^T\left[-Q + P\left(\tfrac{2}{r}BB^T - \tfrac{1}{2\rho^2}LL^T\right)P\right]e + \\ + e^T PB\left(-\tfrac{1}{r}B^T Pe\right) + e^T PL\tilde{d} \Rightarrow\end{gathered} \tag{7.104}$$

$$\begin{gathered}\dot{V} = -\tfrac{1}{2}e^T Qe + \left(\tfrac{2}{r}PBB^T Pe - \tfrac{1}{2\rho^2}e^T PLL^T\right)Pe \\ -\tfrac{1}{r}\left(e^T PBB^T Pe\right) + e^T PL\tilde{d}\end{gathered} \tag{7.105}$$

which after intermediate operations gives

$$\dot{V} = -\tfrac{1}{2}e^T Qe - \tfrac{1}{2\rho^2}e^T PLL^T Pe + e^T PL\tilde{d} \tag{7.106}$$

or, equivalently

$$\begin{gathered}\dot{V} = -\tfrac{1}{2}e^T Qe - \tfrac{1}{2\rho^2}e^T PLL^T Pe + \\ + \tfrac{1}{2}e^T PL\tilde{d} + \tfrac{1}{2}\tilde{d}^T L^T Pe\end{gathered} \tag{7.107}$$

Lemma: The following inequality holds

$$\tfrac{1}{2}e^T L\tilde{d} + \tfrac{1}{2}\tilde{d}L^T Pe - \tfrac{1}{2\rho^2}e^T PLL^T Pe \leq \tfrac{1}{2}\rho^2\tilde{d}^T\tilde{d} \tag{7.108}$$

Proof: The binomial $(\rho\alpha - \frac{1}{\rho}b)^2$ is considered. Expanding the left part of the above inequality one gets

$$\begin{gathered}\rho^2 a^2 + \tfrac{1}{\rho^2}b^2 - 2ab \geq 0 \Rightarrow \tfrac{1}{2}\rho^2 a^2 + \tfrac{1}{2\rho^2}b^2 - ab \geq 0 \Rightarrow \\ ab - \tfrac{1}{2\rho^2}b^2 \leq \tfrac{1}{2}\rho^2 a^2 \Rightarrow \tfrac{1}{2}ab + \tfrac{1}{2}ab - \tfrac{1}{2\rho^2}b^2 \leq \tfrac{1}{2}\rho^2 a^2\end{gathered} \tag{7.109}$$

The following substitutions are carried out: $a = \tilde{d}$ and $b = e^T PL$ and the previous relation becomes

$$\frac{1}{2}\tilde{d}^T L^T Pe + \frac{1}{2}e^T PL\tilde{d} - \frac{1}{2\rho^2}e^T PLL^T Pe \leq \frac{1}{2}\rho^2 \tilde{d}^T \tilde{d} \tag{7.110}$$

Equation (7.110) is substituted in Eq. (7.107) and the inequality is enforced, thus giving

$$\dot{V} \leq -\frac{1}{2}e^T Qe + \frac{1}{2}\rho^2 \tilde{d}^T \tilde{d} \tag{7.111}$$

Equation (7.111) shows that the H_∞ tracking performance criterion is satisfied. The integration of $\dot{V}$ from 0 to T gives

$$\begin{gathered} \int_0^T \dot{V}(t)dt \leq -\frac{1}{2}\int_0^T ||e||_Q^2 dt + \frac{1}{2}\rho^2 \int_0^T ||\tilde{d}||^2 dt \Rightarrow \\ 2V(T) + \int_0^T ||e||_Q^2 dt \leq 2V(0) + \rho^2 \int_0^T ||\tilde{d}||^2 dt \end{gathered} \tag{7.112}$$

Moreover, if there exists a positive constant $M_d > 0$ such that

$$\int_0^\infty ||\tilde{d}||^2 dt \leq M_d \tag{7.113}$$

then one gets

$$\int_0^\infty ||e||_Q^2 dt \leq 2V(0) + \rho^2 M_d \tag{7.114}$$

Thus, the integral $\int_0^\infty ||e||_Q^2 dt$ is bounded. Moreover, $V(T)$ is bounded and from the definition of the Lyapunov function V in Eq. (7.97) it becomes clear that $e(t)$ will be also bounded since $e(t) \in \Omega_e = \{e | e^T Pe \leq 2V(0) + \rho^2 M_d\}$. According to the above and with the use of Barbalat's Lemma one obtains $lim_{t\to\infty} e(t) = 0$.

Elaborating on the above, it can be noted that the proof of global asymptotic stability for the control loop of the autonomous motorcycle is based on Eq. (7.111) and on the application of Barbalat's Lemma. It uses the condition of Eq. (7.113) about the boundedness of the square of the aggregate disturbance and modelling error term $\tilde{d}$ that affects the model. However, as explained above the proof of global asymptotic stability is not restricted by this condition. By selecting the attenuation coefficient ρ to be sufficiently small and in particular to satisfy $\rho^2 < ||e||_Q^2 / ||\tilde{d}||^2$ one has that the first derivative of the Lyapunov function is upper bounded by 0. Therefore for the ith time interval it is proven that the Lyapunov function defined in Eq. (7.97) is a decreasing one. This also assures the Lyapunov function of the system defined in Eq. (7.97) will always have a negative first-order derivative.

7.4.6 Robust State Estimation with the Use of the H-Infinity Kalman Filter

The control loop for the autonomous motorcycle can be implemented with the feedback of a partially measurable state vector and by processing only a small number of state variables. To reconstruct the missing information about the state vector of the autonomous two-wheel vehicle it is proposed to use a filtering scheme which allows to apply state estimation-based control [457]. The recursion of the H_∞ Kalman Filter, for the model of the distributed finance agents, can be formulated in terms of a *measurement update* and a *time update* part

Measurement update:

$$\begin{aligned} D(k) &= [I - \theta W(k)P^{-}(k) + C^{T}(k)R(k)^{-1}C(k)P^{-}(k)]^{-1} \\ K(k) &= P^{-}(k)D(k)C^{T}(k)R(k)^{-1} \\ \hat{x}(k) &= \hat{x}^{-}(k) + K(k)[y(k) - C\hat{x}^{-}(k)] \end{aligned} \tag{7.115}$$

Time update:

$$\begin{aligned} \hat{x}^{-}(k+1) &= A(k)x(k) + B(k)u(k) \\ P^{-}(k+1) &= A(k)P^{-}(k)D(k)A^{T}(k) + Q(k) \end{aligned} \tag{7.116}$$

where it is assumed that parameter θ is sufficiently small to assure that the covariance matrix $P^{-}(k)^{-1} - \theta W(k) + C^{T}(k)R(k)^{-1}C(k)$ will be positive definite. When $\theta = 0$ the H_∞ Kalman Filter becomes equivalent to the standard Kalman Filter. One can measure only a part of the state vector of the system of the autonomous motorcycle, such as the cartesian coordinates of its rear wheels (x, y) and can estimate through filtering the rest of the state vector elements.

7.4.7 Simulation Tests

The performance of the proposed nonlinear optimal (H-infinity) control method for the model of the autonomous motorcycle has been tested through simulation experiments. The simulation results depicted in Figs. 7.31, 7.32, 7.33, 7.34, 7.35, 7.36, 7.37 and 7.38 confirm the stability properties of the control loop that was previously proven through Lyapunov analysis. Moreover, they demonstrate that the state vector elements of the motorcycle could track precisely the reference setpoints and that the two-wheel vehicle could follow accurately the designated paths in the 2D motion plane. This comes to point out that under electronic control, several of the motorcycle's driving tasks such as lane following, lane change or vehicle overtaking can be safely performed. The implementation of the proposed control scheme required the solution at each time step of the algebraic Riccati equation, given in Eq. (7.102).

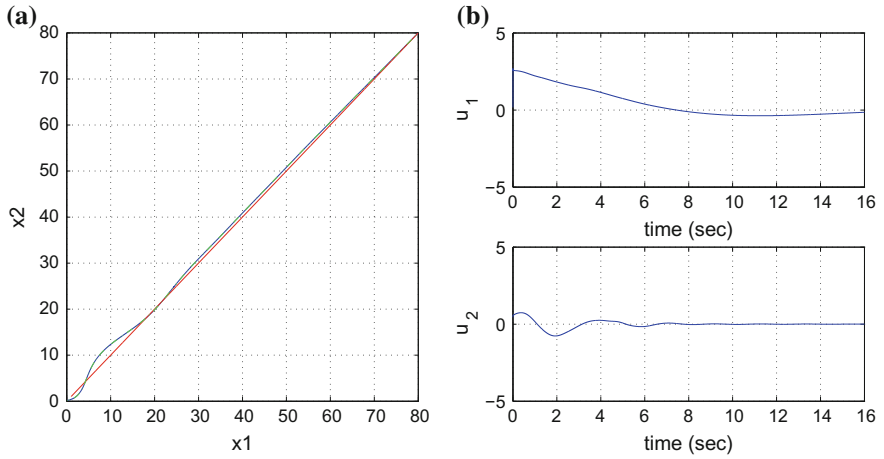

Fig. 7.31 **a** Tracking of reference path 1 (red-line) by the autonomous motorcycle (blue line) and trajectory estimated by the Kalman Filter (green line), **b** control inputs u_1 to u_2 applied to the autonomous motorcycle

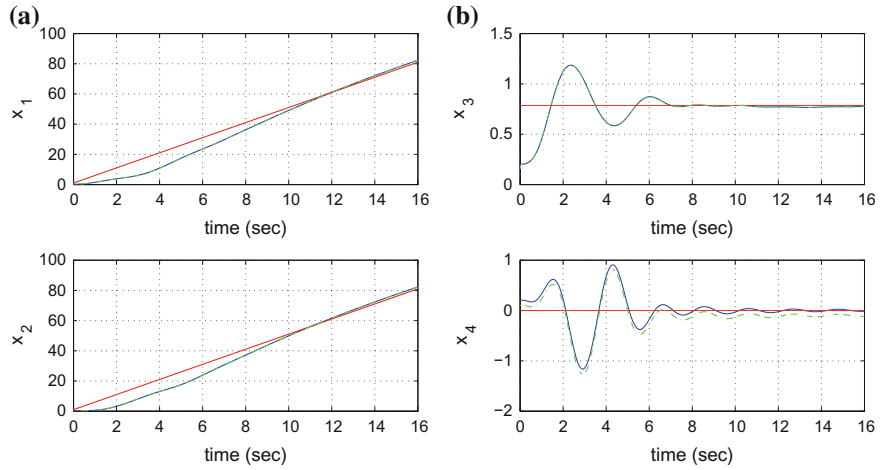

Fig. 7.32 Tracking of reference path 1: **a** convergence of state variables x_1 to x_2 of the autonomous motorcycle to their reference setpoints (red-lines) and estimated state variables provided by the Kalman Filter (green lines), **b** convergence of state variables x_3 to x_4 of the autonomous motorcycle to their reference setpoints (red-lines) and estimated state variables provided by the Kalman Filter (green lines)

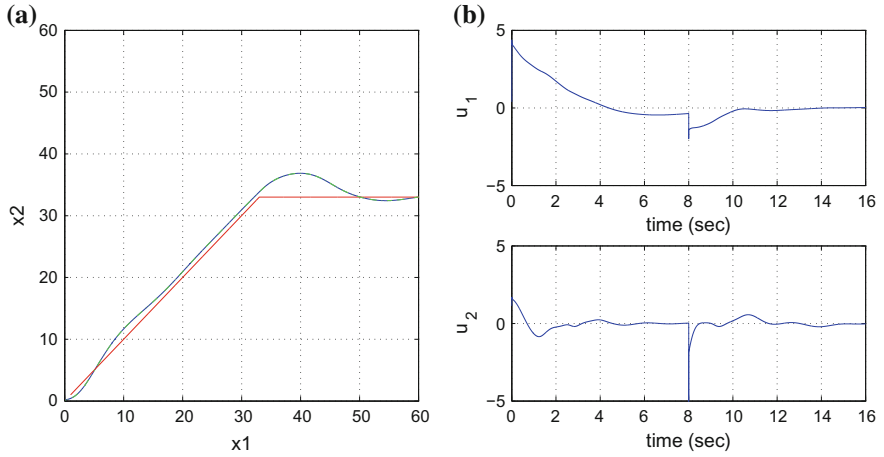

Fig. 7.33 **a** Tracking of reference path 2 (red-line) by the autonomous motorcycle (blue line) and trajectory estimated by the Kalman Filter (green line), **b** control inputs u_1 to u_2 applied to the autonomous motorcycle

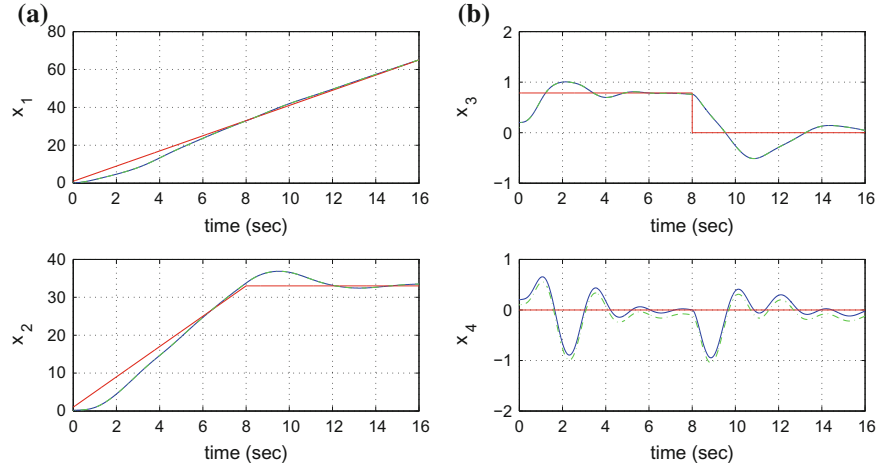

Fig. 7.34 Tracking of reference path 2: **a** convergence of state variables x_1 to x_2 of the autonomous motorcycle to their reference setpoints (red-lines) and estimated state variables provided by the Kalman Filter (green lines), **b** convergence of state variables x_3 to x_4 of the autonomous motorcycle to their reference setpoints (red-lines) and estimated state variables provided by the Kalman Filter (green lines)

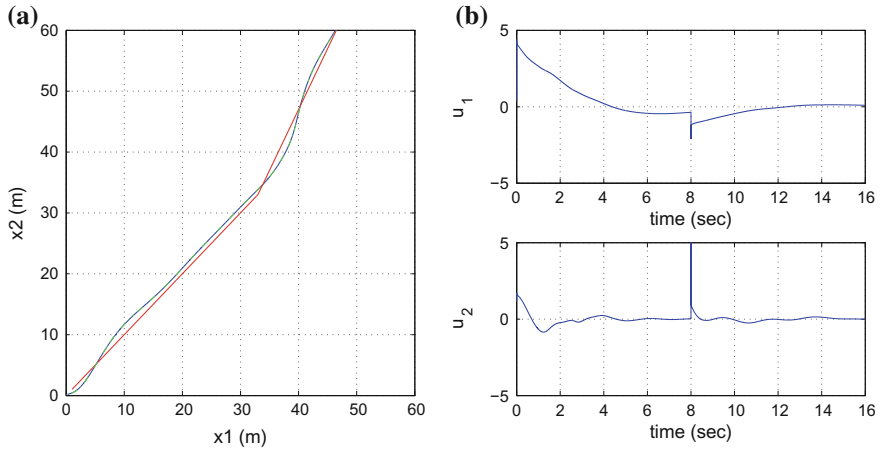

Fig. 7.35 **a** Tracking of reference path 3 (red-line) by the autonomous motorcycle (blue line) and trajectory estimated by the Kalman Filter (green line), **b** control inputs u_1 to u_2 applied to the autonomous motorcycle

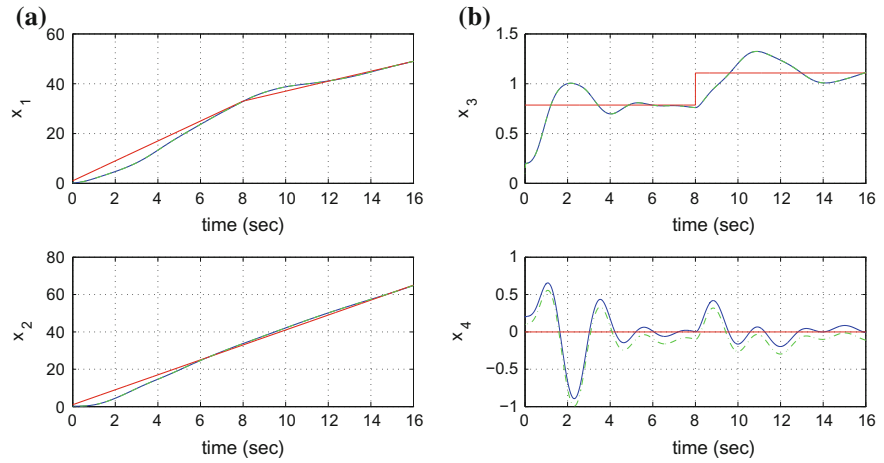

Fig. 7.36 Tracking of reference path 3: **a** convergence of state variables x_1 to x_2 of the autonomous motorcycle to their reference setpoints (red-lines) and estimated state variables provided by the Kalman Filter (green lines), **b** convergence of state variables x_3 to x_4 of the autonomous motorcycle to their reference setpoints (red-lines) and estimated state variables provided by the Kalman Filter (green lines)

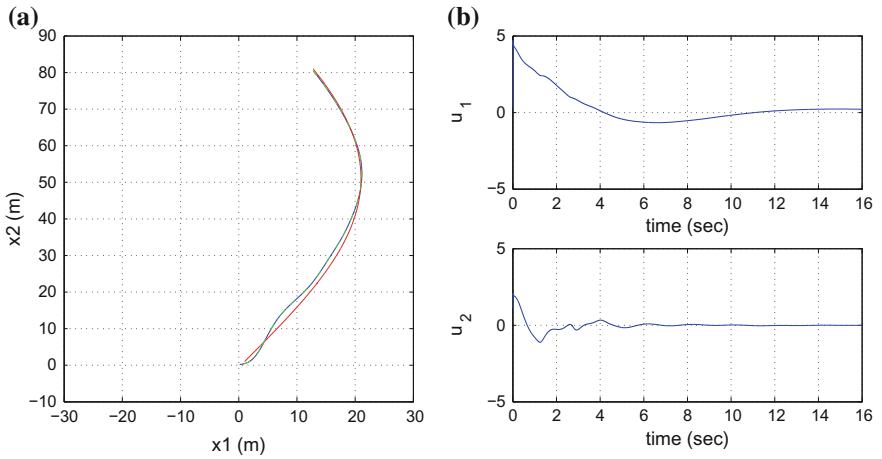

Fig. 7.37 **a** Tracking of reference path 4 (red-line) by the autonomous motorcycle (blue line) and trajectory estimated by the Kalman Filter (green line), **b** control inputs u_1 to u_2 applied to the autonomous motorcycle

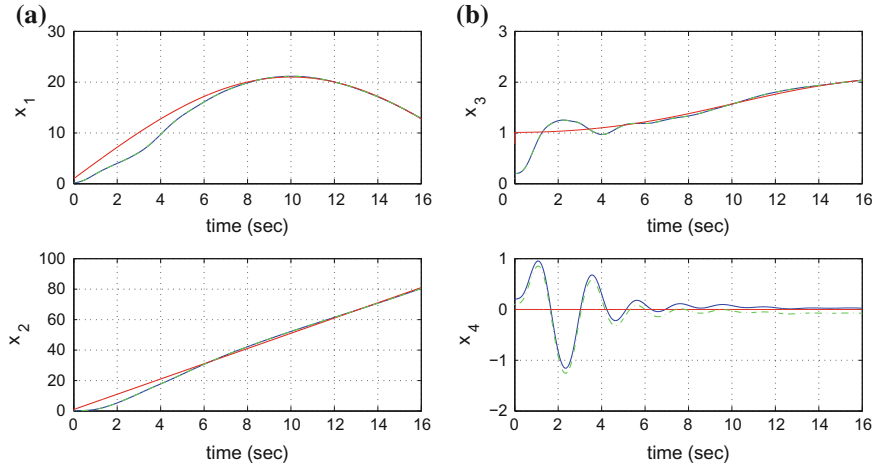

Fig. 7.38 Tracking of reference path 4: **a** convergence of state variables x_1 to x_2 of the autonomous motorcycle to their reference setpoints (red-lines) and estimated state variables provided by the Kalman Filter (green lines), **b** convergence of state variables x_3 to x_4 of the autonomous motorcycle to their reference setpoints (red-lines) and estimated state variables provided by the Kalman Filter (green lines)

To implement state estimation-based control from the autonomous motorcycle through the processing of a small number of on-board sensor measurements, the H-infinity Kalman filter has been used as a robust state estimator. Actually, it was necessary to receive measurements about the cartesian coordinates (x, y) of the vehicle's rear wheel, while the rest of the state vector elements of the motorcycle could be estimated through the H-infinity Kalman Filter. In the simulation diagrams, the real values of the state vector components of the two-wheel vehicle are depicted in blue colour, the estimated values are plotted in green while the associated reference setpoints are printed in red colour. It can be noted that the proposed control method achieved fast and accurate tracking of the reference setpoints, while the variations of the control inputs remained smooth and moderate.

Despite its computational simplicity, the proposed H_∞ control scheme has an excellent performance. Comparing to the control of autonomous vehicles that rely on global linearization methods the presented nonlinear H-infinity control scheme is equally efficient in setpoint tracking while also retaining optimal control features [457]. The tracking accuracy of the presented control method (H_∞) has been monitored in the case of several reference setpoints. By using the Kalman Filter as a robust observer estimates of the state vector of the two-wheel vehicle were obtained thus the implementation of state estimation-based control became possible. The measured state variables were $x_1 = x$, $x_2 = y$. It can be noticed that despite model perturbations the tracking accuracy of the control method remained satisfactory. The RMSE of the tracking reference setpoints by the state variables of the motorcycle is given in Table 7.1. Moreover, the tracking performance of the nonlinear H-infinity control method for the model of the autonomous motorcycle was measured in the case of model uncertainty, imposing an imprecision equal to $\Delta a\%$ about the vehicle's mass m. The obtained results are outlined in Table 7.2. It can be noticed that despite model perturbations the tracking accuracy of the control method remained satisfactory (Tables 7.3 and 7.4).

Table 7.2 Tracking RMSE in motion under disturbances

	$RMSE_x$	$RMSE_y$	$RMSE_\theta$
Path_1	$37.00 \cdot 10^{-4}$	$54.00 \cdot 10^{-4}$	$13.00 \cdot 10^{-4}$
Path_2	$14.00 \cdot 10^{-4}$	$16.00 \cdot 10^{-4}$	$2.41 \cdot 10^{-4}$

Table 7.3 RMSE of the autonomous motorcycle's state variables

Path	RMSE X (m)	RMSE Y (m)	RMSE ψ (rad)	RMSE ϕ (rad)
1	$2.5 \cdot 10^{-3}$	$11.3 \cdot 10^{-3}$	$0.1 \cdot 10^{-3}$	$0.3 \cdot 10^{-3}$
2	$4.8 \cdot 10^{-3}$	$19.7 \cdot 10^{-3}$	$3.0 \cdot 10^{-3}$	$3.2 \cdot 10^{-3}$
3	$1.4 \cdot 10^{-3}$	$6.6 \cdot 10^{-3}$	$0.7 \cdot 10^{-3}$	$1.1 \cdot 10^{-3}$
4	$1.9 \cdot 10^{-3}$	$26.3 \cdot 10^{-3}$	$0.1 \cdot 10^{-3}$	$1.2 \cdot 10^{-3}$

Table 7.4 RMSE of the motorcycle under disturbance

Δa (%)	RMSE X (m)	RMSE Y (m)	RMSE ψ (rad)	RMSE ϕ (rad)
0	$1.9{\cdot}10^{-3}$	$26.3{\cdot}10^{-3}$	$0.1{\cdot}10^{-3}$	$1.2{\cdot}10^{-3}$
10	$1.9{\cdot}10^{-3}$	$26.3{\cdot}10^{-3}$	$0.1{\cdot}10^{-3}$	$1.2{\cdot}10^{-3}$
20	$1.2{\cdot}10^{-3}$	$23.4{\cdot}10^{-3}$	$0.2{\cdot}10^{-3}$	$1.1{\cdot}10^{-3}$
30	$2.4{\cdot}10^{-3}$	$26.9{\cdot}10^{-3}$	$0.1{\cdot}10^{-3}$	$1.3{\cdot}10^{-3}$
40	$3.7{\cdot}10^{-3}$	$16.0{\cdot}10^{-3}$	$0.1{\cdot}10^{-3}$	$0.7{\cdot}10^{-3}$
50	$4.0{\cdot}10^{-3}$	$16.0{\cdot}10^{-3}$	$0.2{\cdot}10^{-3}$	$0.8{\cdot}10^{-3}$
60	$8.5{\cdot}10^{-3}$	$17.1{\cdot}10^{-3}$	$0.5{\cdot}10^{-3}$	$2.3{\cdot}10^{-3}$

Chapter 8
Four-Wheel Autonomous Ground Vehicles

Abstract In the recent years there has been significant effort in the design of intelligent autonomous vehicles capable of operating in variable conditions. The precise modeling of the vehicles dynamics improves the efficiency of vehicles controllers in adverse cases, for example in high velocity, when performing abrupt maneuvers, under mass and loads changes or when moving on rough terrain. Using model-based control approaches it is possible to design a nonlinear controller that maintains the vehicle's motion characteristics according to given specifications. When the vehicle's dynamics is subject to modeling uncertainties or when there are unknown forces and torques exerted on the vehicle it is important to be in position to estimate in real-time disturbances and unknown dynamics so as to compensate for them. In this direction, estimation for the unknown dynamics of the vehicle and state estimation-based control schemes have been developed. Feedback control of robotic ground vehicles can be primarily based on (i) global linearization approaches, (ii) approximate linearization approaches and (iii) Lyapunov methods. The control is applied to (i) 4-wheel vehicles models, and (ii) articulated vehicles. At a second stage, to implement control under model uncertainty, estimation methods can be employed capable of identifying in real-time the vehicles' dynamics. The outcome of the estimation procedure can be used by the aforementioned feedback controllers thus implementing indirect adaptive control schemes. Finally to implement control of the ground vehicles through the measurement of a small number of its state variables, elaborated nonlinear filtering approaches are developed. The topics treated by the chapter are: (a) Nonlinear optimal control of four-wheel autonomous ground vehicles (b) Nonlinear optimal control for an autonomous truck and trailer system (c) Nonlinear optimal control of four-wheel steering autonomous vehicles and (d) Flatness-based control of autonomous four-wheel ground vehicles.

8.1 Chapter Overview

The topics treated by the chapter are: (a) Nonlinear optimal control of four-wheel autonomous ground vehicles (b) Nonlinear optimal control for an autonomous truck and trailer system (c) Nonlinear optimal control of four-wheel steering autonomous

G. Rigatos and K. Busawon, *Robotic Manipulators and Vehicles*,
Studies in Systems, Decision and Control 152,
https://doi.org/10.1007/978-3-319-77851-8_8

vehicles and (d) Flatness-based control of autonomous four-wheel ground vehicles.

With reference to (a) the chapter proposes a new nonlinear optimal control method for solving the problem of path following for four-wheel non-holonomic Automatic Grounded Vehicles (AGVs). The dynamic model of the four-wheel AGVs undergoes first approximate linearization around a temporary operating point that is updated at each iteration of the control algorithm. The linearization takes place through first-order Taylor series expansion and through the computation of the Jacobian matrices of the state-space description of the vehicle. For the approximately linearized model of the four-wheel vehicle an H-infinity feedback controller is computed. Actually, the H-infinity controller stands for the solution of the optimal control problem for the vehicle's kinematics under model uncertainty and external perturbations. For the computation of the feedback gain of the H-infinity controller an algebraic Riccati equation is solved at each time-step of the control method.

With reference to (b) a nonlinear optimal control method is developed, this time for an autonomous truck and trailer system. The dynamic model of the autonomous vehicle undergoes linearization through Taylor series expansion. Adhering to the previously analyzed procedure, the linearization is computed at a temporary equilibrium that is defined at each time instant by the present value of the state vector and the last value of the control inputs vector. The linearization is based on the computation of Jacobian matrices. The modelling error due to approximate linearization is considered to be a perturbation that is compensated by the robustness of the control scheme. For the approximately linearized model of the truck and trailer autonomous vehicle an H-infinity feedback controller is designed. This requires again the solution of an algebraic Riccati equation at each iteration of the control algorithm.

With reference to (c) the chapter introduces a nonlinear optimal control method for feedback control of autonomous four-wheel steering (4WS) robotic vehicles. Comparing to two-wheel steering vehicles, four-wheel steering vehicles can exhibit improved maneuverability. The joint kinematic and dynamic model of such vehicles undergoes approximate linearization around a temporary operating point (equilibrium) which is updated at each iteration of the control method. This operating point comprises the present value of the vehicle's state vector and the last value of the control inputs vector exerted on it. As in previous applications of nonlinear optimal control, the linearization is performed using Taylor series expansion and the computation of the Jacobian matrices of the system's state-space description. For the approximately linearized model of the 4WS vehicle an optimal (H-infinity) feedback controller is designed. The controller's feedback gain requires the solution of an algebraic Riccati equation again at each time step of the control method. The concept of the control scheme is that at each time instant the state vector of the 4WS vehicle is made to converge to the temporary equilibrium, while the equilibrium is also shifted towards the reference setpoints. Thus asymptotically, the state vector of the 4WS vehicle reaches the targeted reference paths. For all cases (a) to (c) asymptotic stability of the control methods is proven through Lyapunov analysis.

With reference to (d) controller design for autonomous 4-wheel ground vehicles is performed with differential flatness theory. Using a 3-DOF nonlinear model of the vehicle's dynamics and through the application of differential flatness theory an

equivalent model in linear canonical (Brunovksy) form is obtained. For the latter model a state feedback controller is developed that enables accurate tracking of velocity setpoints. Moreover, it is shown that with the use of Kalman Filtering it is possible to dynamically estimate the disturbances due to unknown forces and torques exerted on the vehicle. The processing of velocity measurements (provided by a small number of on-board sensors) through a Kalman Filter which has been redesigned in the form of a disturbance observer results in accurate identification of external disturbances affecting the vehicle's dynamic model. By including in the vehicle's controller an additional term that compensates for the estimated disturbance forces, the desirable characteristics of the vehicle's motion are achieved. The global asymptotic stability for the AGV control scheme is assured.

8.2 Nonlinear Optimal Control of Four-Wheel Autonomous Ground Vehicles

8.2.1 Outline

Intelligent four-wheel autonomous vehicles are characterized by the capability to track precisely reference paths and to perform in a dexterous and accurate manner all designated maneuvers [40, 68–70, 392, 523]. The present section proposes a new nonlinear optimal (H-infinity) control method for the kinematic-dynamic model of a four-wheel autonomous vehicle. The considered model describes precisely the motion of four-wheel autonomous vehicles which receive as control inputs the engine's torque and the heading angle provided by the steering wheel, while also taking into account longitudinal and lateral forces exerted on the vehicle's front and rear wheels, as well as torques that result in a change of the vehicle's orientation [26, 72, 228, 622]. To accomplish precision in path following by autonomous vehicles several control approaches have been developed so far. One can primarily distinguish global linearization-based control schemes, requiring a change of state variables for the vehicle's model [317, 319, 332, 333, 419, 571]. Moreover, optimization-based control approaches have been a topic of significant research in autonomous four-wheel vehicles technology [66, 123, 284, 616, 641].

The present section's approach to the solution of the path tracking control problem for autonomous four-wheel land vehicles is based on a nonlinear optimal control concept and on the H-infinity control theory. To implement the considered control method the joint kinematic and dynamic model of the four-wheel vehicle undergoes first approximate linearization around a temporary operating point (equilibrium) which is updated at each iteration of the control method. The temporary equilibrium is defined by the present value of the vehicle's state vector and by the last value of the control inputs vector that was exerted on it [461, 466]. The linearization relies on first-order Taylor series expansion and on the computation of the Jacobian matrices of the vehicle's state-space description [33, 431, 463]. The modelling error which is due to the approximate linearization is considered to be a disturbance term

which is finally compensated by the robustness of the control algorithm. For the approximately linearized model of the four-wheel vehicle an H-infinity (optimal) feedback controller is designed.

The H-infinity feedback controller is the solution to the optimal control problem for the four-wheel vehicle, under model uncertainty and external perturbations [450, 457, 460]. It actually represents the solution to a min-max differential game in which the controller tries to minimize a cost function comprising a quadratic term of the state vector's tracking error, while at the same time the disturbances and model uncertainty terms try to maximize this cost function. The computation of the controller's feedback gain requires the solution of an algebraic Riccati equation taking place at each time step of the control method. The stability properties of the control scheme are analyzed with the use of the Lyapunov method. First, it is proven that the control loop satisfies the H-infinity tracking performance criterion which signifies elevated robustness against model uncertainty and external perturbations [305, 564]. Moreover, under moderate conditions it is proven that the control loop is also globally asymptotically stable. Finally, to implement state estimation-based control through the feedback of a small number of sensor measurements the H-infinity Kalman Filter is proposed as a robust state estimator [169, 511].

8.2.2 Dynamic and Kinematic Model of the Vehicle

8.2.2.1 Definition of Parameters in 4-Wheel Vehicle Dynamic Model

The dynamic model of the four-wheel vehicle has been analyzed in [332, 333, 457, 616]. With reference to Figs. 8.1 and 8.2 (where the lateral forces applied on the wheels are considered to define the vehicle's motion) one has the following parameters: β is the angle between the velocity and the vehicle's transversal angle, V is the velocity vector of the vehicle, ψ is the yaw angle (rotation round the z axis), f_x: is the aggregate force along the x axis, f_y is the aggregate force along the y axis, T_z is the aggregate torque round the z axis and δ is the steering angle of the front wheels.

The motion of the vehicle is described by the following set of equations:

1. Longitudinal motion

$$-mV(\dot{\beta}+\dot{\psi})sin(\beta)+m\dot{V}cos(\beta)=f_x \tag{8.1}$$

2. Lateral motion

$$mV(\dot{\beta}+\dot{\psi})cos(\beta)+m\dot{V}sin(\beta)=f_y \tag{8.2}$$

3. yaw turn

$$I\ddot{\psi}=T_z \tag{8.3}$$

The above described dynamics of the four-wheel vehicle can be also written in matrix form

$$\begin{pmatrix} -sin(\beta) & cos(\beta) & 0 \\ cos(\beta) & sin(\beta) & 0 \\ 0 & 0 & 1 \end{pmatrix} \begin{pmatrix} mV(\dot{\beta}+\dot{\psi}) \\ m\dot{V} \\ I\ddot{\psi} \end{pmatrix} = \begin{pmatrix} f_x \\ f_y \\ T_z \end{pmatrix} \tag{8.4}$$

Finally a matrix relation is provided about the transformation of forces on a tire into forces and torques along the vehicle's axes:

$$\begin{pmatrix} f_x \\ f_y \\ T_z \end{pmatrix} = \begin{pmatrix} -sin(\delta) & 0 \\ cos(\delta) & 1 \\ L_1 cos(\delta) & -L_2 \end{pmatrix} \begin{pmatrix} F_f \\ F_r \end{pmatrix} \tag{8.5}$$

8.2.2.2 Vehicle Dynamic Model with Longitudinal and Lateral Forces

The previous model of Fig. 8.1 is rexamined considering that $\dot{\beta} = 0$ and that ψ is the yaw angle formed between the vehicle's longitudinal axis and the horizontal axis of an inertial reference frame. Moreover, it is assumed that apart from the lateral forces there are traction torques transferred from the engine to the front wheels as well as braking torques on the rear and front wheels. Due to the distance between the wheels axes and the vehicle's center of gravity, torques are also generated along the vehicle's z-axis. With reference to Fig. 8.1 the model of the vehicle's dynamics is formulated as follows [332, 333, 457]:

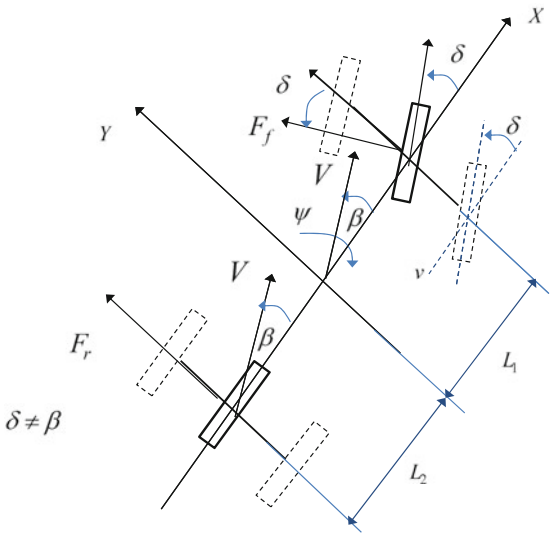

Fig. 8.1 Nonlinear 4-wheeled vehicle model

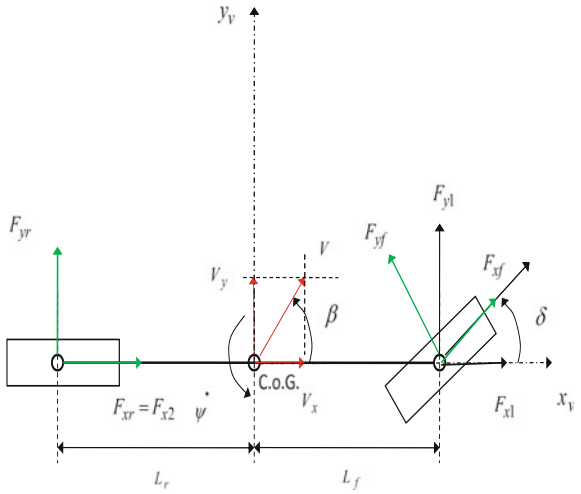

Fig. 8.2 Vehicle model with longitudinal and lateral forces

$$
\begin{aligned}
m\alpha_x &= m(\dot{V}_x - \dot{\psi}\dot{V}_y) = F_{x_1} + F_{x_2} \\
m\alpha_y &= m(\dot{V}_y + \dot{\psi}\dot{V}_x) = F_{y_1} + F_{y_2} \\
I_z\ddot{\psi} &= T_{z_1} + T_{z_2}
\end{aligned} \tag{8.6}
$$

where a_x and a_y are accelerations along the axes of the inertial reference frame and $\dot{V}_x, \dot{V}_y$ in a reference frame that rotates with the yaw rate $\dot{\psi}$. The forces $F_{x_i},\ i = 1, 2$ on the vehicle's longitudinal axis and $F_{y_i},\ i = 1, 2$ on the vehicle's transversal axis are computed from the horizontal and vertical forces applied on the vehicle's wheels as follows:

$$
\begin{aligned}
F_{x_1} &= F_{x_f} cos(\delta) - F_{y_f} sin(\delta) \\
F_{x_2} &= F_{x_r} \\
F_{y_1} &= F_{y_f} sin(\delta) + F_{y_f} cos(\delta) \\
F_{y_2} &= F_{y_r} \\
T_{z_1} &= L_f(F_{y_f} cos(\delta) + F_{x_f} sin(\delta)) \\
T_{z_2} &= -L_r F_{y_r}
\end{aligned} \tag{8.7}
$$

About the longitudinal and the lateral forces applied to the vehicle one has:

1. Longitudinal force on the front wheel

$$
F_{x_f} = \left(\frac{1}{R}\right)(I_r\dot{\omega}_f + T_m - T_{b_f}) \tag{8.8}
$$

2. Longitudinal force on the rear wheel

$$F_{x_r} = -\left(\frac{1}{R}\right)(T_{b_r} + I_r\dot{\omega}_r) \tag{8.9}$$

3. Lateral force on the front wheel (taking that the angle β between the vehicle's longitudinal axis and the wheel's velocity vector is approximated by $\beta = \frac{V_y + \dot{\psi}L_f}{V_x}$)

$$F_{y_f} = C_f\left(\delta - \frac{V_y + \dot{\psi}L_f)}{V_x}\right) \tag{8.10}$$

4. Lateral force on the rear wheel (taking that for the rear wheel the steering angle is $\delta = 0$ and that the angle β between the vehicle's longitudinal axis and the wheel's velocity vector is approximated by $\beta = \frac{V_y - \dot{\psi}L_r}{V_x}$).

$$F_{y_r} = -C_r\frac{V_y - \dot{\psi}L_r}{V_x} \tag{8.11}$$

where C_f and C_r are the cornering stiffness coefficients for the front and rear tires respectively. Nominal values of these cornering stiffness coefficients can be estimated through identification procedures. The substitution of Eqs. (8.8)–(8.11) into (8.6) results into

$$\begin{aligned}
m\dot{V}_x &= m\dot{\psi}V_y - \frac{I_r}{R}(\dot{\omega}_r + \dot{\omega}_f) + \frac{1}{R}(T_m - T_{b_f} - T_{b_r}) + C_f\left(\frac{V_y + \dot{\psi}L_f)}{V_x}\right)\delta - C_f\delta^2 \\
m\dot{V}_y &= -m\dot{\psi}V_x - C_f\left(\frac{V_y + \dot{\psi}L_f}{V_x}\right) - C_r\left(\frac{V_y - \dot{\psi}L_f}{V_x}\right) + \left(\frac{1}{R}\right)(T_m - T_{b_f})\delta + \left(C_f - \frac{I_r}{R}\dot{\omega}_f\right)\delta \\
I_z\ddot{\psi} &= -L_fC_f\left(\frac{V_y + \dot{\psi}L_f)}{V_x}\right) + L_rC_r\left(\frac{V_y - \dot{\psi}L_f)}{V_x}\right) + \frac{L_f}{R}(T_m - T_{b_f})\delta + L_f\left(T_m - \frac{I_r}{R}\right)\delta
\end{aligned} \tag{8.12}$$

The motion of the vehicle along its longitudinal axis is controlled by the traction or braking wheel torque $T_\omega = T_m - T_b$ with $T_b = T_{b_f} + T_{b_r}$ and the lateral movement via the steering angle δ. The two control inputs of the four wheel vehicle model are

$$\begin{aligned}
u_1 &= T_\omega \\
u_2 &= \delta
\end{aligned} \tag{8.13}$$

A first form of the vehicle's dynamic model is

$$\dot{x} = f(x,t) + g(x,t)u + g_1u_1u_2 + g_2u_2^2 \tag{8.14}$$

where

$$f(x,t)=\begin{pmatrix}\frac{I_r}{mR}(\dot{\omega}_r+\dot{\omega}_f)\\ \dot{\psi}V_x+\frac{1}{m}\left(-C_f\frac{(V_y+L_f\dot{\psi})}{V_x}-C_r\frac{(V_y-L_f\dot{\psi})}{V_x}\right)\\ \frac{1}{I_z}\left(-L_fC_f\frac{(V_y+L_f\dot{\psi})}{V_x}+L_rC_r\frac{(V_y-L_f\dot{\psi})}{V_x}\right)\end{pmatrix} \tag{8.15}$$

$$g(x,t)=\begin{pmatrix}\frac{1}{mR} & \frac{C_f}{m}\left(\frac{V_y+L_f\dot{\psi}}{V_x}\right)\\ 0 & \left(\frac{C_fR-I_r\dot{\omega}_f}{mR}\right)\\ 0 & \frac{(L_fC_fR-L_fI_r\dot{\omega}_f)}{I_zR}\end{pmatrix} \tag{8.16}$$

$$g_1=\begin{pmatrix}0\\ \frac{1}{mR}\\ \frac{L_f}{I_zR}\end{pmatrix}\ g_2=\begin{pmatrix}-\frac{C_f}{m}\\ 0\\ 0\end{pmatrix}\ x=\begin{pmatrix}V_x\\ V_y\\ \dot{\psi}\end{pmatrix}\ u=\begin{pmatrix}u_1\\ u_2\end{pmatrix} \tag{8.17}$$

The previously analyzed nonlinear model of the vehicle's dynamics can be simplified if the control inputs u_1u_2 and u_2^2 are not taken into account. In the latter case the dynamics of the vehicle takes the form

$$\dot{x}=f(x,t)+g(x,t)u \tag{8.18}$$

8.2.2.3 Joint Dynamic and Kinematic Model of the Vehicle

Using that the velocity variables of the vehicle V_x and V_y are expressed in a body-fixed orthogonal coordinates frame, and using that the heading angle of the vehicle is ψ one can express next the motion of the vehicle in an inertial reference frame as follows:

$$\begin{aligned}V_X&=cos(\psi)V_x-sin(\psi)V_y\Rightarrow\dot{X}=cos(\psi)V_x-sin(\psi)V_y\\ V_Y&=sin(\psi)V_x+cos(\psi)V_y\Rightarrow\dot{Y}=sin(\psi)V_x+cos(\psi)V_y\end{aligned} \tag{8.19}$$

Using the above, the state-space description of the four-wheel vehicle becomes

$$\begin{pmatrix}\dot{X}\\ \dot{Y}\\ \dot{V}_X\\ \dot{V}_Y\\ \dot{\psi}\\ \ddot{\psi}\end{pmatrix}\begin{pmatrix}cos(\psi)V_x-sin(\psi)V_y\\ sin(\psi)V_x+cos(\psi)V_y\\ \frac{I_r}{mR}(\dot{\omega}_R+\dot{\omega}_f)\\ \dot{\psi}V_x+\frac{1}{m}\left[-C_f\frac{(V_y+L_f\dot{\psi})}{V_x}-C_r\frac{(V_y-L_f\dot{\psi})}{V_x}\right]\\ \dot{\psi}\\ \frac{1}{I_z}\left[-L_fC_f\frac{(V_y+L_f\dot{\psi})}{V_x}+L_rC_r\frac{(V_y-L_f\dot{\psi})}{V_x}\right]\end{pmatrix}+\begin{pmatrix}0 & 0\\ 0 & 0\\ \frac{1}{mR} & \frac{C_f}{m}\frac{V_y+L_f\dot{\pi}}{V_x}\\ 0 & \frac{C_fR-I_r\dot{\omega}_f}{mR}\\ 0 & 0\\ 0 & \frac{L_fC_fR-L_fI_r\dot{\omega}_f}{I_zR}\end{pmatrix}\begin{pmatrix}T_\omega\\ \delta\end{pmatrix} \tag{8.20}$$

Next, by defining the following state variables $x_1 = X$, $x_2 = Y$, $x_3 = V_x$, $x_4 = V_y$, $x_5 = \psi$ and $x_6 = \dot{\psi}$ the state-space description of the system becomes:

$$\begin{pmatrix} \dot{x}_1 \\ \dot{x}_2 \\ \dot{x}_3 \\ \dot{x}_4 \\ \dot{x}_5 \\ \dot{x}_6 \end{pmatrix} \begin{pmatrix} cos(x_5)x_3 - sin(x_3)x_4 \\ sin(x_5)x_3 + cos(x_5)x_4 \\ \frac{I_r}{mR}(\dot{\omega}_R + \dot{\omega}_f) \\ x_6 x_3 + \frac{1}{m}\left[-C_f \frac{(x_5 + L_f x_6)}{x_3} - C_r \frac{(x_4 - L_f x_6)}{x_3}\right] \\ x_6 \\ \frac{1}{I_z}\left[-L_f C_f \frac{(x_4 + L_f x_6)}{x_3} + L_r C_r \frac{(x_4 - L_f x_6}{x_3}\right] \end{pmatrix} + \begin{pmatrix} 0 & 0 \\ 0 & 0 \\ \frac{1}{mR} & \frac{C_f}{m}\frac{x_4 + L_f x_6}{x_3} \\ 0 & \frac{C_f R - I_r \dot{\omega}_f}{mR} \\ 0 & 0 \\ 0 & \frac{L_f C_f R - L_f I_r \dot{\omega}_f}{I_z R} \end{pmatrix} \begin{pmatrix} u_1 \\ u_2 \end{pmatrix} \tag{8.21}$$

In vector field form, one obtains the following state-space description about the vehicle's dynamics

$$\begin{aligned} \dot{x} &= f(x) + G(x)u \Rightarrow \\ \dot{x} &= f(x) + g_1(x)u_1 + g_2(x)u_2 \end{aligned} \tag{8.22}$$

where $f(x) \in R^{6\times 1}$, $G(x) \in R^{6\times 2}$ while its columns are defined as $g_1(x) \in R^{6\times 1}$ and $g_2(x) \in R^{6\times 1}$ with

$$f(x) = \begin{pmatrix} cos(x_5)x_3 - sin(x_3)x_4 \\ sin(x_5)x_3 + cos(x_5)x_4 \\ \frac{I_r}{mR}(\dot{\omega}_R + \dot{\omega}_f) \\ x_6 x_3 + \frac{1}{m}\left[-C_f \frac{(x_5 + L_f x_6)}{x_3} - C_r \frac{(x_4 - L_f x_6)}{x_3}\right] \\ x_6 \\ \frac{1}{I_z}\left[-L_f C_f \frac{(x_4 + L_f x_6)}{x_3} + L_r C_r \frac{(x_4 - L_f x_6}{x_3}\right] \end{pmatrix}$$

$$g_1(x) = \begin{pmatrix} 0 \\ 0 \\ \frac{1}{mR} \\ 0 \\ 0 \\ 0 \end{pmatrix} \quad g_2(x) = \begin{pmatrix} 0 \\ 0 \\ \frac{C_f}{m}\frac{x_4 + L_f x_6}{x_3} \\ \frac{C_f R - I_r \dot{\omega}_f}{mR} \\ 0 \\ \frac{L_f C_f R - L_f I_r \dot{\omega}_f}{I_z R} \end{pmatrix} \tag{8.23}$$

8.2.3 *Approximate Linearization of the Four-Wheel Vehicle Dynamics*

The dynamic model of the four-wheel vehicle undergoes approximate linearization around the temporary operating point (x^*, u^*) which is recomputed at each iteration of the control algorithm. The linearization point (equilibrium) consists of the present value of the vehicle's state vector x^* and of the last value of the control inputs vector u^* that was exerted on it. The linearization is based on first order Taylor

series expansion and on the computation of the Jacobian matrices of the state-space description of the vehicle. This gives:

$$\dot{x} = Ax + Bu + \tilde{d} \tag{8.24}$$

A and B are the system's Jacobian matrices to be defined in the following and $\tilde{d}$ is a model uncertainty term denoting the modelling error due to the truncation of higher-order terms in the Taylor series expansion and the effects of external perturbations. About matrix A one has

$$\begin{gathered} A = \nabla_x [f(x) + G(x)u]|_{(x^*,u^*)} \Rightarrow \\ A = \nabla_x [f(x)]|_{(x^*,u^*)} + \nabla_x [g_1(x)]|_{(x^*,u^*)} + \nabla_x [g_2(x)]|_{(x^*,u^*)} \end{gathered} \tag{8.25}$$

About matrix B one has

$$\begin{gathered} B = \nabla_u [f(x) + G(x)u]|_{(x^*,u^*)} \Rightarrow \\ B = G(x)|_{(x^*,u^*)} \end{gathered} \tag{8.26}$$

The Jacobian matrix $\nabla_x f(x)$ of the state-space description of the system are computed as follows:

$$\nabla_x f(x) = \begin{pmatrix} \frac{\partial f_1}{\partial x_1} & \frac{\partial f_1}{\partial x_2} & \cdots & \frac{\partial f_1}{\partial x_6} \\ \frac{\partial f_2}{\partial x_1} & \frac{\partial f_2}{\partial x_2} & \cdots & \frac{\partial f_2}{\partial x_6} \\ \cdots & \cdots & \cdots & \cdots \\ \frac{\partial f_6}{\partial x_1} & \frac{\partial f_6}{\partial x_2} & \cdots & \frac{\partial f_6}{\partial x_6} \end{pmatrix} |_{(x^*,u^*)} \tag{8.27}$$

The elements of the first row of the Jacobian matrix $\nabla_x f(x)$ are: $\frac{\partial f_1}{\partial x_1} = 0$, $\frac{\partial f_1}{\partial x_2} = 0$, $\frac{\partial f_1}{\partial x_3} = cos(x_5)$, $\frac{\partial f_1}{\partial x_4} = -sin(x_5)$, $\frac{\partial f_1}{\partial x_5} = -x_3 sin(x_5) - x_4 cos(x_5)$, $\frac{\partial f_1}{\partial x_6} = 0$.

The elements of the second row of the Jacobian matrix $\nabla_x f(x)$ are: $\frac{\partial f_2}{\partial x_1} = 0$, $\frac{\partial f_2}{\partial x_2} = 0$, $\frac{\partial f_2}{\partial x_3} = sin(x_5)$, $\frac{\partial f_2}{\partial x_4} = cos(x_5)$, $\frac{\partial f_2}{\partial x_5} = x_3 cos(x_5) - x_4 sin(x_5)$, $\frac{\partial f_2}{\partial x_6} = 0$.

The elements of the third row of the Jacobian matrix $\nabla_x f(x)$ are: $\frac{\partial f_3}{\partial x_1} = 0$, $\frac{\partial f_3}{\partial x_2} = 0$, $\frac{\partial f_3}{\partial x_3} = 0$, $\frac{\partial f_3}{\partial x_4} = 0$, $\frac{\partial f_3}{\partial x_5} = 0$, $\frac{\partial f_3}{\partial x_6} = 0$.

The elements of the fourth row of the Jacobian matrix $\nabla_x f(x)$ are: $\frac{\partial f_4}{\partial x_1} = 0$, $\frac{\partial f_4}{\partial x_2} = 0$, $\frac{\partial f_4}{\partial x_3} = x_6 + \frac{1}{m}[-C_f \frac{-(x_4 + L_f x_6)}{x_3^2} - C_r \frac{-(x_4 + L_f x_6)}{x_3^2}]$, $\frac{\partial f_4}{\partial x_4} = \frac{1}{m}[-C_f \frac{1}{x_3} - C_r \frac{1}{x_3}]$, $\frac{\partial f_4}{\partial x_5} = 0$, $\frac{\partial f_4}{\partial x_6} = x_3 + \frac{1}{m}[-C_f \frac{L_f}{x_3} - C_r \frac{-L_f}{x_3}]$.

The elements of the fifth row of the Jacobian matrix $\nabla_x f(x)$ are: $\frac{\partial f_5}{\partial x_1} = 0$, $\frac{\partial f_5}{\partial x_2} = 0$, $\frac{\partial f_5}{\partial x_3} = 0$, $\frac{\partial f_5}{\partial x_4} = 0$, $\frac{\partial f_5}{\partial x_5} = 0$, $\frac{\partial f_5}{\partial x_6} = 1$.

The elements of the sixth row of the Jacobian matrix $\nabla_x f(x)$ are: $\frac{\partial f_6}{\partial x_1} = 0$, $\frac{\partial f_6}{\partial x_2} = 0$, $\frac{\partial f_6}{\partial x_3} = 0$, $\frac{\partial f_6}{\partial x_4} = \frac{1}{I_z}[-L_f C_f \frac{1}{x_3} + L_f C_r \frac{1}{x_3}]$, $\frac{\partial f_6}{\partial x_5} = 0$, $\frac{\partial f_6}{\partial x_6} = \frac{1}{I_z}[-L_f C_f \frac{L_f}{x_3} + L_f C_r \frac{L_f}{x_3}]$.

The Jacobian matrix $\nabla_x g_1(x)$ of the state-space description of the system are computed as follows:

$$\nabla_x g_1(x) = \begin{pmatrix} \frac{\partial g_{11}}{\partial x_1} & \frac{\partial g_{11}}{\partial x_2} & \cdots & \frac{\partial g_{11}}{\partial x_6} \\ \frac{\partial g_{12}}{\partial x_1} & \frac{\partial g_{12}}{\partial x_2} & \cdots & \frac{\partial g_{12}}{\partial x_6} \\ \cdots & \cdots & \cdots & \cdots \\ \frac{\partial g_{16}}{\partial x_1} & \frac{\partial g_{16}}{\partial x_2} & \cdots & \frac{\partial g_{16}}{\partial x_6} \end{pmatrix} |_{(x^*, u^*)} \tag{8.28}$$

It holds that $\nabla_x g_1(x) = 0_{6\times 6}$.

The Jacobian matrix $\nabla_x g_2(x)$ of the state-space description of the system are computed as follows:

$$\nabla_x g_2(x) = \begin{pmatrix} \frac{\partial g_{21}}{\partial x_1} & \frac{\partial g_{21}}{\partial x_2} & \cdots & \frac{\partial g_{21}}{\partial x_6} \\ \frac{\partial g_{22}}{\partial x_1} & \frac{\partial g_{22}}{\partial x_2} & \cdots & \frac{\partial g_{22}}{\partial x_6} \\ \cdots & \cdots & \cdots & \cdots \\ \frac{\partial g_{26}}{\partial x_1} & \frac{\partial g_{26}}{\partial x_2} & \cdots & \frac{\partial g_{26}}{\partial x_6} \end{pmatrix} |_{(x^*, u^*)} \tag{8.29}$$

The elements of 1st, 2nd, 4th, 5th and 6th row of the Jacobian matrix $\nabla_x g_2(x)$ are 0, while the elements of the third row of the Jacobian matrix $\nabla_x g_2(x)$ are: $\frac{\partial g_{32}}{\partial x_1} = 0$, $\frac{\partial g_{32}}{\partial x_2} = 0$, $\frac{\partial g_{32}}{\partial x_3} = \frac{C_f}{m}(-\frac{(x_4 + L_f x_6)}{x_3^2})$, $\frac{\partial g_{32}}{\partial x_4} = \frac{C_f}{m}(\frac{1}{x_3})$, $\frac{\partial g_{32}}{\partial x_5} = 0$, $\frac{\partial g_{32}}{\partial x_6} = \frac{C_f}{m}(\frac{L_f}{x_3})$.

8.2.4 The Nonlinear H-Infinity Control

8.2.4.1 Tracking Error Dynamics of the Four-Wheel Vehicle

The initial nonlinear model of the automatic ground vehicle is in the form

$$\dot{x} = f(x, u) \;\; x \in R^n, \;\; u \in R^m \tag{8.30}$$

Linearization of the system (four-wheel ground vehicle) is performed at each iteration of the control algorithm round its present operating point $(x^*, u^*) = (x(t), u(t - T_s))$. The linearized equivalent of the system is described by

$$\dot{x} = Ax + Bu + L\tilde{d} \;\; x \in R^n, \;\; u \in R^m, \;\; \tilde{d} \in R^q \tag{8.31}$$

Thus, after linearization round its current operating point, the autonomous ground vehicle's dynamic model is written as

$$\dot{x} = Ax + Bu + d_1 \tag{8.32}$$

Parameter d_1 stands for the linearization error in the vehicle's dynamic model appearing in Eq. (8.32). The reference setpoints for the ground vehicle are denoted by $\mathbf{x_d} = [x_1^d, \ldots, x_6^d]$. Tracking of this trajectory is achieved after applying the control input u^*. At every time instant the control input u^* is assumed to differ from the control input u appearing in Eq. (8.32) by an amount equal to Δu, that is $u^* = u + \Delta u$

$$\dot{x}_d = Ax_d + Bu^* + d_2 \tag{8.33}$$

The dynamics of the controlled system described in Eq. (8.32) can be also written as

$$\dot{x} = Ax + Bu + Bu^* - Bu^* + d_1 \tag{8.34}$$

and by denoting $d_3 = -Bu^* + d_1$ as an aggregate disturbance term one obtains

$$\dot{x} = Ax + Bu + Bu^* + d_3 \tag{8.35}$$

By subtracting Eq. (8.33) from (8.35) one has

$$\dot{x} - \dot{x}_d = A(x - x_d) + Bu + d_3 - d_2 \tag{8.36}$$

By denoting the tracking error as $e = x - x_d$ and the aggregate disturbance term as $\tilde{d} = d_3 - d_2$, the tracking error dynamics becomes

$$\dot{e} = Ae + Bu + \tilde{d} \tag{8.37}$$

The above linearized form of the four wheel vehicle's model can be efficiently controlled after applying an H-infinity feedback control scheme.

8.2.5 Min-Max Control and Disturbance Rejection

The initial nonlinear model of the four-wheel autonomous ground vehicle is in the form

$$\dot{x} = f(x, u) \;\; x \in R^n, \;\; u \in R^m \tag{8.38}$$

Linearization of the system (four-wheel vehicle) is performed at each iteration of the control algorithm round its present operating point $(x^*, u^*) = (x(t), u(t - T_s))$. The linearized equivalent of the system is described by

$$\dot{x} = Ax + Bu + L\tilde{d} \;\; x \in R^n, \;\; u \in R^m, \;\; \tilde{d} \in R^q \tag{8.39}$$

where matrices A and B are obtained from the computation of the vehicle's Jacobians, according to Eqs. (8.25) and (8.26), and vector $\tilde{d}$ denotes disturbance terms due to linearization errors. The problem of disturbance rejection for the linearized model that is described by

$$\dot{x} = Ax + Bu + L\tilde{d}$$
$$y = Cx \tag{8.40}$$

where $x \in R^n$, $u \in R^m$, $\tilde{d} \in R^q$ and $y \in R^p$, cannot be handled efficiently if the classical LQR control scheme is applied. This is because of the existence of the perturbation term $\tilde{d}$. The disturbance term $\tilde{d}$ apart from modeling (parametric) uncertainty and external perturbations can also represent noise terms of any distribution.

As already explained in the previous applications of the H_∞ control approach, a feedback control scheme is designed for trajectory tracking by the system's state vector and simultaneous disturbance rejection, considering that the disturbance affects the system in the worst possible manner. The disturbances' effect are incorporated in the following quadratic cost function:

$$J(t) = \frac{1}{2}\int_0^T [y^T(t)y(t) + ru^T(t)u(t) - \rho^2\tilde{d}^T(t)\tilde{d}(t)]dt, \quad r, \rho > 0 \tag{8.41}$$

Once again, the significance of the negative sign in the cost function's term that is associated with the perturbation variable $\tilde{d}(t)$ is that the disturbance tries to maximize the cost function $J(t)$ while the control signal $u(t)$ tries to minimize it. The physical meaning of the relation given above is that the control signal and the disturbances compete to each other within a min-max differential game. This problem of min-max optimization can be written as

$$min_u max_{\tilde{d}} J(u, \tilde{d}) \tag{8.42}$$

The objective of the optimization procedure is to compute a control signal $u(t)$ which can compensate for the worst possible disturbance, that is externally imposed to the system of the four-wheel autonomous vehicle. However, the solution to the min-max optimization problem is directly related to the value of the parameter ρ. This means that there is an upper bound in the disturbances magnitude that can be annihilated by the control signal.

8.2.5.1 H-Infinity Feedback Control

For the linearized system given by Eq. (8.40) the cost function of Eq. (8.41) is defined, where the coefficient r determines the penalization of the control input and the weight coefficient ρ determines the reward of the disturbances' effects. Once more, it is assumed that (i) The energy that is transferred from the disturbances signal $\tilde{d}(t)$ is bounded, that is $\int_0^\infty \tilde{d}^T(t)\tilde{d}(t)dt < \infty$, (ii) matrices $[A, B]$ and $[A, L]$ are stabilizable, (iii) matrix $[A, C]$ is detectable. Then, the optimal feedback control law is given by

$$u(t) = -Kx(t) \tag{8.43}$$

with

$$K = \frac{1}{r} B^T P \tag{8.44}$$

where P is a positive semi-definite symmetric matrix which is obtained from the solution of the Riccati equation

$$A^T P + PA + Q - P\left(\frac{1}{r} BB^T - \frac{1}{2\rho^2} LL^T\right) P = 0 \tag{8.45}$$

where Q is also a positive definite symmetric matrix. The worst case disturbance is given by

$$\tilde{d}(t) = \frac{1}{\rho^2} L^T P x(t) \tag{8.46}$$

The diagram of the considered control loop is depicted in Fig. 8.3.

8.2.6 Lyapunov Stability Analysis

Through Lyapunov stability analysis it will be shown that the proposed nonlinear control scheme assures H_∞ tracking performance for the control loop of the four-

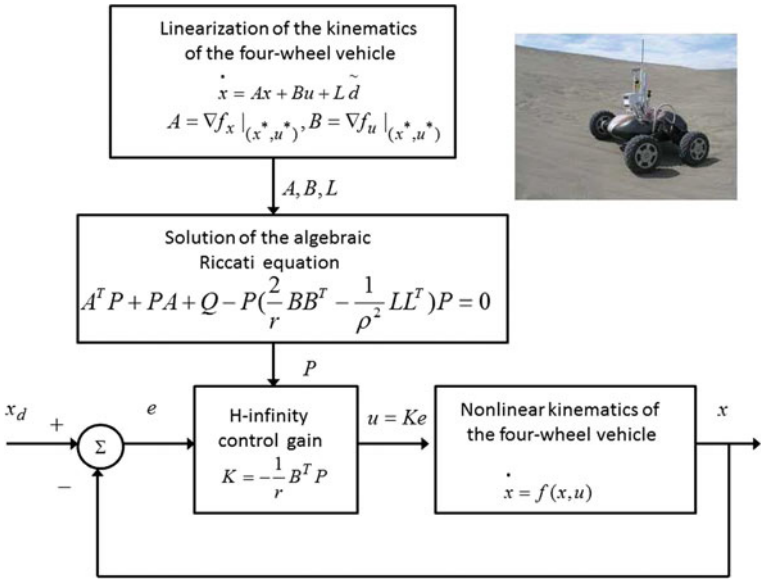

Fig. 8.3 Diagram of the nonlinear optimal control scheme for the four-wheel autonomous ground vehicle

wheel autonomous ground vehicle. Moreover, under moderate conditions asymptotic stability is proven and convergence to the reference setpoints is achieved. The tracking error dynamics for the automatic ground vehicle is written in the form

$$\dot{e} = Ae + Bu + L\tilde{d} \tag{8.47}$$

where in this autonomous vehicle's case $L = I \in R^{6\times 6}$ with I being the identity matrix. Variable $\tilde{d}$ denotes model uncertainties and external disturbances of the vehicle's model. The following Lyapunov function is considered

$$V = \frac{1}{2} e^T P e \tag{8.48}$$

where $e = x - x_d$ is the tracking error. By differentiating with respect to time one obtains

$$\dot{V} = \frac{1}{2}\dot{e}^T P e + \frac{1}{2} e P \dot{e} \Rightarrow$$
$$\dot{V} = \frac{1}{2}[Ae + Bu + L\tilde{d}]^T P + \frac{1}{2} e^T P [Ae + Bu + L\tilde{d}] \Rightarrow \tag{8.49}$$

$$\dot{V} = \frac{1}{2}[e^T A^T + u^T B^T + \tilde{d}^T L^T] P e +$$
$$+ \frac{1}{2} e^T P [Ae + Bu + L\tilde{d}] \Rightarrow \tag{8.50}$$

$$\dot{V} = \frac{1}{2} e^T A^T P e + \frac{1}{2} u^T B^T P e + \frac{1}{2} \tilde{d}^T L^T P e +$$
$$\frac{1}{2} e^T P A e + \frac{1}{2} e^T P B u + \frac{1}{2} e^T P L \tilde{d} \tag{8.51}$$

The previous equation is rewritten as

$$\dot{V} = \frac{1}{2} e^T (A^T P + P A) e + \left(\frac{1}{2} u^T B^T P e + \frac{1}{2} e^T P B u \right) +$$
$$+ \left(\frac{1}{2} \tilde{d}^T L^T P e + \frac{1}{2} e^T P L \tilde{d} \right) \tag{8.52}$$

Assumption: For given positive definite matrix Q and coefficients r and ρ there exists a positive definite matrix P, which is the solution of the following matrix equation

$$A^T P + P A = -Q + P \left(\frac{2}{r} B B^T - \frac{1}{\rho^2} L L^T \right) P \tag{8.53}$$

Moreover, the following feedback control law is applied to the system

$$u = -\frac{1}{r} B^T P e \tag{8.54}$$

By substituting Eqs. (8.53) and (8.54) one obtains

$$\dot{V} = \frac{1}{2} e^T \left[-Q + P \left(\frac{2}{r} B B^T - \frac{1}{2\rho^2} L L^T \right) P \right] e + \\ + e^T P B \left(-\frac{1}{r} B^T P e \right) + e^T P L \tilde{d} \Rightarrow \tag{8.55}$$

$$\dot{V} = -\frac{1}{2} e^T Q e + \left(\frac{2}{r} P B B^T P e - \frac{1}{2\rho^2} e^T P L L^T \right) P e \\ -\frac{1}{r} (e^T P B B^T P e) + e^T P L \tilde{d} \tag{8.56}$$

which after intermediate operations gives

$$\dot{V} = -\frac{1}{2} e^T Q e - \frac{1}{2\rho^2} e^T P L L^T P e + e^T P L \tilde{d} \tag{8.57}$$

or, equivalently

$$\dot{V} = -\frac{1}{2} e^T Q e - \frac{1}{2\rho^2} e^T P L L^T P e + \\ + \frac{1}{2} e^T P L \tilde{d} + \frac{1}{2} \tilde{d}^T L^T P e \tag{8.58}$$

Lemma: The following inequality holds

$$\frac{1}{2} e^T L \tilde{d} + \frac{1}{2} \tilde{d} L^T P e - \frac{1}{2\rho^2} e^T P L L^T P e \leq \frac{1}{2} \rho^2 \tilde{d}^T \tilde{d} \tag{8.59}$$

Proof: The binomial $(\rho\alpha - \frac{1}{\rho} b)^2$ is considered. Expanding the left part of the above inequality one gets

$$\rho^2 a^2 + \frac{1}{\rho^2} b^2 - 2ab \geq 0 \Rightarrow \frac{1}{2} \rho^2 a^2 + \frac{1}{2\rho^2} b^2 - ab \geq 0 \Rightarrow \\ ab - \frac{1}{2\rho^2} b^2 \leq \frac{1}{2} \rho^2 a^2 \Rightarrow \frac{1}{2} ab + \frac{1}{2} ab - \frac{1}{2\rho^2} b^2 \leq \frac{1}{2} \rho^2 a^2 \tag{8.60}$$

The following substitutions are carried out: $a = \tilde{d}$ and $b = e^T PL$ and the previous relation becomes

$$\frac{1}{2}\tilde{d}^T L^T Pe + \frac{1}{2}e^T PL\tilde{d} - \frac{1}{2\rho^2}e^T PLL^T Pe \leq \frac{1}{2}\rho^2\tilde{d}^T\tilde{d} \tag{8.61}$$

Equation (8.61) is substituted in Eq. (8.58) and the inequality is enforced, thus giving

$$\dot{V} \leq -\frac{1}{2}e^T Qe + \frac{1}{2}\rho^2\tilde{d}^T\tilde{d} \tag{8.62}$$

Equation (8.62) shows that the H_∞ tracking performance criterion is satisfied. The integration of $\dot{V}$ from 0 to T gives

$$\int_0^T \dot{V}(t)dt \leq -\frac{1}{2}\int_0^T ||e||_Q^2 dt + \frac{1}{2}\rho^2\int_0^T ||\tilde{d}||^2 dt \Rightarrow$$
$$2V(T) + \int_0^T ||e||_Q^2 dt \leq 2V(0) + \rho^2\int_0^T ||\tilde{d}||^2 dt \tag{8.63}$$

Moreover, if there exists a positive constant $M_d > 0$ such that

$$\int_0^\infty ||\tilde{d}||^2 dt \leq M_d \tag{8.64}$$

then one gets

$$\int_0^\infty ||e||_Q^2 dt \leq 2V(0) + \rho^2 M_d \tag{8.65}$$

Thus, the integral $\int_0^\infty ||e||_Q^2 dt$ is bounded. Moreover, $V(T)$ is bounded and from the definition of the Lyapunov function V in Eq. (8.48) it becomes clear that $e(t)$ will be also bounded since $e(t) \in \Omega_e = \{e|e^T Pe \leq 2V(0) + \rho^2 M_d\}$. According to the above and with the use of Barbalat's Lemma one obtains $lim_{t\to\infty} e(t) = 0$.

8.2.7 *Robust State Estimation with the Use of the H-Infinity Kalman Filter*

The control loop for the four-wheel autonomous vehicle can be implemented with the feedback of a partially measurable state vector and by processing only a small number of state variables. To reconstruct the missing information about the state vector of the autonomous vehicle it is proposed to use a filtering scheme which allows to apply state estimation-based control [457]. The recursion of the H_∞ Kalman Filter, for the model of the distributed finance agents, can be formulated in terms of a *measurement update* and a *time update* part

Measurement update:

$$\begin{aligned} D(k) &= [I - \theta W(k)P^{-}(k) + C^{T}(k)R(k)^{-1}C(k)P^{-}(k)]^{-1} \\ K(k) &= P^{-}(k)D(k)C^{T}(k)R(k)^{-1} \\ \hat{x}(k) &= \hat{x}^{-}(k) + K(k)[y(k) - C\hat{x}^{-}(k)] \end{aligned} \tag{8.66}$$

Time update:

$$\begin{aligned} \hat{x}^{-}(k+1) &= A(k)x(k) + B(k)u(k) \\ P^{-}(k+1) &= A(k)P^{-}(k)D(k)A^{T}(k) + Q(k) \end{aligned} \tag{8.67}$$

where it is assumed that parameter θ is sufficiently small to assure that the covariance matrix $P^{-}(k)^{-1} - \theta W(k) + C^{T}(k)R(k)^{-1}C(k)$ will be positive definite. When $\theta = 0$ the H_{∞} Kalman Filter becomes equivalent to the standard Kalman Filter. One can measure only a part of the state vector of the system of the autonomous ground vehicle, such as the velocities V_x and V_y and the orientation angle ψ, and can estimate through filtering the rest of the state vector elements.

8.2.8 Simulation Tests

The performance of the proposed nonlinear optimal control scheme for the autonomous four-wheel vehicle has been tested in the case of tracking of different reference set-points (Figs. 8.4, 8.5, 8.6, 8.7, 8.8, 8.9, 8.10, 8.11, 8.12 and 8.13). The control scheme exhibited fast and accurate tracking of the reference paths. The computation of the feedback control gain required the solution of the algebraic Riccati equation given in Eq. (8.53), at each iteration of the control algorithm. The obtained results are depicted in Figs. 8.22, 8.23, 8.24, 8.25, 8.26, 8.27, 8.28, 8.29, 8.30, 8.31, 8.32 and 8.33. The measurement units for the state variables of the four-wheel vehicle's model were in the SI system (position coordinates measured in m and heading angle in rad). It can be noticed that the H-infinity controller achieved fast and accurate convergence to the reference setpoints for all elements of the four-wheel vehicle's state-vector. Moreover, the variations of the control inputs, that is of the autonomous vehicle's velocity and of its steering angle were smooth.

As noted, the proposed nonlinear optimal control method for the four-wheel autonomous vehicle was based on an approximate linearization of its joint kinematic and dynamic model. The advantages that the proposed control method exhibits are outlined as follows: (i) it is applied directly on the nonlinear dynamical model of the four-wheel vehicle and not on an equivalent linearized description of it, (ii) It avoids the elaborated linearizing transformations (diffeomorphisms) which can be

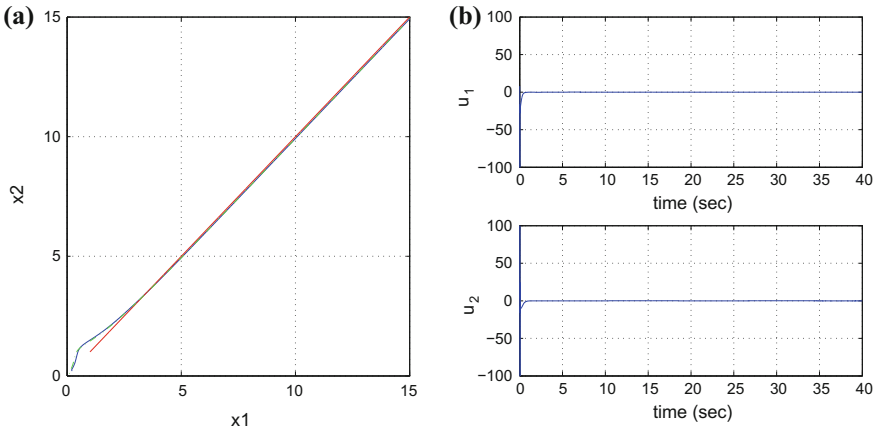

Fig. 8.4 **a** Tracking of reference path 1 (red-line) by the four-wheel autonomous vehicle (blue line) and trajectory estimated by the Kalman Filter (green line), **b** control inputs u_1 and u_2 applied to the vehicle

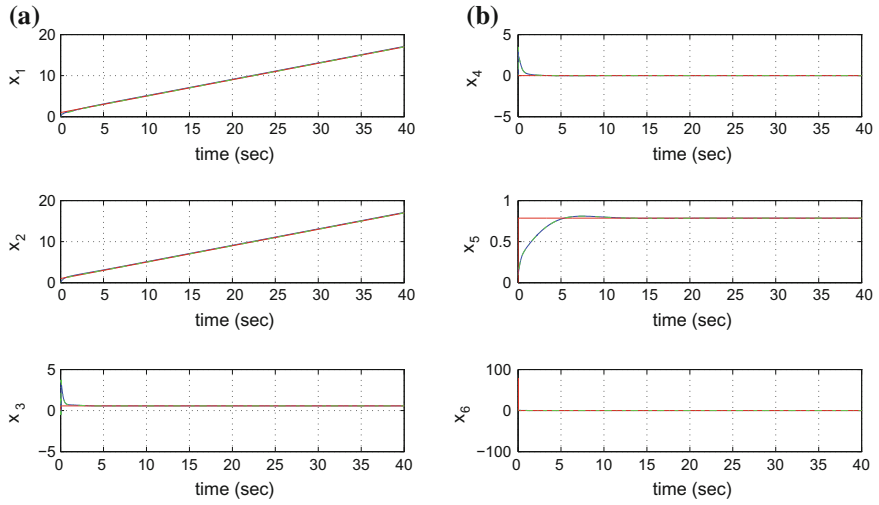

Fig. 8.5 Tracking of reference path 1: **a** convergence of state variables x_1 to x_3 of the four-wheel vehicle to their reference setpoints (red-lines) and estimated state variables provided by the Kalman Filter (green lines), **b** convergence of state variables x_4 to x_6 of the four-wheel vehicle to their reference setpoints (red-lines) and estimated state variables provided by the Kalman Filter (green lines)

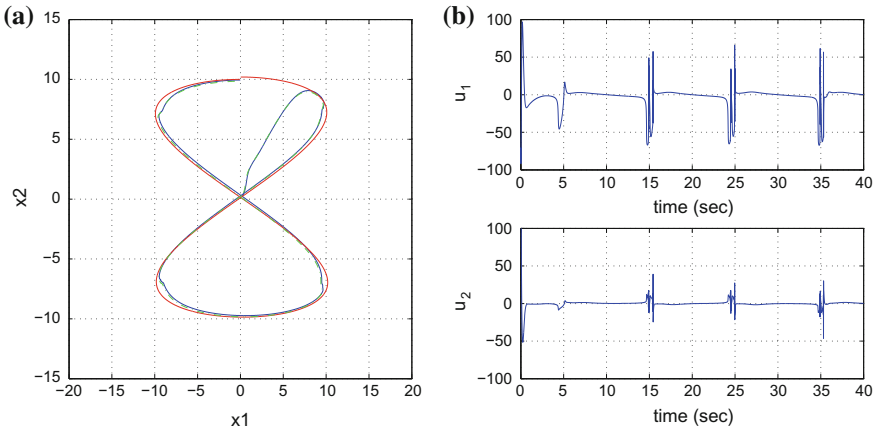

Fig. 8.6 **a** Tracking of reference path 2 (red-line) by the four-wheel autonomous vehicle (blue line) and trajectory estimated by the Kalman Filter (green line), **b** control inputs u_1 and u_2 applied to the vehicle

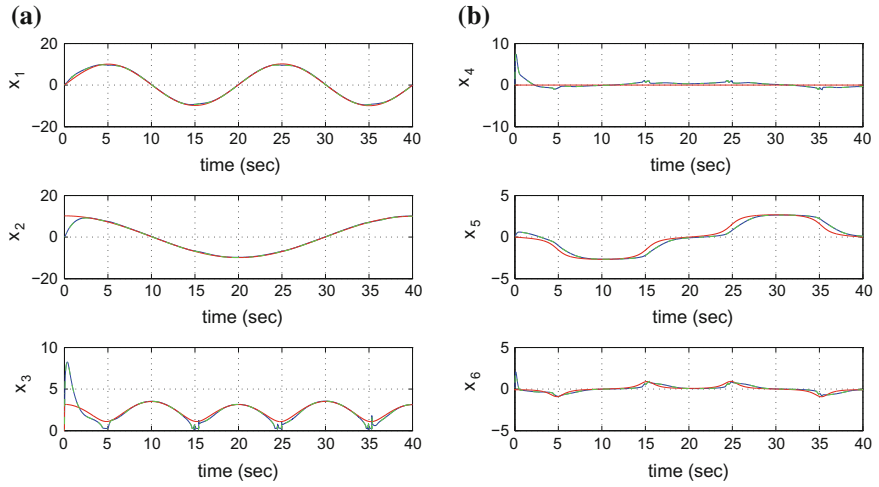

Fig. 8.7 Tracking of reference path 2: **a** convergence of state variables x_1 to x_3 of the four-wheel vehicle-to their reference setpoints (red-lines) and estimated state variables provided by the Kalman Filter (green lines), **b** convergence of state variables x_4 to x_6 of the four-wheel vehicle to their reference setpoints (red-lines) and estimated state variables provided by the Kalman Filter (green lines)

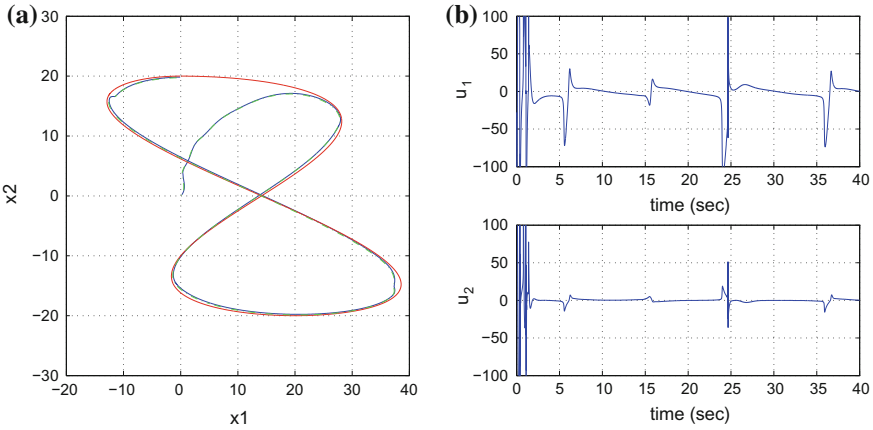

Fig. 8.8 **a** Tracking of reference path 3 (red-line) by the four-wheel autonomous vehicle (blue line) and trajectory estimated by the Kalman Filter (green line), **b** control inputs u_1 and u_2 applied to the vehicle

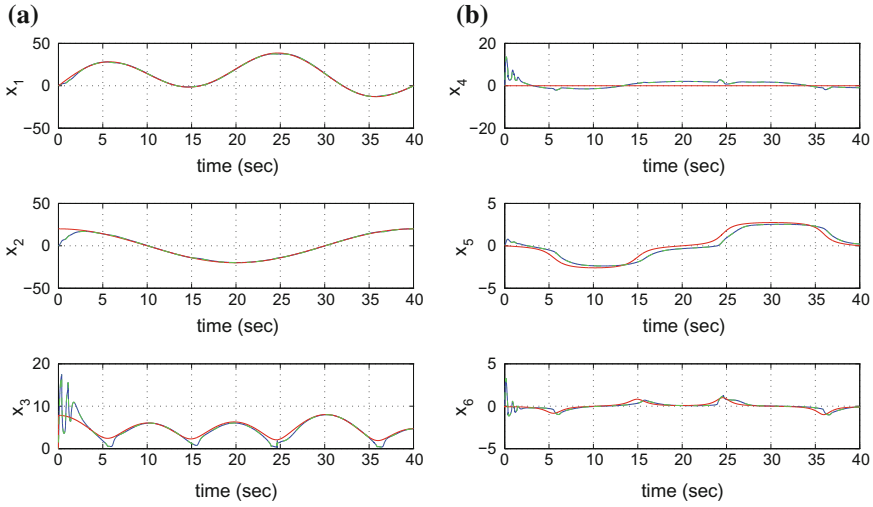

Fig. 8.9 Tracking of reference path 3: **a** convergence of state variables x_1 to x_3 of the four-wheel vehicle to their reference setpoints (red-lines) and estimated state variables provided by the Kalman Filter (green lines), **b** convergence of state variables x_4 to x_6 of the four-wheel vehicle to their reference setpoints (red-lines) and estimated state variables provided by the Kalman Filter (green lines)

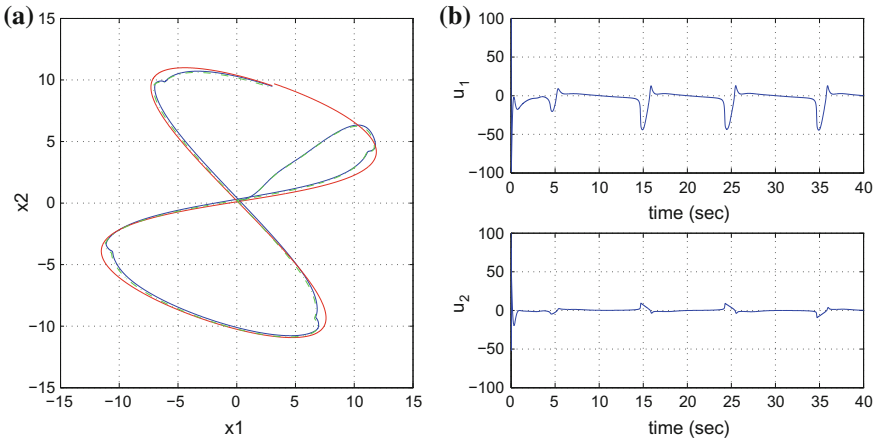

Fig. 8.10 **a** Tracking of reference path 1 (red-line) by the four-wheel autonomous vehicle (blue line) and trajectory estimated by the Kalman Filter (green line), **b** control inputs u_1 and u_2 applied to the vehicle

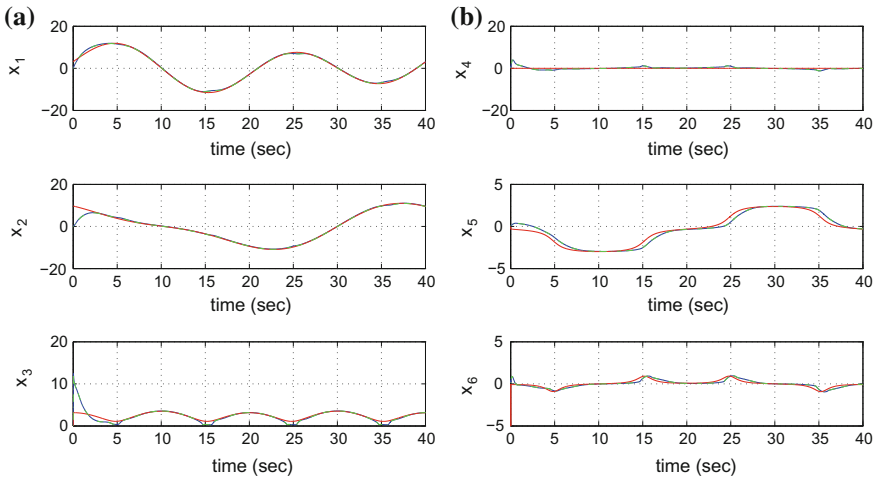

Fig. 8.11 Tracking of reference path 4: **a** convergence of state variables x_1 to x_3 of the four-wheel vehicle to their reference setpoints (red-lines) and estimated state variables provided by the Kalman Filter (green lines), **b** convergence of state variables x_4 to x_6 of the four-wheel vehicle to their reference setpoints (red-lines) and estimated state variables provided by the Kalman Filter (green lines)

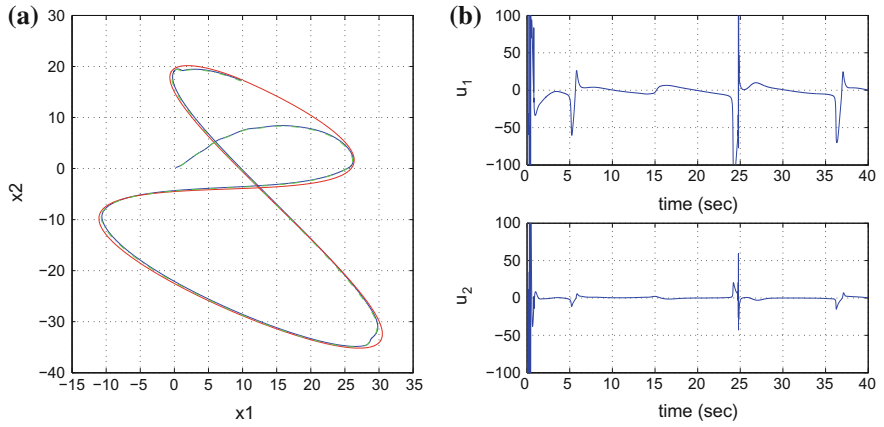

Fig. 8.12 **a** Tracking of reference path51 (red-line) by the four-wheel autonomous vehicle (blue line) and trajectory estimated by the Kalman Filter (green line), **b** control inputs u_1 and u_2 applied to the vehicle

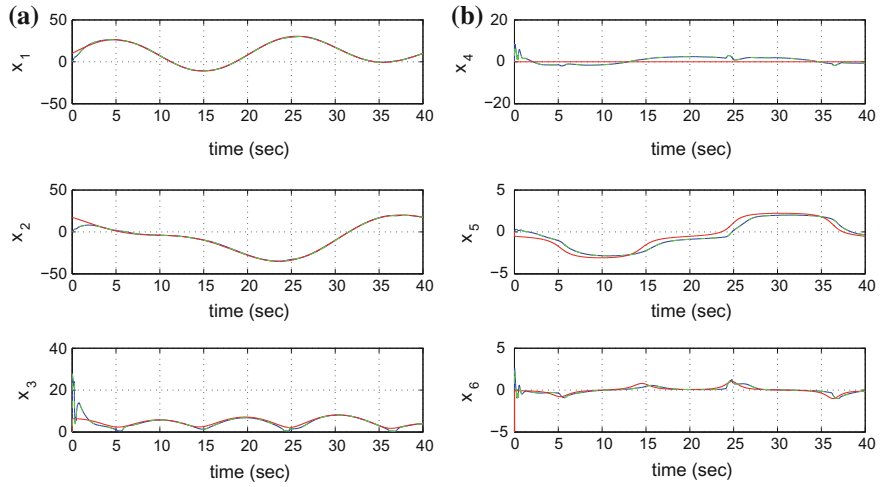

Fig. 8.13 Tracking of reference path 5: **a** convergence of state variables x_1 to x_3 of the four-wheel vehicle to their reference setpoints (red-lines) and estimated state variables provided by the Kalman Filter (green lines), **b** convergence of state variables x_4 to x_6 of the four-wheel vehicle to their reference setpoints (red-lines) and estimated state variables provided by the Kalman Filter (green lines)

met in global linearization-based control methods for autonomous vehicles (iii) the controller is designed according to optimal control principles which implies the best trade-off between precise tracking of the reference setpoints on the one side and moderate variations of the control inputs on the other side (iv) the control method exhibits significant robustness to parametric uncertainty, modelling errors as well as to external perturbations.

Yet computationally simple, the proposed H_∞ control scheme has an excellent performance. Comparing to the control of the automatic ground vehicles that can rely on global linearization methods the presented nonlinear H-infinity control scheme is equally efficient in setpoint tracking while also retaining optimal control features [457]. The tracking accuracy of the presented control method (H_∞) has been monitored in the case of several reference setpoints. By using the Kalman Filter as a robust observer estimates of the state vector of the vehicle were obtained and thus the implementation of state estimation-based control became possible. The measured state variables were $x_3 = V_x$, $x_4 = V_y$ and $x_5 = \psi$. The obtained results are given in Table 8.1.

The tracking performance of the nonlinear H-infinity control method for the model of the four-wheel vehicle was measured in the case of model uncertainty, imposing an imprecision equal to $\Delta a\%$ about the vehicle's moment of inertia I_z. The obtained results are outlined in Table 8.2. It can be noticed that despite model perturbations the tracking accuracy of the control method remained satisfactory.

Table 8.1 RMSE of the vehicle's state variables

Path	RMSE X (m)	RMSE Y (m)	RMSE ψ (rad)
1	$4.5{\cdot}10^{-3}$	$4.5{\cdot}10^{-3}$	$0.1{\cdot}10^{-3}$
2	$15.1{\cdot}10^{-3}$	$5.7{\cdot}10^{-3}$	$17.3{\cdot}10^{-3}$
3	$13.3{\cdot}10^{-3}$	$13.7{\cdot}10^{-3}$	$18.6{\cdot}10^{-3}$
4	$15.3{\cdot}10^{-3}$	$9.3{\cdot}10^{-3}$	$17.0{\cdot}10^{-3}$
5	$8.7{\cdot}10^{-3}$	$15.5{\cdot}10^{-3}$	$17.8{\cdot}10^{-3}$

Table 8.2 RMSE of state variables under disturbance

Δa (%)	RMSE X (m)	RMSE Y (m)	RMSE ψ (rad)
0	$8.7{\cdot}10^{-3}$	$15.5{\cdot}10^{-3}$	$17.8{\cdot}10^{-3}$
10	$9.0{\cdot}10^{-3}$	$16.2{\cdot}10^{-3}$	$16.3{\cdot}10^{-3}$
20	$9.5{\cdot}10^{-3}$	$17.2{\cdot}10^{-3}$	$14.8{\cdot}10^{-3}$
30	$10.1{\cdot}10^{-3}$	$18.3{\cdot}10^{-3}$	$13.4{\cdot}10^{-3}$
40	$10.8{\cdot}10^{-3}$	$19.3{\cdot}10^{-3}$	$12.0{\cdot}10^{-3}$
50	$11.6{\cdot}10^{-3}$	$20.3{\cdot}10^{-3}$	$10.7{\cdot}10^{-3}$
60	$12.7{\cdot}10^{-3}$	$20.9{\cdot}10^{-3}$	$9.5{\cdot}10^{-3}$

8.3 A Nonlinear H-Infinity Control Approach for an Autonomous Truck and Trailer System

8.3.1 Outline

Comparing to the previously analyzed unicycle-type and four-wheel vehicles there exist more complicated and difficult to control models, such as multi-body and articulated autonous vehicles [202, 249, 508]. Due to their complicated kinematic and dynamic model the problems of path planning and path following for the aforementioned types of vehicles is of elevated difficulty [12, 109, 166, 218, 328, 394]. To achieve accurate tracking of reference paths and to assure stability for the vehicles' autonomous navigation system, nonlinear control approaches have been proposed [59, 344, 355, 366, 469]. In [248, 471] one can find results on global linearization-based control of multi-body and articulated vehicles, based on differential flatness theory. In [217] the controller's design for the above mentioned type of vehicles is based on approximate linearization and the description of their kinematics or dynamics with the use of local models. Moreover, in [24] Lyapunov theory-based control methods are developed for such complicated vehicles.

In this section the problems of nonlinear optimal control and the problem of autonomous navigation of a truck and trailer vehicle are considered. The kinematic model of the vehicle is formulated and the controller's design proceeds by carrying out an approximate linearization on this model around a time-varying equilibrium. The linearization procedure relies on Taylor series expansion for the articulated vehicle's kinematic model and on the computation of the associated Jacobian matrices [33, 431, 463]. The linearization point (equilibrium) is updated at each time instant and is defined by the present value of the vehicle's state vector and the last value of the vehicle's control inputs vector. The modelling error which is due to approximate linearization and the cut-off of higher order terms in the Taylor series expansion is considered as a perturbation that is compensated by the robustness of the H-infinity control scheme [461, 466].

For the linearized equivalent model of the truck and trailer vehicle an H-infinity feedback controller is designed. This is an optimal controller for the case of a system subject to model uncertainty and external perturbations [450, 452, 457, 459, 460]. H-infinity control stands for the solution of a min-max differential game. Actually, the control inputs try to minimize a quadratic cost function associated with the deviation of the vehicle's state vector from its reference values, while the perturbations and model uncertainty terms try to maximize this cost function [132, 305, 564]. The feedback gain of the controller is based on the solution of an algebraic Riccati equation that is performed at each iteration of the control algorithm. The stability of the control loop for the truck and trailer system is confirmed through Lyapunov analysis. First, it is shown that the H-infinity tracking performance criterion is satisfied. This signifies elevated robustness of the control loop against model uncertainty and

exogenous disturbances. Moreover, under moderate conditions the global asymptotic stability of the control loop is proven. Finally, ro implement feedback control for the autonomous truck and trailer system when its state vector is only partially measurable, the H-infinity Kalman Filter is proposed [169, 511].

8.3.2 Kinematic Model of the Truck and Trailer

8.3.2.1 State-Space Description of the Truck and Trailer System

The kinematic model of the truck and trailer system is given by

$$\begin{pmatrix} \dot{x}^t \\ \dot{y}^t \\ \dot{\theta} \\ \dot{x}^i \\ \dot{y}^i \\ \dot{\psi} \end{pmatrix} = \begin{pmatrix} vcos(\theta) \\ vsin(\theta) \\ \omega \\ vcos(\theta - \psi)cos(\psi) \\ vcos(\theta - \psi)sin(\psi) \\ \frac{v}{L^i} sin(\theta - \psi) \end{pmatrix} \tag{8.68}$$

where (x^t, y^t) are the cartesian coordinates of the truck in an inertial reference frame, θ is the heading angle of the truck formed by its transversal axis and the OX axis of the reference frame, ω is the turn rate of the truck (turn rate of the steering wheel), (x^i, y^i) are the cartesian coordinates of the trailer, ψ^i is the heading angle of the trailer, v is the longitudinal speed of the truck, and β is the hitch point angle between the truck and the drawbar that connects the truck with the trailer. The parameters of the truck and trailer system are shown in Fig. 8.14.

In the diagram of Fig. 8.14, the following distances are defined: L^t is the distance between the front and the rear axis of the truck, L^i us the distance between the hitch point RJ and the rear axis of the trailer. The state vector of the truck and trailer system is defined as $x = [x^t, y^t, \theta, x^i, y^i, \psi]^T$ while the control inputs vector is defined as $u = [v, \omega]^T$ and thus consists of the velocity of the truck and the turn rate of the steering wheel of the truck.

The kinematic model of the truck and trailer system is justified as follows: The velocity v of point RJ is first projected on the longitudinal axis of the trailer, thus giving $vcos(\theta - \psi)$ and next (a) it is projected on the OX axis thus giving $vcos(\theta - \psi)cos(\psi)$. This variable is the velocity of the trailer along the OX axis (b) it is projected on the OY axis thus giving $vcos(\theta - \psi)sin(\psi)$. Moreover, the trailer performs a rotational motion round point RJ, with rotational speed denoted as $\dot{\psi}$. The linear velocity of point RJ that is parallel to the transversal axis of the vehicle is given by $vsin(\theta - \psi)$. Thus, it holds: $\dot{\psi} = \frac{1}{L_i} vsin(\theta - \psi)$.

The kinematic model of the truck and trailer system is also written in the vector form:

$$\dot{x} = f(x, u) \tag{8.69}$$

where $x \in R^{6\times 1}$, $f \in R^{6\times 1}$ and $u \in R^{2\times 1}$. It also holds that $\beta = \theta - \psi$. With the previous definition of state variables one arrives at the following state-space description

$$\begin{pmatrix} \dot{x}_1 \\ \dot{x}_2 \\ \dot{x}_3 \\ \dot{x}_4 \\ \dot{x}_5 \\ \dot{x}_6 \end{pmatrix} = \begin{pmatrix} u_1 cos(x_3) \\ u_1 sin(x_3) \\ u_2 \\ u_1 cos(x_3 - x_6) cos(x_6) \\ u_1 cos(x_3 - x_6) sin(x_6) \\ \frac{u_1}{L_i} sin(x_3 - x_6) \end{pmatrix} \tag{8.70}$$

8.3.2.2 Approximate Linearization of the Truck and Trailer Model

Approximate linearization is performed to the kinematic model of the truck and trailer system round a temporary equilibrium x^* which is re-computed at each iteration of the control algorithm. The method is based on Taylor series expansion and on the calculation of the associated Jacobian matrices, while the equilibrium consists of the present value of the system's state vector x^* and of the last value of the control inputs vector u^* that was exerted on it. Thus one has the linearization point (x^*, u^*). Using that the kinematic model of the system is $\dot{x} = f(x, u)$ the following linearized description is obtained

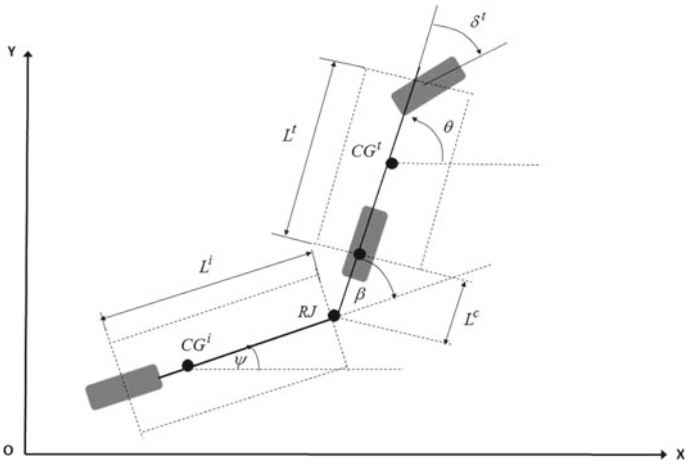

Fig. 8.14 Kinematic model of the truck and trailer

$$\dot{x} = Ax + Bu + \tilde{d} \tag{8.71}$$

where $\tilde{d}$ is the linearization error and the associated Jacobian matrices are:

$$A = \nabla_x f(x,u) \mid_{(x^*,u^*)} \; B = \nabla_u f(x,u) \mid_{(x^*,u^*)} \tag{8.72}$$

The elements of the Jacobian matrices are

$$A = \begin{pmatrix} \frac{\partial f_1}{\partial x_1} & \frac{\partial f_1}{\partial x_2} & \cdots & \frac{\partial f_1}{\partial x_6} \\ \frac{\partial f_2}{\partial x_1} & \frac{\partial f_2}{\partial x_2} & \cdots & \frac{\partial f_2}{\partial x_6} \\ \cdots & \cdots & \cdots & \cdots \\ \cdots & \cdots & \cdots & \cdots \\ \frac{\partial f_6}{\partial x_1} & \frac{\partial f_6}{\partial x_2} & \cdots & \frac{\partial f_6}{\partial x_6} \end{pmatrix} B = \begin{pmatrix} \frac{\partial f_1}{\partial u_1} & \frac{\partial f_1}{\partial u_2} \\ \frac{\partial f_2}{\partial u_1} & \frac{\partial f_2}{\partial u_2} \\ \cdots & \cdots \\ \cdots & \cdots \\ \frac{\partial f_6}{\partial u_1} & \frac{\partial f_6}{\partial u_2} \end{pmatrix} \tag{8.73}$$

With the previous definition of the Jacobian matrices one finds
The first row of the Jacobian matrix $A = \nabla_x f(x,u) \mid_{(x^*,u^*)}$ is $\frac{\partial f_1}{\partial x_1} = 0$, $\frac{\partial f_1}{\partial x_2} = 0$, $\frac{\partial f_1}{\partial x_3} = -u_1 sin(x_3)$, $\frac{\partial f_1}{\partial x_4} = 0$, $\frac{\partial f_1}{\partial x_5} = 0$ and $\frac{\partial f_1}{\partial x_6} = 0$.

The second row of the Jacobian matrix $A = \nabla_x f(x,u) \mid_{(x^*,u^*)}$ is $\frac{\partial f_2}{\partial x_1} = 0$, $\frac{\partial f_2}{\partial x_2} = 0$, $\frac{\partial f_2}{\partial x_3} = u_1 cos(x_3)$, $\frac{\partial f_2}{\partial x_4} = 0$, $\frac{\partial f_2}{\partial x_5} = 0$ and $\frac{\partial f_2}{\partial x_6} = 0$.

The third row of the Jacobian matrix $A = \nabla_x f(x,u) \mid_{(x^*,u^*)}$ is $\frac{\partial f_3}{\partial x_1} = 0$, $\frac{\partial f_3}{\partial x_2} = 0$, $\frac{\partial f_3}{\partial x_3} = 0$, $\frac{\partial f_3}{\partial x_4} = 0$, $\frac{\partial f_3}{\partial x_5} = 0$ and $\frac{\partial f_3}{\partial x_6} = 0$.

The fourth row of the Jacobian matrix $A = \nabla_x f(x,u) \mid_{(x^*,u^*)}$ is $\frac{\partial f_4}{\partial x_1} = 0$, $\frac{\partial f_4}{\partial x_2} = 0$, $\frac{\partial f_4}{\partial x_3} = -sin(x_3 - x_6)cos(x_6)u_1$, $\frac{\partial f_4}{\partial x_4} = 0$, $\frac{\partial f_4}{\partial x_5} = 0$ and $\frac{\partial f_4}{\partial x_6} = [sin(x_3 - x_6) cos(x_6) - cos(x_3 - x_6)sin(x_6)]u_1$.

The fifth row of the Jacobian matrix $A = \nabla_x f(x,u) \mid_{(x^*,u^*)}$ is $\frac{\partial f_5}{\partial x_1} = 0$, $\frac{\partial f_5}{\partial x_2} = 0$, $\frac{\partial f_5}{\partial x_3} = -sin(x_3 - x_6)sin(x_6)u_1$, $\frac{\partial f_5}{\partial x_4} = 0$, $\frac{\partial f_5}{\partial x_5} = 0$ and $\frac{\partial f_5}{\partial x_6} = [sin(x_3 - x_6)sin(x_6) + cos(x_3 - x_6)cos(x_6)]u_1$.

The sixth row of the Jacobian matrix $A = \nabla_x f(x,u) \mid_{(x^*,u^*)}$ is $\frac{\partial f_6}{\partial x_1} = 0$, $\frac{\partial f_6}{\partial x_2} = 0$, $\frac{\partial f_6}{\partial x_3} = \frac{1}{L_i} cos(x_3 - x_6)u_1$, $\frac{\partial f_6}{\partial x_4} = 0$, $\frac{\partial f_6}{\partial x_5} = 0$ and $\frac{\partial f_6}{\partial x_6} = -\frac{1}{L_i} cos(x_3 - x_6)u_1$.

In a similar manner one finds
The first row of the Jacobian matrix $B = \nabla_u f(x,u) \mid_{(x^*,u^*)}$ is $\frac{\partial f_1}{\partial u_1} = cos(x_3)$, $\frac{\partial f_1}{\partial u_2} = 0$,

The second row of the Jacobian matrix $B = \nabla_u f(x,u) \mid_{(x^*,u^*)}$ is $\frac{\partial f_2}{\partial u_1} = sin(x_3)$, $\frac{\partial f_2}{\partial u_2} = 0$,

The third row of the Jacobian matrix $B = \nabla_u f(x,u)\mid_{(x^*,u^*)}$ is $\frac{\partial f_3}{\partial u_1} = 0$, $\frac{\partial f_3}{\partial u_2} = 1$,

The fourth row of the Jacobian matrix $B = \nabla_u f(x,u)\mid_{(x^*,u^*)}$ is $\frac{\partial f_4}{\partial u_1} = cos(x_3 - x_6)cos(x_6)$, $\frac{\partial f_4}{\partial u_2} = 0$,

The fifth row of the Jacobian matrix $B = \nabla_u f(x,u)\mid_{(x^*,u^*)}$ is $\frac{\partial f_5}{\partial u_1} = cos(x_3 - x_6)sin(x_6)$, $\frac{\partial f_6}{\partial u_2} = 0$,

The sixth row of the Jacobian matrix $B = \nabla_u f(x,u)\mid_{(x^*,u^*)}$ is $\frac{\partial f_6}{\partial u_1} = \frac{1}{L^i}sin(x_3 - x_6)$, $\frac{\partial f_6}{\partial u_2} = 0$,

8.3.3 The Nonlinear H-Infinity Control

8.3.3.1 Mini-Max Control and Disturbance Rejection

The initial nonlinear model of the truck and trailer system is in the form

$$\dot{x} = f(x,u) \;\; x \in R^n, \;\; u \in R^m \tag{8.74}$$

Linearization of the system (truck and trailer) is performed at each iteration of the control algorithm round its present operating point $(x^*, u^*) = (x(t), u(t - T_s))$. The linearized equivalent model of the system is described by

$$\dot{x} = Ax + Bu + L\tilde{d} \;\; x \in R^n, \;\; u \in R^m, \;\; \tilde{d} \in R^q \tag{8.75}$$

where matrices A and B are obtained from the computation of the Jacobians matrices of the truck and trailer's state-space model and vector $\tilde{d}$ denotes disturbance terms due to linearization errors. The problem of disturbance rejection for the linearized model that is described by

$$\begin{aligned} \dot{x} &= Ax + Bu + L\tilde{d} \\ y &= Cx \end{aligned} \tag{8.76}$$

where $x \in R^n$, $u \in R^m$, $\tilde{d} \in R^q$ and $y \in R^p$, cannot be handled efficiently if the classical LQR control scheme is applied. This because of the existence of the perturbation term $\tilde{d}$. The disturbance term $\tilde{d}$ apart from modeling (parametric) uncertainty and external perturbation terms can also represent noise terms of any distribution.

Adhering to the previous applications of the H_∞ control approach, a feedback control scheme is designed for trajectory tracking by the system's state vector and

simultaneous disturbance rejection, considering that the disturbance affects the system in the worst possible manner. The disturbances' effect are incorporated in the following quadratic cost function:

$$J(t) = \frac{1}{2}\int_0^T [y^T(t)y(t) + ru^T(t)u(t) - \rho^2 \tilde{d}^T(t)\tilde{d}(t)]dt, \quad r, \rho > 0 \tag{8.77}$$

According to the analysis of the previous sections, the significance of the negative sign in the cost function's term that is associated with the perturbation variable $\tilde{d}(t)$ is that the disturbance tries to maximize the cost function $J(t)$ while the control signal $u(t)$ tries to minimize it. The physical meaning of the relation given above is that the control signal and the disturbances compete to each other within a min-max differential game. This problem of min-max optimization can be written as

$$min_u max_{\tilde{d}} J(u, \tilde{d}) \tag{8.78}$$

As pointed out in previous cases, the objective of the optimization procedure is to compute a control signal $u(t)$ which can compensate for the worst possible disturbance, that is externally imposed to the system of the truck and trailer system. However, the solution to the min-max optimization problem is directly related to the value of the parameter ρ. This means that there is an upper bound in the disturbances magnitude that can be annihilated by the control signal.

8.3.3.2 H-Infinity Feedback Control

For the linearized system given by Eq. (8.76) the cost function of Eq. (8.77) is defined, where the coefficient r determines the penalization of the control input and the weight coefficient ρ determines the reward of the disturbances' effects. As in previous applications of the H-infinity control it is assumed that (i) The energy that is transferred from the disturbances signal $\tilde{d}(t)$ is bounded, that is $\int_0^\infty \tilde{d}^T(t)\tilde{d}(t)dt < \infty$, (ii) matrices $[A, B]$ and $[A, L]$ are stabilizable, (iii) matrix $[A, C]$ is detectable. Then, the optimal feedback control law is given by

$$u(t) = -Kx(t) \tag{8.79}$$

with

$$K = \frac{1}{r}B^T P \tag{8.80}$$

where P is a positive semi-definite symmetric matrix which is obtained from the solution of the Riccati equation

$$A^T P + PA + Q - P\left(\frac{1}{r}BB^T - \frac{1}{2\rho^2}LL^T\right)P = 0 \tag{8.81}$$

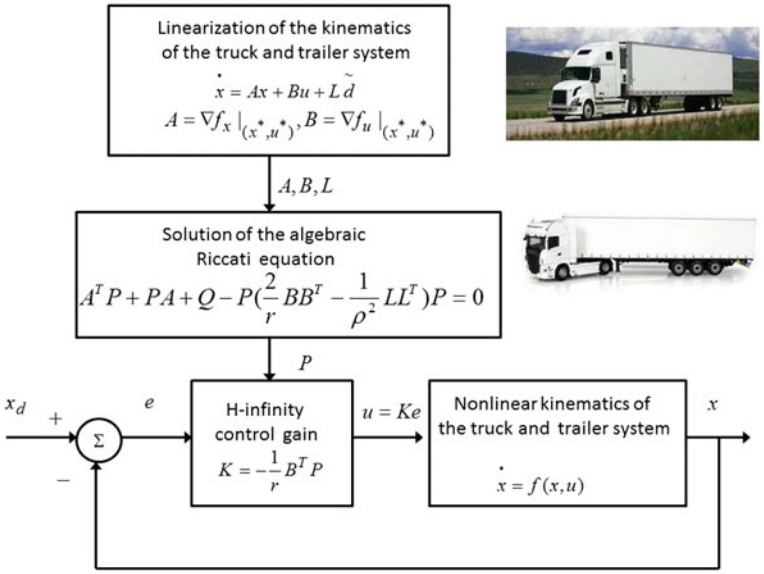

Fig. 8.15 Diagram of the nonlinear optimal control scheme for the truck and trailer system

where Q is also a positive definite symmetric matrix. The worst case disturbance is given by

$$\tilde{d}(t) = \frac{1}{\rho^2} L^T P x(t) \tag{8.82}$$

The diagram of the considered control loop is depicted in Fig. 8.15.

8.3.4 Lyapunov Stability Analysis

Through Lyapunov stability analysis it will be shown that the proposed nonlinear control scheme assures H_∞ tracking performance for the control loop of the truck and trailer system. Moreover, under moderate conditions asymptotic stability is proven and convergence to the reference setpoints is achieved. The tracking error dynamics for the truck and trailer system is written in the form

$$\dot{e} = Ae + Bu + L\tilde{d} \tag{8.83}$$

where in this autonomous vehicle's case $L = I \in R^{6\times 6}$ with I being the identity matrix. Variable $\tilde{d}$ denotes model uncertainties and external disturbances of the truck and trailer model. The following Lyapunov function is considered

$$V = \frac{1}{2} e^T P e \tag{8.84}$$

where $e = x - x_d$ is the tracking error. By differentiating with respect to time one obtains

$$\begin{aligned} \dot{V} &= \frac{1}{2} \dot{e}^T P e + \frac{1}{2} e P \dot{e} \Rightarrow \\ \dot{V} &= \frac{1}{2} [Ae + Bu + L\tilde{d}]^T P + \frac{1}{2} e^T P [Ae + Bu + L\tilde{d}] \Rightarrow \end{aligned} \tag{8.85}$$

$$\begin{aligned} \dot{V} = \frac{1}{2} [e^T A^T + u^T B^T + \tilde{d}^T L^T] P e + \\ + \frac{1}{2} e^T P [Ae + Bu + L\tilde{d}] \Rightarrow \end{aligned} \tag{8.86}$$

$$\begin{aligned} \dot{V} = \frac{1}{2} e^T A^T P e + \frac{1}{2} u^T B^T P e + \frac{1}{2} \tilde{d}^T L^T P e + \\ \frac{1}{2} e^T P A e + \frac{1}{2} e^T P B u + \frac{1}{2} e^T P L \tilde{d} \end{aligned} \tag{8.87}$$

The previous equation is rewritten as

$$\begin{aligned} \dot{V} = \frac{1}{2} e^T (A^T P + P A) e + \left(\frac{1}{2} u^T B^T P e + \frac{1}{2} e^T P B u \right) + \\ + \left(\frac{1}{2} \tilde{d}^T L^T P e + \frac{1}{2} e^T P L \tilde{d} \right) \end{aligned} \tag{8.88}$$

Assumption: For given positive definite matrix Q and coefficients r and ρ there exists a positive definite matrix P, which is the solution of the following matrix equation

$$A^T P + P A = -Q + P \left(\frac{2}{r} B B^T - \frac{1}{\rho^2} L L^T \right) P \tag{8.89}$$

Moreover, the following feedback control law is applied to the system

$$u = -\frac{1}{r} B^T P e \tag{8.90}$$

By substituting Eqs. (8.89) and (8.90) one obtains

$$\begin{aligned} \dot{V} = \frac{1}{2} e^T \left[-Q + P \left(\frac{2}{r} B B^T - \frac{1}{2\rho^2} L L^T \right) P \right] e + \\ + e^T P B \left(-\frac{1}{r} B^T P e \right) + e^T P L \tilde{d} \Rightarrow \end{aligned} \tag{8.91}$$

$$\dot{V} = -\frac{1}{2}e^T Qe + \left(\frac{2}{r}PBB^T Pe - \frac{1}{2\rho^2}e^T PLL^T\right)Pe$$
$$-\frac{1}{r}(e^T PBB^T Pe) + e^T PL\tilde{d} \tag{8.92}$$

which after intermediate operations gives

$$\dot{V} = -\frac{1}{2}e^T Qe - \frac{1}{2\rho^2}e^T PLL^T Pe + e^T PL\tilde{d} \tag{8.93}$$

or, equivalently

$$\dot{V} = -\frac{1}{2}e^T Qe - \frac{1}{2\rho^2}e^T PLL^T Pe +$$
$$+\frac{1}{2}e^T PL\tilde{d} + \frac{1}{2}\tilde{d}^T L^T Pe \tag{8.94}$$

Lemma: The following inequality holds

$$\frac{1}{2}e^T L\tilde{d} + \frac{1}{2}\tilde{d}L^T Pe - \frac{1}{2\rho^2}e^T PLL^T Pe \leq \frac{1}{2}\rho^2\tilde{d}^T\tilde{d} \tag{8.95}$$

Proof: The binomial $(\rho\alpha - \frac{1}{\rho}b)^2$ is considered. Expanding the left part of the above inequality one gets

$$\rho^2a^2 + \frac{1}{\rho^2}b^2 - 2ab \geq 0 \Rightarrow \frac{1}{2}\rho^2a^2 + \frac{1}{2\rho^2}b^2 - ab \geq 0 \Rightarrow$$
$$ab - \frac{1}{2\rho^2}b^2 \leq \frac{1}{2}\rho^2a^2 \Rightarrow \frac{1}{2}ab + \frac{1}{2}ab - \frac{1}{2\rho^2}b^2 \leq \frac{1}{2}\rho^2a^2 \tag{8.96}$$

The following substitutions are carried out: $a = \tilde{d}$ and $b = e^T PL$ and the previous relation becomes

$$\frac{1}{2}\tilde{d}^T L^T Pe + \frac{1}{2}e^T PL\tilde{d} - \frac{1}{2\rho^2}e^T PLL^T Pe \leq \frac{1}{2}\rho^2\tilde{d}^T\tilde{d} \tag{8.97}$$

Equation (8.97) is substituted in Eq. (8.94) and the inequality is enforced, thus giving

$$\dot{V} \leq -\frac{1}{2}e^T Qe + \frac{1}{2}\rho^2\tilde{d}^T\tilde{d} \tag{8.98}$$

Equation (8.98) shows that the H_∞ tracking performance criterion is satisfied. The integration of $\dot{V}$ from 0 to T gives

$$\int_0^T \dot{V}(t)dt \leq -\frac{1}{2}\int_0^T ||e||_Q^2 dt + \frac{1}{2}\rho^2 \int_0^T ||\tilde{d}||^2 dt \Rightarrow$$
$$2V(T) + \int_0^T ||e||_Q^2 dt \leq 2V(0) + \rho^2 \int_0^T ||\tilde{d}||^2 dt \tag{8.99}$$

Moreover, if there exists a positive constant $M_d > 0$ such that

$$\int_0^\infty ||\tilde{d}||^2 dt \leq M_d \tag{8.100}$$

then one gets

$$\int_0^\infty ||e||_Q^2 dt \leq 2V(0) + \rho^2 M_d \tag{8.101}$$

Thus, the integral $\int_0^\infty ||e||_Q^2 dt$ is bounded. Moreover, $V(T)$ is bounded and from the definition of the Lyapunov function V in Eq. (8.84) it becomes clear that $e(t)$ will be also bounded since $e(t) \in \Omega_e = \{e | e^T P e \leq 2V(0) + \rho^2 M_d\}$. According to the above and with the use of Barbalat's Lemma one obtains $lim_{t\to\infty} e(t) = 0$.

8.3.5 Robust State Estimation with the Use of the H-Infinity Kalman Filter

The control loop for the truck and trailer system can be implemented with the feedback of a partially measurable state vector and by processing only a small number of state variables. To reconstruct the missing information about the state vector of the autonomous vehicle it is proposed to use a filtering scheme which allows to apply state estimation-based control [457]. The recursion of the H_∞ Kalman Filter, can be formulated in terms of a *measurement update* and a *time update* part

Measurement update:

$$D(k) = [I - \theta W(k)P^-(k) + C^T(k)R(k)^{-1}C(k)P^-(k)]^{-1}$$
$$K(k) = P^-(k)D(k)C^T(k)R(k)^{-1}$$
$$\hat{x}(k) = \hat{x}^-(k) + K(k)[y(k) - C\hat{x}^-(k)] \tag{8.102}$$

Time update:

$$\hat{x}^{-}(k+1) = A(k)x(k) + B(k)u(k)$$
$$P^{-}(k+1) = A(k)P^{-}(k)D(k)A^{T}(k) + Q(k) \tag{8.103}$$

where it is assumed that parameter θ is sufficiently small to assure that the covariance matrix $P^{-}(k)^{-1} - \theta W(k) + C^{T}(k)R(k)^{-1}C(k)$ will be positive definite. When $\theta = 0$ the H_{∞} Kalman Filter becomes equivalent to the standard Kalman Filter. One can measure only a part of the state vector of the system of the truck and trailer system, such as state variables x_i $i = 1, 2$ (cartesian coordinates of the truck) and can estimate through filtering the rest of the state vector elements.

8.3.6 Simulation Tests

The performance of the proposed nonlinear optimal control scheme for the autonomous truck and trailer vehicle has been tested in the case of tracking of different reference setpoints. The control scheme exhibited fast and accurate tracking of the reference paths. The computation of the feedback control gain required the solution of the algebraic Riccati equation given in Eq. (8.89), at each iteration of the control algorithm. The obtained results are depicted in Figs. 8.16, 8.17 and 8.18. It can be noticed that the H-infinity controller achieved fast and accurate convergence to the reference setpoints for all elements of the vehicle's state-vector. Moreover, the variations of the control inputs, that is of the truck's velocity and of the truck's steering angle were smooth.

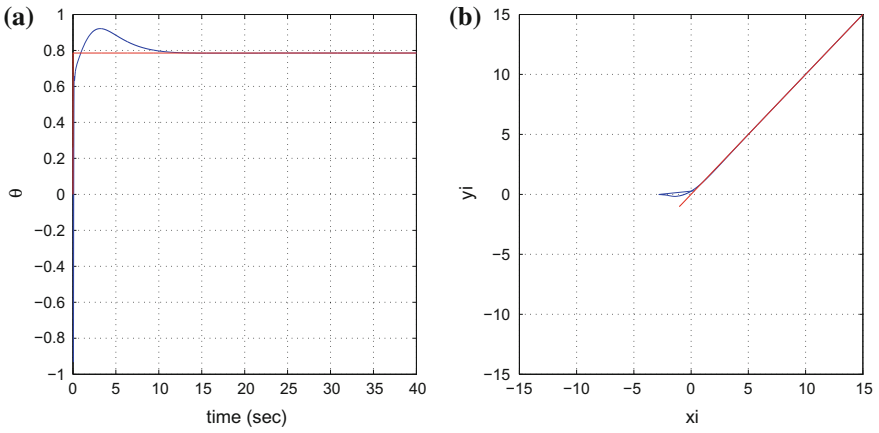

Fig. 8.16 **a** tracking of reference setpoint 1 (red-line) by the heading angle θ of the truck (blue line), **b** tracking of reference path (red line) on the xy-plane by the center of the rear wheel axis of the trailer (blue line)

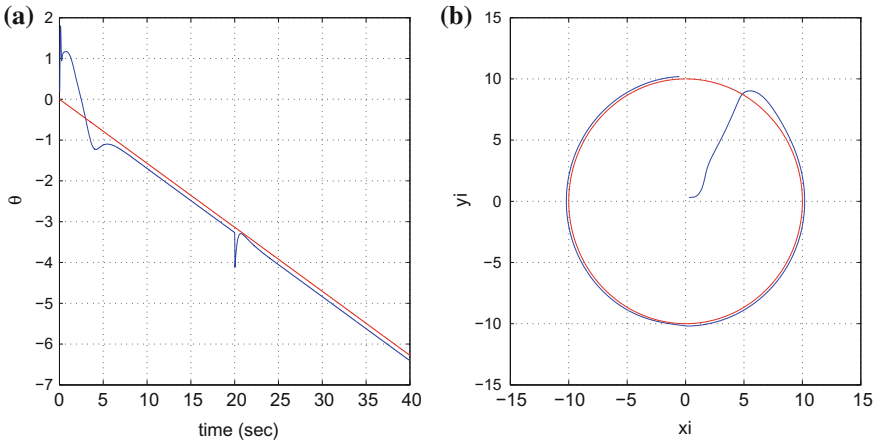

Fig. 8.17 **a** tracking of reference setpoint 2 (red-line) by the heading angle θ of the truck (blue line), **b** tracking of reference path (red line) on the xy-plane by the center of the rear wheel axis of the trailer (blue line)

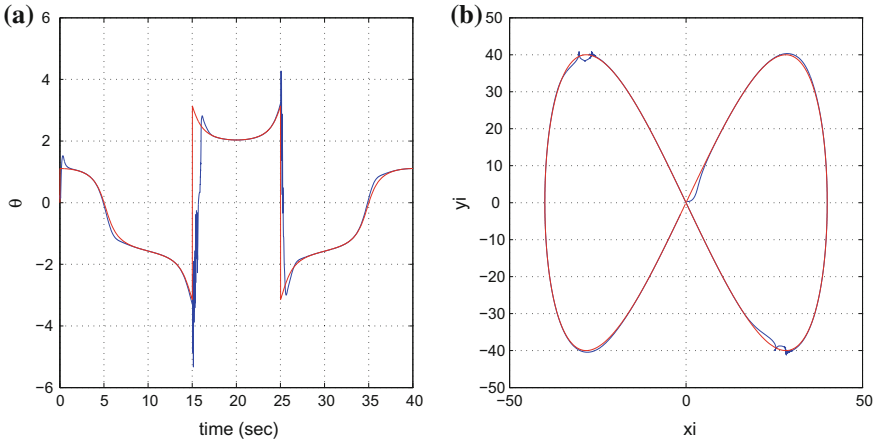

Fig. 8.18 **a** tracking of reference setpoint 3 (red-line) by the heading angle θ of the truck (blue line), **b** tracking of reference path (red line) on the xy-plane by the center of the rear wheel axis of the trailer (blue line)

As noted, the proposed nonlinear optimal control method for the truck and trailer model was based on an approximate linearization of the vehicle's kinematics. Comparing to nonlinear feedback control approaches which are based on exact feedback linearization, the proposed H_∞ control scheme for the autonomous vehicle has the following features: (i) it uses an approximate linear description of the system's kinematics which does not follow the elaborated transformations (diffeomorphisms) met in exact linearization methods, (ii) it is applied directly on the initial nonlinear

model of the vehicle. Thus, the computation of the control inputs which are applied to the vehicle does not require inverse transformations and avoids singularities, (iii) it retains the advantages of typical optimal control, that is accurate tracking of the reference trajectories through moderate variations of the control inputs.

8.4 Nonlinear Optimal Feedback Control of Four-Wheel Steering Autonomous Vehicles

8.4.1 Outline

Four-wheel steering (4WS) autonomous vehicles can exhibit improved maneuverability comparing to two-wheel steering vehicles. There are several examples of applications of 4WS autonomous vehicles in transportation, in security and defense tasks as well as in agriculture [7, 70, 213, 364]. In an aim to improve the steering capabilities of autonomous vehicles and mobile robots there have been several efforts to solve the problem of control of 4WS systems. The description of the kinematics and dynamics of 4WS vehicles typically takes the form of nonlinear models. However under specific assumptions such models can be locally simplified into a linear form and linear control methods can be considered. [67, 195, 381, 478, 586]. One can note also results on nonlinear model-based control for 4WS vehicles [216, 257, 306, 390]. In several approaches it is attempted to decouple the vehicle's multivariable dynamics into simpler loops which are controlled independently [269, 270, 282, 317]. The efficiency of the aforementioned control methods depends on the proximity of the model considered for the controller's design to the real nonlinear dynamics of the vehicle [283, 578, 584].

In the present section, a nonlinear H-infinity (optimal) controller is introduced for the motion control problem of 4WS vehicles [419, 461]. The design of the controller remains consistent with the precise nonlinear dynamics of the four-wheel steering vehicle. As in previous applications of nonlinear optimal control the 4WS vehicle's kinematic and dynamic model undergoes first approximate linearization around a temporary operating point (equilibrium) which is recomputed at each iteration of the control algorithm. The equilibrium is defined by the present value of the system's state vector and the last value of the control inputs vector that was exerted on it. The linearization makes use of first order Taylor series expansion of the state-space description of the vehicle and requires the computation of the associated Jacobian matrices [33, 431, 463]. The modelling error due to truncation of higher order terms in the Taylor series expansion is considered as a perturbation which is asymptotically eliminated by the robustness of the control algorithm. Next, for the approximately linearized model of the 4WS vehicle an H-infinity feedback controller is designed.

The H-infinity controller stands for the solution to the optimal control problem for the 4WS vehicle under model uncertainty and external perturbations. As previously noted, it represents the solution to a min-max differential game in which the controller tries to minimize a cost function that comprises a quadratic term of the state vector's tracking error, whereas the model uncertainty and the external perturbations try to maximize this cost function. To compute the feedback gain of the H-infinity controller an algebraic Riccati equation has to be solved at each time step of the control method [450, 457, 460]. The stability properties of the control scheme are confirmed through Lyapunov analysis. First, it is shown that the control loop satisfies the H-infinity tracking performance criterion, which ascertains elevated robustness against model inconsistencies and external disturbances [305, 564]. Moreover, under moderate conditions the global asymptotic stability of the control scheme is proven. Finally, to implement state estimation-based control for the 4WS vehicle without the need to process measurements from a large number of on-board sensors the H-infinity Kalman Filter is used as a robust state estimator [169, 511].

Comparing to other control methods for the problem of motion control of autonomous vehicles and mobile robots the following can be noted [450, 457, 460]: (i) PID control which is widely used by practitioners in the area of robotics is finally an unreliable methodology because the tuning of such a controller is performed in a heuristic manner around local operating points where the unrealistic assumption is made that the dynamics of the 4WS vehicle remains linear. Such a control method lacks a global stability proof. (ii) On the other side the application of global linearization-based control methods to 4WS vehicles is hindered by the complexity of the associated state-space transformations that finally allow for describing the vehicle's dynamics into a linear canonical form. Besides this method may come against singularity problems because it requires inverse transformations for computing the control signal that will be finally applied to the initial nonlinear system of the 4WS vehicle. (iii) As far as optimal control methods for autonomous vehicles is concerned, the use of model predictive control is unsuccessful because this control method is addressed to linear dynamics and cannot compensate for the nonlinearities of the 4WS vehicle state-space model. On the other side the use of nonlinear model-predictive control for 4WS vehicles can be of questionable performance because its iterative search for an optimum is not of assured convergence and depends on initial parametrization, (iv) Finally, sliding mode control cannot be applied directly to the model of the 4WS vehicles because this is not inherently found into a canonical form. Additionally, the application of backstepping control approaches is hindered by the fact that the state-space description of 4WS vehicles is not found into a triangular form. For the aforementioned reasons, nonlinear optimal (H-infinity) control is one of the most efficient solutions one can have for the control problem of autonomous navigation of 4WS vehicles.

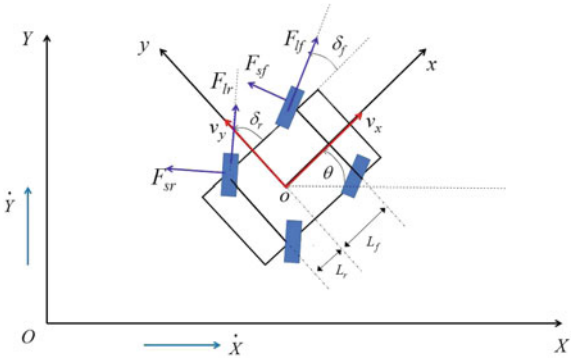

Fig. 8.19 Reference axes for the motion of the 4WS autonomous vehicle: the velocity of the vehicle is decomposed in two components in a body-fixed reference frame xOy. The control inputs for the 4WS vehicle are (i) the longitudinal force F_{lf} and F_{lr} at the wheels of the front and rear axes, provided by the vehicle's engine or actuators, (ii) the turn angle of the front wheels δ_f, (iii) the turn angle of the rear wheels δ_r

8.4.2 Modelling of the Kinematics and Dynamics of the 4WS Autonomous Vehicle

8.4.2.1 Outline of the Model of the 4WS Vehicle

Important parameters and variables in the 4WS vehicle model are: (i) the vehicle's velocity v, which is a vector forming an angle β with the transversal axis of the vehicle. It can be decomposed in two components, a velocity V_x which is aligned with the horizontal axis Ox in a body-fixed reference frame and a velocity V_y which is aligned with the vertical axis Oy in such a body-fixed reference frame (Fig. 8.19), (ii) the vehicle's mass m and its moment of inertia I for rotation around the Oz axis, (iii) the cornering stiffness coefficients c_f and c_r of the front and rear wheels of the vehicle.

The control inputs to the model of the 4WS vehicle are defined as follows: (i) the traction force that is exerted on the vehicle (ii) the turn angle of the front wheels (or the first derivative of this turn angle) (iii) the turn angle of the rear wheels (or the first derivative of this turn angle).

The difference between the turn angle of the vehicle's wheels δ and the angle formed between the vehicle's velocity and the vehicle's transversal axis β, is the side-slip angle of the vehicle and is denoted by $a = \delta - \beta$.

The forces exerted on the 4WS vehicle are defined as follows: (i) the longitudinal force F_l which in turn is defined by the traction force of the vehicle's engine or by the force developed by the vehicle's breaking system, (ii) the side or transversal force F_S which depends on the vehicle's side-slip angle a and on the reaction force F_z developed by the front and rear axle of the vehicle for compensating the vehicle's weight or additional load.

About the X-axis forces, in the body-fixed reference frame for the vehicle one has that [216]:

$$\begin{aligned} F_{xf} &= F_{lf}cos(\delta_f) - F_{sf}sin(\delta_f) \\ F_{xr} &= F_{lr}cos(\delta_f) - F_{sr}sin(\delta_r) \end{aligned} \tag{8.104}$$

Under the assumption of a small turn angle of the vehicle's wheel, that is $cos(\delta_f) \simeq 1$, $sin(\delta_f) \simeq \delta_f$ and $cos(\delta_r) \simeq 1$, $sin(\delta_r) \simeq \delta_r$ one gets [216]:

$$\begin{aligned} F_{xf} &= F_{lf} - F_{sf}\delta_f \\ F_{xr} &= F_{lr} - F_{sr}\delta_r \end{aligned} \tag{8.105}$$

About the Y-axis forces, in the body-fixed reference frame for the vehicle one has that (Fig. 8.20):

$$\begin{aligned} F_{yf} &= F_{sf}cos(\delta_f) + F_{lf}sin(\delta_f) \\ F_{yr} &= F_{sr}cos(\delta_f) + F_{lr}sin(\delta_r) \end{aligned} \tag{8.106}$$

Again, under the assumption of a small turn angle of the vehicle's wheel, that is $cos(\delta_f) \simeq 1$, $sin(\delta_f) \simeq \delta_f$ and $cos(\delta_r) \simeq 1$, $sin(\delta_r) \simeq \delta_f$ one gets:

$$\begin{aligned} F_{yf} &= F_{sf} + F_{lf}\delta_f \\ F_{yr} &= F_{sr} + F_{lr}\delta_r \end{aligned} \tag{8.107}$$

Next, by considering that the vehicle's motion is expressed in a body-fixed frame and that Coriolis effects have to be taken into account, the equations of motion of the 4WS vehicle become

$$m(\dot{v}_x - rv_y) = F_{lf} + F_{lr} - F_{sf}\delta_f - F_{sr}\delta_r - c_a v_x^2 \tag{8.108}$$

$$m(\dot{v}_y + rv_x) = F_{lf}\delta_f + F_{lr}\delta_r + F_{sf} + F_{sr}\delta_r \tag{8.109}$$

$$I\dot{r} = l_f(F_{lf}\delta_f + F_{sf}) - l_r(F_{lr}\delta_r + F_{sr}) \tag{8.110}$$

8.4.2.2 Kinematic and Dynamic Model of the 4WS Vehicle

The dynamic model of the 4WS vehicle was shown to be given by Eqs. (8.108), (8.109) and (8.110). In this model F_{lf} and F_{lr} are the traction forces generated by the engine of the vehicle or by electric actuators and exerted on the wheels of the front rear axles respectively. The control inputs of the vehicle are (i) the traction forces u_1, given by F_{lf} and F_{Lr} (ii) the angle of the wheels of the front axle, that is $\delta_f = u_2$, (iii) the angle of the wheels of the rear axle, that is $\delta_r = u_3$.

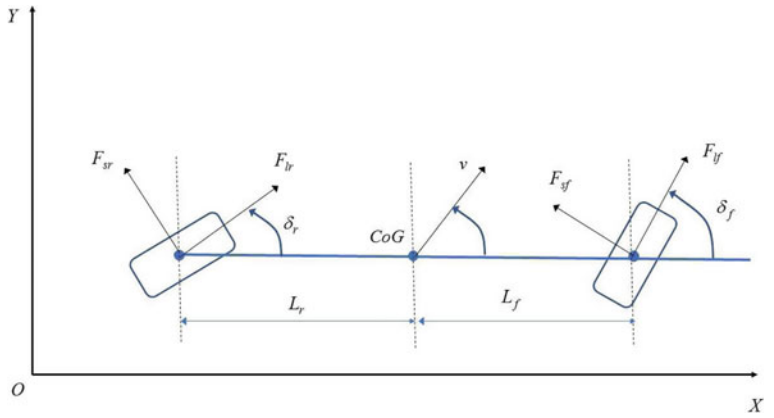

Fig. 8.20 Diagram of the 4 WS vehicle

About the side forces exerted on the front wheels of the vehicle one has

$$F_{s_f} = \frac{m}{l}(gl_r - \dot{v}_x h)c_f a_f \Rightarrow F_{s_f} = \frac{mgl_r}{l}c_f a_f - \frac{m\dot{v}_x h}{l}c_f a_f \tag{8.111}$$

and by considering that $\dot{v}_x << g$ and $h << l$ (h is the height of the center of gravity of the vehicle) one has that the term $\frac{m\dot{v}_x h}{l}c_f a_f$ can be considered as moderate disturbance which can be omitted. Thus, the model of the side force being exerted on the front wheels is given by

$$F_{s_f} = \frac{m}{l}(gl_r - \dot{v}_x h)c_f a_f \Rightarrow F_{s_f} = \frac{mgl_r}{l}c_f a_f \tag{8.112}$$

or equivalently

$$F_{s_f} = \frac{m}{l}(gl_r)c_f\left(u_2 - \frac{v_y + l_f r}{v_x}\right) \tag{8.113}$$

where it has been used that $a_f = \delta_f - \beta_f$ and $\beta_f = \frac{v_y + l_f r}{v_x}$

About the side forces exerted on the rear wheels of the vehicle one has

$$F_{s_r} = \frac{m}{l}(gl_f - \dot{v}_x h)c_r a_r \Rightarrow F_{s_r} = \frac{mgl_f}{l}c_r a_r - \frac{m\dot{v}_x h}{l}c_r a_r \tag{8.114}$$

and by considering that $\dot{v}_x << g$ and $h << l$ one has that the term $\frac{m\dot{v}_x h}{l}c_r a_r$ can be considered as moderate disturbance which can be omitted. Thus, the model of the force being exerted on the front wheels is given by

$$F_{s_r} = \frac{m}{l}(gl_f)c_r a_r \Rightarrow F_{s_r} = \frac{mgl_r}{l}c_r a_r, \tag{8.115}$$

or equivalently

$$F_{s_r} = \frac{m}{l}(gl_f)c_r\left(u_3 - \frac{v_y - l_r r}{v_x}\right) \tag{8.116}$$

where it has been used that $a_r = \delta_r - \beta_r$ and $\beta_r = \frac{v_y - l_r r}{v_x}$.

Consequently, the side forces exerted on the wheels of the vehicle are given by [216]

$$\begin{aligned} F_{s_f} &= \frac{m}{l}(gl_r)c_f\left(u_2 - \frac{v_y + l_r r}{v_x}\right) \\ F_{s_r} &= \frac{m}{l}(gl_f)c_r\left(u_3 - \frac{v_y - l_r r}{v_x}\right) \end{aligned} \tag{8.117}$$

Using Eq. (8.117) in (8.108)–(8.110) one obtains the following equations for the dynamic model of the 4WS autonomous vehicle:

$$\begin{aligned} m\dot{v}_x = mrv_y + u_1 + u_1 - \frac{m}{l}(gl_r)c_f\left(u_2 - \frac{v_y + l_r r}{v_x}\right)u_2 - \\ -\frac{m}{l}(gl_f)c_r\left(u_3 - \frac{v_y - l_r r}{v_x}\right)u_3 - c_a v_x^2 \end{aligned} \tag{8.118}$$

$$\begin{aligned} m\dot{v}_y = -mrv_x + u_1u_2 + u_1u_3 + \frac{m}{l}(gl_r)c_f\left(u_2 - \frac{v_y + l_r r}{v_x}\right) + \\ +\frac{m}{l}(gl_f)c_r\left(u_3 - \frac{v_y - l_r r}{v_x}\right) \end{aligned} \tag{8.119}$$

$$\begin{aligned} I\dot{r} \ = l_f\left[(u_1u_2) + \frac{m}{l}(gl_r)c_f\left(u_2 - \frac{v_y + l_r r}{v_x}\right)\right] - \\ - l_r\left[(u_1u_3) + \frac{m}{l}(gl_f)c_r\left(u_3 - \frac{v_y - l_r r}{v_x}\right)\right] \end{aligned} \tag{8.120}$$

Moreover, taking that (x, y) are the cartesian coordinates and θ is the orientation angle of the vehicle, then the following equations about the 4WS vehicle kinematics are considered:

$$\dot{x} = v_x cos(\theta) - v_y sin(\theta) \tag{8.121}$$

$$\dot{y} = v_x sin(\theta) + v_y cos(\theta) \tag{8.122}$$

$$\dot{\theta} = r \tag{8.123}$$

After a re-arrangement of Eqs. (8.121)–(8.123) and (8.118)–(8.120), the state-space description of the 4WS is given as follows:

$$\dot{x} = v_x cos(\theta) - v_y sin(\theta) \tag{8.124}$$

$$\dot{y} = v_x sin(\theta) + v_y cos(\theta) \tag{8.125}$$

$$\dot{v}_x = r v_y + \frac{2}{m} u_1 - \frac{1}{l}(g l_r) c_f \left(u_2 - \frac{v_y + l_r r}{v_x} \right) u_2 - \\ - \frac{1}{l}(g l_f) c_r \left(u_3 - \frac{v_y - l_r r}{v_x} \right) u_3 - \frac{c_a}{m} v_x^2 \tag{8.126}$$

$$\dot{v}_y = -r v_x + \frac{1}{m} u_1 u_2 + \frac{1}{m} u_1 u_3 + \frac{1}{l}(g l_r) c_f \left(u_2 - \frac{v_y + l_r r}{v_x} \right) + \\ + \frac{1}{l}(g l_f) c_r \left(u_3 - \frac{v_y - l_r r}{v_x} \right) \tag{8.127}$$

$$\dot{\theta} = r \tag{8.128}$$

$$\dot{r} = \frac{l_f}{I} \left[(u_1 u_2) + \frac{m}{Il}(g l_r) c_f \left(u_2 - \frac{v_y + l_r r}{v_x} \right) \right] - \\ - \frac{l_r}{I} \left[(u_1 u_3) + \frac{m}{Il}(g l_f) c_r \left(u_3 - \frac{v_y - l_r r}{v_x} \right) \right] \tag{8.129}$$

By defining the system's state vector as $X = [x, y, v_x, v_y, \theta, r]^T$ one obtains the following state-space description for the 4WS vehicle

$$\dot{x}_1 = x_3 cos(x_5) - x_4 sin(x_5) \tag{8.130}$$

$$\dot{x}_2 = x_3 sin(x_5) + x_4 cos(x_5) \tag{8.131}$$

$$\dot{x}_3 = x_4 x_6 + \frac{2}{m} u_1 - \frac{1}{l}(g l_r) c_f \left(u_2 - \frac{x_4 + l_r x_6}{x_3} \right) u_2 - \\ - \frac{1}{l}(g l_f) c_r \left(u_3 - \frac{x_4 - l_r x_6}{x_3} \right) u_3 - \frac{c_a}{m} x_3^2 \tag{8.132}$$

$$\dot{x}_4 = -x_3 x_6 + \frac{1}{m} u_1 u_2 + \frac{1}{m} u_1 u_3 + \frac{1}{l}(g l_r) c_f \left(u_2 - \frac{x_4 + l_r x_6}{x_3} \right) + \\ + \frac{1}{l}(g l_f) c_r \left(u_3 - \frac{x_4 - l_r x_6}{x_3} \right) \tag{8.133}$$

$$\dot{x_5} = x_6 \tag{8.134}$$

$$\dot{x}_6 = \frac{l_f}{I}\left[(u_1u_2) + \frac{m}{Il}(gl_r)c_f\left(u_2 - \frac{x_4 + l_r x_6}{x_3}\right)\right] - \\ -\frac{l_r}{I}\left[(u_1u_3) + \frac{m}{Il}(gl_f)c_r\left(u_3 - \frac{x_4 - l_r x_6}{x_3}\right)\right] \tag{8.135}$$

Thus, the joint kinematic-dynamic model of the 4WS vehicle is written in the form

$$\dot{x} = f(x, u) \tag{8.136}$$

where $x \in R^{6\times 1}$, $u \in R^{3\times 1}$, and $f \in R^{6\times 1}$.

8.4.3 Approximate Linearization of the Model of the 4WS Vehicle

8.4.3.1 1st Modelling and Linearization Approach

First, linearization of the complete kinematic-dynamic model of the 4WS vehicle is considered. The complete model has been given in Eqs. (8.130)–(8.135). The approximately linearized model of the vehicle is computed around the temporary operating point (equilibrium) (x^*, u^*), where x^* is the present value of the system's state vector and u^* is the last value of the control input vector exerted on the 4WS vehicle. The linearized model is written as

$$\dot{x} = Ax + Bu + \tilde{d} \tag{8.137}$$

where

$$A = \begin{pmatrix} \frac{\partial f_1}{\partial x_1} & \frac{\partial f_1}{\partial x_2} & \cdots & \frac{\partial f_1}{\partial x_6} \\ \frac{\partial f_2}{\partial x_1} & \frac{\partial f_2}{\partial x_2} & \cdots & \frac{\partial f_2}{\partial x_6} \\ \cdots & \cdots & \cdots & \cdots \\ \frac{\partial f_6}{\partial x_1} & \frac{\partial f_6}{\partial x_2} & \cdots & \frac{\partial f_6}{\partial x_6} \end{pmatrix} |_{(x^*,u^*)} \; B = \begin{pmatrix} \frac{\partial f_1}{\partial u_1} & \frac{\partial f_1}{\partial u_2} & \frac{\partial f_1}{\partial u_3} \\ \frac{\partial f_2}{\partial u_1} & \frac{\partial f_2}{\partial u_2} & \frac{\partial f_2}{\partial u_3} \\ \cdots & \cdots & \cdots \\ \frac{\partial f_6}{\partial u_1} & \frac{\partial f_6}{\partial u_2} & \frac{\partial f_6}{\partial u_3} \end{pmatrix} |_{(x^*,u^*)} \tag{8.138}$$

The computation of the Jacobian matrix $A = \nabla_x f(x, u)\,|_{(x^*,u^*)}$ proceeds as follows: For the first row of the Jacobian matrix $A = \nabla_x f(x, u)$ one has: $\frac{\partial f_1}{\partial x_1} = 0$, $\frac{\partial f_1}{\partial x_2} = 0$, $\frac{\partial f_1}{\partial x_3} = cos(x_5)$, $\frac{\partial f_1}{\partial x_4} = -sin(x_5)$, $\frac{\partial f_1}{\partial x_5} = -x_3 sin(x_5) + x_4 cos(x_5)$, $\frac{\partial f_1}{\partial x_6} = 0$.

For the second row of the Jacobian matrix $A = \nabla_x f(x, u)$ one has: $\frac{\partial f_2}{\partial x_1} = 0$, $\frac{\partial f_2}{\partial x_2} = 0$, $\frac{\partial f_2}{\partial x_3} = sin(x_5)$, $\frac{\partial f_2}{\partial x_4} = cos(x_5)$, $\frac{\partial f_2}{\partial x_5} = x_3 cos(x_5) - x_5 sin(x_5)$, $\frac{\partial f_2}{\partial x_6} = 0$,

For the third row of the Jacobian matrix $A = \nabla_x f(x, u)$ one has: $\frac{\partial f_3}{\partial x_1} = 0$, $\frac{\partial f_3}{\partial x_2} = 0$, $\frac{\partial f_3}{\partial x_3} = \frac{gl_r c_f}{l}(-\frac{x_4 + l_f x_6}{x_3^2})u_2 - \frac{gl_f c_r}{l}(-\frac{x_4 - l_r x_6}{x_3^2})u_3 - \frac{c_a}{m}2x_3$, $\frac{\partial f_3}{\partial x_4} = x_6 + \frac{gl_r c_f}{l}\frac{1}{x_3}u_2$, $\frac{\partial f_3}{\partial x_5} = 0$, $\frac{\partial f_3}{\partial x_6} = x_4 + \frac{gl_r c_f}{l}\frac{l_f}{x_3}u_2 - \frac{gl_f c_r}{l}\frac{l_f}{x_3}u_3$

For the fourth row of the Jacobian matrix $A = \nabla_x f(x,u)$ one has: $\frac{\partial f_4}{\partial x_1} = 0$, $\frac{\partial f_4}{\partial x_2} = 0$, $\frac{\partial f_4}{\partial x_3} = -x_6 + \frac{gl_r c_f}{l}\frac{x_4 + l_f x_6}{x_3^2} + \frac{gl_f c_r}{l}\frac{x_4 - l_r x_6}{x_3^2}$, $\frac{\partial f_4}{\partial x_4} = \frac{gl_r c_f}{l} - \frac{1}{x_3}u_2 + \frac{gl_f c_r}{l} - \frac{1}{x_3}u_3$, $\frac{\partial f_4}{\partial x_5} = 0$, $\frac{\partial f_4}{\partial x_6} = -x_3 + \frac{gl_r c_f}{l}(-\frac{l_f}{x_3}) + \frac{gl_f c_r}{l}(\frac{l_r}{x_3})$.

For the fifth row of the Jacobian matrix $A = \nabla_x f(x,u)$ one has: $\frac{\partial f_5}{\partial x_1} = 0$, $\frac{\partial f_5}{\partial x_2} = 0$, $\frac{\partial f_5}{\partial x_3} = 0$, $\frac{\partial f_5}{\partial x_4} = 0$, $\frac{\partial f_5}{\partial x_5} = 0$, $\frac{\partial f_5}{\partial x_6} = 1$.

For the sixth row of the Jacobian matrix $A = \nabla_x f(x,u)$ one has: $\frac{\partial f_6}{\partial x_1} = 0$, $\frac{\partial f_6}{\partial x_2} = 0$, $\frac{\partial f_6}{\partial x_3} = \frac{l_f mgl_r}{Il} c_f \frac{x_4 + l_f x_6}{x_3^2} - \frac{l_r mgl_f}{Il} c_r \frac{x_4 - l_r x_6}{x_3^2}$, $\frac{\partial f_6}{\partial x_4} = \frac{l_f mgl_r}{Il} c_f(-\frac{1}{x_3}) - \frac{l_r mgl_f}{Il} c_r(\frac{1}{x_3})$, $\frac{\partial f_6}{\partial x_5} = 0$, $\frac{\partial f_6}{\partial x_6} = \frac{l_f mgl_r}{Il} c_f(-\frac{l_f}{x_3}) - \frac{l_r mgl_f}{Il} c_r(-\frac{l_r}{x_3})$.

The computation of the Jacobian matrix $B = \nabla_u f(x,u)\,|_{(x^*,u^*)}$ proceeds as follows:
For the first row of the Jacobian matrix $B = \nabla_u f(x,u)$ one has: $\frac{\partial f_1}{\partial u_1} = 0$, $\frac{\partial f_1}{\partial u_2} = 0$, $\frac{\partial f_1}{\partial u_3} = 0$

For the second row of the Jacobian matrix $B = \nabla_u f(x,u)$ one has: $\frac{\partial f_2}{\partial u_1} = 0$, $\frac{\partial f_2}{\partial u_2} = 0$, $\frac{\partial f_2}{\partial u_3} = 0$

For the third row of the Jacobian matrix $B = \nabla_u f(x,u)$ one has: $\frac{\partial f_3}{\partial u_1} = \frac{2}{m}$, $\frac{\partial f_3}{\partial u_2} = -\frac{gl_r c_f}{l}(2u_2 - \frac{x_4 + l_f x_6}{x_3})$, $\frac{\partial f_3}{\partial u_3} = -\frac{gl_f c_f}{l}(2u_3 - \frac{x_4 - l_r x_6}{x_3})$.

For the fourth row of the Jacobian matrix $B = \nabla_u f(x,u)$ one has: $\frac{\partial f_4}{\partial u_1} = \frac{1}{m}u_2 + \frac{1}{m}u_3$, $\frac{\partial f_4}{\partial u_2} = \frac{1}{m}u_1 + \frac{gl_r c_f}{l}$, $\frac{\partial f_4}{\partial u_3} = \frac{1}{m}u_1 + \frac{gl_f c_r}{l}$.

For the fifth row of the Jacobian matrix $B = \nabla_u f(x,u)$ one has: $\frac{\partial f_5}{\partial u_1} = 0$, $\frac{\partial f_5}{\partial u_2} = 0$, $\frac{\partial f_5}{\partial u_3} = 0$.

For the sixth row of the Jacobian matrix $B = \nabla_u f(x,u)$ one has: $\frac{\partial f_6}{\partial u_1} = \frac{l_f}{I}u_2 - \frac{l_r}{I}u_3$, $\frac{\partial f_6}{\partial u_2} = \frac{l_f mgl_r}{Il} c_f + \frac{l_f}{I}u_1$, $\frac{\partial f_6}{\partial u_3} = -\frac{l_r mgl_f}{Il} c_r - \frac{l_r}{I}u_1$

8.4.3.2 2nd Modelling and Linearization Approach

Next, linearization of a simplified kinematic-dynamic model of the 4WS vehicle is considered. This model is obtained from the complete model given in Eqs. (8.130)–(8.135), after omitting terms comprising squares of the control inputs that is u_i^2, or products between the control inputs, such as $u_i u_j$. Under such an approach the kinematic-dynamic model of the 4WS vehicle becomes:

$$\dot{x}_1 = x_3 cos(x_5) - x_4 sin(x_5) \tag{8.139}$$

$$\dot{x}_2 = x_3 sin(x_5) + x_4 cos(x_5) \tag{8.140}$$

$$\dot{x}_3 = x_4 x_6 + \frac{2}{m} u_1 + \frac{1}{l}(gl_r)c_f \left(\frac{x_4 + l_r x_6}{x_3}\right) u_2 - \\ + \frac{1}{l}(gl_f)c_r \left(\frac{x_4 - l_r x_6}{x_3}\right) u_3 - \frac{c_a}{m} x_3^2 \tag{8.141}$$

$$\dot{x}_4 = -x_3 x_6 + \frac{1}{l}(gl_r)c_f \left(u_2 - \frac{x_4 + l_r x_6}{x_3}\right) + \\ + \frac{1}{l}(gl_f)c_r \left(u_3 - \frac{x_4 - l_r x_6}{x_3}\right) \tag{8.142}$$

$$\dot{x}_5 = x_6 \tag{8.143}$$

$$\dot{x}_6 = \frac{l_f}{I}\left[\frac{m}{Il}(gl_r)c_f \left(u_2 - \frac{x_4 + l_r x_6}{x_3}\right)\right] - \\ - \frac{l_r}{I}\left[\frac{m}{Il}(gl_f)c_r \left(u_3 - \frac{x_4 - l_r x_6}{x_3}\right)\right] \tag{8.144}$$

Then, the state-space model of the 4WS autonomous vehicle can be written as:

$$\begin{pmatrix} \dot{x}_1 \\ \dot{x}_2 \\ \dot{x}_3 \\ \dot{x}_4 \\ \dot{x}_5 \\ \dot{x}_6 \end{pmatrix} = \begin{pmatrix} x_3 cos(x_5) - x_4 sin(x_5) \\ x_3 sin(x_5) + x_4 cos(x_5) \\ x_4 x_6 - \frac{c_a}{m} x_3^2 \\ -x_3 x_6 - \frac{1}{l}(gl_r)c_f \left(\frac{x_4 + l_r x_6}{x_3}\right) - \frac{1}{l}(gl_f)c_r \left(\frac{x_4 - l_r x_6}{x_3}\right) \\ x_6 \\ \frac{l_f}{I}\left[\frac{m}{Il}(gl_r)c_f \left(-\frac{x_4 + l_r x_6}{x_3}\right)\right] - \frac{l_r}{I}\left[\frac{m}{Il}(gl_f)c_r \left(-\frac{x_4 - l_r x_6}{x_3}\right)\right] \end{pmatrix} + \\ + \begin{pmatrix} 0 & 0 & 0 \\ 0 & 0 & 0 \\ \frac{2}{m} & \frac{1}{l}(gl_r)c_f \left(\frac{x_4 + l_r x_6}{x_3}\right) & \frac{1}{l}(gl_f)c_r \left(\frac{x_4 - l_r x_6}{x_3}\right) \\ 0 & \frac{1}{l}(gl_r)c_f & \frac{1}{l}(gl_f)c_r \\ 0 & 0 & 0 \\ 0 & \frac{l_f}{I}\frac{m}{Il}(gl_r)c_f & -\frac{l_r}{I}\frac{m}{Il}(gl_f)c_r \end{pmatrix} \begin{pmatrix} u_1 \\ u_2 \\ u_3 \end{pmatrix} \tag{8.145}$$

Thus, the state-space model of the 4WS autonomous vehicle is written in the affine-in-the-input form:

$$\dot{x} = f(x) + g(x)u \tag{8.146}$$

with $x \in R^{6\times 1}$, $f(x) \in R^{6\times 1}$, $g(x) \in R^{6\times 3}$ and $u \in R^{6\times 3}$. For the state-space model of Eq. (8.146) linearization is performed around the temporary operating point (equi-

librium) (x^*, u^*). This operating point which is updated at each iteration of the control method, consists of the present value of the 4WS vehicle state vector x^* and of the last value of the control inputs vector u^* that was exerted on it. By denoting the gain matrix $g(x) = [g_1(x), g_2(x), g_3(x)]$ the approximate linearization procedure gives

$$\dot{x} = Ax + Bu + \tilde{d} \tag{8.147}$$

where matrices A, B are associated with the system's Jacobians, as shown next:

$$A = \nabla_x f(x) \mid_{(x^*,u^*)} + \nabla_x g_2(x) u_2 \mid_{(x^*,u^*)} + \nabla_x g_3(x) u_3 \mid_{(x^*,u^*)} \tag{8.148}$$

$$B = \nabla_u [f(x) + g(x)u] \mid_{(x^*,u^*)} \Rightarrow B = g(x) \mid_{(x^*,u^*)} \tag{8.149}$$

The elements of the Jacobian matrix $\nabla_x f(x) \mid_{(x^*,u^*)}$ are computed as follows:
For the first row of the Jacobian matrix $\nabla_x f(x, u)$ one has: $\frac{\partial f_1}{\partial x_1} = 0$, $\frac{\partial f_1}{\partial x_2} = 0$, $\frac{\partial f_1}{\partial x_3} = cos(x_5)$, $\frac{\partial f_1}{\partial x_4} = -sin(x_5)$, $\frac{\partial f_1}{\partial x_5} = -x_3 sin(x_5) + x_4 cos(x_5)$, $\frac{\partial f_1}{\partial x_6} = 0$.

For the second row of the Jacobian matrix $\nabla_x f(x, u)$ one has: $\frac{\partial f_2}{\partial x_1} = 0$, $\frac{\partial f_2}{\partial x_2} = 0$, $\frac{\partial f_2}{\partial x_3} = sin(x_5)$, $\frac{\partial f_2}{\partial x_4} = cos(x_5)$, $\frac{\partial f_2}{\partial x_5} = x_3 cos(x_5) - x_5 sin(x_5)$, $\frac{\partial f_2}{\partial x_6} = 0$,

For the third row of the Jacobian matrix $\nabla_x f(x)$ one has: $\frac{\partial f_3}{\partial x_1} = 0$, $\frac{\partial f_3}{\partial x_2} = 0$, $\frac{\partial f_3}{\partial x_3} = -2c_a x_3$, $\frac{\partial f_3}{\partial x_4} = x_6$, $\frac{\partial f_3}{\partial x_5} = 0$, $\frac{\partial f_3}{\partial x_6} = x_4$

For the fourth row of the Jacobian matrix $\nabla_x f(x)$ one has: $\frac{\partial f_4}{\partial x_1} = 0$, $\frac{\partial f_4}{\partial x_2} = 0$, $\frac{\partial f_4}{\partial x_3} = -x_4 + \frac{gl_r c_f}{l} \frac{x_4 + l_f x_6}{x_3^2} + \frac{gl_f c_r}{l} \frac{x_4 - l_r x_6}{x_3^2}$, $\frac{\partial f_4}{\partial x_4} = -\frac{gl_r c_f}{l} \frac{1}{x_3} - \frac{gl_f c_r}{l} \frac{1}{x_3}$, $\frac{\partial f_4}{\partial x_5} = 0$, $\frac{\partial f_4}{\partial x_6} = -\frac{gl_r c_f}{l} \frac{l_f}{x_3} + \frac{gl_f c_r}{l} \frac{l_r}{x_3}$.

For the fifth row of the Jacobian matrix $\nabla_x f(x)$ one has: $\frac{\partial f_5}{\partial x_1} = 0$, $\frac{\partial f_5}{\partial x_2} = 0$, $\frac{\partial f_5}{\partial x_3} = 0$, $\frac{\partial f_5}{\partial x_4} = 0$, $\frac{\partial f_5}{\partial x_5} = 0$, $\frac{\partial f_5}{\partial x_6} = 0$.

For the sixth row of the Jacobian matrix $\nabla_x f(x)$ one has: $\frac{\partial f_6}{\partial x_1} = 0$, $\frac{\partial f_6}{\partial x_2} = 0$, $\frac{\partial f_6}{\partial x_3} = \frac{l_f mgl_r}{Il} c_f \frac{x_4 + l_f x_6}{x_3^2} - \frac{l_r mgl_f}{Il} c_r \frac{x_4 - l_r x_6}{x_3^2}$, $\frac{\partial f_6}{\partial x_4} = \frac{l_f mgl_r}{Il} c_f \frac{1}{x_3} + \frac{l_r mgl_f}{Il} c_r \frac{1}{x_3}$, $\frac{\partial f_6}{\partial x_5} = 0$, $\frac{\partial f_6}{\partial x_6} = -\frac{l_f mgl_r}{Il} c_f \frac{l_f}{x_3} - \frac{l_r mgl_f}{Il} c_r \frac{l_r}{x_3}$.

The elements of the Jacobian matrix $\nabla_x g_2(x) \mid_{(x^*,u^*)}$ are computed as follows:

$$\nabla_x g_2(x) \mid_{(x^*,u^*)} = \begin{pmatrix} 0 & 0 & 0 & 0 & 0 & 0 \\ 0 & 0 & 0 & 0 & 0 & 0 \\ 0 & 0 & -\frac{gl_r c_f}{l} \frac{x_4 + l_f x_6}{x_3^2} & \frac{gl_r c_f}{l} \frac{1}{x_3} & 0 & \frac{gl_r c_f}{l} \frac{l_f}{x_3} \\ 0 & 0 & 0 & 0 & 0 & 0 \\ 0 & 0 & 0 & 0 & 0 & 0 \\ 0 & 0 & 0 & 0 & 0 & 0 \end{pmatrix} \tag{8.150}$$

The elements of the Jacobian matrix $\nabla_x g_3(x)\mid_{(x^*,u^*)}$ are computed as follows:

$$\nabla_x g_3(x)\mid_{(x^*,u^*)}=\begin{pmatrix} 0\ 0 & 0 & 0 & 0 & 0 \\ 0\ 0 & 0 & 0 & 0 & 0 \\ 0\ 0 & -\frac{gl_fc_r}{l}\frac{x_4-l_rx_6}{x_3^2} & \frac{gl_fc_r}{l}\frac{1}{x_3} & 0 & \frac{gl_fc_r}{l}-\frac{l_r}{x_3} \\ 0\ 0 & 0 & 0 & 0 & 0 \\ 0\ 0 & 0 & 0 & 0 & 0 \\ 0\ 0 & 0 & 0 & 0 & 0 \end{pmatrix} \tag{8.151}$$

8.4.4 The Nonlinear H-Infinity Control

8.4.4.1 Tracking Error Dynamics for the 4WS Vehicle

The initial nonlinear model of the 4WS automatic ground vehicle is in the form

$$\dot{x} = f(x,u)\ \ x\in R^n,\ u\in R^m \tag{8.152}$$

Linearization of the model of the 4WS ground vehicle is performed at each iteration of the control algorithm round its present operating point $(x^*, u^*) = (x(t), u(t - T_s))$. The linearized equivalent model of the 4WS vehicle is described by

$$\dot{x} = Ax + Bu + L\tilde{d}\ \ x\in R^n,\ u\in R^m,\ \tilde{d}\in R^q \tag{8.153}$$

Thus, after linearization round its current operating point, the 4WS autonomous ground vehicle's kinematic-dynamic model is written as

$$\dot{x} = Ax + Bu + d_1 \tag{8.154}$$

Parameter d_1 stands for the linearization error in the 4WS vehicle's dynamic model appearing in Eq. (8.154). The reference setpoints for the 4WS ground vehicle are denoted by $\mathbf{x_d} = [x_1^d, \cdots, , x_6^d]$. Tracking of this trajectory is achieved after applying the control input u^*. At every time instant the control input u^* is assumed to differ from the control input u appearing in Eq. (8.154) by an amount equal to Δu, that is $u^* = u + \Delta u$

$$\dot{x}_d = Ax_d + Bu^* + d_2 \tag{8.155}$$

The joint kinematics and dynamics of the controlled 4WS vehicle described in Eq. (8.154) can be also written as

$$\dot{x} = Ax + Bu + Bu^* - Bu^* + d_1 \tag{8.156}$$

and by denoting $d_3 = -Bu^* + d_1$ as an aggregate disturbance term one obtains

$$\dot{x} = Ax + Bu + Bu^* + d_3 \tag{8.157}$$

By subtracting Eq. (8.155) from (8.157) one has

$$\dot{x} - \dot{x}_d = A(x - x_d) + Bu + d_3 - d_2 \tag{8.158}$$

By denoting the tracking error as $e = x - x_d$ and the aggregate disturbance term as $\tilde{d} = d_3 - d_2$, the tracking error dynamics becomes

$$\dot{e} = Ae + Bu + \tilde{d} \tag{8.159}$$

The above linearized form of the 4WS vehicle's model can be efficiently controlled after applying an H-infinity feedback control scheme.

8.4.4.2 Min-Max Control and Disturbance Rejection

The initial nonlinear model of the 4WS autonomous ground vehicle is in the form

$$\dot{x} = f(x, u) \;\; x \in R^n, \; u \in R^m \tag{8.160}$$

Linearization of the joint kinematic and dynamic model of the 4WS ground vehicle is performed at each iteration of the control algorithm round its present operating point $(x^*, u^*) = (x(t), u(t - T_s))$. The linearized equivalent of the system is described by

$$\dot{x} = Ax + Bu + L\tilde{d} \;\; x \in R^n, \; u \in R^m, \; \tilde{d} \in R^q \tag{8.161}$$

where matrices A and B are obtained from the computation of the 4WS vehicle's Jacobians, according to Eq. (8.138), and vector $\tilde{d}$ denotes disturbance terms due to linearization errors. The problem of disturbance rejection for the linearized model that is described by

$$\begin{aligned} \dot{x} &= Ax + Bu + L\tilde{d} \\ y &= Cx \end{aligned} \tag{8.162}$$

where $x \in R^n$, $u \in R^m$, $\tilde{d} \in R^q$ and $y \in R^p$, cannot be handled efficiently if the classical LQR control scheme is applied. This is because of the existence of the perturbation term $\tilde{d}$. The disturbance term $\tilde{d}$ apart from modeling (parametric) uncertainty and external perturbation terms can also represent noise terms of any distribution.

As pointed out in previous applications of the H_∞ control approach, a feedback control scheme is designed for trajectory tracking by the 4WS vehicle's state vector and simultaneous disturbance rejection, considering that the disturbance affects the system in the worst possible manner. The disturbances' effect are incorporated in the following quadratic cost function:

$$J(t) = \frac{1}{2}\int_0^T [y^T(t)y(t) + ru^T(t)u(t) - \rho^2 \tilde{d}^T(t)\tilde{d}(t)]dt, \quad r, \rho > 0 \tag{8.163}$$

The significance of the negative sign in the cost function's term that is associated with the perturbation variable $\tilde{d}(t)$ is that the disturbance tries to maximize the cost function $J(t)$ while the control signal $u(t)$ tries to minimize it. The physical meaning of the relation given above is that the control signal and the disturbances compete to each other within a min-max differential game. This problem of min-max optimization can be written as

$$min_u max_{\tilde{d}} J(u, \tilde{d}) \tag{8.164}$$

As in previously examined ground vehicles, the objective of the optimization procedure for the 4WS vehicle is to compute a control signal $u(t)$ which can compensate for the worst possible disturbance, that is externally imposed to the system of the 4WS autonomous vehicle. However, the solution to the min-max optimization problem is directly related to the value of the parameter ρ. This means that there is an upper bound in the disturbances magnitude that can be annihilated by the control signal.

8.4.4.3 H-Infinity Feedback Control

Following previous applications of the H-infinity control, for the linearized system given by Eq. (8.162) the cost function of Eq. (8.163) is defined, where the coefficient r determines the penalization of the control input and the weight coefficient ρ determines the reward of the disturbances' effects. It is assumed that (i) The energy that is transferred from the disturbances signal $\tilde{d}(t)$ is bounded, that is $\int_0^\infty \tilde{d}^T(t)\tilde{d}(t)dt < \infty$, (ii) the matrices $[A, B]$ and $[A, L]$ are stabilizable, (iii) the matrix $[A, C]$ is detectable. Then, the optimal feedback control law is given by

$$u(t) = -Kx(t) \tag{8.165}$$

with

$$K = \frac{1}{r}B^T P \tag{8.166}$$

where P is a positive semi-definite symmetric matrix which is obtained from the solution of the Riccati equation

$$A^T P + PA + Q - P\left(\frac{1}{r}BB^T - \frac{1}{2\rho^2}LL^T\right)P = 0 \tag{8.167}$$

where Q is also a positive definite symmetric matrix. The worst case disturbance is given by

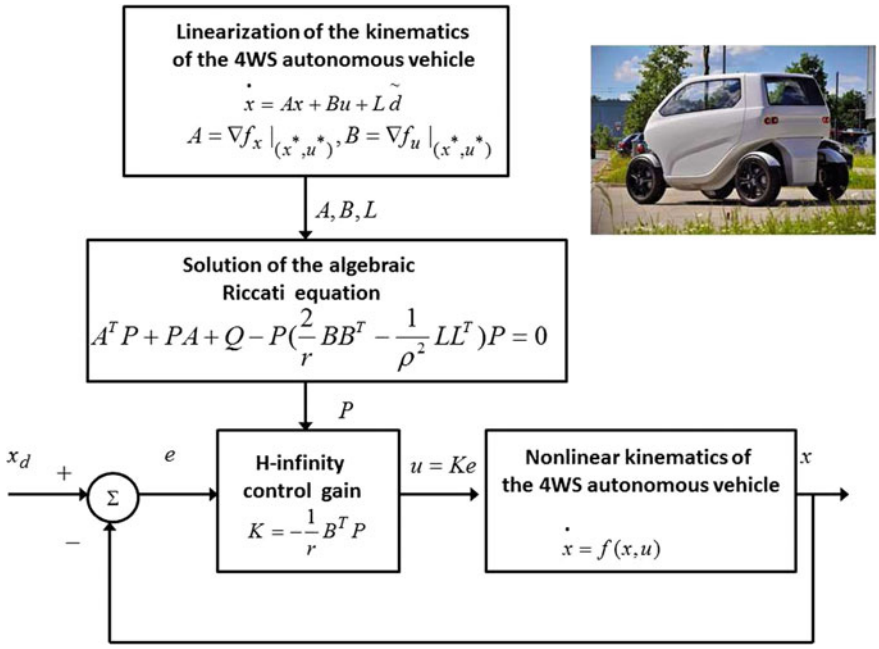

Fig. 8.21 Diagram of the nonlinear optimal control scheme for the 4WS autonomous ground vehicle

$$\tilde{d}(t) = \frac{1}{\rho^2} L^T P x(t) \tag{8.168}$$

The diagram of the considered control loop is depicted in Fig. 8.21.

8.4.5 Lyapunov Stability Analysis

Through Lyapunov stability analysis it will be shown that the proposed nonlinear control scheme assures H_∞ tracking performance for the control loop of the 4WS autonomous ground vehicle. Moreover, under moderate conditions asymptotic stability is proven and convergence to the reference setpoints is achieved. The tracking error dynamics for the 4WS automatic ground vehicle is written in the form

$$\dot{e} = Ae + Bu + L\tilde{d} \tag{8.169}$$

where in this 4WS autonomous vehicle's case $L = I \in R^{6\times 6}$ with I being the identity matrix. Variable $\tilde{d}$ denotes model uncertainties and external disturbances of the vehicle's model. The following Lyapunov function is considered

$$V = \frac{1}{2} e^T P e \tag{8.170}$$

where $e = x - x_d$ is the tracking error. By differentiating with respect to time one obtains

$$\begin{gathered} \dot{V} = \frac{1}{2} \dot{e}^T P e + \frac{1}{2} e P \dot{e} \Rightarrow \\ \dot{V} = \frac{1}{2} [Ae + Bu + L\tilde{d}]^T P + \frac{1}{2} e^T P [Ae + Bu + L\tilde{d}] \Rightarrow \end{gathered} \tag{8.171}$$

$$\begin{gathered} \dot{V} = \frac{1}{2} [e^T A^T + u^T B^T + \tilde{d}^T L^T] P e + \\ + \frac{1}{2} e^T P [Ae + Bu + L\tilde{d}] \Rightarrow \end{gathered} \tag{8.172}$$

$$\begin{gathered} \dot{V} = \frac{1}{2} e^T A^T P e + \frac{1}{2} u^T B^T P e + \frac{1}{2} \tilde{d}^T L^T P e + \\ \frac{1}{2} e^T P A e + \frac{1}{2} e^T P B u + \frac{1}{2} e^T P L \tilde{d} \end{gathered} \tag{8.173}$$

The previous equation is rewritten as

$$\begin{gathered} \dot{V} = \frac{1}{2} e^T (A^T P + P A) e + \left(\frac{1}{2} u^T B^T P e + \frac{1}{2} e^T P B u \right) + \\ + \left(\frac{1}{2} \tilde{d}^T L^T P e + \frac{1}{2} e^T P L \tilde{d} \right) \end{gathered} \tag{8.174}$$

Assumption: For given positive definite matrix Q and coefficients r and ρ there exists a positive definite matrix P, which is the solution of the following matrix equation

$$A^T P + P A = -Q + P \left(\frac{2}{r} B B^T - \frac{1}{\rho^2} L L^T \right) P \tag{8.175}$$

Moreover, the following feedback control law is applied to the system

$$u = -\frac{1}{r} B^T P e \tag{8.176}$$

By substituting Eqs. (2.89) and (2.90) one obtains

$$\begin{gathered} \dot{V} = \frac{1}{2} e^T \left[-Q + P \left(\frac{2}{r} B B^T - \frac{1}{2\rho^2} L L^T \right) P \right] e + \\ + e^T P B \left(-\frac{1}{r} B^T P e \right) + e^T P L \tilde{d} \Rightarrow \end{gathered} \tag{8.177}$$

$$\dot{V} = -\frac{1}{2}e^T Qe + \left(\frac{2}{r}PBB^T Pe - \frac{1}{2\rho^2}e^T PLL^T\right)Pe$$
$$-\frac{1}{r}(e^T PBB^T Pe) + e^T PL\tilde{d} \tag{8.178}$$

which after intermediate operations gives

$$\dot{V} = -\frac{1}{2}e^T Qe - \frac{1}{2\rho^2}e^T PLL^T Pe + e^T PL\tilde{d} \tag{8.179}$$

or, equivalently

$$\dot{V} = -\frac{1}{2}e^T Qe - \frac{1}{2\rho^2}e^T PLL^T Pe +$$
$$+\frac{1}{2}e^T PL\tilde{d} + \frac{1}{2}\tilde{d}^T L^T Pe \tag{8.180}$$

Lemma: The following inequality holds

$$\frac{1}{2}e^T L\tilde{d} + \frac{1}{2}\tilde{d}L^T Pe - \frac{1}{2\rho^2}e^T PLL^T Pe \leq \frac{1}{2}\rho^2\tilde{d}^T\tilde{d} \tag{8.181}$$

Proof: The binomial $(\rho\alpha - \frac{1}{\rho}b)^2$ is considered. Expanding the left part of the above inequality one gets

$$\rho^2 a^2 + \frac{1}{\rho^2}b^2 - 2ab \geq 0 \Rightarrow \frac{1}{2}\rho^2 a^2 + \frac{1}{2\rho^2}b^2 - ab \geq 0 \Rightarrow$$
$$ab - \frac{1}{2\rho^2}b^2 \leq \frac{1}{2}\rho^2 a^2 \Rightarrow \frac{1}{2}ab + \frac{1}{2}ab - \frac{1}{2\rho^2}b^2 \leq \frac{1}{2}\rho^2 a^2 \tag{8.182}$$

The following substitutions are carried out: $a = \tilde{d}$ and $b = e^T PL$ and the previous relation becomes

$$\frac{1}{2}\tilde{d}^T L^T Pe + \frac{1}{2}e^T PL\tilde{d} - \frac{1}{2\rho^2}e^T PLL^T Pe \leq \frac{1}{2}\rho^2\tilde{d}^T\tilde{d} \tag{8.183}$$

Equation (8.183) is substituted in Eq. (8.180) and the inequality is enforced, thus giving

$$\dot{V} \leq -\frac{1}{2}e^T Qe + \frac{1}{2}\rho^2\tilde{d}^T\tilde{d} \tag{8.184}$$

Equation (8.184) shows that the H_∞ tracking performance criterion is satisfied. The integration of $\dot{V}$ from 0 to T gives

$$\int_0^T \dot{V}(t)dt \leq -\frac{1}{2}\int_0^T ||e||_Q^2 dt + \frac{1}{2}\rho^2 \int_0^T ||\tilde{d}||^2 dt \Rightarrow$$
$$2V(T) + \int_0^T ||e||_Q^2 dt \leq 2V(0) + \rho^2 \int_0^T ||\tilde{d}||^2 dt \tag{8.185}$$

Moreover, if there exists a positive constant $M_d > 0$ such that

$$\int_0^\infty ||\tilde{d}||^2 dt \leq M_d \tag{8.186}$$

then one gets

$$\int_0^\infty ||e||_Q^2 dt \leq 2V(0) + \rho^2 M_d \tag{8.187}$$

Thus, the integral $\int_0^\infty ||e||_Q^2 dt$ is bounded. Moreover, $V(T)$ is bounded and from the definition of the Lyapunov function V in Eq. (8.170) it becomes clear that $e(t)$ will be also bounded since $e(t) \in \Omega_e = \{e | e^T P e \leq 2V(0) + \rho^2 M_d\}$. According to the above and with the use of Barbalat's Lemma one obtains $lim_{t\to\infty} e(t) = 0$.

Elaborating on the above, it can be noted that the proof of global asymptotic stability for the control loop of the 4WS vehicle's model is based on Eq. (8.184) and on the application of Barbalat's Lemma. It uses the condition of Eq. (8.186) about the boundedness of the square of the aggregate disturbance and modelling error term $\tilde{d}$ that affects the model. However, as explained above the proof of global asymptotic stability is not restricted by this condition. By selecting the attenuation coefficient ρ to be sufficiently small and in particular to satisfy $\rho^2 < ||e||_Q^2 / ||\tilde{d}||^2$ one has that the first derivative of the Lyapunov function is upper bounded by 0. Therefore for the ith time interval it is proven that the Lyapunov function defined in Eq. (8.170) is a decreasing one. This also assures the Lyapunov function of the system defined in Eq. (8.170) will always have a negative first-order derivative.

8.4.6 *Robust State Estimation Using the H-Infinity Kalman Filter*

The control loop for the 4WS autonomous vehicle can be implemented with the feedback of a partially measurable state vector and by processing only a small number of state variables. To reconstruct the missing information about the state vector of the 4WS autonomous vehicle it is proposed to use a filtering scheme and based on it to apply state estimation-based control [457]. The recursion of the H_∞ Kalman Filter, can be formulated in terms of a *measurement update* and a *time update* part

Measurement update:

$$\begin{aligned} D(k) &= [I - \theta W(k)P^{-}(k) + C^{T}(k)R(k)^{-1}C(k)P^{-}(k)]^{-1} \\ K(k) &= P^{-}(k)D(k)C^{T}(k)R(k)^{-1} \\ \hat{x}(k) &= \hat{x}^{-}(k) + K(k)[y(k) - C\hat{x}^{-}(k)] \end{aligned} \tag{8.188}$$

Time update:

$$\begin{aligned} \hat{x}^{-}(k+1) &= A(k)x(k) + B(k)u(k) \\ P^{-}(k+1) &= A(k)P^{-}(k)D(k)A^{T}(k) + Q(k) \end{aligned} \tag{8.189}$$

where it is assumed that parameter θ is sufficiently small to assure that the covariance matrix $P^{-}(k)^{-1} - \theta W(k) + C^{T}(k)R(k)^{-1}C(k)$ will be positive definite. When $\theta = 0$ the H_{∞} Kalman Filter becomes equivalent to the standard Kalman Filter. One can measure only a part of the state vector of the system of the 4WS autonomous vehicle, such as the velocities V_x and V_y and the orientation angle θ, and can estimate through filtering the rest of the state vector elements.

8.4.7 Simulation Tests

The performance of the proposed nonlinear optimal control scheme for the autonomous 4WS vehicle has been tested in the case of tracking of different reference setpoints. The control scheme exhibited fast and accurate tracking of the reference paths. The computation of the feedback control gain required the solution of the algebraic Riccati equation given in Eq. (8.175), at each iteration of the control algorithm. The obtained results are depicted in Figs. 8.22, 8.23, 8.24, 8.25, 8.26, 8.27, 8.28, 8.29, 8.30, 8.31, 8.32 and 8.33. The measurement units for the state variables of the 4WS vehicle's model were in the SI system (position coordinates measured in m and heading angle in rad). It can be noticed that the H-infinity controller achieved fast and accurate convergence to the reference setpoints for all elements of the 4WS vehicle's state-vector. Moreover, the variations of the control inputs, that is of the 4WS autonomous vehicle's velocity and of its steering angle were smooth.

As noted, the proposed nonlinear optimal control method for the 4WS autonomous vehicle was based on an approximate linearization of its joint kinematic and dynamic model. The advantages that the proposed control method exhibits are outlined as follows: (i) it is applied directly on the nonlinear dynamical model of the 4WS vehicle and not on an equivalent linearized description of it, (ii) It avoids the elaborated linearizing transformations (diffeomorphisms) which can be met in global linearization-based control methods for autonomous vehicles (iii) the controller is

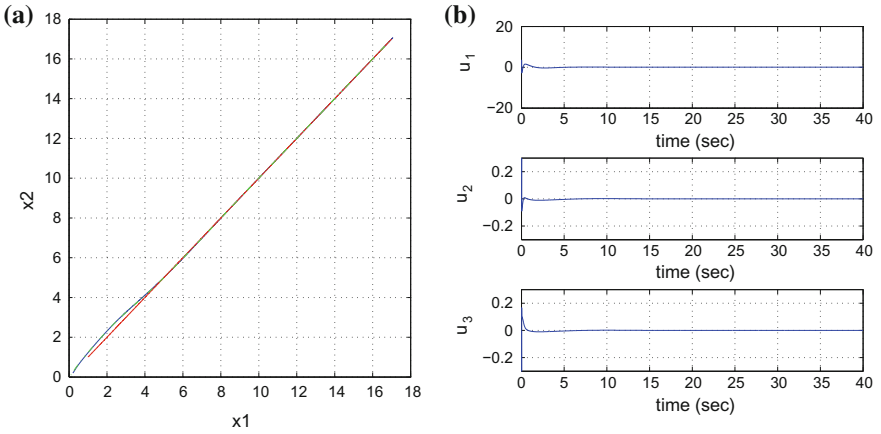

Fig. 8.22 **a** Tracking of reference path 1 (red-line) by the 4WS autonomous vehicle (blue line) and trajectory estimated by the Kalman Filter (green line), **b** control inputs u_1 to u_3 applied to the 4WS vehicle

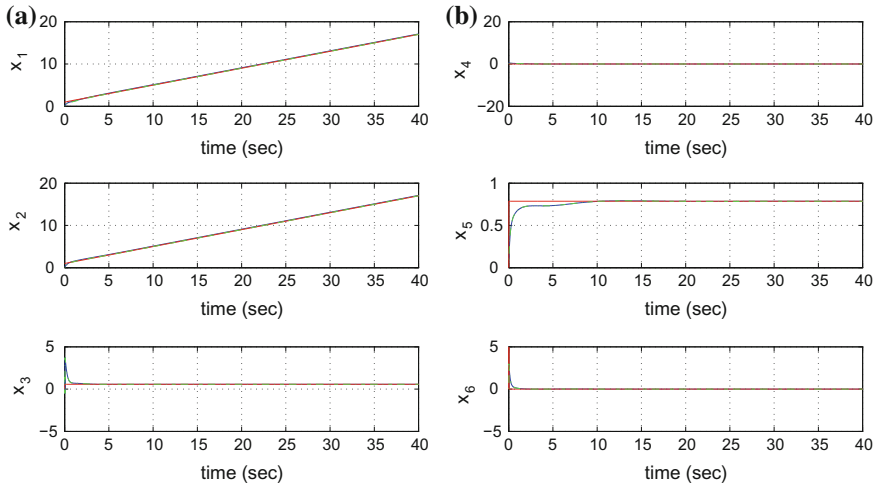

Fig. 8.23 Tracking of reference path 1: **a** convergence of state variables x_1 to x_3 of the 4WS vehicle to their reference setpoints (red-lines) and estimated state variables provided by the Kalman Filter (green lines), **b** convergence of state variables x_4 to x_6 of the 4WS vehicle to their reference setpoints (red-lines) and estimated state variables provided by the Kalman Filter (green lines)

designed according to optimal control principles which implies the best trade-off between precise tracking of the reference setpoints on the one side and moderate variations of the control inputs on the other side (iv) the control method exhibits significant robustness to parametric uncertainty, modelling errors as well as to external perturbations.

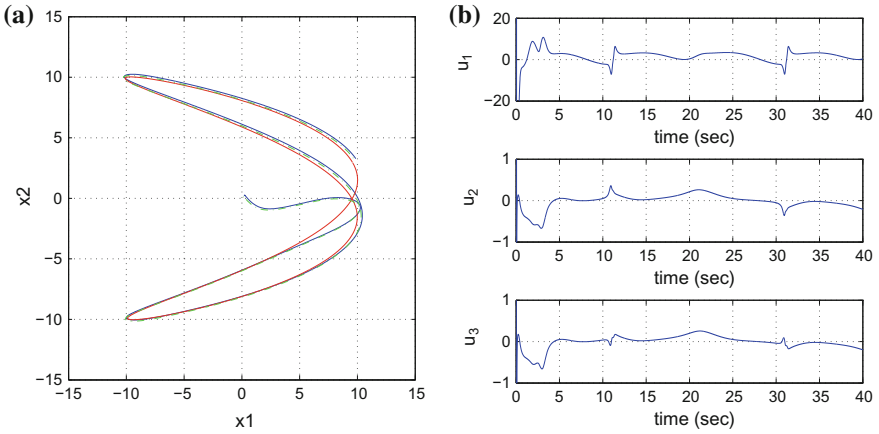

Fig. 8.24 **a** Tracking of reference path 2 (red-line) by the 4WS autonomous vehicle (blue line) and trajectory estimated by the Kalman Filter (green line), **b** control inputs u_1 to u_3 applied to the 4WS vehicle

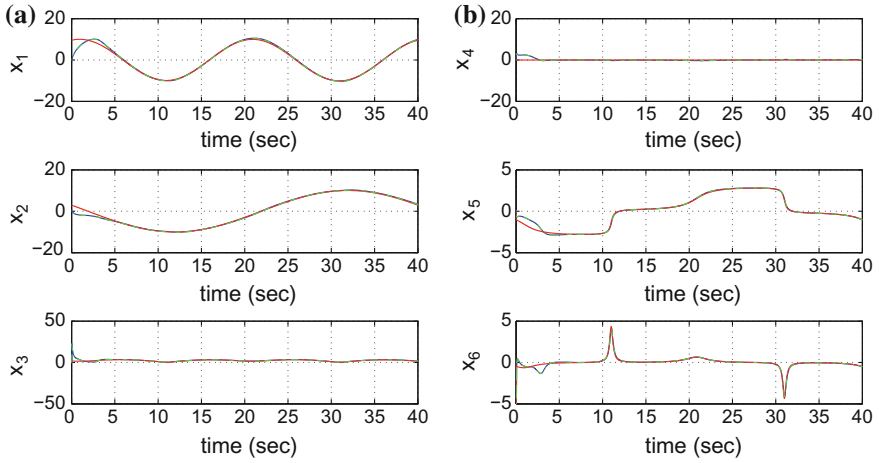

Fig. 8.25 Tracking of reference path 2: **a** convergence of state variables x_1 to x_3 of the 4WS vehicle to their reference setpoints (red-lines) and estimated state variables provided by the Kalman Filter (green lines), **b** convergence of state variables x_4 to x_6 of the 4WS vehicle to their reference setpoints (red-lines) and estimated state variables provided by the Kalman Filter (green lines)

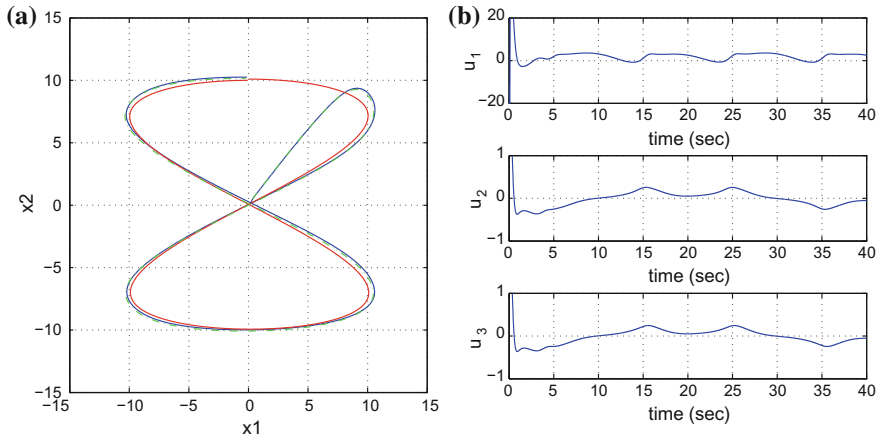

Fig. 8.26 **a** Tracking of reference path 3 (red-line) by the 4WS autonomous vehicle (blue line) and trajectory estimated by the Kalman Filter (green line), **b** control inputs u_1 to u_3 applied to the 4WS vehicle

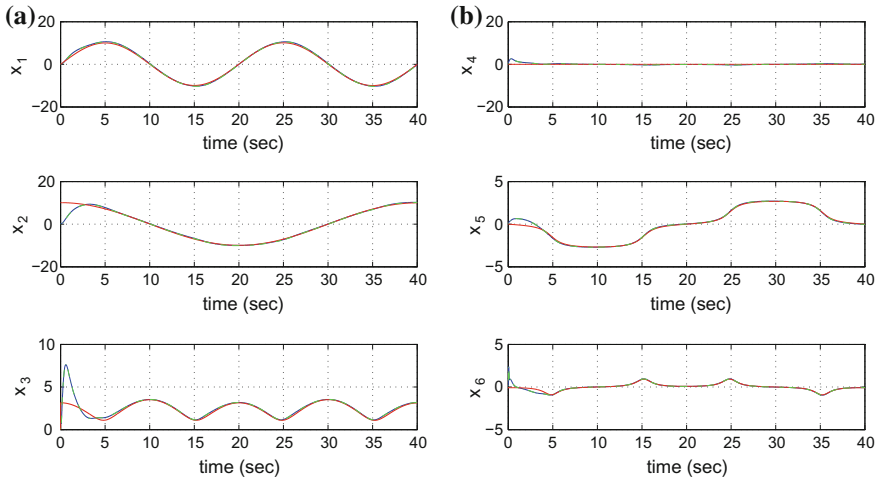

Fig. 8.27 Tracking of reference path 3: **a** convergence of state variables x_1 to x_3 of the 4WS vehicle to their reference setpoints (red-lines) and estimated state variables provided by the Kalman Filter (green lines), **b** convergence of state variables x_4 to x_6 of the 4WS vehicle to their reference setpoints (red-lines) and estimated state variables provided by the Kalman Filter (green lines)

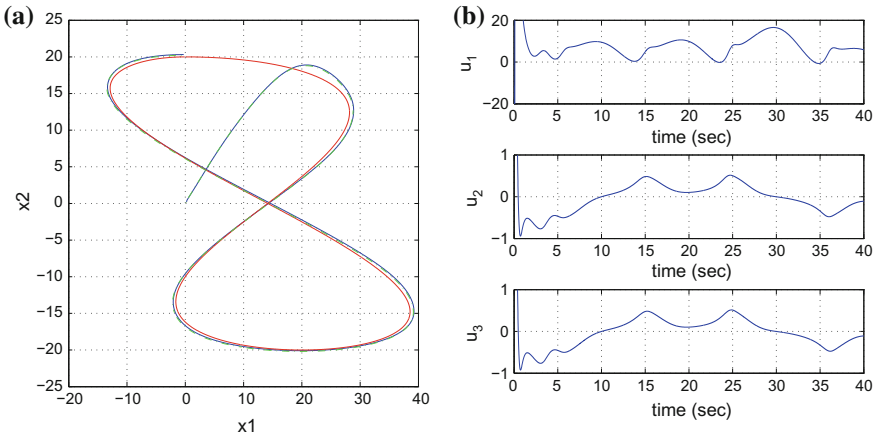

Fig. 8.28 **a** Tracking of reference path 4 (red-line) by the 4WS autonomous vehicle (blue line) and trajectory estimated by the Kalman Filter (green line), **b** control inputs u_1 to u_3 applied to the 4WS vehicle

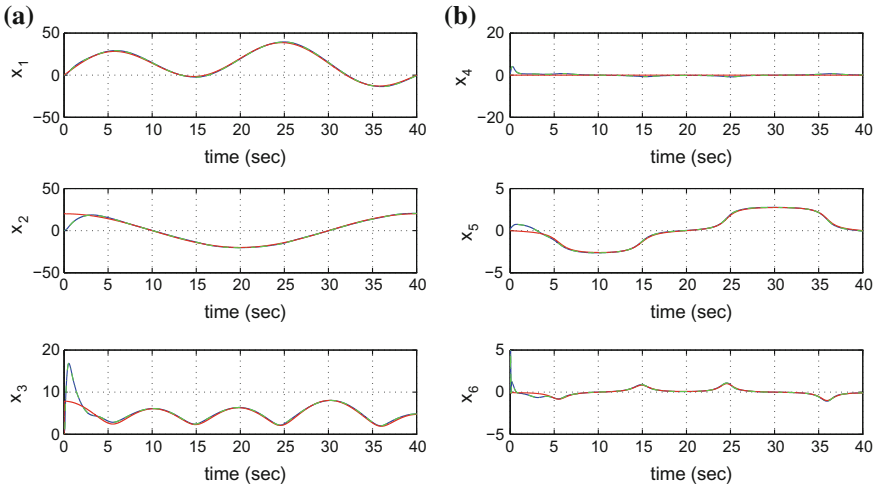

Fig. 8.29 Tracking of reference path 4: **a** convergence of state variables x_1 to x_3 of the 4WS vehicle to their reference setpoints (red-lines) and estimated state variables provided by the Kalman Filter (green lines), **b** convergence of state variables x_4 to x_6 of the 4WS vehicle to their reference setpoints (red-lines) and estimated state variables provided by the Kalman Filter (green lines)

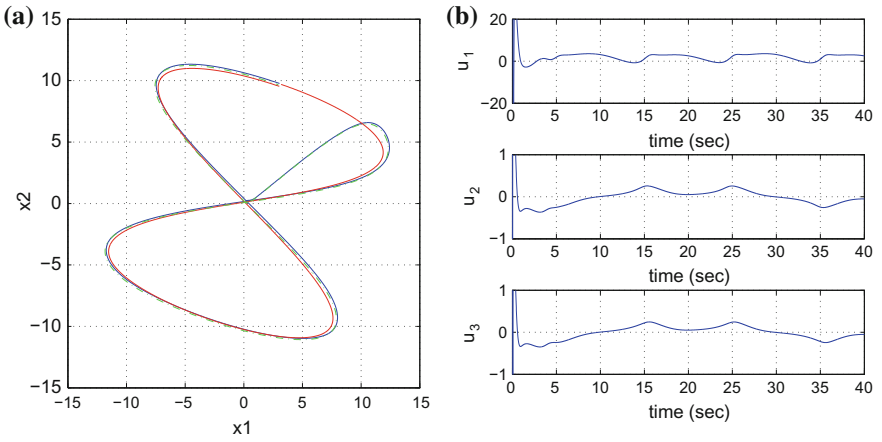

Fig. 8.30 **a** Tracking of reference path 5: (red-line) by the 4WS autonomous vehicle (blue line) and trajectory estimated by the Kalman Filter (green line), **b** control inputs u_1 to u_3 applied to the 4WS vehicle

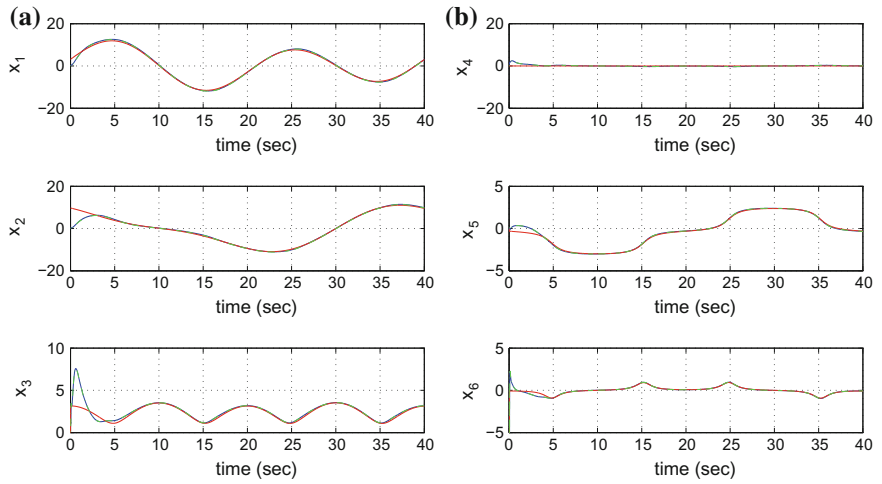

Fig. 8.31 Tracking of reference path 5: **a** convergence of state variables x_1 to x_3 of the 4WS vehicle to their reference setpoints (red-lines) and estimated state variables provided by the Kalman Filter (green lines), **b** convergence of state variables x_4 to x_6 of the 4WS vehicle to their reference setpoints (red-lines) and estimated state variables provided by the Kalman Filter (green lines)

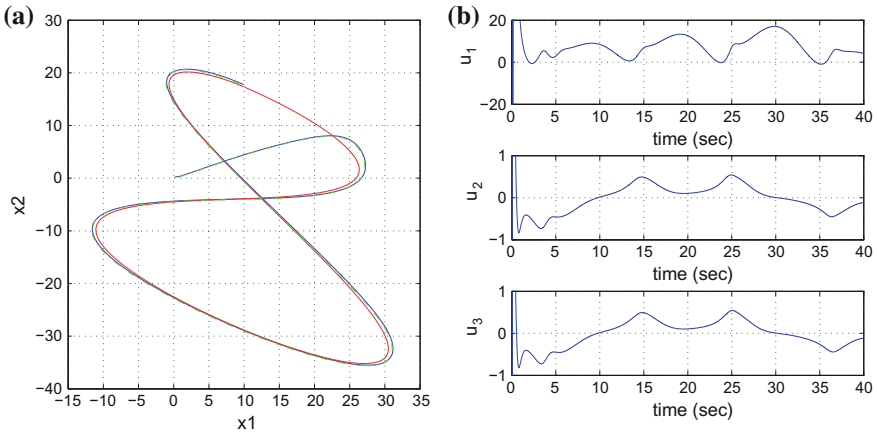

Fig. 8.32 **a** Tracking of reference path 6: (red-line) by the 4WS autonomous vehicle (blue line) and trajectory estimated by the Kalman Filter (green line), **b** control inputs u_1 to u_3 applied to the 4WS vehicle

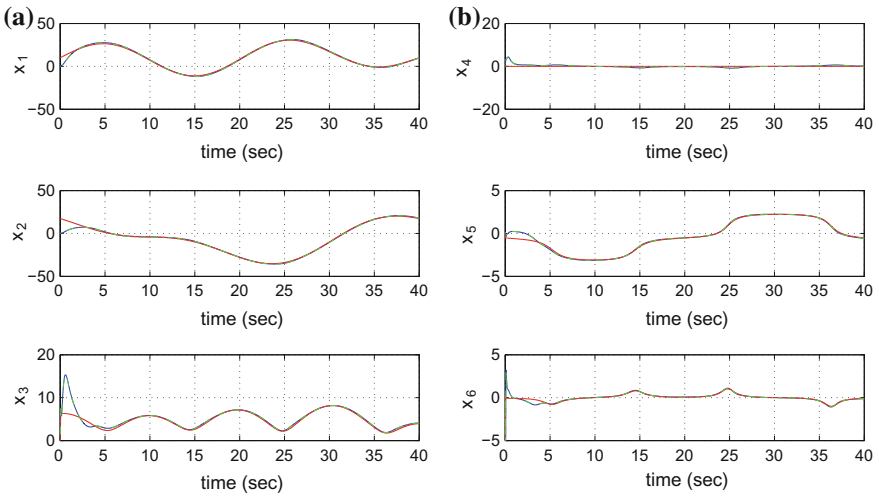

Fig. 8.33 Tracking of reference path 6: **a** convergence of state variables x_1 to x_3 of the 4WS vehicle to their reference setpoints (red-lines) and estimated state variables provided by the Kalman Filter (green lines), **b** convergence of state variables x_4 to x_6 of the 4WS vehicle to their reference setpoints (red-lines) and estimated state variables provided by the Kalman Filter (green lines)

Table 8.3 RMSE of the 4WS vehicle's state variables

Path	RMSE X (m)	RMSE Y (m)	RMSE θ (rad)
1	$3.3{\cdot}10^{-3}$	$3.3{\cdot}10^{-3}$	$0.1{\cdot}10^{-3}$
2	$6.0{\cdot}10^{-3}$	$13.0{\cdot}10^{-3}$	$0.7{\cdot}10^{-3}$
3	$8.2{\cdot}10^{-3}$	$6.0{\cdot}10^{-3}$	$1.1{\cdot}10^{-3}$
4	$13.3{\cdot}10^{-3}$	$11.6{\cdot}10^{-3}$	$2.4{\cdot}10^{-3}$
5	$5.0{\cdot}10^{-3}$	$4.2{\cdot}10^{-3}$	$1.0{\cdot}10^{-3}$
6	$12.2{\cdot}10^{-3}$	$12.6{\cdot}10^{-3}$	$1.2{\cdot}10^{-3}$

Table 8.4 RMSE of the 4WS state variables under disturbance

Δa (%)	RMSE X (m)	RMSE Y (m)	RMSE θ (rad)
0	$8.2{\cdot}10^{-3}$	$6.0{\cdot}10^{-3}$	$1.1{\cdot}10^{-3}$
10	$8.2{\cdot}10^{-3}$	$6.2{\cdot}10^{-3}$	$0.6{\cdot}10^{-3}$
20	$8.2{\cdot}10^{-3}$	$6.3{\cdot}10^{-3}$	$0.8{\cdot}10^{-3}$
30	$8.0{\cdot}10^{-3}$	$6.4{\cdot}10^{-3}$	$1.3{\cdot}10^{-3}$
40	$7.9{\cdot}10^{-3}$	$6.5{\cdot}10^{-3}$	$1.8{\cdot}10^{-3}$
50	$7.9{\cdot}10^{-3}$	$6.6{\cdot}10^{-3}$	$2.3{\cdot}10^{-3}$
60	$7.8{\cdot}10^{-3}$	$6.6{\cdot}10^{-3}$	$2.8{\cdot}10^{-3}$

Yet computationally simple, the proposed H_∞ control scheme has an excellent performance. Comparing to the control of 4WS automatic ground vehicles that rely on global linearization methods the presented nonlinear H-infinity control scheme is equally efficient in setpoint tracking while also retaining optimal control features [457]. The tracking accuracy of the presented control method (H_∞) has been evaluated in the case of several reference setpoints. By using the Kalman Filter as a robust observer estimates of the state vector of the vehicle were obtained, and thus the implementation of state estimation-based control became possible. The measured state variables were $x_3 = V_x$, $x_4 = V_y$ and $x_5 = \theta$. The obtained results are given in Table 8.3.

The tracking performance of the nonlinear H-infinity control method for the model of the 4WS vehicle was measured in the case of model uncertainty, imposing an imprecision equal to $\Delta a\%$ about the vehicle's moment of inertia I. The obtained results are outlined in Table 8.4. It can be noticed that despite model perturbations the tracking accuracy of the control method remained satisfactory.

8.5 Flatness-Based Control for AGVs and Kalman Filter-Based Compensation of Disturbance Forces and Torques

8.5.1 Outline

The present section analyzes the use of a global linearization-based control approach that is based on differential flatness theory to the problem of autonomous navigation of four-wheel robotic vehicles. As previously noted, the precise modeling of the vehicles' dynamics improves the efficiency of vehicles controllers in adverse cases, for example in high velocity, when performing abrupt maneuvers, under mass and loads changes or when moving on rough terrain. Using model-based control approaches it is possible to design a nonlinear controller that maintains the vehicle's motion characteristics within desirable ranges [45, 319, 332, 333, 348, 616]. When the vehicle's dynamics is subject to modeling uncertainties or when there are unknown forces and torques exerted on the vehicle it is important to be in position to estimate in real-time disturbances and unknown dynamics so as to compensate them through the control input and to maintain the satisfactory performance of the vehicle's automated steering system. In this direction, estimation for the unknown dynamics of the vehicle and state estimation-based control schemes have been developed [201, 312, 350, 580].

The objective of the present section is two-fold. On the one side it analyzes the design of a controller for autonomous navigation of automatic ground vehicles (AGVs). On the other side it proposes a solution to the problem of four-wheel vehicle control under model uncertainties and external disturbances. Considering, that only under ideal conditions the dynamic model of the vehicle is precisely known (e.g. there may be variations in the transported mass, or in the cornering stiffness coefficients characterizing the interaction of the tires with the ground, or in the position of the vehicle's center of gravity) and that in several cases there is uncertainty about the forces and torques developed on the vehicle (e.g. traction and braking torques on the wheels, forces due to traction of implements, or lateral forces which generate torques affecting the yaw stability of the vehicle) the need for designing robust controllers of the autonomous vehicles becomes obvious [49, 510, 521, 590]. By compensating efficiently such disturbances forces and torques safety features of the vehicle are improved and its autonomous functioning remains reliable even under adverse road conditions.

Dynamic analysis for the 4-wheel vehicle provided, as in the case of Sect. 8.2. A 3-DOF model is introduced having as elements the vehicle's velocity along the horizontal and vertical axis of an inertial reference frame as well as the rate of change of its orientation angle (this is the angle defined by the vehicle's longitudinal axis and the horizontal axis of the frame). Lateral forces are shown to affect the vehicle's motion and to be dependent on the longitudinal and lateral velocity of the vehicle, on the yaw rate and on the cornering stiffness coefficients for the front and rear tires. The control inputs to the vehicles' dynamic model are the traction/bracking

wheel torque and the turn angle of the steering wheel. Since the parameters of the dynamic model of the vehicle cannot always be known with precision or may be time-varying (e.g. cornering stiffness coefficients, transported mass) and since there may be unmodelled external forces and torques exerted on the vehicle (e.g. due to road condition, disturbances in traction forces) it is important to design a control loop with robustness to the aforementioned sources of uncertainty and disturbances, as well as to be in position to estimate in real-time such disturbances through the processing of measurements from a small number of on-board sensors.

Next, it is shown how a nonlinear controller for the aforementioned vehicle's model can be obtained through the application of differential flatness theory [145, 476, 546, 572]. The flat output for the vehicle's model is a vector comprising the x-axis velocity and a second variable based on a linear relation between the y-axis velocity and the rate of change of the orientation angle [332, 333]. By expressing all state variables and the control input of the four-wheel vehicle model as functions of the flat output and its derivatives the system's dynamic model is transformed into the linear Brunovksy (canonical) form [303, 495]. For the latter model it is possible to design a state feedback controller that enables accurate tracking of the vehicle's velocity set-points.

By exploiting the vehicle's exactly linearized model and its transformation into a canonical form it is possible to design a state estimator for approximating the system's state vector through the processing of measurements coming from a small number of on-board sensors. To this end the concept of *Derivative-free nonlinear Kalman Filtering* is used once again. Unlike the Extended Kalman Filter, the proposed filtering method provides estimates of the state vector of the nonlinear system without the need for derivatives and Jacobians calculation [439, 445, 450]. By avoiding linearization approximations, the proposed filtering method improves the accuracy of estimation of the system's state variables. Moreover, it is shown that it is possible to redesign the Kalman Filter in the form of a disturbance observer and using the estimation of the disturbance to develop an auxiliary control input that compensates for their effects. In this way the vehicle's control and autonomous navigation system can become robust with respect to uncertainties in the model's parameters or uncertainties about external forces and torques. It is also noted that in terms of computation speed the proposed Kalman Filter-based disturbance estimator for the vehicle is faster than disturbance estimators that may be based on other nonlinear filtering approaches (e.g. Extended Kalman Filter, Unscented Kalman Filter or Particle Filter) thus becoming advantageous for the real-time estimation of the unknown vehicle dynamics [438, 457]. The efficiency of the proposed nonlinear control and Kalman Filter-based disturbances estimation scheme is evaluated through numerical simulation tests. It has been shown that by accurately estimating disturbance forces and torques the control loop achieves elimination of the tracking error for all state variables of the vehicle.

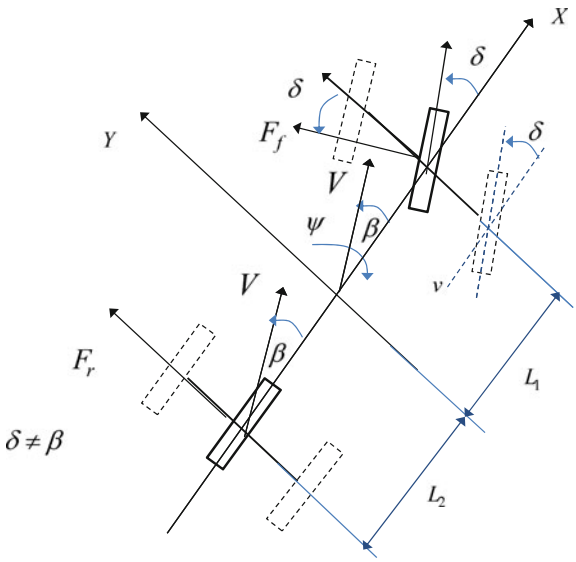

Fig. 8.34 Nonlinear 4-wheeled vehicle model

8.5.2 Dynamic Model of the Vehicle

8.5.2.1 Definition of Parameters in 4-Wheel Vehicle Dynamic Model

The dynamic model of the four-wheel vehicle that was analyzed in a previous section is now re-examined. With reference to Fig. 8.34 (where the lateral forces applied on the wheels are considered to define the vehicle's motion) one has the following parameters: β is the angle between the velocity and the vehicle's transversal angle, V is the velocity vector of the vehicle, ψ is the yaw angle (rotation round the z axis), f_x: is the aggregate force along the x axis, f_y is the aggregate force along the y axis, T_z is the aggregate torque round the z axis and δ is the steering angle of the front wheels [332, 348, 572].

The motion of the vehicle along its longitudinal axis is controlled by the traction or braking wheel torque $T_\omega = T_m - T_b$ with $T_b = T_{b_f} + T_{b_r}$ and the lateral movement via the steering angle δ. The two control inputs of the four wheel vehicle model are

$$\begin{aligned} u_1 &= T_\omega \\ u_2 &= \delta \end{aligned} \tag{8.190}$$

As explained in Sect. 8.2, a first form of the vehicle's dynamic model is

$$\dot{x} = f(x,t) + g(x,t)u + g_1 u_1 u_2 + g_2 u_2^2 \tag{8.191}$$

where

$$f(x,t)=\begin{pmatrix}\frac{I_r}{mR}(\dot{\omega}_r+\dot{\omega}_f)\\ \dot{\psi}V_x+\frac{1}{m}\left(-C_f\frac{(V_y+L_f\dot{\psi})}{V_x}-C_r\frac{(V_y-L_f\dot{\psi})}{V_x}\right)\\ \frac{1}{I_z}\left(-L_fC_f\frac{(V_y+L_f\dot{\psi})}{V_x}+L_rC_r\frac{(V_y-L_f\dot{\psi})}{V_x}\right)\end{pmatrix} \tag{8.192}$$

$$g(x,t)=\begin{pmatrix}\frac{1}{mR} & \frac{C_f}{m}\left(\frac{V_y+L_f\dot{\psi}}{V_x}\right)\\ 0 & \left(\frac{C_fR-I_r\dot{\omega}_f}{mR}\right)\\ 0 & \frac{(L_fC_fR-L_fI_r\dot{\omega}_f)}{I_zR}\end{pmatrix} \tag{8.193}$$

$$g_1=\begin{pmatrix}0\\ \frac{1}{mR}\\ \frac{L_f}{I_zR}\end{pmatrix}\ g_2=\begin{pmatrix}-\frac{C_f}{m}\\ 0\\ 0\end{pmatrix}\ x=\begin{pmatrix}V_x\\ V_y\\ \dot{\psi}\end{pmatrix}\ u=\begin{pmatrix}u_1\\ u_2\end{pmatrix} \tag{8.194}$$

The previously analyzed nonlinear model of the vehicle's dynamics can be simplified if the control inputs u_1u_2 and u_2^2 are not taken into account. In the latter case the dynamics of the vehicle takes the form

$$\dot{x}=f(x,t)+g(x,t)u \tag{8.195}$$

8.5.3 Flatness-Based Controller for the 3-DOF Vehicle Model

8.5.3.1 Flatness-Based Controller for the 4-Wheel Vehicle

To show that the four-wheel vehicle is differentially flat the following flat outputs are defined [332, 333]:

$$\begin{aligned}y_1&=V_x\\ y_2&=L_fmV_y-I_z\dot{\psi}\end{aligned} \tag{8.196}$$

Then it holds that all elements of the system's state vector can be written as functions of the flat outputs and their derivatives. Indeed, for $x=[V_x,\ V_y,\ \dot{\psi}]^T$ it holds

$$V_x=y_1 \tag{8.197}$$

$$V_y=\frac{y_2}{L_fm}-\left(\frac{I_z}{L_fm}\right)\left(\frac{L_fmy_1\dot{y}_2+C_r(L_f+L_r)y_2}{C_r(L_f+L_r)(I_z-L_fL_rm)+(L_fmy_1)^2}\right) \tag{8.198}$$

$$\dot{\psi}=\frac{L_fmy_1\dot{y}_2+C_r(L_f+L_r)y_2}{C_r(L_f+L_r)(I_z-L_fL_rm)+(L_fmy_1)^2} \tag{8.199}$$

Expressing the system's state variables as functions of the flat outputs one has the following state-space description for the system

$$\begin{pmatrix} \dot{y}_1 \\ \ddot{y}_2 \end{pmatrix} = \Delta(y_1, y_2, \dot{y}_2) \begin{pmatrix} u_1 \\ u_2 \end{pmatrix} + \Phi(y_1, y_2, \dot{y}_2) \tag{8.200}$$

where

$$\Delta(y_1, y_2, \dot{y}_2) = \begin{pmatrix} \Delta_{11}(y_1, y_2, \dot{y}_2) & \Delta_{12}(y_1, y_2, \dot{y}_2) \\ \Delta_{21}(y_1, y_2, \dot{y}_2) & \Delta_{22}(y_1, y_2, \dot{y}_2) \end{pmatrix} \tag{8.201}$$

with

$$\Delta_{11}(y_1, y_2, \dot{y}_2) = \frac{1}{mR} \tag{8.202}$$

$$\Delta_{12}(y_1, y_2, \dot{y}_2) = \frac{C_f}{m} \left(\frac{V_y + L_f \dot{\psi}}{y_1} \right) \tag{8.203}$$

$$\Delta_{21}(y_1, y_2, \dot{y}_2) = \frac{C_r(L_f + L_r)(V_y - L_r \dot{\psi}) - L_f m \dot{\psi} y_1^2}{mRy_1^2} \tag{8.204}$$

$$\begin{aligned} \Delta_{22}(y_1, y_2, \dot{y}_2) = & \left(-L_f m y_1 + \frac{L_r C_r (L_f + L_r)}{y_1} \right) \frac{(L_f C_f R - L_f I_r \dot{\omega}_f)}{I_z R} + \\ & + \frac{((C_r(L_f + L_r))(V_y - L_r \dot{\psi}) - L_f m \dot{\psi} y_1^2)}{y_1^2} \cdot \frac{C_f (V_y + L_f \dot{\psi})}{m y_1} - \frac{C_r (L_f + L_r)}{y_1} \frac{RC_f - I_r \dot{\omega}_f}{mR} \end{aligned} \tag{8.205}$$

Moreover about matrix $\Phi(y_1, y_2, \dot{y}_2)$ it holds

$$\Phi(y_1, y_2, \dot{y}_2) = \begin{pmatrix} \Phi_1(y_1, y_2, \dot{y}_2) \\ \Phi_2(y_1, y_2, \dot{y}_2) \end{pmatrix} \tag{8.206}$$

with elements

$$\Phi_1(y_1, y_2, \dot{y}_2) = \dot{\psi} V_y - \frac{I_r}{mR} (\dot{\omega}_r + \dot{\omega}_f) \tag{8.207}$$

$$\begin{aligned} \Phi_2(y_1, y_2, \dot{y}_2) = & -L_f m y_1 f_3(x, t) - \frac{C_r (L_f + L_r)}{y_1} f_2(x, t) + \\ & + \frac{C_f (L_f + L_r)(V_y - L_r \dot{\psi}) - L_f m \dot{\psi} y_1^2}{y_1^2} f_1(x, t) + \frac{L_r C_r (L_f + L_r)}{y_1} f_3(x, t) \end{aligned} \tag{8.208}$$

According to the above the system's control input can be also written as a function of the flat output and its derivatives. Thus one has

$$\begin{pmatrix} \dot{y}_1 \\ \ddot{y}_2 \end{pmatrix} = \Delta(y_1, y_2, \dot{y}_2) \begin{pmatrix} u_1 \\ u_2 \end{pmatrix} + \Phi(y_1, y_2, \dot{y}_2) \tag{8.209}$$

i.e.

$$\begin{pmatrix} u_1 \\ u_2 \end{pmatrix} = \Delta^{-1}(y_1, y_2, \dot{y}_2)^{-1}(\begin{pmatrix} \dot{y}_1 \\ \dot{y}_2 \end{pmatrix} - \Phi(y_1, y_2, \dot{y}_2)) \tag{8.210}$$

which means that provided that matrix $\Delta(y_1, y_2, \dot{y}_2)$ is invertible, the control input $u = [u_1, u_2]^T$ can be written as a function of the flat output and its derivatives. The non-singularity of matrix $\Delta(y_1, y_2, \dot{y}_2)$ depends on the determinant

$$det(\Delta(y_1, y_2, \dot{y}_2)) = \frac{(I_r\dot{\omega}_f - C_f R)(L_f^2 y_1^2 m^2 - C_r(L_f + L_r)L_r L_f m + C_r I_z L_r)}{I_z R^2 y_1 m^2} \tag{8.211}$$

This determinant has non-zero values because it holds:

(i) $(I_r\dot{\omega}_f - C_f R) \neq 0$ since for the wheels rotational acceleration one has $\dot{\omega}_f < \frac{C_f R}{I_r}$, and also

(ii) $(L_f^2 y_1^2 m^2 - C_r(L_f + L_r)L_r L_f m + C_r I_z L_r) \neq 0$ when $I_z > L_f m$.

The differentially flat model of the vehicle can be also written in a canonical form after defining the new control input vector

$$\begin{pmatrix} v_1 \\ v_2 \end{pmatrix} = \Delta(y_1, y_2, \dot{y}_2) \begin{pmatrix} u_1 \\ u_2 \end{pmatrix} + \Phi(y_1, y_2, \dot{y}_2) \tag{8.212}$$

thus one obtains a MIMO system description into canonical form, i.e.

$$\begin{pmatrix} \dot{y}_1 \\ \dot{y}_2 \\ \ddot{y}_2 \end{pmatrix} = \begin{pmatrix} 0 & 0 & 0 \\ 0 & 0 & 1 \\ 0 & 0 & 0 \end{pmatrix} \begin{pmatrix} y_1 \\ y_2 \\ \dot{y}_2 \end{pmatrix} + \begin{pmatrix} 1 & 0 \\ 0 & 0 \\ 0 & 1 \end{pmatrix} \begin{pmatrix} v_1 \\ v_2 \end{pmatrix} \tag{8.213}$$

Once the vehicle's model is written in the differentially flat form the controller that enables tracking of a desirable trajectory defined by y_1^{ref}, y_2^{ref}, $\dot{y}_2^{ref}$ is given by

$$\begin{aligned} v_1 &= \dot{y}_1^{ref} - k_{p_1}(y_1 - y_1^{ref}) \\ v_2 &= \ddot{y}_2^{ref} - k_{d_2}(\dot{y}_2 - \dot{y}_2^{ref}) - k_{p_2}(y_2 - y_2^{ref}) \end{aligned} \tag{8.214}$$

and defining the error variables $e_1 = y_1 - y_1^{ref}$ and $e_2 = y_2 - y_2^{ref}$ one has the following tracking error dynamics for the closed-loop system

$$\begin{aligned} \dot{e}_1 + k_{p_1} e_1 &= 0 \\ \ddot{e}_2 + k_{d_2}\dot{e}_2 + k_{p_2} e_2 &= 0 \end{aligned} \tag{8.215}$$

Therefore, the suitable selection of gains $k_{p_1>0}$ and $k_{p_2} > 0, k_{d_2} > 0$ assures the asymptotic elimination of the tracking errors, i.e. $lim_{t\to\infty} e_1(t) = 0$ and $lim_{t\to\infty} e_2(t) = 0$.

The control input that is finally applied for the vehicle's steering is given by

$$\begin{pmatrix} u_1 \\ u_2 \end{pmatrix} = \Delta(y_1, y_2, \dot{y}_2)^{-1} \left(\begin{pmatrix} v_1 \\ v_2 \end{pmatrix} - \Phi(y_1, y_2, \dot{y}_2) \right) \tag{8.216}$$

or equivalently

$$\begin{pmatrix} u_1 \\ u_2 \end{pmatrix} = \Delta(y_1, y_2, \dot{y}_2)^{-1} [\begin{pmatrix} \dot{y}_1^{ref} - k_{p_1}(y_1 - y_1^{ref}) \\ \ddot{y}_2^{ref} - k_{d_2}(\dot{y}_2 - \dot{y}_2^{ref}) - k_{p_2}(y_2 - y_2^{ref}) \end{pmatrix} - \Phi(y_1, y_2, \dot{y}_2)] \tag{8.217}$$

The transformation of the vehicle's model into a canonical form, through the application of the differential flatness theory, facilitates not only the design of a feedback controller for trajectory tracking but also the design of filters for the estimation of the state vector of the vehicle out of a limited number of sensor measurements.

8.5.4 Estimation of Vehicle Disturbance Forces with the Derivative-Free Nonlinear Kalman Filter

8.5.4.1 State Estimation with the Derivative-Free Nonlinear Kalman Filter

It was shown that the initial nonlinear model of the vehicle can be written in the MIMO canonical form

$$\begin{pmatrix} \dot{y}_1 \\ \dot{y}_2 \\ \ddot{y}_2 \end{pmatrix} = \begin{pmatrix} 0\ 0\ 0 \\ 0\ 0\ 1 \\ 0\ 0\ 0 \end{pmatrix} \begin{pmatrix} y_1 \\ y_2 \\ \dot{y}_2 \end{pmatrix} + \begin{pmatrix} 1\ 0 \\ 0\ 0 \\ 0\ 1 \end{pmatrix} \begin{pmatrix} v_1 \\ v_2 \end{pmatrix} \tag{8.218}$$

Thus one has a MIMO linear model of the form

$$\begin{aligned} \dot{y}_f &= A_f y_f + B_f v \\ z_f &= C_f y_f \end{aligned} \tag{8.219}$$

where $y_f = [y_1, y_2, \dot{y}_2]^T$ and matrices A_f,B_f,C_f are in the MIMO canonical form

$$A_f = \begin{pmatrix} 0\ 0\ 0 \\ 0\ 0\ 1 \\ 0\ 0\ 0 \end{pmatrix} \quad B_f = \begin{pmatrix} 1\ 0 \\ 0\ 0 \\ 0\ 1 \end{pmatrix} \quad C_f^T = \begin{pmatrix} 1\ 0 \\ 0\ 1 \\ 0\ 0 \end{pmatrix} \tag{8.220}$$

where the measurable variables $y_1 = V_x$, $y_2 = L_f m V_y - I_z \dot{\psi}$ are associated with the linear velocity of the vehicle V_x, V_y and with its angular velocity $\dot{\psi}$. For the aforementioned model, and after carrying out discretization of matrices A_f, B_f and C_f with common discretization methods one can perform linear Kalman filtering using Eqs. (8.229) and (8.230). This is *Derivative-free nonlinear Kalman filtering* for the model of the vehicle which, unlike EKF, is performed without the need to compute Jacobian matrices and does not introduce numerical errors.

8.5.4.2 Kalman Filter-Based Estimation of Disturbances

It is assumed that disturbance forces affect the nonlinear vehicle model along its longitudinal and transversal axis and that disturbance torques affect the nonlinear vehicle model on its z axis. For example disturbance forces can be due to a force vector that coincides with the vehicle's longitudinal axis (e.g. traction disturbance) or disturbance torques can be due to unmodelled lateral forces. These disturbance forces and torques change dynamically in time and their dynamics is given by

$$\begin{aligned} \tilde{d}_x &= f_{d_x}(V_x, V_y, \dot{\psi}) \\ \tilde{d}_y &= f_{d_y}(V_x, V_y, \dot{\psi}) \\ \tilde{d}_\psi &= T_{d_\psi}(V_x, V_y, \dot{\psi}) \end{aligned} \tag{8.221}$$

Since the state variables of the vehicle's dynamic model can be written as functions of the flat outputs y_1 and y_2 and of their derivatives it also holds

$$\begin{aligned} \tilde{d}_x^{(i)} &= f_{d_x}^{(i)}(y_1, y_2, \dot{y}_2) \\ \tilde{d}_y^{(i)} &= f_{d_y}^{(i)}(y_1, y_2, \dot{y}_2) \\ \tilde{d}_\psi^{(i)} &= T_{d_\psi}^{(i)}(y_1, y_2, \dot{y}_2) \end{aligned} \tag{8.222}$$

where $i = 1, 2, \ldots$ stands for the ith order derivative of the disturbance variable.

Considering the effect of disturbance functions on the initial nonlinear state equation of the vehicle and the linear relation between the initial state variables $[V_x, V_y]$ and the state variables of the flat system description $[y_1, y_2]$ one has the appearance of the disturbance terms in the canonical form model of Eq. (8.213)

$$\begin{pmatrix} \dot{y}_1 \\ \dot{y}_2 \\ \ddot{y}_2 \end{pmatrix} = \begin{pmatrix} 0 & 0 & 0 \\ 0 & 0 & 1 \\ 0 & 0 & 0 \end{pmatrix} \begin{pmatrix} y_1 \\ y_2 \\ \dot{y}_2 \end{pmatrix} + \begin{pmatrix} 1 & 0 \\ 0 & 0 \\ 0 & 1 \end{pmatrix} \begin{pmatrix} v_1 \\ v_2 \end{pmatrix} + \begin{pmatrix} \frac{1}{m}\tilde{d}_x \\ 0 \\ L_f \dot{\tilde{d}}_y - \dot{\tilde{d}}_\psi \end{pmatrix} \tag{8.223}$$

Next, the state vector of the model of Eq. (8.223) is extended to include as additional state variables the disturbance forces $\tilde{d}_x$, $\tilde{d}_y$ and $\tilde{d}_\psi$. Then, in the new state-space

description one has $z_1 = y_1$, $z_2 = y_2$, $z_3 = \dot{y}_2$, $z_4 = \tilde{f}_a = \frac{1}{m}\tilde{d}_x$, $z_5 = \dot{\tilde{f}}_a$, $z_6 = \dot{\tilde{f}}_b = L_f\dot{\tilde{d}}_y - \dot{\tilde{d}}_\psi$, $z_7 = \ddot{\tilde{f}}_b$, which takes the form of matrix equations

$$\dot{z} = \tilde{A}\cdot z + \tilde{B}\cdot\tilde{v} \tag{8.224}$$

where the control input is

$$\begin{gathered}\tilde{v} = \left(v_1 \; v_2 \; \tfrac{1}{m}\ddot{\tilde{d}}_x \; L_f\tilde{d}_y^{(3)} - \tilde{d}_\psi^{(3)}\right)^T \text{ or} \\ \tilde{v} = \left(v_1 \; v_2 \; \ddot{\tilde{f}}_a \; \tilde{f}_b^{(3)}\right)^T\end{gathered} \tag{8.225}$$

with

$$\tilde{A} = \begin{pmatrix} 0&0&0&1&0&0&0\\ 0&0&1&0&0&0&0\\ 0&0&0&0&0&1&0\\ 0&0&0&0&1&0&0\\ 0&0&0&0&0&0&0\\ 0&0&0&0&0&0&1\\ 0&0&0&0&0&0&0 \end{pmatrix} \quad \tilde{B} = \begin{pmatrix} 1&0&0&0\\ 0&0&0&0\\ 0&1&0&0\\ 0&0&0&0\\ 0&0&1&0\\ 0&0&0&0\\ 0&0&0&1 \end{pmatrix} \quad \tilde{C}^T = \begin{pmatrix} 1&0\\ 0&1\\ 0&0\\ 0&0\\ 0&0\\ 0&0\\ 0&0 \end{pmatrix} \tag{8.226}$$

where the measurable state variables are z_1 and z_2. Since the dynamics of the disturbance terms $\tilde{f}_a$ and $\tilde{f}_b$ are taken to be unknown in the design of the associated disturbances' estimator one has the following dynamics:

$$\dot{z}_o = \tilde{A}_o\cdot z + \tilde{B}_o\cdot\tilde{v} + K(C_o z - C_o\hat{z}) \tag{8.227}$$

where $K \in R^{7\times 2}$ is the state estimator's gain and

$$\tilde{A}_o = \begin{pmatrix} 0&0&0&1&0&0&0\\ 0&0&1&0&0&0&0\\ 0&0&0&0&0&1&0\\ 0&0&0&0&1&0&0\\ 0&0&0&0&0&0&0\\ 0&0&0&0&0&0&1\\ 0&0&0&0&0&0&0 \end{pmatrix} \quad \tilde{B}_o = \begin{pmatrix} 1&0&0&0\\ 0&0&0&0\\ 0&1&0&0\\ 0&0&0&0\\ 0&0&0&0\\ 0&0&0&0\\ 0&0&0&0 \end{pmatrix} \quad \tilde{C}_o^T = \begin{pmatrix} 1&0\\ 0&1\\ 0&0\\ 0&0\\ 0&0\\ 0&0\\ 0&0 \end{pmatrix} \tag{8.228}$$

Defining as $\tilde{A}_d$, $\tilde{B}_d$, and $\tilde{C}_d$, the discrete-time equivalents of matrices $\tilde{A}_o$, $\tilde{B}_o$ and $\tilde{C}_o$ respectively, a Derivative-free nonlinear Kalman Filter can be designed for the aforementioned representation of the system dynamics [438, 459]. The associated Kalman Filter-based disturbance estimator is given by

measurement update:

$$\begin{aligned} K(k) &= P^-(k)\tilde{C}_d^T[\tilde{C}_d \cdot P^-(k)\tilde{C}_d^T + R]^{-1} \\ \hat{x}(k) &= \hat{x}^-(k) + K(k)[z(k) - \tilde{C}_d\hat{x}^-(k)] \\ P(k) &= P^-(k) - K(k)\tilde{C}_d P^-(k) \end{aligned} \tag{8.229}$$

time update:

$$\begin{aligned} P^-(k+1) &= \tilde{A}_d(k)P(k)\tilde{A}_d^T(k) + Q(k) \\ \hat{x}^-(k+1) &= \tilde{A}_d(k)\hat{x}(k) + \tilde{B}_d(k)\tilde{v}(k) \end{aligned} \tag{8.230}$$

To compensate for the effects of the disturbance forces it suffices to use in the control loop the modified control input vector

$$v = \begin{pmatrix} v_1 - \hat{\tilde{f}}_a \\ v_2 - \hat{\tilde{f}}_b \end{pmatrix} \text{ or } v = \begin{pmatrix} v_1 - \hat{z}_4 \\ v_2 - \hat{z}_6 \end{pmatrix} \tag{8.231}$$

8.5.5 Simulation Tests

To evaluate for the performance of the proposed nonlinear control scheme, as well as about the performance of the Kalman Filter-based disturbances estimator simulation experiments have been carried out. Different velocity setpoints had been assumed (for velocity along the horizontal and vertical axis of the inertial reference frame, as well as for angular velocity round the vehicle's z axis). Moroever, different disturbances forces and torques have been assumed to affect the vehicles' dynamic model. Using the representation of the vehicle's dynamics given in Eq. (8.223) two generalized disturbance forces/torques have been considered: the first denoted as $\tilde{f}_a$ was associated with state variable y_1, while the second one denoted as $\tilde{f}_b$ was associated with the state variable y_2. It was also assumed that the change in time of the generalized forces and torques was defined by the second derivative of the associated variable, i.e. $\ddot{\tilde{f}}_a$ and $\ddot{\tilde{f}}_b$. The disturbances dynamics was completely unknown to the controller and their identification was performed in real time by the disturbance estimator. The control loop used in the vehicle's autonomous navigation is given in Fig. 8.35.

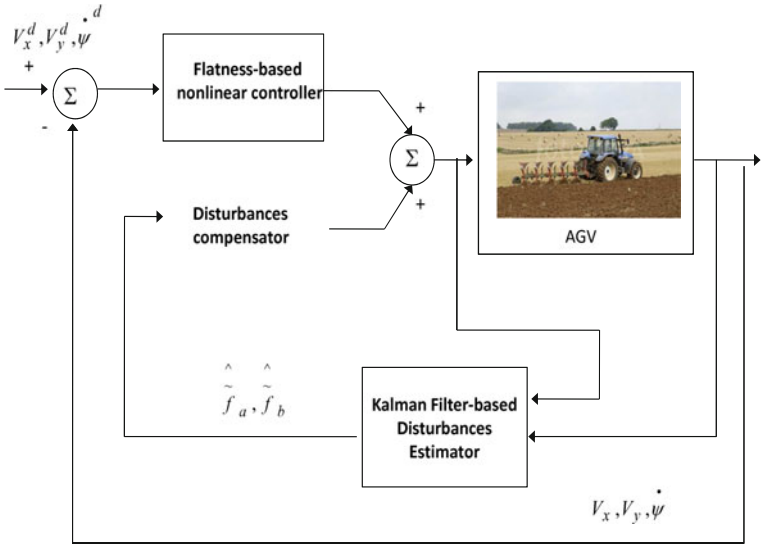

Fig. 8.35 Control loop for the autonomous vehicle comprising a flatness-based nonlinear controller and a Kalman Filter-based disturbances estimator

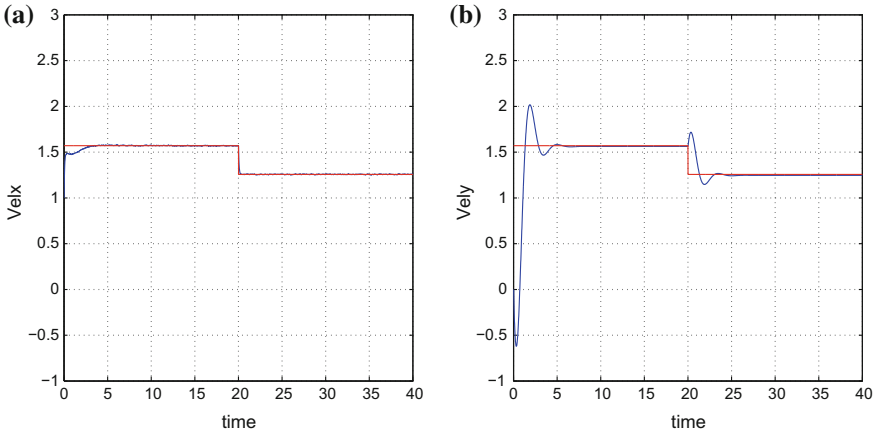

Fig. 8.36 Vehicle control under disturbances profile 1: **a** Convergence of x-axis velocity V_x (blue line) to the desirable setpoint (red line), **b** Convergence of the y-axis velocity V_y (blue line) to the desirable setpoint (red line)

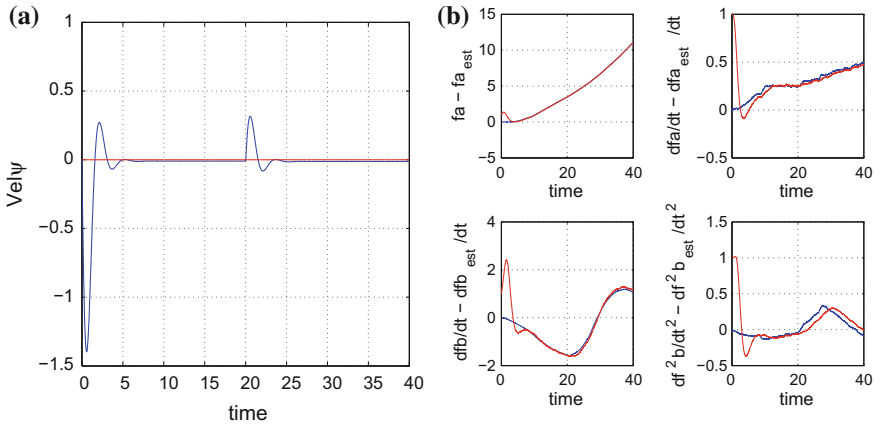

Fig. 8.37 Vehicle control under disturbances profile 1: **a** Convergence of yaw rate $\dot{\psi}$ (blue line) to the desirable setpoint (red line), **b** Estimation of the disturbance terms and of their rate of change (red line) and the associated real values (blue line)

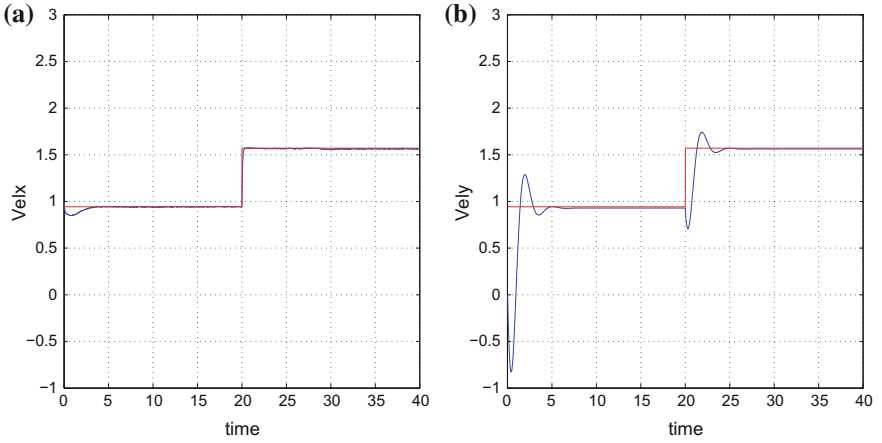

Fig. 8.38 Vehicle control under disturbances profile 2: **a** Convergence of x-axis velocity V_x (blue line) to the desirable setpoint (red line), **b** Convergence of the y-axis velocity V_y (blue line) to the desirable setpoint (red line)

The measurable variables used by the control and disturbances' estimation scheme were the vehicle's velocity V_x along the longitudinal axis, the vehicle's velocity V_y along the lateral axis and the vehicle's yaw rate $\dot{\psi}$. The first two variables can be obtained with the use of onboard accelerometers while the third variable can be

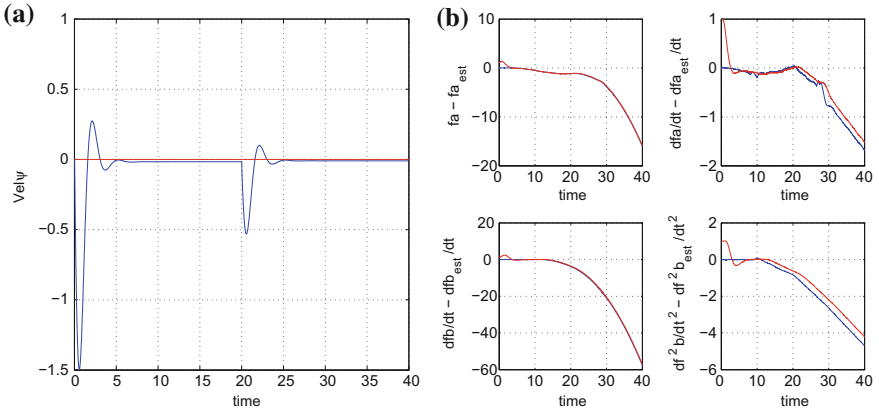

Fig. 8.39 Vehicle control under disturbances profile 2: **a** Convergence of yaw rate $\dot{\psi}$ (blue line) to the desirable setpoint (red line), **b** Estimation of the disturbance terms and of their rate of change (red line) and the associated real values (blue line)

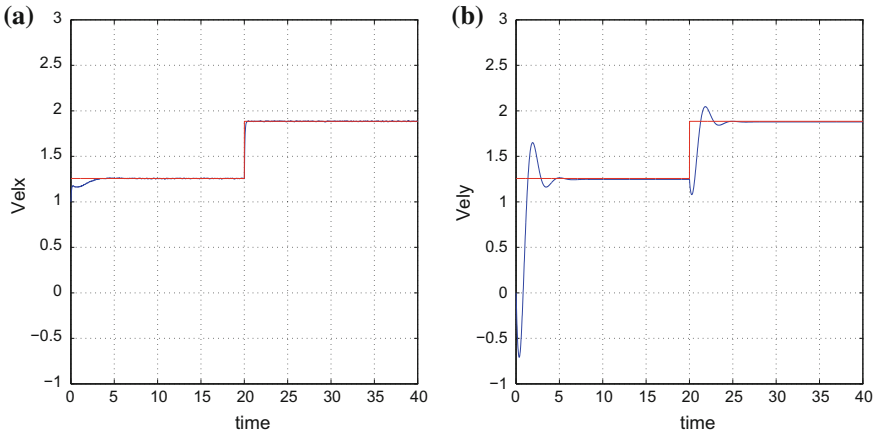

Fig. 8.40 Vehicle control under disturbances profile 3: **a** Convergence of x-axis velocity V_x (blue line) to the desirable setpoint (red line), **b** Convergence of the y-axis velocity V_y to the desirable setpoint (blue line) and the associated real values (red line)

obtained with the use of a gyrocompass. The longitudinal axis of the vehicle is denoted as x-axis, while the lateral axis of the vehicle is denoted as y-axis. As it can be seen in Figs. 8.36, 8.37, 8.38, 8.39, 8.40, 8.41, 8.42 and 8.43 the proposed nonlinear controller achieved accurate tracking of velocity setpoints. Moreover, the efficient

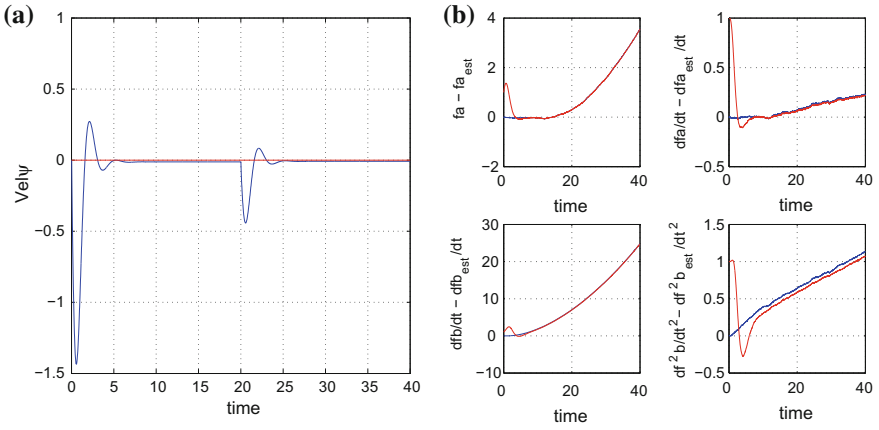

Fig. 8.41 Vehicle control under disturbances profile 3: **a** Convergence of yaw rate $\dot{\psi}$ (blue line) to the desirable setpoint (red line), **b** Estimation of the disturbance terms and of their rate of change (red line) and the associated real values (blue line)

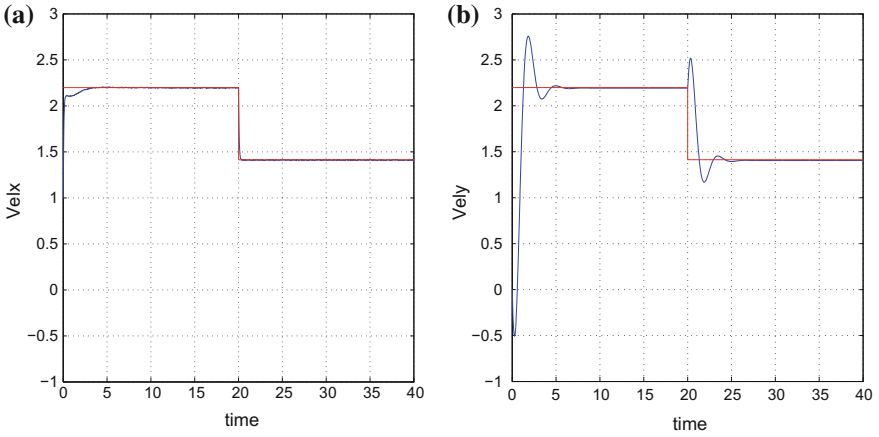

Fig. 8.42 Vehicle control under disturbances profile 4: **a** Convergence of x-axis velocity V_x (blue line) to the desirable setpoint (red line), **b** Convergence of the y-axis velocity V_y (blue line) to the desirable setpoint (red line)

estimation of disturbance forces and torques that was achieved by the Kalman Filter-based disturbance estimator enabled their compensation through the inclusion of an additional control term in the loop.

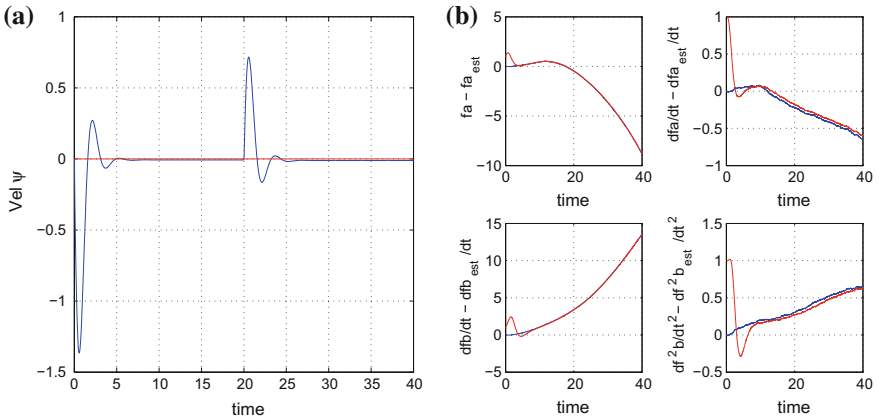

Fig. 8.43 Vehicle control under disturbances profile 4: **a** Convergence of yaw rate $\dot{\psi}$ (blue line) to the desirable setpoint (red line), **b** Estimation of the disturbance terms and of their rate of change (red line) and the associated real values (blue line)

Chapter 9
Unmanned Aerial Vehicles

Abstract The multi-DOF dynamic model of unmanned aerial vehicles (UAVs) is a highly nonlinear one and its control can be performed again with (i) global linearization control methods, (ii) local linearization control methods and (iii) Lyapunov analysis-based methods. In approach (i) the dynamic model of the UAV is transformed into an equivalent linear description through the application of a change of variables (diffeomorphisms). In (ii) the nonlinear model of the UAV is decomposed into local linear models for which linear feedback controllers are designed and next the aim is to select the feedback control gains so as to assure the global asymptotic stability of the control loop. In (iii) the objective is to define an energy function for the UAV (Lyapunov function) and to demonstrate that through suitable selection of the feedback control the first derivative of the energy function is always negative and thus the global stability of the control loop is assured. The latter approach is particularly suitable for model-free control of UAVs and takes the form of adaptive control methods. This chapter analyzes the aforementioned control approaches for UAVs and proves global asymptotic stability for all considered control approaches (i) to (iii). The robustness of the aforementioned control methods to model uncertainty and external perturbations is confirmed. Besides elaborated nonlinear filtering approaches are developed that allow for accurate estimation of the state vector of the UAVs through the processing of measurements coming from a limited number of sensors. In particular this chapter treats the following topics: (a) Control of UAVs based on global linearization methods, (b) Control of UAVs based on approximate linearization methods.

9.1 Chapter Overview

The present chapter treats the following topics: (a) Control of UAVs based on global linearization methods, (b) Control of UAVs based on approximate linearization methods.

With reference to (a) the chapter uses a differential flatness theory-based implementation of the Kalman Filter (known as Derivative-free nonlinear Kalman Filter) for developing a robust controller which can be applied to quadropters. The control

G. Rigatos and K. Busawon, *Robotic Manipulators and Vehicles*,
Studies in Systems, Decision and Control 152,
https://doi.org/10.1007/978-3-319-77851-8_9

problem for quadropters is non-trivial and becomes further complicated if this robot is subject to model uncertainties and external disturbances. Using differential flatness theory it is shown that the model of a quadropter can be transformed into linear canonical form. For the linearized equivalent of the quadropter it is shown that a state feedback controller can be designed. Since certain elements of the state vector of the linearized system cannot be measured directly, it is proposed to estimate them with the use of the previously analyzed Derivative-free nonlinear Kalman Filter. Moreover, by redesigning the Kalman Filter as a disturbance observer, it is is shown that one can estimate simultaneously external disturbances terms that affect the quadropter or disturbance terms which are associated with parametric uncertainty.

With reference to (b) the chapter applies nonlinear H-infinity (optimal) control the dynamic model of 6-DOF UAVs. First, the dynamic model of the UAV undergoes approximate linearization, through Taylor series expansion, round local operating points which are defined at each time instant by the present value of the system's state vector and the last value of the control input that was exerted on it. The linearization procedure requires the computation of Jacobian matrices at the aforementioned operating points. Next, for the linearized equivalent model of the UAV, an H-infinity feedback control loop is designed. The computation of the optimal control input requires the solution of an algebraic Riccati equation at each iteration of the control algorithm. The known robustness properties of H-infinity control enable compensation of model uncertainty and rejection of the perturbation terms that affect the UAV. The stability of the control loop is proven through Lyapunov analysis.

9.2 Control of UAVs Based on Global Linearization

9.2.1 Outline

Quadrotors are four-rotor helicopters characterized by a nonlinear 6-DOF unstable dynamical model. To achieve autonomous navigation of the quadrotors it is necessary to design efficient control algorithms that will exhibit robustness to parametric uncertainties and to external disturbances. One can cite several results on quadrotors' control. An approach for quadrotors' control that is based on the transformation of their dynamical model in the linear canonical form and which is consequently directly associated with differential flatness theory has been given in [576]. Moreover, in [6] a flatness-based control approach is applied to quadrotors' motion control. A predictive controller complemented by an H_∞ term for additional robustness has been analyzed and tested in the quadrotor's flight control problem in [401, 403]. In [55] motion control of the quadrotor was implemented using controllers of the LQR-type and of the PID-type, while Kalman Filtering has been used to provide position estimates out of a visual measurements system. In [77] two control strategies are employed as baseline controllers for the quadrotor's model: a LQR controller which

is based on a linearized model of the quadrotor and a Sliding Mode Controller which is based on a nonlinear model of the quadrotor. Moreover, differential flatness theory has been used for trajectory planning. In [261] and in [135] adaptive control schemes have been proposed for the quadrotor's model. The stability of the control loop is confirmed through the Lyapunov approach. In [48] quadrotor's control with the use of a sliding-mode controller and a sliding-mode disturbance observer has been proposed.

In this section a new control method is developed first for quadrotors after applying global linearization of the UAV's dynamic model. The method comprises differential flatness theory together with the use of a disturbance observer. This state and perturbations observer is also in accordance to differential flatness theory and is the so-called Derivative-free nonlinear Kalman Filter. The differential flatness theory-based design of the controller uses a change of coordinates (diffeomorphism) that transforms the state-space equation of the quadrotor's model into the linear canonical (Brunovsky) form [57, 145, 322, 450, 476, 572]. For the linearized equivalent of the quadrotor it is easier to design a state feedback controller using techniques for linear feedback controllers' synthesis. To provide the quadrotor's control loop with additional robustness a disturbance observer is used. The disturbance observer makes use of the standard Kalman Filter recursion on the linearized model of the quadrotor. It is capable of estimating simultaneously the quadrotor's linear and rotational velocities, as well as the vector of disturbances that affect the quadrotor's model without the need to compute Jacobian matrices. The accurate estimation of the disturbance inputs enables to introduce an additional control term that compensates for the disturbances' effects. The accurate tracking of reference trajectories that is achieved by the quadrotor despite the existence of external disturbances is shown in simulation experiments.

As already analyzed, differential flatness theory has specific advantages when used in nonlinear control systems [57, 145, 322, 457, 476, 572]. Through an exact linearization of the system's state-space description, one can avoid the use of linear models with local validity in the controller's design. The controller performs efficiently despite the change of operating points. After the design of such a state feedback controller, one can consider the inclusion in the control loop of supplementary control terms that provide additional robustness. As mentioned above, it is also possible to use a disturbance estimator-based auxiliary control input for compensating for the effects of disturbances in the feedback control loop. Moreover, the use of differential flatness theory in the design of state estimators and filters has also several strong points. One can perform estimation of the complete state vector of the system without the need to compute partial derivatives and Jacobian matrices. Moreover, by avoiding numerical errors which are due to approximate linearization of the system's dynamic model linear estimation algorithms can be implemented. In the case of Kalman Filter this means that one can perform state estimation with the use of the standard Kalman Filter recursion, thus preserving the method's optimality features and providing state estimates of improved precision (e.g. comparing to Extended Kalman Filtering).

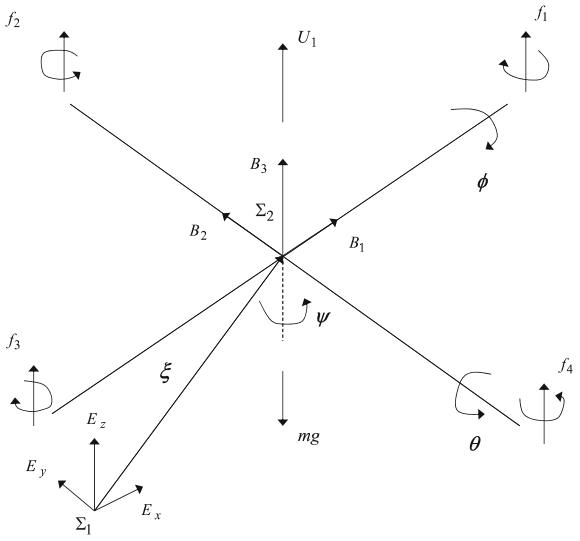

Fig. 9.1 Reference axes for the quadropter

9.2.2 Kinematic Model of the Quadropter

9.2.2.1 State-Space Model of the UAV

Two reference frames are defined [401, 403]. The first one $B = [B_1, B_2, B_3]$ is attached to the quadropter's body, whereas the second $E = [E_x, E_y, E_z]$ is considered to be an inertial coordinates system. As shown in Fig. 9.1, the Euler angles defining rotation round the axes of the body-fixed frame B_1, B_2 and B_3 are defined as θ, ϕ and ψ, respectively. The two reference frames are connected to each other through a rotation matrix

$$R = \begin{pmatrix} C\psi C\theta & C\psi S\theta S\phi - S\psi C\phi & C\psi S\theta C\phi + S\psi S\phi \\ S\psi C\theta & S\psi S\theta S\phi + C\psi C\phi & S\psi S\theta C\phi - C\psi S\phi \\ -S\theta & C\theta S\phi & C\theta C\phi \end{pmatrix} \tag{9.1}$$

where $C = cos(\cdot)$ and $S = sin(\cdot)$.

The connection between velocities in the two reference frames is as follows:

$$V_E = R \cdot V_B \tag{9.2}$$

where $V_E = [u_E, v_E, w_E]$ and $V_B = [u_B, v_B, w_B]$ are the linear velocity vectors expressed in the two reference frames. About the angular velocities in the two reference frames the following relation holds

$$\dot{\eta} = W^{-1}\omega \tag{9.3}$$

that is

$$\begin{pmatrix} \dot{\phi} \\ \dot{\theta} \\ \dot{\psi} \end{pmatrix} = \begin{pmatrix} 1 & sin(\phi)tan(\theta) & cos(\phi)tan(\theta) \\ 0 & cos(\phi) & -sin(\phi) \\ 0 & sin(\phi)sec(\theta) & cos(\phi)sec(\theta) \end{pmatrix} \begin{pmatrix} p \\ q \\ r \end{pmatrix} \tag{9.4}$$

where $\eta = [\phi, \theta, \psi]^T$ is the angular velocities vector in the inertial reference frame and $\omega = [p, q, r]^T$ is the angular velocities vector in the body-fixed reference frame.

9.2.3 Euler–Lagrange Equations for the Quadropter

The Euler–Lagrange equation for the quadropter is formulated as follows

$$\frac{d}{dt}\left(\frac{\partial L}{\partial \dot{q}_i}\right) - \frac{\partial L}{\partial q_i} = \begin{pmatrix} f_\xi \\ \tau_\eta \end{pmatrix} \tag{9.5}$$

where the Lagrangian is defined as $L(q, \dot{q}) = E_{C_{trans}} + E_{C_{rot}} - E_p$, $E_{C_{trans}}$ is the kinetic energy of the quadrotor due to translational motion, $E_{C_{rot}}$ is the kinetic energy of the quadrotor due to rotational motion and E_p is the total potential energy of the quadrotor due to lift. The generalized state vector is $q = [\xi^T, \eta^T]^T \in R^6$, $\tau_\eta \in R^3$ is the torques vector that causes rotation round the axes of the body-fixed reference frame, and $f_\xi = R\hat{f} + \alpha_T$ is the translational force applied to the quadropter due to the main control input U_1 along the z-axis direction, while $\alpha_T = [A_x, A_y, A_z]^T$ are the aerodynamic forces vector, defined along the axes of the inertial reference frame. Since the Lagrangian does not contain cross-coupling between the $\dot{\xi}$ and the $\dot{\eta}$ terms, the Lagrange–Euler equations can be divided into translational and rotational dynamics. The translational dynamics of the quadropter is given by

$$m\ddot{\xi} + mge_3 = f_\xi \tag{9.6}$$

where $e_3 = [0, 0, 1]^T$ is the unit vector along the z axis of the inertial reference frame. Eq. (9.6) can be written using the following three equations

$$\begin{gathered} \ddot{x} = \frac{1}{m}(sin(\psi)sin(\theta)cos(\phi) + sin(\psi)sin(\phi))U_1 + \frac{A_x}{m} \\ \ddot{y} = \frac{1}{m}(sin(\psi)sin(\theta)cos(\phi) - cos(\psi)sin(\phi))U_1 + \frac{A_y}{m} \\ \ddot{z} = -g + \frac{1}{m}(cos(\theta)cos(\phi))U_1 + \frac{A_z}{m} \end{gathered} \tag{9.7}$$

where m is the quadropter's mass and g is the gravitational acceleration. The rotational dynamics of the quadropter is given by

$$M(\eta)\ddot{\eta} + C(\eta, \dot{\eta})\dot{\eta} = \tau_\eta \tag{9.8}$$

where the inertia matrix $M(\eta)$ is defined as

$$M(\eta) = \begin{pmatrix} I_{xx} & 0 & -I_{xx}S\theta \\ 0 & I_{yy}C^2\phi + I_{zz}S^2\phi & (I_{yy} - I_{zz})C\phi S\phi C\theta \\ -I_{xx}S\theta & (I_{yy} - I_{zz})C\phi S\phi C\theta & I_{xx}S^2\theta + I_{yy}S^2\phi C^2\theta + I_{zz}C^2\phi C^2\theta \end{pmatrix} \tag{9.9}$$

and the Coriolis matrix is

$$C(\eta, \dot{\eta}) = \begin{pmatrix} c_{11} & c_{12} & c_{13} \\ c_{21} & c_{22} & c_{23} \\ c_{31} & c_{32} & c_{33} \end{pmatrix} \tag{9.10}$$

where the elements of the matrix are

$$\begin{aligned}
c_{11} &= 0 \\
c_{12} &= (I_{yy} - I_{zz})(\dot{\theta}C\phi S\phi + \dot{\psi}S^2\phi C\theta) + (I_{zz} - I_{yy})\dot{\psi}C^2\phi C\theta \\
c_{13} &= (I_{zz} - I_{yy})\dot{\psi}C\phi S\phi C^2\theta \\
c_{21} &= (I_{zz} - I_{yy})(\dot{\theta}C\phi S\phi + \dot{\psi}S^2\phi C\theta) + (I_{yy} - I_{zz})\dot{\psi}C^2\phi C\theta + I_{xx}\dot{\psi}C\theta \\
c_{22} &= (I_{zz} - I_{yy})\dot{\phi}C\phi S\phi \\
c_{23} &= -I_{xx}\dot{\psi}S\theta C\theta + I_{yy}\dot{\psi}S^2\phi C\theta S\theta + I_{zz}\dot{\psi}C^2\phi S\theta C\theta \\
c_{31} &= (I_{yy} - I_{zz})\dot{\psi}C^2\theta S\phi C\phi - I_{xx}\dot{\theta}C\theta \\
c_{32} &= (I_{zz} - I_{yy})(\dot{\theta}C\phi S\phi S\theta + \dot{\phi}S^2\phi C\theta) + (I_{yy} - I_{zz})\dot{\phi}C^2\phi C\theta + I_{xx}\dot{\psi}S\theta C\theta - \\
&\quad - I_{yy}\dot{\psi}S^2\phi S\theta C\theta - I_{zz}\dot{\psi}C^2\phi S\theta C\theta \\
c_{33} &= (I_{yy} - I_{zz})\dot{\phi}C\phi S\phi C^2\theta - I_{yy}\dot{\theta}S^2\phi C\theta S\theta - \\
&\quad - I_{zz}\dot{\theta}C^2\phi C\theta S\theta + I_{xx}\dot{\theta}C\theta S\theta
\end{aligned} \tag{9.11}$$

Thus, the mathematical model that describes the quadrotor's rotational motion is given by

$$\ddot{\eta} = M(\eta)^{-1}(\tau_\eta - C(\eta, \dot{\eta})\dot{\eta}) \tag{9.12}$$

Denoting $w = M(\eta)^{-1}(\tau_\eta - C(\eta, \dot{\eta})\dot{\eta})$, one has the following notation for the rotational dynamics

$$\begin{pmatrix} \ddot{\phi} \\ \ddot{\theta} \\ \ddot{\psi} \end{pmatrix} = \begin{pmatrix} w_a \\ w_b \\ w_c \end{pmatrix} \tag{9.13}$$

Considering small variations of the heading angle of the quadrotor round $\psi = \frac{\pi}{2}$, denoting $w_1 = U_1/m$ and taking also that the aerodynamic coefficients A_x, A_y, $A_z << m$, a simplified quadropter's model is formulated as follows [576]

$$\begin{array}{lll} \ddot{x} = w_1 sin(\phi) & \ddot{y} = w_1 cos(\phi) sin(\theta) & \ddot{z} = w_1 cos(\phi) cos(\theta) - g \\ \ddot{\phi} = w_a & \ddot{\theta} = w_b & \ddot{\psi} = w_c \end{array}. \tag{9.14}$$

9.2.4 Design of Flatness-Based Control for the Quadrotor's Model

It will be shown, that the quadrotor's model given in Eq. (9.14) is a differentially flat one, i.e. that all its state variables and the associated control inputs can be written as

functions of a new variable called flat output and of its derivatives. The following state variables are introduced $x_1 = x$, $x_2 = \dot{x}$, $x_3 = y$, $x_4 = \dot{y}$, $x_5 = z$, $x_6 = \dot{z}$, $x_7 = \phi$, $x_8 = \dot{\phi}$, $x_9 = \theta$, $x_{10} = \dot{\theta}$, $x_{11} = \psi$, $x_{12} = \dot{\psi}$. Thus, one has the following state-space description for the quadrotor's dynamic model

$$\begin{array}{llll} \dot{x}_1 = x_2 & \dot{x}_2 = w_1 sin(x_7) & \dot{x}_3 = x_4 & \dot{x}_4 = w_1 cos(x_7) sin(x_9) \\ \dot{x}_5 = x_6 & \dot{x}_6 = w_1 cos(x_7) cos(x_9) & \dot{x}_7 = x_8 & \dot{x}_8 = w_a \\ \dot{x}_9 = x_{10} & \dot{x}_{10} = w_b & \dot{x}_{11} = x_{12} & \dot{x}_{12} = w_c \end{array} \tag{9.15}$$

The flat output of the system is taken to be the vector $y_f = [x_1, x_3, x_5, x_7, x_9, x_{11}]^T$. It holds that

$$\begin{array}{llll} x_1 = [1\,0\,0\,0\,0\,0]y_f & x_2 = [1\,0\,0\,0\,0\,0]\dot{y}_f & x_3 = [0\,1\,0\,0\,0\,0]y_f & x_4 = [0\,1\,0\,0\,0\,0]\dot{y}_f \\ x_5 = [0\,0\,1\,0\,0\,0]y_f & x_6 = [0\,0\,1\,0\,0\,0]\dot{y}_f & x_7 = [0\,0\,0\,1\,0\,0]y_f & x_8 = [0\,0\,0\,1\,0\,0]\dot{y}_f \\ x_9 = [0\,0\,0\,0\,1\,0]y_f & x_{10} = [0\,0\,0\,0\,1\,0]\dot{y}_f & x_{11} = [0\,0\,0\,0\,0\,1]y_f & x_{12} = [0\,0\,0\,0\,0\,1]\dot{y}_f \end{array} \tag{9.16}$$

According to Eq. (9.16) all state variables of the quadropter can be written as functions of the flat output and its derivatives. Using this and Eq. (9.15) one also has that the control inputs of the quadropter's model, w_1, w_a, w_b and w_c can be written as functions of the flat output and its derivatives. Therefore, it is confirmed that the system is a differentially flat one. Defining now the new control inputs

$$\begin{array}{lll} v_1 = w_1 sin(x_7) & v_2 = w_1 cos(x_7) sin(x_9) & v_3 = w_1 cos(x_7) cos(x_9) \\ v_4 = w_a & v_5 = w_b & v_6 = w_c \end{array} \tag{9.17}$$

one has the following state-space description for the system

$$\begin{pmatrix} \dot{y}_{f_1} \\ \ddot{y}_{f_1} \\ \dot{y}_{f_2} \\ \ddot{y}_{f_2} \\ \dot{y}_{f_3} \\ \ddot{y}_{f_3} \\ \dot{y}_{f_4} \\ \ddot{y}_{f_4} \\ \dot{y}_{f_5} \\ \ddot{y}_{f_5} \\ \dot{y}_{f_6} \\ \ddot{y}_{f_6} \end{pmatrix} = \begin{pmatrix} 0\,1\,0\,0\,0\,0\,0\,0\,0\,0\,0\,0 \\ 0\,0\,0\,0\,0\,0\,0\,0\,0\,0\,0\,0 \\ 0\,0\,0\,1\,0\,0\,0\,0\,0\,0\,0\,0 \\ 0\,0\,0\,0\,0\,0\,0\,0\,0\,0\,0\,0 \\ 0\,0\,0\,0\,0\,1\,0\,0\,0\,0\,0\,0 \\ 0\,0\,0\,0\,0\,0\,0\,0\,0\,0\,0\,0 \\ 0\,0\,0\,0\,0\,0\,0\,1\,0\,0\,0\,0 \\ 0\,0\,0\,0\,0\,0\,0\,0\,0\,0\,0\,0 \\ 0\,0\,0\,0\,0\,0\,0\,0\,0\,1\,0\,0 \\ 0\,0\,0\,0\,0\,0\,0\,0\,0\,0\,0\,0 \\ 0\,0\,0\,0\,0\,0\,0\,0\,0\,0\,0\,1 \\ 0\,0\,0\,0\,0\,0\,0\,0\,0\,0\,0\,0 \end{pmatrix} \begin{pmatrix} y_{f_1} \\ \dot{y}_{f_1} \\ y_{f_2} \\ \dot{y}_{f_2} \\ y_{f_3} \\ \dot{y}_{f_3} \\ y_{f_4} \\ \dot{y}_{f_4} \\ y_{f_5} \\ \dot{y}_{f_5} \\ y_{f_6} \\ \dot{y}_{f_6} \end{pmatrix} + \begin{pmatrix} 0\,0\,0\,0\,0\,0 \\ 1\,0\,0\,0\,0\,0 \\ 0\,0\,0\,0\,0\,0 \\ 0\,1\,0\,0\,0\,0 \\ 0\,0\,0\,0\,0\,0 \\ 0\,0\,1\,0\,0\,0 \\ 0\,0\,0\,0\,0\,0 \\ 0\,0\,0\,1\,0\,0 \\ 0\,0\,0\,0\,0\,0 \\ 0\,0\,0\,0\,1\,0 \\ 0\,0\,0\,0\,0\,0 \\ 0\,0\,0\,0\,0\,1 \end{pmatrix} \begin{pmatrix} v_1 \\ v_2 \\ v_3 \\ v_4 \\ v_5 \\ v_6 \end{pmatrix} \tag{9.18}$$

and the measurement equation for this system becomes

$$\begin{pmatrix} z_1 \\ z_2 \\ z_3 \\ z_4 \\ z_5 \\ z_6 \end{pmatrix} = \begin{pmatrix} 1\,0\,0\,0\,0\,0\,0\,0\,0\,0\,0\,0 \\ 0\,0\,1\,0\,0\,0\,0\,0\,0\,0\,0\,0 \\ 0\,0\,0\,0\,1\,0\,0\,0\,0\,0\,0\,0 \\ 0\,0\,0\,0\,0\,0\,1\,0\,0\,0\,0\,0 \\ 0\,0\,0\,0\,0\,0\,0\,0\,1\,0\,0\,0 \\ 0\,0\,0\,0\,0\,0\,0\,0\,0\,0\,1\,0 \end{pmatrix} \begin{pmatrix} y_{f_1} \\ \dot{y}_{f_1} \\ y_{f_2} \\ \dot{y}_{f_2} \\ y_{f_3} \\ \dot{y}_{f_3} \\ y_{f_4} \\ \dot{y}_{f_4} \\ y_{f_5} \\ \dot{y}_{f_5} \\ y_{f_6} \\ \dot{y}_{f_6} \end{pmatrix} \tag{9.19}$$

Thus, using differential flatness theory the quadrotor's model has been written in a MIMO linear canonical (Brunovsky) form, which is both controllable and observable. After being written in the linear canonical form the quadrotor's state-space equation comprises 6 subsystems of the form

$$\ddot{y}_{f_i} = v_i,\ i = 1, \ldots, 6 \tag{9.20}$$

For each one of these subsystems a controller can be defined as follows

$$v_i = \ddot{y}^d_{f_i} - k_{d_i}(\dot{y}_{f_i} - \dot{y}^d_{f_i}) - k_{p_i}(y_{f_i} - y^d_{f_i}),\ i = 1, \ldots, 6 \tag{9.21}$$

The control scheme is implemented in the form of two cascading loops. The inner control loop controls rotation angles, while the outer control loop sets the desired values of the rotation angles so as to control position in the xyz-reference system. The computation of the reference setpoints for the rotation angles $\phi_d(t)$, $\theta_d(t)$ and $\psi_d(t)$ and for the cartesian coordinates $x_d(t)$, $y_d(t)$ and $z_d(t)$ takes into account the constraints imposed by the system dynamics.

9.2.5 *Estimation of the Quadrotor's Disturbance Forces and Torques with Kalman Filtering*

It was shown that the initial nonlinear model of the quadrotor can be written in the MIMO canonical form of Eqs. (9.18) and (9.19). Next, it is assumed that the quadrotor's model is affected by additive input disturbances, thus one has

$$\begin{aligned} \ddot{x}_1 &= (w_1 + d_1)sin(x_7) \\ \ddot{x}_3 &= (w_1 + d_1)cos(x_7)sin(x_9) \\ \ddot{x}_5 &= (w_1 + d_1)cos(x_7)cos(x_9) \\ \ddot{x}_7 &= w_a + d_a \\ \ddot{x}_9 &= w_b + d_b \\ \ddot{x}_{11} &= w_c + d_c \end{aligned} \tag{9.22}$$

or using the new state variables $y_{f_i}\ i = 1, \ldots, 12$ of the differential flatness theory-based model and the transformed inputs $v_i, i = 1, \ldots, 6$ one has

$$\begin{array}{c} \ddot{y}_{f_1} = v_1 + d_1 sin(y_{f_7}) \\ \ddot{y}_{f_3} = v_2 + d_1 cos(y_{f_7}) sin(y_{f_9}) \\ \ddot{y}_{f_5} = v_3 + d_1 cos(y_{f_7}) cos(y_{f_9}) \\ \ddot{y}_{f_7} = v_4 + d_a \\ \ddot{y}_{f_9} = v_5 + d_b \\ \ddot{y}_{f_{11}} = v_6 + d_c \end{array} \tag{9.23}$$

while by redefining the disturbance terms as $\tilde{d}_1 = d_1 sin(y_{f_7})$, $\tilde{d}_2 = d_1 cos(y_{f_7}) sin(y_{f_9})$, $\tilde{d}_3 = d_1 cos(y_{f_7}) cos(y_{f_9})$, $\tilde{d}_4 = d_a$, $\tilde{d}_5 = d_b$ and $\tilde{d}_6 = d_c$, the dynamics of the disturbed system can be written as

$$\begin{array}{cc} \ddot{y}_{f_1} = v_1 + \tilde{d}_1 & \ddot{y}_{f_3} = v_2 + \tilde{d}_2 \\ \ddot{y}_{f_5} = v_3 + \tilde{d}_3 & \ddot{y}_{f_7} = v_4 + \tilde{d}_4 \\ \ddot{y}_{f_9} = v_5 + \tilde{d}_5 & \ddot{y}_{f_{11}} = v_6 + \tilde{d}_6 \end{array} \tag{9.24}$$

The system's dynamics can be also written as $\dot{y}_{f_1} = y_{f_2}$, $\dot{y}_{f_2} = v_1 + \tilde{d}_1$, $\dot{y}_{f_3} = y_{f_4}$, $\dot{y}_{f_4} = v_2 + \tilde{d}_2$, $\dot{y}_{f_5} = y_{f_6}$, $\dot{y}_{f_6} = v_3 + \tilde{d}_3$, $\dot{y}_{f_7} = y_{f_8}$, $\dot{y}_{f_8} = v_4 + \tilde{d}_4$, $\dot{y}_{f_9} = y_{f_{10}}$, $\dot{y}_{f_{10}} = v_5 + \tilde{d}_5$, $\dot{y}_{f_{11}} = y_{f_6}$, $\dot{y}_{f_6} = v_6 + \tilde{d}_6$.

Without loss of generality, it is assumed that the dynamics of the disturbances terms are described by their second order derivative, i.e. $\dddot{\tilde{d}}_i = f_{d_i},\ i = 1, \ldots, 6$. Next, the extended state vector of the system is defined so as to include disturbance terms as well. Thus one has the following state variables

$$\begin{array}{cccccc} z_{f_1} = y_{f_1} & z_{f_2} = y_{f_2} & z_{f_3} = y_{f_3} & z_{f_4} = y_{f_4} & z_{f_5} = y_{f_5} & z_{f_6} = y_{f_6} \\ z_{f_7} = y_{f_7} & z_{f_8} = y_{f_8} & z_{f_9} = y_{f_9} & z_{f_{10}} = y_{f_{10}} & z_{f_{11}} = y_{f_{11}} & z_{f_{12}} = y_{f_{12}} \\ z_{f_{13}} = \tilde{d}_1 & z_{f_{14}} = \dot{\tilde{d}}_1 & z_{f_{15}} = \ddot{\tilde{d}}_1 & z_{f_{16}} = \tilde{d}_2 & z_{f_{17}} = \dot{\tilde{d}}_2 & z_{f_{18}} = \ddot{\tilde{d}}_2 \\ z_{f_{19}} = \tilde{d}_3 & z_{f_{20}} = \dot{\tilde{d}}_3 & z_{f_{21}} = \ddot{\tilde{d}}_3 & z_{f_{22}} = \tilde{d}_4 & z_{f_{23}} = \dot{\tilde{d}}_4 & z_{f_{24}} = \ddot{\tilde{d}}_4 \\ z_{f_{25}} = \tilde{d}_5 & z_{f_{26}} = \dot{\tilde{d}}_6 & z_{f_{27}} = \ddot{\tilde{d}}_5 & z_{f_{28}} = \tilde{d}_6 & z_{f_{29}} = \dot{\tilde{d}}_6 & z_{f_{30}} = \ddot{\tilde{d}}_6 \end{array} \tag{9.25}$$

Thus, the disturbed system can be described by a state-space equation of the form

$$\begin{array}{c} \dot{z}_f = A_f z_f + B_f v \\ z_f^{meas} = C_f z_f \end{array} \tag{9.26}$$

where $A_f \in R^{30\times 30}$, $B_f \in R^{30\times 6}$ and $C_f \in R^{6\times 30}$, with

$$A_f = \begin{pmatrix} 0_{1\times1} & 1 & 0_{1\times28} \\ 0_{1\times12} & 1 & 0_{1\times17} \\ 0_{1\times3} & 1 & 0_{1\times26} \\ 0_{1\times15} & 1 & 0_{1\times14} \\ 0_{1\times5} & 1 & 0_{1\times24} \\ 0_{1\times18} & 1 & 0_{1\times11} \\ 0_{1\times7} & 1 & 0_{1\times22} \\ 0_{1\times21} & 1 & 0_{1\times8} \\ 0_{1\times9} & 1 & 0_{1\times20} \\ 0_{1\times24} & 1 & 0_{1\times5} \\ 0_{1\times11} & 1 & 0_{1\times18} \\ 0_{1\times27} & 1 & 0_{1\times2} \\ 0_{1\times13} & 1 & 0_{1\times16} \\ 0_{1\times14} & 1 & 0_{1\times15} \\ 0_{1\times30} & & \\ 0_{1\times16} & 1 & 0_{1\times13} \\ 0_{1\times17} & 1 & 0_{1\times12} \\ 0_{1\times30} & & \\ 0_{1\times19} & 1 & 0_{1\times10} \\ 0_{1\times20} & 1 & 0_{1\times9} \\ 0_{1\times30} & & \\ 0_{1\times22} & 1 & 0_{1\times7} \\ 0_{1\times23} & 1 & 0_{1\times6} \\ 0_{1\times30} & & \\ 0_{1\times25} & 1 & 0_{1\times4} \\ 0_{1\times26} & 1 & 0_{1\times3} \\ 0_{1\times30} & & \\ 0_{1\times28} & 1 & 0_{1\times1} \\ 0_{1\times29} & 1 & \\ 0_{1\times30} & & \end{pmatrix} \quad B_f = \begin{pmatrix} 0_{1\times6} & & \\ 1 & 0_{1\times5} & \\ 0_{1\times1} & 1 & 0_{1\times4} \\ 0_{1\times6} & & \\ 0_{1\times2} & 1 & 0_{1\times3} \\ 0_{1\times6} & & \\ 0_{1\times3} & 1 & 0_{1\times2} \\ 0_{1\times6} & & \\ 0_{1\times4} & 1 & 0_{1\times1} \\ 0_{1\times6} & & \\ 0_{1\times5} & 1 & \\ 0_{18\times6} & & \end{pmatrix} \quad C_f = \begin{pmatrix} 1 & 0_{1\times29} & \\ 0_{1\times2} & 1 & 0_{1\times27} \\ 0_{1\times4} & 1 & 0_{1\times25} \\ 0_{1\times6} & 1 & 0_{1\times23} \\ 0_{1\times8} & 1 & 0_{1\times21} \\ 0_{1\times10} & 1 & 0_{1\times19} \end{pmatrix} \tag{9.27}$$

For the aforementioned model, and after carrying out discretization of matrices A_f, B_f and C_f with common discretization methods one can implement the standard Kalman Filter algorithm using Eqs. (9.29) and (9.30). This is Derivative-free nonlinear Kalman filtering for the model of the quadropter which, unlike EKF, is performed without the need to compute Jacobian matrices and does not introduce numerical errors due to approximate linearization with Taylor series expansion.

The dynamics of the disturbance terms $\tilde{d}_i$, $i = 1, \ldots, 6$ are taken to be unknown in the design of the associated disturbances' estimator. Defining as $\tilde{A}_d$, $\tilde{B}_d$, and $\tilde{C}_d$, the discrete-time equivalents of matrices $\tilde{A}_f$, $\tilde{B}_f$ and $\tilde{C}_f$ respectively, one has the following dynamics:

$$\dot{\hat{z}}_f = \tilde{A}_f \cdot \hat{z}_f + \tilde{B}_f \cdot \tilde{v} + K(z_f^{meas} - \tilde{C}_f \hat{z}_f) \tag{9.28}$$

where $K \in R^{30\times 6}$ is the state estimator's gain. The associated Kalman Filter-based disturbance estimator is given by [439, 445]

Measurement update:

$$\begin{aligned} K(k) &= P^{-}(k)\tilde{C}_d^T[\tilde{C}_d \cdot P^{-}(k)\tilde{C}_d^T + R]^{-1} \\ \hat{z}_f(k) &= \hat{z}_f^{-}(k) + K(k)[z_f^{meas}(k) - \tilde{C}_d\hat{z}_f^{-}(k)] \\ P(k) &= P^{-}(k) - K(k)\tilde{C}_d P^{-}(k) \end{aligned} \tag{9.29}$$

Time update:

$$\begin{aligned} P^{-}(k+1) &= \tilde{A}_d(k)P(k)\tilde{A}_d^T(k) + Q(k) \\ \hat{z}_f^{-}(k+1) &= \tilde{A}_d(k)\hat{z}_f(k) + \tilde{B}_d(k)\tilde{v}(k) \end{aligned} \tag{9.30}$$

To compensate for the effects of the disturbance forces it suffices to use in the control loop the modified control input vector

$$v = \begin{pmatrix} v_1 - \hat{\hat{d}}_1 \\ v_2 - \hat{\hat{d}}_2 \\ v_3 - \hat{\hat{d}}_3 \\ v_4 - \hat{\hat{d}}_4 \\ v_5 - \hat{\hat{d}}_5 \\ v_6 - \hat{\hat{d}}_6 \end{pmatrix} \text{ or } v = \begin{pmatrix} v_1 - \hat{z}_{13} \\ v_2 - \hat{z}_{16} \\ v_3 - \hat{z}_{19} \\ v_4 - \hat{z}_{22} \\ v_5 - \hat{z}_{25} \\ v_6 - \hat{z}_{28} \end{pmatrix}. \tag{9.31}$$

9.2.6 Simulation Tests

Initial simulation experiments were concerned with flight control of the quadropter in the disturbance-free case. The considered reference trajectories are shown in Fig. 9.2. The implementation of the flatness-based control enabled accurate tracking of the reference trajectories. Convergence has been achieved for the linear position and velocity variables to the associated setpoints as it can be seen in Figs. 9.3a, b and 9.4a. Moreover, there has been convergence of the angular position and velocity variables to the associated setpoints as it can be seen in Figs. 9.4a and 9.5a, b.

Additional simulation experiments were concerned with control of the quadropter in flight under disturbance forces and torques. The estimation of the disturbance forces and torques is shown in Fig. 9.6. The implementation of the flatness-based control enabled accurate tracking of the reference trajectories. There has been convergence of the linear position and velocity variables to the associated setpoints as it can be seen in Figs. 9.7a, b and 9.8a. Moreover, there has been convergence of the angular position and velocity variables to the associated setpoints as it can be seen in Figs. 9.8b and 9.9a, b.

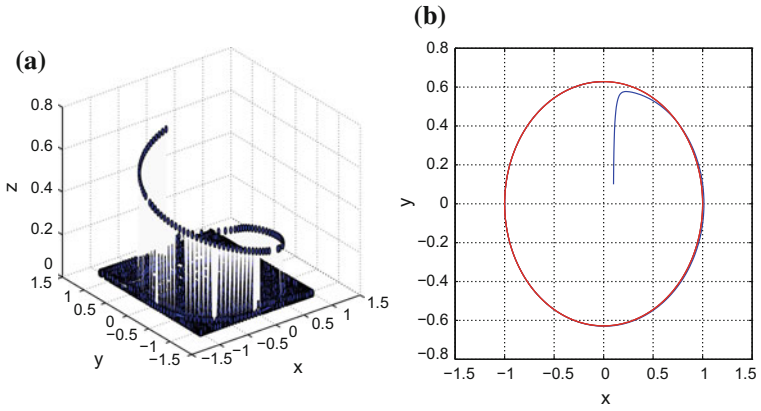

Fig. 9.2 Control of the quadrotor in the disturbance free-case: **a** trajectory of the quadrotor in the cartesian space, **b** projection of the quadrotor's trajectory in the xy plane

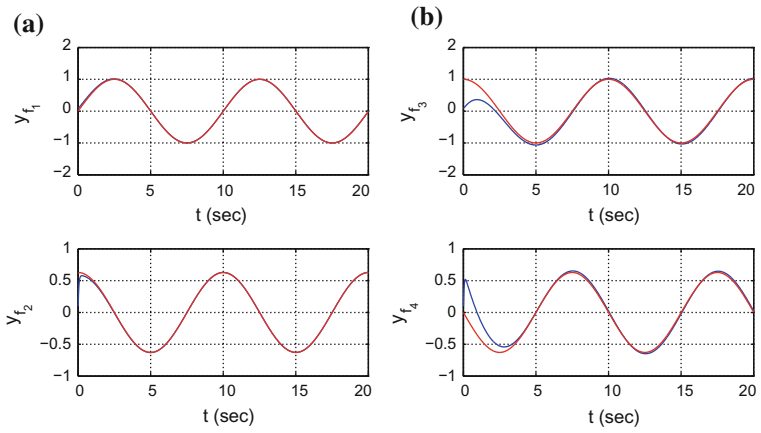

Fig. 9.3 Control of the quadrotor in the disturbance free-case: **a** position and velocity along the x axis, **b** position and velocity along the y axis

9.3 Control of UAVs Based on Approximate Linearization

9.3.1 Outline

The present section analyzes a nonlinear control method for unmanned aerial vehicles (UAVs) which is based on local linearization of the UAVs dynamics and on application of H-infinity control theory. As previously mentioned, the complete 6-DOF dynamic model of the UAV is a highly nonlinear one and its control can be performed with (i) global linearization control methods [6, 77, 152, 430, 438, 452, 457, 576], (ii) local linearization control methods [17, 55, 131, 212, 264, 401, 403, 450, 461, 480, 587] and (iii) Lyapunov analysis-based methods [13, 48, 60, 122,

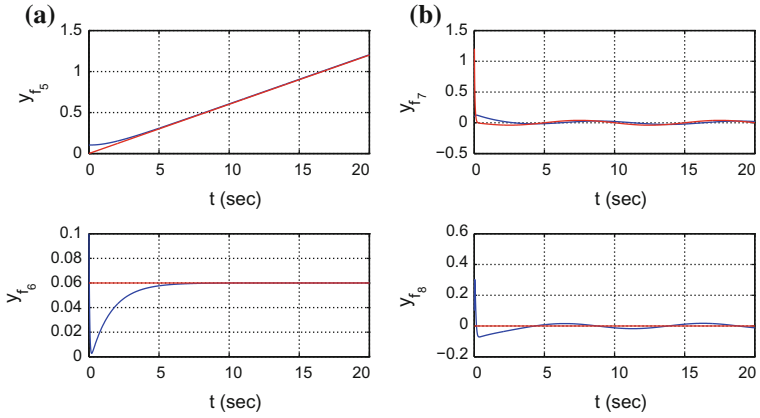

Fig. 9.4 Control of the quadrotor in the disturbance free-case: **a** position and velocity along the z axis, **b** rotation angle ϕ and associated angular speed

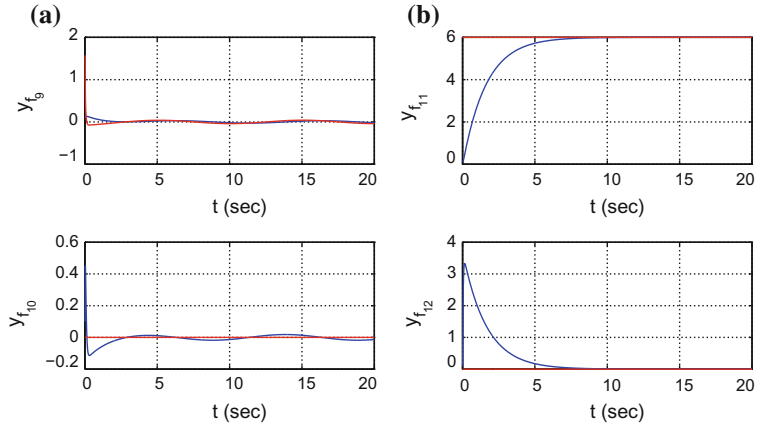

Fig. 9.5 Control of the quadrotor in the disturbance free-case: **a** rotation angle θ and associated angular speed, **b** rotation angle ψ and associated angular speed

135, 193, 261, 653]. In approach (i) the dynamic model of the UAV is transformed into an equivalent linear description through the application of a change of variables (diffeomorphisms). In (ii) the nonlinear model of the UAV is decomposed into local linear models for which linear feedback controllers are designed and next the aim is to select the feedback control gains so as to assure the global asymptotic stability of the control loop. In (iii) the objective is to define an energy function for the UAV (Lyapunov function) and to demonstrate that through suitable selection of the feedback control the first derivative of the energy function is always negative and thus the global stability of the control loop is assured. The latter approach is particularly suitable for model-free control of UAVs as in the case of adaptive control methods.

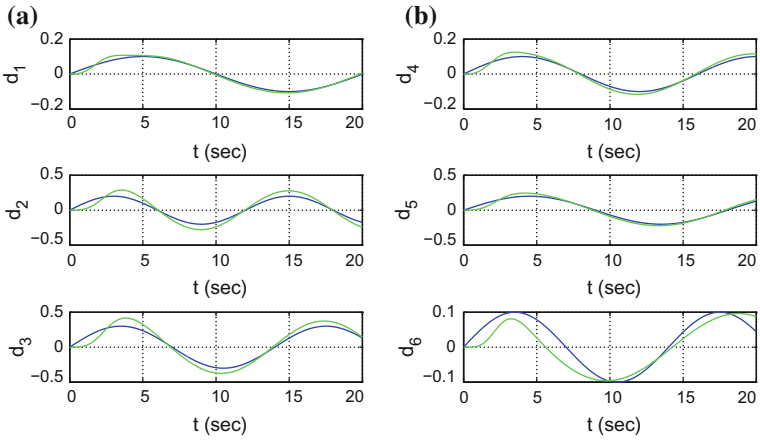

Fig. 9.6 Use of the Derivative-free nonlinear Kalman Filter in estimation of disturbances: **a** associated with linear motion, **b** associated with the rotational motion of the vehicle (blue line: real value, green line estimated value)

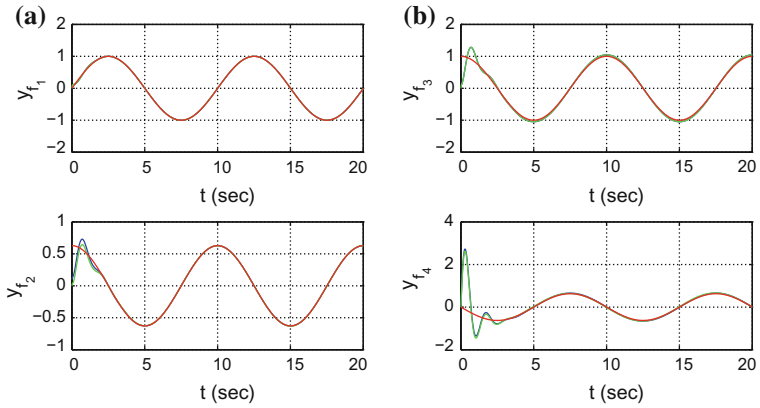

Fig. 9.7 Control of the quadrotor in the presence of external disturbances **a** position and velocity along the x axis, **b** position and velocity along the y axis (blue line: real value, green line estimated value, red line: setpoint)

In this section the control of the UAV makes use of an approach of local linearization. The linearization takes place round the UAV's local operating point which is defined at each time instant by the present value of the state vector and the last value of the control inputs vector [461]. The linearization is based on Taylor series expansion and on the computation of the associated Jacobian matrices. The modelling error, due to truncation of higher order terms in the Taylor series, is considered as perturbation which is compensated by the robustness of the control algorithm. For the linearized model of the UAV an H-infinity feedback controller is designed. A cost

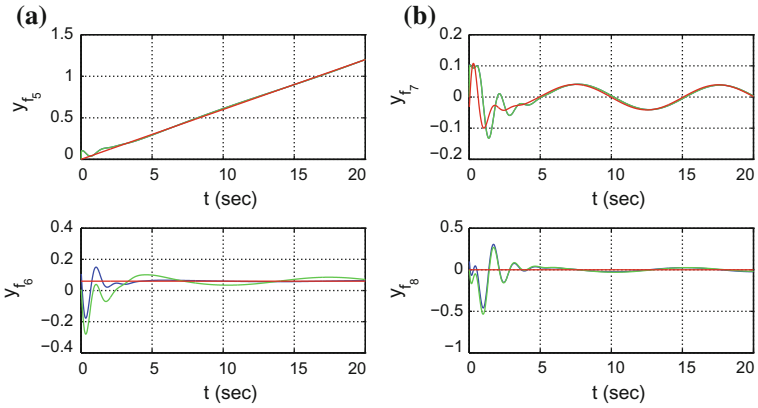

Fig. 9.8 Control of the quadrotor in the presence of external disturbances: **a** position and velocity along the z axis, **b** rotation angle ϕ and associated angular speed (blue line: real value, green line estimated value, red line: setpoint)

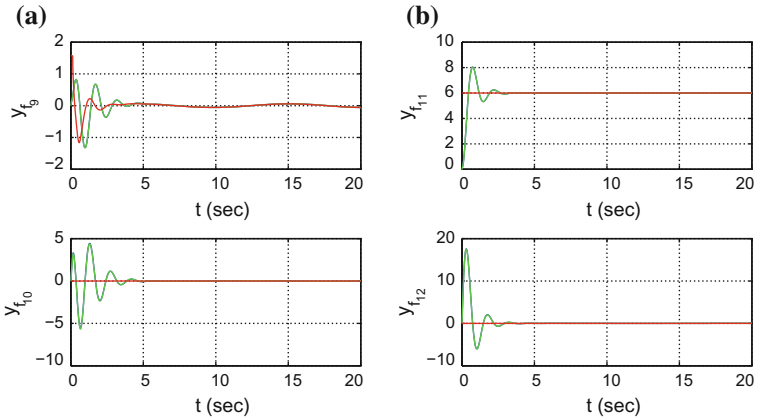

Fig. 9.9 Control of the quadrotor in the presence of disturbances: **a** rotation angle θ and associated angular speed, **b** rotation angle ψ and associated angular speed (blue line: real value, green line estimated value, red line: setpoint)

function is introduced comprising the weighted square of the error of the system's state vector (distance of the state vector from the reference setpoints).

As explained in previous applications of H-infinity control, this control scheme represents a differential game taking place between the control input which tries to minimize the above cost function and between the disturbances which try to maximize this objective function. The computation of the feedback control gain relies on the solution of an algebraic Riccati equation, which is performed at each iteration of the control algorithm. The solution of the Riccati equation provides a positive definite symmetric matrix which is used as a weighting coefficient in the computation of

the controller's feedback gain. The known robustness features of H-infinity control assure the elimination of perturbation effects, which implies compensation of model uncertainty terms, external disturbance inputs as well as of measurement noises. The stability properties of the control scheme are assured with the use of Lyapunov analysis. First, it is shown that the proposed UAV feedback control law results in H-infinity tracking performance which means robustness against modeling uncertainty and external perturbations. Under moderate conditions it is also shown that the control loop is also globally asymptotically stable. The tracking accuracy and the smooth transients in the proposed UAV control method are also confirmed through simulation experiments.

Comparing to nonlinear feedback control approaches which rely on exact feedback linearization of unmanned aerial vehicles (as the ones based on differential flatness theory [452, 457]) the proposed H_∞ control scheme is assessed as follows: (i) it uses an approximate linearization of the system's dynamic model which does not follow the elaborated transformations (diffeomorphisms) of the exact linearization methods, (ii) the method is applied directly on the initial nonlinear model of the UAV, and does not inverse transformations. In this manner it is unlikely to come against singularities in the computation of the UAV's real control inputs, (iii) the method retains the advantages of optimal control techniques, that is the best trade-off between setpoint tracking and moderate variations of the control inputs.

9.3.2 Dynamic Model of the UAV

9.3.2.1 State-Space Description of the UAV

By following the previous analysis of the dynamic model of the UAV, given in Sect. 9.2.3 and by considering that $w_a = \frac{1}{J_x}\tau_\phi$, $w_b = \frac{1}{J_y}\tau_\theta$, and $w_c = \frac{1}{J_z}\tau_\psi$, the following dynamic model of the UAV is obtained:

$$\begin{aligned}
\ddot{x} &= \tfrac{1}{m}[cos(\psi)sin(\theta)cos(\phi) + sin(\psi)sin(\phi)]U_1 + \tfrac{A_x}{m} \\
\ddot{y} &= \tfrac{1}{m}[sin(\psi)sin(\theta)cos(\phi) - cos(\psi)sin(\phi)]U_1 + \tfrac{A_y}{m} \\
\ddot{z} &= \tfrac{1}{m}[cos(\theta)cos(\phi)]U_1 + \tfrac{A_z}{m} - g \\
\ddot{\phi} &= \tfrac{1}{J_x}\tau_\phi \\
\ddot{\theta} &= \tfrac{1}{J_y}\tau_\theta \\
\ddot{\psi} &= \tfrac{1}{J_z}\tau_\psi
\end{aligned} \tag{9.32}$$

where x, y, z are the coordinates of the UAV's center of gravity in a cartesian reference frame, ϕ, θ, ψ are the Euler rotation angles describing roll, pitch and yaw motion respectively, m is the UAV's mass, J_x, J_y, J_z are the UAV's moments of inertia for rotation round the cartesian coordinates axes A_x, A_y, A_z are aerodynamic forces exerted on the UAV for motion along the cartesian axes and g is the acceleration of gravity.

Next, the UAV's dynamic model is written in state-space form by defining the following state variables: $x_1 = x$, $x_2 = \dot{x}$, $x_3 = y$, $x_4 = \dot{y}$, $x_5 = z$, $x_6 = \dot{z}$, $x_7 = \phi$, $x_8 = \dot{\phi}$, $x_9 = \theta$, $x_{10} = \dot{\theta}$, $x_{11} = \psi$, $x_{12} = \dot{\psi}$. Thus, one obtains:

$$\begin{array}{c}
\dot{x}_1 = x_2 \\
\dot{x}_2 = \frac{1}{m}[cos(\psi)sin(\theta)cos(\phi) + sin(\psi)sin(\phi)]U_1 + \frac{A_x}{m} \\
\dot{x}_3 = x_4 \\
\dot{x}_4 = \frac{1}{m}[sin(\psi)sin(\theta)cos(\phi) - cos(\psi)sin(\phi)]U_1 + \frac{A_y}{m} \\
\dot{x}_5 = x_6 \\
\dot{x}_6 = \frac{1}{m}[cos(\theta)cos(\phi)]U_1 + \frac{A_z}{m} - g \\
\dot{x}_7 = x_8 \\
\dot{x}_8 = \frac{1}{J_x}\tau_\phi \\
\dot{x}_9 = x_{10} \\
\dot{x}_{10} = \frac{1}{J_y}\tau_\theta \\
\dot{x}_{11} = x_{12} \\
\dot{x}_{12} = \frac{1}{J_z}\tau_\psi
\end{array} \tag{9.33}$$

or equivalently

$$\dot{x} = f(x, u) \tag{9.34}$$

which is analytically written as

$$\begin{pmatrix} \dot{x}_1 \\ \dot{x}_2 \\ \dot{x}_3 \\ \dot{x}_4 \\ \dot{x}_5 \\ \dot{x}_6 \\ \dot{x}_7 \\ \dot{x}_8 \\ \dot{x}_9 \\ \dot{x}_{10} \\ \dot{x}_{11} \\ \dot{x}_{12} \end{pmatrix} = \begin{pmatrix} x_2 \\ \frac{1}{m}[cos(\psi)sin(\theta)cos(\phi) + sin(\psi)sin(\phi)]u_1 + \frac{A_x}{m} \\ x_4 \\ \frac{1}{m}[sin(\psi)sin(\theta)cos(\phi) - cos(\psi)sin(\phi)]u_1 + \frac{A_y}{m} \\ x_6 \\ \frac{1}{m}[cos(\theta)cos(\phi)]u_1 + \frac{A_z}{m} - g \\ x_8 \\ \frac{1}{J_x}\tau_\phi \\ x_{10} \\ \frac{1}{J_y}\tau_\theta \\ x_{11} \\ \frac{1}{J_z}\tau_\psi \end{pmatrix} \tag{9.35}$$

where the input vector u is defined as $u = [u_1, u_2, u_3, u_4]^T = [U_1, \tau_\phi, \tau_\theta, \tau_\psi]^T$.

9.3.3 Linearization of the UAV's Dynamic Model

Linearization of the previous dynamic model of the UAV $\dot{x} = f(x, u)$ can be performed round local operating points (x^*, u^*), where x^* is the present value of the

UAV's state vector and u^* is the last value of the control input which has been exerted on the system. By applying Taylor series expansion one obtains

$$\dot{x} = J_x f \mid_{(x^*,u^*)} x + J_u f \mid_{(x^*,u^*)} u + \tilde{d} \tag{9.36}$$

or equivalently

$$\dot{x} = Ax + Bu + \tilde{d} \tag{9.37}$$

where $A = J_x f \mid_{(x^*,u^*)}$, $B = J_u f \mid_{(x^*,u^*)}$ and $\tilde{d}$ is the modelling error due to the truncation of higher order terms in the Taylor series expansion. Next, the Jacobian matrices of the UAV's dynamic model with respect to its state variables are computed

$$J_x f = \begin{pmatrix} \frac{\partial f_1}{\partial x_1} & \frac{\partial f_1}{\partial x_2} & \cdots\cdots & \frac{\partial f_1}{\partial x_n} \\ \frac{\partial f_2}{\partial x_1} & \frac{\partial f_2}{\partial x_2} & \cdots\cdots & \frac{\partial f_2}{\partial x_{12}} \\ \cdots & \cdots & \cdots\cdots & \cdots \\ \cdots & \cdots & \cdots\cdots & \cdots \\ \frac{\partial f_{11}}{\partial x_1} & \frac{\partial f_{11}}{\partial x_2} & \cdots\cdots & \frac{\partial f_{11}}{\partial x_{12}} \\ \frac{\partial f_{12}}{\partial x_1} & \frac{\partial f_{12}}{\partial x_2} & \cdots\cdots & \frac{\partial f_{12}}{\partial x_{12}} \end{pmatrix} \tag{9.38}$$

It holds that the 1st row of the Jacobian matrix $J_x f$ is

$$\begin{array}{cccc} \frac{\partial f_1}{\partial x_1} = 0 & \frac{\partial f_1}{\partial x_2} = 1 & \frac{\partial f_1}{\partial x_3} = 0 & \frac{\partial f_1}{\partial x_4} = 0 \\ \frac{\partial f_1}{\partial x_5} = 0 & \frac{\partial f_1}{\partial x_6} = 0 & \frac{\partial f_1}{\partial x_7} = 0 & \frac{\partial f_1}{\partial x_8} = 0 \\ \frac{\partial f_1}{\partial x_9} = 0 & \frac{\partial f_1}{\partial x_{10}} = 0 & \frac{\partial f_1}{\partial x_{11}} = 0 & \frac{\partial f_1}{\partial x_{12}} = 0 \end{array} \tag{9.39}$$

2nd row of the Jacobian matrix $J_x f$

$$\begin{array}{cccc} & \frac{\partial f_2}{\partial x_1} = 0 & \frac{\partial f_2}{\partial x_2} = 0 & \frac{\partial f_2}{\partial x_3} = 0 \\ & \frac{\partial f_2}{\partial x_4} = 0 & \frac{\partial f_2}{\partial x_5} = 0 & \frac{\partial f_2}{\partial x_6} = 0 \\ \frac{\partial f_2}{\partial x_7} = \frac{1}{m}[-cos(x_{11})sin(x_9)sin(x_7) - sin(x_{11}sin(x_7))]u_1 & & & \frac{\partial f_2}{\partial x_8} = 0 \\ & \frac{\partial f_2}{\partial x_9} = \frac{1}{m}[cos(x_{11})cos(x_9)cos(x_7)]u_1 & & \frac{\partial f_2}{\partial x_{10}} = 0 \\ \frac{\partial f_2}{\partial x_{11}} = \frac{1}{m}[-sin(x_{11})sin(x_9)cos(x_7) + cos(x_{11})cos(x_7)]u_1 & & & \frac{\partial f_2}{\partial x_{12}} = 0 \end{array} \tag{9.40}$$

3rd row of the Jacobian matrix $J_x f$

$$\begin{array}{cccc} \frac{\partial f_1}{\partial x_1} = 0 & \frac{\partial f_1}{\partial x_2} = 0 & \frac{\partial f_1}{\partial x_3} = 0 & \frac{\partial f_1}{\partial x_4} = 1 \\ \frac{\partial f_1}{\partial x_5} = 0 & \frac{\partial f_1}{\partial x_6} = 0 & \frac{\partial f_1}{\partial x_7} = 0 & \frac{\partial f_1}{\partial x_8} = 0 \\ \frac{\partial f_1}{\partial x_9} = 0 & \frac{\partial f_1}{\partial x_{10}} = 0 & & \\ \frac{\partial f_1}{\partial x_{11}} = 0 & \frac{\partial f_1}{\partial x_{12}} = 0 & & \end{array} \tag{9.41}$$

4th row of the Jacobian matrix $J_x f$

$$\begin{gathered}
\frac{\partial f_4}{\partial x_1} = 0 \;\; \frac{\partial f_4}{\partial x_2} = 0 \;\; \frac{\partial f_4}{\partial x_3} = 0 \\
\frac{\partial f_4}{\partial x_4} = 0 \;\; \frac{\partial f_4}{\partial x_5} = 0 \;\; \frac{\partial f_4}{\partial x_6} = 0 \\
\frac{\partial f_4}{\partial x_7} = \frac{1}{m}[sin(x_{11})sin(x_9)cos(x_7) - cos(x_{11}cos(x_7))]u_1 \\
\frac{\partial f_4}{\partial x_8} = 0 \;\; \frac{\partial f_4}{\partial x_9} = \frac{1}{m}[sin(x_{11})cos(x_9)cos(x_7)]u_1 \\
\frac{\partial f_4}{\partial x_{10}} = 0 \;\; \frac{\partial f_4}{\partial x_{11}} = \frac{1}{m}[cos(x_{11})sin(x_9)sin(x_7) + sin(x_{11})sin(x_7)]u_1 \;\; \frac{\partial f_4}{\partial x_{12}} = 0
\end{gathered} \tag{9.42}$$

5th row of the Jacobian matrix $J_x f$

$$\begin{gathered}
\frac{\partial f_5}{\partial x_1} = 0 \;\; \frac{\partial f_5}{\partial x_2} = 0 \;\; \frac{\partial f_5}{\partial x_3} = 0 \;\; \frac{\partial f_5}{\partial x_4} = 0 \\
\frac{\partial f_5}{\partial x_5} = 0 \;\; \frac{\partial f_5}{\partial x_6} = 1 \;\; \frac{\partial f_5}{\partial x_7} = 0 \;\; \frac{\partial f_5}{\partial x_8} = 0 \\
\frac{\partial f_5}{\partial x_9} = 0 \;\; \frac{\partial f_5}{\partial x_{10}} = 0 \;\; \frac{\partial f_5}{\partial x_{11}} = 0 \;\; \frac{\partial f_5}{\partial x_{12}} = 0
\end{gathered} \tag{9.43}$$

6th row of the Jacobian matrix $J_x f$

$$\begin{gathered}
\frac{\partial f_6}{\partial x_1} = 0 \;\; \frac{\partial f_6}{\partial x_2} = 0 \;\; \frac{\partial f_6}{\partial x_3} = 0 \\
\frac{\partial f_6}{\partial x_4} = 0 \;\; \frac{\partial f_6}{\partial x_5} = 0 \;\; \frac{\partial f_6}{\partial x_6} = 0 \\
\frac{\partial f_6}{\partial x_7} = \frac{1}{m}[-cos(x_9)sin(x_7)]u_1 \;\; \frac{\partial f_6}{\partial x_8} = 0 \;\; \frac{\partial f_6}{\partial x_9} = \frac{1}{m}[-sin(x_9)cos(x_7)]u_1 \\
\frac{\partial f_6}{\partial x_{10}} = 0 \;\; \frac{\partial f_6}{\partial x_{11}} = 0 \;\; \frac{\partial f_6}{\partial x_{12}} = 0
\end{gathered} \tag{9.44}$$

7th row of the Jacobian matrix $J_x f$

$$\begin{gathered}
\frac{\partial f_7}{\partial x_1} = 0 \;\; \frac{\partial f_7}{\partial x_2} = 0 \;\; \frac{\partial f_7}{\partial x_3} = 0 \;\; \frac{\partial f_7}{\partial x_4} = 0 \\
\frac{\partial f_7}{\partial x_5} = 0 \;\; \frac{\partial f_7}{\partial x_6} = 0 \;\; \frac{\partial f_7}{\partial x_7} = 0 \;\; \frac{\partial f_7}{\partial x_8} = 1 \\
\frac{\partial f_7}{\partial x_9} = 0 \;\; \frac{\partial f_7}{\partial x_{10}} = 0 \;\; \frac{\partial f_7}{\partial x_{11}} = 0 \;\; \frac{\partial f_7}{\partial x_{12}} = 0
\end{gathered} \tag{9.45}$$

8th row of the Jacobian matrix $J_x f$

$$\begin{gathered}
\frac{\partial f_7}{\partial x_1} = 0 \;\; \frac{\partial f_7}{\partial x_2} = 0 \;\; \frac{\partial f_7}{\partial x_3} = 0 \;\; \frac{\partial f_7}{\partial x_4} = 0 \\
\frac{\partial f_7}{\partial x_5} = 0 \;\; \frac{\partial f_7}{\partial x_6} = 0 \;\; \frac{\partial f_7}{\partial x_7} = 0 \;\; \frac{\partial f_7}{\partial x_8} = 0 \\
\frac{\partial f_7}{\partial x_9} = 0 \;\; \frac{\partial f_7}{\partial x_{10}} = 0 \;\; \frac{\partial f_7}{\partial x_{11}} = 0 \;\; \frac{\partial f_7}{\partial x_{12}} = 0
\end{gathered} \tag{9.46}$$

9th row of the Jacobian matrix $J_x f$

$$\begin{gathered}
\frac{\partial f_9}{\partial x_1} = 0 \;\; \frac{\partial f_9}{\partial x_2} = 0 \;\; \frac{\partial f_9}{\partial x_3} = 0 \;\; \frac{\partial f_9}{\partial x_4} = 0 \\
\frac{\partial f_9}{\partial x_5} = 0 \;\; \frac{\partial f_9}{\partial x_6} = 0 \;\; \frac{\partial f_9}{\partial x_7} = 0 \;\; \frac{\partial f_9}{\partial x_8} = 0 \\
\frac{\partial f_9}{\partial x_9} = 0 \;\; \frac{\partial f_9}{\partial x_{10}} = 1 \;\; \frac{\partial f_9}{\partial x_{11}} = 0 \;\; \frac{\partial f_9}{\partial x_{12}} = 0
\end{gathered} \tag{9.47}$$

10th row of the Jacobian matrix $J_x f$

$$\begin{array}{cccc} \frac{\partial f_{10}}{\partial x_1} = 0 & \frac{\partial f_{10}}{\partial x_2} = 0 & \frac{\partial f_{10}}{\partial x_3} = 0 & \frac{\partial f_{10}}{\partial x_4} = 0 \\ \frac{\partial f_{10}}{\partial x_5} = 0 & \frac{\partial f_{10}}{\partial x_6} = 0 & \frac{\partial f_{10}}{\partial x_7} = 0 & \frac{\partial f_{10}}{\partial x_8} = 0 \\ \frac{\partial f_{10}}{\partial x_9} = 0 & \frac{\partial f_{10}}{\partial x_{10}} = 0 & \frac{\partial f_{10}}{\partial x_{11}} = 0 & \frac{\partial f_{10}}{\partial x_{12}} = 0 \end{array} \tag{9.48}$$

11th row of the Jacobian matrix $J_x f$

$$\begin{array}{cccc} \frac{\partial f_{11}}{\partial x_1} = 0 & \frac{\partial f_{11}}{\partial x_2} = 0 & \frac{\partial f_{11}}{\partial x_3} = 0 & \frac{\partial f_{11}}{\partial x_4} = 0 \\ \frac{\partial f_{11}}{\partial x_5} = 0 & \frac{\partial f_{11}}{\partial x_6} = 0 & \frac{\partial f_{11}}{\partial x_7} = 0 & \frac{\partial f_{11}}{\partial x_8} = 0 \\ \frac{\partial f_{11}}{\partial x_9} = 0 & \frac{\partial f_{11}}{\partial x_{10}} = 0 & \frac{\partial f_{11}}{\partial x_{11}} = 1 & \frac{\partial f_{11}}{\partial x_{12}} = 0 \end{array} \tag{9.49}$$

12th row of the Jacobian matrix $J_x f$

$$\begin{array}{cccc} \frac{\partial f_{12}}{\partial x_1} = 0 & \frac{\partial f_{12}}{\partial x_2} = 0 & \frac{\partial f_{12}}{\partial x_3} = 0 & \frac{\partial f_{12}}{\partial x_4} = 0 \\ \frac{\partial f_{12}}{\partial x_5} = 0 & \frac{\partial f_{12}}{\partial x_6} = 0 & \frac{\partial f_{12}}{\partial x_7} = 0 & \frac{\partial f_{12}}{\partial x_8} = 0 \\ \frac{\partial f_{12}}{\partial x_9} = 0 & \frac{\partial f_{12}}{\partial x_{10}} = 0 & \frac{\partial f_{12}}{\partial x_{11}} = 0 & \frac{\partial f_{12}}{\partial x_{12}} = 0 \end{array} \tag{9.50}$$

Next, the Jacobian matrix of the UAV is computed with respect to the elements of the control input vector $U = [u_1, u_2, u_3, u_4]^T = [U_1, \tau_\phi, \tau_\theta, \tau_\psi]^T$. It holds that

$$J_u f = \begin{pmatrix} \frac{\partial f_1}{\partial u_1} & \frac{\partial f_1}{\partial u_2} & \frac{\partial f_1}{\partial u_3} & \frac{\partial f_1}{\partial u_4} \\ \frac{\partial f_2}{\partial u_1} & \frac{\partial f_2}{\partial u_2} & \frac{\partial f_2}{\partial u_3} & \frac{\partial f_2}{\partial u_4} \\ \cdots & \cdots & \cdots & \cdots \\ \cdots & \cdots & \cdots & \cdots \\ \frac{\partial f_{11}}{\partial u_1} & \frac{\partial f_{11}}{\partial u_2} & \frac{\partial f_{11}}{\partial u_3} & \frac{\partial f_{11}}{\partial u_4} \\ \frac{\partial f_{12}}{\partial u_1} & \frac{\partial f_{12}}{\partial u_2} & \frac{\partial f_{12}}{\partial u_3} & \frac{\partial f_{12}}{\partial u_4} \end{pmatrix} \tag{9.51}$$

About the 1st row of the Jacobian matrix $J_u f$ it holds

$$\frac{\partial f_1}{\partial u_1} = 0 \ \frac{\partial f_1}{\partial u_2} = 0 \ \frac{\partial f_1}{\partial u_3} = 0 \ \frac{\partial f_1}{\partial u_4} = 0 \tag{9.52}$$

About the 2nd row of the Jacobian matrix $J_u f$ it holds

$$\begin{array}{cc} \frac{\partial f_2}{\partial u_1} = \frac{1}{m}[cos(x_{11})sin((x_9)cos(x_7) + sin(x_{11})cos(x_7)] & \frac{\partial f_2}{\partial u_2} = 0 \\ \frac{\partial f_2}{\partial u_3} = 0 & \frac{\partial f_2}{\partial u_4} = 0 \end{array} \tag{9.53}$$

About the 3rd row of the Jacobian matrix $J_u f$ it holds

$$\frac{\partial f_1}{\partial u_1} = 0 \ \frac{\partial f_1}{\partial u_2} = 0 \ \frac{\partial f_1}{\partial u_3} = 0 \ \frac{\partial f_1}{\partial u_4} = 0 \tag{9.54}$$

About the 4th row of the Jacobian matrix $J_u f$ it holds

$$\begin{array}{ccc} \frac{\partial f_4}{\partial u_1} = \frac{1}{m}[sin(x_{11})sin((x_9)sin(x_7) - cos(x_{11})sin(x_7)] & \frac{\partial f_4}{\partial u_2} = 0 \\ \frac{\partial f_4}{\partial u_3} = 0 & \frac{\partial f_4}{\partial u_4} = 0 \end{array} \tag{9.55}$$

About the 5th row of the Jacobian matrix $J_u f$ it holds

$$\frac{\partial f_5}{\partial u_1} = 0 \ \frac{\partial f_5}{\partial u_2} = 0 \ \frac{\partial f_5}{\partial u_3} = 0 \ \frac{\partial f_5}{\partial u_4} = 0 \tag{9.56}$$

About the 6th row of the Jacobian matrix $J_u f$ it holds

$$\begin{array}{ccc} \frac{\partial f_6}{\partial u_1} = \frac{1}{m}[cos((x_9)cos(x_7)] & \frac{\partial f_6}{\partial u_2} = 0 \\ \frac{\partial f_6}{\partial u_3} = 0 & \frac{\partial f_6}{\partial u_4} = 0 \end{array} \tag{9.57}$$

About the 7th row of the Jacobian matrix $J_u f$ it holds

$$\frac{\partial f_7}{\partial u_1} = 0 \ \frac{\partial f_7}{\partial u_2} = 0 \ \frac{\partial f_7}{\partial u_3} = 0 \ \frac{\partial f_7}{\partial u_4} = 0 \tag{9.58}$$

About the 8th row of the Jacobian matrix $J_u f$ it holds

$$\frac{\partial f_8}{\partial u_1} = 0 \ \frac{\partial f_8}{\partial u_2} = \frac{1}{J_x} \ \frac{\partial f_8}{\partial u_3} = 0 \ \frac{\partial f_8}{\partial u_4} = 0 \tag{9.59}$$

About the 9th row of the Jacobian matrix $J_u f$ it holds

$$\frac{\partial f_9}{\partial u_1} = 0 \ \frac{\partial f_9}{\partial u_2} = 0 \ \frac{\partial f_9}{\partial u_3} = 0 \ \frac{\partial f_9}{\partial u_4} = 0 \tag{9.60}$$

About the 10th row of the Jacobian matrix $J_u f$ it holds

$$\frac{\partial f_{10}}{\partial u_1} = 0 \ \frac{\partial f_{10}}{\partial u_2} = 0 \ \frac{\partial f_{10}}{\partial u_3} = \frac{1}{J_y} \ \frac{\partial f_{10}}{\partial u_4} = 0 \tag{9.61}$$

About the 11th row of the Jacobian matrix $J_u f$ it holds

$$\frac{\partial f_{11}}{\partial u_1} = 0 \ \frac{\partial f_{11}}{\partial u_2} = 0 \ \frac{\partial f_{11}}{\partial u_3} = 0 \ \frac{\partial f_{11}}{\partial u_4} = 0 \tag{9.62}$$

About the 12th row of the Jacobian matrix $J_u f$ it holds

$$\frac{\partial f_{12}}{\partial u_1} = 0 \ \frac{\partial f_{12}}{\partial u_2} = 0 \ \frac{\partial f_{12}}{\partial u_3} = 0 \ \frac{\partial f_{12}}{\partial u_4} = \frac{1}{J_z} \tag{9.63}$$

9.3.4 Design of an H-Infinity Nonlinear Feedback Controller

9.3.4.1 Equivalent Linearized Dynamics of the Robot

After linearization around its current operating point, the UAV's dynamic model is written as

$$\dot{x} = Ax + Bu + d_1 \tag{9.64}$$

Parameter d_1 stands for the linearization error in the UAV's dynamic model appearing in Eq. (9.64). The reference setpoints for the UAV's state vector are denoted by $\mathbf{x_d} = [x_1^d, \ldots, x_4^d]$. Tracking of this trajectory is achieved after applying the control input u^*. At every time instant the control input u^* is assumed to differ from the control input u appearing in Eq. (9.64) by an amount equal to Δu, that is $u^* = u + \Delta u$

$$\dot{x}_d = Ax_d + Bu^* + d_2 \tag{9.65}$$

The dynamics of the controlled system described in Eq. (9.64) can be also written as

$$\dot{x} = Ax + Bu + Bu^* - Bu^* + d_1 \tag{9.66}$$

and by denoting $d_3 = -Bu^* + d_1$ as an aggregate disturbance term one obtains

$$\dot{x} = Ax + Bu + Bu^* + d_3 \tag{9.67}$$

By subtracting Eq. (9.65) from Eq. (9.67) one has

$$\dot{x} - \dot{x}_d = A(x - x_d) + Bu + d_3 - d_2 \tag{9.68}$$

By denoting the tracking error as $e = x - x_d$ and the aggregate disturbance term as $\tilde{d} = d_3 - d_2$, the tracking error dynamics becomes

$$\dot{e} = Ae + Bu + \tilde{d} \tag{9.69}$$

The above linearized form of the UAV's model can be efficiently controlled after applying an H-infinity feedback control scheme.

9.3.4.2 The Nonlinear H-Infinity Control

The initial nonlinear model of the unmanned aerial vehicle is in the form

$$\dot{x} = f(x, u) \;\; x \in R^n, \;\; u \in R^m \tag{9.70}$$

Linearization of the system (multi-DOF UAV) is performed at each iteration of the control algorithm round its present operating point $(x^*, u^*) = (x(t), u(t - T_s))$. The linearized equivalent of the system is described by

$$\dot{x} = Ax + Bu + L\tilde{d} \;\; x \in R^n, \;\; u \in R^m, \;\; \tilde{d} \in R^q \tag{9.71}$$

where matrices A and B are obtained from the computation of the Jacobians of the UAV's state-space description and vector $\tilde{d}$ denotes disturbance terms due to

linearization errors. The problem of disturbance rejection for the linearized model that is described by

$$\begin{aligned} \dot{x} &= Ax + Bu + L\tilde{d} \\ y &= Cx \end{aligned} \tag{9.72}$$

where $x \in R^n$, $u \in R^m$, $\tilde{d} \in R^q$ and $y \in R^p$, cannot be handled efficiently if the classical LQR control scheme is applied. This is because of the existence of the perturbation term $\tilde{d}$. The disturbance term $\tilde{d}$ apart from modeling (parametric) uncertainty and external perturbations can also represent noise terms of any distribution.

As analyzed in previous applications of the H_∞ control approach, a feedback control scheme is designed for trajectory tracking by the system's state vector and simultaneous disturbance rejection, considering that the disturbance affects the system in the worst possible manner. The disturbances' effects are incorporated in the following quadratic cost function:

$$J(t) = \frac{1}{2}\int_0^T [y^T(t)y(t) + ru^T(t)u(t) - \rho^2 \tilde{d}^T(t)\tilde{d}(t)]dt, \quad r, \rho > 0 \tag{9.73}$$

The significance of the negative sign in the cost function's term that is associated with the perturbation variable $\tilde{d}(t)$ is that the disturbance tries to maximize the cost function $J(t)$ while the control signal $u(t)$ tries to minimize it. The physical meaning of the relation given above is that the control signal and the disturbances compete to each other within a min-max differential game. This problem of min-max optimization can be written as

$$min_u max_{\tilde{d}} J(u, \tilde{d}) \tag{9.74}$$

In the previous cases of applications of the H-infinity control it has been explained that the objective of the optimization procedure is to compute a control signal $u(t)$ which can compensate for the worst possible disturbance, that is externally imposed to the system. However, the solution to the min-max optimization problem is directly related to the value of the parameter ρ. This means that there is an upper bound in the disturbances magnitude that can be annihilated by the control signal.

9.3.4.3 Computation of the Feedback Control Gains

For the linearized system given by Eq. (9.72) the cost function of Eq. (9.73) is defined, where the coefficient r determines the penalization of the control input and the weight coefficient ρ determines the reward of the disturbances' effects.

Once more it is assumed that (i) The energy that is transferred from the disturbances signal $\tilde{d}(t)$ is bounded, that is $\int_0^\infty \tilde{d}^T(t)\tilde{d}(t)dt < \infty$, (ii) the matrices $[A, B]$ and $[A, L]$ are stabilizable, (iii) the matrix $[A, C]$ is detectable. Then, the optimal feedback control law is given by

$$u(t) = -Kx(t) \tag{9.75}$$

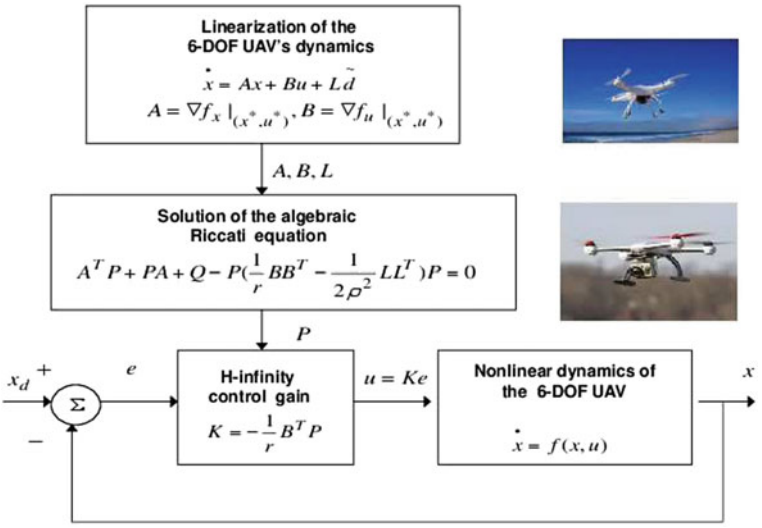

Fig. 9.10 Diagram of the control scheme for the multi-DOF UAV

with

$$K = \frac{1}{r}B^T P \tag{9.76}$$

where P is a positive semi-definite symmetric matrix which is obtained from the solution of the Riccati equation

$$A^T P + PA + Q - P(\frac{1}{r}BB^T - \frac{1}{2\rho^2}LL^T)P = 0 \tag{9.77}$$

where Q is also a positive definite symmetric matrix. The worst case disturbance is given by

$$\tilde{d}(t) = \frac{1}{\rho^2}L^T Px(t) \tag{9.78}$$

The diagram of the considered control loop is depicted in Fig. 9.10.

9.3.5 Lyapunov Stability Analysis

Through Lyapunov stability analysis it will be shown that the proposed nonlinear control scheme assures H_∞ tracking performance for the UAV, and that in case of bounded disturbance terms asymptotic convergence to the reference setpoints is achieved. The tracking error dynamics for the multi-DOF unmanned aerial vehicle is written in the form

$$\dot{e} = Ae + Bu + L\tilde{d} \tag{9.79}$$

where in the robot's case $L = I \in R^{12}$ with I being the identity matrix. Variable $\tilde{d}$ denotes model uncertainties and external disturbances of the UAV's model. The following Lyapunov function is considered

$$V = \frac{1}{2} e^T P e \tag{9.80}$$

where $e = x - x_d$ is the tracking error. By differentiating with respect to time one obtains

$$\begin{gathered} \dot{V} = \frac{1}{2} \dot{e}^T P e + \frac{1}{2} e P \dot{e} \Rightarrow \\ \dot{V} = \frac{1}{2} [Ae + Bu + L\tilde{d}]^T P e + \frac{1}{2} e^T P [Ae + Bu + L\tilde{d}] \Rightarrow \end{gathered} \tag{9.81}$$

$$\begin{gathered} \dot{V} = \frac{1}{2} [e^T A^T + u^T B^T + \tilde{d}^T L^T] P e + \\ + \frac{1}{2} e^T P [Ae + Bu + L\tilde{d}] \Rightarrow \end{gathered} \tag{9.82}$$

$$\begin{gathered} \dot{V} = \frac{1}{2} e^T A^T P e + \frac{1}{2} u^T B^T P e + \frac{1}{2} \tilde{d}^T L^T P e + \\ \frac{1}{2} e^T P A e + \frac{1}{2} e^T P B u + \frac{1}{2} e^T P L \tilde{d} \end{gathered} \tag{9.83}$$

The previous equation is rewritten as

$$\begin{gathered} \dot{V} = \frac{1}{2} e^T (A^T P + P A) e + (\frac{1}{2} u^T B^T P e + \frac{1}{2} e^T P B u) + \\ + (\frac{1}{2} \tilde{d}^T L^T P e + \frac{1}{2} e^T P L \tilde{d}) \end{gathered} \tag{9.84}$$

Assumption: For given positive definite matrix Q and coefficients r and ρ there exists a positive definite matrix P, which is the solution of the following matrix equation

$$A^T P + P A = -Q + P(\frac{2}{r} B B^T - \frac{1}{\rho^2} L L^T) P \tag{9.85}$$

Moreover, the following feedback control law is applied to the system

$$u = -\frac{1}{r} B^T P e \tag{9.86}$$

By substituting Eqs. (9.85) and (9.86) one obtains

$$\begin{gathered} \dot{V} = \frac{1}{2} e^T [-Q + P(\frac{2}{r} B B^T - \frac{1}{\rho^2} L L^T) P] e + \\ + e^T P B (-\frac{1}{r} B^T P e) + e^T P L \tilde{d} \Rightarrow \end{gathered} \tag{9.87}$$

$$\begin{gathered} \dot{V} = -\frac{1}{2} e^T Q e + \frac{1}{r} P B B^T P e - \frac{1}{2\rho^2} e^T P L L^T P e \\ - \frac{1}{r} (e^T P B B^T P e) + e^T P L \tilde{d} \end{gathered} \tag{9.88}$$

which after intermediate operations gives

$$\dot{V} = -\frac{1}{2} e^T Q e - \frac{1}{2\rho^2} e^T P L L^T P e + e^T P L \tilde{d} \tag{9.89}$$

or, equivalently

$$\begin{array}{c}\dot{V} = -\frac{1}{2}e^T Qe - \frac{1}{2\rho^2}e^T PLL^T Pe + \\ +\frac{1}{2}e^T PL\tilde{d} + \frac{1}{2}\tilde{d}^T L^T Pe\end{array} \tag{9.90}$$

Lemma: The following inequality holds

$$\frac{1}{2}e^T PL\tilde{d} + \frac{1}{2}\tilde{d}L^T Pe - \frac{1}{2\rho^2}e^T PLL^T Pe \leq \frac{1}{2}\rho^2\tilde{d}^T\tilde{d} \tag{9.91}$$

Proof: The binomial $(\rho\alpha - \frac{1}{\rho}b)^2$ is considered. Expanding the left part of the above inequality one gets

$$\begin{array}{c}\rho^2a^2 + \frac{1}{\rho^2}b^2 - 2ab \geq 0 \Rightarrow \frac{1}{2}\rho^2a^2 + \frac{1}{2\rho^2}b^2 - ab \geq 0 \Rightarrow \\ ab - \frac{1}{2\rho^2}b^2 \leq \frac{1}{2}\rho^2a^2 \Rightarrow \frac{1}{2}ab + \frac{1}{2}ab - \frac{1}{2\rho^2}b^2 \leq \frac{1}{2}\rho^2a^2\end{array} \tag{9.92}$$

The following substitutions are carried out: $a = \tilde{d}$ and $b = e^T PL$ and the previous relation becomes

$$\frac{1}{2}\tilde{d}^T L^T Pe + \frac{1}{2}e^T PL\tilde{d} - \frac{1}{2\rho^2}e^T PLL^T Pe \leq \frac{1}{2}\rho^2\tilde{d}^T\tilde{d} \tag{9.93}$$

Equation (9.93) is substituted in Eq. (9.90) and the inequality is enforced, thus giving

$$\dot{V} \leq -\frac{1}{2}e^T Qe + \frac{1}{2}\rho^2\tilde{d}^T\tilde{d} \tag{9.94}$$

Equation (9.94) shows that the H_∞ tracking performance criterion is satisfied. The integration of $\dot{V}$ from 0 to T gives

$$\begin{array}{c}\int_0^T \dot{V}(t)dt \leq -\frac{1}{2}\int_0^T ||e||_Q^2 dt + \frac{1}{2}\rho^2\int_0^T ||\tilde{d}||^2 dt \Rightarrow \\ 2V(T) + \int_0^T ||e||_Q^2 dt \leq 2V(0) + \rho^2\int_0^T ||\tilde{d}||^2 dt\end{array} \tag{9.95}$$

Moreover, if there exists a positive constant $M_d > 0$ such that

$$\int_0^\infty ||\tilde{d}||^2 dt \leq M_d \tag{9.96}$$

then one gets

$$\int_0^\infty ||e||_Q^2 dt \leq 2V(0) + \rho^2 M_d \tag{9.97}$$

Thus, the integral $\int_0^\infty ||e||_Q^2 dt$ is bounded. Moreover, $V(T)$ is bounded and from the definition of the Lyapunov function V in Eq. (9.80) it becomes clear that $e(t)$ will be also bounded since $e(t) \in \Omega_e = \{e | e^T Pe \leq 2V(0) + \rho^2 M_d\}$. According to the above and with the use of Barbalat's Lemma one obtains $lim_{t\to\infty} e(t) = 0$.

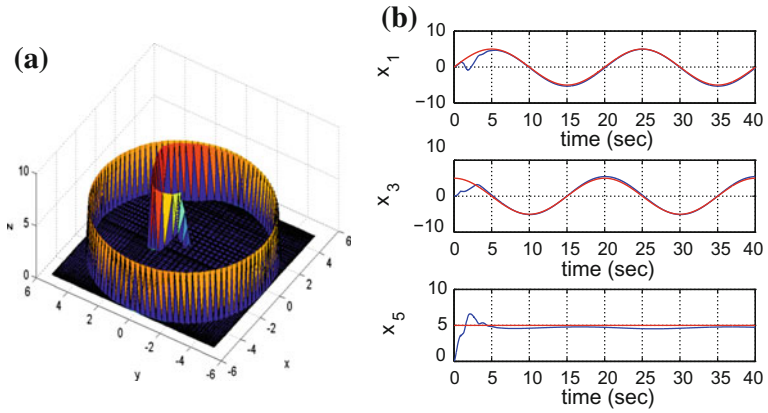

Fig. 9.11 Control of the quadrotor when tracking flight path 1: **a** Three-dimensional plot of tracking of flight path 1 by the quadropter, **b** Cartesian coordinates of the UAV and convergence to the reference setpoints

9.3.6 Robust State Estimation with the Use of the H-Infinity Kalman Filter

Another problem that has to be dealt with in the design of a state feedback controller for the UAV (autonomous quadrotor) is that in several operating conditions the complete state vector might not be measurable. Actually, attempting to measure the complete state vector with the use of suitable sensors is not only costly but is also error-prone because, particularly in the harsh operating environment of the UAVs. Thus the control loop has to be implemented with the use of information provided by a small number of sensors and by processing only a small number of state variables. To reconstruct the missing information about the state vector of the quadrotor it is proposed to use a filtering scheme and based on it to apply state estimation-based control [33, 169, 431, 463, 511].

The recursion of the H_∞ Kalman Filter, for the model of the six-DOF UAV, can be formulated in terms of a *measurement update* and a *time update* part

Measurement update:

$$\begin{aligned} D(k) &= [I - \theta W(k)P^-(k) + C^T(k)R(k)^{-1}C(k)P^-(k)]^{-1} \\ K(k) &= P^-(k)D(k)C^T(k)R(k)^{-1} \\ \hat{x}(k) &= \hat{x}^-(k) + K(k)[y(k) - C\hat{x}^-(k)] \end{aligned} \tag{9.98}$$

Time update:

$$\begin{aligned} \hat{x}^-(k+1) &= A(k)x(k) + B(k)u(k) \\ P^-(k+1) &= A(k)P^-(k)D(k)A^T(k) + Q(k) \end{aligned} \tag{9.99}$$

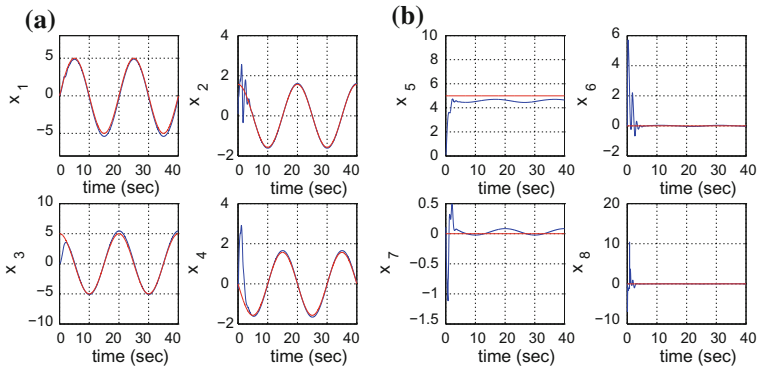

Fig. 9.12 Control of the quadrotor when tracking flight path 1: **a** Convergence of state variables x_1 to x_4 to the reference setpoints, **b** Convergence of state variables x_5 to x_8 to the reference setpoints

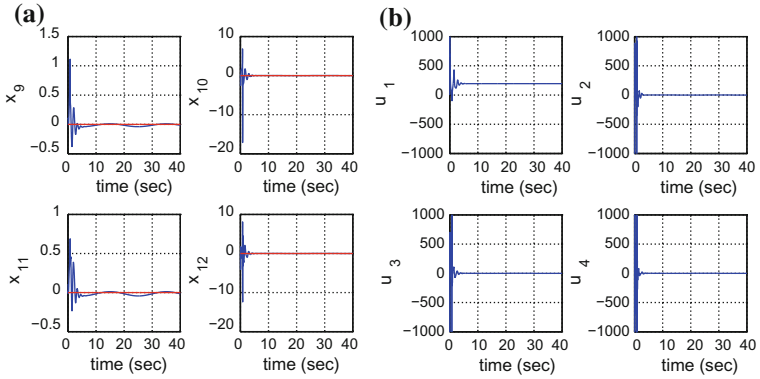

Fig. 9.13 Control of the quadrotor when tracking flight path 1: **a** Convergence of state variables x_9 to x_{12} to the reference setpoints, **b** Control inputs u_1 to u_4 exerted on the UAV

where it is assumed that parameter θ is sufficiently small to assure that the term $P^{-}(k)^{-1} - \theta W(k) + C^{T}(k)R(k)^{-1}C(k)$ will be positive definite. When $\theta = 0$ the H_∞ Kalman Filter becomes equivalent to the standard Kalman Filter. It is noted that apart from the process noise covariance matrix $Q(k)$ and the measurement noise covariance matrix $R(k)$ the H_∞ Kalman filter requires tuning of the weight matrices L and S, as well as of parameter θ.

In the case of UAVs (e.g. autonomous quadropters), the H-infininty Kalman Filter can be used within a state estimation-based control scheme. Actually, one can measure only a part of the state vector of the UAV, such as state variables $x_1 = x, x_3 = y, x_5 = z, x_7 = \phi, x_9 = \theta, x_{11} = \psi$ and estimate through filtering the rest of the state vector elements that is $x_2 = \dot{x}, x_4 = \dot{y}, x_5 = \dot{z}, x_7 = \dot{\phi}, x_9 = \dot{\theta}, x_{11} = \dot{\psi}$. Moreover, the proposed Kalman filtering method can be used for sensor fusion purposes.

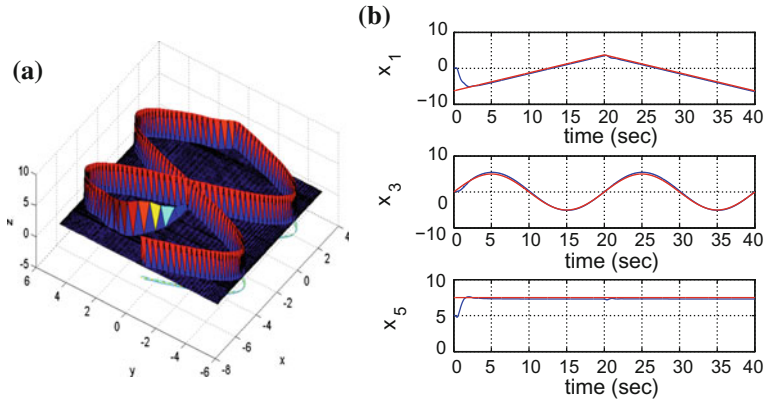

Fig. 9.14 Control of the quadrotor when tracking flight path 2: **a** Three-dimensional plot of tracking of flight path 1 by the quadropter, **b** Cartesian coordinates of the UAV and convergence to the reference setpoints

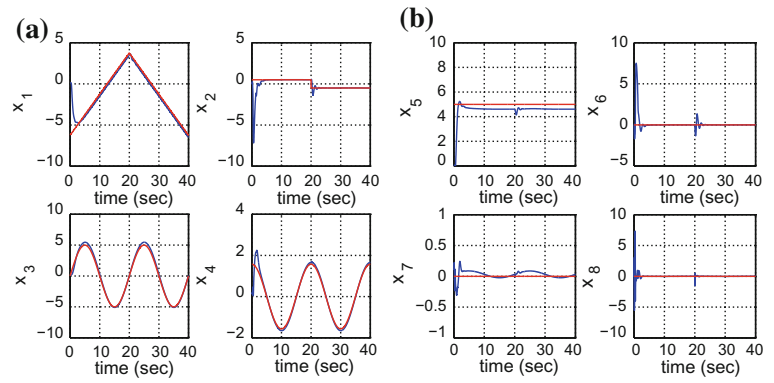

Fig. 9.15 Control of the quadrotor when tracking flight path 2: **a** Convergence of state variables x_1 to x_4 to the reference setpoints, **b** Convergence of state variables x_5 to x_8 to the reference setpoints

9.3.7 Simulation Tests

The tracking performance of the considered nonlinear H-infinity control scheme was tested in the case of several reference flight paths. The first 3D reference trajectory is shown in Fig. 9.11, while the convergence of the UAV's setpoints to their setpoints are shown in Figs. 9.12a, b and 9.13a. The control inputs exerted on the UAV by its actuators are shown in Fig. 9.13b.

The second 3D reference trajectory is shown in Fig. 9.14, while the convergence of the UAV's setpoints to their setpoints are shown in Figs. 9.15a, b and 9.16a. The control inputs exerted on the UAV by its actuators are shown in Fig. 9.16b.

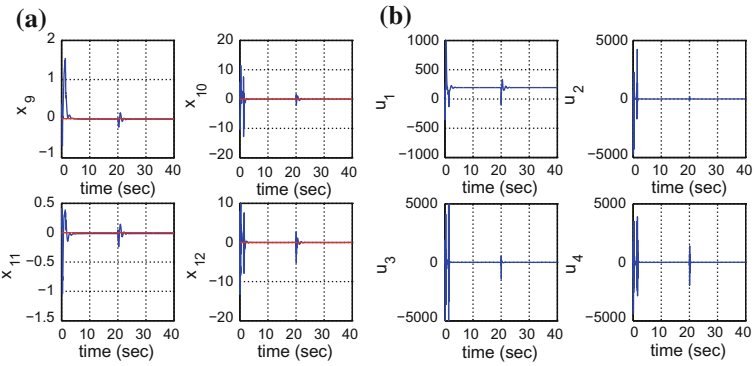

Fig. 9.16 Control of the quadrotor when tracking flight path 2: **a** Convergence of state variables x_9 to x_{12} to the reference setpoints, **b** Control inputs u_1 to u_4 exerted on the UAV

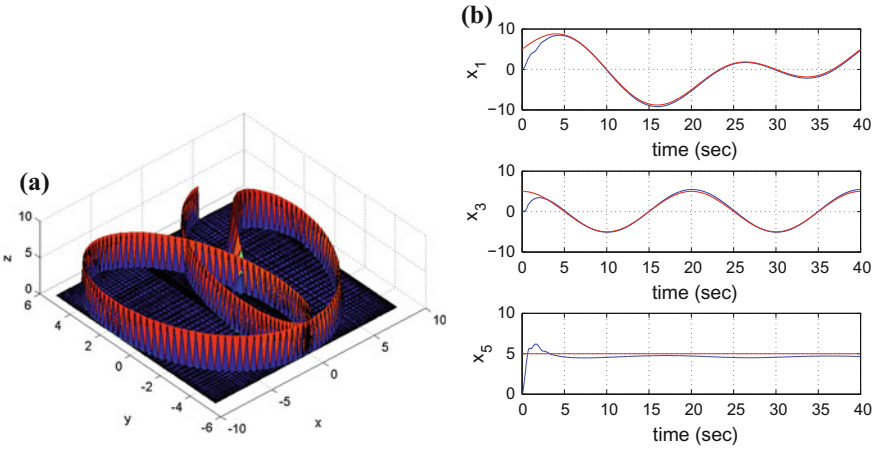

Fig. 9.17 Control of the quadrotor when tracking flight path 3: **a** Three-dimensional plot of tracking of flight path 1 by the quadropter, **b** Cartesian coordinates of the UAV and convergence to the reference setpoints

Finally, the third considered 3D reference trajectory is shown in Fig. 9.17, while the convergence of the UAV's setpoints to their setpoints are shown in Figs. 9.18a, b and 9.19a. The control inputs exerted on the UAV by its actuators are shown in Fig. 9.19b.

It can be noticed that in all cases the nonlinear H-infinity control algorithm for the UAV achieved accurate tracking of the reference path and fast convergence to them. All state variables of the system converged fast and smoothly to the reference setpoints while their tracking error was rapidly eliminated. Moreover, the variation

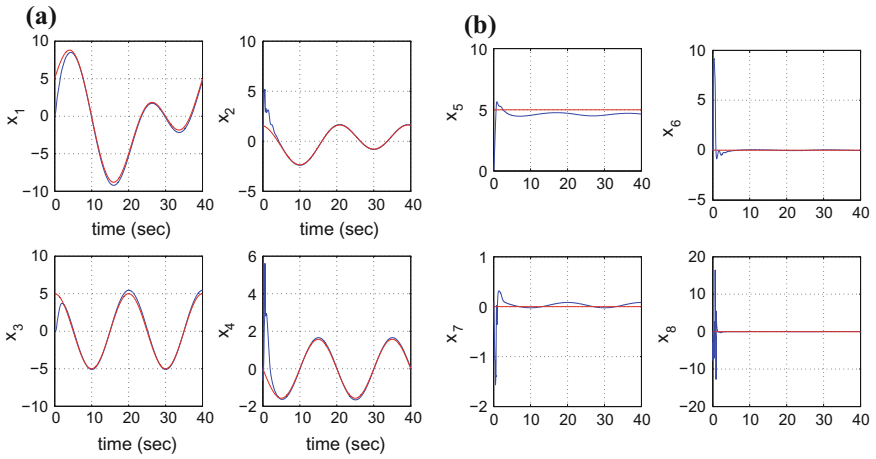

Fig. 9.18 Control of the quadrotor when tracking flight path 3: **a** Convergence of state variables x_1 to x_4 to the reference setpoints, **b** Convergence of state variables x_5 to x_8 to the reference setpoints

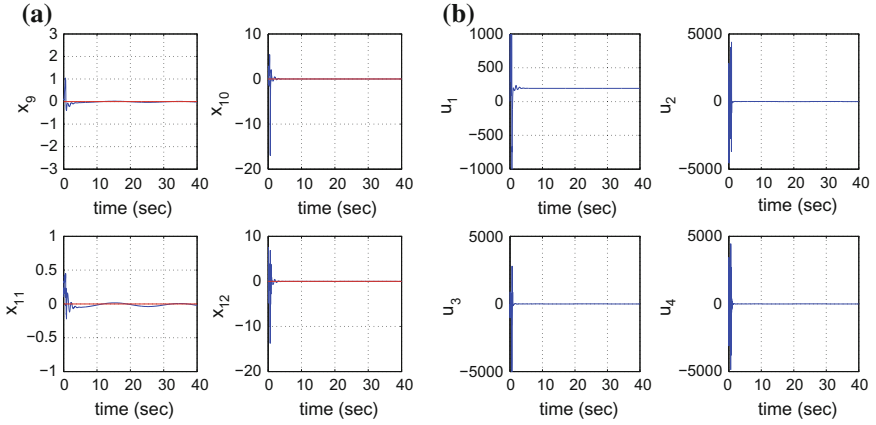

Fig. 9.19 Control of the quadrotor when tracking flight path 3: **a** Convergence of state variables x_9 to x_{12} to the reference setpoints, **b** Control inputs u_1 to u_4 exerted on the UAV

of the control inputs exerted on the UAV by its actuators was smooth and no abrupt changes of the control signal were observed. The above are indicative of the excellent tracking and stability properties of the nonlinear H-infinity control algorithm.

Chapter 10
Unmanned Surface Vessels

Abstract Autonomous navigation of unmanned surface vessels (USVs) (such as ships, hovercrafts, etc), is a significant topic, since it can find use in both security and defence tasks, as well as in maritime transportation. The problem of control and trajectory tracking for unmanned surface vessels (of the ship or hovercraft type) is non-trivial because the associated dynamic and kinematic models are complex nonlinear ones. A first problem that arises in controller design for unmanned surface vessels is that trajectory tracking has to be achieved despite modelling uncertainty and external perturbations and thus the control loop must exhibit sufficient robustness. Another problem that has to be dealt with is that the vessels model is often underactuated (the propulsion system consists of less actuators than the vessel's degrees of freedom). The present chapter treats the problem of control of unmanned surface vessels. Solution to the associated control problem is provided through (i) global linearization methods, (ii) approximate linearization methods and (iii) Lyapunov methods. To solve the control problem for unmanned surface vessels without prior knowledge of the associated dynamic model, elaborated real-time estimation methods are developed. These allow for identifying the unknown dynamic model of the vessel and for implementing an indirect adaptive control scheme. Moreover, for the accurate localization of the vessel and for precise computation of its motion characteristics advanced (and precisely validated) nonlinear filtering and distributed filtering are applied. These enable to perform fusion of the measurements of heterogeneous sensors and of state estimates provided by individual distributed local filters. In particular, the chapter treats the following issues: (a) Nonlinear control and Kalman Filtering for a 3-DOF surface vessel, (b) Flatness-based control for the autonomous hovercraft (c) Nonlinear optimal control for autonomous navigation of unmanned surface vessels, and (d) validation of distributed Kalman Filtering for ship tracking applications.

G. Rigatos and K. Busawon, *Robotic Manipulators and Vehicles*,
Studies in Systems, Decision and Control 152,
https://doi.org/10.1007/978-3-319-77851-8_10

10.1 Chapter Overview

The present chapter treats the following issues: (a) Nonlinear control and Kalman Filtering for a 3-DOF surface vessel, (b) Flatness-based control for the autonomous hovercraft (c) Nonlinear optimal control for autonomous navigation of unmanned surface vessels, and (d) validation of distributed Kalman Filtering for ship tracking applications.

With reference to (a) the chapter examines the problem of dynamic ship positioning with the use of Kalman Filter-based and Particle Filter-based sensor fusion algorithms. The proposed approach enables to estimate accurately the ship's state vector by fusing the vessel's position and heading measurements coming from onboard sensors together with distance measurements coming from sensors located at the coast (e.g. radar). The estimated state vector is used in turn in a control loop, to regulate the horizontal position and heading of the vessel.

With reference to (b) the chapter proposes a nonlinear control approach for the underactuated hovercraft model based on differential flatness theory and uses a new nonlinear state vector and disturbances estimation method under the name of Derivative-free nonlinear Kalman Filter. It is proven that the nonlinear model of the hovercraft is a differentially flat one. It is shown that this model cannot be subject to static feedback linearization, however it admits dynamic feedback linearization which means that the system's state vector is extended by including as additional state variables the control inputs and their derivatives. Next, using the differential flatness properties it is also proven that this model can be subject to input-output linearization and can be transformed to an equivalent canonical (Brunovsky) form. Based on this latter description the design of a state feedback controller is carried out enabling accurate maneuvering and trajectory tracking. Additional problems that are solved in the design of this feedback control scheme are the estimation of the nonmeasurable state variables in the hovercraft's model and the compensation of modeling uncertainties and external perturbations affecting the vessel. To this end, the application of the Derivative-free nonlinear Kalman Filter is proposed. This nonlinear filter consists of the Kalman Filter's recursion on the linearized equivalent model of the vessel and of an inverse nonlinear transformation based on the differential flatness features of the system which enables to compute state estimates for the state variables of the initial nonlinear model. The redesign of the filter as a disturbance observer makes possible the estimation and compensation of additive perturbation terms affecting the hovercraft's model.

With reference to (c) the chapter proposes a new nonlinear optimal control approach for autonomous navigation of unmanned surface vessels. The dynamic model of the surface vessels undergoes approximate linearization round local operating points which are redefined at each iteration of the control algorithm. These temporary equilibria consist of the last value of the vessel's state vector and of the last value of the control signal that was exerted on it. For the approximate linearization of the system's dynamics Taylor series expansion is performed through the computation of the associated Jacobian matrices. The modelling errors are compensated by

the robustness of the control algorithm. Next, for the linearized equivalent model of the vessel an H-infinity feedback controller is designed. This requires the solution of an algebraic Riccati equation at each iteration of the computer control program. It is shown that the control scheme achieves H-infinity tracking performance, which implies maximum robustness to modelling errors and external perturbations. The stability of the control loop is proven through Lyapunov analysis.

With reference to (d) the chapter considers that tracking of ships' motion and monitoring of maritime traffic can be performed with the use of distributed Kalman Filtering. However, some of the local Kalman Filters which constitute distributed estimation schemes may depend on inaccurate models of the vessel's dynamics or kinematics and in such a case the aggregate state estimate provided by the distributed filter is unreliable. To treat this problem the chapter proposes a statistical method of optimized performance for the validation of Fuzzy Kalman Filters used in ship tracking. By showing the equivalence of the local Kalman Filters to ARMAX models, the Fuzzy Kalman Filter is proven to be equivalent to fuzzy weighting of local ARMAX models. Using this equivalent modeling of the Fuzzy Kalman Filter, the local statistical approach to fault diagnosis is applied for validating the accuracy of the distributed filter or in the opposite case for detecting the local Kalman Filter that makes use of an imprecise ship model. By applying the Generalized Likelihood Ratio on the residuals of the Kalman Filtering procedure the proposed validation method finally takes the form of a χ^2 statistical change detection criterion. This statistical validation test is capable of detecting the faulty local filter within the distributed estimation method, even in the case of small errors in the local model's parameters which do not exceed 1% of the associated nominal values.

10.2 Nonlinear Control and Filtering for a 3-DOF Surface Vessel

10.2.1 Outline

During the last years, research on marine navigation systems and on autonomous vessels have grown rapidly. Modern marine vessels are equipped with sophisticated motion-control systems which accomplish various control objectives such as position and heading regulation, trajectory tracking, and wave-induced motion compensation [148, 189, 462]. Motion control operates in the three planar degrees of freedom, i.e. surge (forward motion), sway (transverse motion), and yaw (rotation about the vertical axis, also called heading) and is implemented through the feedback of information from position and heading measurements. To estimate accurately the vessel's position, measurements coming from GPS, radar or an IMU can be used, while to estimate the orientation of the vessel, fusion of measurements coming from magnetic compasses and gyroscopes can be performed. The term "Dynamic positioning" describes the use of the propulsion system, in a control loop, to regulate the horizontal position and heading of the vessel. Early Dynamic Positioning Systems (DPS)

were based on three term PID control with a notch filter in order to counteract high frequency motion due to waves. There exist also results on nonlinear filtering for autonomous navigation systems which have been presented in [110, 310, 567, 592]. The present section studies sensor fusion-based dynamic positioning for ships using Kalman and Particle Filtering methods.

Sensor-fusion based motion estimation using probabilistic inference forms a core component in most modern guidance and navigation systems [234]. The estimator fuses observations from multiple sensors with predictions from a dynamic state-space model of the system under control. The most widely used algorithms for multi-sensor fusion are variants of the Kalman Filter (KF), which in the case of nonlinear dynamical models take the form of the Extended Kalman Filter. Currently, Kalman Filtering is a main element in the design of Dynamic Positioning Systems [163, 477, 547]. A basic assumption made by Kalman Filtering is that of Gaussian process/measurement noise. On the other hand, the Extended Kalman Filter is based on the linearization of the system dynamics, and proceeds with the recursive estimation of the standard Kalman Filter [431, 433, 457].

A different approach to filtering and sensor fusion-based state estimation is Particle Filtering. The Particle Filter is a non-parametric state estimator which unlike the KF or the EKF does not make any assumption on the probability density function of the measurements [23, 555]. The concept of particle filtering comes from Monte-Carlo methods. The Particle Filter (PF) can provide optimal estimation in non-Gaussian state-space models. In the case of nonlinear dynamical models the PF avoids also the calculations associated with the Jacobians which appear in the EKF equations [271, 625]. The main stages of the PF are prediction (time update), correction (measurement update) and resampling for substituting the unsuccessful state vector estimates with those particles that have better approximated the real state vector.

The main developments of the section are outlined in the following: (i) design of a Kalman Filter-based disturbance estimator that enables simultaneous estimation of the ship's state vector and of the vector of external disturbances, through the processing of measurements from various types of sensors, (ii) design of a Particle Filter disturbance estimator that enables simultaneous estimation of the ship's state vector and of the vector of external disturbances, again through the fusion of measurements from various sensors, (iii) implementation of state estimation-based control using these nonlinear filtering methods.

10.2.2 Kinematic and Dynamic Models of Vessels for the Problem of Dynamic Positioning

10.2.2.1 A Generic Kinematic and Dynamic Ship Model

The motion of a ship is described by two reference frames: (i) a local geographical earth-fixed frame and, (ii) a body-fixed frame denoted as $X_b Y_b Z_b$ which is attached

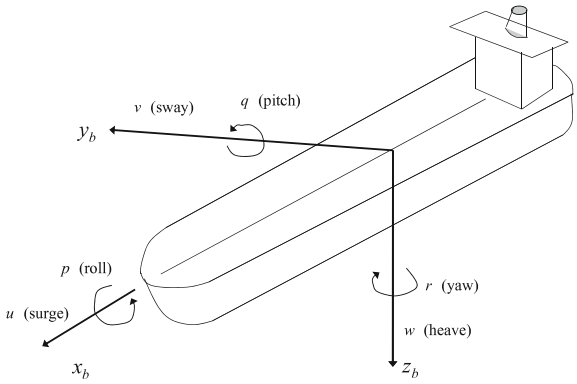

Fig. 10.1 Components of the linear velocity vector of the vessel (surge, sway and heave) and components of the angular velocity of the vessel (roll, pitch and yaw Euler angles)

to the vessel (see Fig. 10.1). The components of the position vector of the vessel are $[x, y, \psi]^T$ where (x, y) are the coordinates of the ship's center of symmetry in a local geographical frame and ψ is the orientation angle with reference to the OX axis of the local coordinates frame [148].

The components of the ship's velocity vector, denoted as $v = [u, v_s, r]^T$, are the surge and sway velocities (u, v_s) and the yaw rate r. A model for vessel kinematics, relating the ship's position vector η to the ship velocity vector v, is

$$\dot{\eta} = R(\psi)v \tag{10.1}$$

The kinematic transformation of Eq. (10.1) relates the body-fixed velocities to the position derivatives in the local geographical frame. The transformation is described by matrix $R(\psi) \in R^{3\times 3}$ which performs a rotation round the z-axis by an angle ψ. The equation of the ship dynamics describes the relation between the ship's velocity and the generalized forces vector (forces and torques $\tau_{control}$, τ_{wind} and τ_{waves}) which is applied to the vessel [148, 167].

$$M\dot{v} + C_{RB}(v)v + d(V_{rc}, \gamma_c) = \tau_{control} + \tau_{wind} + \tau_{waves} \tag{10.2}$$

In the above equation, $C_{RB}(v)v$ denotes Coriolis-centripetal terms while $d(V_{rc}, \gamma_c)$ denotes disturbance terms (e.g. due to wind and currents). The inertia matrix M is the sum of two matrices M_A and M_{RB}, i.e. $M = M_A + M_{RB}$ where

$$M_A = \begin{pmatrix} -X_{\dot{u}} & 0 & 0 \\ 0 & -Y_{\dot{v}_s} & -Y_{\dot{r}} \\ 0 & -Y_{\dot{r}} & -N_{\dot{r}} \end{pmatrix} \; M_{RB} = \begin{pmatrix} m & 0 & 0 \\ 0 & m & mx_g \\ 0 & mx_g & I_z \end{pmatrix} \tag{10.3}$$

In the positive-definite hydrodynamic matrix M_A, the added-mass coefficients $X_{\dot{u}}$, $Y_{\dot{v}}$, and $N_{\dot{r}}$ depend on the hull shape and show the change in momentum in the fluid due to the vessel accelerations. On the other hand in the equation of the positive

definite rigid-body mass matrix M_{RB}, parameter x_g denotes the longitudinal position of the center of gravity of the vessel relative to the body-fixed frame. The Coriolis-centripetal terms matrix C_{RB} is given by

$$C_{RB} = \begin{pmatrix} 0 & 0 & -m(x_g r + v_s) \\ 0 & 0 & mu \\ m(x_g r + v_s) & -mu & 0 \end{pmatrix} \tag{10.4}$$

When a vessel operates under positioning control the velocities are small and thus the Coriolis-centripetal terms $C_{RB}(v)v$ in Eq. (10.2) can be omitted from the ship's dynamic model.

10.2.2.2 Ship Model for the Dynamic Positioning Problem

As noted before, the term $d(V_{rc}, \gamma_c)$ on the left hand side of Eq. (10.2) represents the current and damping forces. The speed of the current is denoted as V_{rc} while the angle of the current is denoted as γ_{rc} and is defined relative to the bow of the vessel [148]. It is common practice to write the current forces in surge, sway and yaw as functions of non-dimensional current coefficients $C_{X_c}(\gamma_{r_c}), C_{Y_c}(\gamma_{rc}), C_{N_c}(\gamma_{r_c})$ which is

$$d(V_{rc}, \gamma_{rc}) = \frac{1}{2}\rho V_{rc}^2 \begin{pmatrix} A_{F_c} C_{X_c}(\gamma_{rc}) \\ A_{L_c} C_{Y_c}(\gamma_{rc}) \\ A_{L_c} L_{0\alpha} C_{N_c}(\gamma_{rc}) \end{pmatrix} \tag{10.5}$$

where ρ is the water density, A_{F_c} and A_{L_c} are frontal and lateral projected areas of the submerged part of the vessel and $L_{0\alpha}$ is the length of the ship. However, the current coefficients $C_{X_c}(\gamma_{r_c})$, $C_{Y_c}(\gamma_{r_c})$, $C_{N_c}(\gamma_{r_c})$ are difficult to estimate with accuracy. In such cases, one can simplify the model of Eq. (10.5), in terms of a linear damping term and a bias term which finally takes the form

$$d(V_{rc}, \gamma_{rc}) \simeq D(v)v - R^T(\psi)d \tag{10.6}$$

$$\text{where } D = D^T = \begin{pmatrix} D_{11} & 0 & \\ 0 & D_{22} & D_{23} \\ 0 & D_{32} & D_{33} \end{pmatrix}, \quad d = \begin{pmatrix} d_1 \\ d_2 \\ d_3 \end{pmatrix} \tag{10.7}$$

The wind forces and moments can be represented in a similar way to the current forces and moments, i.e.

$$\tau_{wind} = \frac{1}{2}\rho_\alpha V_{rw}^2 \begin{pmatrix} A_{Fw} C_{Xw}(\gamma_{rw}) \\ A_{Lw} C_{Yw}(\gamma_{rw}) \\ A_{Lw} L_{0\alpha} C_{Nw}(\gamma_{rw}) \end{pmatrix} \tag{10.8}$$

where ρ_α is the air density, A_{Fw} and A_{Lw} are the frontal and lateral projected wind areas and $L_{0\alpha}$ is the vessel's overall length. The wind speed is V_{rw} and its direction is γ_{rw} in earth-fixed coordinates. The wind model coefficients can be obtained by model tests while with reference to the control problem, obtaining measurements of the wind's speed and direction enables to compensate τ_{wind} using a feed-forward term $\hat{\tau}_{wind}$. The difference (modeling error) between τ_{wind} and $\hat{\tau}_{wind}$ can be described by a bias term $R^T(\psi)d$, as in the case of the current bias term that was given in Eq. (10.6).

Wave forces are usually modeled as the sum of a linear and a nonlinear component, i.e.

$$\tau_{waves} = \tau_{waves}^{lin} + \tau_{waves}^{nlin} \tag{10.9}$$

The low-frequency nonlinear wave forces can be modeled again by a bias term, and considered to be input disturbances. On the other hand the linear wave forces are considered to be output disturbances. Therefore, the observation (measurement) equation of the ship is given by $z = \eta + n_w + v_1$, where n is the vessel's position calculated using the ship's dynamic model of Eqs. (10.1) and (10.2), v_1 is sensor measurement noise and n_w is the ship's displacement due to the linear wave forces.

Using Eq. (10.6) and the above assumptions about the wind and waves forces, the vessel's kinematic and dynamic model described in Eqs. (10.1) and (10.2) respectively, is given by

$$\begin{aligned} &\dot{\eta} = R(\psi)v \\ &\dot{v} + M^{-1}Dv = M^{-1}[R^T(\psi)d + \tau_{\text{control}}] + w \\ &\dot{d} = w \\ &z = \eta + n_w + v_1 \text{ or } z = n + v \end{aligned} \tag{10.10}$$

The bias is an additive disturbance in the ship's dynamic model which can be estimated with the use of a state observer. Once the bias is accurately estimated it can be compensated by a suitable control term in the right hand side of Eq. (10.10). This additional control term provides the required robustness to compensate for the bias effects.

10.2.3 Ship Actuator Model

Without loss of generality the model of a vessel with two propellers and one bow thruster is considered (see Fig. 10.2). The vector of the ship's control forces and torques $\tau \in R^3$ is related to propeller pitch ratios vector u (or propeller revolutions

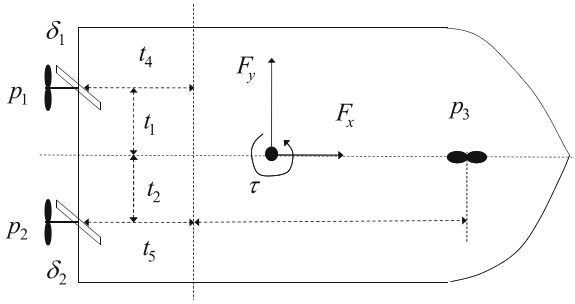

Fig. 10.2 Model of a vessel with two propellers and a bow thruster

for fixed blade propellers) as follows [171]

$$\tau = T \cdot K(U) \cdot u \tag{10.11}$$

where U is the magnitude of the ship's velocity in the xy-plane i.e. $U = \sqrt{u^2 + v^2}$ while u denotes the surge velocity and v denotes the sway velocity. Vector u is defined as $u = [f_1(p_1), f_2(p_2), f_3(p_3), f_4(\delta_1), f_5(\delta_2)]^T$. For the (fully actuated) ship model of Fig. 10.2 with two propellers p_1 and p_2, one thruster p_3 and two rudders δ_1 and δ_2, matrix $T \in R^{3\times 6}$ depends on the position of the actuators p_1, p_2 and p_3, while matrix $K(U) \in R^{6\times 6}$ depends on the ship's velocity and the type of the actuators. The coefficients of matrices T and K are defined as follows: p_i, $(i = 1, 2, 3)$ are the propeller pitch ratios (or for fixed-blade propellers are the propeller revolutions), δ_i, $(i = 1, 2)$ are the rudder angles, t_i, $(i = 1, \ldots, 5)$ are distances to of the actuators from the ship's symmetry axes, and k_i, $(i = 1, \ldots, 5)$ are the force coefficients.

10.2.4 Feedback Linearization for Ship Dynamic Positioning

10.2.4.1 Nonlinear Positioning Control of the Ship Model

As mentioned above, the kinematic and dynamic model of the ship is given by

$$\begin{aligned} \dot{\eta} &= R \cdot v \\ M\dot{v} + D(v)v - R^T d &= \tau \end{aligned} \tag{10.12}$$

From the previous equation one obtains $v = R^{-1}\dot{\eta}$, or since $R^T = R^{-1}$ it can be written as $v = R^T\dot{\eta}$. Similarly one obtains $\dot{v} = \dot{R}^T\dot{\eta} + R^T\ddot{\eta}$. Consequently, this gives [140, 227, 462]

$$J(\eta)\ddot{\eta} + C(\eta, \dot{\eta})\dot{\eta} + F(\eta)\dot{\eta} - d = \tau^* \tag{10.13}$$

where the ship model's parameters are defined as

$$\begin{aligned} J(\eta) = RMR^T \in R^{3\times 3}\ C(\eta,\dot{\eta}) = RM\dot{R}^T \in R^{3\times 3} \\ F(\eta) = RDR^T \in R^{3\times 3} \qquad\qquad \tau^* = R\tau \end{aligned} \tag{10.14}$$

and denoting $sin(\psi)$ and $cos(\psi)$ as S_ψ and C_ψ respectively, while using $m_{ij},\ i, j = 1, \ldots, 3$ to represent the elements of the inertia matrix and $d_{ij},\ i, j = 1, \ldots, 3$ to represent the elements of the damping matrix, the terms of the ship's dynamic model are described by [140]

$$J(\eta) = \begin{pmatrix} m_{11}C_\psi^2 + m_{22}S_\psi^2 & (m_{11} - m_{22})S_\psi C_\psi & -m_{23}S_\psi \\ (m_{11} - m_{12})S_\psi C_\psi & m_{11}S_\psi^2 + m_{22}C_\psi^2 & m_{23}C_\psi \\ -m_{23}S_\psi & m_{23}C_\psi & m_{33} \end{pmatrix} \tag{10.15}$$

$$C(\eta,\dot{\eta}) = \begin{pmatrix} \dot{\psi}(m_{22} - m_{11})S_\psi C_\psi & \dot{\psi}(m_{11}C_\psi^2 + m_{22}S_\psi^2) & 0 \\ -\dot{\psi}(m_{11}S_\psi^2) + m_{22}C_\psi^2)) & \dot{\psi}(m_{22} - m_{11})S_\psi C_\psi & 0 \\ -\dot{\psi}(m_{23}C_\psi & -\dot{\psi}(m_{23}S_\psi & 0 \end{pmatrix} \tag{10.16}$$

$$F(\eta) = \begin{pmatrix} d_{11}C_\psi^2 + d_{22}S_\psi^2 & (d_{11} - d_{12})S_\psi C_\psi & -d_{23}S_\psi \\ (d_{11} - d_{12})S_\psi C_\psi & d_{11}S_\psi^2 + d_{22}C_\psi^2 & d_{23}C_\psi \\ -d_{32}S_\psi & d_{32}C_\psi & d_{23} \end{pmatrix} \tag{10.17}$$

The control signal is chosen to be

$$\begin{aligned} \tau^* = J(\eta)[\ddot{\eta}_d + J(\eta)^{-1}C(\eta,\dot{\eta})\dot{\eta} + \\ + J(\eta)^{-1}F(\eta)\dot{\eta} - J(\eta)^{-1}d - K_D\dot{\tilde{\eta}} - K_P\tilde{\eta}] \end{aligned} \tag{10.18}$$

where $\tilde{\eta} = \eta - \eta_d$ is the tracking error, while

$$\begin{aligned} K_D = diag[k_{d_1}, k_{d_2}, k_{d_3}] \\ K_P = diag[k_{p_1}, k_{p_2}, k_{p_3}] \end{aligned} \tag{10.19}$$

are feedback gain matrices. This finally results into the tracking error dynamics

$$\begin{aligned} \ddot{\eta} - \ddot{\eta}_d + K_D\dot{\tilde{\eta}} + K_P\tilde{\eta} = 0 \\ \text{or } \ddot{\tilde{\eta}} + K_D\dot{\tilde{\eta}} + K_P\tilde{\eta} = 0 \end{aligned} \tag{10.20}$$

10.2.5 Joint Estimation of the Ship's State Vector and of Unknown Additive Disturbances

The sensor fusion-based estimation procedure for obtaining the ship's state vector is affected by uncertainties characterizing the ship's dynamic model. Such uncertainties can be due to parametric variations in the model of Eqs. (10.13) and (10.14) or due to external disturbances, e.g. additive input disturbances as shown in Eqs. (10.2) and (10.10). Simultaneous estimation of a dynamical system's state vector and of the disturbances vector can be achieved using disturbance observers [82, 87, 105, 106, 180, 256, 341, 428, 623].

In the case of a surface vessel, defining the generalized state vector $x = [\eta, d, \dot{\eta}, \dot{d}]^T$ and considering invariance of the disturbance d for specific time periods, one obtains the generalized ship state-space model

$$\begin{aligned} &\ddot{\eta} + J(\eta)^{-1}[C(\eta, \dot{\eta}) + F(\eta)]\dot{\eta} - J^{-1}(\eta)d = J^{-1}(\eta)\tau \\ &\ddot{d} = 0. \end{aligned} \tag{10.21}$$

Setting $x_1 = \eta$, $x_2 = d$, $x_3 = \dot{\eta}$, $x_4 = \dot{d}$ and taking into account the existence of process and measurement noise one obtains a ship's model of the form

$$\begin{aligned} \dot{x} &= Ax + Bu + w \\ z &= \gamma(x) + v \end{aligned} \tag{10.22}$$

where matrices A and B are given by

$$\begin{aligned} A &= \begin{pmatrix} 0_{3\times3} & 0_{3\times3} & I_{3\times3} & 0_{3\times3} \\ 0_{3\times3} & 0_{3\times3} & 0_{3\times3} & I_{3\times3} \\ 0_{3\times3} & J^{-1}(x) & -J^{-1}(x)[C(x,\dot{x}) + F(x)] & 0_{3\times3} \\ 0_{3\times3} & 0_{3\times3} & 0_{3\times3} & 0_{3\times3} \end{pmatrix} \\ B &= \begin{pmatrix} 0_{3\times3} & 0_{3\times3} & J^{-1}(x) & 0_{3\times3} \end{pmatrix}^T \end{aligned} \tag{10.23}$$

The extended state vector is $x = [x_1, x_2, x_3, x_4]^T$ with $x_i \in R^{3\times1}$, $i = 1, 2, 3, 4$. The control input is $\tau \in R^{3\times1}$. The measurement vector of the ship's model is given by $z = [x, y, \psi, d^1]^T$, where x, y are measurements of the ship's cartesian coordinates, ψ is a measurement of the ship's orientation and d^1 is a measurement of the ship's distance from the coast, provided by a coastal sensor (e.g. radar). The vectors of process and measurement noises are denoted as w and v, respectively. Using the above state-space representation, state vector x can be estimated by processing a sequence of output measurements y with the use of a state observer or Kalman Filtering [46, 149, 631].

It is noted that disturbance terms affecting the ship's model, as shown in Eq. (10.10), can be identified with the use of disturbance observers were initially

conceived with a static observer gain [82, 87, 180, 256, 341, 623]. However they can be suitably modified so as to be based on dynamic adaptation of the observer gain through the Kalman Filter recursion [105, 428]. Once the disturbances vector is estimated, a supervisory control term can be introduced in the control law so as to annihilate the disturbances effects. A common technique is the Unknown Input Observer which estimates both the states of the system and the disturbance by augmenting a linear design model with a linear disturbance model. Another approach is based on the Extended State Observer. This has the state and disturbance estimation power of an Unknown Input Observer while being also simpler in tuning. Another solution to the problem of simultaneous state and disturbance estimation comes from the Perturbation Observer. The Perturbation observer is suitable not only for estimation of additive disturbances but also for estimation of unmodeled variations of the monitored system. In place of static observer gain for the aforementioned observers one can consider on-line adaptation of the observer's gain through the Kalman Filter recursion. Therefore it is possible to design Kalman Filter-based disturbance observers exhibiting the advantages of Kalman Filter estimation such as minimization of the estimation error and smoother convergence of the estimated state variables towards the real state variables.

10.2.6 Sensor Fusion for the Surface Vessel Using Kalman Filtering

The application of EKF to the fusion of data that come from different sensors of the monitored surface vessel is examined first. The ship's kinematic and dynamic model is considered again. It is assumed that at each time instant measurements of the ship's cartesian coordinates (x, y) as well as of the ship's heading ψ are available. Moreover the distance of the ship from the coast is provided by a coastal sensor (e.g. radar). Fusing the aforementioned measurements with the use of a stochastic estimation algorithm, such as the Kalman Filter, can provide an accurate estimate of the ship's state vector.

The coordinates of the center of symmetry of the ship with respect to OXY (inertial coordinates system) are (x, y), while the coordinates of a reference point i of the ship (e.g. bridge), with respect to $O'X'Y'$ (body-fixed coordinates system) are $x_i^{'}$, $y_i^{'}$ (Fig. 10.3). The orientation of the ship's reference point with respect to $O'X'Y'$ is $\psi_i^{'}$.

Thus the coordinates of the reference point i with respect to OXY are (x_i, y_i) and its orientation is ψ_i, and are given by

$$\begin{aligned} x_i(k) &= x(k) + x_i^{'} sin(\psi(k)) + y_i^{'} cos(\psi(k)) \\ y_i(k) &= y(k) - x_i^{'} cos(\psi(k)) + y_i^{'} sin(\psi(k)) \\ \psi_i(k) &= \psi(k) + \psi_i \end{aligned} \tag{10.24}$$

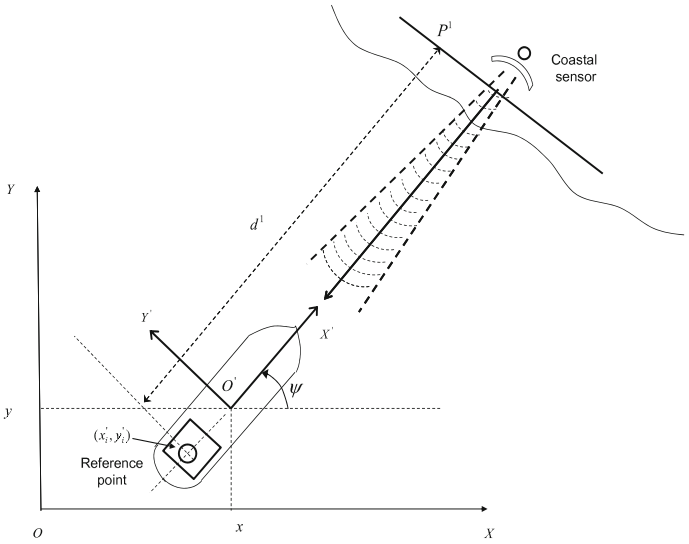

Fig. 10.3 Estimation of the ship's state vector by fusing the measurements of its position and orientation with the measurement of its distance from the coast provided by a coastal sensor (e.g. radar)

Each reference plane P^j on the coast can be represented by P_r^j and P_n^j (Fig. 10.3), where (i) P_r^j is the normal distance of the plane from the origin O, (ii) P_n^j is the angle between the normal line to the plane and the x-direction. Using the above notation, the distance of the ship's reference point i (e.g. bridge), from the reference plane P^j on the coast depends on P_r^j, P_n^j (see Fig. 10.3) [433]:

$$d^1(k) = P_r^j - x_i(k)cos(P_n^j) - y_i(k)sin(P_n^j). \tag{10.25}$$

By definition of the measurement vector one has that the output function $\gamma(x(k))$ is given by

$$\gamma(x(k)) = [x(k), y(k), \psi(k), d^1(k)]^T \tag{10.26}$$

To obtain the Extended Kalman Filter (EKF), the model of the ship is linearized about the estimates $\hat{x}(k)$ and $\hat{x}^-(k)$ as described in the previous subsection. The process noise covariance matrix $Q(k) \in R^{12\times12}$ and the measurement noise matrix $R \in R^{4\times4}$ are taken to be diagonal. The Kalman Filter gain is $K \in R^{12\times4}$. For matrix γ appearing in the ship's output equation it holds

$$\gamma(\hat{x}(k)) = [\hat{x}(k), \hat{y}(k), \hat{\psi}(k), P_r^j - x_i(k))cos(P_n^j) - y_i(k)sin(P_n^j)]^T \tag{10.27}$$

The Jacobian of the ship model's output γ with respect to the state vector $x(k)$ is thus,

$$J_{\gamma}^{T}(\hat{x}^{-}(k)) = \begin{pmatrix} 1 & 0 & 0 & 0_{1\times 9} \\ 0 & 1 & 0 & 0_{1\times 9} \\ 0 & 0 & 1 & 0_{1\times 9} \\ \alpha_{41} & \alpha_{42} & \alpha_{43} & 0_{1\times 9} \end{pmatrix} \tag{10.28}$$

where $\alpha_{41} = -cos(P_n^j)$, $\alpha_{42} = -sin(P_n^j)$ and $\alpha_{43} = \{x_i^{'}cos(\psi - P_n^j) - y_i^{'}sin(\psi - P_n^j)\}$. As analyzed in Sect. 10.2.4, the ship can be steered along the reference trajectory using the estimated state vector and control based on feedback linearization of the ship's dynamic model. Alternatively nonlinear backstepping control can be used [462].

For the dynamic model of the vessel that is described by Eqs. (10.161) and (10.162) sensor fusion-based state estimation can be performed using Kalman Filtering. As shown for instance in Eqs. (4.88) and (4.89) the implementation stages of the Kalman Filter comprise a measurement-update part and a time-update part.

10.2.7 Particle Filter-Based Sensor Fusion for Estimating the Ship's Motion and Disturbances

As in the KF case, the Particles Filter consists also of the measurement update (correction stage) and the time update (prediction stage) [271, 555, 625]. The prediction stage calculates

$$p(x(k)|Z^{-}) \text{ where } Z^{-} = \{z(1), z(2), \ldots, z(k-1)\} \tag{10.29}$$

are output measurements up to time instant $k-1$. It holds that

$$p(x(k-1)|Z^{-}) = \sum_{i=1}^{N} w_{k-1}^{i} \delta_{\xi_{k-1}^{i}}(x(k-1)) \tag{10.30}$$

while from Bayes formula it holds

$$p(x(k)|Z^{-}) = \int p(x(k)|x(k-1))p(x(k-1)|Z^{-})dx \tag{10.31}$$

From the above one finally obtains:

$$\begin{aligned} &p(x(k)|Z^{-}) = \textstyle\sum_{i=1}^{N} w_{k-1}^{i} \delta_{\xi_{k^{-}}^{i}}(x(k)) \\ &\text{with } \xi_{k^{-}}^{i} \sim p(x(k)|x(k-1) = \xi_{k-1}^{i}) \end{aligned} \tag{10.32}$$

The previous relation means that the state equation of the system is executed N times, starting from the N previous values of the state vectors $x(k-1) = \xi_{k-1}^i$. Consequently, the value of the state vector which is calculated in the prediction stage is the result of the weighted averaging of the state vectors which were computed after running the state equation, starting from the N previous values of the state vectors ξ_{k-1}^i.

The a-posteriori probability density is found as follows: a new position measurement $z(k)$ is obtained and the objective is to calculate the corrected probability density

$$p(x(k)|Z) \text{ where } Z = \{z(1), z(2), \ldots, z(k)\} \tag{10.33}$$

From Bayes law it holds that

$$p(x(k)|Z) = \frac{p(Z|x(k))p(x(k))}{p(Z)} \tag{10.34}$$

which can be also written as

$$p(x(k)|Z) = \frac{p(z(k)|x(k))p(x(k)|Z^-)}{\int p(z(k)|x(k), Z^-)p(x(k)|Z^-)dx} \tag{10.35}$$

After intermediate calculations one finally obtains

$$\begin{aligned} p(x(k)|Z) &= \sum_{i=1}^{N} w_k^i \delta_{\xi_{k^-}^i}(x(k)) \\ \text{where } w_k^i &= \frac{w_{k^-}^i p(z(k)|x(k) = \xi_{k^-}^i)}{\sum_{j=1}^{N} w_{k^-}^j p(z(k)|x(k) = \xi_{k^-}^j)} \end{aligned} \tag{10.36}$$

The previous equation denotes the corrected value for the state vector. The recursion of the PF proceeds in a way similar to the update of the Kalman Filter or the Extended Kalman Filter [450, 555].

Measurement update: Acquire $z(k)$ and compute the new value of the state vector

$$\begin{aligned} &p(x(k)|Z) = \textstyle\sum_{i=1}^{N} w_k^i \delta_{\xi_{k^-}^i}(x(k)) \\ &\text{with corrected weights } w_k^i = \frac{w_{k^-}^i p(z(k)|x(k) = \xi_{k^-}^i)}{\sum_{j=1}^{N} w_{k^-}^i p(z(k)|x(k) = \xi_{k^-})^i} \\ &\text{and } \xi_k^i = \xi_{k^-}^i \end{aligned} \tag{10.37}$$

Resampling: Substitute the degenerated particles. The particles of low weight factors are removed and their place is occupied by duplicates of the particles with high weight factors.

Time update: compute state vector $x(k+1)$ according to the pdf

$$\begin{gathered} p(x(k+1)|Z) = \sum_{i=1}^{N} w_k^i \delta_{\xi_k^i}(x(k)) \\ \text{where } \xi_k^i \sim p(x(k+1)|x(k) = \xi_k^i) \end{gathered} \tag{10.38}$$

Knowing the measured value of the ship's position and orientation $[x, y, \psi]$, one can assign a weight to each particle (estimate of the state vector $[\hat{x}, \hat{y}, \hat{\psi}]_i$), according to how closely the particle approaches the measured state vector. Similarly, knowing the distance d^1 from the coastal reference surface, and calculating an estimation of this distance $\hat{d}^1$ for every particle $[\hat{x}, \hat{y}, \hat{\psi}]_i$, one can assign a weight to the particle according to the accuracy of estimation of the distance d^1. Further averaging of these two weight values associated with each particle provides the aggregate particle's weight which is used in the Particle Filter's iteration.

10.2.8 Simulation Tests

10.2.8.1 Dynamic Ship Positioning with the Use of Kalman Filtering

The use of Kalman and Particle Filtering for fusing the data that come from the ship's navigation instruments with the measurements that come from coastal sensors provides an estimation of the state vector $[x(t), y(t), \psi(t)]$ and enables the successful application of nonlinear steering control. In the implementation of the Kalman Filter the process noise covariance matrix $Q \in R^{12\times 12}$ and the measurement noise covariance matrix $R \in R^{4\times 4}$ were taken to be diagonal with nonzero elements equal to $10e^{-3}$. The number of particles used by the PF was $N = 1000$. From the simulation experiments it can be observed that the KF and the PF provide accurate estimations of the external disturbances. Thus, an auxiliary control term based on the disturbances estimation can be included in the right hand side of Eq. (10.18), and can compensate for the disturbances' effects.

The following cases were examined: (i) Kalman Filtering-based ship's Dynamic Positioning (DP) through tracking of a circular trajectory. The associated results are shown in Figs. 10.4, 10.5, 10.6, 10.7 and 10.8 (ii) Kalman Filtering-based ship's DP through tracking of an eight-shaped trajectory. The associated results are shown in Figs. 10.9, 10.10, 10.11, 10.12 and 10.13 (iii) Kalman Filtering-based ship's DP through tracking of a complex curved trajectory. The associated results are shown in Figs. 10.14, 10.15, 10.16, 10.17 and 10.18 (iv) Particle Filtering-based ship's DP through the tracking of a circular trajectory. The associated results are shown in Figs. 10.19, 10.20, 10.21, 10.22 and 10.23 (v) Particle Filtering-based ship's DP through the tracking of an eight-shaped trajectory. The associated results are shown in Figs. 10.24, 10.25, 10.26, 10.27 and 10.28 (vi) Particle Filtering-based ship's DP through the tracking of a complex curved trajectory. The associated results are shown in Figs. 10.29, 10.30, 10.31, 10.32 and 10.33.

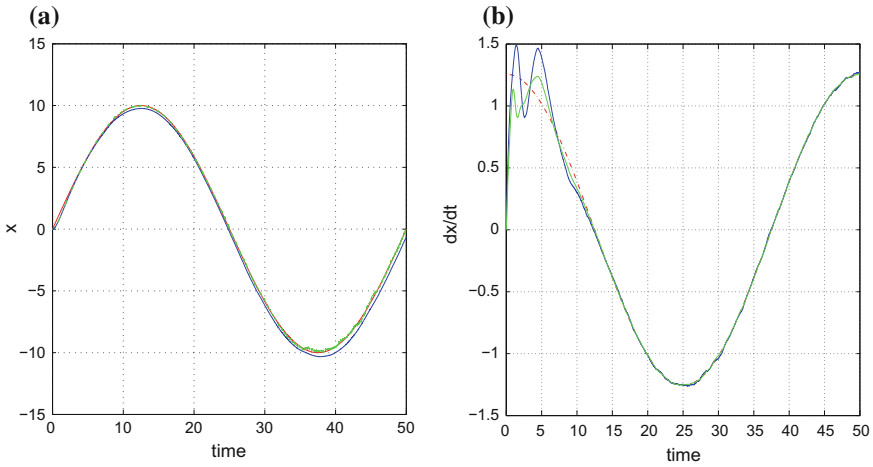

Fig. 10.4 Tracking of a circular trajectory: **a** KF-based estimation of the ship's position along the x-axis (green line) and desirable x-axis position (red line), **b** KF-based estimation of the ship's velocity along the x-axis (green line) and desirable x-axis velocity (red line)

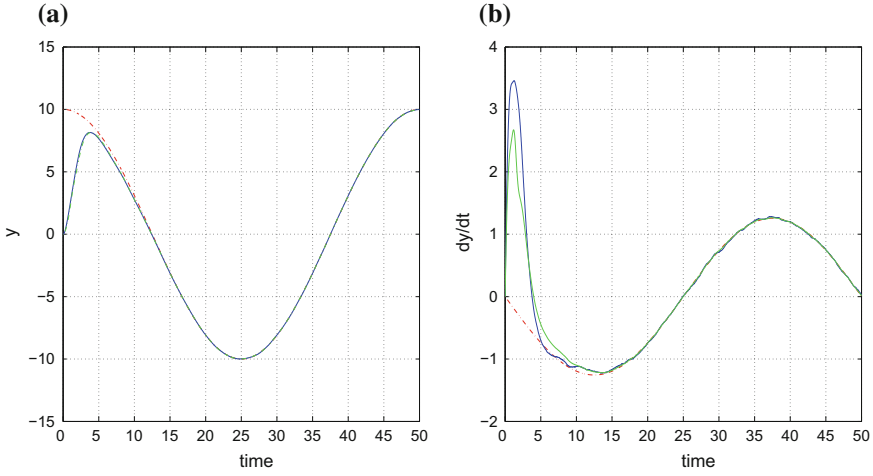

Fig. 10.5 Tracking of a circular trajectory: **a** KF-based estimation of the ship's position along the y-axis (green line) and desirable y-axis position (red line), **b** KF-based estimation of the ship's velocity along the y-axis (green line) and desirable y-axis velocity (red line)

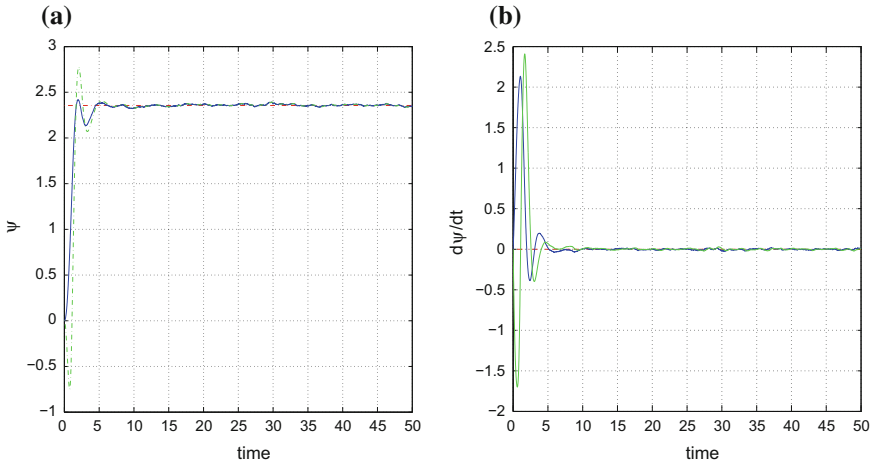

Fig. 10.6 Tracking of a circular trajectory: **a** KF-based estimation of the ship's angle round the z-axis (green line) and desirable z-axis rotation angle (red line), **b** KF-based estimation of the ship's angular velocity round the z-axis (green line) and desirable angular velocity (red line)

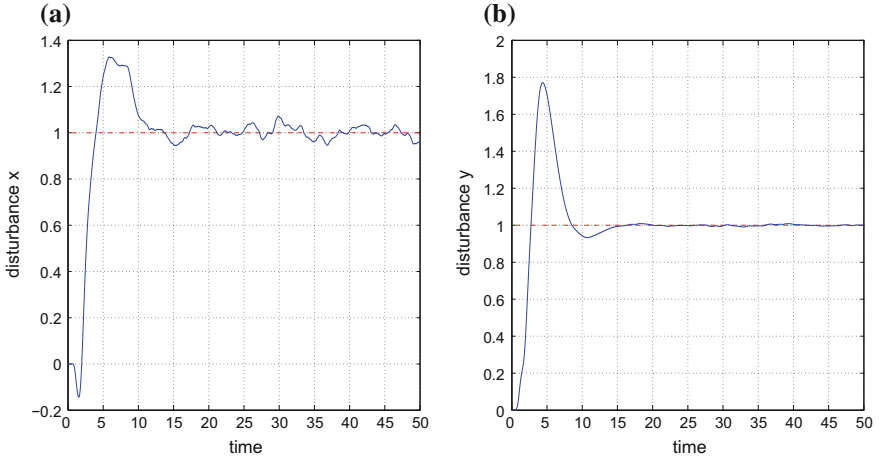

Fig. 10.7 **a** Tracking of a circular trajectory: KF-based estimation of the disturbance along the x-axis (blue line) and real value of the x-axis disturbance (red line), **b** KF-based estimation of the disturbance along the y-axis (blue line) and real value of the y-axis disturbance (red line)

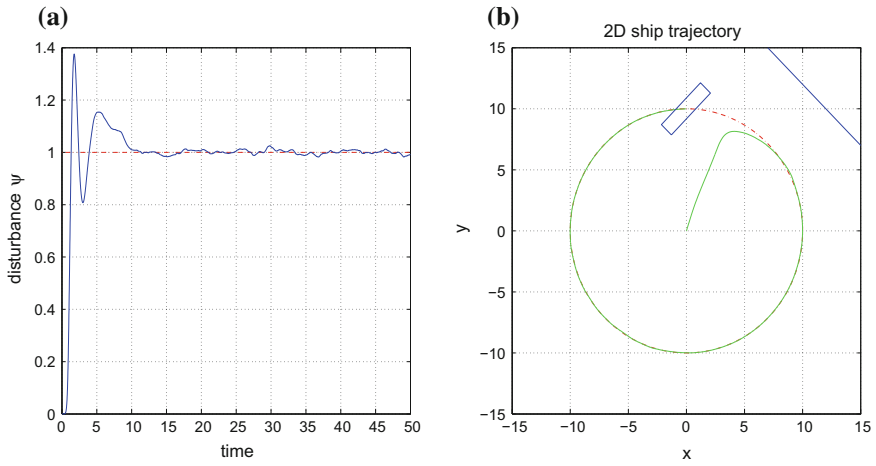

Fig. 10.8 Tracking of a circular trajectory: **a** KF-based estimation of the disturbance torque round the z-axis (blue line) and real value of the z-axis disturbance torque (red line), **b** Trajectory of the ship on the xy-plane (green line) and desirable ship trajectory (red line) in the case of KF-based state estimation

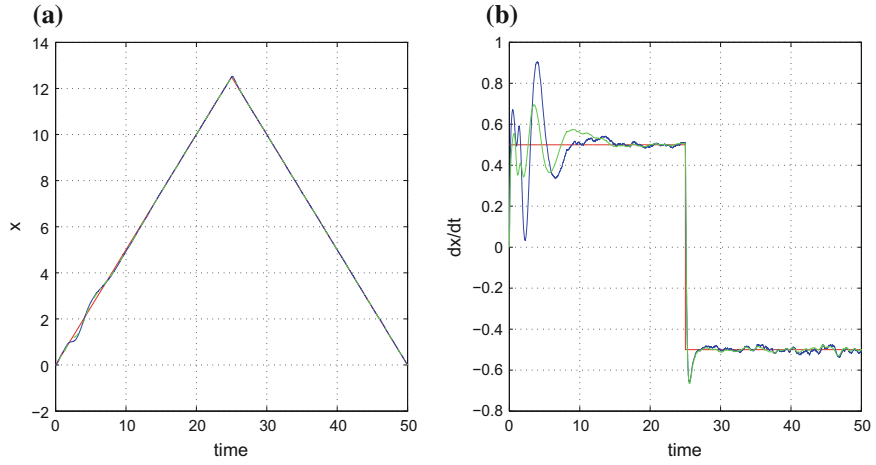

Fig. 10.9 Tracking of an eight-shaped trajectory: **a** KF-based estimation of the ship's position along the x-axis (green line) and desirable x-axis position (red line), **b** KF-based estimation of the ship's velocity along the x-axis (green line) and desirable x-axis velocity (red line)

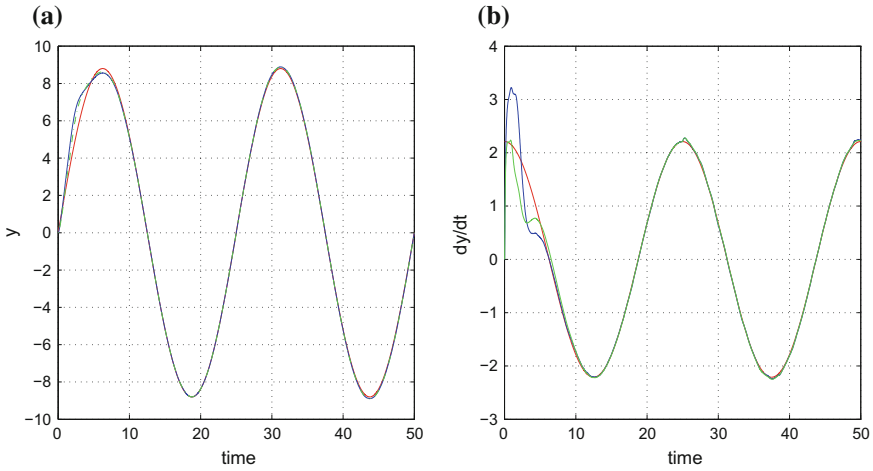

Fig. 10.10 Tracking of an eight-shaped trajectory: **a** KF-based estimation of the ship's position along the y-axis (green line) and desirable y-axis position (red line), **b** KF-based estimation of the ship's velocity along the y-axis (green line) and desirable y-axis velocity (red line)

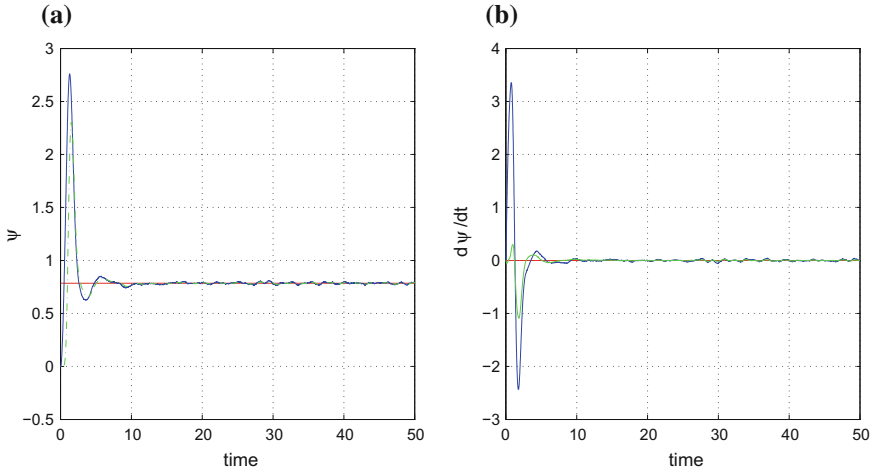

Fig. 10.11 Tracking of an eight-shaped trajectory: **a** KF-based estimation of the ship's angle round the z-axis (green line) and desirable z-axis rotation angle (red line), **b** KF-based estimation of the ship's angular velocity round the z-axis (green line) and desirable angular velocity (red line)

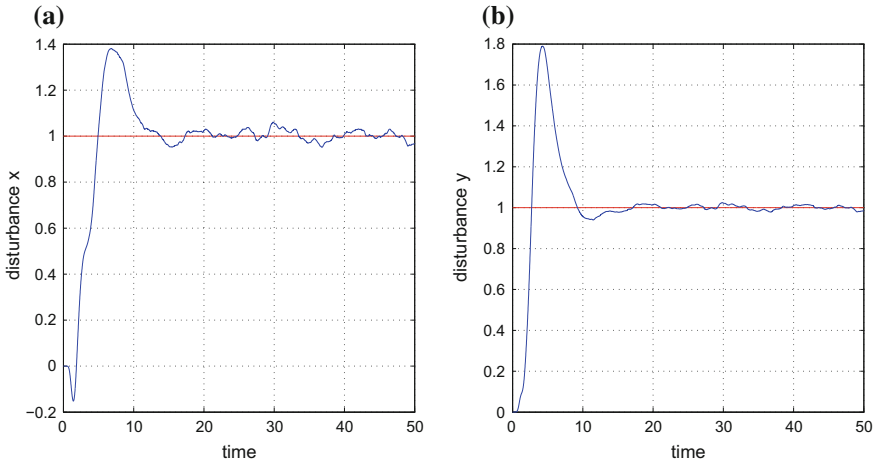

Fig. 10.12 Tracking of an eight-shaped trajectory: **a** KF-based estimation of the disturbance along the x-axis (blue line) and real value of the x-axis disturbance (red line), **b** KF-based estimation of the disturbance along the y-axis (blue line) and real value of the y-axis disturbance (red line)

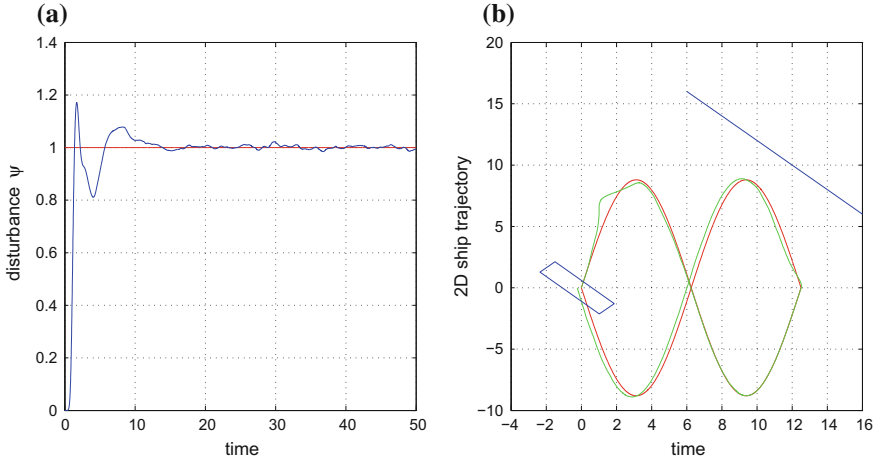

Fig. 10.13 Tracking of an eight-shaped trajectory: **a** KF-based estimation of the disturbance torque round the z-axis (blue line) and real value of the z-axis disturbance torque (red line), **b** Trajectory of the ship on the xy-plane (green line) and desirable ship trajectory (red line) in the case of KF-based state estimation

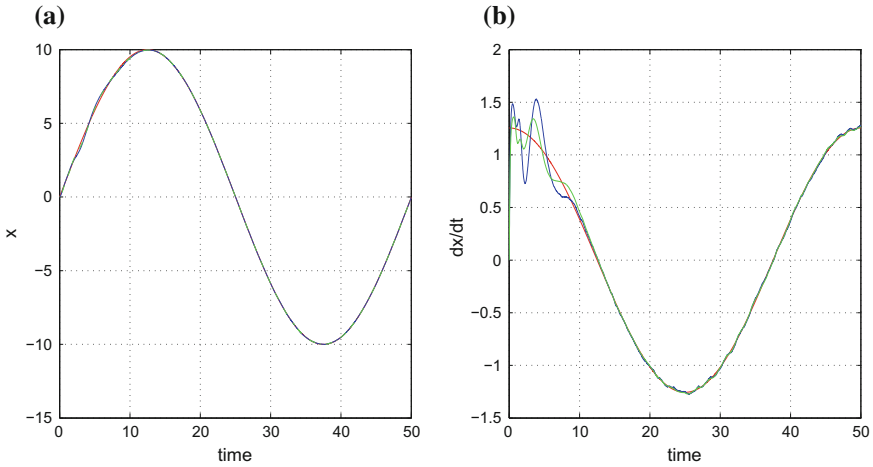

Fig. 10.14 Tracking of a complex-curved trajectory: **a** KF-based estimation of the ship's position along the x-axis (green line) and desirable x-axis position (red line), **b** KF-based estimation of the ship's velocity along the x-axis (green line) and desirable x-axis velocity (red line)

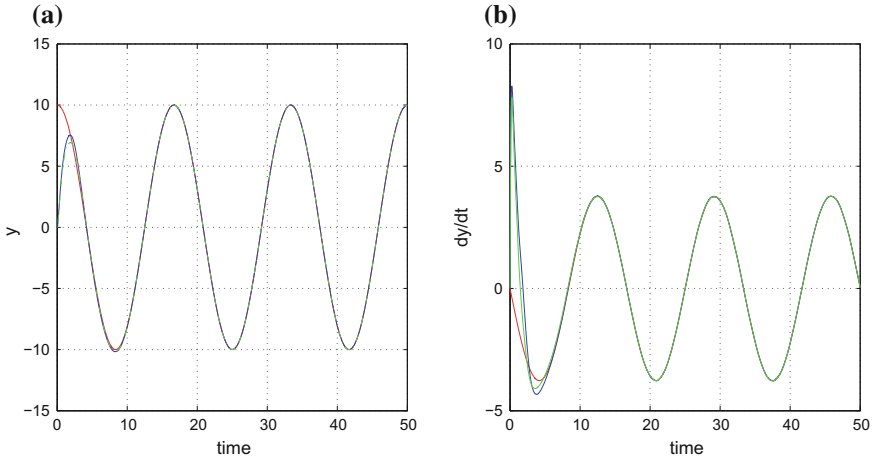

Fig. 10.15 Tracking of a complex-curved trajectory: **a** KF-based estimation of the ship's position along the y-axis (green line) and desirable y-axis position (red line), **b** KF-based estimation of the ship's velocity along the y-axis (green line) and desirable y-axis velocity (red line)

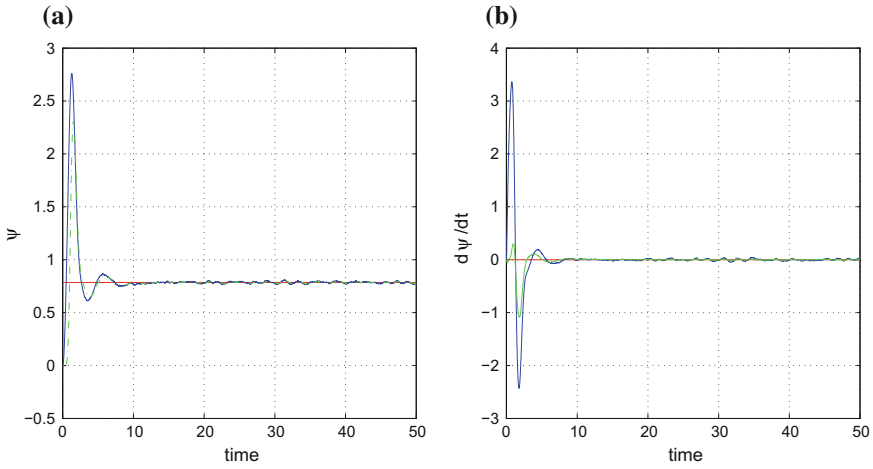

Fig. 10.16 Tracking of a complex-curved trajectory: **a** KF-based estimation of the ship's angle round the z-axis (green line) and desirable z-axis rotation angle (red line), **b** KF-based estimation of the ship's angular velocity round the z-axis (green line) and desirable angular velocity (red line)

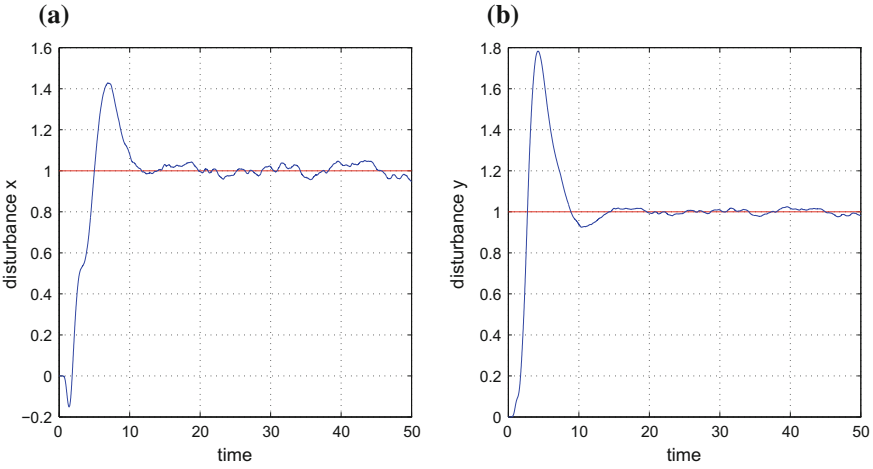

Fig. 10.17 Tracking of a complex-curved trajectory: **a** KF-based estimation of the disturbance along the x-axis (blue line) and real value of the x-axis disturbance (red line), **b** KF-based estimation of the disturbance along the y-axis (blue line) and real value of the y-axis disturbance (red line)

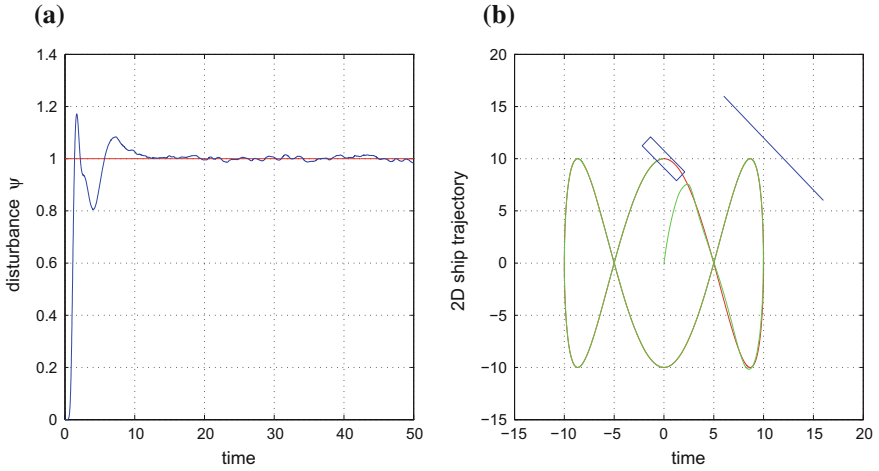

Fig. 10.18 Tracking of a complex-curved trajectory: **a** KF-based estimation of the disturbance torque round the z-axis (blue line) and real value of the z-axis disturbance torque (red line), **b** Trajectory of the ship on the xy-plane (green line) and desirable ship trajectory (red line) in the case of KF-based state estimation

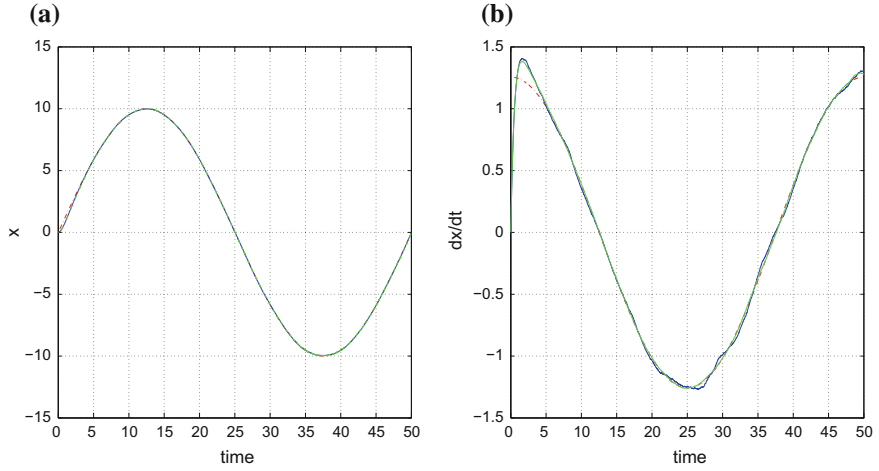

Fig. 10.19 Tracking of a circular trajectory: **a** PF-based estimation of the ship's position along the x-axis (green line) and desirable x-axis position (red line), **b** PF-based estimation of the ship's velocity along the x-axis (green line) and desirable x-axis velocity (red line)

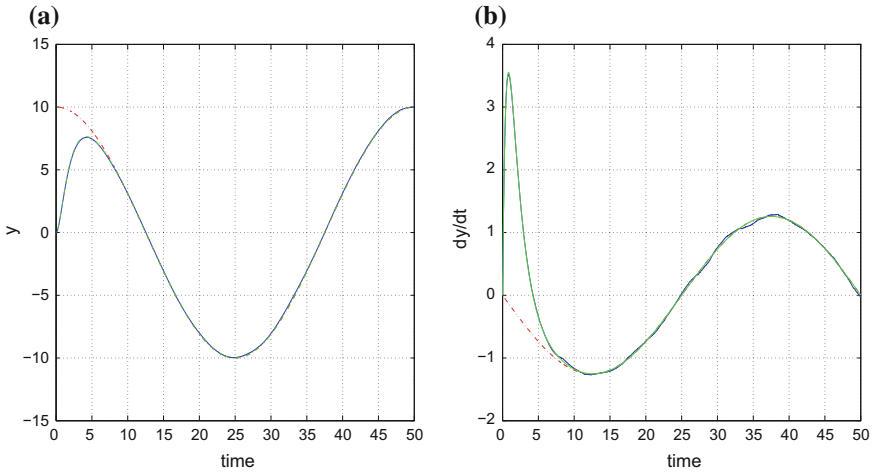

Fig. 10.20 Tracking of a circular trajectory: **a** PF-based estimation of the ship's position along the y-axis (green line) and desirable y-axis position (red line), **b** PF-based estimation of the ship's velocity along the y-axis (green line) and desirable y-axis velocity (red line)

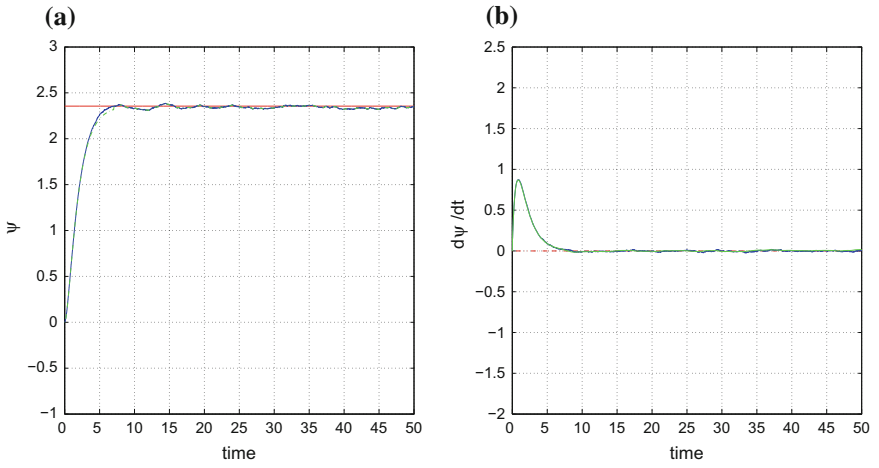

Fig. 10.21 Tracking of a circular trajectory: **a** PF-based estimation of the ship's angle round the z-axis (green line) and desirable z-axis rotation angle (red line), **b** PF-based estimation of the ship's angular velocity round the z-axis (green line) and desirable angular velocity (red line)

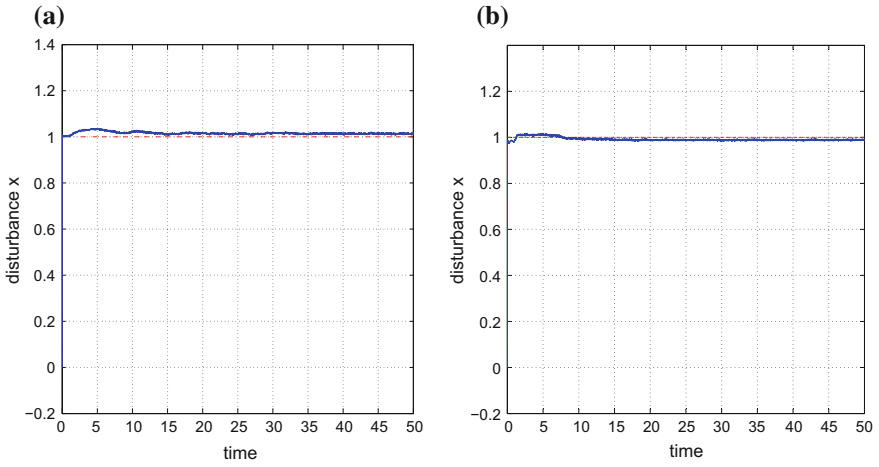

Fig. 10.22 Tracking of a circular trajectory: **a** PF-based estimation of the disturbance along the x-axis (blue line) and real value of the x-axis disturbance (red line), **b** PF-based estimation of the disturbance along the y-axis (blue line) and real value of the y-axis disturbance (red line)

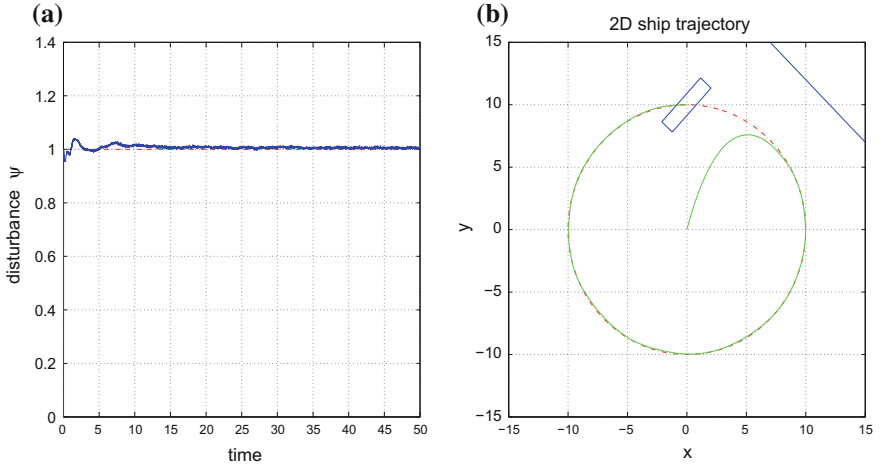

Fig. 10.23 Tracking of a circular trajectory: **a** PF-based estimation of the disturbance torque round the z-axis (blue line) and real value of the z-axis disturbance torque (red line), **b** Trajectory of the ship on the xy-plane (green line) and desirable ship trajectory (red line) in the case of PF-based state estimation

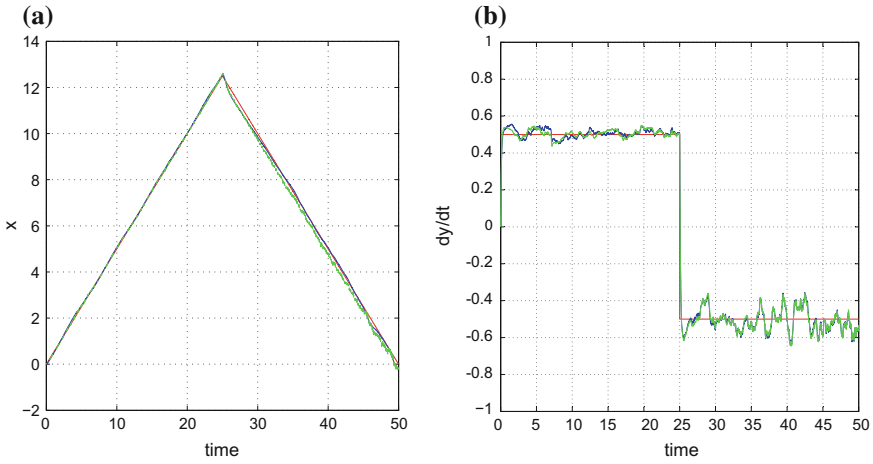

Fig. 10.24 Tracking of an eight-shaped trajectory: **a** PF-based estimation of the ship's position along the x-axis (green line) and desirable x-axis position (blue line), **b** PF-based estimation of the ship's velocity along the x-axis (green line) and desirable x-axis velocity (red line)

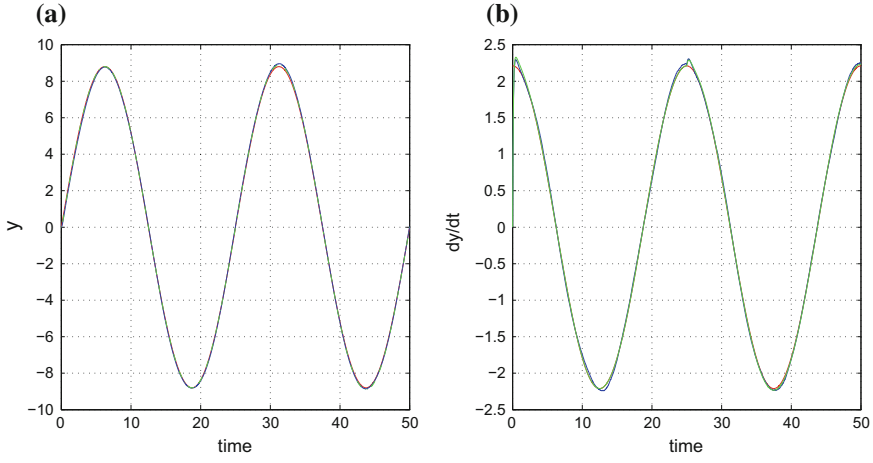

Fig. 10.25 Tracking of an eight-shaped trajectory: **a** PF-based estimation of the ship's position along the y-axis (green line) and desirable y-axis position (red line), **b** PF-based estimation of the ship's velocity along the y-axis (green line) and desirable y-axis velocity (red line)

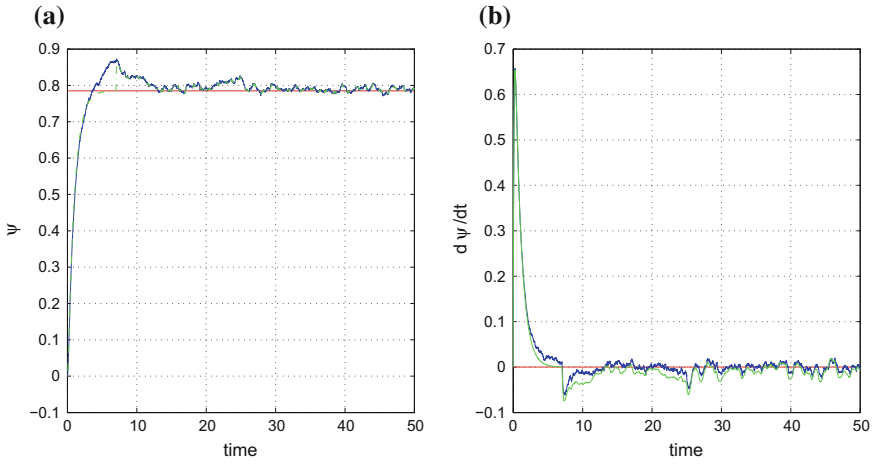

Fig. 10.26 Tracking of an eight-shaped trajectory: **a** PF-based estimation of the ship's angle round the z-axis (blue line) and desirable z-axis rotation angle (red line), **b** PF-based estimation of the ship's angular velocity round the z-axis (blue line) and desirable angular velocity (red line)

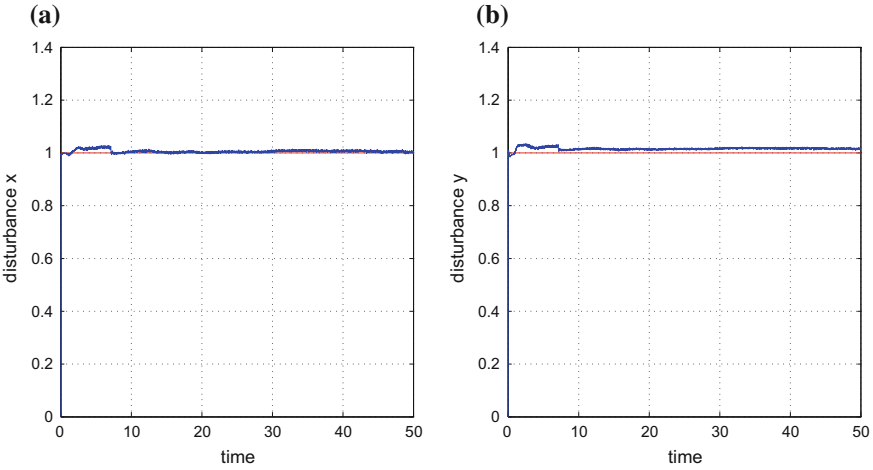

Fig. 10.27 Tracking of an eight-shaped trajectory: **a** PF-based estimation of the disturbance along the x-axis (green line) and real value of the x-axis disturbance (red line), **b** PF-based estimation of the disturbance along the y-axis (green line) and real value of the y-axis disturbance (red line)

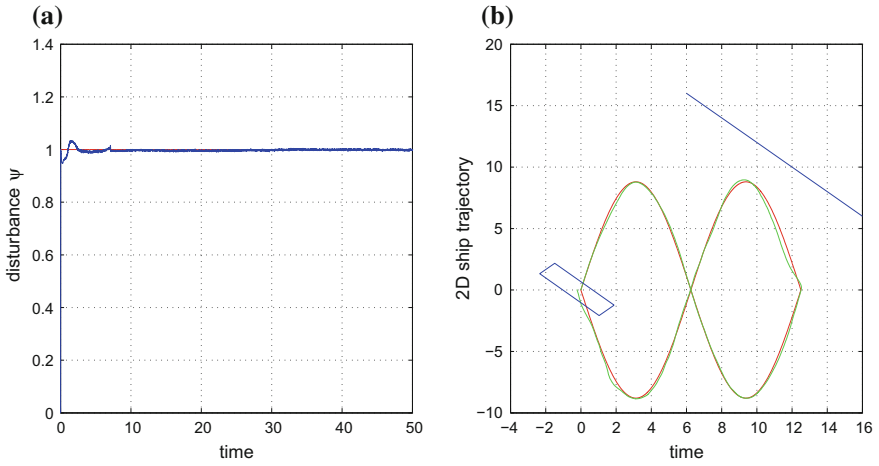

Fig. 10.28 Tracking of an eight-shaped trajectory: **a** PF-based estimation of the disturbance torque round the z-axis (blue line) and real value of the z-axis disturbance torque (red line), **b** Trajectory of the ship on the xy-plane (green line) and desirable ship trajectory (red line) in the case of PF-based state estimation

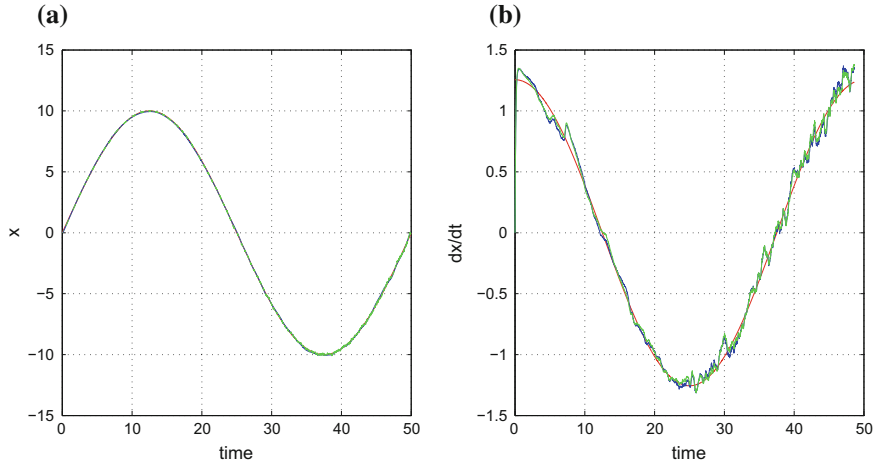

Fig. 10.29 Tracking of a complex-curved trajectory: **a** PF-based estimation of the ship's position along the x-axis (green line) and desirable x-axis position (red line), **b** PF-based estimation of the ship's velocity along the x-axis (green line) and desirable x-axis velocity (red line)

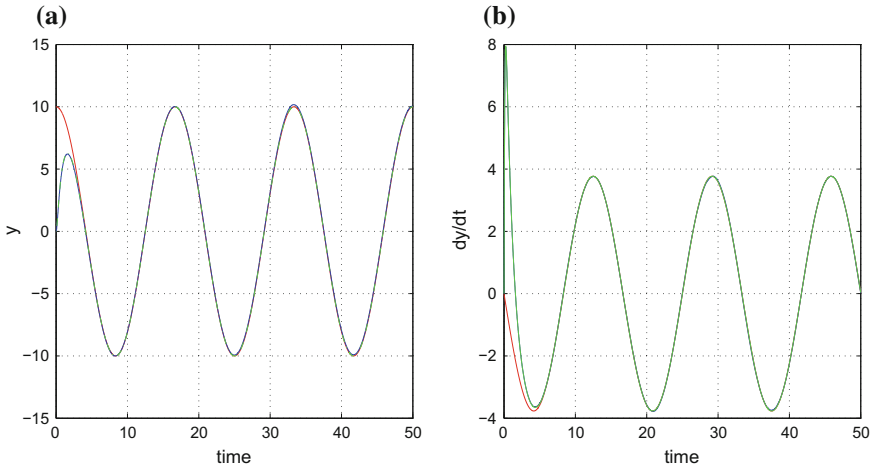

Fig. 10.30 Tracking of a complex-curved trajectory: **a** PF-based estimation of the ship's position along the y-axis (green line) and desirable y-axis position (red line), **b** PF-based estimation of the ship's velocity along the y-axis (green line) and desirable y-axis velocity (red line)

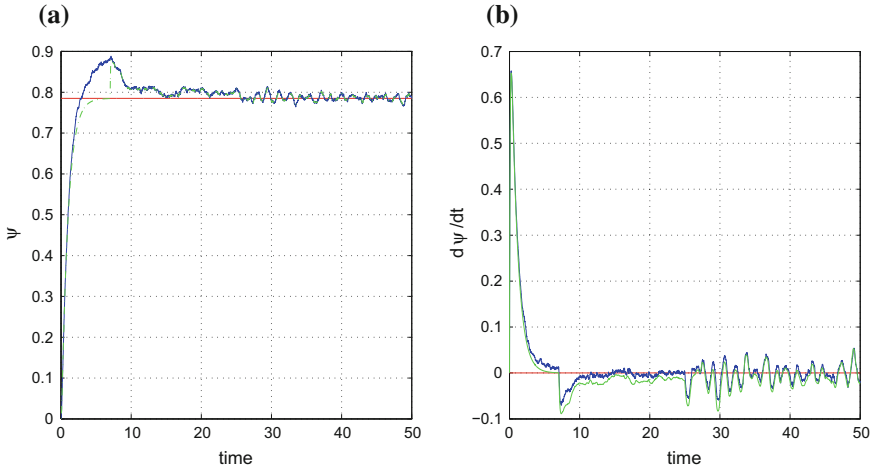

Fig. 10.31 Tracking of a complex-curved trajectory: **a** PF-based estimation of the ship's angle round the z-axis (green line) and desirable z-axis rotation angle (red line), **b** PF-based estimation of the ship's angular velocity round the z-axis (green line) and desirable angular velocity (red line)

10.2.8.2 Evaluation of the Particle Filter-Based State Estimation and Control

From the simulation experiments it can be also noticed that the Particle Filter performs equally well to the Kalman Filter and that it provides accurate estimates of the vessel's

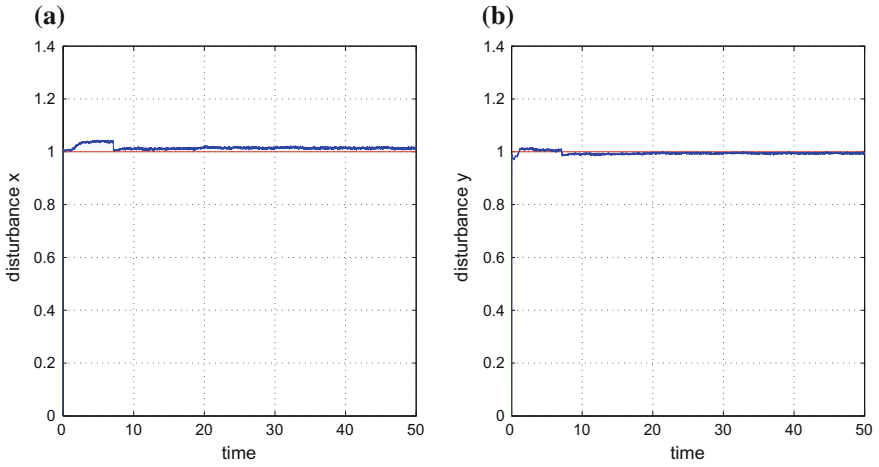

Fig. 10.32 Tracking of a complex-curved trajectory: **a** PF-based estimation of the disturbance along the x-axis (blue line) and real value of the x-axis disturbance (red line), **b** PF-based estimation of the disturbance along the y-axis (blue line) and real value of the y-axis disturbance (red line)

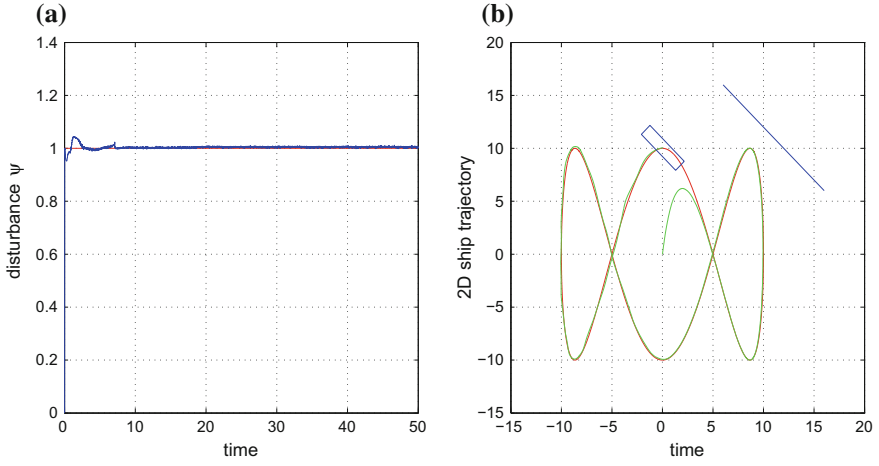

Fig. 10.33 Tracking of a complex-curved trajectory: **a** PF-based estimation of the disturbance torque round the z-axis (blue line) and real value of the z-axis disturbance torque (red line), **b** Trajectory of the ship on the xy-plane (green line) and desirable ship trajectory (red line) in the case of PF-based state estimation

Table 10.1 Variance using KF and PF for N = 1000

State variable	x	y	ψ
KF	$5.24 \cdot 10^{-2}$	$8.52 \cdot 10^{-2}$	$1.94 \cdot 10^{-1}$
PF	$7.03 \cdot 10^{-2}$	$6.80 \cdot 10^{-2}$	$7.47 \cdot 10^{-3}$

Table 10.2 Particle number, simulation time and variance of $\hat{\psi}$

No particles	800	1000	1300	1600	1900	2200
PF cycle time (s)	0.355	0.463	0.577	0.775	0.975	1.097
Variance	$2.733 \cdot 10^{-1}$	$7.473 \cdot 10^{-3}$	$1.153 \cdot 10^{-2}$	$1.647 \cdot 10^{-3}$	$8.905 \cdot 10^{-2}$	$7.817 \cdot 10^{-3}$

state vector. Besides, the Particle Filter is a nonparametric estimator, therefore its application is not constrained by the assumption about Gaussian measurements noise made in the case of the Kalman Filter. Table 10.1 presents results on the variance of the state vector estimates, when considering equal noise levels for the EKF and the PF simulation, and assuming that the number of particles used by the PF was $N = 1000$.The measure used for evaluating the accuracy of the estimation performed by the nonlinear filters, as well as the accuracy of tracking of the state estimation-based control loops was the Root Mean Square Error (RMSE). Alternatively, the Cramer–Rao Lower Bound (CRLB) could have been considered [129, 181, 639].

The cycle time (runtime) of the Particle Filter with respect to the number of particles, using the Matlab platform on a PC with a 2GHz Intel Core Duo processor, is depicted in Table 10.2. Optimization of code of the resampling procedure can improve to some extent the speed of the algorithm. When it is necessary to use more particles, improved hardware and parallel processing available to embedded systems enable real-time implementation of the PF algorithm [53, 340, 611].

When sorting of particles is not performed in the resampling procedure the runtime of Particle Filtering increases linearly with respect to the number of particles [493].

Finally, the accuracy of tracking of the previously described reference trajectories was examined under progressively increasing disturbance magnitude. It was observed that tracking of these trajectories was possible even when the magnitude of the disturbance became several times larger than the initial disturbance of Figs. 10.7, 10.8, 10.9, 10.10, 10.11, 10.12, 10.13, 10.14, 10.15, 10.16, 10.17, 10.18, 10.19, 10.20, 10.21, 10.22, 10.23, 10.24, 10.25, 10.26, 10.27, 10.28, 10.29, 10.30, 10.31, 10.32 and 10.33. Indicative results for disturbance $d_i = 3,\ i = 1, \ldots, 3$ are presented in Fig. 10.34.

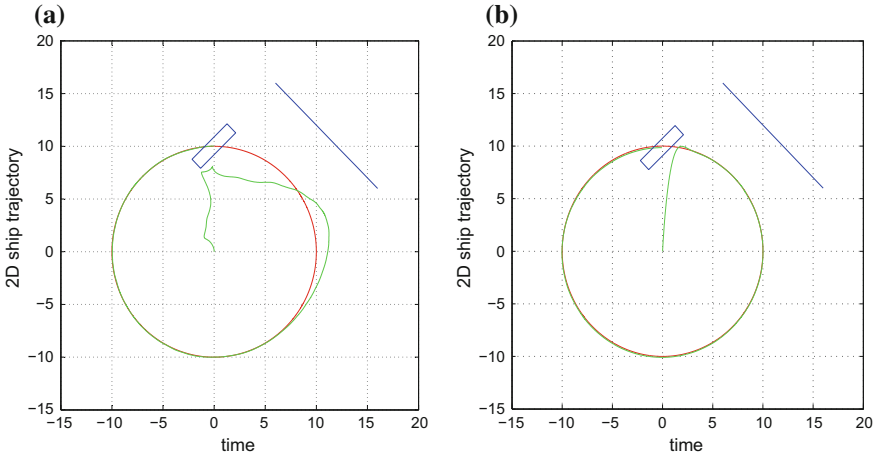

Fig. 10.34 Tracking of a circular trajectory under raised additive disturbances: **a** Trajectory of the ship on the xy-plane (continuous line) and desirable ship trajectory (red line) in the case of KF-based state estimation, **b** Trajectory of the ship on the xy-plane (red line) and desirable ship trajectory (dashed line) in the case of PF-based state estimation

10.3 Flatness-Based Control for the Autonomous Hovercraft

10.3.1 Outline

Autonomous navigation of unmanned surface vessels (USVs) (such as hovercrafts), is a significant topic, since it can find use in both security purposes and passenger transportation [345, 452, 517, 518, 545]. The problem of control and trajectory tracking for unmanned surface vessels of the hovercraft type is non-trivial because the associated kinematic model is a complex nonlinear one [20, 128, 179, 522, 566]. A first problem that arises in controller design for unmanned vessels is that trajectory tracking has to be achieved despite modelling uncertainty and external perturbations and thus the control loop must exhibit sufficient robustness [297, 498]. Another problem that has to be dealt with is that the vessels' model can be underactuated [36, 47, 99, 127, 167, 187, 375, 498, 505, 505, 526, 627]. Indicative results on control of underactuated dynamical systems can be found in [416].

As previously noted, the problem of autonomous navigation of unmanned surface vessels has received particular attention, since it can find use in both security purposes and passenger transportation [2, 111, 452, 517, 518, 545]. In particular, the problem of control and trajectory tracking for unmanned surface vessels of the hovercraft type is non-trivial because the associated kinematic model is a complex nonlinear one [20, 128, 179, 522, 566]. Another problem that has to be dealt with is that the hovercraft's model is underactuated [36, 47, 187, 375, 505, 526]. Indicative results on control of underactuated dynamical systems can be found in [402, 404, 427].

Moreover, the hovercraft's model cannot be subjected to undergo static feedback linearization, but admits only dynamic feedback linearization. This means that to achieve linearization, the state-space description of the system has to be augmented by considering as additional state variables the control inputs and their derivatives. Thus, finally the control input that is applied to the vessel contains integral terms of the tracking error. The present section proposes a solution to the control problem of hovercrafts with the use of differential flatness theory and of a nonlinear filtering method, the so-called Derivative-free nonlinear Kalman Filter.

First it is shown that the hovercraft's model is differentially flat. This means that all its state variables and the control inputs can be written as differential functions of one single algebraic variable which is the flat output [57, 145, 254, 267, 322, 450, 472, 476, 519]. By exploiting the differential flatness properties it is shown that the system can be transformed into the linear canonical form, through dynamic feedback linearization. To achieve this, dynamic extension is performed which means that the state-vector's dimension is increased by considering as additional state variables certain control inputs and their derivatives. For the linearized equivalent model of the system the design of a state feedback controller is possible, through the use of pole placement techniques. Next, to estimate the nonmeasurable state variables of the surface vessel and to identify additive disturbance terms that affect the system, the Derivative-free nonlinear Kalman Filter is redesigned as a disturbance observer [33, 421, 431, 438, 443, 457, 463]. This estimation algorithm consists of the standard Kalman Filter recursion applied on the linearized equivalent model of the surface vessel and of an inverse transformation that makes use of differential flatness theory, which permits to compute estimates of the state variables of the initial nonlinear system.

Comparing to approximate linearization methods [79, 99, 205, 564], nonlinear feedback control approaches which are based on exact feedback linearization of the vessel's model, are assessed as follows: (i) they avoid cumulative numerical errors which are due to the approximate linearization of the system dynamics coming from the application of Taylor series expansion, (ii) the generated control input compensates exclusively for the effects of external perturbations whereas in approximate linearization methods the control input has to compensate both for internal modelling errors and for exogenous disturbances, (iii) they require a smaller number of real-time computations for generating the control inputs, because unlike the approximate linearization methods a large part of the controller's design (e.g. computation of the linearized equivalent model of the system) is performed out of the loop.

10.3.2 State-Space Description of the Underactuated Hovercraft

10.3.2.1 State-Space Equation of the Underactuated Hovercraft

The hovercraft's dynamic and kinematic model stems from the generic ship's model, after setting specific values for the elements of the inertia and Coriolis matrix and

after reducing the number of the available control inputs [452, 517, 518]. The state-space equation of the nonlinear underactuated hovercraft model (Fig. 10.35) is given by

$$\begin{aligned} \dot{x} &= ucos(\psi) - vsin(\psi) \\ \dot{y} &= usin(\psi) + vcos(\psi) \\ \dot{\psi} &= r \\ \dot{u} &= v{\cdot}r + \tau_u \\ \dot{v} &= -u{\cdot}r - \beta v \\ \dot{r} &= \tau_r \end{aligned} \tag{10.39}$$

where x and y are the cartesian coordinates of the vessel, ψ is the orientation angle, u is the surge velocity, v is the sway velocity and r is the yaw rate. Coefficient β is a function of elements of the inertia matrix and hydrodynamic damping matrix of the vessel. The control inputs are the surge force τ_u and the yaw torque τ_r. The hovercraft's model is also written in the matrix form:

$$\begin{pmatrix} \dot{x} \\ \dot{y} \\ \dot{\psi} \\ \dot{u} \\ \dot{v} \\ \dot{r} \end{pmatrix} = \begin{pmatrix} ucos(\psi) - vsin(\psi) \\ usin(\psi) + vcos(\psi) \\ r \\ vr \\ -ur - \beta v \\ 0 \end{pmatrix} + \begin{pmatrix} 0 & 0 \\ 0 & 0 \\ 0 & 0 \\ 1 & 0 \\ 0 & 0 \\ 0 & 1 \end{pmatrix} \begin{pmatrix} \tau_u \\ \tau_r \end{pmatrix} \tag{10.40}$$

or equivalently, one has the description

$$\dot{\tilde{x}} = \tilde{f}(\tilde{x}) + \tilde{g}(\tilde{x})\tilde{v} \tag{10.41}$$

The system's state vector is denoted as $\tilde{x} = [x, y, \psi, u, v, r]^T$, $f(\tilde{x}) \in R^{6\times 1}$, and $\tilde{g}(\tilde{x}) = [\tilde{g}_a, \tilde{g}_b] \in R^{6\times 2}$, while the control input is the vector $\tilde{v} = [\tau_u, \tau_r]^T$.

The system's state vector can be extended by including as additional state variables the control input τ_u and its first derivative $\dot{\tau}_u$. These are denoted as $z_1 = \tau_u$ and $z_2 = \dot{\tau}_u$. The extended state-space description of the hovercraft becomes

$$\begin{pmatrix} \dot{x} \\ \dot{y} \\ \dot{\psi} \\ \dot{u} \\ \dot{v} \\ \dot{r} \\ \dot{z}_1 \\ \dot{z}_2 \end{pmatrix} = \begin{pmatrix} ucos(\psi) - vsin(\psi) \\ usin(\psi) + vcos(\psi) \\ r \\ vr + z_1 \\ -ur - \beta v \\ 0 \\ z_2 \\ 0 \end{pmatrix} + \begin{pmatrix} 0 & 0 \\ 0 & 0 \\ 0 & 0 \\ 0 & 0 \\ 0 & 0 \\ 0 & 1 \\ 0 & 0 \\ 1 & 0 \end{pmatrix} \begin{pmatrix} \ddot{\tau}_u \\ \tau_r \end{pmatrix} \tag{10.42}$$

or equivalently, one has the description

$$\dot{z} = f(z) + g(z)\tilde{v} \tag{10.43}$$

The extended system's state vector is denoted as $z = [x, y, \psi, u, v, r, z_1, z_2]^T$. Moreover, one has $f(z) \in R^{8\times 1}$, and $g(z) = [g_a, g_b] \in R^{8\times 2}$, while the control input is the vector $\tilde{v} = [\ddot{\tau}_u, \tau_r]^T$.

From the previous state-space description it can be noticed that the hovercraft's model is an underactuated one. Underactuation in the considered hovercraft's model means that, to control the vehicle's motion and orientation, one has fewer control inputs that the degrees of freedom. Thus considering the capability of the vessel to move on the xy plane and also to rotate round its z axis by a yaw angle that is denoted by ψ one has three degrees of freedom. On the other hand the vessel is supplied with only two control inputs which are the surge force τ_u and the yaw torque τ_r. In practice, the hovercraft is supplied with a number of fans that inject air mass backwards and which are installed at its rear part, while being also symmetrically placed with respect to the vessel's longitudinal axis (Fig. 10.35). Without loss of generality one can consider the propulsion scheme of Fig. 10.35. The aggregate surge force τ_u is the sum of the two propulsion forces F_L and F_R, which are generated by the left and right fan respectively. The yaw torque τ_r is generated by altering the force produced by the two fans according to the sign of the desirable turn angle. Thus, to turn left F_L is set to be smaller than F_R. On the other hand, to turn right F_R is set to be smaller than F_L. In this manner the steering of the vessel (turn by a specific yaw

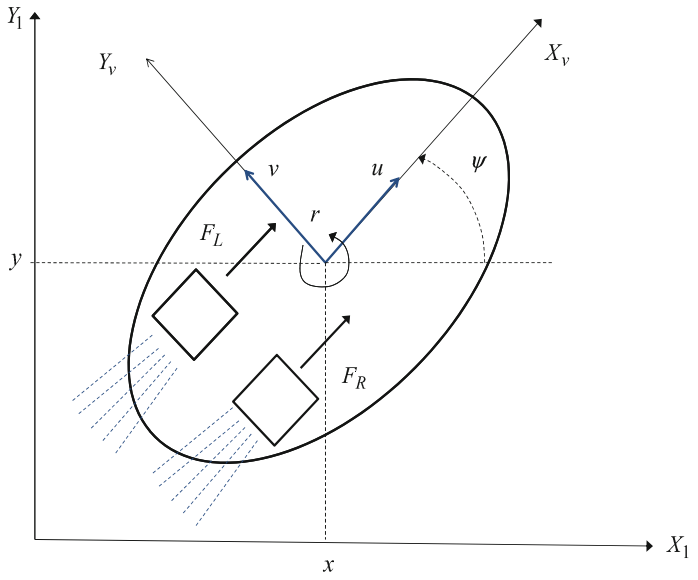

Fig. 10.35 Diagram of the underactuated hovercraft's kinematic model

angle) is achieved without the use of a rudder. Succeeding control of the hovercraft's motion and orientation in case of underactuation is very important, for assuring the efficient navigation of the vessel.

10.3.2.2 Lie Algebra-Based Control of the Underactuated Hovercraft

It will be shown that Lie algebra-based control through the computation of Lie derivatives is an approach equivalent to differential flatness theory-based control for the model of the underactuated hovercraft. The state-space model of the hovercraft that was described in Sect. 10.3.2, and particularly Eq. (10.85), is considered again. The following linearizing outputs of the system are defined

$$z_{1,1} = x \quad z_{2,1} = y \tag{10.44}$$

Moreover, the new state variables are defined

$$\begin{aligned} z_{1,2} &= L_f z_{1,1} \quad z_{2,2} = L_f z_{2,1} \\ z_{1,3} &= L_f^2 z_{1,1} \quad z_{2,3} = L_f^2 z_{2,1} \\ z_{1,4} &= L_f^3 z_{1,1} \quad z_{2,4} = L_f^3 z_{2,1} \end{aligned} \tag{10.45}$$

The system will be brought to a linearized input-output form using

$$\begin{aligned} \dot{z}_{1,4} &= L_f^4 z_{1,1} + L_{g_a} L_f^3 z_{1,1} \ddot{\tau}_u + L_{g_b} L_f^3 z_{1,1} \tau_r \\ \dot{z}_{2,4} &= L_f^4 z_{2,1} + L_{g_a} L_f^3 z_{2,1} \ddot{\tau}_u + L_{g_b} L_f^3 z_{2,1} \tau_r \end{aligned} \tag{10.46}$$

It holds that $z_{1,1} = x$. Thus one has

$z_{1,2} = L_f z_{1,1} \Rightarrow z_{1,2} = \frac{\partial z_{1,1}}{\partial x} f_1 + \frac{\partial z_{1,1}}{\partial y} f_2 + \frac{\partial z_{1,1}}{\partial \psi} f_3 + \frac{\partial z_{1,1}}{\partial u} f_4 + \frac{\partial z_{1,1}}{\partial v} f_5 + \frac{\partial z_{1,1}}{\partial r} f_6 + \frac{\partial z_{1,1}}{\partial z_1} f_7 + \frac{\partial z_{1,1}}{\partial z_2} f_8 \Rightarrow z_{1,2} = 1 \cdot f_1 \Rightarrow z_{1,2} = ucos(\psi) - vsin(\psi).$

Similarly, one obtains

$z_{1,3} = L_f^2 z_{1,1} \Rightarrow z_{1,3} = \frac{\partial z_{1,2}}{\partial x} f_1 + \frac{\partial z_{1,2}}{\partial y} f_2 + \frac{\partial z_{1,2}}{\partial \psi} f_3 + \frac{\partial z_{1,2}}{\partial u} f_4 + \frac{\partial z_{1,2}}{\partial v} f_5 + \frac{\partial z_{1,2}}{\partial r} f_6 + \frac{\partial z_{1,2}}{\partial z_1} f_7 + \frac{\partial z_{1,2}}{\partial z_2} f_8 \Rightarrow z_{1,3} = (-usin(\psi) - vcos(\psi)) f_3 + cos(\psi) f_4 - sin(\psi) f_5 \Rightarrow z_{1,3} = (-usin(\psi) - vcos(\psi)) r + cos(\psi)(vr + z_1) - sin(\psi)(-ur - \beta v) \Rightarrow z_{1,3} = \tau_u cos(\psi) + \beta v sin(\psi).$

Equivalently, it holds that

$z_{1,4} = L_f^3 z_{1,1} \Rightarrow z_{1,4} = L_f z_{1,3} \Rightarrow z_{1,4} = \frac{\partial z_{1,3}}{\partial x} f_1 + \frac{\partial z_{1,3}}{\partial y} f_2 + \frac{\partial z_{1,3}}{\partial \psi} f_3 + \frac{\partial z_{1,3}}{\partial u} f_4 + \frac{\partial z_{1,3}}{\partial v} f_5 + \frac{\partial z_{1,3}}{\partial r} f_6 + \frac{\partial z_{1,3}}{\partial z_1} f_7 + \frac{\partial z_{1,3}}{\partial z_2} f_8,$

while after intermediate operations one obtains

$z_{1,4} = (-\tau_u sin(\psi) + \beta v cos(\psi)) f_3 + \beta sin(\psi) f_5 + cos(\psi) f_7 \Rightarrow z_{1,4} = (-\tau_u sin(\psi) + \beta cos(\psi))r + \beta sin(\psi)(-ur + \beta v) + cos(\psi) z_2 \Rightarrow z_{1,4} = (\dot{\tau}_u sin(\psi) + \beta v cos(\psi))r + \beta sin(\psi)(-ur - \beta v) + cos(\psi) z_2$

or, using the extended state vector variables notation one has

$$\begin{gathered} z_{1,4} = z_2 cos(\psi) - z_1 sin(\psi) r - \beta ur sin(\psi) - \\ -\beta^2 v sin(\psi) + \beta v cos(\psi) r \end{gathered} \tag{10.47}$$

It also holds that

$$\begin{gathered} \dot{z}_{1,4} = L_f^4 z_{1,1} + L_{g_a} L_f^3 z_{1,1} \ddot{\tau}_u + L_{g_b} L_f^3 z_{1,1} \tau_r \Rightarrow \\ \dot{z}_{1,4} = L_f z_{1,4} + L_{g_a} z_{1,4} \ddot{\tau}_u + L_{g_b} z_{1,4} \tau_r \end{gathered} \tag{10.48}$$

where

$$\begin{gathered} L_f z_{1,4} = \frac{\partial z_{1,4}}{\partial x} f_1 + \frac{\partial z_{1,4}}{\partial y} f_2 + \frac{\partial z_{1,4}}{\partial \psi} f_3 + \frac{\partial z_{1,4}}{\partial u} f_4 + \\ + \frac{\partial z_{1,4}}{\partial v} f_5 + \frac{\partial z_{1,4}}{\partial r} f_6 + \frac{\partial z_{1,4}}{\partial z_1} f_7 + \frac{\partial z_{1,4}}{\partial z_2} f_8 \end{gathered} \tag{10.49}$$

which gives

$L_f z_{1,4} = (-z_2 sin(\psi) - z_1 cos(\psi) r - \beta ur cos(\psi) - \beta^2 v cos(\psi) - \beta v sin(\psi) r) r + (-\beta r sin(\psi))(vr + z_1) + (-\beta^2 sin(\psi) + \beta cos(\psi) r)(-ur + \beta v) + (-z_1 sin(\psi) - \beta v sin(\psi) + \beta v cos(\psi))0 + (-sin(\psi) r) z_2$

while after some intermediate computations one obtains

$$\begin{gathered} L_f z_{1,4} = -2 z_2 sin(\psi) r - z_1 cos(\psi) r^2 - \\ -\beta v r^2 sin(\psi) - \beta z_1 r sin(\psi) - \\ -\beta u r^2 cos(\psi) + \beta^2 ur sin(\psi) - \\ -\beta^3 v sin(\psi) - \beta^2 vr cos(\psi) - \beta ur^2 cos^2(\psi) + \beta^2 vr cos(\psi) \\ -\beta v r^2 sin(\psi) \end{gathered} \tag{10.50}$$

In a similar manner one computes

$L_{g_a} z_{1,4} = \frac{\partial z_{1,4}}{\partial x} g_{a_1} + \frac{\partial z_{1,4}}{\partial y} g_{a_2} + \frac{\partial z_{1,4}}{\partial \psi} g_{a_3} + \frac{\partial z_{1,4}}{\partial u} g_{a_4} + \frac{\partial z_{1,4}}{\partial v} g_{a_5} + \frac{\partial z_{1,4}}{\partial r} g_{a_6} + \frac{\partial z_{1,4}}{\partial z_1} g_{a_7} + \frac{\partial z_{1,4}}{\partial z_2} g_{a_8} L_{g_a} z_{1,4} = \frac{\partial z_{1,4}}{\partial z_2} \Rightarrow L_{g_a} z_{1,4} = cos(\psi)$

and also

$L_{g_b} z_{1,4} = \frac{\partial z_{1,4}}{\partial x} g_{b_1} + \frac{\partial z_{1,4}}{\partial y} g_{b_2} + \frac{\partial z_{1,4}}{\partial \psi} g_{b_3} + \frac{\partial z_{1,4}}{\partial u} g_{b_4} + \frac{\partial z_{1,4}}{\partial v} g_{b_5} + \frac{\partial z_{1,4}}{\partial r} g_{b_6} + \frac{\partial z_{1,4}}{\partial z_1} g_{b_7} + \frac{\partial z_{1,4}}{\partial z_2} g_{b_8} L_{g_b} z_{1,4} = \frac{\partial z_{1,4}}{\partial r} \Rightarrow L_{g_b} z_{1,4} = -z_1 sin(\psi) - \beta u sin(\psi) + \beta v cos(\psi)$

In an equivalent way, and using that $z_{2,1} = y_2 = y$ one can compute

$z_{2,2} = L_f z_{2,1} \Rightarrow z_{2,2} = \frac{\partial z_{2,1}}{\partial x} f_1 + \frac{\partial z_{2,1}}{\partial y} f_2 + \frac{\partial z_{2,1}}{\partial \psi} f_3 + \frac{\partial z_{2,1}}{\partial u} f_4 + \frac{\partial z_{2,1}}{\partial v} f_5 + \frac{\partial z_{2,1}}{\partial r} f_6 + \frac{\partial z_{2,1}}{\partial z_1} f_7 + \frac{\partial z_{2,1}}{\partial z_2} f_8 \Rightarrow z_{2,2} = 1 \cdot f_2 \Rightarrow z_{2,2} = usin(\psi) + vcos(\psi)$

Equivalently, one has

$z_{2,3} = L_f^2 z_{2,1} \Rightarrow z_{2,3} = L_f z_{2,2} \Rightarrow z_{2,3} = \frac{\partial z_{2,2}}{\partial x} f_1 + \frac{\partial z_{2,2}}{\partial y} f_2 + \frac{\partial z_{2,2}}{\partial \psi} f_3 + \frac{\partial z_{2,2}}{\partial u} f_4 + \frac{\partial z_{2,2}}{\partial v} f_5 + \frac{\partial z_{2,2}}{\partial r} f_6 + \frac{\partial z_{2,2}}{\partial z_1} f_7 + \frac{\partial z_{2,2}}{\partial z_8} f_8 \Rightarrow z_{2,3} = (ucos(\psi) - vsin(\psi))r + sin(\psi)(vr + z_1) + cos(\psi)(-ur - \beta v) \Rightarrow z_{2,3} = z_1 sin(\psi) + \beta v cos(\psi)$

In an equivalent manner one obtains

$z_{2,4} = L_f^3 z_{2,1} \Rightarrow z_{3,3} = L_f z_{2,3} \Rightarrow z_{2,4} = \frac{\partial z_{2,3}}{\partial x} f_1 + \frac{\partial z_{2,3}}{\partial y} f_2 + \frac{\partial z_{2,3}}{\partial \psi} f_3 + \frac{\partial z_{2,3}}{\partial u} f_4 + \frac{\partial z_{2,3}}{\partial v} f_5 + \frac{\partial z_{2,3}}{\partial r} f_6 + \frac{\partial z_{2,3}}{\partial z_1} f_7 + \frac{\partial z_{2,3}}{\partial z_2} f_8 \Rightarrow z_{2,4} = (cos(\psi) - \beta v sin(\psi)) f_3 + \beta cos(\psi) f_5 + \sin(\psi) f_7 \Rightarrow z_{2,4} = (z_1 cos(\psi) - \beta v sin(\psi))r + (\beta cos(\psi)(-ur - \beta v) + \sin(\psi) z_2 \Rightarrow z_{2,4} = z_1 cos(\psi) r - \beta v r sin(\psi) - \beta u r cos(\psi) + \beta^2 v cos(\psi) + z_2 sin(\psi)$

Moreover, it holds that

$$\dot{z}_{2,4} = L_f^4 z_{2,1} + L_{g_a} L_f^3 z_{2,1} \ddot{\tau}_u + L_{g_b} L_f^3 z_{2,1} \tau_r \tag{10.51}$$

where

$$\begin{aligned} L_f^4 z_{2,1} = L_f z_{2,4} \Rightarrow L_f^4 z_{2,1} = \frac{\partial z_{2,4}}{\partial x} f_1 + \frac{\partial z_{2,4}}{\partial y} f_2 + \frac{\partial z_{2,4}}{\partial \psi} f_3 + \\ + \frac{\partial z_{2,4}}{\partial u} f_4 + \frac{\partial z_{2,4}}{\partial v} f_5 + \frac{\partial z_{2,4}}{\partial r} f_6 + \frac{\partial z_{2,4}}{\partial z_1} f_7 + \frac{\partial z_{2,4}}{\partial z_2} f_8 \Rightarrow \end{aligned} \tag{10.52}$$

which gives

$L_f^4 z_{2,1} = [-z_1 sin(\psi) r - \beta v r cos(\psi) + \beta u r sin(\psi) - \beta^2 v sin(\psi) + z_2 cos(\psi)]r + [-\beta r cos(\psi)](vr + z_1) + [-\beta r sin(\psi) + \beta^2 cos(\psi)](-ur - \beta v) + [z_1 cos(\psi) - \beta v sin(\psi) - \beta u cos(\psi)]0 + [cos(\psi) r] z_2 + [sin(\psi)]0$

and after additional computations one arrives at the form

$L_f^4 z_{2,1} = -z_1 r^2 sin(\psi) - \beta v r^2 cos(\psi) + \beta u r^2 sin(\psi) - \beta^2 v r sin(\psi) + z_2 r cos(\psi) - -\beta v r^2 cos(\psi) - \beta r z_1 cos(\psi) + \beta u r^2 sin(\psi) - \beta^2 r v sin(\psi) - \beta^2 u r cos(\psi) + \beta^2 v cos(\psi) + z_2 r cos(\psi)$

Proceeding as before, one computes

$L_{g_a} L_f^3 z_{2,1} = L_{g_a} z_{2,4} \Rightarrow L_{g_a} L_f^3 z_{2,1} = \frac{\partial z_{2,4}}{\partial x} g_{a_1} + \frac{\partial z_{2,4}}{\partial y} g_{a_2} + \frac{\partial z_{2,4}}{\partial \psi} g_{a_3} + \frac{\partial z_{2,4}}{\partial u} g_{a_4} + \frac{\partial z_{2,4}}{\partial v} g_{a_5} + \frac{\partial z_{2,4}}{\partial v} g_{a_6} + \frac{\partial z_{2,4}}{\partial z_1} g_{a_7} + \frac{\partial z_{2,4}}{\partial z_2} g_{a_8} \Rightarrow L_{g_a} L_f^3 z_{2,1} = \frac{\partial z_{2,4}}{\partial z_2} \Rightarrow L_{g_a} L_f^3 z_{2,1} = sin(\psi)$

Equivalently, one computes

$L_{g_b} L_f^3 z_{2,1} = L_{g_b} z_{2,4} \Rightarrow L_{g_b} L_f^3 z_{2,1} = \frac{\partial z_{2,4}}{\partial x} g_{b_1} + \frac{\partial z_{2,4}}{\partial y} g_{b_2} + \frac{\partial z_{2,4}}{\partial \psi} g_{b_3} + \frac{\partial z_{2,4}}{\partial u} g_{b_4} + \frac{\partial z_{2,4}}{\partial v} g_{b_5} + \frac{\partial z_{2,4}}{\partial r} g_{b_6} + \frac{\partial z_{2,4}}{\partial z_1} g_{b_7} + \frac{\partial z_{2,4}}{\partial z_2} g_{b_8} \Rightarrow L_{g_b} L_f^3 z_{2,1} = \frac{\partial z_{2,4}}{\partial v} \Rightarrow L_{g_b} L_f^3 z_{2,1} = z_1 cos(\psi) = \beta v sin(\psi) - \beta u cos(\psi)$

The aggregate dynamics of the input-output linearized system is

$$\begin{aligned} x^{(4)} &= L_f^4 z_{1,1} + L_{g_a} L_f^3 z_{1,1} \ddot{\tau}_u + L_{g_b} L_f^3 z_{1,1} \tau_r \\ y^{(4)} &= L_f^4 z_{2,1} + L_{g_a} L_f^3 z_{2,1} \ddot{\tau}_u + L_{g_b} L_f^3 z_{2,1} \tau_r \end{aligned} \tag{10.53}$$

By defining the new control inputs

$$\begin{aligned} v_1 &= L_f^4 z_{1,1} + L_{g_a} L_f^3 z_{1,1} \ddot{\tau}_u + L_{g_b} L_f^3 z_{1,1} \tau_r \\ v_2 &= L_f^4 z_{2,1} + L_{g_a} L_f^3 z_{2,1} \ddot{\tau}_u + L_{g_b} L_f^3 z_{2,1} \tau_r \end{aligned} \tag{10.54}$$

one arrives at the following description for the input-output linearized system

$$\begin{aligned} x^{(4)} &= v_1 \\ y^{(4)} &= v_2 \end{aligned} \tag{10.55}$$

which can be also written in the state-space form

$$\begin{pmatrix} \dot{z}_{1,1} \\ \dot{z}_{1,2} \\ \dot{z}_{1,3} \\ \dot{z}_{1,4} \\ \dot{z}_{2,1} \\ \dot{z}_{2,2} \\ \dot{z}_{2,3} \\ \dot{z}_{2,4} \end{pmatrix} = \begin{pmatrix} 0\,1\,0\,0\,0\,0\,0\,0 \\ 0\,0\,1\,0\,0\,0\,0\,0 \\ 0\,0\,0\,1\,0\,0\,0\,0 \\ 0\,0\,0\,0\,0\,0\,0\,0 \\ 0\,0\,0\,0\,0\,1\,0\,0 \\ 0\,0\,0\,0\,0\,0\,1\,0 \\ 0\,0\,0\,0\,0\,0\,0\,1 \\ 0\,0\,0\,0\,0\,0\,0\,0 \end{pmatrix} \begin{pmatrix} z_{1,1} \\ z_{1,2} \\ z_{1,3} \\ z_{1,4} \\ z_{2,1} \\ z_{2,2} \\ z_{2,3} \\ z_{2,4} \end{pmatrix} + \begin{pmatrix} 0\,0 \\ 0\,0 \\ 0\,0 \\ 1\,0 \\ 0\,0 \\ 0\,0 \\ 0\,0 \\ 0\,1 \end{pmatrix} \begin{pmatrix} v_1 \\ v_2 \end{pmatrix} \tag{10.56}$$

while the associated measurement equation is

$$\begin{pmatrix} z_1^m \\ z_2^m \end{pmatrix} = \begin{pmatrix} 1\,0\,0\,0\,0\,0\,0\,0 \\ 0\,0\,0\,0\,1\,0\,0\,0 \end{pmatrix} \begin{pmatrix} z_{1,1} \\ z_{1,2} \\ z_{1,3} \\ z_{1,4} \\ z_{2,1} \\ z_{2,2} \\ z_{2,3} \\ z_{2,4} \end{pmatrix} \tag{10.57}$$

A suitable feedback control law for the linearized system is

$v_1 = x_d^{(4)} - k_1^1(x^{(3)} - x_d^{(3)}) - k_2^1(\ddot{x} - \ddot{x}_d) - k_3^1(\dot{x} - \dot{x}_d) - k_4^1(x - x_d)$, and $v_2 = y_d^{(4)} - k_1^2(y^{(3)} - y_d^{(3)}) - k_2^2(\ddot{y} - \ddot{y}_d) - k_3^2(\dot{y} - \dot{y}_d) - k_4^2(y - y_d)$.

One can also compute the control input that is finally applied to the hovercraft model. It holds that

$$\bar{v} = \tilde{f} + \tilde{M}\tilde{v} \tag{10.58}$$

where matrices and vectors $\bar{v}$, $\tilde{f}$, $\tilde{M}$ and $\tilde{v}$ are defined as

$$\begin{aligned} \bar{v} &= \begin{pmatrix} v_1 \\ v_2 \end{pmatrix} \qquad \tilde{f} = \begin{pmatrix} L_f^4 z_{1,1} \\ L_f^4 z_{2,1} \end{pmatrix} \\ \tilde{M} &= \begin{pmatrix} L_{g,a} L_f^3 z_{1,1} & L_{g_b} L_f^3 z_{1,1} \\ L_{g,a} L_f^3 z_{2,1} & L_{g,b} L_f^3 z_{2,1} \end{pmatrix} \quad \tilde{v} = \begin{pmatrix} \ddot{\tau}_u \\ \tau_r \end{pmatrix} \end{aligned} \tag{10.59}$$

The above equation can be solved with respect to $\tilde{v}$, which finally gives

$$\tilde{v} = \tilde{M}^{-1}(\bar{v} - \tilde{f}) \tag{10.60}$$

The vector $\tilde{u}$ is the control input that is finally applied to the system, which finally means that the control signal contains integrals of the tracking error.

10.3.3 *Differential Flatness Properties of the Hovercraft's Model*

It can be proven that the model of the underactuated vessel (hovercraft) given in Eq. (10.39) is a differentially flat one. This means that all its state variables and the control inputs can be written as functions of a single variable, which is the flat output. In the hovercraft's case the flat output is the vector of the vessel's cartesian coordinates, that is

$$\tilde{y} = [y_1, y_2] = [x, y] \tag{10.61}$$

It holds that

$$\begin{aligned} \ddot{x} &= \dot{u}cos(\psi) - u{\cdot}sin(\psi){\cdot}\dot{\psi} - \dot{v}sin(\psi) - v{\cdot}cos(\psi)\dot{\psi} \\ \ddot{y} &= \dot{u}sin(\psi) + u{\cdot}cos(\psi){\cdot}\dot{\psi} + \dot{v}cos(\psi) - v{\cdot}cos(\psi)\dot{\psi} \end{aligned} \tag{10.62}$$

Moreover, it holds that

$$\begin{aligned} \ddot{x} + \beta\dot{x} &= cos(\psi)(\dot{u} - v\dot{\psi} + \beta u) + sin(\psi)(-u\dot{\psi} - \dot{v} - \beta v) \\ \ddot{y} + \beta\dot{y} &= cos(\psi)(\dot{v} + u\dot{\psi} + \beta v) + sin(\psi)(-v\dot{\psi} + \dot{u} + \beta u) \end{aligned} \tag{10.63}$$

Using Eqs. (10.63) and (10.39), and after computing that

$$\begin{aligned} u\dot{\psi} + \dot{v} + \beta v = u \cdot r - ur - \beta v + \beta v = 0 \\ \dot{u} - v\dot{\psi} + \beta u = vr + \tau_u - vr + \beta u = \tau_u + \beta u \end{aligned} \tag{10.64}$$

one obtains

$$\begin{aligned} \frac{\ddot{y} + \beta \dot{y}}{\ddot{x} + \beta \dot{x}} = \frac{cos(\psi)0 + sin(\psi)(\tau_u + \beta u)}{\cos(\psi)(\tau_u + \beta u) - sin(\psi)0} \Rightarrow \\ \frac{\ddot{y} + \beta \dot{y}}{\ddot{x} + \beta \dot{x}} = tan(\psi) \Rightarrow \psi = atan^{-1}(\frac{\ddot{y} + \beta \dot{y}}{\ddot{x} + \beta \dot{x}}) \end{aligned} \tag{10.65}$$

Thus, through Eq. (10.65) it is proven that the state variable ψ (heading angle of the vessel) is a function of the flat output and of its derivatives.

From Eq. (10.63) one also has that

$$(\ddot{x} + \beta \dot{x})^2 + (\ddot{y} + \beta \dot{y})^2 = (\tau_u + \beta u)^2 \tag{10.66}$$

Moreover, it holds that

$$\begin{aligned} \dot{x}(\ddot{x} + \beta \dot{x}) = (ucos(\psi) - vsin(\psi))cos(\psi)(\tau_u + \beta u) \\ \dot{y}(\ddot{y} + \beta \dot{y}) = (usin(\psi) + vcos(\psi))sin(\psi)(\tau_u + \beta u) \end{aligned} \tag{10.67}$$

while using Eq. (10.66) and after intermediate computations one finally obtains

$$\dot{x}(\ddot{x} + \beta \dot{x}) + \dot{y}(\ddot{y} + \beta \dot{y}) = u(\tau_u + \beta u) \tag{10.68}$$

Dividing Eq. (10.68) with the square root of Eq. (10.66) one obtains

$$\frac{\dot{x}(\ddot{x} + \beta \dot{x}) + \dot{y}(\ddot{y} + \beta \dot{y})}{\sqrt{(\ddot{x} + \beta \dot{x})^2 + (\ddot{y} + \beta \dot{y})^2}} = \frac{u(\tau_u + \beta u)}{(\tau_u + \beta u)} \tag{10.69}$$

which finally give

$$u = \frac{\dot{x}(\ddot{x} + \beta \dot{x}) + \dot{y}(\ddot{y} + \beta \dot{y})}{\sqrt{(\ddot{x} + \beta \dot{x})^2 + (\ddot{y} + \beta \dot{y})^2}} \tag{10.70}$$

It also holds that

$$\begin{aligned} \dot{y}\ddot{x} - \dot{x}\ddot{y} = (usin(\psi) + vcos(\psi))(\dot{u}cos(\psi) - usin(\psi)\dot{\psi} - \dot{v}sin(\psi) - vcos(\psi)\dot{\psi}) - \\ -(ucos(\psi) - vsin(\psi))(\dot{u}sin(\psi) + ucos(\psi)\dot{\psi} + \dot{v}cos(\psi) - vsin(\psi)\dot{\psi}) \end{aligned}$$

which after intermediate computations and substitution of the derivative variables from Eq. (10.39) give

$$\dot{y}\ddot{x} - \dot{x}\ddot{y} = v(\beta u + \tau_u) \tag{10.71}$$

From Eqs. (10.71) and (10.66) one obtains

$$v = \frac{\dot{y}\ddot{x} - \dot{x}\ddot{y}}{\sqrt{(\ddot{x} + \beta\dot{x})^2 + \ddot{y} + \beta\dot{y})^2}} \tag{10.72}$$

From the state-space equations it holds that

$$r = \dot{\psi} \tag{10.73}$$

where from Eq. (10.65) one has that

$$\psi = atan^{-1}\left(\frac{\ddot{y} + \beta\dot{y}}{\ddot{x} + \beta\dot{x}}\right) \tag{10.74}$$

which means that r is also a function of the flat output and of its derivatives. This can be also confirmed analytically. Indeed from Eq. (10.74) it holds that

$$\frac{cos^2(\psi)\dot{\psi} + sin^2(\psi)\dot{\psi}}{cos^2(\psi)} = \frac{(y^{(3)} + \beta\ddot{\psi})(\ddot{x} + \beta\dot{x}) - (\ddot{y} + \beta\dot{y})(x^{(3)} + \beta\ddot{x})}{(\ddot{x} + \beta\dot{x})^2} \tag{10.75}$$

which also gives

$$\frac{\dot{\psi}}{cos^2(\psi)} = \frac{(y^{(3)} + \beta\ddot{\psi})(\ddot{x} + \beta\dot{x}) - (\ddot{y} + \beta\dot{y})(x^{(3)} + \beta\ddot{x})}{(\ddot{x} + \beta\dot{x})^2} \tag{10.76}$$

while using that

$$\frac{1}{\cos^2\psi} = tan^2(\psi) + 1 \tag{10.77}$$

one obtains that

$$\cos^2\psi = \frac{(\ddot{x} + \beta\dot{x})^2}{(\ddot{x} + \beta\dot{x})^2 + (\ddot{y} + \beta\dot{y})^2} \tag{10.78}$$

Thus, from Eqs. (10.76) and (10.73) one has that

$$r = \dot{\psi} \Rightarrow r = cos^2(\psi)\frac{(y^{(3)} + \beta\ddot{\psi})(\ddot{x} + \beta\dot{x}) - (\ddot{y} + \beta\dot{y})(x^{(3)} + \beta\ddot{x})}{(\ddot{x} + \beta\dot{x})^2} \tag{10.79}$$

which after intermediate operations gives

$$r = \frac{y^{(3)}(\ddot{x} + \beta\dot{x}) - x^{(3)}(\ddot{y} + \beta\dot{y}) - \beta^2(\ddot{x}\dot{y} - \ddot{y}\dot{x})}{(\ddot{x} + \beta\dot{x})^2 + (\ddot{y} + \beta\dot{y})^2} \tag{10.80}$$

Equivalently, from the state-space equations one has that

$$\tau_u = \dot{u} - v \cdot r \Rightarrow \tau_u = \frac{d}{dt}\left\{\frac{\dot{x}(\ddot{x}+\beta\dot{x})+\dot{y}(\ddot{y}+\beta\dot{y})}{\sqrt{(\ddot{x}+\beta\dot{x})^2+(\ddot{y}+\beta\dot{y})^2}}\right\} -$$

$$-\frac{\dot{y}\ddot{x}-\dot{x}\ddot{y}}{\sqrt{(\ddot{x}+\beta\dot{x})^2+(\ddot{y}+\beta\dot{y})^2}} \cdot \frac{y^{(3)}(\ddot{x}+\beta\dot{x})-x^{(3)}(\ddot{y}+\beta\dot{y})-\beta^2(\ddot{x}\dot{y}-\ddot{y}\dot{x})}{(\ddot{x}+\beta\dot{x})^2+\ddot{y}+\beta\dot{y})^2} \tag{10.81}$$

which after intermediate operations gives

$$\tau_u = \frac{\ddot{x}(\ddot{x}+\beta\dot{x})+\ddot{y}(\ddot{y}+\beta\dot{y})}{\sqrt{(\ddot{x}+\beta\dot{x})^2+(\ddot{y}+\beta\dot{y})^2}} \tag{10.82}$$

Finally, for the control input τ_r it holds that $\tau_r = \dot{r}$ and using Eq. (10.80) this implies that τ_r is also a function of the flat output and of its derivatives. This can be also shown analytically according to the following:

$$\begin{aligned}
&\tau_r = \dot{r} \Rightarrow \tau_r = \\
&\frac{y^{(4)}(\ddot{x}+\beta x)-x^{(4)}(\ddot{y}+\beta\dot{y})+\beta(y^{(3)}\ddot{x}-x^{(3)}\ddot{y})-\beta^2(x^{(3)}\dot{y}-y^{(3)}\dot{x})}{[(\ddot{x}+\beta\dot{x})^2+(\ddot{y}+\beta\dot{y})^2]\cdot} \\
&-2\frac{[y^{(3)}(\ddot{x}+\beta\dot{x})-x^3(\ddot{y}+\beta\dot{y})-\beta^2(\ddot{x}\dot{y}-\ddot{y}\dot{x})]}{[(\ddot{x}+\beta\dot{x})^2+(\ddot{y}+\beta\dot{y})^2]^2}\cdot \\
&\cdot\{(\ddot{x}+\beta\dot{x})(x^{(3)}+\beta\ddot{x})+(\ddot{y}+\beta\dot{y})(y^{(3)}+\beta\ddot{y})\}
\end{aligned} \tag{10.83}$$

Through Eq. (10.83) it is confirmed that that all state variables and the control input of the hovercraft's model can be written as functions of the flat output and of its derivatives. Consequently, the vessel's model is a differential flat one.

10.3.4 Flatness-Based Control of the Hovercraft's Model

Next, it will be shown that a flatness-based controller can be developed for the hovercraft's model. It has been shown that it holds

$\ddot{x} = \dot{u}cos(\psi) - usin(\psi)\dot{\psi} - \dot{v}sin(\psi) - vcos(\psi)\dot{\psi} \Rightarrow \ddot{x} = (vr + \tau_u)cos(\psi) - usin(\psi)r - (-ur - \beta v)sin(\psi) - vcos(\psi)r \Rightarrow \ddot{x} = \tau_u cos(\psi) + \beta vsin(\psi)$

By differentiating once more with respect to time and after intermediate operations one finally obtains

$$\begin{aligned}
x^{(3)} &= \dot{\tau}_u cos(\psi) - \tau_u sin(\psi)r + \\
&+\beta(-ur - \beta v)sin(\psi) + \beta vcos(\psi)r
\end{aligned} \tag{10.84}$$

Similarly one has

$$\ddot{y} = \dot{u}sin(\psi) + ucos(\psi)\dot{\psi} + \dot{v}cos(\psi) - vsin(\psi)\dot{\psi} \Rightarrow \ddot{y} = (vr + \tau_u)sin(\psi) + ucos(\psi)r + (-ur - \beta v)cos(\psi) - vsin(\psi)r \Rightarrow \ddot{y} = \tau_u sin(\psi) - \beta vcos(\psi)$$

As in Sect. 10.3.2, the state vector of the system is extended so as to include as new state variables the control input τ_u and its first derivative $\dot{\tau}_u$. The new state variables are denoted as $z_1 = \tau_u$ and $\dot{z_1} = \dot{\tau}_u$. The extended state-space description of the system becomes

$$\begin{pmatrix} \dot{x} \\ \dot{y} \\ \dot{\psi} \\ \dot{u} \\ \dot{v} \\ \dot{r} \\ \dot{z}_1 \\ \dot{z}_2 \end{pmatrix} = \begin{pmatrix} ucos(\psi) - vsin(\psi) \\ usin(\psi) + vcos(\psi) \\ r \\ vr + z_1 \\ -ur - \beta v \\ 0 \\ z_2 \\ 0 \end{pmatrix} + \begin{pmatrix} 0 & 0 \\ 0 & 0 \\ 0 & 0 \\ 0 & 0 \\ 0 & 0 \\ 0 & 1 \\ 0 & 0 \\ 1 & 0 \end{pmatrix} \begin{pmatrix} \ddot{\tau}_u \\ \tau_r \end{pmatrix} \tag{10.85}$$

or equivalently, one has the description

$$\dot{z} = f(z) + g(z)\tilde{\nu} \tag{10.86}$$

The system's state vector is again denoted as $z = [x, y, \psi, u, v, r, z_1, z_2]^T$, $f(z) \in R^{8\times 1}$, and $g(z) = [g_a, g_b] \in R^{8\times 2}$, while the control input is the vector $\tilde{\nu} = [\ddot{\tau}_u, \tau_r]^T$.

The extended state-space description of the system given in Eq. (10.85) or in its compact form described by Eq. (10.86), is used. By differentiating once more with respect to time and after intermediate operations one finally obtains

$$\begin{aligned} y^{(3)} &= z_2 sin(\psi) + z_1 cos(\psi)r + \beta urcos(\psi) + \\ &+ \beta^2 vcos(\psi) + \beta vsin(\psi)r \end{aligned} \tag{10.87}$$

It can be noticed that in the equations of the third order derivatives for both x and y only the control input τ_u and its derivative $\dot{\tau}_u$ appear, while the control input τ_r is missing. Therefore, differentiation of $x^{(3)}$ once more with respect to time is performed. This gives

$$x^{(4)} = \ddot{\tau}_u cos(\psi) - 2z_2 sin(\psi)r - z_1 cos(\psi)r^2 - z_1 sin(\psi)\tau_r - \beta vr^2 sin(\psi) - \beta z_1 rsin(\psi) - \beta u\tau_r sin(\psi) - \beta ur^2 cos(\psi) + \beta^2 ursin(\psi) - \beta^3 vsin(\psi) - \beta^2 vrcos(\psi) - \beta ur^2 cos(\psi) + \beta^2 vrcos(\psi) - \beta vr^2 sin(\psi) + \beta vcos(\psi)\tau_r$$

while after substituting the time derivative according to Eq. (10.39) and after regrouping terms one obtains a description of the form

$$x^{(4)} = [-2z_2 sin(\psi)r - z_1 cos(\psi)r^2 - \beta v r^2 sin(\psi) - \beta z_1 r sin(\psi) -$$
$$-\beta u r^2 cos(\psi) + \beta^2 u r sin(\psi) - \beta^3 v sin(\psi) - \beta^2 v r cos(\psi) -$$
$$-\beta u r^2 cos(\psi) + \beta^2 v r cos(\psi) - \beta v r^2 sin\psi] + [cos(\psi)]\ddot{\tau}_u +$$
$$+[-z_1 sin(\psi) - \beta u sin(\psi) + \beta v cos(\psi)]\tau_r$$

Consequently, the fourth derivative of x is finally written in the form

$$x^{(4)} = L_f^4 y_1 + L_{g_a} L_f^3 y_1 \ddot{\tau}_u + L_{g_b} L_f^3 y_1 \tau_r \tag{10.88}$$

where

$$L_f^4 y_1 = -2z_2 sin(\psi)r - z_1 cos(\psi)r - \beta v r^2 sin(\psi) - \beta z_1 r sin(\psi) -$$
$$-\beta u r^2 cos(\psi) + \beta^2 u r sin(\psi) - \beta^3 v sin(\psi) - \beta^2 v r cos(\psi) - \beta u r^2 cos(\psi) +$$
$$\beta^2 v r cos(\psi) - \beta v r^2 sin\psi$$

$$L_{g_a} L_f^3 y_1 = cos(\psi) \tag{10.89}$$

$$L_{g_b} L_f^3 y_1 = -z_1 sin(\psi) - \beta u sin(\psi) + \beta v cos(\psi) \tag{10.90}$$

In a similar manner, differentiating once more with respect to time the expression about $y^{(3)}$ one gets

$$y^{(4)} = \dot{z}_1 cos(\psi)r - z_1 sin(\psi)\dot{\psi}r + z_1 cos(\psi)\dot{r} -$$
$$-\beta \dot{v} r sin(\psi) - \beta v \dot{r} \sin(\psi) - \beta v r cos(\psi)\dot{\psi} -$$
$$-\beta \dot{u} r cos(\psi) - \beta u \dot{r} cos(\psi) + \beta u r sin(\psi)\dot{\psi} + \tag{10.91}$$
$$+\beta^2 \dot{v} cos(\psi) - \beta^2 v sin\psi \dot{\psi} +$$
$$+\dot{z}_2 sin(\psi) + z_2 cos(\psi)\dot{\psi}$$

while after substituting the time derivative according to Eq. (10.39) and after regrouping terms one obtains a description of the form

$$y^{(4)} = [z_2 r cos(\psi) - z_1 r^2 sin(\psi) + \beta u r^2 sin(\psi) - \beta^2 v r sin(\psi) - \beta v r^2 cos(\psi)]$$
$$-\beta v r^2 cos(\psi) - \beta z_1 r cos(\psi) + \beta u r^2 sin(\psi) -$$
$$-\beta u r cos(\psi) + \beta^2 v cos(\psi) - \beta^2 v r sin(\psi) + z_2 r cos(\psi)] +$$
$$+[sin(\psi)]\ddot{\tau}_u + [z_1 cos(\psi) - \beta v sin(\psi) - \beta u cos(\psi)]\tau_r$$

Thus $y^{(4)}$ can be also written in the form

$$y^{(4)} = L_f^4 y_2 + L_{g_a} L_f^3 y_2 \ddot{\tau}_u + L_{g_b} L_f^3 y_2 \tau_r \tag{10.92}$$

where $L_f^4 y_2 = [z_2 r cos(\psi) - z_1 r^2 sin(\psi) + \beta u r^2 sin(\psi) - \beta^2 v r sin(\psi) - \beta v r^2 cos(\psi)] - \beta v r^2 cos(\psi) - \beta z_1 r cos(\psi) + \beta u r^2 sin(\psi) - \beta u r cos(\psi) + \beta^2 v cos(\psi) - \beta^2 v r sin(\psi) + z_2 r cos(\psi)]$, and

$$L_{g_a} L_f^3 y_2 = sin(\psi) \tag{10.93}$$

$$L_{g_b} L_f^3 y_2 = z_1 cos(\psi) - \beta v sin(\psi) - \beta u cos(\psi) \tag{10.94}$$

Consequently, the aggregate input-output linearized description of the system becomes

$$\begin{aligned} x^{(4)} &= L_f^4 y_1 + L_{g_a} L_f^3 y_1 \ddot{\tau}_u + L_{g_b} L_f^3 y_1 \tau_r \\ y^{(4)} &= L_f^4 y_2 + L_{g_a} L_f^3 y_2 \ddot{\tau}_u + L_{g_b} L_f^3 y_2 \tau_r \end{aligned} \tag{10.95}$$

while by defining the new control inputs

$$\begin{aligned} v_1 &= L_f^4 y_1 + L_{g_a} L_f^3 y_1 \ddot{\tau}_u + L_{g_b} L_f^3 y_1 \tau_r \\ v_2 &= L_f^4 y_2 + L_{g_a} L_f^3 y_2 \ddot{\tau}_u + L_{g_b} L_f^3 y_2 \tau_r \end{aligned} \tag{10.96}$$

the following description for the input-output linearized hovercraft model is obtained

$$\begin{aligned} x^{(4)} &= v_1 \\ y^{(4)} &= v_2 \end{aligned} \tag{10.97}$$

For the dynamics of the linearized equivalent model of the system the following new state variables can be defined

$$\begin{aligned} z_{1,1} = x \; z_{1,2} = \dot{x} \; z_{1,3} = \ddot{x} \; z_{1,4} = x^{(3)} \\ z_{2,1} = y \; z_{2,2} = \dot{y} \; z_{2,3} = \ddot{y} \; z_{2,4} = y^{(3)} \end{aligned} \tag{10.98}$$

and the state-space description of the system becomes

$$\begin{aligned} \dot{z} &= Az + Bv \\ z^m &= Cz \end{aligned} \tag{10.99}$$

or equivalently

$$\begin{pmatrix} \dot{z}_{1,1} \\ \dot{z}_{1,2} \\ \dot{z}_{1,3} \\ \dot{z}_{1,4} \\ \dot{z}_{2,1} \\ \dot{z}_{2,2} \\ \dot{z}_{2,3} \\ \dot{z}_{2,4} \end{pmatrix} = \begin{pmatrix} 0\,1\,0\,0\,0\,0\,0\,0 \\ 0\,0\,1\,0\,0\,0\,0\,0 \\ 0\,0\,0\,1\,0\,0\,0\,0 \\ 0\,0\,0\,0\,0\,0\,0\,0 \\ 0\,0\,0\,0\,0\,1\,0\,0 \\ 0\,0\,0\,0\,0\,0\,1\,0 \\ 0\,0\,0\,0\,0\,0\,0\,1 \\ 0\,0\,0\,0\,0\,0\,0\,0 \end{pmatrix} \begin{pmatrix} z_{1,1} \\ z_{1,2} \\ z_{1,3} \\ z_{1,4} \\ z_{2,1} \\ z_{2,2} \\ z_{2,3} \\ z_{2,4} \end{pmatrix} + \begin{pmatrix} 0\,0 \\ 0\,0 \\ 0\,0 \\ 1\,0 \\ 0\,0 \\ 0\,0 \\ 0\,0 \\ 0\,1 \end{pmatrix} \begin{pmatrix} v_1 \\ v_2 \end{pmatrix} \tag{10.100}$$

while the associated measurement equation is

$$\begin{pmatrix} z_1^m \\ z_2^m \end{pmatrix} = \begin{pmatrix} 1\,0\,0\,0\,0\,0\,0\,0 \\ 0\,0\,0\,0\,1\,0\,0\,0 \end{pmatrix} \begin{pmatrix} z_{1,1} \\ z_{1,2} \\ z_{1,3} \\ z_{1,4} \\ z_{2,1} \\ z_{2,2} \\ z_{2,3} \\ z_{2,4} \end{pmatrix} \tag{10.101}$$

A suitable feedback control law for the linearized system is

$v_1 = x_d^{(4)} - k_1^1(x^{(3)} - x_d^{(3)}) - k_2^1(\ddot{x} - \ddot{x}_d) - k_3^1(\dot{x} - \dot{x}_d) - k_4^1(x - x_d)$, and $v_2 = y_d^{(4)} - k_1^2(y^{(3)} - y_d^{(3)}) - k_2^2(\ddot{y} - \ddot{y}_d) - k_3^2(\dot{y} - \dot{y}_d) - k_4^2(y - y_d)$

One can compute again the control input that is finally applied to the hovercraft model. It holds that

$$\bar{v} = \tilde{f} + \tilde{M}\tilde{v} \tag{10.102}$$

where matrices and vectors $\bar{v}$, $\tilde{f}$, $\tilde{M}$ and $\tilde{v}$ are defined as

$$\begin{aligned} \bar{v} &= \begin{pmatrix} v_1 \\ v_2 \end{pmatrix} \qquad & \tilde{f} &= \begin{pmatrix} L_f^4 z_{1,1} \\ L_f^4 z_{2,1} \end{pmatrix} \\ \tilde{M} &= \begin{pmatrix} L_{g,a} L_f^3 z_{1,1} & L_{g_b} L_f^3 z_{1,1} \\ L_{g,a} L_f^3 z_{2,1} & L_{g,b} L_f^3 z_{2,1} \end{pmatrix} & \tilde{v} &= \begin{pmatrix} \ddot{\tau}_u \\ \tau_r \end{pmatrix} \end{aligned} \tag{10.103}$$

The above equation can be solved with respect to $\tilde{u}$, which finally gives

$$\tilde{v} = \tilde{M}^{-1}(\bar{v} - \tilde{f}) \tag{10.104}$$

The vector $\tilde{v}$ is the control input that is finally applied to the system, which finally means that the control signal contains integrals of the tracking error.

For the linearized equivalent model of the system it is possible to perform state estimation using the Derivative-free nonlinear Kalman Filter. Before computing the Kalman Filter stages, the previously defined matrices A, B and C are substituted by their discrete-time equivalents A_d, B_d and C_d. This is done through common discretization methods. The recursion of the filter's algorithm consists of two stages:

Measurement update:

$$\begin{aligned} K(k) &= P^{-}C_d^T[P^{-}C_d^T P + R]^{-1} \\ \hat{z}(k) &= \hat{z}^{-}(k) - K(k)[C_d z(k) - C_d \hat{z}^{-}(k)] \\ P(k) &= P^{-}(k) - K(k)C_d P^{-}(k) \end{aligned} \tag{10.105}$$

Time update:

$$\begin{aligned} P^{-}(k+1) &= A_d^T P(k) A_d + Q(k) \\ \hat{z}^{-}(k+1) &= A_d \hat{z}(k) + B_d u(k) \end{aligned} \tag{10.106}$$

Moreover, by using the nonlinear transformations which are provided by differential flatness theory according to Eqs. (10.70), (10.72), (10.74) and (10.79) one can obtain estimates of the state variables of the initial nonlinear hovercraft model.

10.3.5 Disturbances' Compensation with the Use of the Derivative-Free Nonlinear Kalman Filter

Next, a Kalman Filtering method will be developed for estimating at the same time: (i) the non-measurable state vector elements of the hovercraft and (ii) the external perturbations that affect the vessel's model. It is assumed that the input-output linearized equivalent model of the system, is subject to disturbance terms which express the effects of both modeling uncertainty and of external perturbations. Thus one has

$$\begin{aligned} x^{(4)} &= v_1 + \tilde{d}_1 \\ y^{(4)} &= v_2 + \tilde{d}_2 \end{aligned} \tag{10.107}$$

It is considered that the disturbance signals are equivalently represented by their time derivatives (up to order n) and by the associated initial conditions (however, since disturbances are estimated with the use of the Kalman Filter, finally the dependence on knowledge of initial conditions becomes obsolete). It holds that

$$\tilde{d}_1^{(n)} = f_{d_1} \; \tilde{d}_2^{(n)} = f_{d_2} \tag{10.108}$$

The system's state vector is extended by including as additional state variables the disturbances' derivatives. Thus, taking that the derivative's order is $n = 2$ one has

$$z_{d,1} = \tilde{d}_1 \; z_{d,2} = \dot{\tilde{d}}_1 \; z_{d,3} = \tilde{d}_2 \; z_{d,4} = \dot{\tilde{d}}_2 \tag{10.109}$$

and the extended state-space description of the hovercraft becomes

$$\begin{pmatrix} \dot{z}_{1,1} \\ \dot{z}_{1,2} \\ \dot{z}_{1,3} \\ \dot{z}_{1,4} \\ \dot{z}_{2,1} \\ \dot{z}_{2,2} \\ \dot{z}_{2,3} \\ \dot{z}_{2,4} \\ \dot{z}_{d,1} \\ \dot{z}_{d,2} \\ \dot{z}_{d,3} \\ \dot{z}_{d,4} \end{pmatrix} = \begin{pmatrix} 0\,1\,0\,0\,0\,0\,0\,0\,0\,0\,0\,0 \\ 0\,0\,1\,0\,0\,0\,0\,0\,0\,0\,0\,0 \\ 0\,0\,0\,1\,0\,0\,0\,0\,0\,0\,0\,0 \\ 0\,0\,0\,0\,0\,0\,0\,0\,1\,0\,0\,0 \\ 0\,0\,0\,0\,0\,1\,0\,0\,0\,0\,0\,0 \\ 0\,0\,0\,0\,0\,0\,1\,0\,0\,0\,0\,0 \\ 0\,0\,0\,0\,0\,0\,0\,1\,0\,0\,0\,0 \\ 0\,0\,0\,0\,0\,0\,0\,0\,0\,0\,1\,0 \\ 0\,0\,0\,0\,0\,0\,0\,0\,0\,1\,0\,0 \\ 0\,0\,0\,0\,0\,0\,0\,0\,0\,0\,0\,0 \\ 0\,0\,0\,0\,0\,0\,0\,0\,0\,0\,0\,1 \\ 0\,0\,0\,0\,0\,0\,0\,0\,0\,0\,0\,0 \end{pmatrix} \begin{pmatrix} z_{1,1} \\ z_{1,2} \\ z_{1,3} \\ z_{1,4} \\ z_{2,1} \\ z_{2,2} \\ z_{2,3} \\ z_{2,4} \\ z_{d,1} \\ z_{d,2} \\ z_{d,3} \\ z_{d,4} \end{pmatrix} + \begin{pmatrix} 0\,0\,0\,0 \\ 0\,0\,0\,0 \\ 0\,0\,0\,0 \\ 1\,0\,0\,0 \\ 0\,0\,0\,0 \\ 0\,0\,0\,0 \\ 0\,0\,0\,0 \\ 0\,1\,0\,0 \\ 0\,0\,0\,0 \\ 0\,0\,1\,0 \\ 0\,0\,0\,0 \\ 0\,0\,0\,1 \end{pmatrix} \begin{pmatrix} \ddot{\tau}_u \\ \tau_r \\ f_{d_1} \\ f_{d_2} \end{pmatrix} \tag{10.110}$$

while the associated measurement equation is

$$\begin{pmatrix} z_{1,1} \\ z_{2,1} \end{pmatrix} = \begin{pmatrix} 1\,0\,0\,0\,0\,0\,0\,0\,0\,0 \\ 0\,0\,0\,1\,0\,0\,0\,0\,0\,0 \end{pmatrix} z_e \tag{10.111}$$

where $z_e = [z_{1,1}, z_{1,2}, z_{1,3}, z_{1,4}, z_{2,1}, z_{2,2}, z_{2,3}, z_{2,4}, z_{d,1}, z_{d,2}, z_{d,3}, z_{d,4}]^T$ is the extended state vector. Thus, the extended state-space description of the hovercraft model takes the form

$$\begin{aligned} \dot{z}_e &= A_e z_e + B_e v_e \\ z_e^{meas} &= C_e z_e \end{aligned} \tag{10.112}$$

For the extended state-space description of the system one can design a state estimator of the form

$$\begin{aligned} \dot{\hat{z}}_e &= A_o z_e + B_o v_e + K(z_e^{meas} - C_o \hat{z}_e) \\ \hat{z}_e^{meas} &= C_o \hat{z}_e \end{aligned} \tag{10.113}$$

where for the matrices A_o and C_o it holds $A_o = A_e$ and $C_o = C_e$, while for matrix B_o one has

$$B_o^T = \begin{pmatrix} 0\,0\,0\,1\,0\,0\,0\,0\,0\,0\,0\,0 \\ 0\,0\,0\,0\,0\,0\,0\,1\,0\,0\,0\,0 \\ 0\,0\,0\,0\,0\,0\,0\,0\,0\,0\,0\,0 \\ 0\,0\,0\,0\,0\,0\,0\,0\,0\,0\,0\,0 \end{pmatrix} \tag{10.114}$$

Again the Kalman Filter recursion provides joint estimation of the non-measurable state vector elements, of the disturbances' inputs and of their derivatives. Prior to computing the Kalman Filter stages, the previously defined matrices A, B and C are substituted by their discrete-time equivalents A_{e_d}, B_{e_d} and C_{e_d}. This is done through common discretization methods. The recursion of the filter's algorithm consists of two stages. Thus, one has

Measurement update:

$$\begin{aligned} K(k) &= P_e^- C_{e_d}^T [P_e^- {C_{e_d}}^T P_e + R_e]^{-1} \\ \hat{z}_e(k) &= \hat{z}_e^-(k) - K(k)[C_{e_d} z_e(k) - C_{e_d} \hat{z} e^-(k)] \\ P_e(k) &= P_e^-(k) - K(k) C_{e_d} P_e^-(k) \end{aligned} \tag{10.115}$$

Time update:

$$\begin{aligned} P_e^-(k+1) &= {A_{e_d}}^T P_e(k) A_{e_d} + Q_e(k) \\ \hat{z}_e^-(k+1) &= A_{e_d} \hat{z_e}(k) + B_{e_d} v_e(k) \end{aligned} \tag{10.116}$$

For compensating the disturbances' effects, the modified control input that is applied to the system is

$v_1 = x_d^{(4)} - k_1^1(x^{(3)} - x_d^{(3)}) - k_2^1(\ddot{x} - \ddot{x}_d) - k_3^1(\dot{x} - \dot{x}_d) - k_4^1(x - x_d) - \hat{z}_{d,1}$ and $v_2 = y_d^{(4)} - k_1^2(y^{(3)} - y_d^{(3)}) - k_2^2(\ddot{x} - \ddot{y}_d) - k_3^2(\dot{y} - \dot{y}_d) - k_4^2(y - y_d) - \hat{z}_{d,2}$.

10.3.6 Simulation Tests

The performance of the flatness-based control method for the underactuated hovercraft was evaluated in the case of several reference setpoints. The associated results are presented in Figs. 10.36, 10.37, 10.38, 10.39 and 10.40. It can be observed that in all cases the nonlinear feedback controller achieved fast and accurate tracking of the reference setpoints. The Derivative-free nonlinear Kalman Filter enabled estimation of the nonmeasurable variables of the system's state-vector which were needed for the implementation of the feedback control scheme. Moreover, by using the inverse transformation that was provided by differential flatness theory it was possible to obtain estimates of the state variables of the initial nonlinear system.

The convergence of the state variables of the hovercraft (position x, y to the desirable setpoints is shown in Figs. 10.36a, 10.37a, 10.38a, 10.39a and 10.40a. The estimation of the disturbance terms that were applied to the hovercraft model are depicted in Figs. 10.36b, 10.37b, 10.38b, 10.39b and 10.40b, respectively. It can be noticed again that the proposed feedback nonlinear control scheme achieved fast and accurate tracking to these setpoints.

For the underactuated hovercraft one can succeed exactly the same motion and orientation control as in the case of the fully actuated vessel. Therefore, it is possible

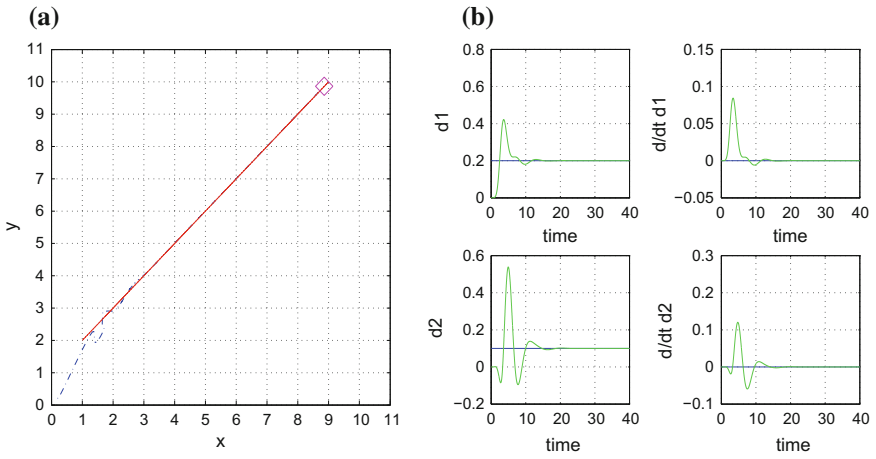

Fig. 10.36 Reference path 1 **a** Trajectory tracking for states x, y of the underactuated hovercraft, **b** Estimation of disturbance inputs affecting the hovercraft, with the use of the Derivative-free nonlinear Kalman Filter

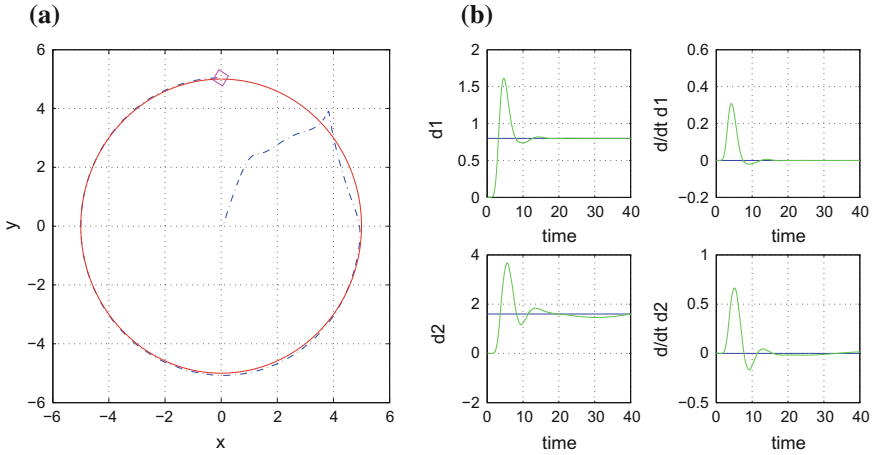

Fig. 10.37 Reference path 2 **a** Trajectory tracking for states x, y of the underactuated hovercraft, **b** Estimation of disturbance inputs affecting the hovercraft, with the use of the Derivative-free nonlinear Kalman Filter

for the hovercraft to track complicated reference paths with excellent accuracy while keeping also the desirable velocity. This has been demonstrated through a series of examples, in the simulation tests section of the manuscript (Figs. 10.36, 10.37, 10.38, 10.39 and 10.40). It is noteworthy that the dynamic feedback linearization procedure which has been implemented on the hovercraft's model, results in the canonical form description of Eqs. (10.100) and (10.101) which is confirmed to

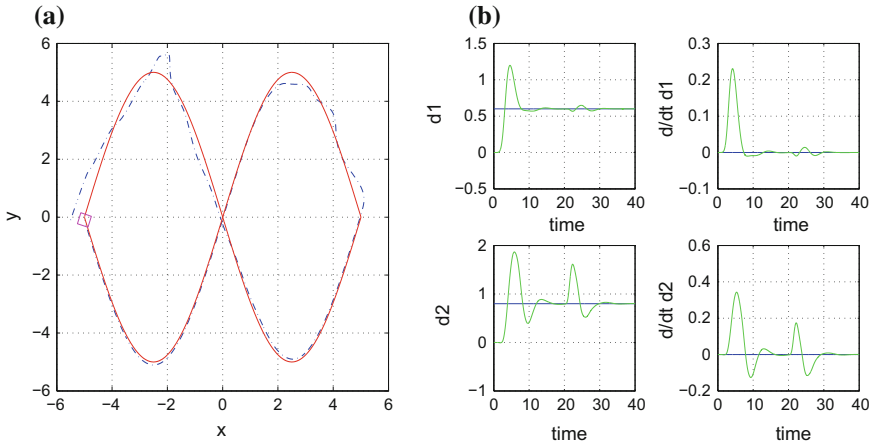

Fig. 10.38 Reference path 3 **a** Trajectory tracking for states x, y of the underactuated hovercraft, **b** Estimation of disturbance inputs affecting the hovercraft, with the use of the Derivative-free nonlinear Kalman Filter

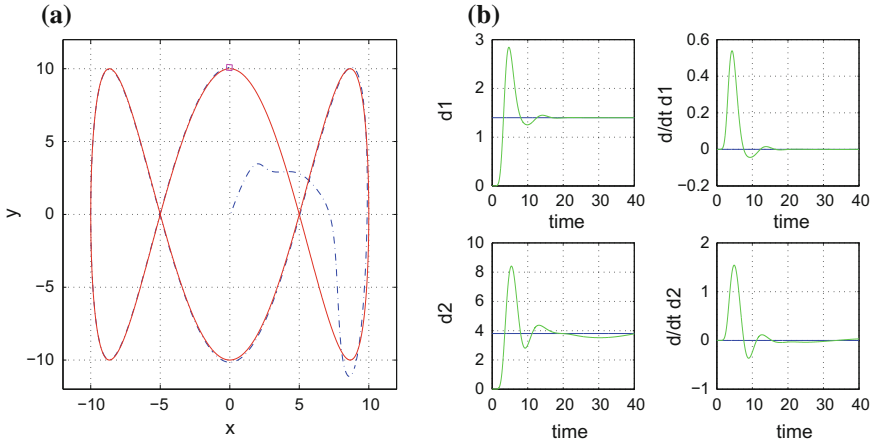

Fig. 10.39 Reference path 4 **a** Trajectory tracking for states x, y of the underactuated hovercraft, **b** Estimation of disturbance inputs affecting the hovercraft, with the use of the Derivative-free nonlinear Kalman Filter

be controllable. Practically, this means that under the proposed control scheme the vessel can reach any point in its motion plane and can track any reference path.

The possibility for the appearance of singularities in the computation of the control signal is present in all static or dynamic feedback linearization algorithms which arrive at a transformed control input of the form $v = f(x,t) + g(x,t)u$, that is $u = g(x,t)^{-1}[v - f(x,t)]$. There are two cases: (i) due to the inherent model of $g(x,t)$ its inverse never becomes 0. In such a case the singularity problem is avoided,

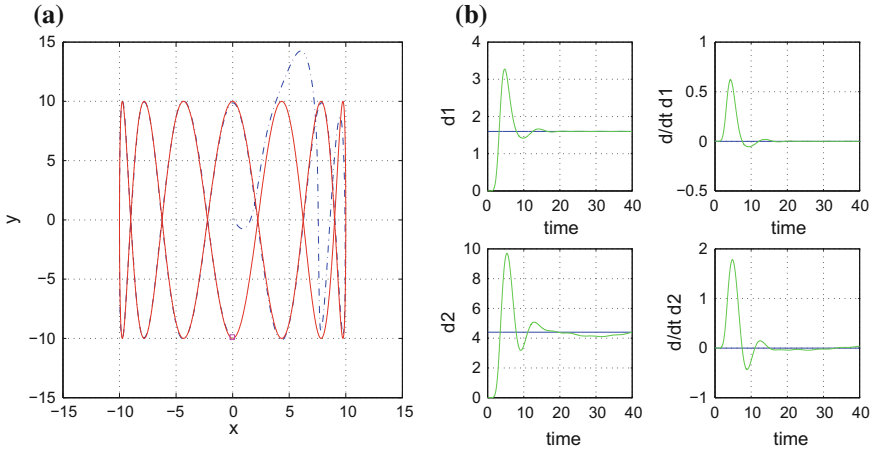

Fig. 10.40 Reference path 5 **a** Trajectory tracking for states x, y of the underactuated hovercraft, **b** Estimation of disturbance inputs affecting the hovercraft, with the use of the Derivative-free nonlinear Kalman Filter

(ii) for certain areas of the state vector space $x \in R^n$ the zeroing of $g(x,t)^{-1}$ cannot be excluded. For the latter case the avoidance of singularities can be succeeded by a state variables transformation into a new state-space representation which does not include any points of singularity.

The presented simulation experiments have been performed under the assumption that the hovercraft was subject to external disturbances such as wind or current. The proposed control scheme is robust to modeling uncertainties and external perturbations. This is a prerequisite in the design of control systems for underactuated surface vessels [127, 167, 297, 345, 498, 627]. First, it has been proven that the feedback control applied on the input-output linearized model of the hovercraft achieved the placement of all poles of the control loop in the left complex semiplane. Next, it can be confirmed that the extended state-space model of the hovercraft, which contains disturbances as additional state variables, has multiple poles at the origin (multiple poles at zero). This means that by output feedback one can achieve infinite gain margin and a sufficiently large phase margin. With the use of the Derivative-free nonlinear Kalman Filter it became possible to identify the perturbation and modeling uncertainty terms in real-time and subsequently to compensate for them through the inclusion of an additional term in the control signal. This amendment in the feedback control scheme provided the control loop with elevated robustness. Finally, it is worth mentioning that the proposed control scheme had an excellent performance although it was not possible to measure directly all elements of the state vector (only the cartesian coordinates of the vessel could be measured) and several state variables had to be estimated with the use of filtering.

The model of the disturbances considered in this section is quite realistic. The disturbance inputs can be represented equally well if their analytical function is known

or if their nth order derivative and the associated initial conditions are known. However, in the latter case and with the Kalman filtering approach followed in the present section, the knowledge of initial conditions becomes obsolete since the Kalman Filter can reconstruct the disturbance inputs and their derivatives without dependance on initial conditions. In conclusion, the numerical simulation performed in this section estimates quite well the disturbances' effects. The disturbance inputs have a clear physical meaning since they represent the effects of wind forces or wave forces exerted on the vessel.

The control method which has been implemented in the present section is a global linearization one. This means that the vessel's dynamic model is transformed through a change of variables into an equivalent linear description for which the design of the feedback controller becomes easier. Moreover, this linearization is an exact one because it does not introduce any numerical errors due to truncation of terms in the linearization procedure. Prior to this transformation the so-called dynamic extension is performed that is the vessel's state-space model is extended by considering as additional state variables the control inputs and their derivatives [382, 634]. A second major class of solutions for the problem of autonomous navigation of underactuated vessels uses methods that asymptotically linearize the vessel's dynamics. This holds for instance in the case of H-infinity control or local models fuzzy control. The vessel's model can be linearized round local operating points. Next, for the linearized model of the vessel a feedback controller is designed, taking also into account that robustness should be exhibited against both approximate linearization errors and external perturbations [79, 99, 205, 564]. A third class of possible solutions comprises Lyapunov methods in which the stabilizing control of the underactuated vessels is obtained from the procedure of minimization of a suitably chosen Lyapunov function. Such solutions can be model-based which means that prior knowledge about the vessel's dynamic model is available and is used by the control algorithm. They can also be model-free taking the form of adaptive control. In the latter case the vessel's dynamic model is considered to be completely unknown and is identified online by an adaptation scheme during the execution of the control algorithm [126, 127, 251, 279, 398]. The comparison of the aforementioned approaches shows that the differential flatness theory-based method for the underactuated vessel is conceptually simpler and straightforward to implement, while also avoiding linearization approximations, numerical errors and constraining assumptions about the structure of the controlled vessel's model.

10.4 A Nonlinear H-Infinity Control Approach for Underactuated Surface Vessels

10.4.1 Outline

In this section control of unmanned surface vessels (USVs) is based on a local linearization approach. The linearization takes place round the USV's local operating

point which is defined at each time instant by the present value of the state vector and the last value of the control inputs vector [461]. The linearization makes use of Taylor series expansion and of the computation of Jacobian matrices [33, 431, 463, 564]. The modelling error, due to truncation of higher order terms in the Taylor series, is considered as perturbation which is compensated by the robustness of the control algorithm. For the linearized model of the USV an H-infinity feedback controller is designed. A cost function is introduced comprising the weighted square of the error of the system's state vector (distance of the state vector from the reference setpoints).

This control method represents a differential game taking place between the control input which tries to minimize the above cost function and between the disturbances which try to maximize this objective function. The computation of the feedback control gain requires the solution of an algebraic Riccati equation, which takes place at each iteration of the control algorithm. The solution of the Riccati equation provides a positive definite symmetric matrix which is used as a weighting coefficient in the computation of the controller's feedback gain. The known robustness features of H-infinity control assure the elimination of perturbation effects, which in turn implies compensation of model uncertainty terms, external disturbance inputs as well as of measurement noises. The stability properties of the control scheme are assured by Lyapunov analysis. It is shown that the proposed feedback control law for USVs results in H-infinity tracking performance which means robustness against modeling uncertainty and external perturbations. Under moderate conditions it is also proven that the control loop is also globally asymptotically stable. The tracking accuracy and the smooth transients in the proposed USV control method are also confirmed through simulation experiments.

Yet computationally simple, the proposed H_∞ control scheme has an excellent performance. Comparing to the control of underactuated vessels that is based on global linearization methods (see [416, 450, 452, 457, 460]), the following features can be attributed to the presented nonlinear H-infinity control scheme (i) it is applied directly on the nonlinear dynamical model of the underactuated vessel and does not require the computation of diffeomorphisms (change of variables) that will bring the system into an equivalent linearized form, (ii) the computation of the feedback control signal follows an optimal control concept and requires the solution of an algebraic Riccati equation at each iteration of the control algorithm, (iii) the method retains the advantages of typical optimal control, that is fast and accurate tracking of the reference trajectories under moderate variations of the control inputs.

10.4.2 Approximate Linearization of the Underactuated Vessel

In the previous section it was shown that the joint kinematic and dynamic model of the underactuated vessel is

$$\begin{pmatrix} \dot{x} \\ \dot{y} \\ \dot{\psi} \\ \dot{u} \\ \dot{v} \\ \dot{r} \end{pmatrix} = \begin{pmatrix} ucos(\psi) - vsin(\psi) \\ usin(\psi) + vcos(\psi) \\ r \\ v \cdot r \\ -ur - \beta v \\ 0 \end{pmatrix} + \begin{pmatrix} 0 & 0 \\ 0 & 0 \\ 0 & 0 \\ 1 & 0 \\ 0 & 0 \\ 0 & 1 \end{pmatrix} \begin{pmatrix} \tau_u \\ \tau_r \end{pmatrix} \tag{10.117}$$

where (x, y) are the cartesian coordinates if the vessel in the inertial reference frame, ψ is the heading angle of the vessel in the inertial reference frame, u is the surge velocity, v is the sway velocity, r is the yaw rate, β is a function of the elements of the inertia matrix of the vessel.

Linearization of the vessel's kinematic and dynamic model will be performed round a local operating point (equilibrium) (x^*, u^*). To this end, the joint kinematics and dynamics model of Eq. (10.117) is written in the form:

$$\dot{x} = f(x) + g(x)u \tag{10.118}$$

where the state vector is $x = [x_1, x_2, x_3, x_4, x_5, x_6]^T = [x, y, \psi, u, v, r]^T$ and

$$f(x) = \begin{pmatrix} x_4 cos(x_3) - x_5 sin(x_3) \\ x_4 sin(x_3) + x_5 cos(x_3) \\ x_6 \\ x_5 x_6 \\ -x_4 x_6 - \beta x_5 \\ 0 \end{pmatrix} \quad g(x) = \begin{pmatrix} 0 & 0 \\ 0 & 0 \\ 0 & 0 \\ 1 & 0 \\ 0 & 0 \\ 0 & 1 \end{pmatrix} \tag{10.119}$$

The linearization of the vessel's model round the temporary equilibrium gives

$$\dot{x} = Ax + Bu \tag{10.120}$$

where

$$A = \nabla_x [f(x) + g(x)u] \mid_{(x^*, u^*)} \Rightarrow A = \nabla_x f(x) \mid_{(x^*, u^*)} \tag{10.121}$$

$$B = \nabla_u [f(x) + g(x)u] \mid_{(x^*, u^*)} \Rightarrow B = g(x) \mid_{(x^*, u^*)} \tag{10.122}$$

For the Jacobian matrix $A = \nabla_x [f(x) + g(x)u] \mid_{(x^*, u^*)}$, it holds that

$$A = \nabla_x [f(x) + g(x)u] \mid_{(x^*, u^*)} \Rightarrow$$

$$A = \begin{pmatrix} \frac{\partial f_1}{\partial x_1} & \frac{\partial f_1}{\partial x_2} & \frac{\partial f_1}{\partial x_3} & \cdots & \frac{\partial f_1}{\partial x_6} \\ \frac{\partial f_2}{\partial x_1} & \frac{\partial f_2}{\partial x_2} & \frac{\partial f_2}{\partial x_3} & \cdots & \frac{\partial f_2}{\partial x_6} \\ \cdots & \cdots & \cdots & \cdots & \\ \frac{\partial f_6}{\partial x_1} & \frac{\partial f_6}{\partial x_2} & \frac{\partial f_6}{\partial x_3} & \cdots & \frac{\partial f_6}{\partial x_6} \end{pmatrix} \tag{10.123}$$

For the first row of the aforementioned Jacobian matrix one has:

$\frac{\partial f_1}{\partial x_1} = 0$, $\frac{\partial f_1}{\partial x_2} = 0$, $\frac{\partial f_1}{\partial x_3} = -x_4 sin(x_3) - x_5 cos(x_3)$, $\frac{\partial f_1}{\partial x_4} = cos(x_3)$, $\frac{\partial f_1}{\partial x_5} = -sin(x_3)$, $\frac{\partial f_1}{\partial x_6} = 0$.

For the second row of the aforementioned Jacobian matrix one has:

$\frac{\partial f_2}{\partial x_1} = 0$, $\frac{\partial f_2}{\partial x_2} = 0$, $\frac{\partial f_2}{\partial x_3} = x_4 cos(x_3) - x_5 sin(x_3)$, $\frac{\partial f_2}{\partial x_4} = sin(x_3)$, $\frac{\partial f_2}{\partial x_5} = cos(x_3)$, $\frac{\partial f_2}{\partial x_6} = 0$.

For the third row of the aforementioned Jacobian matrix one has:

$\frac{\partial f_3}{\partial x_1} = 0$, $\frac{\partial f_3}{\partial x_2} = 0$, $\frac{\partial f_3}{\partial x_3} = 0$, $\frac{\partial f_3}{\partial x_4} = 0$, $\frac{\partial f_3}{\partial x_5} = 0$, $\frac{\partial f_3}{\partial x_6} = 1$.

For the fourth row of the aforementioned Jacobian matrix one has:

$\frac{\partial f_4}{\partial x_1} = 0$, $\frac{\partial f_4}{\partial x_2} = 0$, $\frac{\partial f_4}{\partial x_3} = 0$, $\frac{\partial f_4}{\partial x_4} = 0$, $\frac{\partial f_4}{\partial x_5} = x_6$, $\frac{\partial f_4}{\partial x_6} = x_5$.

For the fifth row of the aforementioned Jacobian matrix one has:

$\frac{\partial f_5}{\partial x_1} = 0$, $\frac{\partial f_5}{\partial x_2} = 0$, $\frac{\partial f_5}{\partial x_3} = 0$, $\frac{\partial f_5}{\partial x_4} = -x_6$, $\frac{\partial f_5}{\partial x_5} = -\beta$, $\frac{\partial f_5}{\partial x_6} = -x_4$.

For the sixth row of the aforementioned Jacobian matrix one has:

$\frac{\partial f_6}{\partial x_1} = 0$, $\frac{\partial f_6}{\partial x_2} = 0$, $\frac{\partial f_6}{\partial x_3} = 0$, $\frac{\partial f_6}{\partial x_4} = 0$, $\frac{\partial f_6}{\partial x_5} = 0$, $\frac{\partial f_6}{\partial x_6} = 0$.

10.4.3 Design of an H-Infinity Nonlinear Feedback Controller

10.4.3.1 Equivalent Linearized Dynamics of the Vessel

After linearization round its current operating point, the USV's dynamic model is written as

$$\dot{x} = Ax + Bu + d_1 \tag{10.124}$$

Parameter d_1 stands for the linearization error in the USV's dynamic model appearing in Eq. (10.124). The reference setpoints for USV's state vector are denoted by $\mathbf{x_d} = [x_1^d, \ldots, x_6^d]$. Tracking of this trajectory is achieved after applying the control input $\tilde{u}^*$. At every time instant the control input $\tilde{u}^*$ is assumed to differ from the control input u appearing in Eq. (10.124) by an amount equal to Δu, that is $\tilde{u}^* = u + \Delta u$

$$\dot{x}_d = Ax_d + Bu^* + d_2 \tag{10.125}$$

The dynamics of the controlled system described in Eq. (10.124) can be also written as

$$\dot{x} = Ax + Bu + Bu^* - Bu^* + d_1 \tag{10.126}$$

and by denoting $d_3 = -B\tilde{u}^* + d_1$ as an aggregate disturbance term one obtains

$$\dot{x} = Ax + Bu + B\tilde{u}^* + d_3 \tag{10.127}$$

By subtracting Eq. (10.125) from (10.127) one has

$$\dot{x} - \dot{x}_d = A(x - x_d) + Bu + d_3 - d_2 \tag{10.128}$$

By denoting the tracking error as $e = x - x_d$ and the aggregate disturbance term as $\tilde{d} = d_3 - d_2$, the tracking error dynamics becomes

$$\dot{e} = Ae + Bu + \tilde{d} \tag{10.129}$$

The above linearized form of the USV's model can be efficiently controlled after applying an H-infinity feedback control scheme.

10.4.3.2 The Nonlinear H-Infinity Control

The initial nonlinear model of the unmanned surface vessel is in the form

$$\dot{x} = \tilde{f}(x, u) \;\; x \in R^n, \;\; u \in R^m \tag{10.130}$$

Linearization of the model of the unmanned surface vessel is performed at each iteration of the control algorithm round its present operating point $(x^*, u^*) = (x(t), u(t - T_s))$, where T_s is the sampling period. The linearized equivalent of the system is described by

$$\dot{x} = Ax + Bu + L\tilde{d} \;\; x \in R^n, \;\; u \in R^m, \;\; \tilde{d} \in R^q \tag{10.131}$$

where matrices A and B are obtained from the computation of the Jacobians

$$A = \begin{pmatrix} \frac{\partial \tilde{f}_1}{\partial x_1} & \frac{\partial \tilde{f}_1}{\partial x_2} & \cdots & \frac{\partial \tilde{f}_1}{\partial x_n} \\ \frac{\partial \tilde{f}_2}{\partial x_1} & \frac{\partial \tilde{f}_2}{\partial x_2} & \cdots & \frac{\partial \tilde{f}_2}{\partial x_n} \\ \cdots & \cdots & \cdots & \cdots \\ \frac{\partial \tilde{f}_n}{\partial x_1} & \frac{\partial \tilde{f}_n}{\partial x_2} & \cdots & \frac{\partial \tilde{f}_n}{\partial x_n} \end{pmatrix} |_{(x^*, u^*)} \;\; B = \begin{pmatrix} \frac{\partial \tilde{f}_1}{\partial u_1} & \frac{\partial \tilde{f}_1}{\partial u_2} & \cdots & \frac{\partial \tilde{f}_1}{\partial u_m} \\ \frac{\partial \tilde{f}_2}{\partial u_1} & \frac{\partial \tilde{f}_2}{\partial u_2} & \cdots & \frac{\partial \tilde{f}_2}{\partial u_m} \\ \cdots & \cdots & \cdots & \cdots \\ \frac{\partial \tilde{f}_n}{\partial u_1} & \frac{\partial \tilde{f}_n}{\partial u_2} & \cdots & \frac{\partial \tilde{f}_n}{\partial u_m} \end{pmatrix} |_{(x^*, u^*)} \tag{10.132}$$

and vector $\tilde{d}$ denotes disturbance terms due to linearization errors. As already analyzed, the problem of disturbance rejection for the linearized model that is described by

$$\dot{x} = Ax + Bu + L\tilde{d}$$
$$y = Cx \tag{10.133}$$

where $x \in R^n$, $u \in R^m$, $\tilde{d} \in R^q$ and $y \in R^p$, cannot be handled efficiently if the classical LQR control scheme is applied. This is because of the existence of the perturbation term $\tilde{d}$. The disturbance term $\tilde{d}$ apart from modeling (parametric) uncertainty and external perturbation terms can also represent noise terms of any distribution.

It has been already noted in the previous application examples of the H_∞ control approach, that a feedback control scheme is designed for trajectory tracking by the system's state vector and simultaneous disturbance rejection, considering that the disturbance affects the system in the worst possible manner. The disturbances' effect are incorporated in the following quadratic cost function:

$$J(t) = \frac{1}{2}\int_0^T [y^T(t)y(t) + ru^T(t)u(t) - \rho^2\tilde{d}^T(t)\tilde{d}(t)]dt, \quad r, \rho > 0 \tag{10.134}$$

It has been pointed out that the meaning of the negative sign in the cost function's term that is associated with the perturbation variable $\tilde{d}(t)$ is that the disturbance tries to maximize the cost function $J(t)$ while the control signal $u(t)$ tries to minimize it. The physical meaning of the relation given above is that the control signal and the disturbances compete to each other within a min–max differential game. This problem of min–max optimization can be written as

$$min_u max_{\tilde{d}} J(u, \tilde{d}) \tag{10.135}$$

As previously explained, the objective of the optimization procedure is to compute a control signal $u(t)$ which can compensate for the worst possible disturbance, that is externally imposed to the system. However, the solution to the min–max optimization problem is directly related to the value of parameter ρ. This means that there is an upper bound in the disturbances magnitude that can be annihilated by the control signal.

10.4.3.3 Computation of the Feedback Control Gains

For the linearized system given by Eq. (10.133) the cost function of Eq. (10.134) is defined, where the coefficient r determines the penalization of the control input and the weight coefficient ρ determines the reward of the disturbances' effects. It is assumed that (i) The energy that is transferred from the disturbances signal $\tilde{d}(t)$ is bounded, that is $\int_0^\infty \tilde{d}^T(t)\tilde{d}(t)dt < \infty$, (ii) the matrices $[A, B]$ and $[A, L]$ are stabilizable, (iii) the matrix $[A, C]$ is detectable. Then, the optimal feedback control

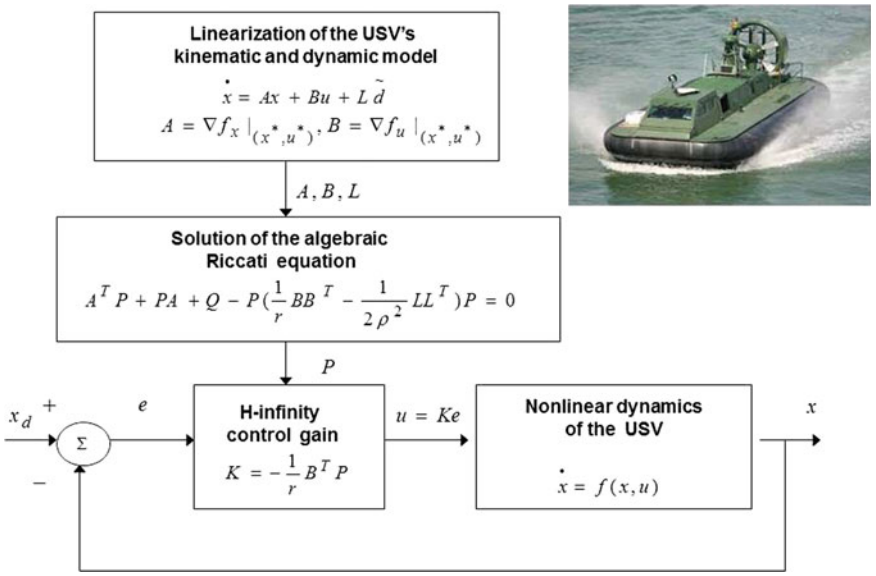

Fig. 10.41 Diagram of the nonlinear H-infinity control scheme for the unmanned surface vessel

law is given by

$$u(t) = -Kx(t) \tag{10.136}$$

with

$$K = \frac{1}{r}B^T P \tag{10.137}$$

where P is a positive semi-definite symmetric matrix which is obtained from the solution of the Riccati equation

$$A^T P + PA + Q - P\left(\frac{1}{r}BB^T - \frac{1}{2\rho^2}LL^T\right)P = 0 \tag{10.138}$$

where Q is also a positive definite symmetric matrix. The worst case disturbance is given by $\tilde{d}(t) = \frac{1}{\rho^2}L^T Px(t)$. The diagram of the considered control loop is depicted in Fig. 10.41.

10.4.4 Lyapunov Stability Analysis

Through Lyapunov stability analysis it will be shown that the proposed nonlinear control scheme assures H_∞ tracking performance for the USV, and that in case of bounded disturbance terms asymptotic convergence to the reference setpoints is

achieved. The tracking error dynamics for the unmanned surface vessel is written in the form

$$\dot{e} = Ae + Bu + L\tilde{d} \tag{10.139}$$

where in the USV's case $L = I \in R^{6\times 6}$ with I being the identity matrix. Variable $\tilde{d}$ denotes model uncertainties and external disturbances of the USV's model. The following Lyapunov function is considered

$$V = \frac{1}{2} e^T P e \tag{10.140}$$

where $e = x - x_d$ is the tracking error. By differentiating with respect to time one obtains

$$\begin{gathered} \dot{V} = \tfrac{1}{2}\dot{e}^T P e + \tfrac{1}{2} e^T P \dot{e} \Rightarrow \\ \dot{V} = \tfrac{1}{2}[Ae + Bu + L\tilde{d}]^T P e + \tfrac{1}{2} e^T P [Ae + Bu + L\tilde{d}] \Rightarrow \end{gathered} \tag{10.141}$$

$$\begin{gathered} \dot{V} = \tfrac{1}{2}[e^T A^T + u^T B^T + \tilde{d}^T L^T] P e + \\ + \tfrac{1}{2} e^T P [Ae + Bu + L\tilde{d}] \Rightarrow \end{gathered} \tag{10.142}$$

$$\begin{gathered} \dot{V} = \tfrac{1}{2} e^T A^T P e + \tfrac{1}{2} u^T B^T P e + \tfrac{1}{2} \tilde{d}^T L^T P e + \\ \tfrac{1}{2} e^T P A e + \tfrac{1}{2} e^T P B u + \tfrac{1}{2} e^T P L \tilde{d} \end{gathered} \tag{10.143}$$

The previous equation is rewritten as

$$\begin{gathered} \dot{V} = \tfrac{1}{2} e^T (A^T P + PA) e + (\tfrac{1}{2} u^T B^T P e + \tfrac{1}{2} e^T P B u) + \\ + (\tfrac{1}{2} \tilde{d}^T L^T P e + \tfrac{1}{2} e^T P L \tilde{d}) \end{gathered} \tag{10.144}$$

Assumption: For given positive definite matrix Q and coefficients r and ρ there exists a positive definite matrix P, which is the solution of the following matrix equation

$$A^T P + PA = -Q + P \left(\frac{2}{r} B B^T - \frac{1}{\rho^2} L L^T \right) P \tag{10.145}$$

Moreover, the following feedback control law is applied to the system

$$u = -\frac{1}{r} B^T P e \tag{10.146}$$

By substituting Eqs. (10.145) and (10.146) one obtains

$$\begin{gathered} \dot{V} = \tfrac{1}{2} e^T [-Q + P(\tfrac{2}{r} B B^T - \tfrac{1}{\rho^2} L L^T) P] e + \\ + e^T P B (-\tfrac{1}{r} B^T P e) + e^T P L \tilde{d} \Rightarrow \end{gathered} \tag{10.147}$$

$$\begin{aligned}\dot{V} = -\tfrac{1}{2}e^T Qe + \tfrac{1}{r}e^T PBB^T Pe - \tfrac{1}{2\rho^2}e^T PLL^T Pe \\ -\tfrac{1}{r}e^T PBB^T Pe + e^T PL\tilde{d}\end{aligned} \tag{10.148}$$

which after intermediate operations gives

$$\dot{V} = -\frac{1}{2}e^T Qe - \frac{1}{2\rho^2}e^T PLL^T Pe + e^T PL\tilde{d} \tag{10.149}$$

or, equivalently

$$\begin{aligned}\dot{V} = -\tfrac{1}{2}e^T Qe - \tfrac{1}{2\rho^2}e^T PLL^T Pe + \\ +\tfrac{1}{2}e^T PL\tilde{d} + \tfrac{1}{2}\tilde{d}^T L^T Pe\end{aligned} \tag{10.150}$$

Lemma: The following inequality holds

$$\frac{1}{2}e^T PL\tilde{d} + \frac{1}{2}\tilde{d}L^T Pe - \frac{1}{2\rho^2}e^T PLL^T Pe \leq \frac{1}{2}\rho^2\tilde{d}^T\tilde{d} \tag{10.151}$$

Proof: The binomial $(\rho\alpha - \frac{1}{\rho}b)^2$ is considered. Expanding the left part of the above inequality one gets

$$\begin{aligned}\rho^2a^2 + \tfrac{1}{\rho^2}b^2 - 2ab \geq 0 \Rightarrow \tfrac{1}{2}\rho^2a^2 + \tfrac{1}{2\rho^2}b^2 - ab \geq 0 \Rightarrow \\ ab - \tfrac{1}{2\rho^2}b^2 \leq \tfrac{1}{2}\rho^2a^2 \Rightarrow \tfrac{1}{2}ab + \tfrac{1}{2}ab - \tfrac{1}{2\rho^2}b^2 \leq \tfrac{1}{2}\rho^2a^2\end{aligned} \tag{10.152}$$

The following substitutions are carried out: $a = \tilde{d}$ and $b = e^T PL$ and the previous relation becomes

$$\frac{1}{2}\tilde{d}^T L^T Pe + \frac{1}{2}e^T PL\tilde{d} - \frac{1}{2\rho^2}e^T PLL^T Pe \leq \frac{1}{2}\rho^2\tilde{d}^T\tilde{d} \tag{10.153}$$

Equation (10.153) is substituted in Eq. (10.150) and the inequality is enforced, thus giving

$$\dot{V} \leq -\frac{1}{2}e^T Qe + \frac{1}{2}\rho^2\tilde{d}^T\tilde{d} \tag{10.154}$$

Equation (10.154) shows that the H_∞ tracking performance criterion is satisfied. The integration of $\dot{V}$ from 0 to T gives

$$\begin{aligned}\int_0^T \dot{V}(t)dt \leq -\tfrac{1}{2}\int_0^T ||e||_Q^2 dt + \tfrac{1}{2}\rho^2\int_0^T ||\tilde{d}||^2 dt \Rightarrow \\ 2V(T) + \int_0^T ||e||_Q^2 dt \leq 2V(0) + \rho^2\int_0^T ||\tilde{d}||^2 dt\end{aligned} \tag{10.155}$$

Moreover, if there exists a positive constant $M_d > 0$ such that

$$\int_0^\infty ||\tilde{d}||^2 dt \leq M_d \tag{10.156}$$

then one gets

$$\int_0^\infty ||e||_Q^2 dt \leq 2V(0) + \rho^2 M_d \tag{10.157}$$

Thus, the integral $\int_0^\infty ||e||_Q^2 dt$ is bounded. Moreover, $V(T)$ is bounded and from the definition of the Lyapunov function V in Eq. (10.140) it becomes clear that $e(t)$ will be also bounded since $e(t) \in \Omega_e = \{e|e^T Pe \leq 2V(0) + \rho^2 M_d\}$. According to the above and with the use of Barbalat's Lemma one obtains $lim_{t\to\infty} e(t) = 0$.

Elaborating on the above, it can be noted that the proof of global asymptotic stability for the control loop of the unmanned surface vessel relies on Eq. (10.154) and on the application of Barbalat's Lemma. It uses the condition of Eq. (10.156) about the boundedness of the square of the aggregate disturbance and modelling error term $\tilde{d}$ that affects the model. However, as explained above the proof of global asymptotic stability is not restricted by this condition. By selecting the attenuation coefficient ρ to be sufficiently small and in particular to satisfy $\rho^2 < ||e||_Q^2 / ||\tilde{d}||^2$ one has that the first derivative of the Lyapunov function is upper bounded by 0. Therefore for the ith time interval it is proven that the Lyapunov function defined in Eq. (10.140) is a decreasing one. This also assures that the Lyapunov function of the system defined in Eq. (10.140) will always have a negative first-order derivative.

10.4.5 Robust State Estimation with the Use of the H-Infinity Kalman Filter

The control loop can be implemented with the use of information provided by a small number of sensors and by processing only a small number of state variables. To reconstruct the missing information about the state vector of the hovercraft it is proposed to use a filtering scheme and based on it to apply state estimation-based control [457]. As previously explained, the recursion of the H_∞ Kalman Filter, for the model of the USV, can be formulated in terms of a *measurement update* and a *time update* part.

Measurement update:

$$\begin{aligned} D(k) &= [I - \theta W(k) P^-(k) + C^T(k) R(k)^{-1} C(k) P^-(k)]^{-1} \\ K(k) &= P^-(k) D(k) C^T(k) R(k)^{-1} \\ \hat{x}(k) &= \hat{x}^-(k) + K(k)[y(k) - C\hat{x}^-(k)] \end{aligned} \tag{10.158}$$

Time update:

$$\begin{aligned} \hat{x}^{-}(k+1) &= A(k)x(k) + B(k)u(k) \\ P^{-}(k+1) &= A(k)P^{-}(k)D(k)A^{T}(k) + Q(k) \end{aligned} \tag{10.159}$$

where it is assumed that parameter θ is sufficiently small to assure that the covariance matrix $P^{-}(k)^{-1} - \theta W(k) + C^{T}(k)R(k)^{-1}C(k)$ will be positive definite. When $\theta = 0$ the H_{∞} Kalman Filter becomes equivalent to the standard Kalman Filter. One can measure only a part of the state vector of the USV, and estimate through filtering the rest of the state vector elements. Moreover, the proposed Kalman filtering method can be used for sensor fusion purposes.

10.4.6 Simulation Tests

The efficiency of the nonlinear H-infinity control method for the problem of autonomous navigation of the underactuated unmanned surface vessels, was tested in the case of tracking of several reference trajectories. The setpoints have been chosen by taking into account the differential flatness properties of the vessel which have been explained in previous sections. In the autonomous vessel's case the flat outputs of the model are the vessel's cartesian coordinates (x, y).

In the presented simulation experiments state estimation-based control has been implemented. Out of the 6 state variables of the USV only the cartesian coordinates of the vessel (x, y) where considered to be measurable. The rest of the state variables were indirectly estimated with the use of the H-infinity Kalman Filter. The real value of each state variable has been plotted in blue, the estimated value has been plotted in green, while the associated reference setpoint has been plotted in red.

The obtained results are presented in Figs. 10.42, 10.43, 10.44, 10.45, 10.46, 10.47, 10.48, 10.49, 10.50 and 10.51. The state variables of the model have been measured in SI units. It has been confirmed that the proposed control method resulted in fast and accurate tracking of the reference paths. The H-infinity controller assured fast elimination of the tracking error for all state variables of the USV while the variation of the control inputs was smooth and remained within moderate ranges. The method exhibited significant robustness both to the modelling error that was due to the approximate linearization of the USV's dynamics and to parametric changes.

The tracking performance of the nonlinear H-infinity control method for the model of the underactuated vessel (in its state estimation-based implementation) is outlined in Table 10.3:

Apart from remarkable tracking accuracy, the proposed control method exhibits also significant robustness. Even if it is considered that the controller is designed under uncertainty about parameter β of Eq. (10.39) and deviation from the parameter's nominal value ($\beta = 15$), the state variables of the hovercraft converged accurately to the reference setpoint and the tracking error was negligible. The robustness of the control method is defined by the attenuation coefficient ρ. Actually, maximum

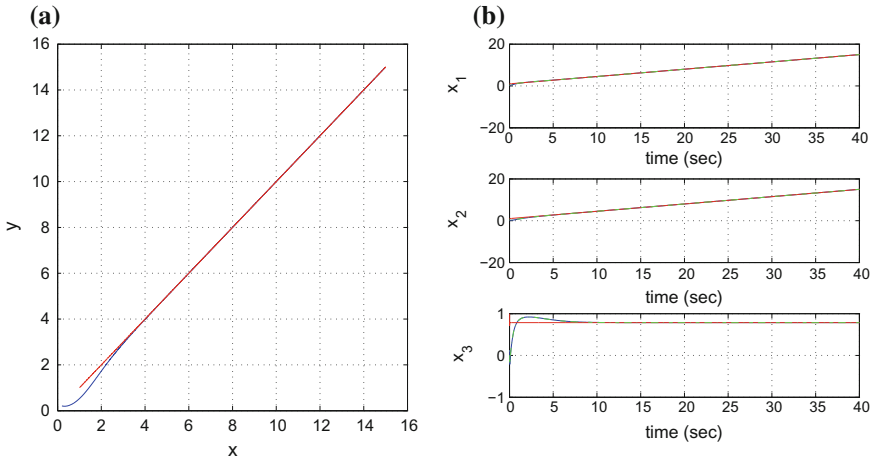

Fig. 10.42 Reference path 1: **a** Tracking of the reference trajectory (red line) in the $x - y$ plane by the unmanned surface vessel (blue line), **b** Convergence of the state variables of the vessel $x_1 = x$, $x_2 = y$ and $x_3 = \psi$ (blue line) to the associated reference values (red line)

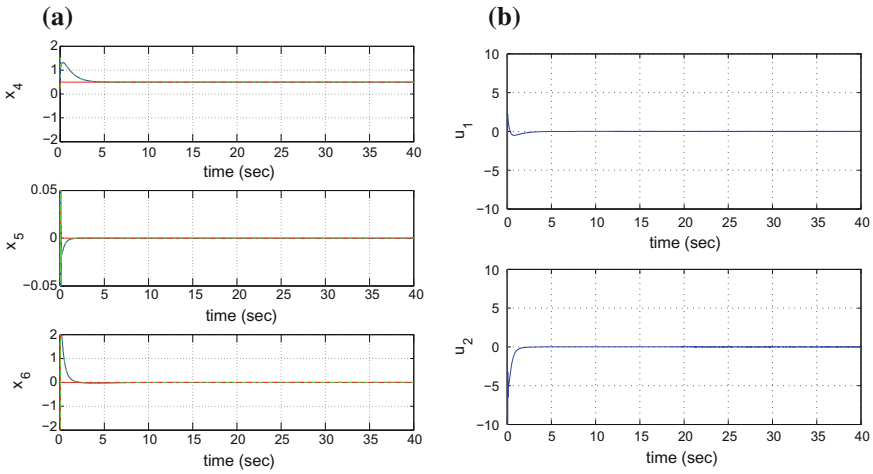

Fig. 10.43 Reference path 1: **a** Convergence of the state variables of the vessel $x_4 = u$, $x_5 = v$ and $x_6 = r$ (blue line) to the associated reference values (red line) **b** Control inputs $u_1 = \tau_u$ and $u_2 = \tau_r$ exerted on vessel

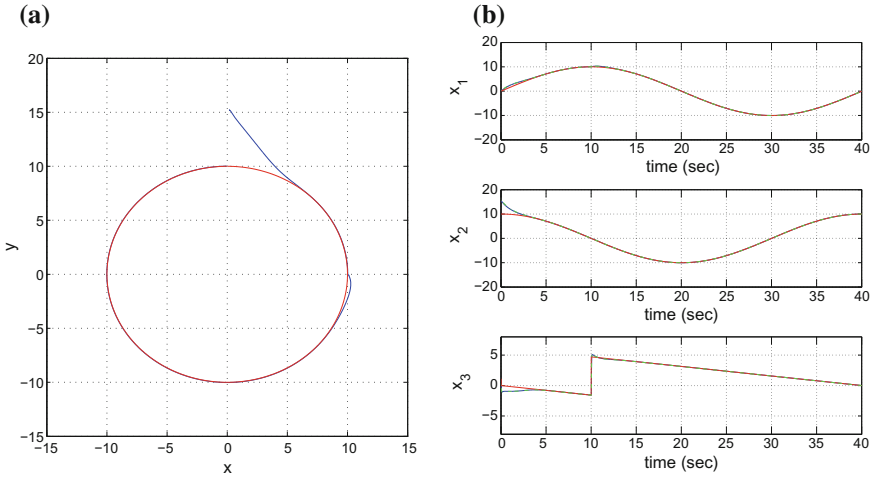

Fig. 10.44 Reference path 2: **a** Tracking of the reference trajectory (red line) in the $x - y$ plane by the unmanned surface vessel (blue line), **b** Convergence of the state variables of the vessel $x_1 = x$, $x_2 = y$ and $x_3 = \psi$ (blue line) to the associated reference values (red line)

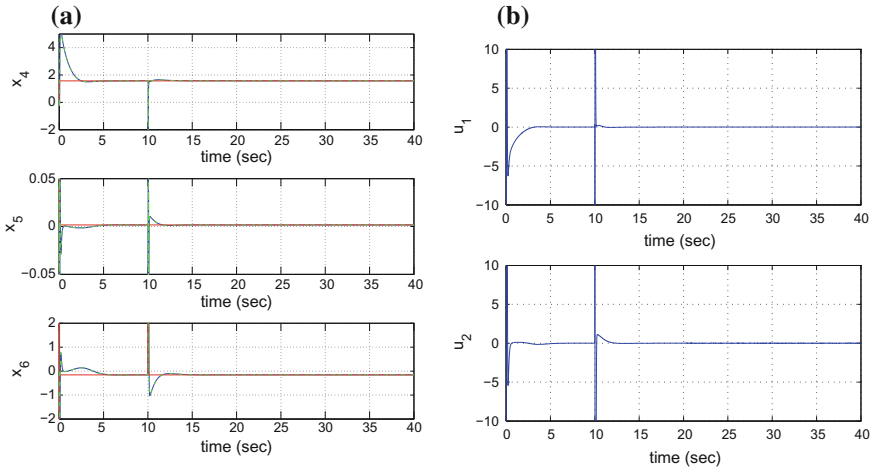

Fig. 10.45 Reference path 2: **a** Convergence of the state variables of the vessel $x_4 = u$, $x_5 = v$ and $x_6 = r$ (blue line) to the associated reference values (red line) **b** Control inputs $u_1 = \tau_u$ and $u_2 = \tau_r$ exerted on vessel

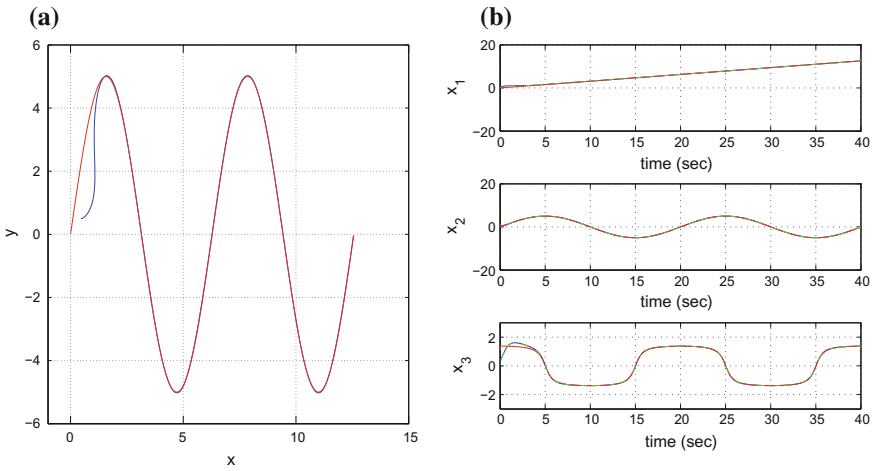

Fig. 10.46 Reference path 3: **a** Tracking of the reference trajectory (red line) in the $x - y$ plane by the unmanned surface vessel (blue line), **b** Convergence of the state variables of the vessel $x_1 = x$, $x_2 = y$ and $x_3 = \psi$ (blue line) to the associated reference values (red line)

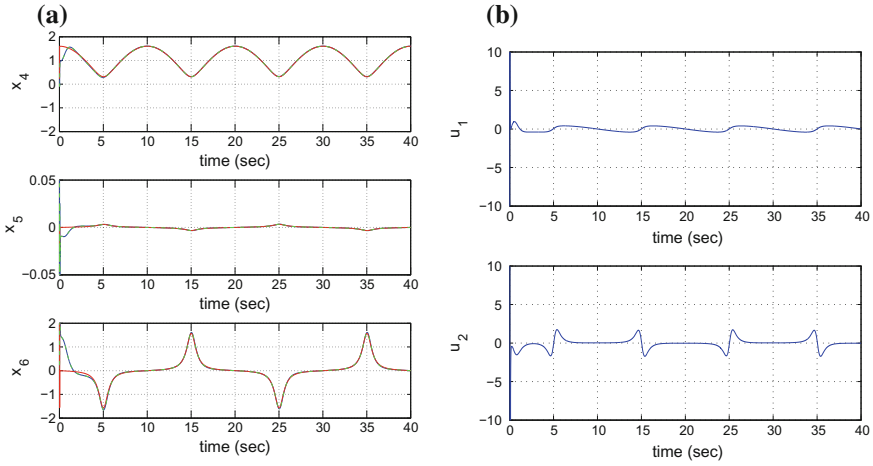

Fig. 10.47 Reference path 3: **a** Convergence of the state variables of the vessel $x_4 = u$, $x_5 = v$ and $x_6 = r$ (blue line) to the associated reference values (red line) **b** Control inputs $u_1 = \tau_u$ and $u_2 = \tau_r$ exerted on vessel

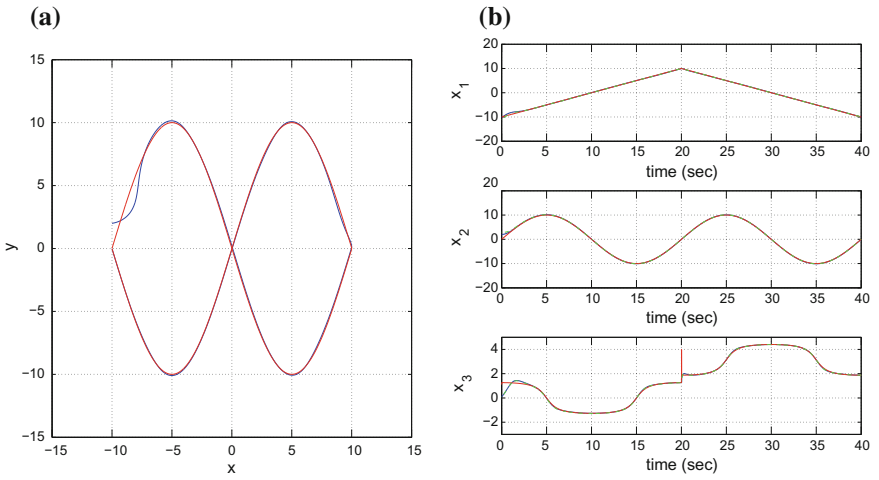

Fig. 10.48 Reference path 4: **a** Tracking of the reference trajectory (red line) in the $x - y$ plane by the unmanned surface vessel (blue line), **b** Convergence of the state variables of the vessel $x_1 = x$, $x_2 = y$ and $x_3 = \psi$ (blue line) to the associated reference values (red line)

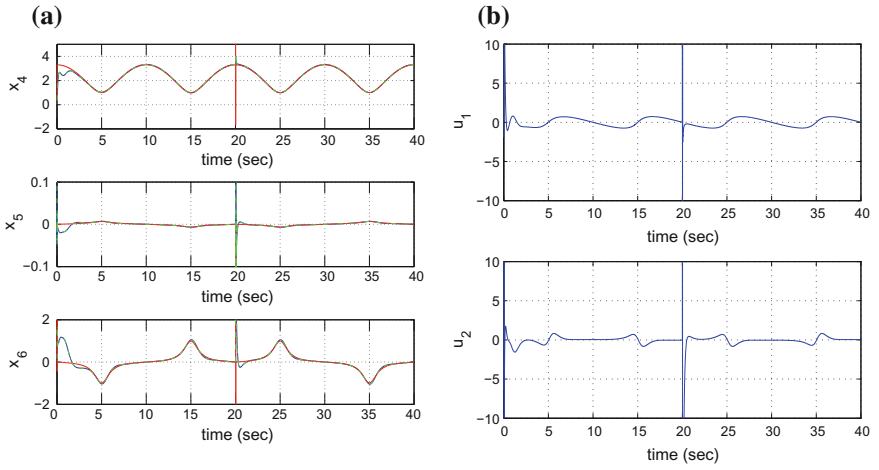

Fig. 10.49 Reference path 4: **a** Convergence of the state variables of the vessel $x_4 = u$, $x_5 = v$ and $x_6 = r$ (blue line) to the associated reference values (red line) **b** Control inputs $u_1 = \tau_u$ and $u_2 = \tau_r$ exerted on vessel

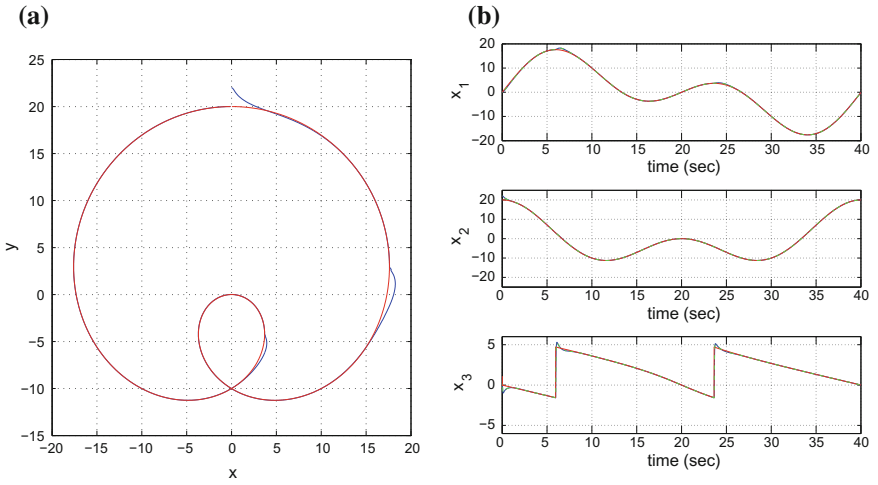

Fig. 10.50 Reference path 5: **a** Tracking of the reference trajectory (red line) in the $x - y$ plane by the unmanned surface vessel (blue line), **b** Convergence of the state variables of the vessel $x_1 = x$, $x_2 = y$ and $x_3 = \psi$ (blue line) to the associated reference values (red line)

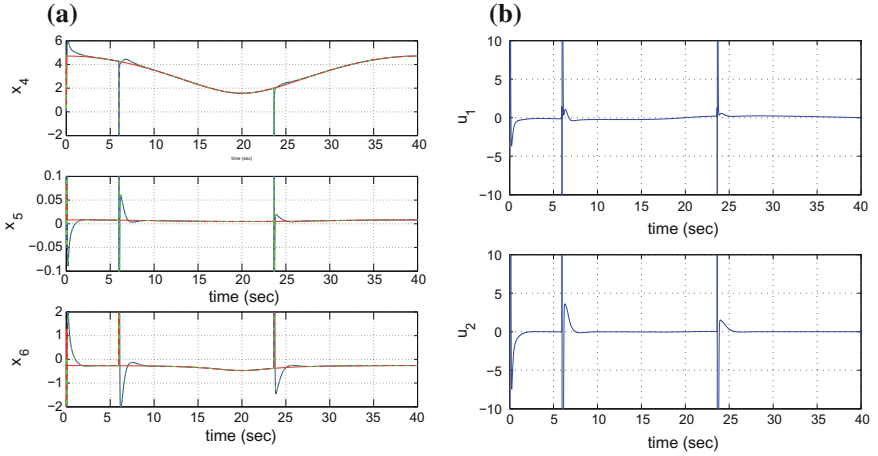

Fig. 10.51 Reference path 5: **a** Convergence of the state variables of the vessel $x_4 = u$, $x_5 = v$ and $x_6 = r$ (blue line) to the associated reference values (red line) **b** Control inputs $u_1 = \tau_u$ and $u_2 = \tau_r$ exerted on vessel

Table 10.3 RMSE of the USV's state variables

Parameter	x	y	ψ	u	v	r
$RMSE_1$	$0.677 \cdot 10^{-4}$	$0.499 \cdot 10^{-4}$	$0.355 \cdot 10^{-4}$	$0.001 \cdot 10^{-4}$	$0.001 \cdot 10^{-4}$	$0.002 \cdot 10^{-4}$
$RMSE_2$	$2.412 \cdot 10^{-4}$	$4.845 \cdot 10^{-4}$	$0.418 \cdot 10^{-4}$	$0.856 \cdot 10^{-4}$	$0.001 \cdot 10^{-4}$	$0.001 \cdot 10^{-4}$
$RMSE_3$	$4.556 \cdot 10^{-4}$	$5.851 \cdot 10^{-4}$	$5.945 \cdot 10^{-4}$	$2.493 \cdot 10^{-4}$	$0.038 \cdot 10^{-4}$	$9.418 \cdot 10^{-4}$
$RMSE_4$	$3.993 \cdot 10^{-4}$	$8.129 \cdot 10^{-4}$	$3.710 \cdot 10^{-4}$	$3.450 \cdot 10^{-4}$	$0.047 \cdot 10^{-4}$	$4.528 \cdot 10^{-4}$
$RMSE_5$	$2.554 \cdot 10^{-4}$	$1.549 \cdot 10^{-4}$	$0.679 \cdot 10^{-4}$	$1.280 \cdot 10^{-4}$	$0.003 \cdot 10^{-4}$	$0.020 \cdot 10^{-4}$

robustness is achieved for the smallest value of ρ for which the algebraic Riccati equation given in Eq. (10.145) can be solved.

As previously noted, the joint kinematic-dynamic model of the surface vessel comes primarily from [517, 518]. The considered model is related to a specific type of surface vessels that is hovercrafts. The model of hovercrafts, is obtained from the generic ship model under specific assumptions about the vessel's parameters and this issue has been analyzed in Ref. [416]. However, the section's results can be applied to more types of surface vessels.

Comparing the H-infinity control approach for the underactuated model of the hovercraft against other control methods such as PID control the following conclusion can be reached: PID control is of questionable performance and unsuitable for the problem of autonomous navigation of unmanned surface vessels. PID controllers are usually tuned round local operating points and assuming a linear dynamics for the controlled system. In the case of the unmanned surface vessel the condition about linearity of the vessel's kinematic-dynamic model does not hold. Moreover, in the problem of autonomous navigation the reference setpoints change continuously, therefore one cannot assume that the operating points of the control loop remain unchanged. Consequently, one cannot select gains of the PID controller that assure the reliable functioning of the vessel's control loop, in terms of global asymptotic stability. Additionally, the PID control is vulnerable to external perturbations. In conclusion PID control is not computationally simpler than the proposed control nonlinear H-infinity control method. Besides it cannot assure the stability of the control loop.

10.5 Validation of Distributed Kalman Filtering for Ship Tracking Applications

10.5.1 Outline

As it has been already pointed out, filtering and control methods of improved accuracy are necessary for developing safe autonomous surface or underwater vessels and reliable maritime transportation systems [222, 271, 555, 625, 631]. By estimating the motion characteristics of a ship through filtering procedures it becomes possible

to implement feedback control for precise trajectory tracking and for avoidance of collisions with nearby vessels [148, 227, 450, 457, 462]. Distributed Kalman filtering is often used for the localization and motion characteristics estimation of ships [189, 234, 309, 329]. Therefore, it is important to develop statistical validation methods for confirming the accuracy of such filtering schemes and for initiating parameters update and corrections in the associated algorithms [30, 33, 58, 107, 170, 221, 430, 652]. To this end, in this section a statistical method is applied for validating the precision of Fuzzy Kalman Filtering, and aiming at a more efficient tracking of the motion of marine vessels.

Fuzzy Kalman Filtering (FKF) is a distributed filtering approach in which a global state estimate is obtained after making use of fuzzy weighting of local estimates provided by distributed Kalman Filters [189, 234, 309, 329]. In the case of autonomous vessels and maritime traffic monitoring, this means that the motion plane of the vessels on the sea surface is covered by spatially distributed Kalman Filters, and that the aggregate estimate of a ship's motion characteristics is computed through a fuzzy averaging procedure. The estimate provided by each local Kalman Filter is attributed a weight which denotes the proximity of a vessel to the center of the area covered by this specific Kalman Filter. To compute an estimate of the ship's state vector each local Kalman Filter makes use of a model of the ship's dynamics. However, the parameters of certain local models may differ from the nominal values of the parameters constituting the real ship dynamics. In such a case inaccurate state estimates are produced, first at a local level, while at a second stage this erroneous state estimates are reflected in the aggregate outcome of the distributed filtering procedure.

The purpose of statistical validation of the Fuzzy Kalman Filter is to detect if the filter provides reliable and precise state estimates about the ship's motion. Moreover, the statistical validation test should detect the local filters which make use of the inaccurate dynamic model of the vessel, thus enabling the update of these models and the removal of errors from the filtering procedure. The Fuzzy Kalman Filter validation method developed in this section is based on the *local statistical approach* to fault diagnosis. To apply the method, it is first shown that local Kalman Filters are equivalent to ARMAX models and next that the Fuzzy Kalman Filter is equivalent to a set of fuzzy weighted ARMAX models [76, 190, 211, 632]. A key element of the proposed validation approach is the Generalized Likelihood Ratio, computed through the processing of the residuals of the estimation procedure (that is the differences between the real and the estimated outputs of the ship's dynamics) [34, 42, 463, 464, 633]. This finally results in the χ^2 change detection test and enables to define an optimal threshold beyond which the distributed filtering procedure and the indicated local dynamical models of the vessels are considered to be unreliable [32, 35, 624]. The efficiency of the proposed validation scheme for the Fuzzy Kalman Filter is confirmed through simulation experiments, making use of a 6th order model of a surface vessel dynamics. It is shown that the statistical validation test is capable of detecting the faulty local filter, even under small errors in the local model's parameters which do not exceed 1% of the associated nominal values.

10.5.2 Dynamic Model of Surface Vessels

10.5.2.1 Estimation of the Ship's State Vector

The sensor fusion-based estimation procedure for obtaining the ship's state vector is affected by uncertainties characterizing the ship's dynamic model. Such uncertainties can be due to parametric variations in the model of Eqs. (10.13) and (10.14) or due to external disturbances, e.g. additive input disturbances as shown in Eqs. (10.2) and (10.10).

In the case of a surface vessel, defining the generalized state vector $x = [\eta, \dot{\eta}]^T$ and considering invariance of the disturbance d for specific time periods, one obtains the generalized ship state-space model

$$\ddot{\eta} + J(\eta)^{-1}[C(\eta, \dot{\eta}) + F(\eta)]\dot{\eta} - J^{-1}(\eta)d = J^{-1}(\eta)\tau \tag{10.160}$$

Setting $x_1 = \eta$, $x_2 = d$, $x_3 = \dot{\eta}$, $x_4 = \dot{d}$ and taking into account the existence of process and measurement noise one obtains a ship's model of the form

$$\begin{aligned} \dot{x} &= Ax + Bu + w \\ z &= \gamma(x) + v \end{aligned} \tag{10.161}$$

where matrices A and B are given by

$$\begin{aligned} A &= \begin{pmatrix} 0_{3\times 3} & I_{3\times 3} \\ 0_{3\times 3} & -J^{-1}(x)[C(x, \dot{x}) + F(x)] \end{pmatrix} \\ B &= \begin{pmatrix} 0_{3\times 3} & J^{-1}(x) \end{pmatrix}^T \end{aligned} \tag{10.162}$$

The extended state vector is $x = [x_1, x_2, x_3, x_4]^T$ with $x_i \in R^{3\times 1}$, $i = 1, 2, 3, 4$. The control input is $\tau \in R^{3\times 1}$. The measurement vector of the ship's model is given by $z = [x, y, \psi]^T$, where x, y are measurements of the ship's cartesian coordinates, and ψ is a measurement of the ship's orientation. The vectors of process and measurement noises are denoted as w and v, respectively. Using the above state-space representation, state vector x can be estimated by processing a sequence of output measurements y with the use of a state observer or Kalman Filtering [222, 555].

10.5.3 Fuzzy Kalman Filtering for Ship Motion Estimation

Fuzzy Kalman Filtering is a distributed filtering approach is which the aggregate state estimate is provided by fuzzy weighting of the estimates generated by local and

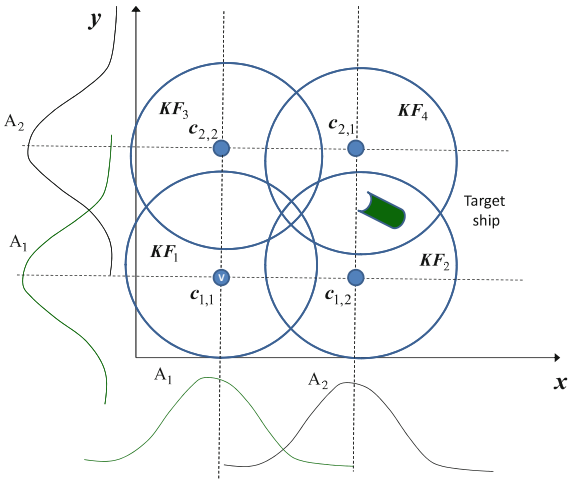

Fig. 10.52 Fuzzy Kalman Filtering for ship tracking applications

spatially distributed Kalman Filters [189, 234, 309, 329]. Here, the sea surface is partitioned into local areas, each one monitored by a different Kalman Filter. The area that each Kalman Filter covers is described by fuzzy rules R^l of the form:

$$R^l \text{ IF } x \text{ is } A_i \text{ AND } y \text{ is } A_j \text{ THEN } KF^l \text{ estimates } \hat{x}^l \tag{10.163}$$

where $i = 1, 2, \ldots, n$, $j = 1, 2, \ldots, n$ and $l = 1, 2, \ldots n \times m$.

Next, it is assumed that the partitioning of the sea surface is as depicted in Fig. 10.52. Then the associated Fuzzy Kalman Filter is described by the following fuzzy rules:

$$\begin{gathered}
\text{IF } x \text{ is } A_1 \text{ AND } y \text{ is } A_1 \text{ THEN } KF_1 \\
\text{IF } x \text{ is } A_1 \text{ AND } y \text{ is } A_2 \text{ THEN } KF_2 \\
\text{IF } x \text{ is } A_2 \text{ AND } y \text{ is } A_1 \text{ THEN } KF_3 \\
\text{IF } x \text{ is } A_2 \text{ AND } y \text{ is } A_2 \text{ THEN } KF_4 \\
\ldots \ldots \ldots \ldots \ldots \ldots \ldots \ldots \\
\text{IF } x \text{ is } A_n \text{ AND } y \text{ is } A_n - 1 \text{ THEN } KF_{n\times n-1} \\
\text{IF } x \text{ is } A_n \text{ AND } y \text{ is } A_n \text{ THEN } KF_{n\times n}
\end{gathered} \tag{10.164}$$

Next, the number of the fuzzy rules is denoted as $M = n \times n$. The aggregate estimate that is provided by the fuzzy Kalman Filter is of the form

$$\hat{x} = \sum_{l=1}^{M} \frac{\prod_{i=1}^{N} A_i^l}{\sum_{j=1}^{M} \prod_{i=1}^{N} A_i^j} \hat{x}_l \Rightarrow \hat{x} = \sum_{l=1}^{M} w_l \hat{x}_l \tag{10.165}$$

According to the above the ship's model was written in the linear state-space form

$$\begin{aligned} \dot{x} &= Ax + Bu + w \\ y &= Cx + v \end{aligned} \tag{10.166}$$

while after discretization, the discrete-time description of the linearized ship dynamics, in discrete-time, is obtained

$$\begin{aligned} x(k+1) &= A_d x(k) + B_d u(k) + w(k) \\ y(k) &= C_d x(x) + v(k) \end{aligned} \tag{10.167}$$

The ith Kalman Filter, which is associated with the lth fuzzy rule is given by

$$\hat{x}^l(k+1) = A_d^l \hat{x}(k) + B_d^l u(k) + K_f^l C_d^l(x^l(k)) - \hat{x}^l(k) \tag{10.168}$$

The difference $\varepsilon(k) = C_d^l(x^l(k)) - \hat{x}^l(k)$ between the real and the estimated output of the vessel's dynamic model, is the residual and follows a zero-mean Gaussian distribution. By applying the z transformation the equivalent description of the Kalman Filter in the z-frequency domain can be obtained, which has a MIMO transfer function form

$$\begin{pmatrix} Y_1(z) \\ Y_2(z) \\ Y_3(z) \end{pmatrix} = \begin{pmatrix} H_{11}^A & H_{12}^A & H_{13}^A \\ H_{21}^A & H_{22}^A & H_{23}^A \\ H_{31}^A & H_{32}^A & H_{33}^A \end{pmatrix} \begin{pmatrix} U_1(z) \\ U_2(z) \\ U_3(z) \end{pmatrix} + \begin{pmatrix} H_{11}^B & H_{12}^B & H_{13}^B \\ H_{21}^B & H_{22}^B & H_{23}^B \\ H_{31}^B & H_{32}^B & H_{33}^B \end{pmatrix} \begin{pmatrix} E_1(z) \\ E_2(z) \\ E_3(z) \end{pmatrix} \tag{10.169}$$

Next, examining for instance the subsystem

$$\begin{aligned} Y_1(z) H_{11}^A U_1(z) + H_{12}^A U_2(z) + H_{13}^A U_3(z) + \\ + H_{11}^B E_1(z) + H_{12}^B E_2(z) + H_{13}^B E_3(z) \end{aligned} \tag{10.170}$$

where each one of the transfer functions H_{1j} $j = 1, 2, 3$ included in the above description has in its denominator the system's characteristic polynomial given by the determinant $|zI - A_d|$. Taking into account that this characteristic polynomial is of 6th order one gets the equivalent ARMAX description

$$\begin{aligned} y_1(k) = \textstyle\sum_{i=1}^{6} a_i y(k-i) + \sum_{j1=1}^{5} b_{j1} u_1(k-j1) + \\ + \textstyle\sum_{j2=1}^{5} c_{j2} u_2(k-j2) + \sum_{j3=1}^{5} c_{j3} u_3(k-j3) + \\ + \textstyle\sum_{m1=1}^{5} p_{m1} \varepsilon_1(k-m1) + \sum_{m2=1}^{5} q_{m2} \varepsilon_2(k-m2) + \\ + \textstyle\sum_{m3=1}^{5} r_{m3} \varepsilon_3(k-m3) \end{aligned} \tag{10.171}$$

where coefficients a_i $i = 1, 2, 3$ are obtained from the system's characteristic polynomial $det|zI - A|$ in descending order. Next, the aforementioned characteristic polynomial is computed. It holds that

$$A = \begin{pmatrix} 0_{3\times 3} & I_{3\times 3} \\ 0_{3\times 3} & -J^{-1}x)[C(x,\dot{x}) + F(x)] \end{pmatrix} \tag{10.172}$$

Furthermore, using the definition of matrices J, C and F given in Eqs. (10.15), (10.16) and (10.17) respectively, and considering that the yaw angle of the ship is 0, that is $\psi = 0$ and $\dot{\psi} = 0$ one obtains $C = 0_{3\times 3}$ while

$$J = \begin{pmatrix} m_{11} & 0 & 0 \\ 0 & m_{22} & 0 \\ 0 & m_{23} & 0 \end{pmatrix} \; F = \begin{pmatrix} d_{11} & 0 & 0 \\ 0 & d_{22} & d_{23} \\ 0 & d_{32} & d_{23} \end{pmatrix} \tag{10.173}$$

To compute the system's description in MIMO transfer function form, one has to calculate first the inverse matrix $(zI - A_d)^{-1}$. It holds that

$$Q = (zI - A_d)^{-1} = \frac{1}{|zI - A_d|} \cdot \begin{pmatrix} Q_{11} & -Q_{21} & Q_{31} & Q_{41} & -Q_{51} & Q_{61} \\ -Q_{12} & Q_{22} & -Q_{32} & -Q_{42} & Q_{52} & -Q_{62} \\ Q_{13} & -Q_{23} & Q_{33} & Q_{43} & -Q_{53} & Q_{63} \\ -Q_{14} & Q_{24} & -Q_{34} & -Q_{44} & Q_{54} & -Q_{64} \\ Q_{15} & -Q_{25} & Q_{35} & Q_{45} & -Q_{55} & Q_{65} \\ -Q_{16} & Q_{26} & -Q_{36} & Q_{46} & -Q_{56} & Q_{66} \end{pmatrix} \tag{10.174}$$

where the elements of the adjoint matrix are

$Q_{11} = (z-1)^2(z-1-T_s\frac{d_{11}}{m_{11}})[(z-1-T_sv_{55})(z-1-T_sv_{66}) - (-1-T_sv_{65})(-1-T_sv_{56})]$, $Q_{12} = 0$, $Q_{13} = 0$, $Q_{14} = 0$, $Q_{15} = 0$ and $Q_{16} = 0$.

$Q_{21} = 0$, $Q_{22} = (z-1)^2(z-1-T_s\frac{d_{11}}{m_{11}})[(z-1-T_sv_{65})(z-1-T_sv_{66}) - (-1-T_sv_{65})(-1-T_sv_{56})]$, $Q_{23} = 0$, $Q_{24} = 0$, $Q_{25} = 0$, and $Q_{26} = 0$.

$Q_{31} = 0$, $Q_{32} = 0$, $Q_{33} = (z-1)^2(z-1-T_s\frac{d_{11}}{m_{11}})[(z-1-T_sv_{55})(z-1-T_sv_{66}) - (-1-T_sv_{65})(-1-T_sv_{56})]$, $Q_{34} = 0$, Q_{35} and $Q_{36} = 0$.

$Q_{41} = (z-1)^2(-T_s)[(z-1-T_sv_{65})(z-1-T_sv_{66}) - (-1-T_sv_{65})(-1-T_sv_{56})]$, $Q_{42} = 0$, $Q_{43} = 0$, $Q_{44} = (z-1)^2[(z-1-T_sv_{55})(z-1-T_sv_{66}) - (-1-T_sv_{65})(-1-T_sv_{56})]$, $Q_{45} = 0$, and $Q_{46} = 0$.

$Q_{51} = 0$, $Q_{52} = -T_s(z-1)^2(z-1-T_s\frac{d_{11}}{m_{11}})(z-1-T_sv_{66})$, $Q_{53} = T_s(z-1)^2(z-1-T_s\frac{d_{11}}{m_{11}})(-1-T_sv_{65})$, $Q_{54} = (z-1)^3(z-1-T_s\frac{d_{11}}{m_{11}})(z-1-T_sv_{66})$, $Q_{55} = (z-1)^3(z-1-T_s\frac{d_{11}}{m_{11}})(z-1-T_sv_{66})$, and $Q_{56} = (z-1)^3(z-1-T_s\frac{d_{11}}{m_{11}})(-1-T_sv_{65})$

$Q_{61} = 0$, $Q_{62} = (z-1^2)(z-1-T_s\frac{d_{11}}{m_{11}})(-T_s)(-1-T_sv_{56})$, $Q_{63} = -(z-1)^2(z-1-T_s\frac{d_{11}}{m_{11}})T_s(z-1-T_sv_{55})$, $Q_{64} - 0$, $Q_{65} = (z-1)^3(z-1-T_s\frac{d_{11}}{m_{11}})(-1-T_sv_{56})$, $Q_{66} = (z-1)^3(z-1-T_s\frac{d_{11}}{m_{11}})(z-1-T_sv_{55})$.

The computation of the associated characteristic polynomial gives:

$$
\begin{aligned}
&det(zI - A) = z^6 + [(-2 - T_s v_{66}) - T_s v_{55} + (-4 + T_s \frac{d_{11}}{m_{11}})]z^5 + \\
&[(T_s v_{66} + T_s v_{65} + T_s^2 v_{55} v_{66} - T_s v_{56} - T_s v_{65} - T_s^2 v_{65} v_{56}) + \\
&+ (-4 + T_s \frac{d_{11}}{m_{11}})(-2 - T_s v_{66} - T_s v_{55}) + (6 + 3T_s \frac{d_{11}}{m_{11}})]z^4 + \\
&[(-4 + T_s \frac{d_{11}}{m_{11}})(T_s v_{66} + T_s v_{65} + T_s^2 v_{55} v_{66} - T_s v_{56} - T_s v_{65} - T_s^2 v_{65} v_{56}) + \\
&+ (6 + 3T_s \frac{d_{11}}{m_{11}})(-2 - T_s v_{66} - T_s v_{55}) + (-4 - 3T_s \frac{d_{11}}{m_{11}})]z^3 + \\
&[(6 + 3T_s \frac{d_{11}}{m_{11}})(T_s v_{66} + T_s v_{65} + T_s^2 v_{55} v_{66} - T_s v_{56} - T_s v_{65} - T_s^2 v_{65} v_{56}) + \\
&+ (-4 - 3T_s \frac{d_{11}}{m_{11}})(-2 - T_s v_{66} - T_s v_{55}) + (1 + T_s \frac{d_{11}}{m_{11}})]z^2 + \\
&[(-4 - 3T_s \frac{d_{11}}{m_{11}})(T_s v_{66} + T_s v_{65} + T_s^2 v_{55} v_{66} - T_s v_{56} - T_s v_{65} - T_s^2 v_{65} v_{56}) + \\
&+ (1 + T_s \frac{d_{11}}{m_{11}})(-2 - T_s v_{66} - T_s v_{55})]z + \\
&[(1 + T_s \frac{d_{11}}{m_{11}})(T_s v_{66} + T_s v_{65} + T_s^2 v_{55} v_{66} - T_s v_{56} - T_s v_{65} - T_s^2 v_{65} v_{56})]
\end{aligned}
\tag{10.175}
$$

where T_s is the sampling period and

$$
\begin{aligned}
v_{55} &= \frac{d_{22} m_{11} m_{33} - d_{33} m_{11} m_{23}}{m_{11}(m_{22} m_{33} - m_{23}^2)} \quad v_{56} = \frac{d_{23} m_{11} m_{33} + d_{33} m_{11} m_{23}}{m_{11}(m_{22} m_{33} - m_{23}^2)} \\
v_{65} &= \frac{d_{22} m_{11} m_{23} + d_{33} m_{11} m_{22}}{m_{11}(m_{22} m_{33} - m_{23}^2)} \quad v_{66} = \frac{-d_{23} m_{11} m_{23} + d_{33} m_{11} m_{22}}{m_{11}(m_{22} m_{33} - m_{23}^2)}
\end{aligned}
\tag{10.176}
$$

Next, to avoid extended computations in the section's example, the ARMAX model of Eq. (10.171) is simplified into the form

$$
\begin{aligned}
y^l(k+1) = a_1^l y^l(k) + a_2^l y^l(k-1) + a_3^l y^l(k-2) + \\
+ b_1^l u_1^l(k) + b_2^l u_2^l(k) + b_3^l u_3^l(k) + \\
+ c_1^l \varepsilon_1^l(k)
\end{aligned}
\tag{10.177}
$$

where $l = 1, 2, 3, 4$ is the lth local model and

$$a_1^l = -[(-2 - T_s v_{66}) - T_s v_{55} + (-4 + T_s \tfrac{d_{11}}{m_{11}})]$$

$$\begin{aligned} a_2^l = -[&(T_s v_{66} + T_s v_{65} + T_s^2 v_{55} v_{66} - T_s v_{56} - T_s v_{65} - T_s^2 v_{65} v_{56}) + \\ &+(-4 + T_s \tfrac{d_{11}}{m_{11}})(-2 - T_s v_{66} - T_s v_{55}) + (6 + 3T_s \tfrac{d_{11}}{m_{11}})] \end{aligned}$$

$$\begin{aligned} a_3^l = -[&(-4 + T_s \tfrac{d_{11}}{m_{11}})(T_s v_{66} + T_s v_{65} + T_s^2 v_{55} v_{66} - T_s v_{56} - T_s v_{65} - T_s^2 v_{65} v_{56}) + \\ &+(6 + 3T_s \tfrac{d_{11}}{m_{11}})(-2 - T_s v_{66} - T_s v_{55}) + (-4 - 3T_s \tfrac{d_{11}}{m_{11}})] \end{aligned} \tag{10.178}$$

Moreover, taking into account that the transfer function matrices given in Eq. (10.169), are $H^A(z) = C_d(zI - A_d)^{-1}B$ and $H^B(z) = C_d(zI - A_d)^{-1}K_f$ (where K_f is the gain of the Kalman Filter), and that the measurement matrix for the ship's model is $C = [I_{3\times 3}\ 0_{3\times 3}]$, it holds

$$\begin{aligned} H^A(z) = &\frac{1}{det(zI - A_d)} \begin{pmatrix} Q_{11} & -Q_{21} & Q_{31} & -Q_{41} & Q_{51} & -Q_{61} \\ -Q_{12} & Q_{22} & -Q_{32} & Q_{42} & -Q_{52} & Q_{62} \\ Q_{13} & -Q_{23} & Q_{33} & -Q_{43} & Q_{53} & -Q_{63} \end{pmatrix} \cdot \\ &\cdot \begin{pmatrix} 0 & 0 & 0 \\ 0 & 0 & 0 \\ 0 & 0 & 0 \\ -\frac{T_s}{m_{11}} & 0 & 0 \\ 0 & -\dfrac{T_s m_{33}}{m_{22}m_{33} - m_{23}^2} & \dfrac{T_s m_{23}}{m_{22}m_{33} - m_{23}^2} \\ 0 & \dfrac{T_s m_{23}}{m_{22}m_{33} - m_{23}^2} & -\dfrac{T_s m_{22}}{m_{22}m_{33} - m_{23}^2} \end{pmatrix} \end{aligned} \tag{10.179}$$

$$H^B(z) = \frac{1}{det(zI - A_d)} \begin{pmatrix} Q_{11} & -Q_{21} & Q_{31} & -Q_{41} & Q_{51} & -Q_{61} \\ -Q_{12} & Q_{22} & -Q_{32} & Q_{42} & -Q_{52} & Q_{62} \\ Q_{13} & -Q_{23} & Q_{33} & -Q_{43} & Q_{53} & -Q_{63} \end{pmatrix} \begin{pmatrix} K_{f_{11}} & K_{f_{12}} & K_{f_{13}} \\ K_{f_{21}} & K_{f_{22}} & K_{f_{23}} \\ K_{f_{31}} & K_{f_{32}} & K_{f_{33}} \\ K_{f_{41}} & K_{f_{42}} & K_{f_{43}} \\ K_{f_{51}} & K_{f_{52}} & K_{f_{53}} \\ K_{f_{61}} & K_{f_{62}} & K_{f_{63}} \end{pmatrix} \tag{10.180}$$

Then for the rest of the parameters of the local ARMAX model of the Kalman Filter one has that:

b_1 is the coefficient multiplying the highest order term of the polynomial $[T_s Q_{41}]/m_{11}$, b_2 is the coefficient multiplying the highest order term of the polynomial

$[-T_s m_{33} Q_{51} - T_s m_{23} Q_{61}]/(m_{22} m_{33} - m_{23}^2)$, b_3 is the coefficient multiplying the highest order term of the polynomial $[T_s m_{23} Q_{51} + T_s m_{22} Q_{61}]/(m_{22} m_{33} - m_{23}^2)$, and c_1 is the coefficient multiplying the highest order term of the polynomial $K_{f_{11}} Q_{11} - K_{f_{21}} Q_{21} + K_{f_{31}} Q_{31} - K_{f_{41}} Q_{41} + K_{f_{51}} Q_{51} - K_{f_{61}} Q_{61}$.

Using the above and Fig. 10.52 the fuzzy Kalman Filter for the ship tracking problem is described by the following fuzzy rule base:

$$
\begin{aligned}
&\text{IF } x \text{ is } A_1 \text{AND } y \text{ is } A_1 \text{ THEN}\\
&\hat{y}^1(k+1) = a_1^1 \hat{y}^1(k) + a_2^1 \hat{y}^1(k-1) + a_3^1 \hat{y}^1(k-2) +\\
&+ b_1^1 u_1^1(k) + b_2^1 u_2^1(k) + b_3^1 u_3^1(k) + c_1^1 \varepsilon_1^1(k)\\
&\text{IF } x \text{ is } A_1 \text{AND } y \text{ is } A_2 \text{ THEN}\\
&\hat{y}^2(k+1) = a_1^1 \hat{y}^2(k) + a_2^1 \hat{y}^2(k-1) + a_3^2 \hat{y}^2(k-2) +\\
&+ b_1^1 u_1^2(k) + b_2^2 u_2^2(k) + b_3^2 u_3^2(k) + c_1^2 \varepsilon_1^2(k)\\
&\text{IF } x \text{ is } A_2 \text{AND } y \text{ is } A_1 \text{ THEN}\\
&\hat{y}^3(k+1) = a_1^3 \hat{y}^1(k) + a_2^3 \hat{y}^3(k-1) + a_3^3 \hat{y}^3(k-2) +\\
&+ b_1^3 u_1^3(k) + b_2^3 u_2^3(k) + b_3^3 u_3^3(k) + c_1^3 \varepsilon_1^3(k)\\
&\text{IF } x \text{ is } A_2 \text{AND } y \text{ is } A_2 \text{ THEN}\\
&\hat{y}^4(k+1) = a_1^4 \hat{y}^4(k) + a_2^4 \hat{y}^4(k-1) + a_3^4 \hat{y}^4(k-2) +\\
&+ b_1^4 u_1^4(k) + b_2^4 u_2^4(k) + b_3^4 u_3^4(k) + c_1^4 \varepsilon_1^4(k)
\end{aligned}
\tag{10.181}
$$

For a properly functioning fuzzy Kalman Filter it should hold $a_j^1 = a_j^2 = a_j^3 = a_j^4$ $j = 1, 2, 3$ and similarly $b_j^1 = b_j^2 = b_j^3 = b_j^4$ $j = 1, 2, 3$, and finally $c_j^1 = c_j^2 = c_j^3 = c_j^4$ $j = 1$. If the above condition does not hold then for at least one local Kalman Filter the parameters of the ship model used in the estimation procedure are incorrect. The statistical change detection test which is proposed in this section is capable of detecting the inconsistent local Kalman Filter.

10.5.4 Consistency of the Kalman Filter

To obtain accurate estimates with the Kalman Filter, previously a tuning process is required. A question that arises is about which state estimates can be considered as reliable. There is need for systematic methods showing when the Kalman Filter is not performing optimally and when its retuning, either in terms of the used dynamic or kinematic model or in terms of the covariance matrices, should be performed. Several methods can be applied to test the consistency of the Kalman Filter, from the desired characteristics of the measurement residuals. These include the normalized error square (NES) test, the autocorrelation test, and the normalized mean error (NME) test and have been analyzed in [30, 107].

(i) It is assumed that a discrete error process e_k with dimension $m \times 1$ is a zero-mean Gaussian white-noise process with covariance given by E_k. This process can be the Kalman Filter's residual associated to the state estimation error or the residual associated to the measurement estimation error. Then, the following *normalized error square* (NES) is defined

$$\varepsilon_k = e_k^T E_k^{-1} e_k \tag{10.182}$$

The normalized error square follows a χ^2 distribution. An appropriate test for the normalized error sum is to numerically show that the following condition is met within a level of confidence (according to the properties of the χ^2 distribution)

$$E\{\varepsilon_k\} = m \tag{10.183}$$

This can be achieved using statistical hypothesis testing, which are associated with confidence intervals. A 95% confidence interval is frequently applied, which is specified using $100(1 - a)$ with $a = 0.05$. Actually, a two-sided probability region is considered cutting-off two end tails of 2.5% each. For M runs of Monte-Carlo experiments the normalized error square that is obtained is given by

$$\bar{\varepsilon}_k = \frac{1}{M}\sum_{i=1}^{M}\varepsilon_k(i) = \frac{1}{M}\sum_{i=1}^{M} e_k^T(i) E_k^{-1}(i) e_k(i) \tag{10.184}$$

where ε_i stands for the ith run at time t_k. Then $M\bar{\varepsilon}_k$ will follow a χ^2 density with Mm degrees of freedom. This condition can be checked using a χ^2 test. The hypothesis holds true if the following condition is satisfied

$$\bar{\varepsilon}_k \in [\zeta_1, \zeta_2] \tag{10.185}$$

where ζ_1 and ζ_2 are derived from the tail probabilities of the χ^2 density. For example, for $m = 2$ and $M = 100$ one has $\chi^2_{Mm}(0.025) = 162$ and $\chi^2_{Mm}(0.975) = 241$. Using that $M = 100$ one obtains $\zeta_1 = \chi^2_{Mm}(0.025)/M = 1.62$ and $\zeta_2 = \chi^2_{Mm}(0.975)/M = 2.41$.

(ii) Another consistency checking method is the *test for whiteness*. This is obtained by using the following sample autocorrelation:

$$\bar{\rho}_{k,j} = \frac{1}{\sqrt{M}}\sum_{i=1}^{M} e_k^T(i)\left[\sum_{i=1}^{M} e_k(i) e_k^T(i) \sum_{i=1}^{M} e_j(i) e_j^T(i)\right]^{-1/2} e_j(i) \tag{10.186}$$

For a sufficiently large value of M, variable $\bar{\rho}_{j,k}$ for $k \neq j$ is zero mean with variance given by $1/M$. Next the application of the central limit theorem provides a normal approximation, and considering a 95% confidence interval one finally obtains

$$\bar{\rho}_{j,k} \in \left[-\frac{1.96}{M}, +\frac{1.96}{M} \right] \tag{10.187}$$

(iii) An additional consistency test is based on the normalized mean error (NME) for the jth element of e_k

$$[\bar{\mu}_k]_j = \frac{1}{M} \sum_{j=1}^{M} \frac{[e_k]_j}{\sqrt{[E_k]_{jj}}}, \quad j = 1, 2, \ldots, M \tag{10.188}$$

Then, since the variance of $[\bar{\mu}_k]_j$ is $\frac{1}{M}$ for a 95% acceptance interval one has

$$[\bar{\mu}_k]_j \in \left[-\frac{1.96}{\sqrt{M}}, +\frac{1.96}{\sqrt{M}} \right] \tag{10.189}$$

The hypothesis holds true, if Eq. (10.189) is satisfied. The NES, NME and autocorrelation consistency tests can be all performed with a single run using N data points. Using a time-averaging approach one obtains a low variability test statistic, which can be executed in real-time. In the latter case the time-average NES is given by

$$\bar{\varepsilon} = \frac{1}{N} \sum_{k=1}^{N} e_k^T E_k^{-1} e_k \tag{10.190}$$

Considering that e_k is a zero mean, white-noise process, then $N\bar{\varepsilon}$ follows a χ^2 density distribution with Nm degrees of freedom. Through the computation of the time-average auto-correlation the whiteness test for e_k is

$$\bar{\rho}_j = \frac{1}{\sqrt{N}} \sum_{k=1}^{N} e_k^T e_{k+j} \left[\sum_{k=1}^{N} e_k^T e_k \sum_{k=1}^{N} e_{k+j}^T e_{k+j} \right]^{\frac{-1}{2}} \tag{10.191}$$

For N sufficiently large, $\bar{\rho}_j$ has zero mean and variance given by $1/N$. With a 95% acceptance interval one has

$$\bar{\rho}_j \in \left[-\frac{1.96}{\sqrt{N}}, +\frac{1.96}{\sqrt{N}} \right] \tag{10.192}$$

The hypothesis is accepted if Eq. (10.192) is satisfied. The aforementioned tests can be applied to the residuals of the Kalman Filter or to the Kalman Filter state errors for checking the consistency of the obtained estimation and for checking the necessary consistency for filter optimality. If the tests are not satisfied then this means that the Kalman Filter is not running optimally, and the filter has to be retuned, or the filter's design has to be reconsidered.

In this section a systematic method, the *local statistical approach to fault diagnosis*, will be introduced for checking the consistency of Fuzzy Kalman Filtering. It will be shown that the method is capable of identifying the elements responsible for the filter's failure, in the dynamic or kinematic model associated with the estimation performed by the local Kalman filters.

10.5.5 Change Detection with the Local Statistical Approach

10.5.5.1 The Global χ^2 Test for Change Detection

The *local statistical approach* to fault diagnosis is a statistical method of fault diagnosis which can be used for consistency checking of the Fuzzy Kalman Filter. Based on a small parametric disturbance assumption, the proposed FDI method aims at transforming complex detection problems concerning a parameterized stochastic process into the problem of monitoring the mean of a Gaussian vector. The local statistical approach consists of two stages: (i) the global test which indicates the existence of a change in some parameters of the fuzzy model, (ii) the diagnostics tests (sensitivity or min–max) which isolate the parameter affected by the change. The method's stages are analyzed first, following closely the method presented in [33, 633].

As shown in Fig. 10.53 the proposed method relies on the definition of the residual e_i described as the difference between the output from the nonlinear ARMAX model of the Fuzzy Kalman Filter obtained with the use of the changed dynamics or kinematics of the system and the output of the nonlinear ARMAX model of the Fuzzy

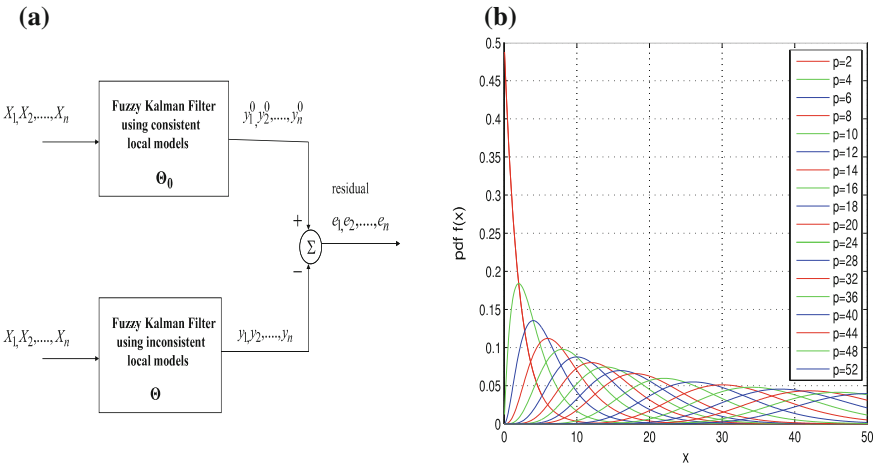

Fig. 10.53 **a** Residual between the Fuzzy Kalman Filter that uses consistent local models and the Fuzzy Kalman Filter that uses inconsistent (distorted) local models, **b** Probability density function of the χ^2 distribution, for various degrees of freedom p

Kalman Filter obtained with the use of the unchanged dynamics or kinematics. The nonlinear ARMAX model is actually a neuro-fuzzy model of the Takagi–Sugeno type that is based on the system's dynamics or kinematics model in an undistorted (fault-free) mode.

The concept of this FDI technique is as follows: there is a nonlinear ARMAX model that represents the unchanged system dynamics. At each time instant the output of the aforementioned reference nonlinear ARMAX model is compared to the output of the nonlinear ARMAX model that represents the changed system dynamics. The difference between these two output measurements is called residual. The statistical processing of a sufficiently large number of residuals through an FDI method provides an index-variable that is compared against a fault threshold' and which can give early indication about deviation of the model used by the Kalman Filter from the real system dynamics or kinematics. Under certain conditions (detectability of changes) the proposed FDI method enables also fault isolation, i.e. to identify the source of fault within the model used by the Fuzzy Kalman Filter. In practical terms this means that the proposed change detection method can find out the ith local Kalman Filter (out of the N local Kalman Filters that constitute the Fuzzy Kalman Filter) which makes use of an inconsistent model of the monitored vessel's dynamics or kinematics.

Considering the representation of the Fuzzy Kalman Filter as a neuro-fuzzy model of the Takagi–Sugeno type, the partial derivative of the residual square is:

$$H(\theta, y_i) = \frac{1}{2}\frac{\partial e_i^2}{\partial \theta} = e_i \frac{\partial \hat{y}_i}{\partial \theta} \tag{10.193}$$

where θ is the vector of model's parameters. The vector H having as elements the above $H(\theta, y_i)$ is called primary residual. Since the nonlinear ARMAX model is a neuro-fuzzy model, the gradient of the output with respect to the consequent parameters $c_{f_i}^l$ is given by

$$\frac{\partial \hat{y}}{\partial c_{f_i}^l} = \frac{x_i \mu_{R^l}(x)}{\sum_{l=1}^{L} \mu_{R^l}(x)} \tag{10.194}$$

The gradient with respect to the center c_i^l has been given in Eq. (10.217) while the gradient with respect to the spread v_i^l has been given in Eq. (10.218).

Next, having calculated the partial derivatives of Eqs. (10.216)–(10.218), the rows of the Jacobian matrix J are found by

$$J(\theta_0, y_k) = \left.\frac{\partial \hat{y}_k(\theta)}{\partial \theta}\right|_{\theta=\theta_0} \tag{10.195}$$

where θ_0 represents the nominal value of the parameters. The problem of change detection with the χ^2 test consists of monitoring a change in the mean of the Gaussian variable which for the one-dimensional parameter vector θ is formulated as

$$X = \frac{1}{\sqrt{N}} \sum_{i=1}^{N} e_k \frac{\partial \hat{y}_k}{\partial \theta} \sim N(\mu, \sigma^2) \tag{10.196}$$

where $\hat{y}_k$ is the output of the neural model generated by the input pattern x_k, e_k is the associated residual and θ is the vector of the model's parameters. It is noted that X is the monitored parameter for the FDI test, which means that when the mean value of X is 0 the system is in the fault-free condition, while when the mean value of X has moved away from 0 the system (Kalman Filter) is in a faulty condition. For a multivariable parameter vector θ should hold $X \sim N(M\delta\theta, S)$, where S denotes the covariance matrix of X. In order to decide if the system (Kalman Filter) is in fault-free operating conditions, given a set of data of N measurements, let θ_* be the value of the parameters vector μ minimizing the RMSE. The notation is introduced only for the convenience of problem formulation, and its actual value does not need to be known. Then the model validation problem amounts to make a decision between the two hypotheses [33, 633]:

$$\begin{aligned} H_0 &: \ \theta_* = \theta_0 \\ H_1 &: \ \theta_* = \theta_0 + \tfrac{1}{\sqrt{N}}\delta\theta \end{aligned} \tag{10.197}$$

where $\delta\theta \neq 0$. It is known from the central limit theorem that for a large data sample, the normalized residual given by Eq. (10.196) asymptotically follows a Gaussian distribution when N$\rightarrow\infty$ [33, 34, 42]. More specifically, the hypothesis that has to be tested is:

$$H_0 : X \sim N(0, S)$$

$$H_1 : X \sim N(M\delta\theta, S)$$

where M is the sensitivity matrix (see Eq. (10.198)), $\delta\theta$ is the change in the parameters' vector and S is the covariance matrix (see Eq. (10.199)). The product $M\delta\theta$ denotes the new center of the monitored Gaussian variable X, after a change on the system's parameter θ. The sensitivity matrix M of $\frac{1}{\sqrt{N}}X$ is defined as the mean value of the partial derivative with respect to θ of the primary residual defined in Eq. (10.215), i.e. $E\{\frac{\partial}{\partial\theta}H(\theta, y_k)\}$ and is approximated by [33, 35, 624, 633]:

$$M(\theta_0) \simeq \frac{\partial}{\partial\theta}\frac{1}{N}\sum\nolimits_{k=1}^{N} H(\theta_0, y_k) \simeq \frac{1}{N} J^T J \tag{10.198}$$

The covariance matrix S is defined as $E\{H(\theta, y_k)H^T(\theta, y_{k+m})\}, m = 0, \pm 1, \ldots$ and is approximated by [32]:

$$\begin{aligned} S \simeq & \sum\nolimits_{k=1}^{N} [H(\theta_0, y_k)H^T(\theta_0, y_k)] + \\ & + \sum\nolimits_{m=1}^{I} \tfrac{1}{N-m} \sum\nolimits_{k=1}^{N-m} [H(\theta_0, y_k)H^T(\theta_0, y_{k+m}) + \\ & + H(\theta_0, y_{k+m})H^T(\theta_0, y_k)] \end{aligned} \tag{10.199}$$

where an acceptable value for I is 3. The decision tool is the likelihood ratio $s(X) = ln\frac{p_{\theta_1}(x)}{p_{\theta_0}(x)}$, where $p_{\theta_1}(X) = e^{[X-\mu(X)]^T S^{-1}[X-\mu(X)]}$ and $p_{\theta_0}(X) = e^{X^T S^{-1} X}$ [633]. The center of the Gaussian distribution of the changed system is denoted as $\mu(X) = M\delta\theta$ where $\delta\theta$ is the change in the parameters vector. The *Generalized Likelihood Ratio* (GLR) is calculated by maximizing the likelihood ratio with respect to $\delta\theta$ [32]. This means that the most likely case of parameter change is taken into account. This gives the global χ^2 test t:

$$t = X^T S^{-1} M (M^T S^{-1} M)^{-1} M^T S^{-1} X \tag{10.200}$$

Since X asymptotically follows a Gaussian distribution, the statistics defined in Eq. (10.200) follows a χ^2 distribution with n degrees of freedom. Mapping the change detection problem to this χ^2 distribution enables the choice of the change threshold. Assume that the desired probability of false alarm is α then the change threshold λ should be chosen from the relation [33, 633]

$$\int_{\lambda}^{\infty} \chi_n^2(s) ds = \alpha, \tag{10.201}$$

where $\chi_n^2(s)$ is the probability density function (p.d.f.) of a variable that follows the χ^2 distribution with n degrees of freedom.

10.5.5.2 Statistical Fault Isolation with the Sensitivity Test

Fault isolation is needed to identify the source of faults in the dynamic or kinematic model of the system used by the Fuzzy Kalman Filter. This means that the fault diagnosis method should also be able to find out (among the N local Kalman Filters that constitute the Fuzzy Kalman Filter) which is the local Kalman Filter that makes use of an inconsistent model. A first approach to change isolation is to focus only on a subset of the parameters while considering that the rest of the parameters unchanged [32]. The parameters vector η can be written as $\eta = [\phi, \psi]^T$, where ϕ contains those parameters to be subject to the isolation test, while ψ contains those parameters to be excluded from the isolation test. M_ϕ contains the columns of the sensitivity matrix M which are associated with the parameters subject to the isolation test. Similarly M_ψ contains the columns of M that are associated with the parameters to be excluded from the sensitivity test.

Assume that among the parameters η, it is only the subset ϕ that is suspected to have undergone a change. Thus η is restricted to $\eta = [\phi, 0]^T$. The associated columns of the sensitivity matrix are given by M_ϕ and the mean of the Gaussian to be monitored is $\mu = M_\phi \phi$, i.e.

$$\mu = MA\phi, \quad A = [0, I]^T \tag{10.202}$$

Matrix A is used to select the parameters that will be subject to the fault isolation test. The rows of A correspond to the total set of parameters while the columns of A correspond only to the parameters selected for the test. Thus the fault diagnosis χ^2 test (sensitivity test) of Eq. (10.200) can be restated as [33, 633]:

$$t_\phi = X^T S^{-1} M_\phi (M_\phi^T S^{-1} M_\phi)^{-1} M_\phi^T S^{-1} X \tag{10.203}$$

10.5.5.3 Statistical Fault Isolation with the Min–Max Test

In this approach the aim is to find a statistic that will be able to detect a change on the part ϕ of the parameters vector η and which will be robust to a change in the non observed part ψ [32]. Assume the vector partition $\eta = [\phi, \psi]^T$. The following notation is used:

$$M^T S^{-1} M = \begin{pmatrix} I_{\varphi\varphi} & I_{\varphi\psi} \\ I_{\psi\varphi} & I_{\psi\psi} \end{pmatrix} \tag{10.204}$$

$$\gamma = \begin{pmatrix} \varphi \\ \psi \end{pmatrix}^T \cdot \begin{pmatrix} I_{\varphi\varphi} & I_{\varphi\psi} \\ I_{\psi\varphi} & I_{\psi\psi} \end{pmatrix} \cdot \begin{pmatrix} \varphi \\ \psi \end{pmatrix} \tag{10.205}$$

where S is the previously defined covariance matrix. The min–max test aims to minimize the non-centrality parameter γ with respect to the parameters that are not suspected for change. The minimum of γ with respect to ψ is given for [33, 463, 633]:

$$\psi^* = \arg\min_\psi \gamma = \varphi^T (I_{\varphi\varphi} - I_{\varphi\psi} I_{\psi\psi}^{-1} I_{\psi\varphi}) \varphi \tag{10.206}$$

and is found to be

$$\begin{aligned} \gamma^* &= \min_\psi \gamma = \varphi^T (I_{\varphi\varphi} - I_{\varphi\psi} I_{\psi\psi}^{-1} I_{\psi\varphi}) \varphi = \\ &= \begin{pmatrix} \varphi \\ -I_{\psi\psi}^{-1} I_{\psi\varphi} \varphi \end{pmatrix}^T \begin{pmatrix} I_{\varphi\varphi} & I_{\varphi\psi} \\ I_{\psi\varphi} & I_{\psi\psi} \end{pmatrix} \begin{pmatrix} \varphi \\ -I_{\psi\psi}^{-1} I_{\psi\varphi} \varphi \end{pmatrix} \end{aligned} \tag{10.207}$$

which results in

$$\gamma^* = \varphi^T \{[I, -I_{\varphi\psi} I_{\psi\psi}^{-1}] M^T \Sigma^{-1}\} \, \Sigma^{-1} \{\Sigma^{-1} M [I, -I_{\varphi\psi} I_{\psi\psi}^{-1}]\} \varphi \tag{10.208}$$

The following linear transformation of the observations is considered:

$$X_\phi^* = [I, -I_{\varphi\psi} I_{\psi\psi}^{-1}] M^T \Sigma^{-1} X \tag{10.209}$$

The transformed variable X_ϕ^* follows a Gaussian distribution $N(\mu_\phi^*, I_\phi^*)$ with mean:

Table 10.4 Stages of the local statistical approach for FDI

1.	Generate the residuals partial derivative given by Eq. (10.215)
2.	Calculate the Jacobian matrix J given by Eq. (10.195)
3.	Calculate the sensitivity matrix M given by Eq. (10.198)
4.	Calculate the covariance matrix S given by Eq. (10.199)
5.	Apply the χ^2 test for change detection of Eq. (10.200)
6.	Apply the change isolation tests of Eq. (10.203) or (10.212)

$$\mu_{\varphi}^{*} = I_{\varphi}^{*}\varphi \tag{10.210}$$

and with covariance:

$$I_{\varphi}^{*} = I_{\varphi\varphi} - I_{\varphi\psi} I_{\psi\psi}^{-1} I_{\psi\varphi} \tag{10.211}$$

The min–max test decides between the hypotheses:

$$H_0^{*} : \mu^{*} = 0$$
$$H_1^{*} : \mu^{*} = I_{\varphi}^{*}\varphi$$

and is described by:

$$\tau_{\varphi}^{*} = X_{\varphi}^{*T} I_{\varphi}^{*-1} X_{\varphi}^{*} \tag{10.212}$$

The stages of fault detection and isolation (FDI) with the use of the local statistical approach are summarized in Table 10.4.

10.5.5.4 Sensitivity of the Fuzzy Kalman Filter to Parametric Changes

It was shown that the Fuzzy Kalman Filter can be represented as a fuzzy weighting of ARMAX models, which is actually the so-called Takagi–Sugeno fuzzy model. These are written as:

$$\begin{aligned} R_l \ : \ & IF\ x_1\ is\ A_1^l AND\ x_2\ is\ A_2^l\ AND\ \cdots AND\ x_n\ is\ A_n^l \\ & THEN\ \bar{y}^l = \textstyle\sum_{i=1}^{n} c_{f_i}^l x_i \ \ l = 1, 2, \ldots, L \end{aligned} \tag{10.213}$$

where R^l is the lth rule, $x = [x_1, x_2, \ldots, x_n]^T$ is the input (antecedent) variable, $\bar{y}^l$ is the output (consequent) variable, and w_i^l, b^l are the parameters of the local linear models. The output of the Takagi–Sugeno model is given by the weighted average of the rules consequents [211, 463]:

$$\hat{y} = \frac{\sum_{l=1}^{L} \bar{y}^l \prod_{i=1}^{n} \mu_{A_i^l}(x_i)}{\sum_{l=1}^{L} \prod_{i=1}^{n} \mu_{A_i^l}(x_i)} \tag{10.214}$$

where $\mu_{A_i^l}(x_i) : R \rightarrow [0, 1]$ is the membership function of the fuzzy set A_i^l in the antecedent part of the rule R^l. The output of the lth local model is given by $\bar{y}^l = \sum_{i=1}^{n} c_{fi}^l x_i$ [211, 463].

First, the residual e_i is defined as the difference between the fuzzy model output $\hat{y}_i$ and the physical system output y_i, i.e. $e_i = \hat{y}_i - y_i$. It is also acceptable to define the residual as the difference between the fuzzy model output and the exact model output, where the exact model replaces the physical system and has the same number of parameters as the fuzzy model (see Fig. 10.53). The partial derivative of the residual square is:

$$H(\theta, y_i) = \frac{1}{2} \frac{\partial e_i^2}{\partial \theta} = e_i \frac{\partial y_i}{\partial \theta} \tag{10.215}$$

The vector H having as elements the above $H(\theta, y_i)$ is called primary residual. Next, the gradients of the output with respect to the model's parameters are computed [463]. In the case of fuzzy models the gradient of the output with respect to the consequent parameters w_i^l is given by

$$\frac{\partial \hat{y}}{\partial w_i^l} = \frac{x_i \mu_{R^l}(x)}{\sum_{l=1}^{L} \mu_{R^l}(x)} \tag{10.216}$$

The gradient with respect to the center c_i^l is

$$\frac{\partial \hat{y}}{\partial c_i^l} = \sum_{l=1}^{L} \frac{\bar{y}^l \frac{2(x_i - c_i^l)}{v_i^l} \mu_{R^l}(x_i) [\sum_{j=1}^{L} \mu_{R^j}(x_i) - \mu_{R^l}(x_i)]}{[\sum_{l=1}^{L} \mu_{R^l}(x_i)]^2} \tag{10.217}$$

The gradient with respect to the spread v_i^l is

$$\frac{\partial \hat{y}}{\partial v_i^l} = \sum_{l=1}^{L} \frac{\bar{y}^l \frac{2(x_i - c_i^l)^2}{v_i^{l\,3}} \mu_{R^l}(x_i) [\sum_{j=1}^{L} \mu_{R^j}(x_i) - \mu_{R^l}(x_i)]}{[\sum_{l=1}^{L} \mu_{R^l}(x_i)]^2} \tag{10.218}$$

It is noted that the equivalence between the fuzzy Kalman filter and a Takagi–Sugeno neurofuzzy model enables to exploit previous results on fault detection and isolation for non-parametric estimators, such as neurofuzzy networks, by making use the *local statistical approach* to fault diagnosis. By describing the Fuzzy Kalman filter in the form of a Takagi–Sugeno neurofuzzy model it becomes easy to complete the intermediate stages for the application of the change detection method, which are described in Table 10.4 [32, 463].

10.5.6 Simulation Tests

The motion of the ship was considered to be monitored by the Fuzzy Kalman Filter of Fig. 10.52. The fuzzy Kalman Filter through local linear models was taken to consist of the following rules:

$$
\begin{aligned}
R^{(1)} &: IF\ x_1\ is\ (c_1^{(1)}, v)\ AND\ x_2\ is\ (c_2^{(1)}, v)\ AND \cdots \\
&\quad AND\ x_n\ is\ (c_n^{(1)}, v) \cdots\ THEN\ \hat{y} = \underline{c_f}^{(1)} \underline{x^T} \\
R^{(2)} &: IF\ x_1\ is\ (c_1^{(2)}, v)\ AND\ x_2\ is\ (c_2^{(2)}, v)\ AND \cdots \\
&\quad AND\ x_n\ is\ (c_n^{(2)}, v) \cdots\ THEN\ \hat{y} = \underline{c_f}^{(2)} \underline{x^T} \\
R^{(3)} &: IF\ x_1\ is\ (c_1^{(3)}, v)\ AND\ x_2\ is\ (c_2^{(3)}, v)\ AND \cdots \\
&\quad AND\ x_n\ is\ (c_n^{(3)}, v) \cdots\ THEN\ \hat{y} = \underline{c_f}^{(3)} \underline{x^T} \\
R^{(4)} &: IF\ x_1\ is\ (c_1^{(4)}, v)\ AND\ x_2\ is\ (c_2^{(4)}, v)\ AND \cdots \\
&\quad AND\ x_n\ is\ (c_n^{(4)}, v) \cdots\ THEN\ \hat{y} = \underline{c_f}^{(4)} \underline{x^T}
\end{aligned}
$$

According to Sect. 10.5.3, the regressor's vector appearing in the consequent part of the previous fuzzy rules is $x^T = [\hat{y}(k), \hat{y}(k-1), \hat{y}(k-2), u_1(k), u_2(k), u_3(k), \varepsilon_1(k)]^T$, while the parameters' vector is $c_f = [a_1, a_2, a_3, b_1, b_2, b_3, c_1]$. The above model implies fusion of local estimates from 4 sub-models. The spread of the membership functions is denoted by v. A 2D projection of the input space partition is demonstrated in Fig. 10.54.

As mentioned before, to reduce the number of parameters in the statistical validation test, only the first three variables were maintained in the AR part of the local ARMAX models, that is $y(k-1)$, $y(k-2)$ and $y(k-3)$. Thus, the parameters set in the new TSK fuzzy model consisted of $4 \times 7 + 4 \times 3 = 40$ parameters (28 linear parameters which were the output layer weights and 12 nonlinear parameters which were the centers of the fuzzy sets in the antecedent part of the rules). This means that by applying the local statistical approach to FDI and the χ^2 change detection test to the considered model, the fault threshold should be equal to 40.

The numerical tests confirmed theory. In case that no fault was assumed for the monitored system the mean value of the χ^2 test over a number of trials was found to be close to the threshold value 40. Such a value was anticipated according to the theoretical analysis of the χ^2 test. For slight deviations of the parameters of the fuzzy Kalman Filter from their nominal (fault-free) values, the global χ^2 test was capable of giving a clear indication about the existence of a fault. Thus for changes which varied between 0.1% and 1% of the nominal parameter's value the score of the χ^2 test deviated significantly from the fault threshold (which as mentioned before was set equal to 40).

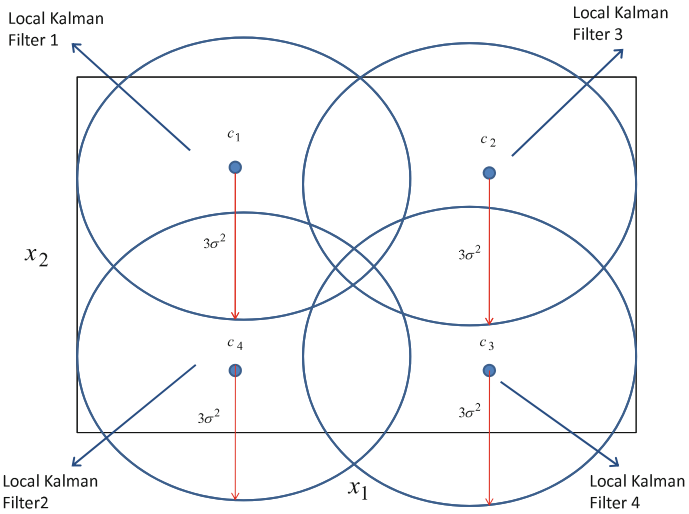

Fig. 10.54 Fuzzy rule base generated with input space partition

Table 10.5 Comparison between χ^2 and MSE tests

% change	χ^2	MSE
0.20	44.45	$1.01 \cdot 10^{-6}$
0.24	60.54	$1.01 \cdot 10^{-6}$
0.30	101.21	$1.01 \cdot 10^{-6}$
0.35	106.99	$1.01 \cdot 10^{-6}$
0.40	172.49	$1.01 \cdot 10^{-6}$
0.45	165.97	$1.02 \cdot 10^{-6}$
0.50	187.87	$1.02 \cdot 10^{-6}$
0.55	230.14	$1.02 \cdot 10^{-6}$
0.60	295.33	$1.02 \cdot 10^{-6}$
0.65	282.00	$1.03 \cdot 10^{-6}$
0.70	330.59	$1.03 \cdot 10^{-6}$
0.75	365.88	$1.03 \cdot 10^{-6}$

A comparison between (i) the proposed χ^2 change detection test based on the local statistical approach and the Generalized Likelihood ratio and (ii) the mean square error (MSE) test, for detecting model inconsistencies in the distributed/fuzzy Kalman Filter is given in Table 10.5 and in Fig. 10.55. It can be clearly noticed that for small parametric changes in the ship's local models used by the fuzzy Kalman Filter, the MSE test gives the erroneous conclusion that the functioning of the Kalman Filter remains accurate. Actually it is observed that there is no change in the MSE value despite changes in the parameters of the model used by the Kalman Filter, and the MSE value remains low as in the case of fault-free operation. Besides in the MSE test

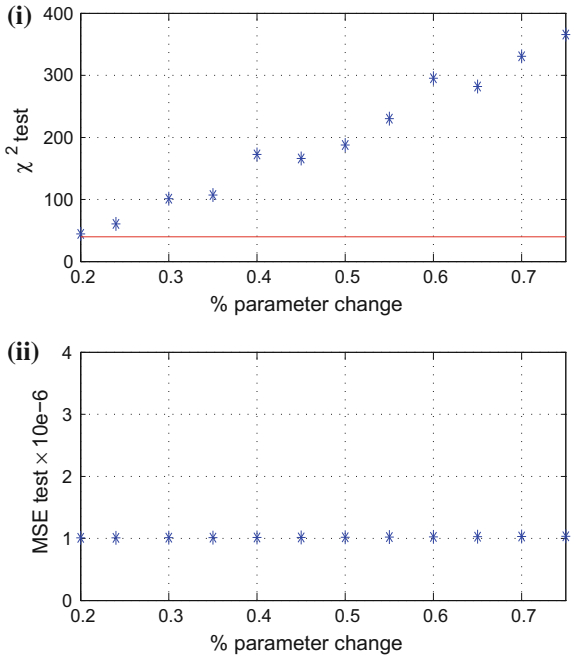

Fig. 10.55 Comparison between **i** the proposed χ^2 test based on the local statistical approach and the Generalized Likelihood ratio and **ii** of the mean square error (MSE) test, for detecting model inconsistencies in the distributed/Fuzzy Kalman Filter

the fault threshold is defined in an ad-hoc manner and this is another reason for the low credibility of this test. On the other hand the proposed χ^2 test based on the local statistical approach and the Generalized Likelihood ratio provides a clear indication about inconsistencies between the models used by the fuzzy Kalman Filter and the dynamics of the real system. Despite the small magnitude of parametric changes, the output of the χ^2 test based on the local statistical approach becomes several times larger than the fault threshold (that is 40). Thus a clear indication is provided about the need to correct the parameters of the local models used by the Fuzzy Kalman Filter.

As far as fault isolation is concerned, the numerical results showed that the sensitivity method for fault isolation was very efficient in distinguishing the parameter subject to fault among all parameters in the fuzzy Kalman Filter's model. The sensitivity fault isolation test and the min–max fault isolation test was performed for the parameters (weight w_i) of the local Kalman Filter. As it can be observed from the test's success rate depicted in Fig. 10.56 the proposed fault isolation methods can detect the local Kalman Filter, that uses an inconsistent model with reference to the

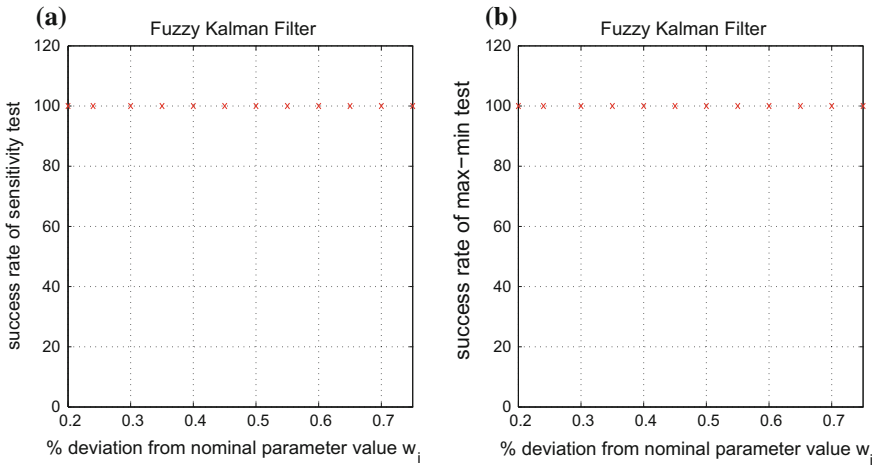

Fig. 10.56 **a** Success rate of the fault isolation test (sensitivity method) for changes in a parameter of the first local Kalman Filter, ranging between 0.1 and 1.0% of the nominal value **b** Success rate of the fault isolation test (max–min method) for changes in a parameter of the first local Kalman Filter, ranging between 0.1 and 1.0% of the nominal value

real system's model. Thus correction of the parameters of this particular filter can be carried out instead of redesign of all local Kalman Filters constituting the Fuzzy Kalman Filter.

Chapter 11
Autonomous Underwater Vessels

Abstract The control of multi-DOF autonomous underwater vessels (AUVs) exhibits particular difficulties which are due to the complicated nonlinear model of the submersible vessels, the coupling between the systems control inputs and outputs, and the uncertainty about the values of their model's parameters. Moreover, the AUVs' dynamic model is subject to external perturbations which are caused by variable sea conditions and sea currents. Consequently, an efficient control scheme for AUVs should not only compensate for the nonlinearities of the associated dynamic model, but should also exhibit robustness to model parameter variations and to external disturbances. To this end, the present chapter provides results on robust control of AUVs, as well as on adaptive control of such submersible vessels. Thus the control problem for autonomous underwater vessels is treated with (i) global linearization methods (ii) approximate linearization methods and (iii) Lyapunov methods. The solution of the control problem requires a more elaborated procedure when the AUVs' dynamic model is underactuated. which means that the number of actuators included in its propulsion system is less than the number of its degrees of freedom.The methods developed in this chapter treat also the case of underactuated AUVs. Moreover, advanced estimation methods are used to identify in real time the unknown dynamics of the underwater vessels or disturbance forces and torques that affect them. This allows for the implementation of indirect adaptive control schemes for the AUVs. Additionally,for the precise localization of the AUVs and their safe navigation elaborated nonlinear filtering methods are developed. These permit to solve problems of multi-sensor fusion as well as problems of decentralized state estimation with the use of spatially distributed nonlinear filters that track the AUVs motion. In particular the chapter treats the following topics: (a) Global linearization-based control of autonomous underwater vessels, (b) Flatness-based adaptive fuzzy control of autonomous submarines, and (c) Nonlinear optimal control of autonomous submarines.

G. Rigatos and K. Busawon, *Robotic Manipulators and Vehicles*,
Studies in Systems, Decision and Control 152,
https://doi.org/10.1007/978-3-319-77851-8_11

11.1 Chapter Overview

The present chapter treats the following topics: (a) Global linearization-based control of autonomous underwater vessels, (b) Flatness-based adaptive fuzzy control of autonomous submarines, and (c) Nonlinear optimal control of autonomous submarines.

With reference to (a) the chapter solves the problem of control and navigation for Autonomous Underwater Vessels (AUVs) using differential flatness theory and the Derivative-free nonlinear Kalman Filter. First, differential flatness is proven for the 6-DOF dynamic model of the AUV. This allows for transforming the AUV model into the linear canonical (Brunovsky) form and for designing a state feedback controller. Uncertainty about the parameters of the AUV's dynamic model, as well external perturbations which affect its motion are issues that have to be taken into account in the controller's design. To compensate for model imprecision and disturbance terms, it is proposed to use a disturbance observer which relies on the previously analyzed the Derivative-free nonlinear Kalman Filter. The considered filtering method consists of the standard Kalman Filter recursion applied on the linearized model of the underwater vessel and of an inverse transformation based on differential flatness theory, which enables to obtain estimates of the state variables of the initial nonlinear model of the vessel. With the use of the Kalman Filter-based disturbance observer, simultaneous estimation of the non-measurable state variables of the AUV and of the perturbation terms that affect its dynamics is achieved. Moreover, after estimating such disturbances, their compensation is also accomplished.

With reference to (b) the chapter proposes adaptive fuzzy control based on differential flatness theory for autonomous submarines. It is proven that the dynamic model of the submarine, having as state variables the vessel's depth and its pitch angle, is a differentially flat one. This means that all its state variables and its control inputs can be written as differential functions of the flat output and its derivatives. By exploiting differential flatness properties the system's dynamic model is written in the multivariable linear canonical (Brunovsky) form, for which the design of a state feedback controller becomes possible. After this transformation, the new control inputs of the system contain unknown nonlinear parts, which are identified with the use of neurofuzzy approximators. The learning procedure for these estimators is determined by the requirement the first derivative of the closed-loop's Lyapunov function to be a negative one. Moreover, the Lyapunov stability analysis shows that H-infinity tracking performance is ascertained for the feedback control loop and this assures improved robustness to the aforementioned model uncertainty as well as to external perturbations.

With reference to (c) the chapter presents a nonlinear H-infinity (optimal) control approach for the problem of the control of the depth and heading angle of an autonomous submarine. This is a multi-variable nonlinear control problem and its solution allows for precise underwater navigation of the submarine. The submarine's dynamic model undergoes approximate linearization around a temporary equilibrium that is recomputed at each iteration of the control algorithm. The linearization procedure is based on Taylor series expansion and on the computation of the submarine's

model Jacobian matrices. For the approximately linearized model, the optimal control problem is solved through the design of an H-infinity feedback controller. The computation of the controller's gain requires the solution of an algebraic Riccati equation, which is repetitively performed at each step of the control method. The stability of the control scheme is proven through Lyapunov analysis.

11.2 Global Linearization-Based Control of Autonomous Underwater Vessels

11.2.1 Outline

The control of 6-DOF autonomous underwater vessels (AUVs) exhibits particular difficulties which are due to the complicated nonlinear model of the vessel, the coupling between the system's control inputs and outputs, and the uncertainty about the values of the model's parameters. Moreover, the AUVs' dynamic model is subject to external perturbations which are due to variable sea conditions and sea currents [143, 144, 191, 411]. Consequently, an efficient control scheme for AUVs should not only compensate for the nonlinearities of the associated dynamic model, but should also exhibit robustness to model parameter variations and to external disturbances. To this end, during the last years, there have been several results on robust control of AUVs [251, 258, 288, 386, 453, 536, 635], as well as on adaptive control of such submersible vessels [253, 346, 462, 618].

In this section a new control method is proposed for the 6-DOF dynamic model of AUVs, based on differential flatness theory [450, 452, 457]. First it is proven, that the 6-DOF dynamic model of the AUV is a differentially flat one. This means that all its state variables and its control inputs can be expressed as differential functions of one single algebraic variable which is the so-called flat output [57, 145, 254, 267, 322, 472, 476, 519, 572]. By exploiting differential flatness properties, the AUVs' model is transformed into the linear canonical (Brunovsky) form. For the latter description of the AUVs the design of a state feedback controller is possible. Unlike approximate linearization methods the aforementioned transformation avoids numerical errors and truncation of nonlinear terms from the AUVs' dynamic model.

Another problem that has to be dealt with is that the control loop should compensate for modelling uncertainties and external perturbation terms affecting the AUVs. To this end, it is proposed to use the Derivative-free nonlinear Kalman Filter as a disturbance observer. This nonlinear filter consists of the Kalman Filter recursion applied on the equivalent linearized model of the AUVs together with an inverse transformation, based again on differential flatness theory, which enables to obtain estimates of the initial nonlinear AUVs' model. The aforementioned disturbance observer provides simultaneously estimates of non-measurable state variables of the AUV and of the external perturbation terms. By identifying external disturbance inputs their compensation becomes also possible.

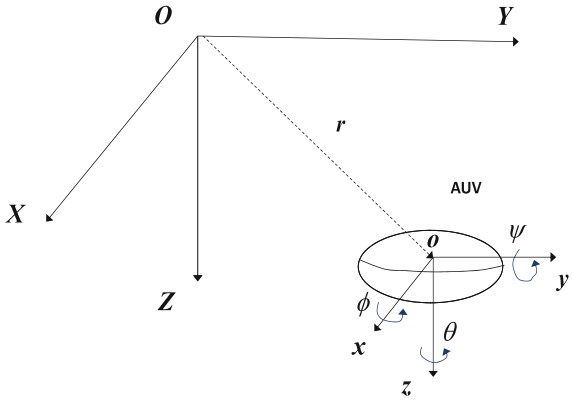

Fig. 11.1 Reference frames for the localization and navigation of the AUV

11.2.2 The 6-DOF Dynamic Model of the AUV

11.2.2.1 Kinematic Model of the AUV

Kinematic and dynamic modelling of AUVs and in general of marine vessels is needed for the development of efficient control for propulsion purposes [373, 388, 416]. In the modelling of AUVs an inertial and a body-fixed reference frame are usually defined. The inertial reference frame of the AUV denoted as $OXYZ$ and the body-fixed reference frame denoted as $Oxyz$, used for the localization and navigation of the underwater vessel are depicted in Fig. 11.1.

The state vector of the AUV in the inertial reference frame is defined as $x = [x_1, x_2]^T = [x, y, z, \phi, \theta, \psi]^T$, where $x_1 = [x, y, z]^T$ denotes linear displacement and $x_2 = [\psi, \theta, \psi]^T$ is the vector of Euler angles which denotes rotational displacement. The associated velocities vector is given by $\dot{x} = [\dot{x}_1, \dot{x}_2]^T = [\dot{x}, \dot{y}, \dot{z}, \dot{\phi}, \dot{\theta}, \dot{\psi}]^T$.

In the body-fixed reference frame the velocity vector of the AUV is denoted as $u = [u_1, u_2]^T = [u, v, w, p, q, r]^T$, where $u_1 = [u, v, w]^T$ is the vector of linear velocities and $u_2 = [p, q, r]^T$ is the vector of angular velocities.

The vector of external forces and torques which can be applied to the 6-DOF AUV is given by $\tau = [F_x, F_y, F_z, T_x, T_y, T_z]^T$. In this representation $\tau_1 = [F_x, F_y, F_z]^T$ is the vector of forces along the X, Y and Z axes respectively and $\tau_2 = [T_x, T_y, T_z]^T$ is the vector of torques causing rotation round the X, Y and Z axes.

The following transformation connects velocities expressed in the inertial reference frame $\dot{\eta}_1 = [\dot{x}, \dot{y}, \dot{z}]^T$ and velocities expressed in the body-fixed frame $v_1 = [u, v, w]^T$:

$\dot{\eta}_1 = J_1 v_1$ where

$$J_1 = \begin{pmatrix} \cos(\psi)cos(\theta) & -sin(\psi)cos(\phi) + cos(\psi)sin(\theta)sin(\phi) & sin(\psi)sin(\phi) + cos(\psi)cos(\phi)sin(\theta) \\ sin(\psi)cos(\theta) & cos(\psi)cos(\phi) + sin(\phi)sin(\theta)sin(\psi) & -cos(\psi)sin(\phi) + sin(\theta)sin(\psi)cos(\phi) \\ -sin(\theta) & cos(\theta)sin(\phi) & cos(\theta)cos(\phi) \end{pmatrix} \tag{11.1}$$

Moreover, the following transformation holds between angular velocities expressed in the inertial and in the body-fixed frame

$$\dot{\eta}_2 = J_2 v_2 \text{ where}$$

$$J_2 = \begin{pmatrix} 1 & sin(\phi)tan(\theta) & cos(\phi)tan(\theta) \\ 0 & cos(\phi) & -sin(\phi) \\ 0 & sin(\phi)/cos(\theta) & cos(\phi)/cos(\theta) \end{pmatrix} \tag{11.2}$$

Therefore, it holds

$$\begin{pmatrix} \dot{\eta}_1 \\ \dot{\eta}_2 \end{pmatrix} = \begin{pmatrix} J_1 & 0 \\ 0 & J_2 \end{pmatrix} \begin{pmatrix} v_1 \\ v_2 \end{pmatrix} \text{ or } \dot{\eta} = J \cdot v \tag{11.3}$$

11.2.2.2 Dynamic Model of the AUV

Dynamic models for AUVs have been extensively analyzed [373, 388]. The dynamic model of the AUV representing an equilibrium in forces and torques is

$$M_{RB}\dot{v} + C_{RB}(v) \cdot v = \tau_{RB} \tag{11.4}$$

where M_{RB} is the inertia matrix of the AUV, $C_{RB}(v)$ is the Coriolis and centrifugal forces matrix, $v = [u, v, w, p, q, r]^T$ is the velocities vector in the body-fixed reference frame and $\tau_{RB} = [F_x, F_y, F_z, T_x, T_y, T_z]^T = 0 \in R^{6\times 1}$ is the vector of external forces and torques exerted on the AUV when the latter is found at an equilibrium. All variables of Eq. (11.4) are expressed in the body-fixed frame.

The inertia matrix M_{RB} is given by

$$M_{RB} = \begin{pmatrix} m & 0 & 0 & 0 & mz_G & -my_G \\ 0 & m & 0 & -mz_G & 0 & mx_G \\ 0 & 0 & m & my_G & -mx_G & 0 \\ 0 & -mz_G & my_G & I_x & -I_{xy} & -I_{xz} \\ mz_G & 0 & -mx_G & -I_{xy} & I_y & -I_{yz} \\ -my_G & mx_G & 0 & -I_{xz} & -I_{yz} & I_z \end{pmatrix} \tag{11.5}$$

where I_x, I_y, I_z are inertia matrices, I_{xy}, I_{xz}, I_{yz} are inertia products and $r_G = [x_G, y_G, z_G]$ are the coordinates of the AUV's center of mass (in the body-fixed frame). The Coriolis matrix of the AUV is given by

$$C_{RB} = \begin{pmatrix} 0 & 0 & 0 & m(y_G q + z_G r) & -m(x_G q - w) & -m(x_G r + v) \\ 0 & 0 & 0 & -m(y_G p + w) & m(z_G r + x_G p) & -m(y_G r - u) \\ 0 & 0 & 0 & -m(z_G p - v) & -m(z_G q + u) & -m(x_G p + y_G q) \\ -m(y_G q + z_G r) & m(y_G p + w) & m(z_G p - v) & 0 & -I_{yz} q - I_{xz} p + I_z r & I_{yz} r + I_{xy} p - I_y q \\ m(x_G q - w) & -m(z_G r + x_G p) & m(z_G q + u) & I_{yx} q + I_{xz} p - I_z r & 0 & I_{xz} r + I_{xy} q + I_x p \\ m(x_G r + v) & m(y_G r - u) & -m(x_G p + y_G q) & -I_{yz} r - I_{xy} p - I_y q & I_{xz} r + I_{xy} q - I_x p & 0 \end{pmatrix} \tag{11.6}$$

The motion of the AUV is also affected by the inertia of the fluid that surrounds it. This is modeled as follows:

$$\tau_A = -M_A \dot{v} - C_A(v) v \tag{11.7}$$

This means that a force / torque is developed against the motion of the vessel and it varies proportionally to the vessel's acceleration. The new inertia matrix M_A is given by

$$M_A = \begin{pmatrix} A_{11} & 0 & 0 & 0 & 0 & 0 \\ 0 & A_{22} & 0 & 0 & 0 & 0 \\ 0 & 0 & A_{33} & 0 & 0 & 0 \\ 0 & 0 & 0 & A_{44} & 0 & 0 \\ 0 & 0 & 0 & 0 & A_{55} & 0 \\ 0 & 0 & 0 & 0 & 0 & A_{66} \end{pmatrix} \tag{11.8}$$

and the new Coriolis matrix is given by

$$C_A = \begin{pmatrix} 0 & 0 & 0 & 0 & A_{33} w & -A_{22} v \\ 0 & 0 & 0 & -A_{33} w & 0 & A_{11} u \\ 0 & 0 & 0 & A_{22} v & -A_{11} u & 0 \\ 0 & A_{33} w & -A_{22} v & 0 & A_{66} r & -A_{55} q \\ -A_{33} w & 0 & A_{11} u & -A_{66} r & 0 & A_{44} p \\ A_{22} v & -A_{11} u & 0 & A_{55} q & -A_{44} p & 0 \end{pmatrix} \tag{11.9}$$

The model is completed by the vector of a force / torque which resists to the motion of the underwater vessel and which is proportional to its velocity

$\tau_{DL} = -D(v)v$ where

$$D(v) = \begin{pmatrix} X_{|u|u}|u| & 0 & 0 & 0 & 0 & 0 \\ 0 & Y_{|v|v}|v| & 0 & 0 & 0 & 0 \\ 0 & 0 & Z_{|w|w}|w| & 0 & 0 & 0 \\ 0 & 0 & 0 & K_{|p|p}|p| & 0 & 0 \\ 0 & 0 & 0 & 0 & M_{|q|q}|q| & 0 \\ 0 & 0 & 0 & 0 & 0 & N_{|r|r}|r| \end{pmatrix} \tag{11.10}$$

while the diagonal elements of matrix $D(v)$ are defined as follows:

$$\begin{array}{ll} X_{|u|u} = \frac{\rho}{2} V^{\frac{2}{3}} C_x(0^o, 0^o) & K_{|p|p} = \frac{\rho}{2} V^{\frac{5}{3}} C_p \\ Y_{|v|v} = \frac{\rho}{2} V^{\frac{2}{3}} C_y(90^o, 0^o) & M_{|q|q} = \frac{\rho}{2} V^{\frac{5}{3}} C_q \\ Z_{|w|w} = \frac{\rho}{2} V^{\frac{2}{3}} C_z(90^o, 90^o) & N_{|r|r} = \frac{\rho}{2} V^{\frac{5}{3}} C_r \end{array} \tag{11.11}$$

where ρ is the specific mass of the water, V is the volume of the submerged vessel and $C_x, C_y, C_z, C_p, C_q, C_r$ are constants.

The weight of the AUV is $W = m \cdot g$, while the lift force exerted on the AUV is $B = \rho g V$, where ρ is the water's specific weight (both expressed in the inertial reference frame). These forces can be expressed in the body-fixed reference frame as follows: $f_W = J_1^{-1}[0, 0, W]^T$ and $f_B = -J_1^{-1}[0, 0, B]^T$. Moreover, there are torques which are generated due to these forces and these are given by $\tau_W = r_G \times f_W$ and $\tau_B = r_B \times f_B$, where $r_G = [x_G, y_G, z_G]^T$ and $r_B = [x_B, y_B, z_B]^T$. Thus, there is an additional vector of forces and torques applied on the AUV which is given by

$$\tau_{WB} = \begin{pmatrix} f_w + f_B \\ \tau_w + \tau_B \end{pmatrix} = \begin{pmatrix} (W - B)sin(\theta) \\ -(W - B)cos(\theta)sin(\phi) \\ -(W - B)cos(\theta)cos(\phi) \\ -(Y_G W - Y_B B)cos(\theta)cos(\phi) + (z_G W - z_B B)cos(\theta)sin(\psi) \\ (z_G W - z_B B)sin(\theta) + (x_G W - x_B B)cos(\theta)cos(\phi) \\ -(x_G W - x_B B)cos(\theta)sin(\phi) - (y_G W - y_B B)sin(\theta) \end{pmatrix} \tag{11.12}$$

By applying one more transformation on the aforementioned vector, the forces and torques due to the effects of weight and lift are finally expressed in the inertial reference frame. Thus, due to the effects of the resistive forces and torques which are generated by the surrounding fluid one has the dynamics

$$M_{RB}\dot{v} + C_{RB}(v)v = \tau_A + \tau_{DL} + \tau_{WB} + \tau \tag{11.13}$$

where $\tau_A = -M_A\dot{v} - C_A(v)v$, $\tau_{DL} = -D(v)v$ stands for forces and torques resisting the vessel's motion), $\tau_{WB} = -g_f$ represents forces and torques due to weight and lift effects, and τ is the vector of external torques and forces defining the vessel's propulsion. By combining Eqs. (11.4) and (11.7) one obtains the aggregate dynamics

$$(M_{RB} + M_A)\dot{v} + (C_{RB}(v) + C_A(v))v + D(v)v + g_f = \tau \tag{11.14}$$

The aggregate inertia matrix is $M = M_{RB} + M_A$, the aggregate Coriolis matrix is $C(v) = C_{RB}(v) + C_A(v)$. Thus, the dynamic and the kinematic model of the AUV are finally written as

$$M\dot{v} + Cv + D(v)v + g_f = \tau \tag{11.15}$$

$$\dot{\eta} = J(\eta)v \tag{11.16}$$

11.2.3 Differential Flatness of the AUV's Model

It will be proven that the dynamic model of the AUV is a differentially flat one, which means that all its state variables and its control inputs can be written as differential functions of the an algebraic variable (vector) which is the so-called flat output [57, 145, 254, 267, 322, 472, 476, 519, 572]. Using that $v = J^{-1}\dot{\eta}$ or $v = R\dot{\eta}$ Eq. (11.15) can be written equivalently as

$$\tilde{M}\ddot{\eta} + \tilde{C}\dot{\eta} + \tilde{D}(\dot{\eta})\dot{\eta} + g_f(\eta) = \tau \tag{11.17}$$

where η has been defined in the inertial reference frame as $\eta = [x, y, z, \phi, \theta, \psi]^T$, $\tilde{M} = MR$, $\tilde{C} = M\dot{R} + CR$ and $\tilde{D} = DR$. By denoting the inverse of the inertia matrix as $\tilde{M}^{-1} = N$ one obtains

$$\ddot{\eta} + N\cdot\tilde{C}\dot{\eta} + N\cdot\tilde{D}(\dot{\eta})\dot{\eta} + N\cdot g_f(\eta) = N\cdot\tau \tag{11.18}$$

Moreover, using the state vector elements notation $z_1 = x$, $z_2 = \dot{x}$, $z_3 = y$, $z_4 = \dot{y}$, $z_5 = z$, $z_6 = \dot{z}$, $z_7 = \phi$, $z_8 = \dot{\phi}$, $z_9 = \theta$, $z_{10} = \dot{\theta}$, $z_{11} = \psi$, $z_{12} = \dot{\psi}$ and by defining the state vector $Z = [z_1, z_2, z_3, z_4, z_5, z_6, z_7, z_8, z_9, z_{10}, z_{11}, z_{12}]^T$, the dynamic model of Eq. (11.18) becomes

$$\begin{array}{ll} \dot{z}_1 = z_2 & \dot{z}_2 + f_1(Z) = N_1(Z)\tau \\ \dot{z}_3 = z_4 & \dot{z}_4 + f_2(Z) = N_2(Z)\tau \\ \dot{z}_5 = z_6 & \dot{z}_6 + f_3(Z) = N_3(Z)\tau \\ \dot{z}_7 = z_8 & \dot{z}_8 + f_4(Z) = N_4(Z)\tau \\ \dot{z}_9 = z_{10} & \dot{z}_{10} + f_5(Z) = N_5(Z)\tau \\ \dot{z}_{11} = z_{12} & \dot{z}_{12} + f_6(Z) = N_6(Z)\tau \end{array} \tag{11.19}$$

where $\tau \in R^{6\times 1}$ is the vector of external forces and torques, $f_i(Z)$ $i = 1, \cdots, 6$ are the row elements of the vector $f = N\cdot\tilde{C}\dot{\eta} + N\cdot\tilde{D}(\dot{\eta})\dot{\eta} + N\cdot g_f(\eta)$, while $N_i(Z)$, $i = 1, \cdots, 6$ are the rows of matrix $N = M^{-1}$. The flat output of the system is taken to be the vector $Y = [z_1, z_3, z_5, z_7, z_9, z_{11}]$. From Eq. (11.19) it holds that $z_2 = \dot{z}_1$, $z_4 = \dot{z}_3$, $z_6 = \dot{z}_5$, $z_8 = \dot{z}_7$, $z_{10} = \dot{z}_9$ and $z_{12} = \dot{z}_{11}$. Therefore, it holds

$$\begin{array}{ll} z_2 = [1\,0\,0\,0\,0\,0]\dot{Y} & z_4 = [0\,1\,0\,0\,0\,0]\dot{Y} \\ z_6 = [0\,0\,1\,0\,0\,0]\dot{Y} & z_8 = [0\,0\,0\,1\,0\,0]\dot{Y} \\ z_{10} = [0\,0\,0\,0\,1\,0]\dot{Y} & z_2 = [0\,0\,0\,0\,0\,1]\dot{Y} \end{array} \tag{11.20}$$

Consequently the state vector elements given above can be written as functions of the flat output Y. Moreover, from Eq. (11.19) one has that

$$\begin{array}{ll} \ddot{z}_1 = v_1 = -f_1 + N_1\tau & \ddot{z}_3 = v_2 = -f_2 + N_2\tau \\ \ddot{z}_5 = v_3 = -f_3 + N_3\tau & \ddot{z}_7 = v_4 = -f_4 + N_4\tau \\ \ddot{z}_9 = v_5 = -f_5 + N_5\tau & \ddot{z}_{11} = v_6 = -f_6 + N_6\tau \end{array} \tag{11.21}$$

Therefore, one has

$$\begin{pmatrix} \ddot{z}_1 \\ \ddot{z}_3 \\ \ddot{z}_5 \\ \ddot{z}_7 \\ \ddot{z}_9 \\ \ddot{z}_{11} \end{pmatrix} = \begin{pmatrix} -f_1 \\ -f_2 \\ -f_3 \\ -f_4 \\ -f_5 \\ -f_6 \end{pmatrix} + \begin{pmatrix} N_1\tau \\ N_2\tau \\ N_3\tau \\ N_4\tau \\ N_5\tau \\ N_6\tau \end{pmatrix} \tag{11.22}$$

which is equivalently written as

$$\begin{gathered} \ddot{z}_a = -f_a(Z) + N\tau \Rightarrow \tau = N^{-1}(\ddot{z}_a + f_a(Z)) \\ \Rightarrow \tau = M(\ddot{z}_a + f_a(Z)) \end{gathered} \tag{11.23}$$

Consequently, the control inputs of the 6-DOF AUV model can be also written as functions of the flat output and its derivatives. Therefore, the AUV model is a differentially flat one.

11.2.4 Flatness-Based Control of the AUV

By exploiting the previously proven differential flatness properties of the AUV it will be shown that a stabilizing feedback controller can be designed for the AUV model. Using Eq. (11.19) the following control inputs are defined.

$$\begin{gathered} v_1 = -f_1 + N_1\tau \; v_2 = -f_2 + N_2\tau \\ v_3 = -f_3 + N_3\tau \; v_4 = -f_4 + N_4\tau \\ v_5 = -f_1 + N_1\tau \; v_6 = -f_1 + N_1\tau \end{gathered} \tag{11.24}$$

or equivalently

$$v = -f_a + N\tau \Rightarrow \tau = N^{-1}(v + f_a) \Rightarrow \tau = M(v + f_a) \tag{11.25}$$

This means that if the transformed control inputs v are computed so as to assure asymptotic tracking of the AUV's reference setpoints, one can also find the real control inputs τ which should be exerted on the AUV for succeeding this objective. According to the above, the dynamic model of Eq. (11.19) can be written into the canonical (Brunovsky) form

$$\begin{gathered} \dot{z}_1 = z_2 \;\; \dot{z}_2 = v_1 \;\; \dot{z}_3 = z_4 \;\; \dot{z}_4 = v_2 \\ \dot{z}_5 = z_6 \;\; \dot{z}_6 = v_3 \;\; \dot{z}_7 = z_8 \;\; \dot{z}_8 = v_4 \\ \dot{z}_9 = z_{10} \; \dot{z}_{10} = v_5 \; \dot{z}_{11} = z_{12} \; \dot{z}_{12} = v_6 \end{gathered} \tag{11.26}$$

which also takes the matrix form

$$\dot{Z} = AZ + BV \tag{11.27}$$

or equivalently one has the following state-space description for the system

$$\begin{pmatrix} \dot{z}_1 \\ \dot{z}_2 \\ \dot{z}_3 \\ \dot{z}_4 \\ \dot{z}_5 \\ \dot{z}_6 \\ \dot{z}_7 \\ \dot{z}_8 \\ \dot{z}_9 \\ \dot{z}_{10} \\ \dot{z}_{11} \\ \dot{z}_{12} \end{pmatrix} = \begin{pmatrix} 0\,1\,0\,0\,0\,0\,0\,0\,0\,0\,0\,0 \\ 0\,0\,0\,0\,0\,0\,0\,0\,0\,0\,0\,0 \\ 0\,0\,0\,1\,0\,0\,0\,0\,0\,0\,0\,0 \\ 0\,0\,0\,0\,0\,0\,0\,0\,0\,0\,0\,0 \\ 0\,0\,0\,0\,0\,1\,0\,0\,0\,0\,0\,0 \\ 0\,0\,0\,0\,0\,0\,0\,0\,0\,0\,0\,0 \\ 0\,0\,0\,0\,0\,0\,0\,1\,0\,0\,0\,0 \\ 0\,0\,0\,0\,0\,0\,0\,0\,0\,0\,0\,0 \\ 0\,0\,0\,0\,0\,0\,0\,0\,0\,1\,0\,0 \\ 0\,0\,0\,0\,0\,0\,0\,0\,0\,0\,0\,0 \\ 0\,0\,0\,0\,0\,0\,0\,0\,0\,0\,0\,1 \\ 0\,0\,0\,0\,0\,0\,0\,0\,0\,0\,0\,0 \end{pmatrix} \begin{pmatrix} z_1 \\ z_2 \\ z_3 \\ z_4 \\ z_5 \\ z_6 \\ z_7 \\ z_8 \\ z_9 \\ z_{10} \\ z_{11} \\ z_{12} \end{pmatrix} + \begin{pmatrix} 0\,0\,0\,0\,0\,0 \\ 1\,0\,0\,0\,0\,0 \\ 0\,0\,0\,0\,0\,0 \\ 0\,1\,0\,0\,0\,0 \\ 0\,0\,0\,0\,0\,0 \\ 0\,0\,1\,0\,0\,0 \\ 0\,0\,0\,0\,0\,0 \\ 0\,0\,0\,1\,0\,0 \\ 0\,0\,0\,0\,0\,0 \\ 0\,0\,0\,0\,1\,0 \\ 0\,0\,0\,0\,0\,0 \\ 0\,0\,0\,0\,0\,1 \end{pmatrix} \begin{pmatrix} v_1 \\ v_2 \\ v_3 \\ v_4 \\ v_5 \\ v_6 \end{pmatrix} \tag{11.28}$$

and the measurement equation for this system becomes

$$\begin{pmatrix} z_1 \\ z_2 \\ z_3 \\ z_4 \\ z_5 \\ z_6 \end{pmatrix} = \begin{pmatrix} 1\,0\,0\,0\,0\,0\,0\,0\,0\,0\,0\,0 \\ 0\,0\,1\,0\,0\,0\,0\,0\,0\,0\,0\,0 \\ 0\,0\,0\,0\,1\,0\,0\,0\,0\,0\,0\,0 \\ 0\,0\,0\,0\,0\,0\,1\,0\,0\,0\,0\,0 \\ 0\,0\,0\,0\,0\,0\,0\,0\,1\,0\,0\,0 \\ 0\,0\,0\,0\,0\,0\,0\,0\,0\,0\,1\,0 \end{pmatrix} \begin{pmatrix} z_1 \\ z_2 \\ z_3 \\ z_4 \\ z_5 \\ z_6 \\ z_7 \\ z_8 \\ z_9 \\ z_{10} \\ z_{11} \\ z_{12} \end{pmatrix} \tag{11.29}$$

Thus, using differential flatness theory the AUV's model has been written in a MIMO linear canonical (Brunovsky) form, which is both controllable and observable. After being written in the linear canonical form the AUV's state-space equation comprises 6 subsystems of the form

$$\ddot{y}_{f_i} = v_i,\ i = 1, \cdots, 6 \tag{11.30}$$

For each one of these subsystems a controller can be defined as follows

$$v_i = \ddot{y}_{f_i}^d - k_{d_i}(\dot{y}_{f_i} - \dot{y}_{f_i}^d) - k_{p_i}(y_{f_i} - y_{f_i}^d),\ i = 1, \cdots, 6 \tag{11.31}$$

Once the transformed control inputs vector $v \in R^{6\times 1}$ has been computed, one can use Eq. (11.25) to find also the torques and forces vector $\tau = M(v + f_a)$ that should be exerted on the AUV so as to achieve convergence to its reference setpoints.

11.2.5 Disturbances Compensation with the Derivative-Free Nonlinear Kalman Filter

It was shown that the initial nonlinear model of the AUV can be written in the MIMO canonical form of Eqs. (11.28) and (11.29). Next, it is assumed that the AUV's model is affected by additive input disturbances, thus one has

$$\begin{array}{l} \ddot{z}_1 = v_1 + \tilde{d}_1 \; \ddot{z}_2 = v_2 + \tilde{d}_2 \\ \ddot{z}_3 = v_3 + \tilde{d}_3 \; \ddot{z}_4 = v_4 + \tilde{d}_4 \\ \ddot{z}_5 = v_5 + \tilde{d}_5 \; \ddot{z}_6 = v_6 + \tilde{d}_6 \end{array} \tag{11.32}$$

The system's dynamics can be also written as $\dot{z}_1 = z_2$, $\dot{z}_2 = v_1 + \tilde{d}_1$, $\dot{z}_3 = z_4$, $\dot{z}_4 = v_2 + \tilde{d}_2$, $\dot{z}_5 = z_6$, $\dot{z}_6 = v_3 + \tilde{d}_3$, $\dot{z}_7 = z_8$, $\dot{z}_8 = v_4 + \tilde{d}_4$, $\dot{z}_9 = z_{10}$, $\dot{z}_{10} = v_5 + \tilde{d}_5$, $\dot{z}_{11} = z_{12}$, $\dot{z}_{12} = v_6 + \tilde{d}_6$.

Without loss of generality, it is assumed that the dynamics of the disturbances terms are described by their second order derivative, i.e. $\dddot{\tilde{d}}_i = f_{d_i}$, $i = 1, \cdots, 6$. Next, the extended state vector of the system is defined so as to include disturbance terms as well. Thus one has the additional state variables

$$\begin{array}{l} z_{13} = \tilde{d}_1 \; z_{14} = \dot{\tilde{d}}_1 \; z_{15} = \ddot{\tilde{d}}_1 \; z_{16} = \tilde{d}_2 \; z_{17} = \dot{\tilde{d}}_2 \; z_{18} = \ddot{\tilde{d}}_2 \\ z_{19} = \tilde{d}_3 \; z_{20} = \dot{\tilde{d}}_3 \; z_{21} = \ddot{\tilde{d}}_3 \; z_{22} = \tilde{d}_4 \; z_{23} = \dot{\tilde{d}}_4 \; z_{24} = \ddot{\tilde{d}}_4 \\ z_{25} = \tilde{d}_5 \; z_{26} = \dot{\tilde{d}}_6 \; z_{27} = \ddot{\tilde{d}}_5 \; z_{28} = \tilde{d}_6 \; z_{29} = \dot{\tilde{d}}_6 \; z_{30} = \ddot{\tilde{d}}_6 \end{array} \tag{11.33}$$

Thus, the disturbed system can be described by a state-space equation of the form

$$\begin{array}{l} \dot{z}_f = A_f z_f + B_f v \\ z_f^{meas} = C_f z_f \end{array} \tag{11.34}$$

where $A_f \in R^{30\times 30}$, $B_f \in R^{30\times 6}$ and $C_f \in R^{6\times 30}$, with

$$A_f = \begin{pmatrix} 0_{1\times1} & 1 & 0_{1\times28} \\ 0_{1\times12} & 1 & 0_{1\times17} \\ 0_{1\times3} & 1 & 0_{1\times26} \\ 0_{1\times15} & 1 & 0_{1\times14} \\ 0_{1\times5} & 1 & 0_{1\times24} \\ 0_{1\times18} & 1 & 0_{1\times11} \\ 0_{1\times7} & 1 & 0_{1\times22} \\ 0_{1\times21} & 1 & 0_{1\times8} \\ 0_{1\times9} & 1 & 0_{1\times20} \\ 0_{1\times24} & 1 & 0_{1\times5} \\ 0_{1\times11} & 1 & 0_{1\times18} \\ 0_{1\times27} & 1 & 0_{1\times2} \\ 0_{1\times13} & 1 & 0_{1\times16} \\ 0_{1\times14} & 1 & 0_{1\times15} \\ 0_{1\times30} & & \\ 0_{1\times16} & 1 & 0_{1\times13} \\ 0_{1\times17} & 1 & 0_{1\times12} \\ 0_{1\times30} & & \\ 0_{1\times19} & 1 & 0_{1\times10} \\ 0_{1\times20} & 1 & 0_{1\times9} \\ 0_{1\times30} & & \\ 0_{1\times22} & 1 & 0_{1\times7} \\ 0_{1\times23} & 1 & 0_{1\times6} \\ 0_{1\times30} & & \\ 0_{1\times25} & 1 & 0_{1\times4} \\ 0_{1\times26} & 1 & 0_{1\times3} \\ 0_{1\times30} & & \\ 0_{1\times28} & 1 & 0_{1\times1} \\ 0_{1\times29} & 1 & \\ 0_{1\times30} & & \end{pmatrix} \quad B_f = \begin{pmatrix} 0_{1\times6} & & \\ 1 & 0_{1\times5} & \\ 0_{1\times1} & 1 & 0_{1\times4} \\ 0_{1\times6} & & \\ 0_{1\times2} & 1 & 0_{1\times3} \\ 0_{1\times6} & & \\ 0_{1\times3} & 1 & 0_{1\times2} \\ 0_{1\times6} & & \\ 0_{1\times4} & 1 & 0_{1\times1} \\ 0_{1\times6} & & \\ 0_{1\times5} & 1 & \\ 0_{18\times6} & & \end{pmatrix} \quad C_f = \begin{pmatrix} 1 & 0_{1\times29} & \\ 0_{1\times2} & 1 & 0_{1\times27} \\ 0_{1\times4} & 1 & 0_{1\times25} \\ 0_{1\times6} & 1 & 0_{1\times23} \\ 0_{1\times8} & 1 & 0_{1\times21} \\ 0_{1\times10} & 1 & 0_{1\times19} \end{pmatrix} \tag{11.35}$$

For the aforementioned model, and after carrying out discretization of matrices A_f, B_f and C_f with common discretization methods one can implement the standard Kalman Filter algorithm, consisting of a *time-update* and a *measurement update* stage [33, 431, 463]. As previously explained,this is Derivative-free nonlinear Kalman filtering for the model of the AUV which, unlike EKF, is performed without the need to compute Jacobian matrices and does not introduce numerical errors.

The dynamics of the disturbance terms $\tilde{d}_i$, $i = 1, \cdots, 6$ are taken to be unknown in the design of the associated disturbances' estimator. Defining as $\tilde{A}_d$, $\tilde{B}_d$, and $\tilde{C}_d$, the discrete-time equivalents of matrices $\tilde{A}_f$, $\tilde{B}_f$ and $\tilde{C}_f$ respectively, one has the following dynamics:

$$\dot{\hat{z}}_f = \tilde{A}_f \cdot \hat{z}_f + \tilde{B}_f \cdot \tilde{v} + K(z_f^{meas} - \tilde{C}_f \hat{z}_f) \tag{11.36}$$

where $K \in R^{30\times 6}$ is the state estimator's gain. The associated Kalman Filter-based disturbance estimator is given by [450, 452, 457]

measurement update:

$$\begin{aligned} K(k) &= P^{-}(k)\tilde{C}_d^T[\tilde{C}_d \cdot P^{-}(k)\tilde{C}_d^T + R]^{-1} \\ \hat{z}_f(k) &= \hat{z}_f^{-}(k) + K(k)[z_f^{meas}(k) - \tilde{C}_d\hat{z}_f^{-}(k)] \\ P(k) &= P^{-}(k) - K(k)\tilde{C}_d P^{-}(k) \end{aligned} \tag{11.37}$$

time update:

$$\begin{aligned} P^{-}(k+1) &= \tilde{A}_d(k)P(k)\tilde{A}_d^T(k) + Q(k) \\ \hat{z}_f^{-}(k+1) &= \tilde{A}_d(k)\hat{z}_f(k) + \tilde{B}_d(k)\tilde{v}(k) \end{aligned} \tag{11.38}$$

To compensate for the effects of the disturbance forces it suffices to use in the control loop the modified control input vector

$$v = \begin{pmatrix} v_1 - \hat{\tilde{d}}_1 \\ v_2 - \hat{\tilde{d}}_2 \\ v_3 - \hat{\tilde{d}}_3 \\ v_4 - \hat{\tilde{d}}_4 \\ v_5 - \hat{\tilde{d}}_5 \\ v_6 - \hat{\tilde{d}}_6 \end{pmatrix} \text{ or } v = \begin{pmatrix} v_1 - \hat{z}_{13} \\ v_2 - \hat{z}_{16} \\ v_3 - \hat{z}_{19} \\ v_4 - \hat{z}_{22} \\ v_5 - \hat{z}_{25} \\ v_6 - \hat{z}_{28} \end{pmatrix} \tag{11.39}$$

11.2.6 Simulation Tests

The efficiency of the proposed control scheme was tested through simulation experiments. First, results are given about tracking a 3D trajectory, having as projection in the xy-plane a circular path (Fig. 11.2). Additional simulation experiments for this first trajectory tracking problem are concerned with control of the AUV under disturbance forces and torques. The estimation of the disturbance forces and torques is shown in Fig. 11.3. Moreover, as shown in Figs. 11.4, 11.5 and 11.6, flatness-based control enabled accurate tracking of the reference trajectories for both the linear position and velocity variables and for the angular position and velocity variables (blue line: real value, green line estimated value, red line: setpoint).

Next, results are given about tracking a 3D trajectory, having as projection in the xy-plane an eight-shaped path (Fig. 11.7). Additional simulation experiments for this second trajectory tracking problem are concerned again with control of the AUV under disturbance forces and torques. The estimation of the disturbance forces and

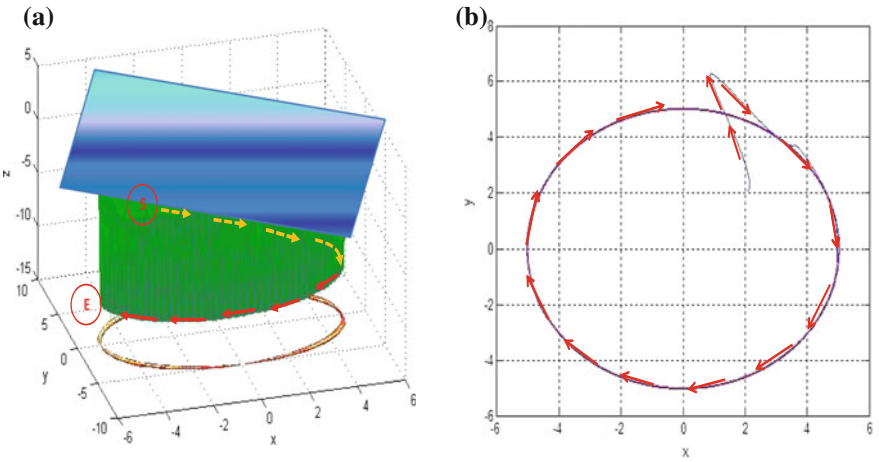

Fig. 11.2 Control of the 6-DOF AUV: **a** trajectory of the AUV in the cartesian space, **b** projection of the AUV's trajectory on the xy plane

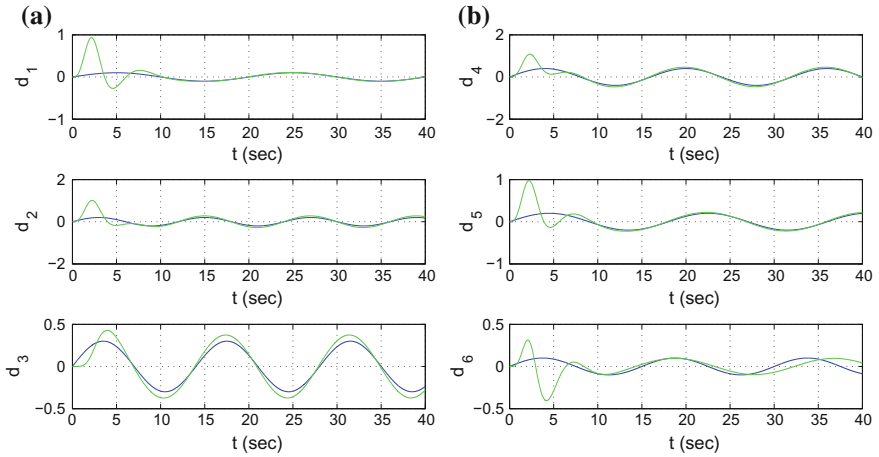

Fig. 11.3 Use of the Derivative-free nonlinear Kalman Filter in estimation of disturbances: **a** associated with linear motion, **b** associated with the rotational motion of the vehicle

torques is shown in Fig. 11.8. Moreover, as demonstrated in Figs. 11.9, 11.10 and 11.11, flatness-based control enabled accurate tracking of the reference trajectories for both the linear position and velocity variables and for the angular position and velocity variables (blue line: real value, green line estimated value, red line: setpoint).

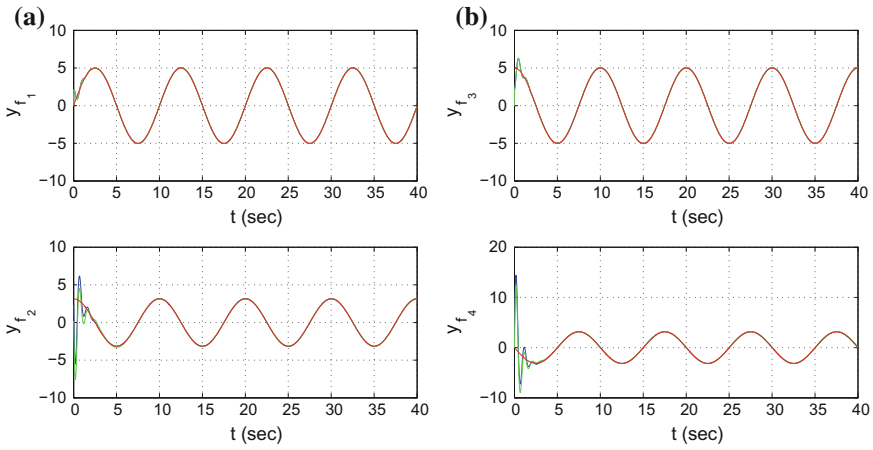

Fig. 11.4 Control of the AUV in the presence of external disturbances **a** position and velocity along the x axis, **b** position and velocity along the y axis

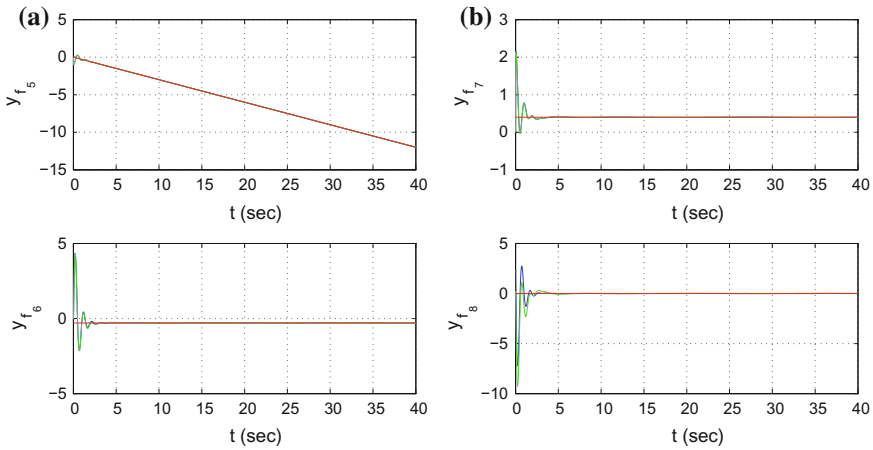

Fig. 11.5 Control of the AUV in the presence of external disturbances: **a** position and velocity along the z axis, **b** rotation angle ϕ and associated angular speed

11.3 Adaptive Fuzzy Control of Autonomous Submarines

11.3.1 Outline

Next, an adaptive control approach to the problem of control of Autonomous Underwater Vessels is presented, comprising both global linearization methods and Lyapunov stability analysis methods. The design of control systems for autonomous underwater vessels (AUVs) and submarines is a non-trivial problem because such

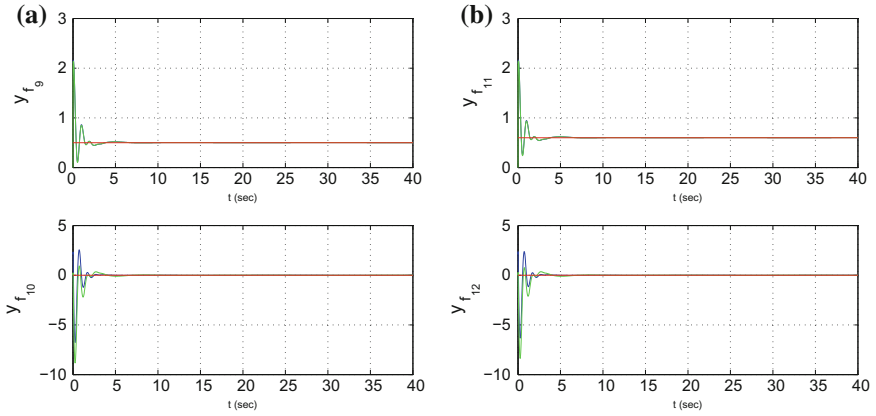

Fig. 11.6 Control of the AUV in the presence of disturbances: **a** rotation angle θ and associated angular speed, **b** rotation angle ψ and associated angular speed

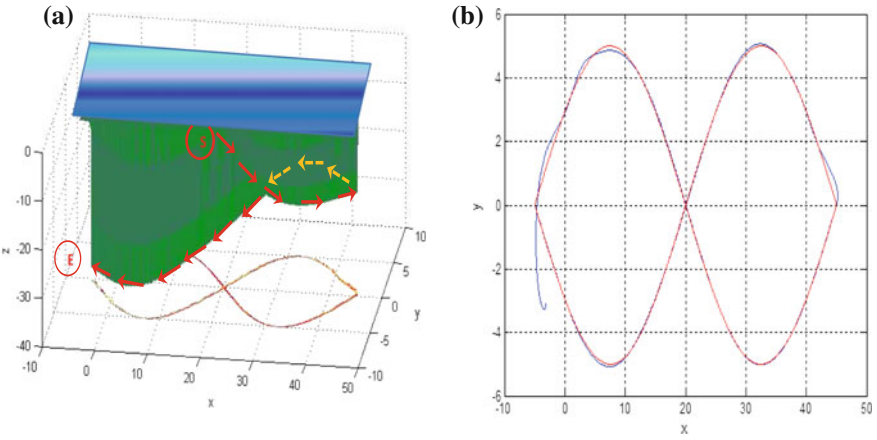

Fig. 11.7 Control of the 6-DOF AUV: **a** trajectory of the AUV in the cartesian space, **b** projection of the AUV's trajectory on the xy plane

systems exhibit a highly nonlinear multivariable dynamics with strong couplings between their inputs and outputs [128, 411, 516]. Besides, such systems function under variable conditions and thus their dynamic model is subject to parametric changes. Moreover, submersible autonomous robots and submarines are exposed to strong perturbations due to variable sea conditions and sea currents. Therefore, it is important to develop feedback control schemes for AUVs and submarines that will be little dependent on prior and exact knowledge of the associated dynamic model and will exhibit sufficient robustness to perturbation inputs [21, 143, 144, 191, 251, 386, 457, 522]. To this end, in the recent years several research results have been presented, in particular on robust control [253, 346, 518] and on adaptive control of AUVs [258, 375, 462, 635].

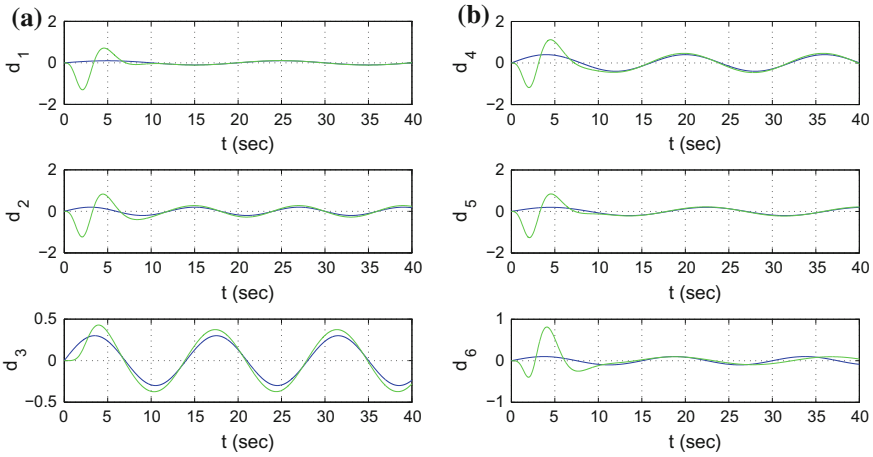

Fig. 11.8 Use of the Derivative-free nonlinear Kalman Filter in estimation of disturbances: **a** associated with linear motion, **b** associated with the rotational motion of the vehicle

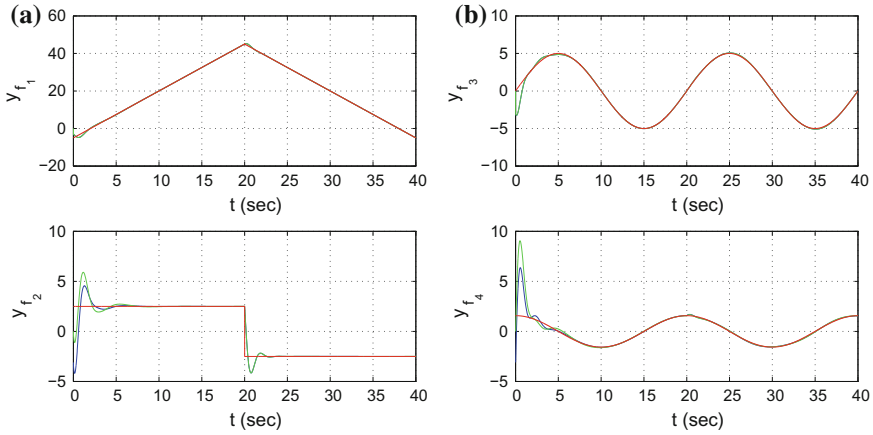

Fig. 11.9 Control of the AUV in the presence of external disturbances **a** position and velocity along the x axis, **b** position and velocity along the y axis

Adaptive fuzzy control methods can provide a solution to the problem of trajectory tracking and stabilization for autonomous submarines. As previously noted, adaptive fuzzy control schemes have been developed for unknown single-input single-output (SISO) and unknown multi-input multi-output (MIMO) dynamical systems. The capability of neurofuzzy controllers to compensate for model parametric uncertainties, external disturbances, as well as for incomplete measurement of the systems state vector has been analyzed in several studies [84, 89, 277, 524, 562]. Adaptive fuzzy control methods usually try to invert the systems dynamics, and thus to achieve convergence of its output to the desirable setpoints, starting from a description of the

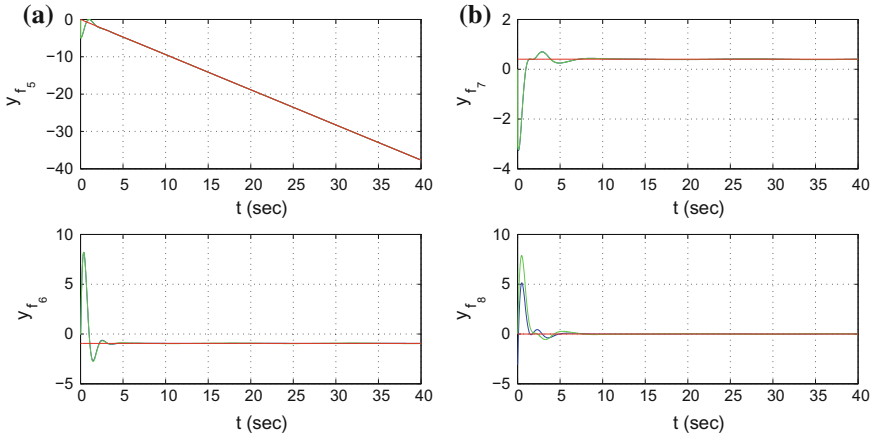

Fig. 11.10 Control of the AUV in the presence of external disturbances: **a** position and velocity along the z axis, **b** rotation angle ϕ and associated angular speed

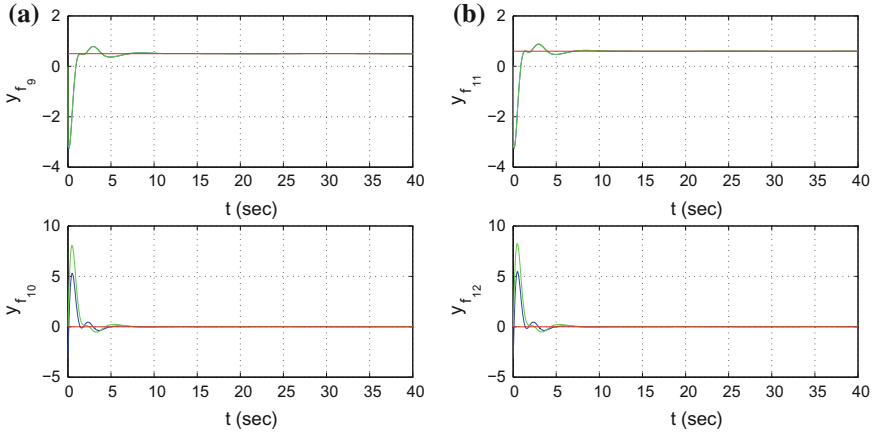

Fig. 11.11 Control of the AUV in the presence of disturbances: **a** rotation angle θ and associated angular speed, **b** rotation angle ψ and associated angular speed

system in the canonical form. On the other hand, differential flatness theory enables to transform the system's generic description $\dot{x} = f(x, u)$ into the canonical form and from that point on to develop adaptive control schemes. Consequently, differential flatness theory extends the class of nonlinear control systems to which adaptive neural / fuzzy control can be applied and this is a significant benefit for adaptive control theory [399, 457, 609, 617].

In this section, an adaptive control scheme is developed for autonomous submarines relying on differential flatness theory and on real-time identification of the unknown dynamics of the system with the use of neurofuzzy approximators

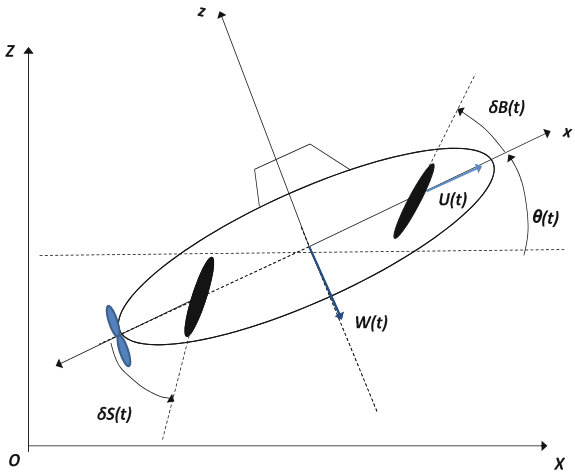

Fig. 11.12 Reference frames for the autonomous submarine

[450, 452]. First, it is proven that the dynamic model of the submersible vessel, comprising as state variables the submarine's depth and its pitch angle, is a differentially flat one. This means that all its state variables and its control inputs can be expressed as differential functions of a specific algebraic variable which is the so-called flat output. By exploiting the differential flatness properties of the submarine's model its transformation into the linear canonical (Brunovsky) form is accomplished. For the latter description of the system's dynamics the design of a MIMO state feedback controller becomes possible [57, 145, 254, 267, 322, 472, 476, 519]. In the transformed state-space model, the new control inputs of the submarine contain unknown nonlinear terms which are identified in real-time with the use of neuro-fuzzy approximators. The learning procedure for these estimators is determined by the requirement the first derivative of the closed-loop's Lyapunov function to be a negative one. Moreover, through Lyapunov stability analysis it is proven that the control system satisfies the H-infinity tracking conditions. This assures the control loop's robustness against model uncertainties and external perturbations. Finally, the efficiency of the submarine's control scheme is confirmed through simulation experiments.

11.3.2 The Dynamic Model of the Autonomous Submarine

The dive-plane nonlinear time-varying dynamic model of the submarine is considered (see. Fig. 11.12). The primary variables of this model are: (i) the diving speed along the vessel's z-axis (in a body-fixed frame), (ii) the pitch angle θ formed between the horizontal reference axis (in an inertial reference frame) and the x-axis of the vessel (in the body-fixed frame) [258].

The equations of motion of the vessel are:

Table 11.1 Parameters of the submarine's dynamic model

Parameter value	Parameter value	Parameter value
$Z_w^{'} = -0.0110$	$Z_{\dot{w}}^{'} = -0.0075$	$Z_{\theta}^{'} = -0.0045$
$Z_{\theta}^{'} = -0.0002$	$Z_{\delta B}^{'} = -0.0025$	$Z_{\delta S}^{'} = -0.0050$
$M_w^{'} = 0.0030$	$M_{\dot{w}}^{'} = -0.0002$	$M_{\theta}^{'} = -0.0025$
$M_{\dot{\theta}}^{'} = -0.0004$	$M_{\delta B}^{'} = 0.0005$	$M_{\delta S}^{'} = -0.0025$
$I_y^{'} = 5.6867{\cdot}10e^{-4}$	$L = 286$ft	$m = 1.52{\cdot}10^5$slug
$Z_g - Z_B = -1.5$ft	$U = 8.43$ft/s	$\rho = 2.0$ slug/ft^3
$I_2^{'} = I_y^{'} - M_B^{'}$	$m = 2m/(\rho L^3))$	$m_3^{'} = m^{'} - Z_w^{'}$

$$\dot{w}(t) = \frac{Z_w^{'}U}{Lm_3^{'}}w(t) + \frac{1}{m_3^{'}}\dot{Z}_{\dot{\theta}}^{'} + m^{'})U\dot{\theta}(t) + \frac{Z_{\dot{Q}}^{'}L}{m_s^{'}}\dot{Q}(t) + \\ + \frac{Z_{\delta B}^{'}U^2}{m_3^{'}L}\delta B(t) + \frac{Z_{\delta S}^{'}U^2}{m_3^{'}L}\delta S(t) + \frac{Z_d(t)}{0.5\rho L^3 m_3^{'}} + Z_{\eta}(w,q) \tag{11.40}$$

$$\dot{Q}(t) = \frac{M_{\dot{w}}^{'}}{LI_2^{'}}\dot{w}(t) + \frac{M_w^{'}U}{L^2I_2^{'}}w(t) + \frac{M_{\dot{\theta}}^{'}U}{LI_2^{'}}\dot{\theta}(t) + \\ + \frac{M_{\delta B}^{'}U^2}{L^2I_2^{'}}\delta B(t) + \frac{M_{\delta S}^{'}U^2}{L^2I_2^{'}}\delta S(t) + \frac{2mg(z_G - z_B)}{\rho L^5 I_2^{'}}\theta(t) + \frac{M_d(t)}{0.5\rho L^5 I_2^{'}} + M_{\eta}(w,q) \tag{11.41}$$

In the above dynamic model of the submarine w is the velocity along the z-axis, h is the depth of the vessel measured in the inertial coordinates system, θ is the pitch angle, $Q = \dot{\theta}$ is the rate of change of the pitch angle, δB is the hydroplane deflection in the bow plane, δS is the hydroplane deflection in the stern plane, and Z_d, M_d are bounded disturbance inputs due to sea currents. Moreover, $Z_{\eta}(w,q)$, $M_{\eta}(w,q)$ are disturbance inputs representing the vessel's cross-flow drag (the latter is a function that contains the terms $w|w|$ and $Q|Q|$, as well as higher-order terms of w and Q).

Actually, for the computation of the mathematical model of the vessel the precise knowledge of the terms $Z_{\eta}(w, Q)$ and $M_{\eta}(w, Q)$ is not necessary since they can be treated by the adaptive control scheme as disturbances. The term $U = U_0$ denotes the x-axis (forward) velocity of the vessel (Table 11.1).

The dynamic model of the submarine is completed by the following coefficients, given in Table I [258]:

The control input of the submarine's model is described by the vector

$$u = [\delta B(t)\ \delta S(t)]^T \tag{11.42}$$

that is the control input consists of the hydroplane deflections in the bow and stern planes. A first description of the vessel's dynamics in matrix form is given by

$$\begin{pmatrix} \dot{w} \\ \dot{Q} \end{pmatrix} = \begin{pmatrix} f_W(w, \theta, Q, t) \\ f_{\theta}(w, \theta, Q, t) \end{pmatrix} + B_o u \tag{11.43}$$

where

$$\begin{pmatrix} f_w(w,\theta,Q,t) \\ f_\theta(f_W(w,\theta,Q,t) \end{pmatrix} = M^{-1}\cdot$$

$$\begin{pmatrix} \frac{Z_w^{'}U}{Lm_3^{'}}w(t) + \frac{1}{m_3^{'}}\dot{Z}_{\dot\theta}^{'} + m^{'})U\dot\theta(t) + \frac{Z_{\dot Q}^{'}L}{m_s^{'}}\dot Q(t) + \frac{Z_d(t)}{0.5\rho L^3 m_3^{'}} + Z_\eta(w,q) \\ \frac{M_{\dot w}^{'}}{LI_2^{'}}\dot w(t) + \frac{M_v^{'}U}{L^2I_2^{'}}w(t) + \frac{M_{\dot\theta}^{'}U}{LI_2^{'}}\dot\theta(t) + \frac{2mg(z_G-z_B)}{\rho L^5 I_2^{'}}\theta(t) + \frac{M_d(t)}{0.5\rho L^5 I_2^{'}} + M_\eta(w,q) \end{pmatrix} \tag{11.44}$$

while for matrices M and B_o it holds

$$M = \begin{pmatrix} 1 & -Z_{\dot Q}L/m_3^{'} \\ -M_{\dot w}(LI_2^{'-1}) & 1 \end{pmatrix} B_o = \begin{pmatrix} \frac{Z_{\delta B}^{'}U^2}{m_3^{'}L} & \frac{Z_{\delta S}^{'}U^2}{m_3^{'}L} \\ \frac{M^{'}\delta BU^2}{L^2I_2^{'}} & \frac{M^{'}\delta SU^2}{L^2I_2^{'}} \end{pmatrix} \tag{11.45}$$

It holds that the depth of the vessel measured in the inertial reference frame and the velocity of the submarine along the z-axis of the body-fixed frame are related as follows:

$$\begin{gathered} \dot h = wcos(\theta) - U_o sin(\theta) \Rightarrow \\ \ddot h = \dot w cos(\theta) - wsin(\theta)\dot\theta - U_o cos(\theta)\dot\theta \Rightarrow \\ \ddot h = \dot w cos(\theta) - wQsin(\theta) - U_o Qcos(\theta) \end{gathered} \tag{11.46}$$

Moreover, solving with respect to w. from the first row of Eq. (11.46) one obtains

$$w = (cos(\theta)^{-1})(\dot h + U_o sin(\theta)) \tag{11.47}$$

Additionally, from Eq. (11.43) one gets

$$\begin{aligned} \dot w &= f_w(w,\theta,Q,t) + B_{o_{11}}u_1 + B_{o_{12}}u_2 \\ \dot Q &= f_\theta(w,\theta,Q,t) + B_{o_{21}}u_1 + B_{o_{22}}u_2 \end{aligned} \tag{11.48}$$

Substituting Eq. (11.47) and the first row of Eq. (11.48) into the third row of Eq. (11.46) gives

$$\ddot h = [f_w(w,\theta,Q,t) + B_{o11}u_1 + B_{o12}u_2]cos(\theta) - \frac{(\dot h + U_0 sin(\theta))}{cos(\theta)}Qsin(\theta) - U_0 Qcos(\theta) \tag{11.49}$$

Next by denoting

$$\begin{aligned} f_w(w,\theta,Q,t) &= g_h(h,\dot h,\theta,\dot\theta,t) \\ f_\theta(w,\theta,Q,t) &= g_\theta(h,\dot h,\theta,\dot\theta,t) \end{aligned} \tag{11.50}$$

from Eq. (11.49) and the second row of Eq. (11.48) one obtains

$$\ddot{h} = g_h(h, \dot{h}, \theta, \dot{\theta}, t)cos(\theta) - \frac{(\dot{h}+U_0 sin(\theta))}{cos(\theta)}\dot{\theta}sin(\theta) - U_0\dot{\theta}cos(\theta) + \\ +B_{0_{11}}cos(\theta)u_1 + B_{0_{12}}cos(\theta)u_2 \tag{11.51}$$

$$\ddot{\theta} = g_\theta(h, \dot{h}, \theta, \dot{\theta}, t) + B_{0_{21}}u_1 + B_{0_{22}}u_2 \tag{11.52}$$

Thus, from Eqs. (11.51) and (11.52) and by defining the state vector

$$x = [h, \dot{h}, \theta, \dot{\theta}]^T \tag{11.53}$$

the dynamic model of the submarine is written as

$$\begin{pmatrix} \ddot{x}_1 \\ \ddot{x}_3 \end{pmatrix} = \begin{pmatrix} g_b(x,t)cos(x_3) - \frac{x_4+U_0 sin(x_3)}{cos(x_3)}x_4 sin(x_3) - U_0 x_4 cos(x_3) \\ g_\theta(x,t) \end{pmatrix} + \\ + \begin{pmatrix} B_{0_{11}} & B_{0_{12}} \\ B_{0_{21}} & B_{0_{22}} \end{pmatrix} \begin{pmatrix} u_1 \\ u_2 \end{pmatrix} \tag{11.54}$$

or equivalently in the MIMO form

$$\begin{pmatrix} \ddot{x}_1 \\ \ddot{x}_3 \end{pmatrix} = \begin{pmatrix} f_1(x,t) \\ f_2(x,t) \end{pmatrix} + \begin{pmatrix} g_{11}(x,t) & g_{12}(x,t) \\ g_{21}(x,t) & g_{22}(x,t) \end{pmatrix} \begin{pmatrix} u_1 \\ u_2 \end{pmatrix} \tag{11.55}$$

11.3.3 Estimation of the Submarine's Unknown Dynamics

11.3.3.1 Differential Flatness of the Submarine's Model

It can be proven that the submarine's MIMO nonlinear model given in Eq. (11.55) is a differentially flat one, having as flat output the vector

$$y = [x_1, x_3]^T = [h, \theta]^T \tag{11.56}$$

As explained above it holds that $x_2 = \dot{x}_1$ and $x_4 = \dot{x}_3$, which also means

$$\begin{aligned} x_2 &= [1\ 0]\dot{y} \\ x_4 &= [0\ 1]\dot{y} \end{aligned} \tag{11.57}$$

Moreover, by solving Eq. (11.55) with respect to the control input u one obtains

$$\begin{pmatrix} u_1 \\ u_2 \end{pmatrix} = \begin{pmatrix} g_{11}(x) & g_{12}(x) \\ g_{21}(x) & g_{22}(x) \end{pmatrix}^{-1} \left(\begin{pmatrix} \ddot{x}_1 \\ \ddot{x}_2 \end{pmatrix} - \begin{pmatrix} f_1(x) \\ f_2(x) \end{pmatrix} \right) \tag{11.58}$$

and since the elements of the state vector x are functions of the flat output, one has $u_1 = f_a(y, \dot{y}, \ddot{y})$ and $u_2 = f_b(y, \dot{y}, \ddot{y})$. Therefore, one finally has that all elements of the submarine's state vector and the control inputs can be written as functions of the flat output and its derivatives [57, 145, 254, 267, 322, 472, 476, 519]. Consequently, the system is a differentially flat one.

By exploiting the differentially flat description of the system. the submarine's model can be written in the linear canonical (Brunovsky) form. To this end the following transformed control inputs are defined

$$\begin{aligned} v_1 &= f_1(x,t) + g_{11}u_1 + g_{12}u_2 \\ v_2 &= f_2(x,t) + g_{21}u_1 + g_{22}u_2 \end{aligned} \tag{11.59}$$

Therefore, one gets

$$\begin{pmatrix} \dot{y}_1 \\ \dot{y}_2 \\ \dot{y}_3 \\ \dot{y}_4 \end{pmatrix} = \begin{pmatrix} 0\,1\,0\,0 \\ 0\,0\,0\,0 \\ 0\,0\,0\,1 \\ 0\,0\,0\,0 \end{pmatrix} \begin{pmatrix} y_1 \\ y_2 \\ y_3 \\ y_4 \end{pmatrix} + \begin{pmatrix} 0\,0 \\ 1\,0 \\ 0\,0 \\ 0\,1 \end{pmatrix} \begin{pmatrix} v_1 \\ v_2 \end{pmatrix} \tag{11.60}$$

while it is considered that the complete state vector of the submarine $y = [h, \dot{h}, \theta, \dot{\theta}]$ is available through measurements.

11.3.3.2 Approximation of the Submarine's Unknown Dynamics

The control signal of the MIMO nonlinear system which has been transformed into the Brunovsky form as described by Eq. (11.60) contains the unknown nonlinear functions $f(x)$ and $g(x)$ which can be approximated by

$$\begin{aligned} \hat{f}(x|\theta_f) &= \Phi_f(x)\theta_f \\ \hat{g}(x|\theta_g) &= \Phi_g(x)\theta_g \end{aligned} \tag{11.61}$$

where

$$\Phi_f(x) = (\xi_f^1(x), \xi_f^2(x), \cdots \xi_f^n(x))^T \tag{11.62}$$

with $\xi_f^i(x), \imath = 1, \cdots, n$ being the vector of kernel functions (e.g. normalized fuzzy Gaussian membership functions), where

$$\xi_f^i(x) = (\phi_f^{i,1}(x), \phi_f^{i,2}(x), \cdots, \phi_f^{i,N}(x)) \tag{11.63}$$

thus giving

$$\Phi_f(x) = \begin{pmatrix} \phi_f^{1,1}(x) & \phi_f^{1,2}(x) & \cdots & \phi_f^{1,N}(x) \\ \phi_f^{2,1}(x) & \phi_f^{2,2}(x) & \cdots & \phi_f^{2,N}(x) \\ \cdots & \cdots & \cdots & \cdots \\ \phi_f^{n,1}(x) & \phi_f^{n,2}(x) & \cdots & \phi_f^{n,N}(x) \end{pmatrix} \tag{11.64}$$

while the weights vector is defined as

$$\theta_f{}^T = \left(\theta_f^1, \theta_f^2, \cdots \theta_f^N\right) \tag{11.65}$$

$j = 1, \cdots, N$ is the number of basis functions that is used to approximate the components of function f which are denoted as $i = 1, \cdots, n$. Thus, one obtains the relation of Eq. (11.61), i.e. $\hat{f}(x|\theta_f) = \Phi_f(x)\theta_f$.

In a similar manner, for the approximation of function g one has

$$\Phi_g(x) = \left(\xi_g^1(x), \xi_g^2(x), \cdots \xi_g^N(x)\right)^T \tag{11.66}$$

with $\xi_g^i(x), \imath = 1, \cdots, N$ being the vector of kernel functions (e.g. normalized fuzzy Gaussian membership functions), where

$$\xi_g^i(x) = \left(\phi_g^{i,1}(x), \phi_g^{i,2}(x), \cdots, \phi_g^{i,N}(x)\right) \tag{11.67}$$

thus giving

$$\Phi_g(x) = \begin{pmatrix} \phi_g^{1,1}(x) & \phi_g^{1,2}(x) & \cdots & \phi_g^{1,N}(x) \\ \phi_g^{2,1}(x) & \phi_g^{2,2}(x) & \cdots & \phi_g^{2,N}(x) \\ \cdots & \cdots & \cdots & \cdots \\ \phi_g^{n,1}(x) & \phi_g^{n,2}(x) & \cdots & \phi_g^{n,N}(x) \end{pmatrix} \tag{11.68}$$

while the weights vector is defined as

$$\theta_g = \left(\theta_g^1, \theta_g^2, \cdots, \theta_g^p\right)^T \tag{11.69}$$

where the components of matrix θ_g are defined as

$$\theta_g^j = \left(\theta_{g_1}^j, \theta_{g_2}^j, \cdots \theta_{g_N}^j\right) \tag{11.70}$$

$j = 1, \cdots, N$ is the number of basis functions that is used to approximate the components of function g which are denoted as $i = 1, \cdots, n$. Thus one obtains about matrix $\theta_g \in R^{N \times p}$

$$\theta_g = \begin{pmatrix} \theta_{g_1}^1 & \theta_{g_1}^2 & \cdots & \theta_{g_1}^p \\ \theta_{g_2}^1 & \theta_{g_2}^2 & \cdots & \theta_{g_2}^p \\ \cdots & \cdots & \cdots & \cdots \\ \theta_{g_N}^1 & \theta_{g_N}^2 & \cdots & \theta_{g_N}^p \end{pmatrix} \tag{11.71}$$

It holds that

$$g = \begin{pmatrix} g_1 \\ g_2 \\ \cdots \\ g_n \end{pmatrix} = \begin{pmatrix} g_1^1 & g_1^2 & \cdots & g_1^p \\ g_2^1 & g_2^2 & \cdots & g_2^p \\ \cdots & \cdots & \cdots & \cdots \\ g_n^1 & g_n^2 & \cdots & g_n^p \end{pmatrix} \tag{11.72}$$

Using the above, one finally has the relation of Eq. (11.61), i.e. $\hat{g}(x|\theta_g) = \Phi_g(x)\theta_g$. If the state variables of the system are available for measurement then a state-feedback control law can be formulated as

$$u = \hat{g}^{-1}(x|\theta_g)[-\hat{f}(x|\theta_f) + y_m^{(r)} - K^T e + u_c] \tag{11.73}$$

where $\hat{f}(x|\theta_f)$ and $\hat{g}(x|\theta_g)$ are fuzzy models to approximate $f(x)$ and $g(x)$, respectively. u_c is a supervisory control term, e.g. H_∞ control term that is used to compensate for the effects of modelling inaccuracies and external disturbances. Using the submarine's state-space description of Eq. (11.60) the control term u_c is defined as

$$u_c = -\tfrac{1}{r} B^T P e \tag{11.74}$$

Moreover, K^T is the feedback gain matrix that assures that the characteristic polynomial of the resulting closed-loop dynamics will be a Hurwitz one.

11.3.4 Flatness-Based Adaptive Fuzzy Control of the Submarine Dynamics

Next, taking into account also the effects of additive disturbances to the submarine the dynamic model of Eq. (11.55) becomes

$$\begin{aligned} \ddot{x}_1 &= f_1(x,t) + g_1(x,t)u + \tilde{d}_1 \\ \ddot{x}_3 &= f_2(x,t) + g_2(x,t)u + \tilde{d}_2 \end{aligned} \tag{11.75}$$

or, in matrix form

$$\begin{pmatrix} \ddot{x}_1 \\ \ddot{x}_3 \end{pmatrix} = \begin{pmatrix} f_1(x,t) \\ f_2(x,t) \end{pmatrix} + \begin{pmatrix} g_1(x,t) \\ g_2(x,t) \end{pmatrix} u + \begin{pmatrix} \tilde{d}_1 \\ \tilde{d}_2 \end{pmatrix} \tag{11.76}$$

The following control input is defined

$$u = \begin{pmatrix} \hat{g}_1(x,t) \\ \hat{g}_2(x,t) \end{pmatrix}^{-1} \cdot \{ \begin{pmatrix} \ddot{x}_1^d \\ \ddot{x}_3^d \end{pmatrix} - \begin{pmatrix} \hat{f}_1(x,t) \\ \hat{f}_2(x,t) \end{pmatrix} - \begin{pmatrix} K_1^T \\ K_2^T \end{pmatrix} e + \begin{pmatrix} u_{c_1} \\ u_{c_2} \end{pmatrix} \} \tag{11.77}$$

where $[u_{c_1}\ u_{c_2}]^T$ is a robust control term that is used for the compensation of the model's uncertainties as well as of the external disturbances and the vector of the feedback gain is $K_i^T = [k_1^i, k_2^i, \cdots, k_{n-1}^i, k_n^i]$.

Substituting Eqs. (11.77) into (11.76) the closed-loop tracking error dynamics of the submarine is obtained

$$\begin{pmatrix} \ddot{x}_1 \\ \ddot{x}_3 \end{pmatrix} = \begin{pmatrix} f_1(x,t) \\ f_2(x,t) \end{pmatrix} + \begin{pmatrix} g_1(x,t) \\ g_2(x,t) \end{pmatrix} \begin{pmatrix} \hat{g}_1(x,t) \\ \hat{g}_2(x,t) \end{pmatrix}^{-1} \cdot \{ \begin{pmatrix} \ddot{x}_1^d \\ \ddot{x}_3^d \end{pmatrix} - \begin{pmatrix} \hat{f}_1(x,t) \\ \hat{f}_2(x,t) \end{pmatrix} - \begin{pmatrix} K_1^T \\ K_2^T \end{pmatrix} e + \begin{pmatrix} u_{c_1} \\ u_{c_2} \end{pmatrix} \} + \begin{pmatrix} \tilde{d}_1 \\ \tilde{d}_2 \end{pmatrix} \tag{11.78}$$

Equation (11.78) can now be written as

$$\begin{pmatrix} \ddot{x}_1 \\ \ddot{x}_3 \end{pmatrix} = \begin{pmatrix} f_1(x,t) \\ f_2(x,t) \end{pmatrix} + \\ + \{ \begin{pmatrix} g_1(x,t) - \hat{g}_1(x,t) \\ g_2(x,t) - \hat{g}_2(x,t) \end{pmatrix} + \begin{pmatrix} \hat{g}_1(x,t) \\ \hat{g}_2(x,t) \end{pmatrix} \} \begin{pmatrix} \hat{g}_1(x,t) \\ \hat{g}_2(x,t) \end{pmatrix}^{-1} \cdot \\ \cdot \{ \begin{pmatrix} \ddot{x}_1^d \\ \ddot{x}_3^d \end{pmatrix} - \begin{pmatrix} \hat{f}_1(x,t) \\ \hat{f}_2(x,t) \end{pmatrix} - \begin{pmatrix} K_1^T \\ K_2^T \end{pmatrix} e + \begin{pmatrix} u_{c_1} \\ u_{c_2} \end{pmatrix} \} + \begin{pmatrix} \tilde{d}_1 \\ \tilde{d}_2 \end{pmatrix} \tag{11.79}$$

and using Eq. (11.77) this results into

$$\begin{pmatrix} \ddot{e}_1 \\ \ddot{e}_3 \end{pmatrix} = \begin{pmatrix} f_1(x,t) - \hat{f}_1(x,t) \\ f_2(x,t) - \hat{f}_2(x,t) \end{pmatrix} + \begin{pmatrix} g_1(x,t) - \hat{g}_1(x,t) \\ g_2(x,t) - \hat{g}_2(x,t) \end{pmatrix} u - \\ - \begin{pmatrix} K_1^T \\ K_2^T \end{pmatrix} e + \begin{pmatrix} u_{c_1} \\ u_{c_2} \end{pmatrix} + \begin{pmatrix} \tilde{d}_1 \\ \tilde{d}_2 \end{pmatrix} \tag{11.80}$$

The following description for the approximation error is defined

$$w = \begin{pmatrix} f_1(x,t) - \hat{f}_1(x,t) \\ f_2(x,t) - \hat{f}_2(x,t) \end{pmatrix} + \begin{pmatrix} g_1(x,t) - \hat{g}_1(x,t) \\ g_2(x,t) - \hat{g}_2(x,t) \end{pmatrix} u \tag{11.81}$$

Moreover, the following matrices are defined

$$A = \begin{pmatrix} 0\ 1\ 0\ 0 \\ 0\ 0\ 0\ 0 \\ 0\ 0\ 0\ 1 \\ 0\ 0\ 0\ 0 \end{pmatrix}, \quad B = \begin{pmatrix} 0\ 0 \\ 1\ 0 \\ 0\ 0 \\ 0\ 1 \end{pmatrix} \tag{11.82}$$

$$K^T = \begin{pmatrix} K_1^1 & K_2^1 & K_3^1 & K_4^1 \\ K_1^2 & K_2^2 & K_3^2 & K_4^2 \end{pmatrix}$$

Using matrices A, B, K^T, Eq. (11.80) is written in the following form

$$\begin{aligned} \dot{e} = (A - BK^T)e + Bu_c + B\{\begin{pmatrix} f_1(x,t) - \hat{f}_1(x,t) \\ f_2(x,t) - \hat{f}_2(x,t) \end{pmatrix} + \\ + \begin{pmatrix} g_1(x,t) - \hat{g}_1(x,t) \\ g_2(x,t) - \hat{g}_2(x,t) \end{pmatrix} u + \tilde{d}\} \end{aligned} \tag{11.83}$$

Next, the following approximators of the unknown system dynamics are defined

$$\hat{f}(x) = \begin{pmatrix} \hat{f}_1(x|\theta_f)\ x \in R^{4\times 1}\ \hat{f}_1(x|\theta_f) \in R^{1\times 1} \\ \hat{f}_2(x|\theta_f)\ x \in R^{4\times 1}\ \hat{f}_2(x|\theta_f) \in R^{1\times 1} \end{pmatrix} \tag{11.84}$$

with kernel functions

$$\phi_f^{i,j}(x) = \frac{\prod_{j=1}^{n} \mu_{A_j^i}(x_j)}{\sum_{i=1}^{N} \prod_{j=1}^{n} \mu_{A_j^i}(x_j)} \tag{11.85}$$

where $l = 1, 2$ and $\mu_{A_j^i}(x)$ is the i-th membership function of the antecedent (IF) part of the l-th fuzzy rule. Similarly, the following approximators of the unknown system dynamics are defined

$$\hat{g}(x) = \begin{pmatrix} \hat{g}_1(x|\theta_g)\ x \in R^{4\times 1}\ \hat{g}_1(x|\theta_g) \in R^{1\times 2} \\ \hat{g}_2(x|\theta_g)\ x \in R^{4\times 1}\ \hat{g}_2(x|\theta_g) \in R^{1\times 2} \end{pmatrix} \tag{11.86}$$

The values of the weights that result in optimal approximation are

$$\begin{aligned} \theta_f^* &= arg\ min_{\theta_f \in M_{\theta_f}} [sup_{x \in U_x} (f(x) - \hat{f}(x|\theta_f))] \\ \theta_g^* &= arg\ min_{\theta_g \in M_{\theta_g}} [sup_{x \in U_x} (g(x) - \hat{g}(x|\theta_g))] \end{aligned} \tag{11.87}$$

where the variation ranges for the weights are defined as

$$\begin{aligned} M_{\theta_f} &= \{\theta_f \in R^h : ||\theta_f|| \leq m_{\theta_f}\} \\ M_{\theta_g} &= \{\theta_g \in R^h : ||\theta_g|| \leq m_{\theta_g}\} \end{aligned} \tag{11.88}$$

For the value of the approximation error defined in Eq. (11.81) that corresponds to the optimal values of the weights vectors θ_f^* and θ_g^* one has

$$w = \left(f(x,t) - \hat{f}(x|\theta_f^*)\right) + \left(g(x,t) - \hat{g}(x|\theta_g^*)\right) u \tag{11.89}$$

which is next written as

$$\begin{aligned} w = &\left(f(x,t) - \hat{f}(x|\theta_f) + \hat{f}(x|\theta_f) - \hat{f}(x|\theta_f^*)\right) + \\ &+ \left(g(x,t) - \hat{g}(x|\theta_g) + \hat{g}(x|\theta_g) - \hat{g}(x|\theta_g^*)\right) u \end{aligned} \tag{11.90}$$

which can be also written in the following form

$$w = \left(w_a + w_b\right) \tag{11.91}$$

where

$$w_a = \{[\hat{f}(x,\theta_f) - \hat{f}(x|\theta_f^*)] + [\hat{g}(x,\theta_g) - \hat{g}(x|\theta_g^*)]\} \cdot u \tag{11.92}$$

$$w_b = \{[f(x,t) - \hat{f}(x|\theta_f)] + [g(x,t) - \hat{g}(x|\theta_g)]\} u \tag{11.93}$$

Moreover, the following weights error vectors are defined

$$\begin{aligned} \tilde{\theta}_f &= \theta_f - \theta_f^* \\ \tilde{\theta}_g &= \theta_g - \theta_g^* \end{aligned} \tag{11.94}$$

Following the previous analysis it is pointed out that the use of differential flatness theory enables to solve the problem of control of the nonlinear dynamics of the autonomous submarine in a conclusive manner: (i) by showing that a dynamical system is differentially flat it is possible to express its dynamics through specific primary variables which are the so-called flat outputs. All state variables of the system can be written as differential functions of the flat outputs, (ii) by showing that a dynamical system is differentially flat it can be assured that its transformation to the linear canonical (Brunovsky) form can be achieved, (iii) by expressing a differentially flat system into its equivalent linearized form the design of a state feedback controller for it can be completed in a few stages.

11.3.5 Lyapunov Stability Analysis

The following quadratic Lyapunov function is defined for the control loop of the autonomous submarine

$$V = \frac{1}{2} e^T P e + \frac{1}{2\gamma_1} \tilde{\theta}_f^T \tilde{\theta}_f + \frac{1}{2\gamma_2} tr[\tilde{\theta}_g^T \tilde{\theta}_g] \tag{11.95}$$

Parameter γ_1 is the learning rate used in the adaptation of the weights of the neurofuzzy approximator for $f(x)$, while parameter γ_2 is the learning rate used in the adaptation of the weights of the neurofuzzy approximation for $g(x)$. It holds that

$$\dot{V} = \tfrac{1}{2}\dot{e}^T P e + \tfrac{1}{2} e^T P \dot{e} + \tfrac{1}{\gamma_1}\dot{\tilde{\theta}}_f^T \tilde{\theta}_f + \tfrac{1}{\gamma_2} tr[\dot{\tilde{\theta}}_g^T \tilde{\theta}_g] \tag{11.96}$$

The tracking error dynamics is described by

$$\begin{aligned} \dot{e} = (A - BK^T)e + Bu_c + B\{\begin{pmatrix} f_1(x,t) - \hat{f}_1(x,t) \\ f_2(x,t) - \hat{f}_2(x,t) \end{pmatrix}\}+ \\ + \begin{pmatrix} g_1(x,t) - \hat{g}_1(x,t) \\ g_2(x,t) - \hat{g}_2(x,t) \end{pmatrix} u + \tilde{d}\} \end{aligned} \tag{11.97}$$

and defining the approximation error

$$w = \begin{pmatrix} f_1(x,t) - \hat{f}_1(x,t) \\ f_2(x,t) - \hat{f}_2(x,t) \end{pmatrix} + \begin{pmatrix} g_1(x,t) - \hat{g}_1(x,t) \\ g_2(x,t) - \hat{g}_2(x,t) \end{pmatrix} u \tag{11.98}$$

the previous relation can be also written as

$$\dot{e} = (A - BK^T)e + Bu_c + B(w + \tilde{d}) \tag{11.99}$$

From Eq. (11.96) one obtains

$$\begin{aligned} \dot{V} = \tfrac{1}{2}\{e^T(A - BK^T)^T + u_c^T B^T + \\ +(w + \tilde{d})^T B^T\} P e + \tfrac{1}{2} e^T P\{(A - BK^T)e + \\ + Bu_c + B(w + \tilde{d})\} + \tfrac{1}{\gamma_1}\dot{\tilde{\theta}}_f^T \tilde{\theta}_f + \tfrac{1}{\gamma_2} tr[\dot{\tilde{\theta}}_g^T \tilde{\theta}_g] \end{aligned} \tag{11.100}$$

which in turn gives

$$\begin{aligned} \dot{V} = \tfrac{1}{2} e^T\{(A - BK^T)^T P + P(A - BK^T)\}e + \\ \tfrac{1}{2} 2 e^T P B u_c + \tfrac{1}{2} 2 B^T P e(w + \tilde{d}) + \\ + \tfrac{1}{\gamma_1}\dot{\tilde{\theta}}_f^T \tilde{\theta}_f + \tfrac{1}{\gamma_2} tr[\dot{\tilde{\theta}}_g^T \tilde{\theta}_g] \end{aligned} \tag{11.101}$$

Assumption 1: For given positive definite matrix Q there exists a positive definite matrix P, which is the solution of the following matrix equation

$$\begin{aligned} (A - BK^T)^T P + P(A - BK^T) - \\ - PB(\tfrac{2}{r} - \tfrac{1}{\rho^2}) B^T P + Q = 0 \end{aligned} \tag{11.102}$$

Substituting Eqs. (11.102) and (11.74) into $\dot{V}$ yields after some operations

$$\begin{gathered}\dot{V}=\tfrac{1}{2}e^{T}\{-Q+PB(\tfrac{2}{r}-\tfrac{1}{\rho^{2}})B^{T}P\}e+\\ e^{T}PB\{-\tfrac{1}{r}B^{T}Pe\}+B^{T}P(w+\tilde{d})+\tfrac{1}{\gamma_{1}}\dot{\tilde{\theta}}_{f}^{T}\tilde{\theta}_{f}+\tfrac{1}{\gamma_{2}}tr[\dot{\tilde{\theta}}_{g}^{T}\tilde{\theta}_{g}]\end{gathered}\tag{11.103}$$

Therefore it holds

$$\begin{gathered}\dot{V}=-\tfrac{1}{2}e^{T}Qe-\tfrac{1}{2\rho^{2}}e^{T}PBB^{T}Pe+e^{T}PB(w+\tilde{d})+\\ \tfrac{1}{\gamma_{1}}\tilde{\theta}_{f}^{T}\tilde{\theta}_{f}+\tfrac{1}{\gamma_{2}}tr[\dot{\tilde{\theta}}_{g}^{T}\tilde{\theta}_{g}]\end{gathered}\tag{11.104}$$

It also holds that

$$\begin{gathered}\dot{\tilde{\theta}}_{f}=\dot{\theta}_{f}-\dot{\theta}_{f}^{*}=\dot{\theta}_{f}\\ \dot{\tilde{\theta}}_{g}=\dot{\theta}_{g}-\dot{\theta}_{g}^{*}=\dot{\theta}_{g}\end{gathered}\tag{11.105}$$

The following weights adaptation law is used (Fig. 11.13)

$$\begin{gathered}\dot{\theta}_{f}=-\gamma_{1}\Phi(x)^{T}B^{T}Pe\\ \dot{\theta}_{g}=-\gamma_{2}\Phi(x)^{T}B^{T}Peu^{T}\end{gathered}\tag{11.106}$$

This is a gradient-type learning method for the weights of the neurofuzzy approximators [33, 431, 463]. Assuming N fuzzy rules and associated kernel functions the matrices dimensions are $\theta_{f}\in R^{N\times 1}$, $\theta_{g}\in R^{N\times 2}$, $\Phi(x)\in R^{2\times N}$, $B\in R^{4\times 2}$, $P\in R^{4\times 4}$ and $e\in R^{4\times 1}$. Therefore it holds

$$\begin{gathered}\dot{V}=-\tfrac{1}{2}e^{T}Qe-\tfrac{1}{2\rho^{2}}e^{T}PBB^{T}Pe+e^{T}PB(w+\tilde{d})+\\ +\tfrac{1}{\gamma_{1}}(-\gamma_{1})e^{T}PB\Phi(x)(\theta_{f}-\theta_{f}^{*})+\\ +\tfrac{1}{\gamma_{2}}(-\gamma_{2})tr[ue^{T}PB\Phi(x)(\theta_{g}-\theta_{g}^{*})]\end{gathered}\tag{11.107}$$

or

$$\begin{gathered}\dot{V}=-\tfrac{1}{2}e^{T}Qe-\tfrac{1}{2\rho^{2}}e^{T}PBB^{T}Pe+e^{T}PB(w+\tilde{d})+\\ +\tfrac{1}{\gamma_{1}}(-\gamma_{1})e^{T}PB\Phi(x)(\theta_{f}-\theta_{f}^{*})+\\ +\tfrac{1}{\gamma_{2}}(-\gamma_{2})tr[ue^{T}PB(\hat{g}(x|\theta_{g})-\hat{g}(x|\theta_{g}^{*})]\end{gathered}\tag{11.108}$$

Taking into account that $u\in R^{2\times 1}$ and $e^{T}PB(\hat{g}(x|\theta_{g})-\hat{g}(x|\theta_{g}^{*}))\in R^{1\times 2}$ it holds

$$\begin{gathered}\dot{V}=-\tfrac{1}{2}e^{T}Qe-\tfrac{1}{2\rho^{2}}e^{T}PBB^{T}Pe+e^{T}PB(w+\tilde{d})+\\ +\tfrac{1}{\gamma_{1}}(-\gamma_{1})e^{T}PB\Phi(x)(\theta_{f}-\theta_{f}^{*})+\\ +\tfrac{1}{\gamma_{2}}(-\gamma_{2})tr[e^{T}PB(\hat{g}(x|\theta_{g})-\hat{g}(x|\theta_{g}^{*}))u]\end{gathered}\tag{11.109}$$

Since $e^{T}PB(\hat{g}(x|\theta_{g})-\hat{g}(x|\theta_{g}^{*}))u\in R^{1\times 1}$ it holds

$$\begin{gathered}tr(e^{T}PB(\hat{g}(x|\theta_{g})-\hat{g}(x|\theta_{g}^{*})u)=\\ =e^{T}PB(\hat{g}(x|\theta_{g})-\hat{g}(x|\theta_{g}^{*}))u\end{gathered}\tag{11.110}$$

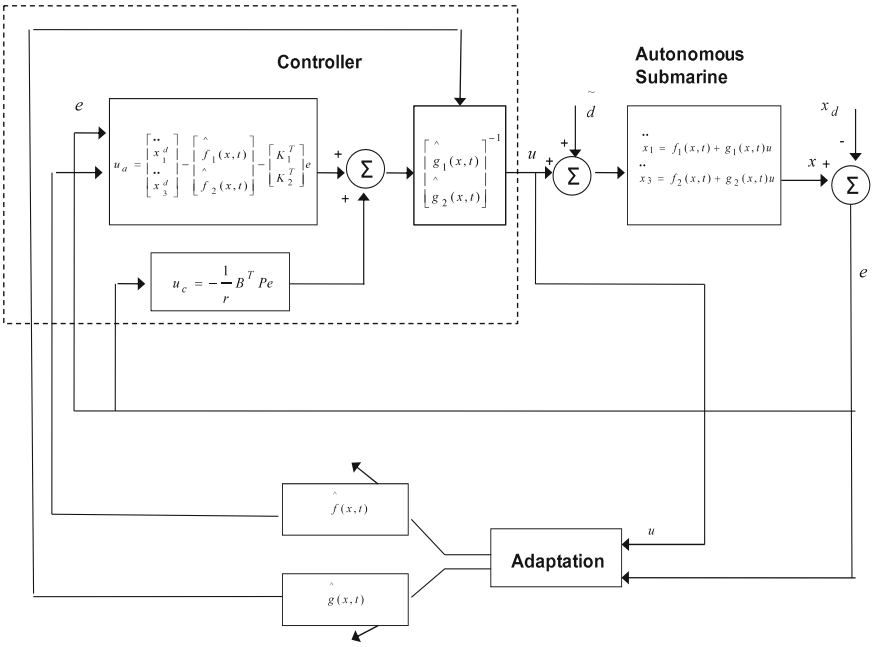

Fig. 11.13 Diagram of the flatness-based adaptive fuzzy controller for the autonomous submarine

Therefore, one finally obtains

$$\begin{aligned}\dot{V} = &-\tfrac{1}{2}e^T Q e - \tfrac{1}{2\rho^2} e^T P B B^T P e + e^T P B(w + \tilde{d}) + \\ &+\tfrac{1}{\gamma_1}(-\gamma_1) e^T P B \Phi(x)(\theta_f - \theta_f^*) + \\ &+\tfrac{1}{\gamma_2}(-\gamma_2) e^T P B(\hat{g}(x|\theta_g) - \hat{g}(x|\theta_g^*))u\end{aligned} \tag{11.111}$$

Next the following approximation error is defined

$$w_\alpha = [\hat{f}(x|\theta_f) - \hat{f}(x|\theta_f^*)] + [\hat{g}(x|\theta_g) - \hat{g}(x|\theta_g^*)]u \tag{11.112}$$

Thus, one obtains

$$\begin{aligned}\dot{V} = &-\tfrac{1}{2}e^T Q e - \tfrac{1}{2\rho^2} e^T P B B^T P e + \\ &+e^T P B(w + \tilde{d}) + e^T P B w_\alpha\end{aligned} \tag{11.113}$$

Denoting the aggregate approximation error and disturbances vector as

$$w_1 = w + \tilde{d} + w_\alpha \tag{11.114}$$

the derivative of the Lyapunov function becomes

$$\dot{V} = -\frac{1}{2}e^T Qe - \frac{1}{2\rho^2}e^T PBB^T Pe + e^T PBw_1 \tag{11.115}$$

which in turn is written as

$$\begin{aligned}\dot{V} = -\frac{1}{2}e^T Qe - \frac{1}{2\rho^2}e^T PBB^T Pe + \\ +\frac{1}{2}e^T PBw_1 + \frac{1}{2}w_1^T B^T Pe\end{aligned} \tag{11.116}$$

Next, the following Lemma is introduced:

Lemma: The inequality given below holds:

$$\frac{1}{2}e^T PBw_1 + \frac{1}{2}w_1^T B^T Pe - \frac{1}{2\rho^2}e^T PBB^T Pe \leq \frac{1}{2}\rho^2 w_1^T w_1 \tag{11.117}$$

Proof: The binomial $(\rho a - \frac{1}{\rho}b)^2 \geq 0$ is considered. Expanding the left part of the above inequality one gets

$$\begin{aligned}\rho^2 a^2 + \frac{1}{\rho^2}b^2 - 2ab \geq 0 \Rightarrow \frac{1}{2}\rho^2 a^2 + \frac{1}{2\rho^2}b^2 - ab \geq 0 \Rightarrow \\ ab - \frac{1}{2\rho^2}b^2 \leq \frac{1}{2}\rho^2 a^2 \Rightarrow \frac{1}{2}ab + \frac{1}{2}ab - \frac{1}{2\rho^2}b^2 \leq \frac{1}{2}\rho^2 a^2\end{aligned} \tag{11.118}$$

The following substitutions are carried out: $a = w_1$ and $b = e^T PB$ and the previous relation becomes

$$\frac{1}{2}w_1^T B^T Pe + \frac{1}{2}e^T PBw_1 - \frac{1}{2\rho^2}e^T PBB^T Pe \leq \frac{1}{2}\rho^2 w_1^T w_1 \tag{11.119}$$

The previous inequality is used in $\dot{V}$, and the right part of the associated inequality is enforced

$$\dot{V} \leq -\frac{1}{2}e^T Qe + \frac{1}{2}\rho^2 w_1^T w_1 \tag{11.120}$$

The attenuation coefficient ρ can be chosen such that the right part of Eq. (11.120) is always upper bounded by 0. For instance, it suffices at every iteration of the control algorithm to have

$$\begin{aligned}-\frac{1}{2}e^T Qe + \frac{1}{2}\rho^2 ||w_1||^2 \leq 0 \Rightarrow -\frac{1}{2}||e||_Q^2 + \frac{1}{2}\rho^2 ||w_1||^2 \leq 0 \Rightarrow \\ \frac{1}{2}\rho^2 ||w_1||^2 \leq \frac{1}{2}||e||_Q^2 + \Rightarrow \rho^2 \leq \frac{||e||_Q^2}{||w_1||^2}\end{aligned} \tag{11.121}$$

Again without knowledge of the uncertainties and disturbance term $||w_1||$ a sufficiently small value of ρ can assure that the above inequality holds and thus that the loop's stability is ascertained. Actually, ρ should be given the least value which permits to obtain a solution of the Riccati equation, given in Eq. (11.102).

Equation (11.120) can be used to show that the H_∞ performance criterion is satisfied. The integration of $\dot{V}$ from 0 to T gives

$$\begin{aligned} &\int_0^T \dot{V}(t)dt \leq -\tfrac{1}{2}\int_0^T ||e||^2 dt + \tfrac{1}{2}\rho^2 \int_0^T ||w_1||^2 dt \Rightarrow \\ &2V(T) + \int_0^T ||e||_Q^2 dt \leq 2V(0) + \rho^2 \int_0^T ||w_1||^2 dt \end{aligned} \tag{11.122}$$

Moreover, if there exists a positive constant $M_w > 0$ such that

$$\int_0^\infty ||w_1||^2 dt \leq M_w \tag{11.123}$$

then one gets

$$\int_0^\infty ||e||_Q^2 dt \leq 2V(0) + \rho^2 M_w \tag{11.124}$$

Thus, the integral $\int_0^\infty ||e||_Q^2 dt$ is bounded and according to Barbalat's Lemma one obtains $lim_{t\to\infty} e(t) = 0$.

It is of worth mentioning that in case that the complete state vector of the submarine is not completely measurable one can implement an observer-based adaptive fuzzy control scheme based on differential flatness theory. The observer-based adaptive fuzzy control, making use of differential flatness theory, extends the class of systems to which indirect adaptive fuzzy control can be applied. This control method enables control of MIMO nonlinear systems without the need to measure all state vector elements [454]. The only assumption needed for the design of the observer-based controller and for succeeding H-infinity tracking performance for the control loop is that there exists a solution for two Riccati equations associated with the linearized error dynamics of the differentially flat model. This assumption holds for several nonlinear systems, thus providing a systematic approach to the design of observer-based controllers.

11.3.6 Simulation Tests

The results about the stability and robustness features of the submarine's control loop were also confirmed through simulation experiments. In the simulation tests, the dynamic model of the submarine was considered to be completely unknown and was identified in real-time by the previously analyzed neurofuzzy approximators. The estimated unknown dynamics of the system was used in the computation of the control inputs which were finally exerted on the submarine's model. The sampling period was set to $T_s = 0.01sec$. Apart from modelling uncertainty it was considered that the submarine's model was also affected by external perturbations. The numerical values of the gains which have been used in the solution of the Riccati equation have been defined as $r = 0.1$ and $\rho = 1.0$.

The state feedback gain was $K \in R^{2\times 4}$. The basis functions used in the estimation of $f_i(x,t),\ i = 1,2$ and $g_{ij}(x,t),\ i = 1,2,\ j = 1,2$ were $\mu_{A_j}(\hat{x}) = e^{(\frac{\hat{x}-c_j}{\sigma})^2},\ j = 1,\cdots,3$. Since there are four inputs x_1, x_2 and x_4, x_4 and the associated definition set

Table 11.2 Parameters of the fuzzy rule base

Rule	$c_1^{(l)}$	$c_2^{(l)}$	$c_3^{(l)}$	$c_4^{(l)}$	$v^{(l)}$
$R^{(1)}$	−1.0	−1.0	−1.0	−1.0	3
$R^{(2)}$	−1.0	−1.0	−1.0	0.0	3
$R^{(3)}$	−1.0	−1.0	−1.0	1.0	3
$R^{(4)}$	−1.0	−1.0	0.0	−1.0	3
$R^{(5)}$	−1.0	−1.0	0.0	0.0	3
$R^{(6)}$	−1.0	−1.0	0.0	1.0	3
...	...	...	...	...	...
...	...	...	...	...	...
$R^{(81)}$	1.0	1.0	1.0	0.5	3

(universe of discourse) consists of 3 fuzzy sets, for the approximation of functions $f_i(x,t)\ i=1,2$, there will be 81 fuzzy rules of the form:

$$\begin{aligned} &R^l: IF\ \ x_1\ \ is\ \ A_1^l\ \ AND\ \ x_2\ \ is\ \ A_2^l \\ &AND\ \ x_3\ \ is\ \ A_3^l\ \ AND\ \ x_4\ \ is\ \ A_4^l\ \ THEN\ \ \hat{f}_i^l\ \ is\ \ b^l \end{aligned} \tag{11.125}$$

and $\hat{f}_i(x,t) = \frac{\sum_{l=1}^{81} \hat{f}_i^l \prod_{i=1}^{4} \mu_{A_i^l}(x_i)}{\sum_{l=1}^{81} \prod_{i=1}^{4} \mu_{A_i^l}(x_i)}$. Indicative (dimensionless) values for the placement on a spatial grid of the centers $c_i^{(l)},\ i=1,\cdots,4$ and the variances $v^{(l)}$ of each rule are as follows (Table 11.2).

As noted, in the considered fuzzy rule-base there are four input parameters in the antecedent parts of the fuzzy rules, i.e. $x_1 = h$, $x_2 = \dot{h}$, $x_3 = \theta$ and $x_4 = \dot{\theta}$. Each parameter is partitioned into 3 fuzzy sets. Therefore, by taking all possible combinations between the fuzzy sets one has $3^4 = 81$ fuzzy rules. The finer the partition of the input variables into fuzzy sets is, the more accurate the approximation of the nonlinear system dynamics by the neuro-fuzzy model is expected to be (although some of the rules of the fuzzy rule base may not be sufficiently activated due to little coverage of the associated region of the state-space by input data). However, considering a large number of fuzzy sets for each input variable induces the curse of dimensionality which means that there is an excessive and rather unnecessary increase in the number of the adaptable parameters that constitute the neuro-fuzzy model.

The associated results are presented in Figs. 11.14, 11.15 and 11.16. It can be observed that the adaptive fuzzy control scheme achieved fast and accurate tracking of the reference setpoints. After finding the solution of the algebraic Riccati equation given in Eq. (11.102) the computation of an H-infinity feedback control term was possible and this provided the submarine's control loop with additional robustness. Taking into account that in real operating conditions the control of a submarine cannot rely on the assumption about a precise mathematical model and about complete knowledge of external perturbations, the significance of the proposed adaptive fuzzy control scheme becomes obvious.

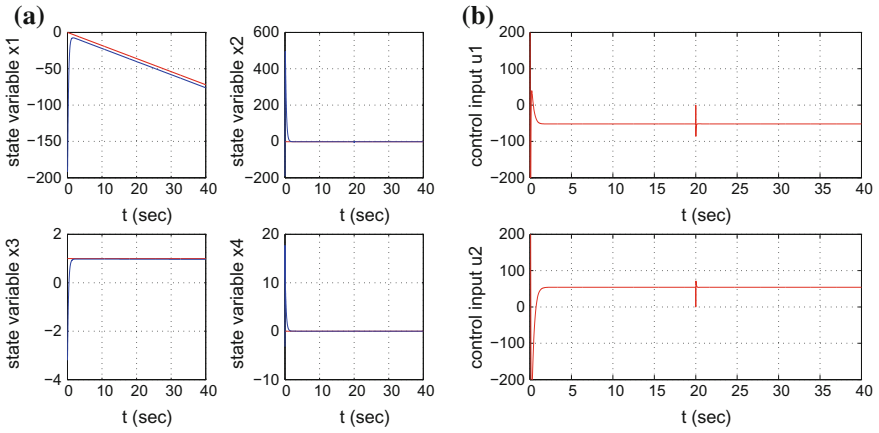

Fig. 11.14 Setpoint 1: **a** Convergence of the state variables x_i, $i = 1, \cdots, 4$ of the submarine to the desirable setpoints, **b** Variations of the control inputs (bow and stern hydroplane reflections)

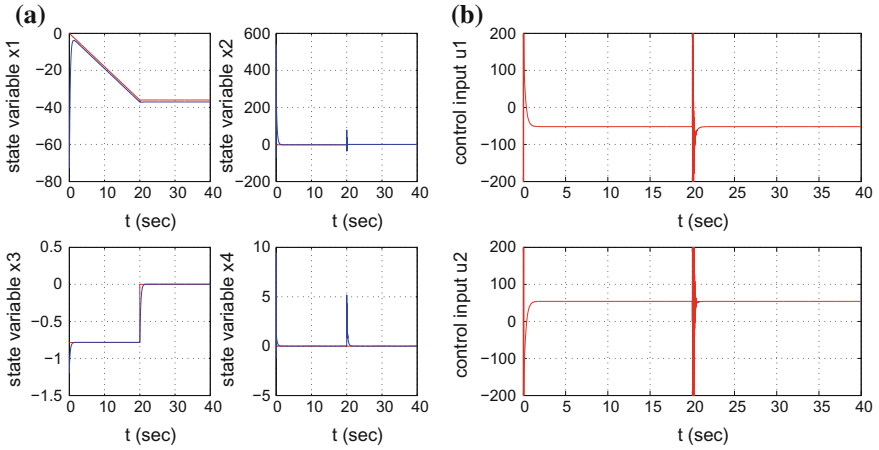

Fig. 11.15 Setpoint 2: **a** Convergence of the state variables x_i, $i = 1, \cdots, 4$ of the submarine to the desirable setpoints, **b** Variations of the control inputs (bow and stern hydroplane reflections)

There have been numerous examples of the use of model-based flatness-based control, given in [450, 457]. If the model of the control system is a precise one flatness-based control is anticipated to have an excellent performance. The control problem becomes more complicated in the case of absence of a precise mathematical model for the controlled system. It is even more difficult when there is no prior knowledge about the system's dynamics that can be used in the design of the flatness-based controller. The solution to the latter control problem is obtained with the use of the proposed flatness-based adaptive fuzzy control method. Although the dynamic model of the system is completely unknown, it is assured through Lyapunov stability

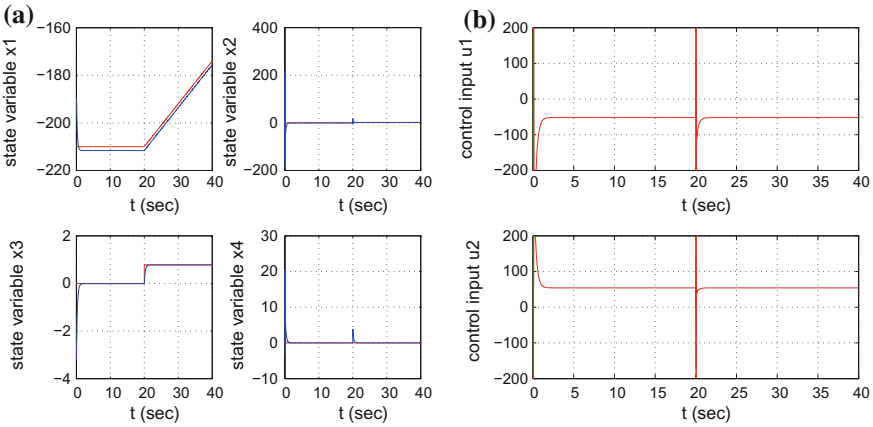

Fig. 11.16 Setpoint 3: **a** Convergence of the state variables x_i, $i = 1, \cdots, 4$ of the submarine to the desirable setpoints, **b** Variations of the control inputs (bow and stern hydroplane reflections)

analysis that this unknown system dynamics will be online identified by neurofuzzy approximators and that the state variables of the system will converge to the desirable setpoints. The robustness of the proposed adaptive fuzzy control method depends on the selection of parameters, such as the attenuation coefficient ρ which is used in the solution of the associated Riccati equation.

The reference trajectories can be generated using the differential flatness properties of the system. This means that all state variables of the system are expressed as differential functions of the flat outputs. Next, reference trajectories are defined for the flat outputs and these are also used for computing the reference setpoints for the rest of the state variables of the submarine's model.

11.4 Nonlinear Optimal Control of Autonomous Submarines

11.4.1 Outline

As previously noted, research on nonlinear control of autonomous underwater vessels has grown rapidly during the last years since there is need to develop robotic systems capable of functioning autonomously in an underwater environment [37, 251, 258, 602]. In this section, a nonlinear optimal (H-infinity) control method is developed aiming at solving the problem of depth and heading control of an autonomous submarine. It has been pointed out that navigation of autonomous underwater vessels (AUVs) and particularly of submarines exhibits several difficulties due to strong nonlinearities and the multivariable coupling characterizing the associated

dynamic model [143, 386, 411, 416, 457, 462]. Moreover, submersible robotized vessels are subject to model uncertainty and parametric variations while they are also affected by external perturbations [253, 275, 420, 500, 635]. For these reasons the control problem of a submarine's depth and heading angle is a nontrivial one. Apart from the developments of the previous sections, other results for the solution of this problem with the use of optimal control theory can be found in [44, 50, 98, 287, 346, 423, 608]. The approach to be developed in this section is relies on approximate linearization of the submarine's dynamics and on application of optimal (H-infinity) control to the model that is obtained from the linearization procedure.

The dynamic model of the submarine, describing coupling between its depth and its heading angle, undergoes approximate linearization, around a temporary operating point (equilibrium) which is recomputed at each iteration of the control algorithm [461, 466]. The equilibrium is defined by the present value of the submarine's state vector and the last value of the control inputs vector that was exerted on it. The linearization takes place through Taylor series expansion and the computation of the associated Jacobian matrices [33, 463, 564]. The modelling error which is due to truncation of higher order terms from the Taylor series is considered to be a perturbation that is compensated by the robustness of the control algorithm.

For the approximately linearized model of the submarine, the optimal (H-infinity) control problem is solved [132, 305, 450, 457, 459]. Actually the designed H-infinity controller stands for a solution to a min-max differential game. In such a game the controller tries to minimize a quadratic cost functional based on the submarine's state vector error, while the model uncertainty and external perturbation terms try to maximize it. The computation of the feedback gain of the H-infinity controller requires the solution of an algebraic Riccati equation which also takes place at each step of the control method.

The stability of the control method is proven through Lyapunov analysis. First, it is demonstrated that the control loop satisfies the H-infinity tracking performance criterion. This provides the control scheme with elevated robustness against model uncertainty and external perturbations. Moreover, under moderate conditions it is shown that the control loop exhibits global asymptotic stability properties. Finally to implement state estimation-based control of the submarine without the need to measure its entire state vector, the H-infinity Kalman Filter is used [169, 511]. This stands for an optimal state estimator, when the monitored system's model is characterized by parametric uncertainty or is subject to external perturbations.

11.4.2 Approximate Linearization of the AUV's Model

Using the description of the state-space model of the submarine given in Eq. (11.54) one has about functions $g_h(x, t)$ and $g_\theta(x, t)$

$$\begin{pmatrix} g_h(x,t) \\ g_\theta(x,t) \end{pmatrix} = \begin{pmatrix} 1 & -Z_Q^{'} L/m_3^{'} \\ -M_{\dot{w}}(LI_2^{'-1}) & 1 \end{pmatrix}^{-1} \cdot \begin{pmatrix} \frac{Z_w^{'} U}{Lm_3^{'}} w(t) + \frac{1}{m_3^{'}}(\dot{Z}_{\dot{\theta}}^{'} + m^{'}) U\dot{\theta}(t) + \frac{Z_d(t)}{0.5\rho L^3 m_3^{'}} + Z_\eta(w, Q) \\ \frac{M_v^{'} U}{L^2 I_2^{'}} w(t) + \frac{M_{\dot{\theta}}^{'} U}{LI_2^{'}} \dot{\theta}(t) + \frac{2mg(z_G - z_B)}{\rho L^5 I_2^{'}} \theta(t) + \frac{M_d(t)}{0.5\rho L^5 I_2^{'}} + M_\eta(w, Q) \end{pmatrix} \tag{11.126}$$

The effects of the wave and currents forces and the effects of hydrodynamic forces are considered as disturbances and thus are omitted from the model of the submarine's dynamics. By grouping coefficients the previous equation given in Eq. (11.126) can be written as

$$\begin{pmatrix} g_h(x,t) \\ g_\theta(x,t) \end{pmatrix} = \begin{pmatrix} m_{11} & m_{12} \\ m_{21} & m_{22} \end{pmatrix} \begin{pmatrix} a_1 \frac{1}{cos(x_3)}[x_2 + U_0 sin(x_3)] + a_2 x_4 \\ b_1 \frac{1}{cos(x_3)}[x_2 + U_0 sin(x_3)] + b_2 x_4 \end{pmatrix} \tag{11.127}$$

or equivalently

$$\begin{pmatrix} g_h(x,t) \\ g_\theta(x,t) \end{pmatrix} = \begin{pmatrix} m_{11} & m_{12} \\ m_{21} & m_{22} \end{pmatrix} \begin{pmatrix} a_1 & a_2 \\ b_1 & b_2 \end{pmatrix} \begin{pmatrix} \frac{1}{cos(x_3)}[x_2 + U_0 sin(x_3)] \\ x_4 \end{pmatrix} \tag{11.128}$$

and by performing additional operations between coefficients one has

$$\begin{pmatrix} g_h(x,t) \\ g_\theta(x,t) \end{pmatrix} = \begin{pmatrix} p_{11} & p_{12} \\ p_{21} & p_{22} \end{pmatrix} \begin{pmatrix} \frac{1}{cos(x_3)}[x_2 + U_0 sin(x_3)] \\ x_4 \end{pmatrix} \tag{11.129}$$

According to the above, the AUV's model is written in the generic form:

$$\begin{pmatrix} \ddot{x}_1 \\ \ddot{x}_3 \end{pmatrix} = \begin{pmatrix} F_1(x) \\ F_2(x) \end{pmatrix} + \begin{pmatrix} G_{11}(x) \\ G_{21}(x) \end{pmatrix} u_1 + \begin{pmatrix} G_{12}(x) \\ G_{22}(x) \end{pmatrix} u_2 \tag{11.130}$$

where one has that

$$F_1(x) = p_{11} \frac{1}{cos(x_3)}(x_2 + U_0 sin(x_3)) + p_{12} x_4 - \frac{x_2 + U_0 sin(x_3)}{cos(x_3)} x_4 sin(x_3) - U_0 x_4 sin(x_3) \tag{11.131}$$

$$F_2(x) = p_{21} \frac{1}{cos(x_3)}(x_2 + U_0 sin(x_3)) + p_{22} x_4 \tag{11.132}$$

while it also holds that

$$\begin{matrix} G_{11}(x) = B_{011} cos(x_3) & G_{12}(x) = B_{012} cos(x_3) \\ G_{21}(x) = B_{021} & G_{22}(x) = B_{022} \end{matrix} \tag{11.133}$$

Next, the Jacobian matrices of the submarine's dynamic model are computed. For the Jacobian matrix $\nabla_x F$ one has:

$$\nabla_x F = \begin{pmatrix} \frac{\partial F_1}{\partial x_1} & \frac{\partial F_1}{\partial x_2} & \frac{\partial F_1}{\partial x_3} & \frac{\partial F_1}{\partial x_4} \\ \frac{\partial F_2}{\partial x_1} & \frac{\partial F_2}{\partial x_2} & \frac{\partial F_2}{\partial x_3} & \frac{\partial F_2}{\partial x_4} \\ \frac{\partial F_3}{\partial x_1} & \frac{\partial F_3}{\partial x_2} & \frac{\partial F_3}{\partial x_3} & \frac{\partial F_3}{\partial x_4} \\ \frac{\partial F_4}{\partial x_1} & \frac{\partial F_4}{\partial x_2} & \frac{\partial F_4}{\partial x_3} & \frac{\partial F_4}{\partial x_4} \end{pmatrix} \tag{11.134}$$

About the first row of the Jacobian matrix $\nabla_x F$ one has: $\frac{\partial F_1}{\partial x_1} = 0$, $\frac{\partial F_1}{\partial x_2} = 1$, $\frac{\partial F_1}{\partial x_3} = 0$, $\frac{\partial F_1}{\partial x_4} = 0$

About the second row of the Jacobian matrix $\nabla_x F$ one has: $\nabla_x F$ one has: $\frac{\partial F_2}{\partial x_1} = 0$, $\frac{\partial F_2}{\partial x_2} = p_{11}\frac{1}{cos(x_3)} - \frac{x_4 sin(x_3)}{cos(x_3)}$, $\frac{\partial F_2}{\partial x_3} = \frac{p_{11}U_0}{cos(x_3)^2} - \frac{U_0 2sin(x_3)cos(x_3)^2 + U_0 sin(x_3)^2}{cos(x_3)^2} - U_0 x_4 cos(x_3)$, $\frac{\partial F_2}{\partial x_4} = p_{12} - \frac{x_2 + U_0 sin(x_3)}{cos(x_3)} sin(x_3) - U_0 sin(x_3)$

About the third row of the Jacobian matrix $\nabla_x F$ one has: $\frac{\partial F_3}{\partial x_1} = 0$, $\frac{\partial F_3}{\partial x_2} = 0$, $\frac{\partial F_3}{\partial x_3} = 0$, $\frac{\partial F_3}{\partial x_4} = 1$

About the fourth row of the Jacobian matrix $\nabla_x F$ one has: $\nabla_x F$ one has: $\frac{\partial F_4}{\partial x_1} = 0$, $\frac{\partial F_4}{\partial x_2} = p_{21}\frac{1}{cos(x_3)}$, $\frac{\partial F_4}{\partial x_3} = p_{21}\frac{U_0}{cos(x_3)^2}$, $\frac{\partial F_4}{\partial x_4} = p_{22}$

For the Jacobian matrix $\nabla_x G_1$ one has:

$$\nabla_x G_1 = \begin{pmatrix} \frac{\partial G_{11}}{\partial x_1} & \frac{\partial G_{11}}{\partial x_2} & \frac{\partial G_{11}}{\partial x_3} & \frac{\partial G_{11}}{\partial x_4} \\ \frac{\partial G_{21}}{\partial x_1} & \frac{\partial G_{21}}{\partial x_2} & \frac{\partial G_{21}}{\partial x_3} & \frac{\partial G_{21}}{\partial x_4} \\ \frac{\partial G_{31}}{\partial x_1} & \frac{\partial G_{31}}{\partial x_2} & \frac{\partial G_{31}}{\partial x_3} & \frac{\partial G_{31}}{\partial x_4} \\ \frac{\partial G_{41}}{\partial x_1} & \frac{\partial G_{41}}{\partial x_2} & \frac{\partial G_{41}}{\partial x_3} & \frac{\partial G_{41}}{\partial x_4} \end{pmatrix} \tag{11.135}$$

About the first row of the Jacobian matrix $\nabla_x G_1$ one has: $\frac{\partial G_{11}}{\partial x_1} = 0$, $\frac{\partial G_{11}}{\partial x_2} = 0$, $\frac{\partial G_{11}}{\partial x_3} = 0$, $\frac{\partial G_{11}}{\partial x_4} = 0$

About the second row of the Jacobian matrix $\nabla_x G_1$ one has: $\frac{\partial G_{21}}{\partial x_1} = 0$, $\frac{\partial G_{21}}{\partial x_2} = 0$, $\frac{\partial G_{21}}{\partial x_3} = -B_{011} sin(x_3)$, $\frac{\partial G_{21}}{\partial x_4} = 0$

About the third row of the Jacobian matrix $\nabla_x G_1$ one has: $\frac{\partial G_{31}}{\partial x_1} = 0$, $\frac{\partial G_{31}}{\partial x_2} = 0$, $\frac{\partial G_{31}}{\partial x_3} = 0$, $\frac{\partial G_{31}}{\partial x_4} = 0$

About the fourth row of the Jacobian matrix $\nabla_x G_1$ one has: $\frac{\partial G_{41}}{\partial x_1} = 0$, $\frac{\partial G_{41}}{\partial x_2} = 0$, $\frac{\partial G_{41}}{\partial x_3} = 0$, $\frac{\partial G_{41}}{\partial x_4} = 0$

For the Jacobian matrix $\nabla_x G_2$ one has:

$$\nabla_x G_1 = \begin{pmatrix} \frac{\partial G_{12}}{\partial x_1} & \frac{\partial G_{12}}{\partial x_2} & \frac{\partial G_{12}}{\partial x_3} & \frac{\partial G_{12}}{\partial x_4} \\ \frac{\partial G_{22}}{\partial x_1} & \frac{\partial G_{22}}{\partial x_2} & \frac{\partial G_{22}}{\partial x_3} & \frac{\partial G_{22}}{\partial x_4} \\ \frac{\partial G_{32}}{\partial x_1} & \frac{\partial G_{32}}{\partial x_2} & \frac{\partial G_{32}}{\partial x_3} & \frac{\partial G_{32}}{\partial x_4} \\ \frac{\partial G_{42}}{\partial x_1} & \frac{\partial G_{42}}{\partial x_2} & \frac{\partial G_{42}}{\partial x_3} & \frac{\partial G_{42}}{\partial x_4} \end{pmatrix} \tag{11.136}$$

About the first row of the Jacobian matrix $\nabla_x G_2$ one has: $\frac{\partial G_{12}}{\partial x_1} = 0$, $\frac{\partial G_{12}}{\partial x_2} = 0$, $\frac{\partial G_{12}}{\partial x_3} = 0$, $\frac{\partial G_{12}}{\partial x_4} = 0$

About the second row of the Jacobian matrix $\nabla_x G_2$ one has: $\frac{\partial G_{22}}{\partial x_1} = 0$, $\frac{\partial G_{22}}{\partial x_2} = 0$, $\frac{\partial G_{22}}{\partial x_3} = -B_{011} sin(x_3)$, $\frac{\partial G_{22}}{\partial x_4} = 0$

About the third row of the Jacobian matrix $\nabla_x G_2$ one has: $\frac{\partial G_{32}}{\partial x_1} = 0$, $\frac{\partial G_{32}}{\partial x_2} = 0$, $\frac{\partial G_{32}}{\partial x_3} = 0$, $\frac{\partial G_{32}}{\partial x_4} = 0$

About the fourth row of the Jacobian matrix $\nabla_x G_2$ one has: $\frac{\partial G_{42}}{\partial x_1} = 0$, $\frac{\partial G_{42}}{\partial x_2} = 0$, $\frac{\partial G_{42}}{\partial x_3} = 0$, $\frac{\partial G_{42}}{\partial x_4} = 0$

By considering the time varying equilibrium (linearization point) (x^*, u^*), where x^* is the present value of the submarine's state vector and u^* is the last value of the control inputs vector that was exerted on it, the linearized description of the AUV's model becomes

$$\dot{x} = Ax + Bu + \tilde{d} \tag{11.137}$$

where matrices A and B are given by

$$A = [\nabla_x F + \nabla_x G_1 u_1 + \nabla_x G_2 u_2] \mid_{(x^*, u^*)} \tag{11.138}$$

$$B = [\nabla_u F + \nabla_u G_1 u_1 + \nabla_u G_2 u_2] \mid_{(x^*, u^*)} = [G_1, G_2] \tag{11.139}$$

and $\tilde{d}$ is a term denoting modelling error and external perturbation effects.

11.4.3 Design of an H-Infinity Nonlinear Feedback Controller

11.4.3.1 Equivalent Linearized Dynamics of the Submarine

After linearization round its current operating point, the submarine's dynamic model is written as

$$\dot{x} = Ax + Bu + d_1 \tag{11.140}$$

Parameter d_1 stands for the linearization error in the submarine's dynamic model appearing in Eq. (11.140). The reference setpoints for the submarine's state vector are denoted by $\mathbf{x_d} = [x_1^d, \cdots, x_4^d]$. Tracking of this trajectory is succeeded after applying the control input u^*. At every time instant the control input u^* is assumed to differ from the control input u appearing in Eq. (11.140) by an amount equal to Δu, that is $u^* = u + \Delta u$

$$\dot{x}_d = Ax_d + Bu^* + d_2 \tag{11.141}$$

The dynamics of the controlled system described in Eq. (11.140) can be also written as

$$\dot{x} = Ax + Bu + Bu^* - Bu^* + d_1 \tag{11.142}$$

and by denoting $d_3 = -Bu^* + d_1$ as an aggregate disturbance term one obtains

$$\dot{x} = Ax + Bu + Bu^* + d_3 \tag{11.143}$$

By subtracting Eq. (11.141) from (11.143) one has

$$\dot{x} - \dot{x}_d = A(x - x_d) + Bu + d_3 - d_2 \tag{11.144}$$

By denoting the tracking error as $e = x - x_d$ and the aggregate disturbance term as $\tilde{d} = d_3 - d_2$, the tracking error dynamics becomes

$$\dot{e} = Ae + Bu + \tilde{d} \tag{11.145}$$

The above linearized form of the submarine's model can be efficiently controlled after applying an H-infinity feedback control scheme.

11.4.4 The Nonlinear H-Infinity Control for the Autonomous Submarine

The initial nonlinear model of the autonomous submarine is in the form

$$\dot{x} = \tilde{f}(x, u) \;\; x \in R^n, \;\; u \in R^m \tag{11.146}$$

Linearization of the system (autonomous submarine) is performed at each iteration of the control algorithm round its present operating point $(x^*, u^*) = (x(t), u(t - T_s))$, where T_s is the sampling period. The linearized equivalent model of the system is described by

$$\dot{x} = Ax + Bu + L\tilde{d} \quad x \in R^n,\ u \in R^m,\ \tilde{d} \in R^q \tag{11.147}$$

where matrices A and B are obtained from the computation of the Jacobians of the submarine's state-space model and vector $\tilde{d}$ denotes disturbance terms due to linearization errors. The problem of disturbance rejection for the linearized model that is described by

$$\begin{aligned} \dot{x} &= Ax + Bu + L\tilde{d} \\ y &= Cx \end{aligned} \tag{11.148}$$

where $x \in R^n$, $u \in R^m$, $\tilde{d} \in R^q$ and $y \in R^p$, cannot be handled efficiently if the classical LQR control scheme is applied. This is because of the existence of the perturbation term $\tilde{d}$. The disturbance term $\tilde{d}$ apart from modeling (parametric) uncertainty and external perturbations can also represent noise terms of any distribution.

As already explained in previous examples on the H_∞ control approach, a feedback control scheme is designed for trajectory tracking by the submarine's state vector and simultaneous disturbance rejection, considering that the disturbance affects the system in the worst possible manner. The disturbances' effects are incorporated in the following quadratic cost function:

$$J(t) = \tfrac{1}{2}\int_0^T [y^T(t)y(t) + ru^T(t)u(t) - \rho^2 \tilde{d}^T(t)\tilde{d}(t)]dt, \quad r, \rho > 0 \tag{11.149}$$

It has already been proven that the significance of the negative sign in the cost function's term that is associated with the perturbation variable $\tilde{d}(t)$ is that the disturbance tries to maximize the cost function $J(t)$ while the control signal $u(t)$ tries to minimize it. The physical meaning of the relation given above is that the control signal and the disturbances compete to each other within a min-max differential game. This problem of min-max optimization can be written as

$$min_u max_{\tilde{d}} J(u, \tilde{d}) \tag{11.150}$$

As already analyzed, the objective of the optimization procedure is to compute a control signal $u(t)$ which can compensate for the worst possible disturbance, that is externally imposed to the system. However, the solution to the min-max optimization problem is directly related to the value of the parameter ρ. This means that there is an upper bound in the disturbances magnitude that can be annihilated by the control signal.

11.4.4.1 Computation of the Feedback Control Gains

For the linearized system given by Eq. (11.148) the cost function of Eq. (11.149) is defined, where the coefficient r determines the penalization of the control input and the weight coefficient ρ determines the reward of the disturbances' effects.

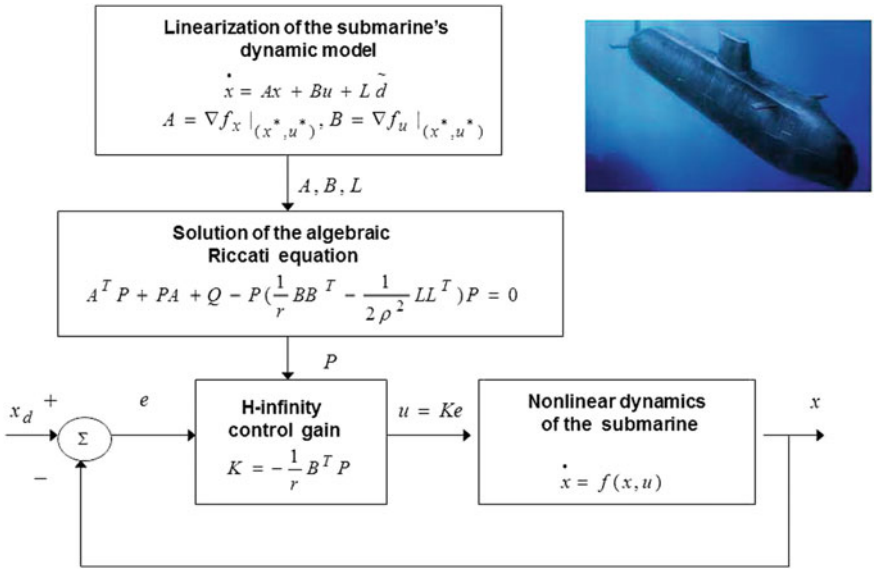

Fig. 11.17 Diagram of the control scheme for the autonomous submarine

Remaining at the assumptions made in previous applications of H-infinity control it is considered that (i) The energy that is transferred from the disturbances signal $\tilde{d}(t)$ is bounded, that is $\int_0^\infty \tilde{d}^T(t)\tilde{d}(t)dt < \infty$, (ii) matrices $[A, B]$ and $[A, L]$ are stabilizable, (iii) matrix $[A, C]$ is detectable. Then, the optimal feedback control law is given by

$$u(t) = -Kx(t) \tag{11.151}$$

with

$$K = \frac{1}{r}B^T P \tag{11.152}$$

where P is a positive semi-definite symmetric matrix which is obtained from the solution of the Riccati equation

$$A^T P + PA + Q - P(\frac{1}{r}BB^T - \frac{1}{2\rho^2}LL^T)P = 0 \tag{11.153}$$

where Q is also a positive definite symmetric matrix. The worst case disturbance is given by

$$\tilde{d}(t) = \frac{1}{\rho^2}L^T Px(t) \tag{11.154}$$

The diagram of the considered control loop is depicted in Fig. 11.17.

11.4.5 Lyapunov Stability Analysis

Through Lyapunov stability analysis it will be shown that the proposed nonlinear control scheme assures H_∞ tracking performance for the submarine, and that in case of bounded disturbance terms asymptotic convergence to the reference setpoints is achieved. The tracking error dynamics for the autonomous submarine is written in the form

$$\dot{e} = Ae + Bu + L\tilde{d} \tag{11.155}$$

where in the submarine's case $L = I \in R^4$ with I being the identity matrix. Variable $\tilde{d}$ denotes model uncertainties and external disturbances of the submarine's model. The following Lyapunov function is considered

$$V = \tfrac{1}{2} e^T P e \tag{11.156}$$

where $e = x - x_d$ is the tracking error. By differentiating with respect to time one obtains

$$\begin{gathered} \dot{V} = \tfrac{1}{2}\dot{e}^T P e + \tfrac{1}{2} e P \dot{e} \Rightarrow \\ \dot{V} = \tfrac{1}{2}[Ae + Bu + L\tilde{d}]^T P e + \tfrac{1}{2} e^T P [Ae + Bu + L\tilde{d}] \Rightarrow \end{gathered} \tag{11.157}$$

$$\begin{gathered} \dot{V} = \tfrac{1}{2}[e^T A^T + u^T B^T + \tilde{d}^T L^T] P e + \\ + \tfrac{1}{2} e^T P [Ae + Bu + L\tilde{d}] \Rightarrow \end{gathered} \tag{11.158}$$

$$\begin{gathered} \dot{V} = \tfrac{1}{2} e^T A^T P e + \tfrac{1}{2} u^T B^T P e + \tfrac{1}{2} \tilde{d}^T L^T P e + \\ \tfrac{1}{2} e^T P A e + \tfrac{1}{2} e^T P B u + \tfrac{1}{2} e^T P L \tilde{d} \end{gathered} \tag{11.159}$$

The previous equation is rewritten as

$$\begin{gathered} \dot{V} = \tfrac{1}{2} e^T (A^T P + P A) e + (\tfrac{1}{2} u^T B^T P e + \tfrac{1}{2} e^T P B u) + \\ + (\tfrac{1}{2} \tilde{d}^T L^T P e + \tfrac{1}{2} e^T P L \tilde{d}) \end{gathered} \tag{11.160}$$

Assumption: For given positive definite matrix Q and coefficients r and ρ there exists a positive definite matrix P, which is the solution of the following matrix equation

$$A^T P + P A = -Q + P(\tfrac{2}{r} B B^T - \tfrac{1}{\rho^2} L L^T) P \tag{11.161}$$

Moreover, the following feedback control law is applied to the system

$$u = -\tfrac{1}{r} B^T P e \tag{11.162}$$

By substituting Eqs. (11.161) and (11.162) one obtains

$$\begin{gathered}\dot{V}=\tfrac{1}{2}e^T[-Q+P(\tfrac{2}{r}BB^T-\tfrac{1}{\rho^2}LL^T)P]e+\\+e^TPB(-\tfrac{1}{r}B^TPe)+e^TPL\tilde{d}\Rightarrow\end{gathered}\tag{11.163}$$

$$\begin{gathered}\dot{V}=-\tfrac{1}{2}e^TQe+\tfrac{1}{r}e^TPBB^TPe-\tfrac{1}{2\rho^2}e^TPLL^TPe\\-\tfrac{1}{r}e^TPBB^TPe+e^TPL\tilde{d}\end{gathered}\tag{11.164}$$

which after intermediate operations gives

$$\dot{V}=-\tfrac{1}{2}e^TQe-\tfrac{1}{2\rho^2}e^TPLL^TPe+e^TPL\tilde{d}\tag{11.165}$$

or, equivalently

$$\begin{gathered}\dot{V}=-\tfrac{1}{2}e^TQe-\tfrac{1}{2\rho^2}e^TPLL^TPe+\\+\tfrac{1}{2}e^TPL\tilde{d}+\tfrac{1}{2}\tilde{d}^TL^TPe\end{gathered}\tag{11.166}$$

Lemma: The following inequality holds

$$\tfrac{1}{2}e^TPL\tilde{d}+\tfrac{1}{2}\tilde{d}L^TPe-\tfrac{1}{2\rho^2}e^TPLL^TPe\leq\tfrac{1}{2}\rho^2\tilde{d}^T\tilde{d}\tag{11.167}$$

Proof: The binomial $(\rho\alpha-\frac{1}{\rho}b)^2$ is considered. Expanding the left part of the above inequality one gets

$$\begin{gathered}\rho^2a^2+\tfrac{1}{\rho^2}b^2-2ab\geq0\Rightarrow\tfrac{1}{2}\rho^2a^2+\tfrac{1}{2\rho^2}b^2-ab\geq0\Rightarrow\\ab-\tfrac{1}{2\rho^2}b^2\leq\tfrac{1}{2}\rho^2a^2\Rightarrow\tfrac{1}{2}ab+\tfrac{1}{2}ab-\tfrac{1}{2\rho^2}b^2\leq\tfrac{1}{2}\rho^2a^2\end{gathered}\tag{11.168}$$

The following substitutions are carried out: $a=\tilde{d}$ and $b=e^TPL$ and the previous relation becomes

$$\tfrac{1}{2}\tilde{d}^TL^TPe+\tfrac{1}{2}e^TPL\tilde{d}-\tfrac{1}{2\rho^2}e^TPLL^TPe\leq\tfrac{1}{2}\rho^2\tilde{d}^T\tilde{d}\tag{11.169}$$

Equation (11.169) is substituted in Eq. (11.166) and the inequality is enforced, thus giving

$$\dot{V}\leq-\tfrac{1}{2}e^TQe+\tfrac{1}{2}\rho^2\tilde{d}^T\tilde{d}\tag{11.170}$$

Equation (11.170) shows that the H_∞ tracking performance criterion is satisfied. The integration of $\dot{V}$ from 0 to T gives

$$\begin{gathered}\int_0^T\dot{V}(t)dt\leq-\tfrac{1}{2}\int_0^T||e||_Q^2dt+\tfrac{1}{2}\rho^2\int_0^T||\tilde{d}||^2dt\Rightarrow\\2V(T)+\int_0^T||e||_Q^2dt\leq2V(0)+\rho^2\int_0^T||\tilde{d}||^2dt\end{gathered}\tag{11.171}$$

Moreover, if there exists a positive constant $M_d>0$ such that

$$\int_0^\infty||\tilde{d}||^2dt\leq M_d\tag{11.172}$$

then one gets

$$\int_0^{\infty} ||e||_Q^2 dt \leq 2V(0) + \rho^2 M_d \tag{11.173}$$

Thus, the integral $\int_0^{\infty} ||e||_Q^2 dt$ is bounded. Moreover, $V(T)$ is bounded and from the definition of the Lyapunov function V in Eq. (11.156) it becomes clear that $e(t)$ will be also bounded since $e(t) \in \Omega_e = \{e | e^T P e \leq 2V(0) + \rho^2 M_d\}$. According to the above and with the use of Barbalat's Lemma one obtains $lim_{t\to\infty} e(t) = 0$.

Elaboratiing on the above, it can be noted that the proof of global asymptotic stability for the control loop of the autonomous submarine relies on Eq. (11.170) and on the application of Barbalat's Lemma. It uses the condition of Eq. (11.172) about the boundedness of the square of the aggregate disturbance and modelling error term $\tilde{d}$ that affects the model. However, the proof of global asymptotic stability is not restricted by this condition. By selecting the attenuation coefficient ρ to be sufficiently small and in particular to satisfy $\rho^2 < ||e||_Q^2 / ||\tilde{d}||^2$ one has that the first derivative of the Lyapunov function is upper bounded by 0. Therefore for the i-th time interval it is proven that the Lyapunov function defined in Eq. (11.156) is a decreasing one. This also ensures that the Lyapunov function of the system defined in Eq. (11.156) will always have a negative first-order derivative.

11.4.6 Robust State Estimation with the Use of the H-Infinity Kalman Filter

The control loop for the autonomous submarine can be implemented with the use of information provided by a small number of sensors and by processing only a small number of state variables. To reconstruct the missing information about the state vector of the autonomous submarine it is proposed to use a filtering scheme and based on it to apply state estimation-based control [169, 457, 511]. The recursion of the H_∞ Kalman Filter, for the model of the submarine, can be formulated in terms of a *measurement update* and a *time update* part

Measurement update:

$$\begin{aligned} D(k) &= [I - \theta W(k) P^-(k) + C^T(k) R(k)^{-1} C(k) P^-(k)]^{-1} \\ K(k) &= P^-(k) D(k) C^T(k) R(k)^{-1} \\ \hat{x}(k) &= \hat{x}^-(k) + K(k)[y(k) - C\hat{x}^-(k)] \end{aligned} \tag{11.174}$$

Time update:

$$\begin{aligned} \hat{x}^-(k+1) &= A(k)x(k) + B(k)u(k) \\ P^-(k+1) &= A(k)P^-(k)D(k)A^T(k) + Q(k) \end{aligned} \tag{11.175}$$

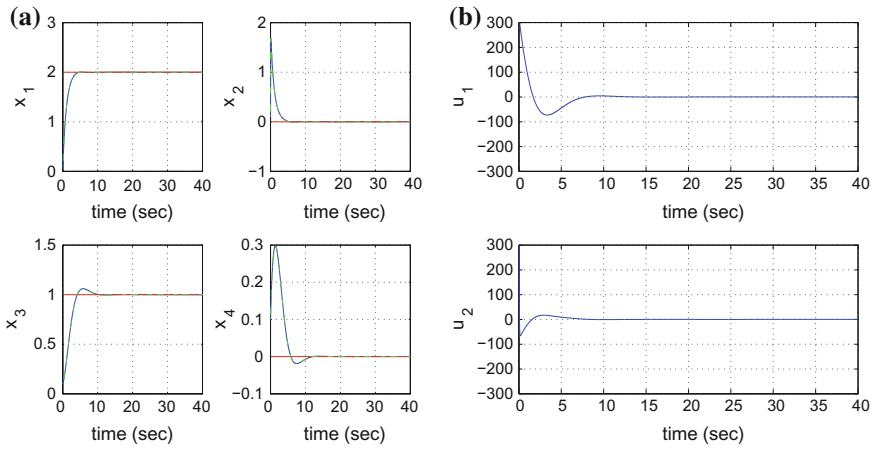

Fig. 11.18 Tracking of setpoint 1: **a** Convergence of the state variables of the submarine x_i $i = 1, \cdots, 4$ (blue lines) to the reference setpoints (red lines) and associated state estimates (green lines) **b** variation of the submarine's control inputs $u_i, i = 1, 2$

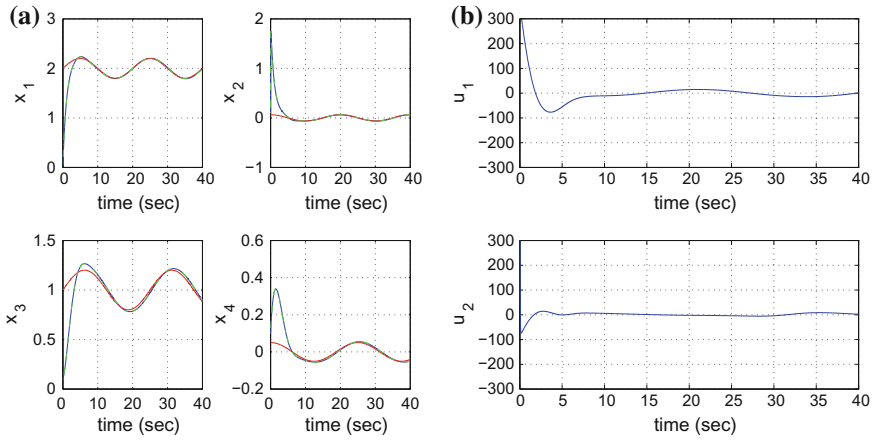

Fig. 11.19 Tracking of setpoint 2: **a** Convergence of the state variables of the submarine x_i $i = 1, \cdots, 4$ (blue lines) to the reference setpoints (red lines) and associated state estimates (green lines) **b** variation of the submarine's control inputs $u_i, i = 1, 2$

where it is assumed that parameter θ is sufficiently small to assure that the covariance matrix $P^{-}(k)^{-1} - \theta W(k) + C^{T}(k)R(k)^{-1}C(k)$ will be positive definite. When $\theta = 0$ the H_{∞} Kalman Filter becomes equivalent to the standard Kalman Filter. One can measure only a part of the state vector of the submarine, and can estimate through filtering the rest of the state vector elements. Moreover, the proposed Kalman filtering method can be used for sensor fusion purposes.

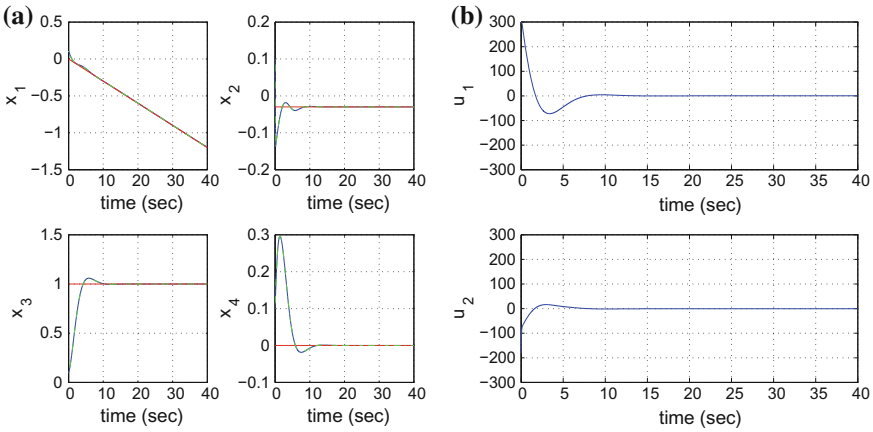

Fig. 11.20 Tracking of setpoint 3: **a** Convergence of the state variables of the submarine x_i $i = 1, \cdots, 4$ (blue lines) to the reference setpoints (red lines) and associated state estimates (green lines) **b** variation of the submarine's control inputs u_i,$i = 1, 2$

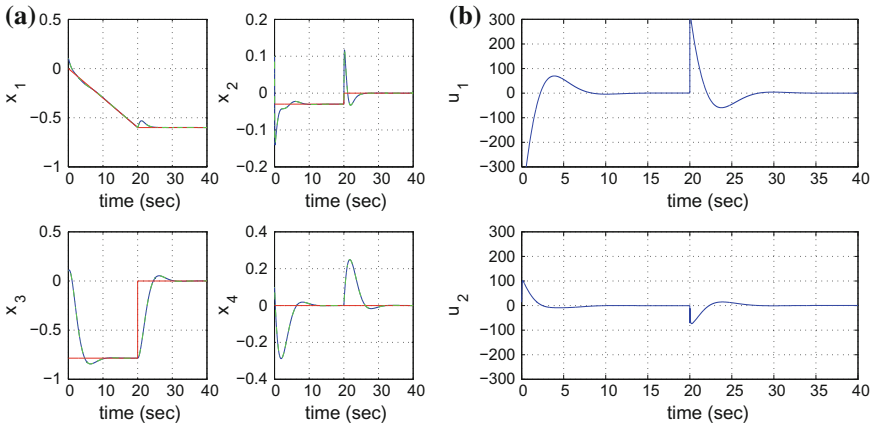

Fig. 11.21 Tracking of setpoint 4: **a** Convergence of the state variables of the submarine x_i $i = 1, \cdots, 4$ (blue lines) to the reference setpoints (red lines) and associated state estimates (green lines) **b** variation of the submarine's control inputs u_i,$i = 1, 2$

11.4.7 Simulation Tests

The performance of nonlinear H-infinity control for the autonomous submarine was tested through simulation experiments.After applying H-infinity control to the dynamic model of the submarine which has been obtained through Taylor series expansion it has become possible to make its state variables converge to the associated reference setpoints. The obtained results are depicted in Figs. 11.18, 11.19, 11.20, 11.21, 11.22 and 11.23. It can be noticed that fast and accurate tracking of

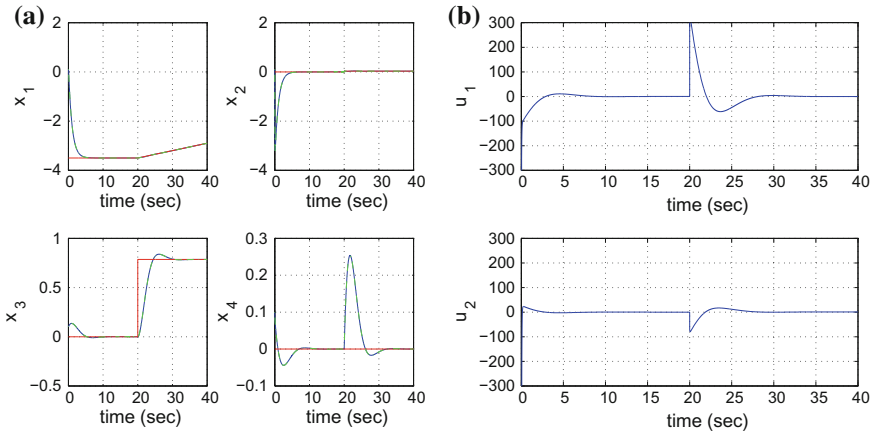

Fig. 11.22 Tracking of setpoint 5: **a** Convergence of the state variables of the submarine x_i $i = 1, \cdots, 4$ (blue lines) to the reference setpoints (red lines) and associated state estimates (green lines) **b** variation of the submarine's control inputs u_i,$i = 1, 2$

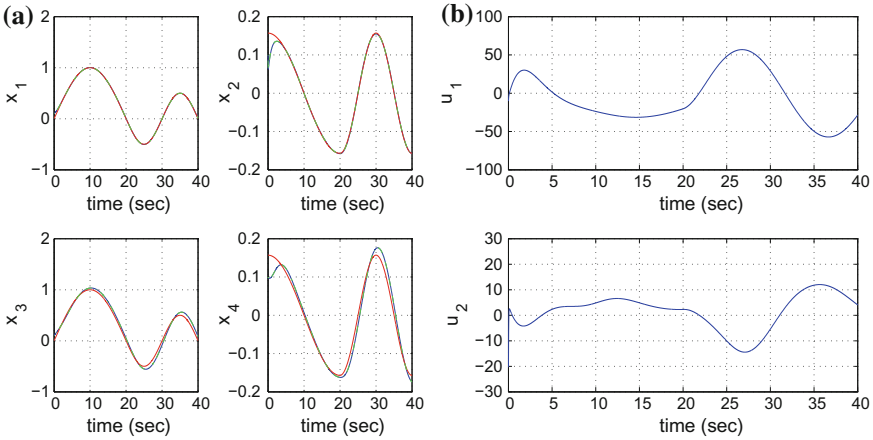

Fig. 11.23 Tracking of setpoint 6: **a** Convergence of the state variables of the submarine x_i $i = 1, \cdots, 4$ (blue lines) to the reference setpoints (red lines) and associated state estimates (green lines) **b** variation of the submarine's control inputs u_i,$i = 1, 2$

the reference setpoints was achieved while the variation of the submarine's control inputs remained smooth and within moderate ranges. For the computation of the feedback control gain the algebraic Riccati equation appearing in Eq. (11.161) had to be repetitively solved at each step of the control method.

In the presented simulation experiments state estimation-based control has been implemented. Out of the 4 state variables of the autonomous submarine only 2 where considered to be measurable. These were the submarine's depth h and its heading angle θ. The rest of the state variables, describing rate of change of the vessel's depth

and rate of change of its heading angle were indirectly estimated with the use of the H-infinity Kalman Filter. The real value of each state variable has been plotted in blue, the estimated value has been plotted in green, while the associated reference setpoint has been plotted in red. It can be noticed that despite model uncertainty the H-infinity Kalman Filter achieved accurate estimation of the real values of the state vector elements. In this manner the robustness of the state estimation-based H-infinity control scheme was also improved.

Comparing to control methods for autonomous underwater vessels which are based on global linearization techniques, the main properties of the nonlinear H-infinity control scheme are outlined as follows: (i) it is applied directly on the nonlinear dynamical model of the submarine and does not require the computation of diffeomorphisms (change of variables) that will bring the system into an equivalent linearized form, (ii) the computation of the feedback control signal follows an optimal control concept and requires the solution of an algebraic Riccati equation at each iteration of the control algorithm, (iii) the control method retains the advantages of optimal control, that is fast and accurate tracking of reference setpoints under moderate variations of the control inputs.

Chapter 12
Cooperating Autonomous Vehicles

Abstract Cooperating autonomous vehicles are analyzed. Distributed and coordinated control of autonomous vehicles (automatic ground vehicles, unmanned aerial vehicles, unmanned surface and underwater vessels) has received significant attention during the last years. In this chapter a solution is developed for the problem of distributed control of cooperating autonomous robots which chase a target. The distributed control aims at achieving the synchronized convergence of the autonomous vehicles towards the target and at maintaining the cohesion of the vehicle's team, while also avoiding collisions between the individuals vehicles and collisions between them and obstacles in their motion plane. To estimate the motion characteristics of the target, distributed filtering is performed. It is shown that to treat the distributed control problem for the cooperating autonomous vehicles a Lyapunov theory-based method is introduced. Moreover, to treat the distributed filtering and state estimation in the multi-vehicle system, decentralized state estimation methods can be applied. The proposed distributed control and filtering method can be used for surveillance and security tasks executed by multi-robot systems. The method for coordinated control of autonomous vehicles is a generic one and thus applicable to various types of autonomous robots, such as automatic ground vehicles, unmanned aerial vehicles, unmanned surface vessels or autonomous underwater vessels. In particular, the chapter treats the following topics: (a) cooperating unmanned surface vessels and (b) Cooperating unmanned ground vehicles

12.1 Chapter Overview

The present chapter treats the following topics: (a) cooperating unmanned surface vessels and (b) Cooperating unmanned ground vehicles.

With reference to (a) the chapter formulates a distributed control problem for unmanned surface vessels (USVs) as follows: there is a number of N USVs which pursue another vessel (moving target). Each USV can be equipped with various sensors, such as IMU, cameras and non-imaging sensors such as sonar, radar and thermal signature sensors. At each time instant each USV can obtain measurements

G. Rigatos and K. Busawon, *Robotic Manipulators and Vehicles*,
Studies in Systems, Decision and Control 152,
https://doi.org/10.1007/978-3-319-77851-8_12

of the target's cartesian coordinates. Additionally, each USV is aware of the target's distance from a reference monitoring station (coastal or satellite monitoring units). The objective is to make the USVs converge in a synchronized manner towards the target, while avoiding collisions between them and avoiding collisions with obstacles in their motion plane. A distributed control law is developed for the USVs which enables not only convergence of the USVs to the goal position, but also makes possible to maintain the cohesion of the USVs ensemble. Moreover, distributed filtering is performed, so as to obtain an estimate of the target vessel's state vector. This provides the desirable state vector to be tracked by each one of the USVs. To this end, a new distributed nonlinear filtering method of improved accuracy and computation speed is introduced. This filtering approach, under the name Derivative-free distributed nonlinear Kalman Filter relies on differential flatness theory and on an exact linearization of the target vessel's dynamic/kinematic model. The stability properties of the distributed oontrol scheme are assured.

With reference to (b) the chapter proposes state estimation-based control for unmanned ground vehicles, such as cooperating robot harvesters. The method is also applicable to a wider class of nonlinear multi-input multi-output vehicle systems. To estimate with accuracy the position of the robotic vehicles as well as their motion characteristics fusion of measurements from multiple sensors is performed with the use of the Derivative-free distributed Kalman Filter., The proposed derivative-free nonlinear filtering method, enables to perform distributed state estimation, by substituting the Extended Information Filter with the standard Information Filter recursion. This filtering approach has significant advantages because unlike the Extended Information Filter it avoids cumulative numerical and modelling errors which are due to approximate linearization of the vehicle's kinematic and dynamic model. The proposed nonlinear control is based on differential flatness theory.

12.2 Cooperating Unmanned Surface Vessels

12.2.1 Outline

Distributed control of unmanned surface and underwater vessels has received significant attention during the last years [11, 54, 316, 554, 598, 621]. In this section a solution is developed for the problem of distributed control of cooperating unmanned surface vessels (USVs) which pursue a target vessel. The distributed control aims at achieving the synchronized convergence of the USVs towards the target and at maintaining the cohesion of the USVs team, while also avoiding collisions between the individuals USVs and collisions between the USVs and obstacles in their motion plane. To estimate the motion characteristics of the target vessel distributed filtering is performed. Actually, each vessel is supplied with equipment which permits to measure the coordinates of the target vessel, such as IMU and cameras, as well as with sonar, radar and thermal signature sensors. Besides each USV receives informa-

tion about the distance of the target vessel from a reference surface, the latter being provided by a coastal or a satellite-based measurement unit. By fusing the aforementioned measurements through a filtering procedure an estimate of the state vector of the target vessel is obtained. Next, to obtain an estimate of improved precision about the motion characteristics of the target vessel distributed filtering is performed which provides fusion of the distributed state vector estimates into one single estimate.

To treat the distributed control problem for the cooperating USVs a Lyapunov theory-based method is introduced. Motion planning for the individual USVs is determined by the minimization of a Lyapunov function which comprises a quadratic term associated with the distance of each USV from the target vessel, as well as quadratic terms which are associated with the distance of the USVs between each other. By applying LaSalle's theorem it is proven that the USVs will follow the target's motion while remaining within a small area that encircles the target.

To treat the distributed filtering and state estimation problems in the multi-USV system one can apply established methods for decentralized state estimation, such as the Extended Information Filter (EIF) and the Unscented Information Filter (UIF). EIF stands for the distributed implementation of the Extended Kalman Filter while UIF stands for the distributed variant of the Unscented Kalman Filter. Moreover, to obtain a distributed filtering scheme in this section the Derivative-free Extended Information Filter (DEIF) is implemented. This stands for the distributed implementation of a differential flatness theory-based filtering method under the name Distributed Derivative-free nonlinear Kalman Filter [57, 450]. The improved performance of DEIF comparing to the EIF and UIF is confirmed both in terms of improved estimation accuracy and in terms of improved speed of computation.

12.2.2 Target Tracking by Multi-robot Systems

12.2.2.1 The Problem of Distributed Target Tracking

It is assumed that there are N USVs (unmanned surface vessels) with positions $p_1, p_2, ..., p_N \in R^2$ respectively, and a target with position $x^* \in R^2$ moving on the sea surface (see Fig. 12.1). Each USV can be equipped with various sensors, such as IMU, cameras, sonar, radar and thermal signature sensors. The USVs can be considered as mobile sensors while the ensemble of the autonomous vehicles constitutes a mobile sensors network. The discrete-time target's kinematic model is given by

$$\begin{aligned} x_t(k+1) &= \phi(x_t(k)) + L(k)u(k) + w(k) \\ z_t(k) &= \gamma(x_t(k)) + v(k) \end{aligned} \tag{12.1}$$

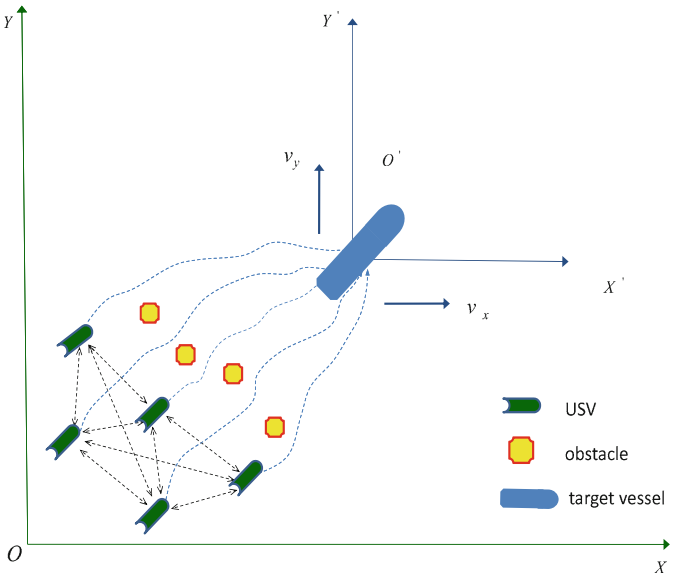

Fig. 12.1 Distributed control for tracking of the target vessel by synchronized USVs

where $x \in R^{m\times 1}$ is the target's state vector and $z \in R^{p\times 1}$ is the measured output, while $w(k)$ and $v(k)$ are uncorrelated, zero-mean, Gaussian zero-mean noise processes with covariance matrices $Q(k)$ and $R(k)$ respectively. The operators $\phi(x)$ and $\gamma(x)$ are defined as $\phi(x) = [\phi_1(x), \phi_2(x), \ldots, \phi_m(x)]^T$, and $\gamma(x) = [\gamma_1(x), \gamma_2(x), \ldots, \gamma_p(x)]^T$, respectively.

At each time instant each USV can obtain a measurement of the target's position. Additionally, each USV is aware of the target's distance from a reference surface measured in an inertial coordinates system (this can be a measurement provided by a coastal observation unit or equivalently by a satellite station). Finally, each USV is aware of the positions of the rest $N - 1$ USVs. The objective is to make the USVs converge in a synchronized manner towards the target, while avoiding collisions between them and avoiding collisions with obstacles in the motion plane. To solve the overall problem, the following steps are necessary: (i) to perform distributed filtering, so as to obtain an estimate of the target's state vector. This estimate provides the desirable state vector to be tracked by each one of the USVs, (ii) to design a suitable control law that will enable individual USVs not only convergence to the target's position but will also preserve the cohesion of the USVs ensemble (see Fig. 12.2).

The exact position and orientation of the target can be obtained through distributed filtering. Actually, distributed filtering provides a two-level fusion of the distributed sensor measurements. At the first level, local filters running at each USV provide an estimate of the target's state vector by fusing the cartesian coordinates of the target with the target's distance from a reference surface which is measured in an inertial coordinates system [573]. At a second level, fusion of the local estimates is performed

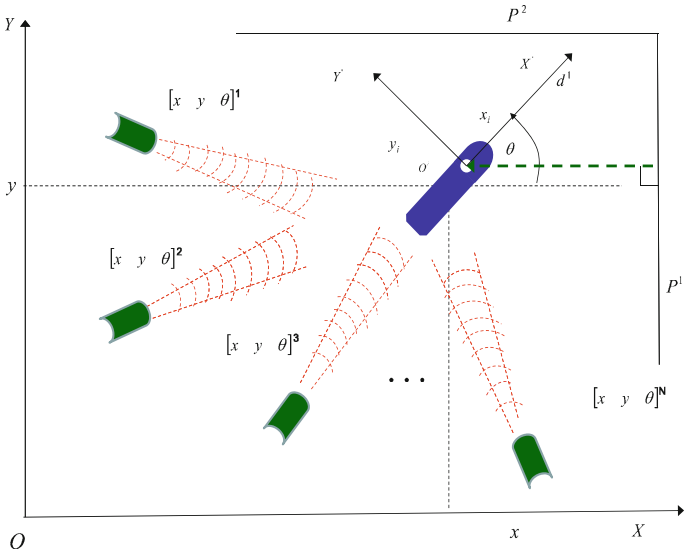

Fig. 12.2 Distributed tracking of the target vessel (blue color) by N unmanned surface vessels (green color) through the fusion of distributed estimates about the target's motion

with the use of the Extended Information Filter and the Unscented Information Filter. It is also assumed that the time taken in the processing of data and in communicating between USVs is small, and that time delays, packet losses and out-of-sequence measurement problems in communication do not distort significantly the flow of the exchanged data.

Comparing to the traditional centralized or hierarchical fusion architecture, the network-centric architectures for the considered multi-USV system has the following advantages: (i) Scalability: since there are no limits imposed by centralized computation bottlenecks or lack of communication bandwidth, and every USV can easily join or quit the multi-USV system, (ii) Robustness: in a decentralized fusion architecture no element of the system is mission-critical, so that the system is survivable in the event of loss of individual USVs, (iii) Modularity: each individual USV is self-coordinated and does not need to possess a global knowledge of the network topology. However, these benefits are possible only if the sensor data can be fused and distributed within the constraints of the available bandwidth.

12.2.2.2 Tracking of the Reference Path by the Target

The complete kinematic and dynamic model of the target vessel, for both the case of fully actuated and underactuated ships, has been analyzed in [416, 450]. In particular, models of the vessel's motion described only by kinematics equations can be found in [62, 252]. Here a simplified kinematic model of the target vessel is considered,

including only surge velocity (forward motion) and without sway velocity. This is given by:

$$\begin{aligned} \dot{x} &= v(t)cos(\theta) \\ \dot{y} &= v(t)sin(\theta) \\ \dot{\theta} &= \omega \end{aligned} \tag{12.2}$$

The target is steered by the dynamic feedback linearization control algorithm which is based on flatness-based control and has been analyzed in Sect. 7.1 [145, 255, 450, 572]:

$$\begin{aligned} u_1 &= \ddot{x}_d + K_{p_1}(x_d - x) + K_{d_1}(\dot{x}_d - \dot{x}) \\ u_2 &= \ddot{y}_d + K_{p_2}(y_d - y) + K_{d_2}(\dot{y}_d - \dot{y}) \\ \dot{\xi} &= u_1 cos(\theta) + u_2 sin(\theta) \\ v &= \xi, \;\; \omega = \frac{u_2 cos(\theta) - u_1 sin(\theta)}{\xi} \end{aligned} \tag{12.3}$$

The linearized equivalent model of the target's kinematics becomes

$$\begin{aligned} \ddot{x} &= u_1 \\ \ddot{y} &= u_2 \end{aligned} \tag{12.4}$$

A linearized model of similar structure is obtained in the case of the more elaborated vessel models as for example those described in [416, 457]. For the complete model of the vessel's kinematics dynamics one arrives at a linearized description of the form $x^{(4)} = u_1$ and $y^{(4)} = u_2$. Therefore, the control and filtering methods to be developed in this manuscript are also applicable to more complicated vessel models.

In case of Eq. (12.4), the dynamics of the tracking error is given by

$$\begin{aligned} \ddot{e}_x + K_{d_1}\dot{e}_x + K_{p_1}e_x &= 0 \\ \ddot{e_y} + K_{d_2}\dot{e}_x + K_{p_2}e_y &= 0 \end{aligned} \tag{12.5}$$

where $e_x = x - x_d$ and $e_y = y - y_d$. The proportional-derivative (PD) gains are chosen as K_{p_i} and K_{d_i}, for $i = 1, 2$. The dynamic compensator of Eq. (12.3) has a potential singularity at $\xi = v = 0$, i.e. when the target is not moving. As it has been previously analyzed, the occurrence of such a singularity is structural for non-holonomic systems. It is assumed that the target follows a smooth trajectory $(x_d(t), y_d(t))$ which is persistent, i.e. for which the nominal velocity $v_d = (\dot{x}_d^2 + \dot{y}_d^2)^{1/2}$ along the trajectory never goes to zero (and thus singularities are avoided).

12.2.3 Distributed Motion Planning for the Multi-USV System

12.2.3.1 Kinematic Model of the Multi-USV System

The objective is to lead the team of N USVs, with different initial positions on the 2-D plane, to converge to the target's position, and at the same time to avoid collisions between the USVs, as well as collisions with obstacles in the motion plane. An approach for doing this is the *potential fields theory*, in which the individual USVs are steered towards an equilibrium by the gradient of an harmonic potential [51, 176, 198, 450]. Variants of this method use nonlinear anisotropic harmonic potential fields which introduce to the USVs' motion directional and regional avoidance constraints [323, 374, 446, 448, 497, 512]. In the examined coordinated target-tracking problem the equilibrium is the target's position, which is not a-priori known and has to be estimated with the use of distributed filtering.

The position of each USV in the 2-D space is described by the vector $x^i \in R^2$. The motion of the USVs is synchronous, without time delays, and it is assumed that at every time instant each USV i is aware about the position and the velocity of the other $N-1$ USVs. The cost function that describes the motion of the ith USV towards the target's position is denoted as $V(x^i): R^n \rightarrow R$. The value of $V(x^i)$ at the target's position in $\nabla_{x^i} V(x^i) = 0$. The following conditions must hold:

(i) The cohesion of the USVs team should be maintained, i.e. the norm $||x^i - x^j||$ should remain upper bounded $||x^i - x^j|| < \varepsilon^h$,
(ii) Collisions between the USVs should be avoided, i.e. $||x^i - x^j|| > \varepsilon^l$,
(iii) Convergence to the target's position should be achieved for each USV through the negative definiteness of the associated Lyapunov function $\dot{V}^i(x^i) = \dot{e}^i(t)^T e^i(t) < 0$, where $e = x - x^*$ is the distance of the ith USV from the target's position.

The interaction between the ith and the jth USV is

$$g(x^i - x^j) = -(x^i - x^j)[g_a(||x^i - x^j||) - g_r(||x^i - x^j||)] \tag{12.6}$$

where $g_a()$ denotes the attraction term and is dominant for large values of $||x^i - x^j||$, while $g_r()$ denotes the repulsion term and is dominant for small values of $||x^i - x^j||$. Function $g_a()$ can be associated with an attraction potential, i.e. $\nabla_{x_i} V_a(||x^i - x^j||) = (x^i - x^j) g_a(||x^i - x^j||)$. Function $g_r()$ can be associated with a repulsion potential, i.e. $\nabla_{x_i} V_r(||x^i - x^j||) = (x^i - x^j) g_r(||x^i - x^j||)$. A suitable function $g()$ that describes the interaction between the USVs is given by [162, 448]

$$g(x^i - x^j) = -(x^i - x^j)(a - be^{\frac{||x^i - x^j||^2}{\sigma^2}}) \tag{12.7}$$

where the parameters a, b and c are suitably tuned. It holds that $g_a(x^i - x^j) = -a$, i.e. attraction has a linear behavior (spring-mass system) $||x^i - x^j|| g_a(x^i - x^j)$.

Moreover, $g_r(x^i - x^j) = be^{\frac{-||x^i - x^j||^2}{\sigma^2}}$ which means that $g_r(x^i - x^j)||x^i - x^j|| \leq b$ is bounded. Applying Newton's laws to the ith USV yields

$$\dot{x}^i = v^i, \quad m^i \dot{v}^i = U^i \tag{12.8}$$

where the aggregate force is $U^i = f^i + F^i$. The term $f^i = -K_v v^i$ denotes a friction-equivalent term, while the term F^i is the propulsion. Assuming zero acceleration $\dot{v}^i = 0$ one gets $F^i = K_v v^i$, which for $K_v = 1$ and $m^i = 1$ gives $F^i = v^i$. Thus an approximate kinematic model for each USV is

$$\dot{x}^i = F^i \tag{12.9}$$

According to the Euler-Langrange principle, the propulsion F^i is equal to the derivative of the total potential of each USV, i.e.

$$\begin{aligned}
&F^i = -\nabla_{x^i}\{V^i(x^i) + \frac{1}{2}\sum_{i=1}^{N}\sum_{j=1, j\neq i}^{N}[V_a(||x^i - x^j|| + V_r(||x^i - x^j||)]\} \Rightarrow \\
&F^i = -\nabla_{x^i}\{V^i(x^i)\} + \sum_{j=1, j\neq i}^{N}[-\nabla_{x^i} V_a(||x^i - x^j||) - \nabla_{x^i} V_r(||x^i - x^j||)] \Rightarrow \\
&F^i = -\nabla_{x^i}\{V^i(x^i)\} + \sum_{j=1, j\neq i}^{N}[-(x^i - x^j)g_a(||x^i - x^j||) - (x^i - x^j)g_r(||x^i - x^j||)] \Rightarrow \\
&F^i = -\nabla_{x^i}\{V^i(x^i)\} - \sum_{j=1, j\neq i}^{N} g(x^i - x^j)
\end{aligned}$$

Substituting in Eq. (12.9) one gets in discrete-time form

$$x^i(k+1) = x^i(k) + \gamma^i(k)[h(x^i(k)) + e^i(k)] + \sum_{j=1, j\neq i}^{N} g(x^i - x^j), \; i = 1, 2, \ldots, M \tag{12.10}$$

The term $h(x(k)^i) = -\nabla_{x^i} V^i(x^i)$ indicates a local gradient algorithm, i.e. motion in the direction of decrease of the cost function $V^i(x^i) = \frac{1}{2} e^i(t)^T e^i(t)$. The term $\gamma^i(k)$ is the algorithms step while the stochastic disturbance $e^i(k)$ enables the algorithm to escape from local minima. The term $\sum_{j=1, j\neq i}^{N} g(x^i - x^j)$ describes the interaction between the ith and the rest $N - 1$ stochastic gradient algorithms [43, 101, 134].

12.2.3.2 Stability of the Multi-USV System

The behavior of the multi-USV system is determined by the behavior of its center (mean of the vectors x^i) and of the position of each USV with respect to this center. The center of the multi-USV system is given by

$$\bar{x} = E(x^i) = \frac{1}{N}\sum\nolimits_{i=1}^{N} x^i \Rightarrow \dot{\bar{x}} = \frac{1}{N}\sum\nolimits_{i=1}^{N} \dot{x}^i \Rightarrow$$
$$\dot{\bar{x}} = \frac{1}{N}\sum\nolimits_{i=1}^{N} [-\nabla_{x^i} V^i(x^i) - \sum\nolimits_{j=1, j\neq i}^{N} (g(x^i - x^j))] \tag{12.11}$$

From Eq. (12.7) it can be seen that $g(x^i - x^j) = -g(x^j - x^i)$, i.e. $g()$ is an odd function. Therefore, it holds that $\frac{1}{N}(\sum_{j=1, j\neq i}^{N} g(x^i - x^j)) = 0$, and

$$\dot{\bar{x}} = \frac{1}{N}\sum_{i=1}^{N} [-\nabla_{x^i} V^i(x^i)] \tag{12.12}$$

Denoting the target's position by x^*, and the distance between the ith USV and the mean position of the multi-USV system by $e^i(t) = x^i(t) - \bar{x}$ the objective of distributed gradient for USV motion planning can be summarized as follows:

(i) $lim_{t\to\infty} \bar{x} = x^*$, i.e. the center of the multi-USV system converges to the target's position,
(ii) $lim_{t\to\infty} x^i = \bar{x}$, i.e. the ith USV converges to the center of the multi-USV system,
(iii) $lim_{t\to\infty} \dot{\bar{x}} = \dot{x}^*$, i.e. the velocity of the multi-USV systems stabilizes at the target's velocity.

If conditions (i) and (ii) hold then $lim_{t\to\infty} x^i = x^*$. Furthermore, if condition (iii) also holds then all USVs will stabilize close to the target's position.

It is known that the stability of local gradient algorithms can be proven with the use of Lyapunov theory [43]. A similar approach can be followed in the case of the distributed gradient algorithms given by Eq. (12.10). The following simple Lyapunov function is considered for each gradient algorithm [162]:

$$V_i = \frac{1}{2} e^{i\,T} e^i \Rightarrow V_i = \frac{1}{2}||e_i||^2 \tag{12.13}$$

Thus, one gets

$$\dot{V}^i = e^{i\,T} \dot{e}^i \Rightarrow \dot{V}^i = (\dot{x}^i - \dot{\bar{x}}) e^i \Rightarrow$$
$$\dot{V}^i = [-\nabla_{x^i} V^i(x^i) - \sum\nolimits_{j=1, j\neq i}^{N} g(x^i - x^j) + \frac{1}{M}\sum\nolimits_{j=1}^{N} \nabla_{x^j} V^j(x^j)] e^i.$$

Substituting $g(x^i - x^j)$ from Eq. (12.7) yields

$$\dot{V}_i = [-\nabla_{x^i} V^i(x^i) - \sum\nolimits_{j=1, j\neq i}^{N} (x^i - x^j) a +$$
$$+ \sum\nolimits_{j=1, j\neq i}^{N} (x^i - x^j) g_r(||x^i - x^j||) + \frac{1}{N}\sum\nolimits_{j=1}^{N} \nabla_{x^j} V^j(x^j)] e^i$$

which gives,

$$\dot{V}_i = -a[\sum_{j=1,j\neq i}^{N}(x^i - x^j)]e^i + \\ + \sum_{j=1,j\neq i}^{N} g_r(||x^i - x^j||)(x^i - x^j)^T e^i - [\nabla_{x^i} V^i(x^i) - \frac{1}{N}\sum_{j=1}^{M} \nabla_{x^j} V^j(x^j)]^T e^i$$

It holds that $\sum_{j=1}^{N}(x^i - x^j) = Nx^i - N\frac{1}{N}\sum_{j=1}^{N} x^j = Nx^i - N\bar{x} = N(x^i - \bar{x}) = Ne^i$, therefore

$$\dot{V}_i = -aN||e^i||^2 + \sum_{j=1,j\neq i}^{N} g_r(||x^i - x^j||)(x^i - x^j)^T e^i - [\nabla_{x^i} V^i(x^i) - \frac{1}{N}\sum_{j=1}^{N} \nabla_{x^j} V^j(x^j)]^T e^i \tag{12.14}$$

It assumed that for all x^i there is a constant $\bar{\sigma}$ such that

$$||\nabla_{x^i} V^i(x^i)|| \leq \bar{\sigma} \tag{12.15}$$

Equation (12.15) is reasonable since for a USV moving on a 2-D plane, the gradient of the cost function $\nabla_{x^i} V^i(x^i)$ is expected to be bounded. Moreover it is known that the following inequality holds:

$$\sum_{j=1,j\neq i}^{N} g_r(x^i - x^j)^T e^i \leq \sum_{j=1,j\neq i}^{N} be^i \leq \sum_{j=1,j\neq i}^{N} b||e^i||.$$

Thus the application of Eq. (12.14) gives:

$$\dot{V}^i \leq -aN||e^i||^2 + \sum_{j=1,j\neq i}^{N} g_r(||x^i - x^j||)||x^i - x^j|| \cdot ||e^i|| + ||\nabla_{x^i} V^i(x^i) - \\ - \frac{1}{N}\sum_{j=1}^{M} \nabla_{x^j} V^j(x^j)||||e^i|| \\ \Rightarrow \dot{V}^i \leq aN||e^i||^2 + b(N-1)||e^i|| + 2\bar{\sigma}||e^i||$$

where it has been taken into account that

$$\sum_{j=1,j\neq i}^{N} g_r(||x^i - x^j||)^T||e^i|| \leq \sum_{j=1,j\neq i}^{N} b||e^i|| = b(N-1)||e^i||,$$

and from Eq. (12.15),

$$||\nabla_{x^i} V^i(x^i) - \frac{1}{N}\sum_{j=1}^{N} \nabla_{x^i} V^j(x^j)|| \leq ||\nabla_{x^i} V^i(x^i)|| + \\ + \frac{1}{N}||\sum_{j=1}^{N} \nabla_{x^i} V^j(x^j)|| \leq \bar{\sigma} + \frac{1}{N}N\bar{\sigma} \leq 2\bar{\sigma}.$$

Thus, one gets

$$\dot{V}^i \leq -aN||e^i||\cdot[||e^i|| - \frac{b(N-1)}{aN} - 2\frac{\bar{\sigma}}{aN}] \tag{12.16}$$

The following bound ε is defined:

$$\varepsilon = \frac{b(N-1)}{aN} + \frac{2\bar{\sigma}}{aN} = \frac{1}{aN}(b(N-1) + 2\bar{\sigma}) \tag{12.17}$$

Thus, when $||e^i|| > \varepsilon$, $\dot{V}_i$ will become negative and consequently the error $e^i = x^i - \bar{x}$ will decrease. Therefore the tracking error e^i will remain in an area of radius ε i.e. the position x^i of the ith USV will stay in the cycle with center $\bar{x}$ and radius ε.

12.2.3.3 Stability in the Case of a Quadratic Cost Function

The case of a convex quadratic cost function is examined, for instance

$$V^i(x^i) = \frac{A}{2}||x^i - x^*||^2 = \frac{A}{2}(x^i - x^*)^T(x^i - x^*) \tag{12.18}$$

where $x^* \in R^2$ denotes the target's position, while the associated Lyapunov function has a minimum at x^*, i.e. $V^i(x^i = x^*) = 0$. The distributed gradient algorithm is expected to converge to x^*. The individual USVs will follow different trajectories on the 2-D plane and will end at the target's position.

Using Eq. (12.18) yields $\nabla_{x^i} V^i(x^i) = A(x^i - x^*)$. Moreover, the assumption $\nabla_{x^i} V^i(x^i) \leq \bar{\sigma}$ can be used, since the gradient of the cost function remains bounded. The USVs will concentrate round $\bar{x}$ and will stay in a radius ε given by Eq. (12.17). The motion of the mean position $\bar{x}$ of the USVs is

$$\dot{\bar{x}} = -\frac{1}{N}\sum_{i=1}^{N} \nabla_{x^i} V^i(x^i) \Rightarrow \dot{\bar{x}} = -\frac{A}{N}\sum_{i=1}^{N}(x^i - x^*) \Rightarrow$$
$$\dot{\bar{x}} = -\frac{A}{N}\sum_{i=1}^{N} x^i + \frac{A}{N}Nx^* \Rightarrow \dot{\bar{x}} - \dot{x}^* = -A(\bar{x} - x^*) - \dot{x}^* \tag{12.19}$$

The variable $e_\sigma = \bar{x} - x^*$ is defined, and consequently

$$\dot{e}_\sigma = -Ae_\sigma - \dot{x}^* \tag{12.20}$$

The following cases can be distinguished:

(i) The target is not moving, i.e. $\dot{x}^* = 0$. In that case Eq. (12.20) results in an homogeneous differential equation, the solution of which is given by

$$\varepsilon_\sigma(t) = \varepsilon_\sigma(0)e^{-At} \tag{12.21}$$

Knowing that $A > 0$ results into $lim_{t\to\infty} e_\sigma(t) = 0$, thus $lim_{t\to\infty} \bar{x}(t) = x^*$.
(ii) the target is moving at constant velocity, i.e. $\dot{x^*} = a$, where $a > 0$ is a constant parameter. Then the error between the mean position of the multi-USV formation and the target becomes

$$\varepsilon_\sigma(t) = \left[\varepsilon_\sigma(0) + \frac{a}{A}\right]e^{-At} - \frac{a}{A} \tag{12.22}$$

where the exponential term vanishes as $t\to\infty$.
(iii) the target's velocity is described by a sinusoidal signal or a superposition of sinusoidal signals, as in the case of function approximation by Fourier series expansion. For instance consider the case that $\dot{x^*} = b{\cdot}sin(at)$, where $a, b > 0$ are constant parameters. Then the nonhomogeneous differential equation (12.20) admits a sinusoidal solution. Therefore the distance $\varepsilon_\sigma(t)$ between the center of the multi-USV formation $\bar{x}(t)$ and the target's position $x^*(t)$ will be also a bounded sinusoidal signal.

12.2.3.4 Convergence Analysis Using La Salle's Theorem

From Eq. (12.16) it has been shown that each USV will stay in a cycle C of center $\bar{x}$ and radius ε given by Eq. (12.17). The Lyapunov function given by Eq. (12.13) is negative semi-definite, therefore asymptotic stability cannot be guaranteed. It remains to make precise the area of convergence of each USV in the cycle C of center $\bar{x}$ and radius ε. To this end, La Salle's theorem can be employed [162, 230].

La Salle's Theorem: Assume the autonomous system $\dot{x} = f(x)$ where $f : D \to R^n$. Assume $C \subset D$ a compact set which is positively invariant with respect to $\dot{x} = f(x)$, i.e. if $x(0) \in C \Rightarrow x(t) \in C \; \forall\, t$. Assume that $V(x) : D \to R$ is a continuous and differentiable Lyapunov function such that $\dot{V}(x) \leq 0$ for $x \in C$, i.e. $V(x)$ is negative semi-definite in C. Denote by E the set of all points in C such that $\dot{V}(x) = 0$. Denote by M the largest invariant set in E and its boundary by L^+, i.e. for $x(t) \in E : lim_{t\to\infty} x(t) = L^+$, or in other words L^+ is the positive limit set of E. Then every solution $x(t) \in C$ will converge to M as $t \to \infty$ (Fig. 12.3).

La Salle's theorem is applicable in the case of the multi-USV system and helps to describe more precisely the area round $\bar{x}$ to which the USV trajectories x^i will converge. A generalized Lyapunov function is introduced which is expected to verify the stability analysis based on Eq. (12.16). It holds that

$$V(x) = \sum_{i=1}^{N} V^i(x^i) + \frac{1}{2}\sum_{i=1}^{N}\sum_{j=1, j\neq i}^{N}\{V_a(||x^i - x^j|| - V_r(||x^i - x^j||)\} \Rightarrow$$

$$V(x) = \sum_{i=1}^{N} V^i(x^i) + \frac{1}{2}\sum_{i=1}^{N}\sum_{j=1, j\neq i}^{N}\{a||x^i - x^j|| - V_r(||x^i - x^j||)$$

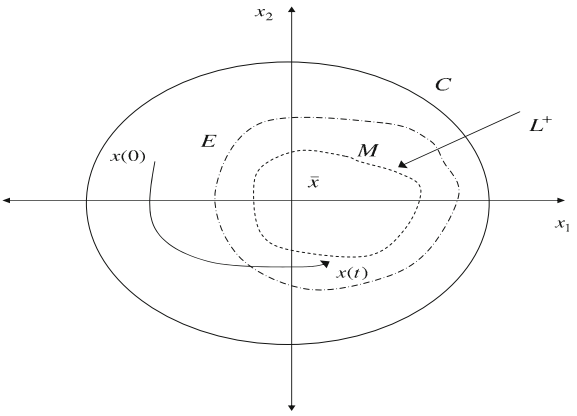

Fig. 12.3 LaSalle's Theorem: C: invariant set, $E \subset C$: invariant set which satisfies $\dot{V}(x) = 0$, $M \subset E$: invariant set, which satisfies $\dot{V}(x) = 0$, and which contains the limit points of $x(t) \in E$, L^+ the set of limit points of $x(t) \in E$

and

$$\nabla_{x^i} V(x) = \left[\sum_{i=1}^{N} \nabla_{x^i} V^i(x^i)\right] + \frac{1}{2}\sum_{i=1}^{N}\sum_{j=1, j\neq i}^{N} \nabla_{x^i}\{a||x^i - x^j|| - V_r(||x^i - x^j||)\} \Rightarrow$$

$$\nabla_{x^i} V(x) = \left[\sum_{i=1}^{N} \nabla_{x^i} V^i(x^i)\right] + \sum_{j=1, j\neq i}^{N} (x^i - x^j)\{g_a(||x^i - x^j||) - g_r(||x^i - x^j||)\} \Rightarrow$$

$$\nabla_{x^i} V(x) = \left[\sum_{i=1}^{N} \nabla_{x^i} V^i(x^i)\right] + \sum_{j=1, j\neq i}^{N} (x^i - x^j)\{a - g_r(||x^i - x^j||)\}$$

and using Eq. (12.10) with $\gamma^i(t) = 1$ yields $\nabla_{x^i} V(x) = -\dot{x}^i$, and

$$\dot{V}(x) = \nabla_x V(x)^T \dot{x} = \sum_{i=1}^{N} \nabla_{x^i} V(x)^T \dot{x}^i \Rightarrow \dot{V}(x) = -\sum_{i=1}^{N} ||\dot{x}^i||^2 \leq 0 \qquad (12.23)$$

Therefore it holds $V(x) > 0$ and $\dot{V}(x) \leq 0$ and the set $C = \{x : V(x(t)) \leq V(x(0))\}$ is compact and positively invariant. Thus, by applying La Salle's theorem one can show the convergence of $x(t)$ to the set $M \subset C$, $M = \{x : \dot{V}(x) = 0\} \Rightarrow M = \{x : \dot{x} = 0\}$.

12.2.4 Distributed State Estimation Using the Extended Information Filter

12.2.4.1 Extended Kalman Filtering at Local Processing Units

To implement the previously analyzed distributed control scheme it is necessary to obtain accurate localization of the target and precise estimation of its motion characteristics. To this end, distributed filtering can be used, which actually performs fusion of estimates of the target's state vector provided by filtering algorithms running locally at each USV [369, 370]. As mentioned, to obtain an accurate estimate of the

target's coordinates, fusion of the distributed sensor measurements can be performed either with the use of the Extended Information Filter or with the use of the Unscented Information Filter. The distributed Extended Kalman Filter, also known as Extended Information Filter, performs fusion of the state estimates which are provided by local Extended Kalman Filters. Thus, the functioning of the local Extended Kalman Filters should be analyzed first. The following nonlinear state-space model is considered again [431, 444]:

$$\begin{aligned} x(k+1) &= \phi(x(k)) + L(k)u(k) + w(k) \\ z(k) &= \gamma(x(k)) + v(k) \end{aligned} \tag{12.24}$$

where $x \in R^{m\times 1}$ is the system's state vector and $z \in R^{p\times 1}$ is the system's output, while $w(k)$ and $v(k)$ are uncorrelated, Gaussian zero-mean noise processes with covariance matrices $Q(k)$ and $R(k)$ respectively. The operators $\phi(x)$ and $\gamma(x)$ are $\phi(x) = [\phi_1(x), \phi_2(x), \ldots, \phi_m(x)]^T$, and $\gamma(x) = [\gamma_1(x), \gamma_2(x), \ldots, \gamma_p(x)]^T$, respectively. It is assumed that ϕ and γ are sufficiently smooth in x so that each one has a valid series Taylor expansion. Following a linearization procedure, ϕ is expanded into Taylor series about $\hat{x}$:

$$\phi(x(k)) = \phi(\hat{x}(k)) + J_\phi(\hat{x}(k))[x(k) - \hat{x}(k)] + \cdots \tag{12.25}$$

where $J_\phi(x)$ is the Jacobian of ϕ calculated at $\hat{x}(k)$:

$$J_\phi(x) = \frac{\partial \phi}{\partial x}|_{x=\hat{x}(k)} = \begin{pmatrix} \frac{\partial \phi_1}{\partial x_1} & \frac{\partial \phi_1}{\partial x_2} & \cdots & \frac{\partial \phi_1}{\partial x_m} \\ \frac{\partial \phi_2}{\partial x_1} & \frac{\partial \phi_2}{\partial x_2} & \cdots & \frac{\partial \phi_2}{\partial x_m} \\ \vdots & \vdots & \vdots & \vdots \\ \frac{\partial \phi_m}{\partial x_1} & \frac{\partial \phi_m}{\partial x_2} & \cdots & \frac{\partial \phi_m}{\partial x_m} \end{pmatrix} \tag{12.26}$$

Likewise, γ is expanded about $\hat{x}^-(k)$

$$\gamma(x(k)) = \gamma(\hat{x}^-(k)) + J_\gamma[x(k) - \hat{x}^-(k)] + \cdots \tag{12.27}$$

where $\hat{x}^-(k)$ is the estimation of the state vector $x(k)$ before measurement at the kth instant to be received and $\hat{x}(k)$ is the updated estimation of the state vector after measurement at the kth instant has been received. The Jacobian $J_\gamma(x)$ is

$$J_\gamma(x) = \frac{\partial \gamma}{\partial x}|_{x=\hat{x}^-(k)} = \begin{pmatrix} \frac{\partial \gamma_1}{\partial x_1} & \frac{\partial \gamma_1}{\partial x_2} & \cdots & \frac{\partial \gamma_1}{\partial x_m} \\ \frac{\partial \gamma_2}{\partial x_1} & \frac{\partial \gamma_2}{\partial x_2} & \cdots & \frac{\partial \gamma_2}{\partial x_m} \\ \vdots & \vdots & \vdots & \vdots \\ \frac{\partial \gamma_p}{\partial x_1} & \frac{\partial \gamma_p}{\partial x_2} & \cdots & \frac{\partial \gamma_p}{\partial x_m} \end{pmatrix} \tag{12.28}$$

The resulting expressions create first order approximations of ϕ and γ. Thus the linearized version of the system is obtained:

$$\begin{aligned} x(k+1) &= \phi(\hat{x}(k)) + J_{\phi}(\hat{x}(k))[x(k) - \hat{x}(k)] + w(k) \\ z(k) &= \gamma(\hat{x}^{-}(k)) + J_{\gamma}(\hat{x}^{-}(k))[x(k) - \hat{x}^{-}(k)] + v(k) \end{aligned} \tag{12.29}$$

Now, the EKF recursion is as follows: First the time update is considered: by $\hat{x}(k)$ the estimation of the state vector at instant k is denoted. Given initial conditions $\hat{x}^{-}(0)$ and $P^{-}(0)$ the recursion proceeds as:

- *Measurement update*. Acquire $z(k)$ and compute:

$$\begin{aligned} K(k) &= P^{-}(k) J_{\gamma}^{T}(\hat{x}^{-}(k)) \cdot [J_{\gamma}(\hat{x}^{-}(k)) P^{-}(k) J_{\gamma}^{T}(\hat{x}^{-}(k)) + R(k)]^{-1} \\ \hat{x}(k) &= \hat{x}^{-}(k) + K(k)[z(k) - \gamma(\hat{x}^{-}(k))] \\ P(k) &= P^{-}(k) - K(k) J_{\gamma}(\hat{x}^{-}(k)) P^{-}(k) \end{aligned} \tag{12.30}$$

- *Time update*. Compute:

$$\begin{aligned} P^{-}(k+1) &= J_{\phi}(\hat{x}(k)) P(k) J_{\phi}^{T}(\hat{x}(k)) + Q(k) \\ \hat{x}^{-}(k+1) &= \phi(\hat{x}(k)) + L(k) u(k) \end{aligned} \tag{12.31}$$

12.2.4.2 Calculation of Local Estimations in Terms of EIF Information Contributions

Again the discrete-time nonlinear system of Eq. (12.24) is considered. The Extended Information Filter (EIF) performs fusion of the local state vector estimates which are provided by the local Extended Kalman Filters, using the *Information matrix* and the *Information state vector* [259, 260, 315, 570]. The Information Matrix is the inverse of the state vector covariance matrix, and can be also associated to the Fisher Information matrix [463]. The Information state vector is the product between the Information matrix and the local state vector estimate

$$\begin{aligned} Y(k) &= P^{-1}(k) = I(k) \\ \hat{y}(k) &= P^{-}(k)^{-1} \hat{x}(k) = Y(k) \hat{x}(k) \end{aligned} \tag{12.32}$$

The update equations for the Information Matrix and the Information state vector are given by

$$\begin{aligned} Y(k) &= P^{-}(k)^{-1} + J_{\gamma}^{T}(k)R^{-1}(k)J_{\gamma}(k) \\ &= Y^{-}(k) + I(k) \end{aligned} \tag{12.33}$$

$$\begin{aligned} \hat{y}(k) &= \hat{y}^{-}(k) + J_{\gamma}^{T}R(k)^{-1}[z(k) - \gamma(x(k)) + J_{\gamma}\hat{x}^{-}(k)] \\ &= \hat{y}^{-}(k) + i(k) \end{aligned} \tag{12.34}$$

where

$$\begin{aligned} &I(k) = J_{\gamma}^{T}(k)R^{(}k)^{-1}J_{\gamma}(k) \text{ is the associated information matrix and} \\ &i(k) = J_{\gamma}^{T}R^{(}k)^{-1}[(z(k) - \gamma(x(k))) + J_{\gamma}\hat{x}^{-}(k)] \text{ is the information state contribution} \end{aligned} \tag{12.35}$$

The predicted information state vector and Information matrix are obtained from

$$\begin{aligned} \hat{y}^{-}(k) &= P^{-}(k)^{-1}\hat{x}^{-}(k) \\ Y^{-}(k) &= P^{-}(k)^{-1} = [J_{\phi}(k)P^{-}(k)J_{\phi}(k)^{T} + Q(k)]^{-1} \end{aligned} \tag{12.36}$$

The Extended Information Filter is next formulated for the case that multiple local sensor measurements and local estimates are used to increase the accuracy and reliability of the estimation of the target's cartesian coordinates and bearing. It is assumed that an observation vector $z^{i}(k)$ is available for N different sensor sites (USVs) $i = 1, 2, \ldots, N$ and each sensor observes a common state according to the local observation model, expressed by

$$z^{i}(k) = \gamma(x(k)) + v^{i}(k), \; i = 1, 2, \ldots, N \tag{12.37}$$

where the local noise vector $v^{i}(k) \sim N(0, R^{i})$ is assumed to be white Gaussian and uncorrelated between sensors. The variance of a composite observation noise vector v_k is expressed in terms of the block diagonal matrix

$$R(k) = diag[R(k)^{1}, \ldots, R^{N}(k)]^{T} \tag{12.38}$$

The information contribution can be expressed by a linear combination of each local information state contribution i^{i} and the associated information matrix I^{i} at the ith sensor site

$$\begin{aligned} i(k) &= \sum\nolimits_{i=1}^{N} J_{\gamma}^{i\,T}(k)R^{i}(k)^{-1}[z^{i}(k) - \gamma^{i}(x(k)) + J_{\gamma}^{i}(k)\hat{x}^{-}(k)] \\ I(k) &= \sum\nolimits_{i=1}^{N} J_{\gamma}^{i\,T}(k)R^{i}(k)^{-1}J_{\gamma}^{i}(k) \end{aligned} \tag{12.39}$$

Using Eq. (12.39) the update equations for fusing the local state estimates become

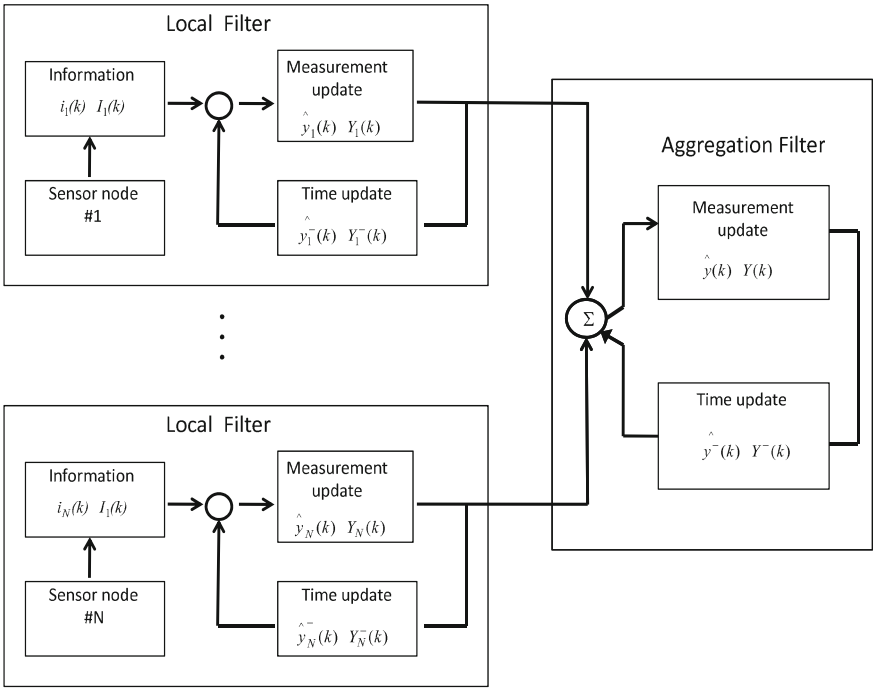

Fig. 12.4 Fusion of the distributed state estimates of the target (obtained by the USVs) with the use of the extended information filter

$$\hat{y}(k) = \hat{y}^-(k) + \sum_{i=1}^{N} J_\gamma^{i\,T}(k) R^i(k)^{-1} [z^i(k) - \gamma^i(x(k)) + J_\gamma^i(k)\hat{x}^-(k)]$$
$$Y(k) = Y^-(k) + \sum_{i=1}^{N} J_\gamma^{i\,T}(k) R^i(k)^{-1} J_\gamma^i(k) \tag{12.40}$$

It is noted that in the Extended Information Filter an aggregation (master) fusion filter produces a global estimate by using the local sensor information provided by each local filter.

As in the case of the Extended Kalman Filter the local filters which constitute the Extended information Filter can be written in terms of *time update* and a *measurement update* equation (Fig. 12.5).

Measurement update: Acquire $z(k)$ and compute

$$Y(k) = P^-(k)^{-1} + J_\gamma^T(k) R(k)^{-1} J_\gamma(k)$$
$$\text{or } Y(k) = Y^-(k) + I(k) \text{ where } I(k) = J_\gamma^T(k) R^{-1}(k) J_\gamma(k) \tag{12.41}$$

$$\hat{y}(k) = \hat{y}^-(k) + J_\gamma^T(k) R(k)^{-1} [z(k) - \gamma(\hat{x}(k)) + J_\gamma \hat{x}^-(k)]$$
$$\text{or } \hat{y}(k) = \hat{y}^-(k) + i(k) \tag{12.42}$$

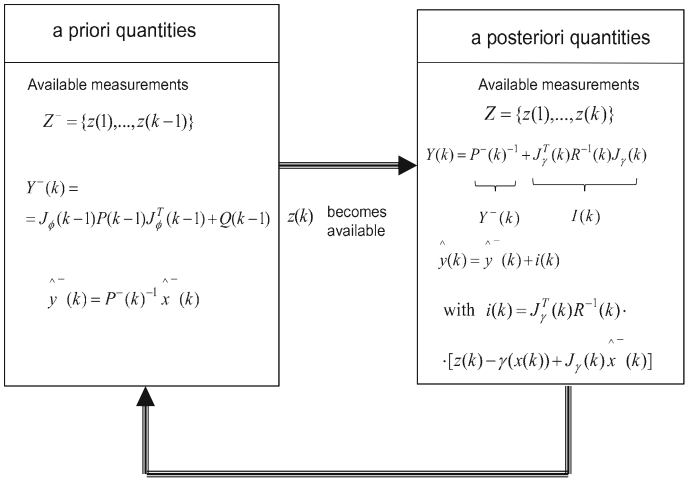

Fig. 12.5 Schematic diagram of the Extended Information Filter loop

Time update: Compute

$$Y^-(k+1) = P^-(k+1)^{-1} = [J_\phi(k)P(k)J_\phi(k)^T + Q(k)]^{-1} \tag{12.43}$$

$$y^-(k+1) = P^-(k+1)^{-1}\hat{x}^-(k+1) \tag{12.44}$$

12.2.4.3 Extended Information Filtering for State Estimates Fusion

In the Extended Information Filter each one of the local filters operates independently, processing its own local measurements. It is assumed that there is no sharing of measurements between the local filters and that the aggregation filter (Fig. 12.4) does not have direct access to the raw measurements feeding each local filter. The outputs of the local filters are treated as measurements which are fed into the aggregation fusion filter [259, 260, 570]. Then each local filter is expressed by its respective error covariance and estimate in terms of information contributions given in Eq. (12.36)

$$\begin{aligned} P_i^{-1}(k) &= P_i^-(k)^{-1} + J_\gamma^T R(k)^{-1} J_\gamma(k) \\ \hat{x}_i(k) &= P_i(k)(P_i^-(k)^{-1}\hat{x}_i^-(k)) + J_\gamma^T R(k)^{-1}[z^i(k) - \gamma^i(x(k)) + J_\gamma^i(k)\hat{x}_i^-(k)] \end{aligned} \tag{12.45}$$

It is noted that the local estimates are suboptimal and also conditionally independent given their own measurements. The global estimate and the associated error covariance for the aggregate fusion filter can be rewritten in terms of the computed estimates and covariances from the local filters using the relations

$$J_{\gamma}^{T}(k)R(k)^{-1}J_{\gamma}(k) = P_i(k)^{-1} - P_i^{-}(k)^{-1}$$
$$J_{\gamma}^{T}(k)R(k)^{-1}[z^i(k) - \gamma^i(x(k)) + J_{\gamma}^{i}(k)\hat{x}^{-}(k)] = P_i(k)^{-1}\hat{x}_i(k) - P_i(k)^{-1}\hat{x}_i(k-1) \tag{12.46}$$

For the general case of N local filters $i = 1, \ldots, N$, the distributed filtering architecture is described by the following equations

$$P(k)^{-1} = P^{-}(k)^{-1} + \sum_{i=1}^{N}[P_i(k)^{-1} - P_i^{-}(k)^{-1}]$$
$$\hat{x}(k) = P(k)[P^{-}(k)^{-1}\hat{x}^{-}(k) + \sum_{i=1}^{N}(P_i(k)^{-1}\hat{x}_i(k) - P_i^{-}(k)^{-1}\hat{x}_i^{-}(k))] \tag{12.47}$$

It is noted that the global state update equation in the above distributed filter can be written in terms of the information state vector and of the information matrix

$$\hat{y}(k) = \hat{y}^{-}(k) + \sum_{i=1}^{N}(\hat{y}_i(k) - \hat{y}_i^{-}(k))$$
$$\hat{Y}(k) = \hat{Y}^{-}(k) + \sum_{i=1}^{N}(\hat{Y}_i(k) - \hat{Y}_i^{-}(k)) \tag{12.48}$$

The local filters provide their own local estimates and repeat the cycle at step $k+1$. In turn the global filter can predict its global estimate and repeat the cycle at the next time step $k+1$ when the new state $\hat{x}(k+1)$ and the new global covariance matrix $P(k+1)$ are calculated. From Eq. (12.47) it can be seen that if a local filter (processing station) fails, then the local covariance matrices and the local state estimates provided by the rest of the filters will enable an accurate computation of the system's state vector.

12.2.5 Distributed State Estimation Using the Unscented Information Filter

12.2.5.1 Unscented Kalman Filtering at Local Processing Units

It is also possible to estimate the cartesian coordinates and bearing of the target through the fusion of the estimates provided by local Sigma-Point Kalman Filters. This can be accomplished using the Distributed Sigma-Point Kalman Filter, also known as *Unscented Information Filter* (UIF) [259, 260]. First, the functioning of the local Sigma-Point Kalman Filters will be explained. Each local Sigma-Point Kalman Filter generates an estimation of the target's state vector by fusing the estimate of the target's coordinates and bearing obtained by each USV with the distance of the target from a reference surface, measured in an inertial coordinates system. Unlike EKF, in Sigma-Point Kalman Filtering no analytical Jacobians of the system equations need to be calculated [219, 220, 492]. This is achieved through a different approach for calculating the posterior 1st and 2nd order statistics of a random variable that undergoes a nonlinear transformation. The state distribution is represented

again by a Gaussian random variable but is now specified using a minimal set of deterministically chosen weighted sample points. The basic sigma-point approach can be described as follows:

1. A set of weighted samples (sigma-points) are deterministically calculated using the mean and square-root decomposition of the covariance matrix of the system's state vector. As a minimal requirement the sigma-point set must completely capture the first and second order moments of the prior random variable. Higher order moments can be captured at the cost of using more sigma-points.
2. The sigma-points are propagated through the true nonlinear function using functional evaluations alone, i.e. no analytical derivatives are used, in order to generate a posterior sigma-point set.
3. The posterior statistics are calculated (approximated) using tractable functions of the propagated sigma-points and weights. Typically, these take on the form of a simple weighted sample mean and covariance calculations of the posterior sigma points.

It is noted that the sigma-point approach differs substantially from general stochastic sampling techniques such as Monte-Carlo integration (e.g Particle Filtering methods) which require significantly more sample points in an attempt to propagate an accurate (possibly non-Gaussian) distribution of the state. The deceptively simple sigma-point approach results in posterior approximations that are accurate to the third order for Gaussian inputs for all nonlinearities. For non-Gaussian inputs, approximations are accurate to at least the second-order, with the accuracy of third and higher-order moments determined by the specific choice of weights and scaling factors.

The Unscented Kalman Filter (UKF) is a special case of Sigma-Point Kalman Filters. The UKF is a discrete time filtering algorithm which uses the unscented transform for computing approximate solutions to the filtering problem for systems in the form

$$\begin{aligned} x(k+1) &= \phi(x(k)) + L(k)U(k) + w(k) \\ y(k) &= \gamma(x(k)) + v(k) \end{aligned} \tag{12.49}$$

where $x(k) \in R^n$ is the system's state vector, $y(k) \in R^m$ is the measurement, $w(k) \in R^n$ is a Gaussian process noise $w(k) \sim N(0, Q(k))$, and $v(k) \in R^m$ is a Gaussian measurement noise denoted as $v(k) \sim N(0, R(k))$. The mean and covariance of the initial state $x(0)$ are $m(0)$ and $P(0)$, respectively.

Some basic operations performed in the UKF algorithm (*Unscented Transform*) are summarized as follows:
(1) Denoting the current state mean as $\hat{x}$, a set of $2n + 1$ sigma points is taken from the columns of the $n \times n$ matrix $\sqrt{(n+\lambda)P_{xx}}$ as follows:

$$\begin{aligned} x^0 &= \hat{x} \\ x^i &= \hat{x} + [\sqrt{(n+\lambda)P_{xx}}]_i, \ i = 1, \ldots, n \\ x^i &= \hat{x} - [\sqrt{(n+\lambda)P_{xx}}]_i, \ i = n+1, \ldots, 2n \end{aligned} \tag{12.50}$$

and the associate weights are computed:

$$\begin{array}{cc} W_0^{(m)} = \frac{\lambda}{(n+\lambda)} & W_0^{(c)} = \frac{\lambda}{(n+\lambda)+(1-\alpha^2+b)} \\ W_i^{(m)} = \frac{1}{2(n+\lambda)}, \ i = 1, \ldots, 2n & W_i^{(c)} = \frac{1}{2(n+\lambda)} \end{array} \tag{12.51}$$

where $i = 1, 2, \ldots, 2n$ and $\lambda = \alpha^2(n + \kappa) - n$ is a scaling parameter, while α, β and κ are constant parameters. Matrix P_{xx} is the covariance matrix of the state x.
(2) Transform each of the sigma points as

$$z^i = h(x^i) \ \ i = 0, \ldots, 2n \tag{12.52}$$

(3) Mean and covariance estimates for z can be computed as

$$\begin{array}{c} \hat{z} \simeq \sum_{i=0}^{2n} W_i^{(m)} z^i \\ P_{zz} = \sum_{i=0}^{2n} W_i^{(c)} (z^i - \hat{z})(z^i - \hat{z})^T \end{array} \tag{12.53}$$

(4) The cross-covariance of x and z is estimated as

$$P_{xz} = \sum_{i=0}^{2n} W_i^{(c)} (x^i - \hat{x})(z^i - \hat{z})^T \tag{12.54}$$

The matrix square root of positive definite matrix P_{xx} means a matrix $A = \sqrt{P_{xx}}$ such that $P_{xx} = AA^T$ and a possible way for calculation is SVD.

Next the basic stages of the *Unscented Kalman Filter* are given:

As in the case of the Extended Kalman Filter and the Particle Filter, the Unscented Kalman Filter also consists of prediction stage (time update) and correction stage (measurement update) [219, 492].
Time update: Compute the predicted state mean $\hat{x}^-(k)$ and the predicted covariance $P_{xx}{}^-(k)$ as

$$\begin{array}{c} [\hat{x}^-(k), P_{xx}^-(k)] = UT(f_d, \hat{x}(k-1), P_{xx}(k-1)) \\ P_{xx}^-(k) = P_{xx}(k-1) + Q(k-1) \end{array} \tag{12.55}$$

Measurement update: Obtain the new output measurement z_k and compute the predicted mean $\hat{z}(k)$ and covariance of the measurement $P_{zz}(k)$, and the cross covariance of the state and measurement $P_{xz}(k)$

$$\begin{array}{c} [\hat{z}(k), P_{zz}(k), P_{xz}(k)] = UT(h_d, \hat{x}^-(k), P_{xx}^-(k)) \\ P_{zz}(k) = P_{zz}(k) + R(k) \end{array} \tag{12.56}$$

Then compute the filter gain $K(k)$, the state mean $\hat{x}(k)$ and the covariance $P_{xx}(k)$, conditional to the measurement $y(k)$

$$\begin{array}{c} K(k) = P_{xz}(k) P_{zz}^{-1}(k) \\ \hat{x}(k) = \hat{x}^-(k) + K(k)[z(k) - \hat{z}(k)] \\ P_{xx}(k) = P_{xx}^-(k) - K(k) P_{zz}(k) K(k)^T \end{array} \tag{12.57}$$

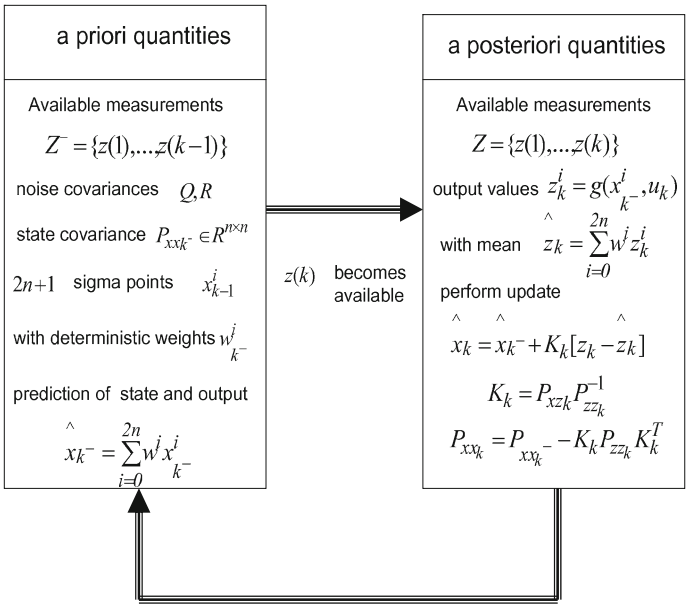

Fig. 12.6 Schematic diagram of the unscented Kalman filter loop

The filter starts from the initial mean $m(0)$ and covariance $P_{xx}(0)$. The stages of state vector estimation with the use of the Unscented Kalman Filter algorithm are depicted in Fig. 12.6.

12.2.5.2 Unscented Information Filtering

The Unscented Information Filter (UIF) performs fusion of the state vector estimates which are provided by local Unscented Kalman Filters, by weighting these estimates with local Information matrices (inverse of the local state vector covariance matrices which are again recursively computed) [259, 260, 570]. The Unscented Information Filter is derived by introducing a linear error propagation based on the unscented transformation into the Extended Information Filter structure. First, an augmented state vector $x_\alpha{}^-(k)$ is considered, along with the process noise vector, and the associated covariance matrix is introduced

$$\hat{x}_\alpha^-(k) = \begin{pmatrix} \hat{x}^-(k) \\ \hat{w}^-(k) \end{pmatrix}, \quad P^{\alpha -}(k) = \begin{pmatrix} P^-(k) & 0 \\ 0 & Q^-(k) \end{pmatrix} \tag{12.58}$$

As in the case of local (lumped) Unscented Kalman Filters, a set of weighted sigma points $X^i_\alpha{}^-(k)$ is generated as

$$\begin{aligned} X^-_{\alpha,0}(k) &= \hat{x}^-_\alpha(k) \\ X^-_{\alpha,i}(k) &= \hat{x}^-_\alpha(k) + [\sqrt{(n_\alpha+\lambda)P^-_\alpha(k-1)}]_i,\ i=1,\ldots,n \\ X^-_{\alpha,i}(k) &= \hat{x}^-_\alpha(k) + [\sqrt{(n_\alpha+\lambda)P^-_\alpha(k-1)}]_i,\ i=n+1,\ldots,2n \end{aligned} \tag{12.59}$$

where $\lambda = \alpha^2(n_\alpha+\kappa) - n_\alpha$ is a scaling, while $0 \leq \alpha \leq 1$ and κ are constant parameters. The corresponding weights for the mean and covariance are defined as in the case of the lumped Unscented Kalman Filter

$$\begin{aligned} W_0^{(m)} &= \tfrac{\lambda}{n_\alpha+\lambda} & W_0^{(c)} &= \tfrac{\lambda}{(n_\alpha+\lambda)+(1-\alpha^2+\beta)} \\ W_i^{(m)} &= \tfrac{1}{2(n_\alpha+\lambda)},\ i=1,\ldots,2n_\alpha & W_i^{(C)} &= \tfrac{1}{2(n_\alpha+\lambda)},\ i=1,\ldots,2n_\alpha \end{aligned} \tag{12.60}$$

where β is again a constant parameter. The equations of the prediction stage (measurement update) of the information filter, i.e. the calculation of the information matrix and the information state vector of Eq. (12.36) now become

$$\begin{aligned} \hat{y}^-(k) &= Y^-(k)\textstyle\sum_{i=0}^{2n_\alpha} W_i^m X_i^x(k) \\ Y^-(k) &= P^-(k)^{-1} \end{aligned} \tag{12.61}$$

where X_i^x are the predicted state vectors when using the sigma point vectors X_i^w in the state equation $X_i^x(k+1) = \phi(X_i^{w-}(k)) + L(k)U(k)$. The predicted state covariance matrix is computed as

$$P^-(k) = \sum_{i=0}^{2n_\alpha} W_i^{(c)}[X_i^x(k) - \hat{x}^-(k)][X_i^x(k) - \hat{x}^-(k)]^T \tag{12.62}$$

As noted, the equations of the Extended Information Filter (EIF) rely on the linearized dynamic model of the system and on the inverse of the covariance matrix of the state vector. However, in the equations of the Unscented Kalman Filter (UKF) there is no linearization of the system dynamics, thus the UKF cannot be included directly into the EIF equations. Instead, it is assumed that the nonlinear measurement equation of the system given in Eq. (12.24) can be mapped into a linear function of its statistical mean and covariance, which makes possible to use the information update equations of the EIF. Denoting $Y_i(k) = \gamma(X_i^x(k))$ (i.e. the output of the system calculated through the propagation of the ith sigma point X^i through the system's nonlinear equation) the observation covariance and its cross-covariance are approximated by

$$\begin{aligned} P^-_{YY}(k) &= E[(z(k) - \hat{z}^-(k))(z(k) - \hat{z}^-(k))^T] \\ &\simeq J_\gamma(k)P^-(k)J_\gamma(k)^T \end{aligned} \tag{12.63}$$

$$\begin{aligned} P^-_{XY}(k) &= E[(x(k) - \hat{x}(k)^-)(z(k) - \hat{z}(k)^-)^T] \\ &\simeq P^-(k)J_\gamma(k)^T \end{aligned} \tag{12.64}$$

where $z(k) = \gamma(x(k))$ and $J_\gamma(k)$ is the Jacobian of the output equation $\gamma(x(k))$. Next, multiplying the predicted covariance and its inverse term on the right side of the information matrix Eq. (12.35) and replacing $P(k)J_\gamma(k)^T$ with $P_{XY}^-(k)$ gives the following representation of the information matrix [259, 260, 570]

$$\begin{aligned} I(k) &= J_\gamma(k)^T R(k)^{-1} J_\gamma(k) \\ &= P^-(k)^{-1} P^-(k) J_\gamma(k)^T R(k)^{-1} J_\gamma^-(k) P^-(k)^T (P^-(k)^{-1})^T \\ &= P^-(k)^{-1} P_{XY}(k) R(k)^{-1} P_{XY}(k)^T (P^-(k)^{-1})^T \end{aligned} \tag{12.65}$$

where $P^-(k)^{-1}$ is calculated according to Eq. (12.62) and the cross-correlation matrix $P_{XY}(k)$ is calculated from

$$P_{XY}^-(k) = \sum_{i=0}^{2n_\alpha} W_i^{(c)} [X_i^x(k) - \hat{x}^-(k)][Y_i(k) - \hat{z}^-(k)]^T \tag{12.66}$$

where $Y_i(k) = \gamma(X_i^x(k))$ and the predicted measurement vector $\hat{z}^-(k)$ is obtained by $\hat{z}^-(k) = \sum_{i=0}^{2n_\alpha} W_i^{(m)} Y_i(k)$. Similarly, the information state vector i_k can be rewritten as

$$\begin{aligned} i(k) &= J_\gamma(k)^T R(k)^{-1} [z(k) - \gamma(x(k)) + J_\gamma(k)^T \hat{x}^-(k)] \\ &= P^-(k)^{-1} P^-(k) J_\gamma(k)^T R(k)^{-1} [z(k) - \gamma(x(k)) + J_\gamma(k)^T (P^-(k))^T (P^-(k)^{-1})^T \hat{x}^-(k)] \\ &= P^-(k)^{-1} P_{XY}^-(k) R(k)^{-1} [z(k) - \gamma(x(k)) + P_{XY}^-(k) (P^-(k)^{-1})^T \hat{x}^-(k)] \end{aligned} \tag{12.67}$$

To complete the analogy to the information contribution equations of the EIF a "measurement" matrix $H^T(k)$ is defined as

$$H(k)^T = P^-(k)^{-1} P_{XY}^-(k) \tag{12.68}$$

In terms of the "measurement" matrix $H(k)$ the information contributions equations are written as

$$\begin{aligned} i(k) &= H^T(k) R(k)^{-1} [z(k) - \gamma(x(k)) + H(k)\hat{x}^-(k)] \\ I(k) &= H^T(k) R(k)^{-1} H(k) \end{aligned} \tag{12.69}$$

The above procedure leads to an implicit linearization in which the nonlinear measurement equation of the system given in Eq. (12.24) is approximated by the statistical error variance and its mean

$$z(k) = \gamma(x(k)) \simeq H(k)x(k) + \bar{u}(k) \tag{12.70}$$

where $\bar{u}(k) = \gamma(\hat{x}^-(k)) - H(k)\hat{x}^-(k)$ is a measurement residual term.

12.2.5.3 Calculation of Local Estimations in Terms of UIF Information Contributions

Next, the local estimations provided by distributed (local) Unscented Kalmans filters will be expressed in terms of the information contributions (information matrix I and information state vector i) of the Unscented Information Filter, which were defined in Eq. (12.69) [259, 260, 570]. It is assumed that the observation vector $\bar{z}_i(k+1)$ is available from N different sensors, and that each sensor observes a common state according to the local observation model, expressed by

$$\bar{z}_i(k) = H_i(k)x(k) + \bar{u}_i(k) + v_i(k) \tag{12.71}$$

where the noise vector $v_i(k)$ is taken to be white Gaussian and uncorrelated between sensors. The variance of the composite observation noise vector v_k of all sensors is written in terms of the block diagonal matrix $R(k) = diag[R_1(k)^T, \ldots, R_N(k)^T]^T$. Then one can define the local information matrix $I_i(k)$ and the local information state vector $i_i(k)$ at the ith sensor, as follows

$$\begin{gathered} i_i(k) = H_i^T(k)R_i(k)^{-1}[z_i(k) - \gamma^i(x(k)) + H_i(k)\hat{x}^-(k)] \\ I_i(k) = H_i^T(k)R_i(k)^{-1}H_i(k) \end{gathered} \tag{12.72}$$

Since the information contribution terms have group diagonal structure regarding their innovation and measurement matrix, the update equations for the multiple state estimations and data fusion are written as a linear combination of the local information contribution terms

$$\begin{gathered} \hat{y}(k) = \hat{y}^-(k) + \sum_{i=1}^{N} i_i(k) \\ Y(k) = Y^-(k) + \sum_{i=1}^{N} I_i(k) \end{gathered} \tag{12.73}$$

Then using Eq. (12.61) one can find the mean state vector for the multiple sensor estimation problem.

As in the case of the Unscented Kalman Filter, the Unscented Information Filter running at the ith measurement processing unit can be written in terms of *measurement update* and *time update* equations (Fig. 12.7):

Measurement update: Acquire measurement $z(k)$ and compute

$$\begin{gathered} Y(k) = P^-(k)^{-1} + H^T(k)R^{-1}(k)H(k) \\ \text{or } Y(k) = Y^-(k) + I(k) \text{ where } I(k) = H^T(k)R^{-1}(k)H(k) \end{gathered} \tag{12.74}$$

$$\begin{gathered} \hat{y}(k) = \hat{y}^-(k) + H^T(k)R^{-1}(k)[z(k) - \gamma(\hat{x}(k)) + H(k)\hat{x}^-(k)] \\ \text{or } \hat{y}(k) = \hat{y}^-(k) + i(k) \end{gathered} \tag{12.75}$$

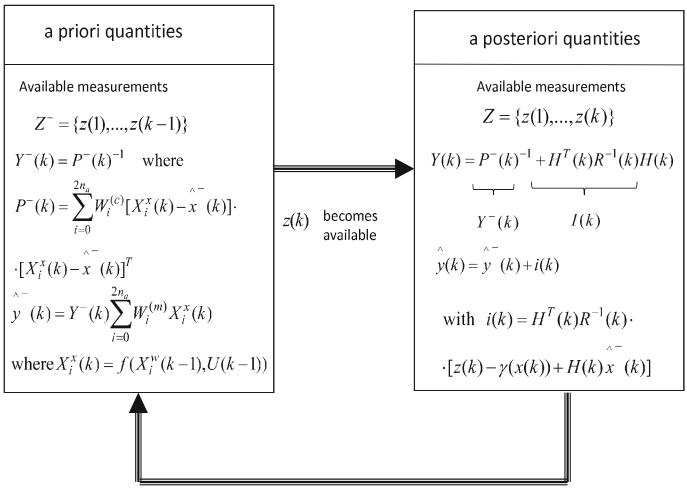

Fig. 12.7 Schematic diagram of the unscented information filter loop

Time update: Compute

$$Y^-(k+1) = (P^-(k+1))^{-1}$$

$$\text{where } P^-(k+1) = \sum_{i=0}^{2n_\alpha} W_i^{(c)}[X_i^x(k+1) - \hat{x}^-(k+1)][X_i^x(k+1) - \hat{x}^-(k+1)]^T \tag{12.76}$$

$$\hat{y}(k+1) = Y(k+1)\sum_{i=0}^{2n_\alpha} W_i^{(m)} X_i^x(k+1)$$
$$\text{where } X_i^x(k+1) = \phi(X_i^w(k)) + L(k)U(k) \tag{12.77}$$

12.2.5.4 Distributed Unscented Information Filtering for State Estimates Fusion

It has been shown that the update of the aggregate state vector of the Unscented Information Filter approach can be expressed in terms of the local information matrices I_i and of the local information state vectors i_i, which in turn depend on the local covariance matrices P and cross-covariance matrices P_{XY}. Next, it will be shown that the update of the aggregate state vector can be also expressed in terms of the local state vectors $x_i(k)$ and in terms of the local covariance matrices $P_i(k)$ and cross-covariance matrices $P_{XY}^i(k)$. It is assumed that the local filters do not have access to each other's row measurements and that they are allowed to communicate only their information matrices and their local information state vectors. Thus each local filter is expressed by its error covariance and estimate in terms of the local information state contribution i_i and its associated information matrix I_i at the ith filter site. Then using Eq. (12.61) one obtains

$$P_i(k)^{-1} = P_i^-(k)^{-1} + H_i^T(k)R_i(k)^{-1}H_i(k)$$
$$\hat{x}_i = P_i(k)(P_i^-(k)\hat{x}_i^-(k) + H_i^T(k)R_i(k)^{-1}[z_i(k) - \gamma^i(x(k)) + H_i(k)\hat{x}^-(k)]) \tag{12.78}$$

Using Eq. (12.78), each local information state contribution i_i and its associated information matrix I_i at the ith filter are rewritten in terms of the computed estimates and covariances of the local filters

$$H_i^T(k)R_i(k)^{-1}H_i(k) = P_i{}^{-1}(k) - P_i^-(k)^{-1}$$
$$H_i^T(k)R_i(k)^{-1}[z_i(k) - \gamma^i(x(k)) + H_i(k)\hat{x}^-(k)]) = P_i(k)^{-1}\hat{x}_i(k) - P_i^-(k)^{-1}\hat{x}_i^-(k) \tag{12.79}$$

where according to Eq. (12.68) it holds $H_i(k) = P_i^-(k)^{-1}P_{XY,i}^-(k)$. Next, the aggregate estimates of the distributed Unscented Information Filtering are derived for a number of N local filters $i = 1, \ldots, N$ and sensor measurements, first in terms of covariances [259, 260, 570].

$$P(k)^{-1} = P^-(k)^{-1} + \sum_{i=1}^N [P_i(k)^{-1} - P_i^-(k)^{-1}]$$
$$\hat{x}(k) = P(k)[P^-(k)^{-1}\hat{x}^-(k) + \sum_{i=1}^N (P_i(k)^{-1}\hat{x}_i(k) - P_i^-(k)^{-1}\hat{x}_i^-(k))] \tag{12.80}$$

and also in terms of the information state vector and of the information state covariance matrix

$$\hat{y}(k) = \hat{y}^-(k) + \sum_{i=1}^N (\hat{y}_i(k) - \hat{y}_i^-(k))$$
$$Y(k) = Y^-(k) + \sum_{i=1}^N [Y_i(k) - Y_i^-(k)] \tag{12.81}$$

State estimation fusion based on the Unscented Information Filter (UIF) is fault tolerant. From Eq. (12.80) it can be seen that if a local filter (processing unit) fails, then the local covariance matrices and local estimates provided by the rest of the filters will enable a reliable calculation of the system's state vector. Moreover, the UIF is computationally more efficient comparing to centralized filters and results in enhanced estimation accuracy.

12.2.6 Filtering Using Differential Flatness Theory and Canonical Forms

12.2.6.1 Transformation of MIMO Systems into Canonical Forms

The conditions for applying differential flatness theory towards transforming a nonlinear MIMO model into the canonical form have been given in Sect. 1.3.3. It is assumed now that after defining the flat outputs of the initial MIMO nonlinear system (this approach will be also shown to hold for the kinematics of the target), and

after expressing the system state variables and control inputs as functions of the flat output and of the associated derivatives, the system can be rewritten in the Brunovsky canonical form:

$$\begin{aligned}
&\dot{x}_1 = x_2 \\
&\cdots \\
&\dot{x}_{r_1-1} = x_{r_1} \\
&\dot{x}_{r_1} = f_1(x) + \textstyle\sum_{j=1}^{p} g_{1_j}(x)u_j + d_1 \\
&\dot{x}_{r_1+1} = x_{r_1+2} \\
&\cdots \\
&\dot{x}_{p-1} = x_p \\
&\dot{x}_p = f_p(x) + \textstyle\sum_{j=1}^{p} g_{p_j}(x)u_j + d_p
\end{aligned} \qquad \begin{aligned}
&y_1 = x_1 \\
&\cdots \\
&y_2 = x_{r_i+1} \\
&\cdots \\
&y_p = x_{n-r_p+1}
\end{aligned} \tag{12.82}$$

where $x = [x_1, \ldots, x_n]^T$ is the state vector of the transformed system (according to the differential flatness formulation), $u = [u_1, \ldots, u_p]^T$ is the set of control inputs, $y = [y_1, \ldots, y_p]^T$ is the output vector, f_i are the drift functions and $g_{i,j}$, $i, j = 1, 2, \ldots, p$ are smooth functions corresponding to the control input gains, while d_j is a variable associated to external disturbances. It holds that $r_1 + r_2 + \cdots + r_p = n$. Having written the initial nonlinear system into the canonical (Brunovsky) form it holds

$$y_i^{(r_i)} = f_i(x) + \textstyle\sum_{j=1}^{p} g_{ij}(x)u_j + d_j \tag{12.83}$$

Next the following vectors and matrices can be defined: $f(x) = [f_1(x), \ldots, f_n(x)]^T$, $g(x) = [g_1(x), \ldots, g_n(x)]^T$, with $g_i(x) = [g_{1i}(x), \ldots, g_{pi}(x)]^T$, $A = diag[A_1, \ldots, A_p]$, $B = diag[B_1, \ldots, B_p]$, $C^T = diag[C_1, \ldots, C_p]$, $d = [d_1, \ldots, d_p]^T$, where matrix A has the MIMO canonical form, i.e. with block-diagonal elements

$$A_i = \begin{pmatrix} 0 & 1 & \cdots & 0 \\ 0 & 0 & \cdots & 0 \\ \vdots & \vdots & \cdots & \vdots \\ 0 & 0 & \cdots & 1 \\ 0 & 0 & \cdots & 0 \end{pmatrix}_{r_i \times r_i} \qquad \begin{aligned} B_i^T &= \begin{pmatrix} 0 & 0 & \cdots & 0 & 1 \end{pmatrix}_{1 \times r_i} \\ C_i &= \begin{pmatrix} 1 & 0 & \cdots & 0 & 0 \end{pmatrix}_{1 \times r_i} \end{aligned} \tag{12.84}$$

As shown in previous chapters, Eq. (12.83) can be written in state-space form

$$\begin{aligned} \dot{x} &= Ax + Bv + B\tilde{d} \\ y &= Cx \end{aligned} \tag{12.85}$$

where the control input is written as $v = f(x) + g(x)u$. The system of Eq. (12.84) and Eq. (12.85) is in controller and observer canonical form.

12.2.6.2 Canonical Forms for the USV Model

It is assumed now that the target's velocity has to be estimated through the processing of the sequence of position measurements by a filtering algorithm. To this end the Derivative-free nonlinear Kalman Filter for MIMO nonlinear dynamical systems can be used. From the application of the differential flatness theory for transforming the initial nonlinear model of the target vessel into a linearized equivalent that is finally written in the Brunovsky form, one has Eq. (12.4) which means $\ddot{x} = u_1$ and $\ddot{y} = u_2$. Next, the state variables $x_1 = x, x_2 = \dot{x}, x_3 = y$ and $x_4 = \dot{y}$ are defined. Considering the state vector $x \in R^{4\times 1}$, the following matrices are also defined

$$A = \begin{pmatrix} 0 & 1 & 0 & 0 \\ 0 & 0 & 0 & 0 \\ 0 & 0 & 0 & 1 \\ 0 & 0 & 0 & 0 \end{pmatrix}, \quad B = \begin{pmatrix} 0 & 0 \\ 1 & 0 \\ 0 & 0 \\ 0 & 1 \end{pmatrix} \qquad C = \begin{pmatrix} 1 & 0 & 0 & 0 \\ 0 & 0 & 1 & 0 \end{pmatrix} \tag{12.86}$$

Using the matrices of Eq. (12.86) one obtains the Brunovsky form of the MIMO model of the target $\dot{x} = Ax + Bv$ and $y = Cx$, where the new input v is given by $v = [u_1(x,t), u_2(x,t)]^T$. This is a state-space model in the form of Eq. (12.85), for which state estimation can be performed using the standard Kalman Filter recursion.

12.2.6.3 Derivative-Free Extended Information Filtering

As mentioned above, for the system of Eq. (12.86), state estimation is possible by applying the standard Kalman Filter. The system is first turned into discrete-time form using common discretization methods, and the discrete-time equivalents of matrices A, B, C are denoted as A_d, B_d and C_d respectively. Then the recursion of the linear Kalman Filter described in Eqs. (12.87) and (12.88) is applied.

Measurement Update:

$$\begin{aligned} K(k) &= P^-(k)C_d^T[C_d \cdot P^-(k)C_d^T + R]^{-1} \\ \hat{x}(k) &= \hat{x}^-(k) + K(k)[z(k) - C_d\hat{x}^-(k)] \\ P(k) &= P^-(k) - K(k)C_dP^-(k) \end{aligned} \tag{12.87}$$

Time Update:

$$\begin{aligned} P^-(k+1) &= A_d(k)P(k)A_d^T(k) + Q(k) \\ \hat{x}^-(k+1) &= A_d(k)\hat{x}(k) + B_d(k)u(k) \end{aligned} \tag{12.88}$$

If the Derivative-free nonlinear Kalman Filter is used in place of the Extended Kalman Filter which has been previously described in Sect. 12.2.4, then in the Extended Information Filter (EIF) equations the following matrix substitutions

should be performed: $J_\phi(k) \rightarrow A_d$, $J_\gamma(k) \rightarrow C_d$, where matrices A_d and C_d are the discrete-time equivalents of matrices A and C which have been defined Eq. (12.86) and which appear also in the measurement and time update of the standard Kalman Filter recursion, given above. Matrices A_d and C_d can be computed using known discretization methods. Moreover, the covariance matrices $P(k)$ and $P^-(k)$ are the ones obtained from the linear Kalman Filter update equations given in the previous Eqs. (12.87) and (12.88).

12.2.7 Simulation Tests

12.2.7.1 Estimation of Target's Position With the Use of the Extended Information Filter

The number of USVs used for target tracking in the simulation experiments was $N = 10$. However, since the USVs team is modular a larger number of USVs could have been also considered. It is assumed that each USV can obtain an estimation of the target's cartesian coordinates and bearing, i.e. the target's cartesian coordinates $[x, y]$ as well as the target's orientation θ. To improve the accuracy of the target's localization, the target's coordinates and bearing are fused with the distance of the target from a reference surface measured in an inertial coordinates system (see Figs. 12.2 and 12.8).

The inertial coordinates system OXY is defined. Furthermore the coordinates system $O'X'Y'$ is considered (Fig. 12.8). $O'X'Y'$ results from OXY if it is rotated by an angle θ (Fig. 12.8). The coordinates of the center of the target vessel with respect to OXY are (x, y), while the coordinates of the reference point i that is on the target vessel (e.g. bridge), with respect to $O'X'Y'$ are $x_i^{'}$, $y_i^{'}$. The orientation of the reference point with respect to $OX'Y'$ is $\theta_i^{'}$. Thus the coordinates of the reference point with respect to OXY are (x_i, y_i) and its orientation is θ_i, and are given by:

$$\begin{aligned} x_i(k) &= x(k) + x_i^{'} sin(\theta(k)) + y_i^{'} cos(\theta(k)) \\ y_i(k) &= y(k) - x_i^{'} cos(\theta(k)) + y_i^{'} sin(\theta(k)) \\ \theta_i(k) &= \theta(k) + \theta_i \end{aligned} \tag{12.89}$$

Each plane P^j in the USV's environment can be represented by P_r^j and P_n^j (Fig. 12.8), where (i) P_r^j is the normal distance of the plane from the origin O, (ii) P_n^j is the angle between the normal line to the plane and the x-direction.

The target's reference point i is at position $x_i(k)$, $y_i(k)$ with respect to the inertial coordinates system OXY and its orientation is $\theta_i(k)$. Using the above notation, the distance of the reference point i, from the plane P^j is represented by P_r^j, P_n^j (see Fig. 12.8):

$$d_i^j(k) = P_r^j - x_i(k) cos(P_n^j) - y_i(k) sin(P_n^j) \tag{12.90}$$

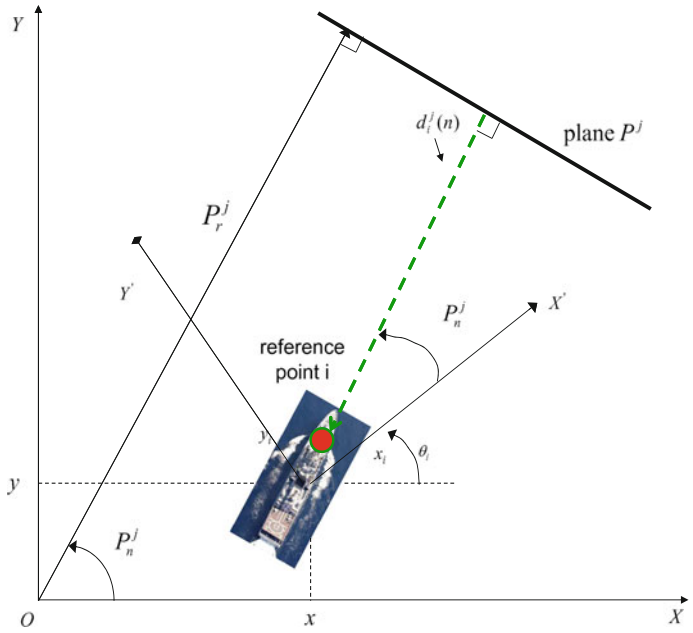

Fig. 12.8 Distance of the target's reference point i from the reference plane P^j, measured in the inertial coordinates system OXY

Assuming a constant sampling period $\Delta t_k = T$ the measurement equation is $z(k+1) = \gamma(x(k)) + v(k)$, where $z(k)$ is the vector containing target's coordinates and bearing estimates obtained from a mobile sensor and the measurement of the target's distance to the reference surface, while $v(k)$ is a white noise sequence $\sim N(0, R(kT))$. The measure vector $z(k)$ can thus be written as

$$z(k) = [x(k) + v_1(k),\, y(k) + v_2(k),\, \theta(k) + v_3(k),\, d_1^j(k) + v_4(k)] \tag{12.91}$$

with $i = 1, 2, \ldots, n_s$, $d_i^j(k)$ to be the distance measure with respect to the plane P^j and $j = 1, \ldots, n_p$ to be the number of reference surfaces. By definition of the measurement vector one has that the output function $\gamma(x(k))$ is given by $\gamma(x(k)) = [x(k), y(k), \theta(k), d_1^1(k)]$.

To obtain the Extended Kalman Filter (EKF), the kinematic model of the target described in Eq. (12.2) is discretized and written in the discrete-time state-space form of Eq. (12.24) [450, 457].

The *measurement update* of the EKF is

$$\begin{aligned}
K(k) &= P^-(k) J_\gamma^T(\hat{x}^-(k))[J_\gamma(\hat{x}^-(k)) P^-(k) J_\gamma^T(\hat{x}^-(k)) + R(k)]^{-1} \\
\hat{x}(k) &= \hat{x}^-(k) + K(k)[z(k) - \gamma(\hat{x}^-(k))] \\
P(k) &= P^-(k) - K(k) J_\gamma^T P^-(k)
\end{aligned}$$

The *time update* of the EKF is

$$P^{-}(k+1) = J_{\phi}(\hat{x}(k))P(k)J_{\phi}^{T}(\hat{x}(k)) + Q(k)$$
$$\hat{x}^{-}(k+1) = \phi(\hat{x}(k)) + L(k)U(k)$$

where

$$L(k) = \begin{pmatrix} Tcos(\theta(k)) & 0 \\ Tsin(\theta(k)) & 0 \\ 0 & T \end{pmatrix}$$

and

$$J_{\phi}(\hat{x}(k)) = \begin{pmatrix} 1 & 0 & -v(k)sin(\theta)T \\ 0 & 1 & -v(k)cos(\theta)T \\ 0 & 0 & 1 \end{pmatrix}$$

while $Q(k) = diag[\sigma^2(k), \sigma^2(k), \sigma^2(k)]$, with $\sigma^2(k)$ chosen to be 10^{-3} and $\phi(\hat{x}(k)) = [\hat{x}(k), \hat{y}(k), \hat{\theta}(k)]^T$, $\gamma(\hat{x}(k)) = [\hat{x}(k), \hat{y}(k), \hat{\theta}(k), d(k)]^T$, i.e.

$$\gamma(\hat{x}(k)) = \begin{pmatrix} \hat{x}(k) \\ \hat{y}(k) \\ \hat{\theta}(k) \\ P_r^j - x_i(k))cos(P_n^j) - y_i(k)sin(P_n^j) \end{pmatrix} \tag{12.92}$$

The vector of the control input is given by $U(k) = [v(k), \omega(k)]^T$. Assuming one reference surface in the target's neighborhood one gets

$$J_{\gamma}^{T}(\hat{x}^{-}(k)) = [J_{\gamma 1}(\hat{x}^{-}(k)), J_{\gamma 2}(\hat{x}^{-}(k)), J_{\gamma 3}(\hat{x}^{-}(k)), J_{\gamma 4}(\hat{x}^{-}(k))]^T, \text{ i.e.}$$

$$J_{\gamma}^{T}(\hat{x}^{-}(k)) = \begin{pmatrix} 1 & 0 & 0 \\ 0 & 1 & 0 \\ 0 & 0 & 1 \\ -cos(P_n^j) & -sin(P_n^j) & \{x_i^{'}cos(\theta - P_n^j) - y_i^{'}sin(\theta - P_n^j)\} \end{pmatrix} \tag{12.93}$$

The use of EKF for fusing the target's coordinates and bearing measured by each USV with the target's distance from a reference surface measured in an inertial coordinates system provides an estimation of the state vector $[x(t), y(t), \theta(t)]$ and enables the successful tracking of the target's motion by the individual USVs (mobile sensors).

The tracking of the target by the team of the USVs was tested in the case of several reference trajectories, both for motion in an environment without obstacles as well as for motion in a plane containing obstacles. The proposed distributed filtering scheme enabled accurate estimation of the target's state vector $[x, y, \theta]^T$ through the fusion of the measurements of the target's coordinates and orientation obtained by each USV with the measurement of the distance from a reference surface in an iner-

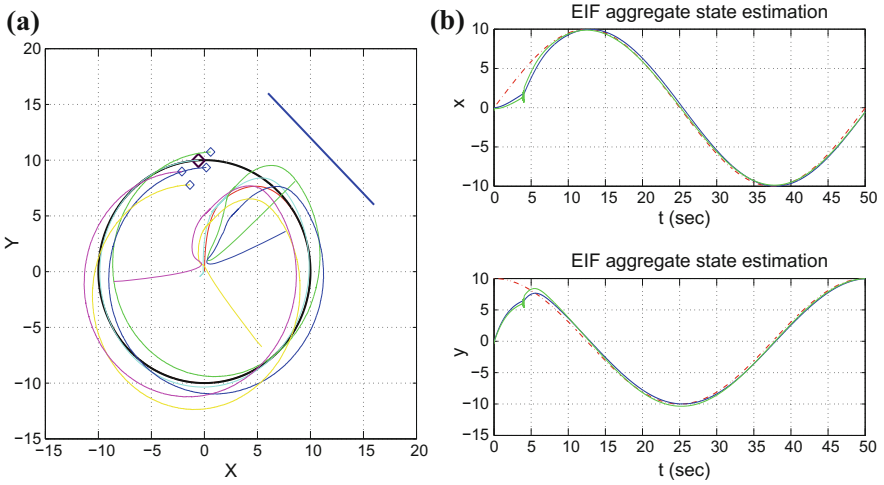

Fig. 12.9 **a** Distributed target tracking by a team of USVs when the target follows a circular trajectory in an obstacles-free motion space, **b** Aggregate estimation of the target's position with the use of Extended Information Filtering (continuous line) and target's reference path (dashed line)

tial coordinates frame. The state estimates provided by the Extended Kalman Filters running at each USV were fused into one single state estimate using Extended Information Filtering. The aggregate estimated coordinates of the target $(\hat{x}^*, \hat{y}^*)$ provided the reference setpoint for the distributed motion planning algorithm. Each USV was made to move along the path defined by $(\hat{x}^*, \hat{y}^*)$. The convergence properties of the distributed motion planning algorithm were described in Sect. 12.2.3. The tracking of the target's trajectory by the USVs as well as the accuracy of the two-level sensor fusion-based estimation of the target's coordinates is depicted in Figs. 12.9, 12.10, 12.11, 12.12 and 12.13. The target is marked as a thick-line rectangle and the associated reference trajectory is plotted as a thick line.

It is noted that using distributed EKFs and fusion through the Extended Information Filter is more robust comparing to the centralized EKF since (i) if a local processing unit is subject to a fault then state estimation is still possible and can be used for accurate localization of the target, as well as for tracking of the target's trajectory by the individual mobile robots (unmanned surface vessels), (ii) communication overhead remains low even in the case of a large number of distributed mobile sensors, because the greatest part of state estimation procedure is performed locally and only information matrices and state vectors are communicated between the local processing units, (iii) the aggregation performed on the local EKF also compensates for deviations in state estimates of local filters (which can be due to linearization errors).

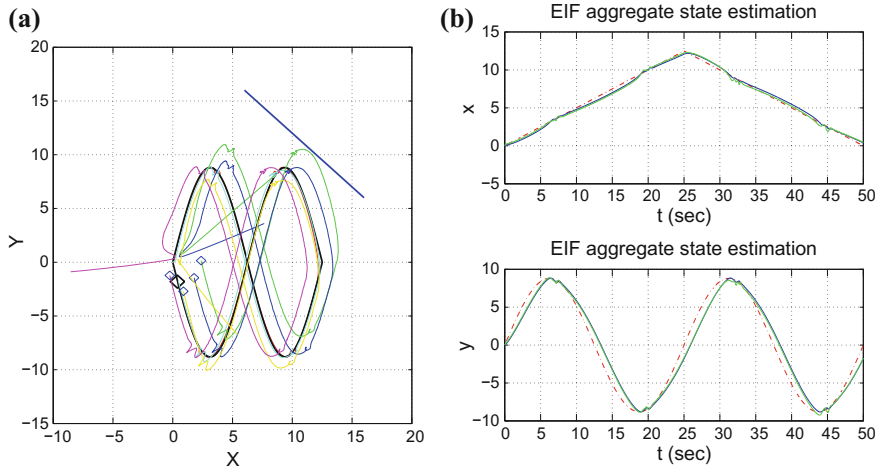

Fig. 12.10 **a** Distributed target tracking by a team of USVs when the target follows an eight-shaped trajectory in an obstacles-free motion space, **b** Aggregate estimation of the target's position with the use of Extended Information Filtering (continuous line) and target's reference path (dashed line)

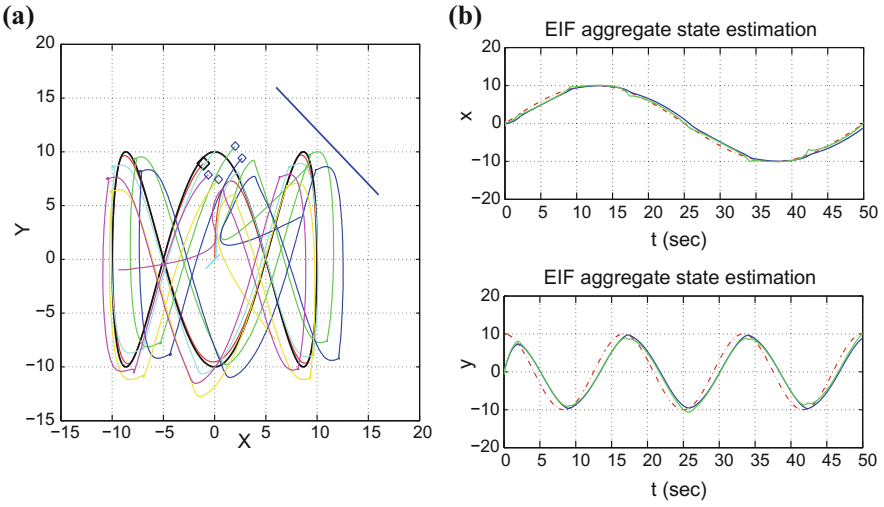

Fig. 12.11 **a** Distributed target tracking by a team of USVs when the target follows a curve-shaped trajectory in an obstacles-free motion space, **b** Aggregate estimation of the target's position with the use of Extended Information Filtering (continuous line) and target's reference path (dashed line)

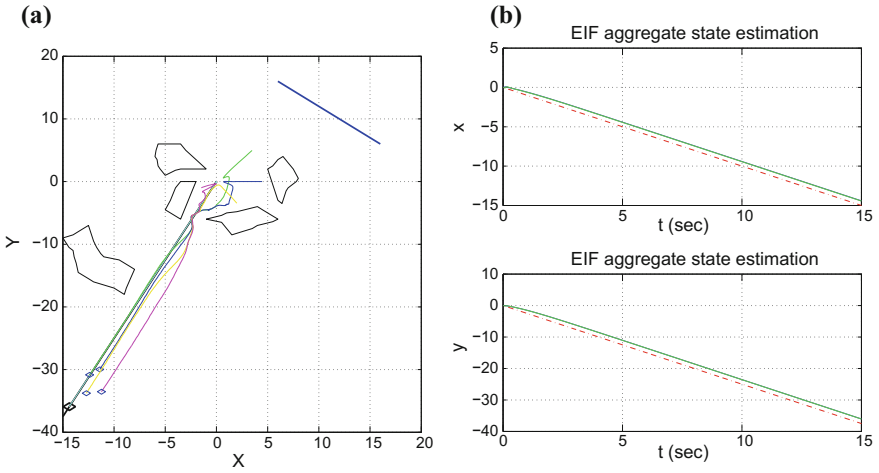

Fig. 12.12 **a** Distributed target tracking by a team of USVs when the target follows a line path in a motion space with obstacles, **b** Aggregate estimation of the target's position with the use of Extended Information Filtering (continuous line) and target's reference path (dashed line)

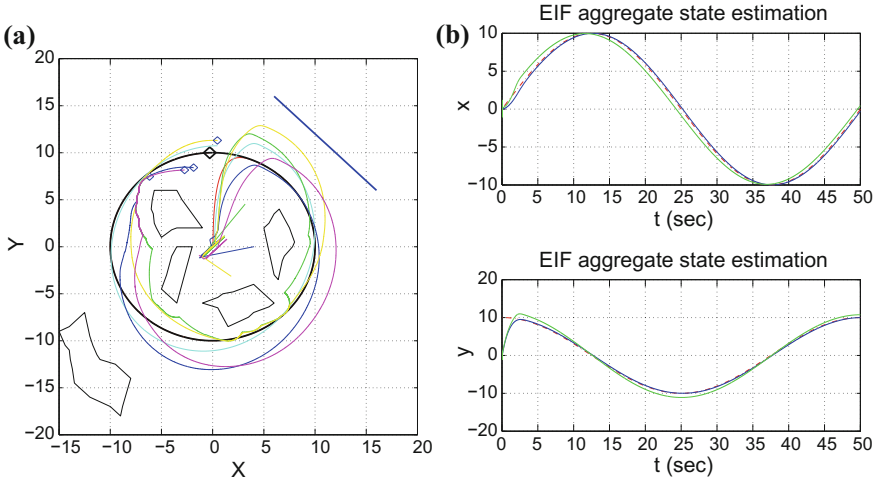

Fig. 12.13 **a** Distributed target tracking by a team of USVs when the target follows a circular path in a motion space with obstacles, **b** Aggregate estimation of the target's position with the use of Extended Information Filtering (continuous line) and target's reference path (dashed line)

12.2.7.2 Estimation of Target's Position With the Use of Unscented Information Filtering

Next, the estimation of the target's state vector was performed using the Unscented Information Filter. Again, the proposed distributed filtering enabled precise estima-

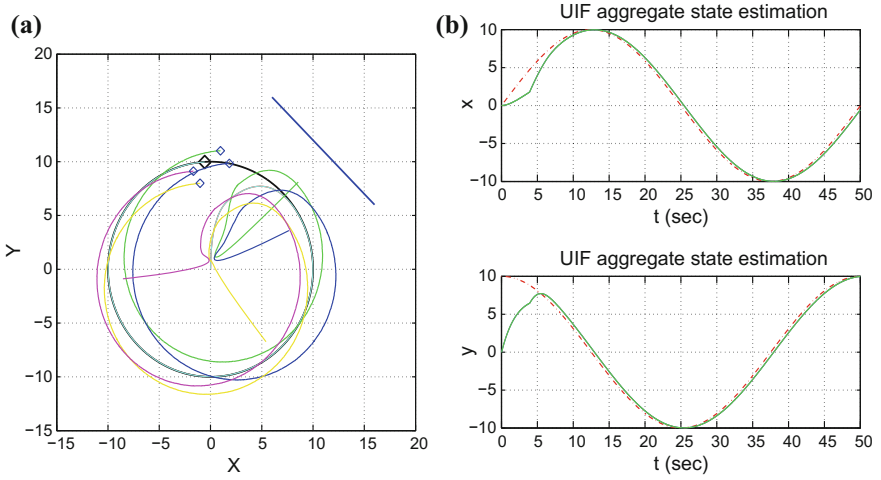

Fig. 12.14 **a** Distributed target tracking by a team of USVs when the target follows a circular trajectory in an obstacles-free motion space, **b** Aggregate estimation of the target's position with the use of Unscented Information Filtering (continuous line) and target's reference path (dashed line)

tion of the target's state vector $[x, y, \theta]^T$ through the fusion of measurements of the target's coordinates and bearing obtained by each mobile sensor with the distance of the target from a reference surface measured in an inertial coordinates system. The state estimates of the local Unscented Kalman Filters running at each USV were aggregated into a single estimation by the Unscented Information Filter. The estimated coordinates $[\hat{x}^*, \hat{y}^*]$ of the target were used to generate the reference path which was followed by the individual mobile robots. The tracking of the target's trajectory by the USVs team as well as the accuracy of the two-level sensor fusion-based estimation of the target's position is shown in Figs. 12.14, 12.15, 12.16, 12.17 and 12.18.

As previously analyzed, the Unscented Information Filter is a derivative-free distributed filtering approach in which the local Unscented Kalman Filters provide estimations of the target's coordinates using the update in-time of a number of suitably chosen sigma-points. Therefore, unlike the Extended Information Filter and the local Extended Kalman Filters contained in it, in the Unscented Information Filter there is no need to calculate Jacobians through the computation of partial derivatives. Additionally, unlike the case of local Extended Kalman Filters there is no truncation of higher order Taylor expansion terms and no linearization errors are introduced at the local estimators. In that sense the Unscented Information Filter provides a robust distributed state estimation and enables accurate tracking of the target by the mobile sensors (USVs).

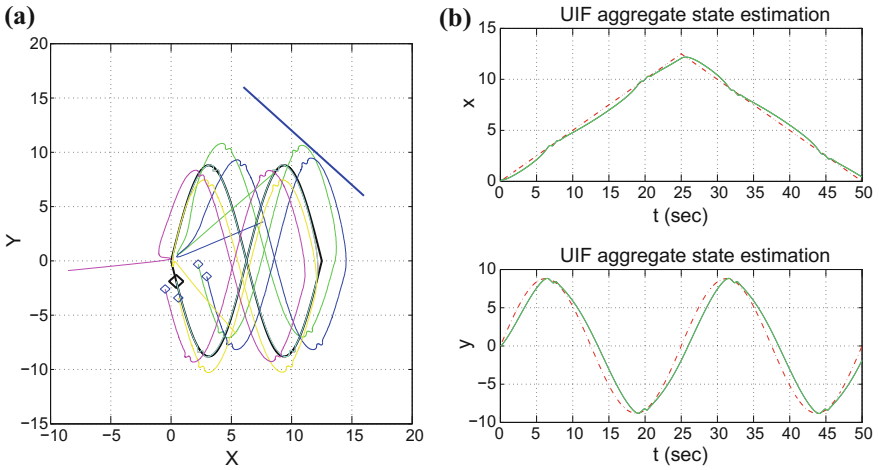

Fig. 12.15 **a** Distributed target tracking by a team of USVs when the target follows an eight-shaped trajectory in an obstacles-free motion space,**b** Aggregate estimation of the target's position with the use of Unscented Information Filtering (continuous line) and target's reference path (dashed line)

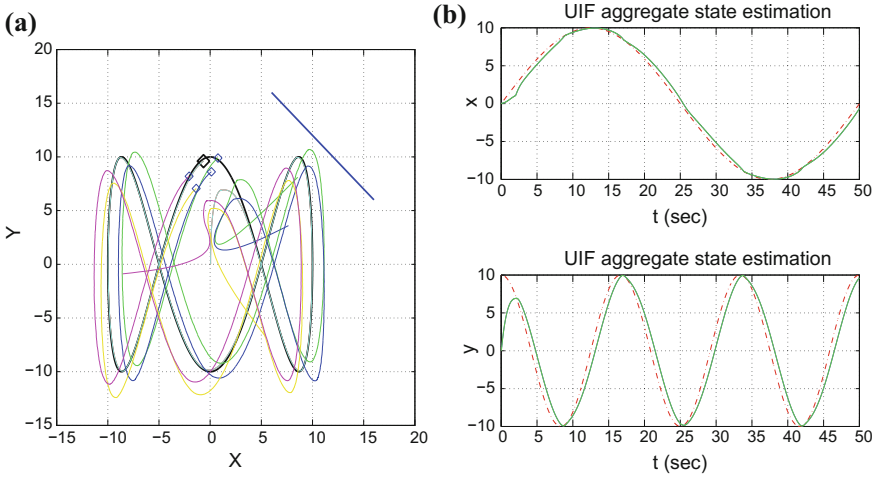

Fig. 12.16 **a** Distributed target tracking by a team of USVs when the target follows a curve-shaped trajectory in an obstacles-free motion space, **b** Aggregate estimation of the target's position with the use of Unscented Information Filtering (continuous line) and target's reference path (dashed line)

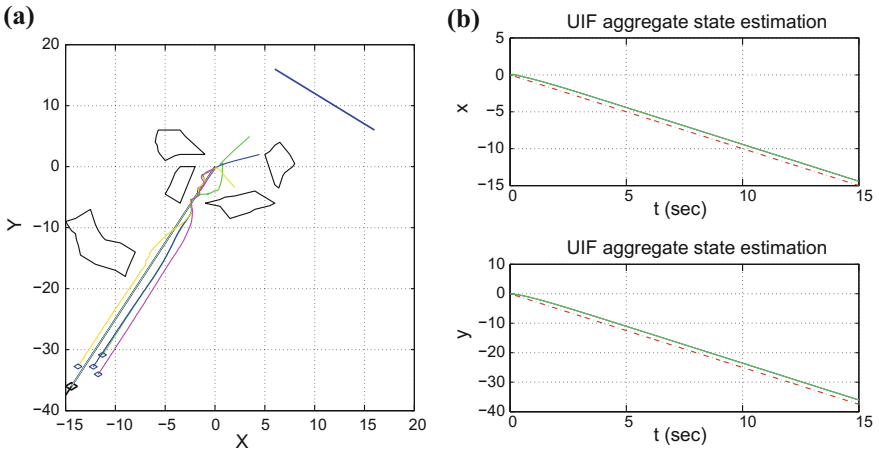

Fig. 12.17 **a** Distributed target tracking by a team of USVs when the target follows a line path in a motion space with obstacles, (b) Aggregate estimation of the target's position with the use of Unscented Information Filtering (continuous line)

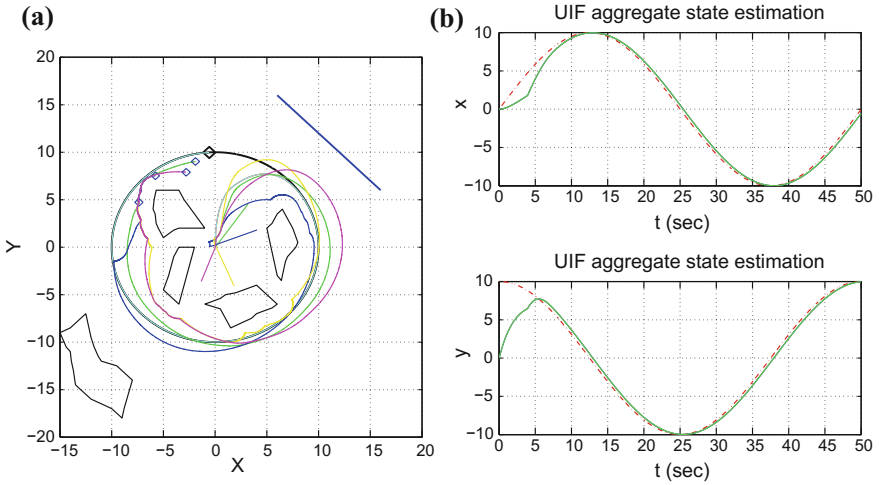

Fig. 12.18 **a** Distributed target tracking by a team of USVs when the target follows a circular path in a motion space with obstacles, **b** Aggregate estimation of the target's position with the use of Unscented Information Filtering (continuous line) and target's reference path (dashed line)

12.2.7.3 Estimation of the Target's Position With the Derivative-Free Distributed Nonlinear Kalman Filter

The Derivative-free Extended Information Filter (DEIF) is also used to solve the problem of the synchronized USVs navigation based on distributed state estimation. In the latter case, local Derivative-free Kalman Filters perform fusion of the target's

coordinates measurements (x_i, y_i) with the distance d_i of the target from a reference surface, as follows:

The target's state vector that was written in the observer canonical form described by Eq. (12.114) is extended through the inclusion of additional state variables that describe the dynamics of the distance measurement d with respect to the reference surface P^j. Thus the extended state vector of the system now becomes $x_e = [x_1, x_2, x_3, x_4, x_5, x_6]^T$ with $x_1 = x$, $x_2 = \dot{x}$, $x_3 = y$, $x_4 = \dot{y}$, $x_5 = d$ and $x_6 = \dot{d}$. The extended output vector is written as $y_e = [y_1, y_2, y_3]^T$, with $y_1 = x$, $y_2 = y$ and $y_3 = d$ which means that measurements of the target's cartesian coordinates (x, y) and of the target's distance d from the reference surface can be obtained. The distance measuring sensor is taken to coincide with the point defining the cartesian coordinates of the target (e.g. center of gravity). In that case, from Eq. (12.89) one has $x_i = x$ and $y_i = y$. The target's kinematics is written in the new state-space form which is also an observer canonical form:

$$\begin{aligned} \dot{x}_e &= A_e x_e + B_e v_e \\ y_e &= C_e x_e \end{aligned} \tag{12.94}$$

while the associated state-space matrices are

$$A_e = \begin{pmatrix} 0 & 1 & 0 & 0 & 0 & 0 \\ 0 & 0 & 0 & 0 & 0 & 0 \\ 0 & 0 & 0 & 1 & 0 & 0 \\ 0 & 0 & 0 & 0 & 0 & 0 \\ 0 & 0 & 0 & 0 & 0 & 1 \\ 0 & 0 & 0 & 0 & 0 & 0 \end{pmatrix} \quad B_e = \begin{pmatrix} 0 & 0 & 0 \\ 1 & 0 & 0 \\ 0 & 0 & 0 \\ 0 & 1 & 0 \\ 0 & 0 & 0 \\ 0 & 0 & 1 \end{pmatrix} \tag{12.95}$$

$$C_e = \begin{pmatrix} 1 & 0 & 0 & 0 & 0 & 0 \\ 0 & 0 & 1 & 0 & 0 & 0 \\ 0 & 0 & 0 & 0 & 1 & 0 \end{pmatrix} \tag{12.96}$$

while the extended inputs vector is defined as $u_e = [u_1, u_2, u_3]^T$ where u_1 and u_2 were defined in Eq. (12.4). Assuming that the incidence angle P_n does not vary in time (as shown in Fig. 12.8), one has

$$u_3 = -\ddot{x}_1 cos(P_n) - \ddot{x}_3 sin(P_n) \tag{12.97}$$

It is noted that knowing the orientation of the reference surface in a cartesian coordinates system, the coordinates of the target at time instant $t = kT_s$ and the coordinates of a reference point on the reference surface, it is always possible to compute the incidence angle P_n. Results about the performance of the Derivative-free Extended Information Filter in estimating the state vector of the target and about using the target's localization procedure for implementing distributed control of the pursuer USVs is given in Figs. 12.19, 12.20, 12.21, 12.22 and 12.23. It can be noticed

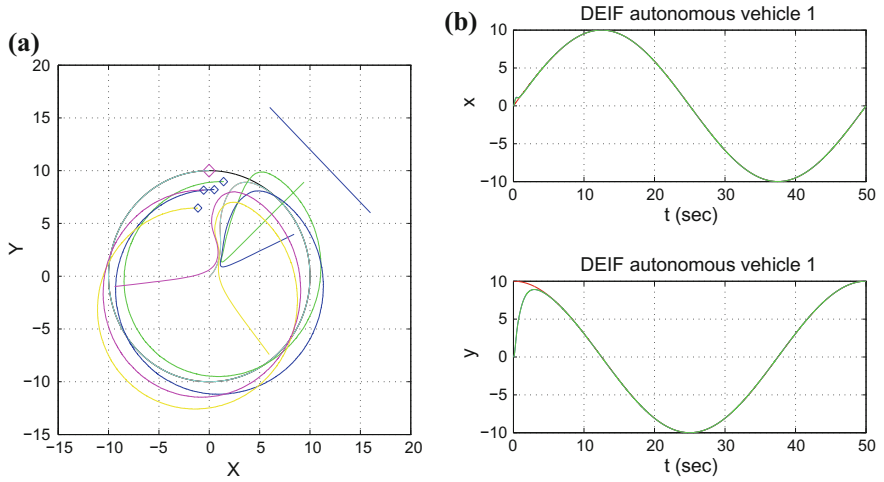

Fig. 12.19 Target following reference path 1 **a** tracking of the target by the USVs **b** estimation of the target's coordinates through sensor fusion and Derivative-free distributed nonlinear Kalman Filtering

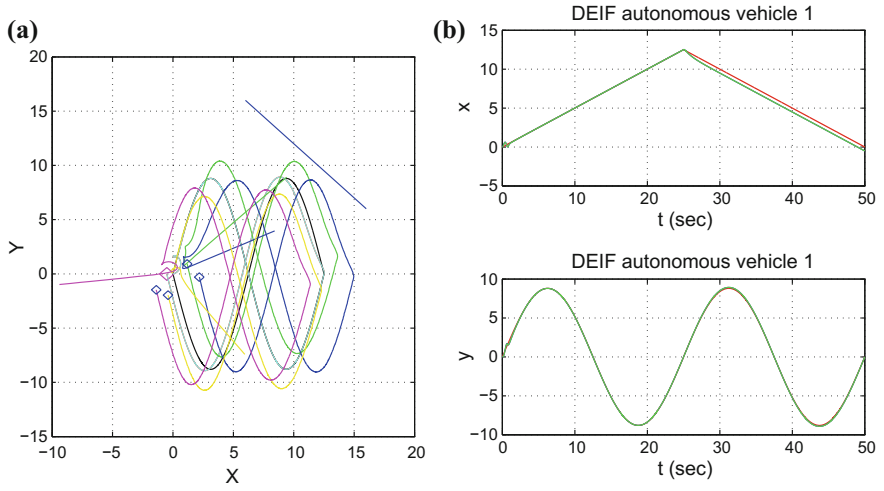

Fig. 12.20 Target following reference path 2 **a** tracking of the target by the USVs **b** estimation of the target's coordinates through sensor fusion and Derivative-free distributed nonlinear Kalman Filtering

that, whilst computationally simpler, the Derivative-free Extended Information Filter provides very accurate estimates of the target's state vector.

Indicative results about the accuracy of estimation provided by the considered nonlinear filtering algorithms (i.e. EIF, UIF and DEIF), as well as about the accuracy of tracking achieved by the associated state estimation-based control loop are given in

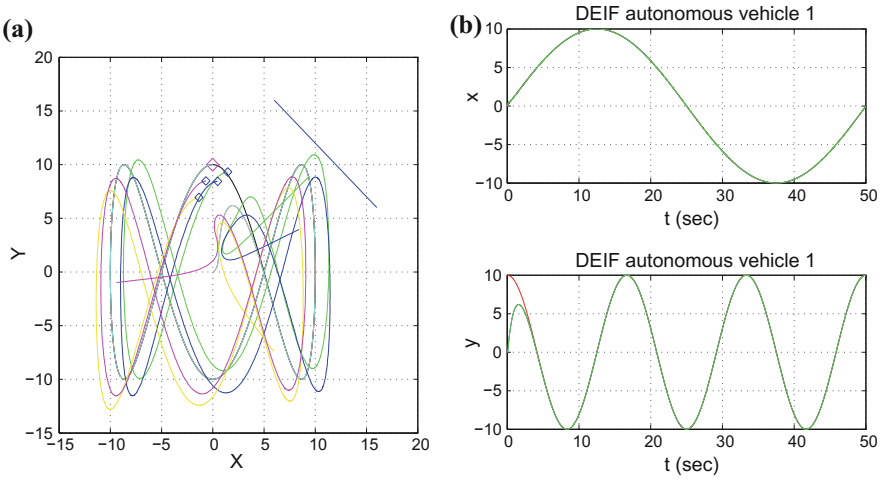

Fig. 12.21 Target following reference path 3 **a** tracking of the target by the USVs **b** estimation of the target's coordinates through sensor fusion and Derivative-free distributed nonlinear Kalman Filtering

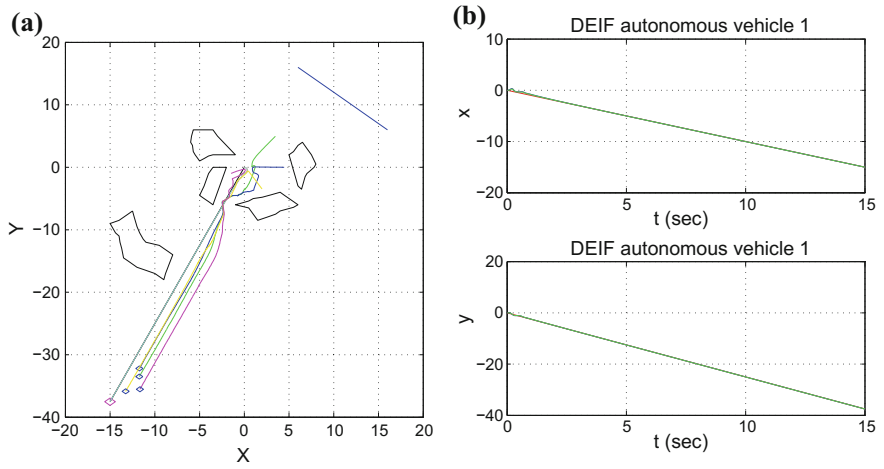

Fig. 12.22 Target following reference path 4, amidst obstacles **a** tracking of the target by the USVs **b** estimation of the target's coordinates through sensor fusion and Derivative-free distributed nonlinear Kalman Filtering

Tables 12.1 and 12.2. It can be noticed that the Derivative-free Extended Information Filter is significantly more accurate and robust than the Extended Information Filter. Its accuracy is comparable to the one of the Unscented Information Filter. Results on the total runtime and the cycle time of the aforementioned distributed filtering

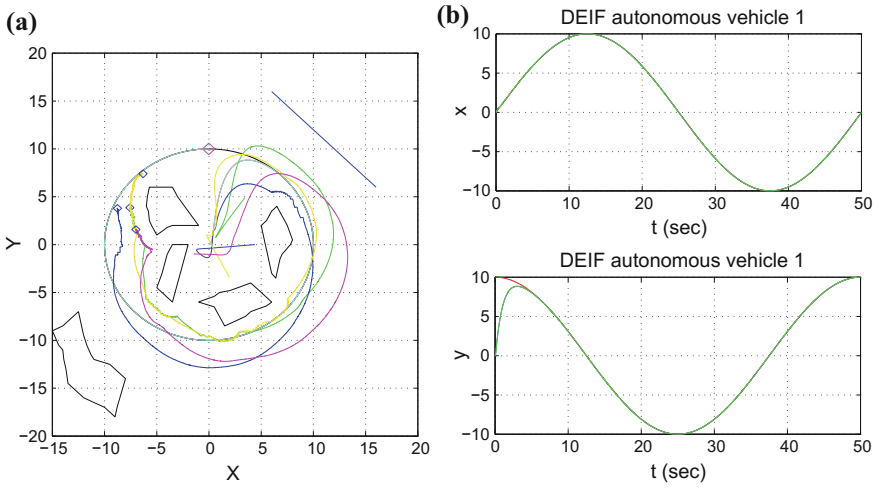

Fig. 12.23 Target following reference path 5, amidst obstacles **a** tracking of the target by the USVs **b** estimation of the target's coordinates through sensor fusion and Derivative-free distributed nonlinear Kalman Filtering

Table 12.1 RMSE of tracking with nonlinear filtering (Gaussian noise)

	RMSE_x	RMSE_y	RMSE_θ
UIF	0.0088	0.0104	0.0013
EIF	0.0123	0.0167	0.0019
DEIF	0.0087	0.0093	0.0013

algorithms are given in Table 12.3 (using the Matlab platform on a PC with an Intel i7 processor at 1.6 GHz).

12.3 Cooperating Unmanned Ground Vehicles

12.3.1 Outline

A second case-study on cooperating autonomous vehicles is concerned with cooperating tractors. There are many types of in-field operations, e.g. agricultural tasks, that can be performed by cooperating tractors. The need for collaborating farming robots that will be able to carry out complicated tasks under synchronization and within desirable precision levels is anticipated to grow in the following years [52]. In several applications a master-slave scheme is required for the robots coordination, which means that a master tractor generates a reference path and the motion

Table 12.2 RMSE of tracking with nonlinear filtering (Rayleigh noise)

	RMSE_x	RMSE_y	RMSE_θ
UIF	0.0089	0.0105	0.0014
EIF	0.0119	0.0163	0.0019
DEIF	0.0089	0.0093	0.0013

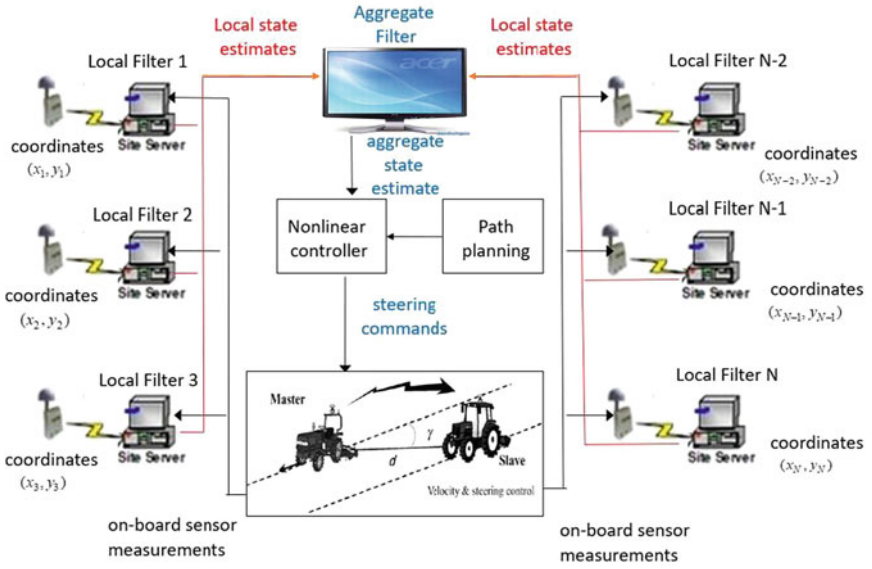

Fig. 12.24 Tracking of the cooperating autonomous ground vehicles: Distributed filtering through the fusion of local state estimates

characteristics (velocity, acceleration, orientation) that the slave tractor has to follow. When harvesting hay on grassland, it is customary for one dump truck and one tractor with a hayfork to be used. When harvesting corn, a combination of one harvester and one tractor with trailer is generally adopted. Therefore, a master-slave system, which uses two vehicles, can be very useful in actual field operations.

In this section, a method for autonomous navigation of agricultural robots under a master-slave scheme is developed. The method comprises the following elements: (i) a path planner for generating automatically the trajectory that has to be followed by the cooperating agricultural robots, (ii) a nonlinear controller that makes the robots track with precision the desirable trajectories, (iii) a distributed filtering scheme for estimating the motion characteristics of the vehicles through the fusion of measurements coming from on-board sensors, as well as measurements about the vehicles' coordinates coming from multiple position sensors (e.g. multiple GPS devices). The autonomous navigation of the cooperating agricultural robots is finally implemented through state estimation-based control where the nonlinear controller uses the estimated state vector of the robots, as provided by distributed filtering, so as to generate the control signal that defines the robots speed and heading angle (see Fig. 12.24).

Table 12.3 Run time of nonlinear estimation algorithms

	UIF	EIF	DEIF
Total runtime (s)	203.97	181.04	162.65
Cycle time (s)	0.0410	0.0366	0.0325

The proposed robotic system performs distributed information processing for estimating the position and motion characteristics of the vehicles. Measurements from on board sensors are combined with measurements from multiple position sensors (e.g. GPS devices) and are initially processed by local filters to provide local state vector estimates. At a second stage the local state estimates for the robotic vehicles are fused using a distributed filtering algorithm. Thus an aggregate state vector of the robotic harvesters is obtained (see Fig. 12.24). Such a filtering approach has several advantages: (i) it is fault tolerant: if a local information processing unit is subject to a fault then state estimation is still possible, (ii) the information processing scheme is scalable and can be expanded with the inclusion of more local information processing units (local filters), (iii) the bandwidth for the exchange of information between the local units and the aggregate filter remains limited since there is no transmission of raw measurements but only transmission of local state estimates and of the associated covariance matrices.

A solution to decentralized information fusion over sensor networks, as the network collecting measurements for the system of the robotic harvesters, can be obtained with the use of distributed Kalman Filtering [157, 358, 369, 370, 553, 589]. Distributed state estimation in the case of non-Gaussian models has been also studied in several other research works [309, 311, 470]. In this section, a solution for the problem of distributed state estimation will be attempted with the use of the Extended Information Filter, which is actually an approach for fusing state estimates provided by local Extended Kalman Filters [260, 450].

Aiming also at finding more efficient implementations of nonlinear distributed Kalman Filtering, in this section a derivative-free approach to Extended Information filtering is introduced. In the proposed derivative-free Kalman Filtering method the system is first subject to a linearization transformation (diffeomorphism) and next state estimation is performed by applying the Kalman Filter to the linearized model. Unlike EKF, the proposed method provides estimates of the state vector of the nonlinear system without the need for derivatives and Jacobians calculation. By avoiding linearization approximations, the proposed filtering method improves the accuracy of estimation of the system state variables, and results in smooth control signal variations and in minimization of the tracking error of the associated control loop. At a second stage, the state estimates which are produced with the use of derivative-free nonlinear Kalman Filters are fused into an aggregate state estimate with the use of the standard Information Filter recursion. Thus, it becomes possible to avoid the inaccuracies introduced by the linearization procedure of the local Extended Kalman filters and to obtain a more robust aggregate state estimate. The Derivative-free distributed

nonlinear Kalman Filtering approach is also useful for compensating delays in the transmission of measurements from the distributed sensors to the local information processing units (local filters) as well as delays in the transmission of the local state estimates to the aggregate filter. By linearization of the system's dynamics through the proposed diffeomorphism one can exploit existing results on the compensation of communication delays and measurements packet drops with the use of the classical linear Kalman Filter recursion [457].

Another issue that has to be taken into account for the autonomous functioning of the robotic harvesters is nonlinear control for precise tracking of desirable trajectories. The present section proposes flatness-based control for steering the robot harvesters along the reference paths. Expressing all system variables as functions of the flat output and its derivatives enables transformation of the robotic vehicle model to a linearized form for which the design of the controller becomes easier.

12.3.2 Localization and Path Planning for Cooperating Agricultural Robots

12.3.2.1 Sensors for Vehicle Localization and Motion Control

Global localization of the tractors can be obtained from the GPS signal. The GPS signal received from the satellites can be corrected by using the signal that is emitted by a GPS reference receiver of well-known location, known as Differential GPS (DGPS). Differential corrections improve data localization considerably, but not all sources of errors can be suppressed. Multi-path and receiver errors are still possible. There are several ways to achieve differential corrections by establishing a network of spatially distributed reference stations (local-area DPGS). The top level of accuracy reachable with GPS is a couple of centimeters and can be accomplished with the Real-Time Kinematic GPS (RTK-GPS). RTK sets contain two receivers, a radio link, and computer software with the purpose of enhancing GPS positioning accuracy by calculating differential corrections from a base station placed in the field, or nearby where the vehicle is operating. The most important disadvantage of the RTK systems is a coverage limitation of about 10km from the vehicle.

The turn angle of the front wheels of the tractor (front-axle steering) or the rear wheels (rear-axle steering) can be measured with three sensors: (i) linear potentiometers which give an indirect measurement of the wheel angle by tracking the displacement of the cylinder rod actuating the steering mechanism, (ii) oil flow meters which provide an indirect measurement of the wheel angle by quantifying the oil flow moving in and out of the cylinders chamber to achieve a turn, (iii) an optical encoder which comprises a free axle attached to a strapped disc that is easily tracked by a light beam.

Tracking of the vehicle's motion requires also estimation of the parameters of the vehicle's state vector, such as position, velocity and acceleration, or even Euler angles such as roll, pitch and yaw. These parameters can be estimated from measurements coming from a limited number of sensors, through the use of filtering techniques such as Kalman Filtering. The position measurements of the vehicle coming from the GPS can be enhanced through information fusion approaches, that process also measurements coming from inertial sensors. The inertial measurement unit combines accelerometers and gyroscopes, typically which are placed along the three orthogonal axes of a Cartesian frame. The accelerometers detect velocity changes over time, i.e. the acceleration, and allow the computation of velocity and position through successive integrations. The gyroscopes, record changes of the angular rates of the vehicle round the Cartesian coordinates axes. The integration over time of the three angular rates provides the yaw, pitch and roll angles of the vehicle. A disadvantage of IMUs is the accumulation of errors after use for an extended time period, which is known as sensor drift. When the agricultural vehicles, operate in flat fields then pitch and roll angles are negligible. Two important parameters for the vehicle's kinematic model are the control inputs which are the rate of change of the heading angle and the forward velocity.

A simplistic method for measuring the vehicle's forward speed is by measuring the number of turns spun by the wheels with the use of a magnetic counter mounted on the chassis. This computation approach is insufficient due to slippage, often taking place in off-road terrains. Therefore, one can estimate the velocity through the processing of GPS measurements by a Kalman Filter, or in complement, can use other types of sensors such as radars. As mentioned above, the heading angle is a crucial parameter in the kinematic model of the vehicle. It provides the orientation of the vehicle with respect to the north. It can be estimated with the use of an inertial measurement unit as the yaw angle is determined by integrating the yaw rate around axes perpendicular to the local tangent plane. An optional sensor to estimate headings is the fluxgate compass.

12.3.2.2 Path Planning

In general, a set of cooperating agricultural robots contains N vehicles of equivalent kinematics which is given by

$$\dot{\bar{x}}_i = f(\bar{x}_i, u_i),\ i = 1, \ldots, N \tag{12.98}$$

where $\bar{x}_i \in R^n$ denotes the states, $u_i \in R^m$ is the control inputs vector and $f()$ is a smooth function. Path planning for such a group consists of finding trajectories that over a time horizon $[t_0, t_f]$ satisfy the kinematic equation given in Eq. (12.98), and the inequality constraints appearing in Eq. (12.99) and Eq. (12.100), as well as minimizing a cost criterion given in Eq. 12.101

$$\bar{g}(x_1, \ldots, x_N, t) \leq \bar{g} \in R^{n_g} \tag{12.99}$$

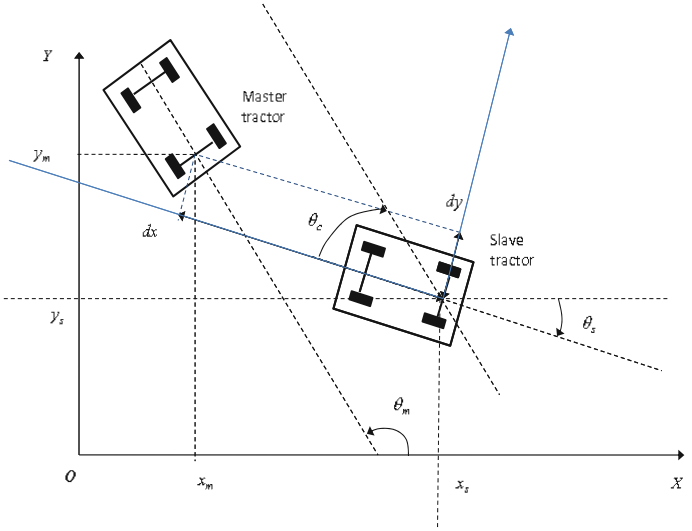

Fig. 12.25 Coordinates systems defining the motion of the master and slave tractor

$$\bar{c}(\bar{x}_1, \ldots, \bar{x}_N, \bar{u}_1, \ldots, \bar{u}_N, y) \leq 0, \ \bar{c} \in R^{n_c} \tag{12.100}$$

$$min \bar{J} = \bar{\Phi}[\bar{x}_1(t_f), \ldots, \bar{x}_N(t_f), t_f] + \int_{t_0}^{t_f} \bar{L}(\bar{x}_1, \ldots, \bar{x}_N, \bar{u}_1, \ldots, \bar{u}_N) dt \tag{12.101}$$

where $\bar{x}_i$ and $u_i, i = 1, \ldots, N$ are the state vector and control vector associated with the trajectory of the ith robotic vehicle, participating in the multi-robot formation. The constraints appearing in Eq. (12.99) are associated to the formation of the multi-robot system. For example, while harvesting, the combine and trailer need to stay within a minimum distance for collision avoidance and maximum distance for avoiding failure of harvest transfer. The constraints appearing in Eq. (12.100) are associated to the state variables of the robotic vehicle, as well as with constraints on the inputs of the kinematic model.

From the above, it can be seen that the trajectory optimization problem for the multi-robot system involves finding $N(n + m)$ state and input trajectories in the presence of $n_g + n_c$ inequality constraints, while satisfying Nn state equations and given terminal constraints. To reduce the complexity of this optimization problem and to make it computationally more tractable one can alleviate some of the constraints going into sub-optimal solutions. For instance, in the case of a master-slave cooperation scheme between two tractors (e.g. combine being the master vehicle and tractor with trailer being the slave vehicle) one has the following formulation of the path planning problem (Fig. 12.25):

Denoting as x_c and y_c the coordinates of the combine in the cartesian motion plane attached to the slave tractor and the heading angle of the combine with respect to the

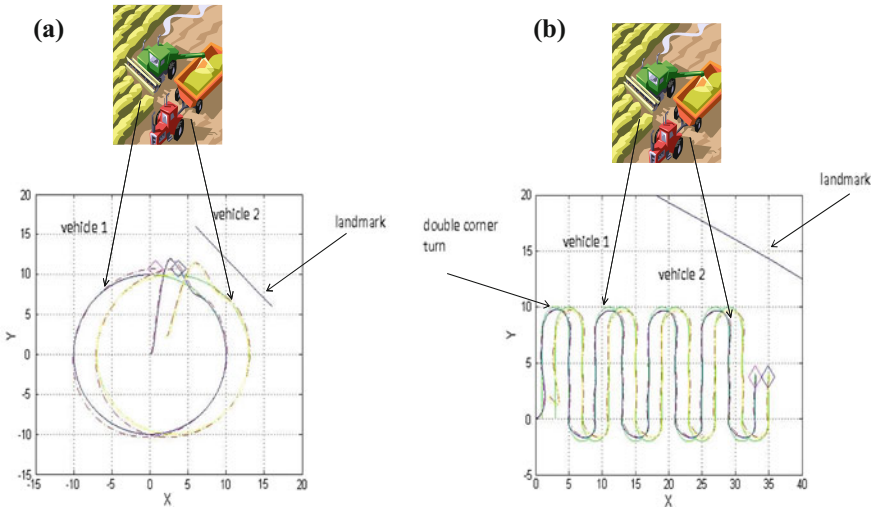

Fig. 12.26 The slave robot's reference trajectory is defined from the master robot's path under a known position offset **a** example reference trajectory 1 **b** example reference trajectory 2

slave tractor as θ_c, the slave tractor's nominal trajectory (x_s, y_s) can be obtained as a function of the reference trajectory of the master tractor (x_m, y_m)

$$\begin{aligned} x_s &= x_m + dx \cdot cos(\theta_c) - dy \cdot sin(\theta_c) \\ y_s &= x_m + dx \cdot sin(\theta_c) - dy \cdot cos(\theta_c) \end{aligned} \tag{12.102}$$

where dx and dy denote the relative position of the master tractor with respect to the slave tractor. The slave tractor's heading angle is then given by

$$\theta_s = tan^{-1}(\frac{\dot{y}_s}{\dot{x}_s}) \tag{12.103}$$

The cost function of Eq. (12.101) aims at minimizing the tractors deviation from the reference trajectory, while ensuring that the non-collision requirement is met (Fig. 12.26).

12.3.3 Derivative-Free Kalman Filtering for Unmanned Ground Vehicles

12.3.3.1 Controller Design for Agricultural Robots

The kinematic model of the agricultural robot is considered. This is given by

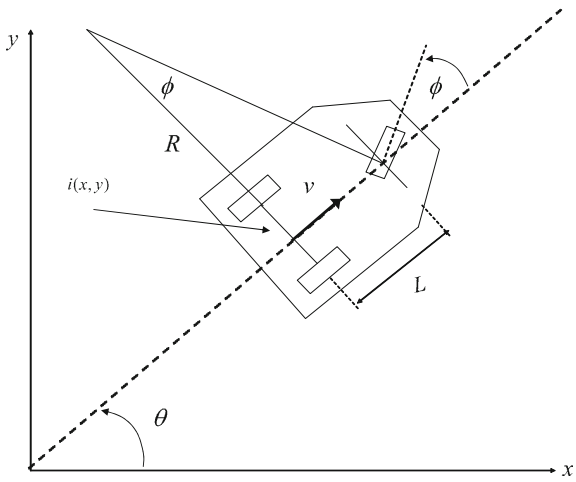

Fig. 12.27 The model of the unicycle autonomous vehicle (cart-like vehicle)

$$\begin{aligned} \dot{x} &= vcos(\theta) \\ \dot{y} &= vsin(\theta) \\ \dot{\theta} &= \omega = \tfrac{v}{L} tan(\phi) \end{aligned} \tag{12.104}$$

where $v(t)$ is the velocity of the vehicle, L is the distance between the front and the rear wheel axis of the vehicle, θ is the angle between the transversal axis of the vehicle and axis OX, and ϕ is the angle of the steering wheel with respect to the transversal axis of the vehicle (Fig. 12.27). The position of such a vehicle is described by the coordinates (x, y) of the center of its rear axis and its orientation is given by the angle θ between the x-axis and the axis of the direction of the vehicle. The steering angle ϕ and the speed u are considered to be the inputs of the system.

Flatness-based control can be used for steering the vehicle along a desirable trajectory. As previously explained in Sect. 7.3, in the case of the autonomous vehicle of Eq. (12.104) the flat output is the cartesian position of the center of the wheel axis, denoted as $\eta = (x, y)$, while the other model parameters can be written as:

$$v = \pm||\dot{\eta}|| \begin{pmatrix} cos(\theta) \\ sin(\theta) \end{pmatrix} = \tfrac{\dot{\eta}}{v}\, tan(\phi) = ldet(\dot{\eta}\ddot{\eta})/v^3 \tag{12.105}$$

One then proceeds by successively differentiating the output until the input appears in a non-singular way. The closed-loop system is then equivalent to a set of decoupled input-output chains of integrators from u_i to η_i. The exact linearization procedure is illustrated for the vehicle's model of Eq. (12.104). As flat output $\eta = (x, y)$ the coordinates of the center of the wheel axis is considered. Following the procedure that was presented in Chap. 7 and differentiating with respect to time yields [371]

$$\dot{\eta} = \begin{pmatrix} \dot{x} \\ \dot{y} \end{pmatrix} = \begin{pmatrix} cos(\theta) & 0 \\ sin(\theta) & 0 \end{pmatrix} \cdot \begin{pmatrix} v \\ \omega \end{pmatrix} \tag{12.106}$$

showing that only v affects $\dot{\eta}$, while the angular velocity ω cannot be recovered from this first-order differential information. To proceed, one needs to add an integrator (whose state is denoted by ξ) on the linear velocity input $v = \xi$, $\dot{\xi} = \alpha \Rightarrow \dot{\eta} = \xi[cos(\theta), sin(\theta)]^T$, where α denotes the linear acceleration of the vehicle. Differentiating further one obtains

$$\ddot{\eta} = \begin{pmatrix} cos(\theta) & -\xi sin(\theta) \\ sin(\theta) & \xi cos(\theta) \end{pmatrix} \begin{pmatrix} \alpha \\ \omega \end{pmatrix} \tag{12.107}$$

and the matrix multiplying the modified input (α, ω) is nonsingular if $\xi \neq 0$. Under this assumption one defines

$$\begin{pmatrix} \alpha \\ \omega \end{pmatrix} = \begin{pmatrix} cos(\theta) & -\xi sin(\theta) \\ sin(\theta) & \xi cos(\theta) \end{pmatrix}^{-1} \cdot \begin{pmatrix} u_1 \\ u_2 \end{pmatrix} \tag{12.108}$$

and $\ddot{\eta}$ is denoted as

$$\ddot{\eta} = \begin{pmatrix} \ddot{\eta}_1 \\ \ddot{\eta}_2 \end{pmatrix} = \begin{pmatrix} u_1 \\ u_2 \end{pmatrix} = u \tag{12.109}$$

which means that the desirable linear acceleration and the desirable angular velocity can be expressed using the transformed control inputs u_1 and u_2. Then, the resulting dynamic compensator is (return to the initial control inputs v and ω)

$$\begin{array}{c} \dot{\xi} = u_1 cos(\theta) + u_2 sin(\theta) \\ v = \xi \\ \omega = \frac{u_2 cos(\theta) - u_1 sin(\theta)}{\xi} \end{array} \tag{12.110}$$

In the new coordinates it holds

$$\begin{array}{l} z_1 = x \\ z_2 = y \\ z_3 = \dot{x} = \xi cos(\theta) \\ z_4 = \dot{y} = \xi sin(\theta) \end{array} \tag{12.111}$$

The extended system is thus fully linearized and described by the chains of integrators, in Eq. (12.109), and can be rewritten as

$$\ddot{z}_1 = u_1, \quad \ddot{z}_2 = u_2 \tag{12.112}$$

On the equivalent and decoupled system of Eq. (12.112), one can easily design an exponentially stabilizing feedback for the desired trajectory, which has the form

$$\begin{array}{l} u_1 = \ddot{x}_d + k_{p_1}(x_d - x) + k_{d_1}(\dot{x}_d - \dot{x}) \\ u_2 = \ddot{y}_d + k_{p_1}(y_d - y) + k_{d_1}(\dot{y}_d - \dot{y}) \end{array} \tag{12.113}$$

and which results in the following error dynamics for the closed-loop system $\ddot{e}_x + k_{d_1}\dot{e}_x + k_{p_1}e_x = 0$ and $\ddot{e}_y + k_{d_2}\dot{e}_y + k_{p_2}e_y = 0$, where $e_x = x - x_d$ and $e_y = y - y_d$.

The proportional-derivative gains are chosen as $k_{p_1} > 0$ and $k_{d_1} > 0$ for $i = 1, 2$. Knowing the control inputs u_1, u_2, for the linearized system one can calculate the control inputs v and ω applied to the vehicle, using Eq. (12.110) [371].

12.3.3.2 Derivative-Free Kalman Filtering for the Field Robots

As explained in the previous section, if the Derivative-free Kalman Filter is used in place of the Extended Kalman Filter then in the equations of the Extended Information Filter (EIF), the following matrix substitutions should be performed: $J_\phi(k) \rightarrow A_d$, $J_\gamma(k) \rightarrow C_d$, where matrices A_d and C_d are the discrete-time equivalents of matrices A_c and C_c which have been defined in the measurement and time update of the standard Kalman Filter recursion. Matrices A_d and C_d can be computed using established discretization methods. Moreover, the covariance matrices $P(k)$ and $P^-(k)$ are the ones obtained from the linear Kalman Filter update equations.

It is assumed now that the vehicle's velocity has to be estimated through the processing of the sequence of position measurements by a filtering algorithm. To this end the Derivative-free Kalman Filter for MIMO nonlinear dynamical systems can been used. From the application of the differential flatness theory presented in Sect. 12.3.3.1 for transforming the initial nonlinear vehicle's model into a linearized equivalent that is finally written in the Brunovsky form, one has Eq. (12.109) which means $\ddot{x} = u_1$ and $\ddot{y} = u_2$. Next, the state variables $x_1 = x$, $x_2 = \dot{x}$, $x_3 = y$ and $x_4 = \dot{y}$ are defined. Considering the state vector $x \in R^{4\times 1}$, the following matrices are also defined

$$A = \begin{pmatrix} 0 & 1 & 0 & 0 \\ 0 & 0 & 0 & 0 \\ 0 & 0 & 0 & 1 \\ 0 & 0 & 0 & 0 \end{pmatrix}, \quad B = \begin{pmatrix} 0 & 0 \\ 1 & 0 \\ 0 & 0 \\ 0 & 1 \end{pmatrix}, \quad C = \begin{pmatrix} 1 & 0 \\ 0 & 0 \\ 0 & 1 \\ 0 & 0 \end{pmatrix} \tag{12.114}$$

Using the matrices of Eq. (12.114) one obtains the Brunovsky form of the MIMO robot model $\dot{x} = Ax + Bv$ and $y = Cx$, where the new input v is given by $v = [u_1(x, t), u_2(x, t)]^T$. This is a robotic model in the form of Eq. (12.85), for which state estimation can be performed using the standard Kalman Filter recursion.

12.3.4 Simulation Tests

12.3.4.1 Autonomous UGV Navigation Using the Extended Indormation Filter

Indicative results about tracking of various reference trajectories, when using the Extended Information Filter for the vehicle's localization, are shown in Figs. 12.28 and 12.29. In these diagrams the green line denotes the reference trajectory, while

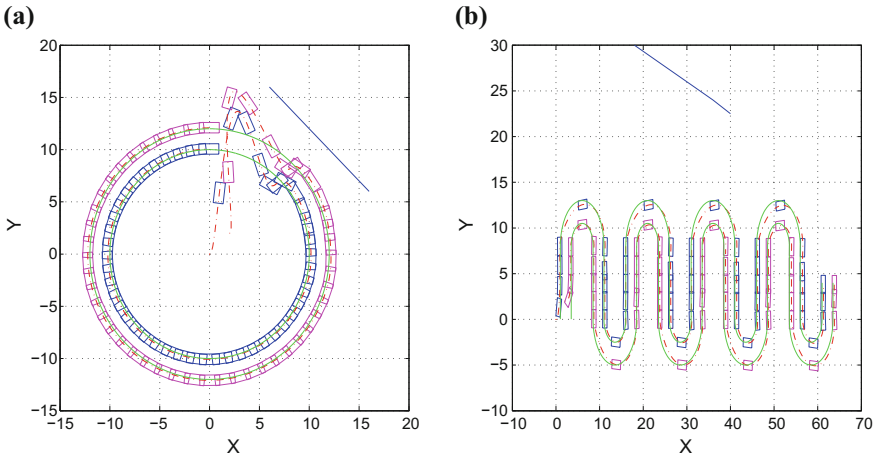

Fig. 12.28 Extended Information Filter and flatness-based control for cooperating robot harvesters: **a** synchronized tracking of reference path 1 **b** synchronized tracking of reference path 2

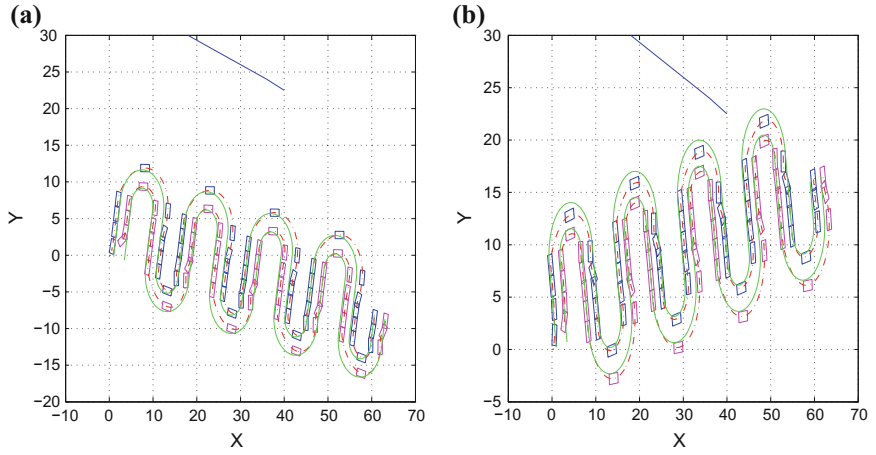

Fig. 12.29 Extended Information Filter and flatness-based control for cooperating robot harvesters: **a** synchronized tracking of reference path 3 **b** synchronized tracking of reference path 4

the red dashed line denotes the real path of the vehicle in the xy plane. The position of the vehicles in plotted every 100 sampling periods.

The performance of the proposed Distributed derivative-free nonlinear Kalman Filter was tested in the problem of state estimation-based control for master-slave cooperation of two agricultural robots (see Fig. 12.26). The master tractor generates a reference path and the motion characteristics (velocity, acceleration, orientation) that the slave tractor has to follow. It was assumed that only measurements of the xy coordinates of the vehicles could be obtained through multiple GPS units (local-

ization of moderate accuracy), or multiple local RTK-GPS stations (localization of elevated accuracy).

12.3.4.2 Autonomous UGV Navigation Using the Distributed Deririvative-Free Nonlinear Kalman Filter

Indicative results about tracking of various reference trajectories, when use the Distributed Derivative-free Nonlinear Kalman Filter for the vehicle's localization, are shown in Figs. 12.30 and 12.31. In these diagrams the green line denotes the reference trajectory, while the red dashed line denotes the real path of the vehicle in the xy plane. The position of the vehicles in plotted every 100 sampling periods.

Comparing the estimation performed by the derivative-free MIMO nonlinear Kalman Filter with the one performed by the Extended Information Filter it can be noticed that the derivative-free filtering approach is significantly more robust and results in more accurate state estimates. This has been confirmed in the results presented in [437]. The following accuracy metrics were obtained in tracking of the reference path of Fig. 12.30: (a) with the use of the derivative-free MIMO nonlinear Kalman Filter: $RMSE_x = 0.0088$, $RMSE_y = 0.0094$, $RMSE_\theta = 0.0013$, (b) with the use of the Extended Information Filter: $RMSE_x = 0.0134$, $RMSE_y = 0.0167$, $RMSE_\theta = 0.0021$.It can be noted that the present section's approach can be applied also to various types of 4-wheel agricultural robots.

Finally, the path tracking error for the autonomous ground vehicles, in the case of tracking of reference path 1, and after using the Distributed Derivative-free nonlinear Kalman Filter for their localization is depicted in Fig. 12.32.

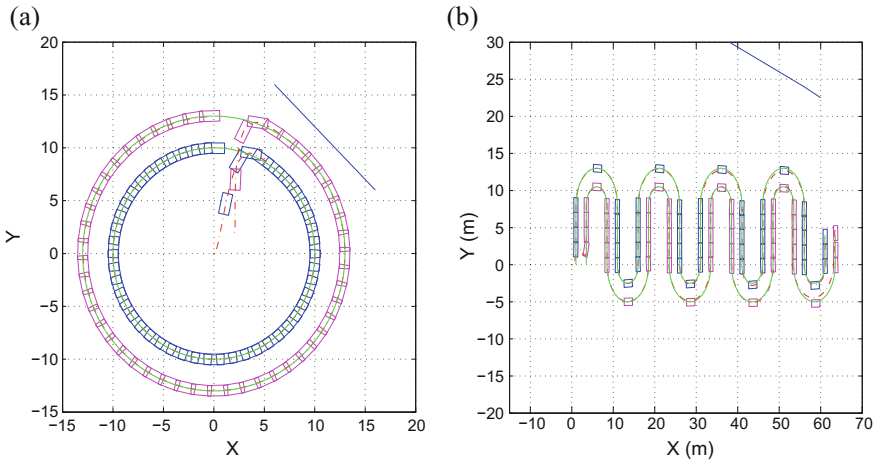

Fig. 12.30 Derivative-free distributed Kalman Filter and flatness-based control for cooperating robot harvesters: **a** synchronized tracking of reference path 1 **b** synchronized tracking of reference path 2

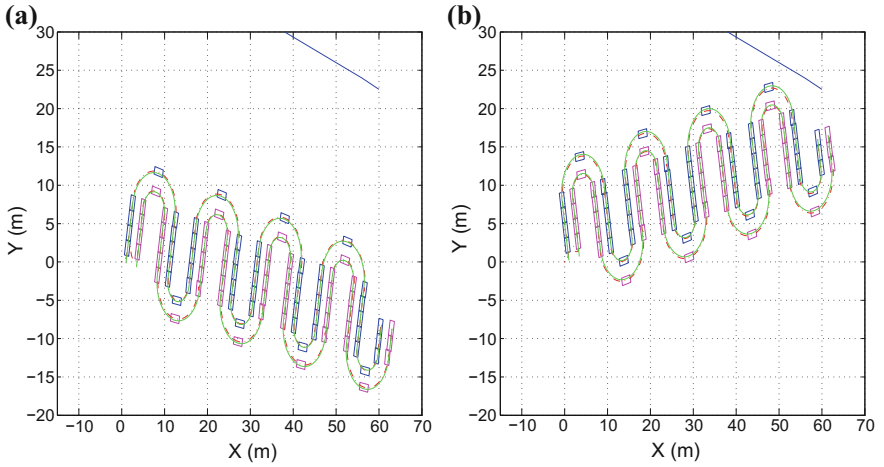

Fig. 12.31 Derivative-free distributed Kalman Filter and flatness-based control for cooperating robot harvesters: **a** synchronized tracking of reference path 3 **b** synchronized tracking of reference path 4

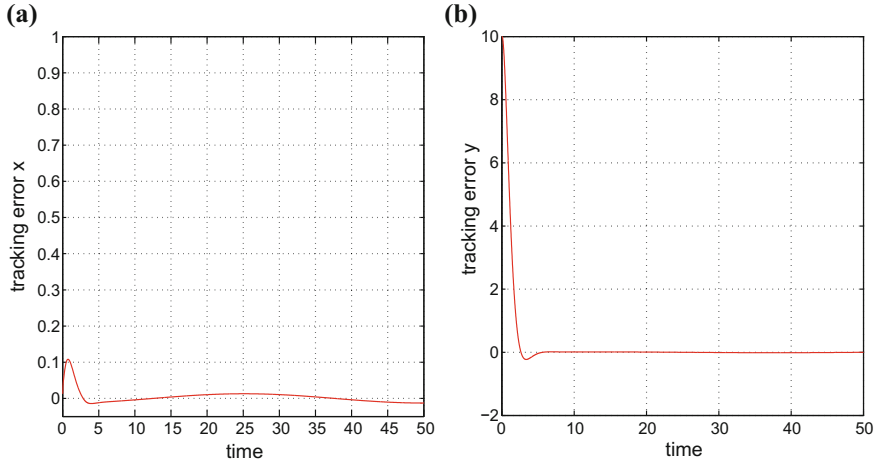

Fig. 12.32 Derivative-free distributed Kalman Filter and flatness-based control for cooperating robot harvesters: **a** path tracking error along the x-axis **b** path tracking error along the y-axis

As a concluding remark it can be stated that the examples on control and filtering of cooperating robots come to complete the analysis of the topics of nonlinear control and estimation for robotic manipulators and autonomous vehicles. This research area remains open and is anticipated to further grow in the forthcoming years.

References

1. Agrawal, S.K., Sangwan, V.: Differentially flat designs of underactuated open-chain planar robots. IEEE Trans. Robot. **24**(6), 1445–1451 (2008)
2. Aguiar, A.P., Hespanha, J.P.: Trajectory-tracking and path-following of underactuated autonomous vehicles with parametric modelling uncertainty. IEEE Trans. Autom. Control **52**(3), 1362–1379 (2007)
3. Aguilar-Avelar, C., Moreno-Valenzuela, J.: A composite controller for trajectory tracking applied to the Furuta pendulum. ISA Trans., Elsevier **57**, 286–294 (2015)
4. Aguilar-Avelar, C., Moreno-Valenzuela, J.: A feedback linearization controller for trajectory tracking of the Furuta pendulum. In: 2014 American Control Conference, Portland, Oregon, USA (2014)
5. Aguilar-Ibanez, C., Sira-Ramirez, H.: Control of the Furuta pendulum based on a linear differential flatness approach. In: IEEE ACC 2002, Proceedings of the American Control Conference, Anchorage, Alaska (2002)
6. Aguilar-Ibnez, C., Sira-Ramirez, H., Surez-Castan, M.S., Martnez-Navarro, E., Moreno-Armendariz, M.A.: The trajectory tracking problem for an unmanned fourrotor system: flatness-based approach. Int. J. Control, Taylor and Francis **85**(1), 69–77 (2012)
7. Akihita, T., Satoh, K.: Development of 4WS control algorithms for a SUV. J. Soc. Autom. Eng. Jpn. **24**, 441–448 (2003)
8. Alamir, M., Hurilo, A.: Swing-up and stabilization of a twin pendulum under state and control constraints by a fast NMPC scheme. Automatica, Elsevier **44**, 1319–1324 (2008)
9. Alhu-Schaffer, A., Petit, C.O.F.: Energy shaping control for a class of underactuated Euler-Lagrange systems. In: 10th IFAC Symposium on Robot Control, Dubrovnik, Croatia, vol. 42, no. 2, pp. 567–575 (2012)
10. Ali, H.S., Boutat-Baddas, L., Becis-Aubry, Y., Darouach, M.: H_∞ control of a SCARA robot using polytopic LPV approach. In: IEEE MED 2006, 14th Mediterranean Conference on Control and Automation, Ancina, Italy (2006)
11. Almeida, J., Silvestre, C., Pascoal, A.M.: Cooperative control of multiple surface vessels with discrete-time periodic communications. Int. J, Robust Nonlinear Control (2011)
12. Altafini, C., Speranzon, A., Eahlberg, B.: A feedback control scheme for reversing a truck snd trailer vehicle. IEEE Trans. Robot. Autom. **17**(6), 915–922 (2001)
13. Ameho, Y., Niel, F., Defay, F., Biannic, J.M., Berard, C.: Adaptive control for quadrotors. In: ICRA 2013 IEEE International Conference on Robotics and Automation, Karlsruhe, Germany (2013)

G. Rigatos and K. Busawon, *Robotic Manipulators and Vehicles*,
Studies in Systems, Decision and Control 152,
https://doi.org/10.1007/978-3-319-77851-8

14. Andone, D., Dobrescu, R., Hossu, A., Dobrescu, M.: Application of fuzzy model prediction control to a drum boiler. Integr. Comput. Aided Eng. **13**(4), 347–359 (2006)
15. Andreo, D., Cerani, V., Deng, D., Regrutto, D.: Experimental results on LPV stabllization of a riderless bicycle, In: IEEE ACC 2009, 2009 Americal Control Conference. St. Louis, MO, USA (2009)
16. Aoustin, Y., Fliess, M., Mounier, H., Rouchon, P., Rudoplh, J.: Theory and practice in the motion planning control of a flexible robot arm using Mikusiǹski operators. In: Proceedings of 4th Symposium on Robotics and Control, pp. 287–293. Nantes (1997)
17. Araar, O., Aouf, N.: Full linear control of a quadrotor UAV, LQ vs H-infinity, UKACC 2014, UK International Conference on Control, Loughborough, UK (2014)
18. Aracil, J., Acosta, J., Gordillo, E.: A nonlinear hybrid controller for swinging-up and stabilizing the Furuta pendulum. Control Eng. Pract., Elsevier **21**, 989–993 (2013)
19. Arai, H., Tanie, K., Shiroma, N.: Nonholonomic control of a three-DOF planar underactuated manipulator. IEEE Trans. Robot. Autom. **14**(5), 681–695 (1998)
20. Ariaei, F., Jonckheere, E.: LDV approach to circular trajectory tracking of the underactuated hovercrafts with modelling parameter uncertainties. In: Proceedings of the 2006 American Control Conference, Minneapolis, Minnesota USA (2006)
21. Arslan, M.S., Fukushima, N., Hagiwara, J.: Nonlinear optimal control of an AUV and its actuator failure compensation. In: 10th International Conference on Control, Automation, Robotics and Vision. Hanoi, Vietnam (2008)
22. Arteaga, M.A., Siciliano, B.: On tracking control of flexible robot arms. IEEE Trans. Autom. Control **45**(3), 520–527 (2000)
23. Arulampalam, S., Maskell, S.R., Gordon, N.J., Clapp, T.: A tutorial on particle filters for on-line nonlinear/non-Gaussian Bayesian tracking. IEEE Trans. Signal Process. **50**, 174–188 (2002)
24. Astolfi, A., Bolzern, P., Locatelli, A.: Path tracking of a tractor-trailer vehicle along rectilinear and circular path: a Lyapunov-based approach. IEEE Trans. Robot. Autom. **20**(1), 154–160 (2004)
25. Atashzar, S.F., Talebi, H.A., Towhidkhah, F., Shahbazi, M.: Tracking control of flexible-link manipulators based on environmental force disturbance observer. In: 49th IEEE Conference on Decision and Control. Atlanta, Georgia, USA (2010)
26. Attia, R., Dijuela, R., Basset, M.: Combined longitudinal and lateral control for automated vehicle guidance. Veh. Syst. Dyn., Taylor and Francis **52**(2), 261–279 (2014)
27. Auestad, O.F., Gravdohl, J.J., Fossen, T.I.: Heave motion estimation on a craft using a strapdown inertial measurement unit. In: 9th IFAC Conference on Control Applications in Marine Systems, Osaka, Japan (2013)
28. Backus, S.B., Dollar, A.M.: An adaptive three-fingered prismatic gripper with passive rotational joints. IEEE Robot. Autom. Lett. **1**(2), 668–675 (2016)
29. Barcelo, J., Rosselo, J.L., Bota, S., Seguro, J., Verd, J.: Electromechanically actuated microbeam resonators at chaotic signal generators: A practical perspective. Commun. Nonlinear Sci. Numer. Simul., Elsevier **30**, 316–327 (2016)
30. Bar-Shalom, Y., Rong Li, X., Kirubarajan, T.: Estimation with Applications to Tracking and Navigation. Wiley, Ney York (2001)
31. Bascetta, L., Rocco, L.: End-point vibration sensing of planar flexible manipulators through visual servoing. Mechatronics, Elsevier **16**, 221–232 (2006)
32. Basseville, M., Benveniste, A., Zhang, Q.: Surveilliance d' installations industrielles: démarche générale et conception de l' algorithmique, IRISA Publication Interne No 1010 (1996)
33. Basseville, M., Nikiforov, I.: Detection of Abrupt Changes: Theory and Applications. Prentice-Hall (1993)
34. Basseville, M.: On fault detectability and isolability. Eur. J. Control **7**(6), 625–637 (2001)
35. Basseville, M., Benveniste, A., Goursat, M., Mevel, L.: In-flight vibration monitoring of aeronautical structures. IEEE Control Syst. Mag. **27**(5), 27–42 (2007)

36. Basturk, H.I., Kristic, M.: Adaptive wave cancellation by acceleration feedback for ramp-connected air-cushion-actuated surface effect ships. Automatica, Elsevier **49**, 2591–2602 (2010)
37. Batista, P., Silvestre, C., Oliveira, P.: A sensor-based controller for homing of underactuated AUVs. IEEE Trans. Robot. **25**(3), 701–716 (2009)
38. Baturone, I., Moreno-Velo, F.J., Blanco, V., Ferruz, J.: Design of embedded DSP-based fuzzy controllers for autonomous mobile robots. IEEE Trans. Ind. Electron. **55**(2), 928–936 (2008)
39. Becker, J., Meurer, T.: Feedforward tracking control for non-uniform Timoshenko beam models: combining differential flatness, modal analysis, and FEM. ZAMM Zeitschrift fur Angewandte Mathematik und Mechanik **87**(1), 37–58 (2005)
40. Beji, L., Bestaoui, Y.: Motion generation and adaptive control method of automated guided vehicles in road following. IEEE Trans. Intell. Transp. Syst. **6**(1), 113–123 (2005)
41. Benosman, A., Le Vey, G.: Control of flexible manipulators: a survey. Robotics **22**(5), 533–545 (2004)
42. Benveniste, A., Basseville, M., Moustakides, G.: The asymptotic local approach to change detection and model validation. IEEE Trans. Autom. Control **32**(7), 583–592 (1987)
43. Benveniste, A., Métivier, M., Priouret, P.: Adaptive Algorithms and Stochastic Approximations. Springer, Berlin (1990)
44. Berhang, E., Pettersen, K., Pavlov, A.: An optimal guidance scheme for cross-track control of under actuated underwater vehicles, IEEE MED 2016. In: 14th Mediterranean Conference on Control and Automation (2006)
45. Berman, S., Edan, Y.: Intelligent automatic guided vehicles. In: Rigatos, G. (ed.) Intelligent Industrial Systems: Modelling, Automation and Adaptive Behavior. IGI Publications (2010)
46. Bernsten, P.I.B., Aamo, O.M., Leira, B.J.: Ensuring mooring line integrity by dynamic positioning: controller design and implementation tests. Automatica, Elsevier **45**, 1285–1290 (2009)
47. Bertini, D., Bittanti, S., Savaresi, S.M.: Decoupled cushion control in ride control systems for air cushion catamarans. Control Eng. Pract., Elsevier **8**, 191–203 (2000)
48. Besnard, L., Shtessel, Y.B., Landrum, B.: Quadrotor vehicle control via sliding mode controller driven by sliding mode disturbance observer. J. Frankl. Inst., Elsevier **349**, 658684 (2012)
49. Bevly, D.M., Ryu, J., Gerdes, J.C.: Integrating INS sensors with GPS measurements for continuous estimation of vehicle sideslip, roll, and tire cornering stiffness. IEEE Trans. Intell. Transp. Syst. **7**(4) (2006)
50. Biggs, J., Hokkerbaum, W.: Optimal kinematic control of an autonomous underwater vehicle. IEEE Trans. Autom. Control **54**(7), 1623–1626 (2009)
51. Bishop, B.E.: On the use of redundant manipulator techniques for control of platoons of cooperative robotic vehicles. IEEE Trans. Syst. Man Cybern. - Part A **33**(5), 608–615 (2003)
52. Blackmore, S., Stout, W., Wang, M., Runov, B.: Robotic agriculture - the future of agricultural mechanisation? In: Stafford, J.V. (ed.) Fifth European Conference on Precision Agriculture, pp. 621–628. Wageningen Academic Publishers, The Netherlands (2005)
53. Bolić, M., Djurić, P.M., Hong, H.: Resampling algorithms and architectures for distributed particle filters. IEEE Trans. Signal Process. **53**, 2242–2450 (2005)
54. Borhaug, E., Pavlov, A., Panteley, E., Pettersen, K.: Straight-line path following for formations of underactuated marine surface vessels. IEEE Trans. Control Syst. Technol. **13**(3), 493–506 (2011)
55. Bosnak, M., Matko, D., Blasic, S.: Quadrocopter control using an on-board video system with off-board processing. Robot. Auton. Syst., Elsevier **60**, 657667 (2012)
56. Boudaond, M., Haddad, Y., Le Gorrec, Y.: Modelling and optimal force control of a nonlinar electrostatic microgripper. IEEE/ASME Trans. Mech. **18**, 1130–1139 (2012)
57. Bououden, S., Boutat, D., Zheng, G., Barbot, J.P., Kratz, F.: A triangular canonical form for a class of 0-flat nonlinear systems. Int. J. Control, Taylor and Francis **84**(2), 261–269 (2011)
58. Brumback, B.D., Srinath, M.D.: A chi-square test for fault-detection in Kalman filters. IEEE Trans. Autom. Control **32**(6), 552–554 (1987)

59. Bugeja, M., Fabri, S., Camilleri, L.: Dual adaptive dynamic control of mobile robots using neural networks. IEEE Trans. Syst. Man Cybern. Part B Cybern. **39**(1), 129–141 (2009)
60. Cabecinhas, D., Cunha, R., Silvestre, C.: A nonlinear quadrotor trajectory tracking controller with disturbance rejection. In: Proceedings of the IEEE American Control Conference (ACC 2014), Portland, Oregon, USA (2014)
61. Cacace, F., Conte, F., Germani, A.: Output transformations and separation results for feedback linearizable delay systems. Int. J, Control Taylor and Francis (2017)
62. Cadre, A., Sonnenberg, C., Du, S., Stilwell, D., Woolsey, C.: Guidance and control of an unmanned surface vehicle exhibiting sternward motion. In: IEEE Oceans. Hampton Roads, USA (2012)
63. Califano, C., Moog, C.H.: Coordinates transformations in nonlinear time-delay systems. In: 53rd, IEEE Conference on Decision and Control, Los Angeles, California, USA (2014)
64. Califano, C., Moog, C.H.: Accessibility of nonlinear time delay systems. IEEE Trans. Autom. Control **62**(3), 1254–1268 (2017)
65. Califano, C., Marquez-Martinez, L.A., Moog, C.H.: Linearization of time-delay systems by input-output injection and output transformation. Automatica Elsevier **49**, 1932–1940 (2013)
66. Canale, M., Fagiano, L., Razza, V.: Approximate NMPC for vehicle stability: design, implementation and SIL testing. Control Eng. Pract., Elsevier **18**, 630–639 (2010)
67. Canale, M., Fagiano, L.: A robust IMC approach for stability control for stability control of 4WS vehicles. In: Proceedings of the 2007 American Control Conference, New York, USA (2007)
68. Caracciolo, L., de Luca, A., Iannitti, S.: Trajectory tracking control of a four-wheel differentially driven mobile robot. In: Proceedings of the 1999 IEEE International Conference on Robotics and Automation, Detroit, Michigan (1999)
69. Cariou, C., Lenain, R., Thuilot, B., Martinet, P.: Adaptive control of four-wheel-steering off-road mobile robots: application to path tracking and heading control in presence of sliding. In: IEEE IROS 2008, IEEE/RSJ International Conference on Intelligent Robots and Systems, Nice, France (2008)
70. Cariou, C., Lenain, R., Thuilot, R., Berducat, M.: Automatic guidance of a four-wheel steering mobile robot for accurate field operations. J. Field Robot. **26**(6–7), 504–518 (2009)
71. Carno, M., Panzani, G., Savaresi, S.: Single-track vehicle dynamics control: state of the art and perspectives. IEEE/ASME Trans. Mech. **20**(4), 1521–1532 (2015)
72. Carvalho, A., Gao, Y., Gray, A., Tseng, H.E., Borrelli, F.: Predictive control of an autonomous ground vehicle using an iterative linearization approach. In: 16th International IEEE Annual Conference on Intelligent Transportation Systems, IEEE ITSC 2013, The Hague, Netherlands (2013)
73. Caswara, F.M., Unbenhauen, H.: A neuro-fuzzy approach to the control of a flexible-link manipulator. IEEE Trans. Robot. Autom. **18**(6), 932–944 (2002)
74. Cerone, V., Andreo, D., Larsson, M., Regrutto, D.: Stabilization of a riderless bicycle: a linear parameter varying approach. IEEE Control Syst. Mag. **30**, 23–32 (2010)
75. Cetinkunt, S., Yu, W.L.: Closed loop behavior of a feedback controlled flexible arm: a comparative study. Int. J. Robot. Res. **10**(3), 263–275 (1991)
76. Chak, C.K., Feng, G., Mia, J.: An adaptive fuzzy neural network for MIMO system model approximation in high dimensional spaces. IEEE Trans. Syst. Man Cybern. Part B: Cybern. **28**(3), 436–446 (1998)
77. Chamseddine, A., Li, T., Zhang, Y., Rabbath, C.A., Theilliol, D.: Flatness-based trajectory planning for a quadrotor unmanned aerial vehicle test-bed considering actuator and system constraints. In: 2012 American Control Conference Fairmont Queen Elizabeth, Montral, Canada, 27–29 June (2012)
78. Chang, D.E.: Stabilizability of controlled Lagrangian systems of two degrees of freedom and one degree of under-actuation by the energy-shaping method. IEEE Trans. Autom. Control **55**(8), 1888–1893 (2010)
79. Chang, N.J., Shih, Y.J.: Fuzzy control of multiplicative noised nonlinear systems subject to actuator saturation and H_∞ performance constraints. Neurocomputing, Elsevier **148**, 512–520 (2015)

80. Chang, S.J., Slotine, J.J.: Cooperative robot control and concurrent synchronization of Lagrangian systems. IEEE Trans. Robot. **25**(3), 686–700 (2008)
81. Chen, C.K., Dao, J.K.: Speed-adaptive path following control of a riderless bicycle via road preview. In: Proceedings of the Biycle and Motorcycle Dynamics Conference: Symposium on the Dynamics and Control of the Single Track Vehicle, p. 2010. Delft, The Nethrlands (2010)
82. Chen, L., Mercorelli, P., Liu, S.: A Kalman Estimator for detecting repetitive disturbances, ACC 2005, American Control Conference, Portland, Oregon, USA (2005)
83. Chen, C.S.: Dynamic structure adaptive neural fuzzy control for MIMO uncertain nonlinear systems. Inf. Sci., Elsevier **179**, 2676–2688 (2009)
84. Chen, C.S.: Dynamic structure adaptive neural fuzzy control for MIMO uncertain nonlinear systems. Inf. Sci. Elsevier **179**, 2676–2688 (2009)
85. Chen, C.S.: Robust self-organising neural-fuzzy control with uncertainty observer for MIMO nonlinear systems. IEEE Trans. Fuzzy Syst. **19**(4), 694–706 (2011)
86. Chen, B.S., Lee, T.S., Feng, J.H.: A nonlinear H_∞ control design in robotic systems under parameter perturbation and external disturbance. Int. J. Control Tayor and Francis **59**(2), 459–461 (1994)
87. Chen, W.H., Ballance, D.J., Gawthrop, P.J., Reilly, J.O.: A nonlinear disturbance observer for robotic manipulators. IEEE Trans. Indust. Electron. **47**(4), 932–938 (2000)
88. Chen, B., Liu, X., Tong, S.: Adaptive fuzzy output tracking control of MIMO nonlinear uncertain systems. IEEE Trans. Fuzzy Syst. **15**(2), 287–300 (2007)
89. Chen, C.H., Lin, C.M., Chen, T.Y.: Intelligent adaptive control for MIMO uncertain nonlinear systems. Expert Syst. Appl. **35**, 865–877 (2008)
90. Chen, H., Ma, M.M., Wang, H., Liu, Z.Y., Cai, Z.X.: Moving horizon tracking H_∞ control of wheeled mobile robots with actuator saturation. IEEE Trans. Control Syst. Technol. **17**(2), 449–457 (2009)
91. Chen, H., Fang, Y., Sun, N.: Optimal trajectory planning and tracking control method for overhead cranes. IET Control Theory Appl. **10**(6), 692–699 (2016)
92. Chiu, C.S.: Mixed feedforward/feedback adaptive fuzzy control for a class of MIMO nonlinear systems. IEEE Trans. Fuzzy Syst. **14**(6), 716–727 (2006)
93. Chladny, R.R., Koch, C.R.: Flatness-based tracking of an electromechanical variable valve timing actuator with disturbance observer feedforward compensation. IEEE Trans. Control Syst. Technol. **16**(4), 652–663 (2008)
94. Cho, Y.W.: Park, C.W., kim, J.H., Park, M.: Indirect model reference adaptive fuzzy control of dynamic fuzzy-state space model. IET Proc. Control Theory Appl. **148**(4), 273–282 (2005)
95. Chu, Y., Sanfilippo, F., Esay, V., Zhang, H.: An effective heave compensation and anti-sway control approach for offshore hydraulic crane application. In: IEEE ICMA 2014, IEEE 2014 International Conference on Mechatronics and Automation, , Tianjin, China (2014)
96. Chu, P.B., Brener, I., Pu, C., Lee, S.S., Dadap, J.J., Park, S., Bergman, K., Bonadeo, N.H., Chou, J., Doran, R.A., Gibson, R., Harel, R., Johnson, J.J., Lee, D., Peale, D.R., Tong, D.T., Tsai, M.J., Wu, Q., Zhang, W., Goldstein, E.L., Linan, L.Y., Walker, J.A.: Design and nonlinear servo control of MEMS mirrors and their performance in a large port-count optical switch. IEEE J. Microelectromech. Syst. **14**(2), 261–273 (2005)
97. Chwa, D.: Nonlinear tracking control of 3-D overhead cranes against the initial swing angle and the variation of the payload weight. IEEE Trans. Control Syst. Technol. **17**(4), 876–893 (2009)
98. Chyba, M., Haberkorn, T., Smith, R., Choi, S.: Design and implementation of time efficient trajectories for autonomous underwater vehicles. Ocean Eng. Elsevier **35**, 63–76 (2006)
99. Cimen, T., Banks, S.P.: Nonlinear optimal tracking control with application to super-tankers for autopilot design. Automatica, Elsevier **40**, 1845–1863 (2004)
100. Coelho, P., Nunes, U.: Path-following control of mobile robots in presence of uncertainties. IEEE Trans. Robot. **21**(2), 252–261 (2005)
101. Comets, F., Meyre, T.: Calcul stochastique et modèles de diffusions. Dunod (2006)

102. Corno, M., Massaro, M., Lot, R., Savaresi, S.M., On linear-parameter varying roll angle controller design for two-wheeled vehicles. In: Proceedings of Bicycle and Motorcycle Dynamics, Symposium on the Dynamics and Control of single-track vehicles, p. 2010. Delft, The Netherlands (2010)
103. Corno, M., Savaresi, S.M., Balas, G.: On linear parameter varying (LPV) slip-controller design for two-wheeled vehicles. Int. J. Robust Nonlinear Control **19**(12), 1313–1336 (2009)
104. Corno, M., Panzani, G., Savaresi, S.: Traction-control-oriented state estimation for motorcycles. IEEE Trans. Control Syst. Technol. **21**(6), 2400–2407 (2011)
105. Cortesao, R.: On Kalman active observers. J. Intell. Robot. Syst., Springer **48**(2), 131–155 (2006)
106. Cortesao, R., Park, J., Khatib, O.: Real-time adaptive control for haptic telemanipulation with Kalman active observers. IEEE Trans. Rob. **22**(5), 987–999 (2005)
107. Crassidis, J.L., Junkins, J.L.: Optimal Estimation of Dynamic Systems, 2nd edn. CRC Press, Boca Raton (2012)
108. Craven, P.J., Sutton, R., Burns, R.S.: Multivariable neurofuzzy control of an autonomous underwater vehicle. Integr. Comput. Aided Eng. **6**(4), 275–288 (1999)
109. Cuesta, F., Gomez-Bravo, F., Ollero, A.: Parking maneuvers of industrial-like electric vehicles with and without trailers. IEEE Trans. Ind. Electron. **51**(2), 257–269 (2004)
110. Cunha, R., Silvestre, C., Hespanha, J.: Output-feedback control for stabilization on SE(3). Syst. Control Lett. **57**(12), 1013–1022 (2008)
111. Dacic, D.B., Subbotin, M.V., Kokotovic, P.V.: Control effort reduction in tracking feedback laws. IEEE Trans. Autom. Control **51**(11), 1831–1837 (2006)
112. Daong, S.C., Uezato, E., Kinga, H., Yamamoto, T.: A hybrid evolutionary algorithm for recurrent neural network control of a three-dimensional tower crane. Autom. Constr., Elsevier **23**, 55–63 (2012)
113. de Filippi, P., Tanelli, M., Corno, M., Savaresi, S.M.: Enhancing active safety of two-wheeled vehicles via electronic stability control. In: 18th IFAC World Congress. Milano, Italy (2011)
114. de Filippi, P., Tanelli, M., Corno, M., Savaresi, S., Fabbri, L.: Semi-active steering damper control in two-wheeled vehicles. IEEE Trans. Control Syst. Technol. **19**(5), 1003–1020 (2011)
115. de Filippi, P., Tanelli, M., Corno, M., Savaresi, S., Santucci, M.: Electronic stability control for powered two wheelers. IEEE Trans. Control Syst. Technol. **22**(1), 265–272 (2014)
116. De Luca, A., Ianitti, S., Mattone, R., Oriolo, G.: Control problems of underactuated manipulators. In: 2001 IEEE/ASME International Conference on Advanced Intelligent Mechatronics, Como, Italy (2001)
117. De Luca, A., Oriolo, G.: Motion planning and trajectory control of an underactuated three-link robot via dynamic feedback linearization. In: Proceedings of IEEE ICRA 2000, IEEE International Conference on Robotics and Automation, San Francisco, USA (2000)
118. De Luca, A., Oriolo, G.: Trajectory planning and control for planar robots with passive last joint. Int. J. Robot. Res. **51**(5–6), 575–590 (2002)
119. De Luca, A., Siciliano, B.: Regualation of flexible arms under gravity. IEEE Trans. Robot. Autom. **9**, 463–467 (1993)
120. de Martinis, B.E., Butterfield, H.B., Moehli, J., Turner, K.L.: Chaos for a microelectromechanical oscillator governed by the nonlinear Mathieu equation. IEEE J. Microelectromech. Syst. **16**(6), 1314–1323 (2007)
121. Deng, M., Inoue, A., Henmi, T., Ueki, N.: Analysis and experiment on simultaneous swing-up of a parallel cart-type double inverted pendulum. Asian J. Control, Wiley **10**(1), 121–138 (2010)
122. Derafa, I., Benallegue, A., Fridman, L.: Super-twisting control algorithm for the attitude tracking control of a four rotors UAV. J. Frankl. Inst., Elsevier **949**, 685–699 (2013)
123. Dingle, P., Guzella, L.: Optimal emergency maneuvers on highways for passenger vehicles with two and four-wheel active strategy. In: 2010 American Control Conference, Baltimore, MD, USA (2010)
124. Do, K.D., Pan, J.: High-performance control of an active heave compensation system. In: Proceedings of the IFAC 17th World Congress, Seoul, Korea (2008)

125. Do, D., Pan, J.: Nonlinear control of an active heave compensation system. Ocean Eng., Elsevier **35**(56), 558–571 (2008)
126. Do, K.D.: Practical control of underactuated ships. Ocean Eng., Elsevier **37**, 1111–1119 (2010)
127. Do, K.D.: Practical formation control of multiple underactuated ships with limited sensing ranges. Robot. Auton. Syst., Elsevier **59**, 457–471 (2011)
128. Do, K.D., Pan, J.: Global tracking control of underactuated ships with nonzero off-diagonal terms in their system matrices. Automatica, Elsevier **41**, 87–95 (2005)
129. Dodin, P., Minvielle, O., Le Cadre, J.P.: Re-entry vehicle tracking observability and theoretical bound. In: 2005 8th IEEE International Conference on Information Fusion (2005)
130. Dofler, F., Bullo, F.: Synchronization incomplex networks of phase oscillators: a survey. Elsevier, Automatica (2014)
131. Donadel, R., Raffo, G.V., Becker, L.B.: Modeling and control of a tiltrotor UAV for path tracking. In: 19th World Congress The International Federation of Automatic Control Cape Town, South Africa (2014)
132. Doyle, J.C., Glover, K., Khargonekar, P.P., Francis, B.A.: State-space solutions to standard H_2 and H_∞ control problems. IEEE Trans. Autom. Control **34**, 831–847 (1989)
133. Du, H., Zhang, N.: H_∞ control of active vehicle suspensions with actuator time delay. J. Sound Vib. Elsevier **301**, 236–252 (2007)
134. Duflo, M.: Algorithmes stochastiques, Mathématiques et Applications, vol. 23. Springer, Berlin (1996)
135. Dydek, Z.T., Annaswamy, A.M., Lavretsky, E.: Adaptive control of quadrotor UAVs: a design trade study with flight evaluations. IEEE Trans. Control Syst. Technol. **21**(4), 1400–1406 (2013)
136. Etxebarria, V., Sanz, A., Lizarraga, L.: Control of a lightweight flexible robotic arm using sliding modes. Int. J. Adv. Robot. Syst. **2**(2), 103–110 (2005)
137. Fabbri, T., Fenucci, D., Falasca, S., Gamba, M., Bicchi, A.: Packet-based dynamic control of a Furuta pendulum over ethernet. In: IEEE MED 2013, 21st Mediterranean Conference on Control and Automation, Crete, Greece (2013)
138. Fahsi, A., Belhaq, M., Lakrad, F.: Suppression of hysteresis in a Van der Pol - Duffing oscillator. Commun. Nonlinear Sci. Numer. Simul., Elsevier **14**, 1609–1616 (2009)
139. Fang, Y., Dixon, W., Dawson, D., Zergeloglu, E.: Nonlinear coupling control laws for an underactuated overhead crane system. IEEE/ASME Trans. Mechatron. **8**(3), 418–423 (2003)
140. Fang, Y., Zergeroglu, E., de Queiroz, M.S., Dawson, D.M.: Global output feedback control of dynamically positioned surface vessels: an adaptive control approach. Mechatronics, Elsevier **14**, 341–356 (2004)
141. Fang, Y., Wang, P., Sun, N., Zhang, Y.: Dynamics analysis and nonlinear control of an offshore boom crane. IEEE Trans. Ind. Electron. **61**(2), 414–427 (2014)
142. Fei, J., Zhou, J.: Robust adaptive control of MEMS triaxial gyroscope using fuzzy compensator. IEEE Trans. Syst. Man Cybern. - Part B: Cybern. **42**(6), 1599–1607 (2012)
143. Fischer, N., Hughes, D., Walters, P., Swartz, E.M., Dixon, W.E.: Nonlinear RISE-based control of an autonomous underwater vehicle. IEEE Trans. Robot. **30**(4), 845–852 (2014)
144. Fishcer, N., Bhasin, S., Dixon, W.E.: Nonlinear control of an autonomous underwater vehicle: A RISE-based approach. Am. Control Conf. San Francisco, USA (2011)
145. Fliess, M., Mounier, H.: Tracking control and π-freeness of infinite dimensional linear systems. In: Picci, G., Gilliam, D.S (eds.) Dynamical Systems, Control, Coding and Computer Vision, vol. 258, pp. 41–68. Birkhaüser (1999)
146. M. Fliess, H. Mounier, P. Rouchon and J. Rudolph, Systèmes lineaires sur les operateurs de Mikusiǹski et commande d' une poutre flexible, In: ESAIM Proc. Élasticité, viscoélasticité et contrôle optimal, huitièmes entretiens du Centre Jacques Cartier, Lyon, 1996
147. Fliess, M., Mounier, H.: On a class of linear delay systems often arising in practice. Kybernetika **37**(3), 235–308 (2001)
148. Fossen, T.I., Perez, T.: Kalman Filtering heading control of ships and offshore rigs. In: IEEE Control Systems Magazine, pp. 32–46 (2009)

149. Fossen, T.I., Strand, J.P.: Passive nonlinear observer design for ships using Lyapunov methods: full scale experiments with a supply vessel. Automatica, Elsevier **35**, 3–16 (1999)
150. Franch, J., Agrawal, S.K., Sangwan, V.: Differential flatness of a class of -DOF planar manipulators driven by 1 or 2 actuators. IEEE Trans. Autom. Control **55**(2), 548–554 (2010)
151. Franch, J., Reyes, A., Agrawal, S.K.: Differential flatness of a class of n-DOF planar manipulators driven by an arbitrary number of actuators, : European Control Conference, July 2013. Zurich, Switzerland (2013)
152. Freddi, A., Lanzon, A., Longhi, S.: A feedback linearization approach to fault tolerance in quadrotor vehicles. In: 18th IFAC World Congress, Italy, Milan (2011)
153. Freidovich, L., Shiriaev, A., Gordillo, F., Gmez-Estern, F., Aracil, J.: Partial-energy-shaping control for orbital stabilization of high-frequency oscillations of the Furuta pendulum. IEEE Trans. Control Syst. Technol. **17**(4), 853–858 (2009)
154. Frezza, R., Beghi, A.: A virtual motorcycle driver for closed-loop simulations: Multi-body tools for evaluating system performance. IEEE Control Syst. Mag. **5**, 62–77 (2006)
155. Fu, K.S., Gonzalez, R.C., Lee, G.S.G.: Robotics: Control. Sensing. Vision and Intelligence. McGraw-Hill, New York (1987)
156. Galicki, M.: Finite-time control of robotic manipulators. Automatica Elsevier **51**, 49–54 (2015)
157. Gan, Q., Harris, C.J.: Comparison of two measurement fusion methods for Kalman-filter-based multisensor data fusion. IEEE Trans. Aerosp. Electron. Syst. **37**(1), 273–280 (2001)
158. Gao, Y., Er, M.J.: Online adaptive fuzzy neural identification and control of a class of MIMO nonlinear systems. IEEE Trans. Fuzzy Syst. **11**(4), 462–477 (2003)
159. Gao, H., Song, X., Ding, L., Xia, K., Li, N.: Adaptive motion control of wheeled mobile robot with unknown slippage. Int. J. Control **87**(8), 1513–1522 (2014)
160. Garcia-Ramirez, E., Califano, C., Marquez-Martinez, L.A., Moog, C.H.: Observer design based on linearization via input-output injection of time-delay systems, NOLCOS2 2016. In: 10th IFAC Conference on Nonlinear Control Systems, Monterey, California (2016)
161. Garcia-Ramirez, E., Moog, C.H., Califano, C., Marquez-Martinez, L.A.: Linearization via input-output injection of time-delay systems. Int. J. Control Taylor and Francis **89**(6), 1125–1136 (2016)
162. Gazi, V., Passino, K.: Stability analysis of social foraging swarms. IEEE Trans. Syst. Man Cybern. - Part B. Cybernetics **34**(1), 539–557 (2004)
163. Ge, Q.-B., Wen, G.-L.: Relative ship positioning based on information fusion in the Marine Intelligent Transportation System (MITS). In: Proceeding of the 7th International Conference on Machine Learning and Cybernetics, Kunming, China (2008)
164. Ge, S.S., Lee, T.H., Zhu, G.: Energy-based robust controller design for multi-link flexible robots. Mechatronics, Elsevier **6**(7), 779–798 (1996)
165. Ghanes, M., DeLeon, J., Barbot, J.P.: Simultaneous observation and identification for nonlinear systems under unknown time-varying delay. J. Frankl. Inst. Elsevier **353**, 2305–2318 (2016)
166. Ghilardelli, F., Lini, G., Piazzi, A.: Path generation using n^4 splines for a track and trailer vehicle. IEEE Trans. Autom. Sci. Eng. **11**(1m), 187–203 (2014)
167. Ghommam, J., Mnif, F.: Coordinated path-following control for a group of underactuated surface vessels. IEEE Trans. Industr. Electron. **56**(5), 3951–3963 (2009)
168. Gian, Y., Fang, Y.: A learning strategy based partial feedback linearization control method for an offshore boom crane. In: 2015 IEEE 54th Annual Conference on Decision and Control (CDC), Osaka, Japan (2013)
169. Gibbs, B.P.: Advanced Kalman Filtering, Least Squares and Modelling: A Practical Handbook. Wiley, New York (2011)
170. Gibbs, R.G.: New Kalman filter and smoother consistency tests. Automatica, Elsevier **49**(10), 3141–3144 (2013)
171. Godhavn, J.M., Fossen, T.I., Berge, S.P.: Nonlinear and adaptive backstepping designs for tracking control of ships. J. Adapt. Control Signal Process. Special Issue on Marine Syst. Control, Wiley **12**(8), 649–670 (1998)

172. Granle, M., Zhu, G., Saydy, L.: Sliding-mode tracking control of an electrostatic parllel-plate MEMs, 2010 IEEE/ASME International Conference on Advanced Intelligent Mechatronics. Montréal, Canada (2010)
173. Grasser, F., d' Arrigo, A., Colombi, S., Rafer, A.C.: JOE: a mobile inverted pendulum. IEEE Trans. Ind. Electron. **49**, 107–114 (2002)
174. Green, A., Sasiadek, J.Z.: Fuzzy adaptive vibration suppression and noise filtering for flexible robot control. In: American Control Conference, p. 2005. Portland, Oregon, USA (2005)
175. Greichen, K., Treurer, H., Zeitz, M.: Swing-up of the double pendulum on a cart by feedforward and feedback control with experimental validation. Automatica, Elsevier **43**, 63–71 (2007)
176. Groß, R., Bonani, M., Mondada, F., Dorigo, M.: Autonomous self-assembly in swarm-bots. IEEE Trans. Robot. **22**(6), 1115–1130 (2006)
177. Gu, P., Walid, A., Iskandarani, Y., Karimi, H.R.: Int. J. Mach. Learn. Cybern., Springer **4**, 85–98 (2013)
178. Guan, X.P., Chen, C.L.: Delay-dependent guaranteed cost control for TS fuzzy systems with time delays. IEEE Trans. Fuzzy Syst. **12**(2), 236–249 (2004)
179. Guo, S., Xie, W., Ma, B.: Robust position stabilization of underactuated hovercrafts with modelling parameter uncertainties. In: Proceedings of the 32nd Chinese Control Conference, Xian China (2013)
180. Gupta, A., Malley, M.K.O.: Disturbance-observer-based force estimation for haptic feedback. ASME J. Dyn. Syst. Meas. Control **133**(1), 014505 (2011)
181. Gustafsson, F.: Particle filter theory and practice with positioning applications. IEEE Aerosp. Electron. Syst. Mag. **25**(7), 53–81 (2010)
182. Hagenmeyer, V., Delaleau, E.: Robustness analysis of exact feedforward linearization based on differential flatness. Automatica, Elsevier **39**, 1941–1946 (2003)
183. Hagenmeyer, V., Delaleau, E.: Robustness analysis with respect to exogenous perturbations for flatness-based exact feedforward linearization. IEEE Trans. Autom. Control **55**(3), 727–731 (2010)
184. Haghighi, H.S., Markazi, A.M.: Chaos prediction and control in MEMS resonators. Commun. Nonlinear Sci. Numer. Simul. **15**, 3091–3099 (2010)
185. Haidar, I., Nicolau, F., Barbot, J.P., Aggune, W.: Further remarks on input-output linearization of SISO time-varying delay systems. In: 2017 SIAM Conference on Control and Applications, Pittsburg, USA (2017)
186. Halse, K.H., Easy, V., Ponkratov, D., Chen, Y., Xu, J., Pedersen, E.: Lifting operations for subsea installations using small construction vessels and active heave compensation systems: a simulation approach. In: Proceedings of the ASME 2014, 33rd International Conference on Ocean, Offshore and Arctic Engineering, San Francisco, California (2014)
187. Han, T.T., Ge, S.S.: Cooperative control design for circular flocking of underactuated hovercrafts. In: 2011 IEEE Conference on Decision and Control and European Control Conference (CDC-ECC), Orlando Florida USA (2011)
188. Hao, Y.J., Shime, Y.K.: Adaptive coupling control for overhead crane systems. Mechatronics, Elsevier **17**, 143–152 (2007)
189. Harris, C.J., Gan, Q.: State estimation and multi-sensor data fusion using data-based neurofuzzy local linearization process models. Information Fusion, Elsevier **2**, 17–29 (2001)
190. Harris, C., Hong, X., Gan, Q.: Adaptive Modelling. Estimation and Fusion From Data. Springer, Berlin (2002)
191. He, B., Wang, B.R., Yan, T.H., Han, Y.Y.: A distributed parallel motion control for the multithruster autonomous underwater vehicle. Mech based Des. Struct. Mach. Taylor and Francis **41**(2), 236–257 (2013)
192. He, G., Gang, Z.: Finite-time stabilization of a comb-drive electrostatic microactuator. IEEE/ASME Trans. Mechatron. **17**(1), 107–115 (2012)
193. He, Y., Pei, H., Sun, T.: Robust tracking control of helicopters using backstepping with disturbance observers. Asian J. Control **16**(6), 116 (2014)

194. Hernandez-Guzman, V.M., Antonio-Cruz, M., Ortigoza, R.S.: Linear state feedback regulation of the Furuta pendulum: design based on differential flatness and root locus. IEEE Access **4**, 8721–8736 (2016)
195. Hiraoka, T., Nishikara, O., Kamamoto, H.: Automatic path tracking controller of a four-wheel steering vehicle. J. Veh. Syst. Dyn., Taylor and Francis **42**(10), 1205–1223 (2009)
196. Hong, K.S., Ngo, G.H.: Dynamics of the container crane on a mobile harbor. Ocean Eng., Elsevier **53**, 16–24 (2012)
197. Hong, K.S.: An open-loop control for underactuated manipulators using oscillatory inputs: steering capability of an unactuated joint. IEEE Trans. Control Syst. Technol. **10**(3), 469–479 (2002)
198. Hong, Y., Gao, L., Cheng, D., Hu, J.: Luapunov-based approach to multi-agent systems with switching jointly connected interconnection. IEEE Trans. Autom. Control **52**(5), 943–948 (2007)
199. Hosseini, M., Zhu, G., Peter, Y.A.: A new formulation of fringing capacitance and its application to the control of parallel-plate electrostatic micro-actuators. Analog Integr. Circuits Signal Process., Springer **53**, 119–128 (2007)
200. Hsu, H.R., He, W.H., Chen, J.H.: Stable and quadratic optimal control fot TS fuzzy model-based time-delay control systems. IEEE Trans. Syst. Man Cybern. - Part B Cybern. **39**(2), 503–516 (2009)
201. Hua, J.S., Yin, D., Hori, Y.: Fault-tolerant traction control of electric vehicles. Control Eng. Pract., Elsevier **19**, 204213 (2011)
202. Huang, J., Turn, H.S.: Development and validation of an automated steering control system for bus revenue service. IEEE Trans. Autom. Sci. Eng. **13**(1), 227–237 (2016)
203. Huang, Y.S., Zhou, D.Q., Xiao, S.P., Ling, D.: Coordinated deventralized hybrid adaptive output feedback fuzzy control for a class of large-scale nonlinear systems with strong interconnections. IET Control Theory Appl. **3**(9), 1261–1274 (2009)
204. Hui, D., Fuchun, S., Zengqi, S.: Observer-based adaptive controller design of flexible manipulators using time-delay neuro-fuzzy networks. J. Intell. Robot. Syst., Springer **34**(4), 453–466 (2002)
205. Hwang, C.N.: The integrated design of fuzzy collission-avoidance and H_∞ autopilots on ships. J. Navig., Cambridge University Press **55**, 117–136 (2002)
206. Hwang, C.L., Shih, C.Y.: A distributed active-vision network-space approach for the navigation of a car-like wheeled robot. IEEE Trans. Ind. Electron. **56**(3), 846–855 (2009)
207. Hwang, C.L., Chang, L.J., Yu, Y.S.: Network-based fuzzy decentralized sliding-mode control for car-like mobile robots. IEEE Trans. Ind. Electron. **54**(1), 574–585 (2007)
208. Iannitti, S., de Luca, A.: Dynamic feedback control of $XYn\bar{R}$ planar robots with n rotational passive joints. J. Field Robot., Wiley **20**(5), 251–270 (2003)
209. Imura, J., Kobayashi, K., Yoshikawa, T.: Nonholonomic control of 3-link planar manipulator with a free joint. In: Proceedings of the 35th Conference on Decision and Control, Kobe, Japan (1996)
210. Ito, M., Toda, N.: Control of a three-joint underactuated planar manipulator: interconnection and damping assignment passivity-based control approach. In: Kozlowski, K. (ed.) Robot Motion and Control 2007. Lecture Notes in Control and Information Sciences, vol. 360, pp. 109–117 (2007)
211. Jang, J.S.R., Sun, C.T., Mizutani, E.: Neurofuzzy and Soft-Computing. A computational Approach to Learning and Machine Intelligence. Prentice-Hall, Upper Saddle River (1997)
212. Jasim, W., Gu, D.: H-infinity for quadrotor attitude stabilization, UKACC 2014, UK International Conference on Control, Loughborough, UK (2014)
213. Jiang, D., Li, D., Wang, S., Tian, L., Yang, L.: Additional yaw movement control of a 4WS and 4WID agricultural data acquisition vehicle. Int. J. Adv. Robot. Syst. 1–10 (2015). Sage Publications
214. Jimenez-Triana, A., Zhu, G., Saydy, L.: Chaos synchronization of an electrostatic MEMS resonator in the presence of parametric uncertainties. In: IEEE ACC 2011, IEEE American Control Conference. San Francisco, California, USA (2011)

215. Jimenez-Triana, A., Zhu, G., Saydy, L.: Oscillation amplitude enhancement of an electrostatic MEMS resonatorvia chaos control. In: IEEE ACC 2013, IEEE American Control Conference. Washington DC, USA (2014)
216. Jin, Y.: Robust control with decoupling performance for steering and traction of 4WS vehicles under velocity-varying motion. IEEE Trans. Control Syst. Technol. **8**(3), 554–569 (2000)
217. Jing, Y., Jing, N., Zhang, Y., Dimirovksi, G.: Fuzzy robust and non-fragile minimax control of a trailer-truck model. In: Proceedings of the 46th IEEE Conference on Decision and Control, New Orleans, USA (2001)
218. Jujnowich, B., Cebon, D.: Path-following steering control for articulated vehicles. J. Dyn. Syst. Meas. Control **135**(3) (2013)
219. Julier, S.J., Uhlmann, J.K.: Unscented filtering and nonlinear estimation. Proc. IEEE **92**, 401–422 (2004)
220. Julier, S., Uhlmann, J., Durrant-Whyte, H.F.: A new method for the nonlinear transformations of means and covariances in filters and estimators. IEEE Trans. Autom. Control **45**(3), 477–482 (2000)
221. Jwo, D.J., Cho, T.S.: A practical note on evaluating Kalman filter performance optimality and degradation. Appl. Math. Comput., Elsevier **193**(2), 482–505 (2007)
222. Kamen, E.W., Su, J.K.: Introduction to Optimal Estimation. Springer, Berlin (1999)
223. Kanghyun, N., Fujimoto, M., Hori, Y.: Advanced motion control of electric vehicles based on robust lateral tire force control via active front steering. IEEE/ASME Trans. Mechatron. **19**(1), 289–299 (2014)
224. Kanoh, H., Tzafestas, S.G., Lee, H.G., Kalat, J.: Modelling and control of flexible robot arms. In: Proceedings of 25th Conference on Decision and Control, Athens, Greece, pp. 1866–1870 (1986)
225. Karlsson, R., Norrlöf, M.: Bayesian position estimation of an industrial robot using multi sensors. Technical Report-ISY-R-2613, University of Linköping (2004)
226. Karlsson, R., Norrlöf, M.: Bayesian position estimation of an industrial robot using multiple sensors. In: Proceedings of IEEE International Conference on Control Applications, Taipei, Taiwan, pp. 303–308 (2004)
227. Katebi, M.R., Yamamoto, I., Matsuura, M., Grimble, M.J., Hiroyama, H., Okamoto, N.: Robust dynamic ship positioning control system design and application. Int. J. Robust Nonlinear Control, Wiley **11**, 1257–1284 (2001)
228. Keviczky, T., Falcone, P., Borelli, F., Asgari, J., Hrovat, D.: Predictive control approach to autonomous vehicle steering. In: IEEE ACC: American Control Conference, June 2016, Minneapolis, USA (2006)
229. Khalhoub, N.G., Kfoury, G.A., Bazzi, B.A.: Design of robust controllers and a nonlinear observer for the control of a single-link flexible robotic manipulator. J. Sound Vib., Elsevier **291**, 437–461 (2006)
230. Khalil, H.K.: Nonlinear Systems, 2nd edn. Prentice Hall, Englewood Cliffs (1996)
231. Khorrami, F., Jain, S., Tzes, A.: Experimental results on adaptive nonlinear control and input preshaping for multi-link flexible manipulators. Automatica **31**(1), 83–97 (1995)
232. Kim, Y., Park, C., Joo, J., Jeong, S.: Extended Kalman filter for wireless LAN based indoor positioning. Decis. Support Syst., Elsevier **45**, 960–971 (2008)
233. Kim, M.J., Choi, Y., Chung, W.K.: Bringing nonlinear H_∞ optimality to robot controllers. IEEE Trans. Rob. **31**(3), 682–698 (2015)
234. Kobayashi, K., Cheok, K.C., Watanabe, K., Munekata, F.: Accurate differential global positioning system via fuzzy logic Kalman Filtering. IEEE Trans. Industr. Electron. **45**(3), 510–518 (1998)
235. Koch, C., Lynch, A., Chung, S.: Flatness-based automotive solenoid valve control. In: Proceedings of 6th IFAC Symposium on Nonlinear Control Systems (NOLCOS), pp. 1091–1096 (2004)
236. Koluda, P., Perlikowski, P., Czolezynski, K., Kapitaniak, T.: Synchronization configurations of two coupled double pendula. Commun. Nonlinear Sci. Numer. Simul., Elsevier **19**, 979–990 (2014)

237. Kopernick, B., Graichen, K.: Tranformation of output constraints in optimal control applied to a double-pendulum on a cart. In: NOLCOS 2013, 9th IFAC Symposium on Nonlinear Control Systems, Toulouse, France (2013)
238. Ku, C.C., Lee, K.Y.: Diagonal recurrent neural networks for dynamic systems control. IEEE Trans. Neural Netw. **6**(1), 144–156 (1995)
239. Kuchler, S., Preziger, C., Eberharter, J.K., Schneider, K., Sawodny, O.: Real-time estimation of a ship's attitude. In: 2011 American Control Conference, San Francisco, California, USA (2011)
240. Kuchler, S., Sawodny, O.: Nonlinear control of an active heave compensation system with time-delay. In: 2010 IEEE International Conference on Control Applications, Part of 2010 IEEE Multi-conference on Systems and Control, Yokohama, Japan (2010)
241. Kuchler, S., Mehi, T., Neipert, J., Schneider, K., Sawodhy, O.: Active control for an offshore crane using prediction of the vessel's motion. IEEE/ASME Trans. Mechatron. **16**(2), 297–309 (2010)
242. Kulcher, S., Eberharter, J.K., Langer, K., Schneider, K., Sawodny, O.: Heave motion estimation of a vessel using acceleration measurements. In: 18th IFAC World Congress, Milano, Italy (2011)
243. Kurylowicz, A., Jaworska, I., Tzafestas, S.G.: Robust stabilizing control : an overview. In: Tzafestas, S.G. (ed.) Applied Control - Current Trends and Modern Methodologies, pp. 289–324. Marcel Dekker, New York (1993)
244. La Hera, P., Freidovich, L., Shiriaev, A., Mettin, U.: New approach for swinging-up the Furuta pendulum: theory and experiments. Mechatronics, Elsevier **19**, 1240–1250 (2009)
245. Lai, X.Z., Pan, C.Z., Wu, M., Yang, S.X.: Unified control of n-link underactuated manipulator with single passive joint: a reduced order approach. Mech. Mach. Theory, Elsevier **56**, 170–185 (2012)
246. Lai, X.Z., She, J.H., Yang, S.X., Wu, M.: Comprehensive unified control strategy for underactuated two-link manipulators. IEEE Trans. Syst. Man Cybern. Part B Cybern. **39**(2), 389–398 (2009)
247. Lai, X.Z., Yang, S.X., Yu, M.: Comprehensive unified control strategy for underactuated two-link manipulators. IEEE Trans. Syst. Man Cybern. **39**(2), 389–398 (2009)
248. Lamiraux, F., Laumond, J.P.: Flatness and small-time controllability of multi-body mobile robots: application to motion planning. IEEE Trans. Autom. Control **45**(10), 1878–1881 (2000)
249. Lamiraux, F., Laumond, J.P., Van Geem, C., Boutonnet, D., Raust, G.: Trailer-truck trajectory optimization: the transportation of components for the Airbus A380. IEEE Robot. Autom. Mag. **12**(1), 14–21 (2005)
250. Lamiraux, F., Laumond, J.P., Van Geem, C., Boutonnet, D., Raust, G.: Trailer-truck trajectory optimization: the transportation of components for the Airbus A380. IEEE Robot. Autom. Mag. **12**(1), 14–21 (2005)
251. Lapierre, L., Saetanto, D.: Nonlinear path-following control of an AUV. Ocean Eng., Elsevier **34**, 1734–1744 (2007)
252. Lapierre, L., Soetanto, D., Pascoal, A.: Coordinated motion control of marine robots. In: IFAC Conference on Maneuvering and control of marine crafts, Girona, Spain (2003)
253. Lapierre, L.: Robust diving control of an AUV. Ocean Eng. Elsevier **36**, 92–104 (2009)
254. Laroche, B., Martin, P., Petit, N.: Commande par platitude: Equations différentielles ordinaires et aux derivées partielles. Ecole Nationale Supérieure des Techniques Avancées, Paris (2007)
255. Léchevin, N., Rabbath, C.A.: Sampled-data control of a class of nonlinear flat systems with application to unicycle trajectory tracking. ASME J. Dyn. Syst. Meas. Control Trans. ASME **128**(3), 722–728 (2006)
256. Lee, S.C., Ahn, H.S.: Sensorless torque estimation using Adaptive Kalman Filter and disturbance estimator. In: 2010 IEEE/ASME International Conference on Mechatronic and Embedded Systems and Applications, QingDao, China (2010)
257. Lee, M.H., Li, T.H.S.: Kinematics, dynamics and control design of 4WIS4WID mobile robots. IET Engineering, p. 11 (2015)

258. Lee, K.W., Singh, S.N.: Multi-input submarine control via L_2 adaptive feedback despite uncertainties. J. Syst. Control Eng., Sage Publications **228**(5), 330–347 (2014)
259. Lee, D.J.: Unscented information filtering for distributed estimation and multiple sensor fusion. In: AIAA Guidance, Navigation and Control Conference and Exhibit, Hawai, USA (2008)
260. Lee, D.J.: Nonlinear estimation and multiple sensor fusion using unscented information filtering. IEEE Signal Process. Lett. **15**, 861–864 (2008)
261. Lee, T.: Robust adaptive attitude tracking on SO(3) with an application to a quadrotor UAV. IEEE Trans. Control Syst. Technol. **2**(5), 1924–1930 (2012)
262. Lee, T.C., Tsai, C.Y., Song, K.T.: Fast parking control of mobile robots: a motion planning approach with experimental validation. IEEE Trans. Control Syst. Technol. **12**(5), 661–676 (2004)
263. Leland, R.P.: Adaptive control a MEMS gyroscope using Lyapunov methods. IEEE Trans. Control Syst. Technol. **14**(2), 278–283 (2006)
264. Lendek, Z., Berna, A., Guzman-Gimenez, J., Sala, A., García, P.: Application of Takagi-Sugeno observers for state estimation in a quadrotor. In: 2011 CDC-ECC, 50th IEEE Conference on Decision and Control and European Control Conference Orlando, FL, USA (2011)
265. Lerbet, J.: About the synchronization of MEMS. Nonlinear Anal., Elsevier **10**, 266–276 (2009)
266. Leung, A.Y., Guo, Z., Yang, H.X.: Residue harmonic balance analysis for the damped Duffing resonator driven by a a Van der Pol oscillator, Intl. J. Mech. Sci., Elsevier **67**, 59–65 (2012)
267. Lévine, J.: On necessary and sufficient conditions for differential flatness. Appl. Algebra Eng. Commun. Comput., Springer **22**(1), 47–90 (2011)
268. Lewis, F.L., Jagannathan, S., Yesildirek, A.: Neural Network Control of Robot Manipulators and Nonlinear Systems. Taylor and Francis, London (1999)
269. Li, M., Jia, Y., Matsuno, F.: Attenuating diagonal decoupling with robustness for velocity-varying 4WS vehicles. Control Eng. Pract., Elsevier **54**, 49–59 (2016)
270. Li, M., Jia, Y.: Decoupling and robust control of velocity-varying four-wheel-steering vehicle wirh uncertainties via solving attenuating diagonal decoupling problem. J. Frankl. Inst., Elsevier **354**, 105–122 (2017)
271. Li, P., Kadirkamanathan, V.: Particle filtering based likelihood ratio approach to fault diagnosis in nonlinear stochastic systems. IEEE Trans. Syst. Man Cybern. Part C: Appl. Rev. **31**, 337–343 (2001)
272. Li, J.H., Lee, P.M.: Design of an adaptive nonlinear controller for depth control of an autonomous underwater vehicle. Ocean Eng., Elsevier **32**, 2165–2181 (2005)
273. Li, B., Su, T.: Nonlinear heading control of an autonomous underwater vehicle with internal actuators. Ocean Eng., Elsevier **125**, 103–112 (2016)
274. Li, Y., Jiang, Y.: Real-time control of the robot manipulators by neural networks. Integr. Comput. Aided Eng. **2**(3), 241–248 (1995)
275. Li, J.H., Lee, P.M.: Design of an adaptive nonlinear controller for depth control of an autonomous underwater vehicle. Ocean Eng. Elsevier **32**, 2165–2181 (2005)
276. Li, W., Lin, P.X.: Robust adaptive tracking control of uncertain electrostatic microactuators with H-infinity performance. Mechatronics, Elsevier **19**, 591–597 (2009)
277. Li, H.X., Tong, S.: A hybrid adaptive fuzzy control for a class of nonlinear MIMO systems. IEEE Trans. Fuzzy Syst. **11**(1), 24–35 (2003)
278. Li, T.H.S., Chang, S.J., Chen, Y.X.: Implementation of human-like driving skills by autonomous fuzzy behavior control on an FPGA-based car-like mobile robot. IEEE Trans. Ind. Electron. **50**(5), 867–880 (2003)
279. Li, J.H., Lee, P.M., Jun, B.H., Lim, Y.K.: Point-to-point navigation of underactuated ships. Automatica, Elsevier **44**, 3201–3205 (2008)
280. Li, T.S., Tong, S.C., Feng, G.: A novel robust adaptive-fuzzy-tracking control for a class of nonlinear multi-input multi-output systems. IEEE Trans. Fuzzy Syst. **18**(1), 150–160 (2010)
281. Li, T.H.S., Yeh, Y.C., Wu, J.D., Hsiao, M.Y., Chen, C.Y.: Multifunctional intelligent autonomous parking controllers for carlike mobile robots. IEEE Trans. Ind. Electron. **57**(5), 1687–699 (2010)

282. Li, M., Jia, Y., Du, J.: LPV control with decoupling performance of 4WS vehicles under velocity-varying motion. IEEE Trans. Control Syst. Technol. **22**(5), 1708–1724 (2014)
283. Li, B., Du, H., Li, W., Zhang, Y.: Side-slip angle estimation based on lateral dynamics control for omni-directional vehicles with optimal steering angle and traction/brake torque distribution. Mechatronics, Elsevier **30**, 348–362 (2015)
284. Li, L., Lu, Y., Wang, R., Chen, J.: A three-dimensional dynamics control framework of vehicle lateral stability and rollover presentation via active breaking with MPC. IEEE Trans. Ind. Electron. **64**(4), 3389–3401 (2017)
285. Li, S., Wu, J., Guo, K., Zhu, W.L.: Nonlinear robust prediction control of hybrid active-passive heave compensation with extended disturbance observers. IEEE Trans. Ind. Electron. **64**(8), 6681–6694 (2017)
286. Lian, K.Y., Chiu, C.S., Liu, P.L.: Semi-decentralized adaptive fuzzy control for cooperative multirobot systems with H-infinity motion/internal force tracking performance. IEEE Trans. Syst. Man Cybern. Part B Cybern. **32**(3), 269–280 (2002)
287. Liceaga-Castro, E., van der Molen, G.M.: Submarine H_∞ depth control under wave disturbances. IEEE Trans. Control Syst. Tech. **3**(3), 338–346 (1995)
288. Liceaga-Castro, E., van der Molen, G.M.: Submarine H_∞ depth control under wave disturbances. IEEE Trans. Control Syst. Tech. **3**(3), 338–346 (1995)
289. Lin, D.T., Guo, W.P., Yi, J.G.: Composite sliding-mode fuzzy control for double-pendulum type overhead crane. In: Proceedings of the Fourth International Conference on Machine Learning and Cybernetics, Guangzhou, China (2005)
290. Lin, J., Lewis, F.L.: Improved measurement / estimation technique for flexible-link robot arm control. In: Proceedings of the 32nd Conference on Decision and Control, San Antonio Texas (1993)
291. Lin, J.M., Lin, M.C., Wang, H.P.: LEQG/LTR controller design with extended Kalman filter for sensorless brushless DC driver. Comput. Methods Appl. Mech. Eng., Elsevier **190**, 5481–5494 (2001)
292. Lin, C.M., Ting, A.B., Hsu, C.F., Chung, C.M.: Adaptive control for MIMO uncertain nonlinear systems using recurrent wavelet neural network. Int. J. Neural Syst. **21**(6) (2011)
293. Lin, S.C., Tsai, C.C., Huang, H.C.: Nonlinear adaptive sliding-mode control design for two-wheeled human transportation vehicle. In: Proceedings of the 2009 IEEE International Conference on Systems, Man and Cybernetics, San Antonio, Texas, USA (2009)
294. Lin, Y.J., Wang, W.: Adaptive fuzzy control for a class of uncertain non-affine nonlinear systems. Inf. Sci., Elsevier **177**, 3901–3917 (2007)
295. Lin, J., Lewis, F.L.: Fuzzy controller for flexible-link robot arm by reduced-order techniques. IEE Proc. Control Theory Appl. **149**(3), 177–187 (2002)
296. Liu, S., Davidson, A., Lin, Q.: Simulation studies on nonlinear dynamics and chaos in a MEMS cantilever control system. J. Micromech. Microeng., Institute of Physics Publishing **14**, 1064–1073 (2004)
297. Liu, Y., Guo, C., Zhou, R.: Robust feedback stabilization control of an underactuated surface vessel. In: IEEE WRI 2009 World Congress on Computer Science and Information Engineering, Los Angeles, California, USA (2009)
298. Liu, M., Zhang, S.: An LMI approach to design H_∞ controllers for discrete-time nonlinear systems based on unified models. Int. J. Neural Syst., World Scientific **18**(5), 443–452 (2008)
299. Liu, S.: Stable synchronization of two Furuta pendulums network based on the model of controlled Lagrangian. In: Proceedings of the 33rd Chinese Control Conference, Niajing, China (2014)
300. Liu, Y.C., Chopra, N.: Control of robotic manipulators under input/output communication delays: theory and experiments. IEEE Trans. Rob. **23**(3), 742–751 (2012)
301. Liu, Y., Zhu, Z.Q., Howe, D.: Instantaneous torque estimation in sensorless direct-torque-controlled brushless DC Motors. IEEE Trans. Ind. Appl. **42**(5), 1275–1283 (2006)
302. Lo, J.C., Kuo, Y.H.: Decoupled fuzzy sliding-mode control. IEEE Trans. Fuzzy Syst. **6**(3), 426–435 (1998)

303. Lu, W.C., Duan, L., Hsiao, F.B., Mora-Camino, F.: Differential flatness applied to vehicle trajectory tracking. In: Proceedings of the 27th Chinese Control Conference, 16–18 July 2008, Kunming, Yunnan, China (2008)
304. Lu, B., Feng, Y., Sun, N., Wang, X.: Antiswing control of offshore boom cranes with ship roll disturbances. IEEE Trans. Control Syst. Technol. 1–8 (2017)
305. Lublin, L., Athans, M.: An experimental comparison of and designs for interferometer testbed. In: Francis B., Tannenbaum A. (eds.) Lectures Notes in Control and Information Sciences: Feedback Control, Nonlinear Systems and Complexity, pp. 150–172. Springer (1995)
306. Lucet, E., Lenain, R., Girard, G.: Dynamic path tracking control of a vehicle on slippery terrain. Control Eng. Pract., Elsevier **42**, 60–73 (2016)
307. Lynch, K., Shiroma, N., Arai, H., Tanie, K.: Collision-free trajectory planning for a 3-DOF robot with a passive joint. Int. J. Robot. Res., Sage Publications **19**, 1171–1184 (2000)
308. Mahindrakar, A.D., Rao, S., Banavar, R.N.: Point-to-point control of a 2R planar horizontal underactuated manipulator. Mech. Mach. Theory, Elsevier **41**, 838–844 (2006)
309. Mahler, R.P.S.: Statistical Multisource-multitarget Information Fusion. Artech House Inc, Boston (2007)
310. Mahony, R., Hamel, T., Pflimlin, J.M.: Nonlinear complementary filters on the special orthogonal group. IEEE Trans. Autom. Control **53**(5), 1203–1218 (2008)
311. Makarenko, A., Durrany-Whyte, H.: Decentralized Bayesian algorithms for active sensor networks. Inf. Fusion, Elsevier **7**, 418–433 (2006)
312. Mammar, S., Glaser, S., Netto, M.: Vehicle lateral dynamics estimation using unknown input proportional-integral observers. In: American Control Conference (2006)
313. Man, W.S., Lin, J.S.: Nonlinear control design for a class of underactuated systems. In: 2010 IEEE International Conference on Control Applications, Proceedings of the 2010 IEEE Multi-Conference on Systems and Control, Yokohama, Japan (2010)
314. Man, W.S., Lin, J.S.: Nonlinear control design for a class of underactuated systems. In: 2010 IEEE International Conference on Control Applications, Proceedings of the 2010 IEEE Multi-conference on Systems and Control, Yokohama, Japan (2010)
315. Manyika, J., Durrant-Whyte, H.: Data Fusion and Sensor Management: A Decentralized Information Theoretic Approach. Prentice Hall, Englewood Cliffs (1994)
316. Marco, B., Cacciu, M., Lapierre, L., Gabriele, B.: Control of unmanned surface vehicles: experiments in vehicle following. In: IEEE Robotics and Automation Magazine, pp. 92–102 (2012)
317. Marino, R., Cinili, F.: Input-output decoupling control by measurement feedback in four-wheel-active-steering vehicles. In: IEEE CDC 2006, Proceedings of the 45th IEEE Conference on Decision and Control, San Diego, CA, USA (2006)
318. Marino, R.: Adaptive observers for single output nonlinear systems. IEEE Trans. Autom. Control **35**(9), 1054–1058 (1990)
319. Marino, R., Cinili, F.: Input-output decoupling control by measurement feedback in four-wheel-active-steering vehicles. IEEE Trans. Control Syst. Technol. **17**(5), 1163–1172 (2009)
320. Marino, R., Tomei, P.: Global asymptotic observers for nonlinear systems via filtered transformations. IEEE Trans. Autom. Control **37**(8), 1239–1245 (1992)
321. Marquez-Martinez, L.A., Moog, C.H.: Input-output feedback linearization of time-delay systems. IEEE Trans. Autom. Control **49**(5), 781–786 (2004)
322. Martin, P., Rouchon, P.: Systèmes plats: planification et suivi de trajectoires. Ecole des Mines de Paris, Journées X-UPS, Mai (1999)
323. Masoud, M.A., Masoud, A.A.: Motion planning in the presence of directional and regional avoidance constraints using nonlinear, anisotropic, harmonic potential fields: a physical metaphor. IEEE Trans. Syst. Man Cybern. - Part A **32**(6), 705–723 (2002)
324. Massar, M., Lot, R.: A virtual rider fir two-wheeled vehicles. In: 48th IEEE Conference on Decision and Control, IEEE CDC 2012, Athens, GA, USA (2012)
325. Massoud, Z., Nayfeh, A., Mook, D.: Cargo pendulation reduction of ship-mounted cranes. Nonlinear Dyn., Springer **35**(3), 299–311 (2004)

326. Mathew, N.J., Rao, K.K., Sivakumaran, N.: Swing-up and stabilization control of a rotary inverted pendulum. In: 10th IFAC Symposium on Dynamics and Control of Process Systems, Mumbai, India (2013)
327. Mathuswamy, J., Okandan, M., Jain, T., Gilletti, A.: Electrostatic microactuators for precise positioning of neural microelectrodes. IEEE Trans. Biomed. Eng. **52**(10), 1742–1755 (2005)
328. Matsushita, K., Murakami, T.: Nonholonomic equivalent disturbance-based backward motion control of a tractor-trailer with virtual steering. IEEE Trans. Ind. Electron. **55**(1), 280–287 (2008)
329. McGinnity, S., Irwin, G.: Nonlinear Kalman filtering using fuzzy local linear models. In: Proceedings of the American Control Conference, Albuquerque, New Mexico, pp. 3299–3300 (1997)
330. Medina Martinez, J.I., Sawat, U., Nakano, K.: Application of non-linear observer with simultaneous perturbation stochastic approximation method to single flexible-link SMC. In: SICE Annual Conference 2008, The University of Electro-Communications, Japan (2008)
331. Melo Linares, T., Onirama, J., Limaverde Filh, A., Cueller, W., Feitoza Fortaleza, E.L., Active heave compensator using Kalman Filter disturbance estimator. In: Proceedings of CBA 2016, 21st Brasilian Congress of Automation, Votoria, Brasil (2016)
332. Menhour, L., dAndrea-Novel, B., Boussard, C., Fliess, M., Mounier, H.: Algebraic nonlinear estimation and flatness-based lateral/longitudinal control for automotive vehicles. In: 14th International IEEE Conference in Intelligent Transportation Systems, Washington (2011)
333. Menhour, L., dAndréa-Novel, B., Fliess, M., Mounier, H.: Commande couplée longitudinale/latérale de véhicules par platitude et estimation algébrique, Manuscrit publié dans "7e Conférence Internationale Francophone d'Automatique, Grenoble, France (2012)
334. Menhour, L., d'Andre'a-Novel, B., Fliess, M., Mounier, H.: Coupled nonlinear vehicle control: flatness-based setting with algebraic estimation techniques, Control Eng. Pract., Elsevier **22**, 135–146 (2014)
335. Mercorelli, P., Lehmann, K., Liu, S.: Robust flatness based control of an electromagnetic linear actuator using adaptive PID controller. In: Proceedings of IEEE Decision and Control Conference, pp. 3790–3795 (2003)
336. Mestrom, R.M., Fey, R.H., Nijmeijer, H.: On phase feedback for nonlinear MEMS resonators. In: IEEE International Frequency Control Symposium, 2007 Joint with the 21st European Frequency and Time Forum, Geneva, Switzerland (2007)
337. Meurer, T., Zeitz, M.: A modal approach to flatness-based control of flexible structures. PAMM Proc. Appl. Math. Mech. **4**, 133–134 (2004)
338. Miandoab, E.M., Pishkenari, H.N., Youssefi-Koma, A., Tojaddodianfar, T.F.: Chaos prediction in MEMS-NEMS resonators, Int. J. Eng. Sci., Elsevier **82**, 74–83 (2014)
339. Miandoab, E.M., Youssefi-Koma, A., Pishkenari, H.N., Tojaddodianfar, T.F.: Study of nonlinear dynamics and chaos in MEMS/NEMS resonators. Commun. Nonlinear Sci. Numer. Simul., Elsevier **22**, 611–622 (2015)
340. Míguez, J.: Analysis of parallelizable resampling algorithms for particle filtering. Signal Process., Elsevier **87**, 3155–3174 (2007)
341. Miklosovic, R. Radke, A., Gao, Z.: Discrete implementation and generalization of the extended state observer. In: Proceedings of the Americal Control Conference, p. 2006. Minneapolis, Minnesota, USA (2006)
342. Mills, A., Wills, A., Ninness, B.: Nonlinear model predictive control of an inverted pendulum. In: 2009 American Control Conference, St. Louis, MO, USA (2009)
343. Möller, B., Deutscher, J., Grodde, S.: Continuous curvature trajectory design and feedforward control for parking a car. IEEE Trans. Control Syst. Technol. **15**(3), 541–553 (2007)
344. Morales, J., Martinez, J., Mandow, A., Garcia-Cereza, A.: Steering the low trailer as a virtual tractor for vehicles with passive on and off - axle hitches. IEEE Trans. Ind. Electron. **60**(12), 5721–5736 (2013)
345. Moreira, L., Fossen, T.I., Soares, G.G.: Path following control system for a tanker ship model. Ocean Eng., Elsevier **34**(14–15), 2074–2085 (2007)

346. Moreira, L., Soares Gueda, C.: H_2 and H_∞ design for diving and course control of an autonomous underwater vehicle in presence of waves. IEEE J. Oceanic Eng. **33**(2), 69–88 (2008)
347. Morena-Valenzuela, J., Aguilar-Avelar, C., Puga-Guzman, S., Santibanex, V.: Adaptive neural network control for the trajectory tracking of the Furuta pendulum. IEEE Trans. Cybern. **46**, 1–14 (2016)
348. Moriwaki, K., Tanaka, K.: Navigation control for electric vehicles using nonlinear state feedback H-infinity control. Nonlinear Anal., Elsevier **71**, 2920–2933 (2009)
349. Mounier, H., Rudolph, J.: Trajectory tracking for π-flat nonlinear dealy systems with a motor example. In: Isidori, A., Lamnabhi-Lagarrigue, F., Respondek, W. (eds.) Nonlinear Control in the Year 2000, vol. 1. Lecture Notes in Control and Information Sciences, vol. 258, pp. 339–352. Springer, Berlin (2001)
350. M'Sirdi, N.K., Jaballah, B., Rabhi, A., Messaoud, H., Naamane, A.: Differential estimators for state observers in vehicle dynamics: HOSM and ALIEN. In: 18th IFAC World Congress Milano, Italy (2011)
351. Mudgal, V., Kwong, W.A., Passino, K.M., Yurkovich, S.: Fuzzy learning control for a flexible-link robot. IEEE Trans. Fuzzy Syst. **3**(2), 199–210 (1995)
352. Mullhaupt, P., Shrinivasan, B., Bonvin, D.: Analysis of exclusively-kinetic two-link underactuated mechanical systems. Automatica, Elsevier **38**(9), 1565–1573 (2006)
353. Nagarkatti, S.P., Rahn, C.D., Dawson, D.M., Zergeroglou, E.: Observer-based modal control of flexible systems using distributed sensing. In: Proceedings of the 40th IEEE Conference on Decision and Control, Orlando, Florida, USA (2001)
354. Najdecka, A., Kapetaniak, T., Wierigroch, M.: Synchronous rotational motion of parametric pendulums. Elsevier, Int. J. Nonlinear Mech (2017)
355. Nakamura, Y., Ezak, H., Yuegang, T., Wooyan, C.: Design of steering mechanism and control of nonholonomic trailer systems. IEEE Trans. Robot. Autom. **17**(3), 967–974 (2001)
356. Narikiyoa, T., Sahashib, J., Misao, K.: Control of a class of underactuated mechanical systems. Nonlinear Anal. Hybrid Syst. Elsevier **2**, 231–241 (2008)
357. Neipert, J., Muhl, T., Huessig, B., Sawodny, O., Schneider, K.: A heave compensation approach for offshore cranes. In: 2008 American Control Conference, Seattle, Washington, USA (2008)
358. Nettleton, E., Durrant-Whyte, H., Sukkarieh, S.: A robust architecture for decentralized data fusion. In: ICAR03 11th International Conference on Advanced Robotics. Coimbra, Portugal (2003)
359. Ng, G.W.: Intelligent Systems - Fusion. Research Studies Press, Tracking and Control (2003)
360. Ngo, Q.H., Hong, K.S.: Sliding-mode antiswing control of an offshore container crane. IEEE/ASME Trans. Mechatron. **17**(2), 201–209 (2012)
361. Nguyen, T.D., Egeland, O.: Observer design for a flexible robot arm with a tip load. In: 2005 American Control Conference, Portland, Oregon, USA (2005)
362. Nguyen, V.B., Morris, A.S.: Genetic algorithm tuned fuzzy logic controller for a robot arm with two-link flexibility and two-joint elasticity. J. Intell. Robot. Syst., Springer **49**(1), 3–18 (2007)
363. Nilsen, U.D., Jensen, J.J.: A novel approach for navigational guidance of ships using onboard monitoring systems. Ocean Eng, Elsevier **38**, 444–455 (2011)
364. Nizard, A., Thilot, B., Lenain, R,, Mezouar, Y.: Nonlinear path tracking controller for bi-steerable vehicles in cluttered environments. In: 8th IFAC Symposium on Intelligent Autonomous Vehicles, IAV 2016, Leipzig, Germany (2016)
365. O' Connor, W.J.: IEEE Trans. Robot. Wave-based analysis and Control of Lump-Modeled Flexible Robots. **23**(1), 342–352 (2007)
366. Odhams, A., Roebock, R., Jujnovich, B., Cebon, D.: Active steering of a tractor semi-trailer. Proc. Inst. Mech. Eng. Part D J. Automob. Eng. **226**(7), 847–869 (2011)
367. Ohnishi, K.: Disturbance observation - cancellation technique. In: Wilamowski, B.M., Irwin, J.D. (eds.) Control and Mechatronics. CRC Press, Boca Raton (2010)

368. Oiuakad, H.M., Nayfeh, A.H., Chaira, S., Najar, F.: Nonlinear feedback controller of a microbeam resonator. J. Vib. Control, Sage Publications **21**(3m), 1680–1697 (2015)
369. Olfati-Saber, R., Distributed Kalman filter with embedded consensus filters. In: Proceedings of 44th IEEE Conference on Decision and Control, pp. 8179–8184. Seville, Spain (2005)
370. Olfati-Saber, R.: Distributed Kalman filtering and sensor fusion in sensor networks. Lecture Notes in Control and Information Sciences **331**, 157–167 (2006)
371. Oriolo, G., De Luca, A., Vendittelli, M.: WMR control via dynamic feedback linearization: design, implementation and experimental validation. IEEE Trans. Control Syst. Technol. **10**, 835–852 (2002)
372. Ortega, M.G., Vargas, M., Vivas, C., Rubio, F.R.: Robustness improvement of a nonlinear H_∞ controller for robot manipulators via saturation functions. J. Robot. Syst. **22**(8), 421–437 (2005)
373. Ovalle, D.M., García, J., Periago, F.: Analysis and numerical simulation of a nonlinear mathematical model for testing the manoeuvrability capabilities of a submarine. Nonlinear Anal. Real World Appl. **12**(3), 1654–1669 (2011)
374. Pagello, E.: D' Angelo, A., Menegatti, E.: Cooperation issues and distributed sensing for multi-robot systems. Proc. IEEE **94**(7), 1370–1383 (2006)
375. Pan, C.Z., Lai, X.Z., Yang, S.X., Wu, M.: An efficient neural network approach to tracking control of an autonomous surface vehicle with unknown dynamics. Expert Syst. Appl. **40**, 1629–1635 (2013)
376. Pandey, M., Rand, R., Zehander, A.T.: Frequency locking in forced Mathieu - Van der Pol - Duffing system. Nonlinear Dyn., Springer **54**, 7–12 (2008)
377. Park, J., Chung, W.: Design of a robust H_∞ PID control for industrial manipulators. Trans. ASME J. Dyn. Syst. Meas Control **122**(4), 801–812 (2000)
378. Park, M.S., Chwa, D.: Swing-up stabilization control of inverted pendulum systems with coupled sliding-mode contorl method. IEEE Trans. Ind. Electron. **56**(9), 3541–3555 (2009)
379. Park, M.D., Chwwa, D.: Swing-up and stabilization control of inverted pendulum systems via coupled sliding-mode control method. IEEE Trans. Ind. Electron. **56**(9), 3541–3555 (2009)
380. Pena-Ramirez, J., Cuestra-Garcia, R., Alvarez, J.: Synchronization of two inverted pendula via dynamic coupling. In: 2016 Australian Control Conference, Newcastle, Australia (2016)
381. Peng, S.T.: On one approach to constraining the combined wheel slip in the autonomous control of a 4WS 4WD vehicle. IEEE Trans. Control Syst. Technol. **15**(1), 168–175 (2007)
382. Perera, L.K., Soares, C.G.: Lyapunov and Hurwitz based controls for input-output linearization applied to nonlinear vessel steering. Ocean Eng., Elsevier **66**, 58–68 (2013)
383. Perez Polo, M.F. Perez Molina, M.: Steady-state self-oscillations and chaotic behavior of a controlled electromechanical deviceby using the first 'Lyapunov value and the Melnikov theory. J. Sound Vib., Elsevier **333**, 1163–1181 (2014)
384. Perez Polo, M.F., Perez Molina, M., Gil Chico, J.: Chaotic dynamics and control for micro-electromechanical systems of massive storage with harmonic base excitation. Chaos, Solitons Fractals, Elsevier **39**, 1356–1370 (2009)
385. Perez, T., Steinmann, P.: Modelling and performance of an active heave compensation for offshore operations. In: 10th IFAC Conference on Control Applications of Marine Systems, Trondheim, Norway (2016)
386. Petersen, K.Y., Egeland, O.: Time-varying exponential stabilization of the position and attitude of an underactuated autonomous underwater vehicle. IEEE Trans. Autom. Control **44**(1), 112–115 (1999)
387. Petkovic, D., Pavlovic, N.D., Cozbasic, Z., Pavlovic, N.T.: Adaptive neuro fuzzy estimation of underactuated robotic gripper contact forces. Expert Syst. Appl., Elsevier **40**, 281–286 (2013)
388. Pinheiro Gomes, S.C., Motea Moraes, C.E., Lil Drews, P., Garcia Moreira, T.: Underwater vehicle dynamic modelling. In: Proceedings of COBEM 2005 18th International Congress of Mechanical Engineering, Ouro Preto, Brazil (2005)
389. Piyabongkarn, D., Sun, Y., Rajamani, R., Sezen, A., Nelson, B.J.: Travel range extension of a MEMS electrostatic microactuator. IEEE Trans. Control Syst. Technol. **13**(1), 138–145 (2005)

390. Portlui, R., Singh, A.K.: Path tracking control of an autonomous 4WS4WD electric vehicle using its using its natural feedback loops. IEEE Trans. Control Syst. Technol. **21**(5), 2053–2062 (2015)
391. Post, B.K., Book, W.J.: A robust nonlinear observation strategy for the control of flexible manipulators. In: IEEE ICRA 2011, International Conference on Robotics and Automation. Shanghai, China (2011)
392. Pozdersk, D., Kozlowski, K.: Trajectory tracking of underactuated skid-steering robot. In: 2008 American Control Conference, Seattle Washington, USA (2008)
393. Pozzi, M., Malvezzi, M., Prattichizzo, D.: On grasp quality measures: grasp robustness and contact force distribution in underactuated and compliant robotic hands. IEEE Robot. Autom. Lett. **2**(1), 329–336 (2017)
394. Pradalier, C., Usher, K.: Robust trajectory tracking for a reversing tractor-trailer. J. Field Robot., Wiley **25**(6–7), 378–399 (2008)
395. Purwar, S., Kar, I.N., Jha, A.N.: Adaptive control of robot manipulators using fuzzy logic systems under actuator constraints. Fuzzy Sets Syst. **152**, 651–664 (2004)
396. Puscasu, G., Codres, B.: Nonlinear system identification and control based on modular neural networks. Int. J. Neural Syst., World Scientific **21**(4), 319–334 (2011)
397. Pyrkin, A.A., Bobtsov, A.A.: Output control for nonlinear system with time-varying delay and stability analysis. In: 50th IEEE Conference on Decision and Control and European Control Conference, IEEE CDC- ECC 2011, Orlando, Florida (2011)
398. Qi, X.: Adaptive coordinated tracking control of multiple autonomous underwater vehicles. Ocean Eng., Elsevier **91**, 84–90 (2014)
399. Qi, R., Tao, G., Tan, C., Yao, X.: Adaptive control of discrete-time state-space TS fuzzy systems with general relative degree. Fuzzy Sets Syst. Elsevier **217**, 2240 (2013)
400. Quen, W., Liu, Y., Zhang, Z., Li, X., Liu, C.: Scale model test of a semi-active heave compensation system for deep-sea testbed ROVs. Ocena Eng., Elsevier **126**, 353–360 (2016)
401. Raffo, G.V., Ortega, M.G., Rubio, F.R.: MPC with nonlinear H_∞ control for path tracking of a quad-rotor helicopter. In: Proceedings of the 17th World Congress The International Federation of Automatic Control Seoul, Korea, 6–11 July 2008
402. Raffo, G.V., Ortega, M.G., Rubio, F.R.: Nonlinear H-infinity controller for the quad-rotor helicopter with input coupling. In: 18th World Congress of the IFAC, 2011, Milan, Italy (2011)
403. Raffo, G.V., Ortega, M.G., Rubio, F.R.: An integral predictive/nonlinear H_∞ control structure for a quadratic helicopter. Automatica, Elsevier **46**(1), 29–39 (2010)
404. Raffo, G.V., Ortega, M.G., Rubio, F.R.: Path tracking of a UAV via an underactuated H-infinity control strategy. Eur. J. Control Elsevier **17**, 194–213 (2011)
405. Ramirez-Neria, M., Sira-Ramirez, H., Garrido-Moctezuma, R., Luviano-Suarez, A.: On the linear active disturbance rejection control of the furuta pendulum, In: IEEE ACC 2014, American Control Conference, Portland, Oregon, USA (2014)
406. Ramirez-Neria, M., Sira-Ramirez, H., Garrido-Moctezuma, R., Luviano-Juarez, A.: Linear active disturbance rejection control of underactuated systems: the case of the Furuta pendulum. ISA Trans. **53**, 920–928 (2014)
407. Randrianandrasana, M., Wei, X., Lowe, D.: A preliminary study into emergent behaviours in a lattice of interacting nonlinear resonators and oscillators. Commun. Nonlinear Sci. Numer. Simul., Elsevier **16**, 2945–2956 (2011)
408. Randrianandrasana, M., Wei, X., Lowe, D.: Collective behavior in a square lattice of driven Duffing resonators coupled to Van der Pol oscillators. In: 2010 IEEE 10th International Conference on Computer and Information Technology (CIT), Bradford, UK (2010)
409. Randrianandrasana, M., Wei, X., Lowe, D.: Collective behaviorn a square lattice of driven Duffing resonators coupled to Van der Pol oscillators. In: 2010 IEEE 10th International Conference on Computer and Information Technology (CIT). Bradford, UK (2010)
410. Ravichandran, M., Mahindrakar, A.D.: Robust stabilization of a class of underactuated mechanical systems, using time-scaling and Lyapunov redesign. IEEE Trans. Ind. Electron. **58**(9), 4299–4313 (2011)

411. Refsnes, J.B., Sorensen, A.J., Petersen, K.Y.: Model-based output feedback control of slender-body underactuated AUVs: theory and experiments. IEEE Trans. Control Syst. Technol. **16**(5), 930–946 (2008)
412. Renno, J.M.: Inverse dynamics-based tuning of a fuzzy logic controller for a single-link flexible manipulator. J. Vib. Control, Sage Publications **13**(12), 1741–1759 (2007)
413. Ri, S.H., Huang, J., Wang, Y., Kim, M.H., An, S.: Terminal sliding mode control of mobile wheeled inverted pendulum system with nonlinear disturbance observer. Math. Probl. Eng. **2014**, 1–8 (2014)
414. Rigatos, G., Al-Khazraji, A.: Flatness-based adaptive fuzzy control for MIMO nonlinear dynamical systems. In: Nonlinear Estimation and Applications to Industrial Systems Control, Nova Publications (2011)
415. Rigatos, G.G., Flatness-based adaptive fuzzy control for nonlinear dynamical systems. In: AIM 2011, IEEE/ASME, International Conference on Advanced Intelligent Mechatronics, Budapest, Hungary (2011)
416. Rigatos, G., Raffo, G.: Input-output linearizing control of the underactuated hovercraft using the derivative-free nonlinear Kalman filter. J. Unmanned Syst., World Scientific **3**(2), 1–15 (2015)
417. Rigatos, G., Siano, P., Cecati, C.: A new nonlinear H-infinity feedback control approach for three-phase voltage source converters. In: Electric Power Components and Systems, Taylor and Francis (2015)
418. Rigatos, G., Siano, P., Cecati, C.: An H-infinity feedback control approach for three-phase voltage source converters. In: IECON 2014–40th Annual Conference of the IEEE 1Industrial Electronics Society. Dallas, TX, 1227–1232 (2014)
419. Rigatos, G., Siano, P., Ingention, G.: Controller design for AGVs and Kalman filter-based compensation of disturbance forces and torques. J. Intell. Ind. Syst., Springer **2**(3), 197–216 (2016)
420. Rigatos, G., Siano, P., Raffo, G.: An H-infinity nonlinear control approach for multi-DOF robotic manipulators, IFAC MIM, 2016. In: 8th IFAC Conference on Manufacturing, Modelling, Management and Control. Troyes, France (2016)
421. Rigatos, G., Siano, P., Zervos, N., Cecati, C.: Derivative-free nonlinear Kalman Filtering for control of three-phase voltage source converters. In: IEEE IECON 2013, 39th IEEE Conference on Industrial Electronics, Vienna, Austria (2013)
422. Rigatos, G., Siano, P., Zervos, N.: A nonlinear H-infinity control approach for autonomous navigation of under actuated vessels. In: 16th International Conference on Control, Automation and Systems. Gyeongju, Korea (2016)
423. Rigatos, G., Siano, P., Zervos, N.: A nonlinear H-infinity control approach for autonomous navigation of underactuated vessels. In: 16th International Conference on Control, Automation and Systems, Gyeongju, Korea (2016)
424. Rigatos, G., Siano, P., Zervos, N.: PMSG sensorless control with the use of the Derivative-free nonlinear Kalman filter. In: IEEE ICCEP 2013, IEEE International Conference on Clean Electrical Power, Alghero, Sardinia Italy (2013)
425. Rigatos, G., Siano, P.: An H-infinity feedback control approach to autonomous robot navigation, In: IECON 2014–40th Annual Conference of the IEEE Industrial Electronics Society, pp. 2689–2694. TX, Dallas (2014)
426. Rigatos, G., Siano, P.: Control of quadrotors with the use of the Derivative-free nonlinear Kalman Filter. J. Intell. Ind. Syst. **1**(3) (2015)
427. Rigatos, G., Siano, P.: Control of underactuated robotic systems with the use of the Derivative-free nonlinear Kalman filter. In: ICNAAM 2013, 11th International Conference on numerical analysis and applied mathematics, AIP Conference Proceedings, vol. 1558, pp. 2551–2556 (2013)
428. Rigatos, G., Siano, P.: Distributed nonlinear filtering and sensorless control under disturbances and model uncertainties. In: MASCOT 2011. IMACS Workshop on Scientific Computation, Italian Institute for Calculus Applications, Roma, Italy (2011)

429. Rigatos, G., Siano, P.: Flatness-based adaptive fuzzy control of autonomous submarines. J. Intell. Ind. Syst., Springer **1**(3), 187–200 (2015)
430. Rigatos, G., Siano, P.: Fuzzy Kalman Filter validation using the local statistical approach. J. Intell. Ind. Syst., Springer **1**(1), 15–28 (2015)
431. Rigatos, G.G., Tzafestas, S.G.: Extended Kalman filtering for fuzzy modelling and multi-sensor fusion. Math. Comp. Model. Dyn. Syst., Taylor and Francis **13**, 251–266 (2007)
432. Rigatos, G., Zhang, Q.: Fuzzy model validation using the local statistical approach. In: Publication Interne IRISA No 1417, Rennes, France (2001)
433. Rigatos, G.G.: A derivative-free Kalman Filtering approach for sensorless control of nonlinear systems. In: IEEE ISIE 2010, IEEE International Symposium on Industrial Electronics, Bari, Italy (2010)
434. Rigatos, G.: A differential flatness theory approach to adaptive fuzzy control of chaotic dynamical systems. In: IEEE SSCI 2014, Orlando, Florida, USA (2014)
435. Rigatos, G.G.: Adaptive fuzzy control for field-oriented induction motor drives. Neural Comput. Appl., Springer **21**(1), 9–23 (2012)
436. Rigatos, G.G.: Adaptive fuzzy control of DC motors using state and output feedback. Electr. Power Syst. Res., Elsevier **79**(11), 1579–1592 (2009)
437. Rigatos, G.G.: Adaptive fuzzy control of MIMO dynamical systems using differential flatness theory. In: IEEE ISIE 2012, 21st International Symposium on Industrial Electronics. Hangzhou, China (2012)
438. Rigatos, G.G.: Distributed filtering over sensor networks for autonomous navigation of UAVs. In: Intelligent Service Robotics. Springer, Berlin (2012)
439. Rigatos, G.G.: Extended Kalman and particle filtering for sensor fusion in motion control of mobile robots. Math. Comput. Simul., Elsevier **81**(3), 590–607 (2010)
440. Rigatos, G.G.: Kalman Filter-based sliding-mode control of flexible-link robots. In: IFAC CESCIT 2012, 1st Conference on Embedded Systems, Computational Intelligence and Telematics in Control. Wuerzburg, Germany (2012)
441. Rigatos, G.G.: Model-based and model-free control of flexible-link robots: a comparison between representative methods. Appl. Math. Model., Elsevier **33**, 3906–3925 (2008)
442. Rigatos, G.G.: Model-free control of flexible-link robots. In: IC-SCCE 2006, 2nd International Conference From Scientific Computing to Computational Engineering, Athens, Greece (2006)
443. Rigatos, G.G.: Nonlinear Kalman filters and particle filters for integrated navigation of unmanned aerial vehicles. Robot. Auton. Syst., Elsevier **60**, 978–995 (2012)
444. Rigatos, G.G.: Sigma-point Kalman filters and particle filters for integrated navigation of unmanned aerial vehicles. In: International Workshop on Robotics for Risky Interventions and Environmental Surveillance RISE 2009. Brussels, Belgium (2009)
445. Rigatos, G.G.: Particle Filtering for state estimation in industrial robotic systems. IMeche J. Syst. Control Eng. **222**(6), 437–455 (2008)
446. Rigatos, G.G.: Coordinated motion of autonomous vehicles with the use of a distributed gradient algorithm. J. Appl. Math. Comput. Elsevier **199**(2), 494–503 (2008)
447. Rigatos, G.G.: Adaptive fuzzy control with output feedback for H_∞ tracking of SISO nonlinear systems. Int. J. Neural Syst. World Scientific **18**(4), 1–16 (2008)
448. Rigatos, G.G.: Distributed gradient and particle swarm optimization for multi-robot motion planning. Robotica Cambridge University Press **26**(3), 357–370 (2008)
449. Rigatos, G.G.: Particle filtering for state estimation in nonlinear industrial systems. IEEE Trans. Instrum. Meas. **58**(11), 3885–3901 (2009)
450. Rigatos, G.G.: Modelling and Control for Intelligent Industrial Systems: Adaptive Algorithms in Robotcs and Industrial Engineering. Springer, Berlin (2011)
451. Rigatos, G.G.: A derivative-free Kalman Filtering approach to state estimation-based control of nonlinear dynamical systems. IEEE Trans. Industr. Electron. **59**(10), 3987–3997 (2012)
452. Rigatos, G.: Advanced Models of Neural Networks: Nonlinear Dynamics and Stochasticity in Biological Neurons. Springer, Berlin (2013)
453. Rigatos, G.G.: Sensor fusion-based dynamic positioning of ships using extended kalman and particle filtering. Robotica Camb. Univ. Press **31**(3), 389–403 (2013)

454. Rigatos, G.: A differential flatness theory approach to observer-based adaptive fuzzy control of MIMO nonlinear dynamical systems. Nonlinear Dyn. Springer **76**(2), 1335–1354 (2014)
455. Rigatos, G.G.: Robust control of valves in ship diesel engines with the use of the Derivative-free nonlinear Kalman Filter. Sage Publications, IMeche J. Syst. Control Eng (2014)
456. Rigatos, G.: A differential flatness theory approach to adaptive fuzzy control of chaotic dynamical systems, IEEE SSCI 2014. Orlando, Florida, USA (2014)
457. Rigatos, G.: Nonlinear Control and Filtering Using Differential Flatness Approaches: Applications to Electromechanical Systems. Springer, Berlin (2015)
458. Rigatos, G.: Control and disturbances compensation in underactuated robotic systems using the derivative-free nonlinear Kalman filter. Cambridge University Press, Robotica (2015)
459. Rigatos, G.: Intelligent Renewable Energy Systems: Modelling and Control. Springer, Berlin (2017)
460. Rigatos, G.: State-Space Appproaches for Modelling and Control in Financial Engineering: Systems Theory and Machine Learning Methods. Springer, Berlin (2017)
461. Rigatos, G., Siano, P.: A new nonlinear h-infinity feedback control approach to the problem of autonomous Robot navigation. J. Intel. Ind. Syst. Springer. **1**(3), 179–186 (2015)
462. Rigatos, G.G., Tzafestas, S.G.: Adaptive fuzzy control for the ship steering problem. J. Mechatron. Elsevier **16**(6), 479–489 (2006)
463. Rigatos, G., Zhang, Q.: Fuzzy model validation using the local statistical approach. Fuzzy Sets Syst. Elsevier **60**(7), 882–904 (2009)
464. Rigatos, G.G., Siano, P., Piccolo, A.: A neural network-based approach for early detection of cascading events in electric power systems. IET J. Gener. Transm. Distrib. **3**(7), 650–665 (2009)
465. Rigatos, G., Siano, P., Zervos, N.: Sensorless Control of distributed power generators with the derivative-free nonlinear Kalman Filter. IEEE Trans. Ind. Electron. **61**(11), 6369–6382 (2014)
466. Rigatos, G., Siano, P., Wira, P., Profumo, F.: Nonlinear H-infinity feedback control for asynchronous motors of electric trains. J. Intel. Ind. Syst. Springer **1**(2), 85–98 (2015)
467. Rigatos, G., Siano, P., Zervos, N., Cecati, C.: Control and disturbances compensation for doubly fed induction generators using the derivative-free nonlinear Kalman Filter. IEEE Trans. Power Electron. **30**(10), 5532–5547 (2015)
468. Rigatos, G., Zervos, N., Melkikh, A.: A flatness-based control approach to drug infusion for cardiac function regulation. IET Syst. Biol. **11**(1), 8–18 (2017)
469. Ritzen, P., Roenbroek, E., De Wouw, N., Jiang, J.P., Nijmeijer, H.: Trailer steering control of a tractor-trailer robot. IEEE Trans. Control Syst. Technol. **24**(4), 1240–1252 (2016)
470. Rosencrantz, M., Gordon, G., Thrun, S.: Decentralized data fusion with distributed particle filtering. In: Proceedings of the Conference of Uncertainty in AI (UAI), Acapulco, Mexico (2003)
471. Rouchon, P., Fliess, M., Lévine, J., Martin, P.: Flatness, motion planning and trailer systems. In: Proceedings of the 32nd IEEE Conference on Decision and Control, San Antonio, Texas (1993)
472. Rouchon, P.: Flatness-based control of oscillators. J. Appl. Math. Mech. J. Wiley **85**(6), 411–421 (2005)
473. Roy, B., Asad, H.: Nonlinear feedback control of a gravity assisted underactuated manipulator with application to aircraft assembly. IEEE Trans. Rob. **25**(5), 1125–1133 (2009)
474. Rubio, J.J.: Adaptive least square control in discrete time of robotic arms. Soft Comput. (2014). https://doi.org/10.1007/s00500-014-1300-2
475. Rubio, J.J., Zamudio, Z., Pacheco, J., Mujica-Vargas, D.: Proportional derivative control with inverse dead-zone for pendulum systems. Math. Probl. Eng. **2013**, 1–9 (2013)
476. Rudolph, J.: Flatness Based Control of Distributed Parameter Systems. Shaker Verlag, Aachen, Examples and Computer Exercises from Various Technological Domains (2003)
477. Ruiz, A.R.J., Granja, F.S.: A short-range ship navigation system based on Ladar imaging and target tracking for improved safety and efficiency. IEEE Trans. Intell. Transp. Syst. **10**(1), 186–197 (2009)

478. Russel, H., Gerdes, J.: Design of variable vehicle holding characteristics using four-wheel steer-by-wire. IEEE Trans. Control Syst. Technol. **24**(5), 1529–1540 (2016)
479. Saccon, A., Hauser, J., Beghi, A.: A virtual rider for motorcycles maneuver regulation of a multi-body vehicle model. IEEE Trans. Control Syst. Technol. **21**(2), 332–346 (2013)
480. Safarian, M., Fahimi, F.: Control of helicopter's formation using non-iterative nonlinear model predictice approach. In: 2008 American Control Conference, Seattle, Washington, USA (2008)
481. Saidbakhih, D., Zhang, Y., Yi, J.: Stability analysis of human rider: balance control of stationary bicycles. In: IEEE ACC 2012, 2012 IEEE American Control Conference, Montreal, Canada (2012)
482. Saleh, M.H., Aldvidyan, K.M., Tatlicioglu, E., Dawson, D.M.: Robust backstepping nonlinear control for parallel-plate micro electrostatic actuators. In: Proceedings of the 49th IEEE Conference on Decision and Control, Atlanta, Georgia, USA, (2010)
483. Salgado, I., Kamal, S., Bandyopadhyay, B., Chairez, I., Fridman, L.: Control of discrete time systems based on recurrent Super-Twisting-like algorithm. ISA Trans., Elsevier **64**, 47–55 (2016)
484. Salvucci, V., Kimura, Y., Sehoon, O., Koseki, T., Hori, Y.: Comparing approaches for actuator redundancy resolution in biarticularly-actuated robot arms. IEEE Trans. Mechatron. **19**(2), 765–776 (2014)
485. Sanchez, B., Ordaz, P., Garcia-Barrientos, A., Vera, E.: Nonlinear suboptimal control for a class of underactuated mechanical systems. In: 12th IEEE International Conference on Electrical Engineering, Computing Science and Automatic Control, Mexico City, Mexico (2015)
486. Sanchez-Solano, S., Cabrera, A.J., Baturone, I., Moreno-Velo, F.J., Brox, M.: FPGA implementation of embedded fuzzy controllers for robotic applications. IEEE Trans. Ind. Electron. **54**(4), 1937–1945 (2007)
487. Sandler, M., Wahl, A., Zimmermann, R., Faul, M., Kabatek, U., Gilles, E.D.: Autonomous guidance of ships on waterways. Robot. Auton. Syst., Elsevier **18**, 327–335 (1996)
488. Sanfilippo, F., Hatfield, H., Zhang, H.: A wave simulator and active heave compensation framework for demanding offshore crane operations. In: IEEE CCECE 2015, 28th Canadian Conference on Electrical and Computer Engineering, Halifax, Canada (2015)
489. Sangwan, V., Koebler, H., Agrawal, S.: Differentially flat design of underactuated planar robot: experimental results. In: 2008 International Conference on Robotics and Automation, Pasadena, California, USA (2008)
490. Sanz, A., Etxebarria, V.: Experimental control of a 2-DOF flexible robot manipulator by optimal and sliding methods. J. Intell. Robot. Syst., Springer **46**, 95–110 (2000)
491. Sanz, A., Etxebarria, V.: Experimental control of a single-link flexible robot arm using energy shaping. Int. J. Syst. Sci., Taylor and Francis **38**(1), 61–71 (2007)
492. Särrkä, S.: On unscented Kalman filtering for state estimation of continuous-time nonlinear systems. IEEE Trans. Autom. Control **52**(9), 1631–1641 (2007)
493. Schön, T.B., Törnqvist, D., Gustafsson, F.: Fast particle filters for multi-rate sensors. In: EUSIPCO 2007 Conference, Proceedings of the 15th European Signal Processing Conference, Poznan, Poland (2007)
494. Seguritan, A., Rotuno, M.: Torque pulsation compensation for a DC motor using an extended Kalman filter approach. In: Proceedings of the 41sl IEEE Conference on Decision and Control Las Vegas, Nevada USA (2002)
495. Sekhavat, S., Rouchon, P., Hermosillo, J.: Computing the flat outputs of engel differential systems: the case study of the bi-steerable car. In: American Control Conference (2001)
496. Selaim, A., Towfighiar, S., Delande, E., Abdel-Rahman, E., Happler, G.: Dynamics of a closed-loop controller MEMS resonator. Springer, Nonlinear Dynamics (2011)
497. Sepulchre, R., Paley, D.A., Leonard, N.E.: Stabilization of planar collective motion: all to all communication. IEEE Trans. Autom. Control **52**(5), 811–824 (2007)
498. Serrano, M.E., Scaglia, G.J.E., Godoy, S.A., Mut, V., Ortiz, O.A.: Trajectory tracking of underactuated surface vessels: a linear algebra approach. IEEE Trans. Control Syst. Technol. **22**(3), 1103–1111 (2014)

499. Shang, W., Cong, S.: Robust nonlinear control of a planar 2-DOF parallel manipulator with redundant actuation. Robot. Comput. Integr. Manuf. Elsevier **30**, 597–804 (2014)
500. Sharkar, M., Nandy, S., Vadali, S., Roy, S., Shome, S.: Modelling and simulation of a robust energy efficient AUV controller. Math. Comput. Simul., Elsevier **121**, 34–47 (2016)
501. Shcheglov, K., Jiang, X., Toch, R., Chang, Z., Yang, E.H.: Hybrid linear microactuators and their control models for mirror shape correction. J. Micro-Nano Mechatron., Springer **4**, 159–167 (2008)
502. Shem, J., Zhang, A., Lai, X., Wu, M.: Global stabilization of 2-DOF underactuated mechanical systems: an equivalent input-disturbance approach. Nonlinear Dyn., Springer **69**, 495–509 (2012)
503. Shi, L.Z., Trabia, M.B.: Design and tuning of importance-based fuzzy logic controller for a flexible-link manipulator. J. Intell. Fuzzy Syst., IOS press **17**(3), 313–323 (2006)
504. Shih, M.C., Wang, T.Y.: Active control of electro-rheological fluid embedded pneumatic vibration isolator. Integr. Comput. Aided Eng. **15**(3), 267–276 (2008)
505. Shimizu, Y., Ohtsuka, T., Diehl, M.: Nonlinear receding horizon control of an underactuated hovercraft with a multiple-shooting-based algorithm. In: Proceedings of the 2006 IEEE International Conference on Control Applications, Munich, Germany (2006)
506. Shiriaev, A., Freidovich, L., Robertsson, A., Johansson, R., Sandberg, A.: Virtual-holonomic-constraints-based design of stable oscillations of furuta pendulum: theory and experiments. IEEE Trans. Rob. **23**(4), 827–832 (2007)
507. Shrinivashan, P., Gallash, C.O., Kraft, M.: Three-dimensional electrostatic actuators for tunable optical micro-cavities. Sens. Actuators A phys. **161**, 191–198 (2010)
508. Shue, H.S., Huang, J.: Design of a high-performance automation steering controller for bus revenue service based on how drivers steer. IEEE Trans. Rob. **30**(5), 1137–1147 (2014)
509. Siciliano, B., Villani, L.: An inverse kinematics algorithm for interaction control of a flexible arm with a compliant surface. Control Eng. Pract., Elsevier **9**, 191–198 (2001)
510. Sienel, W.: Estimation of the tire cornering stiffness and its application to active car steering. In: Proceedings of the 36th Conference on Decision & Control, San Diego, California USA (1997)
511. Simon, D.: A game theory approach to constrained minimax state estimation. IEEE Trans. Signal Proces. **54**(2), 405–412 (2006)
512. Sinha, A., Ghose, D.: Generalization of linear cyclic pursuit with application to rendezvous of multiple autonomous agents. IEEE Trans. Autom. Control **51**(11), 1819–1824 (2006)
513. Siqueira, A., Terra, M.: Nonlinear H-infinity controllers for underactuated cooperative manipulators. In: IFAC 16th Triennial World Congress, Czech Republic, Prague (2005)
514. Siqueira, A., Terra, M.: Nonlinear H-infinity controllers for underactuated cooperative manipulators. Robotica, Cambridge University Press **25**(4), 425–432 (2007)
515. Siqueiraa, A., Terra, M.: Neural network-based H-infinity control for fully actuated and underactuated cooperative manipulators. Control Eng. Pract., Elsevier **17**(3), 418425 (2009)
516. Sira-Ramirez, H., Aguilar-Ibanez, C.: On the control of the hovercraft system. Dyn. Control, Springer **10**, 151–163 (2000)
517. Sira-Ramirez, H., Ibanez, C.A.: the control of the hovercraft system: a flatness based approach. In: Proceedings of the 2000 IEEE International Conference on Control Applications, Anchorage, Alaska, USA (2000)
518. Sira-Ramirez, H.: Dynamic second-order sliding-mode control of the hovercraft vessel. IEEE Trans. Control Syst. Tech. **10**(6), 860–865 (2002)
519. Sira-Ramirez, H., Agrawal, S.: Differentially Flat Systems. Marcel Dekker, New York (2004)
520. Siriaev, A., Perman, J.W., Canudas-de-Wit, C.: Constructive tool for orbital stabilization of underactuated nonlinear systems: virtual constraints approach. IEEE Trans. Autom. Control **50**(8), 1166–1176 (2005)
521. Sivaramakrishnan, S.: Simultaneous identification of tire cornering stiffnesses and vehicle center of gravity. In: 2008 American Control Conference, Seattle, Washington, USA (2008)
522. Soltun, R.A., Ashrafiuon, H., Muske, K.R.: ODE-based obstacle avoidance and trajectory planning for unmanned surface vessels. Robotica **29**, 691–703 (2010)

523. Song, P., Zong, C., Tomizuka, M.: Combined longitudinal and lateral control for automated lane guidance of full-drive-by-wire vehicles. SAE Int. J. Passeng. Cars - Electron. Electr. Syst. **8**(2), 419–424 (2015)
524. Song, T., Bin, C., Wang, Y.: Fuzzy adaptive output feedback control for MIMO nonlinear systems. Fuzzy Sets Syst. Elsevier **156**, 285–299 (2005)
525. Sorensen, A.J.: A survey of dynamic ship positioning control systems. Annu. Rev. Control, Elsevier **35**, 123–136 (2011)
526. Sorensen, A.J., Egeland, O.: Design of ride control system for surface effect ships using dissipative control. Automatica, Elsevier **31**, 183–199 (1995)
527. Stamens, O.N., Aamo, O.M., Kaasa, G.O.: A constructive speed observer design for optimal Euler-Lagrange systems. Automatica, Elsevier **47**, 2233–2238 (2011)
528. Stout, W.L., Sawan, M.E.: Application of H-infinity theory to robot manipulator control. In: First IEEE Conference on Control Applications, Dayton, Ohio, USA (1992)
529. Su, Z., Khorasani, K.: A neural-network-based controller for a single link flexible manipulator using the inverse dynamics approach. IEEE Trans. Ind. Electron. **48**, 1074–1086 (2001)
530. Subudhi, B., Morris, A.S.: Fuzzy and neuro-fuzzy approaches to control a flexible single-link manipulator. J. Syst. Control Eng., Proc. IMechE **217**, 387–399 (2003)
531. Subudhi, B., Morris, A.S.: Soft computing methods applied to the control of a flexible robot manipulator. Appl. Soft Comput. **9**(1), 149–158 (2009). https://doi.org/10.1016/j.asoc.2008.02.2004
532. Sun, N., Fang, Y., Chen, H.: Adaptive control of underactuated crane systems subject to bridge length limitation and parametric uncertainties. In: Proceedings of the 33rd Chinese Control Conference, Nanjing, China (2014)
533. Sun, N., Feng, Y., Chen, H., Fu, Y., Lu, B.: Nonlinear stabilizing control for ship-mounted cranes with ship roll and heave measurement: design, analysis and experiments. IEEE Trans. Syst. Man Cybern. Part B: Syst. 1–13 (2017)
534. Sun, N., Fang, Y.: New energy analytical results for the regulation of underactuated overhead cranes: an end-effector motion-based approach. IEEE Trans. Ind. Electron. **59**(12), 4723–4734 (2012)
535. Sun, N., Fang, Y., Zhang, X.: Energy coupling output feedback control of 4-DOF underactuated cranes with saturated inputs. Automatica **49**(5), 1318–1325 (2013)
536. Sun, B., Zhu, D., Yang, S.X.: A bioinspired filtered backstepping tracking control of 7000-m manned submarine vehicle. IEEE Trans. Indu. Electron. **61**(7), 3682–3693 (2014)
537. Sun, Z.Y., Song, Z.B., Li, T., Yang, S.H.: Output feedback stabilization of high-order uncertain feed-forward time-delay nonlinear systems. J. Frankl. Inst. Elsevier **352**, 5308–5326 (2015)
538. Sun, N., Fang, Y., Chen, H., Lu, B., Fu, Y.: Slew/Translation positioning and swing suppression for 4-DOF tower cranes with parametric uncertainties, design and hardware experimentation. IEEE Trans. Ind. Electron. **63**(10), 6407–6418 (2016)
539. Sun, N., Fang, Y., Chen, H., Lu, B.: Amplitude-saturated nonlinear output feedback antiswing control for underactuated cranes with double-pendulum cargo dynamics. IEEE Trans. Ind. Electron. **64**(3), 2135–2146 (2017)
540. Sun, N., Fang, Y., Chen, H., Lu, B.: Output-saturated nonlinear output feedback antiswing control for underactuated cranes with double-pendulum cargo dynamics. IEEE Trans. Industr. Electron. **64**(3), 2135–2146 (2017)
541. Suresh, S., Kannan, N., Sundararajan, N., Saratchandran, P.: Neural adaptive control for vibration suppression in composite fin-tip of aircraft. Int. J. Neural Sys., World Scientific **18**(3), 219–231 (2008)
542. Suzuki, S., Furuta, K., Pan, Y.: State-dependent sliding vector VS control and application to swing-up control of pendulum. In: Proceedings of the 42nd IEEE Conference on Decision and Control, Maui, Hawai, USA (2003)
543. Talebi, H.A., Khorasani, K., Patel, R.V.: Neural network based control schemes for flexible-link manipulators: simulations and experiments. Special Issue Neural Control Robot. Biol. Technol. **11**, 1357–1377 (1998)

544. Tanaka, S., Xiu, X., Yamasaki, T.: New results on energy-based swing-up control for rotational pendulum. In: Proceedings of the 18th IFAC World Congress, Milan, Italy (2011)
545. Tanaka, K., Iwasaki, M., Wang, H.O.: Switching control of an R/C hovercraft: stabilization and smooth switching. IEEE Trans. Syst. Man Cybern. **31**(6), 853–863 (2001)
546. Tang, C.P., Miller, P.T., Krovi, V.N., Ryu, J.C., Agrawal, S.K.: Differential flatness-based planning and control of a wheeled mobile manipulator - theory and experiment. IEEE/ASME Trans. Mechatron. **16**(4), 768–773 (2011)
547. Tannuri, E.A., Morishita, H.M.: Experimental and numerical evaluation of a typical dynamic positioning system. Appl. Ocean Res., Elsevier **28**, 133–146 (2006)
548. Tao, C.W., Tanr, J., Chang, J.H., Su, S.F.: Adaptive fuzzy switched swing-up and sliding control for the double-pendulum and cart system. IEEE Trans. Syst. Man Cybern. Part B: Cybern. **40**(1), 241–252 (2010)
549. Tee, K.P., Ge, S.S., Tay, E.H.: Output feedback adaptive control of electrostatic microactuators. In: 2009 American Control Conference, St. Louis, MO USA (2009)
550. Tee, K.P., Ge, S.S., Tay, F.E.H.: Adaptive control of electrostatic microactuators with bidirectional drive. IEEE Trans. Control Syst. Technol. **17**(2), 340–352 (2009)
551. Terzic, B., Jadric, M.: Design and implementation of the extended Kalman filter for the speed and rotor position estimation of brushless DC motor. IEEE Trans. Ind. Electron. **48**(6) (2011)
552. Tham, Y.K., Wang, H., Teoh, E.K.: Multi-sensor fusion for steerable four-wheeled industrial vehicles. Control Eng. Pract., Elsevier **7**, 1233–1248 (1999)
553. Tharmarasa, R., Kirubarajan, T., Peng, J., Lang, T.: Optimization-based dynamic sensor management for distributed multitarget tracking. IEEE Trans. Syst. Man Cybern. - Part C **39**(5), 534–546 (2009)
554. Thorvaldsen, C., Skjetne, R.: Formation control of fully actuated marine vessels using group agreement protocols. In: 50th IEEE Conference on Decision and Control and European Control Conference (CDC-ECC), Orlando Florida, USA (2011)
555. Thrun, S., Burgard, W., Fox, D.: Probabilistic Robotics. MIT Press, Cambridge (2005)
556. Tian, L., Wang, J., Mao, Z.: Constrained motion control of flexible robot manipulators based on recurrent neural networks. IEEE Trans. Syst. Man Cybern. Part B: Cybern. **34**(3), 1541–1552 (2004)
557. Tian, L., Collins, C.: Adaptive neuro-fuzzy control of a flexible manipulator. Mechatronics **15**(10), 1305–1320 (2005)
558. Timmermann, J., Khatab, S., Ober-Blobaum, S., Trachtler, A.: Discrete mechanics and optimal control and its application to a double pendulum on a cart. In: IFAC WC 2011, Proceedings of the 18th IFAC World Congress, Milan, Italy (2011)
559. Tonati, Y., Djouani, K., Amirat, Y.: Neuro-fuzzy based approach for hybrid force/position robot control. Integr. Comput. Aided Eng. **11**(1), 85–98 (2004)
560. Tong, S., Chen, B., Wang, Y.: Fuzzy adaptive output feedback control for MIMO nonlinear systems. Fuzzy Sets Syst., Elsevier **156**, 285–299 (2005)
561. Tong, S., Li, H.-X., Chen, G.: Adaptive fuzzy decentralized control for a class of large-scale nonlinear systems. IEEE Trans. Syst. Man Cybern. - Part B: Cybern. **34**(1), 770–775 (2004)
562. Tong, S., Li, Y.: Observer-based adaptive control for strict-feedback nonlinear systems. Fuzzy Sets Syst. Elsevier **160**, 1749–1764 (2009)
563. Torres, C., Rubio, J.J.: Aguilar-Iba*ñ*ez, C., Perez-Cruz, J.H.: Stable optimal control applied to a cylindrical robotic arm. Neural Comput. Appl. **24**(3–4), 937–944 (2014)
564. Toussaint, G., Basar, T., Bullo, F.: H_∞ optimal tracking control techniques for nonlinear under actuated systems. In: Proceedings of the 39th IEEE Conference on Decision and Control Sydney. Australia (2000)
565. Tsai, C.C., Huang, H.C., Lin, S.C.: Adaptive neural network control of a self-balancng two-wheeled scooter. IEEE Trans. Ind. Electron. **57**(4), 1420–1428 (2010)
566. Tyner, D.R., Lewis, A.D.: Controllability of a hovercraft model (and two general results). In: 43rd IEEE Conference on Decision and Control, Atlantis, Paradise Island, Bahamas (2004)
567. Vasconcelos, J.F.,Cunha, R., Silvestre, C., Oliveira, P.: Landmark based nonlinear observer for rigid body attitude and position estimation. In: Proceedings 46th IEEE Conference on Decision and Control, USA (2007)

568. Vasquez, C., Collado, J., Fridman, L.: Control of a prametrically excited crane: a vector Lyapunov approach. IEEE Trans. Control Syst. Technol. **21**(6), 2332–2340 (2013)
569. Vepa, R.: Nonlinear unscented H_∞ suspension and tracking control of mobile vehicles. IEEE Trans. Veh. Technol. **61**(4), 1543–1553 (2012)
570. Vercauteren, T., Wang, X.: Decentralized sigma-point information filters for target tracking in collaborative sensor networks. IEEE Trans. Signal Process. **53**(8), 2997–3009 (2005)
571. Villagra, J., Horreo-Perez, D.: A comparison of control techniques for robust docking maneuvers of an AGV. IEEE Trans. Control Syst. Technol. **20**(4), 1116–1125 (2012)
572. Villagra, J., d'Andrea-Novel, B., Mounier, H., Pengov, M.: Flatness-based vehicle steering control strategy with SDRE feedback gains tuned via a sensitivity approach. IEEE Trans. Control Syst. Tech. **15**, 554–565 (2007)
573. Vissière, D., Bristeau, P.J., Martin, A.P., Petit, N.: Experimental autonomous flight of a small-scaled helicopter using accurate dynamics model and low-cost sensors. In: Proceedings of the 17th World Congress the International Federation of Automatic Control Seoul, pp. 6–11. Korea (2008)
574. Wada, M., Yoon, K., Hashimoto, H.: Development of advanced parking assistance system. IEEE Trans. Ind. Electron. **50**(1), 4–17 (2003)
575. Wai, R.J., Lee, M.C.: Intelligent optimal control of a single-link, flexible robot arm. IEEE Trans. Ind. Electron. **51**(1), 201–220 (2004)
576. Wang, J., Boussaada, I., Cela, A., Mounier, H., Niculescu, S.I.: Analysis and control of quadrotor via a normal form approach. In: IEEE International Symposium on Mathematical Theory of Networks and Systems, Melbourne, Australia (2012)
577. Wang, Z., Chiu, Y., Fang, N.: Minimum-time swing-up of a rotary inverted pendulum by iterative impulsive control. In: IEEE ACC 2004, Proceedings of the: American Control Conference, Boston, Massachusetts (2004)
578. Wang, R., Hu, C., Wang, Z., Chen, V.: Integrated optimal dynamics control of two 4WD 4WS electric ground vehicle with tire-road frictional coefficient estimation. Mech. Syst. Signal Process., Elsevier **60–61**, 728–741 (2015)
579. Wang, Y.Z., Li, F.M.: Dynamic properties of Duffing- Van der Pol oscillator subject to both external and parametric excitations with time-delayed feedback control, J. Vib. Control, Sage Publications **21**(2), 371–387 (2013)
580. Wang, Y., Nam, K., Fujimoto, H., Hori, Y.: Robust roll and yaw integrated control using 4 wheel steering based on yaw moment and lateral force observers. Proceedings of the IEEJ Technical Meeting Record, IIC-11-138 (2011)
581. Wang, L.X.: Adaptive Fuzzy Systems and Control: Design and Stability Analysis. Prentice Hall, Englewood Cliffs (1994)
582. Wang, L.X.: A Course in Fuzzy Systems and Control. Prentice-Hall, Englewood Cliffs (1998)
583. Wang, F.-Y., Gao, Y.: Advanced Studies of Flexible Robotic Manipulators. World Scientific, Singapore (2004)
584. Wang, R., Wang, J.: Actuator-redundancy-based fault diagnosis for four-wheel independently actuated electric vehicles. IEEE Trans. Intell. Transp. Syst. **15**(1), 239–249 (2014)
585. Wang, Z., Goodall, D.P., Burnham, K.J.: On designing observers for time-delay systems with nonlinear disturbances. Int. J. Control Taylor and Francis **75**(11), 803–811 (2002)
586. Wang, R., Zhang, H., Wang, J.: Linear parameter-varying controller design for four-wheel independently actuated electric ground vehicles with active steering system. IEEE Trans. Control Syst. Technol. **22**(4), 1281–1286 (2014)
587. Wang, Z., Wang, Q., Dong, C.: Asynchronous H-infinity control for unmanned aerial vehicles: switched polytopic system approach. IEEE/CAA J. Autom. Sin. **2**(2), 207–216 (2015)
588. Wang, S., Sun, Y., Chen, H., Han, G.: Kinematics and force analysis of a novel offshore crane combined compensation system. IMech J. Eng. Maritime Environ. **231**(2), 633–648 (2017)
589. Watanabe, K., Tzafestas, S.G.: Filtering, smoothing and control in discrete-time stochastic distributed-sensor networks. In: Tzafestas, S.G., Watanabe, K. (eds.) Stochastic Large-Scale Engineering Systems, pp. 229–252. Marcel Dekker (1992)

590. Wesemeier, D., Isermann, R.: Identification of vehicle parameters using stationary driving maneuvers. Control Eng. Pract., Elsevier **17**, 14261431 (2009)
591. Witkowski, B.: Modeling of the dynamics of two coupled spherical pendula. Eur. Phys. J. **223**(4), 631–648 (2014)
592. Wondergen, M., Lefeber, E., Petersen, K.Y., Nijmeijer, H.: Output feedback tracking of ships. IEEE Trans. Control Syst. Technol. **19**(2), 442–448 (2011)
593. Woodcore, J.K., Brauer, R.J., Irani, R.A.: A review of vertical motion heave compensation systems. Ocean Eng., Elsevier **104**, 140–154 (2015)
594. Wu, X., He, X., Qu, X.: A coupling control method applied to 2D overhead cranes. In: Proceedings of the 35th Chinese Control Conferences, Changdu, China (2016)
595. Wu, T.S., Karkoub, N., Yu, W.S., Chen, C.T., He, M.G., Wu, K.W.: Anti-swing tracking control of tower cranes with delayed uncertainty using a robust adaptive fuzzy control. Fuzzy Sets Syst., Elsevier **290**, 118–137 (2016)
596. Wu, X., He, X.: Enhanced damping-based anti-swing control method for underactuated overhead cranes. IET Control Theory Appl. **9**(12), 1893–1900 (2015)
597. Wu, X., He, X.: Nonlinear energy-based regulation control of three-dimensional overhead cranes. IEEE Trans. Autom. Sci, Eng (2016)
598. Xiang, X., Zheng, J., Yu, C., Xu, G.: Nonlinear path following control of autonomous underwater vehicles: under-actuated and fully-actuated cases. In: Proceedings of the 33rd Chinese Control Conference. Nanjing, China (2014)
599. Xin, X., Tanaka, S., She, J., Yamasaki, T.: New analytical results of energy-based swing-up control for the Pendubot. Int. J. Non-Linear Mech., Elsevier **52**, 110118 (2013)
600. Xin, X.: Analysis of the energy-based swing-up control for the double pendulum on a cart. Int. J. Robust Nonlinear Control, Wiley **21**, 387–403 (2011)
601. Xiong, J.: An Introduction to Stochastic Filtering Theory. Oxford University Press, Oxford (2008)
602. Xiong, X., Lapierre, L., Jouvencel, B.: Smooth transition of AUV motion control: from fully actuated to underactuated configuration. Robot. Auton. Syst. Elsevier **67**, 14–22 (2015)
603. Xu, L., Hu, Q.: Output-feedback stabilization control for a class of under-actuated mechanical systems. IET Control Theory Appl. **7**(7), 985–996 (2013)
604. Yamaguchi, Y., Murakami, T.: Adaptive control for virtual steering characteristics on electric vehicle using steer-by-wire system. IEEE Trans. Ind. Electron. **56**(5), 1585–1594 (2009)
605. Yamashita, M., Fujimori, K., Hakayawa, K., Kimura, H.: Application of H_∞ control to active suspension systems. Automatica Elsevier **30**(11), 1717–1729 (1994)
606. Yan, Q.: Output tracking of underactuated rotary inverted pendulum by nonlinear controllers. In: IEEE CDC 2003, Proceedings of the 42nd IEEE Conference on Decision and Control, Maui, Hawaii, USA (2003)
607. Yang, Q., Jagannathan, S.: A suite of robust controllers for the manipulation of microscale objects. IEEE Trans. Syst. Man Cybern. - Part B: Cybern. **38**(1), 113–125 (2008)
608. Yang, Q., Sun, H., Tang, G., Gao, D.: Optimal internal model control with specified decay time rate for AUV under irregular move forces. In: Proceedings of the 35th Chinese Control Conference. Changdu, China (2016)
609. Yang, Y., Zhou, C., Jia, X.: Robust adaptive fuzzy control and its application to ship roll stabilization. Inf. Sci., Elsevier **142**, 177194 (2002)
610. Yang, C., Murakami, T.: Full-speed range self-balancing electric motorcycles without the handlebar. IEEE Trans. Ind. Electon. **63**(3), 1911–1922 (2016)
611. Yang, N., Tian, W.F., Jin, Z.H., Zhang, C.B.: Particle Filter for sensor fusion in a land vehicle navigation system. Meas. Sci. Technol. **16**, 677–681 (2005)
612. Yazdizadeh, A., Khorasani, K., Patel, R.V.: Identification of a two-link flexible manipulator using adaptive time delay neural networks. IEEE Trans. Syst. Man Cybern. Part B **30**, 165–172 (2000)
613. Yi, J., Yabazaki, N., Hirota, K.: A new fuzzy controller for stabilization of parallel-type double inverted pendulum system. Fuzzy Sets Syst., Elsevier **126**, 105–119 (2002)

614. Yi, J., Yabazaki, N., Hirota, K.: Stabilization control of series-type double inverted pendulum systems using the SIRM dynamically connected fuzzy inference model. Artif. Intell. Eng., Elsevier **15**, 297–308 (2001)
615. Yi, J., Zhang, Y., Song, D.: Autonomous motorcycles for agile maneuvers. In: Part I: Dynanic Modellinng, 2019 IEEE CDC, Joint IEEE Decision and Control Conference and Chinese Control Conference. Shanghai, China (2009)
616. Yoon, Y., Shin, J., Kim, H.J., Park, Y., Sastry, S.: Model-predictive active steering and obstacle avoidance for autonomous ground vehicles. Control Eng. Pract., Elsevier **17**, 741–750 (2009)
617. Yousef, H.A., Hamdy, M., Shafiq, M.: Flatness-based adaptive fuzzy output tracking excitation control for power system generators. J. Frank. Inst. **350**, 23342353 (2013)
618. Yu, J.C., Zhang, A.Q., Wang, X.H.: Adaptive neural network control with control allocation for a manned submersible in deep sea. China Ocean Eng. **21**(1), 147161 (2007)
619. Yuan, O.H.: Actively damped heave compensation system. In: 2010 American Control Conference, Baltimore MD USA (2010)
620. Yue, H., Li, J.: Output-feedback adaptive fuzzy control for a class of nonlinear time-varying delay systems with unknown control directions. IET Control Theory Appl. **6**, 1266–1280 (2012)
621. Yung, E., Gu, D.: Nonlinear formationn-keeping and mooring control of multiple autonomous underwater vehicles. IEEE/ASME Trans. Mechatron. **12**(2), 164–178 (2011)
622. Zanon, M., Frasch, J.V., Vukov, M., Sager, S., Diehl, M.: Model predictive control of autonomous vehicles. Optimization and Optimal Control in Automotive Systems. Lecture Notes in Control and Information Sciences, vol. 455, pp. 41–47. Springer, Switzerland (2014)
623. Zarei, J., Poshtan, J., Poshtan, M.: Robust fault detection of nonlinear systems with unknown disturbances. In: 2010 IEEE International Conference on Control Applications (Part of 2010 IEEE Multi-Conference on Systems and Control), Yokohama, Japan (2010)
624. Zhang, Q., Basseville, M.: Advanced numerical computation of chi2-tests for fault detection and isolation. In: Safeprocess'03 - 5th IFAC/IMACS Symposium on Fault Detection. Supervision and Safety of Technical Processes, Washington DC (2003)
625. Zhang, Q., Campillo, F., Cérou, F., Legland, F.: Nonlinear fault detection and isolation based on bootstrap particle filters. In: Proceedings of the 44th IEEE Conference on Decision and Control, and European Control Conference, Seville Spain (2005)
626. Zhang, Y., Li, J., Yi, J., Song, D.: Balance control and analysis of stationary riderless motorcycles. In: 2011 IEEE ICRA International Conference on Robotics and Automation. Shanghai, China (2011)
627. Zhang, B., Ma, B.: Robust stabilization of underactuated surface vessels with parameter uncertainties. In: 29th Chinese Control Conference, Beijing, China (2010)
628. Zhang, A., Qiu, J., Yang, C., He, H.: Stabilization of underactuated four-link gymanst robot using torque-coupled method. Int. J. Nonlinear Mech., Elsevier **77**, 299–306 (2015)
629. Zhang, Z., Wu, Y., Huang, J.: Motion and anti-swing control of underactuated bridge cranes using differential flatness. In: Proceedings of the 35th Chinese Control Conference, Chengdu, China (2015)
630. Zhang, J., Zhang, Y.: Optimal linear modelling and its applications on swing-up and stabilization control for rotary inverted pendulum. In: Proceedings of the 30th Chinese Control Conference, Yantai, China (2011)
631. Zhang, Q.: Adaptive observer for Multiple-Input-Multiple-Output (MIMO) linear time-varying systems. IEEE Trans. Autom. Control **47**(3), 525–529 (2002)
632. Zhang, Q.: Nonlinear system identification with an integrable continuous time nonlinear ARX model. J. Européen des Systèmes Automatisés **46**(6–7), 691–710 (2012)
633. Zhang, Q., Basseville, M., Benveniste, A.: Fault detection and isolation in nonlinear dynamic systems: a combined input-output and local approach. Automatica, Elsevier **34**(11), 1359–1373 (1998)
634. Zhang, R., Chen, Y., Sun, Z., Sun, F., Xu, H.: Path control of a surface ship in restricted waters using sliding mode. IEEE Trans. Control Syst. Technol. **8**(4), 722–732 (2000)

635. Zhang, L.J., Qi, X., Pang, Y.J.: Adaptive output feedback control based on DFRNN for AUV. Ocean Eng. Elsevier **36**, 716–722 (2009)
636. Zhang, C., Franch, J., Agrawal, S.K.: Differentially flat design of a closed-chain planar underactuated 2-DOF system. IEEE Trans. Robot. **29**(1), 277–282 (2013)
637. Zhang, Y., Yu, X., Yin, Y., Peng, C., Fan, Z.: Singularity-conquering ZG controllers of z2g1 type for tracking control of the IPC systems. Int. J. Control **87**(9), 1729–1746 (2014)
638. Zhang, A., Yang, C., Gang, S., Giu, J.: Nonlinear stabilizing control of underactuated inertia wheel pendulum based on coordinates transformation and time-reverse strategy. Springer, Nonlinear Dyn. (2016)
639. Zhao, Z., Chen, H., Chen, G., Kwan, C., Rong Li, X.: Comparison of several ballistic target tracking filters. In: IEEE ACC 06, American Control Conference, Minneapolis, Minnesota, USA (2006)
640. Zhao, X., Zhang, Z., Huang, J.: Energy-based swing-up control of rotary parallel inverted pendulum. In: IEEE WCICA 2016, Proceedings of the 12th World Congress on Intelligent Control and Automation, Guilin, China (2016)
641. Zhao, H., Ga, B., Ren, B., Chen, H., Deng, W.: Model predictive control allocation for stability improvement of four-wheel drive electric vehicles in critical driving condition. IET Control Theory Appl. **9**(18), 2688–2696 (2015)
642. Zheng, G., Barbot, J.P., Boutat, D., Floquet, T., Richard, J.P.: Finite-time observation of nonlinear time-delay systems under unknown inputs. In: IFAC NOLCOS 2010, IFAC Conference on Nonlinear Control Systems, Bologna, Italy (2010)
643. Zheng, G., Barbot, J.P., Boutat, D., Floquet, T., Richard, J.P.: On observation of time-delay systems with unknown inputs. IEEE Trans. Autom. Control **56**(8), 1973–1978 (2011)
644. Zheng, G., Barbot, J.P., Boutat, D.: Identification of the delay parameter for nonlinear time-delay systems with unknown inputs. Automatica Elsevier **49**(6), 1755–1760 (2013)
645. Zheng, G., Bejarano, F.J., Rerruquetti, W., Richard, J.P.: Unknown-input observer for linear time-delay systems. Automatica Elsevier **61**, 35–41 (2015)
646. Zhou, Y., Wu, X.: Control of the double-container overhead crane. In: Proceedings of the 34th Chinese Control Conference, Hangzhou, China (2015)
647. Zhou, L., Yan, Z.: H_∞ networked control of two inverted pendulums coupled by a spring. In: Proceedings of the 34th Chinese Control Conference, Hangzhou, China (2015)
648. Zhu, G., Agudelo, G.G., Saydy, L., Packirisamy, M.: Torque multiplication and singularity avoidance in the control of electrostatic torsional micro-mirrors. In: Proceedings 17th IFAC World Congress. Seoul, Korea (2008)
649. Zhu, G., Packirisamy, M., Hosseini, M., Peter, Y.A.: Modelling and control of an electrostatically actuated torsional micromirror. J. Micromech. Microeng., Institute of Physics Publishing **16**, 20442052 (2006)
650. Zhu, G., Saydy, L., Hosseini, M., Chiannetta, J.F., Peter, Y.A.: A robustness apporach for handling modelling errors in parallel-plate electrostatic MEMS control. J. Microelectromech. Syst. **17**(6), 1902–2007
651. Zhu, G., Lévine, J., Praly, L., Peter, Y.A.: Flatness-based control of electrostatically actuated MEMS with application to adaptive optics: a simulation study. IEEE J. Microelectromech. Syst. **15**(5), 1165–1174 (2006)
652. Zolghadri, A.: An algorithm for real-time failure detection in Kalman filters. IEEE Trans. Autom. Control **41**(10), 1537–1539 (1996)
653. Zuo, Z.: Adaptive trajectory tracking control design with command filtered compensation for a quadrotor. JVC/J. Vib. Control **19**(1), 94–108 (2013)

Index

A

Accelerometers, 688
Active joint, 140
Adapative fuzzy control, 222, 234
Adaptation of weights, 172, 180
Adaptive control, 162, 170, 344, 593, 595, 607, 608
Adaptive control of Furuta's pendulum, 207, 215
Adaptive control of underactuated robots, 207, 215
Adaptive fuzzy control, 212, 220, 609, 626
Additive input disturbances, 510, 603, 617
Affine-in-the-input system, 13, 206, 208, 214, 216, 436
Aggregate fusion filter, 660
Aggregate state estimate, 686
Agricultural robots, 694
Algebraic Riccati equation, 27, 94, 101, 106, 115, 124, 140, 149, 151, 178, 186, 207, 210, 213, 215, 218, 221, 251, 262, 263, 265, 274, 277, 302, 316, 321, 322, 325, 330, 335, 342, 348, 352, 373, 382, 392, 394, 404, 405, 408, 415, 420, 422, 425, 428, 440, 442, 445, 470, 483, 492, 493, 503, 555, 560, 570, 595, 625, 626, 629, 635, 636, 641
Approximate kinematic model of USVs, 650
Approximate linearization, 1, 66, 67, 86, 89, 100, 103, 115, 118, 138, 207, 214, 215, 222, 234, 239, 251, 325, 327, 342, 343, 373, 393, 415, 417, 434, 469, 470, 484, 490, 502, 533, 554, 594, 629
Approximate linearization-based control, 305
Approximate linearization methods, 1, 469
Approximation error, 173, 181, 191, 198, 199, 206, 248, 250, 260, 262, 314, 618, 619, 623
ARMAX model of the Kalman Filter, 577
Articulated vehicles, 391, 415
Asymptotic stability, 208, 216, 279
Attenuation coefficient, 79, 109, 165, 173, 624
Autocorrelation test, 578
Automatic ground vehicles, 453, 643
Autonomous agricultural robots, 685
Autonomous four-wheel ground vehicles, 391, 392
Autonomous Ground Vehicles (AGVs), 354, 695
Autonomous hovercraft, 501, 502, 532
Autonomous motorcycle, 341, 342, 373, 374, 377, 380
Autonomous navigation of ground vehicles, 453
Autonomous submarines, 593, 594, 610, 636, 640
Autonomous underwater vessels, 593, 594, 607, 628, 642, 643
Autonomous unicycle vehicle, 344
AUVs dynamic model, 593
AUVs model, 630

B

Backstepping control, 101, 374, 428

G. Rigatos and K. Busawon, *Robotic Manipulators and Vehicles*,
Studies in Systems, Decision and Control 152,
https://doi.org/10.1007/978-3-319-77851-8

Barbalat's Lemma, 41, 79, 96, 109, 127, 153, 200, 208, 215, 223, 253, 265, 320, 334, 350, 383, 407, 424, 444, 494, 563, 625, 638
Basis functions, 187, 195
Bayes law, 514
Bellman's optimality principle, 47
Body-fixed reference frame, 596

C

Canonical Brunovsky form, 11, 14, 183, 184, 191, 192, 223, 234, 235, 246, 247, 258, 259, 301, 303, 342, 354, 358, 393, 454, 458, 460, 471, 502, 551, 594, 595, 601, 602, 615, 670, 693
Canonical form of MIMO models, 671
Car-like vehicles, 355
Cart and double-pendulum system, 65, 66, 115, 116, 122, 128
Cart-like vehicles, 355
Change detection method, 587
Change threshold, 584
Chaotic dynamics, 325
Characteristic polynomial, 167, 175, 307, 309, 574
Closed-chain robotic manipulator, 224, 236
Closed-chain robotic mechanism, 221, 233, 256, 257, 260–262, 268, 269, 272–274
Closed-chain robots, 221, 233
Collaborating farming robots, 684
Computed torque method, 7
Consistency checking of the Fuzzy Kalman Filter, 581
Consistency of the Kalman Filter, 578
Contact force, 284
Control and navigation for AUVs, 594
Control in cascading loops, 476
Controllable system, 602
Controller canonical form, 15, 670
Control of UAVs, 469
Control problem of hovercrafts, 533
Cooperating agricultural robots, 685
Cooperating autonomous vehicles, 643
Cooperating robot harvesters, 644
Cooperating unmanned ground vehicles, 643
Cooperating unmanned surface vessels, 643, 644
Coordinated control, 643
Coordinated target tracking problem, 649
Coordinates transformation matrices, 11
Coriolis effects, 430
Coriolis matrix, 4, 506, 597, 598
Coupled MEMS, 335
Coupled nonlinear oscillators, 327
Covariance matrix, 296, 583, 668
Cramer Rao Lower Bound (CRLB), 531
Curvature radius, 355
Cycle time of filtering algorithms, 531

D

Data fusion, 511, 667
Decentralized state estimation, 643, 645
Denavit-Hartenberg method, 4
Derivative-free distributed nonlinear Kalman Filter, 644, 681, 687
Derivative-free extended information filter, 681, 686
Derivative-free nonlinear Kalman Filter, 20, 222, 234, 239, 245, 251, 257, 342, 354, 358, 364, 454, 460, 462, 469, 471, 478, 502, 533, 548, 550, 594, 595, 604, 671, 686, 693
Detectable system, 37, 76, 92, 106, 124, 262, 274, 330, 380, 403, 420, 440, 491, 559, 635
Diagnostics tests (sensitivity or min–max), 581
Diffeomorphisms, 101, 207, 215, 223, 235, 245, 256, 257, 268, 303, 309, 374, 408, 426, 445, 471, 481, 548, 555, 642, 686
Differential flatness of AUVs, 595, 600, 601
Differential flatness of four-wheel vehicle, 456
Differential flatness of MEMS, 335
Differential flatness of quadrotor's model, 474
Differential flatness of submarine, 611, 614
Differential flatness of the 6-DOF AUV, 601
Differential flatness theory, 11, 303, 342, 344, 354, 454, 470, 471, 502, 594, 610, 693
Differential flatness theory-based filtering, 2, 645
Differential flatnessof USV, 564
Differential game, 483, 555
Differential geometry, 306
Differential GPS, 687
Differential kinematic model, 281
Differentially flat dynamical system, 247, 259
Differentially flat four-wheel vehicle, 458
Differentially flat MIMO systems, 669

Differentially flat systems, 1, 11, 308, 620
Discretization methods, 296
Distributed control, 643, 644, 681
Distributed derivative-free nonlinear Kalman Filter, 645, 672, 694, 695
Distributed filtering, 572, 643–646, 655, 674, 685
Distributed filtering-based fusion, 686
Distributed gradient algorithms, 651, 653
Distributed Kalman Filtering, 503, 571, 573, 644, 686
Distributed motion planning, 675
Distributed Sigma-Point Kalman Filters, 661
Distributed state estimation, 686
Distributed Unscented Kalman Filters, 664, 667
Disturbance estimator, 223, 235, 461, 478, 604
Disturbance inputs, 553, 612
Disturbance observer, 2, 50, 222, 234, 393, 454, 470, 471, 502, 510, 533, 594, 595
Disturbance rejection, 105, 123, 148, 261, 273, 379, 419, 439, 559, 634
Dive-plane dynamics of submarine, 611
3-DOF surface vessel, 501, 502
6-DOF autonomous underwater vessels, 595
Driftless systems, 13
Duffing oscillator, 302, 325, 326, 335
Dynamic extension, 101, 246, 258, 554
Dynamic feedback linearization, 253, 265, 356, 502, 533, 551, 648
Dynamic model of 4WS vehicle, 430
Dynamic model of AUVs, 597, 600
Dynamic model of motorcycles, 373
Dynamic model of robotic manipulator, 50
Dynamic model of submarine, 612, 614
Dynamic model of UAVs, 484
Dynamic positioning of vessels, 503
Dynamic positioning systems, 504
Dynamics of four-wheel vehicle, 453
Dynamics of the tracking error, 648

E

Elastic force, 283
Electrostatic microactuators, 302, 304, 308
Electrostatically actuated MEMS, 301
Energy-based control, 85, 272, 277, 286
Euler-Bernoulli model, 274
Euler–Lagrange analysis, 3, 69, 101, 116, 225, 237, 246, 258, 650
Euler–Lagrange equations, 473
Euler rotation angles, 472, 484
Exact linearization, 343, 484, 533, 691
Exact linearization of MEMS, 303
Extended Information Filter, 644, 645, 647, 656–658, 660, 671, 675, 686, 693
Extended Kalman Filter, 20, 353, 359, 454, 512, 675, 693
Extended state observer, 511
Extended state-space model, 57, 239, 251, 534, 544, 549, 553
Extended state vector, 239, 251, 477

F

Fault isolation, 584
Fault isolation test, 584
Fault threshold, 582, 588, 590
Flatness-based adaptive control, 301
Flatness-based adaptive fuzzy control, 163, 171, 221, 233, 246, 253, 258, 265, 301, 303, 309, 321, 593, 594, 610, 627
Flatness-based control, 221, 223, 233, 235, 273, 341, 355, 391, 392, 470, 479, 501, 502, 543, 605, 644, 687, 691
Flat output, 11, 235, 247, 307, 454, 456, 540–542, 600, 615, 620, 669, 687
Flexible-link robot dynamics, 292
Flexible-link robotic manipulator, 271, 272, 280
Flexible-link robots, 272
Flexible modes, 277
Four-wheel ground vehicle, 391, 392, 394, 408, 453
Four-wheel steering vehicle, 391, 392, 427
Four-wheel vehicle dynamic model, 455, 460
Furuta's pendulum, 101, 110, 207, 215
Fusion-based state estimation, 675
Fusion of distributed sensor measurements, 656
Fusion of distributed state estimates, 656, 658, 675
Fuzzy Kalman Filter, 572, 578, 586–588
Fuzzy-weighted ARMAX models, 571, 586

G

Generalized Likelihood Ratio, 503, 584, 589
Generalized Lyapunov function, 654
Global asymptotic stability, 42, 79, 96, 109, 115, 140, 155, 252, 264, 265, 277, 302, 325, 342, 383, 416, 424, 428,

444, 469, 484, 494, 555, 563, 625, 629, 638
Global linearization, 1, 245, 256, 257, 268, 352, 469, 554, 642
Global linearization-based control, 101, 255, 267, 305, 428, 445, 593, 594
Global linearization methods, 1, 469
Global linearization of tractors' kinematics, 687
Global linearization transformations, 27
Global stability proof, 374
Global test for fault detection, 581
Global χ^2 test for fault detection, 584
GNSS measurement, 688
GPS sensor, 359, 687
Gradient algorithm, 197, 205, 313, 318
Gradient-type learning, 622
Gravitational forces matrix, 4
Grid partitioning of state-space, 206, 214
Ground vehicle's dynamic model, 395, 397
Gyroscopes, 688

H
Hamiltonian matrix, 93, 150, 177, 185, 201, 209, 321
H-infinity control, 27, 37, 66, 75, 86, 91, 115, 124, 149, 176, 184, 188, 196, 204, 310, 325, 329, 335, 342, 343, 373, 379, 392–394, 403, 414, 415, 419, 428, 439, 480, 491, 497, 559, 617, 629, 634
H-infinity feedback control, 74, 100, 123, 139, 207, 215, 256, 260, 261, 268, 272, 273, 329, 346, 378, 402, 439, 470, 482, 490, 503, 555, 558, 633
H-infinity Kalman Filter, 79, 80, 96, 101, 110, 128, 140, 155, 256, 266, 268, 278, 302, 326, 334, 339, 373, 384, 389, 394, 407, 416, 425, 428, 444, 495, 563, 564, 629, 638, 642
H-infinity norm, 165, 173
H-infinity performance index, 176, 184, 252, 264
H-infinity tracking performance, 78, 95, 101, 106, 127, 154, 176, 183, 184, 191, 200, 208, 215, 216, 223, 248, 260, 262, 274, 319, 325, 331, 333, 380, 394, 404, 407, 415, 421, 424, 484, 492, 503, 560, 562, 594, 611, 624, 625, 629, 637
Homogeneous transformation matrix, 8
Hovercraft's input-output linearized model, 553
Hovercraft's kinematic and dynamic model, 533, 555
Hovercraft's linearized equivalent model, 546
Hovercraft's motion, 536
Hurwitz polynomial, 167, 175, 307, 309

I
Inconsistent model, 582, 584
Indirect adaptive control, 161, 169
Indirect adaptive fuzzy control, 625
Inertial measurement unit, 688
Inertial reference frame, 596
Inertia matrix, 4, 292, 505, 597
Infinite dimensional systems, 271
Infinite number of DOF, 271
Information Filter recursion, 686
Information matrix, 657, 661, 665–668
Information state vector, 657, 661, 665–668
Input-output linearization, 502
Input-output linearized form, 54, 546
Input-output linearized hovercraft's model, 546
Input-output linearized system, 539
Input-space partition, 588
Input-to-state linearizable systems, 254, 266
Input-to-state linearization, 227, 239
Inverse dynamics control, 271–273, 275, 300
Inverse kinematics, 284

J
Jacobian matrices, 27, 36, 71, 86, 100, 103, 118, 139, 146, 208, 216, 222, 234, 256, 257, 268, 269, 302, 325, 327, 342, 343, 345, 346, 373, 392, 393, 400, 415, 418, 427, 434, 470, 482, 486, 502, 555, 558, 595, 629, 631, 634, 656

K
Kalman Filter-based control, 241, 253
Kalman Filter-based disturbance estimation, 224, 236, 479
Kalman Filter-based disturbance estimator, 241, 253, 454, 466, 504, 605
Kalman Filter-based disturbance observer, 56, 511, 594
Kalman Filter-based sensor fusion, 502, 515
Kalman Filter-based sliding-mode control, 292, 300
Kalman Filter recursion, 19, 292, 550, 693

Kalman Filter's residuals, 574, 587
Kalman Filtering, 19, 272, 291, 296, 393, 501, 502, 504, 688
Kernel functions, 166, 171, 174, 179, 182, 187, 195, 197, 205, 249, 261, 314, 615, 619, 622
Kinematic analysis of rigid link robots, 8
Kinematic and dynamic model of AUVs, 596, 599
Kinematic-dynamic model of 4WS vehicle, 434, 435, 438
Kinematic-dynamic model of four-wheel vehicle, 393
Kinematic model of agricultural vehicle, 690
Kinematic model of motorcycles, 373
Kinematic model of truck and trailer system, 416, 417
Kinematic model of unicycle AGVs, 354

L

Lagrangian, 229, 241
La Salle's theorem, 645, 654, 655
Learning rate, 208, 216
Lie algebra, 223, 235
Lie algebra-based control, 536
Lie-algebra theory, 232, 244
Lie Bracket, 14
Lie derivatives, 14, 306
Likelihood ratio, 584
Linearization error, 31, 74, 260, 272, 328, 352, 438
Linearization of vessel's model, 556
Linearization point, 399
Linearized dynamic model of AUV, 632
Linearized input-output form, 536
Linearized MEMS dynamics, 306, 309
Linear matrix inequalities, 323
Local gradient algorithm, 650
Local linearization, 27, 554
Local linearization-based control, 255, 267
Local linear models, 1, 344, 469, 588
Local operating point, 485, 556
Local statistical approach to fault diagnosis, 503, 571, 581, 587, 589
LQG control, 240, 245, 252, 257
LQR control, 36, 75, 105, 124, 261, 273, 329, 347, 379, 403, 419, 439, 491, 559, 634
LQR/LQG control, 46
Lyapunov analysis, 27, 93, 101, 140, 208, 216, 222, 234, 342, 352, 484, 555, 629
Lyapunov function, 39, 76, 79, 106, 151, 194, 202, 215, 223, 263, 265, 275, 277, 303, 331, 333, 348, 350, 405, 421, 441, 444, 469, 481, 493, 494, 561, 563, 594, 611, 620, 623, 636, 638, 645
Lyapunov function in adaptive control, 172, 180, 315
Lyapunov stability analysis, 39, 106, 125, 151, 163, 171, 250, 256, 262, 268, 274, 302, 325, 331, 348, 373, 380, 392, 404, 421, 441, 470, 492, 503, 560, 595, 611, 628, 636, 651
Lyapunov theory-based control, 305, 344
Lyapunov theory-based motion planning, 643

M

Manipulator's decoupled dynamics, 7
Marine vessels, 503
Master-slave cooperation scheme, 689, 694
Master-slave robots coordination, 684
Meas Square Error (MSE) test, 589
Measurement noise covariance matrix, 58
Membership function, 313
MEMS nonlinear dynamics, 306, 327
Microactuator dynamics, 305
Microactuators, 301
Microelectromechanical Systems (MEMS), 301, 321, 325
Micromanipulation, 302
Microrobotics, 301
MIMO canonical form, 15, 459, 476, 603
MIMO controller, 177, 185
MIMO transfer function, 574
Min-max differential game, 27, 68, 75, 92, 100, 115, 124, 149, 201, 209, 325, 330, 373, 394, 415, 629
Min–max fault diagnosis test, 585
Min–max optimization, 105, 261, 273, 347, 379, 420, 440, 491, 559, 634
Min–max test, 586
Model-based control, 1
Model-free adaptive control, 161, 169
Model Predictive Control (MPC), 68, 85, 101, 374, 428
Monte-Carlo integration, 662
Motion control, 344
Motor's power, 278
Multi-DOF robotic manipulators, 1
Multi-DOF UAV, 492
Multi-pendulum system, 115

Multi-robot systems, 643
Multi-sensor fusion, 644
Multi-USV system, 654
Multivariable canonical Brunovsky form, 594
Multivariable nonlinear control, 594
Multi-vehicle system, 643

N
Networked control of robotic manipulators, 49
Neurofuzzy approximators, 161, 169, 171, 179, 208, 216, 246, 249, 258, 261, 303, 321, 582, 594, 610, 619, 621, 625, 628
Neurofuzzy controllers, 162, 170, 609
Neurofuzzy estimators, 216, 224
Neurofuzzy networks, 207, 215
Nonholonomic constraints, 355
Nonholonomic systems, 355
Nonlinear control, 501, 502
Nonlinear estimation methods, 245, 257
Nonlinear H-infinity control, 66, 344, 350, 564, 640
Nonlinear Kalman Filter, 244, 256
Nonlinear model of truck and trailer system, 419
Nonlinear Model Predictive Control, 68, 85, 101, 374, 428
Nonlinear multivariable dynamics, 608
Nonlinear optimal control, 65, 221, 233, 266, 278, 301, 302, 341, 384, 391, 392, 408, 415, 425, 427, 470, 501, 502, 593, 594, 628
Normalized error square, 579
Normalized Error Square (NES) test, 578
Normalized Gaussian membership functions, 166, 174
Normalized Mean Error (NME) test, 578

O
Observable system, 602
Observation error, 196, 204, 313
Observation gain, 312
Observation gain matrix, 189, 197
Observer-based adaptive fuzzy control, 183, 191, 194, 202, 625
Observer-based control scheme, 291, 625
Observer canonical form, 15, 670, 681
Optimal (H-infinity) control, 325
Orthogonal basis functions, 274
Output feedback, 302, 303
Overhead cranes, 65, 67

P
Partial feedback linearization, 100, 102
Particle Filter-based disturbance estimator, 504
Particle Filter-based sensor fusion, 502, 515
Particle filter's correction stage, 513
Particle filter's prediction stage, 513
Particle Filtering, 454, 504, 513, 662
Passive joint, 140
Path planning, 688
Path tracking error, 695
Payload positioning system, 87
PD joint controller, 284
Perturbation observer, 511
PID control, 45, 245, 257, 374, 428, 570
Pole placement method, 240, 252
Positive definite symmetric matrix, 38
Potential energy, 277
Potential fields theory, 649
Primary residual, 582, 587
Prismatic joint, 9
Process noise covariance matrix, 58

Q
Quadratic cost function, 75, 91, 105, 200, 208, 320, 347, 379, 403, 420, 439, 491, 559, 634
Quadropters, 470, 472, 473
Quadrotors, 470
Quadrotor's dynamic model, 474, 486

R
Regressor's vector, 588
Regulation problem, 248, 260
Residuals of the Kalman Filter, 580, 581
Revolute joint, 9
Riccati equations, 195, 201, 203, 209
Rigid-link robotic manipulator, 1, 161, 167, 169, 175
Robot dynamics, 1
Robot kinematics, 1
Robot operating in free-space, 3
Robot performing compliance tasks, 3
Robot's Lagrangian, 4
Robotic ground vehicles, 391
Robotic unicycles, 341
Robust control, 608
Robust control of AUVs, 593, 595
Robustness, 570, 625

Robust observer, 414, 452
Robust state estimator, 339, 389, 428
Root Mean Square Error (RMSE), 180, 188, 204, 212, 242, 254, 531
Rotary pendulum, 65, 66, 207, 214, 215, 222
Rotation frame, 280
Rotation matrix, 280, 472
Rotation-translation matrix, 9
RTK-GPS, 366, 687

S
Self-tuning controller, 181, 189
Sensitivity matrix, 583
Sensitivity test for fault diagnosis, 585
Sensor fusion, 564, 639
Sensor fusion-based estimation, 572
Sensor fusion-based motion estimation, 504
Ship motion control systems, 503
Ship-mounted cranes, 65, 66, 85
Ship tracking, 501, 502
Ship's control forces, 507
Ship's dynamic model, 507
Ship's kinematic and dynamic model, 508
Sigma-Point Kalman Filters, 661, 662
Sigma-points, 662
Singularity problem, 552
Sliding mode control, 101, 271, 272, 291, 292, 300, 428
Sliding-mode control law, 294
Sliding surface vector, 294
Solution of the inverse kinematics problem, 285
Stability of local gradient algorithms, 651
Stabilizable system, 37, 76, 92, 106, 124, 262, 274, 330, 380, 403, 420, 440, 491, 559, 635
Stabilizing feedback control, 209, 217, 692
Stabilizing H-infinity controller, 321
State estimation-based control, 266, 278, 295, 342, 389, 428, 453, 495
State observer, 189, 197, 303, 311
State-space model of 4-wheel vehicle, 398
Static feedback linearization, 253, 265, 533
Static state feedback, 27
Statistical change detection test, 578
Statistical validation of Fuzzy Kalman Filter, 571
Stochastic gradient algorithm, 650
Stochastic sampling techniques, 662
Submarine's dynamic model, 614, 631
Suppression of vibrations, 286
Switching control gains, 295
Synchronized motion of AGVs, 643
Synchronized motion of USVs, 644, 646

T
Takagi-Sugeno neurofuzzy networks, 313
Takagi-Sugeno neurofuzzy system, 582, 587
Target tracking, 644, 646
Taylor series expansion, 2, 27, 67, 71, 86, 100, 103, 138, 145, 208, 216, 222, 234, 239, 251, 256, 257, 268, 269, 302, 325, 342, 343, 373, 392, 393, 400, 415, 427, 470, 482, 486, 502, 555, 594, 629, 640, 656
Temporary operating point, 89, 115, 118, 138, 208, 216, 325, 342, 436, 594
Time-delays, 1, 88
Tracking error, 263, 275, 293–295, 303, 329, 350, 422, 493
Tracking error dynamics, 74, 91, 106, 123, 148, 191, 199, 209, 217, 309, 331, 348, 380, 402, 405, 441, 561, 618, 621, 636, 692
Tracking of ships' motion, 503
Trajectory optimization, 689
Transfer function matrices, 577
Transformed control inputs, 357
Triangular systems, 206, 214
Truck and trailer system, 391, 392, 415, 424, 425
Two-wheel unmanned vehicle, 341, 376
Two-wheel vehicles, 342

U
Underactuated closed-chain manipulator, 222, 234, 241, 253
Underactuated 3-DOF robotic manipulator, 65, 66, 137, 155
Underactuated electromechanical systems, 67
Underactuated hovercraft, 502, 532, 534, 550
Underactuated overhead crane, 65, 69, 70
Underactuated robotic manipulators, 65, 136
Underactuated rotary pendulum, 98
Underactuated vessels, 501, 532, 540
Underactuation, 123, 221, 233, 245, 536
Underatuated MEMS, 301
Unicycle robotic vehicles, 341–343, 691
Unicycle's kinematic model, 344
Unicycle's linearization, 346
Unknown input observers, 511
Unmanned aerial vehicles, 469, 643

Unmanned ground vehicles, 344, 353, 644
Unmanned surface vessels, 501, 502, 532, 554, 643, 644
Unmanned underwater vessels, 644
Unscented Information Filter, 645, 647, 661, 664, 668, 677
Unscented Kalman Filter, 454, 662
Unscented Kalman Filter's recursion, 663
Unscented transform, 662
USV's kinematic and dynamic model, 558
USVs synchronized motion, 644

V
Validation of distributed Kalman Filter, 501, 571
Validation of distributed Kalman Filtering, 502
Validation of Fuzzy Kalman Filter, 503, 571
Van-der-Pol oscillator, 302, 325, 326, 335
Variable structure control, 291
Vessel's dynamic model, 505, 507
Vessel's kinematic model, 505, 507
Vibration modes, 271, 274, 295, 300

W
Weights adaptation law, 197, 205, 250, 262, 622
Weights vector, 187, 195
Wind and wave forces on ship, 507
4WS autonomous vehicle, 427–429, 432, 436, 438, 439, 444
4WS vehicle kinematics, 432

X
χ^2 change detection test, 571, 582, 588
χ^2 distribution, 579

Z
Zero-mean Gaussian distribution, 574
Zero mean Gaussian process, 579